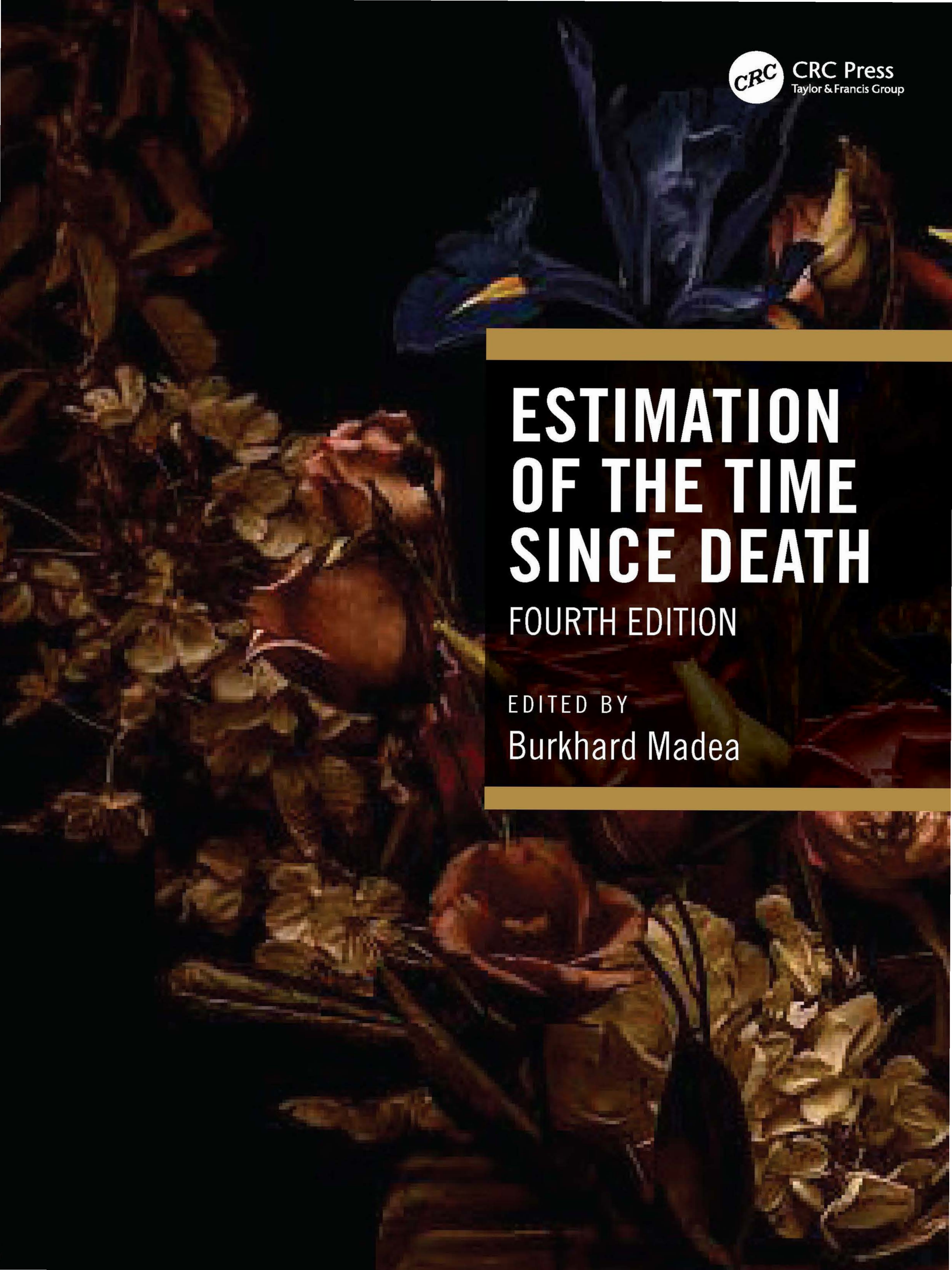

CRC Press
Taylor & Francis Group

ESTIMATION OF THE TIME SINCE DEATH

FOURTH EDITION

EDITED BY
Burkhard Madea

Fourth Edition

Estimation of the Time Since Death

Estimation of the Time Since Death remains the foremost authoritative book on scientifically calculating the estimated time of death post-mortem. Building on the success of previous editions, which covered the early post-mortem period and the third edition's coverage of the later post-mortem period, this edition includes a new chapter on DNA/RNA degradation and a new chapter on drug testing in hair, widening the scope of the material.

Chapters have been improved, updated and expanded, and they include new and additional images to enhance the text. A unique work of synthesis combining rigorous science with practical guidance, this edition reinforces the book's reputation as an invaluable resource—and also the standard—for the estimation of the time since death.

Taylor & Francis
Taylor & Francis Group
http://taylorandfrancis.com

Fourth Edition

Estimation of the Time Since Death

Fourth Edition

Edited by

Burkhard Madea

CRC Press
Taylor & Francis Group
Boca Raton London New York

CRC Press is an imprint of the
Taylor & Francis Group, an **informa** business

Cover image—Getty © 685478291

Fourth edition published 2023
by CRC Press
4 Park Square, Milton Park, Abingdon, Oxon, OX14 4RN

and by CRC Press
6000 Broken Sound Parkway NW, Suite 300, Boca Raton, FL 33487-2742

© 2023 selection and editorial matter, Burkhard Madea; individual chapters, the contributors

First edition published by Elsevier 1995

CRC Press is an imprint of Informa UK Limited

The right of Burkhard Madea to be identified as the author of the editorial material, and of the authors for their individual chapters, has been asserted in accordance with sections 77 and 78 of the Copyright, Designs and Patents Act 1988.

This book contains information obtained from authentic and highly regarded sources. While all reasonable efforts have been made to publish reliable data and information, neither the author[s] nor the publisher can accept any legal responsibility or liability for any errors or omissions that may be made. The publishers wish to make clear that any views or opinions expressed in this book by individual editors, authors or contributors are personal to them and do not necessarily reflect the views/opinions of the publishers. The information or guidance contained in this book is intended for use by medical, scientific or health-care professionals and is provided strictly as a supplement to the medical or other professional's own judgement, their knowledge of the patient's medical history, relevant manufacturer's instructions and the appropriate best practice guidelines. Because of the rapid advances in medical science, any information or advice on dosages, procedures or diagnoses should be independently verified. The reader is strongly urged to consult the relevant national drug formulary and the drug companies' and device or material manufacturers' printed instructions, and their websites, before administering or utilizing any of the drugs, devices or materials mentioned in this book. This book does not indicate whether a particular treatment is appropriate or suitable for a particular individual. Ultimately it is the sole responsibility of the medical professional to make their own professional judgements, so as to advise and treat patients appropriately. The authors and publishers have also attempted to trace the copyright holders of all material reproduced in this publication and apologize to copyright holders if permission to publish in this form has not been obtained. If any copyright material has not been acknowledged please write and let us know so we may rectify in any future reprint.

All rights reserved. No part of this book may be reprinted or reproduced or utilised in any form or by any electronic, mechanical, or other means, now known or hereafter invented, including photocopying and recording, or in any information storage or retrieval system, without permission in writing from the publishers.

For permission to photocopy or use material electronically from this work, access www.copyright.com or contact the Copyright Clearance Center, Inc. (CCC), 222 Rosewood Drive, Danvers, MA 01923, 978-750-8400. For works that are not available on CCC please contact mpkbookspermissions@tandf.co.uk

Trademark notice: Product or corporate names may be trademarks or registered trademarks and are used only for identification and explanation without intent to infringe.

British Library Cataloguing-in-Publication Data
A catalogue record for this book is available from the British Library

ISBN: 978-1-032-13553-3 (hbk)
ISBN: 978-1-003-24497-4 (ebk)

DOI: 10.1201/9781003244974

Typeset in Melior
by Apex CoVantage, LLC

Contents

Preface to the Third Edition vii
Preface to the Fourth Edition ix
Editor Biography xi
List of Contributors xiii

1 General Remarks on Estimating the Time Since Death 1
Burkhard Madea and Claus Henssge

2 Historical Review on Early Work on Estimating the Time Since Death 9
Bernard Knight and Burkhard Madea

3 Supravitality in Tissues 25
Burkhard Madea

4 Rigor Mortis: Estimation of the Time Since Death by Evaluation of Cadaveric Rigidity 51
Thomas Krompecher

5 Post-mortem Lividity: Hypostasis and Timing of Death 71
Burkhard Madea and Bernard Knight

6 Post-mortem Body Cooling and Temperature-Based Methods 77
Claus Henssge, Michael Hubig, Michał Kaliszan, Gita Mall,
Holger Muggenthaler, Stefan Potente, Guy Rutty

6.1 Basics and Application of the 'Nomogram Method' at the Scene 79
Claus Henssge

6.2 Finite Element Method in Temperature-Based Death Time Determination 132
Michael Hubig, Holger Muggenthaler, Gita Mall

6.3 The Prism Method 152
Stefan Potente

6.4 The Use of Temperatures Recorded from the External Auditory Canal for the Estimation of the Post-mortem Intervalt 162
Guy Rutty

6.5 Eye Temperature and the Time Since Death 181
Michał Kaliszan

7 Autolysis, Putrefactive Changes and Post-mortem Chemistry 187
Elke Doberentz, Claus Henssge, Bernhard Knight, Burkhard Madea,
Frank Musshoff, Angela Pittner, Stefan Pittner, Torleiv Ole Rognum, Brita Zilg

7.1 Autolysis (Self-digestion) 189
Burkhard Madea

7.2a Eye Changes After Death 201
Burkhard Madea and Claus Henssge

7.2b Potassium Levels Combined with Age and Temperature 229
Brita Zilg

7.2c **Estimation of Time Since Death Based on Vitreous Humour Hypoxanthine and Temperature Measurement** 232
Torleiv Ole Rognum

7.3 **Cerebrospinal Fluid Chemistry** 240
Burkhard Madea and Claus Henssge

7.4 **Estimation of Duration of Immersion** 245
Elke Doberentz and Burkhard Madea

7.5 **H^3-Magnetic Resonance Spectroscopy** 259
Frank Musshoff and Burkhard Madea

7.6 **Post-mortem Protein Degradation** 264
Stefan Pittner and Angela Pittner

8 **DNA/RNA Degradation and Time Since Death** 283
Akihiko Kimura and Toshikazu Kondo

9 **Gastric Contents and Time Since Death** 295
Burkhard Madea, Bernard Knight, Elke Doberentz

10 **Immunohistochemical Methods as an Aid in Estimating the Time Since Death** 309
Burkhard Madea

11 **Practical Casework** 313
Claus Henssge, Burkhard Madea and Stefan Potente

11.1 **Integration of Different Methods in Casework** 313
Claus Henssge and Burkhard Madea

11.2 **Conditional Probability in Death Time Estimation** 328
Stefan Potente

12 **Forensic Entomology** 335
Saskia Reibe

13 **Radiocarbon Dating: Basic Principles and Applications** 345
Wilfried Rosendahl and Doris Döppes

14 **Cross-Sectional Imaging and the Post-mortem Interval** 355
Guy Rutty

15 **Drug Testing in Hair for the Estimation of the Time Since Death** 371
Christopher Wiedfeld and Frank Musshoff

Index 375

Preface to the Third Edition

Estimation of the time since death is a practical task in daily forensic casework. Already the physicians of the 19th century were familiar with the difficulties to estimate the time since death. As a historical review will indicate, the problem of determining to estimate the postmortem interval has absorbed doctors and scientists for at least one century and a half, yet accuracy still remains beyond our grasp. For about the last 50 years, forensic scientists have tried hard to solve the problem of estimating the time since death by developing methods that would permit the determination of the exact time of death. But the results of all these often even very extensive studies clearly show that the moment of death can only be determined within certain limits of probability. According to Francis E. Camps the establishment of the time since death must have a true scientific backing both on an experimental and statistical basis. Otherwise the evidence might possibly be dangerous to the aims of justice. The main aim should be to obtain a figure with the smallest range of error as possible. In fact, it would be better to prove without contradiction that death could have occurred at a time when a certain person was present rather than it did occur at a certain exact time.

This book is based on basic research and this basic research should always be the background for time since death estimation in practice. However, a practical case does sometimes not fit into the experimental background of scientific research. Instead of analysing a case and evaluate it which information on postmortem changes is possible to obtain some practitioners rely only on environmental evidence instead of seeking an intellectual challenge to find solutions based on an examination of the scene of death and the body.

Relying just on environmental evidence is often not more than certain convenience or even laziness of the forensic pathologist who may feel unpleasant to study the results of research.

Since the last edition of this book numerous papers on estimation of the time since death have been published. Most of them have in common that they are of no value for practice.

The main criterion for the quality of any new method is that it helps to solve a case better, easier and with greater accuracy compared to traditional methods.

Progress in the field of death time estimation usually requires long lasting research.

Real progress will not be achieved by just writing a paper but if research focuses for **years** on a special problem rising from the basic idea to validation of the method over field studies which prove the accuracy and reliability of the method.

In practice, estimating the time of death is not always an exact science. The best we can achieve is often only a reasoned guess taking into account all known factors. Our aim should be to limit the margin of error inherent in assessing the effects of these factors. Aim of methods of estimating the time since death is according to Camps to give true scientific evidence and to avoid at all costs a miscarriage of justice. However, in some cases the time of death resembles somewhat the value attributed in some peoples mind to the lie detector. It is hoped that this new book edition will continue to be the main work in English language to provide up to date data and references on this important subject. In this 3rd edition we have included new developments in death time estimation. All chapters of the previous edition were revised and new chapters were added. These new chapters are for instance: Forensic aspects of decomposition: how immunohistochemistry and magnetic resonance spectroscopy can contribute to death time estimation. Estimation of duration of immersion based on decomposition in relation to the actual water temperature. Entomology and the Radiocarbon test have been included as well since they may be of importance already in the early postmortem period. In times of increasing importance of postmortem imaging a chapter on cross sectional imaging and the postmortem interval was included as well. Furthermore a new mathematical approach to narrow down the postmortem interval derived from the compound method (conditional probability in death time estimation) is described in detail.

I have to thank all contributors to the third edition and hope that the book will be a valuable source of information for forensic practitioners and scientists dealing with the estimation of the time since death. Many thanks to my secretary Elke Weinland and the staff of the Institute of Forensic Medicine in Bonn for continuous support.

Burkhard Madea

Taylor & Francis
Taylor & Francis Group
http://taylorandfrancis.com

Preface to the Fourth Edition

Seven years after the third edition, the preparation of a fourth edition of *Estimation of the Time Since Death* was necessary.

The first edition was published in 1995, edited by Professor Bernard Knight, who brought together some forensic pathologists working on time since death.

Without Bernard, this book would never have been born, and the book still seems to be viable.

I still remember the time more than 25 years ago, when I prepared my contributions for the first edition. This is nearly a generation ago and much has been published on time since death in the meanwhile.

Four authors of the first edition are still contributing to the book, but like the previous edition, new aspects of death time estimation had to be considered and presented by new authors. New aspects are, for instance, post-mortem protein degradation, DNA/RNA degradation, circadian rhythm, recent mathematical approaches, taking into account influencing factors such as ambient temperature for a more precise estimation of TSD using vitreous humour, cross-sectional imaging and time since death. These methods should be further developed, and the practical applicability should be carefully observed.

It is hoped that this new edition will continue to be an informative work in the English language to provide up-to-date data and references on this important subject.

It is furthermore hoped that the book inspires research in this field. As already outlined in the previous edition, real success in the field and scientific breakthrough require years of undisturbed research.

The editor of this book has to review many papers submitted to international journals on death time estimation. When the abstract or the paper begins like 'death time estimation is a crucial part in forensic case work' since methods are imprecise and then many papers that have nothing to do with death time estimation in real casework are cited, and the relevant literature is missing, you can already be convinced that the authors are familiar with neither time since death estimation nor forensic medicine. Then either animal experiments are reported on killed rats ('rat and mice forensic pathology') with highly sophisticated biochemical or molecular approaches, which however solve no problem in practice, or a meta-analysis is carried out—mainly done by students supervised by a professor—which do not delve deep into the real problems.

Papers on time since death estimation are abundant and most—even the published papers—are either nonsense or superfluous: waste of time and money. As in the previous editions, this book focuses on time since death in practice. The forensic pathologist going to the scene of crime should use it and benefit from it.

The 'rat forensic pathologist' with biochemical or molecular background should at least learn something about the essentials of death time estimation in practice.

One of the co-authors of this book, Professor Claus Henssge, aged 85, died last year (Figure 0.1).

Born on June 3, 1936, in Dresden, he later studied medicine at the Humboldt University in East Berlin where he also received his MD. He started his career in physiology at the Institute of Applied Physiology, collaborating with Professor Adolf-Henning Frucht (1913–1993). The institute had three research departments: biophysics, physiology, and applied physiology, with a focus on sports and performance physiology. Since the head of the department was also interested in biomathematics, he studied this, too.

This education in physiology and later also in sports medicine formed the essential basis for his scientific work in forensic medicine. In 1966, Dr Henssge was then board-certified as a physiologist.

For political reasons he had to leave his job in sports medicine in 1975 and was offered another job at the Humboldt-University in East Berlin. He was allowed to choose the field, and so he decided to start a second career at

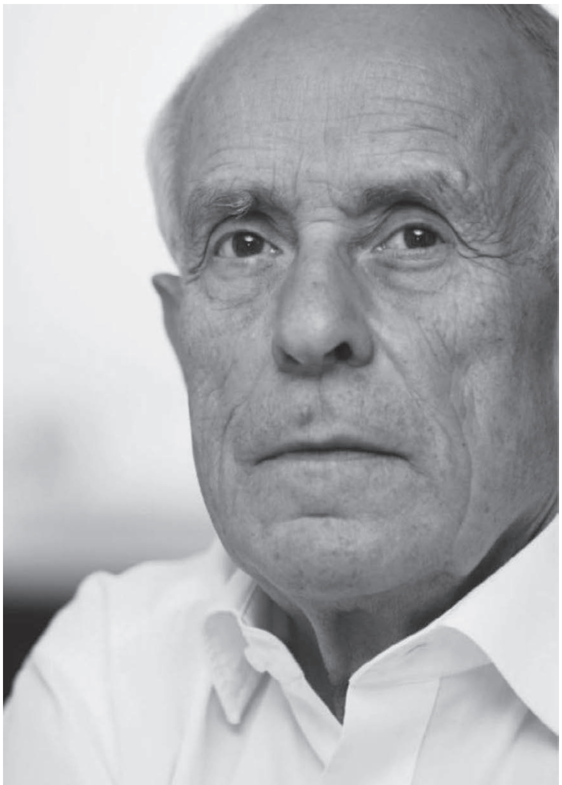

Figure 0.1 Professor Claus Henssge.

(Photo: ® Timo Bobert, Berlin)

the Institute of Forensic Medicine led by Professor Otto Prokop.

He soon started with his experiments on human body cooling and found empirical solutions for the two-exponential formula by Marshall and Hoare.

He developed the nomogram for time of death estimation under standard cooling conditions (rectal-temperature-time of death nomogram).

For ambient temperatures above 23°C, he used the material of De Saram et al.

In 1980 he was board-certified as an expert in forensic medicine and in 1982 received the licence to lecture (habilitation).

Meanwhile, he had also carried out extensive investigations on body cooling under non-standard conditions.

In 1983 he moved from East to West Germany and was appointed deputy at the Institute of Forensic Medicine of the University of Münster.

Further steps in his scientific career were investigations on central brain temperature and body cooling in water-immersed bodies.

He was always in further contact with physiologists. In Münster, for example, with a cardiac physiologist with whom first results on the supravital electrical stimulation of skeletal muscle using a force transducer for objectifying the muscle contraction were produced.

In 1986 he was appointed Professor of Forensic Medicine at the University of Cologne, and in 1993 Professor and Director at the Institute of Forensic Medicine at the University of Essen. The focus of his own scientific work was always the time of death using the decrease of body temperature. He used cooling dummies for simulation of body cooling. Further main research fields were the empirical evaluation of body corrective factors for body cooling under non-standard conditions, evaluating the dependence of the corrective factors from the real body weight and estimation of the time since death in cases of change of the ambient temperature.

Furthermore, he carried out single- and multicentre studies on the reliability of the nomogram method. Besides his own research, he stimulated research on other methods of death time estimation, for instance, supravital electrical excitability and chemical methods, especially on vitreous humour, amongst others.

In 1988 the first German monograph on death time estimation was published and in 1995 an English monograph, titled *The Estimation of the Time Since Death in the Early Postmortem Period*, originally edited by Bernard Knight, followed. This monograph is now published in a fourth edition.

Professor Henssge worked not only in research but also in practice in the whole field of forensic medicine, and he was a very respected expert at court, especially in difficult trials.

His practical work in forensic medicine was very much influenced by the school of Otto Prokop in East Berlin.

However, his first postgraduate training in physiology was the basis of all the research on death time estimation and without his experimental and mathematical training in physiology, this career in forensic medicine would not have been possible.

In 2003 Professor Henssge retired, but even after his retirement, he was available to give younger colleagues advice on their further research.

He was a genuine and focused man and colleague, free from any vanities. Until his death he was clearheaded and interested but due to underlying conditions physically limited.

Not only the German forensic medicine but forensic medicine worldwide has lost one of the leading scientists in the field.

I have to thank all contributors to the fourth edition and hope that the book will be a valuable source of information for both practitioners and scientists.

Burkhard Madea

Editor Biography

Professor Burkhard Madea is a world-renowned forensic pathologist and is the author of approximately 40 books and 700 papers. He earned his medical licence in 1982, working as a medical doctor in the German army from 1983 to 1984. He completed his postgraduation degree in forensic medicine from the University of Münster, further continuing his forensic studies at the University of Cologne from 1985 to 1989. In 1991 he was appointed as Professor of Forensic Medicine at the University of Cologne. In 1996 he was appointed as Professor of Forensic Medicine at the University of Bonn. He also served as the Head of the Institute of Forensic Medicine until his retirement in autumn of 2022.

Taylor & Francis
Taylor & Francis Group
http://taylorandfrancis.com

Contributors

Elke Doberentz
Institute of Forensic Medicine
University of Bonn, Germany

Doris Döppes
World Cultures and Natural History
Reiss-Engelhorn-Museum, Mannheim, Germany

Claus Henssge†
Institute of Forensic Medicine
University of Essen, Germany

Michael Hubig
Institute of Forensic Medicine
Jena University Hospital
Friedrich Schiller University Jena, Germany

Michał Kaliszan
Department of Forensic Medicine
Medical University of Gdansk, Poland

Akihiko Kimura
Department of Forensic Medicine
Wakayama Medical University, Wakayama, Japan

Bernard Knight
University of Wales
College of Medicine
Cardiff, Wales

Toshikazu Kondo
Department of Forensic Medicine
Wakayama Medical University, Japan

Thomas Krompecher
University of Lausanne, Switzerland

Gita Mall
Institute of Forensic Medicine
Jena University Hospital
Friedrich Schiller University Jena, Germany

Holger Muggenthaler
Institute of Forensic Medicine
Jena University Hospital
Friedrich Schiller University Jena, Germany

Frank Musshoff
Forensic Toxicological Centre
Munich, Germany

Angela Pittner
Department of Environment and Biodiversity
Paris Lodron University of Salzburg
Salzburg, Austria

Stefan Pittner
Department of Forensic Medicine
Paris Lodron University of Salzburg
Salzburg, Austria

Stefan Potente
Institute of Legal Medicine
University of Saarland, Germany

Saskia Reibe
Institute of Forensic Medicine
University of Bonn, Germany

Torleiv Ole Rognum
Institute of Forensic Medicine
University of Oslo, Norway

Wilfried Rosendahl
Reiss-Engelhorn-Museen
Curt-Engelhorn-Centre of Archaeometry
Head German Mummy Project, Germany
Mannheim, Germany

Guy Rutty
East Midlands Forensic Pathology Unit
University of Leicester, UK

Christopher Wiedfeld
Forensic Toxicological Centre
Munich, Germany

Brita Zilg
Institute of Forensic Medicine
Karolinska Institute, Sweden

Taylor & Francis
Taylor & Francis Group
http://taylorandfrancis.com

1 General Remarks on Estimating the Time Since Death

Burkhard Madea and Claus Henssge

Contents

1.1 Estimation of the Time Since Death 1
  1.1.1 Design of Study (Methodology) 3
    1.1.1.1 Case Material 4
    1.1.1.2 Analyses of Results 4
  1.1.2 Conclusions 4
1.2 Errors in Estimating the Time Since Death 4
  1.2.1 Time Since Death as Evidence at Court 6
    1.2.1.1 Case Example (for the Basics on body cooling See Also Chapter 6.1) 6

1.1 Estimation of the Time Since Death

Bernard Knight [12] began the general introduction to the previous edition with the following words:

> The importance of estimating the time since death must have been appreciated for centuries, probably millennia. Even in the most unsophisticated societies, when homicides took place the community would inevitably have correlated the location and movements of the prime suspects with the apparent time of death—however crude that comparison might have been—to test what would later become the defence of alibi.
>
> Little has changed from those early days, except that their data acquisition equipment was merely the back of a hand to test the coolness of the corpse's skin, and their eyes and nose to evaluate decomposition. We now have multichannel thermometry with thermocouples sensitive to a fraction of a degree, enzyme methods, vitreous chemistry, muscular reactivity and several other avenues for collecting data. Regrettably, the accuracy of estimating the postmortem interval has by no means kept pace with the enormous strides made in technological sophistication.

Estimation of the time since death is a practical task in daily forensic casework. The main objective is to give the police a first estimation of the time since death already at the place where the body was found. Methods of estimating the time since death should, of course, be as precise as possible, but even more important is its reliability. Reliability as the most important principle can only be provided empirically by statistical analysis of mistakes (deviation between calculated and real time since death) in field studies (Camps, Figure 1.1).

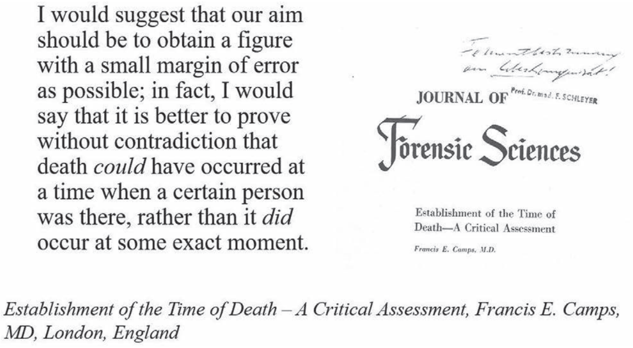

I would suggest that our aim should be to obtain a figure with a small margin of error as possible; in fact, I would say that it is better to prove without contradiction that death *could* have occurred at a time when a certain person was there, rather than it *did* occur at some exact moment.

JOURNAL OF Prof. Dr. med. F. SCHLEYER

Forensic Sciences

Establishment of the Time of Death—A Critical Assessment

Francis E. Camps, M.D.

Establishment of the Time of Death – A Critical Assessment, Francis E. Camps, MD, London, England

Figure 1.1 Copy of the article of Professor Camps dedicated to Professor Schleyer (1913–1995) Bonn, a leading German expert on time since death estimation at that time.

The demands of practice are to be precise, to be reliable and to give an immediate result. The main principle of determining the time since death is the calculation of a measurable date along a time-dependent curve back to the starting point. Characteristics of the curve (e.g. the slope) and the starting point are influenced by internal and external, antemortem and post-mortem conditions.

Therefore, the estimation of the time since death will never reveal a time point, but rather an interval.

Methods of estimating the time since death are based on two different approaches:

1 Which antemortem changes, either physiological or pathological, can be detected and allow, together with police investigations, a conclusion on the

DOI: 10.1201/9781003244974-1

time since death (survival time)? Methods such as wound-age estimation and gastric emptying when time and volume of the last meal are known follow this approach.
2 Which post-mortem changes allow a conclusion to be made on the time since death? Most methods used in practice follow this second approach.

There is extensive literature on methods proposed for estimating the time since death. However, most of these methods have never gained practical importance. Many papers on 'estimating the time since death' simply describe the time dependence of an analyte or parameter. However, the search for new analytes on post-mortem changing parameters does not make any sense because nearly all parameters are changing more or less with an increasing post-mortem interval. Furthermore, just applying new technologies ('time since death markers have lagged behind the advance in technology over the past 50 years') does not involve any breakthrough for the practical purposes of death time estimation.

The various methods proposed for estimating the time since death are completely different from each other:

- Predominantly physical processes such as body cooling and hypostasis.
- Metabolic processes such as concentration changes of metabolites, substrates and activity of enzymes.
- Autolysis (loss of selective membrane permeability, diffusion according to Fick's law with increase or decrease of analytes in various body fluids, morphological changes).
- Physicochemical processes (supravital reagibility, rigor mortis, immunological reactivity).
- Bacterial processes (putrefaction).

Furthermore, the methods for estimating the time since death are not only different but also have widely varying scientific value in terms of the underlying scientific background, the mode of investigation and the validation of the method (Table 1.1). Already Camps wrote in his critical assessment that time since death estimation must have a true scientific backing both on an experimental and statistical basis for otherwise the evidence must possibly be dangerous to the interests of justice.

Methods of the highest scientific value do, of course, comprise methods with a quantitative measurement of post-mortem changes and a mathematical description that takes into account influencing factors quantitatively. Clear data on the precision of the method are available, and the data on precision have been proved on independent material and in field studies.

Conversely, the evidence for death time estimation of the lowest scientific value involves methods with only a subjective description of the post-mortem change. The progression of a post-mortem change is entirely dependent on ambient factors. However, these ambient factors cannot be taken into account quantitatively.

Table 1.1 Grading of Methods of Estimating the Time Since Death Regarding Mode of Registration of Post-mortem Changes, Description, Considering Influencing Factors; Calculation of Confidence Limits

1. Quantitative measurement, mathematical description, taking into account influencing factors quantitatively, declaration of precision, proof of precision on independent material. Examples: body cooling (nomogram method), potassium in vitreous humour.
2. Subjective description (grading), considering influencing factors, declaration of precision, proof of precision on independent material. Example: supravital reactions.
3. Subjective description of post-mortem changes; influencing factors known 'in principle', empirical estimations instead of statistically evaluated reference values. Examples: rigor mortis, lividity.
4. Subjective description; analogous conclusions based on empiricism and assumptions instead of statistically evaluated reference values. Example: gastric contents.
5. Subjective description, velocity of progression of post-mortem changes entirely depending on ambient factors; because of the broad spectrum of ambient factors, no sound empirical estimation possible. Example: putrefaction.

Table 1.2 Objectives of Estimating the Time Since Death

1. To give the police a preliminary idea on the time of an assault in criminal connotations.
2. To check whether the time since death is consistent with the alibi of a suspect.
3. When two deaths occur, especially of spouses or siblings, the order of deaths and hence survivorships.
4. Registration purposes: 'Enquire where, when and by what means a person came to death'.

The estimation of the time since death at the scene of crime has, as already mentioned, two different objectives (Table 1.2):

1 To give the police a preliminary idea of the time of an assault. The time since death gives information on the time of an assault only in those instances in which the survival period after an injury was short.
2 To check whether the time since death is consistent or inconsistent with the alibi of a suspect. Only in rare cases does the time of death play a major role in court as the only evidence for or against the guilt of a suspect [20] (see also the case example at the end of this chapter).

However, the coroner, medical examiner or other authority needs to know the time and date of death for registration purposes. Indeed, the legal basis of the English coroner's jurisdiction is to 'enquire where, when and by what means a person came to his death'.

Other matters besides usual criminal connotations concern insurance and contract and culpability issues, as well as situations in which two deaths, especially of spouses or siblings, occur close together, and the order of those deaths—and hence survivorship—may have profound effects on the transfer of estate and property [12].

Before any suspect is questioned or charged, knowledge of the approximate time of death is essential if the investigating officers are to direct their enquiries in the appropriate direction. The relationship of the time of death with other events, with persons in the vicinity and with those who could not have been in the vicinity, will automatically channel investigative efforts along certain lines. When several suspects are being considered, the best estimate of the time of death forms a primary screening procedure to eliminate some putative killers, who could not have had access to the deceased at the material time, and it may strengthen suspicion against others whose movements coincided with an estimated time. There is thus a heavy responsibility on the doctor who offers an opinion as to the probable time of death—if they are significantly in error, an investigation may be dislocated at its earliest and perhaps most vulnerable stage.

To offer an unreasonably accurate time of death is worse than providing such a wide range of times that the police can derive no help from it. In the latter situation, police officers do at least then know that they have to use other methods in their investigations, but to mislead the police by some outrageously precise time runs the risk of excluding the true culprit, as well as falsely implicating an innocent party [12].

For estimating the post-mortem interval, different sources are used [22]:

1. Evidence from the body of the deceased (post-mortem changes).
2. Information from the environment in the vicinity of the body (date of the newspaper, open television programme).
3. Anamnestic factors concerning the deceased's habits (leaving a flat, arriving at work, day-to-day activities).

For the forensic investigation of the time since death, all sources of information on the time since death always should be kept in mind. In forensic medicine much research has been carried out on post-mortem changes. The progression of all post-mortem changes is influenced by many internal or external factors, mainly the ambient temperature. The longer the post-mortem interval, the less accurate is the estimation of the time since death based on post-mortem changes [22].

Post-mortem changes, especially body cooling, have been investigated with sophisticated methods, and formulas developed to calculate the time since death are full of mathematics. Despite the high level of research in estimating the time since death, in practice we can often achieve not more than a reasoned guess on the time elapsed since death.

1.1.1 Design of Study (Methodology)

If new parameters are studied, the following should be kept in mind: What is the nature of the underlying process studied [3, 6,17] (Figure 1.1)?

- Predominantly physical processes (body cooling, hypostasis).
- Metabolic processes (e.g. concentration of metabolites and substrates, activity of enzymes).
- Autolysis (loss of selective membrane permeability, diffusion, morphological changes).
- Physicochemical processes (supravital reagibility, rigor mortis, immunological reactivity).
- Bacterial process (putrefaction).

Analysing the underlying process may already prevent wrong expectations. In theory, it could be expected that a parameter with just a post-mortem increase that is solely caused by diffusion would correlate much more strongly with the time since death than would a parameter that increases as a result of vital/post-mortem degradation (metabolic process) and diffusion [19]. Furthermore, a clear definition of the site of measurement or site of sample acquisition is necessary. Post-mortem changes should preferably be investigated in longitudinal studies with objective measurements of these changes, although it should be kept in mind that the objective measurement contributes only in a small part to a more accurate death time estimation.

For the early post-mortem interval with body cooling and supravital reactions, standards in practice have been established, and applicability and reliability were confirmed in field studies that can hardly be improved by other studies [1,4–10,14–19]. Therefore, research should focus on the later post-mortem interval. However, investigations on the time course of any analyte do not make any sense without also verifying the variability because

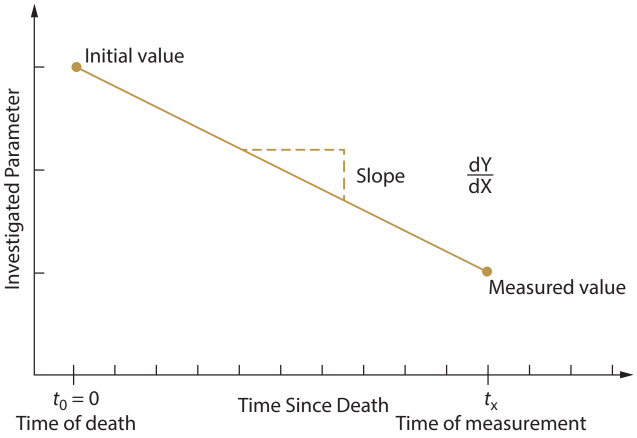

Figure 1.2 Main principle of the determination of the time since death (calculation from a measured value along a curve back to the initial value).

it is often the interindividual variability that prevents the application of a parameter in practice (besides the fact that *in corpore* measurements at the scene are, from the standpoint of practicability, always of higher value compared with *in vitro* measurements).

Therefore, at some different times (10, 20, 30,. . ., hpm), post-mortem (time-dependent) investigations and taking samples from some bodies should be carried out; however, the ambient temperature or temperature history of the bodies should differ markedly (e.g. differing ambient temperature for identical post-mortem intervals). This time-saving procedure already allows a first estimation of the variability in comparison with established methods. If new parameters or methods are recommended for death time estimation, their reliability and accuracy should always be compared with those of methods developed for the same post-mortem period. Besides the same post-mortem interval, a comparison of methods should always address the practicability and the time interval until results are available. Influencing factors governing the change of an investigated parameter should be studied (preferably in longitudinal studies), and they should be taken into account for the death time estimation quantitatively. Without considering influencing factors, a wide period will result. Control studies on independent case material must be carried out to prove the accuracy of the method. Furthermore, field studies on cases with a known time since death are necessary to check the practicable applicability, reliability and accuracy compared with standard methods. Additionally, the combination of different methods for a common result of death time estimation should be investigated [9,15].

1.1.1.1 Case Material

The case material should comprise different causes of death; diseases and the duration of the terminal episode may be vital points for the strength of correlations between investigated parameter and time since death, and they must be addressed [16,18].

1.1.1.2 Analyses of Results

For statistical analysis, it is not sufficient to present only mean values of the correlation between investigated parameters and time since death or correlation coefficients. Instead, statistical parameters of the deviation of single values from the mean correlation such as confidence limits are necessary.

1.1.2 Conclusions

The huge amount of literature, especially on chemical methods of estimating the time since death [24], is still increasing. However, most of these methods have never gained any practical relevance because they do not meet the demands of practice (being precise, being reliable and giving immediate results). Field studies are good indicators of the practical value of a method, but, to our knowledge, field studies on most methods of estimating the time since death are nearly completely missing in the literature compared, for instance, with studies of body cooling or supravital reactions [1,8,9,15]. Thus, most methods proposed for an estimation of the time since death are of only academic interest because they describe just post-mortem changes. These methods gain practical relevance only if the following criteria are fulfilled: quantitative measurements, mathematical descriptions, taking into account influencing factors quantitatively and declarations of precision and proof of precision on independent material.

Without validation of a method and field studies, the application of novel approaches in practice may be misleading, a miscarriage of justice and irresponsible.

1.2 Errors in Estimating the Time Since Death

Camps [2] stated that estimating the time of death is not an exact science:

> The best we can achieve is a reasoned guess taking into account all the known factors and our aim should be to limit the margin of error inherent in assessing the effect of these factors. Aim of estimating the time since death is to give true scientific evidence and avoid at all costs a miscarriage of justice. . . . in other words, I feel that at present the time of death resembles somewhat the value in some people's minds to the lie detector [2].

Van den Oever [25] proposed that for greater accuracy in the estimation of the time since death, it seems that the proper way is to find a suitable combination of the most efficient known methods. Using different methods with a different background concerning post-mortem changes and analytical approaches increases the reliability of the estimation of the time since death and the self-confidence of the investigator. Therefore, in the protocol of a medicolegal autopsy, as in the report of the crime scene investigation, it is better to describe ten findings that prove to be of no significance than to omit a single finding that may be critical [21].

In his famous paper on classical mistakes in forensic pathology, Alan R. Moritz [21] summarized some errors of omission in the collection of evidence required for establishing the time of death:

1. Failure to record the rectal temperature of the body.
2. Failure to observe changes that may occur in the intensity and distribution of rigor mortis—before, during and after autopsy.
3. Failure to observe the ingredients of the last meal and its location in the alimentary tract.

A further classical mistake, especially concerning estimating the time since death, may be to talk too soon, too much or to the wrong people. This was outlined by Moritz [21] with an illustrative case example. The danger of releasing opinions prematurely is illustrated by the following case: because the dead woman's body was still warm and there was no rigor, Dr X, the pathologist, told the district attorney, who was eager to know the time of death, that the woman probably died early that morning. Dr X provided this information before the autopsy had actually been started. The district attorney immediately passed this information to news reporters. Shortly before the noon edition of the newspapers reached the streets, the pathologist realized that the news was released too soon. The degree of autolysis of the parenchymatous organs, together with the presence of intravascular haemolysis, indicated a considerably longer post-mortem interval than he originally thought. The noon edition of the newspaper carried two items on the first page: the district attorney's news release to the effect that Dr X had established that the woman was murdered early that morning, and a recent news bulletin stating that the murderer had just confessed and took the responsibility of killing the woman during the evening of the preceding day. Approximately 12 hours after the murder, and 2 hours before the body was found, the murderer moved the woman's body from the warm room where the crime occurred to the cool basement where the police found the victim. The interior of the body was warm because it had been in a warm place during most of the post-mortem period. There was no rigor because rigor had developed and regressed. If the murderer had not confessed and was able to establish an alibi for the time that the murder was supposed to have been committed, the murderer could have been proved to be innocent by using the pathologist's premature and incorrect guess.

General problems in estimating the time since death can be summarized as follows:

- Most methods are of help only in the first 1 or 2 days post-mortem.
- Does the actual case meet the requirements of experimental investigations (e.g. unusual cooling conditions with no reference values)?
- High ambient temperature is a problem.
- Is experimental reference material with calculation of the margin of error available or not (e.g. preservation of decomposing bodies in plastic bags)?
- Being unfamiliar with the scientific background, the requirements and limitations of a method is a problem.

The main errors in estimating the time since death can be summarized as follows:

- Not taking into account the post-mortem temperature plateau.
- Using rules of thumb.
- No careful examination of the scene of the crime (severe changes in cooling conditions).
- Calculation of a mean value without confidence limits.
- Using a wrong temperature site for calculation (e.g. outer ear temperature is used as body core temperature in the nomogram).
- Not taking into account influencing factors.
- Post-mortem changes not seen in a context.

Factors that can introduce errors into the calculation of the time since death by body cooling include the following:

- The ambient temperature can vary widely and rapidly in certain conditions and can swing both higher and lower than the final temperature as measured on discovery of the body. The temperature of the environment is, of course, partly determined by some of the other factors.
- Wind and draughts affect body temperature by increasing convection and conduction from the surface and by evaporating moisture.
- Rain, humidity and snow, apart from the direct temperature effect, alter the evaporative properties of the skin and clothing.
- The body posture alters the rate of heat loss, by varying the effective exposed surface area per unit mass available for convection and conduction.
- The body size also alters the mass/surface area ratio. Infants and children cool more quickly for this reason because the heat gradient from the core is steeper.
- Naturally, clothing (or its lack) makes a very great difference to cooling rates. Other coverings, such as bedclothes, other fabrics, even debris or another adjacent body, can dramatically alter the cooling characteristics.
- In the same way as clothing, body fat acts as an insulator, and its deficiency or absence accelerates cooling, and *vice versa*.
- However debatable the applicability of Newton's law of cooling may be to human cooling, there is no doubt that the original body temperature at the time of death affects the progress of heat loss. This is partly by the Newtonian principle of a higher cooling rate where the excess of body temperature above ambient is large, but also from the smaller fall of temperature remaining above ambient.
- Further problems are the result of fever at death, a longer agonal period and hypothermia.

Table 1.3 Calculations of the Time Since Death for Different Ambient Temperatures and Corrective Factors for the Body Weight

Henssge (www.AMA-soft.de)			
	TU 27,5	**27,5/27,8**	**28,33/28,3**
f **= 1**	15,5 +/– 3,2 12,3–18,7		
Time	7.08–13.32		
f **= 1,1**	16,9 h +/– 4,5 12,4–21,4	17,8 +/– 4,5 13,3–22,3	19,7 +/– 7 12,7–26,7
Time	4.26–13.26	3.32–12.32	23.08–13.08
f **= 1,2**	18,2 +/– 4,5 13,7–22,7	19,2 +/– 4,5 14,7–23,7	21,2 +/– 7 14,2–28,2
Time	3.08–12.08	2.08–11.08	21.38–11.38

Abbreviation: f = corrective factor

One of the few published accounts of an estimation of actual errors was made by James and Knight [11,13]. In this investigation, 110 bodies with a known time of death were examined by two experienced forensic pathologists, each pathologist making the estimation alternately with no knowledge of the real time of death. The estimates were then compared with the true interval to evaluate the errors.

Of the 100 bodies, the true time since death was correctly estimated in only 11 cases, whereas underestimations occurred in 57 cases and overestimations in 32 cases. In 35 of the 100 cases, the error was less than 10 per cent, in 54 cases less than 20 per cent, in 70 cases less than 30 per cent, in 90 cases less than 40 per cent and in 95 cases less than 50 per cent. In two cases, there was an error of 100 per cent. The absolute error increased as the interval grew longer, but, in percentage terms, appreciable errors can also exist even near the time of death.

The general experience gained from this investigation was that in deaths occurring less than 4 hours before estimation, the major problem was the variable 'plateau'. Seven bodies had rectal temperatures at or even above 37°C up to 4 hours post-mortem—a phenomenon constantly encountered since the early days of research in the mid-nineteenth century.

1.2.1 Time Since Death as Evidence at Court

1.2.1.1 Case Example (for the Basics on body cooling, see also Chapter 6.1)

A prostitute was found murdered in her apartment in an Eros Center. A main question at court was if she was killed in the afternoon or already 12 hours earlier in the early morning. According to the prosecution, time of death was in the early afternoon. During the main hearing, the criminal court changed the time of death to early morning, that is 12 hours prior. The case was twice overturned by the Supreme Court because the time change was not sufficiently proved. For the preparation of the third trial, a further physical opinion was ordered on the temperature time course in the room of the prostitute in the last 24 hours. This physical evidence revealed a temperature profile and was the basis for the calculation of the time since death using the nomogram method. Time since death in the afternoon could be excluded; time since death in the early hours of the morning was probable.

The prostitute was found in a prone position on a mattress of her bed. Room temperature at the floor at 1.47 am: 27,3°C. Temperature directly near the body: 27,5°C. Deep rectal temperature at 1.50 am: 30,7°C. Supravital electrical excitability of skeletal muscle: negative. Fully developed rigor mortis in all joints. No reestablishment of rigor mortis. Post-mortem lividity according to a prone position. Incomplete disappearance of post-mortem lividity on sharp pressure.

According to the temperature profile in the room of the prostitute, the time since death was calculated for different ambient temperatures and corrective factors for the body weight. According to the scene findings (lying naked in a prone position on a mattress) at least a corrective factor of 1.1 was necessary. A time of death in the afternoon could be ruled out and a time since death to 12 hours prior was very probable.

References

1. Albrecht A, Gerling I, Henssge C, Hochmeister M, Kleiber M, Madea B, Oehmichen M, Pollak S, Püschel K, Seifert D, Teige K. Zur Anwendung des Rektaltemperatur-Todeszeit-Nomogramms am Leichenfundort. *Z Rechtsmed* 1990;*103*:257–78.
2. Camps F. Establishment of the time since death: a critical assessment. *J Forensic Sci* 1959;*4*:73–6.
3. Henssge C. Todeszeitbestimmung: eine Methodenkritik. *Beitr Gerichtl Med* 1986;*44*:109–16.
4. Henssge C. Rectal temperature time of death nomogram: dependence of corrective factors on the body weight under stronger thermic isolation conditions. *Forensic Sci Int* 1992;*54*:51–6.
5. Henssge C. Temperature-based methods II. In: Henssge C, Knight B, Krompecher T, Madea B, Nokes L (eds.). *The*

Estimation of the Time Since Death in the Early Postmortem Period. 2nd ed. London, Edward Arnold, 2002.

6. Henssge C, Madea B. Methoden zur Bestimmung der Todeszeit an Leichen. In: *Arbeitsmethoden der medizinischen und naturwissenschaftlichen Kriminalistik*, vol. 18. Lübeck, Schmidt-Römhild, 1988.
7. Henssge C, Madea B. Estimation of the time since death in the early post-mortem period. *Forensic Sci Int* 2004;*144*:167–75.
8. Henssge C, Althaus L, Bolt J, Freislederer A, Haffner HT, Henssge CA, Hoppe B, Schneider V. Experiences with a compound method for estimating the time since death. I. Rectal temperature nomo-gram for time since death. *Int J Legal Med* 2000;*113*:303–19.
9. Henssge C, Althaus L, Bolt J, Freislederer A, Haffner HT, Henssge CA, Hoppe B, Schneider V. Experiences with a compound method for estimating the time since death. II. Integration of non–temperature-based methods. *Int J Legal Med* 2000;*113*:320–31.
10. Henssge C, Knight B, Krompecher T, Madea B, Nokes L. (eds.). *The Estimation of the Time Since Death in the Early Postmortem Period*. London, Edward Arnold, 1995 (2nd ed., 2002).
11. James E, Knight B. Errors in estimating the time since death. *Med Sci Law* 1965;*5*:111–16.
12. Knight B. General introduction. In: Henssge C, Knight B, Krompecher T, Madea B, Nokes L (eds.). *The Estimation of the Time Since Death in the Early Postmortem Period*. 2nd ed. London, Edward Arnold, 2002, pp 1–2.
13. Knight B. Errors in estimating the time since death. In: Henssge C, Knight B, Krompecher T, Madea B, Nokes L (eds.). *The Estimation of the Time Since Death in the Early Postmortem Period*. 2nd ed. London, Edward Arnold, 2002, pp 30–1.
14. Madea B. Is there recent progress in the estimation of the postmortem interval by means of thanatochemistry? *Forensic Sci Int* 2005;*151*:139–49.
15. Madea B, Henssge C. Electrical excitability of skeletal muscle postmortem in casework. *Forensic Sci Int* 1990;*47*:207–27.
16. Madea B, Henssge C. Eye changes after death. In: Henssge C, Knight B, Krompecher T, Madea B, Nokes L (eds.). *The Estimation of the Time Since Death in the Early Postmortem Period*. 2nd ed. London, Edward Arnold, 2002, pp 103–33.
17. Madea B, Henssge C. Time since death. In: Payne-James J, Busuttil A, Smock W (eds.). *Forensic Medicine: Clinical and Pathological Aspects*. London, Greenwich Medical Media Limited, 2003, pp 91–114.
18. Madea B, Henssge C, Hönig W, Gerbracht A. References for determining the time of death by potassium in vitreous humor. *Forensic Sci Int* 1989;*40*:231–43.
19. Madea B, Käferstein H, Hermann N, Sticht G. Hypoxanthine in vitreous humor and cerebrospinal fluid: marker of postmortem interval and prolonged (vital) hypoxia? *Forensic Sci Int* 1994;*65*:19–31.
20. Madea B, Potente S, Duval I. Time since death as evidence at court? *Arch f Kriminol*. 2021;*248*:11–30 (in German).
21. Moritz AR. Classical mistakes in forensic pathology. *Am J Clin Pathol* 1956;*26*:1383–92.
22. Pounder D. Postmortem changes and time since death. In: *Department of Forensic Medicine*. Scotland, Dundee, University of Dundee, 1995.
23. Sabucedo AJ, Furton KG. Cardiac troponin I: a time since death marker. *Forensic Sci Int* 2003;*134*:11–16.
24. Schleyer F. Determination of the time since death in the early post-mortem interval. In: Lundquist F (ed.). *Methods of Forensic Sciences*, vol. 2. London, Interscience Publishers, 1963, pp. 253–95.
25. Van den Oever R. A review of the literature as to the present possibilities and limitations in estimating the time of death. *Med Sci Law* 1976;*16*:269–76.

Taylor & Francis
Taylor & Francis Group
http://taylorandfrancis.com

2 Historical Review on Early Work on Estimating the Time Since Death

Bernard Knight and Burkhard Madea

Contents

2.1 Temperature Measuring Scales 9
  2.1.1 Fahrenheit 9
  2.1.2 Centigrade 9
  2.1.3 Réaumur 9
2.2 Early Work on Temperature and Time of Death 9
2.3 Post-mortem Electrical Excitability of Skeletal Muscle—Historical Review 15
2.4 Rigor Mortis 18
  2.4.1 Cadaveric Spasm 19
2.5 Post-mortem Lividity 20
2.6 Putrefactive Changes 21
2.7 Vitreous Potassium as a Measure of the Post-mortem Interval 22

2.1 Temperature Measuring Scales

2.1.1 Fahrenheit

This scale was devised in about 1714 by the German instrument maker Gabriel Fahrenheit (1686–1736). He used a mixture of ammonium chloride and ice for his 0 degrees and his own body temperature for the 100-degree mark. On this scale, the freezing point of water was 32 degrees, and its boiling point was 212 degrees.

2.1.2 Centigrade

This scale is divided into 100 degrees, with the freezing point of water as 0 and its boiling point at 100. It is often misnamed 'Celsius', after Anders Celsius (1701–1744), a Swedish astronomer, who proposed a 100-degree scale in 1742. However, he placed the freezing point of water at 100 and the boiling point at 0 degrees; it was reversed 8 years later by his pupil Martin Stromer.

2.1.3 Réaumur

This scale was devised in France in 1731 by René Réaumur (1683–1757). He used an alcohol thermometer, with the freezing point of water as 0, then graduating the stem into degrees, each of which contained one-thousandth of the volume of the bulb and stem up to the 0-degree mark. Arbitrarily, the boiling point of water lay at 80 degrees on his scale.

2.2 Early Work on Temperature and Time of Death

Although the general principle that corpses cool progressively after death has been appreciated since time immemorial, the first attempts to place the phenomenon on a scientific footing appeared towards the middle of the nineteenth century, as far as writings in English are concerned [36,37].

In 1839, a book was published in London by Dr John Davey [14], titled *Researches, Physiological and Anatomical*, in which Chapter 13 dealt with 'Observations on the Temperature of the Human Body after Death'. This chapter described the author's experiments in thermometry conducted on the bodies of eight British soldiers in Malta in 1828 and subsequently on ten others after returning to the cooler climate of the British Isles. Considering that Davey was such a pioneer in this field, as well as considering the primitive facilities of his day, Davey's methodology and his insight into the results were remarkably modern. In Malta, the bodies were placed, soon after death, on a wooden table in a large room and were covered only with a sheet, thus ensuring relatively uniform environmental conditions. Davey recorded the ambient temperature in all cases. No details of his thermometer are given, other than it had a (presumably mercury) bulb and was calibrated in degrees Fahrenheit. Unlike many workers who followed him, Davey did not confine his measurements to only one body site, but he recorded the temperatures in various places within the tissues. No skin, mouth, axillary or rectal temperatures were taken, and it seems

DOI: 10.1201/9781003244974-2

obvious that the measurements were recorded during the course of autopsies. They were taken between 3 and 29 hours after death, and most were later than 12 hours post-mortem. Davey made no attempt to estimate the time of death from his data—much of the discussion in relation to the Malta bodies concerned the very high temperatures discovered in some corpses, which reached 108°F and even 113°F some hours after death. Davey decided that the hot climate and the common infective causes of death contributed to this phenomenon, but he also began the long-running speculation about post-mortem production of heat in the organs and tissues. However, Davey rejected this hypothesis after some discussion. Following his return to England, Davey decided to continue his measurements in a more temperate climate, and he conducted similar tests on soldiers dying in Chatham General Hospital in Kent. In his preamble to this section, Davey offered the first mention of the forensic use of body temperature:

> It may often be a question, how long a body has been dead. By attention to its temperature, particularly of the deep-seated parts, taking into consideration the circumstances affecting temperature, probably in most instances an answer may be given approximating to the truth and which may be of considerable use in evidence [14].

Davey's final comments are worth recording, because although in hindsight the first part has proved overly optimistic, his last caution is as true today as when first written, more than 150 years ago:

> These observations may enable the enquirer, instituting similar trials and reasoning analogically, to arrive at a tolerably positive conclusion, in doubtful cases of death, as to the time which may have elapsed between the fatal event and the postmortem examination. Much judgement, however, and nice discrimination may be requisite on the part of the medical man in appreciating the circumstances likely to modify temperature, so as to enable him, when called on for his opinion, to give one which will be satisfactory to the legal officers and to himself, on reflection.

Soon after Davey, there were some brief records published in the United States, in the journal *The Medical Examiner* of Philadelphia, although this general clinical publication has no medico-legal connection with the modern office of medical examiner. In June 1845, this journal published an abstract from an article in the *Western Journal of Medicine and Surgery* for June and October 1844 by Dr Bennett Dowler of New Orleans, concerning his temperature measurements of a variety of corpses. This abstract was followed, in August, September and October 1845, by letters from Dr Dowler with further information. His main interest was again the 'postmortem caloricity' noted by John Davey—the frequent marked rise in body temperature after death. Dowler took temperatures at different sites, both on the body surface and internally, and he also measured these temperatures at intervals. His records are a mixture of Fahrenheit and Réaumur, but he does not describe his thermometer. However, he seems to have had not the slightest interest in using his data for medico-legal purposes [37].

Dowler's publications stimulated another letter to *The Medical Examiner* of Philadelphia in January 1846, this time from a Dr Benjamin Hensley [22], who gave an address in Marietta, Ohio. He said that he used the thermometer mentioned by Dr Dowler, which was composed of a large glass cylinder with a bulb at one extremity, the large cylinder enclosing a smaller one, which was graduated in degrees Réaumur. The boiling and freezing points were found to be correct to within less than half a degree on the scale.

Hensley took many temperatures from various sites, including the skin, axilla, rectum, vagina, antecubital fossae, muscle and under internal organs. He repeated these measurements at varying intervals and built up quite a mass of data, although he seems to have made no real use of it. He also took the temperature of the 'dead-house' and in some cases, measured the body temperature several hours before death, presumably in those of his patients whom he knew were going to die.

After these rather futile beginnings, as far as a post-mortem interval is concerned, there was a gap of some 17 years before the subject was tackled again. In 1863, a substantial paper was published in London, which is often cited as if it had been the very first in the field, in spite of its quoting Davey, Dowler and Hensley. However, it was the first English-language paper to concentrate on the forensic aspects of the topic. It was a long article by Taylor and Wilkes [85] from Guy's Hospital in London and was published in the *Reports* of that institution.

Alfred Swaine Taylor was a Lecturer in Medical Jurisprudence at Guy's Hospital and was the author of the famous book *Taylor's Principles and Practice of Medical Jurisprudence*, which was first published in 1865 and was for a century the premier textbook of forensic medicine in the English language. The article had a typically lengthy title for that era, being called 'On the Cooling of the Human Body after Death—Inferences Respecting the Time of Death: Observations of Temperature made in 100 Cases'. The 30-page paper is largely anecdotal and discursive and, although very interesting, is rather disappointing from the scientific aspect. It begins with several pages devoted to putrefaction, a subject hardly relevant to the title.

Taylor and Wilkes' experimental results are marked by several major faults, which cannot be blamed on the facilities available in the middle of the nineteenth century. First, almost all the hundreds of temperature measurements were made ‘by placing the naked bulb of a good thermometer uncovered on the skin of the abdomen’. This is highly unsatisfactory because the thermometer readings must have varied with air temperature, stray draughts, humidity and also with the inconstant area of contact of the curved bulb with the abdomen—to say nothing of the variable relationship of any such small area of skin with the deep tissue temperature.

The other error, which is admitted in the paper, was that for the first 27 cases of the series of 100, the authors omitted to record when the bodies were brought from the hospital wards to the ‘dead-house’, so it was quite unknown for how long there was a different environmental temperature.

All but four of the hundreds of measurements were taken on the skin surface, and the results were grouped into four ranges: 2–3, 4–6, 6–8 and 12 or more hours after death. Because the variation of temperature within each group was very wide, and also because the size of each group varied from 29 to 76 people, the statistical value of the results is very limited. As with previous authors, Taylor and Wilkes made no effort to derive any formula from their data, to assist in calculating the time of death.

Among the generalizations and numerous anecdotal cases, there are some interesting observations and speculations. Like previous writers, Taylor and Wilkes noted that there is sometimes a post-mortem rise in temperature, and they discussed possible mechanisms for this increase. These included, of course, the frequent infections that were a common cause of death. They also noted, although without giving it a name, the temperature ‘plateau’ that still gives rise to controversy and that was to become so important in later research. Other aspects discussed were the effect of environmental temperature, clothing and the effect of immersion in hastening cooling. The first concept of a heat gradient from the interior to the surface is discussed, as well as the obvious fact that the interior of the body can remain warm after the skin is cold.

Two other phenomena were quoted from other authors, which have passed into forensic mythology and still appear, without any scientific foundation, in some textbooks today—although to be fair to Taylor and Wilkes, they were partly dismissive of the claims. The first phenomenon was quoted from Dr W. B. Richardson, who also wrote in 1863, although the reference is not offered. Richardson stated that ‘a loss of blood, as in cases of death from haemorrhage, whether the blood is effused externally or internally or even temporarily withdrawn from the heart as in syncope, is a cause of rapid cooling of the body’. Taylor and Wilkes point out that ‘the sudden cold of collapse is here confounded with the slow and progressive cooling of the dead body’. To Richardson’s claim that ‘if the body is left dead from direct and absolute loss of blood, cooling to the temperature of the surrounding medium is completed in regard to the external surface in two hours’, they comment that ‘this may lead to a serious error and implicate an innocent person in a charge of murder’.

The second myth is quoted from Nysten, although again no reference is provided. Nysten claimed that ‘the bodies of persons who have died from asphyxia by hanging or suffocation or from the inhalation of carbonic acid gas, do not cool until from 2–48 hours after death and that sometimes, even three days have elapsed before the body has become completely cold’. Taylor and Wilkes disparaged this statement by saying: ‘Too much importance must not be attached to this statement, since it is quite certain that in some cases of fatal asphyxia, the body has cooled just as rapidly as in death from other causes.’ However, this justifiable criticism is contradicted elsewhere in the paper, when the authors are describing the death of the Prince of Conde, Duke of Bourbon, who was found hanging by his cravat from a window shutter. Here they say, ‘As in asphyxia from hanging, the warmth of the body is preserved longer than under common circumstances.’ They also made the unfounded assertion that ‘[w]here death has taken place suddenly, as from accident or acute disease or apoplexy, a body has sometimes been found to retain its heat for a long period’.

To summarize, although the article of Taylor and Wilkes has been acclaimed as the earliest paper on post-mortem temperatures, it is in fact neither the earliest nor particularly erudite, even though it has great interest in other ways, such as a record of a hundred common causes of death in mid-nineteenth-century London and a series of Victorian anecdotes, which throw a fascinating light on both patients and doctors of that era.

In the German-speaking countries it was R. Seydeler [79] who wrote on ‘Nekrothermometrie’. Like the others, he measured the temperature of the axilla. Temperature measurements were not made for the purpose of estimating the time since death but to prevent apparent deaths. Seydeler wanted to determine which temperature increase or decrease could be found in various causes of death. However, he also developed a method to determine the time since death.

The next important contribution to the literature came 3 years later, and it was of a different scientific calibre altogether. It was written in 1868 by Harry Rainy (Figure 2.1) [72], professor of medical jurisprudence at the University of Glasgow, who wrote with a clarity of thought and the use of mathematics that at least equal many modern papers on the subject.

Rainy acknowledged the publications of previous authors and credited the collection of his own data to Dr Joseph Coates of Glasgow Royal Infirmary. They measured abdominal skin and rectal temperatures on 100 bodies but sensibly discarded all the surface readings in favour of those from the rectum. They also rejected 54 cases because the temperature of the mortuary was not constant during their experiments. Four, and sometimes five, serial temperatures were measured on each body,

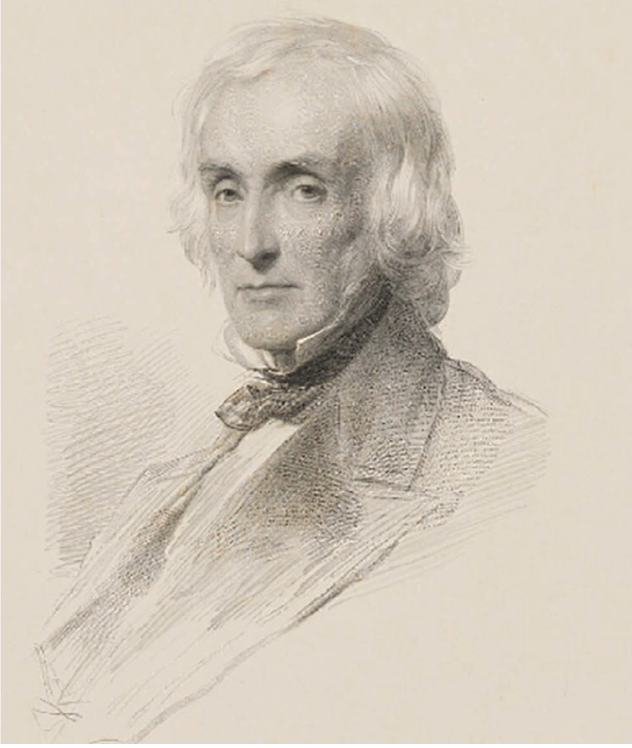

Figure 2.1 Harry Rainy, professor of medical jurisprudence at the University of Glasgow.

between limits of 30 minutes and 63 hours after death. Rainy then calculated the 'ratio of cooling per hour' for each measurement, by expressing the proportion that the excess of temperature above the ambient at the end of an hour bore to the excess at its commencement, the latter being taken as unity. Rainy was the first to mention Newton's law of cooling, but he rightly declared that it was not absolutely correct when applied to dead bodies. 'Bodies recently dead are not found to cool in conformity with this law', he stated, and went on to recount that some temperatures actually rise after death, again quoting Davey, Dowler, Taylor and Wilkes in this respect. 'We scarcely hesitate to ascribe this rise in temperature in these cases to physiological processes which are continued after the action of the heart ceases.' Rainy commented on the 'plateau', although again he did not name it as such. He said, 'It follows that the cooling may be retarded in the earlier stages by the continuance of obscure vital processes . . . these processes must be kept in view in estimating the time which has elapsed since death.'

Like Fiddes and Patten [18], Marshall and Hoare [56–60] and others in the twentieth century, Rainy stated categorically that more than one temperature reading is needed to determine the time since death:

> It will be obvious that it is important to ascertain, not merely the relative temperature of the body and the surrounding medium when the body is found, but also the rate at which the process of cooling is going on during that period. This requires two observations at an interval of an hour, or if possible, two or three hours.

He went on to state another truth, which is still disregarded by many pathologists and police surgeons even today: '[H]aving obtained these data, though we cannot exactly calculate the period which has elapsed since death, we can almost always determine a minimum and a maximum of time within which that period will be included.' This is a statutory warning, from well over a century ago, for doctors not to be so rash as to volunteer a single time of death, but rather to give a preferred range within which they consider that death occurred.

Rainy [72] was the first to offer a formula for calculating the central point of that range of time since death.

> Let the excess of temperature of the rectum at the first observation be t, and at one hour later t—n: and let the excess of temperature of the body at death be n + D, where D = the rectal temperature at death minus environmental temperature. Further, let t/t1 = R and because t is greater than n and consequently will be greater than unity, then:
>
> $$\frac{\log D - \log t1}{\log \mathrm{R}} = \chi eq1.tif$$
>
> which is the number of hours that have elapsed since death. The number of hours, x, determined by this calculation will in almost every case be less than the actual time which has elapsed since death. This arises from the fact that in the early stages, the cooling proceeds more slowly than the assumed (Newton's) law and that the calculation furnishes us with a minimum time.

Here, Rainy was acknowledging the plateau and went on to say:

> It is more difficult to fix a maximum time with precision, but a careful comparison of recorded cases will show that in all cases in which the temperature of the rectum is found to be below 85°F, the time elapsed since death has been less than the minimum multiplied by 1.5 [72].

Rainy then offered the delightful comment, still often appropriate in respect of the mathematical ability of many doctors, that '[p]ersons unacquainted with logarithms may make the necessary observations when the body is found—and the proper inferences may be deduced by competent parties afterwards!'

This article was the first that can truly be recognized as a proper scientific contribution to the subject, and in spite of its relatively early date, the style and content compare favourably with many modern publications.

Indeed, the theoretical content of Rainy's publications was more important than that of many publications that were published 100 years later. He transferred the Newton rule of cooling to the cooling of corpses and thus considered the environmental temperature. By measuring the temperature several times, he could even determine experimentally the individual steepness of the temperature drop curve according to the Newton coefficient. Additionally, Rainy already identified the post-mortal temperature plateau as declination of the single-exponential model (Newton) and consistently designated the calculated death time as minimum time.

Interest increased in the topic, both in English and in Continental journals. In 1870, Goodhard [20] published a report, although he contributed little that was useful.

Wilkie Burman [10], a medical officer at a mental asylum in Wiltshire, published papers in 1874 and 1880, describing his experiments with a special thermometer that he had designed. This thermometer was bent at right angles so that the bulb could be left in the axilla while the mercury level was read. Burman first reviewed the writings of Hensley [22] and Dowler [37] (whom he called 'Fowler') and of Taylor [85], on whose failure to record the time of removal to the mortuary he seized. In his own experiments, all of which were carried out on skin temperatures, Burman found no plateau—again showing that the delay in the fall of core temperature must be the result of the interval needed for the establishment of a heat gradient. Burman tested a number of cases from a 'lunatic asylum' in Yorkshire and pointed out that 'his results were of greater value than those of Taylor and Wilkes', because his special thermometer could be read without disturbing its position in the axilla and also because all his estimations began either at the moment of death or even before death took place. Burman's article was the first to exhibit a graph of results, which indicates an almost linear fall over the first 12 hours, with no trace of a plateau. He calculated that the mean drop in temperature was 1.6°F per hour. One of his deaths showed a slight post-mortem temperature increase and, in common with the material of many of the early writers, the temperatures at death are often markedly elevated, presumably because of infective disease.

Burman stated that cooling was much faster in the immediate post-mortem period because there was no plateau in skin measurements. The mean rate of cooling for hyperthermic bodies was 4.4°F per hour. As a recommendation for calculating the time since death, he advocated dividing the observed drop in temperature in degrees Fahrenheit by his factor of 1.6, which is really the same rule-of-thumb method recommended right up to the present day by some authors. In fact, Burman suggested, in 1880, that the factor be rounded down to 'one and a half'—exactly the figure given in standard books for so many years. To give credit to Burman, he added all the usual cautions and advocated modifying the result according to environment, clothing and so on.

The first author writing in English to move to the Centigrade system was Womack [91] in 1887. Womack used a special mercury thermometer with a flattened bulb of very thin glass, which he strapped to the abdominal wall with a white adhesive tape. This obviously gave better results than the Taylor and Wilkes method because it reduced cooling of the bulb by draughts and convection. However, Womack claimed that the thermometer could be read to an accuracy of 'better than a fortieth of a degree', which seems unrealistic even by today's standards, and for 1887, it seems unlikely that comparably exact calibration could have been available.

Womack used sophisticated mathematics, including calculus, to apply Newtonian theory to his 118 cases, and he illustrated his article with several graphs. He referred to these as 'woodcuts', as they were white on a black background—perhaps an early precursor of our 'reverse video'!

Once again, Womack found no initial plateau, as a result of his choice of the skin as a measuring site. Although Womack's paper is an impressive piece of mathematics, it is marred in retrospect by the unrealistic accuracy with which he computed the time of death. In his first illustrative case, he apologized for estimating the time of death as minutes to 5 o'clock, whereas it was really 5 minutes past 5 . . . yet the first temperature reading was not taken until half past 12. In his second example, Womack again calculated to within a few minutes of the true time, more than 5 hours after the death, from two skin temperatures taken 30 minutes apart. Over his series of 118 cases, he recorded an accuracy of better than 25 minutes from the true time for 57 deaths—an impossible result given the method used.

One of the best-known of the 'modern' publications in the field of temperature and time of death is that of De Saram et al. [15,16], who carried out their research in Sri Lanka (formerly known as Ceylon). This work appeared in 1955 and began a new era of investigation into the subject. Some of the interest stemmed possibly from the rather macabre fact that the work was carried out on victims of judicial execution, but the intrinsic worth of the research is undoubted, even though the algorithm produced has never enjoyed widespread use in practice.

De Saram and his collaborators worked in a tropical country where the ambient temperature was high, so their results were not readily applicable to temperate climates. They investigated the cooling rates of 41 executed criminals under strictly observed conditions, by taking hourly rectal temperatures usually beginning an hour after execution.

These investigators noted a 'lag period' or plateau of about 45 minutes and added this to their estimates of time since death arrived at from their calculations. De Saram et al. recommended using a formula that incorporated all the known variables, rather than the use of a general calculation followed by further modifications according to local circumstances. The actual submission is as follows: 'The time of death (should) be estimated, not, as at present, by a generalised formula where the influence of modifying factors are assessed, so as to say, empirically, but by the use of a formula which itself embodies the influence of these factors.' De Saram et al. included the humidity of the environment, which in Ceylon varied between 70 and 90 per cent saturation, considering that this was a potent factor in altering the cooling rate. The presence of thick cotton overalls on the bodies was dismissed as having little influence because five of the bodies from a different prison were measured unclothed.

The De Saram formula combined heat losses from convection, radiation and conduction, and the mathematical principles of his methods are discussed in Chapter 6.1. His discussion from first principles is an excellent review of the whole problem and well repays study even from this distance of many years.

An interesting case on death time estimation is reported by Sir Sidney Smith in his book *Mostly Murder* [83].

In this case, there were three main facts to be considered in fixing the time of death by the medical evidence:

- Temperature of the body
- Extent of rigor mortis
- State of food in the stomach and bowel

A woman was found dead in the garage of the house after 3 pm. The husband had left the house by taxi at 10.35 am, and he could prove it. He had a complete alibi for the rest of the day. Therefore, he could have had no part in the murder if it occurred after that time.

And the simple question was death before or after 10.35 am.

Professor Smith adds: 'An interval of time as fine as a hair but as deep as a grave.'

Professor De Saram estimated the time since death between 10 and 11.30 am.

Some days later the cook William 'confessed' that he had helped his master (the husband) to kill the lady of the house before 9 am. He further confessed that he went to a jeweller and sold objects at 9.30 am. However, three other witnesses asserted independently that they had seen or heard the woman alive an hour or more later. One witness, who was familiar with the voice of the woman, said he had a telephone conversation with her at some time between 10.25 am and 12 noon.

The woman had breakfast consisting of string hoppers after 8.15 am.

Professor De Saram had been fortunate in obtaining three bodies of young murderers immediately after they had been executed. Approximately seven hours were required for these bodies to lose 5.2 degrees. This information was of crucial importance, for it was obvious that the much lighter body of the dead woman would have taken less time to cool to the same extent; and therefore, she would have died much later than 10.30 am. The time food takes to pass from the stomach along the 22 feet of the small intestine varies very considerably, being affected by many circumstances—physiological, psychological and physical.

When Professor Sydney Smith, who was also serving as an expert in the trial, was cross-examined, he was asked how long it took for food to pass from the mouth to the lower end of the small intestine. He replied that though it was simple enough to give an average time, that average could not apply to a particular case. It was much the same as asking how long it took a horse to run a mile. It depended on the breed of the horse, its condition at the time, upon the trainer and upon the jockey. Although the trial had been going on for over three months, the jury came to the unanimous verdict of 'Not Guilty'.

This case report is of importance concerning several aspects:

- Gastric contents and time since death
- Degree of rigor mortis
- Body cooling in high ambient temperatures

Professor De Saram started his experiments on body cooling in high ambient temperature, which are still today the basics for death time estimation.

Professor Sydney Smith added a further important point: do not use mean values for death time estimation.

In 1956, Lyle and Cleveland [45] entered the scene with new technology in the form of a six-channel thermocouple device that continuously recorded temperatures at a number of sites, these being plotted on a strip chart every minute. These sites were from the skin of the chest, forehead, rectum, liver, brain and thigh muscle. Valuable data were acquired, demonstrating that the rate of heat loss was widely different at different sites, but that extrinsic variables had less effect on brain than on rectal temperature. These investigators also pointed out the well-known fact that time of death could not be determined satisfactorily after 24 hours or where the difference in environmental and body temperature was only a few degrees. Lyle and Cleveland did not derive any practical formula from their work, and the main legacy of this research is some of the actual data from the recordings.

Karl Sellier [78] from the Bonn Institute published a paper of considerable mathematical complexity in 1958, based on the concept of the infinite cylinder. Most of his work was pure mathematics and heat mechanics, and it was a very useful dissection of the theoretical basis of the problems. Sellier was obviously very much influenced by the work of De Saram et al. [15,16], to whom he referred constantly. He stated that the experimental material in his own institute was not usable because the environmental temperature was too variable and the bodies did not stay long enough, so he used the data of De Saram and his collaborators for his manipulations.

Sellier made the interesting assertion that the retardation of cooling in fat bodies was not the result of the insulating effect of the 'fatty pads', as he called them, but rather was caused by the fact that the excess adipose tissue increased the radius of his cylinder.

Also in 1958, the seminal paper of Fiddes and Patten [18] appeared, which, like that of De Saram et al. [15,16], is still held up as one of the models of theorizing about the use of temperature in death time estimation. Fiddes and Patten pinned their hopes on assessing the rate of fall of the temperature, by using two or more temperature measurements. They also developed the concept of 'virtual cooling time', the time taken to cool through 85 per cent of the difference between normal body temperature (not defined but assumed to be 37°C) and the environmental temperature. This is discussed in more detail in Chapter 3.

Fiddes and Patten devised a 'percentage cooling rate', in which the fall in temperature from 'normal' is expressed as a percentage of the difference in temperature between 37°C and the ambient. This is calculated for two or more points separated in time, and the post-mortem interval calculated by applying the data to a standard graph offered by the authors from 100 known cases. The method can be applied only if the ambient temperature remains constant throughout the whole investigation and if the initial body temperature is assumed to be 37°C (or some other fixed assumption). It may also be noted that when James and Knight [31] used the Fiddes and Patten double-measurement method in their research into errors, they found it to give no added accuracy compared with a simple single-exponential method.

Professor T. K. Marshall [55–60] of Belfast is one of the most prolific writers of recent years (up to the 1970s) and, with several collaborators, produced a doctoral thesis and six other publications on temperature and time since death. The best-known paper is that by Marshall and Hoare [55], which was published in 1962. The paper showed that a dead body did not cool according to Newtonian principles during the first 12 hours after death. These authors suggested that the deviation from Newton's law is caused by post-mortem metabolism and the development of temperature gradients in the surface layers of the body, resulting in a sigmoid rather than a single-exponential cooling curve. However, after about 12 hours, the curve approximates to an exponential expression and is then amenable to use for post-mortem interval calculation because the rate of heat loss is then directly proportional to the excess temperature of the body over its surroundings.

The rate of cooling per degree of temperature difference (the 'cooling factor') was then said by Marshall to be proportional to the ratio of the effective radiating surface of the corpse to its mass (the 'size factor').

Marshall and Hoare devised a formula, discussed later in this chapter, which expressed two exponential terms: first, the cooling proportional to the excess of the temperature excess of the body over its environment, and, second, the influence of modifying factors.

With reference to many experimental results, which provided 'standard cooling curves', the use of this formula was held to provide satisfactory results. Their data have been reworked several times by other investigators, although with conflicting results. The more recent computer and nomogram methods of Henssge et al. [23–25], described at length in later chapters of this book, are substantially based on the Marshall and Hoare material. In the many other papers by Marshall, with and without collaborators, the basic theory was discussed and refined. Perhaps one of the most useful comments of this prolific author is contained in the very last sentence of an article in the *Journal of Forensic Sciences*: 'It would seem that the timing of death by means of temperature can never be more than an approximation' [56].

2.3 Post-mortem Electrical Excitability of Skeletal Muscle—Historical Review

Studies on the electrical excitability of skeletal muscle post-mortem began with Luigi Galvani's discovery of 'animal electricity' [19].

The great period of electrophysiology during the nineteenth century was accompanied by many studies on the post-mortem electrical excitability of skeletal muscle, studies that were performed mainly by physiologists, but also by French and German pathologists. At the beginning of the nineteenth century, the aim of these studies was mainly to exclude apparent death (Table 2.1), and only those bodies in which electrical excitability had ceased completely were buried [13].

As late as 1872, Rosenthal [76] wrote that the loss of electrical excitability was the most reliable sign of death. However, as early as 1811, Nysten [64] described (in analogy to the onset of rigor mortis—Nysten's rule) the regular loss of electrical excitability in different regions of the body, '*In musculis trunci citius periit irritabilitas, quam in musculis membrorum; musculi extremitatum inferiorum eam citius perdunt quam musculi extremitatum superiorum.*' This rule proved to be quite exact in succeeding investigations.

Several papers on anatomical and physiological investigations in executed bodies provided information on the duration of electrical excitability [21,38]. According to

Table 2.1 Development of Electrical Excitability of Skeletal Muscle Post-mortem in the Nineteenth Century

Galvani	1780	— Animal electricity.
Klein	1794	Studies on electrical excitability of skeletal muscle post-mortem to detect and prevent apparent death.
Creve	1796	
Hüpsch	1800	
Heidmann	1804	
Struwe	1805	
Sommer	1833	
Rosenthal	1872	
Bichat	1800	Studies on electrical excitability of skeletal muscle post-mortem that provide some knowledge for determining the time since death.
Nysten	1811	
Devergie	1841	
Harless	1851	
Kölliker	1851	
Rosenthal	1871	
Onimus	1880	

these authors, indirect electrical excitability of skeletal muscle ceases some minutes after death. However, Du Bois Reymond (in Kölliker and Virchow) and Kölliker and Virchow [38] saw intensive muscle contractions after exciting the nerve at 1.5 hours post-mortem. This finding was confirmed more than 100 years later by Krause et al. [40] on amputated limbs. Figure 2.2 shows experiments by Aldini on human bodies after decapitation. Aldini examined the electrical excitability of the muscles of the trunk, limbs and facial muscles of two criminals decapitated in Bologna in 1804 [87]. Aldini (1762–1834) was a nephew of Galvani.

After having performed animal experiments, he wanted to study further questions regarding 'animal electricity' on human bodies. He thought that the bodies of persons dying of chronic diseases were not suitable for his experiments because the diseases would destroy the 'fibre structure of muscles'. Therefore, Aldini used bodies

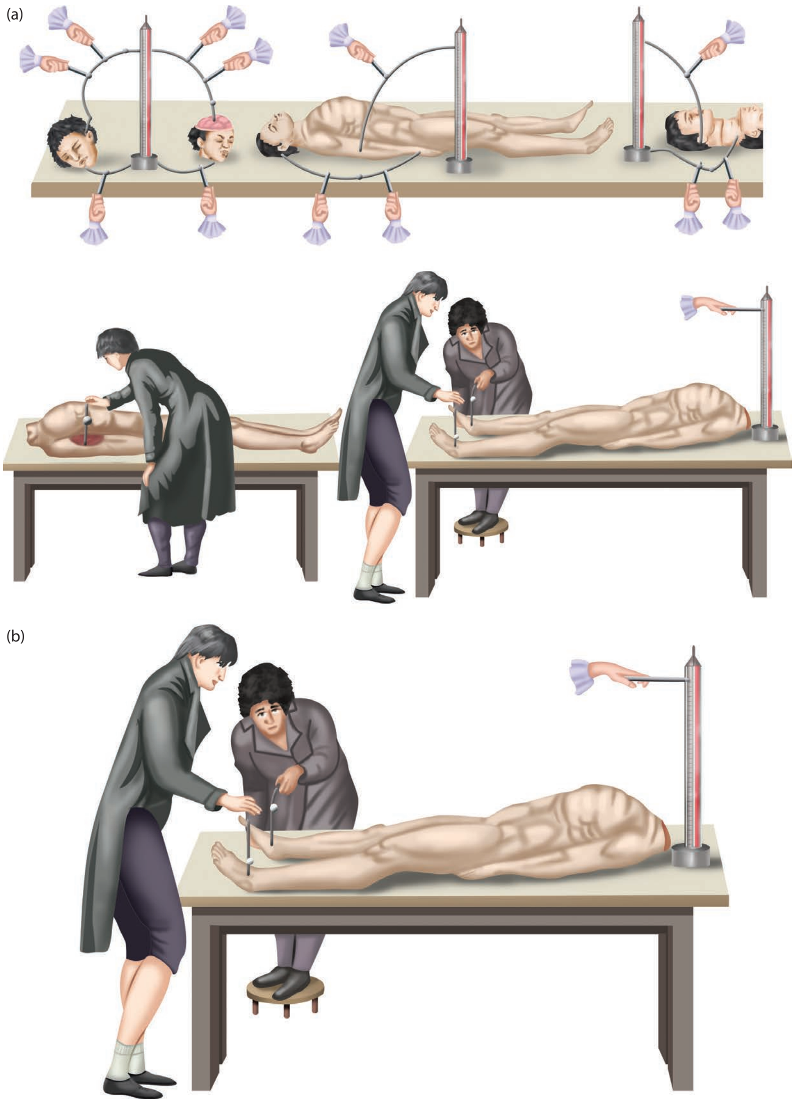

Figure 2.2 (a–c) Experiments on electrical excitability of skeletal muscles post-mortem conducted after decapitation, by J. Aldini in 1804.

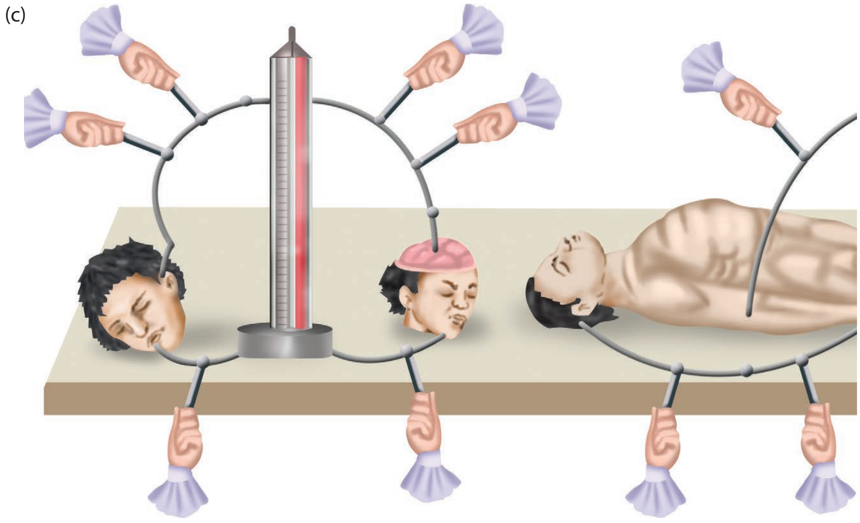

Figure 2.2 (a–c) (Continued)

whose vital force would be preserved after death. 'Therefore I stood so to speak near the scaffold to receive from the hangman's hand the exsanguinated bodies . . . It was for advantage to me that two criminals in Bologna were decapitated and the government understood my physical curiosity.' The copperplate print shows the experiments being carried out.

On direct excitation, excitability remained preserved for several hours, according to Nysten [64], up to 26 hours post-mortem. In several executed bodies (decapitation), he was able to detect the following intervals of electrical excitability:

1. Left chamber of the heart: 'short'.
2. Bowel and stomach: 45 minutes.
3. Right chamber of the heart: 3 hours.
4. Oesophagus: 1.5 hours.
5. Iris: 1.75 hours
6. Muscles of the trunk shorter than muscles of the lower limbs shorter than muscles of the upper limbs.

Nysten [64] investigated the influence of the cause of death on electrical excitability in 40 hospital cases and found a loss of electrical excitability after:

- 2.75 hours in cases with peritonitis.
- 3–6 hours in cases with phthisis, carcinoma and scirrhous.
- 9 hours in cases of fatal haemorrhage or injuries of the heart.
- 12 hours in cases with apoplexy with paralysis.
- 10–15 hours in cases with 'adynamic fever'.
- 13–15 hours in cases with pneumonia.
- 5–27 hours in cases with aneurysm of the heart.

In 1872, Rosenthal [76] stated that the sphincter palpebrarum remains the longest excitable muscle; this finding was confirmed more than 100 years later by Klein and Klein [33].

Figure 2.3 Professor Otto Prokop and the editor of this book as a young man in 1987.

The fact that Rosenthal was working in the 1870s indicates that it was recognized quite early that electrical excitability of skeletal muscles may be a suitable method for determining the time since death in the early post-mortem interval. This conclusion was also reached by Onimus [65] and Tidy [86]. However, Lochte [44] and Puppe [70] rejected electrical excitability as a method of death time estimation—Lochte having no experimental experience and Puppe working with already outdated time intervals.

The renaissance of post-mortem electrical excitability of skeletal muscles began with investigations stimulated by Prokop (Figure 2.3) [69].

Several papers on the construction of square-wave generators and a large series on human bodies followed [5,8,32–35,39–41,52,62,66,71–73–75–88–92].

In 1912 the Hungarian psychiatrist István Zsakó (1882–1966) reported the existence of a mechanical muscle phenomenon in the early post-mortem interval. Using a carefully developed methodology, he performed a systematic study to examine the reaction of skeletal muscle after mechanical excitation. In the early post-mortem interval, he was able to produce a propagated contraction of the whole muscle region. After a period of about 2–2½ hours, he was able to produce only an idiomuscular pad. Already in his first publication he suggested that his findings may be useful for the estimation of the time since death. Later important investigations were carried out by Popwassiliew and Palm in Berlin and especially by Dotzauer in Hamburg. The investigations by Dotzauer are probably the most important reference for routine casework.

2.4 Rigor Mortis

In 1964 and 1971, Mallach [53,54] published his well-known table on the time course of rigor mortis based on potations in the classical textbooks of forensic medicine. He also used the data of Eduard von Hofmann (1876/77) (Figure 2.4) [27,28], which were some of the rare data

LEHRBUCH
DER
GERICHTLICHEN MEDICIN.

MIT BESONDERER BERÜCKSICHTIGUNG
DER
ÖSTERREICHISCHEN UND DEUTSCHEN GESETZGEBUNG.

VON
DR. EDUARD HOFMANN,
K. K. OBERSANITÄTSRATH, O. Ö. PROFESSOR DER GERICHTLICHEN MEDICIN
UND LANDESGERICHTSANATOM IN WIEN.

WIEN, 1878.
URBAN & SCHWARZENBERG.
MAXIMILIANSTRASSE 4.

LEHMANN'S MEDIZIN.
HANDATLANTEN.
BAND XVII.

ATLAS
der
Gerichtlichen Medizin
nach Originalen von Maler **A. Schmitson**
von
Hofrat Professor Dr. E. Ritter von Hofmann.
Director des gerichtlich medizin. Institutes
in Wien.

Mit 56 farbigen Tafeln und 193 ſchwarzen Abbildungen.

ICH HAB'S GEWAGT

München.
Verlag von J. F. Lehmann.
1898.

Figure 2.4 (a–c) Eduard von Hofmann (1837–1897).

Table 2.2 Time Course of Rigor Mortis in Adults (According to Mallach 1971 and Mittmeyer 1971)

	Rigor related to the time since death (hpm) and standard deviation			
Author	Complete rigidity	Beginning of resolution	Complete resolution	Number of cases
von Hofmann (1877)	48 ± 14 65% (117)	47 ± 14 28% (51)	50 ± 6¼ 7% (13)	181
Mallach (1962)	57 ± 27 25% (57)	76 ± 24 53% (126)	86 ± 29 22% (54)	238

Note: Adults (24–86 years old), children (1 day–13 years old)

Table 2.3 Time Course of Rigor Mortis in Adults and Children; Own Calculations on the Data of von Hofmann (1876/77) with Differences to the Calculations of Mallach

	Adults (24-86 years old)				Children (1 day - 13 years old)			
	n	Variation	$\bar{x}$	s	n	Variation	$\bar{x}$	S
Complete rigidity	118	24–96	47,1	14,3	31	18–66	47	14
Beginning of resolution/ missing rigidity	51	30–86	48	14,2	34	28–80	55,4	15,4
Complete resolution of rigor mortis	13	36–62	50	6,1	76	25–72	52,2	12,9

from the nineteenth century that could be used for statistical analysis of the time course of rigor mortis.

In 1964, Mallach had already calculated mean values and standard deviations for the various degrees of rigor mortis published by von Hofmann (1877) (Tables 2.2 and 2.3). These data are still of relevance more than 100 years later. At the same time, Niderkorn (1872) (Tables 2.2 and 2.3) [63] published his observation on the time course of rigor mortis.

Of special importance is that the mean values for the degrees of rigor mortis are nearly the same. However, this must not lead to the conclusion that between fully developed rigor mortis and complete resolution is only a time course of 3 hours.

He noticed the time until complete development of rigor mortis. These data could also be used for a statistical analysis and recalculated mean values and standard deviations. The random sample consisted of 113 cases; complete rigor mortis was established after 5.6 hours. The variation was between 2 and 13 hours, and the 95 per cent limits of confidence were between 1.2 and 10.1 hours post-mortem. The variations in 95 per cent limits of confidence are quite similar in the case material of von Hofmann and Niderkorn; however, the mean value for complete development of rigor mortis in the case material of von Hofmann is, at 8 hours, much higher than in the material of Niderkorn, at 5.6 hours. One reason may reflect the composition of the case material and the influencing factors on the time course of rigor mortis [39].

In an 1811 anthology, *Recherches de physiologie et de chimie pathologiques*, Pierre-Hubert Nysten (born in Liège, 1771, died in Paris, 1818) published a range of observations on rigor mortis in humans and animals, many of which are still considered valid today. After him, a rule describing the onset and sequence in which rigor mortis develops has been named: at first in the muscles of the trunk, then neck, before spreading to arms and legs, before finally resolving in the same sequence. Other authors have published similar observations, for instance, Devergie. Since the discovery of ATP and the importance of the glycogen content of skeletal muscle for the development of rigor mortis, it became clear that there is no single general sequence of development of rigor mortis. However, his name is still today used to describe a rule for the onset and development of rigor mortis [89].

2.4.1 Cadaveric Spasm

With irreversible circulatory arrest and/or respiratory arrest, striated muscle loses its tone and becomes flaccid. According to changes in elasticity of mammalian muscles undergoing rigor mortis, Bate-Smith and Bendall [1,2] developed 3 phases:

- A delay period with high elasticity of muscle
- A rapid phase with decreasing elasticity and
- A post rigor phase with constant elasticity on a lower level

Bate-Smith and Bendall [1,2] studied also the factors determining the time course of rigor mortis. Even in animals with ante mortem energy exhaustion (e.g. after strychnine injection) a short delay period was observed.

The experiments of Bate-Smith and Bendall [1,2] are of course of great heuristic value for forensic practice since they describe the influencing factors governing the time course of rigor mortis (ambient temperature, pre-existing diseases, violent exercise prior to death [energy depletion], poisoning, electrocution) based on a biochemical and physical level.

The delay period until the onset or complete development of rigor mortis is used for estimating the time since death by examining the electrical excitability of skeletal muscles.

In forensic practice many conditions have been described that may accelerate or delay the onset of rigor mortis. For instance, an accelerated onset of rigor mortis can be seen in cases of electrocution when the body remains in direct or indirect contact with electrical current up to the moment of discovering the cadaver. The term ‘cadaveric spasm’ is defined either as ‘accelerated rigor mortis’ or as ‘instantaneous rigor mortis’ [3,50].

According to Bernard Knight [36] cadaveric spasm may well be an extreme variant of accelerated rigor mortis. It is defined as a rare form of virtually instantaneous rigor that develops at the time of death with a lacking period of post-mortem flaccidity. Furthermore, according to Knight cadaveric spasm has meanwhile received a disproportional amount of notice in renowned textbooks compared to its practical importance. Many forensic pathologists claim to have observed such a phenomenon far too soon after death for this to be normal rigor mortis. Although the authors are sceptical about the phenomenon, Bernard Knight has described one or two cases to be genuine enough to be remarkably early for veritable rigor. The phenomenon usually affects only one group of muscles such as the flexors of one arm rather than the whole body. Cadaveric spasm seems to be confined to those deaths that occur in the midst of intense physical and/or emotional activity. According to Knight, it must be initiated by motor nerve activity but for some reason there is a failure of normal relaxation. To diagnose cadaveric spasm, the body must be examined before ordinary rigor mortis might be expected to have developed. Otherwise, the presence of cadaveric spasm cannot be assumed. According to Krompecher, instantaneous rigor mortis or cadaveric spasm are also defined as complete rigor mortis occurring at the moment of death and involving a hand, limb or even the entire body (cataleptic rigor). According to Baumann [3] who carried out a survey on cataleptic rigor in 1923, two possibilities for establishing the diagnosis have to be differentiated:

Either the person is observed while dying and instantaneous rigor is noted at the moment of death.

Or the observation is made some time after death with body parts erected against gravity.

In both cases, the whole body or parts of it have remained in the same position as prior to death and the position has not been changed by gravity. Baumann [3] surveyed the literature on this subject and concluded that the majority of instantaneous rigor mortis cases are seen in cases with brain injuries. He stated already in 1923 that many reports on cadaveric spasm are misdiagnoses because the development of rigor mortis has not been observed. Up to now there is no pathophysiological concept of cadaveric spasm. Laves and Prokop proposed that the cause of cadaveric spasm or cadaveric rigidity may be decerebration rigidity according to Sherrington. However, decerebration rigidity is an intravital phenomenon. It has also to be strengthened, that many reports on cataleptic rigidity originate from war times (French-German-War 1870/71, World War I). Unusual positions were more likely to have resulted from blast waves. Mueller, a famous German forensic pathologist, who worked also during World War II, searched for cases of cataleptic rigidity but failed to observe a single case of instantaneous rigor mortis. Altogether, there is no pathophysiological basis of instantaneous rigor mortis or cadaveric spasm. Therefore, as recommended by Bedford and Tsokos [4], the term ‘cadaveric spasm’ should not be used any longer.

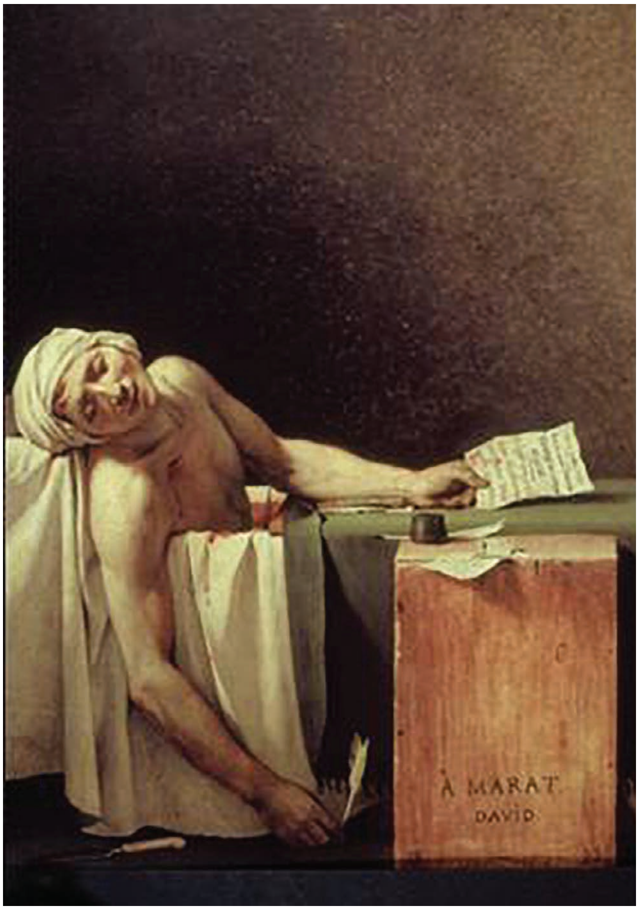

Figure 2.5 Death of Marat by Jacques Louis David, Royal Museum of Art, Brussels.

Most cases are misreported because the development of rigor mortis has not been observed. The presence of objects in a hand is not an extraordinary finding and does not prove an instantaneous development of rigor mortis. For example, in the famous painting ‘Death of Marat’ by Jacques Louis David, the paper in the left hand and the quill in the right hand of the dead Marat is consistent with law of gravity.

Note the post-mortem lividity in the lower right arm and hand, after Marat was stabbed by Charlotte Corday, the convent ordered a painting and the painter, Jacques Louis David, decided to paint Marat, as he has seen him last alive, also sitting in the bathtub. Cause of death was obviously cardiac tamponade due to step wound of the pulmonary artery, therefore intense post-mortem lividity.

2.5 Post-mortem Lividity

Concerning rigor mortis, Hofmann has published detailed observations, which allow still today a statistical analysis

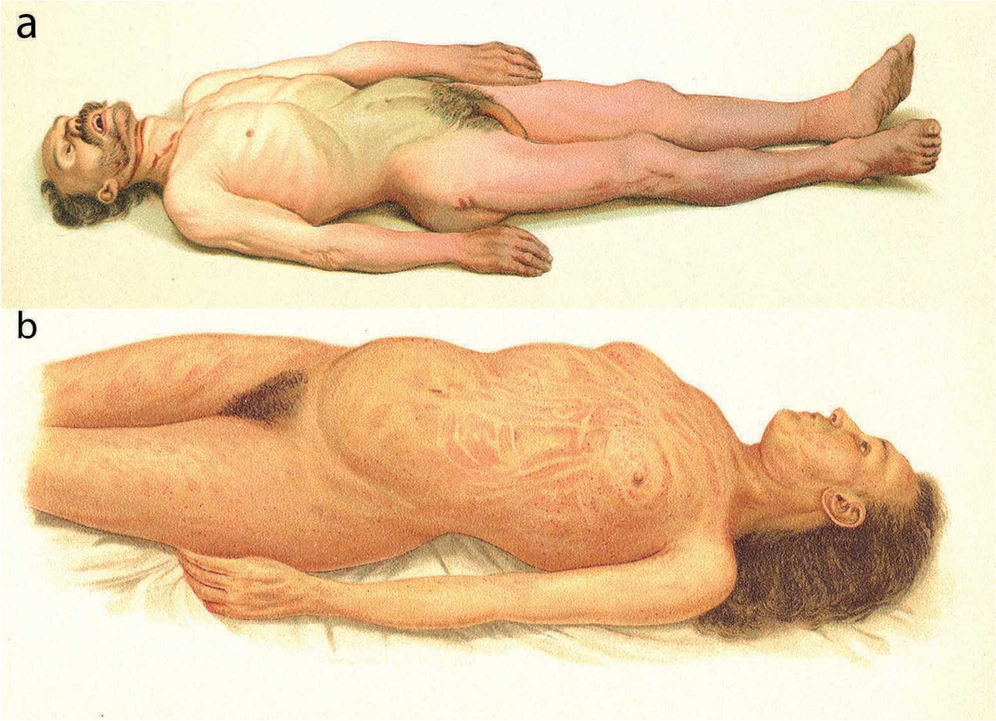

Figure 2.6 (a) Suicide by hanging. After hanging for several days, the body displayed livor mortis in the lower extremities (stocking-shaped in the legs, glove-shaped in the lower arms and hands). Initial greenish discolouration of the belly. (b) Livor mortis of a body lying face down.

(Tables 2.2 and 2.3). In his review on forensically important post-mortem changes, he mentions post-mortem lividity but gives no detailed description on the time course and different criteria of lividity for estimating the time since death [67].

He writes that post-mortem lividity develops in the first 3–10 hours of the death. In his *Atlas of Forensic Medicine* [26], there are however two illustrations with fixed post-mortem lividity in hanging (Figure 2.6a) and at the front of the body due to prone position for 12–24 hours post-mortem (Figure 2.6b).

2.6 Putrefactive Changes

Putrefactive changes have already been described in detail in the textbooks of the nineteenth century. Johann Ludwig Casper (Figure 2.7) studied putrefactive changes in the air, water and earth grave and wrote that the same state of decomposition is achieved in air after one week (month), in water after two weeks (months) and in the earth grave after eight weeks (months) (Casper's rule). He published in his *Atlas of Forensic Medicine* also colour plates of advanced decomposition of bodies recovered from water (Figure 2.8).

An interesting case on putrefactive changes and entomology was described by Professor Keith Simpson in his autobiography *Forty Years of Murder* [82].

Figure 2.7 Johann Ludwig Casper (1796–1874), forensic pathologist in Berlin and the author of a well-known textbook on forensic medicine.

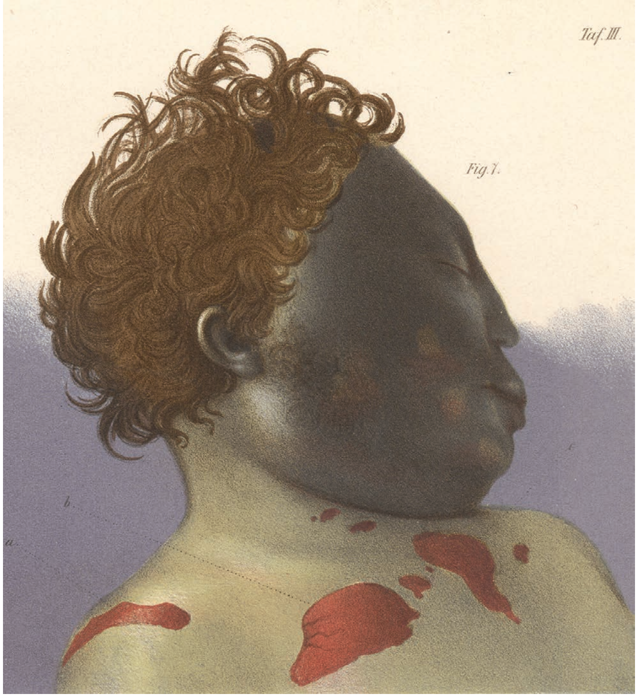

Figure 2.8 Colour plate of a body recovered from water with severe decomposition, bloating, greenish discolouration, loss of epidermis.

A man had disappeared from his home on 16 June 1964. He was found dead on 28 June. The man was lying on his back, fully clothed with his head wrapped in towelling. The body was disintegrating, and police assumed it must have been dead for six or eight weeks.

Professor Simpsons estimation was ‘at least nine or ten days, but probably not more than 12’. He based his estimation on the maggots, which were larvae of the bluebottle *Calliphora erythrocephala*. The larvae he was looking at were mature, indeed elderly, fat, indolent, third-stage maggots, but they were not in pupa cases. Therefore, he estimated that the eggs had been laid nine or ten days earlier. Adding a little more time to allow the bluebottles to get to the dead body, he reckoned death had occurred on 16 or 17 June.

However, there were witnesses who claimed to have seen the deceased on 20 June. Professor Keith Simpson found this statement as being wholly inconsistent with his own findings. The condition of the body when examined in the wood suggested in the first instance, while still at the scene, ‘some nine or ten days, possibly more’, which was a minimum period. Nothing in the post-mortem state of the body suggested any special conditions likely to have accelerated the ordinary process of maggot infestation and disintegration of the body.

Although there were further alibis, which claimed to have seen the deceased even on 21 June, the jury decided the maggots were more reliable in the hatching habits than the alibis of the defence.

2.7 Vitreous Potassium as a Measure of the Post-mortem Interval

Chemical tests for determining the post-mortem interval have been largely developed since the 1950s. Among these tests, the most widely used one is the vitreous potassium concentration. Naumann [62] was the first to study extensively the human post-mortem vitreous fluid in 1959, and he demonstrated a rise in the vitreous potassium values but did not attempt to correlate this increase with the post-mortem interval. Since then, numerous papers have been published [30], and in 1963 Sturner [84] published his observation on the post-mortem rise of vitreous potassium with very narrow 95 per cent limits of confidence in the post-mortem interval up to 1 hour post-mortem. The development of formulae on vitreous potassium as a measure of the post-mortem interval was summarized by Coe (Figure 2.9) [12].

Figure 2.9 Professor John Coe (1919–2011).

References and further reading

1. Bate-Smith EC. Changes in elasticity of mammalian muscles undergoing rigor mortis. *J Physiol* 1939;*96*:176–93.
2. Bate-Smith EC, Bendall JR. Factors determining the time course of rigor mortis. *J Physiol* 1949;*110*:47–65.
3. Baumann J. Über kataleptische Totenstarre. *Deutsche Zeitschrift Gesamte Gerichtliche Medizin* 1923;*2*:647–70.
4. Bedford PJ, Tsokos M. The occurrence of cadaveric spasm is a myth. *Forensic Sci Med Pathol* 2013;*9*:244–8.
5. Berg S. Nervensysteme und Totenstarre. *Dtsch Z Gerichtl Med* 1948/49;*39*:429–34.
6. Bichat X. *Recherches physiologiques sur la vie et la mort (1800). German trans*. Barth JA, Leipzig, 1912.
7. Billroth T, Fick A. Postmortale Temperatursteigerung. *Vierteljahresschr Naturforsch Ges (Zürich) VIII B*, 1863.
8. Böhm E. Anmerkungen zu Reizbarkeit und Starreeintritt der Skelettmuskulatur. *Beitr Gerichtl Med* 1986;*44*:439–50.
9. Brown A, Marshall T. Body temperature as a means of estimating the time of death. *Forensic Sci Int* 1974; *4*:125–33.
10. Burman J. On the rate of cooling of the human body after death. *Edinb Med J* 1880;*25*:993–1003.
11. Casper J. *Praktisches Handbuch der gerichtlichen Medizin*. Berlin, 1857.
12. Coe JI. Vitreous potassium as a measure of the postmortem interval: an historical review and critical evaluation. *Forensic Sci Int* 1989;*42*:201–13.
13. Creve CC. *Vom Metallreize, einem neuentdeckten untrüglichen Prüfungsmittel des wahren Todes*. Germany, Leipzig und Gera, 1796.
14. Davey J. Observations on the temperature of the human body after death. *Res Physiol Anat (Lond)* 1839;*1*:228–48.
15. De Saram G, Webster G, Kathirgamatamby N. Post-mortem temperature and the time of death. *J Crim Law Criminol Police Sci* 1955;*1*:562–77.
16. De Saram G. Estimation of death by medical criteria. *J Forensic Med* 1957;*4*(2):47.
17. Dittrich, Gerlach, Herz. Beobachtungen an den Leichen von 2 Hingerichteten. *Prag Vierteljahresschr* 1851;*31B*.
18. Fiddes F, Patten TA. Percentage method for representing the fall in body temperature after death. *J Forensic Med* 1958;*5*:2–15.
19. Galvani L. Cited by Rothschuh KE. In *Physiologie. Der Wandel ihrer Konzepte, Probleme und Methoden vom 16. bis 20. Jahrhundert*. Freiburg-München, Germany, Karl Alber, 1968.
20. Goodhard JF. Thermoelectric observations in clinical medicine. *Guy's Hosp Rep* 1870;*15*:365–419.
21. Harless E. Untersuchungen an einem Hingerichteten. *Jenaer Analen II 2*, 1850; *Zit, nach Schmids Jahrbuch* 1851;*72*:10–11.
22. Hensley B. Experiments on the temperature of bodies after death. *Med Examiner (Philadelphia)* 1846;*2*:149–52.
23. Henssge C, Madea B, Gallenkemper E. Death time estimation in casework; integration of different methods. *Forensic Sci Int* 1988;*38*:77–87.
24. Henssge C. Death time estimation in case work. I. The rectal temperature time of death nomogram. *Forensic Sci Int* 1988;*38*:209–36.
25. Henssge C. *Methoden zur Bestimmung der Todeszeit-Leichenabkühlung und Todeszeitbestimmung*. Dissertation B. Berlin, Berlin, Humboldt University, 1982.
26. Hofmann EV. *Atlas der Gerichtlichen Medizin*. München, Lehmanns, 1898.
27. Hofmann EV. Die forensisch wichtigsten Leichenerscheinungen. *Vierteljahresschr Gerichtl Med* 1876;*25*:229–61.
28. Hofmann EV. Die forensisch wichtigsten Leichenerscheinungen. *Vierteljahresschr Gerichtl Med* 1877;*26*:17–40.
29. Hofmann EV. *Lehrbuch der Gerichtlichen Medizin*. Wien, Urban und Schwarzenberg, 1878.
30. Jaffe FA. Chemical post-mortem changes in the intraocular fluid. *J Forensic Sci* 1962;*7*:231–7.
31. James W, Knight B. Errors in estimating time since death. *Med Sci Law* 1965;*5*:111–16.
32. Joachim H, Feldmann U. Eine quantitative Methode der Todeszeitbestimmung durch Untersuchung der galvanischen Reizschwelle. *Z Rechtsmed* 1980;*85*:5–22.
33. Klein A, Klein S. *Die Todeszeitbestimmung am menschlichen Auge*. Medical Dissertation, B, Dresden, Germany, Medical Academy, 1978.
34. Klein A, Krause D, Hamann B. Praktische Erfahrungen mit einem neuen elektronischen Reizgerät zur Todeszeitbestimmung. *Kriminal Forens Wiss* 1975;*19*:126.
35. Kliese U, Henssge C, Madea B. Reizgenerator zur Prüfung der elektrischen Erregbarkeit der Skelettmuskulatur. *Unpublished manuscript*, 1985.
36. Knight B. *Forensic Pathology*. London, Edward Arnold, 1991.
37. Knight B. The evolution of methods for estimating the time of death from body temperature. *Forensic Sci Int* 1988;*36*:47–55.
38. Kölliker A, Virchow R. Über einige an der Leiche eines Hingerichteten angestellte Versuche und Beobachtungen. *Wiss Zool* 1851;*III*:37–52.
39. Krause D, Klein A, Mattig W, Waltz H. Praktische Erfahrungen mit dem Reizgerät D 76 zur Todeszeitbestimmung. *Kriminal Forens Wiss* 1980;*40*:83–6.
40. Krause D, Klein A, Zett L. Todeszeitbestimmung mittels indirekter Muskelreizung über den N. ischiadicus und N. radialis. *Kriminal Forens Wiss* 1976;*26*:66–7.
41. Krause D, Schöning R, Kuchheuser W. Stimulator M 85—Ein kommerzielles Reizgerät zur Todeszeitbestimmung. In: Liebhardt E, Schuck M, Eisenmenger W (eds.). *Medizin und Recht. Festschrift fur Wolfgang Spann*. Berlin, Springer, 1986, pp 639–44.
42. Krompecher T. Rigor mortis: estimation of the time since death by evaluation of cadaveric rigidity. In: Henssge C, Knight B, Krompecher T, Madea B, Nokes L. (eds.). *The Estimation of the Time Since Death in the Early Post Mortem Period*. London, Edward Arnold, 2002, 2nd ed., pp 144–60.
43. Laves W. Über die Totenstarre. *Deutsche Zeitschrift Gerichtliche Medizin* 1948/49;*39*:186–98.
44. Lochte Th. Über die Absterbeerscheinungen der Skelettmuskulatur, insbesondere über die Totenstarre in gerichtlich-medizinischer Beziehung. *Z Ges Gerichtl Med* 1923;*2*:169–90.
45. Lyle H, Cleveland F. Determination of the time since death by heat loss. *J Forensic Sci* 1956;*1*:11–24.
46. Madea B. Importance of supravitality in Forensic Medicine. *For Sci Int* 1994;*69*:221–41.
47. Madea B, Henssge C. Electrical excitability of skeletal muscle postmortem in casework. *For Sci Int* 1990;*47*:207–27.
48. Madea B, Henssge C, Honig W, Gerbracht A. References for determining the time of death by potassium in vitreous humor. *Forensic Sci Int* 1989;*8*:231–43.
49. Madea B, Henssge C. Historisches zur Todeszeitbestimmung. *Z Rechtsmed* 1985;*95*:19–25.
50. Madea B. Cadaveric spasm. *For Sci, Med Path* 2013:*9*:249–50.

51. Madea B. *History of Forensic Medicine*. Berlin, Lehmanns Media.
52. Madea B. *Supravitale elektrische Erregbarkeit der Skelettmuskulatur: Längsschnittuntersuchungen zur Objektivierung der muskulären Reaktion an 70 Leichen*. Cologne, Germany, Habil. Schrift, 1989.
53. Mallach HJ, Mittermeyer HJ. Totenstarre und Totenflecke. *Z Rechtsmed* 1971;*69*:70–8.
54. Mallach HJ. Zur Frage der Todeszeitbestimmung. *Berl Med* 1964;*18*:577–82.
55. Marshall T, Hoare F. Estimating the time of death: the rectal cooling after death and its mathematical representation. *J Forensic Sci* 1962;*7*:56–81.
56. Marshall T. Estimating the time of death. *J Forensic Sci* 1962;*7*:189–210.
57. Marshall T. Estimating the time of death. *J Forensic Sci* 1962;*7*:210–21.
58. Marshall T. Temperature methods of estimating the time of death. *Med Sci Law* 1965;*5*:224–32.
59. Marshall T. *The Cooling of the Body After Death*. MD thesis. Leeds, University of Leeds, 1960.
60. Marshall T. The use of body temperature in estimating the time of death and its limitations. *Med Sci Law* 1969;*9*:178–82.
61. Nagy J. The postmortem excitability of the skeletal muscles. *Acta Med Leg Soc (Liege)* 1968:177–8.
62. Naumann HN. Postmortem chemistry of the vitreous body in man. *Arch Ophthalmol* 1959;*62*:356–63.
63. Niderkorn PF. Zitiert nach Tidy CM. The period of cadaveric rigidity (rigor mortis). In: *Legal Medicine*, vol. 1. London, Smith Elder, 1872/1882, pp 62–9.
64. Nysten PH. Von der Erstarrung, welche die Körper der Menschen und Tiere nach dem Tode befällt. *Recherches de physiologie et chemie pathologique*, Paris, 1811. German trans. and with additional material by Mayer AC, Bern. *Hufeland-Journal* 1816;*43*.
65. Onimus M. Modification de l'excitabilité des nerfs et des muscles après la mort. *J Anat Physiol Normale Pathol* 1880:629.
66. Popwassilew J, Palm W. Über die Todeszeitbestimmung in den ersten 10 Stunden. *Z Arztl Fortbild* 1960;*54*:734–7.
67. Potente S, Wirth I. Perspektiven der Todeszeitschätzung seit Henßge. *Archf. Kriminol* 2022;*249*:27–40.
68. Prokop O. *Forensische Medizin*. Berlin, Volk und Gesundheit, 1975.
69. Prokop O. *Lehrbuch der gerichtlichen Medizin*. Berlin, Verlag Volk und Gesundheit, 1960.
70. Puppe G. Der Scheintod und seine Diagnose. *Med Wochenschr* 1920;*14/15*:383–5.
71. Radam G. Ein elektronisches Reizgerät zur Todeszeitbestimmung. *Gesundheitswes* 1963;*18*:1400–1.
72. Rainy H. On the cooling of dead bodies as indicating the length of time since death. *Glasg Med J* 1868;*1*:323–30.
73. Raszeja S, Bardzik S. Studies on the "intralethal" excitability of muscles following stimuli obtained from an electronic stimulator. *Bull Pol Med Sci Hist* 1971;*14*:93.
74. Ravache-Quiriny J. *Les moments de la mort. Cahiers de médicine légale, droits medicales no. 3: Association Lyonnaise Médicine legale*. Lyon, Editions Alesandre Lacasagne, 1986.
75. Ravache-Quiriny J. The time of death: some thoughts on the trustworthiness of our response. *Int Acad Leg Med Soc Med* 1982;*1*(Newsletter):9–11.
76. Rosenthal M. Untersuchungen und Beobachtungen über das Absterben der Muskeln und den Scheintod. *Wiener Medizinisches Jahrbuch* 1872:389–413.
77. Saukko P, Knight B. *Knight's Forensic Pathology*, 3rd ed. London, Edward Arnold, 2004.
78. Sellier K. Determination of the time of death by extrapolation of the temperature decrease curve. *Acta Med Leg Soc* 1958;*2*:279–301.
79. Seydeler R. Nekrothermometrie. *Prag Viertelsjahresschr* 1869;*104B*:137–48.
80. Shapiro H. Medico-legal mythology: the time of death. *J Forensic Med* 1954;*1*(3):1–159.
81. Shapiro H. The post-mortem temperature plateau. *J Forensic Med* 1965;*12*:137–41.
82. Simpson K. *Forty Years of Murder. An Autobiography*. London and Glasgow, Grafton Books, 1980.
83. Smith S. *Mostly Murder*. Dorset Press, 1989.
84. Sturner WQ. The vitreous humour: post-mortem potassium changes. *The Lancet* 1963;*1*:807–8.
85. Taylor A, Wilkes D. On the cooling of the human body after death. *Guy's Hosp Rep* 1863;*9*:180–211.
86. Tidy CM. Changes in the muscle and in the general condition of the body after death. In: *Legal Medicine*. Part 1. London, Smith-Elder, 1882.
87. Vogt H. *Das Bild des Kranken*. Munich, Germany, JF Bergman, 1980.
88. Waltz H, Mattig W. Elektrische Messungen an Leichen für die Konstruktion eines elektronischen Reizgerätes zur Todeszeitbestimmung. *Kriminal Forens Wiss* 1974;*16*:159–78.
89. Wirth I, Krocker K, Geserick G. Über die Nysten'schen Regel—eine Literaturstudie. *Archiv f Kriminol* 2020;*246*:11–25.
90. Wirth I, Kroker K, Geserick G. Über das Zsakó-Muskelphänomen—eine Literaturstudie. *Archiv f. Kriminol* 2021:*247*:9–21.
91. Womack F. The rate of cooling of the body after death. *St Barts Hosp Rep* 1887;*23*:193–200.
92. Zink P, Reinhardt G. Die Todeszeitbestimmung bei der ärztlichen Leichenschau. *Bayer Arztebl* 1972;*27*:109–15.

3 Supravitality in Tissues

Burkhard Madea

Contents

3.1 Definitions 25
  3.1.1 Spontaneous Supravital Activity 28
  3.1.2 Supravital Reagibility 28
  3.1.3 Supravital Metabolism 28
  3.1.4 Physiological Peculiarities of Supravital Reagibility 29
3.2 Post-mortem Mechanical Excitation of Skeletal Muscle 32
3.3 Post-mortem Electrical Excitability of Skeletal Muscles in Casework 34
  3.3.1 Current State 34
  3.3.2 Recommendations for Practical Use 36
  3.3.3 Re-examination of the Data of Klein and Klein 38
  3.3.4 Conclusions 39
3.4 Longitudinal Studies of Electrical Excitability 40
  3.4.1 Objectifying Supravital Muscular Contraction 40
  3.4.2 Is There a Higher Precision of Death Time Estimation When Using the Time Since Death as a Dependent Variable? 45
  3.4.3 Are There Any Differences Between Contralateral Muscle Groups? 45
  3.4.4 Are There Differences among Muscle Groups? 46
  3.4.5 Could the Original Data on the Precision of Death Time Estimation Be Confirmed on the Remodelled Reference and Control Sample? 46
  3.4.6 Conclusions 47
  3.4.7 Current Recommendations 47

As far as we know, the last review in the English literature on determination of the time since death in the early post-mortem interval (PMI) (dealing also in detail with supravital reactions) was published by Schleyer in 1963 in Volume II of Lundquist's *Methods of Forensic Science* [68]. Since then, much work has been carried out on supravital reactions, and some progress has been made. This, and the fact that many scientific papers in this field have been published in German, may justify a new review on supravital reactions in English. Those supravital reactions that are of practical value in casework (mechanical excitability of skeletal muscles, electrical excitability of skeletal muscle with subjective grading of muscular contraction, chemical excitability of the iris) are mentioned briefly again in Chapter 11.

The objective of this chapter is to present some basic considerations on supravitality, to review the work on mechanical and electrical excitability of skeletal muscles and to present some recent longitudinal studies on electrical excitability that have no current practical value in casework but may be of some heuristic interest and may also form the basis of future work on influencing factors. A complete summary of supravital reactions was published in German in 1988 by Henssge and Madea [17].

3.1 Definitions

Irreversible circulatory arrest represents the starting point for a period of survival of some tissues under the condition of global ischaemia; this is called the 'supravital period' or 'intermediary life'.

Investigations on global ischaemia in various organs have been performed mainly with regard to the survival period and to the resuscitation period (Figure 3.1) [6,10,23,33,51–53,67,69,70].

The *latency period* is an undisturbed period characterized by continuing aerobic energy production.

The *survival period* is the interval up to the point after which every aspect of life ceases. During the survival period, there is still spontaneous activity of organs (e.g. spontaneous but decreasing myocardial contractility), as well as reagibility (e.g. the response of muscles to stimulation) on excitation (e.g. evoked potentials on acoustic stimulation, nerve action potentials on electrical stimulation of nerves) [15,18–22,77].

The *resuscitation period* is the duration of global ischaemia after which the ability to recover expires. The resuscitation period is mainly defined as the interval when complete recovery of fine morphological, functional and

DOI: 10.1201/9781003244974-3

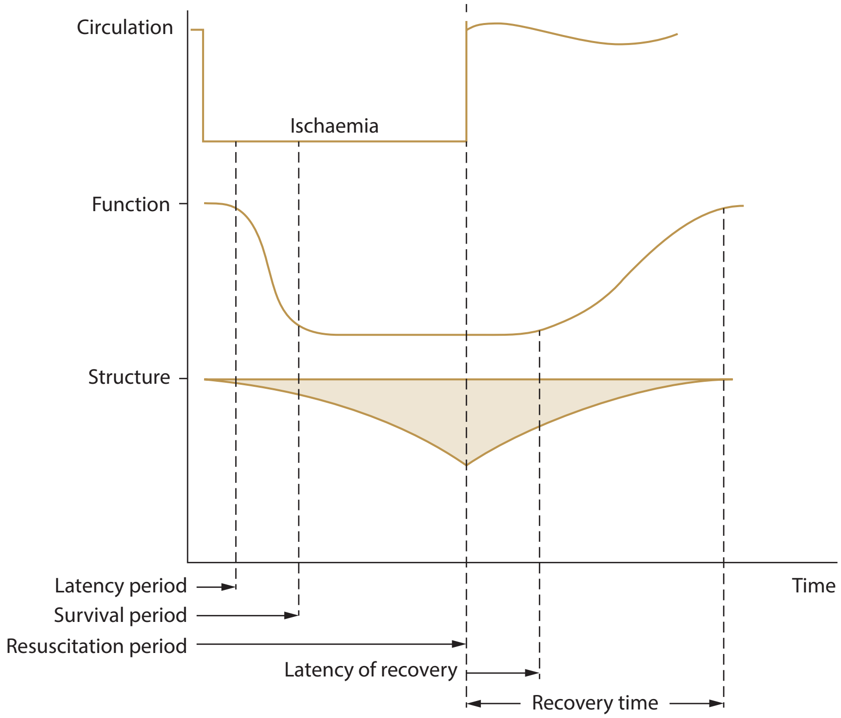

Figure 3.1 Survival and resuscitation periods of organs after temporary global ischaemia and reperfusion.

biochemical parameters in the post-ischaemic period is possible. The time required for complete recovery of these parameters is termed the 'recovering time'. The latency period is limited by the oxygen reserve as the basis of aerobic energy production characterized biochemically by the exhaustion of creatinine phosphate and a small decrease of adenosine triphosphate (ATP). During the resuscitation period, there is a breakdown of ATP to less than 60 per cent of the normal value and a steep increase in lactic acid (Figure 3.2) [10,74].

Ischaemia, resulting in cessation of nutrition and waste product removal, not only causes reversible consequences ('effects') but also, after a longer duration, results in irreversible changes ('damage').

The end of the resuscitation period demarcates both these steps of deficiency—reversible effects and irreversible damage [6,51,53,69].

Although 'survival period' and 'resuscitation period' are terms of great importance in physiology, organ preservation and transplantation because they describe the maximal ischaemic damage that is completely reversible in terms of structure and function, forensic medicine is also interested in the subsequent period—the period characterized by increasingly irreversible damage to structures and functions.

Although the definition of the resuscitation period of organs and tissues is based on complete recovery of different functional and biochemical parameters in the post-ischaemic period, supravitality is mainly defined by reagibility on excitation in the ischaemic period itself, irrespective of whether the damage to function is reversible (Figure 3.3).

As a result, the data on the duration of the resuscitation period, on the one hand, and the supravital period, on the other, are not comparable. The resuscitation period of skeletal muscles under normothermic conditions is 2–3 hours; supravital reagibility of skeletal muscles may be maintained in some cases for up to 20 hours post-mortem [9,27,36,44].

The resuscitation period of the heart under normothermia is 3.5–4 minutes (without cardiac massage in the post-ischaemic period), but supravital electrical excitability of cardiac muscle, according to Raule et al. [63], is preserved for up to 100–120 minutes post-mortem.

One difference between the resuscitation period and the supravital period is described by the 'reversibility/irreversibility' of damage. Another important difference is that physiologists and experimental surgeons are working on the restoration of the function of organs after ischaemic damage within an intact organ system, whereas forensic medicine is concerned with the functions of tissues because organ functions cannot be restored after an irreversible loss of the function of the major systems and their coordination.

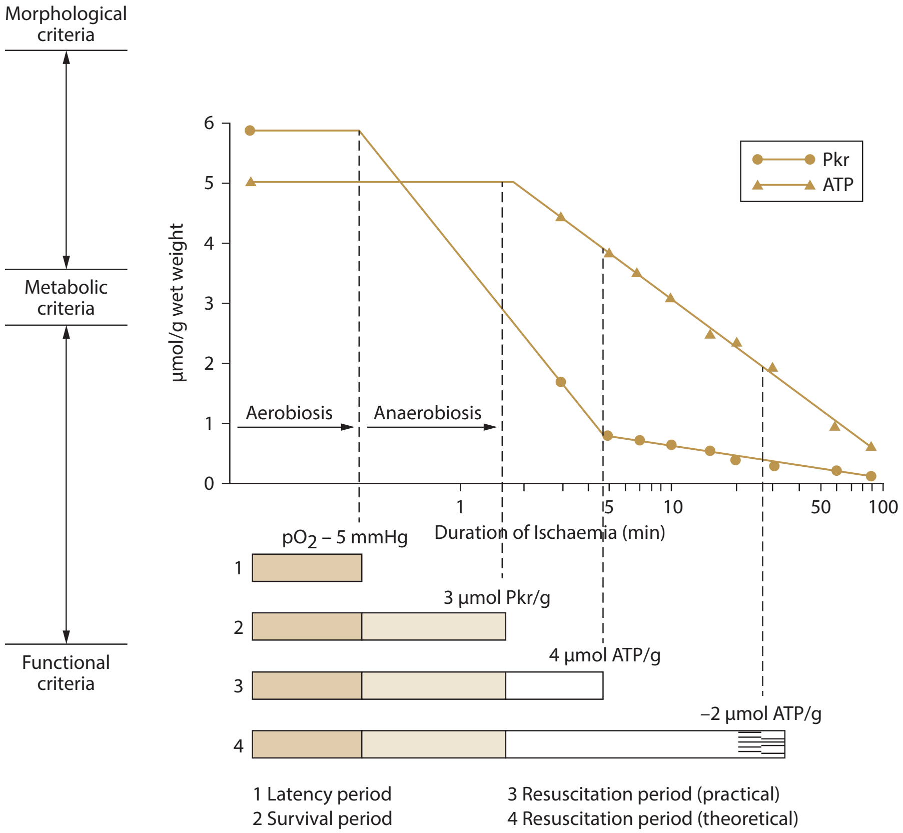

Figure 3.2 Latency, survival and resuscitation periods of the heart compared with the state of energy-rich phosphates. ATP, adenosine triphosphate; ^{18}Pkr, phosphocreatine.

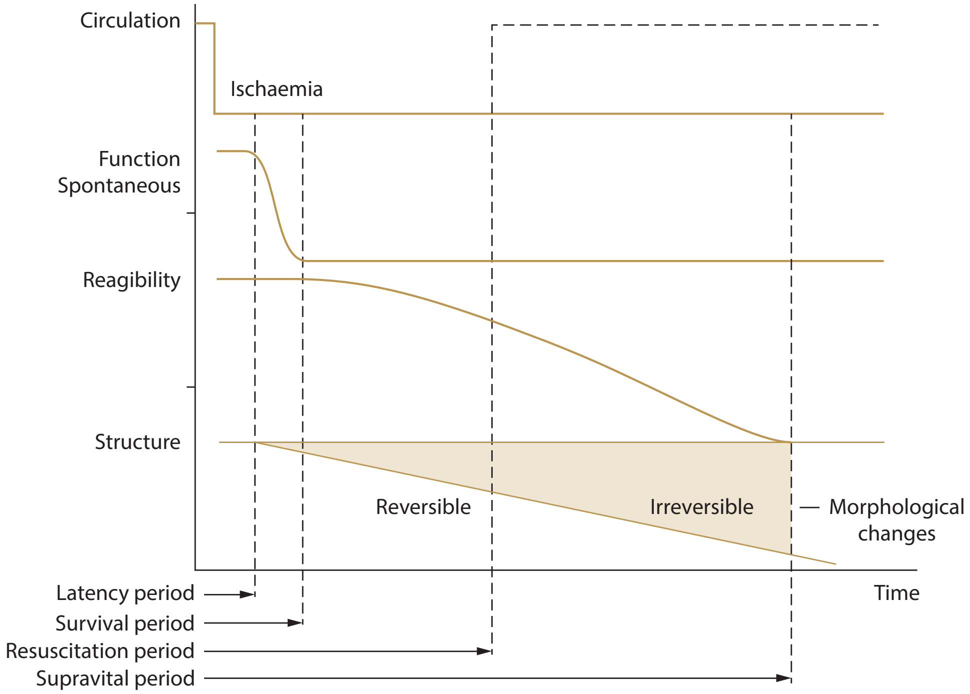
Circulation
Ischaemia
Function
Spontaneous
Reagibility
Structure
Reversible
Irreversible
Morphological changes
Time
Latency period
Survival period
Resuscitation period
Supravital period

Figure 3.3 Post-mortem course of functions (spontaneous function and reagibility) and structures after continuous global ischaemia (compare this with Figure 3.1).

Supravitality is compared with the resuscitation period the longer survival on a morphologically deeper step of organization. On a yet deeper step (the cell) reagibility of the myofibrils may be preserved even longer than in tissues.

Up to 104 days post-mortem, muscle cells in frozen muscle pulp may react to ATP administration with strong contractions; weak contractions end after 5 minutes [54].

3.1.1 Spontaneous Supravital Activity

These introductory definitions are not only of theoretical value but may also be of great practical importance, for instance, in cases where spontaneous supravital activity is in question.

This can be illustrated by a short case history published in *Medicine, Science and the Law* [50]. A 78-year-old woman—cause of death: spontaneous cerebral haemorrhage—displayed coordinated motor movements of her right lower limb, especially of the right foot, for 2 hours post-mortem. These motor movements were thought to be coordinated by the spinal cord and are analogous to movements of the decapitated chicken. However, this interpretation of the authors requires that, at 2 hours post-mortem, spontaneous activity of the spinal cord and of peripheral nerves is still preserved. According to all basic investigations on the supravital period and resuscitation period of spinal cord and nerves, spontaneous activity of spinal cord tissue is impossible 2 hours post-mortem [7,31,67,77].

In my opinion, there was no spontaneous supravital activity; this was the spontaneous activity of a woman still alive but who was declared dead.

3.1.2 Supravital Reagibility

From the definition of supravital reactions—obtainable vital reaction patterns of special tissues on proper excitations beyond individual death—it becomes evident that no fixed PMI can be given for the supravital period.

The supravital period is specific for each tissue; it depends on the tissue-specific metabolism (enzymes, substrates) under the condition of global ischaemia. Within the same tissue, it depends on the topographical localization within the body (different cooling velocity at different sites of the body depending on the diameter). Finally, the post-mortem duration of supravital reagibility depends on the mode of excitation and recording of the reaction (Figure 3.4). For instance, Popwassilew and Palm [55] reported the maximum duration of electrical excitability of the thenar muscles to be 5.5 hours post-mortem, whereas in my own investigations, with different modes of excitation and by objectifying muscular contractions of thenar muscles, reactions could be obtained up to 13–15 hours post-mortem.

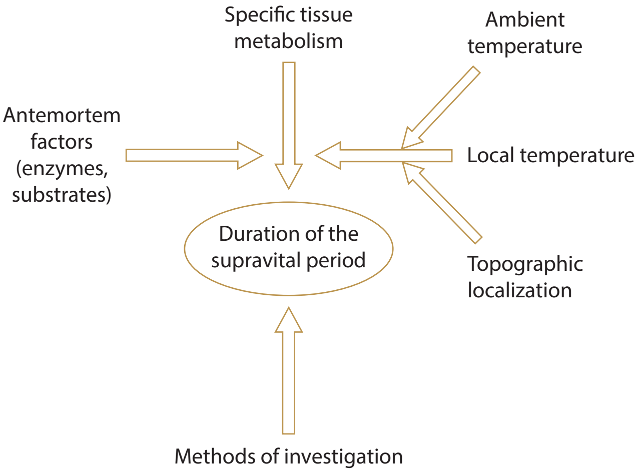
Specific tissue metabolism
Ambient temperature
Antemortem factors (enzymes, substrates)
Local temperature
Duration of the supravital period
Topographic localization
Methods of investigation

Figure 3.4 Factors determining the time course of supravitality.

3.1.3 Supravital Metabolism

The basis of supravital reactions is the vital metabolism, which, after death, runs down until substrates (e.g. glycogen) are exhausted or (and just as important) until reaction-limiting changes of the milieu intérieur cease (e.g. cessation of anaerobic glycolysis at pH 6.3).

Post-mortem anaerobic glycolytic metabolism proceeds at a high rate during the first 10 hours post-mortem, but only at a low rate thereafter. Correspondingly, lactic acid shows its steepest increase within the first 6–8 hours post-mortem, as shown by Schourup [71] in cerebrospinal fluid (Figure 3.5). In contrast, the pH shows its steepest decrease in the same time interval (Figure 3.6) [14], the decrease of the blood in the heart being steeper than that of the blood in the peripheral veins. This finding can be attributed to the higher glycogen content of heart muscle and to the different cooling velocity at central and peripheral measuring points, as shown by Dotzauer and Naeve [13].

During the first 10 hours post-mortem, the partial pressure of carbon dioxide (pCO_2) shows its steepest increase, as well as the accumulation of lactic acid, as was shown in vitreous humour by Klein and Klein [27]. After 10 hours post-mortem, the pCO_2 is decreasing very slowly by diffusion; even after 120 hours post-mortem, it has not yet reached its original level.

Although blood gases and substrates and metabolites of anaerobic glycolytic metabolism show the most marked changes of concentration within the first 10 hours post-mortem, all authors agree that these parameters are of only limited value for determining the time since death because of the great interindividual variability.

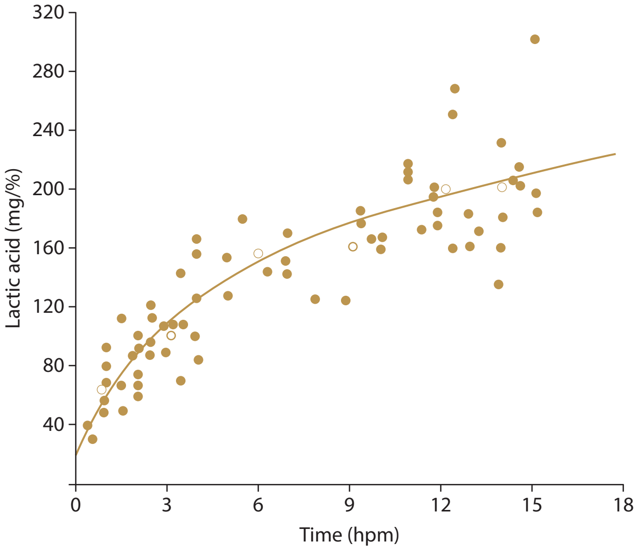

Figure 3.5 Lactic acid in mg per cent of cerebrospinal fluid over the PMI. Closed circles, single values; open circles, mean values; hpm, hours post-mortem.

(From Schourup K. *Determination of the Time Since Death* (Danish, English summary). Medical dissertation, Copenhagen, 1950.)

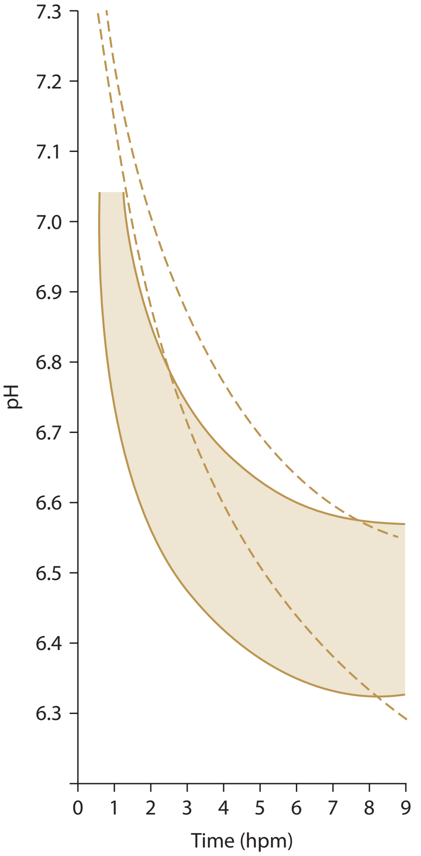

Figure 3.6 pH of cerebrospinal fluid (dashed lines) and heart blood (shaded area) in the first 9 hours post-mortem (hpm).

(From Dotzauer G, Naeve W. Wasserstoffionenkonzentration im Liquor post mortem. *Zentralbl Allg Pathol Anat* 1959;**100**:516–524.)

The interindividual variability of supravital reactions cannot, of course, be smaller than that of the substrates and metabolites of the basic metabolic processes [17].

3.1.4 Physiological Peculiarities of Supravital Reagibility

The smooth iris muscle is reactive to electrical and pharmacological stimulation for a longer time period than skeletal muscles. Klein and Klein [27] presented extensive experimental data on death time estimation using the smooth iris muscle (electrical and pharmacological stimulation). These authors examined 18 different pupillomotor drugs in different concentrations. The onsets of reactions vary between 5 and 30 minutes; the reactions lasted at least 1 hour. The drug concentrations had no influence on the durations and strengths of reaction. The onsets of reaction were later with increasing PMIs, the maximum reactions being reached later; the intensities of reactions (pupil dilatation in millimetres) decreased with an increasing PMI (Table 3.1 and Figure 3.7). The post-mortem pharmacological excitability to adrenaline, atropine and cyclopentolate covers three different PMIs; additionally, adrenaline and acetylcholine have the longest post-mortem efficiencies (Table 3.2). For practical use of pharmacological excitability of the iris in casework, see Chapter 10.

The strongest and longest post-mortem effects of acetylcholine and noradrenaline, as the natural transmitters of cholinergic and adrenergic fibres, reflect Cannon and Rosenblueth's law of denervation. According to this law, each denervated structure becomes supersensitive to the humoural mediator. This supersensitivity also becomes evident from the concentration of the drugs used in the cadaver experiments, which would cause no change or only a small change in the pupillary diameter in living individuals.

The physiological mechanism of supersensitivity of denervated smooth muscles to adrenergic drugs is related to the loss of the main mechanism for the regulation of adrenergic drugs at the receptor–neuronal

Table 3.1 Pharmacological Excitability of the Iris

Investigation of 5765 eyes from bodies.
Subconjunctival injection instead of injection into the anterior chamber; reaction after 5–30 minutes.
Duration of reaction at least 1 hour.
Concentration of drugs has no influence on the intensity and duration of reaction.

Source: Data from Klein A, Klein S. *Die Todeszeitbestimmung am menschlichen Auge*. Dresden, Germany, Medical Academy, Dresden University, MD thesis, 1978.

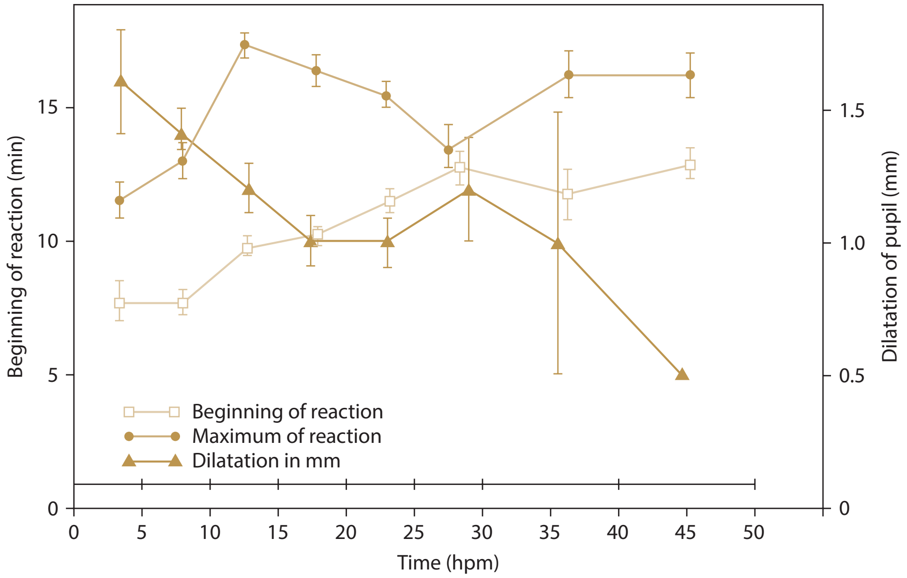

Figure 3.7 Post-mortem excitability of the iris after injection of noradrenaline. *x* axis = hours post-mortem (hpm); left *y* axis = beginning of the reaction after injection (in minutes); right *y* axis = dilatation of pupil (in millimetres). For each classified time interval, the mean value and 95 per cent confidence limits are given.

(The figure is designed using original data from Klein A, Klein S. *Die Todeszeitbestimmung am menschlichen Auge*. Dresden, Germany, Medical Academy, Dresden University, MD thesis, 1978.)

Table 3.2 Pharmacological Excitability of the Iris: Post-mortem Duration of Excitability after Injection of Different Drugs*

		Number of bodies		
		Post-mortem excitability (h)	**Subconjunctival (*n*)**	**Anterior chamber (*n*)**
Mydriatica				
Noradrenaline/ adrenaline	1.00%	14–46	573	737
Tropicamide	0.25%	5–30	307	320
Atropine/ cyclopentolate	1%/0.50%	3–10	131	145
Miotica				
Acetylcholine	5.00%	14–46	586	721

* In two cases there was no mydriasis in the interval 3–12 hours post-mortem.

re-uptake. It is a presynaptic specific supersensitivity (Figure 3.8).

For acetylcholine, the physiological mechanism of supersensitivity after denervation is a decrease in activity of the cholinesterase.

A recent study warned to use these data for forensic death time estimation (29). However, these data (Table 3.2) were checked in routine casework in numerous cases, furthermore in field studies and proved to be reliable (see also Chapter 11.1).

Discussing Cannon and Rosenblueth's law of denervation, we have seen that denervated structures may be supersensitive to physiological excitations; however, other tissues, with increasing PMIs, need much stronger excitations than vital tissues. Although impulses 0.2 millisecond in duration are a common means of excitation in clinical neurophysiology, skeletal muscle fails to react 2 hours post-mortem to a stimulus of such a short duration, whereas impulses 1 second in duration stimulate muscular contractions (Figure 3.9).

Although muscular contractions on mechanical excitation in the early PMI are characterized by contraction of the whole muscle (i.e. propagated excitation), with an increasing PMI the contraction is confined to the place of excitation; a local contraction called 'idiomuscular contraction' or 'idiomuscular pad' then results [12,25,30,48,73]. This change from propagated excitation to local contraction can also be seen after electrical excitation in both skeletal and smooth muscles [27].

For instance, on electrical excitation, in the early PMI, the smooth iris muscle reacts by a miosis (propagated excitation), but in the later PMI, there is only a drawing out of muscle fibres into the direction of the electrodes—a local contraction (Figure 3.10).

Decreasing ciliary motility of nasal cells or cells of the respiratory tract, as well as motility of spermatozoa, as supravital phenomena with potential importance for estimating the time since death have already been described in the older literature. More recently, the working group around Romanelli and Solarino et al. [66] carried out *in vitro* experiments on nasal ciliary motility. These investigators evaluated the diagnostic usefulness of ciliary

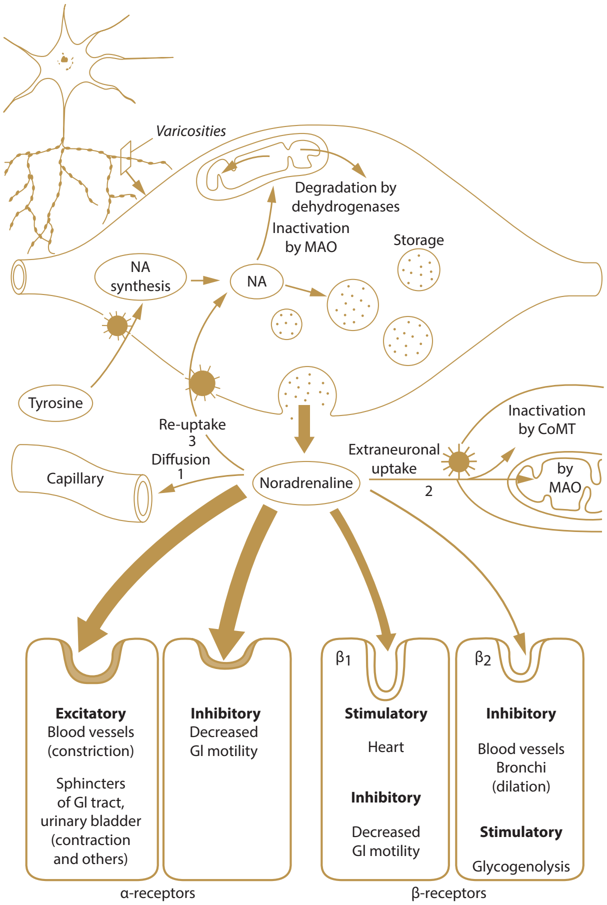
Varicosities
Degradation by dehydrogenases
Inactivation by MAO
Storage
NA synthesis
NA
Tyrosine
Re-uptake 3
Diffusion 1
Capillary
Noradrenaline
Extraneuronal uptake
2
Inactivation by CoMT
by MAO
Excitatory
Blood vessels (constriction)
Sphincters of GI tract, urinary bladder (contraction and others)
Inhibitory
Decreased GI motility
β1
Stimulatory
Heart
Inhibitory
Decreased GI motility
β2
Inhibitory
Blood vessels Bronchi (dilation)
Stimulatory
Glycogenolysis
α-receptors
β-receptors

Figure 3.8 Synthesis, metabolism and effects of noradrenaline (NA). Neuronal re-uptake (3) is the main mechanism for the regulation of adrenergic activity at the receptor; it ceases after denervation. CoMT, Catechol-O-methyltransferase; GI, gastrointestinal; MAO, monoamine oxidase.

(Data from Silbernagel S, Despopoulos A. *Taschenatlas der Physiologie*, 3rd ed. Stuttgart, Germany, Thieme, 1988.)

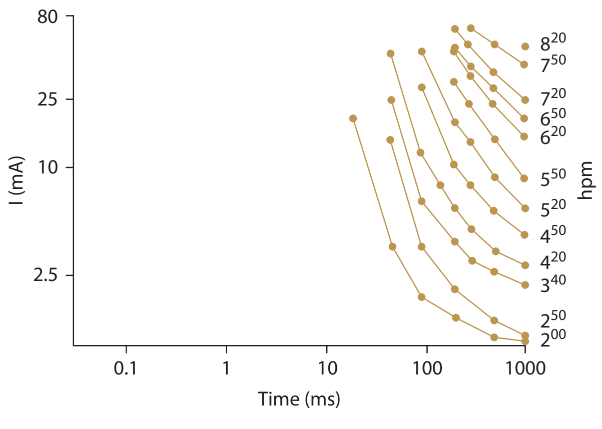

Figure 3.9 Strength-duration curve. *y* axis = current intensity (in ln milliamperes); *x* axis = duration of stimulus in milliseconds. At the right: time of death in hours and minutes. Using stimuli with a duration of less than 10 milliseconds, at 2 hours post-mortem (hpm) no muscular reaction can be obtained.

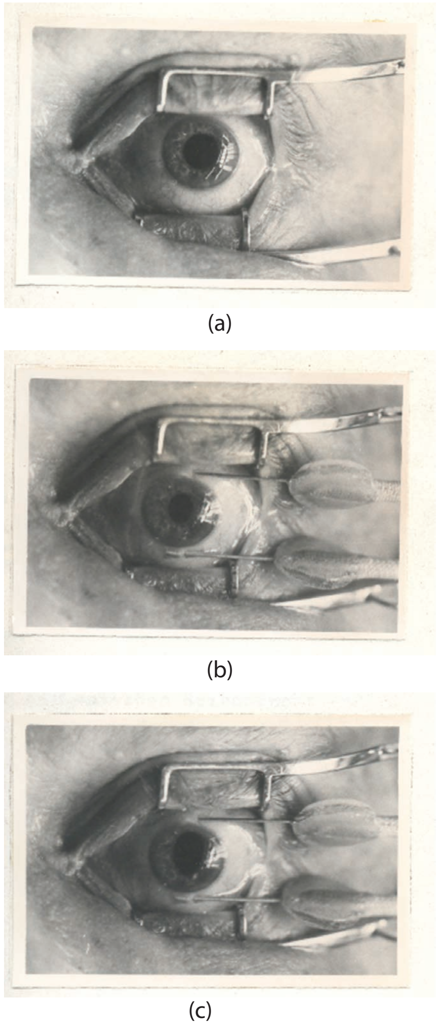

Figure 3.10 Electrical excitability of the iris. (a) Pupil before excitation. (b) Miosis after excitation (propagated excitation). (c) Drawing out of the pupil in the direction of the electrodes (local contraction).

(From Klein A, Klein S. *Die Todeszeitbestimmung am menschlichen Auge*. Dresden, Germany, Medical Academy, Dresden University, MD thesis, 1978.)

motility as a potential tool in estimating the time since death. Specimens of ciliated epithelium from 100 consecutive bodies were obtained by scraping the nasal mucosa at three different PMIs. The samples were then smeared on a slide, and an *in vitro* evaluation of ciliary movement was analysed by phase-contrast microscopy. Post-mortem nasal ciliary motility was observed, and a statistically significant relationship between decreasing ciliary movements and increasing PMI was detected even in the presence of putrefactive changes to nasal ultrastructure integrity. Some peculiar causes of death seemed to influence ciliary motility in the early PMI, whereas no significant correlations with gender or age were observed. According to the results of this study by Romanelli et al. [66], post-mortem evaluation of nasal ciliary motility should be studied further.

These few comments on supravitality can be summarized as follows:

1. Supravitality, especially reagibility on excitation, covers a much longer post-mortem period than latency, survival and resuscitation times. Clinically oriented investigations on latency, survival and resuscitation periods may form the only scientifically safe basis for the explanation of spontaneous supravital activity, but they do not provide an explanation for the upper margin for vital actions and reactions beyond the end of the resuscitation period. The portion of the supravital period beyond the end of the resuscitation period requires further scientific investigation.
2. The correlation of functional and biochemical parameters, which have been investigated for the latency, survival and resuscitation periods, should be extended over the whole supravital period. The aim of these investigations would be to improve the precision of death time estimation using supravital reactions, by narrowing the great interindividual variability of supravital reagibility by considering complementary parameters of metabolism.
3. With an increasing PMI, the supravital reaction pattern differs not only quantitatively but also qualitatively from physiological conditions. Investigations of supravital reagibility should address this issue, with the aim of extending the investigations over a post-mortem period for as long as possible.

3.2 Post-mortem Mechanical Excitation of Skeletal Muscle

Zsako's phenomenon [79,80] and the idiomuscular contraction [12] are different phases of the post-mortem mechanical excitability of skeletal muscles. Whereas Zsako's phenomenon seems to be a propagated excitation of muscle fibres, the idiomuscular contraction or idiomuscular pad is a local contraction of the muscle.

Investigations on post-mortem mechanical excitability of skeletal muscles were mainly carried out during the nineteenth century and during the first half of the twentieth century [12,48,55,57,72,79,80] (the more recent investigations are listed in Table 3.3).

In these older investigations, different muscles were investigated and different modes of excitation were used (including pinching and hitting with the hand, the back of the hand, the back of a knife or a chisel). The heavier the blow, the stronger is the reaction. Different names were used for the same phenomenon, for instance, 'Zsako's muscle phenomenon', which is just a propagated contraction of the muscle after mechanical excitation in the very early PMI. Some authors confined their experiments to the very early post-mortem period [79,80], and they recommended as many as eight different locations to examine this phenomenon (Figure 3.11); however, clear values for the duration of post-mortem excitability of these different muscles are lacking. Therefore, the literature on mechanical excitation of skeletal muscles is somewhat confusing, and different studies are hardly comparable. For practical use, the extensive studies on idiomuscular contraction by Dotzauer [12] and by Popwassilew and Palm [55] should be considered because they present relatively detailed information on the mode of excitation and the results obtained (Table 3.4 and Figure 3.12; see also Figure 3.11).

According to Dotzauer [12] and the detailed review of Joachim [25] on post-mortem mechanical excitability of skeletal muscle, three phases or degrees of mechanical excitability of skeletal muscles can be distinguished (see Figure 3.11; Table 3.5):

Table 3.3 Investigations on Idiomuscular Pad with Random Samples, Muscles Investigated and Results Obtained

Reference	Random sample	Results	Muscles investigated
Näcke [48]	20 mentally ill men	Mechanical excitability of skeletal muscles expired after 3–4 hours	Mimic muscles, neck muscles, limb muscles
Dotzauer [12]	595 examinations on 176 bodies	Idiomuscular pad can be induced up to 12 hpm; $\bar{x}$ = 6.9 hpm	M. pectoralis M. deltoideus M. biceps brachii
Popwassilew and Palm [55]	60 examinations	Idiomuscular pad can be induced in the interval of 1.5–8 hpm; $\bar{x}$ = 4.25 hpm	M. biceps brachii
Semmler[72]	102 bodies	2 hpm idiomuscular pad positive in 90.3%, 8 hpm negative in all cases; $\bar{x}$ = 4.21 hpm	Right thigh
Warther et al. [76]	270 bodies hospital cases and cases of sudden death	Up to 13 hpm	Musculus biceps brachii, Musculus quadriceps femoris, left and right sides of the body

Abbreviations: hpm, hours post-mortem; M., musculus; $\bar{x}$, mean value.

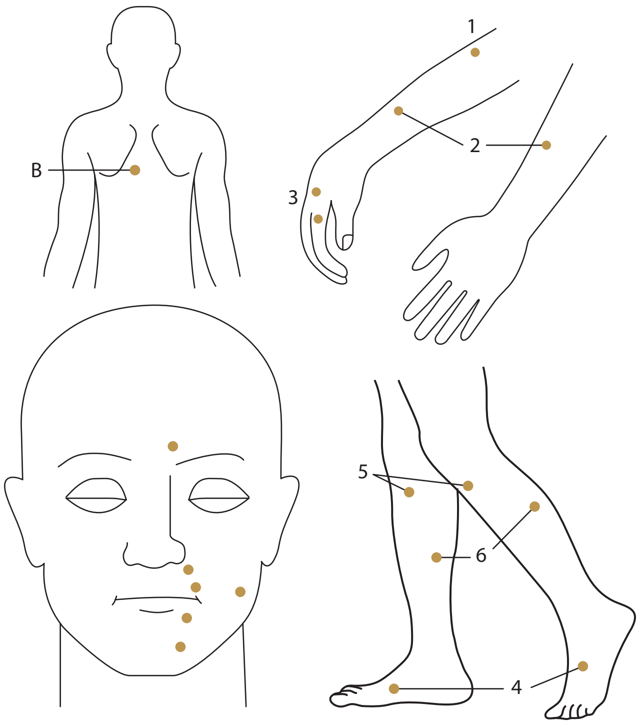

Figure 3.11 Examining Zsako's phenomenon (mechanical excitability of skeletal muscle in the very early PMI). The points give the places where optimum reactions can be obtained.

(From Joachim H. Mechanische und elektrische Erregbarkeit der Skelettmuskulatur. In: Henssge C, Madea B (eds.). *Methoden zur Bestimmung der Todeszeit an Leichen*. Lübeck, Schmidt-Römhild, 1988, pp 32–82.)

Table 3.4 Post-mortem Mechanical Excitability

Zsako's phenomenon/ idiomuscular pad	Grading	
	++	+
Idiomuscular pad	0–5.5	1.5–8
(Musculus biceps brachii)	$\bar{x} = 2.25$	$\bar{x} = 4.25$
	$n = 77$	$n = 60$
Zsako's phenomenon		0–2.5
Hitting on the musculi interossei at the back of the hand		$\bar{x} = 1.5$
Hitting on the musculus quadriceps femoris		$n = 41$

Abbreviations: +, only weak reaction, idiomuscular pad just to touch; ++, stronger reaction, idiomuscular pad is good, visible; $\bar{x}$, mean value.

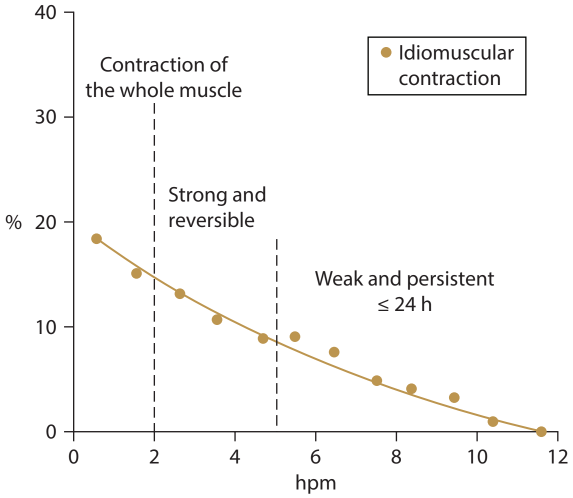

Figure 3.12 Percentage frequency of positive results in mechanical excitability of skeletal muscles. The mechanical excitability is graded in three phases (see also Table 3.5). hpm, hours post-mortem.

Table 3.5 Mode of Excitation and Grading of the Three Phases of Post-mortem Mechanical Excitability of Skeletal Muscles

Phase one	Contraction of the whole muscle; 1.5–2.5 hpm
Phase two	Strong and typical reversible idiomuscular pad; 4–5 hpm
Phase three	Weak idiomuscular pad which may persist for a longer period (up to 24 hours); 8–12 hpm

Note: Mode of excitation: hitting vigorously with the back of a knife or a chisel on the musculus biceps brachii at a right angle to the arm axis.

1. In the first phase, mechanical excitation of the muscle reveals a contraction of the whole muscle (propagated excitation). This first phase of idiomuscular contraction is identical to Zsako's muscle phenomenon [79,80]. Zsako himself gave eight methods of examining the mechanical excitability of skeletal muscles at different regions of the body (see Figure 3.11). Although these methods are quoted in the literature, very few investigators seem to have experience with Zsako's methods, as stated by Dotzauer [12]. Prokop [57] recommended the following procedure for Zsako's method: hit the lower third of the thigh with four to five cross-fingers above the patella. This first degree of idiomuscular contraction (propagated excitation) can be seen up to 1.5–2.5 hours post-mortem [12,25]. Figures 3.13 and 3.14 show the frequency of idiomuscular contraction post-mortem within three temperature classes.
2. In the second phase, a strong and typically reversible idiomuscular pad develops. This phase may be seen as long as 4–5 hours post-mortem. The mechanical excitation of the muscle causes membrane depolarization. The shortening of the muscle spreads very slowly, at only 0.2 cm/second, over the whole length of the muscle; the duration of shortening is 0.7 second. Shortening is initiated by action potentials. The local excitation and contraction comprise a relatively stable process, with

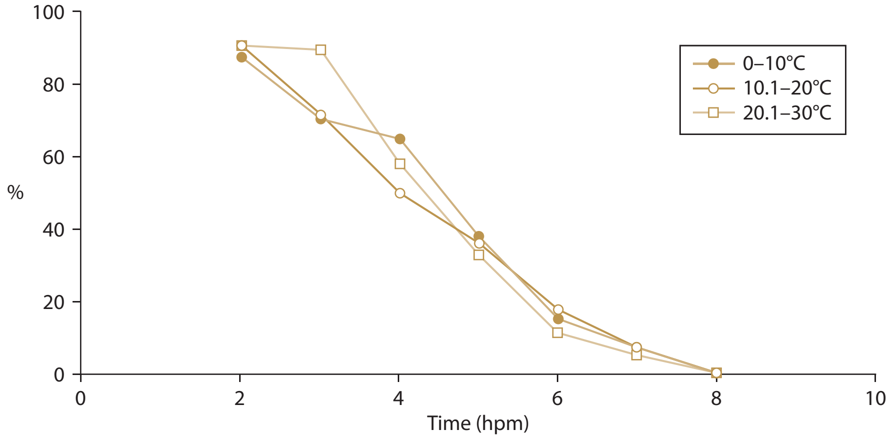

Figure 3.13 Percentage frequency of positive results in mechanical excitability of skeletal muscles (idiomuscular pad and Zsako's phenomenon). There is no obvious temperature dependency for the duration of mechanical excitability. The reason for the shorter post-mortem period in which idiomuscular pad could be induced, compared with Figure 3.12, is probably that Semmler used hospital cases, whereas Dotzauer (see Figure 3.12) used coroner cases for his investigations. hpm, hours post-mortem.

(Diagram was drawn using original data from Semmler [72].)

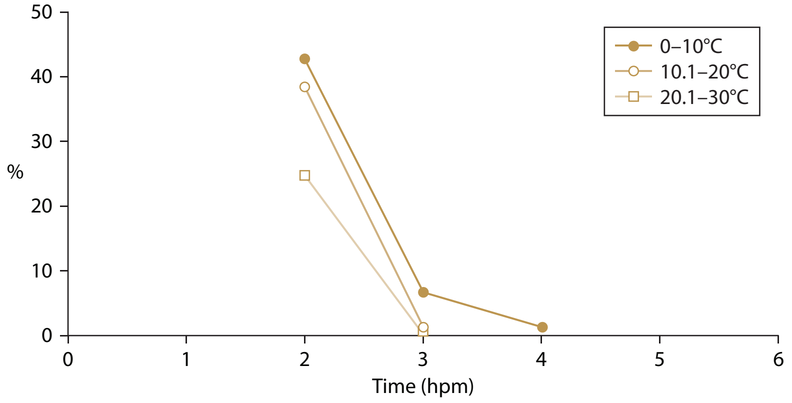

Figure 3.14 Percentage frequency of Zsako's phenomenon within three temperature classes. Mode of excitation: hitting onto the musculi interossei between metacarpal 3 and 4 with a reflex hammer. hpm, hours post-mortem.

(Drawn using original data from Semmler J. Einfluss der Umgebungstemperatur auf die Todeszeitbestimmung durch elektrische Reizung der Oberlidmuskulatur menschlicher Leichen. Magdeburg, Germany, Magdeburg University, MD thesis, 1979.)

mechanical excitability lasting longer than electrical excitability, according to older literature as referenced by Dotzauer [12].

3. In the last phase, a weak idiomuscular pad develops which may persist over a rather long period (up to 24 hours). The weak idiomuscular pad can be seen in the time interval up to 8–12 hours post-mortem.

This time interval (upper limit of 13 hpm) was recently confirmed (76). However, this finding would be in contrast to another study of the same group (1,11), which claimed reestablishment of rigor mortis up to 20 hpm, which is, of course, completely impossible (43).

Semmler [72], working on the influence of ambient temperatures on the duration of electrical excitability, also examined idiomuscular contractions and Zsako's phenomenon. The idiomuscular pad was examined by hitting on the right thigh with a reflex hammer. At about 2 hours post-mortem, an idiomuscular pad was present in 90.3 per cent of the bodies investigated; at 8 hours post-mortem, it was absent in all of the 102 bodies (median value, 4.21 hours post-mortem). No temperature dependency of the idiomuscular pad could be demonstrated (see Figure 3.13). The shorter time period in which an idiomuscular pad could be demonstrated in Semmler's study compared with Dotzauer's study [12] may reflect the composition of the samples. Dotzauer worked on forensic pathology material, and Semmler studied clinical pathology material.

Zsako's phenomenon was also investigated by hitting the interosseous muscles between metacarpals 3 and 4 with a reflex hammer. At 2 hours post-mortem, Zsako's phenomenon was seen in 35.5 per cent of all bodies, but at 3 hours post-mortem only two bodies showed positive results, and at 4 hours post-mortem, none had positive results for this phenomenon. (Figure 3.14 shows the frequency of Zsako's phenomenon.) For practical use regarding death time estimation in casework, we recommend that the data in Table 3.5 should be used.

3.3 Post-mortem Electrical Excitability of Skeletal Muscles in Casework

3.3.1 Current State

The renaissance of post-mortem electrical excitability of skeletal muscles began with investigations stimulated by Prokop [56]. These studies were followed by several papers on the construction of square-wave generators [8,32,47,49,55,59–61,75,78] and a large series on human bodies [24–32,36,38–41,62–65].

Most investigators of the post-mortem electrical excitability of skeletal muscles have worked with a verbal description and subjective grading of the muscular response to excitation—the muscular contraction—according to

1. the strength of contraction;
2. the spread of movement to areas distant from the electrodes.

For example, the results of the first large study on electrical excitability of orbicularis oculi muscle, orbicularis oris muscle and muscles of the hand and forearm on 102 bodies are shown in Figure 3.15 and Table 3.6. The muscle contraction is graded into three degrees [55].

During the early PMI there is strong contraction of the muscles, and the excitation also spreads to muscles distant from the electrodes (+++; Figure 3.16). Conversely, with an increasing PMI, muscle contraction becomes weaker, and the muscular response is confined to the place of excitation (+). Table 3.7 gives the results of this first major investigation (mean values for the special degree, ranges of scatter and number of cases).

Succeeding investigations modified the subjective grading of electrical excitability for the electrode positions in the orbicularis oculi muscle: the three degrees by Popwassilew and Palm [55] were changed to six degrees by Klein and Klein [27]and to four degrees by Krause et al. [28,30,32] (Table 3.8).

Not only was the subjective grading changed but also the position of electrodes was altered, even for the same investigated muscle (Table 3.9). Most investigators use

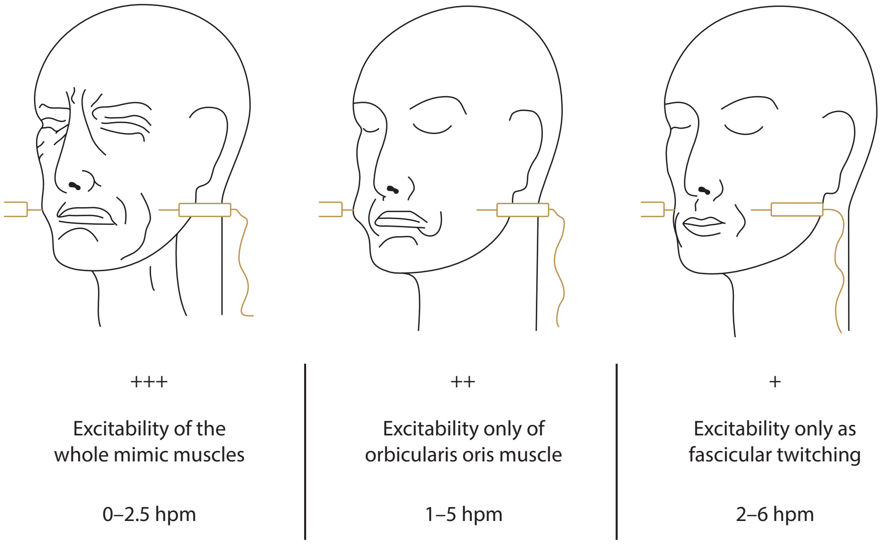
+++
Excitability of the whole mimic muscles
0–2.5 hpm
++
Excitability only of orbicularis oris muscle
1–5 hpm
+
Excitability only as fascicular twitching
2–6 hpm

Figure 3.15 Positions of electrodes and grading of muscular contractions of the orbicularis oris muscles according to Popwassilew and Palm [55] with the post-mortem duration of electrical excitability for the special degree. +, this degree is found in any case up to 2 hours post-mortem (hpm) and in some cases up to 6 hours post-mortem [55].

Table 3.6 Grading by Popwassilew and Palm

	Grading		
	+++	++	+
Orbicularis oculi	Contraction of the whole mimic muscles.	Contraction of the eyelids.	Fibrillar twitching.
Orbicularis oris	Contraction of orbicularis oris, neck muscles and eyelids.	Contraction of orbicularis oris.	Fibrillar twitching.
Hand	Contraction of the whole arm.	Contraction of the hand and the forearm.	Fibrillar twitching.

Source: Data from Popwassilew J, Palm W. Über die Todeszeitbestimmung in den ersten 10 Stunden. *Z Arztl Fortbildg* 1960;**54**:734–737.

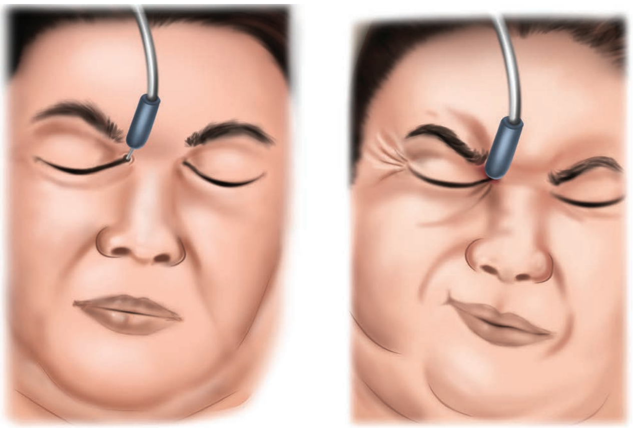

Figure 3.16 Contraction of the whole mimic muscles on excitation. Degree +++ according to Popwassilew and Palm [55] or degree VI according to Klein and Klein [27] (see Tables 3.7 and 3.8).

Table 3.7 Random Sample of 102 Cases of Popwassilew and Palm*

	Grading		
	1	2	3
	+++	++	+
Orbicularis oculi			
Range	0–2.5 h	1–5 h	2–8 h
Mean	1.25 h	2.25 h	4.25 h
N	64	79	75
Orbicularis oris			
Range	0–2.5 h	1–5 h	2–6 h
Mean	1 h	1.75 h	3.75 h
N	56	67	56
Hand			
Range	0–2.5 h	1–4 h	1–5.5 h
Mean	0.75 h	1.25 h	3.25 h
N	53	55	51

* For grading, see Table 3.6.

Source: Data from Popwassilew J, Palm W. Über die Todeszeitbestimmung in den ersten 10 Stunden. *Z Arztl Fortbildg* 1960;**54**:734–737.

Table 3.8 Subjective Grading of Muscular Responses to Excitation for the Orbicularis Oculi Muscle

Popwassilew and Palm [55]	Klein and Klein [27]	Krause et al. [30]
+++ Whole mimic muscles.	VI upper and lower eyelid and forehead and cheek.	IV heavy contraction spreading to the surrounding muscles.
	V upper and lower eyelid and forehead.	III contraction in whole length of the excited muscle.
++ Upper and lower eyelid.	IV upper and lower eyelid. III whole upper eyelid.	II incomplete contraction of the excited muscle.
+ Fibrillar twitching.	II 1/3–2/3 upper eyelid. I local upper eyelid.	I fibrillar twitching.

puncture electrodes; only Zink and Reinhardt [78] recommend surface electrodes.

The depth of insertion of the puncture electrodes varies between 3 mm and 2 cm.

Finally, the physical parameters of excitation also differ (Table 3.10). Some authors work with differing repetition rate-voltage combinations [27,30], for example, rectangular-like impulses of some milliseconds duration, a repetition rate of 10, 30, 70 and 120 per second, and a voltage of 10, 30 or 50 V, which means 12 repetition rate-voltage combinations [27]. Together with the 6 (7) degrees of muscular reaction, 75 combinations between mode of excitation and degree of reaction result. In this way, examining electrical excitability becomes very complicated, without any rise in the precision of the death time estimation.

Table 3.9 Positions of Electrodes in the Orbicularis Oculi Muscle According to Different Authors

Positions of electrodes	Reference
Puncture electrodes in a horizontal distance of 10 mm in the medial part of the left upper eyelid 3 mm deep or Puncture electrodes in a vertical distance of 10 mm into the right upper eyelid, inner angle, 3 mm deep	Krause et al. [30]
Surface electrodes beside the eye angles of the same eye	Zink and Reinhardt [78]
Puncture electrodes from lateral into the upper eyelid (musculus orbicularis oculi, pars palpebralis)	Popwassilew and Palm [55]
Needle electrodes at a distance of 15–20 mm into the nasal part of the upper eyelid 5–7 mm deep	Klein and Klein [27]
Like Popwassilew and Palm—2 cm deep	Walz and Mattig [75]

These few tabular summaries show that all elements of methods (position of electrodes, parameters of excitation, grading of muscular contraction) have been modified. Therefore, it is not surprising that the results of different authors are hardly comparable (Table 3.11). For instance, the Popwassilew and Palm [55] three degrees are comparable to the six degrees of Klein and Klein [27]; however, according to the parameters of excitation and the position of electrodes, the mean values and ranges of scatter for the degrees differ widely. The same is the case for the results on the orbicularis oris muscle.

In practice, there arises the question of which investigation (mode of excitation and results) to use as a reference. If experts wish to use different studies as references, they must apply different square-wave generators.

3.3.2 Recommendations for Practical Use

One of the most extensive investigations was presented by Klein and Klein [27], on case material of 447 bodies. The position of electrodes and the grading of muscular contraction are seen in Tables 3.8 and 3.9 and in Figures 3.17 and 3.18. From this extensive case material, Henssge [17] calculated the 95 per cent confidence limits for the six degrees of muscular contraction.

The data originally referred to stimulation by rectangular-like impulses of some milliseconds duration, with a repetition rate of 30–70 per second, a voltage of 50 V and resistance of 1 kOhm. These data are completely transferable to excitation with constant-current rectangular impulses of 30 mA, of 10 milliseconds duration and a repetition rate 50 per second. At the scene of a crime, we use a small, self-constructed generator (Figure 3.19), with the previously mentioned physical parameters of excitation.

Table 3.10 Differing Parameters of Excitation According to Different Authors

Parameters of excitation	Investigated muscles	Reference
Probably rectangular impulses of 6 ms duration, 9 V, repetition rate 100/s; voltage peaks >4000 V.	M. orbicularis oculi M. orbicularis oris Flexors of the forearm	Popwassilew and Palm [55]
Rectangular impulses of some ms duration, repetition rate 10–120/s; 10, 30, 50 V; resistance 1 kOhm.	M. orbicularis oculi M. orbicularis oris	Klein and Klein [27] Klein et al. [28]
Triangular impulses; repetition rate probably 50/s; 10 voltage steps between 9 and 70 V.		Mattig and Waltz [47]
Rectangular impulses of 'a few ms duration', 10–50 V, repetition rate between 10 and 100/s.	M. orbicularis oculi M. orbicularis oris M. biceps brachii M. brachioradialis	Krause et al. [30]
Constant-current rectangular impulses of 10 ms duration, 30 mA, repetition rate 50/s.	M. orbicularis oculi M. orbicularis oris	Henssge and Madea [16,38]
Rectangular impulses of 1 s duration; 200 V; current intensities according to the muscular threshold.	Different muscles	Joachim and Feldmann [26] Madea [36] Madea and Henssge [44] Ravache-Quiriny [64,65]
Rectangular impulses of 30 V; repetition rate 50/s.		Waltz and Mattig [75]
Non-sinus-like voltage with voltage peaks up to 1000 V.	M. orbicularis oculi	Zink and Reinhardt [78]
Constant-current rectangular impulses of 1 s duration, current intensity between 0.1 and 80 mA according to muscular threshold or definite supraliminal strength.	Thenar, hypothenar, M. biceps brachii, M. quadriceps, M. orbicularis oculi	Madea [36]

Abbreviation: M, musculus.

Table 3.11 Mean Values and 95 Per Cent Limits of Confidence (Klein and Klein) or Ranges of Scatter (Popwassilew and Palm) of Differing Degrees of Electrical Excitability (in Hours)*

		Klein and Klein [27]		Popwassilew and Palm [55]	
		x	95% limits	x	Range of scatter
Musculus orbicularis oculi					
I	Upper eyelid, nasal part	13.5	5–22		
II	1/3–2/3 upper eyelid	10.5	5.16 J+++	4.25	2–8
III	Whole upper eyelid	8.25	3.5–13		
IV	Plus lower eyelid	5.5	3–8.00 J+++	2.25	1–5
V	Plus cheek	4.5	2–7		
VI	Plus forehead	3.5	1–6 J+	1.25	0–2.5
Musculus orbicularis oris		7	3–11	3.25	2–6

* The three degrees of Popwassilew and Palm are comparable to the six degrees of Klein and Klein. Different time values according to position of electrodes and mode of excitation.

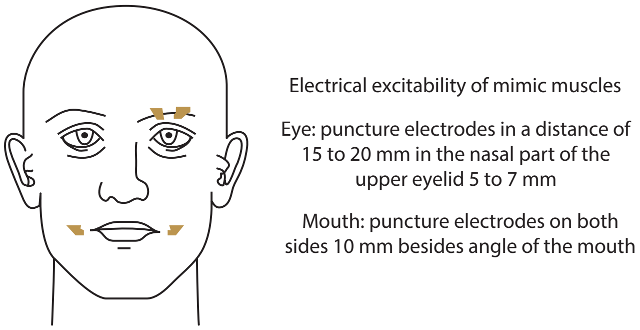
Electrical excitability of mimic muscles
Eye: puncture electrodes in a distance of 15 to 20 mm in the nasal part of the upper eyelid 5 to 7 mm
Mouth: puncture electrodes on both sides 10 mm besides angle of the mouth

Figure 3.17 Positions of electrodes for the stimulation of mimic muscles (musculus orbicularis oculi, musculus orbicularis oris) according to Klein and Klein [27].

The 95 per cent confidence limits for the six degrees of electrical excitability of the orbicularis oculi muscle were calculated on forensic pathology case material. In cases with a longer terminal episode (clinical pathology), the duration of electrical excitability is shorter (see Table 3.10).

In cases with haematomas or emphysema of the eyelid, electrical excitability may last much longer than that corresponding to the upper 95 per cent confidence limits for the special degree of the forensic pathology case material (Table 3.12 and Figure 3.20). This response may result from aerobic glycolysis in these cases, with a 19-fold greater energy profit [2,3,5,36] and a post-mortem Feng effect [36].

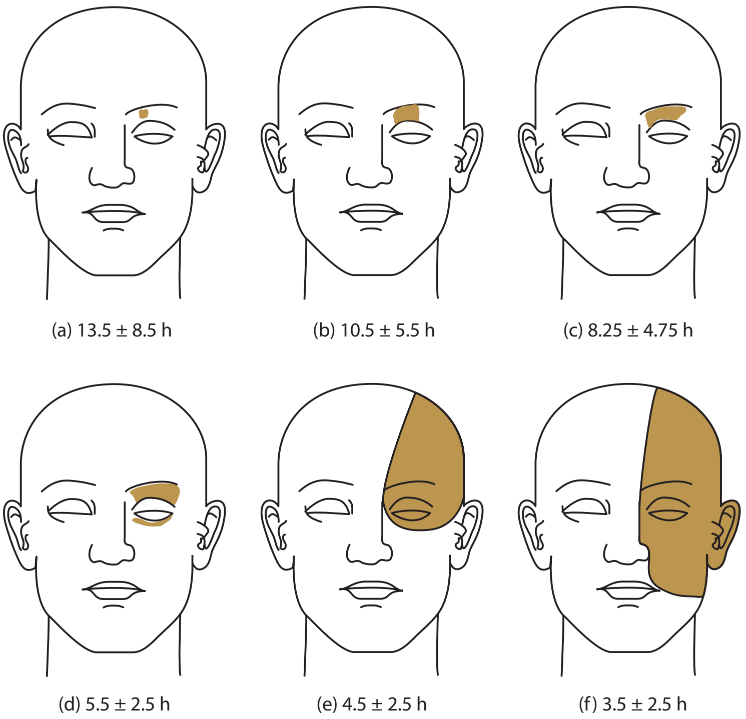

Figure 3.18 (a–f) Degrees of a positive reaction for stimulating the orbicularis oculi muscles according to Klein and Klein [27] with mean values and 95 per cent limits of confidence (in hours) for the special degree

(Calculated by Henssge from data of Klein and Klein [27]).

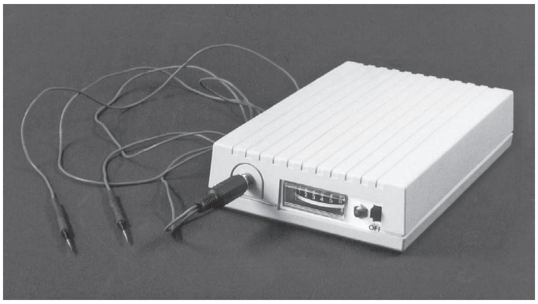

Figure 3.19 Self-constructed generator for examining electrical excitability at the scene of a crime. The output consists of constant-current rectangular impulses of 30 mA, 10 milliseconds duration, at a repetition rate of 50/second.

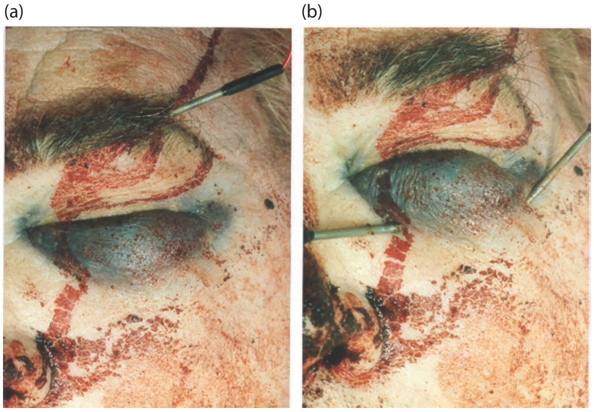
(a) (b)

Figure 3.20 Electrical excitability of the upper eyelid (a) at 16 hours post-mortem, while the whole bloodshot lower eyelid is still contracting (b).

Table 3.12 Upper and Lower 95 Per Cent Limits of Confidence for the Six Degrees of Electrical Excitability in Two Different Random Samples: Forensic Pathology and Clinical Pathology*

Degree		Forensic pathology (hours)	Clinical pathology (longer-lasting terminal episode) (hours)
I	Local upper eyelid	5–22	3–16
II	1/3–2/3 upper eyelid	5–16	0–16
III	Whole upper eyelid	3.5–13	1.5–9
IV	Upper and lower eyelid	3–8	1–7
V	Upper and lower eyelid and forehead	2–7	1–7
VI	Upper and lower eyelid and forehead and cheek	1–6	1–6

* In clinical pathological cases (longer-lasting terminal episode), the duration of electrical excitability is shorter.

3.3.3 Re-examination of the Data of Klein and Klein

My colleagues and I performed investigations on 30 bodies (traumatic or sudden natural death without long-lasting terminal episodes) with about 300 excitations, to re-examine whether the calculated 95 per cent confidence limits for the different degrees are valid.

The time period investigated ranged from 2 to 13 hours post-mortem. The mode of excitation was constant-current rectangular impulses of 1 second duration at 30 mA.

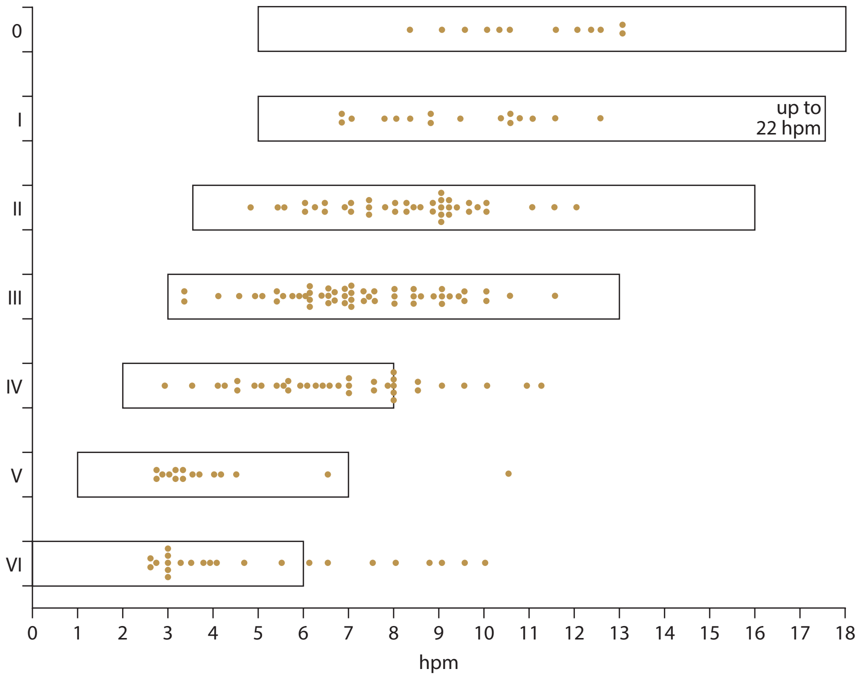

Figure 3.21 Re-examination of the calculated 95 per cent limits of confidence for the forensic pathology case material. I to VI: The degree of electrical excitability according to grading by Klein and Klein. The boxes represent the upper and lower 95 per cent limits of confidence. Each point corresponds to one excitation (about 300 excitations on 30 bodies). The points outside the boxes (the upper 95 per cent limits of confidence) for degrees IV to VI were observed in two cases of fatal hypothermia. hpm, hours post-mortem.

Table 3.13 Duration of Electrical Excitability in Cases of Traumatic Emphysema, Post-mortem Artificial Emphysema and Traumatic Haematoma of the Eyelid

Circumstances	Duration of electrical excitability (hpm)
Traumatic emphysema (vital)	Up to 29
Post-mortem emphysema (air insufflation into the eyelid)	27.3–52
Traumatic haematoma of the eyelid	Up to 32

Abbreviation: hpm, hours post-mortem.

The boxes represent the upper and lower 95 per cent confidence limits for the special degree (Figure 3.21).

In spite of the slightly differing mode of excitation, the 95 per cent confidence limits proved to be valid (see Figure 3.21). Each point represents one single excitation and all points are within the boxes, except some points for the degrees IV to VI, which represent several excitations in two cases of fatal hypothermia. In hypothermia, electrical excitability may last much longer.

3.3.4 Conclusions

Examining the electrical excitability of skeletal muscles post-mortem is a very easy procedure, which can be performed at the scene of a crime. It takes less than 1 minute to perform, and information on the time since death is available immediately.

Because, in almost all previous papers, either the mode of excitation or the grading of muscular contraction has changed, the investigator must adhere to one method. I recommend examining electrical excitability using a square-wave generator with rectangular impulses of 10 milliseconds duration, 30 mA and a repetition rate of 50 per second. The positions of electrodes and the grading of muscular contractions are according to Klein and Klein, with the 95 per cent confidence limits calculated by the method of Henssge. These times are valid for forensic cases (exceptions: fatal hypothermia; haematoma or emphysema of the eyelid, where longer times are possible) (Table 3.13).

By combining electrical excitability with the nomogram method of Henssge et al. in the early PMI, the precision and the accuracy of the death time estimation may be raised considerably (see Chapter 6.1). Using two independent methods to obtain a common result increases the investigator's confidence for the calculation of the time since death. When the temperature method cannot be used, examining electrical excitability alone may provide valuable additional information on the time of death. In my opinion, the examination of electrical excitability should be included in the minimum standard of methods used in the early PMI for determining the time since death. In those countries where, for legal reasons, the insertion of needle electrodes before autopsy is not permitted, the use of surface electrodes may be an alternative. However, this would require further investigations if the 95 per cent confidence limits for the six degrees are to be valid for this modified mode of excitation.

3.4 Longitudinal Studies of Electrical Excitability

One of the main reasons for the unsatisfactory comparability among different studies on electrical excitability of skeletal muscle is that the subjective grading of muscular contractions was made only by visual perception of the muscular reactions or their intensity (spread). The first improvement must therefore be the introduction of a method for objectifying muscular contraction. Another reason for the lack of comparability among different studies is that different authors worked with:

- Different modes of excitation
- Insufficiently defined physiological parameters of excitation

This second point for improvement must therefore be the introduction of well-defined electrical stimuli.

An electrical stimulus is defined, according to its biological efficiency, by:

1. Strength or intensity
2. Rise
3. Duration in one direction
4. Repetition rate

3.4.1 Objectifying Supravital Muscular Contraction

The preceding studies showed variation in all elements of excitation. The aim of this study was to analyse the objectified muscular contraction in relation to electrical stimuli. Therefore, according to the practice in clinical neurophysiology, we used only constant-current rectangular impulses of 1 second duration as single impulses. These impulses are characterized by an infinitely high rise, sufficient duration in one direction and a defined strength. Our experimental studies with a much shorter duration of stimulus—for instance, 0.2 millisecond, as it is usual in physiology—revealed that even by 2 hours post-mortem the muscle failed to give any response on excitation.

The third defect in preceding investigations was that longitudinal studies on the electrical excitability of the same muscle, until excitability expired, were virtually non-existent (with the exception of the post-mortem rise of galvanic threshold).

After an encouraging pilot study in 1984 that avoided these three defects of the preceding investigation [16], an accurate, standardized and reproducible method was developed for assessing the contractions of skeletal muscles after death by means of electrical stimulation, by assessing this phenomenon serially and then relating it to the time elapsed since death [16,35,36,39–41,45,46].

For objectifying muscular contractions, we used a sensitive force transducer (originally constructed for investigations in experimental cardiac surgery [34,35]) inserted in a hypodermic needle. Below the top of the force transducer is a lateral window, in which a flexural bar can be seen (Figure 3.22 [a]).

When the force transducer was inserted into the muscle, the contracting muscle fibres pressed on the flexural bar and caused it to lose its axial position in the force transducer; this signal will be quantified by the strain gauge. The signal measured the centripetal force acting on the bar in response to the contracting muscle fibres (Figure 3.22 [c]).

The measured force of the muscle fibres compressing the bar and the electrical stimulus were registered by a two-channel writer (Figure 3.22 [d]).

The force transducer was pricked into the muscle, and puncture electrodes were inserted on either side (Figure 3.23). Investigations were performed mainly on the thenar and hypothenar muscles. The muscle was stimulated half hourly, using rectangular impulses of 1 second duration at 2, 4, 8, 16, 32, 64 and/or 80 mA, by use of a commercial square-wave generator (Siemens Neurotron 726 S) until the electrical excitability expired for the applied or for highest current intensity (Table 3.14).

Electrical excitation and registration were usually performed at contralateral positions. When electrical excitability expired at one position, the electrodes and the force transducer were inserted into another muscle. The random sample consisted of 50 cases of sudden natural or traumatic death. Afterwards, a control group of 21 cases was also investigated. The experiments took place in a constant ambient temperature of 20°C (Table 3.15). Continuous measurement of the deep rectal temperature was made, as well as the local temperature at the location of measurement.

Two graphical forms of muscular contraction must be distinguished:

1. A two-peak shape during the first hours after death.
2. A one-peak shape in the later PMI (Figure 3.24).

The continuous change of the shape of muscular contraction could be studied in some cases where the start of investigation could be made very soon after death,

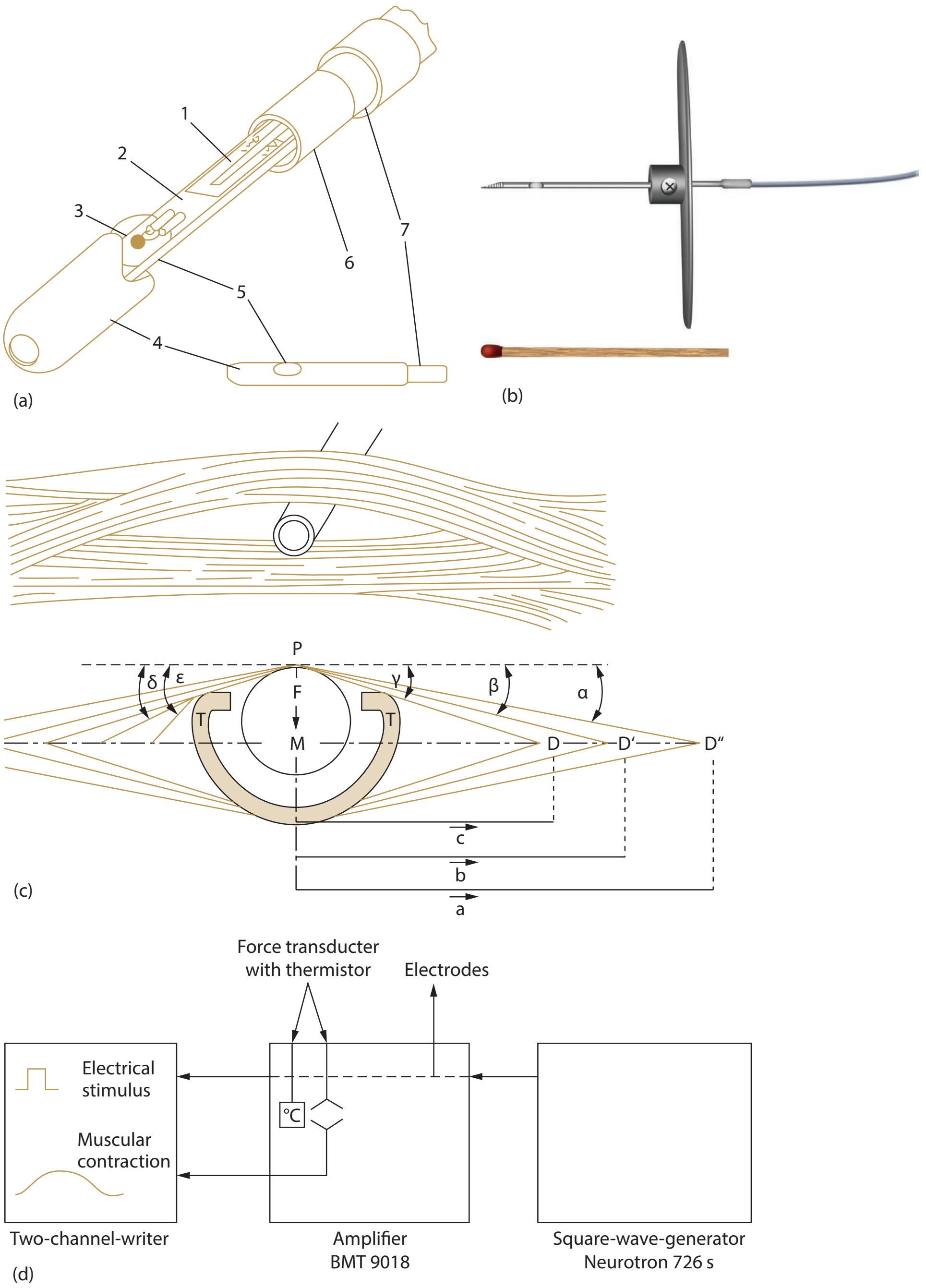
1
2
3
4
5
6
7
(a)
(b)
P
δ
ε
γ
β
α
F
T
T
M
D
D′
D″
c
b
a
(c)
Force transducter with thermistor
Electrodes
Electrical stimulus
Muscular contraction
°C
Two-channel-writer
Amplifier BMT 9018
Square-wave-generator Neurotron 726 s
(d)

Figure 3.22 (a) Schematic presentation of the force transducer: 1, DMS (strain gauge); 2, flexural bar; 3, thermistor; 4, outer tube; 5, lateral window; 6, bar support; 7, PE-catheter. (b) Size of the force transducer compared with a match. (c) Schematic drawing of the force transducer pricked into a skeletal muscle. The resulting force measured is the centripetal on the bar (M) acting force (F) of different layers of the contracting muscle fibres. (d) Schematic drawing of the experimental design.

with a long duration of electrical excitability (Figure 3.25 [a]).

In the early PMI, the muscular contraction is characterized by a two-peak shape: a closing and opening contraction at the beginning and the end of the 1-second electrical stimulus (see Figure 3.25). The closing and opening contractions have their own contraction and relaxation periods.

In the early PMI, the closing contraction has a higher maximum force than the opening contraction (see Figure 3.25 [a]). When the relaxation period of the closing contraction becomes weaker, the opening contraction begins at a higher force level and shows a higher force maximum (see Figure 3.25 [d]). This results in a superimposition of the closing contraction on the opening contraction.

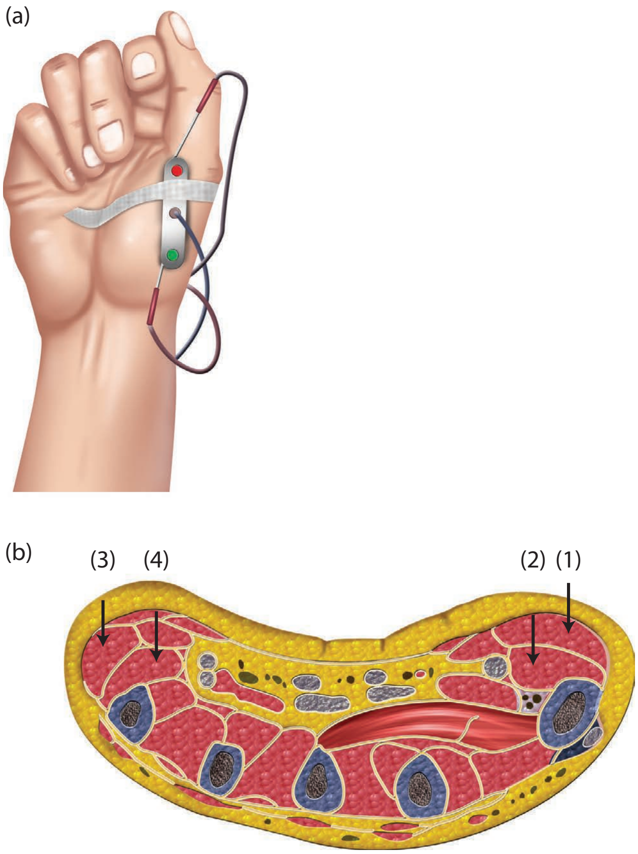

Figure 3.23 (a) *In corpore* insertion of force transducer and puncture electrodes on the right thenar. (b) Cross section of the hand with muscles investigated: thenar (musculus abductor pollicis brevis (1)); musculus opponens pollicis (2); hypothenar (musculus abductor digiti minimi) (3); musculus opponens digiti minimi (4).

Table 3.14 Experimental Procedure and Equipment

Measurement mostly at contralateral positions (thenar, hypothenar, biceps of right and left side).
Mode of excitation: rectangular impulses of 1 second duration of supraliminal strength (2, 4, 8, 16, 32, 64, 80 mA) each half hour until electrical excitability expired for the applied or highest current intensity. Then change to another location (of the same muscle) or to another muscle.
Puncture electrodes (steel, 2-mm diameter, 10 mm long) were pricked into the muscle at a distance of 3–4 cm, 5–7 cm deep.
Generator: Neurotron 726 S (Siemens).
Objectifying muscular contraction by a force transducer pricked into the muscle (see text).

Table 3.15 Composition of the Reference and Control Samples

Reference sample	Control sample
50 cases of sudden natural or traumatic death with a short terminal episode.	21 cases of sudden natural or traumatic death with a short terminal episode.
Male: 26; $\bar{x}$ 54.2 years (21–80 years)	10; $\bar{x}$ 38.3 years (19–69 years)
Female: 24; $\bar{x}$ 53.5 years (16–76 years)	11; $\bar{x}$ 66.3 years (40–79 years)
Beginning of the experiments	
2–11 hpm ($\bar{x}$ 3.9 hpm)	2–8 hpm ($\bar{x}$ 4.3 hpm)
Duration of the experiments	
1–9 h ($\bar{x}$ 4.9 h)	1–9 h ($\bar{x}$ 4.3 h)

Abbreviations: hpm, hours post-mortem; $\bar{x}$, mean value.

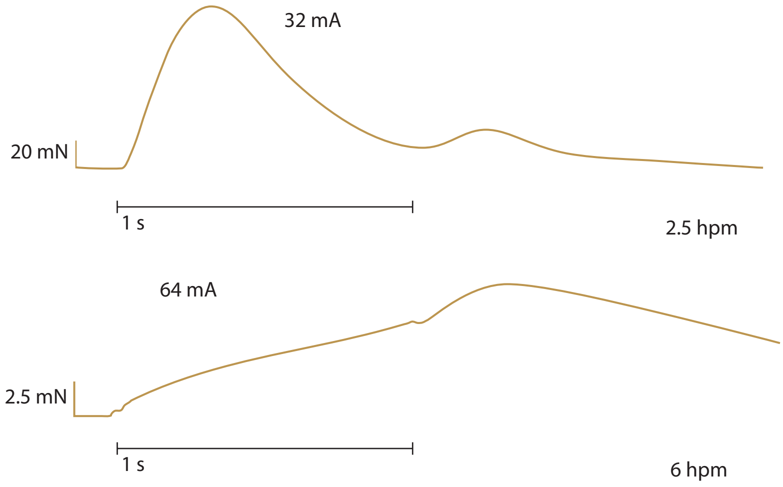

Figure 3.24 Two principal graphical forms of muscular contraction after stimulation with rectangular impulses of 1 second duration and supraliminal strength. Top, Two-peak-shaped contractions corresponding to a closing and opening contraction at beginning and end of the stimulus. Fast relaxation of the closing, as well as the opening contraction. Bottom, One-peak-shaped muscular contraction. The maximum force is achieved following the end of the stimulus; an opening contraction is missing. Return of the contracted muscle fibres to the starting tension is retarded. hpm, hours post-mortem.

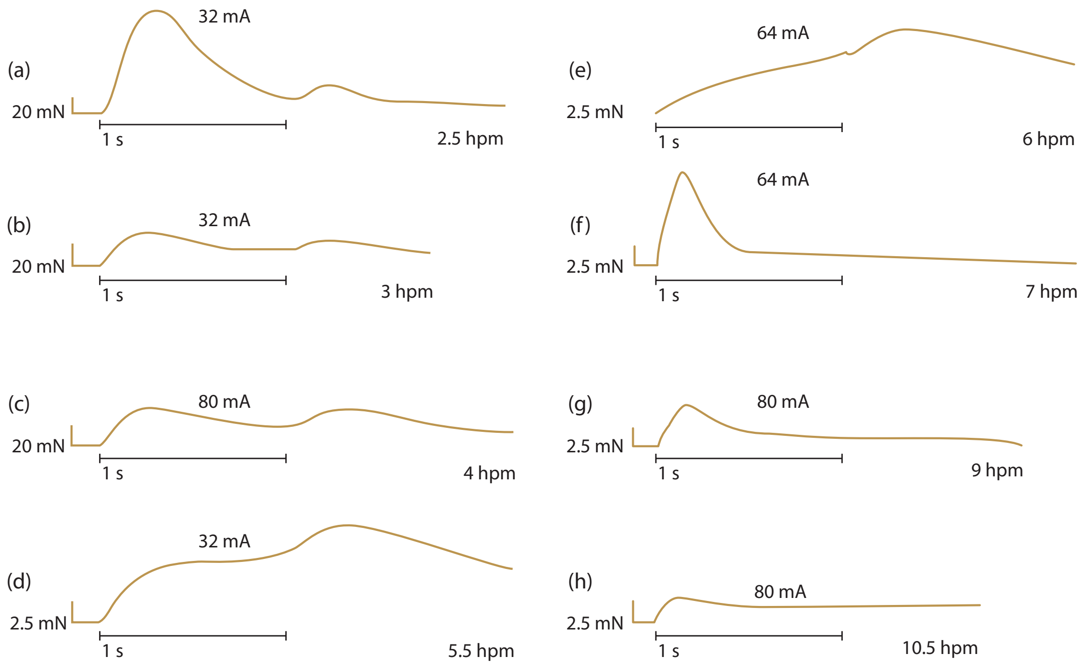

Figure 3.25 Post-mortem change in the shape of muscular contraction. Left, force in millinewtons; bottom, duration of the 1-second electrical stimulus in relation to the time course of muscular contraction; current intensities; time since death in hours. The curves (a) to (e) were registered at 100 mm/second, the curves (f) to (h) at 10 mm/second paper speed. hpm, hours post-mortem.

As the contraction velocity of the closing contraction decreases, the contraction period of the closing contraction is continued through the contraction period of the opening contraction. Consequently, a one-peak shape of muscular contraction results. At 80 mA current intensities, the one-peak shape appears, on average, at 5 hours post-mortem.

This one-peak shape of muscular contraction becomes increasingly weaker with the increasing PMI (see Figure 3.25 [f to h]). The reason that this pattern of muscular contraction has not yet been described in the literature may be that long-lasting stimuli, such as used here, are not normally used for physiology investigations.

The first appearance of a one-peak shape of muscular contraction depends not only on the current intensity used for stimulation but also on the temperature history of the body. The deeper the rectal temperature is at the beginning of the investigations, the later the one-peak shape of muscular contraction will appear.

With this method the following criteria for extrapolating the time since death from the objectified muscular contraction could be derived:

- Decrease of the maximum force of the muscular contraction after excitation with various current intensities (Figure 3.26)
- Increase of the relaxation time (Figure 3.27)
- Increase of the galvanic threshold (Figure 3.28)

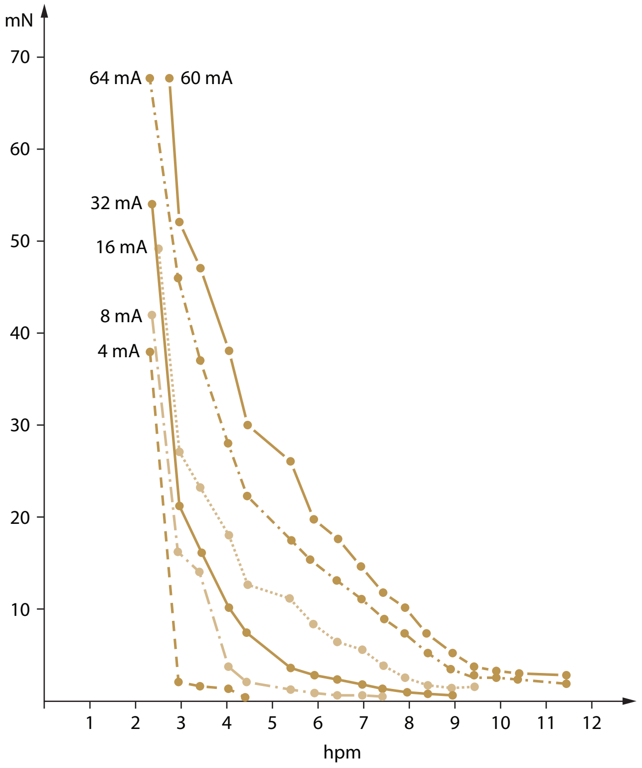

Figure 3.26 Decrease of maximum force (in millinewtons, mN) on the right thenar over the PMI for current intensities from 4 to 80 mA (one case). Exponential decrease of the maximum force for the same current intensity over the PMI. hpm, hours post-mortem.

The original investigations were carried out on different muscles: biceps brachii, thenar and hypothenar. The

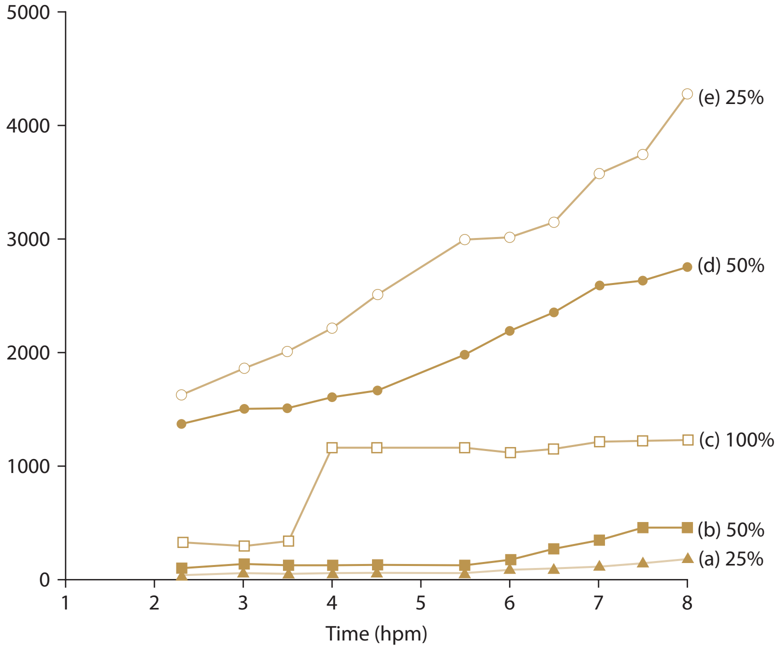

Figure 3.27 Contraction and relaxation time over the PMI. Contraction time up to 25 per cent (a), 50 per cent (b), 100 per cent (c) of the maximum force; relaxation time up to 50 per cent (d) or 25 per cent (e) of the maximum force achieved during muscular relaxation. The relaxation time up to 25 per cent of the maximum force shows the steepest increase over the PMI. Each point is a mean value for at least three muscular contractions registered at the same time post-mortem after excitation with different current intensities. hpm, hours post-mortem.

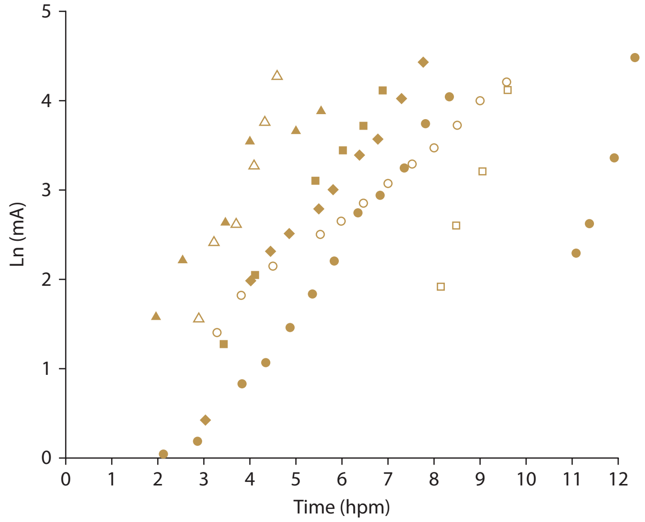

Figure 3.28 Post-mortem rise of galvanic threshold (ln mA) for eight cases marked with different symbols. Linear relationship between natural logarithm (ln) of galvanic threshold (rheobase) and time since death. hpm, hours post-mortem.

consecutive cases 1–50 were used as reference—the following 21 cases comprised the control sample. It could be shown that a decrease of the maximum force after stimulation with definite current intensities, an increase of the relaxation time in the form of force-related relaxation time and an increase of the galvanic threshold were suitable criteria for extrapolating the time since death.

In the original investigation, consecutive cases were used as references or control sample. Because they were not matched concerning beginning of the investigations, duration of electrical excitability, age and other factors, a matched reference and control sample was remodelled from the original data set [46] (Table 3.16). On the remodelled references and control sample, the calculations described after this list were performed to answer the following questions:

Table 3.16 Remodelled Reference and Control Sample at the Beginning of the Experiments (Minutes Post-mortem) and Duration of Electrical Excitability (Minutes Post-mortem)

	Reference sample	Control sample
N	28	28
Age (in years)	21–80; $\bar{x}$ 52.86	16–78; $\bar{x}$ 53.64
Beginning of the experiments (min pm) $\bar{x}$ ± SD	269.21 ± 126.71	233.21 ± 91.46
Duration of electrical excitability (min) $\bar{x}$ ± SD	282.71 ± 116.43	306.07 ± 118.72

Abbreviation: SD, standard deviation.

1. Is there an increase in the precision of death time estimation by using the PMI as dependent variable? From statistical calculations on the correlation between analyte concentrations in vitreous humour and time since death, it is known that using the analyte concentration as an independent variable reveals a statistically significant higher precision of death time estimation compared with its use as a dependent variable.
2. Are there systematic differences between contralateral muscles?
3. Are there differences among muscles (biceps brachii muscle, thenar, hypothenar muscles) in the duration of the electrical excitability?

4 Can the original data on precision of death time estimation be confirmed on the remodelled reference and control sample?

From the original data set of 71 cases, 2 reference and control groups, each comprising 28 cases, were remodelled and matched concerning post-mortem beginning of the experiments, duration of electrical excitability and ambient temperature until beginning of the experiments. The relevant data for the reference and control samples are shown in Table 3.10. Questions 1–4 were checked on the reference group. The precision of death time estimation is always given as 95 per cent confidence limits in hours. The calculations were performed for various criteria of objectified muscular contraction (decrease of maximum force, increase of relaxation time, increase of galvanic threshold). To achieve a clear structure, the results for one criterion (e.g. decrease of maximum force) are presented when questions 1–4 are addressed, although calculations have been carried out with other criteria (e.g. increase of galvanic threshold), also with the same results. The results were checked against those of the control group (e.g. by calculation of the accuracy of death time estimation on the data of the control sample in comparison with the reference group).

3.4.2 Is There a Higher Precision of Death Time Estimation When Using the Time Since Death as a Dependent Variable?

For the regression between time since death and decrease of the maximum force on the left thenar muscle after stimulation with a current intensity of 80 mA, the hypothesis was checked for using the PMI as a dependent variable or for using it as an independent variable. This revealed a higher precision of death time estimation. Thus, if in the regression analysis the PMI was used as a dependent variable, the precision of death time estimation was much greater with a standard deviation [SD] of ±1.93 hours compared with a linear regression with the PMI as an independent variable (SD ±3.4 hours) (Table 3.17). The precision of death time estimation calculated on the reference sample was confirmed on the control sample.

3.4.3 Are There Any Differences between Contralateral Muscle Groups?

Contralateral muscle groups normally show a very similar pattern, for instance, for the decrease of the maximum force after stimulation with the same current intensity or the increase of the galvanic threshold. When the 95 per cent confidence limits of precision of death time estimation (e.g. for the increase of the galvanic threshold or the decrease of the maximum force after stimulation with the same current intensity) were compared for contralateral muscle groups, nearly identical data were revealed (Figures 3.29 [a] and 3.30 [a]). Furthermore, the data on the

Table 3.17 Calculation of Precision of Death Time Estimation Using the Post-mortem Interval as a Dependent or an Independent Variable in Correlation between Decrease of Maximum Force and Time Since Death

	Reference sample	Control sample
N (number of cases)	28	28
n (number of measurements)	130	154
PMI residues*		
PMI as dependent variable	1.93	2.01
PMI as independent variable	3.41	3.96

* Standard deviation in hours.

Abbreviation: PMI, post-mortem interval.

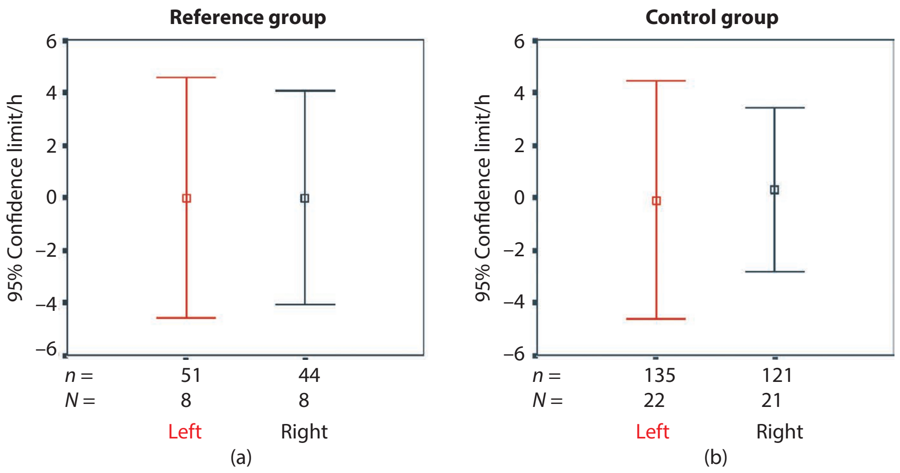

Figure 3.29 (a and b) 95 per cent confidence limit for estimating the time since death using the increase of the galvanic threshold on the left and right thenar muscles. *N* = number of cases; *n* = number of measurements.

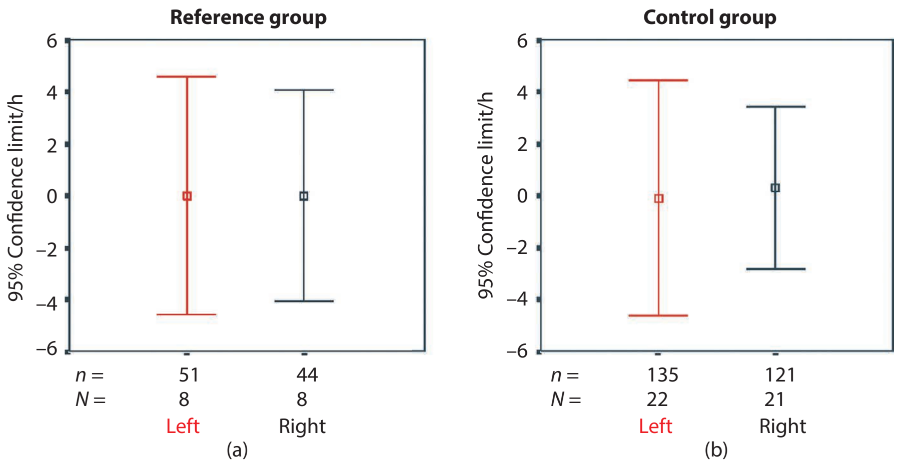

Figure 3.30 (a and b) Precision of estimating the time since death based on the decrease of the maximum force after stimulation with a current intensity of 80 mA on the right and left thenar muscles. Precision calculated on the reference sample confirmed on the control sample. *N* = number of cases; *n* = number of measurement.

precision of death time estimation for contralateral muscle groups could be confirmed for the control samples (see Figures 3.29 [b] and 3.30 [b]).

3.4.4 Are There Differences among Muscle Groups?

The mean duration of electrical excitability for different muscle groups for current intensities between 2 and 80 mA was calculated. The duration of electrical excitability was systematically shorter for the biceps brachii muscle compared with the thenar and hypothenar muscles. For the highest current intensity of 80 mA, thenar and hypothenar muscles showed a nearly identical duration of electrical excitability (Figure 3.31).

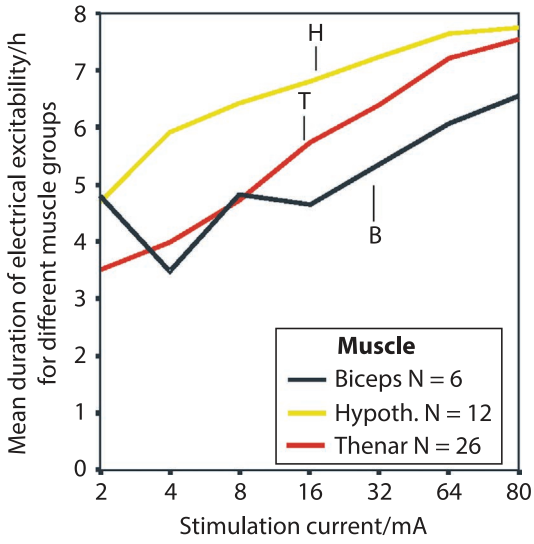

Figure 3.31 Mean duration of electrical excitability (hour) for different muscle groups (biceps brachii, hypothenar, thenar) and current intensities.

3.4.5 Could the Original Data on the Precision of Death Time Estimation Be Confirmed on the Remodelled Reference and Control Sample?

For the criteria decrease of maximum force, increase of the galvanic threshold and increased force-related relaxation time, 95 per cent confidence limits of death time estimation between ±2.69 hours (force-related relaxation time) and ±4.27 hours (decrease of maximum force) were calculated for the original reference group. These data on the precision of death time estimation could be confirmed for the decrease of the maximum force and the increase of the force-related relaxation time on the remodelled reference sample. For the increase of the galvanic threshold, systematically higher 95 per cent confidence limits were calculated on the remodelled reference sample (Table 3.18).

Table 3.18 Precision of Death Time Estimation (95 Per Cent Confidence Limits in Hours) of the Original Reference Sample and of the Remodelled Reference Sample

		Original reference sample	Remodelled reference sample
Decrease of maximum force	95% confidence limit	±4.27	±3.68
	n	445	280
	N	35	28
Increase of galvanic threshold	95% confidence limit	±3.27	±4.15
	n	267	182
	N	17	15
Increase of force-related relaxation time	95% confidence limit	±2.69	±2.87
	n	346	150
	N	35	16

Abbreviations: N, number of cases; *n*, number of measurements.

3.4.6 Conclusions

For regression analysis between analytical parameters and time since death, the analytical parameters should always be used as independent variables because this approach reveals a higher precision of death time estimation compared with a change of variables.

There is no difference in duration of electrical excitability between contralateral muscle groups. Thus, investigations can be carried out at either side.

The thenar and hypothenar muscles are much more suitable for examination of electrical excitability compared with the biceps brachii muscle, perhaps because of the higher tension of the biceps brachii muscle during development of rigor mortis compared with the thenar or hypothenar muscles (the greater the tension, the higher is the oxygen demand). Another point is the higher local temperature of the biceps brachii muscle compared with the thenar and hypothenar muscles (greater diameter of the upper arm compared with thenar or hypothenar; the greater the diameter, the more slowly the temperature will drop).

The original data on the precision of death time estimation using different criteria of objectified muscular contraction were proved to be valid for the decrease of the maximum force and the increase of the force-related relaxation time, but not for the increase of the galvanic threshold. Therefore, the results of the original work were confirmed on the matched remodelled reference and control samples. Different criteria of the objectified muscular contraction allow a much more precise estimation of the time since death than do other criteria of electrical excitability, especially subjective grading. However, great interindividual variability in the duration of electrical excitability still remains. The main factors determining the time course of the supravital period of skeletal muscles are the glycogen content of the muscles at the moment of death and the environmental and, of course, local temperatures at the places of excitation. With the described method of objectifying muscular contraction, the role of the glycogen content at the moment of death and the ambient temperature should be examined in further investigations.

3.4.7 Current Recommendations

1. Objectifying of supravital muscular contractions reveals a higher precision of death time estimation compared with the subjective grading of muscular excitability.
2. For regression analysis between the analytical parameters and death time estimation, the analytical parameters should always be used as independent variables because they reveal a higher precision of death time estimation compared with a change of variables.
3. In contralateral muscle groups, the duration of electrical excitability is almost identical; however, among different muscles of the same body, the duration of electrical excitability differs widely (in the thenar and hypothenar muscles, it is longer than in the biceps brachii muscle).
4. Differences in the duration of electrical excitability among different muscles of the same body may be the result of the variations in the glycogen content of different muscles, the varying cooling velocity depending on the diameter of the muscles and their topographical localization and the extension of the muscles (the greater the extension, the sooner the electrical excitability will expire). These influence factors have to be taken into consideration in further studies.

References and further reading

1. Anders S, Raupach T, Sehner S. Zeitgrenzen nichttemperaturbasierter Faktoren der Komplexmethode zur forensischen Todeszeitdiagnostik. *Rechtsmedizin* 2019;*29*:248–52.
2. Bate-Smith EC, Bendall JR. Factors determining the time course of rigor mortis. *J Physiol* 1949;*110*:47–65.
3. Bate-Smith EC, Bendall JR. Rigor mortis and adenosine-triphosphate. *J Physiol* 1947;*106*:177–85.
4. Bedford PJ, Tsokos M. The occurrence of cadaveric spasm is a myth. *Forensic Sci Med Pathol* 2013;*9*(2):244–8.
5. Bendall JR. Postmortem changes in muscle. In: Bourne DH (ed.). *The Structure and Function of Muscle, Vol. II. Structure*, part 2. London, Academic Press, 1973, pp 244–309.
6. Blasius W, Zimmermann H. Comparative studies on the functional, structural and histochemical changes of the anterior horn ganglion cells of rabbit spinal cord in gradually receding ischemia [in German]. *Pflugers Arch Physiol* 1957;*264*(6):618–50.
7. Blasius W. Allgemeine Physiologie des Nervensystems. In: Rosemann H (ed.). *Lehrbuch der Physiologie des Menschen*, vols. 2, 28. Munich, Germany, Urban und Schwarzenberg, 1962, pp 629–62.
8. Böhm E. Anmerkungen zu Reizbarkeit und Starreeintritt der Skelettmuskulatur. *Beitr Gerichtl Med* 1986;*44*:439–50.
9. Bohn HJ. *Status energiereicher Phosphate und glykolytischer Metabolite in der Extremitälenmuskulatur der Ratte bei Ischämie und in der postischämischen Erholung*, MD thesis. Cologne, Germany, University of Cologne, 1974.
10. Bretschneider HJ, Hübner G, Knoll D, Lohr B, Nordbeck H, Spieckermann PG. Myocardial resistance and tolerance to ischaemia: physiological and biochemical basis. *J Cardiovasc Surg* 1975;*16*:241–60.
11. Crostack C, Sehner S, Raupach T, Anders S. Re-establishment of rigor mortis: evidence for a considerably longer post-mortem time span. *Int J Legal Med* 2017;*131*(4):1039–42. https://doi.org/10.1007/s00414-017-1558-x
12. Dotzauer G, Naeve W. Die aktuelle Wasserstoffionenkonzentration im Leichenblut. *Zentralbl Pathol* 1955;*93*:360–70.
13. Dotzauer G, Naeve W. Wasserstoffionenkonzentration im Liquor post mortem. *Zentralbl Allg Pathol Anat* 1959;*100*:516–24.

14. Dotzauer G. Idiomuskulärer Wulst und postmortale Blutung bei plötzlichen Todesfällen. *Dtsch Z Gerichtl Med* 1958;*46*:761–71.
15. Gerard RW. The response of nerve to oxygen lack. *Am J Physiol* 1930;*92*:498–541.
16. Henssge C, Lunkenheimer PP, Salmon O, Madea B. Zur supravitalen elektrischen Erregbarkeit der Muskulatur. *Z Rechtsmed* 1984;*93*:165–74.
17. Henssge C, Madea B. *Methoden zur Bestimmung der Todeszeit an Leichen*. Lübeck, Schmidt-Römhild, 1988.
18. Hirsch H, Hohmann V, Kaegler M, Sickel B. Auditory evoked potentials during and after complete ischaemia of the brain. *Adv Neurosurg* 1986;*14*:364–7.
19. Hirsch H, Hohmann V, Kaegler M, Sickel B. Recovery of auditory evoked potentials after long-term complete brain ischaemia. *Neurosurg Rev* 1989;*12*(Suppl 1):313–16.
20. Hirsch H, Kaegler M, Hohmann V, Mues B. Latency of recovery and electrical silence of auditory potentials and the electrocorticogram after peracute complete brain ischaemia of 2–30 minutes duration. *Adv Neurosurg* 1989;*17*:254–8.
21. Hirsch H, Tesch P. Recovery of the electrocorticogram of canine brains after complete cerebral ischaemia at 37 and 32°C. *Neurosurg Rev* 1982;*5*:49–54.
22. Hirsch H. Recovery of the electrocorticogram after incomplete and complete ischaemia of the brain. *Acta Neurochir* 1982;*66*:147–58.
23. Isselhard W. Akuter Sauerstoffmangel und Wiederbelebung. *Dtsch Med Wochenschr* 1965;*90*:349–55.
24. Joachim H, Feldmann U. Eine quantitative Methode der Todeszeitbestimmung durch Untersuchung der galvanischen Reizschwelle. *Z Rechtsmed* 1980;*85*:5–22.
25. Joachim H. Mechanische und elektrische Erregbarkeit der Skelettmuskulatur. In: Henssge C, Madea B (eds.). *Methoden zur Bestimmung der Todeszeit an Leichen*. Lübeck, Schmidt-Römhild, 1988, pp 32–82.
26. Joachim H. *Probleme der frühen Todeszeitbestimmung und die sogenannten supravitalen Reaktionen des Muskels im Tierversuch*. Freiburg, Germany, Habil 26Schrift, 1976.
27. Klein A, Klein S. *Die Todeszeitbestimmung am menschlichen Auge*, MD thesis. Dresden, Germany, Medical Academy, Dresden University, 1978.
28. Klein A, Krause D, Hamann B. Praktische Erfahrungen mit einem neuen elektronischen Reizgerät zur Todeszeitbestimmung. *Kriminal Forens Wiss* 1975;*19*:126.
29. Koehler K, Sehner S, Riemer M, Gehl A, Raupach T, Anders S. Post-mortem chemical excitability of the iris should not be used for forensic death time diagnosis. *Int J Legal Med* 2018;*132*(6):1693–7. https://doi.org/10.1007/s00414-018-1846-0
30. Krause D, Klein A, Mattig W, Waltz H. Praktische Erfahrungen mit dem Reizgerät D 76 zur Todeszeitbestimmung. *Kriminal Forens Wiss* 1980;*40*:83–6.
31. Krause D, Klein A, Zett L. Todeszeitbestimmung mittels indirekter Muskelreizung über den N. ischiadicus und N. radialis. *Kriminal Forens Wiss* 1976;*26*:66–7.
32. Krause D, Schöning R, Kuchheuser W. Stimulator M 85—Ein kommerzielles Reizgerät zur Todeszeitbestimmung. In: Liebhardt E, Schuck M, Eisenmenger W (eds.). *Medizin und Recht. Festschrift fur Wolfgang Spann*. Berlin, Springer, 1986, pp 639–44.
33. Lochte T. Über die Absterbeerscheinungen der Skelettmuskulatur, insbesondere über die Totenstarre in gerichtlich-medizinischer Beziehung. *Z Gesamte Gerichtl Med* 1923;*2*:169–90.
34. Lunkenheimer PP, Lunkenheimer A, Stroh N, Köhler F, Welham K, Graham G, Kirk E, Sonnenblick E, Kröller J. Vergleich klassischer und neuer Zugänge zum intramyokardialen Kraftverteilungsmuster. *Zentralbl Vet Med A* 1982;*29*:557–601.
35. Lunkenheimer PP, Lunkenheimer A, Torrent-Guasp F. *Kardiodynamik: Wege zur strukturgerechten Analyse der Myokardfunktion. Beiträge zur Kardiologie*, vol. 33. Erlangen, Germany, Perimed-Fachbuch-Verlagsges, 1985.
36. Madea B, Henssge C. Electrical excitability of skeletal muscle postmortem in casework. *Forensic Sci Int* 1990;*47*:207–27.
37. Madea B, Henssge C. Zum postmortalen Verhalten der Rheobase. *Z Rechtsmed* 1990;*103*:435–52.
38. Madea B, Rödig A. Precision of estimating the time since death using different criteria of supravital muscular excitability. *Forensic Sci Med Pathol* 2006;*2*(2):127–33.
39. Madea B. Cadaveric spasm. *Forensic Sci Med Pathol* 2013;*9*:249–50.
40. Madea B. Estimating time of death from measurement of the electrical excitability of skeletal muscle. *J Forensic Sci Soc* 1992;*32*:117–29.
41. Madea B. Längsschnittuntersuchungen zur supravitalen elektrischen Erregbarkeit der Skelettmuskulatur. I. Objektivierung der supravitalen Muskelkontraktion. *Z Rechtsmed* 1992;*2*:107–21.
42. Madea B. Längsschnittuntersuchungen zur supravitalen elektrischen Erregbarkeit der Skelettmuskulatur. II. Quantifizierung der supravitalen Muskelkontraktion. *Z Rechtsmed* 1993;*3*:44–50.
43. Madea B. *Handbook of Forensic Medicine*, 2nd ed. Chichester, Blackwell Wiley 2022.
44. Madea B. Postmortem electrical excitability of skeletal muscle in casework. In: Henssge C, Knight B, Krompecher T, Madea B, Nokes L. (eds.). *The Estimation of the Time Since Death in the Early Postmortem Period*. London, Arnold, 2002, pp 164–206.
45. Madea B. *Supravitale elektrische Erregbarkeit der Skelettmuskulatur—Längsschnittuntersuchungen zur Objektivierung der muskulären Reaktion an 70 Leichen*. Cologne, Germany, Habil Schrift, 1989.
46. Madea B. Zum postmortalen Verhalten von Reizzeit—Reizstromstärkekurven. *Beitr Gerichtl Med* 1991;*49*:233–46.
47. Mattig W, Waltz H. Untersuchungen zur Todeszeitbestimmung mittels elektrischer Reizung. *Kriminal Forens Wiss* 1976;*26*:68–71.
48. Näcke P. Die Dauer der postmortalen mechanischen Muskulaturerregbarkeit bei chronisch Geisteskranken, speziell Paralytikern. *Z Gesamte Neurol Psychiatr* 1911;*7*:424–46.
49. Nagy J. The postmortem excitability of the skeletal muscles. *Acta Med Leg Soc (Liege)* 1968:177–8.
50. Nokes LD, Barasi S, Knight BH. Case report: co-ordinated motor movement of a lower limb after death. *Med Sci Law* 1989;*29*:265.
51. Opitz E, Schneider M. Über die Sauerstoffversorgung des Gehirns und den Mechanismus von Mangelwirkungen. *Ergebn Physiol* 1950;*46*:126–260.
52. Opitz E. Der Stoffwechsel des Gehirns und seine Veränderungen bei Kreislaufstillstand. *Verh Dtsch Ges Kreislaufforsch* 1953;*19*:26–44.
53. Opitz E. Physiologie der Erstickung und des Sauerstoffmangels. In: Ponsold A (ed.). *Lehrbuch der Gerichtlichen Medizin*. Stuttgart, Germany, Thieme, 1950, pp 174–218.
54. Partmann W. Zur Frage der postmortalen Reaktionsfähigkeit des kontraktilen Mechanismus der Muskulatur. *Naturwissenschaften* 1955;*42*:161–2.

55. Popwassilew J, Palm W. Über die Todeszeitbestimmung in den ersten 10 Stunden. *Z Arztl Fortbildg* 1960;*54*:734–7.
56. Prokop O. *Forensische Medizin*. Berlin, Verlag Volk und Gesundheit, 1975.
57. Prokop O. *Lehrbuch der gerichtlichen Medizin*. Berlin, Verlag Volk und Gesundheit, 1960.
58. Puppe G. Der Scheintod und seine Diagnose. *Med Wochenschr* 1920;*14/15*:383–5.
59. Radam G. Ein elektronisches Reizgerät zur Todeszeitbestimmung. *Gesundheitswes* 1963;*18*:1400–1.
60. Ramme H, Staak M. Vergleichende Untersuchungen zur Methodik der Todeszeitschätzung. *Beitr Gerichtl Med* 1983;*41*:365–9.
61. Rampitsch D. *Todeszeitbestimmung im frühpostmortalen Stadium*, Medical dissertation. Graz, Austria, University of Graz, 2010.
62. Raszeja S, Bardzik S. Studies on the "intralethal" excitability of muscles following stimuli obtained from an electronic stimulator. *Bull Pol Med Sci Hist* 1971;*14*:93.
63. Raule P, Forster B, Joachim H, Ropohl D. Tierexperimentelle Untersuchungen zur Erregbarkeit des absterbenden Herzmuskels. *Z Rechtsmed* 1974;*74*:99–110.
64. Ravache-Quiriny J. Les moments de la mort. Cahiers de Médiane légale, Droits medicales, no. 3. In: *Association Lyonnaise Médicine Legale*. Lyon, Editions Alesandre Lacasagne, 1986.
65. Ravache-Quiriny J. The time of death: some thoughts on the trustworthiness of our response. *Int Acad Leg Med Soc Med* 1982;*1*(Newsletter):9–11.
66. Romanelli MC, Gelardi M, Fiorella ML, Tattoli L, Di Vella G, Solarino B. Nasal ciliary motility: a new tool in estimating the time of death. *Int J Legal Med* 2012;*126*(3):427–33.
67. Rotter W. Über die postischämische Insuffizienz überlebender Zellen und Organe, ihre Erholungszeit und die Wiederbelebungszeit nach Kreislaufunterbrechung. *Thoraxchir* 1958/59;*6*:107–24.
68. Schleyer F. Determination of the time of death in the early postmortem interval. In: Lundquist F (ed.). *Methods of Forensic Science*, vol. 2. London, Interscience, 1963, pp 253–93.
69. Schneider M. Die Wiederbelebungszeit verschiedener Organe nach Ischämie. *Langenbecks Arch Klin Chir* 1964;*308*:252–64.
70. Schneider M. Über die Wiederbelebung nach Kreislaufunterbrechung. *Thoraxchir* 1958;*6*:95–106.
71. Schourup K. *Determination of the Time Since Death* (Danish, English summary), Copenhagen, Medical dissertation, Dansk Videnskabs Kobenhavn, 1950.
72. Semmler J. *Einfluss der Umgebungstemperatur auf die Todeszeitbestimmung durch elektrische Reizung der Oberlidmuskulatur menschlicher Leichen*, MD thesis. Magdeburg, Germany, Magdeburg University, 1979.
73. Silbernagel S, Despopoulos A. *Taschenatlas der Physiologie*, 3rd ed. Stuttgart, Germany, Thieme, 1988.
74. Spieckermann PG. *Überlebens—und Wiederbelebungszeit des Herzens. Anaesth and Resuscit 66*. Berlin, Springer, 1973.
75. Waltz H, Mattig W. Elektrische Messungen an Leichen für die Konstruktion eines elektronischen Reizgerätes zur Todeszeitbestimmung. *Kriminal Forens Wiss* 1974;*16*:159–78.
76. Warther S, Sehner S, Raupach T, et al. Estimation of the time since death: post-mortem contractions of human skeletal muscles following mechanical stimulation (idiomuscular contraction). *Int J Legal Med* 2012;*126*:399–405.
77. Wright EB. A comparative study of the effects of oxygen lack on peripheral nerve. *Am J Physiol* 1946;*147*:78–89.
78. Zink P, Reinhardt G. Die Todeszeitbestimmung bei der ärztlichen Leichenschau. *Bayer Ärztebl* 1972;*27*:109–15.
79. Zsako S. Die Bestimmung der Todeszeit durch die muskelmechanischen Erscheinungen. *Munch Med Wochenschr* 1916;*3*:82.
80. Zsako S. Die Bestimmung des Todeszeitpunktes. *Psychiatr Neurol Wochenschr* 1941;66–9.

Taylor & Francis
Taylor & Francis Group
http://taylorandfrancis.com

4 Rigor Mortis

Estimation of the Time Since Death by Evaluation of Cadaveric Rigidity

Thomas Krompecher

Contents

4.1 Explanation of the Mechanism of Rigor Mortis 51
  4.1.1 First Phase: Delay Period 53
  4.1.2 Second Phase: Onset Period (Reversible) 53
  4.1.3 Third Phase: Rigor (Irreversible) 53
  4.1.4 Fourth Phase: Resolution 53
4.2 Description of Cadaveric Rigidity in the Literature 54
  4.2.1 Description Based on Subjective Examinations 54
    4.2.1.1 Nysten's Law 54
  4.2.2 The Chronology of the Development of Rigor Mortis 54
  4.2.3 Reestablishment 55
  4.2.4 The Influence of Temperature 55
  4.2.5 The Influence of the Central Nervous System 56
  4.2.6 Instantaneous Rigor or Cadaveric Spasm 57
  4.2.7 Objective Measurements of Rigor Mortis 57
  4.2.8 Serial Objective Measurements to Follow the Development of Rigor Mortis 59
    4.2.8.1 Effect of Difference in the Muscle Mass 60
    4.2.8.2 Effect of Physical Exercise 60
    4.2.8.3 Effect of Different Temperatures 61
    4.2.8.4 Effect of Intoxication 61
    4.2.8.5 Effect of Electrocution 61
    4.2.8.6 Effect of Breaking 63
    4.2.8.7 Nysten's Law: Does It Apply to Rats? 65
    4.2.8.8 Effect of the Central Nervous System 65
    4.2.8.9 Estimation of the Time Since Death by Repeated Measurements of the Intensity of Rigor Mortis 65
4.3 Recommendations for Practice 67

Rigor mortis is certainly the most fascinating cadaveric sign. Because it gives the deceased person a petrified appearance, rigor mortis is noticed by everybody who encounters a corpse. It is therefore often used to estimate the time since death, even (and especially) by the non-initiated. It is generally accepted that a watch must be tested, perhaps even under various circumstances, before it is used to measure time. In addition, one is expected to read the user's manual. Alas, I fear we lack such a user's manual in the case of rigor mortis—and, if this is so, it is certainly not for want of related literature; in fact, publications about cadaveric rigidity abound. A brief summary of our present knowledge concerning this phenomenon is presented here.

4.1 Explanation of the Mechanism of Rigor Mortis

According to our current understanding, rigor mortis is the result of post-mortem muscle contraction. Therefore, to understand the development of rigidity, we must first study the mechanism of muscle contraction and hence the structure of the muscle.

In the 1940s, Szent-Györgyi [91,92], whose laboratory gave us numerous basic data concerning the composition and the function of the muscle, described the muscle fibre as 'the loveliest toy ever provided by nature for the

DOI: 10.1201/9781003244974-4

biochemist . . . like most children, the biochemist, when he finds a toy, usually pulls it to pieces.'

Szent-Györgyi's attempts to pull the muscle fibre to pieces resulted in the discovery of two proteins, which he named actin and myosin. These two proteins form interdigitating thick (myosin) and thin (actin) filaments, which build the sarcomere, the contractile unit of the muscle. The sarcomeres are organized from head to tail in series (4000 per cm) that form the fibrils. The muscle cell is a fibre composed of 1000–2000 fibrils (Figure 4.1).

The contraction of the muscle can be explained by the adenosine triphosphate (ATP) theory of Erdös [21] and the sliding filament model of contraction proposed by Hanson and Huxley [31]. According to this sliding filament model, contraction or tension in the muscle is achieved by the contrary motion of the interdigitating filaments. The myosin filament carries myosin heads on both ends. These heads attach to the actin filament and act as cross-bridges to form the actin-myosin complex. During contraction, the heads swivel and the thin filament is pulled past the thick filament. As the heads on each end of the myosin filament swivel in opposite directions, the Z-lines approach each other and the sarcomere shortens. The limit of contraction is reached when the thick myosin filaments butt against the Z-line (see Figure 4.1).

Both filaments slide without changing their length. Motion is achieved by cyclical formation and breaking of the cross-bridges. The fibrils may shorten by 30–50 per cent, thus requiring that the swivel cycle be repeated many times.

The driving force for the sliding motion comes from the myosin heads. The kinetic energy is derived from chemical processes. The myosin heads bind ATP and form myosin-ATP, which in turn has a very high affinity for actin, resulting in the actin-myosin complex. When the actin-myosin complex is formed, the low ATPase activity displayed by free myosin heads is increased, and ATP is hydrolyzed. The energy released through ATP hydrolysis is used for the dissociation of the actin-myosin complex.

The ATP used is almost immediately regenerated. This may be achieved through three different processes:

1. The hydrolysis of creatine phosphate, which furnishes rapidly available energy within short time limits. As a consequence, brief but violent exercise may be accomplished (e.g. a 100-metre sprint). The creatine phosphate used in this process is restored by means of the energy generated by anaerobic glycolysis.
2. For continued exercise, the glycogen content of the muscle must be used. Glycogen can be transformed entirely to lactic acid by anaerobic hydrolysis. This process is limited by the accumulation of lactic acid.
3. Oxidative phosphorylation is the combustion of glucose in the presence of oxygen. It results in the production of carbon dioxide and water and, although it liberates great amounts of ATP, it is a relatively slow process.

If ATP is not regenerated, as is the case when ATP is consumed after death, the actin-myosin complex is not split; rather, it persists and the muscle remains inextensible. This stable actin-myosin complex is the basis for the development of rigor mortis in the post-mortem state.

In summary, rigor mortis is a normal muscle contraction occurring after death and fixed by lack of ATP.

The *in vitro* experiments of Erdös [21] and Krause and Zett [44,45] demonstrated that rigidity disappears after the addition of ATP or oxygen. Consequently, the onset of

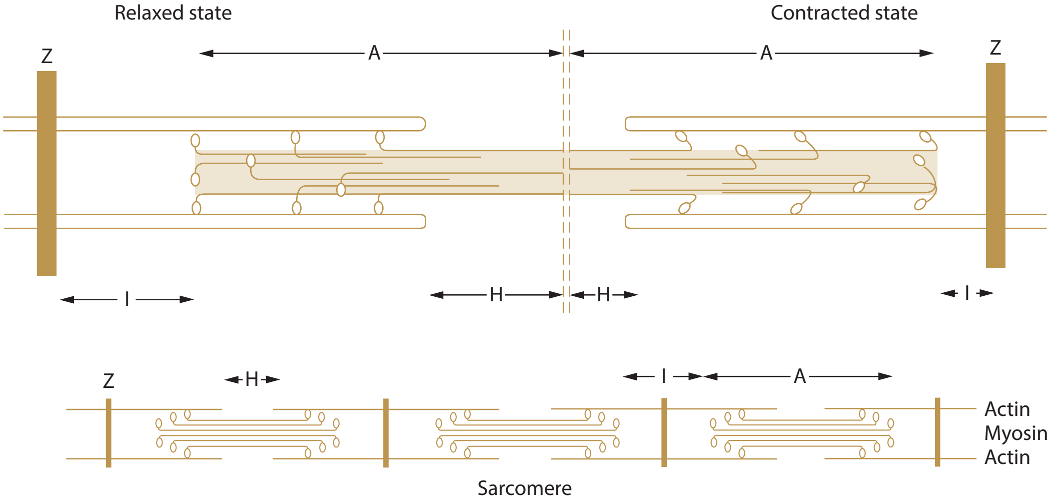

Figure 4.1 Schematic representation of the contraction and relaxation of an isolated sarcomere. The cross-bridges (myosin heads) pull the actin filaments and the attached Z-lines towards each other. The swivel cycle is repeated until the myosin filaments butt against the Z-line. The H zone and I band shorten, and the A band remains constant.

rigor mortis can be considered a supravital phenomenon; in fact, it is the last evident vital event in the muscle.

Given this explanation, it is easy to understand the mechanism of development of cadaveric rigidity, which unfolds in four different phases.

4.1.1 First Phase: Delay Period

After clinical death, the muscle survives in a normal state for a short time and stays relaxed as long as the ATP content remains sufficiently high to permit the splitting of the actin-myosin cross-bridges. This fact was first proven by Erdös [21], who compared the hardness of the muscle with its ATP concentration. The two curves showed mirror images: the decrease in ATP levels was matched by an increase in hardness (confirmed by Bate-Smith and Bendall [3]). The rate of ATP depletion depends on its content at the time of death, on the possibility of post-mortem ATP production and on the rate of ATP hydrolysis.

According to a recently published paper by Saber et al. [79], a treatment by boldenone (an anabolic androgenic synthetic steroid used by bodybuilders) results in a significant increase in the level of ATP, ADP, glycogen, and hydroxyproline in skeletal muscle of rats and thus can delay the onset of rigor mortis.

4.1.2 Second Phase: Onset Period (Reversible)

The ATP content of the muscle falls below a critical threshold. The cross-bridges remain intact and rigidity appears. However, this state is still reversible: the addition of ATP (reported by Erdös [21] and confirmed by Bendall [7]) or oxygen [44] results in relaxation, indicating that the muscle is still able to function.

According to Bendall [7], the rigor-tension development of post-mortem muscles is very feeble compared with a living muscle; the maximal tension is about 150 g/cm^2 compared with about 4000 g/cm^2 in tetanus.

4.1.3 Third Phase: Rigor (Irreversible)

Rigidity is fully developed and becomes irreversible. Post-mortem modifications of muscle fibres destroy their ability to relax.

4.1.4 Fourth Phase: Resolution

Rigidity disappears and the muscle becomes limp. The cause of resolution is not definitely established. Nevertheless, I believe that, according to our present knowledge, one can accept the suggestions of Erdös [21] and Szent-Györgyi [91] that resolution is a denaturation process. Morphological evaluations confirm this hypothesis [15,20,46,73].

Bendall [7] proposed that the process is strongly pH dependent and added, ‘Thus there may be no further need to search about, apparently hopelessly, for a protease (cathepsin) which could break the rather specific linkages probably involved.’

The foregoing phases are valid only for isolated fibres. In everyday practice, one is confronted with muscles that are made up of a multitude of fibres. The timing of the onset of rigor mortis cannot be determined precisely because rigor mortis is a progressive event, evolving from less apparent to more pronounced. The progression can be explained by the coexistence of fibres at different stages of developing rigidity.

Although the timing of the onset of rigor mortis in a fibre may depend on its ATP content, there are other reasons for heterogeneity.

The human skeletal muscles contain two types of fibres:

- Type I (red): rich in mitochondria, with a predominantly oxidative metabolism and slow myosin
- Type II (white): relatively poor in mitochondria, with a predominantly glycolytic metabolism [11,22,64] and fast myosin [10]

The onset of rigor mortis in these two types of fibres is expected to occur at different times.

During a given period of time after the onset of rigor mortis, rigidity that is broken (by forcing the movement of a joint) is restored. This re-establishment of rigor mortis can be explained as follows: those fibres that are still slack, and perhaps those that are not fully contracted retain their capacity for reversible binding of the myosin heads to the actin filaments. The contraction of such fibres causes the re-establishment of rigor mortis.

The progressive nature of the resolution of rigor mortis may be caused by a similar phenomenon. The different fibres relax at different times as the number of fibres destroyed by post-mortem reactions increases.

The development of rigor mortis in canine cardiac muscle has been also investigated [62,85,96]. Seelye et al. [85] found that

> at 37°C the physical onset of rigor mortis commenced after 40 min . . . and complete rigor was attained at 100 min. The onset of rigor mortis commenced when the adenine content of the muscle had fallen by 62 per cent and was complete when a 75 per cent loss had occurred.

Evidence for rigor in smooth muscle was described by Wuytack and Casteels [99] in guinea pig taenia coli and in rabbit aorta, mesenteric artery and vena portae. These investigators concluded that ‘this contracture occurring during metabolic depletion corresponds to a rigor mortis of smooth muscle'.

4.2 Description of Cadaveric Rigidity in the Literature

4.2.1 Description Based on Subjective Examinations

4.2.1.1 Nysten's Law

In 1811, the French physician and chemist P. H. Nysten [70] published the first scientific description of rigor mortis. The law named after him states: 'The rigidity in humans begins in the trunk and the neck, followed by the upper extremities and after that by the lower limbs. It follows the same order during the resolution.' The development of rigor mortis is thus descending, a finding thought to be related to the varying distances between the different muscles and the central nervous system (CNS). However, Nysten himself noticed that the destruction of the CNS did not affect the order of the development of rigidity.

Although Naumann [68] confirmed the descending development of rigor mortis, he added that in some special cases (e.g. in weak individuals or those diminished by illness), rigidity may show an ascending pattern.

Based on 271 protocols carried out by the same forensic pathologist, Mittmeyer [65] concluded that 'with increasing time interval from death, the joints were seen absolutely rigid and completely released in the following order: nape, elbow, jaw, knee and leaping joints'.

Shapiro [86,87] wrote:

> It is difficult to understand why a physico-chemical process which takes place in recently dead tissues should follow the sequence usually described. It appears more likely that, because we are dealing with a physico-chemical process in what is virtually a lump of clay, this will take place *simultaneously* in all the recently dead muscles. If that be the case, it would be reasonable to expect that small masses of muscle would be involved completely much more rapidly than large masses of muscle.
>
> The account of the invariable progression of death stiffening from the top to the bottom of the body as generally given in the textbooks must, therefore, be modified. The explanation may have to be sought along the lines indicated, viz., that rigor mortis does not progress from the upper end to the lower end of the body in a well-defined fashion, but occurs simultaneously in the recently dead muscles; and that the fixation of a joint depends, among other things, on the involvement by rigor mortis of the quantity of muscle which controls that joint. Variations in the sizes of different joints and in the muscle masses which control them determine the surface, from where further heat loss occurs to the atmosphere by radiation and convection.

I found a possible confirmation of this hypothesis in the paper of Tarrant and Mothersill [94]. These investigators found that in beef carcasses the pH values decreased with distance from the surface and as muscle temperature increased. The time required for the pH to fall to 6.0 in six major hindquarter muscles ranged from 2.2 to 13.6 hours, and it varied with the muscle and depth in the carcass. Moreover, these investigators observed a good correlation between the rate of ATP turnover and muscle temperature. Much of our knowledge of the chemical changes underlying the rigor process was discovered in laboratories working for the meat industry because the tenderness (i.e. the quality of the meat) depends on this process. New data are continually emerging, and they help create a better understanding of this phenomenon [29,90]. For example, one article is titled 'Meat toughening does not occur when rigor shortening is prevented' [43]. Reading some of these articles [36,39,40], we can appreciate the complexity of the physicochemical and structural changes that occur during the conversion of muscle to meat.

Textbooks of forensic medicine often suggest exceptions to Nysten's law, implying that

- Nysten's law is often valid.
- Considering the exceptions, we must not rely on it.

4.2.2 The Chronology of the Development of Rigor Mortis

In this respect, it is interesting to recall the observations of Niderkorn [69], who in 1872 determined the times necessary for the completion of rigor mortis in 113 bodies. In 76 corpses (67 per cent), rigor mortis was fully established after 4–7 hours (in 31 cases, after 4 hours; in 14 cases, after 5 hours; in 20 cases, after 6 hours; and in 11 cases, after 7 hours). In two cases, rigidity was complete 2 hours post-mortem, and in two others, only 13 hours after death.

Mallach's chronology of the development of rigor mortis [61,62], which was based on a survey of the literature from 1811 to 1960, is shown in Table 4.1 [81].

This summary has been criticized, however [33]. Indeed, it is hazardous to compare and evaluate 'feelings' statistically: the observations are highly subjective and were gathered by examiners over 150 years (1811–1960). Moreover, these observations were not codified: various authors often used different classifications in their determination of the state of development of cadaveric rigidity. Nonetheless, we lack a better survey.

Table 4.1 Time Course of Cadaveric Rigidity

Rigor phase	Mean with standard deviation(s)*	Hours post-mortem				Number of publications evaluated
		Limits of 95.5% probability (2 s)		Variations		
		Lower limit	Upper limit	Lower limit	Upper limit	
Delay period	3 ± 2	—	7	<1/2	7	26
Re-establishment possible	Up to 5	—	—	2	8	—
Complete rigidity	8 ± 1	6	10	2	20	28
Persistence	57 ± 14	29	85	24	96	27
Resolution	76 ± 32	12	140	24	192	27

* Mean and standard deviation calculated from the literature data of 150 years (1811–1960) by Mallach 1964.

Source: Modified from Schleyer F. Leichenveränderungen. Todeszeitbestimmung im früh postmortalen Intervall. In: Muller B (ed.). *Gerichtliche Medizin,* vol. 1. Berlin, Springer, 1975.

In spite of the subjective nature of the information, I believe that every individual estimate is highly valuable. In fact, our predecessors, with observation as the sole method at their disposal, used this simple means expertly, and their conclusions are of great worth. In our own work on cadaveric rigidity, we often base our experiments on statements provided by ancient authors. If our measurements happen to contradict these statements, we regard the results with scepticism. Once an experiment is repeated, and if our results are confirmed, we always seek a valid explanation for the discrepancy.

If these observations are valid (and in my mind, they are indeed in most cases), what are the reasons for the great differences in the development of rigor mortis between one corpse and another? The answer stems from the realization that the process is biological or, more precisely, biochemical, and that it can be affected by a number of intrinsic and extrinsic factors.

First, we must consider the physical condition of the individual before death (i.e. the factors that influence the energetic reserves).

H. A. Husband [37], in his 1877 *Student's Hand-Book of Forensic Medicine*, summarized such factors as follows:

- Effects of enfeebling disease before death: rapid in its invasion, passing off rapidly.
- Effects of a robust frame at period of death: the accession may be prolonged, but, other things being equal, it is more strongly manifested and continues longer.
- Effects of violent exercise before death: supervenes and disappears rapidly.
- Effects of poison. Poisons that cause violent contractions for some time before death (e.g. strychnine) influence the rapid invasion of the rigor mortis, its short duration and the subsequent putrefaction.
- Where death in poisoning by strychnine is almost instantaneous, with a short convulsive stage, the rigor mortis comes on rapidly and remains for a long time.

Today, more than 100 years later, textbooks include very similar statements.

In 1984, Vock et al. [98] published a case of tetany involving instantaneous rigor. Electrocution may also hasten the onset of cadaveric rigidity. In the three electrocution cases reported by Schneider in 1985 [82], stiffness was complete after 1 hour 40 minutes, 1 hour 45 minutes and 2 hours 5 minutes after death. In one of our cases [48], rigidity was fully established 1 hour post-mortem in the upper limbs located in the path of the electrical current, but no rigidity was observed elsewhere. Another individual who was found in the bathtub with a hairdryer was in a state of complete rigidity only 3 hours after being seen alive for the last time.

Several cases of accelerated rigidity after certain intoxications have been reported, with organophosphate com pounds [63] and strychnine [54].

4.2.3 Reestablishment

According to Mallach's [61] chronology of the development of rigor mortis, the re-establishment of the rigidity is possible between 2 and 8 hours post-mortem, with a mean time up to 5 hours. In current textbooks and publications [34,35,42,80], we found the same upper limit (i.e. 8 hours, sometimes 8–12 hours [76,93]).

In a more recent publication, Anders et al. [1] examined 314 joints (elbow and knee) of 79 deceased persons. These investigators found that re-establishment—tested manually—occurred in 38.5 per cent of joints at 7.5–19 hours post-mortem.

4.2.4 The Influence of Temperature

Considering that the onset of rigor mortis depends on biochemical processes, and that its resolution results from the degradation of cellular structures, it is easy to understand that its overall development is affected by the temperature of the body and consequently by that of the surroundings. Naturally, this fact was noticed long ago. In 1811, Nysten [70] stated that rigidity persists longer in cold, dry air than in warm, wet air.

In 1856, Kussmaul [58] wrote: ‘The corpses of strong persons can stay stiff till 8–10 and more days in air of 2.5 to 7.5°C, while at 18.8 to 30°C the last traces of rigidity disappear in 4 to 6 days.’

In his 1877 textbook, Husband [37] summed up the effect of low temperature as follows: ‘[Rigor mortis is] prolonged by dry cold air and cold water.’

In 1888, Bierfreund [9] examined the influence of temperature on the development of cadaveric rigidity on the lower limbs of rabbits. His observations are shown in Table 4.2.

Morgenstern’s [66] experiments in 1927 on rabbits and cats of various ages showed that temperature has spectacular effects on the development of rigor mortis. These experiments also revealed differences related to the species studied and the various ages of the animals. Morgenstern also recorded an important acceleration in the onset of rigidity when human corpses were immersed in warm water (35–37°C).

In 1974, Forster et al. [26] observed the duration of cadaveric rigidity in the lower limbs of human corpses kept at low temperatures (4–11°C). Based on the observations made during the entire period when the corpses were available, the following conclusions were made:

> If we address the question raised in the beginning specifically the persistence of complete rigidity 130 hours after death, we must come to the conclusion that at low temperatures, rigidity can be demonstrated well after this period, even if we take into account slight fluctuations in temperature and a possible error (of a few hours) in the estimate of time of death.

In one of Forster’s cases, a corpse kept at +4°C exhibited strong rigidity, even after 234 hours.

Duncan et al. [18] published a case of malignant hyperthermia (42°C) in a dog secondary to ingestion of hops where ‘the onset of rigor mortis was evident in <15 minutes’. Varetto and Curto [97] tested the mobility of the knee on corpses kept at a constant temperature of +4°C. These investigators found a persistence of complete rigor lasting for 10 days in all the cadavers, and in one case, rigor lasted for 16 days.

In our practice, the opposite situation was illustrated by the case of two corpses found on an exceptionally hot summer day (40°C) in a closed car exposed to the sun. At the examination, carried out less than 8 hours after death, the corpses appeared strongly affected, with parts that were blackened and, naturally, without the faintest sign of rigidity. At the other temperature extreme, an interesting observation was made by Bendall [7]: ‘If a muscle is frozen in the pre-rigor state while ATP and PC [phosphocreatine] levels are high, after thawing out rigor sets in.’ However, because this experiment was carried out on very thin strips of muscle, which were rapidly frozen at −20°C, it is difficult to imagine the occurrence of this phenomenon in the forensic practice.

4.2.5 The Influence of the Central Nervous System

As noted earlier, the descending pattern in the development of rigor mortis was thought to be caused by the

Table 4.2 Effect of Temperature on the Development of Rigor Mortis on the Lower Limbs of Rabbits

		Beginning of the onset of rigidity post-mortem		Complete development of rigidity		Beginning of resolution post-mortem		Complete resolution post-mortem	
Number	**Temperature of air (°C)**	**Hours**	**Min**	**Hours**	**Min**	**Hours**	**Min**	**Hours**	**Min**
1	4.0	1	30	7	—	38	—	48	—
2	20.0	1	—	5	15	26	—	36	—
3	22.5	1	—	4	20	—	—	36	—
4	29.0	—	50	3	20	24	—	28	—
5	37.5	—	35	2	—	2	25	4	10
6	41.0	—	45	1	5	1	22	2	30
7	52.5	—	15	—	45	1	—	1	40
8	54.0	—	—	—	50	1	—	1	50
9	55.0	—	2–5	—	37	—	40	1	40
10	60.0	Almost instantly		—	10	—	35	1	10

Source: Data from Bierfreund M. Untersuchungen über die Totenstarre. *Pflügers Arch* 1888;**43:**195–216.

varying distances from the CNS. In 1904, Fuchs [28] described the brain as the initial site of death, followed by the proximal part of the spinal cord, and suggested that the process then progressed towards the caudal spinal cord: the presumed impulsions arose from catabolic changes in the nerve cells. In 1819, Busch [12] observed that the removal of the brain and spinal cord resulted in an early onset of rigidity; moreover, rigidity was more pronounced and lasted longer.

In experiments conducted on animals, Eiselberg [19] in 1881 demonstrated that when the sciatic nerve was sectioned on one side, in more than 70 per cent of the cases rigidity developed later than on the other side.

Gendre [30] and Aust [2] confirmed this finding. Aust, in particular, obtained this result in 12 of a total of 13 experiments. Having conducted *in vivo* sectioning of the left side of the spinal cord in rabbits (underneath the pyramidal crossing), Bierfreund [9] in 1888 made the following statement: ‘I was very surprised to find that after a few hours following death, the right half of the body became very rigid, while the left half remained almost normally mobilisable.’ Bierfreund thought that the ‘accelerating’ effect of the CNS on the appearance of cadaveric rigidity was the result of weak excitation of the muscular system, and if this excitation really did exist, it was too weak to cause a visible contraction. To prove this hypothesis, Bierfreund conducted animal experiments that involved weak irritation by the sciatic nerve. The results were the very opposite of what he had hoped for.

In the 1940s, Berg [8] determined that, following death, cholinesterase retains its full or partial activity in the muscle until an advanced stage of muscular degradation. Moreover, during the delay period, the muscular system was found to release small amounts of acetylcholine. The onset of cadaveric rigidity was found to be hastened by the inhibition of acetylcholinesterase, by the addition of acetylcholine or by thermal irritation of the contralateral motor region. The inhibition of transmitters retarded the onset of rigidity.

In 1976, Krause et al. [46] made the following interesting observation: ‘The irritation of sciatic and radial nerves in amputated arms and legs caused violent muscular reactions for up to two hours, but action potentials in the nerves were detectable even after this period of time.’

The experimental results described in this section are partially contradictory. Therefore, it remains unclear what role the nervous system may play in the development of cadaveric rigidity.

4.2.6 Instantaneous Rigor or Cadaveric Spasm

Instantaneous rigor is defined as complete rigor mortis occurring at the moment of death and involving a hand, limb or even the entire body. In 1923, Baumann [4] surveyed the literature on this subject and concluded that most of the reported cases of instantaneous rigor mortis involving lesions in the head, brain, brainstem and thorax were caused by death from internal lesions and also probably by gas embolism. Laves [59] and Prokop [77,78] proposed that the cause could be decerebrate rigidity as also suggested by Sherrington in 1908 [88].

Polson and Gee [75] cited many such instances in the literature, but during their 20-year practice in Leeds, they reported only two cases. In our own practice, I have never encountered an example of truly instantaneous rigor mortis, nor have I been able to gather acceptable examples in my colleagues’ cases.

Some of the cases published in the literature, especially the more spectacular ones, were based on observations made during war time [75,77]. Interestingly, Mueller [67], a German forensic pathologist, searched but failed to observe a case of instantaneous rigor during the Second World War, in spite of his surveys of military medics.

In their paper, titled ‘The occurrence of cadaveric spasm is a myth’, Bedford and Tsokos [5] state that there is no recognized pathophysiological basis for the process of ‘cadaveric spasm’.

My colleagues and I have encountered numerous cases of electrocution in which the body apparently remained in the position of the spasm caused by the electric shock [82]. In these cases, the facies was also found to be contracted. However, the term ‘instantaneous rigidity’ does not apply here. Indeed, in all our observed cases [48], the body remained in direct or indirect contact with the electrical current up to the moment of discovery of the cadaver. Because of the accelerated onset of rigor mortis (see earlier), it is reasonable to assume that rigor mortis fixed the body in a given position while the spasm was still occurring.

Pirch et al. [74] presented the case of a young woman found dead in an upright standing position. These investigators concluded that ‘whereas the position of the body is most unusual, a detailed analysis reveals that it is a stable position even without rigor mortis. Therefore, this case does not further support the controversial concept of IR’.

In our practice, my colleagues and I encountered an identical case.

Ultimately, we believe that even if instantaneous rigor mortis does exist, it is a very rare event. Consequently, before accepting such an explanation, it is important to study all the other possibilities (e.g. changes in the position of the body and/or of the surrounding objects, electrocution).

4.2.7 Objective Measurements of Rigor Mortis

Rigor mortis, the stiffening of the muscles after death, immobilizes the joints. The resistance in the joints can be used to make a qualitative or even a quantitative estimate of the degree of rigor.

In the situations described so far, the conclusions were drawn based on estimates of the force necessary to bend a knee or an elbow immobilized by cadaveric rigidity. Such manual estimates are necessarily subjective and cannot be compared among different observers. Moreover, this method is not applicable when the degree of rigidity rises above a certain level. For example, one feels the same when asked to lift 200 or 500 kg—the weight makes no difference because one cannot move either. The same situation can be found in the case of rigidity. When rigidity in a knee or jaw joint cannot be broken, it is not clear whether rigidity increases or decreases until its intensity falls down to the levels commensurate with human strength.

It is, of course, desirable to determine the exact degree of rigidity, to obtain reproducible numerical values that can be compared and to extend the measurements in situations where human strength is insufficient.

As far as we know, the first objective measurements of rigidity were reported in 1919 by Oppenheim and Wacker [71], who gave a detailed description of their method to measure the force necessary to bend a leg with a knee joint immobilized by rigidity; this is referred to as ‘breaking’ the rigidity of a joint. Oppenheim and Wacker expressed their results relative to the mass of the relevant muscles. They discussed the influence of the cause of death on the development of rigor mortis, so their results could not be used to estimate the time of death.

Subsequently, two German research teams further developed methods to measure the force necessary to break the cadaveric rigidity of a knee joint. One team was headed by Forster in Freiburg, and the other by Beier in Munich. However, before reviewing their findings, a few general comments about the development of cadaveric rigidity may be useful.

In forensic practice, one examines the degree to which muscular rigidity fixes or immobilizes a joint. Hence, the measure of cadaveric rigidity is a measure of the force necessary to move a joint. The development of rigidity is the process of change in the intensity of rigidity over time. This intensity is weak at first, but it then increases, reaches a maximum, decreases and finally practically disappears after a variable period of time. This process can be represented by a curve, although such a curve is valid only for one given corpse under clearly defined conditions.

Although only two points are necessary (and sufficient) to define a straight line, multiple points are needed to define a curve, which cannot be determined by a single point. This is the basis of the difficulty in attempting to characterize the development of cadaveric rigidity by using a single measurement (it is not even possible to make two measurements because the development of cadaveric rigidity is different in the two lower limbs of the same corpse; this is discussed later). Forster et al. [27] proposed standardizing the measurements using the following formula:

$$\text{FRR (Freiburger Rigor Index)} = p \cdot I_1/U2 \cdot I_2 \times 100$$

where p is the traction force (kp), I_1 is the length of the leg (cm), I_2 is the distance from the rotation axis of the knee joint to the anterior surface of the knee cap (cm) and U is the circumference of the thigh (cm) (Table 4.3).

This formula may be used to correct (at least partially) for the differences among individual cases. However, it does not take into account individual factors, such as the difference in muscle mass between two thighs with the same circumference.

The actual worth of this formula remains unknown. Although Forster et al. published the formula on several occasions [23,25,27], they did not communicate any numerical data to justify the entries made in their table. They also published a schematic curve of the development of rigor mortis [23,25,27], which was apparently based on the results calculated using their formula, but without explaining how they obtained it. Lacking conclusive reports, these conclusions should be treated with great caution.

Beier et al. [6] relied on a similar approach to measure the intensity of cadaveric rigidity. The experiments consisted of determining the torque necessary to break the rigor mortis of arms and legs. The measurements were made on 17 female and 35 male cadavers stored at a temperature of 4°C. The authors concluded that

> The values show differences between male and female cadavers to an extent that both groups have to be treated separately. Relating the torque to the diameter of the cross-section of the limb does not eliminate the difference. Frequently, considerable differences between left and right limbs were obtained, however, without preference for one side over the other. There is no direct functional relationship between postmortem time and the intensity of rigor mortis, but the values occasionally allow estimates on the maximum time postmortem.

Table 4.3 Proposed Standardized Measurements of Cadaveric Rigidity

Rigor index	Degree of rigidity	Subjective observation
>5.5	1	Complete rigidity
<5.5–4.0	2	Very difficult to break
<4.0–2.5	3	Relatively easy to break
<2.5–1.3	4	Soft
<1.3–0.2	5	Weak
<0.2	6	Complete resolution

In a second series of reports [83,84], the following observations were made:

> The torque to overcome rigor mortis was determined for each leg by bending the lower leg of the prone cadaver toward the fixed thigh. The device ensures that the force is kept perpendicular to the tibia. The force is read from a spring balance with an accuracy of 5 Nm. For the lever arm, the distance from the knee joint, or the epicondylus lateralis, to the site of attachment of the spring balance was taken. Torque values ranging from 10 to 500 Nm were measured to an accuracy of 3 Nm and, above 100 Nm, to 3 per cent. Before measurement the cadavers were kept in storage rooms at 4–6°C.
>
> The rigor mortis of the legs of 101 male human cadavers were investigated. These were selected from the cadavers brought to the Institute by the following criteria: age at least 14 years, no pathological findings at the investigated extremities, time of death known exactly to within one hour.
>
> There seems to exist an upper limit for the torque of rigor mortis, depending on the lay-time, above which no value was found. Below this limit, however, every value could be found. By calculating the 90% tolerance limits of lay-times grouped at 12-hourly intervals, this upper limit was found to decrease exponentially with lay-time. This plot may be used for the estimation of maximum lay-times from rigor mortis measurements.

4.2.8 Serial Objective Measurements to Follow the Development of Rigor Mortis

Beier's investigations and results have probably reached the limits of the possibilities offered by this method. Considering that only a single measurement can be made per joint (or limb), and that the obtained value represents a random time point in the development of rigor mortis, one can appreciate the large degree of freedom in constructing a curve depicting the development of rigidity.

Given these limitations, I developed a different method for the objective measurement of the intensity of cadaveric rigidity in rats [49–52]. The apparatus used is shown in Figure 4.2. The principle of the method is to determine the force necessary to cause a movement of small amplitude (4 mm) in the limb under examination.

Because this movement does not break rigor mortis, serial measurements can be taken. Our apparatus measured the resistance caused by rigor both in the knee and in the hip joints.

Initially, the force was measured by hooking successively heavier weights to obtain the standardized movement of the limb [49–52]. Subsequently, a slight modification was introduced: the hook was attached to the plate of a digital balance, which was placed on a jack (see Figure 4.2, label d). When the balance was lowered to produce the standardized small amplitude movement of

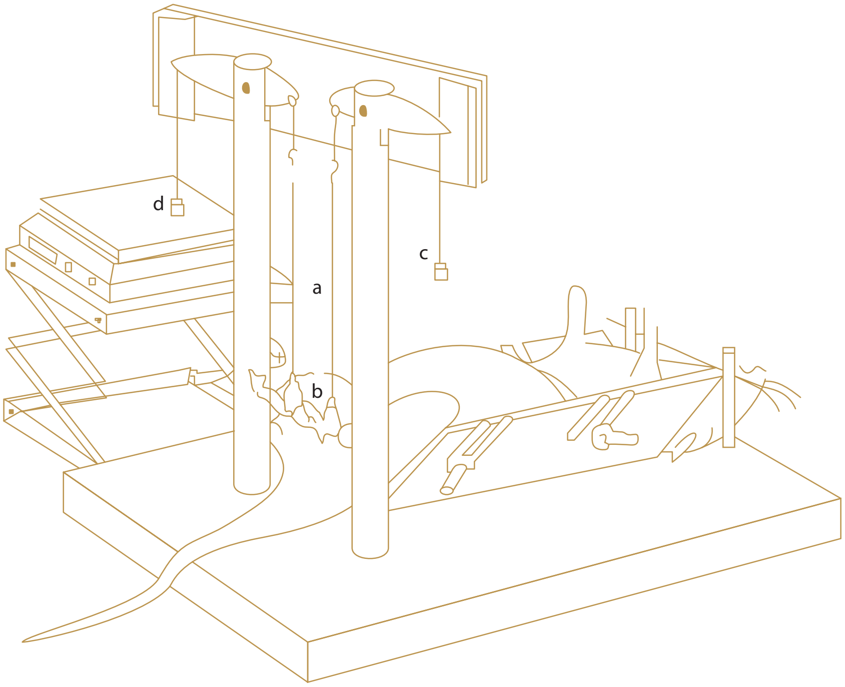

Figure 4.2 Apparatus for the measurement of rigor mortis intensity: cord attached to hind limb (a), steel hooks permitting attachment of cord to limbs (b), hook supporting weights (previous technique) (c), hook attached to a digital balance (d).

the limb, the resistance caused by rigidity could be read directly from the balance (a negative value, as traction was exerted).

All the experiments were conducted on male albino rats. Each study involved animals of the same age and weight.

We reproduce here the curve of the development of the rigor mortis as first obtained on a rat at a temperature of 24.5°C (Figure 4.3).

4.2.8.1 Effect of Difference in the Muscle Mass

In the following experiment [50], we demonstrated that there is essentially no difference in the time course of the development of rigor mortis in the hind and front limbs, even though the muscular mass of the hind limbs is 2.89 times greater than that of the front limbs. At the same time, in the initial phase, rigor mortis was more pronounced in the front limbs. Moreover, resolution was initially faster in the front limbs, although both hind and front limbs reached complete resolution at the same time.

The development of rigor mortis was also studied in rats of varying ages and weights [52]. Although the time course of the development was always the same, the intensity of rigor was found to be directly proportional to the increase in the animal's body weight.

4.2.8.2 Effect of Physical Exercise

Because the method appeared to be suitable for studying the development of rigor mortis in rats, we decided to determine the effects of physical exercise before death [51]. The animals were subjected to a treadmill exercise lasting 1 hour, with the distance covered being approximately 1020 metres. For rats raised in small cages, a 1000-metre run must represent a considerable effort, but the experimental animals tolerated it quite well. The results of this experiment are presented in Figure 4.4.

The development of rigor mortis in rats that had exercised before death differed from that of the control. The following features were noted for the exercised animals:

- There was a higher intensity in the initial phase.
- Maximum development was reached at the same time as in the controls.
- Higher maximum values were reached (in our experiments, 1.39 times the maximum values in the controls).
- The higher values were maintained from 100 minutes to 16 hours, with statistically significant differences.
- Resolution occurred at the same time.

Table 4.4 summarizes the development of rigor mortis in the exercised and in the control groups, relative to the maximum value of the control group (33.8 g) normalized to 100 per cent. The results illustrate the types of errors that can occur when a single, manual estimate of rigor made on a cadaver with an unknown history is used to establish the time of death. For example, the values obtained at 100 minutes and 16 hours in the exercised group are both very close to 100 per cent, which could be interpreted, erroneously, as fully developed rigidity (compared with the control group).

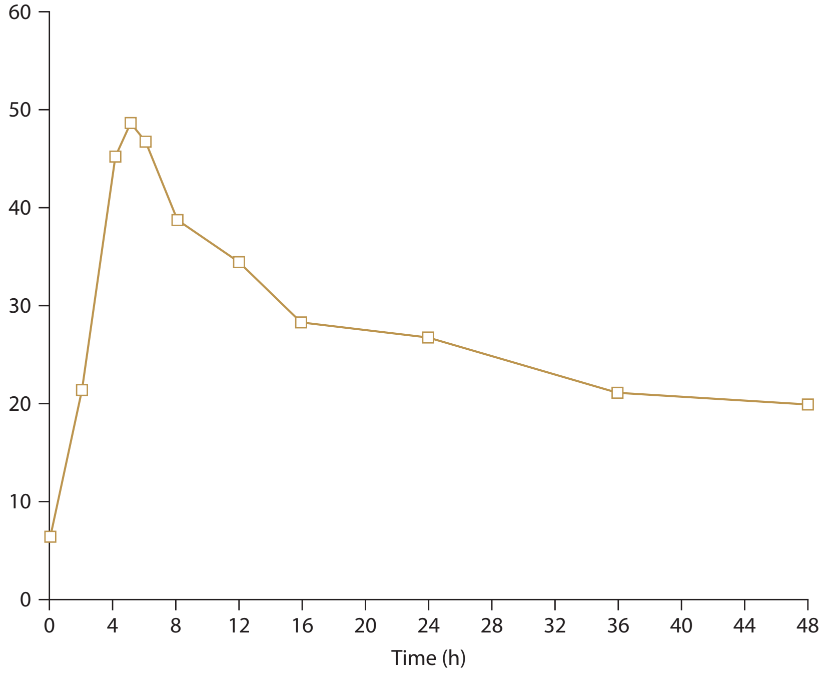

Figure 4.3 Evolution of the intensity of rigor mortis in the hind limb of a rat weighing 350 g.

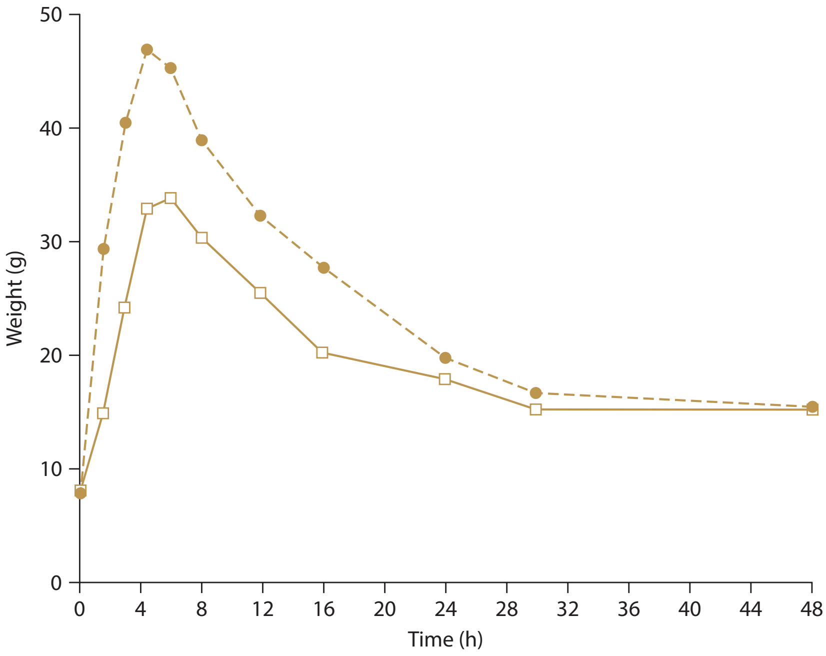

Figure 4.4 The evolution of rigor mortis in the hind limbs of rats in control (solid lines) and exercised (dashed lines) groups. Values given are always an average for ten animals (20 hind limbs).

Table 4.4 Evolution of Rigor Mortis in the Two Groups Relative to the Maximum Value of the Control Group (33.8 g) Taken as 100 Per Cent

	Time post-mortem (h)						
	1.66	**3**	**4.5**	**6**	**8**	**12**	**16**
Treadmill exercise (%)	86.5	119.5	139.2	134.6	115.8	95.6	82.3
Control (%)	44.4	72.3	97.8	100.0	89.8	76.0	60.3

4.2.8.3 Effect of Different Temperatures

The development of rigor mortis at different temperatures is shown in Figure 4.5. Figure 4.6 illustrates the development of rigor at 6°C. By transferring the cadavers to 24°C for 24 hours between 216 and 240 hours post-mortem, we wished to accelerate decomposition, thus causing the possible remnants of rigor mortis to disappear. The consecutive transfer to 6°C for 24 hours was made to determine whether the decrease in temperature alone could cause rigidity. Indeed, a marked increase in resistance could be seen between the measurements taken at 240 hours post-mortem at 24°C and those taken 24 hours later at 6°C. The only difference between the specimens at these two time points was the decrease in rectal temperature from 24°C to 6°C (note that the muscles were not frozen). The increase in resistance (from 17.3 to 27.6 g) led us to conclude that a decrease in temperature alone enhances the stiffness of the muscles and perhaps the resistance in the joints as well, thus leading to what can be called ‘cold rigidity’. The increase in our case was 59.53 per cent, which was highly significant [53].

4.2.8.4 Effect of Intoxication

Figure 4.7 illustrates the effects of fatal intoxication by strychnine, carbon monoxide and curare on the development of intensity of rigor mortis [54]. Our findings can be summarized as follows:

- Strychnine intoxication hastens the onset and the passing of rigor mortis.
- Carbon monoxide intoxication delays the resolution of rigor mortis.
- The intensity of rigor may vary depending on the cause of death.

4.2.8.5 Effect of Electrocution

In one of our electrocution cases, our first investigation at the scene of death revealed that the arms of the victim, which were in direct contact with the electrical current, displayed severe rigor. The victim’s husband, suspected of the murder of his wife, asserted that he had left her alive 1 hour earlier.

Our experiments on electrocution [48] were conducted on rats as follows:

- Group 1, a control set killed in the usual manner by nitrogen asphyxia.
- Group 2, electrocution with 140 V, 50 Hz alternating current applied for 50 seconds, with the electrodes clamped on the left front and the right hind limb of the animal.
- Group 3, same as group 2, but electrocution for 90 seconds.
- Group 4, animals killed by nitrogen asphyxia, followed by electrocution (same as group 3), 10 minutes later.

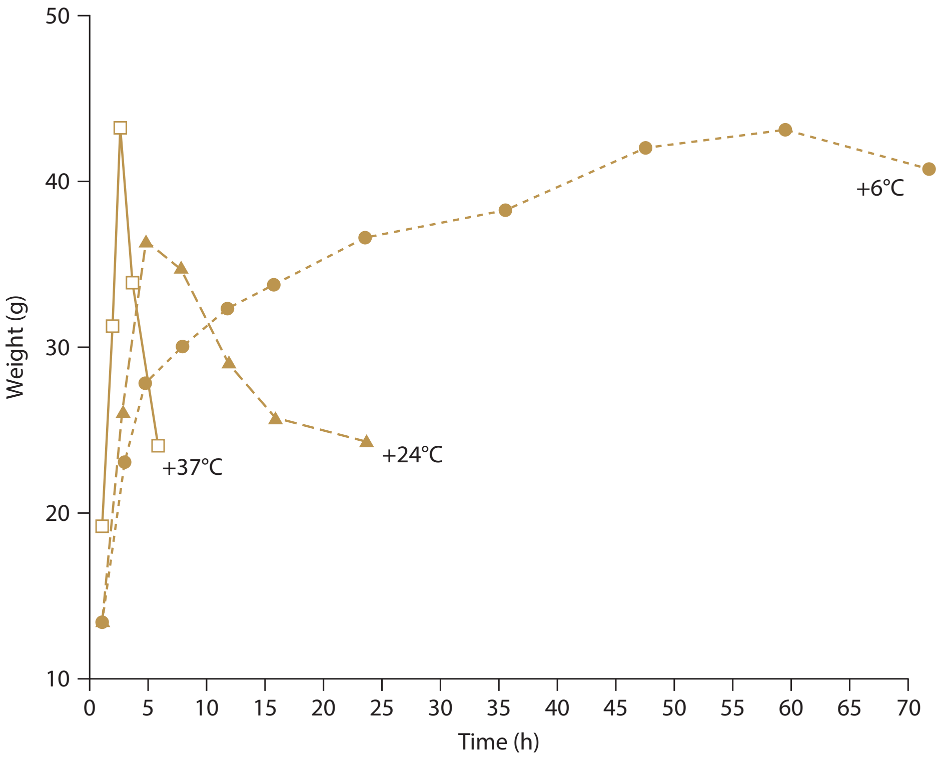

Figure 4.5 The evolution of the intensity of rigor mortis in the hind limbs of rats at different temperatures. Values given are always an average for ten animals (20 hind limbs).

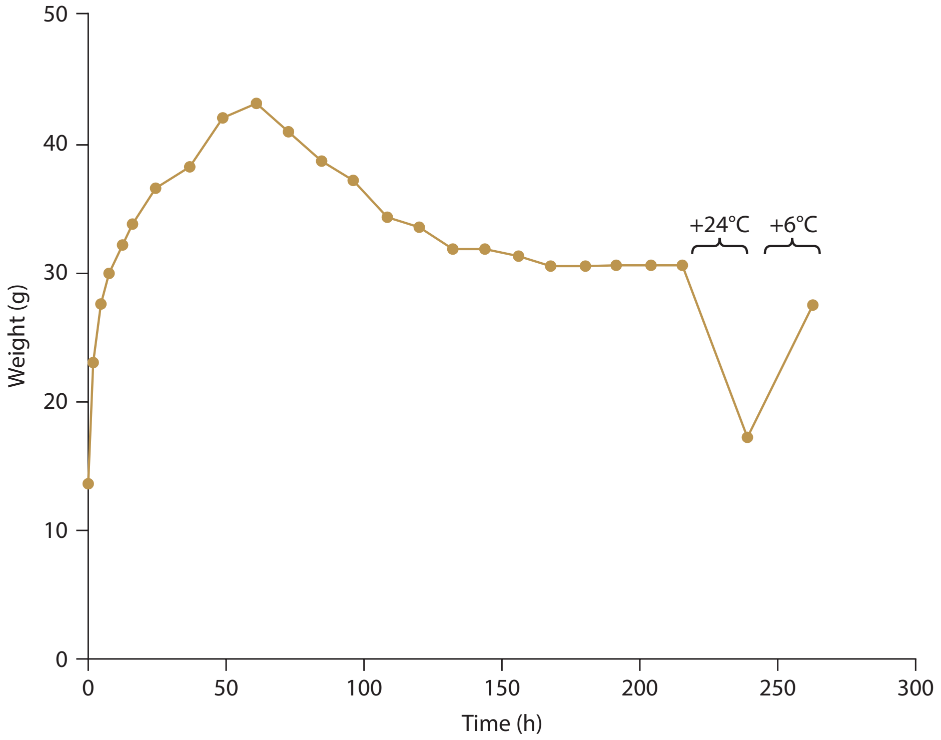

Figure 4.6 The evolution of the intensity of rigor mortis in the hind limbs of rats at +6°C. Values given are always an average for ten animals (20 hind limbs).

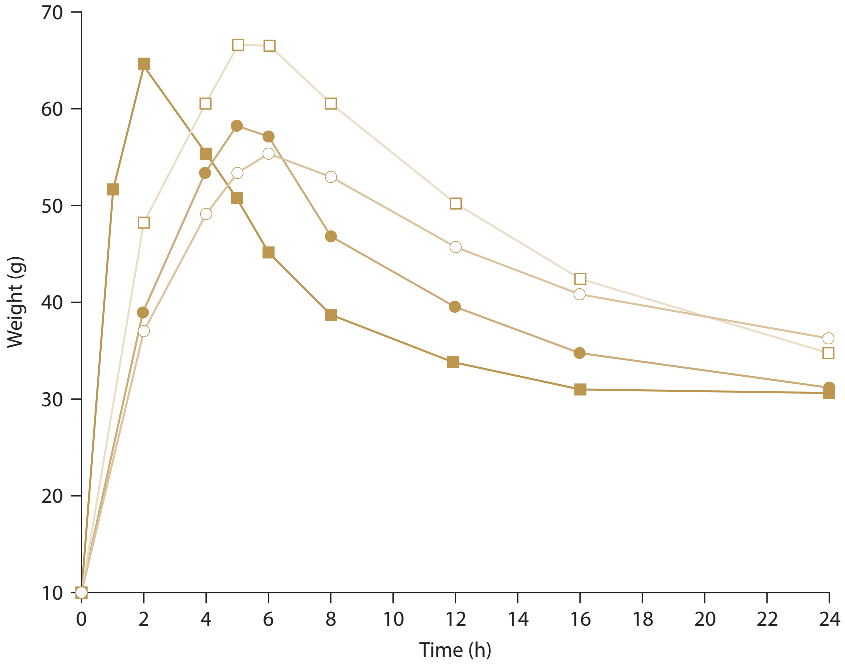

Figure 4.7 Evolution of the intensity of rigor mortis in the hind limbs of rats in the case of nitrogen asphyxia (open squares); fatal intoxication by strychnine (closed squares); carbon monoxide (open circles); and curare (closed circles). Mean values are for ten animals (20 hind limbs).

The results of this experiment, shown in Figure 4.8, led to the following conclusions:

1. Electrocution hastens the onset of rigor mortis. After a 90-second electrocution, rigor mortis developed as rapidly as 1 hour post-mortem, compared with 5 hours for the controls.
2. Electrocution hastens the disappearance of rigor mortis.
3. In the case of post-mortem electrocution, the observed changes were slightly less pronounced.

The changes in the development of rigor mortis were less pronounced in the limbs that were not directly affected by the electrical current (left hind limbs in our experiments).

Our results were confirmed by different authors [13,17,72]. For example, Owens and Sams [72] wrote: ‘Electrical stimulation accelerated rigor mortis development.’

Moreover, we have found a good explanation for the rapid resolution of the rigidity in the case of electrocution in the article of Iwamoto et al. [38]. They wrote: ‘the gas stunned chickens maintained a good fibre structure for 4 hours or more, but the electrically stunned had already lost intact fibre structure at 4 hours.’

4.2.8.6 Effect of Breaking

The influence of the breaking (mechanical solution) is shown in Figures 4.9 and 4.10.

Our experiments [57] showed that

- Cadaveric rigidity can re-establish after breaking.
- Significant rigidity can reappear if the breaking occurs before the process is complete.
- Rigidity is considerably weaker after the breaking.
- The time course of the intensity does not change in comparison with the controls:
- The re-establishment begins immediately after the breaking.
- Maximal values are reached at the same time as in the controls.
- The course of the resolution is the same as in the controls.

To explain the phenomenon of the re-establishment of rigor mortis after ‘breaking’, our hypothesis is as follows.

In the course of the development of rigidity, muscle fibres enter the rigid state progressively (i.e. one by one according to their different metabolism). The less fibres are rigid, the more easily rigor mortis can appear anew. When full rigor is installed, there remain no more muscle fibres which could reproduce rigidity after the breaking.

After the breaking at 6 hours post-mortem (i.e. after the rigor was fully established), we still observed an increase in resistance, but the maximal values were lower than those measured in the control group 24 hours post-mortem, after complete resolution. We thus conclude that this resistance is not caused by rigor mortis. Every person dealing with dead bodies can observe that, on human corpses, after resolution of rigor mortis—which requires 2–3 days depending on the ambient temperature—in spite

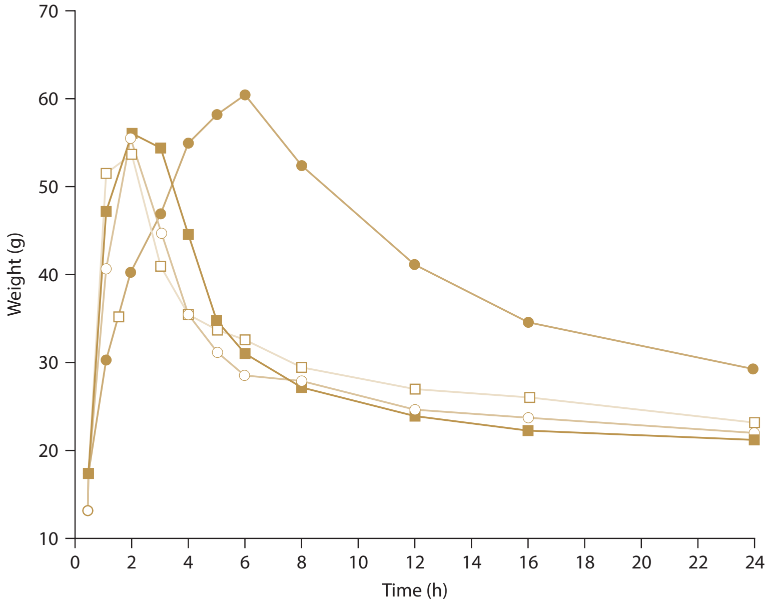

Figure 4.8 Evolution of the intensity of rigor mortis in the hind limbs of rats in the case of nitrogen asphyxia (closed circles); 'direct' electrocution for 50 seconds (open circles); 'direct' electrocution for 90 seconds (open squares); 'direct' post-mortem electrocution for 90 seconds (closed squares). Mean values are for ten animals (20 hind limbs) in the control group and for ten animals (20 hind limbs) in the 'electrocution' groups.

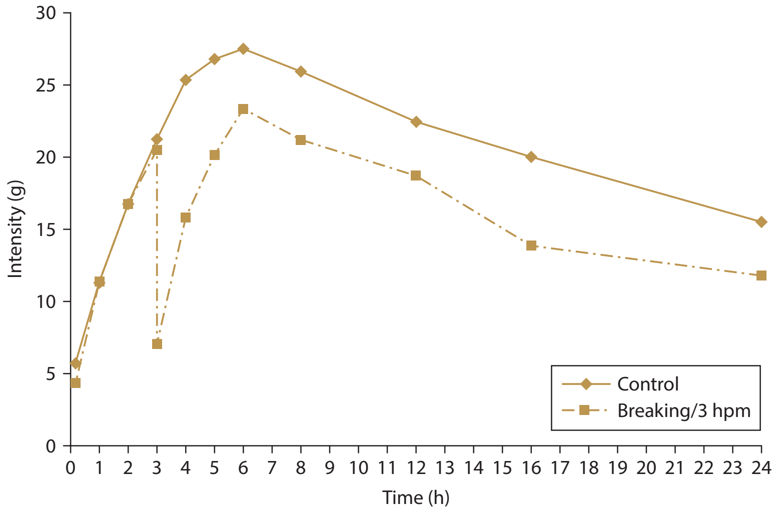

Figure 4.9 Influence of breaking on rigor mortis. Breaking 3 hours post-mortem.

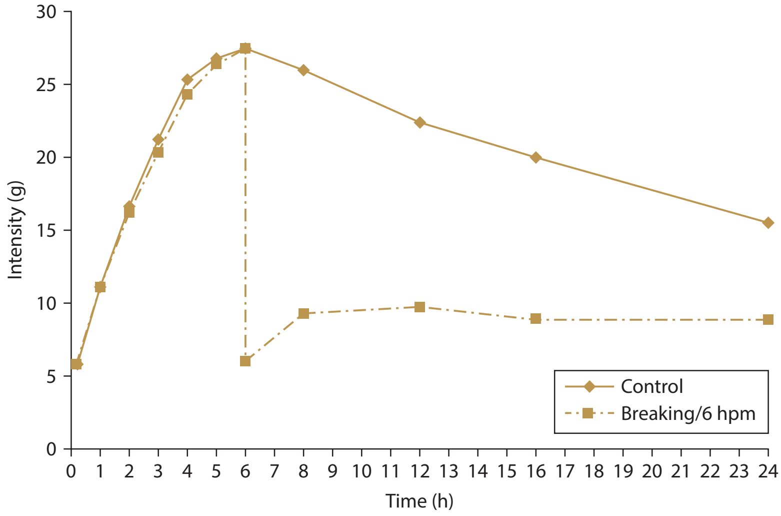

Figure 4.10 Influence of breaking on rigor mortis. Breaking 6 hours post-mortem.

of complete resolution, the joints are not as mobile as during the initial few minutes post mortem. Certain rigidity remains, and it can be easily broken. We believe that this residual rigidity is not caused by muscular rigidity *per se*, but rather by the resistance of all the periarticular tissues. We base our opinion also on the finding that when the rigidity was broken after 6 hours post mortem, there was a significant rise in the resistance after breaking, but no more changes were noted in the resistance after the maximal values were reached (i.e. no 'resolution').

Anders and his collaborators [1, 14] found a re-establishment of rigor mortis on human corpses following mechanical loosening up to 20 hpm. Taking into consideration the post-mortem cellular decay, such a late re-instalment of rigor mortis cannot be explained by the known biological processes. Therefore, it cannot be accepted as a "classical" rigor mortis. It may be the result of a stiffening of the periarticular tissues. The causes and mechanism of its apparition must be investigated—especially carefully concerning the circumstances of its development.

Nevertheless, this observation shows us the necessity to be very cautious with the appreciation of the re-establishment of rigor mortis, using it for the estimation of the time since death.

For daily forensic practice, we recommend taking into consideration the possibility of the higher upper limit of the possible re-establishment of rigor mortis proposed by Anders et al., being that in practice we use manual estimation.

4.2.8.7 Nysten's Law: Does It Apply to Rats?

We tried to determine the validity of Nysten's law in the case of rats. For this purpose, we adapted our method to perform parallel measurements in the masticatory muscles, the neck, the front limbs and the hind limbs in rats while respecting the same principles of measurements [56].

- In group 1: hind limbs, the maximal values of the intensity of rigor mortis were reached at 5 hours post-mortem
- In group 2: front limbs, at 5 hours post-mortem
- In group 3: neck, at 3 hours post-mortem
- In group 4: masticatory muscles, at 2 hours post-mortem

No significative differences were found concerning the resolution of rigor mortis among the four groups.

Consequently, Nysten's law seems to apply to rats as far as the onset of rigor mortis is concerned.

4.2.8.8 Effect of the Central Nervous System

To evaluate the possible influence of the CNS on the evolution of rigor mortis, the following experiments were conducted on four groups of rats [55]:

- Group 1: control
- Group 2: section of the sciatic nerve
- Group 3: destruction of the spinal cord with a needle introduced in the spinal canal
- Group 4: section of the medulla oblongata

No significant difference was found in the development of rigor mortis among the four groups. We can thus state that in a 'normal' condition the CNS has no significant influence on the intensity or on the time course of the rigor mortis. These experiments do not exclude the possibility of the influence of the CNS on the development of cadaveric rigidity in some pathological conditions.

Although it is clear that the results of our experiments are not directly applicable to humans, our method is the only means to evaluate the effects of different intrinsic and extrinsic factors on the development of rigor mortis, under a set of well-defined conditions. Moreover, these experiments do provide us with an overall idea on the time course of the various changes.

In terms of practical applications based on our experiments, if the stage of rigidity is used to estimate the time of death, it is necessary to perform a succession of objective measurements of the intensity of rigor mortis and to verify the possible presence of factors that can play a role in the modification of the development of rigor mortis.

4.2.8.9 Estimation of the Time Since Death by Repeated Measurements of the Intensity of Rigor Mortis

We applied these two principles and tested our method by deriving an estimate of time elapsed since death [47]. The experiment consisted of monitoring the development of the intensity of rigor mortis in nine groups of six rats each. The animals were killed by nitrogen asphyxia at an ambient temperature of 24°C. Measurements were initiated after 2, 4, 5, 6, 8, 12, 15, 24 and 48 hours post-mortem and lasted 5–9 hours, which would be the usual procedure when a corpse is discovered.

The results of these experiments are shown in Figure 4.11 and Table 4.5. The measurements, which were initiated 2 hours post-mortem and covered a period of 9 hours, resulted in a curve composed of a rising portion, a plateau and a descending slope. When the measurements were started 4 hours post-mortem, the rising portion was small, and this was followed by a long descending slope. At the later time points, the rising part was absent: after 8 hours post-mortem, for example, the curve showed a plateau and a descent.

Thus, three different phases were observed that can help estimate the time since death:

1. If an increase in intensity is observed, measurements are made no later than 5 hours post-mortem.

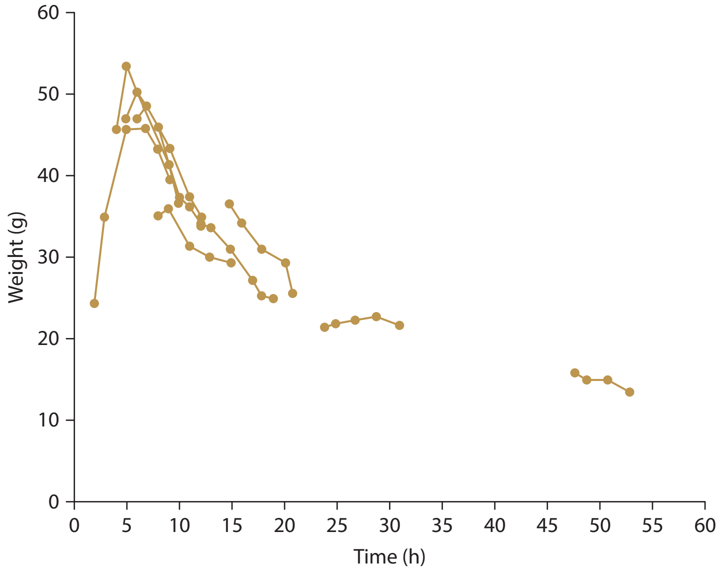

Figure 4.11 Changes in the intensity of rigor mortis in rats in different post-mortem periods.

Table 4.5 Experimental Evaluation of Rigor Mortis

Time post-mortem (h)	Intensity changes
2–9	2 ↑ 3 ↑ 5 — 7 ↓ 8 ↓ 9
4–10	4 ↑ 5 — 7 ↓ 9 ↓ 10
5–12	5 ↑ 6 — 8 ↓ 10 — 11 ↓ 12
6–12	6 — 7 ↓ 9 ↓ 11 ↓ 12
8–15	8 — 9 ↓ 11 — 13 — 14 — 15
12–19	12 — 13 ↓ 15 ↓ 17 ↓ 18 — 19
15–21	15 — 16 ↓ 18 — 20 ↓ 21
24–31	24 — 25 — 27 — 29 — 31
48–53	48 — 49 — 51 ↓ 53

Abbreviations: ↑, Increase. ↓, Decrease. } Significant changes.

—, No significant changes.

2. If a decrease in intensity is observed, measurements are made no earlier than 7 hours post-mortem.
3. At 24 hours post-mortem, the resolution is complete; there are no more changes in intensity.

It should also be noted that the totality of the curves assembled in Figure 4.11 gives a form very similar to that of a normal curve (compare this with Figure 4.3).

The results presented here demonstrate that, in comparison with the single measurement method used earlier, repeated measurements of the intensity of rigor mortis in rats allow the derivation of a more accurate estimate of the time since death.

The question remains whether this method is applicable to human corpses. In theory, it should be, and although we can attest that its practical realization is not simple, we are nevertheless attempting to build a measuring device.

In terms of objective methods of evaluation of rigor mortis, several new methods deserve mention. Hasan and Mason [32] described a technique for measuring the propagation velocity of a mechanical pulse along a muscle. The pulse was generated by piezoelectric crystals (bimorph benders). They used this method for the evaluation of the mechanics of rigor.

Vain et al. [95] used the myotonometer to grade rigor mortis. The instrument gives a mechanical impact against the muscle. The muscle responds with a damped vibration, which is registered and treated mathematically. The method gives quantitative information on the muscular stiffness and can be used, according to the authors, when estimating the time of death.

De-Giorgio et al. [16] used ultrasound elastographic measurement assessing the level of rigidity and stated that it can play a promising role in the quantitative determination of cadaveric rigidity.

Kliewer et al. [41] used the same method for measuring the muscle stiffness on pigs and found that 'two-dimensional shear wave ultrasound elastography can quantifiably measure the trajectory of rigor mortis in an animal model'.

Hopefully one or more of these new methods could be useful in the future in the forensic medical practice.

4.3 Recommendations for Practice

First, I would like to quote a remark made by Keith Simpson [89]: 'Rigor mortis is the best known, though the most uncertain and unreliable postmortem event.'

I hope that this chapter has convinced readers of the validity of this statement, and that they should exercise great caution if they use cadaveric rigidity to estimate the time since death.

Having studied cadaveric rigidity for a long time, I have come to believe that it is not the 'good method', or not 'the method' to estimate the time since death. Indeed, it requires experience (i.e. regular examinations of corpses made over a long period of time). Moreover, one must remember that there are no tables with values necessarily applicable to a given case.

Nevertheless, I am sure that rigor mortis could be a useful complement to the estimation of the time since death. Under such circumstances, I can make only the following recommendations:

1. We must base estimates on our own personal experience.
2. It is important to consult the data in the literature, in particular the descriptions of individual experiences made by a number of persons.
3. In Mallach's table (see Table 4.1), the extreme values, and not the averages, must be considered.
4. We must always seek and appreciate factors that may affect the development of rigor mortis.

Finally, I hope that the method of repeated measurements of the intensity of rigor mortis, once adapted to the human corpse, will permit a better use of this phenomenon for the estimation of time since death.

References

1. Anders S, Kunz M, Gehl A, Sehner S, Raupach T, Beck-Borholdt HP. Estimation of the time since death: reconsidering the re-establishment of rigor mortis. *Int J Legal Med* 2013;**127**:127–30.
2. Aust G. Zur Frage über den Einfluss des Nervensystems auf die Todtenstarre. *Pflugers Arch* 1886;**39**:241–4.
3. Bate-Smith EC, Bendall JR. Rigor mortis and adenosine triphosphate. *J Physiol* 1947;**106**:177–85.
4. Baumann J. Ueber kataleptische Totenstarre. *Dtsch Z Gesamte Gerichtl Med* 1923;**2**:647–70.
5. Bedford PJ, Tsokos M. The occurrence of cadaveric spasm is a myth. *Forensic Sci Med Pathol* 2013;**9**(2):244–8.
6. Beier G, Liebhardt E, Schuck M, Spann W. Totenstarremessungen an menschlichen Skelettmuskeln *in situ*. *Z Rechtsmed* 1977;**79**:277–83.
7. Bendall JR. Postmortem changes in muscle. In: Bourne GH (ed.). *The Structure and Function of Muscle, Vol. II, Structure*, part 2. London, Academic Press, 1973, pp 24–309.
8. Berg S. Nervensystem und Totenstarre. *Dtsch Z Gesamte Gerichtl Med* 1948/49;**39**:429–34.
9. Bierfreund M. Untersuchungen über die Totenstarre. *Pflügers Arch* 1888;**43**:195–216.
10. Billeter R, Weber H, Lutz H, Howald H, Eppenberger HM, Jenny E. Myosin types in human skeletal muscle fibres. *Histochemistry* 1980;**65**:249–59.
11. Brooke MH, Kaiser KK. The use and abuse of muscle histochemistry. *Ann N Y Acad Sci* 1974;**228**:121–44.
12. Busch H. *Experimenta quaedam de morte*. Halae, 1819. Cited by Bierfreund M. Untersuchungen über die Totenstarre. *Pflugers Arch* 1888;**43**:195–216.
13. Cavitt LC, Sams AR. Evaluation of physical dimension changes as nondestructive measurements for monitoring rigor mortis development in broiler muscles. *Poultry Sci* 2003;**82**:1198–204.
14. Crostack C, Sehner S, Raupach T, Anders S. Re-establishment of rigor mortis: evidence for a considerably longer post-mortem time span. *Int J Legal Med*. 2017;**131**(4):1039–42.
15. David H, David S. Submikroskopische Veränderungen der Skelettmuskulatur während der postmortalen Autolyse. *Acta Biol Med Ger* 1965;**14**:423–35.
16. De-Giorgio F, Ciasca G, D'Amico R, Trombatore P, D'Angelo A, Rinaldi P, Milano F, Locci E, De Spirito M, d'Aloja E, Colosimo C, Pascali VL. An evaluation of the objectivity and reproducibility of shear wave elastography in estimating the post-mortem interval: a tissue biomechanical perspective. *Int J Legal Med* 2020;**134**(5):1939–48.
17. Devine CE, Payne SR, Peachey BM, Lowe TE, Ingram JR, Cook CJ. High and low rigor temperature effects on sheep meat tenderness and ageing. *Meat Sci* 2002;**60**:141–6.
18. Duncan KL, Hare WR, Buck WB. Malignant hyperthermia-like reaction secondary to ingestion of hops in five dogs. *J Am Vet Med Assoc* 1997;**210**:51–4.
19. Eiselberg AV. Zur Lehre von der Todtenstarre. *Pflugers Arch* 1881;**24**:229–31.
20. Eisenmenger W, Peschel O, Bratzke H, Welsch U, Herzog V. Electronenoptische Untersuchungen zur Totenstarre. In: Bauer G (ed.). *Gerichtsmedizin: Festschrift für W. Holczabek*. Vienna, F. Deuticke Verlag, 1988, pp 251–66.
21. Erdös T. Rigor, contracture and ATP. In: *Studies from the Institute of Medical Chemistry*, vol. 3. Hungary, University of Szeged, 1943, pp 51–6.
22. Essen B, Jansson E, Henriksson J, Taylor AW, Saltin B. Metabolic characteristics of fibre types in human skeletal muscle. *Acta Physiol Scand* 1975;**95**:153–65.
23. Forster B. Der Arzt am Tatort. Todeszeitbestimmung. *Hippokrates* 1978;**49**:22–40.
24. Forster B, Ropohl D. *Rechtsmedizin 2*. Stuttgart, Germany, Ferdinand Enke Verlag, 1979.

25. Forster B, Ropohl D. *Medizinische Kriminalistik am Tatort*. Stuttgart, Germany, Ferdinand Enke Verlag, 1983.
26. Forster B, Ropohl D, Prokop O, Riemer K. Tierexperimentelle und an menschlichen Leichen gewonnene Daten zur Frage der Dauer der Totenstarre. *Kriminal Forens Wiss* 1974;**13**:35–45.
27. Forster B, Ropohl D, Raule P. Eine neue Formel zur Beurteilung der Totenstarre. Die Feststellung des FRR-Index. *Z Rechtsmed* 1977;**80**:51–4.
28. Fuchs Z. *Allg Physiol* 1904;**4**:359. Cited by Berg S. Nervensystem und Totenstarre. *Dtsch Z Gesamte Gerichtl Med* 1948/49;**39**:429–34.
29. Geesink G, Sujang S, Koohmaraie M. Tenderness of pre- and post-rigor lamb longissimus muscle. *Meat Sci* 2011;**88**:723–6.
30. Gendre AV. Ueber den Einfluss des Nervensystems auf die Todtenstarre. *Pflugers Arch* 1885;**35**:45–8.
31. Hanson J, Huxley HE. The structural basis of contraction in striated muscle. *Symp Soc Exp Biol* 1955;**9**:228–64.
32. Hasan H, Mason P. Pulse propagation in muscle. *Phys Med Biol* 1978;**23**:917–27.
33. Henssge CI, Madea B. *Methoden zur Bestimmung der Todeszeit am Leichen*. Lübeck, Schmidt-Römhild, 1988.
34. Henssge C, Madea B. Estimation of the time since death in the early post-mortem period. *Forensic Sci Int* 2004;**144**:167–75.
35. Henssge C, Madea B. Leichenerscheinungen und Todeszeitbestimmung. In: Brinkmann B, Madea B (eds.). *Handbuch gerichtliche Medizin*, vol. 1. Berlin, Springer, 2004, pp 79–225.
36. Huff Lonergan E, Zhang W, Lonergan SM. Biochemistry of postmortem muscle: lessons in mechanism of meat tenderization. *Meat Sci* 2010;**86**:184–95.
37. Husband HA. *The Student's Hand-Book of Forensic Medicine and Medical Police.* Edinburgh, E. and S. Livingstone, 1877.
38. Iwamoto H, Ooga T, Moriya T, Miyachi H, Matsuzaki M, Nishimura S, Tabata S. Comparison of the histological and histochemical properties of skeletal muscles between carbon dioxide and electrically stunned chickens. *Br Poultry Sci* 2002;**43**:551–9.
39. Kemp CM, Parr T. Advances in apoptotic mediated proteolysis in meat tenderization. *Meat Sci* 2012;**92**:252–9.
40. Kemp CM, Sensky PL, Bardsley RG, Buttery PJ, Parr T. Tenderness: an enzymatic view. *Meat Sci* 2010;**84**:248–56.
41. Kliewer MA, Mao L, Weigman BJ, Walker DC, Gettle LM, Corliss RF. Ultrasound elastographic measurement of rigor mortis in an animal model: a feasibility study for improved time-of-death estimates in forensic investigations. *Am J Roentgenol*. 2021;**216**(4):1126–33.
42. Knight B (ed.). *The Estimation of the Time Since Death in the Early Postmortem Period*, 2nd ed. London, Edward Arnold, 2002.
43. Koohmaraie M, Doumit ME, Wheeler TL. Meat toughening does not occur when rigor shortening is prevented. *J Anim Sci* 1996;**74**:2935–42.
44. Krause D, Zett L. Experimentelle Untersuchungen über den Einfluss von Sauerstoff auf Mechanogramm und Membranpotential bei der Ausbildung der Totenstarre. *Beitr Gerichtl Med* 1973;**30**:252–7.
45. Krause D, Zett L. Physiologische und morphologische Untersuchungen zu Mechanismus und Verlauf der Totenstarre. *Z Rechtsmed* 1973;**72**:245–54.
46. Krause D, Klein A, Zett L. Todeszeitbestimmung mittels indirekter Muskelreizung über den N. ischiadicus und N. radialis. *Kriminal Forens Wiss* 1976;**26**:66–7.
47. Krompecher T. Experimental evaluation of rigor mortis. VIII. Estimation of the time since death by repeated measurements of the intensity of rigor mortis on rats. *Forensic Sci Int* 1994;**68**:149–59.
48. Krompecher T, Bergerioux C. Experimental evaluation of rigor mortis. VII. Effect of ante- and postmortem electrocution on the evolution of rigor mortis. *Forensic Sci Int* 1988;**38**:27–35.
49. Krompecher T, Fryc O. Experimentelle Untersuchungen an der Leichenstarre. II. Das Entstehen der Leichenstarre unter Einfluss von körperlicher Anstrengung. *Beitr Gerichtl Med* 1978;**36**:345–9.
50. Krompecher T, Fryc O. Experimental evaluation of rigor mortis. III. Comparative study of the evolution of rigor mortis in differ ent sized muscle groups in rats. *Forensic Sci Int* 1978;**12**:97–102.
51. Krompecher T, Fryc O. Experimental evaluation of rigor mortis. IV. Change in strength and evolution of rigor mortis in the case of physical exercise preceding death. *Forensic Sci Int* 1978;**12**:103–7.
52. Krompecher T, Fryc O. Zur Frage der Todeszeitbestimmung auf Grund der Leichenstarre. *Beitr Gerichtl Med* 1979;**37**:285–9.
53. Krompecher T, Fryc O. Experimental evaluation of rigor mortis. V. Effects of temperature on the evolution of rigor mortis. *Forensic Sci Int* 1981;**17**:19–26.
54. Krompecher T, Bergerioux C, Brandt-Casadevall C, Gujer HR. Experimental evaluation of rigor mortis. VI. Effect of various causes of death on the evolution of rigor mortis. *Forensic Sci Int* 1983;**22**:1–9.
55. Krompecher T, Gilles A, Brandt-Casadevall C, Horisberger B, Mangin P. Experimental evaluation of rigor mortis: the influence of the central nervous system on the evolution of the intensity of rigor mortis. *Proc Am Acad Forensic Sci* 2005;**11**:261.
56. Krompecher T, Gilles A, Brandt-Casadeval C, Mangin P. Experimental evaluation of rigor mortis. Nysten's law: does it apply to rats? *Proc Am Acad Forensic Sci* 2004;**10**:255–6.
57. Krompecher T, Gilles A, Brandt-Casadevall C, Mangin P. Experimental evaluation of rigor mortis IX. The influence of the breaking (mechanical solution) on the development of rigor mortis. *Forensic Sci Int* 2008;**176**:157–62.
58. Kussmaul A. Ueber die Todtenstarre und die ihr nahe ver wandtem Zustande von Muskelstarre, mit besonderer Berücksichtigung auf die Staatsarzneikunde. *Vierteljahrsschr prakt Heilk (Prag)* 1856;**13**:67–115.
59. Laves W. Ueber die Totenstarre. *Dtsch Z Gerichtl Med* 1948/49;**39**:186–98.
60. Lowe JE, Jennings RB, Reimer KA. Cardiac rigor mortis in dogs. *J Mol Cell Cardiol* 1979;**11**:1017–31.
61. Mallach HJ. Zur Frage des Todeszeitbestimmung. *Berlin Med* 1964;**18**:577–82.
62. Mallach HJ, Mittmeyer HJ. Totenstarre und Totenflecke. *Z Rechtsmed* 1971;**69**:70–8.
63. Maresch W. Die Vergiftung durch Phosphor säureester. *Arch Toxikol* 1957;**16**:285–319.
64. Meijer AEFH, Elias EA. The value of enzyme histochemical techniques in classifying fibre types of human skeletal muscle. I. Adult skeletal muscles with no apparent disease of the neuromuscular system. *Histochemistry* 1976;**48**:257–67.
65. Mittmeyer HJ. Abhängigkeit der Totenstarre und Totenflecke vom Leichenalter. *Beitr Gerichtl Med* 1971;**28**:101–7.

66. Morgenstern S. Experimentelle Ergebnisse zur Frage des Temperatureinflusses auf die Leichenstarre. *Dtsch Z Gesamte Gerichtl Med* 1927;**9**:718–22.
67. Mueller B. *Gerichtliche Medizin*. Berlin, Springer, 1953.
68. Naumann E. Untersuchungen über den Gang der Totenstarre. *Pflugers Arch* 1917;**169**:517–36.
69. Niderkorn PF. Cited by Polson CJ. *The Essentials of Forensic Medicine*. Oxford, Pergamon Press, 1962.
70. Nysten PH. *Recherches de physiologie et de chimie pathologiques, pour faire suite à celles de Bichat sur la vie et la mort*. Paris, J.A. Brosson, 1811, pp 384–420.
71. Oppenheim F, Wacker L. Das Ausbleiben der postmortalen Saurebildung im Muskel als Ursache der verschiedenen Intensität der Totenstarre menschlicher Leichen. *Berl Klin Wochenschr* 1919;**42**:990–4.
72. Owens CM, Sams AR. Muscle metabolism and meat quality of pectoralis from turkeys treated with postmortem electrical stimulation. *Poultry Sci* 1997;**76**:1047–51.
73. Peschel O, Bratzke H, Eisenrnenger W, Welsch U. Zur Mikromorphologie der Totenstarre im menschlichen Skelettmuskel. *Beitr Gerichtl Med* 1989;**47**:31–42.
74. Pirch J, Schutz Y and Klintschar M. A case of instantaneous rigor? *Int J Legal Med* 2013;**127**:971–4.
75. Polson CJ, Gee DJ. *The Essentials of Forensic Medicine*. Oxford, Pergamon Press, 1973.
76. Pounder DJ. Postmortem interval. In: Payne-James J, Byard RW, Corey TS, Henderson C (eds.). *Encyclopedia of Forensic and Legal Medicine*, vol. 3. Oxford, Elsevier, 2005, pp 382–8.
77. Prokop O. Supravitale erscheinungen. In: Prokop O, Göhler W (eds.). *Forensische Medizin*. Berlin, Volk und Gesundheit Verlag, 1975, pp 16–27.
78. Prokop O. Die Totenstarre (Rigor Mortis). In: Prokop O, Göhler W (eds.). *Forensische Medizin*. Stuttgart, Germany, G. Fischer Verlag, 1976.
79. Saber TM, Omran BHF, El Deib MM, El-Sharkawy NI, Metwally MMM, Abd-Elhakim YM. Early postmortem biochemical, histological, and immunohistochemical alterations in skeletal muscles of rats exposed to boldenone undecylenate: Forensic implication. *J Forensic Leg Med* 2021;**83**:1–8
80. Saukko P, Knight B. *Knight's Forensic Pathology*. London, Arnold, 2004.
81. Schleyer F. Leichenveränderungen. Todeszeitbestimmung im früh postmortalen Intervall. In: Muller B (ed.). *Gerichtliche Medizin*, vol. 1. Berlin, Springer, 1975.
82. Schneider V. Zum Elektrotod in der Badewanne. *Arch Kriminol* 1985;**176**:89–95.
83. Schuck M, Beier G, Liebhardt E, Spann W. On the estimation of lay-time by measurement of rigor mortis. *Forensic Sci Int* 1979;**14**:171–6.
84. Schuck M, Beier G, Liebhardt E, Spann W. Zur Schätzung der Liegezeit durch Messungen der Totenstarre. *Beitr Gerichtl Med* 1978;**36**:339–43.
85. Seelye RN, Nevalainen TJ, Gavin JB, Webster VJ. Physical and biochemical changes in rigor mortis of cardiac muscle. *Biochem Med* 1979;**21**:323–32.
86. Shapiro HA. Rigor mortis. *Br Med J* 1950;**2**:304.
87. Shapiro HA. Medico-legal mythology: some popular forensic fallacies. *J Forensic Med* 1953/54;**1**:144–69.
88. Sherrington CS. *The Integrative Action of the Nervous System*. London, A. Constable and Co, 1908.
89. Simpson K. *Forensic Medicine*. London, Edward Arnold, 1974.
90. Swatland HJ. Observations on rheological, electrical, and optical changes during rigor development in pork and beef. *J Anim Sci* 1997;**75**:975–85.
91. Szent-Györgyi A. Studies on muscle. *Acta Physiol Scand* 1945;**9**(Suppl 25).
92. Szent-Györgyi A. *Chemistry of Muscular Contraction*. New York, Academic Press, 1947.
93. Tacqui A. Time since death. In: Siegel JA, Saukko PJ, Knupfer GC (eds.). *Encyclopedia of Forensic Sciences*, vol. 3. London, Academic Press, 2000, pp 1357–63.
94. Tarrant PV, Mothersill C. Glycolysis and associated changes in beef carcasses. *J Sci Food Agric* 1977;**28**:739–49.
95. Vain A, Kauppila R, Humal LH, Vuori E. Grading rigor mortis with myotonometry: a new possibility to estimate time of death. *Forensic Sci Int* 1992;**56**:147–50.
96. Vanderwee MA, Humphrey SM, Gavin JB and Armiger LC. Changes in the contractile state, fine structure and metabolism of cardiac muscle cells during development of rigor mortis. *Virchows Arch (Cell Pathol)* 1981;**35**:159–67.
97. Varetto L, Curto O. Long persistence of rigor mortis at constant low temperature. *Forensic Sci Int* 2005;**147**:31–4.
98. Vock R, Hein PM, Metter D. Tod im tetanischen Anfall. *Z Rechtsmed* 1984;**92**:231–7.
99. Wuytack F, Casteels R. Evidence for rigor in smooth muscle. *Arch Int Physiol Biochim* 1975;**83**:340–1.

Taylor & Francis
Taylor & Francis Group
http://taylorandfrancis.com

5 Post-mortem Lividity
Hypostasis and Timing of Death

Burkhard Madea and Bernard Knight

Contents

5.1 Definition 71
5.2 Attempts to Objectify Post-mortem Blanching 74
5.3 Stages of Post-mortem Lividity 75

5.1 Definition

Hypostasis is one of the most obvious post-mortem changes; alternative names are ‘post-mortem lividity’ and the older term, ‘suggillation’.

Hypostasis is the staining of the skin surface—and of internal organs—by the settling of blood under the influence of gravity after circulation has ceased [3–6,10,11–15].

After irreversible circulatory arrest, post-mortem lividity develops early and therefore is one of the initial post-mortem changes. Following circulatory arrest, in blood vessels the hydrostatic pressure becomes the leading force within the parallelogram of forces consisting of blood pressure, structural barriers, tissue turgor and pressure of underlying surfaces. ‘Hypostasis’ means the movement of body fluids according to gravity. All fluid compartments are involved in hypostasis, both intravascular and transcellular fluids. Hypostasis in internal organs has misled inexperienced pathologists into regarding hypostasis in the intestines and myocardium as true infarctions, as a result of the dark, congested appearance in organs. Influenced by gravity, blood is sinking into the lowest parts within the vascular system of the body, in a supine position towards the back, the buttocks, thighs, calves and back of the neck. Where the body is pressed onto a firm supporting surface, these contact areas remain pale because the vascular channels are obliterated by pressure; this is commonly seen over the buttocks and the shoulder blades. Irregular pink patches over the face, especially over the cheeks in the agonal period, are caused by local stasis and in German are called ‘Kirchhofrosen’ (Table 5.1). Post-mortem lividity visible on the skin is a result of the sinking of blood into the capillaries of the corium. Post-mortem lividity may be visible within 20–30 minutes after death, in the early stages, as pink patches that regularly and gradually become confluent with an increasing post-mortem interval. Because of consumption of oxygen, the pink colour of lividity changes to dark pink and then to bluish (Figure 5.1).

Table 5.1 Lividity: Causes, Consequences and Phenomena Checked on the Body

Cause	Consequence(s)	Phenomenon
Decrease in intensity of myocardial contraction	Stasis	‘Kirchhofrosen’, local stasis with patchy discolouration during the agonal period resulting from centralization of the circulation.
Cardiac arrest, hydrostatic pressure	Hypostasis	Livores with a ‘shifting’ quality and ‘disappearance on pressure’.
Vascular permeability	Haemoconcentration	Decrease of shifting and disappearance on pressure.
Autolysis, putrefaction	Diffusion of haemoglobin	No shifting, no disappearance on pressure.

In the areas of deep hypostasis, cutaneous petechial haemorrhages secondary to capillary rupture may develop; these are called ‘vibices’ (see Figure 5.1 [b]). Of diagnostic and criminal investigation relevance is not only the development but also the colour of lividity, its distribution over the body and the phenomena of fixation (disappearance after turning the body) and disappearance (blanching) on blunt thumb pressure.

The colour of hypostasis varies; it is darker red or blue when the contained haemoglobin is less oxygenated. In hypothermia, or if the body has been in refrigeration or other cold environmental surroundings, the colour may be bright pink.

In cases of intoxication such as with carbon monoxide and cyanides, the colour of hypostasis usually appears cherry pinkish, and in methaemoglobin intoxication it is brownish (Table 5.2; see also Figure 5.1 [d]). Because of the lack of dissociation of oxyhaemoglobin,

DOI: 10.1201/9781003244974-5

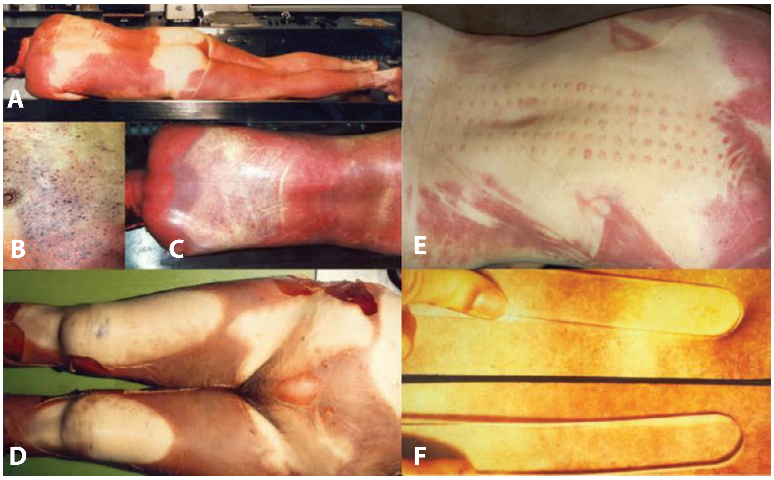

Figure 5.1 Post-mortem lividity. (a) Post-mortem lividity in a supine position, with pink colour resulting from storage in a refrigerator. (b) Petechial-like haemorrhages secondary to capillary ruptures in areas of deep hypostasis (vibices). (c) Zonal segmentation of hypostasis: partly dark blue, partly red. (d) Brownish colour of hypostasis in the case of methaemoglobin intoxication. (e) Patterned hypostasis of the back resulting from the underground. (f) Complete disappearance of lividity on light blunt pressure.

Table 5.2 Post-mortem Lividity Discolouration

Aetiology	Colour	Mechanism
Normal	Blue-purplish	Venous blood
Carbon monoxide	Pink, cherry red	Carboxyhaemoglobin
Cyanide	Pink, cherry red	Excessively oxygenated blood resulting from inhibition of cytochrome oxidase
Fluoroacetate	Pink, cherry red	Same as above
Refrigeration/ hypothermia	Pink, cherry red	Oxygen retention in cutaneous blood by cold air left shifting of the haemoglobin-oxygen dissociation curve
Sodium chloride/ nitrite, nitrate	Brown	Methaemoglobin
Hydrogen sulphide	Green	Sulfhaemoglobin

Source: Modified from Spitz WU. *Spitz & Fisher's Medicolegal Investigation of Death*. 3rd ed. Springfield, Illinois, Charles C Thomas, 1993.

Table 5.3 Time of Onset of Hypostasis (from 10)

Textbook authors	Onset	Maximum hours
Adelson	30 min–4 h	8–12
Polson and Gee	30 min–2 h	6–12
Spitz and Fisher	2–4 h	8–12
Taylor (ed. Simpson)	0 h	12
Taylor (ed. Mant)	1 h	12
Gradwohl (ed. Camps)	20–30 min	6–12
Glaister	—	8–12
DiMaio	30 min–2 h	8–12
Sydney Smith	0 h	12
Mant	0 h	12
Gordon and Shapiro	'Few' h	12

a bright pink colour of lividity may be seen in cases of hypothermia as well. If a body is transferred from a cold environment to normal room temperature, a typical zonal segmentation of hypostasis may be seen, with the colour turning dark blue in the rewarmed areas (see Figure 5.1 [c]).

True post-mortem hypostasis develops at very variable rates following cardiac arrest. The standard forensic medicine textbooks offer a wide range of the time of onsets (Table 5.3).

Several authors have attempted to use subjective measurements of hypostasis, by using stages such as 'beginning, confluence, maximum intensity, displacement by slight pressure, complete shifting and incomplete shifting'. Mallach [14] analysed such data, but the wide scattering of results and the doubtful specificity of such subjective descriptions make the results of little practical value in casework, other than to add a further general corroboration to better results obtained by other techniques.

Given these wide ranges, it is obvious that the use of hypostasis in estimating the time of death is of little evidential use. All that can be said about hypostasis is that it usually appears between 30 minutes and 4 hours after death, it reaches maximum intensity in up to about 12 hours following death and it persists in an undisturbed corpse until putrefactive changes set in, usually a number of days later. Under tropical conditions, hypostasis may be destroyed by decomposition on the first day after death if the body undergoes rapid dissolution.

Apart from the initial time of the onset of hypostasis, it has been claimed over a long period of time that its permanent fixation is time related. Numerous textbooks have stated that, after a certain (but very variable) time, primary

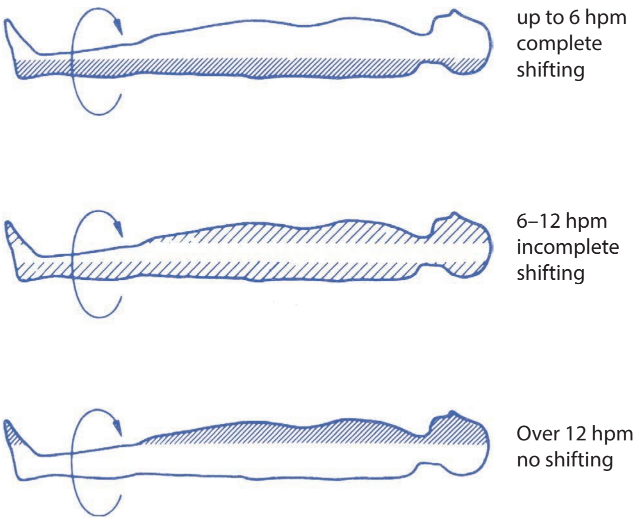

Figure 5.2 Shifting of lividity after turning the body.

(Modified from Patscheider/Hartmann, *Leitfaden der Rechtsmedizin*, 3rd ed., Göttingen, Verlag Hans Huber, 1993.)

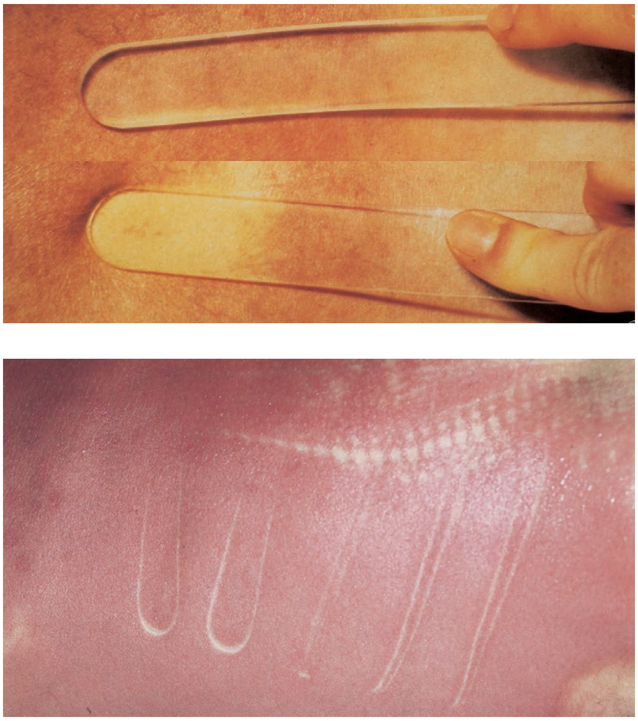

Figure 5.3 Complete disappearance on soft pressure disappearance only after pressure with tweezers.

hypostasis becomes fixed and will not move again under the influence of gravity, even if the body position is altered.

Of predominant criminal investigation significance regarding lividity are the phenomena **disappearance on pressure** and **disappearance after turning the body**. In early stages, lividity completely disappears on soft thumb pressure. With an increasing post-mortem interval, the pressure must increase as well. Later, lividity disappears only incompletely on blunt pressure, and finally, it does not disappear at all.

If the body is turned in the early post-mortem interval, some or all of the hypostasis may move down to the most dependent areas as a result of gravity. In a comparatively later post-mortem interval, only some of the hypostasis will slip down to the newly dependent area, and only faint blanching of the lividity will be noted in the formerly dependent areas (Figure 5.2).

With an increasing post-mortem interval, disappearance of hypostasis on thumb pressure and relocation after shifting decrease and then cease completely (Figure 5.3).

This effect is caused by an increasing haemoconcentration of intravascular erythrocytes in response to transcapillary extravasation of plasma. The intravascular haemoconcentration is the main reason that the disappearance of hypostasis gradually decreases on thumb pressure and after shifting. In a comparatively later post-mortem interval, haemolysis and haemoglobin diffusion into the perivasal tissues start, but these are only secondary mechanisms contributing to the fixation of hypostasis.

For instance, Hunnius et al. [7] could demonstrate an exponential relation between necessary pressure for disappearance of lividity and time since death (Figure 5.4). The dependence between pressure and time since death can best be described by a semi-logarithmic curve. However, these data cannot be used in practice since the pressures used were too high (kPa up to 300 kPa) and the pressure time too short (1 sec) (5).

All different elements of hypostasis such as beginning, confluence, maximum, disappearance on thumb pressure and complete or incomplete disappearance after shifting change with an increasing post-mortem time interval.

Longitudinal studies of these criteria in large random samples are lacking, and cross-sectional studies are of only limited value. The best statistical data available were summarized by Mallach [14], who calculated mean values, standard deviations and 95 per cent limits of confidence based on a number of textbook reports (Table 5.4). Because better data are lacking, these data are still undisputed. However, these data do not represent absolute threshold values. Investigations using a quantitative measurement of livor mortis have not yet gained practical importance.

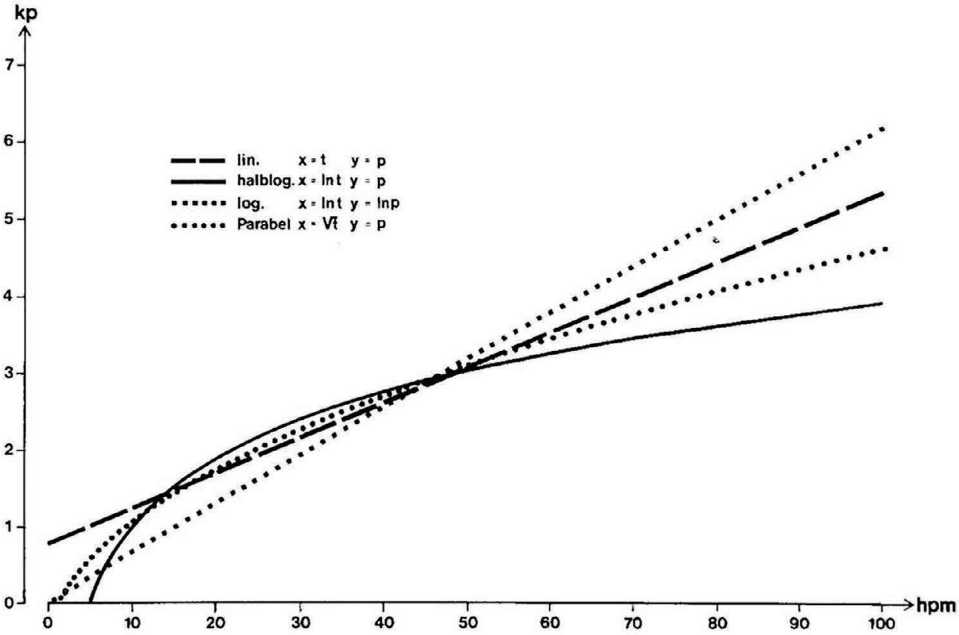

Figure 5.4 Force (kp) necessary for blanching over the post-mortem interval (hpm). The relationship between force and time since death can best be described by semi-logarithmic curve.

(From Hunnius et al. 1973)

Table 5.4 Time Course of Different Criteria of Lividity: Statistical Calculations by Mallach Based on Textbook Reports*

			2 SD		**Range of scatter**		
	$\bar{x}$	**SD**	**Lower limit**	**Upper limit**	**Lower limit**	**Upper limit**	**Number of quotations**
Development	¾	½	—	2	¼	3	17
Confluence	2½	1	¾	4¼	1	4	5
Greatest distension and intensity	9½	4½	½	18¼	3	16	7
Disappearance							
1. Complete on thumb pressure.	5½	6	—	17½	1	20	5
2. Incomplete on sharp pressure (forceps).	17	10½	—	37½	10	36	4
Displacement after turning the body							
1. Complete	3¾	1	2	5½	2	6	11
2. Incomplete	11	4½	2¼	20	4	24	11
3. Only little pallor	18½	8	2½	34½	10	30	7

* The statistical calculations are not based on cross-sectional or longitudinal studies but on empirical knowledge quoted in textbooks.

Abbreviations: $\bar{x}$, mean value; SD, standard deviation.

Source: Data from Mallach HJ. Zur Frage der Todeszeitbestimmung. *Berlin Med* 1964;**18**:577–582.

5.2 Attempts to Objectify Post-mortem Blanching

Crude methods of detecting fixation have been used in which local pressure is applied to the hypostatic skin, to determine whether the colour can be blanched.

Suzutani et al. [17] examined 430 bodies by pressing the side of forceps against the dependent skin. These authors discovered that hypostasis could not be squeezed out in about 30 per cent of cases where death had occurred 6–12 hours previously. More than 50 per cent of cases were fixed after a post-mortem interval of 12–24 hours, and no fading took place in about 70 per cent of those who had died 1–3 days earlier.

Suzutani et al. [17] also found a significant number of cases in which hypostasis was not fixed for up to at least 3 days. In addition, there was some seasonal variation, with less movement in the summer months; cases of

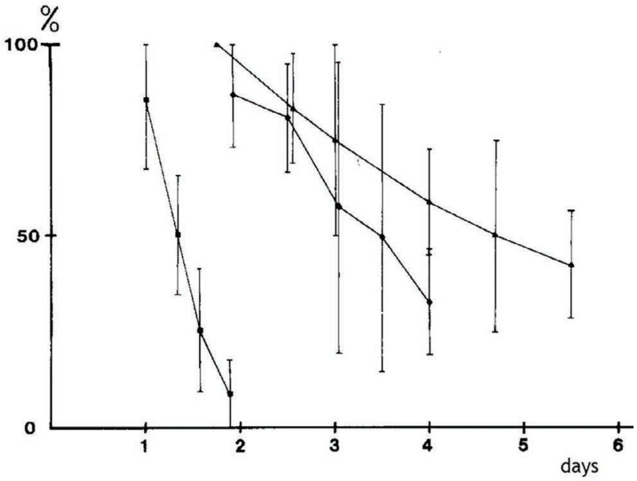

Figure 5.5 Influence of temperature and blanching of post-mortem lividity over the post-mortem interval (days). *x*-axis represents time since death in days; *y*-axis represents blanching of post-mortem lividity; defined pressure (3.5 kPa) and pressure time (10 min). ▲ 5°C, ◊ 14–15°C, ■ 25°C.

(From Fechner et al. 1984.)

asphyxial deaths and those with intracranial lesions also had delayed fixation rates.

Fechner et al. [2] examined 28 cases of sudden death in which the bodies were stored at different temperatures and found a variation of hypostatic fixation with temperature, but no linear relationship and very wide individual variation relative to the time of death (Figure 5.5).

Although there seems to be a temperature dependence between pressure and time since death for the disappearance of lividity. The pressure times were with 10 and 30 minutes much too long.

Although the foregoing commentary seems to indicate that hypostasis is almost valueless in the determination of time since death, more recent research—some of which is still in progress—is attempting to improve this situation with the use of sophisticated optical equipment.

Schuller et al. [16] began to use colorimetry on hypostasis. When examining seven corpses over a period from 3 to 35 hours after death, these investigators observed an increasing paleness of the hypostasis between 3 and 15 hours post-mortem. These authors concluded that there was a colour change from a wavelength of 575 nm at 3 hours at an average rate of 2 nm per hour.

Ongoing research by Vanezis [18] uses a tri-stimulus colorimeter. A standard xenon light source and filter illuminate the bodies, conforming to standard illumination D 65, which resembles daylight. A constant, small area of hypostasis on each corpse is illuminated, and the reflected light is split into blue, green and red for measurement. The body, which had developed primary hypostasis in the supine position, was turned to a prone position, and an area of lumbar skin was examined at 30-minute intervals to determine changes in colour as secondary movement took place over a period of 3–8 hours.

In a pilot study of 41 corpses, Vanezis [18] claimed that there is a linear relationship between the fading colour of the hypostasis and time during the first 24 hours, after which the relationship is unpredictable.

In 1996, Vanezis and Trujillo [19] reported further on the use of colorimetry in measuring the hypostasis from 93 corpses. Measurements were taken over a 4-hour period, and the rate of change of colour intensity of the hypostasis was plotted over a post-mortem interval. A regression formula was reported with a correlation coefficient *r* of 0.538. These authors commented that the shift in hypostasis was marked during the first 12 hours and decreased thereafter. They also claimed that hypostasis could be a useful means for determining the post-mortem period up to 48 hours.

Further photometric measurements of colour changes in livor mortis were published by Kaatsch et al. [8,9] and Bohnert et al. [1]. They have up to now not replaced the traditional subjective investigation of post-mortem lividity.

Methods to replace the subjective examination of post-mortem lividity by objectifying post-mortem blanching had been previously unsuccessful [5,6].

Further experimental approaches of objective measurement of post-mortem lividity must consider the following points: amount of pressure, time of pressure applied, area where the pressure is applied. Pressure, time and area should be comparable to conditions in forensic practice.

5.3 Stages of Post-mortem Lividity

- **Beginning** is stated if mottled patches at lower parts of the body (e.g. over the neck in a supine position) are observed.
- **Confluence** is stated if separate areas of discolouration of moderate intensity are noted.
- **Maximum** can be stated if during death scene investigation and autopsy hypostasis did not increase.
- The criterion **thumb pressure** is positive if lividity disappears completely on soft thumb pressure.
- **Complete relocation** is given when all hypostasis shifts down to the newly dependent areas. This may be observed at the scene when a body is turned from a face-down into a supine position.
- In **incomplete shifting**, hypostasis remains in the formerly dependent areas, but it also shifts to a greater or lesser extent to the newly dependent areas.

References

1. Bohnert M, Weinmann W, Pollak S. Spectrophotometric evaluation of postmortem lividity. *Forensic Sci Int*. 1999;*99*(2): 149–58.
2. Fechner G, Koops E, Henssge C. Cessation of livor in defined pressure conditions. Z Rechtsmed 1984;93:238–87.
3. Henssge C, Madea B. Methoden zur Bestimmung der Todeszeit an Leichen. Lübeck, Schmidt-Römhild, 1988.
4. Henssge C, Madea B. Leichenerscheinungen und Todeszeitbestimmung. In: Brinkmann B, Madea B (eds.). Handbuch Gerichtliche Medizin, vol. I. Berlin, Springer, 2004, pp 79–150.
5. Henssge C, Madea B. Estimation of the time since death in the early postmortem period. Forensic Sci Int 2004;144(2–3):167–75.
6. Henssge C, Madea B. Estimation of time since death. Forensic Sci Int 2007;165:182–4.
7. Hunnius PV, Mallach HJ, Mittmeyer HJ. Quantitative pressure measurements of livores mortis relative to the determination of the time of death. Z Rechtsmed 1973;73:325–1244.
8. Kaatsch HJ, Stadler M, Nietert M. Photometric measurement of colour changes in livor mortis as a function of pressure and time. *Int J Leg Med* 1993;106:91–7.
9. Kaatsch HJ, Schmidtke E, Nietsch W. Photometric measurement of pressure-induced blanching of livor mortis as an aid to estimating time of death. *Int J Leg Med*. 1994;*106*:109–214.
10. Knight B. Hypostasis and timing of death. In: Henssge C, Knight B, Krompecher T, Madea B, Nokes L (eds.). *Estimation of the Time Since Death in the Early Postmortem Period*. London, Arnold, 2002, pp 206–8.
11. Madea B. Death: time of. In: Jamieson A, Moenssens A (eds.). Wiley Encyclopaedia of Forensic Sciences, vol. 2. Chichester, John Wiley and Sons, 2009, pp 697–716.
12. Madea B. Time of death determination. In: Jamieson A, Moenssens A (eds.). Wiley Encyclopaedia of Forensic Sciences, vol. 5. Chichester, John Wiley and Sons, 2009, pp 2466–79.
13. Madea B, Henssge C. Timing of death. In: Payne-James J, Busuttil A, Smock W (eds.). Forensic Medicine: Clinical and Pathological Aspects. London, Greenwich Medical Media, 2003, pp 91–114.
14. Mallach HJ. Zur Frage der Todeszeitbestimmung. Berlin Med 1964;18:577–82.
15. Schuller E, Pankratz H, Liebhardt E. Farbortmessungen an Totenflecken. Beitr Gerichtl Med 1987;45:169–73.
16. Patscheider H, Hartmann H. *Leitfaden der Gerichtsmedizin*. 3 Auflage, Huber, Bern, Stuttgart, Toronto, 1993.
17. Suzutani T, Ishibashi H, Takatori T. Studies on the estimation of the post-mortem interval. 2 The post-mortem lividity. Hokkaido Zasshi 1978;52:259–67.
18. Vanezis P. Assessing hypostasis by colorimetry. Forensic Sci Int. 1991;52:1–3.
19. Vanezis P, Trujillo O. Evaluation of hypostasis using a colorimeter measuring system and its application to the assessment of the post-mortem interval (time of death). Forensic Sci Int 1996;78:19–28.

6 Post-mortem Body Cooling and Temperature-Based Methods

Claus Henssge

Contents

6.1 Basics and Application of the 'Nomogram Method' at the Scene 79
  6.1.1 Scientific Investigation of Experimental Body Cooling under Controlled Conditions 79
    6.1.1.1 Basic Conditions 79
    6.1.1.2 Cooling Dummy 80
    6.1.1.3 Heat Exchange to Surroundings 80
    6.1.1.4 Heat Flow Measurements on Body Surfaces 82
    6.1.1.5 Rectal Temperature Probe Sites 84
    6.1.1.6 Mathematically Modelling the Rectal Cooling Curve by the Two Exponential Formulae of Marshall and Hoare 85
    6.1.1.7 The Individual Value of the Constant *B* (The Newtonian Cooling Coefficient) 86
    6.1.1.8 Body Cooling in Constantly, Even Slightly Moving, Air 92
    6.1.1.9 The Cooling of Clothed Bodies 92
    6.1.1.10 Clothed Bodies in Moving Air 92
    6.1.1.11 Covered Bodies in Still Air 92
    6.1.1.12 Body Cooling in Still Water 92
    6.1.1.13 Body Cooling in Flowing Water 94
    6.1.1.14 Body Cooling in Cases of Wet Clothing or Covering, or Unclothed Wet Body Surface 95
    6.1.1.15 Investigations on Dummies 96
    6.1.1.16 Influence of the Type of Supporting Base on Body Cooling 99
    6.1.1.17 The Individual Value of the Plateau-related Constant *A* 101
    6.1.1.18 The Temperature at Death 103
    6.1.1.19 Accuracy of Calculated Time Since Death 104
    6.1.1.20 How Is the Death Time Obtained? 107
  6.1.2 Application of the 'Nomogram Method' in Casework 116
    6.1.2.1 Evaluation of the Mean Ambient Temperature 118
    6.1.2.2 Evaluating the Corrective Factor 121
    6.1.2.3 Known Changes of Cooling Conditions 123
    6.1.2.4 Uncertainty in the Value of Corrective Factors 123
    6.1.2.5 When the Method Must Not Be Used 124
    6.1.2.6 Special Problems 125
    6.1.2.7 Accuracy of Calculated Time Since Death 126
    6.1.2.8 Reconstruction of Body Cooling 129
    6.1.2.9 Investigation of Central Brain Temperature 129
    6.1.2.10 Combined Brain and Rectal Temperatures 130
6.2. Finite Element Method in Temperature-Based Death Time Determination 132
Michael Hubig, Holger Muggenthaler, Gita Mall 132

  6.2.1 Introduction: Physical Methods in Temperature-Based Death Time Determination 132
  6.2.2 The Physics of Body Cooling 133

DOI: 10.1201/9781003244974-6

6.2.2.1 Heat Transfer Mechanisms 133
6.2.2.2 Differential Equation of Heat Transfer 136
6.2.3 Solving the Heat Equation 137
6.2.3.1 The Finite Element Method 137
6.2.3.2 Implementation of the Finite Element Method 140
6.2.4 The Body Cooling Finite Element Model 140
6.2.4.1 Mapping the Cooling Scenario: Geometry 140
6.2.4.2 Thermodynamical Properties of Biological Materials 141
6.2.4.3 Starting the Cooling Process: Initial Conditions 142
6.2.4.4 Connecting the Cooling Process to the World: Boundary Conditions 143
6.2.4.5 Reconstructing Time Since Death 143
6.2.5 Model Validation 146
6.2.5.1 Comparison to the Model of Marshall and Hoare 147
6.2.5.2 Comparison to Real Body Cooling 147
6.2.6 FE Error Analysis 149
6.2.7 Application Examples 150
6.2.7.1 Case A 150
6.2.7.2 Case B 150
6.2.7.3 Case C 151
6.2.7.4 Case D 151
6.3 The Prism Method 152
Stefan Potente *152*

6.4 The Use of Temperatures Recorded from the External Auditory Canal for the Estimation of the Post-mortem Interval 162
Guy Rutty

6.4.1 Introduction 162
6.4.2 Anatomy of the External Ear 163
6.4.3 Human Thermoregulation 163
6.4.4 Ear Thermometry 165
6.4.4.1 Clinical Infrared Thermometry 165
6.4.4.2 Problems with Clinical IT Readings 166
6.4.5 Early Human Cadaveric Experimental Data 167
6.4.6 Cadaveric Animal Experimental Data 168
6.4.7 Human Cadaveric Experimental Data 169
6.4.8 Variables That Could Influence a PMI Calculation 175
6.4.9 Application in Practice 176
6.4.10 Summary 177
6.5 Eye Temperature and the Time Since Death 181
Michał Kaliszan *181*

6.5.1 Introduction 181
6.5.2 Method of Temperature Measurement and TSD Calculation 181
6.5.3 Limitations of the Method 185
6.5.4 Application in Practice 185
6.5.4.1 Case 1 185
6.5.4.2 Case 2 185
6.5.4.3 Case 3 186
6.5.4.4 Case 4 186

6.1 Basics and Application of the ‘Nomogram Method’ at the Scene

■ *Claus Henssge*

The main topic of this chapter is the rectal temperature ‘nomogram method’ for determining the time of death, which was developed for practical use at the scene of death. It provides a time range immediately at the scene, and it may considerably assist criminal investigations at their earliest stage. Beyond that, evidence may be provided regarding the guilt or innocence of a suspect as a result of the denial or corroboration of an alibi.

The main object is to be able to use the method in a wide spectrum of casework. For that purpose, the circumstances at the scene of death must be analysed thoroughly and the findings taken into account. This process requires personal experience. Additional rapid methods used at the scene are helpful for reducing the range of the interval limited by the nomogram, and these methods are described in Chapter 10.

Chapter 6.1 is divided into two main sections. The first section discusses basic physical considerations, including mathematically modelling body cooling by two exponential equations and verifying them on experimental body and dummy cooling under various controlled conditions. The second section describes the practical means of applying the nomogram method in casework, with references to the first section where essential.

6.1.1 Scientific Investigation of Experimental Body Cooling under Controlled Conditions

6.1.1.1 Basic Conditions

Body cooling results from non-stationary heat conduction inside a body of low thermal diffusivity.

1. With failure of circulation, convectional transport of heat inside the body ceases. (In hanged bodies, hypostasis could theoretically distort rectal temperature by warm blood descending from above, but this has no practical significance.)
2. Exchange of heat between the core and the surface of the body takes place only by conduction. Heat transfer inside the body by radiation and convection is negligible.
3. The post-mortem rate of heat production is very low. Heat is produced mainly by anaerobic glycolysis, which is ongoing for about the first 10 hours post-mortem, in a non-linear fashion. Lundquist [37] calculated roughly that heat release per gram of glycogen was 0.4 kcal, so the glycogen store of the body (350 g) corresponds to 140 kcal heat release. A body of about 70 kg and a specific heat of 0.8 kcal/kg would be heated by 2.5°C over the first 10 hours after death. With that, one-sixth of the post-mortem temperature plateau could be explained as a rough estimation. The rate of heat release from autolysis and putrefaction is even lower during the early post-mortem phase of cooling the body to ambient temperature so that its influence on cooling is negligible. Fulminant putrefaction in the early post-mortem period may markedly decelerate the cooling.
4. The thermal diffusivity of body tissues is much lower than that of metals. (Thermal diffusivity of water is 0.00143; that of fat is 0.001; and that of aluminium is 1.0 [10^{-4} m^2 per s^{-1}]. Note the small difference between water and fat.) Given its lower thermal conductivity, fat conducts heat more slowly than muscle. Because of its lower specific heat and specific weight, the fall in temperature is greater when leaving a hotter object. Because the thermal diffusivity is the quotient from thermal conductivity and specific heat times specific weight, only a small difference results between water and fat (e.g. [51]).
5. The cooling of a body is nearly ‘non-stationary’ and unsteady. As a consequence, the ‘thermal diffusivity’ is the measure of any heat transfer inside the body, but not the ‘thermal conductivity’.
6. The body is not ‘thermally thin’.
7. Newton’s law of cooling is not adequate to describe the cooling curve of any central probe site.
8. With the start of cooling, a temperature gradient develops from the surface to the core of any part of the body.
9. First, heat is lost from the most superficial layers of the body, whereas the deeper layers are initially unaltered. Because of the low velocity of heat transport inside the body, it takes some time for heat to be conducted from the deeper layers to the more superficial (colder) layers, until, eventually, the temperature gradient reaches the core.
10. The temperature gradient has an almost radial direction. The cooling curve of any central temperature probe site has a sigmoidal shape, with the physically determined ‘postmortal temperature plateau’ occurring during the first cooling phase.

6.1.1.2 Cooling Dummy

Any solid body consisting of a substance of low thermal diffusivity and without significant heat release cools in the same manner. Thus, a body configured like a human trunk, consisting of a layer of coated material or caoutchouc (natural rubber) and filled with a gel mixture of glycerine (47.5 per cent), water (47.5 per cent) and agar (5 per cent) (Figure 6.1) provides cooling curves that resemble those of cadavers, including the plateau (Figure 6.2). Similarly, the two exponential equations (see Equation 6.14), although investigated empirically on dead human bodies, also apply to the dummy (Figure 6.3). This is because of the similar thermal diffusivity and the similar relationship between surface area and volume of both dead human bodies and dummies. Therefore, a dummy cools under controlled conditions as does a cadaver of a specified body weight, depending on its cross-sectional dimensions (Table 6.1 and Figure 6.4.) The conformity of cooling curves of bodies and dummies has been confirmed in numerous experiments conducted under different conditions (see Figure 6.18). Therefore, in test cooling, dummies can replace bodies [20,29,30,35,41,53,56].

6.1.1.3 Heat Exchange to Surroundings

The actual mechanisms of heat exchange between body and surroundings (conduction, convection, radiation, evaporation) depend on the individual circumstances at the scene and therefore cannot be stated in generally valid terms for any cooling conditions.

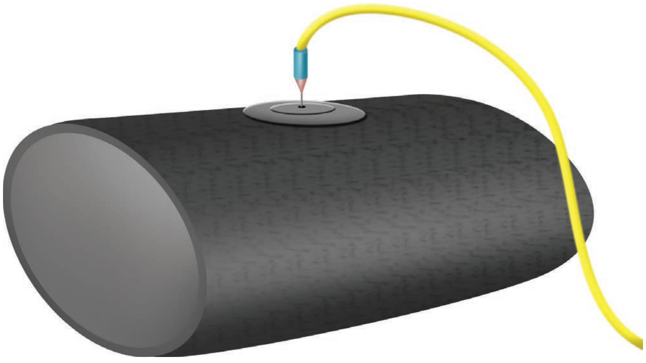

Figure 6.1 Example of a cooling dummy. The 1.5-m m-thick wrap is made of caoutchouc. It is filled with a gel mixture (Wirodouble, BEGO, Bremen, Germany: 47.5 per cent glycerine and water, 5 per cent agar) at 90°C, at which it is molten. At lower temperatures the consistency becomes solid and elastic. The dimensions are 19 cm (sagittal), 38 cm (transverse) and 50 cm (longitudinal). The real weight is 31 kg. The temperature probe is inserted in the middle, 9.5 cm deep, corresponding to half of the sagittal diameter.

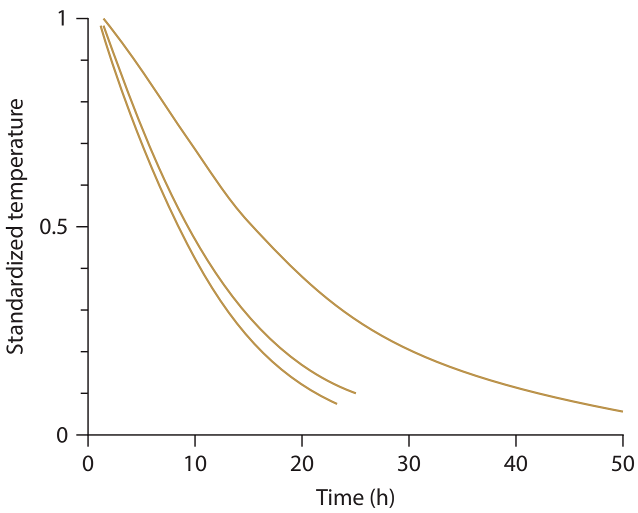

Figure 6.2 Cooling curves of two different-sized dummies. Abscissa: time (hours) after taking the 37°C heated dummy out of the incubator. Ordinate: standardized temperature (central temperature of the dummy—ambient temperature) divided by (37°C—ambient temperature). Each of six test coolings occurred under chosen standard conditions at each of three different places in nearly constant ambient temperatures between 0.1°C and 14.1°C. The upper cooling curves are as good as the curve of a 73-kg body, and the lower curves are as accurate as the curve of a 42-kg body when cooling under comparable 'standard' conditions. Even the 'postmortal temperature plateau' is equally developed. The model curves of a 73-kg body and a 42-kg body computed according to Equation 6.14 would fit into the middle of each of the six curves (see Figure 6.3).

Conductive heat exchange results from the temperature difference between the body and the surroundings, from the intermediate material between the body surface and the surroundings (e.g. clothing, covering) and from the surrounding medium (e.g. water, air). At the contact zones of the body with the supportive surface, conductive heat exchange plays the decisive role. The heat capacity and the thermal conductivity of the supporting surface must be noted (see Figures 6.19–6.21).

At non-contact areas of naked bodies, the convectional mechanism of heat exchange dominates, even without forced convection such as wind. In the case of a naked body, the heat exchange at the non-contact surface usually exceeds that of the contact surface (see Figures 6.7, 6.8 and 6.22), unless the supporting base conducts heat exceptionally well (see Figure 6.19).

Under standard conditions, heat exchange by radiation is extensive for the first hour post-mortem, but it decreases during the later process of cooling, depending on the rapid decrease in skin temperature [39,40]. However, under special conditions, such as sun radiating on

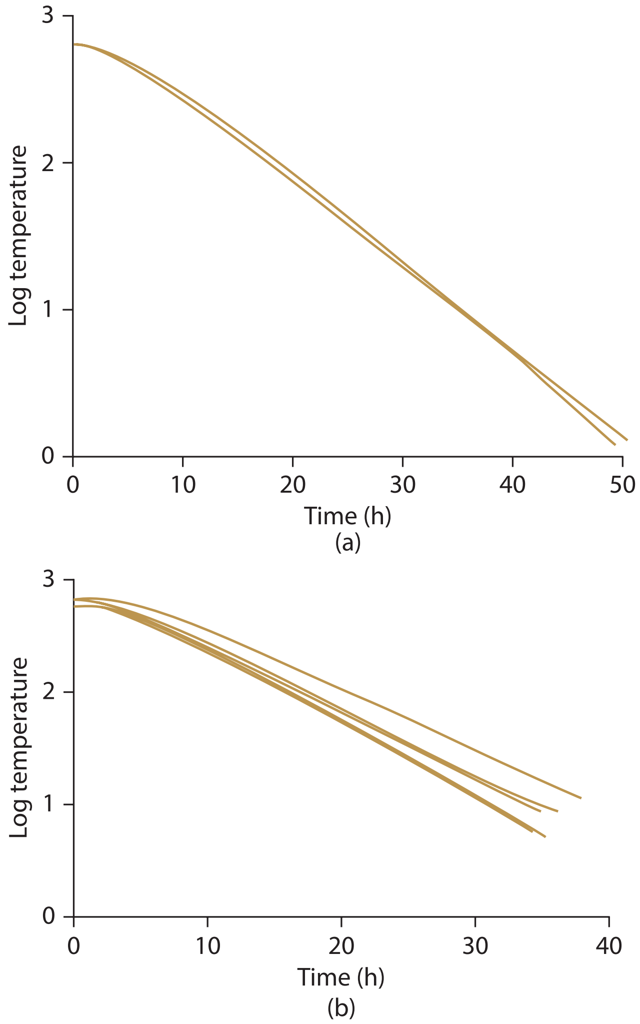

Figure 6.3 Experimental cooling curves of dummies and their modelling by the two exponential equations using the figures of constants investigated on bodies (equations 6.5 and 6.14) 10 years before the dummies were 'born'. Abscissa: time (hours); ordinate: logarithm of (central temperature of the dummy—ambient temperature). (a) Cooling curve of the dummy in Figure 6.1. The 36.5°C heated dummy cooled in a nearly constant mean ambient temperature of 20.1°C. The stars without connecting lines are the original values of measurements. The crosses linked by connecting lines represent the model curve of a 67-kg dead human body. The differences between the real and the model-computed cooling times do not exceed −0.8 to 1.1 hours up to the 40th hour. After this time, the differences increase to 1.8 hours. (b) Experimental cooling and model curves of a dummy and two bodies under identical circumstances. Naked bodies lying on a wooden board in a closed room.

Table 6.1 Mean Radius of Cross Section of Some Different-sized Dummies and the Resulting Body Weight ('Virtual Weight') Calculated from the Newtonian Coefficient *B* of the Cooling Curves According to Equation 6.3 (see Figure 6.4)

Real weight (kg)	Mean radius (mm)	Virtual weight (kg)	Wrap
0.70	42.8	6.9	0.5-mm-thick
1.02	49.6	14.3	PVC-coated
2.82	67.8	17.3	material
3.35	78.1	32.8	or
8.20	110.9	36.8	0.5-mm-thick
10.00	115.6	38.0	transparent
21.80	152.9	64.8	PVC foil
22.00	152.9	66.5	
27.50	161.2	72.5	
24.00	162.3	72.4	
25.00	162.3	76.5	
31.00	177.0	67.0	1.5-mm-thick caoutchouc

Abbreviation: PVC, polyvinyl chloride.

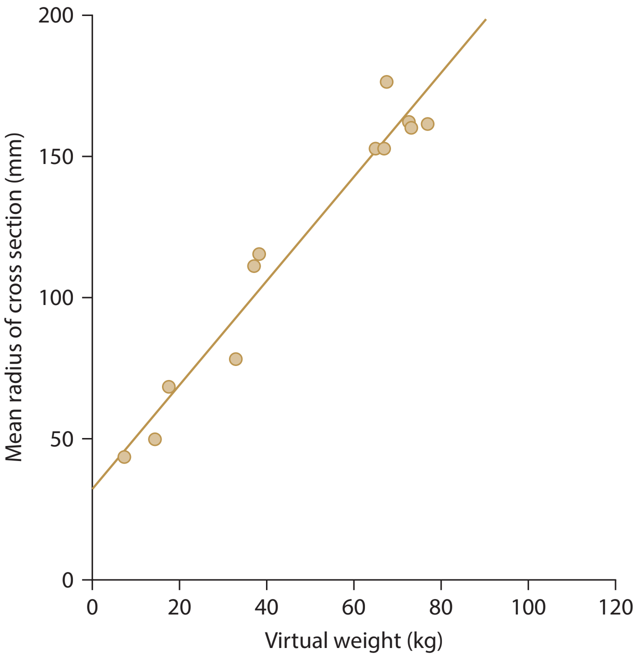

Figure 6.4 Close relationship between mean radius of cross section and 'virtual weight' of some different-sized dummies (see Table 6.1). The virtual weight results from the Newtonian coefficient *B* of the cooling curves set in Equation 6.3.

the body, the net exchange of heat between body and surroundings is influenced to a large degree. There are no reports about this in the literature.

The loss of heat from the dry surface of the body by evaporation does not have any significant influence on cooling. The loss of heat would correspond to 580 kcal/l of evaporated water. The weight of the body does not diminish during the early post-mortem interval to such an extent that considerable acceleration of cooling would result from such fluid loss.

	Uppermost body	Intermediate body	Lowest body
Ambient temperature (°C)	19.5	20.5	20.6
First measurement (hpm)	3	1	0
°C	35.7	37.6	36.5
Real body weight (kg)	80.8	67.0	—
Calculated body weight (Equation 6.3)	78.0	69.8	64.6
Cooling coefficient	−0.0558	−0.0618	−0.0663

Abbreviation: hpm = hours post-mortem.

Noting the almost radial direction of heat conduction inside the body, it is essential to take into account which parts of the body contribute to total heat transfer.

6.1.1.4 Heat Flow Measurements on Body Surfaces

By using new, highly sensitive heat flow sensors (HY-CAL Engineering Sensable; Santa Fe Springs, California; types used: BI-6 and LO-6) (Figure 6.5), the heat exchange on both the contact and the non-contact surfaces can be investigated in combination with superficial and central temperatures (Figures 6.6–6.8). Using the analogy of Ohm's law, the heat flow corresponds with the power of an electric current. With the temperature measurements corresponding to the voltage, the resistance can be calculated as the third, but unknown, quantity of Ohm's law. Thus, a complete circuit of the heat exchange between body and environment can be established (Figure 6.9). Heat flow measurements on body surfaces support the incorporation of influencing factors of body cooling such as clothing, wetness or supporting surfaces [35,41,56].

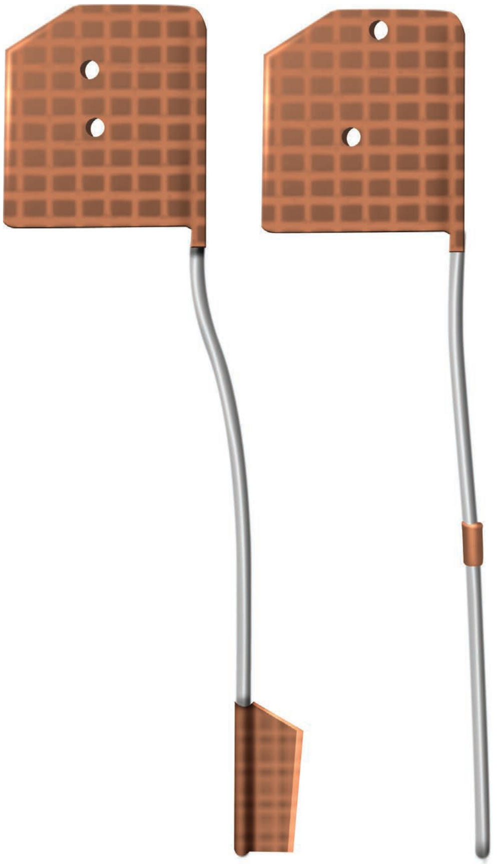

Figure 6.5 Heat flow sensor. The active thermoelectric sensor transduces the whole absorbed or emitted heat flow of a surface area into a voltage. The sensitivity of the two sensors was 149 and 46 mV per 500 Btu ft^{-2} h^{-1}. The range of measurements was limited from minus to plus 11.38 Btu ft^{-2} h^{-1} and the discrimination was set to 0.01 Btu ft^{-2} h^{-1}. Into each heat flow sensor a thermocouple (10 mV/°C) is integrated to measure the surface temperature beside the heat flow. The gauge can be attached easily using double-sided tape.

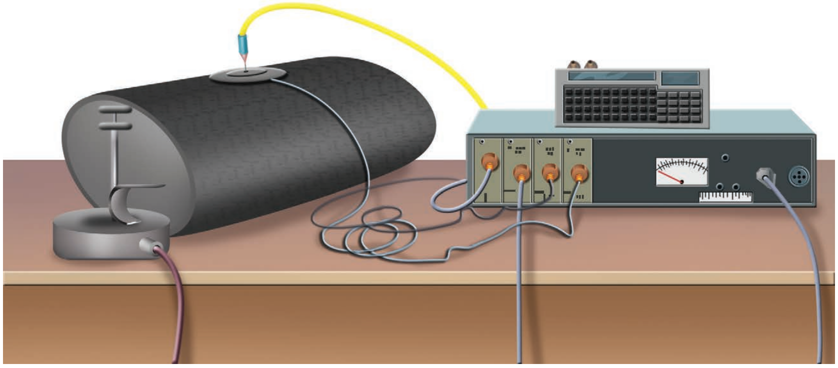

Figure 6.6 Experimental arrangement for measurements of ambient temperature (air and base), the central temperature of the dummy, surface temperatures and heat flow on both the contact and non-contact surfaces. To control and store the seven automatic measurements, the handheld computer HP 71B is used. This picks up the measurements in optional intervals from the data logger at the right. After the programmed end of measurements the HP 71B is connected to a plotter, a printer and a digital cassette drive. To analyse the data, special algorithms corresponding to the given equations are used. Development of the device including construction of the probes, integration of thermocouples into the heat flow sensors (seen in Figure 6.5) and calibration: BMT Messtechnik GmbH—Dr Ing F. Wallner, Berlin.

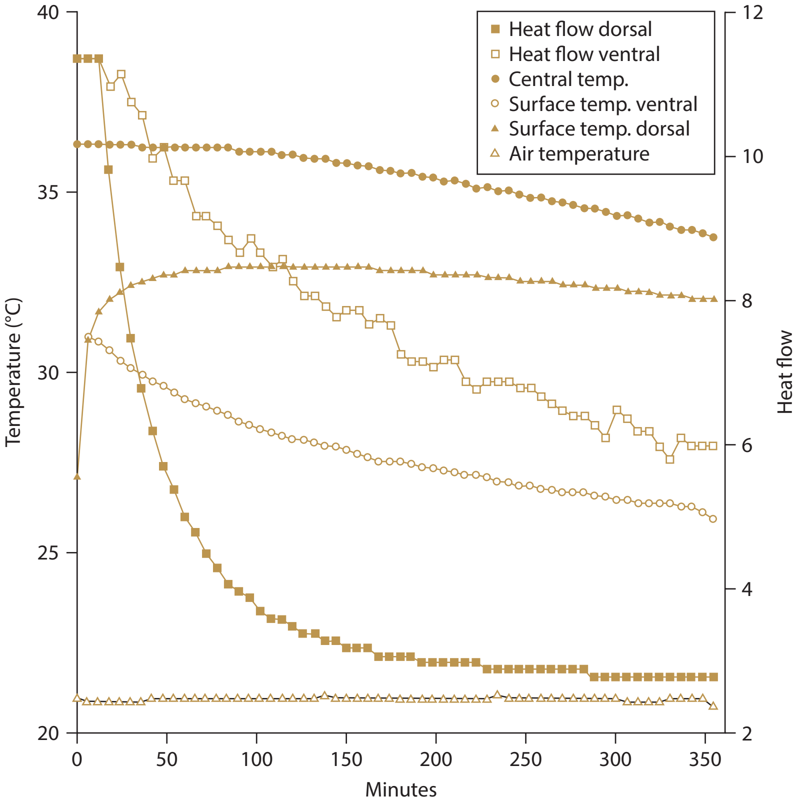

Figure 6.7 Heat flow measurements on the surfaces of the dummy of Figure 6.6. Central temperature, ventral (non-contact) and dorsal (contact), both surface temperatures and heat flow curves of a 36.5°C heated dummy during the first 6 hours of cooling in still air of 21°C. The supporting base was a wood board 2 cm thick. Left ordinate: temperature (°C); right ordinate: heat flow Btu ft^{-2} h^{-1}. Abscissa: cooling time (min). Interval of measurements: 6 minutes. The initially great heat flow at the contact surface (dorsal) heats the base quickly (see the curve of dorsal surface temperature). The subsequent very low dorsal heat flow is combined with a very slow decrease of the dorsal surface temperature, indicating that the wood board has a low thermal conductivity. The curves of ventral heat flow and surface temperature initially show the heating of the bound layer, and afterwards, with the start of thermic air movement (convectional heat exchange), the greater heat loss combined with a steeper fall of the ventral surface temperature compared with the dorsal surface. Note the more irregular curve of the ventral ('naked') heat flow in comparison with the dorsal flow.

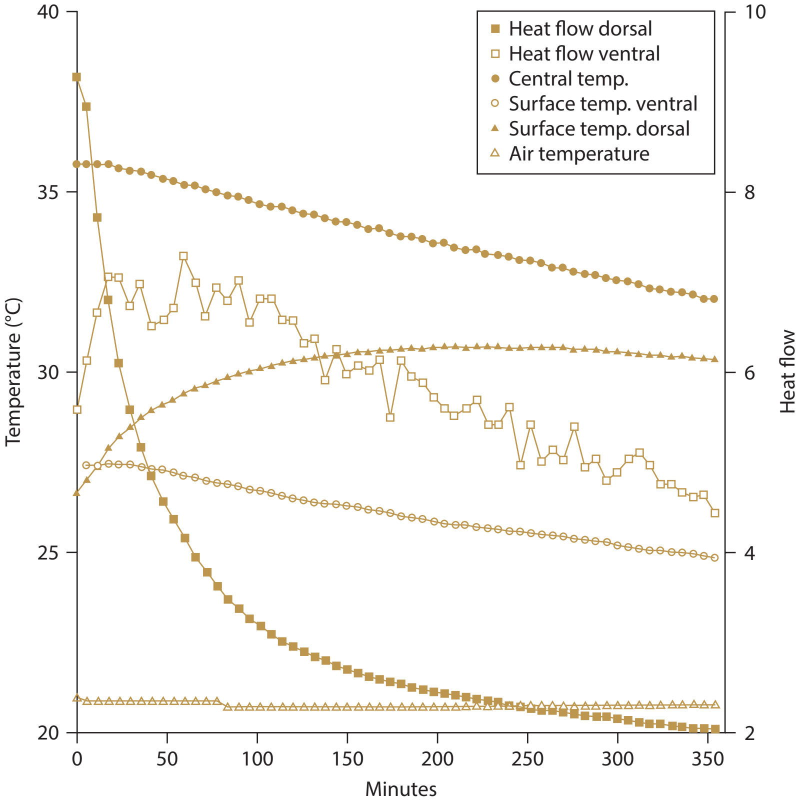

Figure 6.8 Heat flow measurements on the surfaces of a body. Rectal and ambient temperatures, dorsal and ventral surface temperatures and heat flows of a naked 69.5-kg body lying on a wood board 2 cm thick in still air at 20.7°C. Left ordinate: temperature (°C); right ordinate: heat flow (Btu ft^{-2} h^{-1}). Abscissa: cooling time after the start of measurements 3.1 hours post-mortem with a rectal temperature of 35.8°C. Interval of measurements 6 minutes. Considering the death time of 3.1 hours at the beginning of measurements with advanced post-mortal plateau, the curves agree well with those of the dummy in Figure 6.7. The more irregular curve of the ventral heat flow curve is apparent, indicating that it is unsuitable for short interval analysis, at least on naked surfaces.

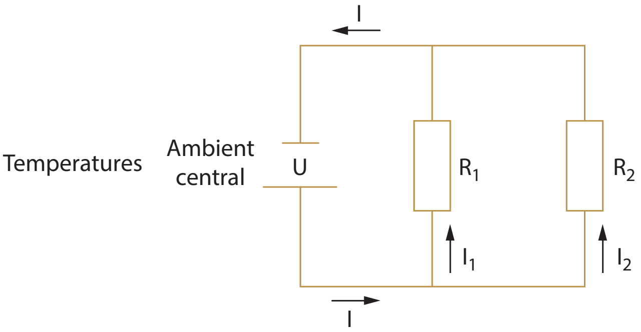

$$R = \frac{U}{I} = \text{Resistance} = \frac{\text{Difference temperature}}{\text{Heat flow}}$$

Figure 6.9 Circuit of heat exchange between body and environment analogous to Ohm's law. Calculating both the total and the parts of resistance (R_1, R_2) and flow (I_1, I_2) at lying and non-lying surfaces, the parts of their surface areas must be taken into account.

6.1.1.5 Rectal Temperature Probe Sites

Keeping the non-stationary heat conduction inside a body of low 'thermal conductivity' in mind, the time course of any body temperature depends first of all on the temperature probe site. Because surface temperatures may be susceptible even to transient, minute alterations of the actual cooling circumstances, they seem to be unsuitable for measuring 'the' body temperature. (The measurement of surface temperatures is problematic [e.g., Newitt C, Green MA. J *Forensic Sci Soc* 1979;**19:**179–181]. In addition, surface temperatures approach the ambient temperature more quickly and complicate the procedure once more.) At present, the deep rectal temperature and central brain temperature are the most thoroughly investigated probe sites. Because of the greater radius of the trunk compared with the radius of the head, the cooling curve of the rectal temperature probe site has a shallower slope and therefore gives information about the time since death over a longer post-mortem interval than the steeper cooling curve of the brain. Conversely, in general, the steeper the cooling curve, the more exact the calculated time since death will be. Therefore, temperature probe sites on different parts of the body having a different radius are not alternative methods but can complement each other (e.g. brain and rectal probe site [28] as well as multiple probe sites).

Besides the location of the temperature probe, another question should be discussed: the infliction of injuries by measuring brain temperature and the disturbance of traces such as semen during measurement of rectal temperature. The injuries caused by central brain temperature measurements are minute and discernible [6,7,26,49].

The disturbance of traces by rectal temperature measurement can be avoided by taking a swab before inserting the temperature probe into the sphincter. The securing of micro-traces by the criminal investigators must be finished before any removal of the clothing or cutting through the crotch area of trousers can be done. Co-operation is required with other investigators to avoid conflict of interests.

In my opinion, the rectal probe site provides the most reliable determination of the time since death, compared with other probe site measurements.

Nevertheless, there is some discussion concerning the exact probe site in the rectum. Joseph and Schickele [34] suggested that variation of the exact location of thermometers in the rectum from body to body (and from one experiment to another) could explain the wide variation of Marshall and Hoare's cooling curves [42–44]. They criticized the rectal probe site for not being at the centre of the body, and they proposed a convenient standardized location—a more defined point 2.5 cm (1 inch) above the symphysis—at which the thermometer would be inserted through an incision to a depth half the distance of the anteroposterior diameter. However, this impracticable procedure could cause injury (e.g. of the bladder, possibly followed by an outflow of urine into the peritoneal cavity).

The site of a straight, non-flexible probe inserted at least 8 cm inside the anal sphincter [42–44] is in fact not at the centre of the lower trunk but at a level corresponding to the junction between the posterior third and anterior two-thirds of the anteroposterior diameter of the trunk, at a longitudinal level that is not defined exactly [31]. If a straight, non-flexible probe is inserted deep into the rectum via the anal sphincter without undue force, a convenient standardized point is given; a great variation of the so-called location factor (by Joseph and Schickele) from body to body is not of practical significance, in our opinion.

Hiraiwa et al. [32] analysed the location of the rectal probe by computed tomography in ten patients after inserting the thermometer about 10–15 cm beyond the anus close to the anterior wall of the sacrum. The ratio of the length between the centre of the rectum and the middle of the back to the distance between the surface of the lower abdomen and the middle of the back was found to have a mean of 0.27. Our own simple measurements of the sagittal and transverse diameter of the lower trunk at the level of the greater trochanter and the anterior inferior iliac spine (corresponding to the actual level of a straight rigid temperature probe when inserted via the anus into the rectum as deep as possible without resort to force) resulted in ratios between 0.42 and 0.47, depending on whether the insertion was more ventral or more dorsal.

Standardization of the temperature probe site is absolutely necessary and is much more important than its exactly central location. All experience of death time estimation from body cooling is limited to a distinct probe site. Experience can be extended more by systematic measurements based on a few standardized probe sites than by a surfeit of 'new' temperature probe sites. I therefore decided to adhere to Marshall and Hoare's procedure [42–44], including the rectal probe site, as described earlier, when I started my studies of body cooling in 1975.

The rectal temperature and the ambient temperature were measured online by an electronic device within an accuracy of 0.1°C.

6.1.1.6 Mathematically Modelling the Rectal Cooling Curve by the Two Exponential Formulae of Marshall and Hoare

In 1962, Marshall and Hoare [42–44] published a formula for modelling rectal body cooling mathematically by using different notation:

$$\begin{aligned} Q &= \frac{Tr - Ta}{To - Ta} \\ &= A \times \exp(B \times t) + (1 - A) \times \exp\left(\frac{A \times B}{A - 1} \times t\right) \end{aligned} \tag{6.1}$$

where Q is the standardized temperature; Tr is the rectal temperature at any time t; To is the rectal temperature at death ($t = 0$); Ta is the ambient temperature; A is the constant; B is the constant; and t is the time of death.

There are two exponential terms: the first (with the constant B as exponent) expresses the exponential drop of the temperature after the plateau according to Newton's law of cooling (Figure 6.10). The second (with the constant A as a part of the exponent) describes the 'post-mortal temperature plateau'.

The formula by Marshall and Hoare is the ultimate success in modelling body cooling for the purpose of estimation of the time since death. The formula requires only two constants besides the body temperature at death, but it nevertheless provides a sufficient mathematical description of real cooling curves of different parts of the body (e.g. rectum, brain), as well as of the cooling dummy. As demonstrated by Brown and Marshall [8], more than two exponential terms complicate the model without improving results.

Although there are some difficulties in identifying the individual values of the only two constants in any specific case, the solution is not to look for a better model, but rather for the best way to identify the individual values of the constants A and B. They depend on the body build and the ambient cooling conditions, including the thermal factors on the surface of the body. Besides great variation of body build, the cooling conditions at the scene may vary over a wide range. In addition, some of the actual influencing factors at the scene may be unknown to the forensic pathologist. Furthermore, the ambient conditions can change between the time of death and the time of investigation. The question of identifying the representative values of the required constants seems to be insoluble.

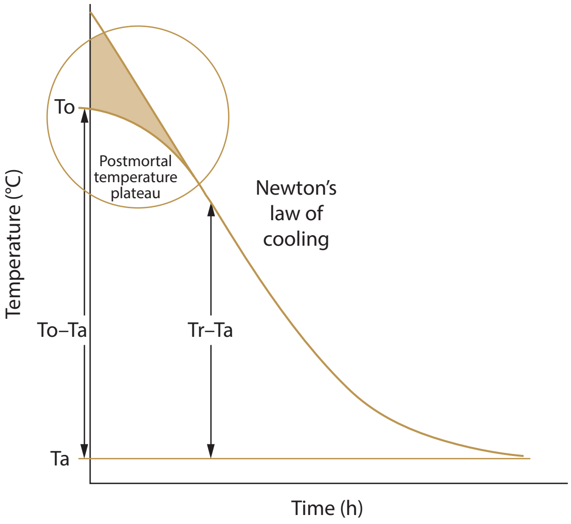

Figure 6.10 Sigmoidal shape of cooling curve. A single exponential term such as Newton's law of cooling is insufficient to describe this mathematically. The two-exponential term (Equation 6.1) of Marshall and Hoare provides a close mathematical description. The quotient Tr-Ta/To-Ta (standardized temperature) is a good measure of the progress of cooling.

First, we must accept that the problem cannot be solved in all cases. Second, we must accept that the problem cannot be solved *exactly* in many cases. However, we can at least *approximate* the value of the required constants.

There are two different ways to identify the individual values of the constants. The first is to estimate the values by analysing the whole experimental cooling curve. Then we can decide whether a short part of the cooling curve is able to give representative values of the constants for the whole curve. The second way uses the effect of the constants on whole cooling curves, as a means to find rules approximating the representative individual values of the constants indirectly by taking the most important features of body build and ambient cooling conditions into account.

Theoretically, both ways have some inherent advantages and disadvantages. The decision whether the first or the second way is better can only be made under the conditions of practice at the scene in many cases.

Although the formulae of Marshall and Hoare validate the earlier observation of Rainy in 1868 [48] that bodies would cool more slowly in the first phase after death than expected by Newton's law of cooling, and even though the excellent papers of Marshall and Hoare gave an adequate and easily applied mathematical expression of post-mortem cooling, including the post-mortal plateau, progress concerning their application to the important field of forensic practice was incomprehensibly insignificant. Instead, for example, pathologists continued to use simplistic methods such as the rule of thumb that bodies would cool 1°C per hour: this persisted as if Rainy [48] and Marshall and Hoare [42–44] had not existed. Only James and Knight [33] reported errors in estimating the time since death in coroners' cases, and Prokop [47] stated that Marshall and Hoare's data would be much more useful than the earlier data of Schwarz and Heidenwolf [50], who produced a sigmoidal curve of rectal body cooling in 1953.

As has been said, the main question is to identify the individual values of the constants *A* and *B* in individual cases at the scene where the circumstances do not allow extensive measurements. The constant *B* has greater significance for the reproduction of the cooling curve from the measurement at the scene to the moment of death because it describes the cooling rate for as long as there is a difference of temperature between the body and the ambient. In comparison, the constant *A* is of less significance; it expresses the relative duration of the plateau phase and ceases its function after that. Both these constants are discussed here.

6.1.1.7 The Individual Value of the Constant *B* (the Newtonian Cooling Coefficient)

6.1.1.7.1 Estimation of *B* by Multiple Temperature Measurements

The individual value of *B* can be exactly computed by a linear regression line with time *t* (hours) as the independent variable (*X*) and logarithm of temperature difference between rectum and ambient ln $(Tr - Ta)$ as the dependent variable (*Y*) of the cooling curve after the plateau (Figure 6.11 [c]). The exact estimation of *B* as the slope of the regression line (regression coefficient b_{yx}) requires a long period of temperature measurements after the plateau, without any change of the cooling conditions (including constant ambient temperature). The more slowly the body cools (e.g. high body weight, covering with thick clothing or bedclothes), the more the requirement has to be met. Shorter periods of temperature measurement of the order of 1–4 hours and/or actual changes of the cooling conditions shortly before or during the measurements may result in erroneous values of *B*. The inability to estimate reliably the representative cooling rate *B* to the whole period between death and time of investigation by multiple temperature measurements within a few hours at the scene is the main reason that these methods give unsatisfactory results in estimating the time since death (Table 6.2).

Without any question, it would be an important breakthrough, similar to that of Marshall and Hoare [42–44], to obtain a measurement of the individual slope of the temperature drop of any case, instead of evaluating it indirectly from the 'size factor' [42–44], or the body weight with 'corrective factors' for particular circumstances (nomogram method; see later).

The methods of De Saram et al. [10], Fiddes and Patten [11], Marshall and Hoare [42–44] and Green and Wright [12,13] are based on the principle of measurement of the individual slope, by measuring the temperature at least twice. The most sophisticated method of this type is that published by Green and Wright [12,13].

We therefore examined these methods, especially that of Green and Wright [12,13], on all our experimental material, as well as on the more problematic part of our casework [23].

Experiments on a series of 30 cooling curves of dummies under different, but controlled, constant conditions [36] gave the same results as in body cooling [15]—we obtained worse results than with the nomogram method (see later).

In my opinion, there are three main reasons for these inferior results from multiple temperature measurements:

1. There is only a small decrease in the rectal temperature over an interval of 1–3 or 4 hours, especially in cases of obesity, thick clothing or high ambient temperature: thus, even a small mismeasurement of either one or both rectal temperatures, of the order of 0.1°C, may lead to a relatively large error in the cooling rate. In computing the time of death, this small error in the rate is multiplied and may result in a large error in the calculated time of death. To reduce this source of error, Marshall and Hoare [42–44], recommended taking the second measurement 3 or 4 hours apart. To avoid any inaccuracy of the rate by small mismeasurements, Green and Wright [12,13] used, in addition to a double measurement, an 11-fold measurement of the rectal temperature, with measurements taken at intervals of 6 minutes over a period of 1 hour for computing a regression line, but without success, as demonstrated by the experiments of Koppes-Koenen [36].
2. The actual measured rate of the decrease in rectal temperature is valid only for the cooling conditions during the period of measurement. When the cooling conditions[*] —including the ambient temperature—

---

[*] Common situations at the scene: a thick bedspread was taken off the body; the ambient temperature is changed by the investigators opening windows and doors or using special lamps, which generate heat, or by the sun rising and shining on the body. Such changes can occur before the temperature measurements of the body can be made.

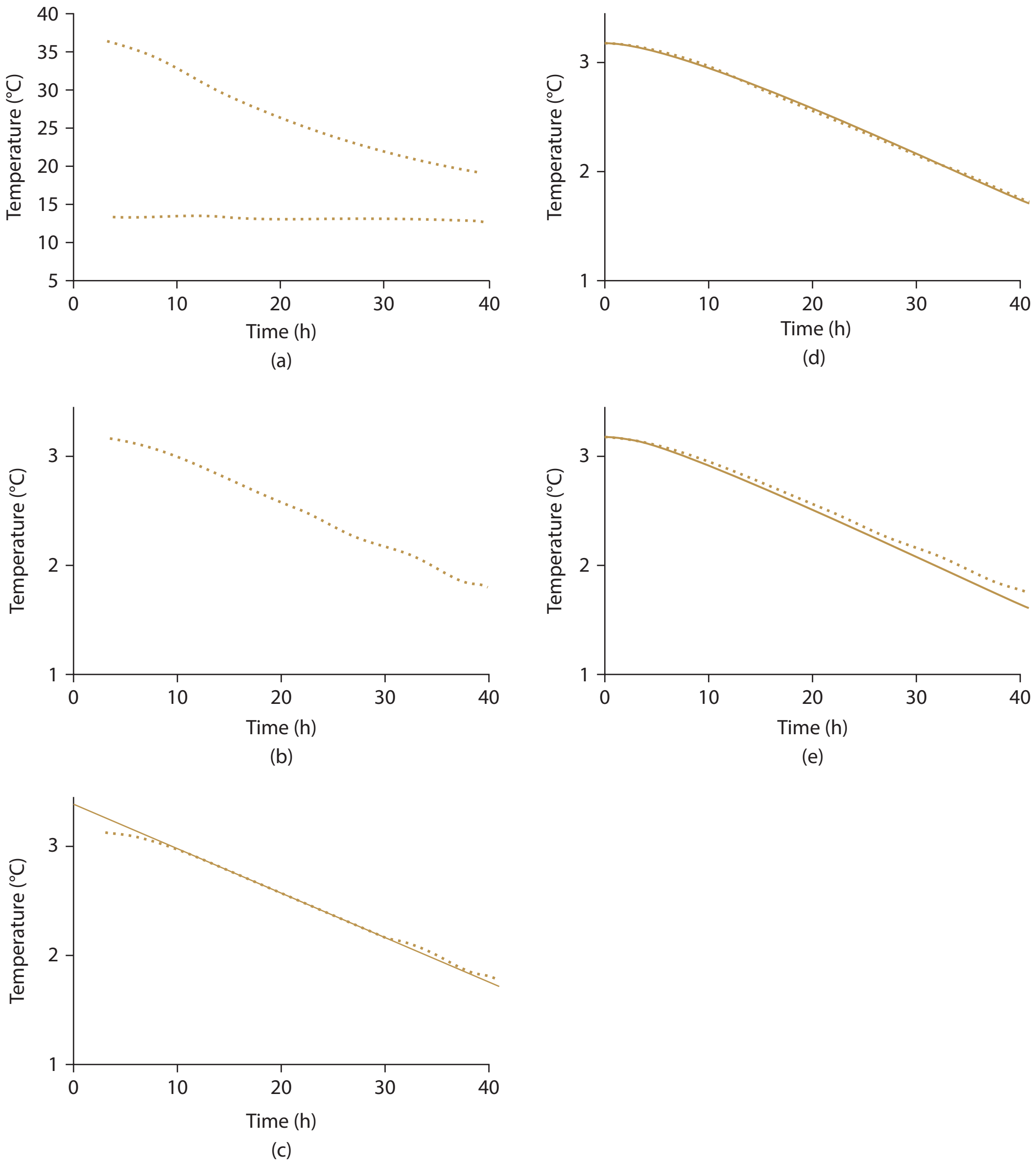

Figure 6.11 The cooling of a body and its modelling. Hourly measurements of rectal (*Tr*) and ambient (*Ta*) temperatures from the beginning of the third hour post-mortem of a naked body of 99.5 kg lying extended on the back on a thermally indifferent base in a closed room. Abscissa: time since death (t) in hours; ordinate: temperature (°C). Compare with Table 6.2. (a) Data points of rectal and ambient temperatures in linear measures. The mean of the ambient temperature is 13.3°C (*Ta*). (b) Logarithm of temperature differences 'rectal–ambient'. There is apparently a linear relationship between 'time' and 'ln temperature difference' from the 8th to the 28th hour post-mortem. (c) Regression line 'time' (X) against 'ln temperature difference' (Y) computed from the data points between the 8th and the 28th hour post-mortem: $\ln(Tr - Ta) = a_{yx} + b_{yx} \times t$. Regression coefficient $b_{yx} = \mathrm{B}$ (slope) $= -0.0408$ 'Newtonian cooling coefficient'. Intercept $a_{yx} = \ln(Tr - Ta)$ at $t_0 = 0 = 3.3677$; $\exp(a_{yx}) = 29.01$(°C). Correlation coefficient $r = 0.9996$. (d) Model curve according to Equation 6.2. $\mathrm{B} = -0.0408$ as computed from all the data points between the 8th and the 28th hour; therefore called 'direct examined B'. $A = 1.25$ as an empirically investigated constant. $To = 37.2$°C as a chosen constant; $Ta = 13.3$°C. The computed death times are estimations. The errors (see Table 6.2) are caused by the inevitable use of empirically investigated constants (A and T_o) and not by the use of an insufficient model. (e) Model curve according to Equations 6.1 and 6.2. Instead of the use of the real existing figure of B (−0.0408), which can only be known exactly by many hourly data points after the post-mortal plateau and without any tendency change of cooling conditions, $B = -0.0439$ is used as calculated from the real body weight (99.5 kg) according to the empirically investigated Equation 6.2; therefore called 'indirect estimated B'. The real figure of B (−0.0408) would be calculated (Equation 6.2) from a body of 106.6 kg according to Equation 6.3. The difference between the real, direct examined figure of B (−0.0408) and the body weight-related, indirect estimated figure of B (−0.0439) causes additional errors in computation of the time of death (see Table 6.2). The error increases with the progress of cooling, as in this case. This disadvantage yields a great gain for practical application in casework. Now, the time of death can be computed from a single measurement of rectal temperature at any time in the process of cooling.

Table 6.2 The Cooling of a Body and Tts Modelling*

	Real temperatures (°C)		Model error (h)	
Time (h)	Rectal	1n difference	*B* = −0.0408 (Figure 6.11[d])	*B* = −0.0439 (Figure 6.11[e])
0	—	—	—	—
1	—	—	—	—
2	—	—	—	—
3	36.1	3.1274	0.9	0.6
4	35.7	3.1097	0.7	0.4
5	35.4	3.0962	0.2	−0.1
6	35.0	3.0780	−0.1	−0.5
7	34.6	3.0594	−0.4	−0.9
8	34.2	3.0405	−0.8	−1.3
9	33.4	3.0015	−0.5	−1.1
10	32.8	2.9712	−0.6	−1.2
11	32.0	2.9293	−0.4	−1.1
12	30.9	2.8687	0.3	−0.5
13	30.3	2.8341	0.3	−0.6
14	29.7	2.7982	0.2	−0.7
15	28.9	2.7482	0.6	−0.5
16	28.3	2.7090	0.6	−0.6
17	27.7	2.6682	0.6	−0.6
18	27.1	2.6257	0.7	−0.6
19	26.5	2.5813	0.8	−0.5
20	26.1	2.5506	0.6	−0.8
21	25.7	2.5189	0.4	−1.1
22	25.1	2.4693	0.7	−0.9
23	24.7	2.4349	0.5	−1.1
24	24.1	2.3809	0.9	−0.9
25	23.7	2.3432	0.8	−1.0
26	23.5	2.3238	0.3	−1.5
27	22.9	2.2633	0.8	−1.2
28	22.5	2.2208	0.8	−1.2
29	22.3	2.1989	0.4	−1.7
30	21.9	2.1535	0.5	−1.6
31	21.7	2.1300	0.1	−2.1
32	21.5	2.1059	−0.4	−2.5
33	21.1	2.0560	−0.1	−2.4
34	20.9	2.0301	−0.5	−2.8
35	20.5	1.9761	−0.2	−2.6
36	20.1	1.9191	0.2	−2.3
37	19.7	1.8586	0.7	−1.9
38	19.7	1.8586	−0.3	−2.9
39	19.5	1.8269	−0.5	−3.2
40	19.3	1.7942	−0.7	−3.4

* Mean ambient temperature = 13.3°C.

Source: Data from Figure 6.11.

have been changed, even shortly before, the body cooling rate also changes. Nevertheless, it is used multiplicatively for the whole period between time of death and time of investigation. There is no way to take into account even well-recognized changes of the cooling conditions*—including the ambient temperature. Figures 6.12 and 6.13 illustrate the great change in the cooling rate *B* after the cooling conditions had been altered. The cooling conditions inevitably change at the scene of death because the forensic pathologist is never the first to arrive. The question is whether we can recognize and reconstruct the changes in cooling conditions more or less approximately. If not, no temperature-based method can be applied. If this is possible, the method used should be able to take the changes into account, even approximately (compare the recommended strategy of the nomogram method; see Figure 6.38). Therefore, the main advantage of the enlightened method of Green and Wright [12,13]—measuring instead of evaluating the individual factors—is reduced by the impossibility of taking into account even known changes of the cooling conditions.

3. The plateau must have ended before estimating constant *B*. In casework at the scene, the doctor cannot decide whether the plateau is over or not. Only the method of Green and Wright [12,13] avoids this particular problem, which could introduce great errors during the very early phase after death.

The real inability to estimate reliably the representative cooling rate *B* by multiple temperature measurements within a few hours at the scene led to the concept of indirect estimation of the individual values of the constants *A* and *B* by ascertaining rules from a mass of experimental body cooling under various controlled conditions. This took the main influencing factors of body cooling into account in calculating the time since death at the scene of death.

6.1.1.7.2 Indirect Estimation of *B* under Chosen Standard Conditions of Cooling

As said earlier, the values of the constants *A* and *B* depend on the body build and the ambient cooling conditions, including the thermal factors on the surface of the body. To investigate empirically the dependency of the constants on the body build, at first, I kept the other influencing factors uniform, except for the ambient temperature, which was relatively constant during a single experiment but was at different levels (between 5.8°C and 22°C) in different experiments.

The chosen standard conditions (Figure 6.14) of the cooling used in this sequence of experiments are the same as described by Marshall and Hoare [42,44]:

- Naked body—lying extended—on the back—on a thermally indifferent base—in still air—in a closed room—without any sources of strong heat radiation

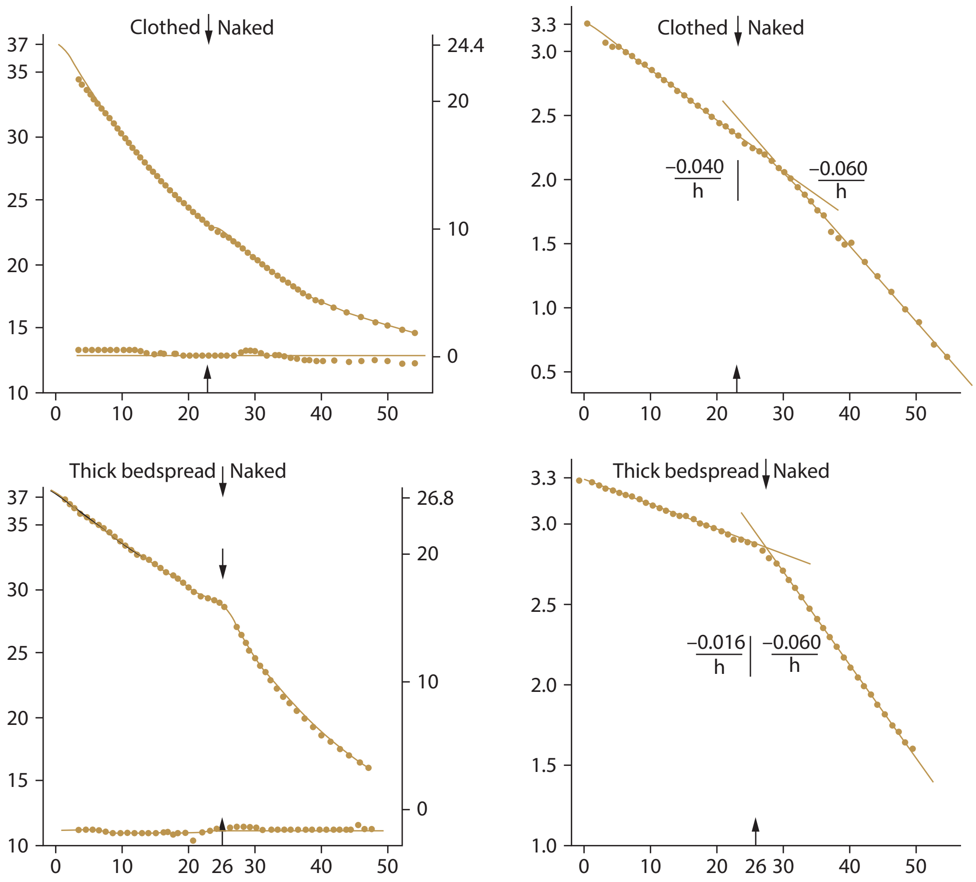

Figure 6.12 'Broken' cooling experiments. Change from clothes to naked (upper graphs) and from being covered by a thick bedspread to naked (lower graphs). On the left: rectal and ambient temperature (scale in the left margin) and temperature difference 'rectum-ambient' (scale in the right margin) in linear measures. On the right: logarithm of the temperature difference 'rectal–ambient' [17,19].

In the first sequence of experimental body cooling under almost identical conditions of the chosen standard (same investigator, room and random circumstances), I estimated the true value of *B* by the procedure shown in Figure 6.11 (c) and investigated it in relation to some measures of body build. The strongest correlation was found between the 'body weight to the power of –0.625' and the 'directly estimated' value of *B* (see Figure 6.14 and Equation 6.1).

The correlation between the 0.8-fold of the quotient 'body surface/body weight' ('size factor' according to Marshall and Hoare [42–44]) and the value of *B* was less strong but not significantly so in this sample of 29 bodies, which ranged between 30 and 112 kg body weight [12,16]. I concluded that the body build described as the relation of height and weight (by the size factor) does not give a more precise estimation of the cooling coefficient *B* than the more simple measure of the body weight (bw) in kilograms only. Therefore, I preferred the simpler procedure of calculating the value of *B* from the body weight. In addition, the quantity of fatty tissue of a body had no apparent influence on the value of *B*, in accordance with theoretical aspects [51] (see footnote 4, earlier).

A combined series of 53 body-cooling experiments by different investigators conducted at different places (though under the chosen standard conditions of cooling) confirmed this correlation. The variance was greater than in the first series because of similar, but not identical, cooling conditions [54]. In consequence, the individual value of *B* can be computed under 'chosen standard conditions' of cooling by:

$$B = -1.2815(bw^{-0.625}) + 0.0284 \tag{6.2}$$

The power of –0.625 seems to be an analogy to the 'rule of surface': the surface is proportional to the body weight to the power of 0.67 according to the cubic root of the squared body weight. If the individual value of *B* is investigated experimentally from the whole cooling curve of the body (Figure 6.11 [c]), the body weight can

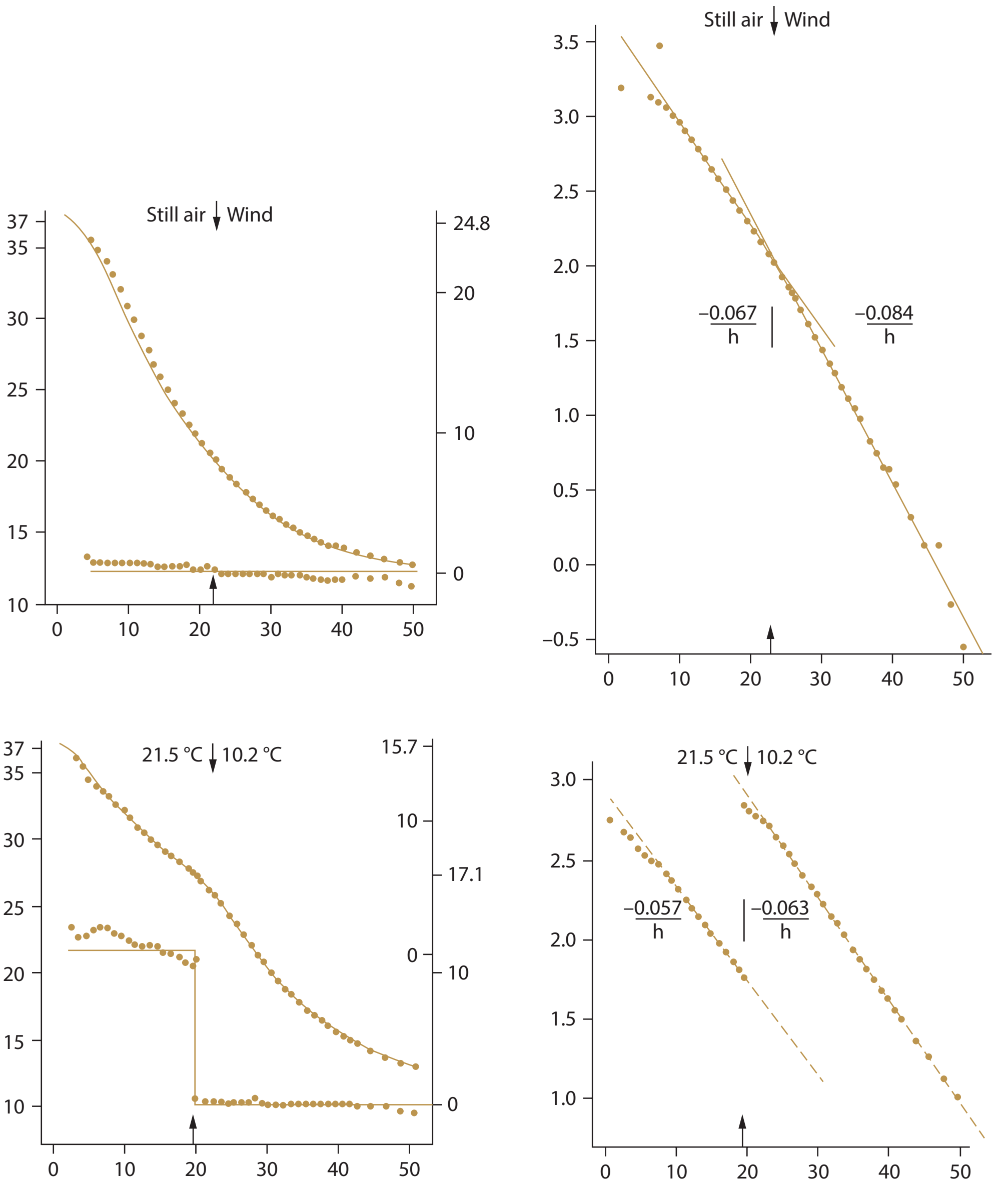

Figure 6.13 'Broken' cooling experiments. Change from cooling in still air to permanently moving air ('wind'; upper graphs). As a control experiment (lower graphs): change of the ambient temperature only, from 21.5°C to 10.2°C [17,19]. For further details, see Figure 6.12.

be computed [23] by solving for the variable body weight (*bw*) in Equation 6.2:

$$bw(kg) = \left[\frac{-1{\cdot}2815}{B - 0{\cdot}0284}\right]^{1{\cdot}6} \tag{6.3}$$

In 46 cases, this agreed with the real body weight within a standard deviation of ±6.1 kg. That means that body weight–related estimation of the value of *B* results in a rather moderate inaccuracy, compared with the direct estimation by multiple temperature measurements over a period of a few hours, possibly after a change in the cooling conditions. Nevertheless, this moderate inaccuracy can lead to a moderate systematic error in computing the time since death, which increases with progress of cooling related to the standardized temperature, *Q*.

A typical but pronounced example is the case of Figure 6.11. The body of 99.5 kg cooled somewhat slower than expected compared with the body weight–related value of *B* according to Equation 6.2, which would be −0.0439, so providing a progressive overestimation of the calculated time since death, as can be seen by comparing Figure 6.11 (d) and Table 6.2 with Figure 6.11 (e) and Table 6.2. The actual observed value of *B* (−0.0408) would correspond to a body weight of 106.6 kg according to Equation 6.3.

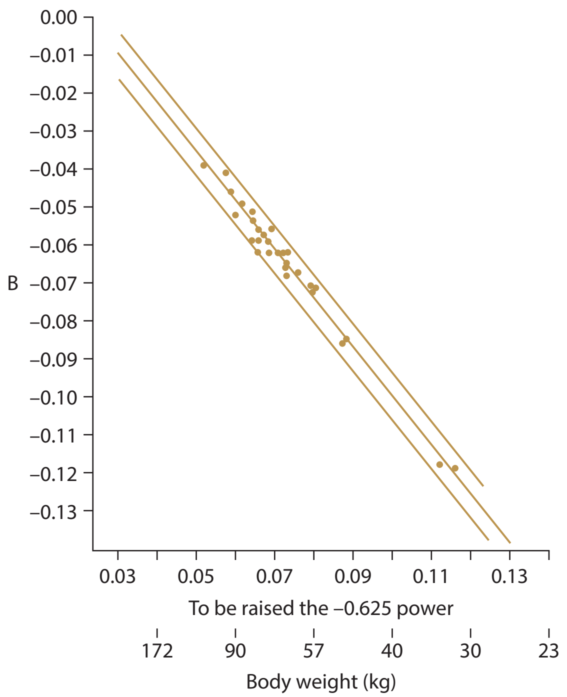

Figure 6.14 Relation between the exponent B (Equation 6.2) and the body weight to the power of −0.625 under chosen standard conditions of cooling. Regression line and permissible variation of 95 per cent [17,19].

6.1.1.7.3 Indirect Estimation of *B* under Cooling Conditions Differing from the Chosen Standard

See Figures 6.12 and 6.13.

6.1.1.7.4 Investigations on Bodies

For a clear decision as to whether there is a significant influence of clothing, covering and wind on the body cooling [42,44,17] or not [46,51], I performed some special 'broken' experiments (see Figures 6.12 and 6.13). A body was allowed to cool for the first few hours clothed or covered, the covering was removed and the body then cooled naked in still air (chosen standard) (see Figure 6.12). The graphs on the left show the original points of measurement with the computed cooling curves (lines) according to Equations 6.1 and 6.2 using the individual calculated values of the constant *B*, which can be seen in the graphs on the right. These graphs demonstrate the cooling curves as the logarithm of the temperature difference between the rectum and the surroundings. Here, the given lines are the regression lines and the given figures are the slopes, which are identical to the constant *B* of each of the two parts of the cooling curves (see Figure 6.11 [c]).

Figure 6.12 clearly illustrates the results. The clothed body (upper graphs) cools with a slope of $B = -0.04$, which corresponds to the slope of a naked body of 109 kg according to Equation 6.3. After taking the clothing off the body, the same body now cools with a slope of $B = -0.06$, corresponding to 72 kg. The actual body weight was 76 kg. The influence of the clothing (underwear, shirt, suit and thicker coat) is significant. The influence of a covering such as a thick bedspread (lower graphs of Figure 6.12) is much more pronounced: the body cools with $B = -0.016$, corresponding to 217 kg. After taking the covering off the body, it cools with $B = -0.06$, corresponding to 72 kg. The actual body weight was 73 kg. In analogy (see Figure 6.13, upper graphs), if a body first cools naked in still air (chosen standard), then later in permanently moving air (by switching on a small fan; 25 watts, mounted on the ceiling at a distance of about 2 m from the body surface, thus giving only a very slight air movement), the slope *B* equals −0.067 (64 kg) under the chosen standard conditions (still air) and is closely related to the real body weight of 65 kg. This changes to $B = -0.084$ under the conditions of moving air corresponding to 49 kg. The conclusion of this experiment indicates that even a slight but permanent air movement results in a significant acceleration of the cooling of a naked body.

Conversely (see lower part of Figure 6.13), there is no significant change in the slope of the cooling curve when the ambient temperature changes only rectangularly. As a control experiment, this naked body of 71 kg body weight cooled in still air, first in an ambient temperature of about 21.5°C and later, after a quick transfer to another room, in about 10°C ambient temperature. The slope *B* changed from −0.057 (76 kg) to −0.063 (68 kg), which is insignificant.

6.1.1.7.4.1 The Principle of Corrective Factors of the Body Weight

Taking as an example the upper part of Figure 6.12, a clothed body cools like a naked body 1.4 times heavier: 109 kg/76 kg = 1.4. This corrective factor of the body weight (*C*) equals the body weight calculated according to Equation 6.3 from *B* of the cooling curve (*bw calc*) divided by the real body weight (*bw*):

$$C = \frac{bw\ calc}{bw} \tag{6.4}$$

So, Equation 6.2 is now:

$$B = -1.2815\,(C\ x\ bw)^{-0.0625} + 0.0284 \tag{6.5}$$

where *C* is the corrective factor of the body weight taking into account any difference of the cooling conditions from the chosen standard.

In the case of the lower part of Figure 6.12 (thick bedspread):

$$C = \frac{217\ kg}{73\ kg} = 3.0$$

In the case of the upper part of Figure 6.13 (wind):

$$C = \frac{49\,\text{kg}}{65\,\text{kg}} = 0.75$$

In the case of the lower part of Figure 6.13 (chosen standard, rectangular change of the ambient temperature only):

$$C = \frac{76\,\text{kg}}{71\,\text{kg}} = 1.07, \quad \text{and} \quad \frac{68\,\text{kg}}{71\,\text{kg}} = 0.96$$

In comparison with the chosen standard ($C = 1$), thermic insulation conditions result in a corrective factor greater than 1. Conditions that cause an acceleration of the cooling result in a corrective factor less than 1.

After the pilot experiments, we made several series of cooling experiments under various cooling conditions, all differing from the chosen standard, using naked bodies in constantly moving air, different types of dry clothing and covering [54,57], wet clothing, wet, naked body surface with or without wind [22] and body cooling in still water [27]. From each experimental body cooling curve, the real value of B (analogous to the graphs on the right in Figures 6.12 and 6.13), the corresponding body weight according to Equation 6.3 and the resulting corrective factor according to Equation 6.4 were calculated.

6.1.1.8 Body Cooling in Constantly, Even Slightly Moving, Air

The cooling curves of ten naked bodies of actual body weight between 52 and 89 kg, lying extended on the back beneath a 25-watt fan mounted at a distance of 2 m on the ceiling of the room and producing a slight movement of air, provided values of B equal to 0.75 times the real body weight on average (Table 6.3). The corrective factor varied only a little, from 0.66 to 0.81, corresponding to lower errors of computed death times (standard deviation ±0.9 hours) in comparison with body cooling in still air (standard deviation ±1.3 hours) in the same series of body coolings [17].

Table 6.3 Body Cooling in Permanently Moving Air*

Case	Body weight	B_{wind}	bw_{calc}	Corrective factor
01	52.0	−0.095	42.3	0.81
02	57.0	−0.098	40.7	0.71
27	65.0	−0.094	42.8	0.66
28	65.0	−0.084	49.1	0.76
29	66.5	−0.082	50.5	0.76
30	89.0	−0.063	68.4	0.77
38	56.0	−0.091	44.3	0.79

* Body weight calculated (bw_{calc}) according to Equation 6.3.

Source: From Henssge C. Estimation of death-time by computing the rectal body cooling under various cooling conditions (German, English summary). *Z Rechtsmed* 1981;**87:**147–178.

6.1.1.9 The Cooling of Clothed Bodies

The data of experimental cooling of clothed bodies in still air (Table 6.4) show the relationship between the verbal description of clothing and the corrective factor. However, they also show that this relationship is not without exception, and therefore it is not possible to estimate a corrective factor true to within ± one-tenth from a verbal description. A further conclusion is that only the clothing of the lower trunk is relevant for the retardation of rectal body cooling. The almost radial direction of heat transfer inside the body and the rectal temperature probe site theoretically support this conclusion.

6.1.1.10 Clothed Bodies in Moving Air[33]

A study of Table 6.3 (naked bodies in moving air) and Table 6.4 (clothed bodies in still air) shows that the influence of moving air on clothed bodies becomes less as the clothing or covering becomes thicker. Moving air accelerates cooling in very thinly clothed bodies (Table 6.5; H12, H15), compensates the slightly decelerating influence of thin clothing (H14, H11) and seems to be without any accelerating influence on thicker-clothed bodies (B66, B67). Moving air accelerates the cooling by forced convection of heated air from the body surface. Clothing decelerates the cooling, mainly by fixation of a layer of heated air at the surface of the body. This principle should be borne in mind when estimating a corrective factor in cases of clothed bodies lying in moving air.

6.1.1.11 Covered Bodies in Still Air

The corrective factors for taking usual coverings into account are rather uniform, although it is pointed out that the cooling experiments listed in Table 6.6 were made by laying the bodies on 'thermally indifferent' bases (e.g. on a simple covered stretcher). When bodies are lying on more thermally insulating bases (couch, divan, bed), somewhat higher corrective factors may be required, even in covered bodies. The corrective factors of bed-like covered bodies are rather non-uniform. In Table 6.6, the different corrective factors for cases H09 and H06, and H08 and H10 may be explained by the great difference in body weight because the cooling conditions were nearly identical in these cases. This is one clue that lower corrective factors are necessary for higher thermic insulation conditions (e.g. a bedspread) on heavier bodies, and vice versa (see later).

6.1.1.12 Body Cooling in Still Water

Nineteen bodies (body weights between 48.5 and 108.5 kg) were suspended undressed in a tub holding 1000 L of almost still water at temperatures of approximately 20°C and 10°C, from the third hour post-mortem (Table 6.7).

Table 6.4 Corrective Factors for Clothed Bodies Lying on a 'Thermally Indifferent' Base in Still Air

Case number	Whole clothing	Clothing of lower trunk	Real body weight	Calculated body weight	Corrective factor
B61	Work jacket, trousers displaced upwards, downwards, vest, short pants	Short pants	92.0	92.0	1.0
B63	Vest, panties	Panties	110.0	121.0	1.1
H66	Sweater, vest, drawers, short pants	Drawers, short pants	92.5	94.4	1.02
B64	Shirt, displaced upwards, vest, short pants, trousers	Short pants, trousers	82.0	90.2	1.1
B58	Trousers, thin sweater, two vests, short pants	Trousers, short pants	68.0	74.8	1.1
B37	Open anorak, sweater, trousers, drawers	Trousers, drawers	79.0	85.3	1.08
B57	Anorak, jacket, sweater, vest, trousers, drawers	Trousers, drawers	76.5	86.4	1.26
H2	Jacket, sweatshirt, shirt, vest, short pants, trousers	Trousers, drawers	84.5	110.7	1.31
H6	Sweater, shirt, vest, trousers, two drawers	Trousers, two drawers	68.0	72.8	1.07
B53	Parker, jacket, waistcoat, shirt, vest, trousers, drawers	Parker, trousers, drawers	79.0	104.3	1.32
H4	Jacket, vest, roll-on panty, two short pants, trousers	Trousers, roll-on panty, two short pants	86.5	102.9	1.19
B60	Waistcoat, shirt, two vests, short pants, trousers, corselet, tights	Trousers, corselet, tights, short pants	55.5	79.4	1.43
B54	Jacket, shirt, long cardigan, vest, trousers, thick drawers	Long cardigan, trousers, thick drawers	63.5	91.4	1.44
B36	Woollen coat, jacket, waistcoat, vest, shirt, short pants, trousers	Woollen coat, trousers, short pants	85.0	126.7	1.49
B59	Jacket, sweater, vest, drawers, trousers, truss with pad	Trousers, drawers, truss with pad	78.5	125.6	1.6
B60	Lining trench coat, thick woollen dress, slip, short panty, tights	Lining trench coat, thick woollen dress, slip, short panty, tights	52.0	93.6	1.8

Source: Data from Henssge C, Madea B. *Methoden zur Bestimmung der Todeszeit an der Leiche*. Lübeck, Schmidt-Römhild, 1988; and Stipanits E, Henssge C. Präzisionsvergleich von Todeszeitrückrechnungen ohne und mit Berücksichtigung von Einflussfaktoren (German, English summary). *Beitr Gerichtl Med* 1985;**43:**323–329.

Table 6.5 Corrective Factors for Clothed Bodies in Permanently Moving Air

Case number	Clothing of lower trunk	Real body weight	Calculated body weight	Corrective factor
H12	Nightwear, short panty	73.3	55.7	0.76
H15	Short panty	67.5	60.8	0.9
H14	Trousers, drawers	78.0	75.6	0.97
H11	Trousers, drawers	73.0	80.3	1.10
B66	Thin trench coat, short panty, trousers	78.5	110.7	1.41
H13	Dress, slip, short panty, roll-on panty, truss	63.7	77.7	1.21
B67	Thick coat, skirt, slip, corselet, tights, short panty	83.5	138.7	1.66

Source: From Henssge C, Madea B. *Methoden zur Bestimmung der Todeszeit an der Leiche*. Lübeck, Schmidt-Römhild, 1988.

Table 6.6 Corrective Factors for Covering of Naked and Partly Clothed Bodies, Respectively

Case number	Clothing	Covering	Real body weight	Calculated body weight	Corrective factor
Thinner covering—thermically indifferent supporting base					
B62	Naked	Simple cover	66.0	79.2	1.2
B51	Naked	Double cover	91.0	106.2	1.17
B56	Drawers, short panty	Simple cover	92.5	119.3	1.29
B52	Drawers, short panty	Simple blanket	74.0	100.2	1.34
Bed-like covering—mattress on supporting base					
B33	Short panty	Thick bedspread	73.0	157.7	2.16
H08	Naked	Two thick blankets	77.0	110.4	1.44
H07	Nightwear		93.0	124.0	1.33
H10	Trousers, drawers		113.0	152.2	1.35
H06	Skirt, drawers		64.5	127.0	1.97
H09	Two napkins, short panty		6.3 6.25	16.4 25.0	2.6 4.0

Source: From Henssge C, Madea B. *Methoden zur Bestimmung der Todeszeit an der Leiche*. Lübeck, Schmidt-Römhild, 1988.

Table 6.7 Body Cooling in Still Water

Case number	Body weight (kg)	B_{standard}* calculated	Water temperature (°C)	B_{water} real	bw_{calc} (kg)	Corrective factor
01	65.0	−0.066	19.3	−0.128	28.9	0.445
20	68.0	−0.063	20.0	−0.107	36.5	0.536
21	59.5	−0.071	20.3	−0.137	26.6	0.447
22	84.5	−0.052	20.2	−0.091	44.6	0.528
24	108.5	−0.040	20.2	−0.074	57.4	0.529
25	100.5	−0.043	19.8	−0.082	50.5	0.502
27	97.5	−0.045	19.7	−0.084	49.0	0.503
28	77.5	−0.056	19.9	−0.113	34.1	0.439
30	71.5	−0.061	20.5	−0.111	35.0	0.489
						0.491
						±0.036
02	92.0	−0.048	9.8	−0.074	57.4	0.623
03	48.5	−0.085	9.8	−0.156	22.2	0.457
04	75.0	−0.058	10.0	−0.098	40.7	0.543
05	58.5	−0.063	9.9	−0.104	36.4	0.631
08	88.0	−0.050	10.2	−0.103	38.2	0.435
10	70.0	−0.062	10.2	−0.127	29.2	0.417
11	83.5	−0.052	10.0	−0.099	40.2	0.482
12	77.5	−0.056	8.3	−0.133	27.5	0.355
13	56.5	−0.075	10.0	−0.150	23.5	0.415
14	85.5	−0.051	9.1	−0.092	44.3	0.518
						0.488
						±0.086
06	44.2	−0.092	0.6	−0.140	25.8	0.583
07	75.5	−0.058	0.0	−0.071	60.3	0.798
09	83.5	−0.052	0.0	−0.079	52.9	0.633
15	95.5	−0.046	0.0	−0.044	99.7	1.040
16	79.0	−0.055	0.0	−0.092	44.0	0.557
17	80.0	−0.054	−0.1	−0.055	79.0	0.988
18	49.0	−0.084	−0.1	−0.121	31.1	0.638
19	69.5	−0.062	0.0	−0.073	57.6	0.828
23	58.0	−0.073	0.0	−0.090	44.9	0.775
29	66.5	−0.065	1.2	−0.082	50.6	0.761
						0.760
						±0.155

* B_{standard} according to Equation 6.2; body weight$_{\text{calculated}}$ (bw_{calc}) according to Equation 6.3; corrective factor according to Equation 6.4.

Source: From Henssge C, Brinkmann B, Püschel K. Determination of time of death by measuring the rectal temperature in corpses suspended in water (German, English summary). *Z Rechtsmed* 1984;**92:**255–276.

The rectal temperature was measured, usually until the 33rd hour post-mortem. The bodies cooled as quickly as naked bodies of half the real body mass in still air of the same temperature, corresponding to a corrective factor of 0.5 as a mean (ranging from 0.36 to 0.63). However, ten further bodies (body weights between 44 and 95 kg), suspended in nearly still water at approximately 0°C, yielded a distinctly smaller temperature decrease, which was especially marked at rectal temperatures lower than about 11°C in all bodies, without regard to body mass. In bodies of great body weight and small body surface in proportion to body mass, the lower cooling rate was pronounced, the cooling curve corresponding to corrective factors tending to 1.0. This can be explained by a decrease in the thermal conductivity of the subcutaneous adipose tissue with a decrease in tissue temperature [27].

6.1.1.13 Body Cooling in Flowing Water

Brown and Marshall [8] characterized the cooling curve of a very small body (size factor: 320 cm^2/kg) suspended in flowing water (velocity 5 m/hour) by a four-exponential model. Transcribed to the two-exponential Equation 6.1 and the body weight relation of *B* according to Equation 6.2, this would result in a corrective factor of the body weight in order of 0.35, which relates well to all the other corrective factors.

6.1.1.14 Body Cooling in Cases of Wet Clothing or Covering, or Unclothed Wet Body Surface

Some cooling experiments of 'wet-through' clothed or covered bodies, and of naked bodies with a wet body surface were made in a closed room, and by night in the open air under a cloudless sky when reconstructing a special case [22].

According to the accused husband, his wife had fallen from a boat into the water and drowned. The real time of death could not have been earlier than 22:10 hours and not later than 22:20 hours, averaging 22:15 hours according to his declaration. Some 15 minutes later, the body was detected by the husband and salvaged by witnesses. The body was laid on a lawn. At 00:23 hours, the deep rectal temperature was measured as 28°C, and at 00:40 hours as 27.5°C. The law court decided on a 28.3°C rectal temperature at 00:23 hours after examining the thermometer. The body weight of the woman was 53 kg, and her height was 159 cm. Until the temperature measurement, the body was clothed with a slip, a corselette, Silastic trousers, a shirt, a brassiere and a long waterproof anorak. The day in August was sunny. During the windless night there was a cloudless sky. The weather station stated the following temperatures: 20.7°C (16:00 hours), 20.1°C (19:00 hours), 15.6°C (21:00 hours), 14.3°C (22:00 hours), 13.8°C (23:00 hours), 12.6°C (00:00 hours) and 11.9°C (01:00 hours). From these data there resulted a mean temperature of 12.8°C between 23:00 and 01:00 hours. The water temperature within the harbour measured approximately 20°C. The decisive question was whether the rectal body cooling to 28.3°C at 00:23 hours could be compatible with a death time at 22:15 hours.

To solve this question, some cooling experiments were made (Table 6.8), which led to the following conclusions:

1. Naked bodies suspended in water for a short time (~10 minutes) cool in still air as a result of their wet body surface at the same rate as bodies 0.75 times the real body weight.
2. Bodies with thin but 'wet-through' clothing/covering seem to cool in moving air like bodies of 0.7 times the real body weight.
3. Bodies with more layers of wet-through clothing/covering seem to cool in moving air like bodies of the real body weight without any corrective adjustment.
4. One layer of thin, wet-through clothing/covering does not seem to have a marked influence on the velocity of body cooling in still air, compared with cooling under chosen standard conditions. Therefore, no corrective adjustment of the real body weight is necessary. Conversely, thick, wet-through clothing/covering, especially of several layers, provides a reduced velocity of body cooling in still air that is similar to dry clothing/covering and corresponding to corrective factors between 1.1 and 1.4.

Table 6.8 Body Cooling under Wet-through Clothing/Covering and Respective Wet Body Surface

Case number	Cooling conditions	Real body weight	Corrective factor
	Closed room, still air, wet body surface		
50		45.0	0.77
52		65.0	0.75
	Wet-through covering or clothing		
41	One smock	84.5	1.00
42	Two smocks	57.2	1.10
51	Roll-on panty, trousers, three smocks	69.5	1.10
44	Roll-on panty, trousers, three smocks	65.0	1.30
	Permanently moving air		
68	Drawers, trousers, skirt, pullover, jacket	64.5	0.7
55	Drawers, trousers, pullover, coat	91.0	0.9
47	Three smocks	91.5	0.7
	Under cloudless sky, wet lawn, still air		
80	Drawers, dress, one smock	59.5	1.2
81	Drawers, skirt, one smock	67.5	1.4
82	Drawers, dress, one smock	58.0	1.4

Source: From Henssge C, Brinkmann B. Todeszeitbestimmung aus der Rektaltemperatur. *Arch Kriminol* 1984;**174:**96–112.

On the basis of these results, corrective factors from 1.1 to 1.4 were used to test the husband's account of events. However, another technical expert maintained that the body would have cooled more because of the influence of radiation against the cloudless sky at night, which would be equal to a corpse at −30°C. To examine this argument, the cooling experiments of cases 80, 81 and 82 in Table 6.8 were made by night in the open air under a cloudless sky by laying the bodies on a wet lawn. The results were the same as for a closed room, showing that radiation from the surface of the body to the cloudless sky by night had no marked influence on body cooling. The computation was made using the following:

- Mean ambient temperature 12.8°C
- Body weight 53 kg
- Averaged corrective factor 1.2
- Rectal temperature 28.3°C
- Rectal temperature at death 36.5°C (as agreed by the law court)

This equals (according to Equations 6.1 and 6.5) 9.4 hours before 00:23 hours as a mean value. Using the range of corrective factors from 1.0 to 1.4, which could be possible according to the special cooling experiments (see Table 6.8), the time of death ranges between 5.6 hours (corrective factor = 1.0) and 13.5 hours (corrective factor = 1.4), corresponding to 3.8 hours around the mean of 9.4 hours, which is in close agreement with three times the experienced standard deviation of cooling experiments under various conditions (see Figures 6.29 and 6.30 and Table 6.14). Therefore, a time of death at 22:15 hours (22:10–22:30 hours) could be excluded.

6.1.1.15 Investigations on Dummies

Using dummies to replace bodies of average weight, we obtained results that correspond well with the corrective factor for various cooling conditions. An exception was experiments with wet-surfaced dummies and dummies suspended in water, where somewhat lower corrective factors were found compared with bodies (Figure 6.15).

6.1.1.15.1 Dependence of Corrective Factors on the Body Weight

Although the corrective factors established on bodies include a wide spectrum of frequently occurring cooling conditions, nearly all these experiences resulted from bodies of average body weight [20,53]. Only a few cases support the assumption that bodies of a very high body weight and, at the same time, strong thermic insulation conditions (see Table 6.6) would require lower corrective factors and, conversely, bodies of a low body weight would require higher corrective factors. To correct these deficiencies, 98 cooling experiments on five different-sized dummies under five different cooling conditions, besides standard ones, were made. The dummies were cooled under standard conditions equivalent to human bodies of 14, 33, 41, 83 and 104 kg, respectively.

6.1.1.15.2 Characteristics of the Cooling Conditions

The dummies were laid on a thick, foam-upholstered supported base and exposed permanently to a slightly

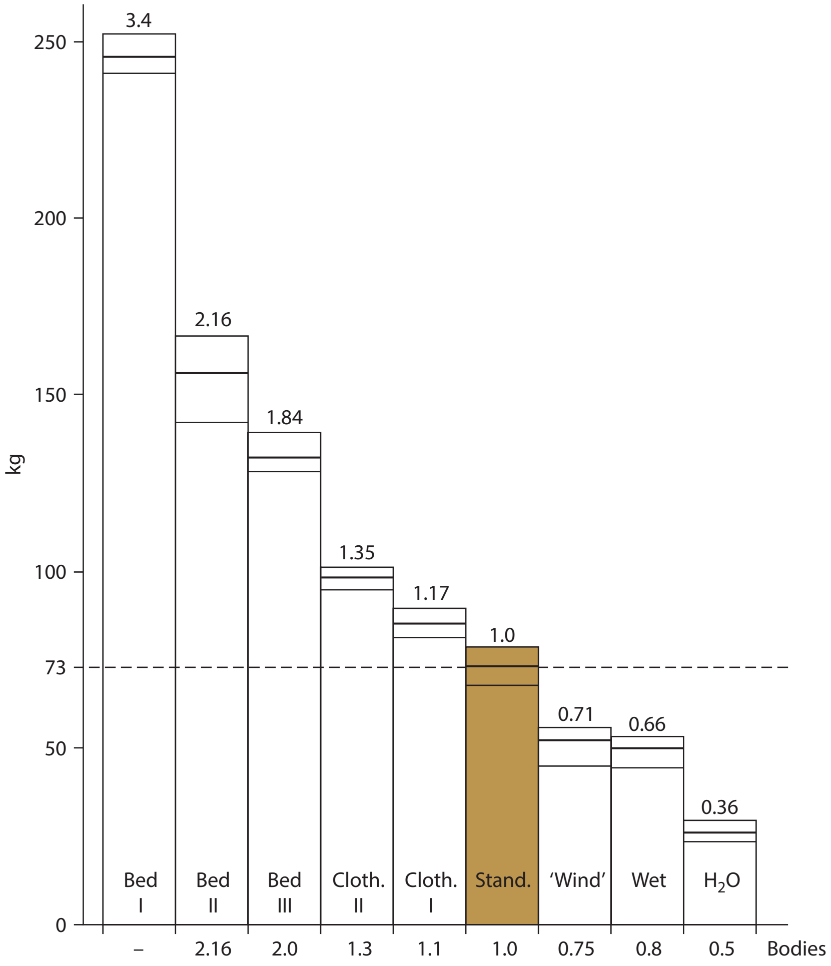

Figure 6.15 Comparison of corrective factors investigated on bodies and on a dummy cooling under various, but very similar, conditions. The dummy replaces a body of 73 kg. The corrective factors resulting from dummy experiments are given at the top of the columns. Beneath the baseline the corrective factors of bodies are shown as they resulted from the previously reported experimental body investigations.

(Data from Henssge C, Madea B, Schaar U, Pitzken C. Die Abkühlung eines Dummy unter verschiedenen Bedingungen im Vergleich zur Leichenabkühlung (German, English summary). *Beitr Gerichtl Med* 1987;**45:**145–149.)

moving air, produced by a small fan (25 watts) mounted on the ceiling at a distance of approximately 2 m.

- Clothing I: two layers. One layer was thin (cotton textile, like pants), and the second layer was rather thick (blue jeans).
- Clothing II: three layers. Additional to 'clothing I', a second thin layer was applied.
- Covering I: A wool blanket, loose-fitting.
- Covering II: A thick feather eiderdown. The dummies were laid on an additional mattress, which was placed on the upholstered support base used for the other dummies.

After repeated test cooling measurements under chosen standard conditions, the coefficient B was calculated. From these 'experimental' values of B, '*virtual*' weights were calculated according to Equation 6.3. The virtual weight represents the weight of a body whose cooling curve is identical to cooling under standard conditions.

Just as under standard conditions of cooling, a close linear relationship results between 'experimental' B and 'virtual weight' to the power of −0.625 for each condition differing from the standard (Figure 6.16 and Table 6.9).

Because of the common point of intersection, the dependence of B for each cooling condition is differentiated only by the slope S. Therefore, the coefficient B can be calculated for each cooling condition, depending on the body weight (standard) according to its own slope S:

$$B_{\text{condition}} = \left[(bw^{-0.625} - 0.028)S_{\text{condition}}\right] - 0.007 \qquad (6.6)$$

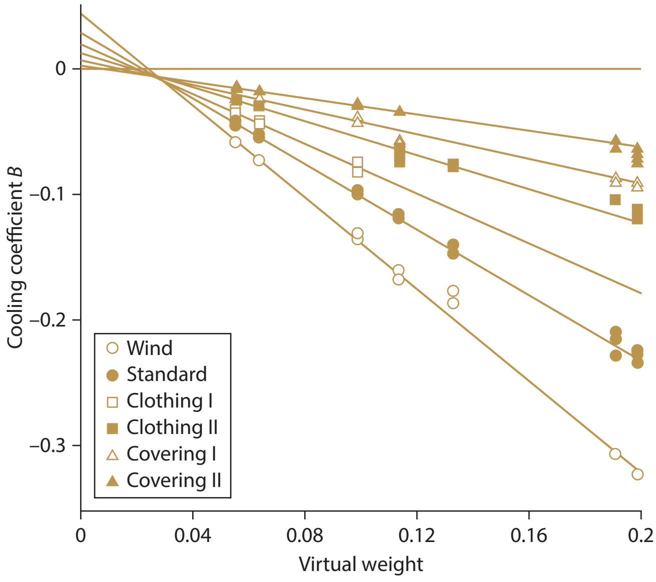

Figure 6.16 Regression lines (see Table 6.9) of the dependence of cooling coefficient B (ordinate) on virtual weight to the power of −0.625 (abscissa) for the various cooling conditions. The common point of intersection has the coordinates Y = −0.007 and X = 0.028 [20,53].

Table 6.9 Regression Lines of Cooling Coefficient B (Ordinate) against Virtual Weight to the Power of −0.625 (Abscissa) for the Various Cooling Conditions (see Figure 6.16)

Condition	Number of experiments	Regression line Slope 'S'	Regression line Intercept
Wind	20	−1.8083	0.0436
Standard	24	−1.2815	0.0289
Clothing I	07	−0.9591	0.0199
Clothing II	12	−0.6431	0.0110
Covering I	17	−0.4828	0.0065
Covering II	18	−0.3218	0.0020

Source: Data from Henssge C. Rectal temperature time of death nomogram: dependence of corrective factors on the body weight under stronger thermic insulation conditions. *Forensic Sci Int* 1992;**54:**51–56; and Stadtmüller K. *Zur Todeszeitbestimmung aus der Leichenabkühlung: Die Normierung der Abkühlgeschwindigkeit unterschiedlicher Körper auf verschiedene äussere Bedingungen*. Cologne, Germany, University of Cologne, MD thesis, 1991.

$B_{\text{condition}}$ can be used to calculate the body weight (kg) by:

$$bw_{\text{condition}} = \left[-1.2815 / B_{\text{condition}} - 0.0284\right]\left[61{,}143\right] \qquad (6.7)$$

The *bw* condition represents the weight that is apparently changed by the special cooling conditions. Dividing the virtual weight (standard) by the apparently changed weight, the corrective factor can be determined. Conversely, the virtual weight of the dummy (standard) multiplied by the corrective factor provides for a special cooling condition.

The corrective factors of the investigated cooling conditions can be calculated universally for any virtual weight (Figure 6.17):

$$\frac{\left[\dfrac{-1.2815}{(S_{\text{condition}} \times bw_{\text{standard}} + I_{\text{condition}})}\right]^{1.6}}{bw_{\text{standard}}} = \text{F} \qquad (6.8)$$

where $S_{\text{condition}}$ is the slope; $I_{\text{condition}}$ is the intercept from Table 6.9; and bw_{standard} is the virtual weight under standard conditions.

The dependence of the corrective factors on the virtual dummy weight (acting for body weight) is evident. If the dependence on body weight did not exist, the lines for all the cooling conditions in Figure 6.17 would have to be horizontal, just as they are for the standard condition and, approximately, for the cooling condition 'wind'. The dynamics of the dependence on body weight become pronounced with the power of the thermic insulation. The curves of Figure 6.17 demonstrate a non-linear regularity of the cooling conditions. The dependence between virtual weight and the corrective factor of the investigated cooling conditions can also be used to interpolate the relation to non-examined cooling conditions of any distinct weight, as shown in Figure 6.18 for an average body

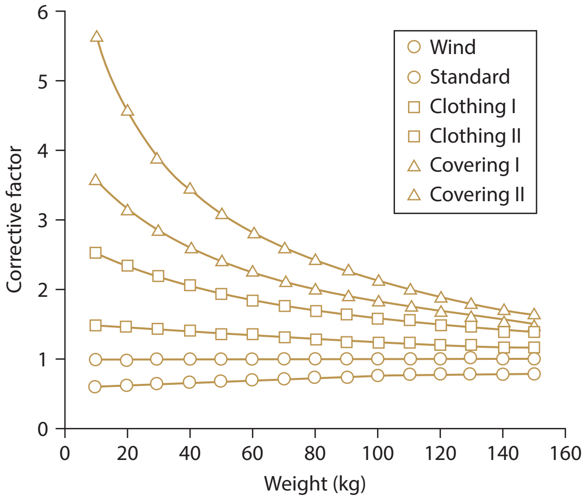

Figure 6.17 Generalization of the dependence of the corrective factors on the virtual weight of dummies (acting for body weight) for the investigated cooling conditions [20,53].

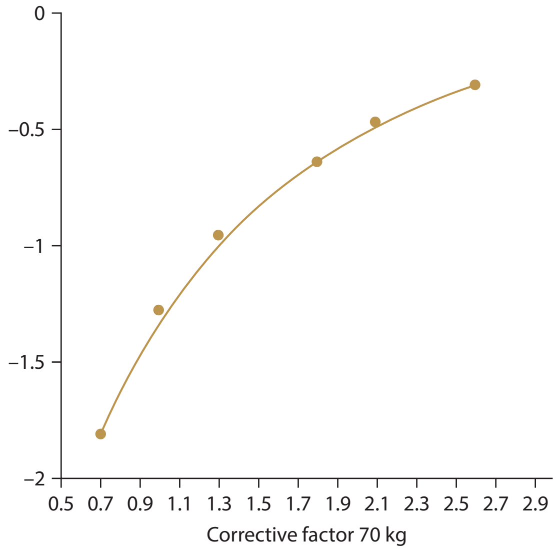

Figure 6.18 The relation between corrective factors (abscissa) and slope S of the correlation between cooling coefficient and weight according to Figure 6.16 and Table 6.9 (ordinate) for a dummy of approximately 70 kg. The points represent, from below: wind, standard, clothing I, clothing II, covering I, covering II.

(Data from Henssge C. Rectal temperature time of death nomogram: dependence of corrective factors on the body weight under stronger thermic insulation conditions. *Forensic Sci Int* 1992;**54**:51–56.)

weight of 70 kg. The 'best fit' curve of the measurement points drawn is expressed mathematically:

$$S = 3.24596 \times \exp(-0.89959 \times C_{70}) \tag{6.9}$$

where S is the slope to calculate the cooling coefficient B from body weight to the power of −0.625 (see Figure 6.16), and C_{70} is the corrective factor valid for a special cooling condition to a body of 70 kg.

The interpolation can only be made, in the first instance, on the range of the actually investigated cooling conditions (from wind to thick bedspread) and for those corrective factors (from 0.75 to 3.0) valid for 'average' body weights.

Using the same principle, the corrective factor (C) can be calculated for any actual body weight (kg) according to Equation 6.8, provided that the corrective factor for an 'average body weight' of 70 kg (C_{70}), for any actual cooling condition, is known:

$$\frac{\left[\dfrac{-1.2815}{(bw^{-0.625}-0.028)(-3.24596 \times \exp(-0.89959 \times C_{70}))-0.0354}\right]^{1.6}}{\text{kg}} = C \tag{6.10}$$

Using Equation 6.10, the corrective factors were calculated for body weights ranging from 4 to 150 kg, related to the corrective factors of 70 kg (see Table 6.17).

Equation 6.10 can be used to demonstrate that special thermic insulating conditions, which require a corrective factor of 2.0 on a dummy of 70 kg virtual weight, would require a higher corrective factor of approximately 3.2 on a dummy of virtual 10 kg; and, in the case of a 110-kg dummy, a lower corrective factor of 1.7. In these experiments, the corrective factor for one of the different-sized dummies of one of the applied cooling conditions can be calculated by Equation 6.10 if the corrective factor of a different-sized dummy is known.

Because of the close conformity of the previous investigations in comparing the cooling of dummies and bodies under various conditions (see Figure 6.15) it is concluded that the result of the dependence of corrective factors on the body weight is applicable to bodies.

Intuitively, it appears obvious that, in the case of a 150-kg body, a special bedspread does not cause a deceleration of cooling proportional to the body weight corresponding to 525 kg (3.5 × 150 kg), such as in a case of a 4-kg body corresponding to 14 kg (3.5 × 4). The physical explanation for this effect is, however, more difficult. The model of a cylinder of infinite length [14] applied to body cooling [31,32,51] may be helpful. A special bedspread has a distinct layer thickness. The enlargement of the radius is, in the case of a 4-kg body, relatively much greater than in the case of a 150-kg body; it is not proportional to the radius of the body, but it enlarges the radius cumulatively. In addition, the bedspread causes a deceleration of heat loss by its comparatively smaller heat conductivity against body tissues. The effect of this component on the velocity of body cooling is proportional to the surface area of the body. The surface area itself is proportional to the body weight to the power of 0.67 (see Figure 6.4; 'geometric likeness'). Therefore, it may be concluded that the deceleration of body cooling by a bedspread is provided by the enlargement of the radius of a body as an additive component, as well as by the low heat conductivity as a proportional component [20,53].

However, although these considerations may be helpful in understanding, they do not lead to practicable solutions useful for casework.

6.1.1.16 Influence of the Type of Supporting Base on Body Cooling

In a series of cooling experiments utilizing heat flow sensors (see Figures 6.5–6.9), 'naked' dummies were lain on supporting bases with very different thermic features [35,41,56] (Table 6.10 and Figures 6.19–6.21).

Related to a 'thermally indifferent base', insulating bases slow down the cooling rate by corrective factors of up to 1.3. As may be seen in Table 6.10, it was not possible to slow down the cooling beyond this level by adding more insulating material (see experiment numbers 200–310) but not covering the dummies' flanks. Conversely, some bases accelerate the cooling, requiring corrective factors in the order of 0.75–0.5.

Figure 6.19 (a–c) demonstrates not only the dependence of the heat flow at the contact surface but also the slope of central temperature on that type of base. Even the heat flow at the non-contact surface is slightly influenced by the type of base, which is comprehensible in view of the parallel circuit of the surfaces in Figure 6.9. This also explains why the cooling cannot be further decelerated by adding more insulating features to the supporting base. Finally, the heating of the ground by the heat flow from the contact surface of the dummy to the base

Table 6.10 Type of Supporting Base and Its Influence of Cooling of a 'Naked' Dummy Related to a 'Thermally Indifferent Base' as Used at 'Standard Conditions'*

Experiment number	Supporting base	Real *B*	Body weight calculated	Corrective factor
	Thick foam-upholstered base			
200		−0.0514	84.9	1.31
201		−0.0524	83.3	1.29
202		−0.0528	82.6	1.28
270	Thick foam-upholstered base + polystyrene (Styropor) plate	−0.0529	82.4	1.27
300	Thick foam-upholstered base + polystyrene (Styropor) plate + cushion	−0.0514	85.0	1.31
310	Armchair	−0.0526	82.9	1.28
	Table + cover 'indifferent'			
210		−0.0646	66.4	1.03
211		−0.0669	63.9	0.99
212		−0.0659	65.1	1.01
225		−0.0672	63.6	0.98
	Floor of a room covering with PVC			
230		−0.0840	49.1	0.76
231		−0.0838	49.2	0.76
232		−0.0829	49.9	0.77
	Loft			
	Ground of cellar			
240		−0.0859	47.8	0.74
250		−0.0863	47.5	0.73
251		−0.0864	47.5	0.73
252		−0.0953	42.1	0.65
260	Stone slab outside	−0.0867	47.3	0.73
	Steel plate on concrete-ground wash round			
290		−0.1095	35.4	0.55
291		−0.1106	34.9	0.54
292		−0.1116	34.5	0.53

* Calculation of the body weight according to Equation 6.3. Calculation of the corrective factor according to Equation 6.4 with an average 'standard' weight of 64.7 kg. The nearly constant ambient temperatures ranged between 14°C and 19°C, except in experiment number 260, where it was 6.1°C [35].

Abbreviation: PVC, polyvinyl chloride.

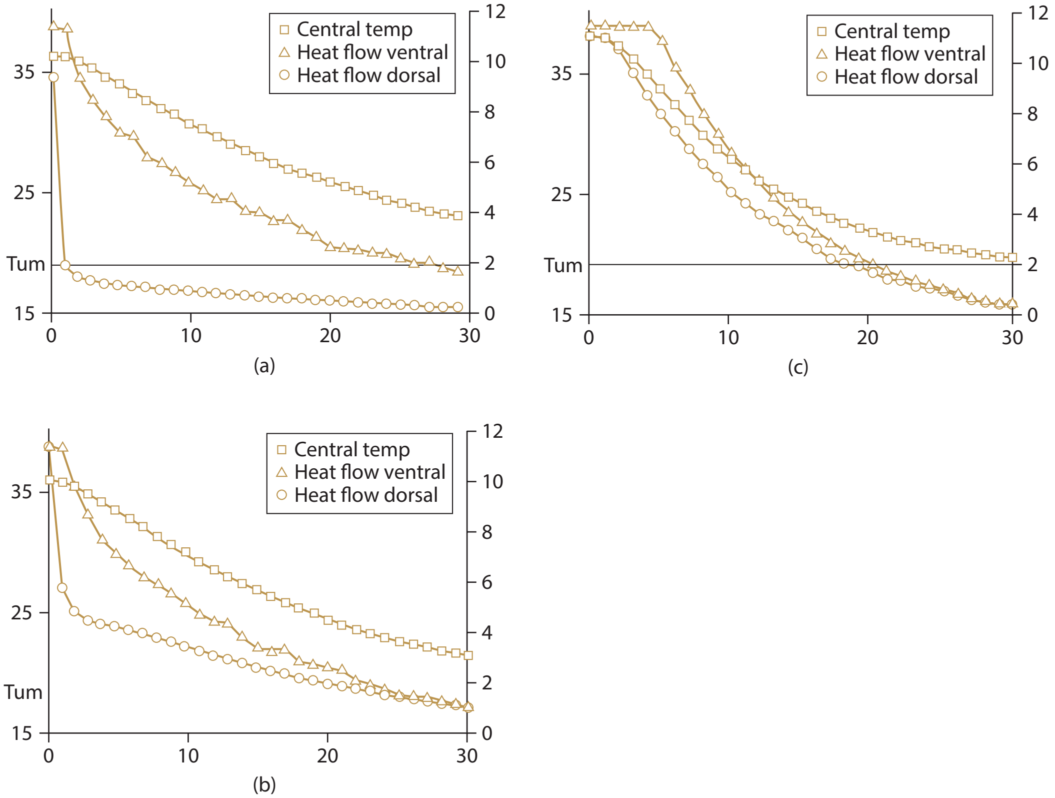

Figure 6.19 Heat flow on the contact and the non-contact surfaces of a 'naked' dummy in still air lying on different supporting bases. Abscissa: cooling time (hours); ordinate: heat flow (Btu ft^{-2} h^{-1}) [35]. (a) Isolating base. Experiment number 201 from Table 6.10. (b) Indifferent base. Experiment number 211 from Table 6.10. (c) Well-conducting base. Experiment number 292 from Table 6.10.

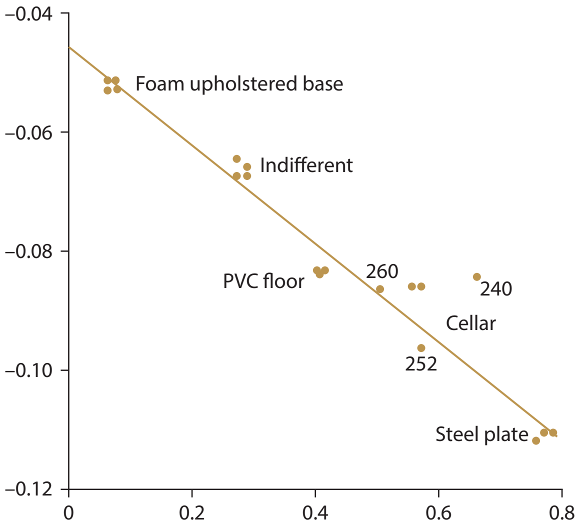

Figure 6.20 Relationship between the slope of central temperature against heat flow on the contact surface (abscissa) and cooling coefficient B (ordinate) of the experiments with different thermal features of the base listed in Table 6.10.

(Data from [35].)

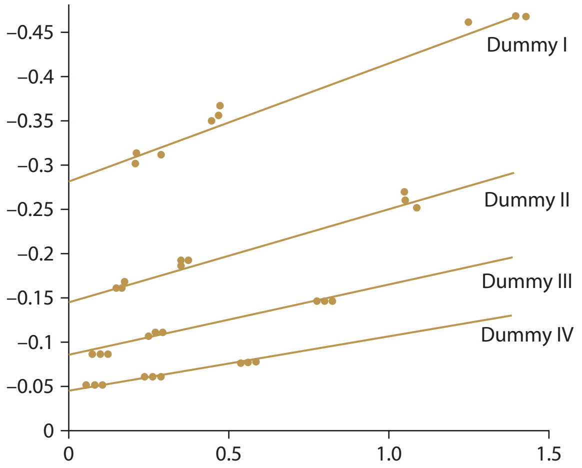

Figure 6.21 Relationship between the slope of heat flow against central temperature (abscissa) and cooling coefficient B (ordinate) investigated in four different-sized dummies (I = 6.9 kg; II = 17.3 kg; III = 36.8 kg; IV = 72.5 kg) and three thermally different bases (double-covered table; thick, foam-upholstered base; concrete cellar floor).

(Data from [56].)

itself, immediately after contact, causes a more reduced temperature difference between base and contact surface, as can be clearly seen in the first parts of the curves in Figures 6.7 and 6.8. In accordance with this, there is a linear relationship between central temperature (X) and heat flow at the contact surface (Y) during cooling after the plateau. The slope of this regression line best characterizes the influence of the type of base on the cooling velocity, because there is a strong correlation with the cooling coefficient B (see Figure 6.21), which means the slope of logarithm of temperature difference against cooling time (see Figure 6.11 [c]).

In a second series of experiments by Unland [56] with different-sized dummies, it was shown that this relation depends on the size of dummy (see Figure 6.21). According to Figure 6.21, the cooling coefficient B can be computed for any body weight and any kind of base by:

$$\begin{aligned} B = {} & (bw \times 0.4774 + 13.3462)^{-0.725} \\ & \times sFT - (bw \times 0.3210 + 1.5299)^{-0.98} \end{aligned} \tag{6.11}$$

where bw is body weight in kg, and sFT is the slope of central temperature against the heat flow at the lying surface.

The importance of Equation 6.11 is the replacement of the estimation of a corrective factor for any cooling condition, by the measurement of the heat flow at surfaces, in addition to the measurement of ambient and central (rectal) temperatures and body weight.

6.1.1.16.1 Body Cooling under the Condition of Lying on Leaves and Covered by Leaves

Cooling experiments of two different dummies were carried out using first ‘standard conditions of cooling’, second with a 2-cm-thick compressed layer of leaves on the floor and third covered by a 10-cm-thick layer of leaves additionally [4]. Under chosen standard conditions of cooling, the dummies cooled like bodies of virtual weights of 60.4 kg and 67.6 kg (calculation according to Equation 6.3). When the dummies were lying on wet-through leaves at the beginning of the measurements, cooling was not different from standard conditions. Over a period of several days, the leaves became drier and drier, and the cooling retarded, corresponding to higher virtual body weights related to corrective factors of about 1.3 (calculation according to Equation 6.4). When the dummies were lying on totally dry leaves, corrective factors of the order of 1.5 are adequate (Table 6.11). In contrast, corrective factors greater than 1.3 could not be achieved in the experiments of Table 6.10 when using smooth and rigid insulating bases that did not cover the flanks of the dummies. In the experiments using leaves, the material is flexible and adapts itself to the body surface. In consequence, the insulating area is enlarged by the flanks of the dummy, thus providing corrective factors up to 1.5. When the dummies were lying on leaves and covered by a nearly 10-cm-thick layer of leaves, corrective factors of 1.8–2.7 were determined (Table 6.12). The great variability of the insulating effect of apparently identical layers of leaves can be explained by different amounts of enclosed air.

Table 6.11 Corrective Factors Determined by Experiments Using Leaves on the Floor

Virtual weight under standard conditions of cooling [kg]	Virtual weight lying on leaves [kg]	Humidity of the leaves	Resulting corrective factor
67.6	68.1	Wet through	1.01
67.6	86.5	More or less dry	1.28
67.6	84.7	More or less dry	1.25
60.4	88.0	Totally dry	1.46
60.4	93.7	Totally dry	1.55
60.4	93.4	Totally dry	1.54

Table 6.12 Corrective Factors Using Leaves on the Floor and Covered by Leaves

Virtual weight under standard conditions of cooling [kg]	Virtual weight laying on and covered by leaves [kg]	Resulting corrective factor
67.6	120.0	1.77*
67.6	154.6	2.28
67.6	136.7	2.02
67.6	159.2	2.35
67.6	165.5	2.45
67.6	177.2	2.62
67.6	155.8	2.30
60.4	142.3	2.35
60.4	140.9	2.33
60.4	136.7	2.26
60.4	146.2	2.41
60.4	154.0	2.54
60.4	164.5	2.72
60.4	147.0	2.43

* The factor could have been influenced by low humidity of the leaves.

6.1.1.17 The Individual Value of the Plateau-related Constant *A*

6.1.1.17.1 Estimation of *A* on Bodies

The empirical investigation of the dependency of the constant A in experimental body cooling was much more difficult than that of the constant B because A describes the ‘post-mortal temperature plateau’ [52], and the temperature at death was really unknown in our cases, given that the bodies investigated came in between 0.8 and 6 hours post-mortem. In the first series of experiments, the duration of the plateau varied from 5 to 14 hours, which is equivalent to a period without any drop of the rectal temperature between 1 and 6 hours [16]. Nevertheless, there was a significant relationship between the duration of the plateau and the rate of the temperature drop after the plateau. Bodies with a low rate (high body weight) also had a longer plateau phase than bodies with a high rate (low body weight). There is a relationship between the values of the exponent of the first and second terms of the model (see Equation 6.2). Within the investigated range of the ambient temperature, between 5°C and 22°C, the value of the second exponent was found to be five times the value of the first exponent (*B*), resulting in an approach of $A = 1.25$ as a mean [16]. In the example of the body in Figure 6.11, the temperature measurement began 3 hours after death. The intercept of the regression line (Figure 6.11 [b]) was 3.3677, corresponding to 29.01°C above ambient temperature (13.3°C) in a linear measure. The best fit of the curve was made using a value of *A* equal to 1.25, assuming a starting temperature at death of 37.2°C (see Figure 6.11 [d]).

If the value of *A* really equals 1.25, then the starting temperature must have been 36.5°C, because (29.01/1.25) + 13.3 gives 36.5°C. In contrast, if the starting temperature was 37.2°C, then the value of *A* must equal 1.21 (29.01/[37.2 −13.3]). This example demonstrates the difficulties in investigating the 'true' value of *A* in bodies where the starting temperature at death is unknown.

Marshall and Hoare [42–44] did not discover any distinct relation between the first exponent (*B*) and the second one (inherent in *A*). In practice, they set the value of the second exponent at a fixed value of −0.4 for all bodies, independent of its general cooling velocity. This procedure leads to additional errors in calculating the time since death, especially in cases of a greater or a lower cooling rate *B*. This error is avoidable by linking the second exponent to the first one, which is provided by a distinct value of *A*.

Using the value 1.25 for *A*, the rectal cooling curves published in 1955 by De Saram et al. [10] (which were obtained in ambient temperatures between 26°C and 31°C) systematically overestimated the time of death. The reason for this was solely an overestimation of the relative length of the plateau related to $A = 1.25$. By means of an approach of $A = 1.11$ (where the value of the second exponent is 10 times that of the first), corresponding to a relatively shorter length of the plateau, the overestimation was removed. Theoretically, the plateau also depends on the magnitude of the difference in temperature between the rectum and surroundings at death [34] so that the empirical result in modelling De Saram's cooling curves would establish a real dependency of the value of *A* (relative length of the post-mortal temperature plateau) on the ambient temperature. The ambient temperatures of our own experimental body coolings ($A = 1.25$) did not usually exceed 23°C. In De Saram's material it ranged between 26°C and 31°C ($A = 1.11$). The dependency of *A* on the ambient temperature seems to be non-linear but pronounced in ambient temperatures above 23°C. Certainly, a jump in the value of *A* from 1.25 to 1.11 at 23°C, or at any other level of an ambient temperature, is not to be expected but, lacking more experimental data of rectal cooling curves in higher ambient temperatures, we were unable to pursue the matter any further.

6.1.1.17.2 Determination of *A* on Dummies

The rule of the close relationship between the first exponent (*B*) and the second exponent of Equation 6.1, corresponding to the value of *A* according to:

$$\text{Second exponent} = A \times B \,/\, A - 1 \qquad (6.12)$$

can be better studied on dummies than on bodies because of the exact measurement of the starting point of cooling (*To*) immediately after removing the dummy from the incubator because:

$$A = \exp(a_{yx}) \,/\, To - \mathrm{Ta} \qquad (6.13)$$

whereas the *To* of bodies is usually unknown.

By extrapolation of the later part of the cooling curves to $t = 0$ according to the procedure shown in Figure 6.11 (c), the value of 'exp (a_{yx})' is easy to obtain.

Dividing exp (a_{yx}) by *To* – *Ta* gives the value of *A*.

Cooling curves of a dummy corresponding to a body weight of 70 kg in ambient temperatures of 2°C and 28°C (Figure 6.22) show an identical duration of the plateau if the value of *A* remains the same at 1.25. The plateau is equivalent to a period of 3.7 hours without any drop of the central temperature, independent of the ambient temperature. However, the cooling curves of two dummies

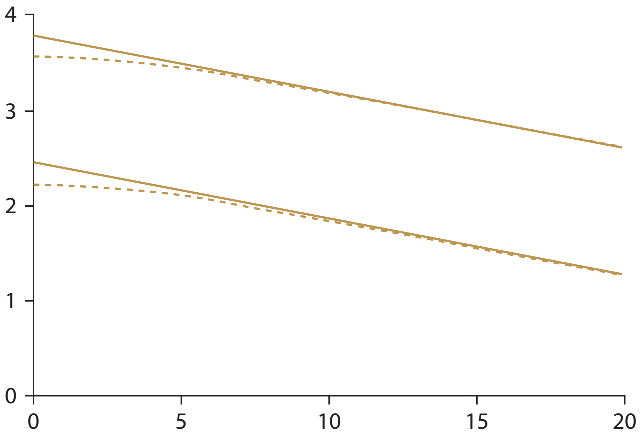

Figure 6.22 Cooling curves equivalent to a 70-kg body ($B = -0.0617$) starting at 37.2°C in ambient temperatures of 2°C (upper curve) and 28°C (lower curve) with identical values of *A* (1.25). The regression lines reach 37.2°C at the same time of 3.7 hours. Abscissa: time (hours); ordinate: ln (*Tr* – *Ta*).

of different body weights (10 and 110 kg) show a different duration of their plateaux (Figure 6.23), equivalent to periods of 6.3 hours (110 kg) and 0.8 hours (10 kg) without any drop of central temperature, assuming the same value of *A* (1.25). These data are comparable to those of our first sequence of cooling experiments on 29 bodies with real body weights between 30 and 112 kg, which led to the best fit of the actually observed durations of the plateau using 1.25 as value of *A*. If the plateau is really shorter (Figure 6.24), as it is in De Saram's cooling curves, a value of *A* lower than 1.25 must be chosen (e.g. 1.11), for best fitting the plateau.

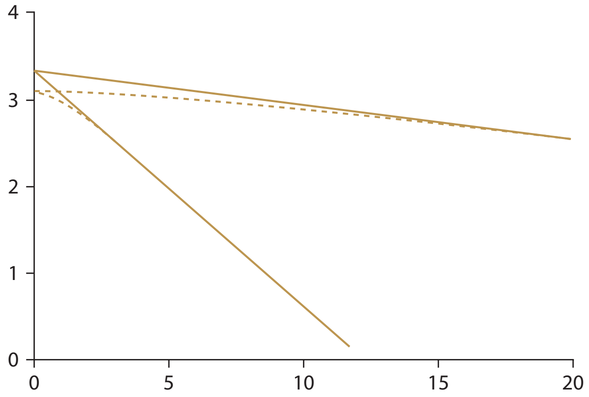

Figure 6.23 Post-mortal temperature plateau dependent on the body weight. Cooling curves are equivalent to a 110-kg body (B = −0.0395, upper curve) and a 10 kg body (B = −0.2755, lower curve) both starting at 37.2°C in 15°C ambient temperature. The value of A is 1.25. The regression line of the 110-kg body reaches 37.2°C as late as 5.7 hours after the start of cooling, but that of the 10-kg body reaches 37.2°C 0.9 hours after start of cooling. Abscissa: time (hours); ordinate; ln ($Tr - Ta$).

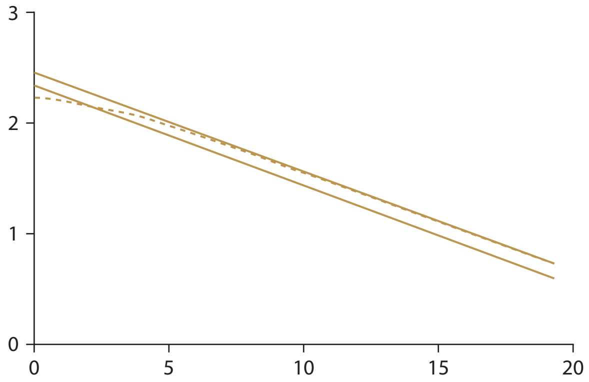

Figure 6.24 The figure of *A* and its influence on the duration of post-mortal plateau in model curves. Model cooling curves of a 50-kg body (B = −0.0827) starting at 37.2°C in an ambient temperature of 28°C. Modelling with A = 1.25 (upper curve); modelling with A = 1.11 (lower curve). The time till regression lines reach 37.2°C is different: 2.7 hours (A = 1.25) and 1.3 hours (A = 1.11), respectively. After the end of the plateau the curves proceed in parallel with a time difference of 1.4 hours.

From 216 cooling experiments conducted on dummies corresponding to body weights of between 7 and 104 kg, and under different ambient temperatures and a wide range of different cooling conditions (including variable conditions such as clothing, covering, wind, wet surface, grounds of very different thermal conductivity and capacity), a mean value of *A* of 1.16 with a standard variation of ±0.14 was found. A systematic analysis [2] could not confirm any dependence of the figure of the constant *A* on the ambient temperature as supposed in body cooling. Nevertheless, the magnitude of *A* showed a slight dependence on the virtual weight of dummies in cooling experiments under standard conditions. The magnitude of *A* also varied with the magnitude of *B* resulting from the virtual weight and the corrective factor for various cooling conditions differing from standard. The cooling curves could not be modelled more accurately mathematically using these 'new' results than using the 'old' value of 1.25 for the constant *A*.

The value of *A* may also depend on the homogeneity of body temperature when death occurs. If the superficial layers of the body are already cool because of the peripheral vasoconstriction (e.g. during haemorrhagic shock without any central hypothermia), a gradient in body temperature, directed from the shell to the core of the body, is present when death occurs; the post-mortem temperature plateau, so to speak, has started during life. The real post-mortem plateau will be shorter in such cases than in cases with a short duration of agony. This particular event cannot be reproduced by dummies.

6.1.1.18 The Temperature at Death

The temperature at death, *To*, is the third constant of Marshall and Hoare's formula [42–44]. Any temperature-based method for calculating the time since death needs a distinct value of this constant. If the rectal temperature at death is unknown, as is usual in casework at the scene, it is necessary to use a fixed value. Because the central body temperature has a circadian rhythm, a detailed discussion about the 'true' value of *To*, which should be used as the fixed value in the formula, is meaningless—the more so as physiological mechanisms can change the central temperature (e.g. the menstrual cycle or strong physical activity shortly before death). We used the same fixed value (37.2°C) as used by Marshall and Hoare [42–44].

In giving evidence at court, one can extrapolate the rectal temperature to limiting values of the physiological range of rectal temperature (36.5°C to 37.5°C), instead of using the fixed value. Actually, this would be an unimportant part of the overall range of uncertain factors (mean ambient temperature, corrective factor of the body weight, approximation of the constants *B* and *A*) in calculating the time since death in any particular case. In addition, the overall limits of error resulting from many investigated body coolings include the partial errors resulting from the physiological range of rectal temperature. One of the most widely discussed sources of error in calculating the time since death by extrapolating the body temperature is 'fever at death'. Equation 6.1 is open for electing a greater value than 37.2°C if there is actual information concerning a fever of the decedent (this usually comes from the physician, other witnesses and/or as a result of autopsy) (examples in Figure 6.25). Nevertheless, this is an exception to the rule.

Conversely, an unrecognized rise of temperature ante mortem during agony may be present in certain cases (especially in intracranial injuries, certain poisonings, febrile illness without any pathomorphological findings, struggle or physical work shortly before death). What errors can be expected in cases of unrecognizable fever? The error caused by fever is greatest during the first hours post-mortem and decreases with time. Because of the higher gradient between the rectal and the ambient temperature, the drop of the rectal temperature is at first steeper than the stated value of 37.2°C at death (Figure 6.26 and Table 6.13). As long as the measured rectal temperature is 37.2°C or higher, the decedent is 'still alive' according to the formula's value of 37.2°C. When the rectal temperature falls to 37.1°C, the real possibility of an error caused by a fever exists. In the example of Table 6.13, the death time is 0.8 hours in a case of 37.2°C at death. In a case with a real starting point of 40.2°C, the death time would be 4.8 hours and, in using Equation 6.1 with the stated starting point of 37.2°C, an error of −4 hours would result. This is the maximum error in this case. However, this error should be recognized by rigor mortis, hypostasis and the reduced mechanical and electrical excitability after a real time since death of about 5 hours (see Chapter 10).

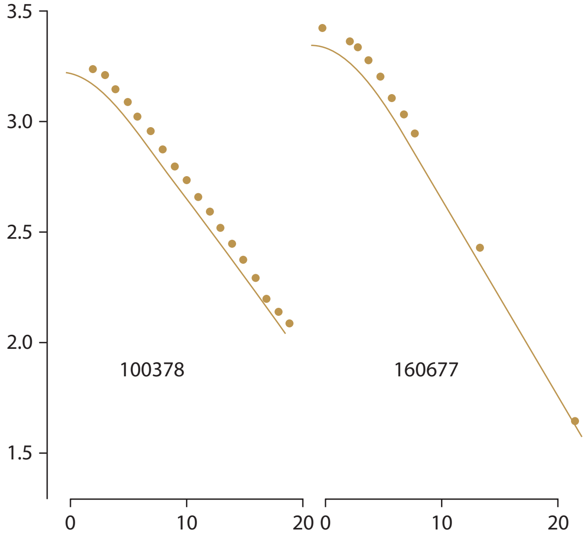

Figure 6.25 Real cooling curves and model curves according to Equation 6.2 with stated 37.2°C as '*To*' of two bodies with fever at death [23]. Abscissa: time of death in hours; ordinate: ln (rectal–ambient temperature). Case 100378: measured temperature 37.8°C 2 hours post-mortem and 37.0°C 3 hours post mortem, respectively. Result of autopsy: acute tuberculosis of the lungs with pneumonia and pleuritis. Case 160677: chronic leukaemia with final blast crisis. Last measured temperature 4 hours before death occurred was 39.6°C.

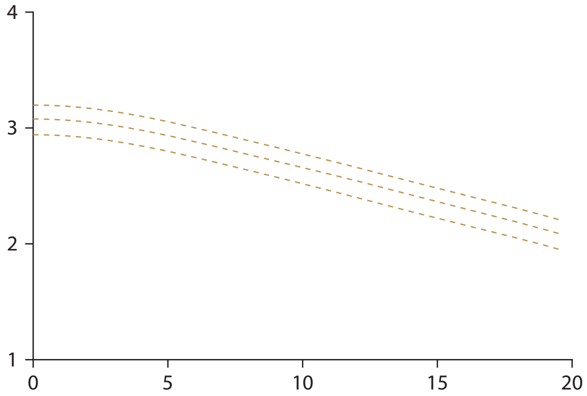

Figure 6.26 Errors caused by fever or slight hypothermia at death. Model cooling curves of a 70 kg body ($B = -0.0617$) in 15°C ambient temperature starting at 40.2°C (upper curve), 37.2°C (middle curve) and 34.2°C (lower curve), respectively. The errors of computed death times according to Equation 6.2 using 37.2°C as the value for *To* are seen in Table 6.13.

Later on, when the rectal temperature decreases further, the error caused by a fever diminishes to a level of about 2.5–2 hours (see Table 6.13).

More serious, in relation to large errors of calculated time since death, is a fall of rectal temperature during the period between fatal injury and death (or general hypothermia). This is because an antemortal decrease of rectal temperature can become greater than any increase caused by fever. As long as the antemortal decrease of rectal temperature is of the same order, but with changed sign, the overestimation of the calculated death time is also of the same order (see Table 6.13 and Figure 6.26). Nevertheless, if there is any suspicion of general hypothermia, any temperature method of calculating the time since death must not be used. Hypothermia should be suspected if a long agonal period existed under ambient conditions conducive to hypothermia. In the very early post-mortem interval of the first 10 hours, a threatened error can be avoided by applying other tests of death time estimation (especially the examination of mechanical and electrical excitability of skeletal muscle), which gives results inconsistent with the low rectal temperature in cases of hypothermia (see Chapter 10).

6.1.1.19 Accuracy of Calculated Time Since Death

When plotting the errors in calculated death time against the post-mortem time scale, there was first a decrease in error, which reached a minimum about 16–22 hours

Table 6.13 Errors Caused by Fever or Slight Hypothermia at Death*

Measured rectal temperature (°C)	Stated 37.2°C at death	Really 40.2°C at death		Really 34.2°C at death	
Time of death	Calculated	Error	Calculated	Error	
37.2	0.0	4.6	−4.6	—	—
37.1	0.8	4.8	−4.0	—	—
34.2	5.0	7.6	−2.6	0.0	5.0
34.0	5.4	7.8	−2.4	1.2	4.2
28.0	12.2	14.4	−2.2	9.8	2.4
22.0	22.4	24.4	−2.0	20.0	2.4

* Errors of computed death times (Equation 6.1) using 37.2°C as the value for T_0 if the temperature at death is really 40.2°C and 34.2°C, respectively. Example of a 70-kg body in 15°C ambient temperature (see Figure 6.28) [146].

post-mortem in a series of 28 bodies between 31 and 112 kg body weight [16]. This phenomenon is mainly caused by the use of a fixed (but actually unknown) value of rectal temperature at death *To* of 37.2°C, which provides larger errors in the early cooling phase than later on, as discussed earlier (see Table 6.13). A second reason was the usually unknown cooling conditions between death and the beginning of examination, before the body had been transported to the mortuary. This was called 'pre-analytic error' [26].

After the minimum phase of error, there is a continuous increase in error because the mean value of the constants *A* (1.25) and *B* (Equations 6.2 and 6.5, respectively) and the low accuracy of temperature measurements become progressively more disturbing as the temperature difference between body and ambient temperature decreases. In addition, even small changes of ambient temperature, as well as of any other cooling condition, cause larger errors, as the difference between body and ambient becomes lower.

Plotting the errors against the progress of death time is not a good way of obtaining information about errors because of the great variation in the time taken to reach the ambient temperature, which depends on the body weight (Table 6.14). The body of a baby reaches the ambient temperature corresponding to increased errors in a much shorter time than does the obese body of an adult, where the larger errors develop much later.

In summarizing cases of different body weights, the errors of computed death time should not be plotted against the progress of death time, but against the progress of cooling—which is the real cause of the increase in errors. A good measure of the progress of cooling is the standardized temperature *Q* (see Figure 6.10 and Equation 6.1). Its value is 1 at death, and 0 when the rectal temperature has reached the ambient temperature. So, a value of 0.5 means that the original difference between the rectal and the ambient temperature at death has been reduced to 50 per cent. Dependent on the body weight, a defined value of *Q* corresponds to different times of death (see Table 6.14). Relating the errors of calculated time since death to the standardized temperature, *Q*, the values from bodies of very different weights become comparable. In our own experiments under controlled conditions in ambient temperatures between 5°C and 22°C, the computed time of death, according to Equations 6.1 and 6.2 (see Equation 6.14), had errors that could be classified into three groups (Figures 6.27 and 6.28 and Table 6.15).

Table 6.14 Death Time at Defined Levels of the Standardized Temperature '*Q*' Dependent on the Body Weight

Level of *Q*	Body weight (kg)				
30	50	70	90	100	
0.5	7	11	15	19	23
0.3	12	17	23	29	36
0.2	15	22	30	38	46

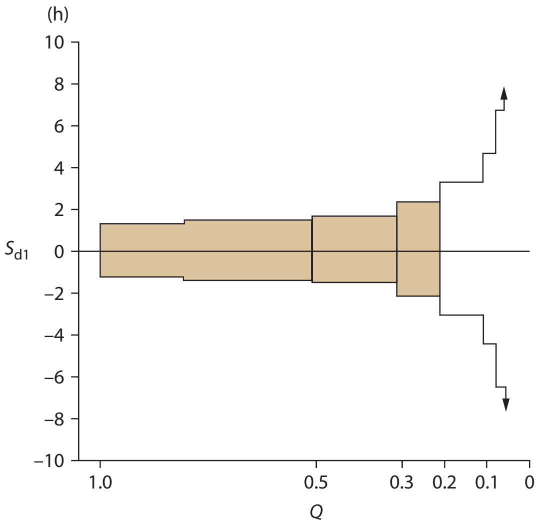

Figure 6.27 Standard deviation S_{dt} of calculated death time dependent on the progress of cooling *Q*. Chosen standard conditions of cooling. Fifty-three bodies were used; body weights of 9–112 kg; age 1– 87 years; ambient temperature 5.8–22°C; start of temperature measurement 0.8– 6 hours post-mortem to end 10–75 hours post-mortem. Most bodies were cases of a sudden unexpected death, all of them with time of death known to within some minutes. Calculation of the death time according to Equations 6.1 and 6.2 [19,54].

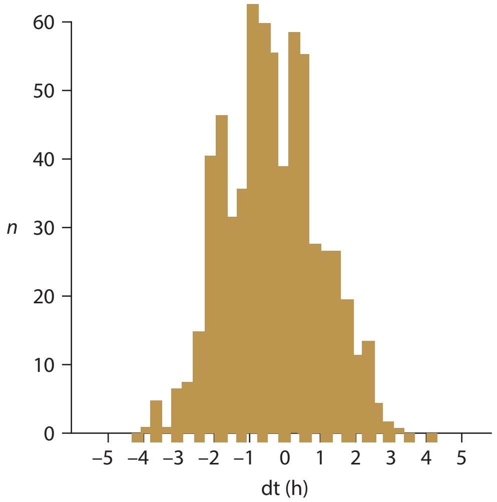

Figure 6.28 Histogram of the errors of calculated death time for $1 > Q > 0.5$ in addition to Figure 6.27. Standard conditions of cooling [19,54].

Table 6.15 Standard Deviation of 'Calculated-real Death Time' Dependent on the Progress of Cooling *Q* of 53 Bodies under Chosen Standard Conditions of Cooling*

		Calculations according to	
***Q* range**	***n***	**Equations 6.1 and 6.2**	**Rule of thumb**
$1.0 > Q > 0.90$	117	1.3	1.4
$0.9 > Q > 0.80$	126	1.3	2.0
$0.8 > Q > 0.70$	142	1.4	2.5
$0.7 > Q > 0.60$	140	1.4	3.2
$0.6 > Q > 0.50$	155	1.4	4.0
$0.5 > Q > 0.40$	181	1.6	5.1
$0.4 > Q > 0.30$	208	1.6	6.7
$0.3 > Q > 0.20$	208	2.2	10.8
$0.2 > Q > 0.10$	224	3.1	16.1
$0.1 > Q > 0.07$	67	4.5	18.1

* In comparison with the calculation of death time according to the two exponential formulae, the figures are also given for calculation of the death time according to the rule of thumb '1°C decrease of rectal temperature per hour plus 3 hours' [54].

These corresponded to values of *Q* between 1 and 0.5—the permissible variation of 95 per cent is ±2.8 hours. For more progressive cooling, corresponding to values of *Q* between 0.5 and 0.3, the permissible variation of 95 per cent is ±3.2 hours. For values of *Q* between 0.3 and 0.2, the permissible variation of 95 per cent is ±4.5 hours [54]. Below a *Q* value of 0.2, we obtained very large errors in some cases. Therefore, and in compliance with Fiddes and Patten [11], the reliability of computing the time since death cannot be assessed.

Computing the time since death of the cooling curves reported by De Saram et al. [10] in ambient temperatures between 26°C and 31°C according to Equation 6.15, the standard deviation was ±1 hour [16], which corresponded to the permissible variation of 95 per cent of about ±2 hours. Nevertheless, we recommend the use of the given permissible variation of 95 per cent of our own experimental cooling curves in lower ambient temperatures because the computation of death time ended at 8 hours post-mortem in the material of De Saram et al.

In computing the time since death of the experimental body cooling under various cooling conditions, and the resulting error statistics (Table 6.16), we assumed a variation in the corrective factor of ±0.1 around the real one. If the investigated corrective factor was, for example, 1.4 in a case, we also supplied 1.3 and 1.5. This was done in casework where the selection of a corrective factor is really somewhat uncertain. Depending on the progress of cooling *Q*, we obtained the listed permissible variations (see Table 6.16; Figures 6.29 and 6.30) [16].

Table 6.16 Standard Deviation of 'Calculated-real Death Time' Dependent on the Progress of Cooling Q of 26 Bodies under Various Cooling Conditions*

		Calculations according to	
***Q* range**	***n***	**Equations 6.1 and 6.5**	**Rule of thumb**
$1.0 > Q > 0.5$	464	1.3	3.9
$0.5 > Q > 0.3$	142	2.2	9.2
$0.3 > Q > 0.2$	42	3.4	18.3

* For the 'rule of thumb' see Table 6.15.

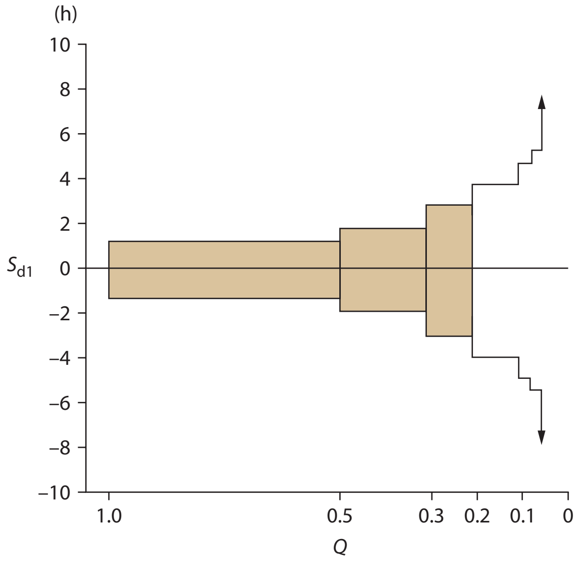

Figure 6.29 Standard deviation S_{dt} of calculated death time dependent on the progress of cooling *Q*. Various cooling conditions differing from the chosen standard. Twenty-six bodies were used. Calculation of the death time was according to Equations 6.2 and 6.6. For further details see Figure 6.30 [19,54].

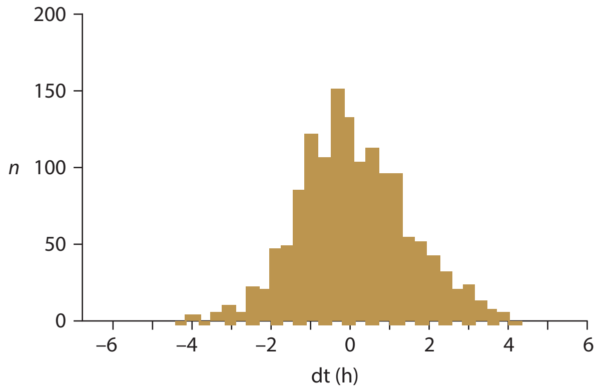

Figure 6.30 Histogram of the errors of calculated death time for 1 > Q > 0.5 in addition to Figure 6.29. Various cooling conditions differing from the chosen standard [19,54].

6.1.1.20 How Is the Death Time Obtained?

To apply all the basic considerations raised by mathematical modelling of the body cooling, and the experience of experimental body and dummy coolings to casework, a simple means is required for the quick calculation of the interval of death at the scene without any mental arithmetic.

The basis for calculating the time of death is Equation 6.1, which has the three constants *To, B* and *A*, and the two measures *Tr* (rectal temperature) and *Ta* (ambient temperature). As discussed earlier, we defined:

- *To* as 37.2°C
- *B* as [–1.2815 × (corrective factor × body weight)$^{-0\ 625}$ + 0.0284] (Equation 6.5)
- *A* for ambient temperatures up to 23°C as 1.25.

Equation 6.1 can now be written as:

$$Q = \frac{\mathrm{Tr}-\mathrm{Ta}}{37.2-\mathrm{Ta}} = 1.25\times\exp(B\times t) - 0.25\exp(5\times B\times t) \qquad (6.14)$$

The cooling curves published by De Saram et al. [10] were obtained in ambient temperatures between 26°C and 31°C and could be better fitted by *A* = 1.11, giving:

$$Q = \frac{\mathrm{Tr}-\mathrm{Ta}}{37.2-\mathrm{Ta}} = 1.11\times\exp(B\times t) - 0.11\exp(10\times B\times t) \qquad (6.15)$$

Equations 6.14 and 6.15 cannot be solved to time *t*, and therefore an approximation is necessary. There are two ways to calculate the time since death at a scene of death, neither of which requires the use of any mental arithmetic:

1. By means of a computer program. ‘Professor, I get thanks from the whole world for putting the formulae that you worked out into a computer form that police officers now carry on their cell phones’, wrote Ed Friedlander MD (Kansas City) to the author. His free online program (Java) calculates the time since death following this method (www.pathguy.com/TimeDead.htm). The self-explanatory program (Figure 6.31) operates on the basis of Table 6.18. It also gives the 95 per cent confidence limits according to Tables 6.15 and 6.16 and points to high uncertainty of the result when the temperature difference between rectum and surrounding is too low. Some adjustment is reminded in cases of known fever or hypothermia. The influence of the kind of supporting base on the corrective factor according to Table 6.19 is not taken into account just as the dependence of corrective factors on the body weight according to Table 6.20 or Equation 6.10. In such cases adjustment is necessary.

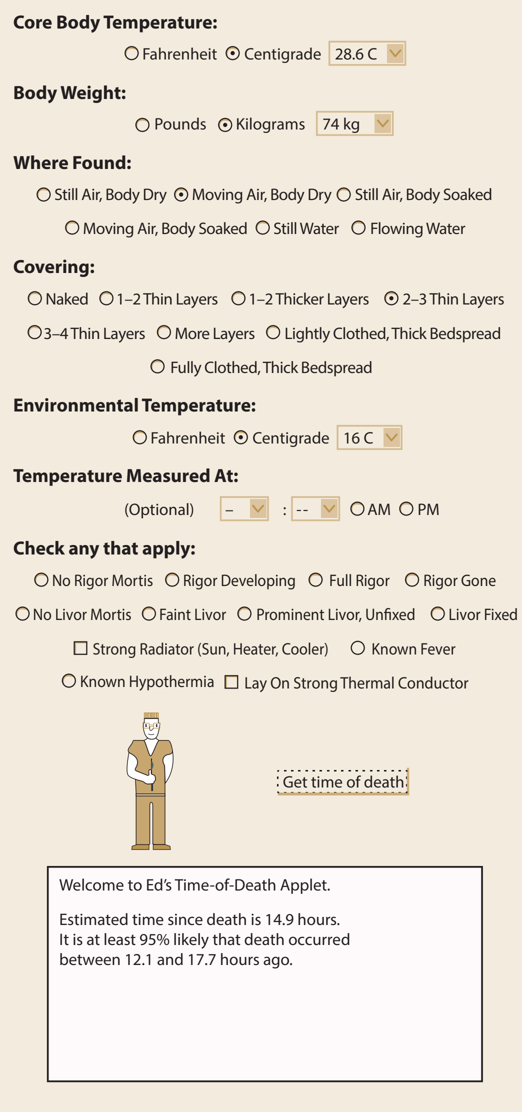

Core Body Temperature:

○ Fahrenheit ● Centigrade 28.6 C

Body Weight:

○ Pounds ● Kilograms 74 kg

Where Found:

○ Still Air, Body Dry ● Moving Air, Body Dry ○ Still Air, Body Soaked
○ Moving Air, Body Soaked ○ Still Water ○ Flowing Water

Covering:

○ Naked ○ 1–2 Thin Layers ○ 1–2 Thicker Layers ● 2–3 Thin Layers
○ 3–4 Thin Layers ○ More Layers ○ Lightly Clothed, Thick Bedspread
○ Fully Clothed, Thick Bedspread

Environmental Temperature:

○ Fahrenheit ● Centigrade 16 C

Temperature Measured At:

(Optional) – : -- ○ AM ○ PM

Check any that apply:

○ No Rigor Mortis ○ Rigor Developing ○ Full Rigor ○ Rigor Gone
○ No Livor Mortis ○ Faint Livor ○ Prominent Livor, Unfixed ○ Livor Fixed
☐ Strong Radiator (Sun, Heater, Cooler) ○ Known Fever
○ Known Hypothermia ☐ Lay On Strong Thermal Conductor

Welcome to Ed’s Time-of-Death Applet.

Estimated time since death is 14.9 hours.
It is at least 95% likely that death occurred
between 12.1 and 17.7 hours ago.

Figure 6.31 Computation of a case example by Ed Friedlander’s computer program.

(Courtesy of E. Friedlander, www.pathguy.com/TimeDead.htm)

Table 6.17 Data of Instructive Cases of a Field Study

Case number	Cooling conditions	Correction factor		Real body weight (kg)	Ambient temperature (°C)		Rectal temperature (°C)	Time estimated lower upper limit (hpm)		Time ascertained lower upper limit (hpm)		Comment
		Mean	Range		Measured	Used						
11	Outside, LB on asphalt, trousers, pants, short panty, moving air[*].	1.1	1.0–1.2	60	16.0/16.3	14.0[*]/163	22.1	16.7	25.7	?	?	[*] According to local weather station for the period in question.
13	Room, floor, LB, open trousers, short panty.	1.1	1.0–1.2	98	19.8/19.8	16.0[*]/18.0	33.2	07.2	12.8	08.3	[†]08.3	[*] Reconstruction of the room temperature by night 1 day later with automatically turned off central heating system. The body was found in the morning. [†] Stop of destroyed wrist watch.
15	Street, LL, wet-through tracksuit trousers, short panty, rain, moving air.	0.7	0.6–0.8	76	12.8/12.8	11.8/13.8	35.0	00.3	05.9	04.3	04.5	
22	Outside, soil, LP, wet-through work trousers, short panty, wind, rain.	0.7	0.6–0.8	93	09.9/09.9	08.9/10.9	36.2	00.0	04.9	02.7	02.9	
25	Room, floor, LB, pyjamas, briefs, temporarily moving air.	1.0	0.9–1.1	56	15.7/17.2	15.7/17.2	25.4	10.7	17.1	12.9	13.0	
26	Concrete staircase ground floor, LB, jeans, short panty.	1.0	0.9–1.1	82	073[*]/11.1[†]	04.2[‡]/11.1	30.2	06.3	11.9	07.4	07.4	[*] Ground floor near the body. [†] Staircase second floor. [‡] Outside, open front door.
27	Metal road, LL, jeans pulled down to knee-joints, moving air.	0.7	0.5–0.9	68	14.2/14.2	07.0[*]/14.2	30.6	02.8	08.4	01.5	6.3	[*] Lowest temperature at night before finding in the morning.
31	Outside, soil, LL, remnants of carbonized[*] clothing, wet body surface, moving air.	0.7	0.6–0.8	57	06.2[†]/10.3[‡]	06.2/10.3	33.3	00.3	05.9	03.8	04.3	[*] Some minutes after inflammation of the person extinguishing began, first with dry fire-fighting equipment, subsequently with water.

(*Continued*)

Table 6.17 (*Continued*) **Data of Instructive Cases of a Field Study**

Case number	Cooling conditions	Correction factor		Real body weight (kg)	Ambient temperature (°C)		Rectal temperature (°C)	Time estimated lower upper limit (hpm)		Time ascertained lower upper limit (hpm)		Comment
		Mean	Range		Measured	Used						
							Second measurement 1 hour later:					†Soil.
							31.2	01.4	07.0	04.8	05.3	‡Air.
							Method not used.					Estimation of the period since death by non-temperature-based methods only; see Table 6.7
33	LB on bed covered with thick blanket, trousers, boxing shorts, short panty.	2.2	2.0–2.4	62	18.5/18.5		41.6	(04.7	10.3) Not used (lack of expertise) 12.1*	00.5 35.3*	25.5	*On the supposition of malignant hyperthermia with temperature at death of 43.5°C: Subtraction of 6.3°C from the measured rectal and ambient temperatures as the difference between the supposed rectal temperature at death (43.5°C) and the 37.2°C-norm of the formula (nomogram).
42	Room of attic flat, floor, open skylight*, jeans, short panty.	1.1	1.0–1.2	57	22.5/22.5	12.8*/22.5	24.8	12.6	33.0	15.4	16.2	*Mean temperature at night outside: 12.8°C (weather station). Examination at noon (summertime).
43	Room, floor, LL, naked, temporarily moving air*.	0.9	0.75–1.0	67	19.0/21.0	18.0/22.0	34.5	02.1	07.7	02.7	?	*Open windows.
44	Room, floor, carpet, LB, trousers, short panty, moving air*.	1.0	0.9–1.1	71.5	15.4†/21.3‡	15.4/21.3	35.5	01.1	06.7	03.6	04.3	*Open windows and doors. †At time of examination beside body. ‡Within cupboards, beneath carpets near the body.
45	Situation at finding: outside, head-stand-like position within a big bale of straw, jeans, short panty.	1.8?	1.5–2.0?	83	18.6* 11.5† 12.2‡			32.8	Method not used: no experience as to particular cooling condition.	04.5	07.5	*Within straw. †Air at examination. ‡Soil at examination. §Air for the period in question (weather station) Estimation of the time since death by non-temperature-based methods only; see Table 6.7.

(*Continued*)

Table 6.17 (*Continued*) **Data of Instructive Cases of a Field Study**

Case number	Cooling conditions	Correction factor		Real body weight (kg)	Ambient temperature (°C)		Rectal temperature (°C)	Time estimated lower upper limit (hpm)		Time ascertained lower upper limit (hpm)		Comment
		Mean	Range		Measured	Used						
	4 hours before examination: Outside soil, LB, jeans, short panty, temporarily moving air.	1.0	0.9–1.1		16.0–18.0§							
48	Room, LL on sofa with his back in contact with the back-rest of sofa, blanket between tights, short underpants.	1.2	1.1–1.3	78	27.3/27.3	25.0*/27.3	33.3	08.8	14.4	11.0	14.0	*According to crime police on coming to the scene 2 hours before examination.
49	Outside, soil, LB, jeans, trousers, leggings, panty, moving air	1.35	1.3–1.4	45.5	16.6*/20.3†	13.0‡/20.3	25.4	11.2	21.6	16.3	16.8	*Soil. †Air. ‡Mean temperature at night before finding the body at the early afternoon.
54	Room, LL on couch, tracksuit, short panty, moving air*	1.05	0.9–1.2	77	21.5/21.5	17.0†/20.0†	29.8	10.5	16.4	04.8	13.8	*Open window. †The open window of the very small room was closed by investigators 1 hour before examination. At this time the room temperature was 18.5°C measured by crime police.
55	Street, LL on asphalt, jeans, short panty, moving air.	0.9	0.8–1.0	80	05.5*/07.2†	05.5/07.2	33.2	02.2	07.8	03.8	05.2	*Asphalt. †Air.
56	Room, LL on bed, trousers, short panty, moving air*.	1.05	0.9–1.2	78	15.7/16.2	10.0†/16.2	26.9	11.2	19.1	04.7	20.7	*The window was open at finding the body 4.5 hours before examination. Then it was closed. It was opened again for 30 minutes a short time before examination and was closed again. †The temperature outside at night before examination at noon was around 0°C.

(*Continued*)

Table 6.17 (*Continued*) Data of Instructive Cases of a Field Study

Case number	Cooling conditions	Correction factor		Real body weight (kg)	Ambient temperature (°C)		Rectal temperature (°C)	Time estimated lower upper limit (hpm)		Time ascertained lower upper limit (hpm)		Comment
		Mean	Range		Measured	Used						
64	Outside LP[*] on lawn, jeans, short panty, temporarily moving air.	1.0	0.9–1.1	98	10.3/11.0	10.3/11.0	33.8	03.9	09.5	06.3	06.6	[*] Found LP, changed to LB by first aid doctor.
62	LB on bed, naked.	1.15	1.0–1.2	60	18.0/20.5	18.0/20.5	27.5	10.9	17.3	13.2	19.7	
66	Room, LB on bed, covered with eiderdown until 2.5 hours before examination, boxer shorts.	1.8	1.6–2.0[*]	116	26.9[†]/26.9[†]	26.4/27.4	33.0	24.1	34.2	24.8	?	[*] Because of strong insulation condition and high body weight adaptation to 1.4–1.7 according to [20]. [†] Temperature at any place in the near and wider surrounding of bodies.
72	Behind open entrance-door of shop, floor, LL, trousers, short panty, temporarily moving air.	1.0	0.9–1.1	82	17.1/17.5	17.1/17.5	33.9	03.9	09.5	05.1	05.4	

Abbreviations: hpm, hours post-mortem; LB, lying back; LL, lying laterally; LP, lying prone.

Source: From Henssge C, Althaus L, Bolt J, Freislederer A, Henssge CA, Hoppe B, Schneider V. Experiences with a compound method for estimating the time since death. I. Rectal temperature nomogram for time since death. *Int J Legal Med* 1999;**113:**303–319.

Table 6.18 Empirical Corrective Factors of the Body Weight for Cooling Conditions Differing from the Chosen Standard*

Dry clothing/covering	Air	Corrective factor	Wet-through clothing/ covering wet body surface	In air	In water
		0.35	Naked		Flowing
		0.5	Naked		Still
		0.7	Naked	Moving	
		0.7	One to two thin layers	Moving	
Naked	Moving	0.75			
One to two thin layers	Moving	0.9	Two or more thicker layers	Moving	
Naked	Still	1.0			
One to two thin layers	Still	1.1	Two thicker layers	Still	
Two to three thin layers		1.2	More than two thicker layers	Still	
One to two thicker layers	Moving	1.2			
Three to four thin layers	or	1.3			
More thin/thicker layers	Still	1.4			
	Without influence	. . .			
Thick blanket		1.8			
+		. . .			
Clothing combined		. . .			
		2.4			
Lying on		1.8			
+		. . .			
covered by		. . .			
dry leaves		2.7			

* The listed values apply to bodies of average weight (reference: 70 kg), in an extended position on a 'thermically indifferent' base.
From Henssge C. Death time estimation in case work. I. The rectal temperature time of death nomogram. *Forensic Sci Int* 1988;**38:**209–236.

Table 6.19 Influence of the Kind of Supporting Base on the Corrective Factor

Supporting base		Clothing?	Corrective factor
Indifferent	Usual floor of rooms, dry soil, lawn, asphalt	Yes/no	
Insulating	Excessively thickly upholstered	Thick	+0.1
		Thin	+0.3
		No	+1.3
	Mattress (bed), thick carpet	Yes	+0.1
		No	+1.1/+1.2
	About 2 cm wettish leaves	No	+1.3
		No	+1.5
	About 2 cm totally dry leaves		
Accelerating	Concrete, stony, tiled	Thick	−0.1
		Very thin	−0.2
		No	−0.75

W. Schweitzer MD (Zürich) implemented a pHp written program (www.swisswuff.ch/calculaors/todeszeit.php). The appended three tables analogous to Tables 6.18, 6.19 and 6.20 assist in choosing an appropriate empirical corrective factor that also takes into account the supporting base and the dependence of corrective factors on the body weight (Figure 6.32). The generally used initial temperature at death of the order of 37.2°C can be changed if indicated. The result can be rounded to arbitrary 'smallest output unit [minutes]' (e.g. 30 minutes). The given 95 per cent tolerances are in accord with Tables 6.15 and 6.16.

The commercial Windows-operated program of C.A. Henssge MD (Magdeburg) [21] (www. AMAsoft.de) is flexible and interactive. Instead of an exact single value, a range for ambient temperature and corrective factor can be entered alternatively because in many cases it is impossible to appoint exact values to the found circumstances at the scene. A range of body weight first estimated at the scene can also be entered (Figure 6.33; compare with Figures 6.38 and 6.40). Two superimposed tables analogous to Tables 6.18 and 6.19 assist in choosing an appropriate empirical corrective factor that also takes into account the supporting base where required. The adjustment of corrective factors in dependence on the body weight (see Table 6.20) operates automatically according to Equation 6.10 whenever it is required. The generally used starting temperature at death of the order of 37.2°C can be changed if there is a history of fever during life. In addition, the program involves some non-temperature-based methods/criteria within a compound method (see Chapter 10). When the temperature-based nomogram method must not be used

Table 6.20 Chart of the Dependence of Corrective Factors on the Body Weight*

	Real body weight (kg)																	
	4	**6**	**8**	**10**	**20**	**30**	**40**	**50**	**60**	**70**	**80**	**90**	**100**	**110**	**120**	**130**	**140**	**150**
Cooling conditions										Average range								
										1.3								
Clothing,	1.6	1.6	1.6	1.6	1.5					**1.4**					1.3	1.2	1.2	1.2
more layers	2.1	2.1	2.0	2.0	1.9	1.8				**1.6**				1.4	1.4	1.4	1.3	1.3
Bedspread	2.7	2.7	2.6	2.5	2.3	2.2	2.1	2.0		**1.8**			1.6	1.6	1.6	1.5	1.4	1.4
	3.5	3.4	3.3	3.2	2.8	2.6	2.4	2.3		**2.0**		1.8	1.8	1.7	1.6	1.6	1.5	1.5
	4.5	4.3	4.1	3.9	3.4	3.0	2.8	2.6	2.4	**2.2**	2.1	2.0	1.9	1.8	1.7	1.7	1.6	1.6
Clothing +	5.7	5.3	5.0	4.8	4.0	3.5	3.2	2.9	2.7	**2.4**	2.3	2.2	2.1	1.9	1.9	1.8	1.7	1.6
bedspread	7.1	6.6	6.2	5.8	4.7	4.0	3.6	3.2	2.9	**2.6**	2.5	2.3	2.2	2.1	2.0	1.9	1.8	1.7
Feather bed	8.8	8.1	7.5	7.0	5.5	4.6	3.9	3.5	3.2	**2.8**	2.7	2.5	2.3	2.2	2.0	1.9	1.8	1.7
	10.9	9.8	8.9	8.3	6.2	5.1	4.3	3.8	3.4	**3.0**	2.8	2.6	2.4	2.3	2.1	2.0	1.9	1.8

* The average range of body weight, which is the base of the corrective factors 'known by experience' (Table 6.18), has been chosen at 70 kg (bold numbers). Below a corrective factor of 1.4 (up to 0.75), the dependence on the body weight can be neglected (see Table 6.1).

Source: From Henssge C. Rectal temperature time of death nomogram: dependence of corrective factors on the body weight under stronger thermic insulation conditions. *Forensic Sci Int* 1992;**54:**51–56.

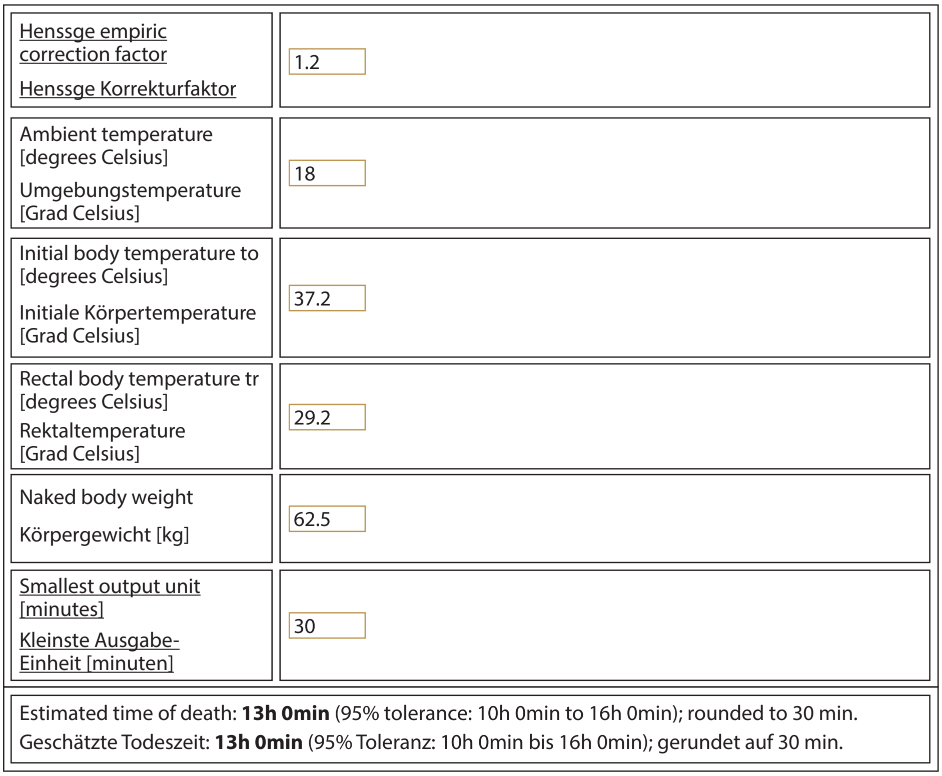

Henssge empiric correction factor Henssge Korrekturfaktor	1.2
Ambient temperature [degrees Celsius] Umgebungstemperature [Grad Celsius]	18
Initial body temperature to [degrees Celsius] Initiale Körpertemperature [Grad Celsius]	37.2
Rectal body temperature tr [degrees Celsius] Rektaltemperature [Grad Celsius]	29.2
Naked body weight Körpergewicht [kg]	62.5
Smallest output unit [minutes] Kleinste Ausgabe-Einheit [minuten]	30

Estimated time of death: **13h 0min** (95% tolerance: 10h 0min to 16h 0min); rounded to 30 min.
Geschätzte Todeszeit: **13h 0min** (95% Toleranz: 10h 0min bis 16h 0min); gerundet auf 30 min.

Figure 6.32 Example of Schweitzer's free online program.

(Courtesy of W. Schweitzer, www.swisswuf.ch/calculators/todeszeit.php)

because of contrary circumstances, the examination of the body should instead begin with any of the non-temperature-based methods/criteria. The result is displayed in hours post-mortem decimal as well as in date and time.

2. By means of nomogram (Figures 6.34 and 6.35) [17,18]. The calculation of the period since death by a computer program should be the preferred method of implementation of nomogram forms nowadays because it has more convenient handling, provides more accurate results and avoids significant errors caused by using potentially distorted scales of reproduced nomograms [9]. For the first step (see Figure 6.36), the points of the scales of the measured rectal temperature (e.g. 27°C in the left margin) and ambient temperature (e.g. 15°C in the right margin) have been joined by a straight line, which crosses the diagonal of the nomogram at a specific point. For the second step, a second straight line must be drawn passing

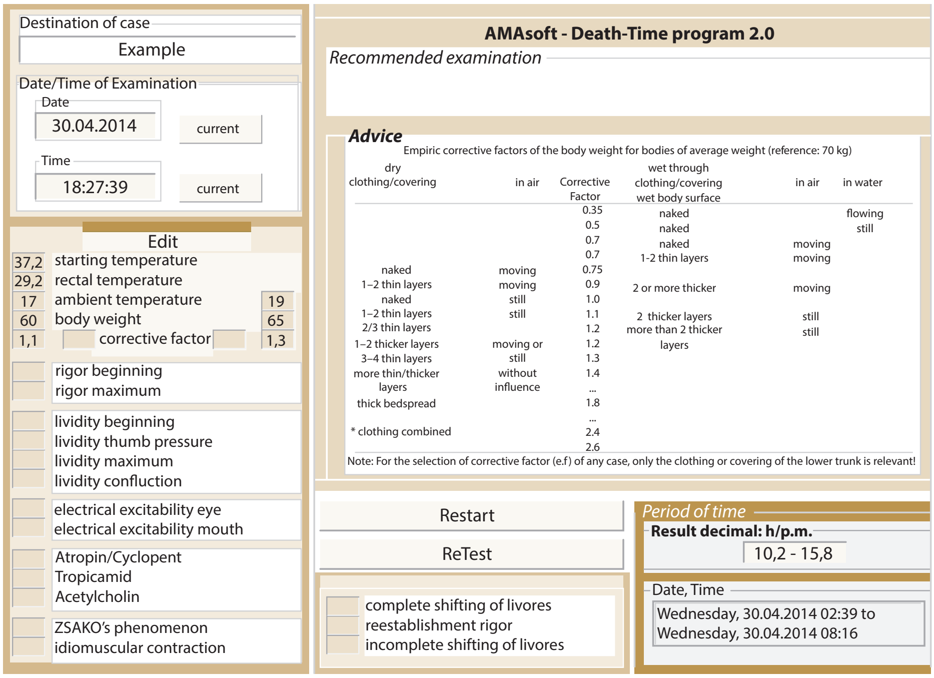

Destination of case

Example

Date/Time of Examination

Date: 30.04.2014 current

Time: 18:27:39 current

Edit

37,2 starting temperature

29,2 rectal temperature

17 ambient temperature 19

60 body weight 65

1,1 corrective factor 1,3

rigor beginning

rigor maximum

lividity beginning

lividity thumb pressure

lividity maximum

lividity confluction

electrical excitability eye

electrical excitability mouth

Atropin/Cyclopent

Tropicamid

Acetylcholin

ZSAKO's phenomenon

idiomuscular contraction

AMAsoft - Death-Time program 2.0

Recommended examination

Advice

Empiric corrective factors of the body weight for bodies of average weight (reference: 70 kg)

dry clothing/covering	in air	Corrective Factor	wet through clothing/covering wet body surface	in air	in water
		0.35	naked		flowing
		0.5	naked		still
		0.7	naked	moving	
		0.7	1-2 thin layers	moving	
naked	moving	0.75			
1–2 thin layers	moving	0.9	2 or more thicker	moving	
naked	still	1.0			
1–2 thin layers	still	1.1	2 thicker layers	still	
2/3 thin layers		1.2	more than 2 thicker layers	still	
1–2 thicker layers	moving or	1.2			
3–4 thin layers	still	1.3			
more thin/thicker layers	without influence	1.4 ...			
thick bedspread		1.8 ...			
* clothing combined		2.4 2.6			

Note: For the selection of corrective factor (e.f) of any case, only the clothing or covering of the lower trunk is relevant!

complete shifting of livores

reestablishment rigor

incomplete shifting of livores

Period of time

Result decimal: h/p.m. 10,2 - 15,8

Date, Time

Wednesday, 30.04.2014 02:39 to
Wednesday, 30.04.2014 08:16

Figure 6.33 Computation of a case example by the PC program of C.A. Henssge (www.AMAsoft.de) with ranges of body weight, ambient temperature and corrective factor [21].

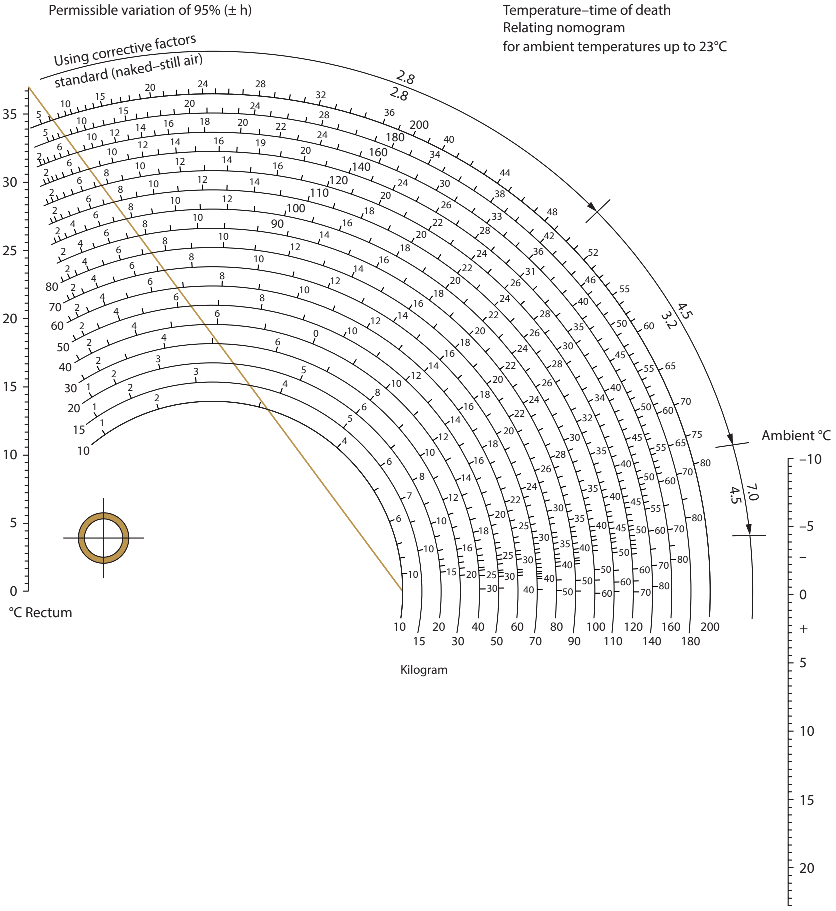

Figure 6.34 Nomogram for reading off the time of death from a single measurement of rectal and ambient temperature and from the body weight for ambient temperatures up to 23°C according to Equation 6.14. Without any corrective factor the nomogram is related to the chosen standard conditions of cooling. Reproduction of this form can provoke erroneous results by even slight distortion of the scales [9]. Download and print the original form at www.rechtsmedizin.uni-bonn.de/dienstleistungen/for_Med/todeszeit

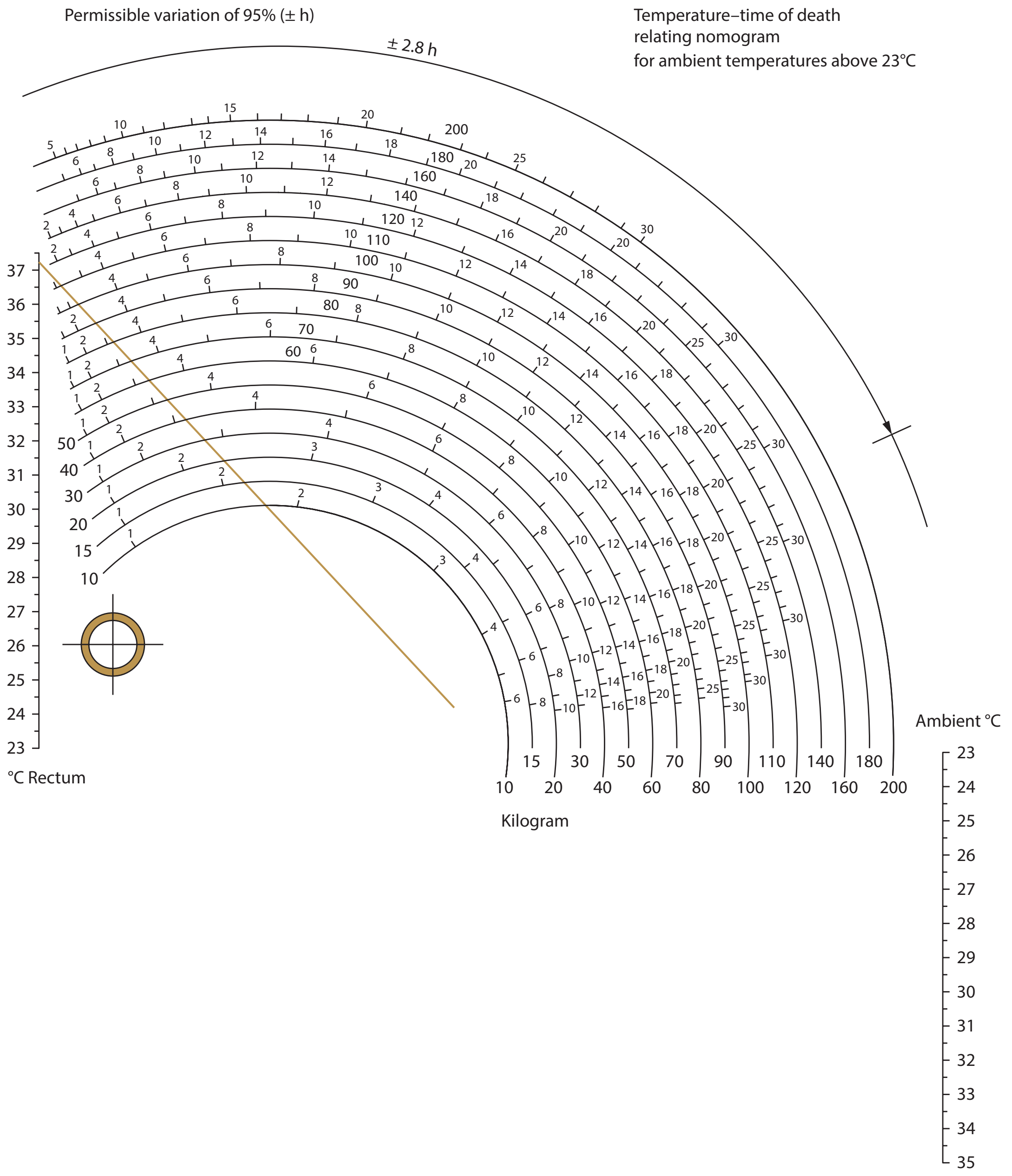
Permissible variation of 95% (± h)
± 2.8 h
Temperature–time of death
relating nomogram
for ambient temperatures above 23°C
37
36
35
34
33
32
31
30
29
28
27
26
25
24
23
°C Rectum
50
40
30
20
15
10
15
30
50
70
90
110
140
180
10
20
40
60
80
100
120
160
200
Kilogram
Ambient °C
23
24
25
26
27
28
29
30
31
32
33
34
35

Figure 6.35 Nomogram for reading off the time of death from a single measurement of rectal and ambient temperature and from the body weight for ambient temperatures above 23°C according to Equation 6.15. Without any corrective factor the nomogram is related to the chosen standard conditions of cooling. Reproduction of this form can provoke erroneous results by even slight distortion of the scales [9]. Download and print the original form at www.rechtsmedizin.uni-bonn.de/dienstleistungen/for_Med/todeszeit

through the centre of the circle (below left of the nomogram) and the intersection of the first line and the diagonal (Figure 6.37). The second line crosses the semicircles, which represent the different body weights, each with a calibration of the death time. The time since death (e.g. 13.5 hours post-mortem) can be read off at the intersection of the semicircle of the given body weight (e.g. 70 kg). The body weight used can be the real (chosen standard conditions of cooling) or the corrected body weight (using corrective factors). The second straight line touches the outermost semicircle, where the permissible variation of 95 per cent can be seen respectively levelling off the range of reliability. In bodies found under standard conditions of cooling, the figures ‘standard (naked-still air)’ are true (see Table 6.15). The figures ‘using corrective factors’ should be used when the body is found under cooling conditions differing from the chosen standard (see Table 6.16).

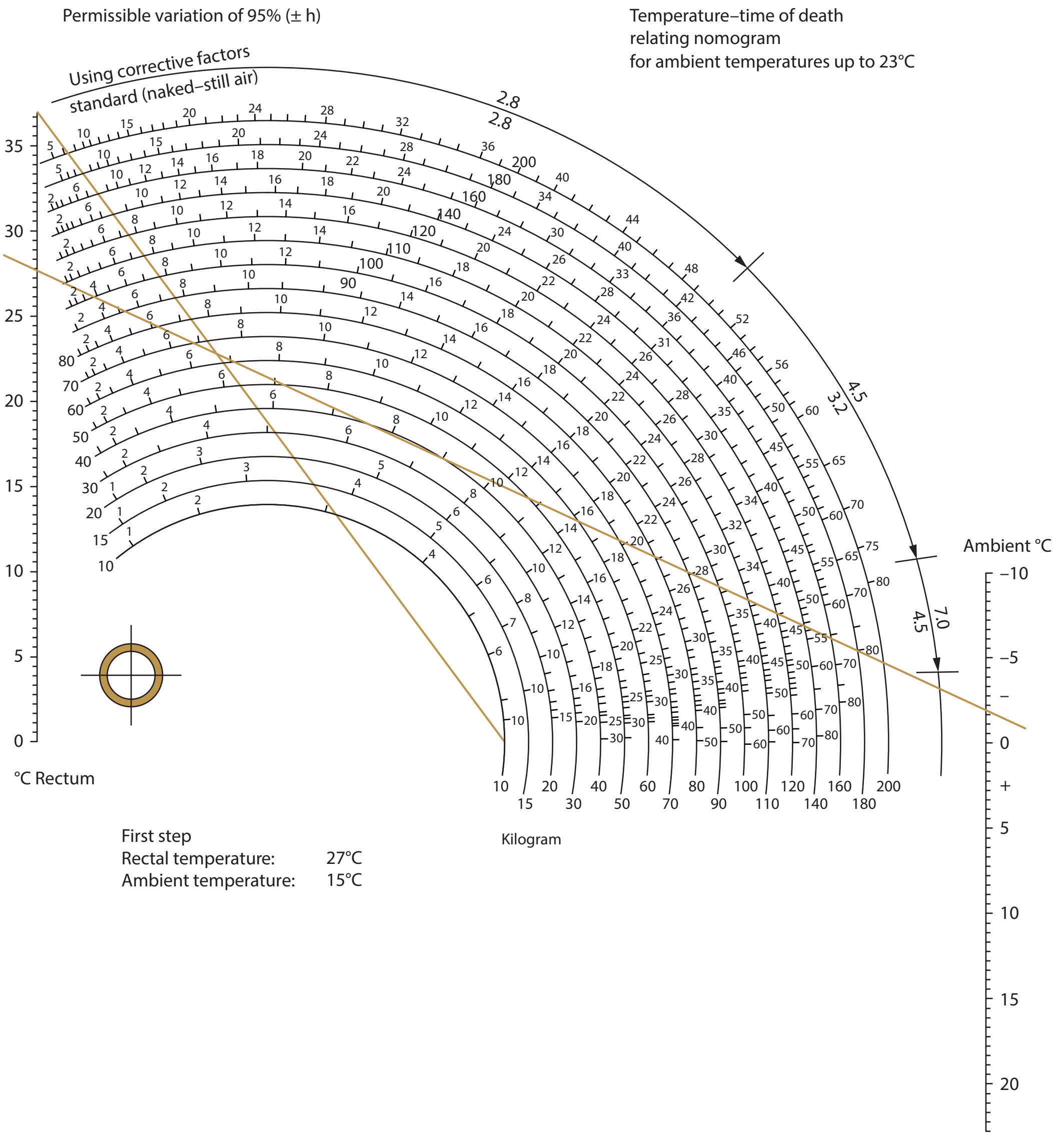
Permissible variation of 95% (± h)
Using corrective factors
standard (naked–still air)
Temperature–time of death
relating nomogram
for ambient temperatures up to 23°C
2.8
2.8
4.5
3.2
7.0
4.5
°C Rectum
Kilogram
Ambient °C
First step
Rectal temperature: 27°C
Ambient temperature: 15°C

Figure 6.36 The use of the nomograms. First step [19]. Reproduction of this form can provoke erroneous results by even slight distortion of the scales [9]. Download and print the original form at www.rechtsmedizin.uni-bonn.de/dienstleistungen/for_Med/todeszeit

6.1.2 Application of the 'Nomogram Method' in Casework

The estimation of the time since death at the scene of death using the nomogram form (see Figures 6.34–6.37) or computation by means of a computer program requires:

1. Single measurement of the 'deep' rectal temperature.
2. Estimation of the body weight.
3. Evaluation of the mean ambient temperature.
4. Evaluation of the corrective factor, if necessary.
5. Consideration of the features where the method must not be used.
6. Calculation of the interval of death.

The nomogram form itself (or Equations 6.14 and 6.15) is the result of experimental body coolings under chosen standard conditions of cooling reported earlier.

The chosen standard conditions of cooling are defined as follows:

- Naked body with dry surfaces
- Lying extended on the back
- On a thermally indifferent base
- In still air
- In surroundings without any source of strong heat radiation

If a body is found under conditions similar or comparable to the chosen standard conditions of cooling, the time of death can be computed or read off according to

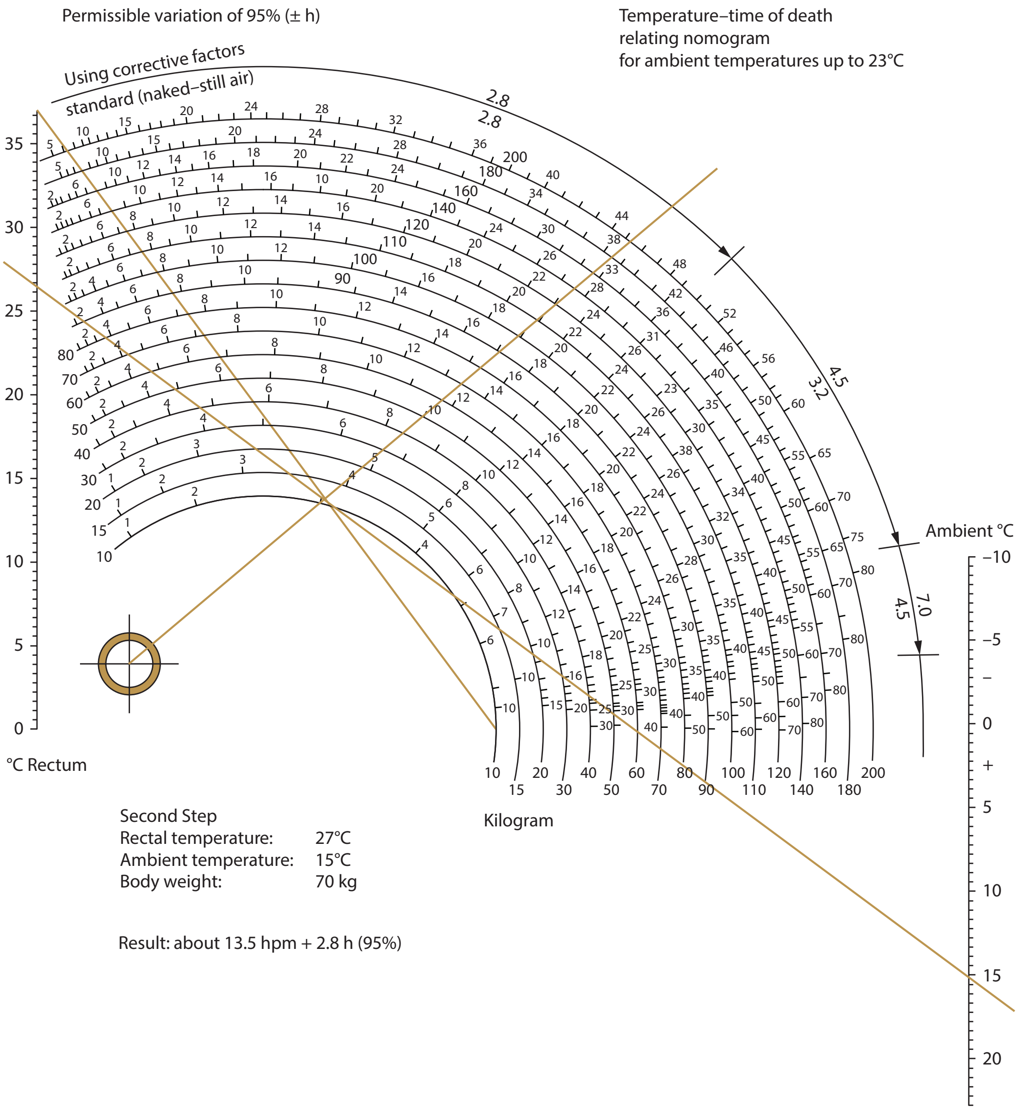
Permissible variation of 95% (± h)
Using corrective factors
standard (naked–still air)
Temperature–time of death relating nomogram for ambient temperatures up to 23°C
2.8
2.8
4.5
3.2
7.0
4.5
Ambient °C
°C Rectum
Kilogram

Second Step
Rectal temperature: 27°C
Ambient temperature: 15°C
Body weight: 70 kg

Result: about 13.5 hpm + 2.8 h (95%)

Figure 6.37 The use of the nomograms. Second step [19]. Reproduction of this form can provoke erroneous results by even slight distortion of the scales [9]. Download and print the original form at www.rechtsmedizin.uni-bonn.de/dienstleistungen/for_Med/todeszeit

the measured deep rectal temperature, the mean ambient temperature and the body weight. Provided it is made as exactly as possible, the time of death read from the nomogram closely approaches the computed time. The given permissible variation of 95 per cent at the outermost semicircle 'standard (naked-still air)' corresponds to the data of Table 6.15 and Figures 6.27 and 6.28.

If the cooling conditions differ from the chosen standard, they have to be taken into account by evaluating a corrective factor. The real body weight must be multiplied by the evaluated corrective factor. The time of death has to be read from the nomogram at the semicircle of the corrected body weight. The permissible variation of 95 per cent at the outermost semicircle 'using corrective factors' is then valid corresponding to Table 6.15 and Figures 6.29 and 6.30. By analogy, *B* must be calculated by Equation 6.5 when computing the time of death.

The successful use of the nomogram method requires experience, as with any medico-legal procedure. It is very easy to read off the time since death from the nomogram or to compute it. However, especially after computing the time of death without adding the permissible variation of 95 per cent, this gives the impression of high accuracy, which leads to the danger of misuse and misinterpretation.

First, the estimation of the time since death by any method of examination of the body is really the task of a forensic pathologist.

Second, the indicated value read from the nomogram or the computed time of death, is a mean value—a misleading part of the full result. *The interval limited by the* *permissible variation of 95 per cent is the one and only result: the death occurred, with the probability of 95 per cent, within this interval. A more precise indication of the interval since death cannot be obtained according to all the results of scientific investigations. A central mean value must not be offered (see Figure 6.33*).

Third, when using the nomogram method, the interval of death that is obtained is calculated using factors that are themselves either measures or evaluations. *It is possible to use the right rules but obtain the wrong results if the factors are wrong. The most important thing is to analyse these factors carefully at the scene of the crime. Fragmentary analysis of the facts at the scene often result in significant false estimation of the period since death.*

The estimation of the body weight at the scene of death is a question of personal experience. A serious mistake could be remedied quickly by weighing the body after its removal from the scene.

In the following subsection, evaluation of the 'mean ambient temperature' and of the 'corrective factor', as well as consideration of the features where the method must not be used, are discussed in more detail.

To enable handling of the method, it is referenced to special cases of a field study that are listed in Tables 6.17 and 6.21. The field study [24] includes 72 consecutive cases of an inspection of the scene of crime by a forensic pathologist before autopsies were carried out. The period of death was estimated by using the temperature-based nomogram method as a primary method (see Table 6.17), followed by the use of other non-temperature-based methods to confirm or improve the primary result (see Chapter 10).

6.1.2.1 Evaluation of the Mean Ambient Temperature

Theoretically, Equations 6.1, 6.14 and 6.15 require a constant ambient temperature. In fact, the mean ambient temperature of the whole period between the time of death and the time of investigation is employed [19,23]. The actual measured ambient temperature at a scene of crime need not necessarily be the mean. At first, the actual ambient temperature should be measured close to the body, and particularly at the same level above the base. It is recommended that not only the air temperature be measured but also the temperature of the underlying surface itself—if possible probing into the earth, into gaps between stones or beneath a carpet. If there are differences among ambient temperatures around the body, take the mean or use the range (Figures 6.38 and 6.39).

Furthermore, it is advisable to measure the temperature of the wider surroundings of the body, for example in the next room, the corridor and the landing, respectively, to obtain a view of temperature distribution (e.g. case 26 in Table 6.17). Some additional observation is necessary: in a closed room, look for the heating system and note its operating state (e.g. case 13 in Table 6.17). Were the windows and doors open or closed when the body was found? What about the outside temperature or sunshine through windows, and its possible influence on the room temperature (e.g. cases 44, 54 and 56 in Table 6.17)? The course of the ambient temperature from night (time of death) into day (finding the body) should be taken into account for evaluation of the mean ambient temperature of the period in question (e.g. cases 27, 42, 49 and 56 in Table 6.17). If the body is found outside, contact the weather station and ask for hourly temperatures and periods of rain, wind and sunshine (e.g. cases 11 and 42 in Table 6.17). Later, for example in court, this can be an advantage if the ambient temperature comes into question. Then consider the mean ambient temperature during the interval between death and the examination of body. The actual measured ambient temperature(s) and the concomitant temperature-related circumstances allow an evaluation of the required mean ambient temperature of the period in question, at least as a range in most cases (see Figure 6.38).

If ambient temperature *decreases* more or less continuously, its mean value for the period in question can be used successfully. A continuous *increase* of the ambient temperature is more problematic if a long death time comes into question (see later). The difference between rectal and ambient temperature should then be considered. If there is only a small difference, the method should not be used. The progression of cooling can be estimated quickly by calculation of the value of Q (Equations 6.1, 6.14 or 6.15). Conversely, the calculated mean of the ambient temperature can be used if the progression of cooling is still low ($Q > 0.5$).

When a range of ambient temperature is applied, two death times are computed or read from the nomogram—a shorter time corresponding to the lower ambient temperature, and a longer time corresponding to the higher ambient temperature (see Figures 6.38 and 6.39).

A peculiarity is a sudden great change in ambient temperature. Two murder cases in which the bodies had been transported from high ambient temperatures (scene of the crime) to low ambient temperature (place of finding the body) were the reason for cooling experiments with a sudden decrease and increase of ambient temperature of the order of 15°C in the course of the cooling process [3]. The experiments were performed with the aforementioned cooling dummies. In the case of a sudden *decrease* in ambient temperature, after cooling in a higher ambient temperature (about 21°C) for several hours to about 4°C, a second 'temperature plateau' occurred that was shorter than the known plateau at the beginning of body cooling. The second plateau at the beginning of the second cooling phase in a sudden decreased ambient temperature required a lower value of the constant A (1.15) compared with the known value (1.25) at the beginning of cooling. The period since death could be computed if the body was transported at a known time from a known high level

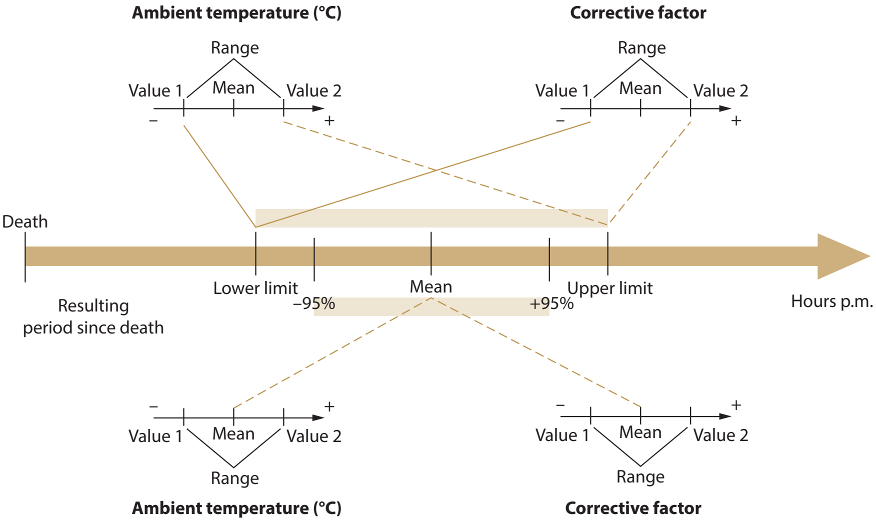
Ambient temperature (°C)
Range
Value 1
Mean
Value 2
–
+
Corrective factor
Range
Value 1
Mean
Value 2
–
+
Death
Lower limit
–95%
Mean
+95%
Upper limit
Hours p.m.
Resulting
period since death
Value 1
Mean
Value 2
Range
Ambient temperature (°C)
Value 1
Mean
Value 2
Range
Corrective factor

Figure 6.38 Scheme of the resulting periods since death using: (mode 1) mean values of the elevated ranges of ambient temperature and corrective factor and adding the empirical permissible variation of 95 per cent (see Tables 6.15 and 6.16); and (mode 2) the upper and lower brackets of the evaluated ranges of ambient temperature and corrective factor. If the evaluated ranges of both ambient temperature and corrective factor are very wide, the resulting period since death using mode 2 calculation may be greater than that using mode 1 calculation. It is recommended that both modes of calculation be applied and to use the wider period since death for expert opinion.

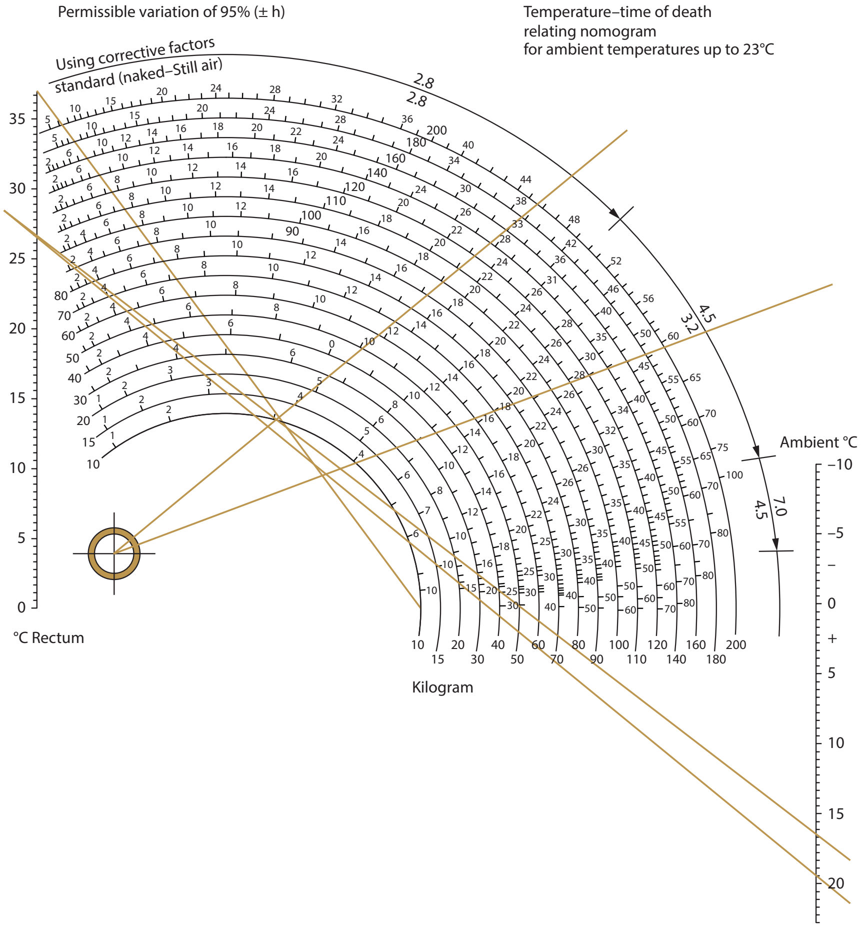

Figure 6.39 The use of the nomogram in a case with ranges of the ambient temperature (17–20°C) and the corrective factor (1.2–1.5) of a real body weight of 75 kg corresponding to corrected body weights between 90 and 110 kg [19].

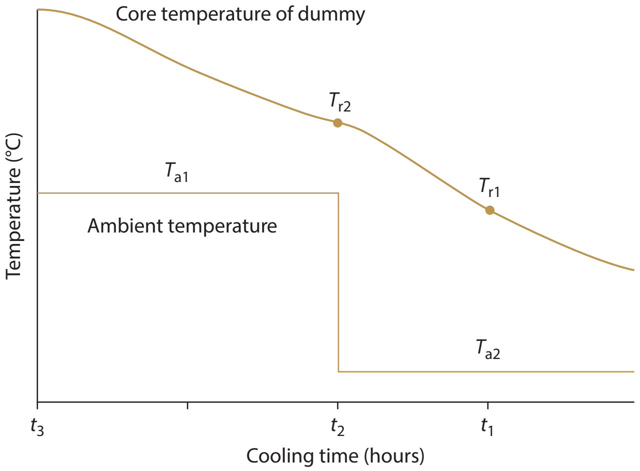

Figure 6.40 The scheme for the three-step procedure.

of ambient temperature to a low ambient temperature by means of the following three-step procedure (Figure 6.40).

6.1.2.1.1 Step 1

Going from the dummy temperature (T_{r1}) at any time of the second cooling phase (t_1) in low ambient temperature (T_{a2}), the body temperature (T_{r2}) at the known time (t_2) of rapid decrease of the ambient temperature can be calculated by transforming Equation 6.14 using a value of 1.15 for the constant A:

$$T_{r2} = \frac{T_{r1} - T_{r2}}{\mathrm{Q}} + T_{r2} \tag{6.16}$$

with

$$\begin{aligned} \mathrm{Q} &= 1.15 \times \exp[\mathrm{B} \times (t_1 - t_2) - 0.15 \\ &\quad \times \exp\left[\frac{1.15 \times \mathrm{B}}{0.15} \times (t_1 - t_2)\right] \end{aligned} \tag{6.17}$$

6.1.2.1.2 Step 2

Using the calculated body temperature (T_{r2}) at the known moment of moving the body according to Equations 6.17 and 6.18, the unknown period (t_2–t_3) of the first cooling phase in the known higher ambient temperature (T_{a1}) can be calculated by the standard method, either nomographically or by computing as usual according to Equation 6.15.

6.1.2.1.3 Step 3

The whole cooling period (*t*w) analogous to the period since death results from the addition of times of both cooling phases:

$$t_1 - t_3 = (t_1 - t_2) + (t_2 - t_3) \tag{6.18}$$

The errors of the calculated cooling times were within the known confidence limits of the method. The estimated period of death calculated by the three-step procedure was in agreement with the investigated period in the murder cases. One experimental online cooling curve of a body cooling for the first 10 hours at an ambient temperature of 22.5°C, and for the next 9 hours at 7.8°C, could also be sufficiently modelled by the three-step procedure.

In contrast, Althaus and I [3] were not able to model mathematically the cooling curves of the experiments with a sudden increase of ambient temperature from 4°C to 21°C. Nevertheless, an engineering induced team [5] provided a four-step procedure to estimate the cooling period analogous to the period of death in the dummy experiments with sudden increase of ambient temperature [3]. The main principle is to compute a theoretical body temperature T'_r at the time of temperature measurement t_1 that would have been measured if no sudden increase of ambient temperature had taken place. That results in a difference ΔT between the measured temperature T_r and the lower theoretical temperature T'_r.

$$\Delta T = T_r - T_r \tag{6.19}$$

This difference is caused by the sudden increase of ambient temperature from T_{a1} to T_{a2} at t_2. A standardization of ΔT with respect to its cause, the increase ΔT_a, is denoted by R. In its mathematical expression the whole cooling time t is replaced by the known cooling period after the sudden increase of ambient temperature $t_1 - t_2 = \Delta t$. The denotation of t follows Figure 6.40.

Step 1

$$R = A\exp[B(\Delta t - d)] - (A-1)\exp\left[\frac{AB}{A-1}(\Delta t - d)\right] \tag{6.20}$$

with $d = \dfrac{0.07}{\mathrm{R}}$

But according to Equation 6.5; 6.14 $A = 1.25$

Step 2

$$\Delta T = \Delta T_a(1 - R) \tag{6.21}$$

Step 3

$$T_r = T_r - \Delta \mathrm{T} \tag{6.22}$$

6.1.2.1.4 Step 4

This step involves estimation of the whole cooling time t analogous to the time since death by the standard method of Equation 6.14 with T'_r and T_{a1} by means of computation or nomographically.

The cooling times of the dummy experiments [3] could be calculated without systematic error within small confidence limits as demonstrated by the histograms of errors [5].

The study may provide evidence that the period since death can be calculated by the four-step procedure if the ambient temperature undergoes a rapid increase at a known time from a known level to a higher level.

6.1.2.2 Evaluating the Corrective Factor

The experience of all the experimental body and dummy cooling reported earlier is shown in Tables 6.18–6.21. The listed corrective factors are valid for typical situations whenever a body is found in a roughly extended position or sitting.

The corrective factor for cooling conditions in air that differ from the standard conditions should be evaluated under three aspects:

1. Clothing/covering of the lower trunk, dry (left-hand side) or 'wet-through' (right-hand side).
2. Resting or moving air.
3. Type of supporting base (accelerating or decelerating) compared with 'indifferent'.

Should the occasion arise, it is useful to re-examine the experimental background that provided the corrective factors listed in Table 6.18:

1. With the exclusively radial transfer of heat from the body to surroundings (as well as the probe site within the rectum) in mind, only the clothing or covering and other special cooling conditions (the ground, wetness, wind) of the lower trunk are relevant for evaluating the corrective factor.
2. The corrective factors listed in Table 6.18 were investigated experimentally on bodies lying on a simple covered stretcher, which was declared to be a 'thermally indifferent' base. Different grounds such as floor, asphalt and dry lawn (e.g. cases 11, 55 and 64 in Table 6.17) dummy experiments have shown that insulating bases may require corrective factors up to 1.3, and excessively heat-conducting bases to 0.5 in naked bodies (see Table 6.10). Therefore, the base on which the body lies should be checked for both its thermal conductivity and its heat capacity. For example, thin sheet metal has a high conductivity but a low heat capacity, and so will not markedly accelerate body cooling. In contrast, the concrete floor of a cellar has both a higher conductivity and capacity. The cooling of a naked body will be accelerated according to a corrective factor of 0.75. The effect of the type of base on clothed bodies seems to be diminished more (thicker clothes) or less (thin clothes). Instructive examples in Table 6.17 are cases 15, 26, 28 and 46 for accelerating bases and cases 47, 48, 62 and 70 for insulating bases.
3. The position of the body (i.e. whether it is extended or crouched) influences cooling. Exact data are not yet known.
4. The influence of even slow but permanently moving air on body cooling is significant as long as the body is naked or is only thinly clothed (covered) or if the surface of the naked or clothed (covered) body is wet through. Therefore, attention should be paid to even slightly moving air (e.g. cases 25, 43 and 72 in Table 6.17).
5. The corrective factors listed in Table 6.18 were investigated on bodies of average body weight. Systematic investigations of the cooling of different-sized dummies under various conditions resulted in a clear dependency of the corrective factors on body weight in cases of a low or high body weight and, at the same time, higher thermic insulation conditions [20]. Higher body weights need lower factors and, vice versa, lower body weights need higher factors, as listed in Table 6.18. Insulation conditions that require a corrective factor up to 1.3 according to the experience on bodies of medium body weights (see Table 6.18)—reference 70 kg—can be used independently of the real body weight. Table 6.20 should be used whenever a special case requires a corrective factor of 1.4 or greater, according to Table 6.18, and the body weight exceeds 80 kg or is less than 60 kg at the same time. In such a case, evaluation of the corrective factor should be made, in the first instance, relative to the actual cooling conditions by experience from average body weights (e.g. Table 6.18). The corrective factor chosen in the first instance must be applied to the real high or low body weight either by Table 6.20 or by Equation 6.10. Using Equation 6.10 removes the need for interpolation. One of the previously mentioned computer programs, www.AMAsoft.de (see Figure 6.33), automatically takes into account this adaptation whenever the body weight and the corrective factor according to Table 6.18 require it. Examples can be seen in Table 6.17 (cases 6 and 66) and Table 6.20 (case 37).
6. As in many cases involving cooling conditions significantly different from standard conditions, the initial commitment to an exact corrective factor is impossible, and it is advisable to choose a range for the corrective factor (see Figures 6.38 and 6.39). If it is necessary to use Table 6.20 or Equation 6.10, the threshold values of that chosen range of corrective factors must be modified. Once the time of death has been taken from the nomogram at two corrected body weights, the result is a range for the time of death (see Figures 6.38 and 6.39).

   Example: A scene may lead to the choice of a range of corrective factors, perhaps between 1.8 and 2.2; the choice is based on experience of particular conditions (e.g. a bedspread) for an average body weight (see Table 6.18). The actual body weight may be evaluated to approximately 20 kg.

Table 6.21 **Data of Paired Cases**

Case number	Cooling conditions	Correction factor		Real body weight (kg)	Ambient temperature (°C)		Rectal temperature (°C)	Time estimated lower upper limit (hpm)		Time ascertained lower upper limit (hpm)		Comment
		Measured	Used		Mean	Range						
6	LB on bed, covered with two thick blankets together about 30 cm thick, night dress, short panty.	2.4	2.0–2.8*	89	20.6/20.6	19.6/21.6	36.9	02.0	07.6	01.8	15.0	*Because of strong insulation condition and high body weight: adaption according to Table 6.3: 1.8–2.5.
7	Room, hanging at door, short panty.	1.05	1.0–1.1	78	20.6/20.6	19.6/21.6	35.0	03.0	08.6	01.8	15.0	The wife was strangled by the husband, who committed suicide by hanging thereafter.
36	Apartment house, stony staircase, LP, thicker pyjamas.	1.0	0.9–1.1	62	15.6/16.1	15.5/16.5	33.1	03.0	08.6	07.1	08.1	The mother and her 3-year-old son were killed by the culprit.
37	Room, floor, carpet, thicker pyjamas, disposable nappies.	1.5	1.3–1.7*	14	15.8/16.3	15.5/16.5	28.3	02.5	08.1	06.8	07.8	*There is no experience with one-way nappies concerning the correction factor. The used range was speculated. Because of strong insulation condition and low body weight the correction factor of 1.7 was adapted to 2.2 according to [20].
46	Windowless basement room, LP on tiled floor, jeans, bodice.	1.0	0.9–1.1	57	22.5/23.0	22.5–23.0	32.8	04.9	10.5	05.8	06.1	The woman was killed by the man who committed suicide immediately thereafter.
47	Windowless basement room, leaned back sitting on a pail with a dust-filled bag on it, jeans, short panty.	1.3*	1.2–1.4*	77	as 46	as 46	35.5	03.5	09.1	07.3	07.6	*The pail with a dust-filled bag on it looks like a stronger thermic insulation.
70	Room, sitting position on thick upholstered couch, back and left region of the lower trunk leaning against thick cushions, pyjamas, pants, in front open bathing gown.	1.3	1.2–1.4	96	18.0/19.0	18.0/19.0	33.5	08.5	14.1	04.0	17.5	The man committed suicide at an unclear time after having killed his wife at a time that could be exactly investigated.
71	Room, LL, floor, carpet, pyjamas, briefs.	1.2	1.1–1.3	64	18.0/19.0	18.0/19.0	26.5	14.4	23.4	17.2	17.7	

Abbreviations: hpm, hours post-mortem; LB, lying back; LL, lying in a lateral position; LP, lying prone.

Source: From Henssge C, Althaus L, Bolt J, Freislederer A, Henssge CA, Hoppe B, Schneider V. Experiences with a compound method for estimating the time since death. I. Rectal temperature nomogram for time since death. *Int J Legal Med* 1999;**113:**303–319.

Using Table 6.20, a corrective factor range of 2.4 (from 1.8) to 3.6 (from 2.2) would be the result. Using Equation 6.10, the exact range would be 2.3–3.4. The corrected weight, taking the bedspread in the case of a 20-kg body into account, would range between 50 and 70 kg. If the ambient temperature is 18°C and the rectal temperature is 29°C, the range of the time of death would be 9.4 hours (50 kg) to 12.6 hours (70 kg) according to the nomogram, corresponding to 11 ± 1.6 hours. However, this range of the time of death resulting from the range of corrective factor is smaller than the ±2.8 hours permissible variation of 95 per cent given by the nomogram (see Figures 6.38 and 6.39). We recommend, in all cases, using the wider range (11 ± 2.8 hours) in official statements to avoid misleading the investigation. In fact, it is impossible to limit that range without loss of reliability. The previously mentioned computer programs operate according to this recommendation. On the contrary, the use of additional methods for estimating the time of death is recommended (see Chapter 10).

A few cases of the bodies of babies and infants covered with a bedspread may confirm the data of Table 6.20. The victims of a triple murder were a baby (3.2 kg), a child (8.1 kg) and their mother (44 kg). The bodies of the children were found in bed, fully clothed and covered by a thick bedspread. The body of the mother was found lying on a bed, clothed in ski trousers and covered partly by a bedspread. The time of death would be met exactly in the case of the 3.2-kg body by nomographical read-off of the time of death using a corrective factor of 9.0, which corresponds to 2.8 in the case of a 70-kg body (see Table 6.20). The real time of death would be recorded by the upper limit of the permissible variation of 95 per cent (2.8 hours) to the examined time applying a corrective factor of 4.0, which corresponds to 2.0 in the case of a 70-kg body. Corrective factors of between 7.0 (2.7 at 70 kg) and 3.0 (1.9 at 70 kg) would be correct for the 8.1-kg body. In the case of the 44-kg body, the real time of death would be recorded by the application of 3.2 (1.9 at 70 kg) and 1.4 (1.4 at 70 kg) as corrective factors. The three cases can be solved sufficiently by the combined application of Tables 6.18 and 6.20. Further actual cases (numbers 36 and 37 in Table 6.21) may also confirm adoption of the corrective factor in dependence of the body weight in cases of strong thermic insulation conditions according to Equation 6.10 (see Table 6.20).

7 Evaluating the corrective factor of body weight for special cooling conditions differing from the chosen standard conditions is often the most difficult problem, particularly when clothing or covering, special bases, moving air and wetness overlap. The difficulty can be avoided by complying with the previously mentioned order of the three aspects in evaluating the corrective factor: (1) clothing or covering; (2) resting or moving air and (3) accelerating or decelerating base. The difficulty can be further avoided if, instead of a point value, a range of corrective factors is chosen appropriate to the actual cooling conditions (see Table 6.18 and Figures 6.38 and 6.39). Instructive examples are cases 15, 22, 27 and 54 in Table 6.17.

6.1.2.3 Known Changes of Cooling Conditions

If the changes in cooling conditions are known, they can often be taken into account without loss of reliability and without a significant reduction in accuracy. The one common situation is a change of the cooling conditions by the investigators before the temperature measurements can be made.

For example, a thick bedspread was taken off a body 1 hour before the temperature measurement. Nevertheless, a corrective factor of about 1.8 (see Table 6.18) was used for calculating the death time. Although the drop of the rectal temperature starts to become steeper during the 1 hour after the bedspread was removed from the body, the resulting error will be negligible because it is additive (compare the lower graphs in Figure 6.13; 26–28 hours post-mortem). Certainly, if such a significant change of the cooling conditions has lasted several hours, it can no longer be neglected. The probable cooling curve should then be reconstructed from the time of temperature measurements by using a computer.

Sometimes, the ambient temperature is significantly changed by the person who found the body, or by the investigators (e.g. closing or opening windows, using special lamps that heat a small room quickly), a short time before temperature measurement. If the ambient temperature was changed 1 or 2 hours before body temperature measurement, body cooling becomes accelerated or decelerated after the change of ambient temperature, and the resulting error will again be negligible so far as the ambient temperature before its change is used.

A second temperature plateau provides a lag of the ‘reaction’ of the rectal temperature curve (see the example in Figure 6.40). If such a significant change of the ambient temperature has lasted for several hours, the range or the mean ambient temperature should be used as discussed earlier.

6.1.2.4 Uncertainty in the Value of Corrective Factors

There is often uncertainty about point values of mean ambient temperature, body weight and, especially, corrective factors for special cooling conditions. It is a good strategy to evaluate possible upper and lower limits (see Figure 6.38). The nomogram (see Figure 6.39) or a computer program helps in this calculation by taking a range of each factor. The available computer program [21] requires range on principle.

Example (see Figure 6.39): For a body of 75 kg actual body weight and a rectal temperature of 27°C, evaluate a mean ambient temperature between 17°C and 20°C and a corrective factor between 1.2 and 1.5 for special clothing. Using the nomogram, draw 2 × 2 straight lines: connect a 27°C rectal temperature with both 17°C and 20°C. Now draw two more lines crossing the semicircles. Read off the time since death on both lines at the two intersections of the following semicircles: 75 × 1.2 = 90 kg and 75 × 1.5 = 112.5 (110) kg. The result will be four values for a death time: about 19, 23.5, 23 and 28.5 hours post-mortem. Thus, it could be stated that death occurred between 19 and 28.5 hours before the time of investigation, which means 23.5 ± 4.5 hours. This example also demonstrates clearly that the given permissible variation at the outermost semicircle (± 4.5 hours; see Figure 6.39) includes some uncertainties.

This method is recommended if the points of contact (mean ambient temperature, corrective factor, body weight at scene) are not closely defined, so that a range must be taken into account.

The computer program www.AMAsoft.de generally computes the period of death in two ways [21] (see Figures 6.38 and 6.39):

1. The time of death is computed using the mean values of the chosen ranges of corrective factor, and mean ambient temperature, respectively. The period of death results by adding the empirical permissible variation of 95 per cent (see Tables 6.10 and 6.13).
2. In addition, the period of death is computed using the lower and upper brackets of the evaluated ranges of ambient temperature and corrective factor, thus giving the lower and the upper limit of the period of death.

If the second method results in a wider range of the period than the first method, it is used as the final result (see Figure 6.38). There were some such cases in the previously mentioned field study [24] (e.g. cases 42, 49 and 56 in Table 6.17).

6.1.2.5 When the Method Must Not Be Used

This method cannot be used, however, under a number of conditions. Having analysed the situation at the scene carefully, it must be decided whether this approach is feasible:

1. Strong radiation. There is no experience in taking solar or other radiation into account. If a body is found with direct sun on its surface, the situation is apparent. If a body is found at a place where the sun is not actually shining, the question of sun radiation must be checked, to establish whether direct sun radiation on the body may have been possible. For example, a body was found at night in a closed room lying on the floor near the southwest window. Using the apparent factors—especially the darkness—a death time of early afternoon was given. Because at this time the body would have been in direct sun radiation, we did not give any statement concerning the time of death. Situations such as this are open to inappropriate use of any temperature method. Conversely, a short period of direct sun radiation on the body just before examination is not a contraindication to the method.
2. Uncertain severe change of cooling conditions. In contrast to methods with multiple temperature measurements at the scene for direct estimation of the individual values of the required constants, the nomogram method with a single measurement of rectal temperature can still be used when even severe changes of the cooling conditions occur for a short period before examination, if they can be reconstructed in relation to time and type (see earlier). If the changes in the cooling conditions are assumed but are really unknown in extent and direction, the method must not be used. A common situation of this type is a presumed severe change of cooling conditions during the interval between discovering the body and the beginning of the examination by the crime police.

Example: A body of 51 kg was found lying on its back, extended in a room on the floor. It was clothed only with a gown open at the front. Even the crime police could not decide later whether the windows and the doors were originally open because the body was found 4.5 hours previously. The actual measured room temperature was 12.4°C. The radiator in the room felt warm. The room thermostat showed 21°C and the heating system was found to be working. The rectal temperature was 21°C. If the windows and doors were open during the whole time interval since death occurred, the mean room temperature would have been similar to the actual measured temperature of about 12°C. A corrective factor of 0.75 for permanently moving air should be applied (51 kg corrected 38 kg). The death time interval would have been 12.5 ± 2.8 hours (95 per cent) according to the nomogram. Conversely, supposing the windows and doors had been closed between the moment of death and finding the body 4.5 hours before examination, the mean room temperature until examination would have been close to 21°C; its fall to 12.4°C must have developed only when windows and doors were opened 4.5 hours before. A special corrective factor (still air) would then be out of the question. In this case, no reliable reading from the nomogram could be made because of the 21°C figure of both the ambient and the rectal temperature. Later on, the death time could have been calculated as 27 hours before examination at the scene in accord with the following reconstruction. The body cooling had not yet reached the ambient temperature (about 21°C) when the unidentified person found the body and opened the windows and doors. If the rectal temperature was about 24°C at this moment, the mean nomographic death time would be 23 hours (51 kg; corrective factor 1.0; ambient temperature 21°C). During the following 4.5 hours with changed cooling conditions, the rectal temperature fell to the measured 21°C. This example demonstrates the advice to 'analyse carefully the factors at the scene' before giving an estimate of death time. No special knowledge is necessary, but only general physical thinking about the carefully analysed situation at the scene.

3. Unusual cooling conditions. This point is not only a matter of formally selecting a corrective factor (from Table 6.18) for the special cooling conditions but is also a matter of personal experience. In cases of unusual cooling conditions without any personal experience, the examination at the scene should still be performed. Nevertheless, a statement of the time since death cannot be given from this method (e.g. cases 31 and 45 in Table 6.17). After a test cooling of the dummy, an opinion can be given later on whether the question of death time becomes of greater importance (see later).
4. Repeated extensive climatic changes. The method must not be used if repeated extensive climatic changes have occurred that do not allow the evaluation of representative mean figures for ambient temperature and corrective factors for the whole period between death and investigation.
5. Transported body. If the place where the body was found is not the same as the place of death, the method must not be used except when both the place of death and the date of transportation of the body are known. This is uncommon, but the circumstances of transportation become apparent later on. Therefore, the examination of the body at the place where it was found should still be made. Under certain circumstances, a restricted statement of the time since death can be given to support the investigation.

   It is strongly recommended not to use the method after the removal of the body to the mortuary if there is only reported information about the place where the body was found. Conversely, there are no arguments against measurement of the rectal temperature and examination of the other methods estimating the time since death after the removal of the body to the mortuary, provided the forensic investigator has already inspected the scene of crime and the period of the transportation has not been too long. Marty and Baer [45] investigated the influence on body cooling of storing bodies in a closed compartment such as a coffin, a closet or a car boot. Whereas storing a body in a closet or a car boot did not affect the cooling rate significantly, bodies stored in a wooden coffin showed a lower cooling rate corresponding to a mean corrective factor of 1.2 (variation 1.0–1.3).
6. Suspicion of general hypothermia. See earlier and Figure 6.26. An example of suspected malignant hyperthermia is shown in case 33 in Table 6.17.

6.1.2.6 Special Problems

Besides the questions referred to earlier, some further problems are encountered.

High ambient temperature

As discussed in connection with constant *A* and its uncertain dependence on the ambient temperature, it is emphasized that the nomogram (see Figure 6.35) and Equation 6.15 for ambient temperatures above 23°C are based on the data from De Saram et al. [10]. Among our own data on experimental body cooling, there are no cases that cooled in ambient temperatures above 23°C. In the casework of a multicentre study ($n = 46$) [2] are seven cases where the ambient temperature was above 23°C. In the field study ($n = 72$) [24] reported earlier (see Tables 6.17 and 6.21) are seven cases where the mean ambient temperature was above 23°C (e.g. cases 48 and 66 in Table 6.17) and four further cases where the upper bracket of the range of ambient temperature was above 23°C. The estimated death times of these cases using the nomogram of Figure 6.35 or Equation 6.5 with the 1.11 value of constant *A* are in accord with the true times of death. However, more experience of body cooling in high ambient temperatures has yet to be gained.

6.1.2.6.1 Fever at Death

In our cooling experiments reported earlier, we had some cases with fever at death (see Figure 6.25). The errors caused by fever are included in the given permissible variations of 95 per cent and are greatest for the first post-mortal hours, decreasing later (see Table 6.13 and Figure 6.26). By computation, the temperature at death can be changed from 37.2°C to a higher figure when adequate investigation or autopsy findings suppose fever at death. When using the nomogram form, the difference between the supposed temperature at death and the normal 37.2°C must be subtracted both from the measured rectal temperature and from the ambient temperature (e.g. case 33 in Table 6.17).

6.1.2.6.2 Longer Agony

If there is a long period between the time of fatal injury and death, the estimate of the time since death should be supplemented by emphatically warning the investigators of a possibly longer interval. Stating only the time since death in cases of a possible longer period of agony can lead to a misunderstanding. In addition, the nomographically estimated time of death may be loaded with a greater error because the regulation of body temperature can be markedly disturbed during agony, either from a central fever or from hypothermia. In the latter case, cooling may develop even more quickly during agony than on a dead body. During agony, the circulation acts as convectional heat transfer from the centre of the body to the surface. At the same time, the regulation of homeostasis of body temperature by additional heat production can be reduced. A clear decision on whether a longer period of agony comes into question or not can be made only after autopsy. The preliminary examination of the body at the scene may suggest a very short agony, even if this is not the case. An immediate autopsy after the procedure at the scene is the best way to recognize such a mistake. The stated death time can be corrected quickly after autopsy before misleading the investigation. Later on, the findings of toxicological (e.g. ratio of metabolites) or histological (e.g. age of wounds, signs of organ shock) examination may provide evidence of a distinct interval between fatal injury and death.

6.1.2.7 Accuracy of Calculated Time Since Death

In 1990, Albrecht et al. [1] published a multicentre study on the accuracy of calculated time since death. The range of accuracy stated previously (see Figures 6.27–6.30) at the outermost circle of the nomogram results from experimental body cooling under controlled conditions in various research institutes.

Representative assessments of accuracy in using the nomogram method at the scene are difficult to obtain because of technical problems. A single forensic pathologist does not deal with sufficient cases to constitute a scientific study. Therefore, a multicentre study was made using 11 forensic pathologists from six forensic institutes in Germany, Austria and Switzerland [1]. Seventy-six cases were examined at the scene. All bodies were later examined by autopsy. The cooling conditions at the scene varied over a wide range corresponding to evaluated corrective factors between 0.3 (bodies found in flowing water) and 2.1 (thick bedspread). Ambient temperatures varied between −6°C and 26°C. The differences (nomographically estimated – actual interval of death) were calculated as follows (Figure 6.41). Because the investigated time of death was known with certainty in most cases, the mean figure and the upper and the lower limits of this interval were related to the mean of nomographically estimated time of death. In consequence, three values of error (*dt* 1, *dt* 2 and *dt* 3) of each case entered into the statistical analysis of error. The 76 cases were divided into two groups.

6.1.2.7.1 Group I

These 46 cases had clearly defined points of contact. The standard deviation of the differences between nomographic and actual death times resulted in ±1.3 hours, equivalent to permissible variation of 95 per cent of ±2.6 hours (Figures 6.42 and 6.43). The progress of cooling corresponded in 37 cases to values of $Q > 0.5$, and in nine cases the cooling was more advanced, corresponding to values of $0.5 > Q > 0.2$. There was no trend towards increased errors with advance of cooling, as expected theoretically and from experimental body coolings.

In 20 cases, the real death time was less than 4 hours. Among these were five cases in which the nomographic death time did not agree closely with the actual time but did not contradict it. These cases could be explained by the problem of stated 37.2°C for *To*, as discussed earlier. The errors may be avoided by means of examining the

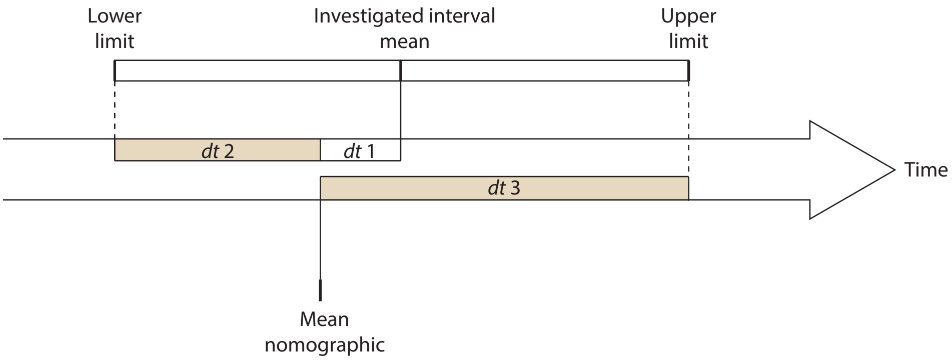

Figure 6.41 Differences between nomographically calculated time of death and mean (*dt* 1), lower limit (*dt* 2) and upper limit (*dt* 3) of the investigated time of death used in the statistical analysis of errors.

(Data from Albrecht A, Gerling I, Henssge C, Hochmeister M, Kleiber M, Madea B, Oehmichen M, Pollak St, Püschel K, Seifert D, Teige K. Zur Anwendung des Rektaltemperatur-Todeszeit-Nomogramms am Leichenfundort (German, English summary). *Z Rechtsmed* 1990;**103:**257–278.)

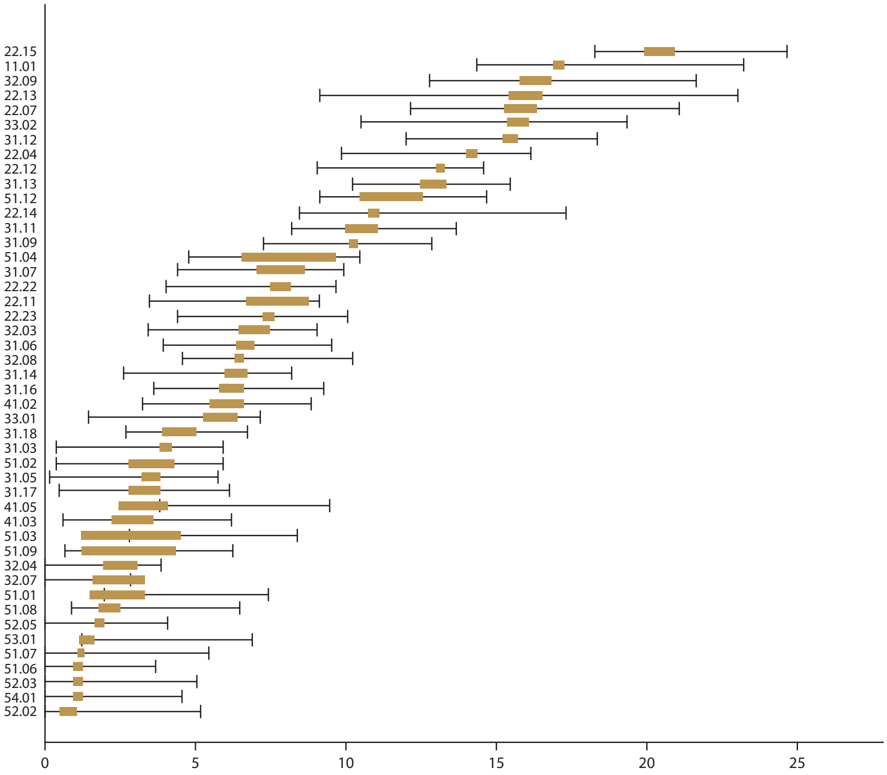

Figure 6.42 The thin bars represent the nomographically calculated interval according to the permissible variation of 95 per cent given at the nomogram, and the thick bars represent the investigated interval of death in group I of casework.

(Data from Albrecht A, Gerling I, Henssge C, Hochmeister M, Kleiber M, Madea B, Oehmichen M, Pollak St, Püschel K, Seifert D, Teige K. Zur Anwendung des Rektaltemperatur-Todeszeit-Nomogramms am Leichenfundort (German, English summary). *Z Rechtsmed* 1990;**103:**257–278.)

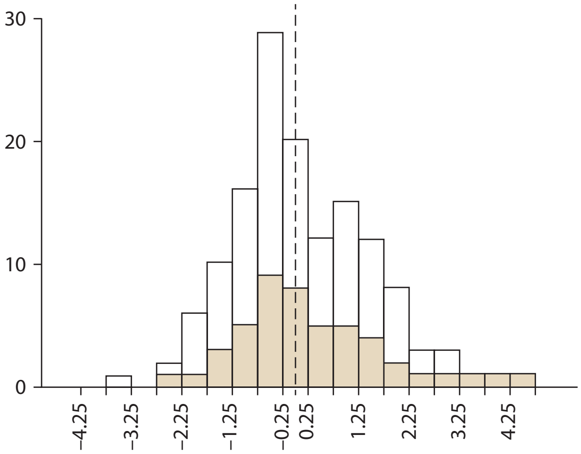

Figure 6.43 Histogram of errors of all the 46 cases of group I according to Figures 6.41 and 6.42.

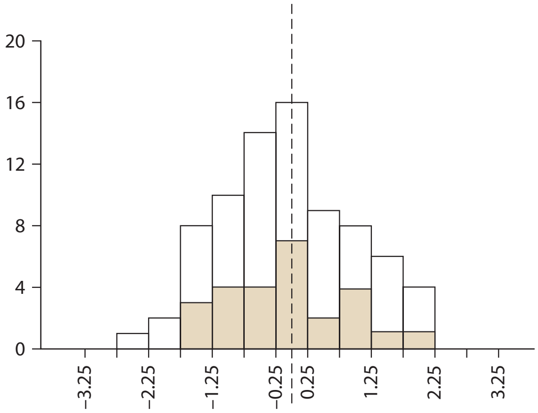

Figure 6.44 Histogram of errors of that part of the cases of group I having investigated death times greater than 4 hours (26 cases; compare with Figure 6.45).

(Data from Albrecht A, Gerling I, Henssge C, Hochmeister M, Kleiber M, Madea B, Oehmichen M, Pollak St, Püschel K, Seifert D, Teige K. Zur Anwendung des Rektaltemperatur-Todeszeit-Nomogramms am Leichenfundort (German, English summary). *Z Rechtsmed* 1990;**103:**257–278.)

mechanical and electrical excitability of muscles (see Chapter 10). Separating the 26 cases with a real death time greater than 4 hours, the standard deviation was ±1 hour—equivalent to a permissible variation of ±2 hours (Figures 6.44 and 6.45), which is significantly smaller than both the total group I and that suggested by the nomogram. The latter result seems to indicate lower errors in casework than in experimental body coolings. This rather surprising result could be explained by the previously discussed 'pre-analytic' error inherent in experimental body cooling but usually absent in casework. Nevertheless, the results of this group confirm the reliability of the nomogram method within the 95 per cent permissible variation.

6.1.2.7.2 Group II

These additional 30 cases had uncertain corrective factors. The nomographic death time interval does not agree with

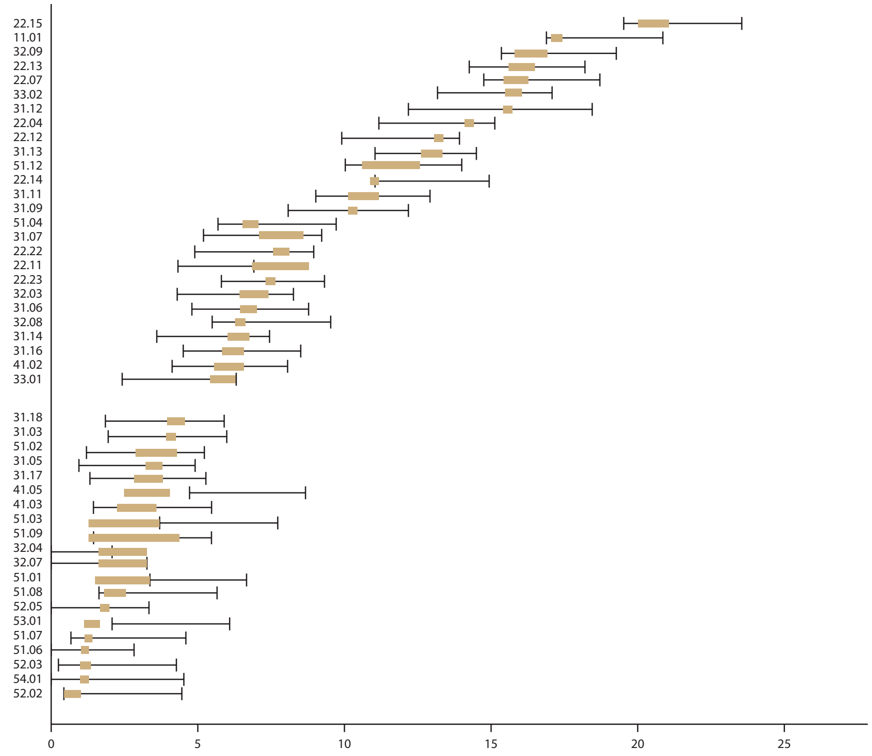

Figure 6.45 The thin bars represent the nomographically calculated time of death but with interval according to the permissible variation of 95 per cent of that part of casework having investigated death times greater than 4 hours (see Figure 6.44). The thick bars represent the investigated interval of death. The calculated interval does not agree with the investigated interval in case numbers 41.05, 51.01 and 53.01.

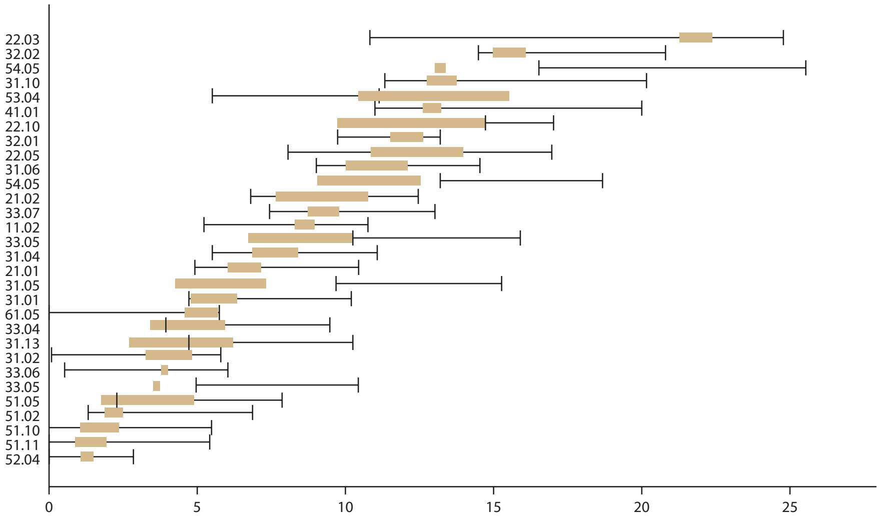

Figure 6.46 Nomographically calculated (thin bars) and investigated interval of death (thick bars) of group II including 30 cases with recognizable unsure point of contact.

the real investigated interval in five cases, thus demonstrating that an estimate of the death time should not be given at all where points of contact are unsure (Figure 6.46).

In 1999, Henssge et al. [24] published a single-centre field study on the experiences with a compound method for estimating the time since death at the scene in 72 consecutive cases. The computer-assisted nomogram method [21] was used as the primary method (examples in Table 6.17 and 6.21), followed by non-temperature-based methods [25] (see Chapter 10).

The reliability of the estimated period since death by the temperature-based nomogram method could be considered in 60 cases where the period of death could be determined by the police investigations with certainty. In all these cases, the estimated period since death was consistent with the investigated period. In 50 cases, the estimated period since death corresponded completely to the investigated period, and partially in ten cases. In the latter ten cases, death could have occurred within the overlapping range between the estimate and the investigated period.

In each of four cases two bodies were found at the same scene, and the question of the sequence of deaths arose. These paired cases (see Table 6.21) provide evidence for the degree of differentiation that is achieved with the nomogram method. Despite the different rectal temperatures, congruent periods of death resulted because of different cooling conditions and body weights (cases 6/7, 36/37 and 46/47). In the paired cases 36/37 and 46/47, the police investigation ascertained nearly simultaneous death of the two persons. In the paired case 6/7, the police investigation could not verify the times of death. In the paired case 70/71, the time of the wife's death could be exactly verified by the investigation, but the time of the husband's death remained unclear. In contrast to the other three paired cases, the different cooling conditions and body weights did not compensate the different rectal temperatures, with the result that different periods since death were calculated at the 95 per cent level of permissible variation.

6.1.2.8 Reconstruction of Body Cooling

When a body is found under special cooling conditions where there is no experience of a corrective factor, test cooling of a 37°C heated dummy at the place and under the special conditions where the body was found can provide evidence of the true corrective factor. Before a dummy can be used for such a reconstruction, its cooling under the chosen standard conditions must be investigated by several test coolings. As a result of these tests (see Figure 6.2), the weight of the body can be calculated (Equation 6.3), and this is replaced by the dummy. This weight stands for the chosen standard conditions of cooling. It acts as the real body weight (*bw*) in calculating the corrective factor according to Equation 6.4. The weight resulting from the test cooling under the special conditions at the place where the body was actually found acts as *bw calc* in Equation 6.4.

The additional measurement of heat flow and temperatures on the surfaces of body, especially on the supporting surface, may assist the detection of special influencing factors of the body cooling (see Figures 6.19–6.21), including the influence of heat radiation.

Besides additional measurements concerning the body cooling in special cases, it is recommended in all cases to apply other, simple methods in addition to the nomogram method [25]; these are described in Chapter 10.

6.1.2.9 Investigation of Central Brain Temperature

Beyond our investigation of the rectal temperature probe site, we investigated the central brain temperature. The theory of modelling the central brain temperature mathematically is the same as described in connection with the rectal temperature (see Equation 6.1).

The central brain temperature was recorded in 53 bodies, stored at nearly constant ambient temperatures between 10°C and 30°C in still air. The measurements were started on average 1.6 hours post-mortem and were continued for 8–50 hours. The diameters of the temperature probes were 0.5 and 1 mm. The probes were inserted via the upper part of the superior orbital fissure into the brain with a depth of half the sagittal diameter of the head. The computation of the time of death according to Equation 6.1 (Tr replaced by Tb = brain temperature) with average values for the starting temperature, To (37.2°C), and the constants B (−0.127) and A (1.135) provided margins of error for the 95 per cent tolerance limits of ±1.5 hours up to 6.5 hours post-mortem, ± 2.5 hours between 6.5 and 10.5 hours post-mortem, and ±3.5 hours between 10.5 and 13.5 hours post-mortem. Compared with the margins of error based on rectal body cooling (see Figures 6.27–6.30 and Tables 6.15 and 6.16), a more precise estimation of the time of death can be obtained up to 6.5 hours post-mortem only. For practical applications, a 'brain temperature–time of death nomogram' was constructed (Figure 6.47). The nomogram is related only to 'standard conditions' of cooling (see earlier). Even uniformly moving air alters the time relations—the constant B changes from −0.127 to −0.158 [23]. The cooling coefficient B was also influenced by the amount of hair. Nevertheless, taking this into account, the estimated time of death did not become significantly more accurate. Other influencing factors have not yet been fully investigated. The often-expressed opinion that the cooling curve of the brain would be less affected by factors that could affect the cooling of other temperature probe sites [6,38] cannot be confirmed, either physically or empirically. Nevertheless, this concept may be correct because the head is less often clothed or covered than the trunk.

Inserting temperature probes on both sides via the upper part of the superior orbital fissure, the measured brain temperatures differed by up to 1.5°C, corresponding to a difference of computed death times up to 1 hour. This result required further studies into the optimal way to insert the probes into the centre of the brain. The best method of obtaining a well-standardized probe site was found by Ratermann [49] to be as follows: the probe is placed on the palpebral conjunctive of the lower eyelid within the temporal part of the first medial third of the infraorbital margin at an angle of 50–60 degrees to the nasal septum (Figure 6.48). Using this technique and using an insertion depth of half the sagittal diameter of

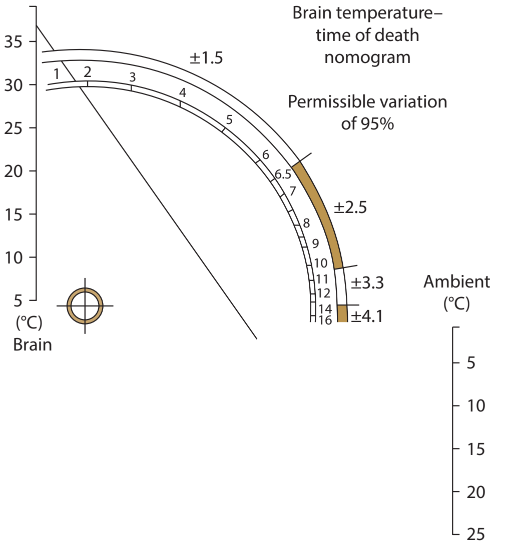

Figure 6.47 Central brain temperature–time of death nomogram related to 'standard conditions' of cooling. For the first step the points of the scales of the measured brain temperature (in the left margin) and ambient temperature (in the right margin) have been connected by a straight line, which crosses the diagonal of the nomogram at a particular point. The second step is to draw a second straight line through the centre of the circle, below left of the nomogram, and the intersection of the first line and the diagonal. The latter touches the outermost semicircle where the permissible variation of 95 per cent can be seen (see Figures 6.36 and 6.37).

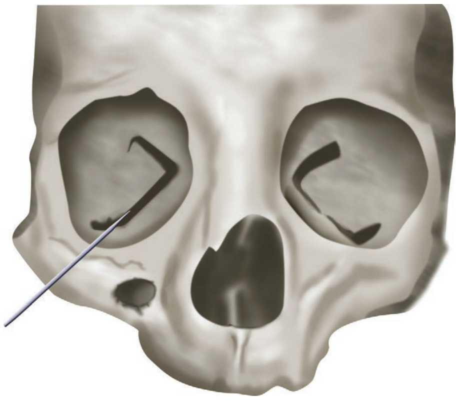

Figure 6.48 Standardized method of inserting the temperature probe into the 'centre' of brain providing more instant positioning than other procedures of insertion.

(Data from Ratermann J. Postmortale Hirntemperaturmessungen zur Todeszeitbestimmung—Untersuchungen zur Insertionstechnik der Temperaturmesssonden. Münster, Germany, University of Münster, MD thesis, 1986.)

the head, the temperature probe will be situated at the centre of the brain. The temperature differences between probes on both sides will be only minutely variable. In a study of 25 bodies using this procedure, the margin of error for the 95 per cent tolerance limits of computed time of death was ±1.3 to 6.5 hours post-mortem.

6.1.2.10 Combined Brain and Rectal Temperatures

Estimating the time of death on the basis of simultaneous measurements of brain and rectal temperatures on 21 bodies cooling under standard conditions, the following margins of error for the 95 per cent tolerance limits were obtained [28]. Up to 6.5 hours post-mortem, the most precise computation of time of death was achieved by the exclusive application of brain temperature, which gave a time of death within ±1.5 hours. Between 6.5 and 10.5 hours post-mortem, the brain-rectum combined computation of time of death balanced in the ratio of 6:4 (Figure 6.49) was the most precise, at ±2.4 hours. Beyond 10.5 hours post-mortem, the most precise computation of time of death was achieved by exclusive application of rectal temperature and gave a time of death within ±3.2 hours. These data agree well with those of a series of 53 bodies [26] that was based on the brain temperature only, as well as of the series that was based on the rectal temperature only.

Integrating Equation 6.1 applied to brain temperature and then again to rectal temperature with an equation common to both by dividing them into each other eliminates the starting temperature, *To*:

$$\frac{Tb-Ta}{Tr-Ta}=\frac{1.135\exp(-0.127\times t)-0.135\exp(-1.0677\times t)}{1.25\exp(B\times t)-0.25(5\times B\times t)} \tag{6.23}$$

where *Tb* is brain temperature; *Tr* is rectal temperature; *Ta* is ambient temperature; *B* is constant; and *t* is time of death (hours) (see Equations 6.1, 6.2, 6.14 and 6.15).

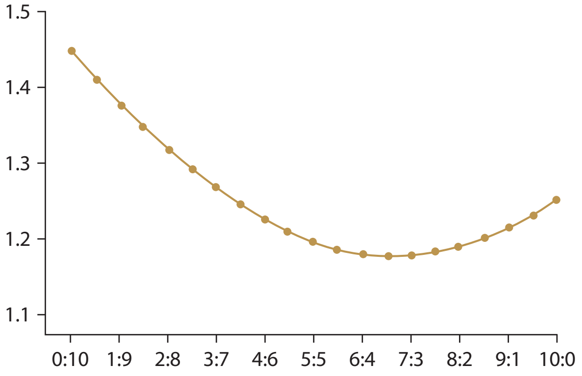

Figure 6.49 Relationship between standard deviation of errors of the computed time of death (ordinate) and the ratio of the balance of brain to rectal temperatures (abscissa) in combined computation of the time of death during the interval from 6.5 to 10.5 hours post-mortem corresponding to the standardized temperature 'Q' (Equation 6.1) of the brain.

(Data from Henssge C, Frekers R, Reinhardt S, Beckmann E-R. Determination of time of death on the basis of simultaneous measurement of brain and rectal temperature (German, English summary). *Z Rechtsmed* 1984;**93**:123–133.)

This procedure may avoid major errors, for example, in cases involving fever in the occurrence of death, as in 2 cases in the previously mentioned series. The rectal temperature, first measured 2 hours post-mortem, was 38°C in both cases. The fever-induced errors of computed death times in the later period when the rectal temperature had fallen below 37°C was reduced from about 3 hours (underestimation) to about 1 hour and virtually 0 hours, respectively.

References

1. Albrecht A, Gerling I, Henssge C, Hochmeister M, Kleiber M, Madea B, Oehmichen M, Pollak St, Püschel K, Seifert D, Teige K. Zur Anwendung des Rektaltemperatur-Todeszeit-Nomogramms am Leichenfundort (German, English summary). *Z Rechtsmed* 1990;*103*:257–78.
2. Altgassen X. *Untersuchungen zum 'postmortalen Temperaturplateau' an Abkühlkurven von Kunstkörpern*, MD thesis. Cologne, Germany, University of Cologne, 1992.
3. Althaus L, Henssge C. Rectal temperature time of death nomogram: sudden change of ambient temperature. *Forensic Sci Int* 1999;*99*:171–8.
4. Althaus L, Stückradt S, Henssge C, Bajanowski T. Cooling experiments using dummies covered by leaves. *Int J Legal Med* 2006;*121*:112–14.
5. Bisegna P, Henssge C, Althaus L, Giusti GEstimation of the time since death: sudden increase of ambient temperature. *Forensic Sci Int* 2008;*176*:196–9.
6. Brinkmann B, May D, Riemann U. Post mortem temperature equilibration of the structures of the head (German, English summary). *Z Rechtsmed* 1976;*78*:69–82.
7. Brinkmann B, Menzel G, Riemann U. Environmental influences to postmortem temperature curves (German, English summary). *Z Rechtsmed* 1978;*81*:207–16.
8. Brown A, Marshall TK. Body temperature as a means of estimating the time of death. *Forensic Sci* 1974;*4*:125–33.
9. Burger E, Dempers, J, Steiner S, Shepherd R. Henssge nomogram typesetting error. *Forensic Sci Med Pathol* 2013;*9*:615–17.
10. De Saram G, Webster G, Kathirgamatamby N. Post-mortem temperature and the time of death. *J Crim Law Criminol Police Sci* 1955;*46*:562–77.
11. Fiddes FS, Patten TD. A percentage method for representing the fall in body temperature after death. Its use in estimating the time of death. *J Forensic Med* 1958;*5*:2–15.
12. Green MA, Wright JC. Postmortem interval estimation from body temperature data only. *Forensic Sci Int* 1985;*28*:35–46.
13. Green MA, Wright JC. The theoretical aspects of the time-dependent Z equation as a means of postmortem interval estimation using body temperature data only. *Forensic Sci Int* 1985;*28*:53–62.
14. Grober H, Erk S, Grigull U. *Wärmeübertragung*. Berlin, Springer, 1957.
15. Gruner K. *Todeszeitbesimmung aus der Rektaltemperatur*, Medical thesis. Berlin, Humboldt University, 1985.
16. Henssge C. Precision of estimating the time of death by mathematical expression of rectal body cooling (German, English summary). *Z Rechtsmed* 1979;*83*:49–67.
17. Henssge C. Estimation of death-time by computing the rectal body cooling under various cooling conditions (German, English summary). *Z Rechtsmed* 1981;*87*:147–78.
18. Henssge C. Temperatur-Todeszeit-Nomogramm für Bezugs standardbedingungen der Leichenlagerung. *Kriminal Forens Wiss* 1982;*46*:109–15.
19. Henssge C. Death time estimation in case work. I. The rectal temperature time of death nomogram. *Forensic Sci Int* 1988;*38*:209–36.
20. Henssge C. Rectal temperature time of death nomogram: dependence of corrective factors on the body weight under stronger thermic insulation conditions. *Forensic Sci Int* 1992;*54*:51–6.
21. Henssge CA. *Beitrag zur Standardisierung eines komplexen Verfahrens zur Todeszeitbestimmung am Leichenfundort: Interaktives Computerprogramm*, MD thesis. Essen, Germany, University of Essen, 1999. www.AMAsoft.de
22. Henssge C, Brinkmann B. Todeszeitbestimmung aus der Rektaltemperatur. *Arch Kriminol* 1984;*174*:96–112.
23. Henssge C, Madea B. *Methoden zur Bestimmung der Todeszeit an der Leiche*. Lübeck, Schmidt-Römhild, 1988.
24. Henssge C, Althaus L, Bolt J, Freislederer A, Henssge CA, Hoppe B, Schneider V. Experiences with a compound method for estimating the time since death. I. Rectal temperature nomogram for time since death. *Int J Legal Med* 1999;*113*:303–19.
25. Henssge C, Althaus L, Bolt J, Freislederer A, Henssge CA, Hoppe B, Schneider V. Experiences with a compound method for estimating the time since death. II. Integration of non-temperature-based methods. *Int J Legal Med* 1999;*113*:320–31.
26. Henssge C, Beckmann ER, Wischhusen F, Brinkmann B. Determination of time of death by measuring central brain temperature (German, English summary). *Z Rechtsmed* 1984;*93*:1–22.
27. Henssge C, Brinkmann B, Püschel K. Determination of time of death by measuring the rectal temperature in corpses suspended in water (German, English summary). *Z Rechtsmed* 1984;*92*:255–76.
28. Henssge C, Frekers R, Reinhardt S, Beckmann E-R. Determination of time of death on the basis of simultaneous measurement of brain and rectal temperature (German, English summary). *Z Rechtsmed* 1984;*93*:123–33.
29. Henssge C, Hahn S, Madea B. Praktische Erfahrungen mit einem Abkühlungsdummy (German, English summary). *Beitr Gerichtl Med* 1986;*44*:123–6.
30. Henssge C, Madea B, Schaar U, Pitzken C. Die Abkühlung eines Dummy unter verschiedenen Bedingungen im Vergleich zur Leichenabkühlung (German, English summary). *Beitr Gerichtl Med* 1987;*45*:145–9.
31. Hiraiwa K, Kudo T, Kuroda F, Ohno Y, Sebetan IM, Oshida S. Estimation of postmortem interval from rectal temperature by use of computer-relationship between the rectal and skin cooling curves. *Med Sci Law* 1981;*21*:4–9.
32. Hiraiwa K, Ohno Y, Kuroda F, Sebetan IM, Oshida S. Estimation of postmortem interval from rectal temperature by use of computer. *Med Sci Law* 1980;*20*:115–25.
33. James WRL, Knight BH. Errors in estimating time since death. *Med Sci Law* 1965;*5*:111–16.
34. Joseph A, Schickele E. A general method for assessing factors controlling postmortem cooling. *J Forensic Sci* 1970;*15*:364–91.
35. Knörle T. *Normierungsvarianten für die Wärmeflussmessung an einem Kunstkörper*, MD thesis. Cologne, German, University of Cologne, 1991.
36. Koppes-Koenen KM. *Untersuchungen zum parameterfreien Verfahren der Todeszeitbesimmung aus Körpertemperaturen von Green und Wright*, MD thesis. Cologne, Germany, University of Cologne, 1991.

37. Lundquist F. Physical and chemical methods for the estimation of the time of death. *Acta Med Leg Soc* 1956;*9*:205–13.
38. Lyle HP, Cleveland FP. Determination of the time of death by body heat loss. *J Forensic Sci* 1956;*1*:11–23.
39. Mall G, Hubig M, Beier G, Eisenmenger W. Energy loss due to radiation in post-mortem cooling. Part A. Quantitative estimation of radiation using the Stefan-Boltzmann Law. *Int J Legal Med* 1998;*111*:299–304.
40. Mall G, Hubig M, Beier G, Büttner A, Eisenmenger W. Energy loss due to radiation in post-mortem cooling. Part B. Energy balance with respect to radiation. *Int J Legal Med* 1999;*112*:233–40.
41. Malt M. *Das Abkühlverhalten eines Kunstkörpers unter Berücksichtigung seines Wärmeflusses*, MD thesis. Cologne, Germany, University of Cologne, 1991.
42. Marshall TK, Hoare FE. Estimating the time of death. I. The rectal cooling after death and its mathematical expression. *J Forensic Sci* 1962;*7*:56–81.
43. Marshall TK, Hoare FE. Estimating the time of death. II. The use of the cooling formula in the study of post mortem body cooling. *J Forensic Sci* 1962;*7*:189–210.
44. Marshall TK, Hoare FE. Estimating the time of death. III. The use of the body temperature in estimating the time of death. *J Forensic Sci* 1962;*7*:211–21.
45. Marty W, Baer W. Cooling of cadavers in a coffin (German, English summary). *Rechtsmedizin* 1993;*3*:51–3.
46. Mueller B. Das Verhalten der Mastdarmtemperatur der Leiche unter verschiedenen äusseren Bedingungen. *Dtsch Z Gesamte Gerichtl Med* 1938;*29*:158–62.
47. Prokop O. Die Abkühlung der Leiche. In: Prokop O, Gohler W (eds.). *Forensische Medizin*. Berlin, Verlag Volk und Gesundheit, 1975.
48. Rainy H. On the cooling of dead bodies as indicating the length of time that has elapsed since death. *Glasgow Med J* (new series) 1868;*1*:323–30.
49. Ratermann J. *Postmortale Hirntemperaturmessungen zur Todeszeitbestimmung—Untersuchungen zur Insertionstechnik der Temperaturmesssonden*, MD thesis. Münster, Germany, University of Münster, 1986.
50. Schwarz F, Heidenwolf H. Le refroidissement post mortem: sa signification quant à l'heure du décès. *Intern Pol Rev* 1953;*8*:339–44.
51. Sellier K. Determination of the time of death by extrapolation of the temperature decrease curve. *Acta Med Soc* 1958;*11*:279–302.
52. Shapiro HA. The post-mortem temperature plateau. *J Forensic Med* 1965;*12*:137–41.
53. Stadtmüller K. *Zur Todeszeitbestimmung aus der Leichenabkühlung: Die Normierung der Abkühlgeschwindigheit unterschiedlicher Körper auf verschiedene äussere Bedingungen*, MD thesis. Cologne, Germany, University of Cologne, 1991.
54. Stipanits E, Henssge C. Präzisionsvergleich von Todeszeitrückrechnungen ohne und mit Berücksichtigung von Einflussfaktoren (German, English summary). *Beitr Gerichtl Med* 1985;*43*:323–9.
55. Szpak D, Groszek B, Obara M, Kusiak K. Thermoregulatory dysfunction secondary to acute ethanol poisoning. *Przegl Lek* 1995;*52*:281–3.
56. Unland M. *Ein Modell zur Bestimmung der Todeszeit aus dem Wärmefluss*, MD thesis. Cologne, Germany, University of Cologne, 1991.
57. Wessel H. *Leichenabkühlung bei Bettlagerung*, MD thesis. Münster, Germany, University of Münster, 1989.

6.2 Finite Element Method in Temperature-Based Death Time Determination

■ *Michael Hubig, Holger Muggenthaler, Gita Mall*

6.2.1 Introduction: Physical Methods in Temperature-Based Death Time Determination

One of the main targets of forensic medicine in homicide cases is death time determination. Various methods estimate the time of death by evaluating post-mortem changes of physiological body parameters [Henßge, Madea 1988]. A long history of forensic casework culminated in the realization that post-mortem core temperature decline is the most reliable of those parameters. The general guiding idea is to use a temperature-time-diagram showing the post-mortem temperature progression of the body core: the *model curve* $T(t)$.

All temperature-based death time determination methods merely differ in the way of calculating the model curve $T(t)$. Since decline of body temperature cannot be measured on-site, the model curve must be known a priori. Body core temperature and the parameter values necessary for calculating the model curve like ambient temperature, body mass and height or clothing are measured or determined at the crime scene. Once the model curve $T(t)$ is calculated from the parameters the time difference between death and core temperature measurement—called *time since death* t_S—can be determined starting from the measured *core temperature* T_M on the abscissa and reading t_S from the ordinate. This can be expressed by a simple formula:

$$T\left(t_S\right) = T_M \qquad (6.2.1\text{–}1)$$

While this strategy is easily realized in a time-temperature diagram (see Figure (6.2.1–1) given the model curve $T(t)$, it will be complicated in most cases to directly solve Equation (6.2.1–1) numerically by computing:

$$t_S = T^{-1}\left(T_M\right) \qquad (6.2.1\text{–}2)$$

Temperature time diagram for body core cooling–based death time estimation. $T(t)$ (dashed curve) body core temperature as a function of time t starting at the core temperature T_0 of the living. Death time estimation: horizontally moving from left to right starting at the measured rectal temperature T_M on the abscissa until the model curve is

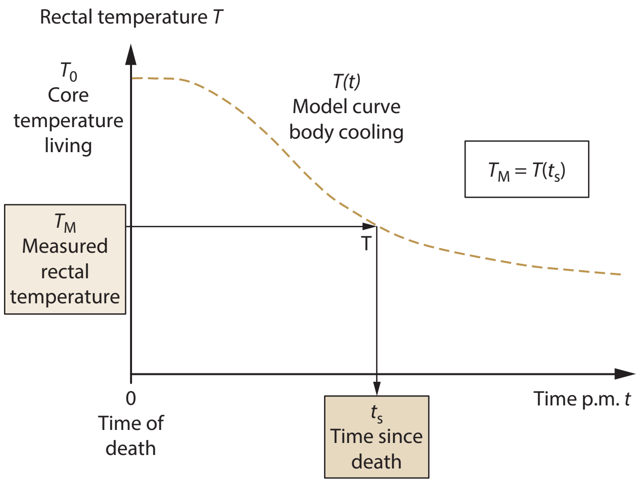

Figure 6.2.1–1 The model curve in death time estimation.

met. Then moving orthogonally down on the time axis, which is gauged to have 0 at the time of death, to read t_S the time since death estimate.

Two classes of methods to calculate a model curve $T(t)$ can be differentiated: the so-called *mathematical approaches* and the *physics-based approaches.* While the mathematical approaches use general knowledge of physical cooling processes as well as information about the general geometrical form of cooling curves, the physics-based approaches try to implement the physics of body cooling completely by taking into account the different heat exchange mechanisms, the geometry of the special cooling scenario and the material properties of the cooling body as well as the thermodynamically relevant parts of the scene. Mathematical approaches use fitting parameters not directly tied to physical measurements—to compute the model curve, e.g. the corrective factor in the method of Marshall and Hoare and Henßge, which is described in Chapter 6.1. This often leads to problems in the estimation of those parameters since the values derive for somehow fuzzily defined classes of cooling scenarios. Physics-based methods in contrast use only measurable parameters of thermodynamics and are frequently affected by the problem that not all values can be achieved at the crime scene or a posteriori and have therefore to be reasonably estimated.

A typical example for the mathematical death time estimation–type approaches is the method of Marshall and Hoare with the parameters of Henßge, also called the Nomogram method, presented in Chapter 6.1. In contrast, the Finite Elemente Method (FEM) described in the following paragraphs is a typical member of the physics methods class.

6.2.2 The Physics of Body Cooling

Body cooling—like all cooling processes of objects in our universe—can be described as a physical process. The physical quantity relevant in body cooling is the temperature field $T(r,t)$, which is a function of the three coordinates in space $r = (x,y,z)$ and the time coordinate t. The temperature field states the temperature $T(r,t)$ for every location r at a specified time t. For computational purposes in FEM, the temperature $T(r,t)$ has to be specified on an absolute scale starting from absolute zero at −273°C. Therefore, the scale of choice for this purpose is the *Kelvin* scale with the unit °K. A temperature value expressed in the Kelvin scale can be easily transformed to the Celsius scale by changing the unit '°K' to '°C' and subtracting 273°C.

If the temperature field $T_0 = T(r,t_0)$ is known at a certain time t_0 for all relevant locations r in space, the theory of thermodynamics allows to compute the temperature field $T = T(r,t)$ for all times t later than t_0. The temperature field T_0 is called the *initial condition* of the actual cooling problem. For example, the temperature field of the body at the moment of death is supposed to be a priori known, e.g. from literature or measurements; this temperature field is usually part of the initial condition of a cooling problem in death time determination. Since the region Ω in space which is relevant for the cooling problem considered is bounded, we have to define the temperature field T for all relevant times t in the time interval I of interest on the boundary $\partial\Omega$ of the region Ω. This partial fixing of the temperature field T on the boundary $\partial\Omega$ of the relevant region Ω is called the *boundary condition* of the cooling problem. In the case of a body cooling problem in death time determination the relevant region Ω might be a room where the boundary $\partial\Omega$ consists of the walls, the ceiling and the floor and the temperature has to be fixed throughout the whole cooling process as a boundary condition.

The science of *thermodynamics* represents the time evolution of the cooling process by a solution $T(r,t)$ of the so-called *heat equation* (see [Baehr, Stephan 1996] or [Cengel 1998]), which in the general case of body cooling is a second order partial differential equation, under the relevant initial and boundary conditions.

6.2.2.1 Heat Transfer Mechanisms

Three main mechanisms are considered for body cooling: *conduction*, *convection* and *radiation*. While the first two can be interpreted as pure mechanical processes on a microscopic scale, the last one, radiation, includes mechanics and electrodynamics. In our representation of heat transfer mechanisms relevant for body cooling, we rely mainly on the books by Cengel (1998); Gerthsen, Vogel (1993) and Alonso, Finn (1977).

The last section of this chapter does not deal with heat transfer mechanism per se but with a mechanism of post-mortem heat production in the body. Nevertheless, we see the solution to deal with the post-mortem heat source in the section of heat transfer mechanisms as adequate since convection and radiation are at play in the FE model as heat sinks.

The microscopical theory of thermodynamics discovered and quantified the interpretation of a medium's temperature essentially as the mean velocity of its particles. Quantum mechanics later showed that a certain temperature of a medium leads to a specific spectrum of quantum leaps of the outer electrons in the hull of its constituent atoms and therefore to irradiation of electromagnetic waves.

Heat conduction means heat flux from a static medium into another static medium. The terminus static is used to emphasize that no macroscopic movement like a flux phenomenon in a fluid is involved in this heat transport mechanism. Conduction is governed by the heat equation which interprets heat flux as a sort of energy transport phenomenon. In principle, conduction can be fully understood by applying the conservation-of-energy principle and the proposition, that heat flux power is proportional to the temperature difference between start and destination, which shall be demonstrated here in a simple linear case: Let R be a rod with cross section *A* and length *L*; let further T_1 be the temperature at the right end of the rod R and T_2 be the temperature at the left end. The rod R shall consist of a homogeneous material of *conductivity* λ with a unit of W/(°K m). The heat power of conductivity between the right and the left end of the rod can be quantified as:

$$P_{\text{cond}} = A \cdot \lambda \cdot \frac{T_1 - T_2}{L} \qquad (6.2.2\text{–}1)$$

This means that P_{cond} is proportional to the cross section *A*, to the temperature difference T_1–T_2 and inversely proportional to the length *L* of rod R. The proportionality constant is the conductivity λ.

Convection is the term used for heat energy transfer from a stationary medium into a medium with nonzero average particle velocity. Usually, the moving target medium of heat transport is a *fluid*, which can be a gas as well. Body cooling in moving air is a good example of convective heat transfer: heat is transferred from the skin as the stationary medium into the surrounding air, which is moved by wind, and represents the moving fluid. Due to the intricate nature of convective heat transfer processes involving fluid dynamics, the thermodynamic theory of convection is the most complex of all heat transfer mechanism theories and can only be applied in a linearized and approximated form. The convection process depends on the following parameters of flow in the target fluid:

- Dynamic viscosity μ [kg/(m s)]
- Mass density ρ [kg/m^3]
- Coefficient of volume expansion β [1/°K]
- Specific heat C_P [kJ/(kg °K)]
- Free stream fluid velocity v_E [m/s]
- Thermal conductivity λ [W/(°K m)]

When the convection process has reached a steady state, a temperature gradient in the fluid can be registered: Most of the fluid in the free stream region is of temperature T_E but near the surface of the stationary medium the fluid temperature rises continuously and monotonously with falling distance to the surface up to the surface temperature $T_{S.}$ We can interpret this as the existence of a thin *film* of fluid near the surface where the temperature gradient changes with changing distance from the surface. For computational purposes a so-called *film temperature* T_F is introduced as the mean of T_E and T_S:

$$T_F = \left(T_S + T_E\right)^{/2} \qquad (6.2.2\text{–}2)$$

An analogous film of fluid can be imagined for the fluid velocity, which depends on the distance to the surface only near the surface, where the velocity v of the fluid drops continuously from the free-stream velocity v_E to the value 0 directly on the surface.

Fluid dynamic distinguishes two types of flows, known as *flow regimes*: *laminar flows* and *turbulent flows*. Flow regimes can be characterized by purely kinematic criteria: a laminar flow is a highly ordered motion, it has smooth streamlines, whereas a turbulent flow is a highly disordered motion with strong velocity vector fluctuations in time and space and curly streamlines. Turbulent flows usually lead to faster mixing of the fluid and therefore mostly increase heat transfer in comparison to laminar flows.

Due to the highly complex nature of flow phenomena, the convective heat power P_{conv} is approximated as a linear function of the temperature difference $T_E - T_S$ with good results. The proportionality constant of this approach is called *convection coefficient h*. The dependency of *h* on the geometry of the scenario, that is the shape of the cooling stationary surface and the direction of the fluid flow, is expressed in the formulae by two terms:

- The characteristic length δ, a constant depending solely on the specific geometry of the convection scenario, for example if the scenario is a cooling cylinder of diameter *D* with a fluid flowing orthogonally to the rotational axis around the cylinder, the characteristic length is $\delta = D$.
- A function *f* connecting the so-called Nusselt number (see formula [6.2.2–5], [6.2.2–6], [6.2.2–7]) to the Prandtl number Pr (see formula [6.2.2–8]) and the Reynolds number Re (see formula [6.2.2.1–9]) or the Grashof number Gr (see formula [6.2.2–10]).

Both quantities can be found in tables containing specific scenario geometries in textbooks (e.g. in Cengel [1998]).

The theory of thermodynamics differentiates two types of convection: *natural convection* where the movement of the target fluid is caused by buoyancy forces and *forced convection* if the target medium is moved by other forces. Because of the complex nature of the mechanisms involved, the convective heat transfer power P_{conv} is modelled as a linear approximation called *Newton's law of cooling* to the heat transfer equation:

$$P_{\text{conv}} = h \cdot A \cdot \left(T_S - T_E\right) \qquad (6.2.2\text{–}3)$$

In formula (6.2.2–3) the symbol h stands for *the convection heat transfer coefficient*, A is the area through which convective heat transfer takes place, the temperature of the cooling stationary surface is named T_S and T_E is the fluid temperature sufficiently far from the surface. Numerical computation of the convective heat transfer coefficient is done via the *Nusselt number* Nu:

$$h = \mathrm{Nu} \cdot \frac{\delta}{\lambda} \qquad (6.2.2\text{–}4)$$

The symbol Nu in formula (6.2.2–4) is for the Nusselt number, λ the heat conductivity of the fluid and δ the characteristic length of the cooling scenario. Three dimensionless quantities Pr, Re and Gr, called numbers, are most important for computation of the Nusselt number Nu. In the case of forced convection, we have a functional dependency:

$$\mathrm{Nu} = f\left(\mathrm{Pr},\ \mathrm{Re}\right) \qquad (6.2.2\text{–}5)$$

whereas in the case of free convection we may write:

$$\mathrm{Nu} = f\left(\mathrm{Pr}, \mathrm{Gr}\right) \qquad (6.2.2\text{–}6)$$

The function f is dependent of the geometry of the cooling scenario as previously mentioned and has to be measured or taken from textbooks such as Cengel (1998) or original literature (Colin, Houdas 1967).

If both mechanisms, forced and free convection, are involved in one cooling scenario, a common Nusselt number Nu has to be computed depending on the Nusselt numbers $\mathrm{Nu}_{\mathrm{forced}}$ and $\mathrm{Nu}_{\mathrm{free}}$ for the forced convection and the free convection part of the scenario, respectively. The following formula was yielded by evaluation of experimental data. The plus sign stands for the case where the mixing forced and free flows have the same direction, whereas the minus sign is valid if the free flow and the forced flow have opposite directions:

$$\mathrm{Nu} = \left(\mathrm{Nu}_{\mathrm{forced}}{}^{n} \mp \mathrm{Nu}_{\mathrm{free}}{}^{n}\right)^{1/n} \qquad (6.2.2\text{–}7)$$

The parameter $n = 3$ is used for horizontal surfaces, while $n = 4$ better matches the cases of vertical surfaces.

Nu is a function of the *Prandtl number* Pr, which can be interpreted as the ratio between molecular quasi-diffusivity of momentum and the molecular diffusivity of heat in the fluid. This interpretation leads to the formula:

$$\mathrm{Pr} = \frac{\mu \cdot C_P}{\lambda} \qquad (6.2.2\text{–}8)$$

which can be expressed as Pr being proportional to the dynamical viscosity μ, the specific heat capacity C_P and inversely proportional to the conductivity λ of the fluid.

In the case of forced convection, the *Reynolds number* Re describes the flow regime. It is defined as the ratio between inertia forces and viscous forces in the fluid. This leads to the following formula for the Reynolds number Re:

$$Re = \frac{\rho \cdot v_E \cdot \delta}{\mu} \qquad (6.2.2\text{–}9)$$

A large Reynolds number means that inertia forces are large in comparison to viscous forces. Therefore, a large Reynolds number indicates that viscous forces are too weak to preserve ordered motion of the fluid which leads to rapid and random changes of the local velocity vector in the fluid. The result is a turbulent flow. On the other hand, a small Reynolds number leads to an ordered and thus laminar flow. For a given fluid and a given flow scenario a critical Reynolds number $\mathrm{Re}_{\mathrm{crit}}$ can be found separating laminar flows from turbulent flows.

The *Grashof number* Gr governs the flow regime in the case of free convection just as the Reynolds number does in the case of forced convection. In analogy to the definition of the Reynolds number it is defined as the ratio of buoyancy force and viscous force in the fluid. Transformation of this definition leads to the following formula for the Grashof number Gr:

$$\mathrm{Gr} = \frac{g \cdot \beta \cdot \left(T_S - T_E\right) \cdot \rho^2 \cdot \delta^3}{\mu^2} \qquad (6.2.2\text{–}10)$$

As in forced convection a critical Grashof number $\mathrm{Gr}_{\mathrm{crit}}$ can be found for a specific free convection cooling scenario meaning that for $\mathrm{Gr} > \mathrm{Gr}_{\mathrm{crit}}$ the flow is turbulent and laminar otherwise. For example for the cooling process of a vertical plate the critical Grashof number $\mathrm{Gr}_{\mathrm{crit}}$ is about 10^9.

Radiation is the third mechanism to be considered in body cooling. A so-called *black body*, which has a surface of area A absorbing all electromagnetic waves of all frequencies and reflecting none of them, of a specific surface temperature T irradiates with a power $P_{\text{black body}}$ described by the famous *Stefan–Boltzmann law*:

$$P_{\text{black body}} = A \cdot \sigma \cdot T^4 \qquad (6.2.2\text{–}11)$$

The factor σ in the equation is the *Stefan–Boltzmann constant*:

$$\frac{\sigma = \frac{4}{15} \cdot \pi^{\mathrm{s}} \cdot \frac{k^4}{c^2 \cdot h^3} = 5.6703 \cdot 10^{-8}\,\mathrm{w}}{m^2 \cdot {}^{\circ}K^4} \qquad (6.2.2\text{–}12)$$

Radiation heat transfer includes not only energy loss by radiation but also the absorption of thermal radiation arriving at the surface from other surfaces which in some cases even belong to the same body. This among other aspects makes radiation heat transfer a complicated task for computation. The other cause is that most real bodies are no black bodies in the technical sense: they reflect a certain proportion of irradiation and absorb the other part. This fact is taken into account by using *emissivity* factors ε_i for all approximately plane homogeneous surfaces of a scenario. The factor ε_i is the quotient of the radiation power emitted by the surface and the radiation power emitted by a black body surface of equal geometry at the same temperature. This factor actually depends on the radiation frequency. In practical computations the *grey body approximation* is often used which states that the irradiation spectrum of the real surface A_i of temperature T can be generated by multiplying the spectrum of the black body of temperature T by ε_i. Additionally, it is assumed that the surface A_i is *opaque*, which means not transparent, and that it does not reflect radiation but backscatters it *diffusively*.

Another point to be considered is the position of every surface A_i in space relative to the positions of all other surfaces $A_1, \ldots, A_n$ involved in the scenario. This is done by *sight factors* $\mathrm{SF}(A_i,A_k)$ for each pair A_i,A_k of surfaces in the scenario. The sight factor $\mathrm{SF}(A_i,A_k)$ is defined as the quotient of the area of the surface A_k seen from the surface A_i and the area of A_i. This factor is used to compute the ratio of the radiation leaving surface A_i and striking surface A_k.

Let A_1 and A_2 be two surfaces of area A_1 and A_2, of temperatures T_1 and T_2 and emissivities ε_1 and ε_2, respectively. Let $\mathrm{SF}(A_1,A_2)$ be the sight factor of this scenario, then the power irradiated from surface A_1 on A_2 can be computed as:

$$P_{1,2} = A_1 \cdot \mathrm{SF}(A_1,A_2) \cdot \sigma \cdot \left(\varepsilon_1 \cdot T_1^{4} - \varepsilon_2 \cdot T_2^{4}\right) \qquad (6.2.2\text{–}13)$$

It is a well-known fact that heat-producing mechanisms in the body do not come to an abrupt halt with the heart stopping (see Lundquist [1956] and Mall et al. [2002]). Different causes for this p.m. *inner energy production* are discussed in literature. The overall thermodynamical effect is modelled in FE death time determination by attributing a fast-decreasing heat power P_{inner} to certain compartments of the human body in a FE cooling scenario model. A physiologically plausible approach models the overall inner energy production of the body as an exponentially dropping function of time:

$$P_{\text{inner}}(t) = P_0 \cdot \exp(-\alpha \cdot t) \qquad (6.2.2\text{–}14)$$

The inner energy production rate P_0 at the time of death was assumed to be the basal metabolic rate (see e.g. Klinke, Silbernagl (1994)) multiplied by the body mass m, whereas the factor α, which determines half-life, was fitted (Mall, Eisenmenger (2005)) using the cooling model of Marshall and Hoare to a value of $\alpha = 0.0000770164\ \mathrm{s}^{-1}$. The inner energy production rate is implemented in the FE model as a power density varying in the different body compartments (see Stolwijk, Hardy [1977]): 60% of the basal metabolic rate are attributed to the trunk core, 18% to the muscles, 17% to the brain and 5% to the connective tissue and the skeleton.

6.2.2.2 Differential Equation of Heat Transfer

The present section of the FEM article relies on the textbooks of Steinbuch (1998), Baehr, Stephan (1996) and Thomas (1998).

Essentially, heat transfer processes can be seen as energy transport phenomena which are governed by a sort of diffusion equation. The temperature field $T(r,t)$ is modelled as a function of space r and time t, which is differentiable two times. It is essential to define a specific spatial range Ω, where the heat equation shall be solved resulting in the temperature field $T(r,t)$ with the location vector r in the range Ω. Deriving a differential equation for the quantification of body cooling starts from the well-known *basic equation for heat transfer* of Fourier, which states that the stream density of heat energy at location r is proportional to the gradient grad $T(r,t)$ of the temperature field $T(r,t)$ at this location r. The proportionality constant $\lambda(r,t)$ is as usual in body cooling applications, a scalar function of space and time and is called *conductivity*. Introduction of another material constant, called the *specific heat capacity* c, states how much heat energy is necessary for warming up a mass unit of a specific material by 1°K turns out to be necessary to eliminate the heat stream density. The specific heat capacity c is a function $c(r,t)$ of space and time as well as the mass density $\rho(r,t)$. Applying the Gaussian integral theorem eventually leads to the well-known *homogeneous heat equation*. Additionally, considering the role of *heat sources* and *sinks* in the heat energy transportation process by introducing *heat source and sink densities* p(r,t) results in the *general inhomogeneous form of the heat equation*:

$$(\mathrm{P}) \qquad \frac{\partial}{\partial t} T = \frac{\lambda}{c \cdot \rho} \cdot \Delta T + \frac{1}{c \cdot \rho} \cdot p \qquad (6.2.2\text{–}15)$$

The Laplace operator Δ applied to the temperature field $T(r,t)$ is an abbreviation for the following sum of second order spatial partial derivations of $T(r,t)$:

$$\Delta T(r,t) = \frac{\partial^2 T}{\partial x^2}(r,t) + \frac{\partial^2 T}{\partial y^2}(r,t) + \frac{\partial^2 T}{\partial z^2}(r,t) \qquad (6.2.2\text{–}16)$$

The spatial position vector r has the components x,y and z. In equation (P) the symbol ρ stands for the mass density. The symbol p represents the heat power density of all heat generating or heat consuming entities in the spatial range Ω of the equation. It is important to remember that the transport process equation (*P*) models heat conduction only, so processes like warming by irradiation or cooling by convection have to be coped with by implementing specifically designed heat sources or sinks at the locations in Ω, where radiation heat transfer or convective warming or cooling takes place. This can be done since the heat powers of those processes are known from (6.2.2–3) and (6.2.2–13). The heat power (6.2.2–14) of p.m. energy production is modelled as a heat source in (*P*) as well.

To yield a unique solution $T(r,t)$ of the inhomogeneous heat equation (*P*) in the spatial range Ω for all points of a time interval $I = [t_0,t_1]$ of interest, we need to specify *initial conditions*: one has to define the temperature field $T_0(r) = T(r,t_0)$ at the beginning t_0 of the cooling process for every point r in the spatial range Ω:

$$\text{(I)} \qquad \forall r \in \Omega : T\left(r,t_0\right) = T_0\left(r\right) \qquad \text{(6.2.2–17)}$$

The second condition to guarantee uniqueness of the solution of the cooling problem is connected to the edge ∂Ω of the spatial range Ω. Since the FEM cannot compute $T(r,t)$ on an infinite space, we have to specify the bounded region Ω as definition range for the temperature field $T(r,t)$. On the edge ∂Ω of Ω the solution cannot be computed, it has to be specified as a function $T_\partial(r,t)$—called the *boundary condition*—a priori for r in ∂Ω and for all points t in the time interval $I = [t_0,t_1]$ of this process:

$$\text{(B)} \qquad \forall t \in \left[t_0,t_1\right] : \forall r \in \partial\Omega : T\left(r,t\right) = T_\partial\left(r,t\right) \qquad \text{(6.2.2–18)}$$

The three conditions (I), (B) and (P) together are now sufficient for the existence and uniqueness of a solution $T(r,t)$ in the range Ω and for all times *t* in *I*.

6.2.3 Solving the Heat Equation

As sources for the material presented in the following section, we mention the textbooks of Steinbuch (1998) and Zienkiewicz, Taylor (1997). The following presentation is only loosely based on those texts.

From the theory of partial differential equations, we know that there is a unique solution to the boundary and initial value problem posed by ((I),(B),(P)). Nevertheless, it is impossible to find exact formulae for such solutions in most practical cases. This is a fortiori true in the real body cooling cases, which are relevant in homicide cases. Since the beginning of the computer age, there have been several approaches to compute good approximations to solutions of problems like ((I),(B),(P)). The Finite Difference Scheme as well as Boundary Element Method have to be named in this context. One of the most effective and widely used methods is the FEM, which was developed in the sixties and seventies. It provides a general approximation method for vector fields, which leads in a natural way to an approach for computing approximate solutions of partial differential equations like (P) under conditions (I) and (B).

6.2.3.1 The Finite Element Method

In the next paragraphs the term *mathematically easy* will be used extensively. A function is called mathematically easy if it and all its derivations of sufficiently high order can be computed by hand in a finite and exact form. This implies that the function itself and also its necessary derivations can be easily implemented in a computer program.

The first step of the FEM is to find a discrete approximation of the temperature field $T(r,t)$, which is defined on the spatial range Ω at a certain point t in the relevant time interval I. For this purpose, the range Ω is approximated by a spatial volume *E*, which is assembled of small volumes $E_1, \ldots, E_n$ (see Figure (6.2.3–1). Every small volume E_n can be described as the result of a mathematically easy transformation $f_n = (f_n^x, f_n^y, f_n^z)$, called *element transformation*, with the three vector components f_n^x, f_n^y, f_n^z, which maps Euklidean space IR³ into itself. The element transformation f_n is applied to an elementary mathematical volume E^*, which is called the *pre-element*, for example, of the unit cube or of a tetrahedron in IR³ (see Figure 6.2.3–2) to generate the volume E_n:

$$E_n = f_n\left(E^*\right) \qquad \text{(6.2.3–1)}$$

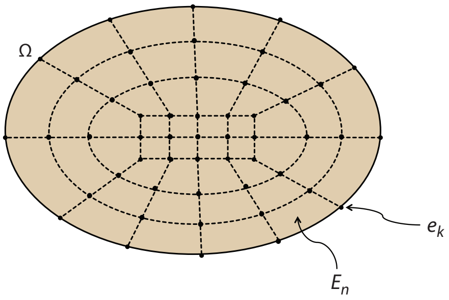

Figure 6.2.3–1 Finite element model of a two-dimensional ellipsoid.

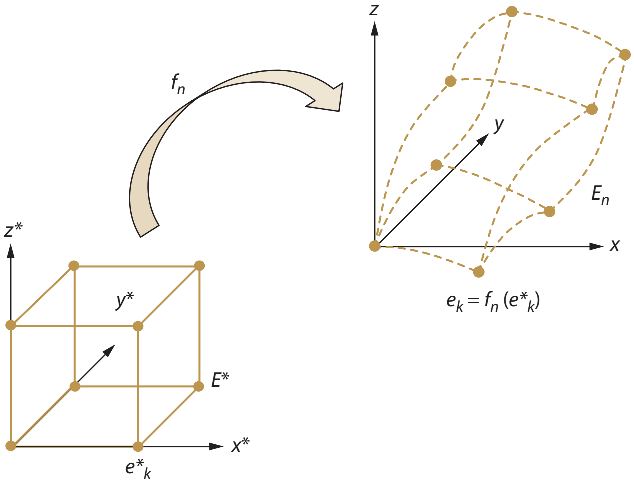

Figure 6.2.3–2 Element transformation.

The vertices $e^*_1, \ldots, e^*_K$ of the volume E^* are called *pre-nodes* of E_n whereas their images $e_1 := f_n(e^*_1), \ldots, e_K := f_n(e^*_K)$ under the transformation f_n, which are the vertices of E_n, are called *nodes* of E_n. For every node index k there is a mathematically easy function h^*_k defined on E^*, which maps E^* into the real numbers IR. The function h^*_k takes the value 1 on the pre-node e^*_k and the value 0 on all other pre-nodes e^*_j of E^*. Moreover, for all indices k the value $h^*_k(r^*)$ of the function h^*_k is falling monotonously with rising distance between e^*_k and the point r^* in E^*. The functions $h^*_1, \ldots, h^*_K$ are called *pre-shape functions*. One can define *shape functions* on any E_n by 'pulling back' the point r in E_n, where the shape function h_k is to be defined, to the volume E^* via f_n^{-1} and applying the pre-shape functions h^*_k from E^* to E_n via the function f_n:

$$h_k(r) = h^*_k\left(f_n^{-1}(r)\right) \tag{6.2.3–2}$$

A volume E_n together with its nodes e_k and its shape functions h_k and its element transformation f_n is called a *finite element*. For convenience we will often use the term 'finite element E_n'.

For any function g^* on E^*, assigning a real number $g^*(r^*)$ to each r^* in E^*, the pre-shape functions h^*_k on E^* can be used to generate a simpler function $g^{*\#}$ on E^* which approximates g^*, if g^* is sufficiently smooth on E^*:

$$g^{*\#}\left(r^*\right) := \sum_{k=1}^{K} g^*\left(e^*_k\right) \cdot h^*_k\left(r^*\right) \tag{6.2.3–3}$$

This means to compute an approximate $g^{*\#}$ of g^* by a linear combination of g^*'s values $g^*(e^*_k)$ on the pre-nodes of E^* with the values of the pre-shape functions $h^*_k(r^*)$ as weights. This idea can be applied to a function g (e.g. temperature distribution T) with a range in the real numbers on the volume E_n analogously:

$$g^{\#}(r) := \sum_{k=1}^{K} g(e_k) \cdot h_k(r) = \sum_{k=1}^{K} g(e_k) \cdot h^*_k\left(f_n^{-1}(\mathrm{r})\right) \tag{6.2.3–4}$$

To apply this idea to partial differential equation solving it is necessary to define the approximation of a partial derivation of a function g from E_n into the set IR of the real numbers. This can be done consistently by defining it as the partial derivative of the approximation $g^\#$ with respect to the metavariable ξ, which can be the variable x, y or z:

$$\left(\frac{\partial g(r)}{\partial \xi}\right)^{\#} := \frac{\partial g^{\#}(r)}{\partial \xi} \tag{6.2.3–5}$$

Computing this formula with the help of the chain rule and of definition (6.2.3–4) the partial derivations of the pre-shape functions h_n as well as of the inverted element transformations f_n^{-1} appear. In the following we will use matrix representation for convenience. Note that all matrices are defined for only one element E_n initially. This is indicated by appending the index n onto the matrix names. Later we will use the matrices' names without index n indicating that all matrices X_n—where X can be H, B, T^+ or J—of the same type for all finite elements $E_1, \ldots, E_n$ are concatenated in an obvious way by the enumeration of the shape functions h_k^n of the elements E_n to assemble the matrix X for the whole cooling system from the $K \times K$—element matrices X_n and from matrices of the same dimensions $K \times K$ filled with 0s. The $K \times K$—matrices completely filled with zeros are represented simply by the single symbol 0 in formula (6.2.3–6):

$$X = \bigcup_{n=1}^{N} X_n := \begin{pmatrix} X_1 & \cdots & 0 \\ \vdots & \ddots & \vdots \\ 0 & \cdots & X_N \end{pmatrix} \tag{6.2.3–6}$$

Analogously, vectors related to the whole cooling system are assembled from the specific element vectors. For example the concatenation T^+ of the element-related temperature vectors T_n^+ defined in (6.2.3–11) is defined simply by putting all components of all vectors T_n^+ in a column vector T^+ following the scheme $T^+ = (T_1^+, \ldots, Tn^+)^T$.

We define the vector H_n of the shape functions h_k evaluated at r in E_n and the vector H^*_n of the pre-shape functions h^*_k evaluated at r^* with $r = f_n(r^*)$ by:

$$H_n(r) = \left(h_1(r) \;\; \ldots \;\; h_K(r)\right) \tag{6.2.3–7}$$

$$H^*_n\left(r^*\right) = \left(h^*_1\left(r^*\right) \;\; \ldots \;\; h^*_K\left(r^*\right)\right) \tag{6.2.3–7*}$$

Their derivations $B_n = H_n'$ and $B^*_n = H^*_n{}'$, evaluated at r in E_n and r^* in E^*, respectively, is therefore:

$$B_n(r) = H_n'(r) := \begin{pmatrix} \dfrac{\partial h_1(r)}{\partial x} & \cdots & \dfrac{\partial h_K(r)}{\partial x} \\ \dfrac{\partial h_1(r)}{\partial y} & \cdots & \dfrac{\partial h_K(r)}{\partial y} \\ \dfrac{\partial h_1(r)}{\partial z} & \cdots & \dfrac{\partial h_K(r)}{\partial z} \end{pmatrix} \tag{6.2.3–8}$$

$$B^*_n\left(r^*\right) = H^{*\prime}_n(r) := \begin{pmatrix} \dfrac{\partial h^*_1\left(r^*\right)}{\partial x^*} & \cdots & \dfrac{\partial h^*_K\left(r^*\right)}{\partial x^*} \\ \dfrac{\partial h^*_1\left(r^*\right)}{\partial y^*} & \cdots & \dfrac{\partial h^*_K\left(r^*\right)}{\partial y^*} \\ \dfrac{\partial h^*_1\left(r^*\right)}{\partial z^*} & \cdots & \dfrac{\partial h^*_K\left(r^*\right)}{\partial z^*} \end{pmatrix} \tag{6.2.3–8*}$$

For computing derivations the *Jacobi matrix* $J_n(r^*)$ of the spatial partial derivatives of the element transformation f_n evaluated at the point $r^* = f_n^{-1}(r)$ in E^* and its inverse $J_n(r^*)^{-1}$, which is identical to the matrix of the partial derivations of the inverted element transformation f_n^{-1}, at the location vector r is useful:

$$J_n\left(r^*\right)=\begin{pmatrix} \dfrac{\partial f_n{}^x\left(r^*\right)}{\partial x^*} & \dfrac{\partial f_n{}^y\left(r^*\right)}{\partial x^*} & \dfrac{\partial f_n{}^z\left(r^*\right)}{\partial x^*} \\ \dfrac{\partial f_n{}^x\left(r^*\right)}{\partial y^*} & \dfrac{\partial f_n{}^y\left(r^*\right)}{\partial y^*} & \dfrac{\partial f_n{}^z\left(r^*\right)}{\partial y^*} \\ \dfrac{\partial f_n{}^x\left(r^*\right)}{\partial z^*} & \dfrac{\partial f_n{}^y\left(r^*\right)}{\partial z^*} & \dfrac{\partial f_n{}^z\left(r^*\right)}{\partial z^*} \end{pmatrix} \qquad (6.2.3\text{–}9)$$

$$J_n{}^{-1}\left(r\right)=\begin{pmatrix} \dfrac{\partial f_n{}^{-1x}\left(r\right)}{\partial x^*} & \dfrac{\partial f_n{}^{-1y}\left(r\right)}{\partial x^*} & \dfrac{\partial f_n{}^{-1z}\left(r\right)}{\partial x^*} \\ \dfrac{\partial f_n{}^{-1x}\left(r\right)}{\partial y^*} & \dfrac{\partial f_n{}^{-1y}\left(r\right)}{\partial y^*} & \dfrac{\partial f_n{}^{-1z}\left(r\right)}{\partial y^*} \\ \dfrac{\partial f_n{}^{-1x}\left(r\right)}{\partial z^*} & \dfrac{\partial f_n{}^{-1y}\left(r\right)}{\partial z^*} & \dfrac{\partial f_n{}^{-1z}\left(r\right)}{\partial z^*} \end{pmatrix} \qquad (6.2.3\text{–}10)$$

The *determinant* of the Jacobi matrix $J_n(r^*)$ is $|J_n(r^*)|$.

If finally the vector $T_n{}^+$ of the values $T(e_1,t), \ldots, T(e_K,t)$ of the temperature field $T(r,t)$ at the node points $e_1, \ldots, e_K$ of E_n is defined (with the script T indicating transposition of the vector) as:

$$T_n{}^+\left(t\right) = \left(T\left(e_1,t\right),\ldots,T\left(e_K,t\right)\right)^T \qquad (6.2.3\text{–}11)$$

we can write the approximating field $T^\#$ (r,t) as well as the approximation (grad T)$^\#$ of its *spatial gradient* grad T and the time derivations $(\partial T/\partial t)$ approximation $(\partial T/\partial t)^\#$ in matrix form:

$$T^\#\left(r,t\right)=H\left(r\right)\cdot T^+\left(t\right) \qquad (6.2.3\text{–}12)$$

$$\left(grad\ T\right)^\#\left(r,t\right)=B\left(r\right)\cdot T^+\left(t\right) \qquad (6.2.3\text{–}13)$$

$$\left(\frac{\partial T}{\partial t}\right)^\#\left(r,t\right)=H\left(r\right)\cdot\left(\frac{\partial T^+}{\partial t}\right) \qquad (6.2.3\text{–}14)$$

The second step of FEM is to transform the partial differential equation (P) into an equation that can be solved with the finite and essentially linear numerical methods which can be implemented on computers. Using Green's integral theorem and a weak representation of the equation with the help of test functions, formula (P) is transformed to an equation, where the finite element approximations, yielded in the first step, can be inserted. This leads to the following form of the partial differential equation, which is stated here for the sake of simplicity in the homogeneous form:

$$c\cdot\rho\cdot\left(\int_\Omega H^T H\,d\Omega\right)\cdot\left(\frac{\partial T^+}{\partial t}\right)+\lambda\cdot\left(\int_\Omega B^T B\,d\Omega\right)\cdot T^+=0 \qquad (6.2.3\text{–}15)$$

In this equation the integrals over the region Ω are pure spatial integrations referring to the variable r. Further, it is obvious that the functions to be integrated $H^T H$ and $B^T B$ are solely dependent on the shape functions h_k; they do not depend on the actual temperature field T or on its derivations.

For convenience, we introduce the following abbreviations:

$$C=\lambda\cdot\left(\int_\Omega B^T B\,d\Omega\right) \qquad (6.2.3\text{–}16)$$

$$M=c\cdot\rho\cdot\left(\int_\Omega H^T H\,d\Omega\right)$$

The matrix C is called the *conductivity matrix* and M is called the *heat capacity matrix*.

Both integrals in (6.2.3–16) have the same integration range Ω, which consists of the element regions E_n's set union. The set union sign U is used here, in contrary to formula (6.2.3–6), in its conventional denotation:

$$\Omega=\bigcup_{n=1}^{N} E_n \qquad (6.2.3\text{–}17)$$

Therefore, C and M can be represented as the following sums, where the set union symbol U has to be interpreted as assembling a matrix from the element matrices:

$$C=\bigcup_{n=1}^{N}\lambda_n\cdot\left(\int_{E_n} B_n{}^T B_n\,dE_n\right)$$

$$M=\bigcup_{n=1}^{N}c_n\cdot\rho_n\left(\int_{E_n} H_n{}^T H_n\,dE_n\right) \qquad (6.2.3\text{–}18)$$

Using the transformation theorem for integrals the integrations in (6.2.3–18) can be computed via the Jacobi matrices J_n and the element transformations f_n as integrations on the pre-element E^* for all elements E_n:

$$C=\bigcup_{n=1}^{N}\lambda_n\cdot\left(\int_{E^*} J_n{}^{-1T}\cdot B^*{}_n{}^T\cdot B^*{}_n\cdot J_n{}^{-1}\left|J_n\right|dE^*\right)$$

$$M=\bigcup_{n=1}^{N}c_n\cdot\rho_n\left(\int_{E^*} H^*{}_n{}^T\cdot H^*{}_n\left|J_n\right|dE^*\right) \qquad (6.2.3\text{–}19)$$

Additionally, introducing the heat source and sink power density $p(r,t)$, the vector $p_n{}^+$ of its values on the nodes of element E_n, the vector p^+ of all node values and the approximation equation $p \approx H\,p^+$ after inserting (6.2.3–19) in (6.2.3–15) yields the *FEM heat equation* for the inhomogeneous case:

$$M\cdot\left(\frac{\partial T^+}{\partial t}\right)+C\cdot T^+=H\cdot p^+ \qquad (6.2.3\text{–}20)$$

The FEM heat equation represents a major step for approximately solving the original partial differential equation system ((P),(B),(I)) since the equation contains *no more spatial derivations* of the temperature field. Only an ordinary differential equation system of first order is left which can be numerically treated.

6.2.3.2 Implementation of the Finite Element Method

Given the FEM heat equation it is now possible to compute an approximated solution using a finite difference method for time integration of the system where only linear algebra operations have to be used in every time step.

6.2.4 The Body Cooling Finite Element Model

Generating an FE model of the human body for death time determination via body cooling was performed for the first time by G. Mall in her habilitation thesis [Mall 2000]. The FE models used at the forensic medicine institute in Jena up to 2014 are derived from this model. Modelling and pre-processing were done with the *FEM-Preprocessor* MENTAT, which also performs features of post-processing and is currently distributed by the MSC Software company. The program allows to define an FE model interactively by constructing 3D-geometrical objects, setting nodes, defining element areas, element types and material properties. The program also allows to define a start temperature field $T_0(r,t)$ of the body as initial condition (I) and to define boundary conditions (B), for example the ambient temperature $T_A(r,t)$ or ground temperature. The pre-processor transforms input data into the actual FEM input data file, which contains the whole information in a purely numerical style, for example the nodes are transferred to its coordinate tuples. The FE computation consists in the computation of the heat capacity matrix M, the conductivity matrix C for the whole scenario, in stating the FE heat equation in the general inhomogeneous form which takes into account all of the boundary conditions and in solving the FE heat equation. These steps are performed by the *FE processor* program, which in the case of the actual model is MARC of the MSC Software company. The result of its computations is a sequence of temperature field approximations $T^{\#}$ (r,t_j) which give for each of J°+°1 timesteps t_0, t_1, . . ., t_j the node temperatures T^{+} (r,t_j) at any node location of the whole model. This information is passed back to the pre-/post-processor, which allows the user to visualize and check the results.

6.2.4.1 Mapping the Cooling Scenario: Geometry

The human body was approximated by elementary geometrical forms. The forms were filled with ca. 8000 solid, nearly exclusively cuboid, 8-node so-called HEX-8 elements, which are the elements E_n, determining the element area E_n as well as the shape functions h_k, in our explanations earlier. Using the fact that the human body has a median-sagittal symmetry approximately, it was possible to do the FE computations for half of the body saving a huge amount of computing time (which was more important in the 1990 years than it is nowadays). The *meshing*, which means setting the nodes (ca. 10000) and relating them to elements, was done exclusively manually. The complex body anatomy geometry prevented the usage of automatic-meshing software.

The original FE model (see Figures 6.2.4–1 and 6.2.4–2), from which application models can be derived by scaling the spatial dimensions, had a length of 2 m, the (half) trunk had a width of 0.2 m and sagittal depth of 0.2 m. The inner elements have a mean edge length of ca. 0.025 m. The whole body is covered by a layer of solid cuboid elements of thickness 0.005 m maximum representing the skin except the part on the symmetry plane. On the skull this layer covers another layer of thickness 0.01 m representing the skull bone. The model is lying on its ‘back’ with arm and leg slightly abducted. The arm and leg were modelled with semi-ellipsoid cross sections.

As support surface of the underground material a trough, consisting of a 0.01 m thick element layer matching the body contours was generated. This trough can be

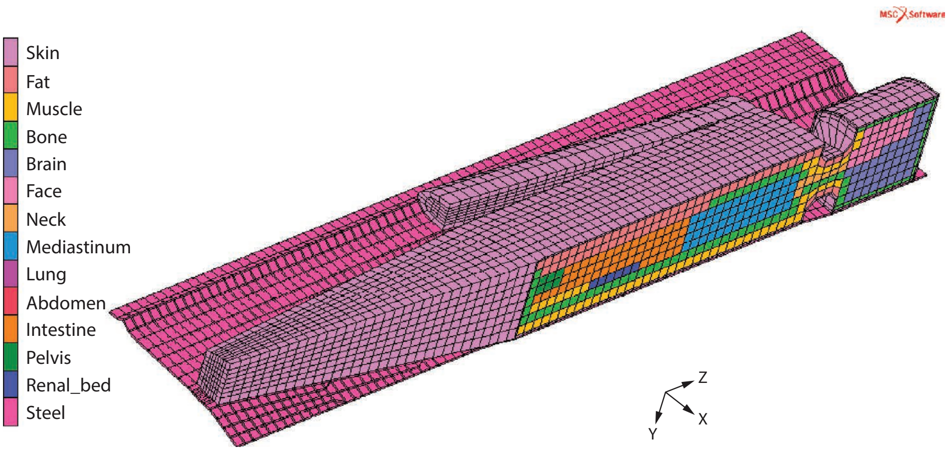

Figure 6.2.4–1 Finite element model of cooling body: outside view.

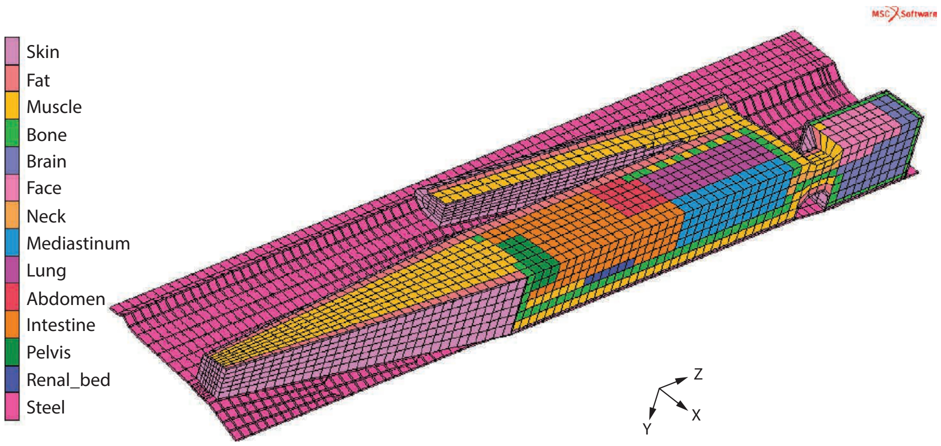

Figure 6.2.4–2 Finite element model of cooling body: view with ventral layers removed.

thickened by scaling and its material properties can be adapted to the actual underground of a case by changing the material properties. The projection of the trough onto the *x*-*y* plane is a rectangle. The models of body and trough together include ca. 10,000 elements and ca. 13,000 nodes.

For the FE model presented we differentiated the tissue compartments in the human body which are represented in Table (6.2.4–1) together with their numbers of elements and their volume proportion in the FE model:

6.2.4.2 Thermodynamical Properties of Biological Materials

All of the thermodynamical constants given in the following chapter are taken from the literature (e.g. Cengel (1998), Duck (1990) The FEM presupposes the knowledge of the relevant material constants for the case scenario considered. In practical casework we are confronted with the difficulties of gaining reliable values for the materials relevant for the cooling process. In many cases one has to rely on published parameter values of similar materials or has to estimate values making reasonable assumptions. Each of the three parameters λ, c, ρ is dependent on the location r in the scene.

Table (6.2.4–1) Body Compartments with Numbers of Elements and Volume Proportion

Body tissue	Number of elements	Volume proportion in %
Skin	2740	10.3
Fat tissue	1798	26.2
Muscle	2019	28.0
Skeleton	680	10.0
Brain	174	4.2
Face soft tissue	91	2.3
Cervical organs	14	0.2
Mediastinum	104	2–6
Lungs	220	5.0
Upper abdominal organs	97	2.2
Gastrointestinal tract	259	6.0
Renal bed	42	0.8
Retroperitoneum	47	1.2
Pelvic organs	43	1.0
Sum	8328	100

Heat conductivity λ is defined as the heat transfer rate through a unit thickness of the material per unit area per unit temperature difference.

Defining specific heat *c* of a material means to state the energy required to raise a unit mass of a substance by one temperature unit.

The mass density ρ, measuring mass per volume, seems to be the most uncomplicated physical quantity in the heat equation at first sight. In principle for any object of homogeneous consistency immersion of an object into water yields the volume and weighing the object leads to the mass. But since the individual body can deviate a great deal from the standardized mean body geometry and in many cases, there is no access to individual organs of the body, even this parameter ρ can be unknown.

A special role is played by the radiation connected emissivity ε. It takes values between 0 and 1 and it measures the ratio of emitting radiation power of the real surface and the black body under equal temperature conditions. The values of this parameter have to be taken from literature as well.

In real casework we are confronted with the problem of identifying and separating homogeneous regions in the body (*segmentation problem*) and to assign material properties to them. Up to now, the solution consists in using published anatomical knowledge and data about organ geometry in the human body as well as material constants published in biomechanics (Duck 1990) and physiology literature (Werner, Buse 1988) and (Stolwijk, Hardy 1977) or elsewhere (deDear et al. 1997). At present the desirable solution to have a CT body scan of a body in a real case and to automatically generate an individual FE model from it is not yet realized.

For the model presented, the material constants of single organ parts could be taken from literature. Since the FE model should not include too many details due to computational capacity reasons, it was often necessary to combine several organs to one compartment. So every material property of any compartment was assembled as linear combination of the material properties of its components with the volume proportions as weight factors (which are given in parentheses in the following listings). For the face soft tissue, the material properties of eyes (1/6), connective tissue (1/3), muscle (1/3) and fat (1/6) were used, whereas the cervical organs were composed of oesophagus (1/4) trachea (1/4), thyroid (1/4) and connective tissue (1/4). For the mediastinum a mixture of heart (1/2), trachea (1/6), oesophagus (1/6) and connective tissue (1/6) was used, the upper abdominal organs were assumed to consist of liver (3/4) and spleen (1/4) and the gastrointestinal tract of stomach (1/6), bowel (2/3) and fat (1/6). The renal bed was combined of kidney (2/3) and fat (1/3), the pelvic organs compartment of bladder (1/2), connective tissue (1/4) and muscle (1/4), whereas the retroperitoneum was assumed to consist of muscle by 100%.

6.2.4.3 Starting the Cooling Process: Initial Conditions

Solving a differential equation needs a fixed initial condition $T_0(r) = T(t_D,r)$ at the time of death t_D as a starting point. In practical casework the temperature distribution $T_0(r)$ of the cooling body is strictly spoken unknown. For many cases a reasonable guess can be made by assuming the standard mean temperature field $T(r)$ in the living body which is published in physiology literature. This approach does not take into account singular circumstances, for example, fever, hypothermia or strong physical stress at the time of death t_D. It is in most cases adequate to assume that there is a temperature gradient from body core to the peripheral body parts.

For the initial condition temperature field $T_0(r)$ in a case of body cooling at room temperature the results of Klinke, Silbernagl (1994) can be assumed. Additionally, we set the temperature of the body core at 37.2°C like in Marshall, Hoare (1962). The resulting temperature field of the body model is shown in Figure (6.2.4–3). Table (6.2.4–3) shows the values used for $T_0(r)$.

The initial temperature field of those parts of the scenario not belonging to the body, for example the floor or the surrounding air should be measured. If there is no further information about the latter temperature field but the statement, that the scenario was not heated up or cooled down by external causes like a heating switched on during

Table (6.2.4–2) Body Compartments with Heat Conductivity λ, Specific Heat Capacity *c* and Mass Density ρ

Body tissue	λ (W m^{-1} °C^{-1})	c (J kg^{-1} °C^{-1})	ρ (kg m^{-3})
Skin	0.47	3680	1085
Fat tissue	0.21	2300	920
Muscle	0.51	3800	1085
Skeleton	0.75	1700	1357
Brain	0.49	3850	1080
Facial soft tissue	0.51	3245	1056
Cervical organs	0.48	3363	1006
Mediastinum	0.47	3375	1033
Lungs	0.28	3520	560
Upper abdominal organs	0.48	3730	1080
Gastrointestinal tract	0.46	3346	933
Renal bed	0.39	3158	1026
Retroperitoneum	0.51	3800	1085
Pelvic organs	0.49	3350	1008

Note: The emissivity ε of the skin was assumed to be ε = 0.95, a value which can be found in Cengel (1998).

Table (6.2.4–3) Initial Temperature Node Sets in the Body with Number of Nodes and Initial Temperature T_0

Node set	Number of nodes	Temperature T_0 (°C)
Head (outer)	355	35
Head (middle)	254	36
Head (inner)	450	37.2
Neck (outer)	60	35
Neck (middle)	45	36
Neck (inner)	60	37.2
Trunk (outer)	816	35
Trunk (middle)	854	36
Trunk (inner)	1873	37.2
1: Arm (outer)/Arm (inner)	60/139	35/36
2: Arm (outer)/Arm (inner)	36/132	34/35
3: Arm (outer)/Arm (inner)	64/132	33/34
4: Arm (outer)/Arm (inner)	64/132	32/33
5: Arm (outer)/Arm (inner)	64/132	31/32
6: Arm (outer)/Arm (inner)	64/132	30/31
7: Arm (outer)/Arm (inner)	64/132	29/30
8: Arm (outer)/Arm (inner)	64/132	28/29
9: Arm (outer)/Arm (inner)	33/33	27/28
1: Leg (outer)/Leg (inner)	107/345	35/36
2: Leg (outer)/Leg (inner)	128/324	34/35
3: Leg (outer)/Leg (inner)	128/324	33/34
4: Leg (outer)/Leg (inner)	128/324	32/33
5: Leg (outer)/Leg (inner)	128/324	31/32
6: Leg (outer)/Leg (inner)	128/324	30/31
7: Leg (outer)/Leg (inner)	128/324	29/30
8: Leg (outer)/Leg (inner)	128/324	28/29
9: Leg (outer)/Leg (inner)	81/81	27/28

the cooling process or a window opened during investigations but some hours before temperature measurement, it can be reasonable to assume that the scenario without the cooling body was in a temperature steady state. Then the room air temperature T_A can be taken as a raw approximation for the initial condition temperature field $T_0(r) = T_A$ of the scenarios non-body parts.

6.2.4.4 Connecting the Cooling Process to the World: Boundary Conditions

Solution of the initial and boundary value problem ((I),(B),(D)) involves defining boundary conditions in the sense of (B) for the whole duration of the cooling process. This means specifying the temperature field $T_\partial\ (r)$ for all locations r on the boundary $\partial\Omega$ of the range considered. For example this could mean to assign a fixed and constant temperature T_∂ for all points r on the walls (modelled as two-dimensional objects) of a small room where cooling takes place, during all times t for which the cooling process is computed: $T_\partial\ (r,t) = T_\partial$. In most cases the boundary condition (B) assigns a constant temperature T_A to the surrounding air and neglects the minor effect of air heating by body cooling.

The problem of setting boundary values reflects the more basic problem of choosing a finite range Ω for the scenario of body cooling. In principle, the range Ω could be modelled as the whole earth and its atmosphere. This is certainly absurd, since time, storage and computing capacity is finite and costly in most application cases. Therefore, one takes advantage of the fact that in some distance to the cooling body temperature effects, caused by body cooling, cannot be detected anymore. The usual solution will be to implement the range Ω's boundary ∂Ω in at least such a distance of the cooling body. An erroneous choice of the boundary ∂Ω can be the source of major errors in computing death time. If, for example a cooling body is situated on a stony and wet underground, which is a good heat conductor, it would be fallacious to choose part of the boundary ∂Ω to be the surface of the underground and to assign a constant temperature (far below the body core temperature of 37.2°C) to it. This would lead to a heat flow from the body into the underground which is not slowed down by the warming of the part of the ground directly below the body. Therefore, this heat flow would be much too strong leading to accelerated cooling and to death time estimation t_D^ which is too late (t_D^ >> t_D) in comparison to the true time of death t_D. The correct solution would have been to model a part of thickness D of the underground in Ω and to include its outer walls as a part of ∂Ω. It would have been necessary to model several Ω's with different values of D, for example $D = 0.25$ m, $D = 0.5$ m and $D = 1.0$ m to test, whether the outer walls of the underground heat up essentially at a given D value. For the final computation such a value of D would have been chosen to fix the cooling scenario.

6.2.4.5 Reconstructing Time Since Death

Once the model described in the earlier sections is equivalent to the complete initial and boundary value problem ((P),(I),(B)), the FE computation can be started. As was already mentioned, the result of the solving process is a series of temperature fields $(T(r,t_j))_{j^\circ=^\circ 1,\ldots,J}$, where each $T(r,t_j)$ describes the temperature distribution on the spatial region Ω containing the cooling body (see Figures 6.2.4–4(a)–6.2.4–4(h)). Let now r_M be a node in the FE model corresponding to the top of the rectal temperature probe during rectal temperature measurement at the crime scene which produces the value T_M. By extracting the point series $(t_j,\ T(r_M,t_j))_{j^\circ=^\circ 1,\ldots,J}$ from the series of temperature fields $(T(r,t_j))_{j^\circ=^\circ 1,\ldots,J}$ and applying interpolation of the point series $(t_j,\ T(r_M,t_j))_{j^\circ=^\circ 1,\ldots,J}$ the model curve $T(t)$ can be reconstructed, which gives the deep rectal

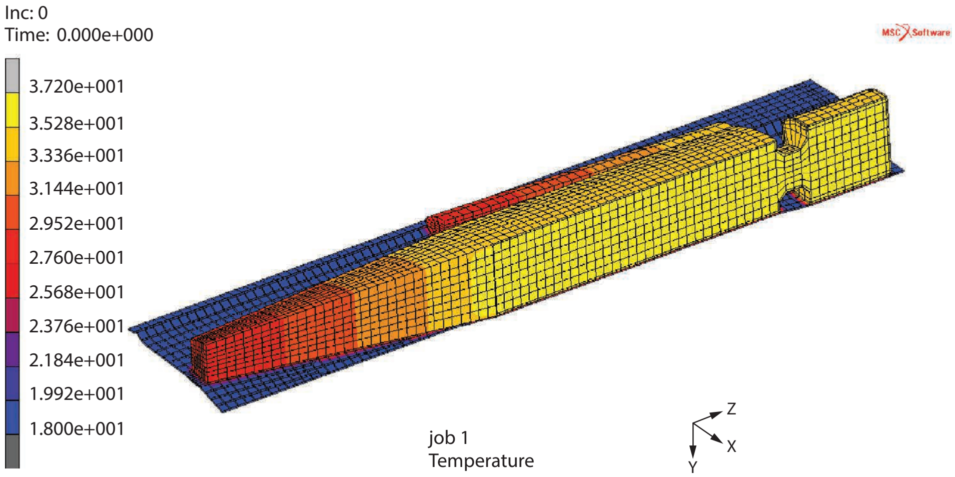

Figure 6.2.4–3 Initial condition: temperature field of the living.

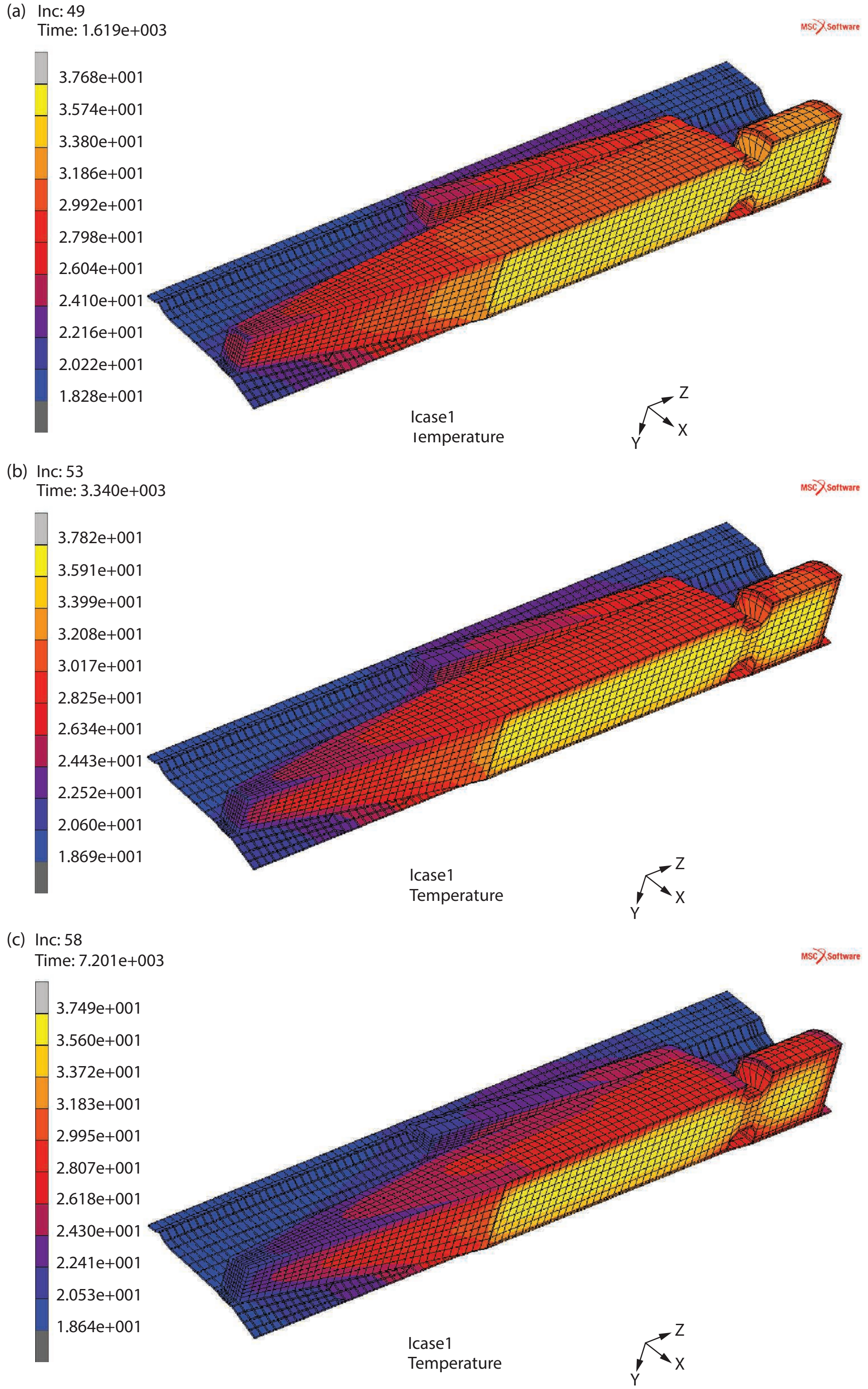
(a) Inc: 49
Time: 1.619e+003
MSC Software
3.768e+001
3.574e+001
3.380e+001
3.186e+001
2.992e+001
2.798e+001
2.604e+001
2.410e+001
2.216e+001
2.022e+001
1.828e+001
Icase1
Temperature
Z
X
Y
(b) Inc: 53
Time: 3.340e+003
MSC Software
3.782e+001
3.591e+001
3.399e+001
3.208e+001
3.017e+001
2.825e+001
2.634e+001
2.443e+001
2.252e+001
2.060e+001
1.869e+001
Icase1
Temperature
Z
X
Y
(c) Inc: 58
Time: 7.201e+003
MSC Software
3.749e+001
3.560e+001
3.372e+001
3.183e+001
2.995e+001
2.807e+001
2.618e+001
2.430e+001
2.241e+001
2.053e+001
1.864e+001
Icase1
Temperature
Z
X
Y

Figure 6.2.4–4 Phases of body cooling: time evolution of the body's temperature field. (a). Time *t* = 1619 seconds = 0.45 hours. (b). Time *t* = 3340 seconds = 0.93 hours. (c). Time *t* = 7201 seconds = 2.00 hours. (*Continued*)

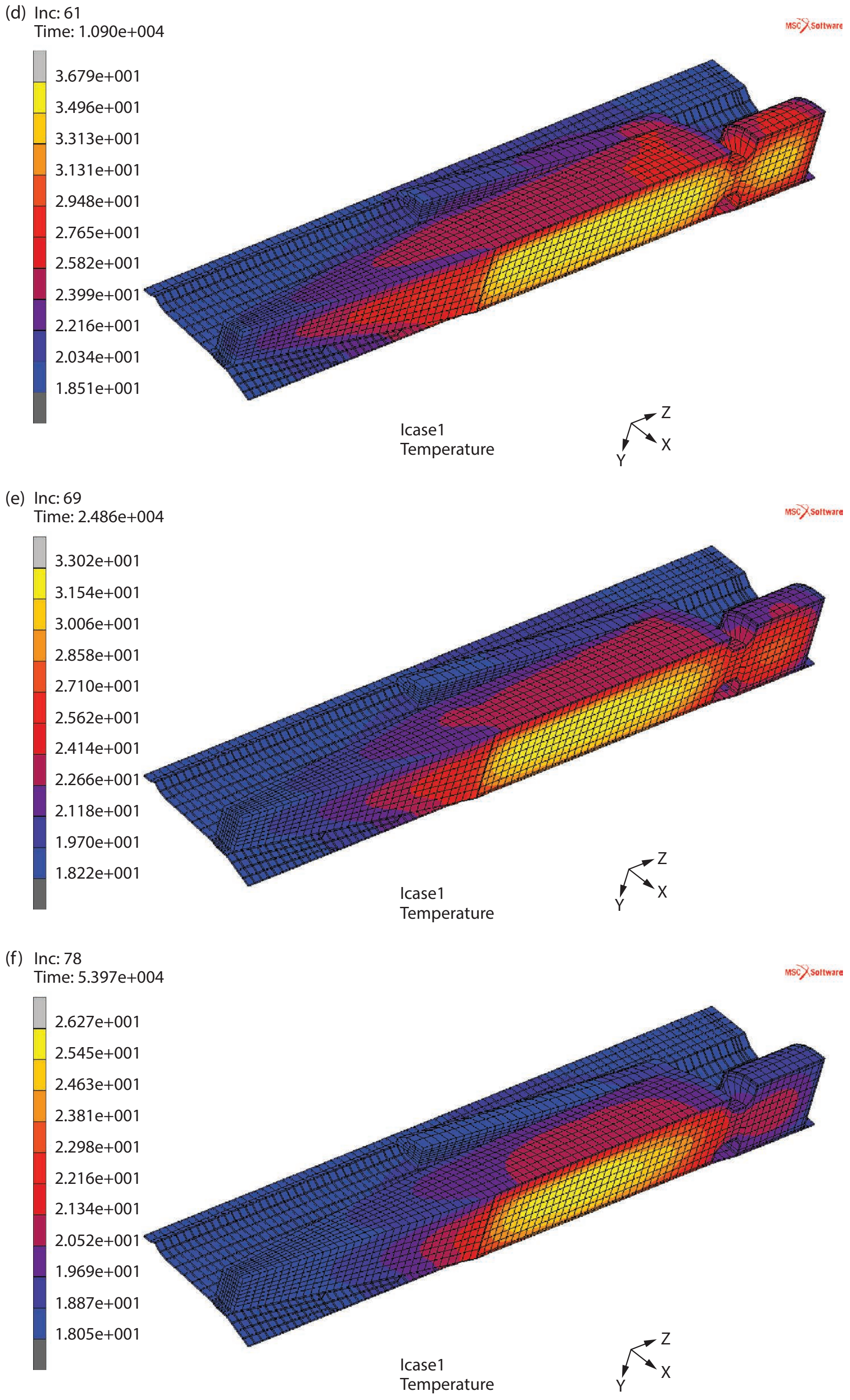
(d) Inc: 61
Time: 1.090e+004
3.679e+001
3.496e+001
3.313e+001
3.131e+001
2.948e+001
2.765e+001
2.582e+001
2.399e+001
2.216e+001
2.034e+001
1.851e+001
MSC Software
Icase1
Temperature
Z
X
Y
(e) Inc: 69
Time: 2.486e+004
3.302e+001
3.154e+001
3.006e+001
2.858e+001
2.710e+001
2.562e+001
2.414e+001
2.266e+001
2.118e+001
1.970e+001
1.822e+001
MSC Software
Icase1
Temperature
Z
X
Y
(f) Inc: 78
Time: 5.397e+004
2.627e+001
2.545e+001
2.463e+001
2.381e+001
2.298e+001
2.216e+001
2.134e+001
2.052e+001
1.969e+001
1.887e+001
1.805e+001
MSC Software
Icase1
Temperature
Z
X
Y

Figure 6.2.4–4 (*Continued*) Phases of body cooling: time evolution of the body's temperature field. (d). Time *t* = 10900 seconds = 3.03 hours. (e). Time *t* = 24860 seconds = 6.91 hours. (f). Time *t* = 53970 seconds = 14.99 hours. (*Continued*)

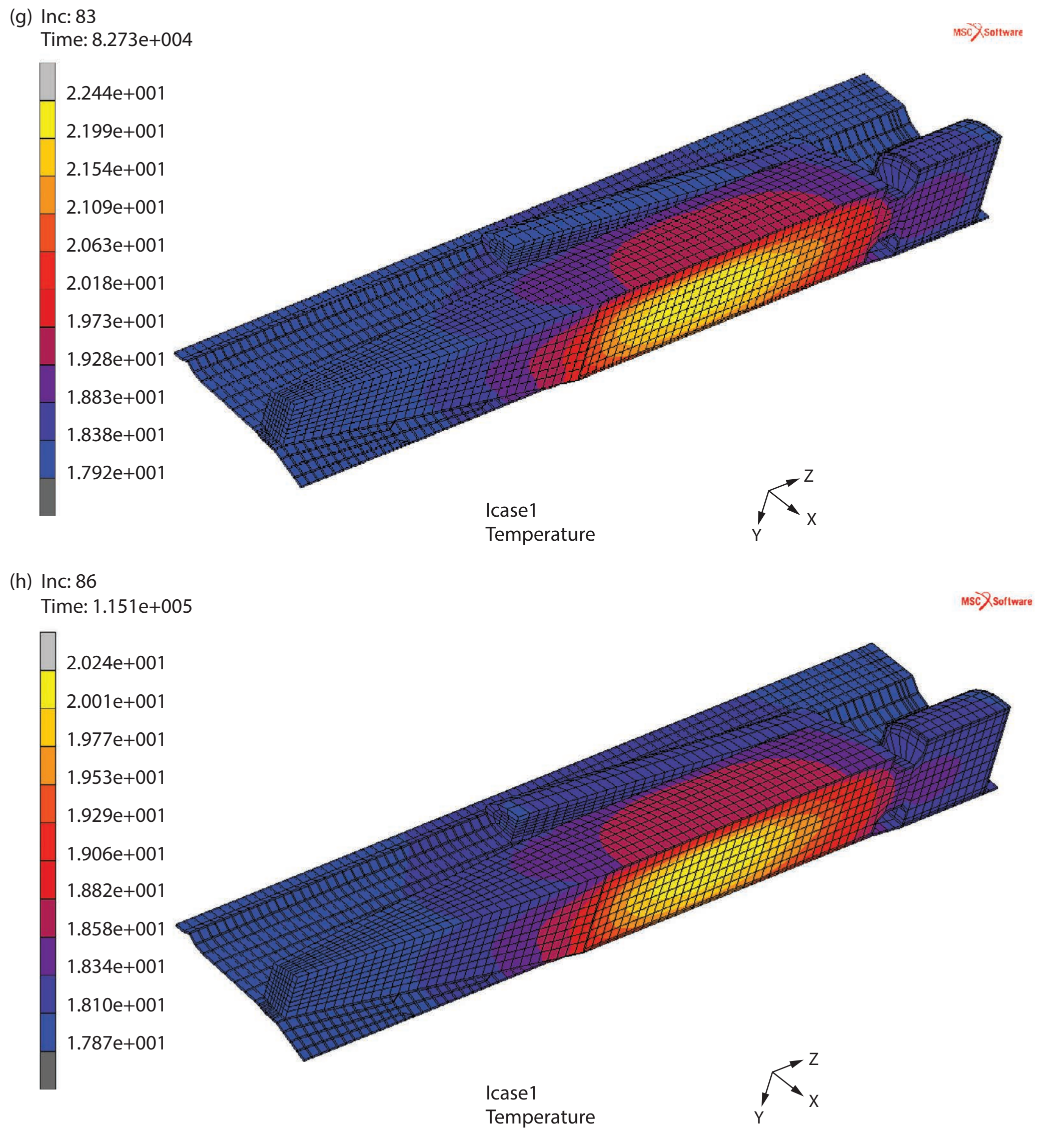
(g) Inc: 83
Time: 8.273e+004
2.244e+001
2.199e+001
2.154e+001
2.109e+001
2.063e+001
2.018e+001
1.973e+001
1.928e+001
1.883e+001
1.838e+001
1.792e+001
MSC Software
Icase1
Temperature
Z
X
Y
(h) Inc: 86
Time: 1.151e+005
2.024e+001
2.001e+001
1.977e+001
1.953e+001
1.929e+001
1.906e+001
1.882e+001
1.858e+001
1.834e+001
1.810e+001
1.787e+001
MSC Software
Icase1
Temperature
Z
X
Y

Figure 6.2.4–4 (*Continued*) Phases of body cooling: time evolution of the body's temperature field. (g). Time t = 82730 seconds = 22.98 hours. (h). Time t = 115100 seconds = 31.97 hours.

temperature at any time t in the interval $[t_0, t_j]$. Since $t_0 = 0$ is set in the FE calculation, we can now read time since death t_S directly from the model curve $T(t)$ diagram by looking up the value t_S, which satisfies the equation:

$$T\left(t_S\right) = T_M \qquad (6.2.4\text{–}1)$$

as described in Section 6.2.1.

6.2.5 Model Validation

As for all parts or applications of theories in science there is no verification for cooling models. This is a direct consequence of Popper's epistemology. The only possibility to be reasonably sure that a scientific method actually works is to have as many tests as possible in practical situations, where viability can be checked. This tactic is called validation. The FE-based death time determination is in a comparably comfortable situation with respect to validation. The heat equation (P) as well as the algorithms for computing all heat transfer mechanisms were tested in many varying scenarios. The situation for the FEM in thermodynamics seems to be even better. Since its development in the sixties and seventies there have been legions of applications to technical problems, where the predictions of the FEM could be directly compared to measurements. The only part of the temperature and FE-based death time estimation to be validated is the FE model of the cooling body itself.

Validation of any cooling model can be done by comparison to real cooling cases as well as to established models in scenarios where they are known to work well. In the next section the matching of FEM to the well-established Marshall and Hoare model is shown in four hypothetical case scenarios. In the second next section comparison to real cooling cases is presented.

One major problem in the FEM validation of body cooling consists in the fact that real cases regularly show special conditions which have to be implemented in the FE model. For example the FE model of a very obese body has to be generated starting from the original model by adding layers of fat tissue under the skin. The model of a body half-covered by a blanket will be constructed by adding additional element layers onto the skin layer. Such 'handmade model variants' involve an immense expenditure of work in every single case. Therefore, the validation of a large number of cases, necessary to compute quantitative statistical measures, for example, confidence intervals, is extremely costly. The next stage of the FEM death time estimation method development will involve automatic or semi-automatic FEM mesh generating from CT or MRT images bypassing this bottleneck.

6.2.5.1 Comparison to the Model of Marshall and Hoare

For the comparison of FEM the model of Marshall and Hoare (1962) was chosen. This model takes into account the cooling body's height, which at first sight seems to be an important geometrical parameter: it determines not only the 'linear distribution' of body mass in the direction of the body's main axis but also the body's surface area. Since FEM takes into account the body constitution a model with the parameters body mass m and body height L seems to be adequate. The *model of Marshall and Hoare* like the *model of Henßge* is a double exponential model of the following form:

$$\frac{T(t)-T_A}{T_0-T_A}=\frac{p}{p-Z}\cdot e^{-Z\cdot t}-\frac{Z}{p-Z}\cdot e^{-p\cdot t} \qquad (6.2.5–1)$$

where the following parameter values were fixed: The parameter Z depending on the *size factor* S:

$$Z=0.0573+0.000625\cdot S$$

with the size factor S being defined by the quotient of body surface area estimate A given in cm^2 and body mass m in kg:

$$S=0.8\cdot\frac{A}{m}$$

In the formula for the size factor S, the body surface estimate A is computed using the DuBois formula (see e.g. Klinke, Silbernagl (1994)):

$$A=0.007184\cdot L^{0.725}\cdot m^{0.425}$$

The parameter p is given together with a value $p_{\min}$, which leads to a temperature curve $T_{\min}(t)$ lying below the model curve $T(t)$ as a lower boundary and a value $p_{\max}$ with a corresponding temperature curve $T_{\max}(t)$ as an upper bound.

$$p=0.4,\ p_{\min}=0.275,\ p_{\max}=0.6$$

Rectal cooling curves $T(t)$ were computed for four different cooling scenarios varying three important parameters: Ambient temperature T_A, body mass m and body height L. The scenario was cooling of the naked body on a steel trolley lying on the back with stretched legs and arms parallel to the body. The surrounding air was assumed to be static and the parameters of the four scenarios were:

(M1) $T_A = 18°\mathrm{C}$, $m = 80$ kg, $L = 1.75$ m Figure (6.2.5–1(a))
(M2) $T_A = 8°\mathrm{C}$, $m = 80$ kg, $L = 1.75$ m Figure (6.2.5–1(b))
(M3) $T_A = 13°\mathrm{C}$, $m = 61$ kg, $L = 1.60$ m Figure (6.2.5–1(c))
(M4) $T_A = 13°\mathrm{C}$, $m = 103$ kg, $L = 1.90$ m Figure (6.2.5–1(d))

Figures (6.2.5–1(a))–(6.2.5–1(d)) show the resulting FEM-computed rectal cooling curves (yellow), the Marshall and Hoare model curve $T(t)$ (red) and the lower and upper Marshall and Hoare boundary curve (blue) of the scenarios (M1)–(M4). The resulting FE curve $T(t)$ approximates the Marshall and Hoare curve well in all cases. In all of the scenarios the lower and upper boundary curves are not crossed by the FEM curve. For times of up to 25 hpm the back calculation results can be seen to be in the order of magnitude of 1 hour or smaller.

6.2.5.2 Comparison to Real Body Cooling

For real-case validation of the FE model, cooling experiments were conducted in the Munich Institute of Legal Medicine by Gita Mall and Inga Sinicina in 2003–2007. The bodies of suddenly deceased persons whose times of death were well documented were transferred into a climate chamber in the institute where their cooling processes could be plotted by rectal and skin thermometers while the chamber held the air temperature on the constant level T_A measured and documented at the death scene. The experiments are described in Muggenthaler et al. (2012). For comparison the rectal temperature curves measured in the chamber are represented together with the FEM-generated model curve.

To demonstrate FE model validation, we chose two cases of very similar body constitution from literature (Muggenthaler et al. (2011)). Case 1 was used to calibrate the FE model to the specific body constitution by changing the thickness of the subcutaneous fat layer of the torso so that the simulation results matched the corresponding experimental rectal temperature curve for case 1. The calibration result is shown in Figure (6.2.5–2(a)),

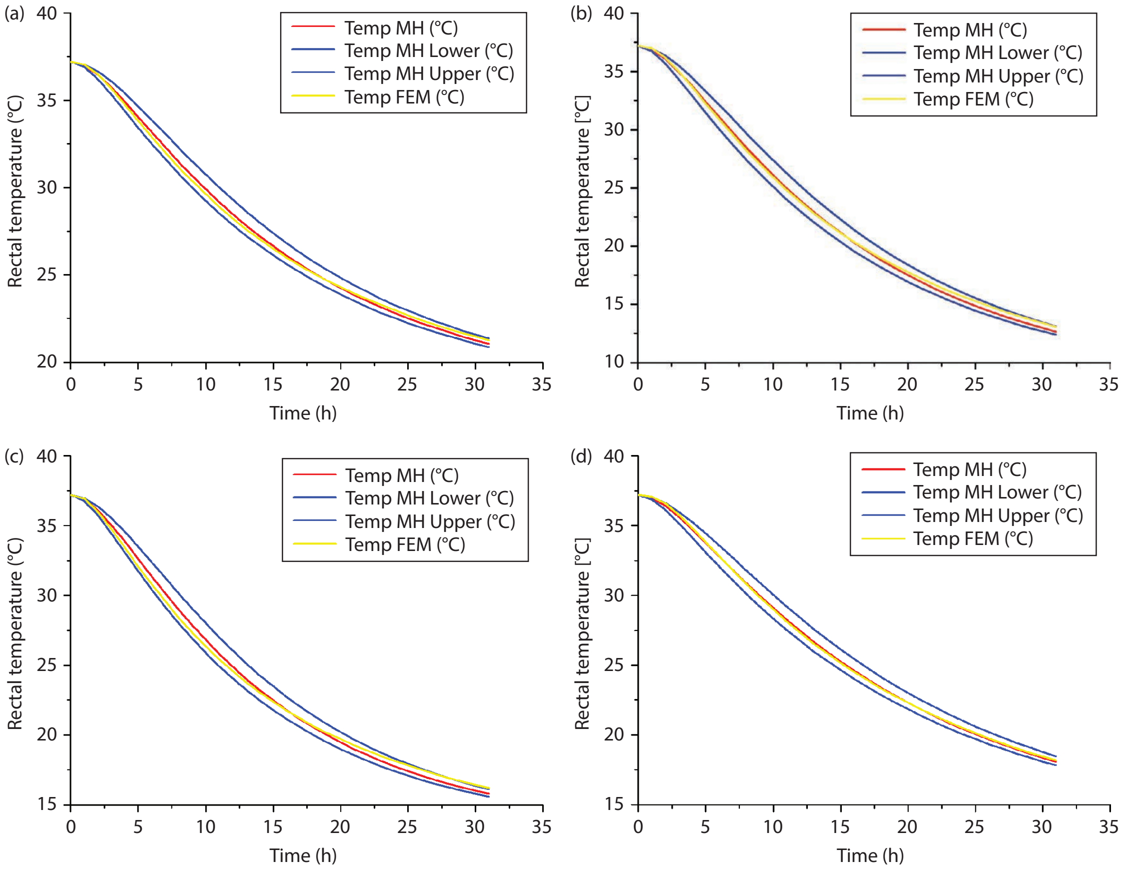

Figure 6.2.5–1 Validation with Marshall and Hoare model: cooling curves. (a). Scenario M1: $T_A = 18$°C, $m = 75$ kg, $L = 1.75$ m. (b). Scenario M2: $T_A = 8$°C, $m = 75$ kg, $L = 1.75$ m. (c). Scenario M3: $T_A = 13$°C, $m = 61$ kg, $L = 1.60$ m. (d). Scenario M4: $T_A = 13$°C, $m = 103$ kg, $L = 1.90$ m.

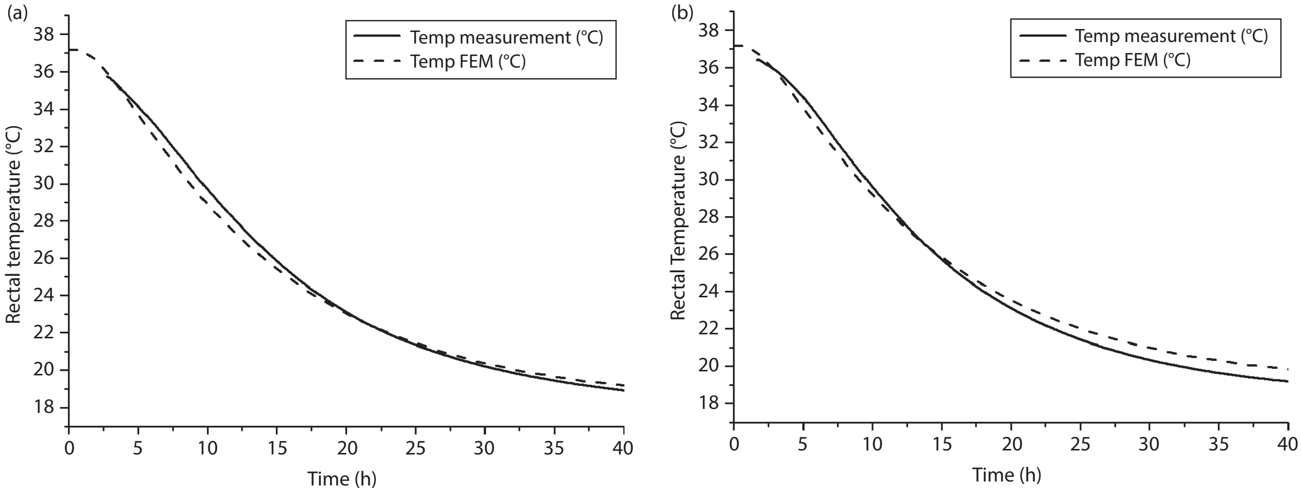

Figure 6.2.5–2 Calibration and validation on similar cases of experimental cooling. (a). Case 1: calibration. (b). Case 2: validation.

where the solid black line represents the measured data and the dashed line stands for the FE-computed result. Though the result is very good—up to 45 hpm there are back calculation errors of order smaller than 2 hours only—one can notice local systematic deviations of the FEM-computed rectal temperature–time curve from the one yielded by measurement. For example the FE-generated curve lies consistently below the measured curve between 5 hpm and 20 hpm, a typical deviation which most probably is caused by a structural model mismatch: The inner geometry and the material parameters of the FE model do not exactly represent the real cooling body. For validation purpose, the modified model was then scaled and adapted to the boundary conditions for case 2 and a simulation was performed without any further model modifications.

The environmental conditions of our validation cases (unclothed body, normal constitution, ambient temperature constant at about 18°C) are close to Henßges standard conditions (see e.g. Henßge, Madea (1988)) which correspond to a corrective factor value $c = 1$. According to the experimental setup, the support was modelled as a thin steel sheet representing the surface of the steel trolley used in the experimental measurements.

Case 1 was a male subject of 1.64 m body height and 64 kg body weight. He committed suicide in a bathtub by shooting himself immediately after announcing his suicide via telephone. This led to the discovery of the body only some minutes after death. The constant ambient temperature was 18°C and the body lay in the bathtub in approximately dorsal position. The time t_D between death and start of the rectal temperature measurement in the climatic chamber was t_D = 2 hours 44 minutes.

The male subject of case 2 died on a public staircase and was discovered immediately. He had a body height of 1.68 m and his body weighed 65.3 kg. The ambient temperature was 18.7°C and the time delay between death and measurement begin was t_D = 1 hour 40 minutes.

Figure (6.2.5–2(b)) shows the temperature–time courses measured in the climatic chamber (solid) and calculated with the finite element model (dashed). The curves in Figure (6.2.5–2(b)) represent the FE model validation. The FE-simulation-derived cooling curve exhibits strong correlation with the corresponding experimental data. Nevertheless, the matching is poorer than in the calibration diagram Figure (6.2.5–2(a)), which had to be expected. Maximum back calculation error can be bounded to values smaller than 3 hours for times of up to 30 hpm. As in the calibration diagram the locally systematic deviations are noticeable, which have to be attributed to structural model mismatch.

6.2.6 FE Error Analysis

The field of FE error analysis can be split into three subfields. The first one is *numerical stability* of the FE algorithm: Numerical stability is a necessary condition for the algorithm to produce reasonable results, but it does not guarantee the results to be correct. The second topic is errors in the input data caused by measurement, for example, flaws in rectal temperature measurement value or deviations of the model geometry from the cooling scenario. Those errors are called here *input data error*. The last subject area comprises errors generated by the so-called *model error*, which is a lack of the model assumptions to match the real-world conditions of the modelled scenario. This sort of error may come from simplifying assumptions, for example the approximation of the convection constant to be independent of the actual surface temperature where the convection takes place. It was discussed in paragraph 6.2.5 as structural model mismatch. Frequently, this kind of error leads to a *systematic deviation* of the estimated value—the time of death—from the true value.

A problem arising from time integration step of FEM is the choice of appropriate time step widths Δt. Since computation time rises with diminishing time step size Δt, it would be convenient to have large step sizes. On the other hand, approximation error and computational error grow with increasing step size Δt. An analogous argumentation shows that very small mesh widths Δx are computational infeasible while they yield better approximation results.

The numerical stability of the FEM depends on a condition (see e.g. Thomas (1998), Zienkiewicz, Taylor (1997)) connecting the maximum allowed spatial mesh width Δx between two neighbouring nodes of the same element to the maximum allowed time step size Δt:

$$\Delta t \leq \frac{1}{4} \cdot \left(\frac{\lambda}{c \cdot \rho} \right) \cdot \Delta x^2 \qquad (6.2.6\text{–}1)$$

FE calculations regularly need tests of *convergence*. This means testing whether the result of the FE computations is independent from the mesh width and from the time step size. Convergence testing is usually done by doubling the element number for testing element size convergence by subdivision of elements and decreasing the maximum time step size. If those two operations lead to a calculated cooling curve which is identical—in sufficient approximation—to the cooling curve calculated with larger element size and larger time steps the model is assumed to be convergent for practical purposes.

Investigating the input data error of a method means on one hand to find out the amount of change in the output data of the method caused by a given change in the input data. This is the classical form of the *error propagation problem* which could be answered for FEM in principle by an approach derived using the Gaussian error propagation formula. This approach allows computing the input data error as the standard deviation of the estimated quantity—the time since death—as a function of the standard deviations of the input data. In the case of FEM, the numerical computation of the partial derivations necessary for an actual evaluation is a practical problem.

The model error, which quantifies the models matching to the physics represented, requires comparison of the computation results to the real-world measurements.

Controlling the model error is usually called *validation*. It must be taken into account that the naïve comparison of computation and measurement results usually comprises both sorts of errors: the model error and the input data error. In the case of the FE model, the validation step using the model of Marshall and Hoare (see Section 6.2.5) as well as the real-case validation (see Section 6.2.5) combines both types of errors.

6.2.7 Application Examples

The four typical cases of FE application given here were taken from the paper (Mall, Eisenmenger (2005)). They demonstrate the applicability of the FEM-based death time estimation in cases of nonstandard conditions. Case A made it necessary to model an abrupt change of the body's position during cooling. For case B an abrupt change in ambient temperature was modelled. In case C and in case D clothing had to be modelled.

6.2.7.1 Case A

A 30-year-old woman was found dead in front of her apartment at 7:35 p.m. The body was fully clothed with a slip, brassiere, thin long-sleeved pullover of cotton-like material, jeans, nylon knee-high socks, ankle-high boots and an outdoor quilted anorak, which was open in front. The body was found in a ventral position and turned to a dorsal position around 7:50 p.m. by the emergency doctor. The emergency doctor testified death. The deep rectal temperature was measured at 12 p.m. with 29.7°C.

The environmental temperature at the same time was 16.6°C. The body height was 1.69 m. The body weighed 57.9 kg. The victim had last been seen alive at 3:30 p.m. Furthermore, the post-mortem rigidity, which had been broken at the crime scene in the left cubital joint, had strongly recurred.

The standard FE model was scaled according to the actual body height (1.69 m) and mass (57.7 kg) by applying a scaling factor in *z*-direction and a different scaling factor in *x*- and *y*-directions. The standard thermal tissue properties were attributed to the tissue compartments. The clothing of the upper part of the body was modelled by a 2.5 mm thick element layer with the thermal material properties of cotton to account for the cotton-like pullover. The quilted anorak was modelled on the back and around the arms with two element layers, the inner 30 mm thick with the thermal material properties of cellulosic insulation material and the outer 2.5 mm thick with the thermal material properties of polyester. The trousers were modelled by a 2.5 mm thick element layer with the material properties of cotton and the bootees by a 5 mm thick element layer with the material properties of leather. The standard initial temperature field with a temperature gradient of 37°C in the core and 27°C at the surfaces of the distal extremities was implemented. The nodes at the clothing surface were set to room temperature (20°C) since the victim had presumably been in her apartment before death. Natural convection and heat loss by thermal radiation were modelled. The initial amount of the internal energy production or the basal metabolic rate was converted to a heat flux density by division by the body volume and produced the standard initial heat flux density (1250 W/m^3) which was distributed in the standard manner to the different compartments (750 W/m^3 to the core, 225 W/m^3 to the muscle, 212.5 W/m^3 to the brain and 62.5 W/m^3 to the skeletal system).

The standard internal power decrease rate was implemented. First an FE analysis was performed assuming a ventral position throughout cooling from death till the rectal temperature measurement producing a time since death of 7.5 hours. Then an analysis was performed assuming a ventral position for 3 hours and then a dorsal position producing slightly longer times. The FE results would correspond to a time of death around 4:15 p.m.

The perpetrator meanwhile confessed to have killed the victim between 4:00 and 4:30 p.m.

6.2.7.2 Case B

An 18-year-old boy was found dead aside a street on a small asphalt path at 6:40 a.m. At 9 a.m. the deep rectal temperature was measured with 22.3°C. According to meteorological data from a nearby weather station, the air temperature was about 5°C during the night, the wind velocity (measured at a height of 10 m) was around 2 m/s and there was almost no rain. The boy had been last seen alive at 8:55 p.m. some 50 km away. The perpetrator was observed by a witness stopping the car presumably for depositing the victim aside the street at 11 p.m. The body was fully clothed with a thick woollen pullover, T-shirt, jeans, slip, socks and shoes. The body had a length of 1.87 m and a mass of 68.3 kg.

The standard FE model was again scaled to the actual body length and body mass. The thick woollen pullover was realized by a 5 mm thick element layer with the thermal properties of wool, the jeans by a 2.5 mm thick element layer with the thermal properties of cotton and the shoes by a 5 mm thick element layer with the thermal properties of leather. The standard initial temperature field with a maximum core to shell gradient from 37°C to 27°C was assumed. The standard initial energy production with the standard decrease rate was implemented. Then two different cooling phases were analysed: the first phase during the transportation in the car and the second phase after deposition outside. In the first phase room temperature (20°C) and natural convection were assumed. In the second phase, the outside temperature of 5°C and forced convection were assumed. The wind velocity was estimated with 0.25 m/s near the ground at the location where the body was found. According to formulae from the literature convection coefficients between 4.5 W/(m^2 °C) and 6.1 W/(m^2 °C) were calculated. Alternative analyses were performed with the first transportation phase lasting 1 or 2 hours. The assumption of a 1-hour transportation phase produced a total time since death of 11 hours, which would correspond to a time of death at 10 p.m. and deposition of the body at 11 p.m. The assumption of a 2-hour transportation phase produced a time since death of 11.5 hours, which would correspond to a time of death at 9:30 p.m. and deposition of the body at 11:30 p.m.

The perpetrator meanwhile confessed to have met the victim at 9 p.m. and killed him between 9 and 10 p.m. and deposited the victim at 11 p.m. corresponding to the observations of the witness.

6.2.7.3 Case C

A 49-year-old woman was found dead in her apartment at 8:45 a.m. The deep (insertion of the probe: 10 cm) rectal temperature was measured at 12:15 a.m. with 30.9°C. The environmental temperature was 23.5°C, the ground temperature 22.0°C. There was no sun or other irradiation. The body was fully clothed with a cotton pullover, undershirt, jeans, underpants, socks and shoes. The body height was 1.60 m, the body mass 48.7 kg.

The standard FE model was scaled to the actual body height and mass. The pullover was modelled by a 3 mm thick element layer with the thermal properties of cotton, the jeans by a 2.5 mm thick element layer with the thermal properties of cotton as well and the shoes by a 5 mm thick element layer with the thermal properties of leather. The standard tissue properties, the standard initial temperature field and the standard internal energy production were implemented. Natural convection and radiation heat loss were modelled.

The development of the temperature fields over 12 hours was analysed and evaluated at the node corresponding to the measurement site of the deep rectal temperature. A time since death of 8 hours was read from the model curve, which would correspond to a time of death around 4:15 a.m.

Investigations had meanwhile shown that the perpetrator was busy at the telephone till 4 a.m. and then went to the victim.

6.2.7.4 Case D

A 60-year-old man was found dead in his apartment at 6 p.m. The deep rectal temperature was measured at 10 p.m. with 27.1°C. The victim had been last seen alive at 8:20 p.m. the evening before. The body lay in a ventral position and was clothed with shirt, undershirt, trousers, underpants and socks. The underpants and trousers were dragged down below the buttocks. The ground (floor heating) was covered with a carpet. The room temperature was 25°C. The body height was 1.78 m, the body mass 83.3 kg.

The individually scaled standard FE model was complemented with a 2.5 mm thick element layer for the clothing with the material properties of cotton. The standard tissue properties, the standard initial temperature field and the standard internal energy production were implemented. Natural convection and radiation heat loss were modelled.

The temperature fields were analysed over 32 hours. A time since death of 25 hours could be read from the model curve which would correspond to a time of death around 9 p.m. The perpetrators meanwhile confessed to have entered the apartment at 8:30 p.m.

References

Alonso M, Finn EJ. *Physik*, Amsterdam: Addison-Wesley, Inter European Editions, 1977.

Baehr HD, Stephan K. *Wärme- und Stoffübertragung*, Berlin: Springer, 1996.

Cengel YA. *Heat Transfer. A Practical Approach*, Boston: McGraw-Hill, 1998.

Colin J, Houdas Y. Experimental determination of coefficient of heat exchange by convection of human body. *Journal of Applied Physiology*. 1976; **22**(1): 31–38.

deDear RJ, Arens E, Hui Z, Oguro M. Convective and radiative heat transfer coefficients for individual human body segments. *International Journal of Biometeorology*. 1997; **40**: 141–56.

Duck FA. *Physical Properties of Tissue*, London: Academic Press, 1990.

Gerthsen C, Vogel H. *Physik. Ein Lehrbuch zum Gebrauch neben Vorlesungen*, Berlin: Springer, 1993.

Henßge C, Madea B. *Methoden zur Bestimmung der Todeszeit an Leichen*, Lübeck: Schmidt-Römhild, 1988.

Klinke R, Silbernagl SA (eds.). *Lehrbuch der Physiologie*, Stuttgart: Thieme, 1994.

Lundquist F. Physical and chemical methods for the estimation of the time of death. *Acta Medicinae Legalis et Socialis*. 1956; **9**: 205–213.

Mall G. *Temperaturgestützte Bestimmung der Todeszeit mit Hilfe der Methode der Finiten Elemente*, Habilitationsschrift, München: Ludwig-Maximilians-Universität, 2000.

Mall G, Hubig M, Beier G, Büttner A, Eisenmenger W. Supravital energy production in early post-mortem phase—Estimate based on heat loss due to radiation and natural convection. *Legal Medicine*. 2002; **4**: 71–8.

Muggenthaler H, Hubig M, Mall G. Heat-flow finite-element models in death time estimation. In: Turk EE (ed.). *Forensic Pathology Reviews*, Vol. 6, Berlin: Springer Science + Business Media, 2011: 259–75.

Muggenthaler H, Sinicina I, Hubig M, Mall G. Database of post-mortem rectal cooling cases under strictly controlled conditions: a useful tool in death time estimation. *International Journal of Legal Medicine*. 2012; **126**(1): 79–87.

Steinbuch R. *Finite Elemente—Ein Einstieg*, Berlin: Springer, 1998.

Stolwijk JAJ, Hardy JD. Control of body temperature. In: Lee DHK, Falk HL, Murphy SD (eds.). *Handbook of Physiology*, Section 9: Reactions to environmental agents, Bethesda: American Physiological Society, 1977.

Thomas JW. *Numerical Partial Differential Equations. Finite Difference Methods*, New York: Springer, 1998.

Werner J, Buse M. Temperature profiles with respect to inhomogeneity and geometry of the human body. *Journal of Applied Physiology*. 1988; **65**(3): 1110–18.

Zienkiewicz OC, Taylor RL. *The Finite Element Method*, Volume 1, 2, London: McGraw-Hill, 1997.

6.3 The Prism Method

Stefan Potente

The approach to time since death (TsD) estimation after Marshall, Hoare and Henssge (MHH), most prominently the nomogram method (NM), is based on single rectal temperature readings only.[1] Methods for TsD estimation, which aim to exploit two or more rectal temperature readings over time, such as [1, 7, 8, 27, 30], have not gained widespread use. Here, we present the Prism method as yet another method to implement multiple rectal temperature readings. However in this method, parts of the whole cooling curve will be exploited. The Prism method was designed to reduce subjectivity in the assumption of parameters to be used in Henssge's equation:

$$\begin{aligned} Q &= \frac{Tr - Ta}{To - Ta} \\ &= A \times \exp(B \times t) + (1 - A) \times \exp\left(\tfrac{A \times B}{A - 1} \times t\right) \end{aligned} \qquad (6.1)$$

A and B, both constants, are mathematically connected. A describes the length of the plateau phase of the cooling curve. It is in itself dependent on T_a. Henssge emphasizes that this dependency is pronounced in high T_a. The chosen cut-off for T_a at 23.2°C makes two separate nomograms necessary. Correction factors (CF) are executed on the physical body weight to reflect crime scene conditions, which either promote or inhibit cooling compared to standard conditions.[2] However, CF themselves must be scaled for (physical) body weight [11]. CF may be difficult to assess for non-standard cooling conditions, with varying degrees of subjectivity. Rectal temperature at the time of death ($T_{r@D}$) is assumed as 37.2°C in MHH and ante mortem temperature elevation is very problematic in TsD estimation [6, 26, 33, 37]. Prism, however, was demonstrated to reliably detect formerly elevated T_r, even when it had already fallen below 37.2°C.

In the NM, parameters must be assumed. Correctness of such parameter assumptions is problematic for different reasons:

Corrective factors (CF) as a concept are very powerful [15] since they allow to take crime scene conditions into account. Conditions, which either promote or hinder body cooling, are translated into body weight changes in a simple and intuitive way. This follows the logic that heavy bodies cool slower than light bodies and conditions which slow down cooling effectively make the body cool 'as if it was heavier'.

In practice, however, the number of defined conditions is limited and some definitions leave room for interpretation. Individual determination of CF is theoretically possible but only rarely executed in practice, for example when investigating the effects of covering the body with leaves on cooling [3].

The examiner must therefore often fall back on experience when applying CF, introducing subjectivity. Direct, objective CF determination would be an important improvement in TsD estimation methodology [17]. For reasons of *scaling*, CF must be corrected for physical body weight [11, 13, 25, 31]. Simply put, a similar blanket does not result in similar changes to the cooling behaviour on differently sized bodies. Agreement between the calculated and the true physical body weight was within ±12.2 kg (2 SD) for 46 cases in [12].

Failure to correct CF relative to body weight may severely increase overall error, especially for extreme body weights and very large or very small CF [29].

Also, the concept of CF, their correction procedure and the concept of body weight in NM assume a fundamentally similar relationship of torso proportions, where rectal temperature is measured, and total body weight between any dead body in question and the underlying cooling models. In other words, valid results can be expected only when the torso of the dead body in question shows a comparable cooling behaviour to the assumed torso of an equal body weight in the MHH model. For example, when a body of 100 kg does not cool as predicted in the MHH model, because it is missing a limb or simply because of different proportions of the torso versus the rest of the body, this discrepancy cannot be resolved from within the NM.

Rectal temperature at the time of death ($T_{r@D}$) is generally assumed as 37.2°C in the NM. As a starting temperature, it is a very important parameter.

Elevated $T_{r@D}$ is a known problem in TsD estimation, for example in antemortem brain trauma, intoxication/medication, infection, stress [36] and other causes [6, 33].

A *post-mortem* temperature rise [37] is not generally accepted.

Once the body has cooled below 37.2°C, the NM in itself can neither detect such anomaly, even though discrepancy between NM results and compound method findings as well as police investigation may raise suspicion. For example, when the rectal temperature reading is 37.0°C, yet the body has been found 8 hours ago and/or rigor has already developed in full.

As pointed out by Muggenthaler et al. [26] 'the most considerable errors [. . .] occur in the first few hours post-mortem. With decreasing body core temperature and increasing post-mortem time the error diminishes and stagnates at a nearly constant level'.

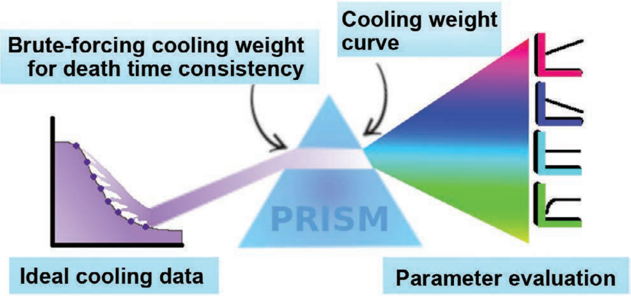

Figure 6.59 Prism method, illustration of the principle. Note minimized cooling curves on the right (from top to bottom): assumed ambient temperature too high, assumed ambient temperature too low, correct parameters, regular rectal temperature assumed as normal while in fact being elevated.

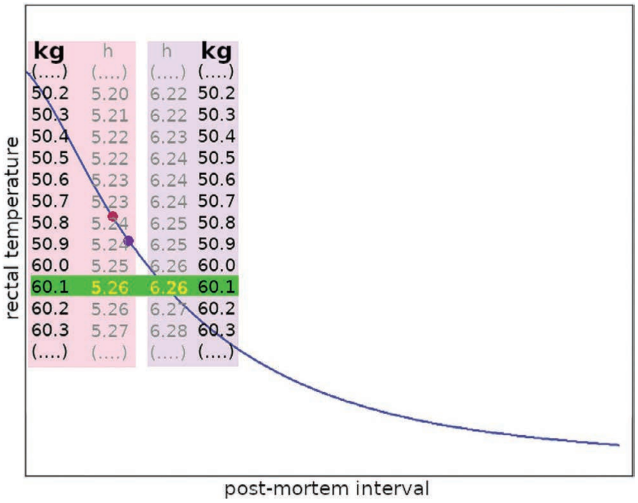

kg	h	h	kg
(....)	(....)	(....)	(....)
50.2	5.20	6.22	50.2
50.3	5.21	6.22	50.3
50.4	5.22	6.23	50.4
50.5	5.22	6.24	50.5
50.6	5.23	6.24	50.6
50.7	5.23	6.24	50.7
50.8	5.24	6.25	50.8
50.9	5.24	6.25	50.9
60.0	5.25	6.26	60.0
60.1	5.26	6.26	60.1
60.2	5.26	6.27	60.2
60.3	5.27	6.28	60.3
(....)	(....)	(....)	(....)

Figure 6.60 Brute-force calculations simplified: for two rectal temperatures (pink and purple dots on blue cooling curve) one hour apart, expected values (in hours, h) are calculated for a multitude of cooling weights (kg) in small increments. In the example, 60.1 kg is accepted as the momentary cooling weight (green), fulfilling the target condition for equal death time (yellow: 5.26 and 6.26, 1 hour apart).

Ambient temperature (T_a) should be reasonably constant [20] in TsD estimation. For moderate changes, mean ambient temperature is generally used while special considerations are applied to sudden and significant changes [2, 4]. Uncertainties and missing information regarding ambient temperature have led to attempts at estimating TsD independently from ambient temperature altogether [19].

To limit the potentially negative effects of parameter estimation, the **Prism method** was developed (named for its potential to break the rectal cooling curve up into its factors much like a Prism breaks up light (see Figure 6.59).

It aims at resolving uncertainties of parameters by using the underlying MHH equation in brute-force calculations. Such brute-force calculations are usually applied to problems such as the picking of a combination lock by trying out all possible number combinations (with ‘opening of the lock’ as the target condition) but also to more complex mathematical problems, where an equation is solved by putting in all possible values. Drawbacks of this approach are relative inefficiency when alternative solving mechanisms are available, crudity and reliance on computing power.

For the application of Prism, rectal temperature at the time of death, cooling weight[3] and ambient temperature are considered *uncertain*.

Cooling weight should however be *constant* when body mass, proportions and cooling conditions remain constant over the course of cooling.

Furthermore, estimated time of death itself (as in ‘10.00 a.m.’) must be *constant* over the course of cooling when all parameters are correct. The mathematical description in the NM uses relative time in the calculation of the expected value. The results are expressed in relation to the time of measurement.

Logically, if for one rectal temperature the calculated time since death is calculated as *X* (hours before measurement), it must be calculated as *X*°+°1 (hours before measurement) for the rectal temperature *one hour later*.

Generally, Prism first uses brute-force calculation to establish the cooling weight between two points. In a second step, the consistency of cooling weight over time is evaluated. In doing so, the problem of unknown parameters is split into a finite number of cases, which are then tested individually using the individual case’s cooling data (see Figure 6.60).

More specifically in the Prism method two times since death (expected values) are calculated for two rectal temperatures with known time difference to each other. For each, the assumed rectal temperature at the time of death and ambient temperature are used with a multitude of cooling weights in small increments to calculate thousands of slightly different expected values. Each expected value for time *X* and a known time interval later is then compared. Accounting for the known time difference, the cooling weight which produces the expected value difference closest to zero is accepted as the momentary cooling weight and the target condition ‘consistency of death time’ is fulfilled.

This process is repeated for the next rectal temperature pair and so on until ideally the whole cooling curve is processed. Momentary cooling weights are then plotted as a cooling weight curve which may be evaluated for ‘consistency of cooling weight over time’.

For **proof of principle**, the Prism method was utilized first on artificial cooling data. This data was modelled following the NM equation and its parameters by rearranging the equation and solving for rectal temperature, given points in time.

Such ‘ideal’ data has several benefits over experimental cooling data for proof of principle operations: it may be calculated to absolute precision and in a resolution of choice without rounding. In contrast, external factors in experimental settings are difficult to control or may even be unknown (elevated rectal temperature at the time of death). For modelled cooling data sets, all variation and uncertainty are eliminated.

The modelled cooling data was then subjected to Prism and several scenarios were simulated. Both the modelling of cooling data and the brute-forcing procedure were performed using scripts written in the computer language Python [34, 35]. The brute-forcing script follows a similar approach to a program published by Henssge in 1988.[4] The ideal rectal temperature data is used as input with ambient temperature and rectal temperature at the time of death set by the user. TsD (expected value) is calculated according to the NM equation, iterating over a large number of cooling weights in small increments. By comparing expected values, the momentary cooling weight is found. Finally, momentary cooling weights are graphed over time as cooling weight curves and 'consistency of cooling weight' over time is evaluated.

Rectal cooling data sets were *generated* for defined parameter sets (such as 80.0 kg cooling weight, 10.0°C ambient temperature and 37.2°C rectal temperature at the time of death). These included data sets for elevated rectal temperature at the time of death.

Then, the following Prism calculations were performed:

1. Prism assuming *correct parameters only*.
2. Prism assuming *false-low ambient temperature* compared to known parameters.
3. Prism assuming *false-high ambient temperature* compared to known parameters.
4. Prism assuming 37.2°C rectal temperature at death even though ideal data was calculated for elevated rectal temperature at death.

- Scenario 1 acted as control.
- Scenarios 2 and 3 are simulating a misjudgement about ambient temperature, for example if it has been changed after finding of the body and before inspection by the examiner.
- Scenario 4 simulates how elevated $T_{r@D}$ may not be recognized and calculations may be performed for regular $T_{r@D}$ instead.

For these different calculations, typical cooling weight curves were identified (see Figures 6.61 and 6.62):

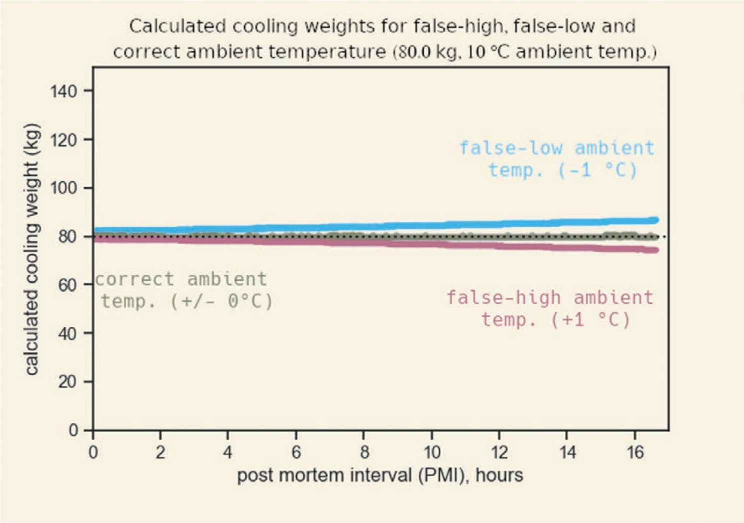

Figure 6.61 Cooling weight curve for correct (green), false-high (red) and false-low (blue) ambient temperature. False ambient temperature may be identified and correct temperature may be inferred.

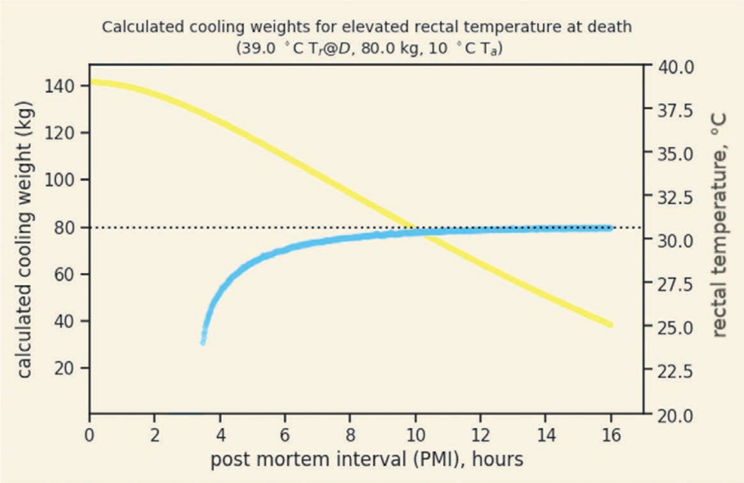

Figure 6.62 Cooling weight curve (blue) for an elevated rectal temperature at death dataset, assuming non-elevated rectal temperature at death for calculation. Note the delayed start of the cooling weight curve, its sharp rise and the time interval until normalization (correct cooling weight 80.0 kg). Yellow curve: rectal temperature.

As expected, assuming *correct parameters* (ambient temperature and rectal temperature at death) Prism generated a linear cooling weight curve at the correct cooling weight (e.g. 80.0 kg) which was constant over time.

Assuming *false-high ambient temperature* and *false-low ambient temperature* (true ambient temperature ±1°C) generated characteristic sloping of the cooling weight curve. For false-high ambient temperature the cooling weight curve remained linear, but with negative slope. Accordingly, assumption of false-low ambient temperature produced a positive slope. These effects can be explained intuitively:

When false-high ambient temperature is assumed, the body (which cools at a factually lower ambient temperature) cools 'too fast' in relation to the assumed (false-high) ambient temperature. Since ambient temperature is fixed, the body weight must calculate 'lighter' over time in order to reach the known rectal temperature in the known time.

The opposite holds true for false-low ambient temperature, where accordingly the body cools 'too slow' and must 'become heavier over time' to be consistent with rectal temperature for the given time interval.

For Prism falsely assuming regular $T_{r@D}$ of 37.2°C when it was in fact **elevated rectal temperature at the time of death (38.0°C)**, as displayed in Figure 6.62, the cooling weight curve starts only after rectal temperature has fallen below 37.2°C. Then, the initially calculated cooling weights are extremely low, and it takes a considerable time for these false-low cooling weights in the cooling weight curve to finally reach true cooling weight. These effects may again be explained intuitively:

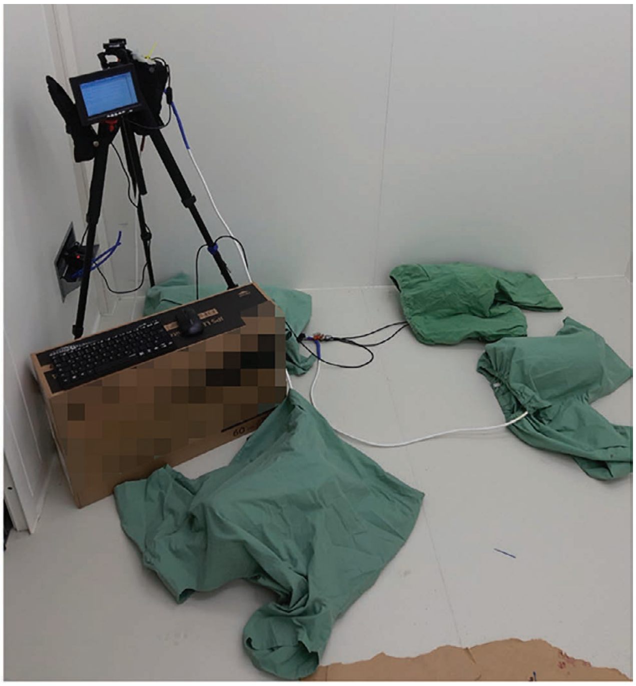

Figure 6.63 Experimental setup: cooling dummies covered with surgical gowns.

Since the MHH parameters assume $T_{r@D}$ as 37.2°C, the computations necessary for Prism cannot be performed for higher temperatures.[5] However, since the initial 'starting point' of the rectal temperature curve is elevated, the slope of cooling is comparatively steep at 37.2°C. Compared to regular cooling, the body cools 'extremely fast'. With all other parameters fix, the cooling weight is calculated as extremely low to accommodate for extremely fast cooling. Notably, this effect persists over a considerable length of time. Thus, in theory this characteristic shape of the cooling weight curve with sharp rise and gradual levelling to a horizontal line may serve as an indicator of elevated rectal temperature at death, even when the actual rectal temperature is no longer elevated.

This finding corresponds well with observations of Muggenthaler et al. that negative impact from elevated rectal temperature at death is most prominent in the early stages of cooling and later fades away.

To verify the theoretically observed properties from this proof of principle (PoP) [28], where unlike Marshall & Hoare [21–24] and Henssge [5, 9, 13, 18] numerous data points were used in brute forcing, experiments on cooling dummies were then conducted.

For such real-life experiments, thermometer accuracy and resolution must be considered. Thermometer rounding is a known error source for TsD estimation [14, 16]. Data smoothing, such as Savitzky and Golay's smoothing filter [32], poses as a possible solution to this problem.

Over-fitting of calculations by feeding too many known parameters may threaten baseline error statistics and should be avoided ('uninformed approach').

Ten cooling dummies with physical weights between 5.9 kg and 26.9 kg were fabricated. For the outer shell, 'dry bags'[6] with an extra layer of cling film were used (see Figures 6.63 and 6.64).

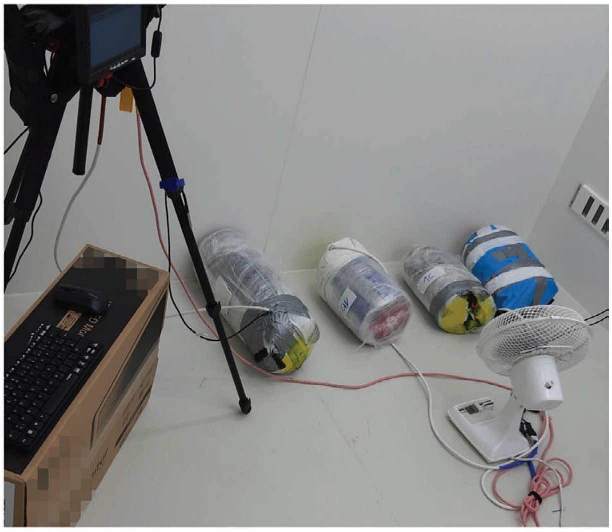

Figure 6.64 Experimental setup: 'naked' cooling dummies and fan at room temperature.

Table 6.25 Overview of Cooling Dummies (Grouped as Light, Medium and Heavy Weight) and Experiments.

Dummy Name (Weight Group)	Circumference x Length, Weight	Experi-ments, n	Cooling Hours	T_{start}	T_a	CF
1a (medium weight)	62 x 40 cm, 11.8 kg	15	386.1	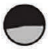	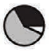	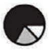
1b (light weight)	62 x 32 cm, 9.7 kg	14	398.6	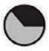	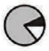	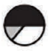
1c (light weight)	54 x 28 cm, 6.8 kg	15	375.9	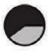	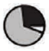	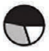
2a (medium weight)	60 x 42 cm, 12.3 kg	11	235.6	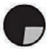	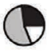	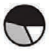
2b (light weight)	61 x 27 cm, 8.6 kg	13	256.5	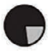	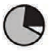	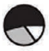
2c (light weight)	60 x 29 cm, 8.7 kg	10	214.6	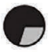	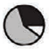	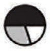
3a (heavy weight)	93 x 39 cm, 26.9 kg	12	388.8	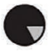	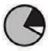	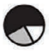
3b (heavy weight)	75.5 x 44 cm, 21.5 kg	9	324.9	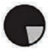	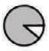	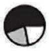
4a (light weight)	60 x 30 cm, 8.5 kg	12	210.2	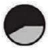	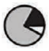	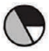
4b (light weight)	54 x 24 cm, 5.9 kg	16	327.8	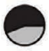	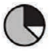	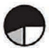
TOTAL		127	3119 (**) (130 days)	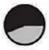	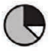	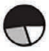

Notes: Cooling hours: the average cooling time for experiments was 24.6 hours, with heavy dummies 3a and 3b averaging 32.4 hours/36.1 hours. Pie charts: starting temperature (T_{start}) up to 38°C (black) and above 38°C (grey); the ambient temperature T_a as cold (< 10°C, black), medium (10–23.2°C, grey) or warm (> 23.2°C). **Correction factors** (CF), standard conditions (CF°=°1.0, black), conditions promoting cooling (CF < 1.0, grey) and conditions inhibiting cooling (CF > 1.0, white). (**) 2082 hours with Q > 0.2 used.

As filling material, Wirodouble® duplicating hydrocolloid was used in one dummy (dummy '4a', see Table 6.25) as suggested in [17].

The remaining nine dummies were filled with a preparation according to the recipe given in the same publication.[7]

For temperature recording, individual dummies were permanently fitted with two or more thermometer probes (Maxim Integrated DS 18b20, 12-bit (= 0.0625°C) resolution, ±0.5°C accuracy). T_a was recorded using similar probes. All probes were connected to a Raspberry Pi 3 Model B microcomputer. Dedicated scripts, written in the Python programming language on the microcomputer recorded timestamps and temperatures continually in 1-minute intervals as comma separated value (.csv) files. Even though not used in the current experiments, this setup allows battery operation and remote access.

Dummy heating prior to cooling was performed in warming cabinets (manufacturers Memmert ® and Ehret®) with a target temperature of 37.2°C. Some dummies were heated to higher temperatures to simulate elevated $T_{r@D}$.

For cooling environments, different lab rooms were chosen for medium to high T_a (10–24°C), cold body storage units for low T_a (0–10°C), and a large 'cabinet style'

Table 6.26 Overview of Errors for Various Experimental Settings, in Early, Medium and Late Cooling as well as the Total Length of Cooling.

Setting, Number of Experiments (n)	Total (Q = 1.0–0.2) $\mu \pm 2$ SD	Early (Q = 1.0–0.5) $\mu \pm 2$ SD	Medium (Q = 0.5-0.3) $\mu \pm 2$ SD	Late (Q = 0.3–0.2) $\mu \pm 2$ SD
all dummies (n = 127)	-0.29 ± 5.24	-0.45 ± 3.76	-0.1 ± 5.86	-0.43 ± 8.42
light (< 10 kg) dummies (n = 80)	-0.35 ± 5.32	-0.42 ± 3.26	-0.06 ± 6.1	-0.63 ± 8.7
medium (10–20 kg) dummies (n = 26)	0.13 ± 3.48	-0.21 ± 3.34	0.81 ± 3.06	0.06 ± 4.14
heavy (> 20 kg) dummies (n = 21)	-0.5 ± 5.54	-0.65 ± 4.6	-0.12 ± 6.42	-0.44 ± 8.98
elevated $T_{r@D}$ (n = 45)	-0.56 ± 4.3	-1.02 ± 2.62	+ 0.14 ± 4.8	+0.14 ± 6.66
NE $T_{r@D}$ (n = 85)	-0.13 ± 5.6	-0.17 ± 4.06	+ 0.11 ± 6.34	-0.52 ± 9.44
sub-zero T_a, NE* (n = 11)	-0.52 ± 4.28	-0.37 ± 2.22	-0.16 ± 3.26	-4.57 ± 7.14
< 10°C T_a, NE* (n = 20)	+0.02 ± 4.02	-0.18 ± 2.56	+ 0.54 ± 4.56	-0.55 ± 8.68
10–23.2°C T_a, NE* (n = 57)	-0.22 ± 6.3	-0.14 ± 4.62	-0.16 ± 7.2	-0.71 ± 9.96
> 23.2 °C T_a, NE* (n = 5)	+0.17 ± 3.12	-0.43 ± 3.02	+0.9 ± 2.28	+1.4 ± 2.06
CF = 1, NE* (n = 43)	-0.34 ± 6.44	-0.3 ± 4.48	-0.07 ± 7.04	-1.08 ± 10.62
CF‡ 1, NE* (n = 38)	0.16 ± 4.28	-0.01 ± 3.56	0.42 ± 5.16	0.6 ± 5.9
CF > 1, NE* (n = 12)	0.57 ± 5.1	+0.41 ± 4.42	+0.84 ± 6.84	+1.58 ± 6.2
CF < 1, NE* (n = 26)	-0.03 ± 3.8	-0.25 ± 2.84	+0.3 ± 4.52	+0.3 ± 5.68

Notes: Note that < 10.0°C ambient temperature includes sub-zero ambient temperature experiments. CF unequal to 1.0 combines both CF smaller than and larger than 1.0. *) NE°=°non-elevated rectal temperature at the time of death (defined as 37.0–38.0°C).

freezer unit for sub-zero T_a as low as −14°C. The body storage facility could only be used in a few experiments.

In addition to MHH's 'standard' cooling conditions, special ambient conditions for cooling were created using various covers (ski jacket, thick bedspread, wet and dry layers of surgical gowns) as well as air flow from a household fan. One hundred and twenty-seven cooling experiments were conducted in total; see Tables 6.25 and 6.26.

The **computational workflow** described in PoP was expanded: the cooling data sets were cropped to a minimum 'relative cooling' Q of 0.2 and run through Savitzky and Golay's smoothing filter [32] to create continuous, non-repetitive, high-resolution cooling data. This data was then fed into the Python script for Prism brute-force calculations. Insight into elevated $T_{r@D}$—if applicable—was ignored. Calculations were started only below 37.2°C dummy temperature and a 'starting temperature' of 37.2°C was assumed in TsD estimation. No further adjustments were made to compensate for elevated $T_{r@D}$. Only momentary cooling weights, without operations such as mean values, best fit or other modifications, were used for the TsD calculations according to MHH. No correction factors were applied. The brute-forcing interval between data points was set to sixty minutes.

For each experiment, three Prism calculations were performed over the whole course of cooling (T_a as measured and ±1.0°C). For each Prism calculation, a CWC was graphed and the (most) horizontal CWC was accepted as correct without further adjustments. Finally, TsD calculations according to MHH were performed for each data point, using the T_a from the horizontal CWC, the momentary brute-forced cooling weight at that data point, and 37.2°C for $T_{r@D}$.

As a result, general CWC-shapes, as demonstrated in PoP, were confirmed for elevated $T_{r@D}$ and for false-low/false-high T_a assumptions (see Figure 6.65).

The effect of non-standard cooling conditions on cooling weight in our experiments was limited.

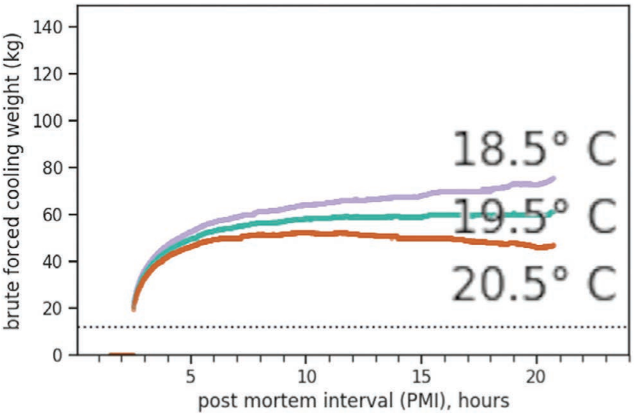

Figure 6.65 Different cooling weight curves for one experiment of dummy 1a (physical weight 11.8 kg). Note initial increase of cooling weight for all three curves, indicating elevated starting temperature. Green cooling weight curve (19.5°C assumed ambient temperature) accepted as correct.

For non-elevated starting temperature cases (defined as 37–38°C), non-standard cooling conditions did not impact error distribution negatively compared to standard cooling scenarios.

For example, at room temperature and covered with one wet layer, dummy "2a" (physical weight 12.3 kg) displayed a cooling weight in Prism of ≈ 40 kg. When covered with a thick bed spread, the cooling weight was determined as around 100 kg, which translates to an *unscaled* CF of roughly 2.1 for the bed spread. Note that no CF was used in Prism calculations, only the cooling weight.

Generally, the relationship between physical dummy weights and their respective cooling weights was comparable to published data published in [13]. Light dummies in particular (< 10 kg physical weight) revealed 'childlike' to slim proportions. For example dummies '4a' and '4b',

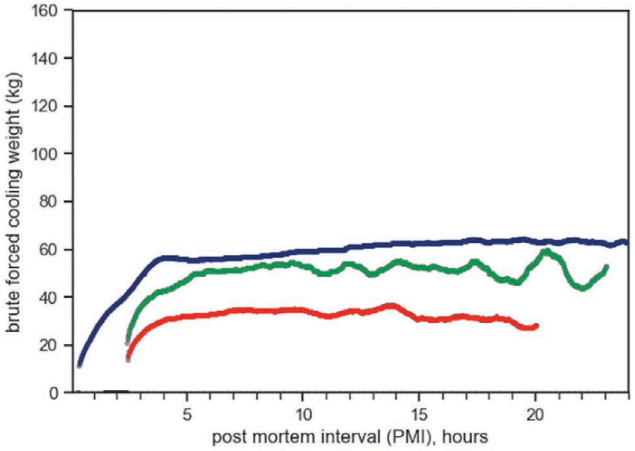

Figure 6.66 Cooling weight curves for dummy 4a (physical weight 8.5 kg). Red: room temperature, standard cooling. Green: room temperature and winter jacket cover. Blue: 5.9°C T_a, one wet layer of cover.

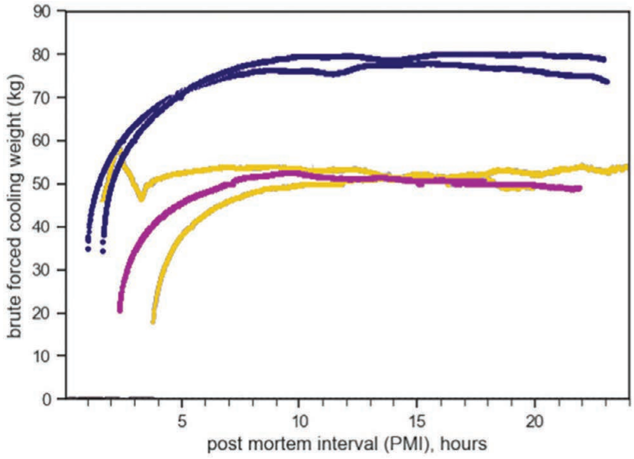

Figure 6.68 Different experiments for dummy 1a (physical weight 11.8 kg, mostly elevated T_{start}). Standard cooling conditions, low T_a (dark blue, –15.0°C) and high T_a (yellow: 22.1°C/22.5°C). Purple: blowing fan, 19.4°C T_a. Cooling weights over time (CWC).

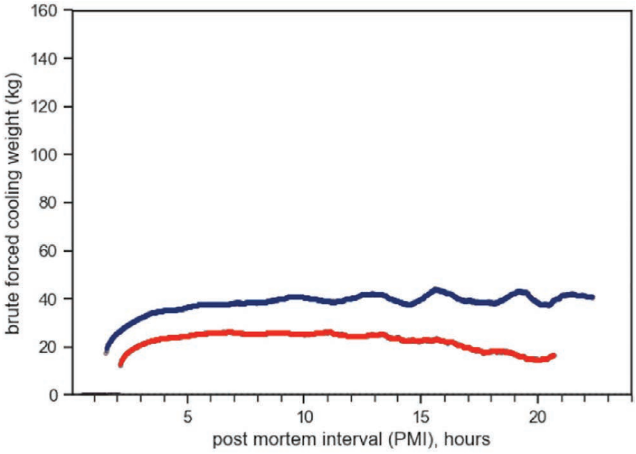

Figure 6.67 Cooling weight curves for dummy 4b (physical weight 5.9 kg). Red: room temperature, no cover. Blue: 5.5°C T_a, no cover.

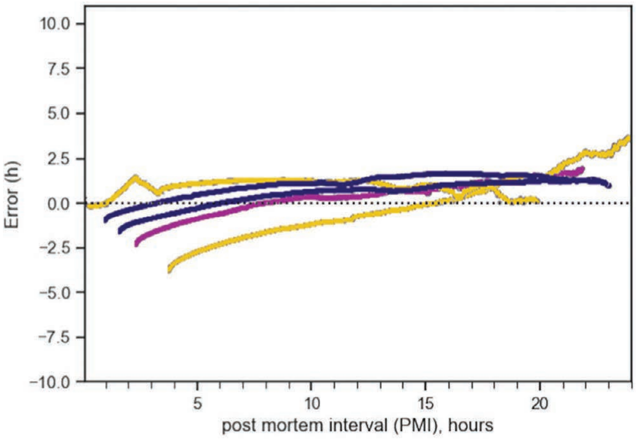

Figure 6.69 Same experiments for dummy 1a as in Figure 6.68. Standard cooling conditions, low T_a (dark blue, –15.0°C) and high T_a (yellow: 22.1°C/22.5°C). Purple: blowing fan, 19.4°C T_a. Errors (hours) over time.

under standard cooling conditions, displayed cooling weights of around 20–30 kg (see Figures 6.66 and 6.67).

For *low and sub-zero ambient temperature*, however, cooling weights were calculated as drastically higher: while at room temperature the cooling weight for dummy "1a" (physical weight 11.8 kg) was determined as ≈ 50 kg, it calculated as ≈ 75 kg for −15.0°C T_a (see Figures 6.68 and 6.69).

For dummy '4a' (physical weight 8.5 kg), cooling weight for room temperature (defined as 18–21°C) and standard cooling was ≈30 kg. Here, cover with a thick winter jacket at room temperature had a similar effect as only a single layer of wet cover but in cold T_a of 5.9°C (≈ 50 kg/55 kg, respectively).

For dummy '1b' (physical weight 9.7 kg) the cooling weight was ≈ 30 kg at room temperature while ≈ 58 kg in cold T_a of 5.3°C (each standard cooling conditions). Dummy '2c' (physical weight 8.7 kg) showed a cooling weight of ≈ 40 kg in room temperature yet ≈ 60 kg for T_a of −10.0°C (each standard cooling conditions).

When calculating TsD estimation errors for cold and sub-zero conditions, utilizing the brute-forced heavy cooling weights, errors were comparable—if not smaller—compared to room temperature conditions and lighter cooling weights (see Figure 6.69 and Table 6.26).

The momentary cooling weights were utilized in the MHH equation to calculate the expected value ('t'). This was then compared against the known true 'time since death' (time since beginning of the experiment) to calculate the

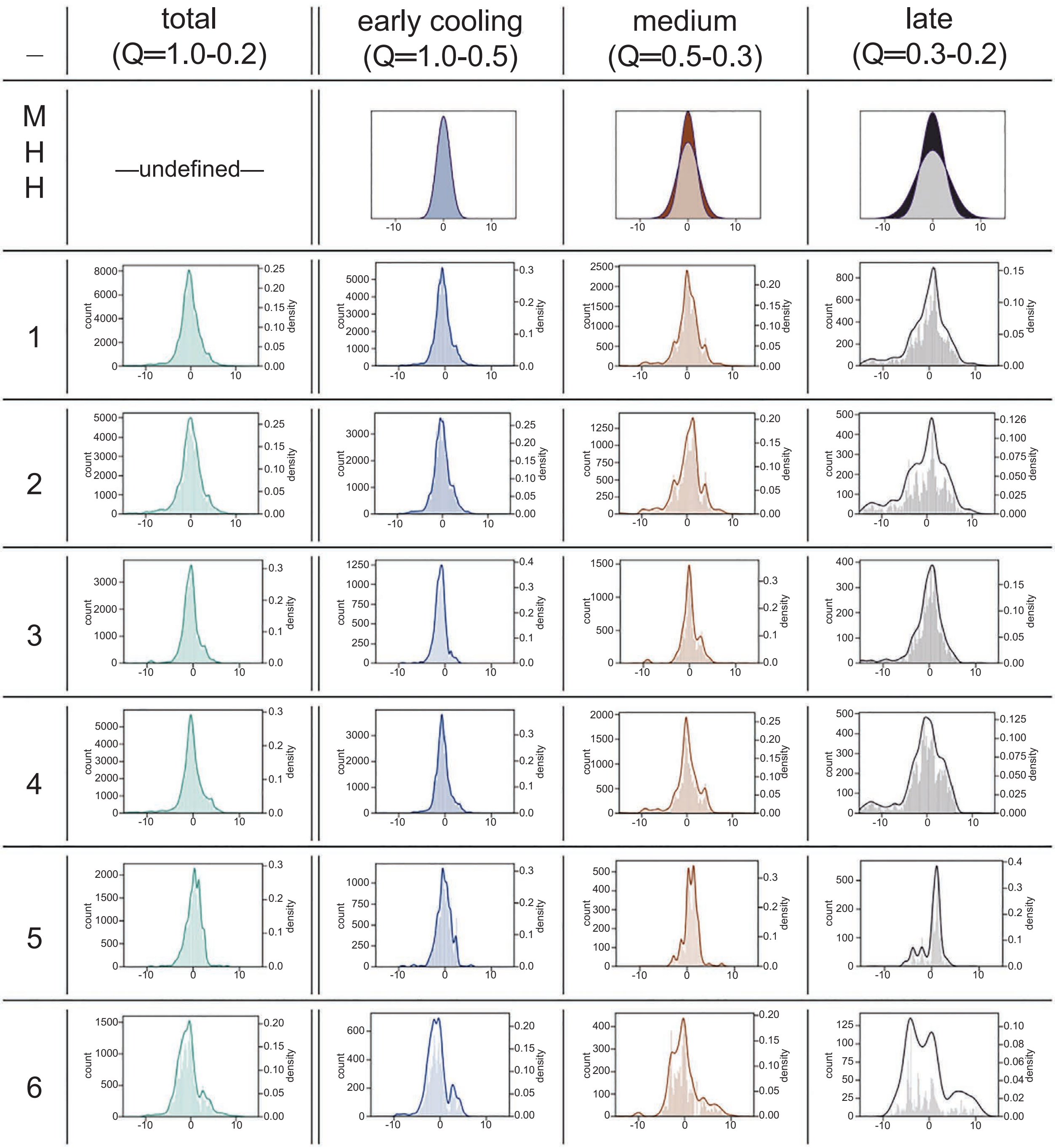

Figure 6.70 Error distribution, value count and density curves in different stages of cooling, for different cooling scenarios: **Marshall, Hoare & Henssge/MHH)** Inner and outer curves for standard and non-standard cooling. No benchmarks for total course of cooling defined.

1) All dummy experiments (*n* = 127).
2) Non-elevated $T_{r@D}$ dummy experiments (*n* = 85)
3) Elevated $T_{r@D}$ dummy experiments (*n* = 45).
4) Light weight (<10 kg) dummy experiments (*n* = 80).
5) Medium weight (10–20 kg) dummy experiments (*n* = 26).
6) Heavy weight (>20 kg) dummy experiments (*n* = 21).

estimation errors. Error distribution was visualized for different stages of cooling (Q ranges), equivalent to the MHH documentation, for various subgroups and conditions (see Figure 6.70). For additional results, see Table 6.26.

Elevated $T_{r@D}$ did produce a significant shift of the expected value when compared to non-elevated cases (−0.56 hours versus −0.13 hours in total, pronounced in the early stages of cooling (see Table 6.26).

At large, the MHH benchmarks were not (yet) met using the Prism method, with slight underestimation of TsD (negative expected value) and wider 2-SD intervals when compared to the benchmarks for MHH.

The Prism method, after first theoretical demonstrations on modelled data, was successfully applied to real-world experimental cooling data. In direct comparison of Prism to MHH, the published error distribution benchmarks for MHH were not (yet) met.

When comparing the strengths and weaknesses of the two methods, several aspects should be considered:

- Elevated $T_{r@D}$ negatively impacts both Prism and MHH. While MHH does not provide means to either detect or correct such elevation, in Prism, such elevation was detected and may be compensated for theoretically.
- MHH benchmarks assume, among others, correctly applied, valid correction factors, which may be difficult to obtain in case work for reasons such as scaling or lack of reference data. In contrast, Prism does not require correction factors.
- MHH benchmarks are not necessarily achievable when using the nomogram, due to rounding. Prism as a purely electronic method does not suffer from such drawbacks.
- MHH performance may suffer from 'childlike' body proportions. In Prism, proportions are irrelevant.
- MMH performance may suffer from the static parameter A in low ambient temperature, which is not (yet) reflected in the MHH error benchmarks. The results for low and sub-zero ambient temperature were unexpected.
- A number of potential approaches for future improvements to the Prism method have emerged.

Considering these preliminary limitations, Prism has performed reasonably well. As a downside, Prism is much less 'tangible' and more abstract compared to conventional MHH and the nomogram method in particular.

As an unexpected experimental result, Prism calculated the cooling weight of dummies dramatically higher for cooling experiments in low and sub-zero ambient temperatures as compared to regular ambient temperature. These findings were encountered consistently for different dummies. Yet, no 'correction factor'-like conditions were present to justify such weight elevation. However, using the resulting high cooling weights for TsD estimation yielded good results. Experimental findings indicate, that in Prism the target value 'cooling weight', in addition to reflecting the physical body weight and general cooling conditions, may potentially incorporate 'factor A' and act as a sort of 'super-parameter'. In MHH, particularly the nomogram method, A has been recognized as depending on ambient temperature, with 23.2°C as the chosen cut-off (A = 1.25 for <23.2°C, A = 1.11 for >23.2°C ambient temperature). Cooling experiments were performed by Henssge et al. for T_a > 5.0°C. It may be theorized, that since in Prism A is static and cooling weight is variable (brute-forcing target), changes of cooling, which would otherwise result in a higher value for A must result in/be compensated for by a larger cooling weight. This theory is supported by modelling of cooling curves for different A: Higher values corresponded to a slower cooling with a more shallow cooling curve, similar to a higher cooling weight (see Figure 6.71).

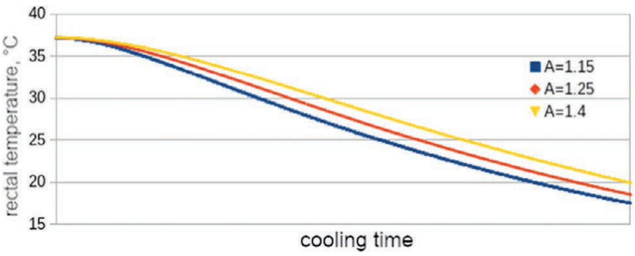

Figure 6.71 Modelled cooling curves for different values of A, 100 kg, 15°C T_a.

Finally, as a result of the current experiments, a number of potential approaches for future improvements to Prism as well as potential applications have emerged.

- Elevated $T_{r@D}$, when detected using Prism, may potentially be accounted for in calculations.
- Non-momentary cooling weights may be constructed, for example by averaging of cooling weights over a stable portion of the cooling curve.
- Prism allows for the assessment of consequences of change of ambient conditions, such as ambient temperature or cover, which will have a delayed, yet detectable effect on body core temperature. 'Broken experiments' with sudden changes of ambient conditions and temperature, will be conducted in the future.
- As a purely electronic method, Prism may also incorporate a finer parameter resolution of parameters, which cannot be implemented into a graphical solution and/or would require additional versions of the nomograms. Such may be a finer resolution of interval width for additional ranges of cooling or of 'factor A' for additional ranges of T_a.

The Prism method potentially both simplifies and complicates several aspects of TsD estimation. The complication is caused by the method's complexity, which makes troubleshooting and quality control more demanding, as well as a more demanding technical setup. On the other hand, substantial simplification is provided by the elimination of CF, possible marginalization of ‘Factor A’ and its absorption into cooling weight.

Future research will include application to pigs and humans, implementation of an ‘informed’ approach as well as ‘broken experiments’ with deliberate changes to ambient temperature and ambient conditions.

For the practical application of Prism, the application of the Savitzky-Golay-filter proved essential, as it delivered high-resolution, yet continuously decreasing temperature values. The method was applicable to the dummy cooling experiments. For future experiments and applications, we advise to use button-type thermometers (for example iButton DS 1925L-F5#) instead of probes, as our current experiments were difficult to set up and in particular non-mobile.

The biggest challenge overall will be to transform the experimental setup into a usable workflow for routine case work. This is however true for many new methods and approaches.

Notes

1 Multiple temperature readings at the crime scene are recommended to ensure proper alignment of thermometer probe and body/ambient temperature.

2 Uncovered (‘naked’) body in supine position on thermally indifferent surfaces without air movement or dampness.

3 We use the term ‘cooling weight’ to indicate that identical torsos and CF may belong to different true physical body weights. Cooling weight therefor describes the ‘hypothetical weight, according to which the body cools’ without underlying physical weight.

4 The program was written in BASIC and intended for the programmable calculator HP 71B [10]. It solved the NM equation by trying out a multitude of values for ‘t’ followed by a simple ‘left side minus right side’ calculation. The program solved the expected value for one set of parameters in up to 500 such calculations, for which Henssge reported about 1–2 minutes computation time.

5 In real-case work, the examiner would of course notice any rectal temperature elevated above 37.2°C. Likewise to electronic calculations, rectal temperature above 37.2°C cannot be entered into the nomograms either.

6 Waterproof cylindrical bags for water sports and other outdoor activities.

7 By volume: 47.5% water, 47.5% agar agar powder, 5.0 % glycerine.

References

[1] Louay M al Alousi, Robert A Anderson, Diana M Worster, and David V Land. “Factors influencing the precision of estimating the postmortem interval using the triple-exponential formulae (TEF). Part II. A study of the effect of body temperature at the moment of death on the postmortem brain, liver and rectal cooling in 117 forensic cases.” In: *Forensic Sci. Int.* 125.2-3 (2002), pp. 231–6. ISSN: 0379-0738. URL: www.ncbi.nlm.nih.gov/pubmed/11909669.

[2] L Althaus and C Henssge. “Rectal temperature time of death nomogram: sudden change of ambient temperature.” In: *Forensic Sci. Int.* 99.3 (Jan. 1999), pp. 171–8. ISSN: 0379-0738. URL: www.ncbi.nlm.nih.gov/pubmed/10098255.

[3] L Althaus, S Stückradt, C Henssge, and T Bajanowski. “Cooling experiments using dummies covered by leaves.” In: *Int. J. Legal Med.* 121.2 (Mar. 2007), pp. 112–14. ISSN: 0937-9827. http://doi.org/10. 1007/s00414-006-0108-8.

[4] Paolo Bisegna, C Henssge, Lars Althaus, and Giusto Giusti. “Estimation of the time since death: sudden increase of ambient temperature.” In: *Forensic Sci. Int.* 176.2–3 (Apr. 2008), pp. 196–9. ISSN: 0379-0738, 1872–6283. http://doi.org/10.1016/j.forsciint.2007.09.007.

[5] C Henssge, L Althaus, J Bolt, A Freislederer, H-T Haffner, C A Henssge, B Hoppe, and V Schneider. “Experiences with a compound method for estimating the time since death. I. Rectal temperature nomogram for time since death.” In: *Int. J. Legal Med.* 113 (2000), pp. 303–19. ISSN: 0937-9827.

[6] N Demierre, D Wyler, U Zollinger, S Bolliger, and T Plattner. “Elevated body core temperature in medico-legal investigation of violent death.” In: *Am. J. Forensic Med. Pathol.* 30.2 (June 2009), pp. 155–8. ISSN: 0195-7910, 1533-404X. http://doi.org/10.1097/PAF.0b013e31819a04a6.

[7] F Fiddes. “A percentage method for representing the fall in body temperature after death.” In: *J. Forensic Med.* 5 (1958), pp. 2–15. ISSN: 0022-1171. URL: https://ci.nii.ac.jp/naid/10012201405/.

[8] M A Green and J C Wright. “Postmortem interval estimation from body temperature data only.” In: *Forensic Sci. Int.* 28.1 (May 1985), pp. 35–46. ISSN: 0379-0738. URL: www.ncbi.nlm.nih.gov/pubmed/4018680.

[9] C Henssge. “Death time estimation in case work. I. The rectal temperature time of death nomogram.” In: *Forensic Sci. Int.* 38.3–4 (Sept. 1988), pp. 209–36. ISSN: 0379-0738. URL: www.ncbi.nlm.nih.gov/pubmed/3192144.

[10] C Henssge. “Ambulatory electronic data processing using the hand-held computer (HP 71B).” In: *Beitr. Gerichtl. Med.* 47 (1989), pp. 327–31. ISSN: 0067-5016. URL: www.ncbi.nlm.nih.gov/pubmed/2818498.

[11] C Henssge. “Rectal temperature time of death nomogram: dependence of corrective factors on the body weight under stronger thermic insulation conditions.” In: *Forensic Sci. Int.* 54.1 (Apr. 1992), pp. 51–66. ISSN: 0379-0738. URL: www.ncbi.nlm.nih.gov/pubmed/1618454.

[12] C Henssge and B Madea. Methoden zur Bestimmung der Todeszeit an Leichen. In: *Arbeitsmethoden der medizinischen und naturwissenschaftlichen Kriminalistik*. Ed. M. Schmidt-Römhild, 1988. ISBN: 9783795006242. URL: https://books.google.de/books?id=Ta0hAQAAMAAJ.

[13] Claus Henssge and Burkhard Madea. “Estimation of the time since death.” In: *Forensic Sci. Int.* 165.2–3 (2007), pp. 182–4. ISSN: 0379-0738. http://doi.org/10.1016/j.forsciint.2006.05.017.

[14] M Hubig, H Muggenthaler, and G Mall. “Influence of measurement errors on temperature-based death time determination.” In: *Int. J. Legal Med.* 125.4 (July 2011), pp. 503–17. ISSN: 09379827, 1437–1596. http://doi.org/10.1007/s00414-010-0453-5.

[15] Michael Hubig, Holger Muggenthaler, Inga Sinicina, and GiTaMall. “Body mass and corrective factor: impact on

temperature based death time estimation.” In: *Int. J. Legal Med.* 125.3 (May 2011), pp. 437–444. ISSN: 0937-9827, 1437–1596. http://doi.org/10.1007/s00414-011-0551-z.

[16] Y Kanawaku, J Kanetake, Atsuki Komiya, Shigenao Maruyama, and Masato Funayama. “Effects of rounding errors on postmortem temperature measurements caused by thermometer resolution.” In: *Int. J. Legal Med.* 121.4 (July 2007), pp. 267–73. ISSN: 0937-9827. http://doi.org/10.1007/s00414-006-0088-8.

[17] Burkhard Madea. *Estimation of the Time Since Death*, Third Edition. CRC Press, 2015. ISBN: 9781444181777. URL: http://books.google.de/books/about/Estimation_of_the_Time_Since_Death_Third.html?hl=&id=WNKYCgAAQBAJ.

[18] Burkhard Madea. “Methods for determining time of death.” In: *Forensic Sci. Med. Pathol.* 12.4 (Dec. 2016), pp. 451–85. ISSN: 1547-769X, 1556–2891. http://doi.org/10.1007/s12024-016-9776-y.

[19] G Mall, Mona Eckl, Inga Sinicina, Oliver Peschel, and M Hubig. “Temperature-based death time estimation with only partially known environmental conditions.” In: *Int. J. Legal Med.* 119.4 (July 2005), pp. 185–194. ISSN: 0937-9827. http://doi.org/10.1007/s00414004-0461-4.

[20] G Mall, M Hubig, Mona Eckl, Andreas Büttner, and Wolfgang Eisenmenger. “Modelling postmortem surface cooling in continuously changing environmental temperature.” In: *Leg. Med.* 4.3 (Sept. 2002), pp. 164–73. ISSN: 1344-6223. URL: www. ncbi.nlm.nih.gov/pubmed/12935664.

[21] T K Marshall. “Temperature methods of estimating the time of death.” In: Med. Sci. Law 5.4 (Oct. 1965), pp. 224–232. issn: 00258024. url: www.ncbi.nlm.nih.gov/pubmed/5849645.

[22] T K Marshall and F E Hoare. “Estimating the time of death: the use of the cooling formula in the study of post-mortem body cooling.” In: *J. Forensic Sci.* 7 (1962), pp. 189–210. ISSN: 0022-1198.

[23] Thomas K Marshall. “The use of body temperature in estimating the time of death and its limitations.” In: *Med. Sci. Law* 9.3 (1969), pp. 178–82. ISSN: 0025-8024. http://doi.org/10.1177/002580246900900304. URL: http://msl.sagepub.com/content/9/3/178.short.

[24] Thomas K Marshall and F E Hoare. “Estimating the time of death. The rectal cooling after death and its mathematical expression.” In: *J. Forensic Sci.* 7.1 (1962), pp. 56–81. ISSN: 0022-1198.

[25] K Meeh. “Oberflächenmessungen des menschlichen Körpers.” In: *Z. Biol.* 15 (1897), pp. 425–58.

[26] H Muggenthaler, M Hubig, S Schenkl, and G Mall. “Influence of hypo- and hyperthermia on death time estimation—A simulation study.” In: *Leg. Med.* 28 (Sept. 2017), pp. 10–14. ISSN: 13446223, 1873-4162. http://doi.org/10.1016/j.legalmed.2017.06.005.

[27] E L Nelson. “Estimation of short-term postmortem interval utilizing core body temperature: a new algorithm.” In: *Forensic Sci. Int.* 109.1 (Mar. 2000), pp. 31–8. ISSN: 0379-0738. URL: www.ncbi.nlm.nih.gov/pubmed/10759069.

[28] S Potente, L Henneicke, and P Schmidt. “Prism—A novel approach to dead body cooling and its parameters.” In: *Forensic Sci. Int.* 325 (June 2021), p. 110870. ISSN: 0379-0738, 1872-6283. http://doi.org/10.1016/j.forsciint.2021.110870.

[29] Stefan Potente, Mattias Kettner, and Takaki Ishikawa. “Time since death nomographs implementing the nomogram, body weight adjusted correction factors, metric and imperial measurements.” In: *Int. J. Legal Med.* 133.2 (Sept. 2018), pp. 491–9. ISSN: 0937-9827, 1437–1596. http://doi.org/10.1007/s00414-018-1928-z.

[30] Keith W Proctor, William J Kelch, and John C New. “Estimating the time of death in domestic canines.” In: *J. Forensic Sci.* 54.6 (Nov. 2009), pp. 1433–7. ISSN: 0022-1198, 1556–4029. http://doi.org/10.1111/j.1556-4029.2009.01156.x

[31] M Rubner. “Über den Einfluss der Körpergrösse auf Stoff- und Kraftwechsel.” In: *Z. Biol.* 19 (1883), pp. 536–62.

[32] Abraham Savitzky and M J E Golay. “Smoothing and differentiation of DaTaby simplified least squares procedures.” In: *Anal. Chem.* 36.8 (1964), pp. 1627–39. ISSN: 0003-2700. http://doi.org/10.1021/ac60214a047.

[33] J L Smart and M Kaliszan. “The post mortem temperature plateau and its role in the estimation of time of death. A review.” In: *Leg. Med.* 14.2 (Mar. 2012), pp. 55–62. ISSN: 1344-6223, 1873–4162. http://doi.org/10.1016/j.legalmed.2011.11.002.

[34] G Van Rossum and F L Drake Jr. *Python Reference Manual*. Amsterdam: Centrum voor Wiskunde en Informatica Amsterdam, 1995.

[35] G Van Rossum and F L Drake. *Python 3 Reference Manual*. Scotts Valley, CA: CreateSpace, 2009. ISBN: 1441412697.

[36] Christiaan H Vinkers, Renske Penning, Juliane Hellhammer, Joris C Verster, John H G M Klaessens, Berend Olivier, and Cor J Kalkman. “The effect of stress on core and peripheral body temperature in humans.” In: *Stress* 16.5 (Sept. 2013), pp. 520–30. ISSN: 1025-3890, 1607–8888. http://doi.org/10.3109/10253890.2013.807243.

[37] T Vojtíšek, Š Kučerová, J Krajsa, B Eren, P Vysočanová, and P Hejna. “Postmortem increase in body core temperature: How inaccurate we can be in time since death calculations.” In: *Am. J. Forensic Med. Pathol.* 38.1 (Mar. 2017), pp. 21–23. ISSN: 0195-7910, 1533-404X. http://doi.org/10.1097/PAF.0000000000000286.

6.4 The Use of Temperatures Recorded from the External Auditory Canal for the Estimation of the Post-mortem Interval

■ *Guy Rutty*

6.4.1 Introduction

Over the years a number of authors have published cadaveric animal and human research related to the recording of temperatures from the external auditory canal (EAC) for the purpose of estimating a post-mortem interval (PMI) [1–19]. This chapter summarises this published literature and draws upon the doctorate work of

Rutty [20], which remains to date the largest body of work concerning the use of the ear for the estimation of the post-mortem interval, to illustrate how a temperature recorded from the EAC can be used to estimate a PMI and the problems that may be encountered by using this anatomical site.

6.4.2 Anatomy of the External Ear

Prior to considering how a temperature may be taken from the EAC or applied for the purpose of estimating the PMI one should understand the anatomy of the ear and why, for example in clinical medical practice, the taking of a temperature from the ear to record 'core' body temperature has become common practice both in the pre- and in-hospital environment.

The human ear is composed of three parts: the external ear composed of the auricle or pinna and the external auditory canal; the middle ear or tympanic cavity; and the inner ear or labyrinth [21]. In terms of this chapter, it is the external ear that needs to be considered further.

In terms of the embryology of the external ear the auricle commences development at the sixth week of gestation when a series of external 'hillocks' develops on the dorsal margins of the first and second branchial arches. Of these six mesenchymal thickenings, the majority of the auricle develops from the second branchial arch with the tragus developing from the first arch. These then fuse together which results in the individual variation in the shape of the final auricle. The auricle then shifts its position in relation to the developing mandible, by going from a ventrocaudal to a dorsocranial position. Errors in this positional change account for malpositioned ears. The typical relief structure of the auricle then forms during the third to sixth month of development [22]. The external auditory canal develops from the dorsal portion of the first branchial arch. The primary external meatus forms in the eighth week as the first branchial pouch deepens towards the tympanic cavity. This forms the outer third of the canal, which is initially separated from the first pharyngeal pouch, from which the tympanic cavity arises, by a pad of mesoderm. This remains in place up to the 21st week. The plug is then hollowed out and the inner cells degenerate. By the seventh month the canal is completely formed. The residual medial cells of the epithelial plug become the outer layer of the tympanic membrane [23].

The auricle or pinna is an external elastic cartilaginous structure, covered by skin, which serves to collect air vibrations for the purpose of hearing. It is composed of four parts: the helix, the lobule, the tragus and the concha. In addition to these main landmarks are a number of other anatomically defined points. The skin of the auricle turns inwards into the external auditory canal (EAC). The outer part of the canal is elastic cartilage with the inner part composed of bone of the tympanic plate. The canal serves to conduct sound waves to the tympanic membrane. Although the tympanic membrane and the contents of the middle ear are of adult size at birth, the external auditory canal continues to develop up to about the age of 9 years. Initially the canal is straight, with the tympanic membrane in a horizontal position. Over the next 9 years, the characteristic 'S' shape of the canal develops and the membrane becomes orientated at approximately 45-degree to the horizontal plane (Figure 6.72). These bends divide the canal arbitrarily into three sections: the first and second being the cartilaginous sections and the third the bony section [24]. In an adult the canal is approximately 2.5 cm long (the anterio-inferior wall is longer at 3.1 cm), tapering towards the tympanic membrane where the diameter is narrowest at approximately 0.5 cm. The volume of the canal, in the adult, is approximately 0.85 mL.

The external and middle parts of the ear are separated by the tympanic membrane. The membrane is composed of three layers: an outer layer of squamous epithelium, a middle layer of fibrous tissue and an inner layer of columnar epithelium. The membrane is roughly circular in shape, approximately 0.074 mm thick and measures 1.0 cm high and 0.8 cm in width. In the adult it is orientated obliquely, facing downwards, forwards and laterally at approximately 45 degrees to the floor of the canal. The handle of the malleus (bone of the middle ear) is attached to the inner surface. The blood supply to the external surface of the membrane is from the deep auricular artery. The internal surface receives blood from the stylomastoid branch of the posterior auricular artery and from the tympanic branch of the maxillary artery. Venous drainage is to the external jugular vein, transverse sinus and the veins of the dura mater.

6.4.3 Human Thermoregulation

Humans are mammals and homeotherms: by this one means that, under a number of conditions, humans are able to maintain a normal, steady-state temperature. This is achieved by the central regulation of body temperature mediated through receptors located within the hypothalamus. Humans maintain their temperature within a range with the internal 'thermostat' set between 36.9 and 37.1°C, which in turn regulates core temperature between 35.5 and 37.5°C [25]. Humans have a 'core temperature', that is the temperature within the body. This is different to the 'shell temperature' which is the temperature of the skin and underlying subcutaneous tissue [26].

Body temperature is maintained by balancing heat production against heat loss. The temperature regulating area of

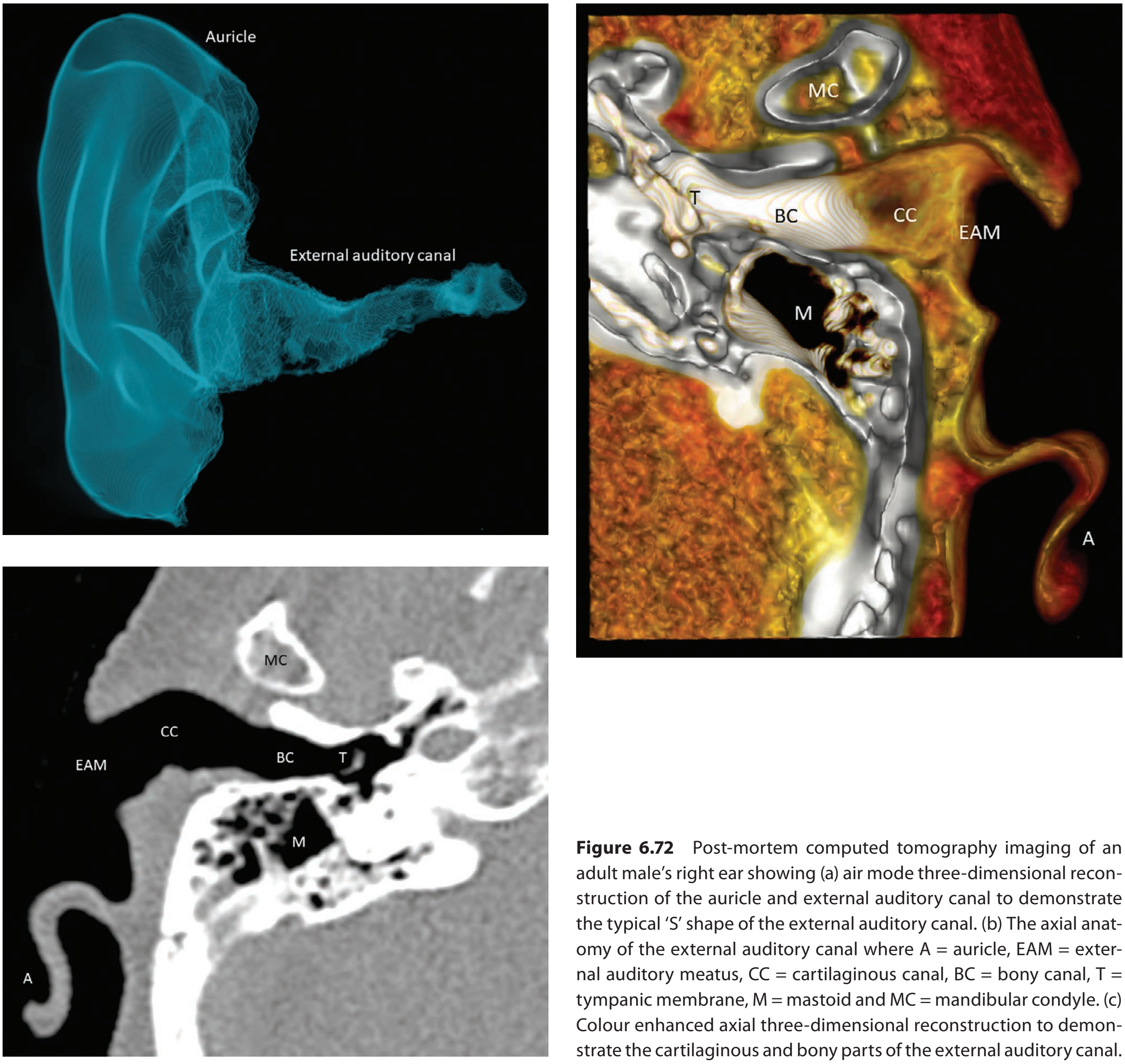

Figure 6.72 Post-mortem computed tomography imaging of an adult male's right ear showing (a) air mode three-dimensional reconstruction of the auricle and external auditory canal to demonstrate the typical 'S' shape of the external auditory canal. (b) The axial anatomy of the external auditory canal where A = auricle, EAM = external auditory meatus, CC = cartilaginous canal, BC = bony canal, T = tympanic membrane, M = mastoid and MC = mandibular condyle. (c) Colour enhanced axial three-dimensional reconstruction to demonstrate the cartilaginous and bony parts of the external auditory canal.

the body is found in the pre-optic area of the hypothalamus. This area has input from the temperature receptors of the skin and mucous membranes as well as the internal central thermoreceptors of the hypothalamus. When the temperature of the blood increases it causes peripheral vasodilation, perspiration and decreased metabolism. In contrast, if the blood temperature falls then there is vasoconstriction, shivering and an increase in the metabolic rate.

The central parts of the body are kept at 'core temperature', which is regulated by gaining or losing heat from the outer aspects. However, as noted earlier, humans are not only a homeotherm but also rhythmic creatures. By this, one means that our body temperature follows a circadian rhythm, that is it fluctuates up and down during the 24-hour day [27]. This raises the questions of what do we mean by a 'core temperature' and what should it be?

Humans are usually considered to have an average body temperature of 37°C (98.6°F), which is accredited to Wunderlich who claimed to have analysed 1 million axillary temperatures from 25,000 patients [28]. He is also accredited with indicating that there is a potential range of core temperature and that the body temperature is at its lowest between 0200 and 0800 hours and at its peak between 1600 and 1900 hours, that is the circadian rhythm [29]. In addition to this diurnal variation, the core temperature is said to be higher in blacks than whites, and females compared to males, which is in part attributed to the menstrual cycle. It is affected by the environment within which one is, and the clothes one is wearing [30–32]. The temperature will be different if one is resting and asleep compared to if one is undertaking exercise where the temperature may be up to 1°C higher than the resting temperature [33]. It can also be affected by the use of drugs including alcohol and caffeine, bright light, and atmospheric pressure [34–37]. These observations are important if using a 'core temperature' within a PMI calculation. As most PMI algorithms are based on a starting temperature of 37°C, if this is not the case then the result from the calculation will be incorrect. Peyron et al. caution us that temperature-based methods cannot be applied to hypo- or hyperthermic patients [19], although, of course, in relation to forensic cadaver casework the forensic pathologist may not know this to be the case but should bear this in mind when undertaking and applying such estimations.

6.4.4 Ear Thermometry

Although Benzinger [38] is cited in almost all publications concerning the recording of temperatures from the EAC as the original author who drew attention to the ability to record body core temperature from the EAC, it was in fact Williams and Thompson who had first described a device to measure body temperature from the EAC [39]. They described the use of a Western Electric V611 thermistor, which was incorporated into a plastic ear mould, moulded to the contour of the EAC so that it was insulated from the environmental temperature, to record the temperature of the EAC in one patient, in one ear during the night. The temperatures obtained were approximately 0.25°C lower than simultaneous readings taken from the sublingual region. This temperature is within the range reported in more recent publications which report that the EAC temperature may be between 0.06 and 0.74°C lower than the sublingual temperature [40].

The reason why Benzinger is accredited with the first reporting of core temperatures from the EAC, and not Williams and later Carlson, is because these two previous authors had measured the temperature of the ear canal and not the tympanic membrane. In the 1963 paper it is described how three different types of fixation method were used to apply a thermocouple to the tympanic membrane. The temperatures were then recorded and compared to those from the anterior ethmoid sinus, anterior wall of the sphenoid sinus and Rosenmueller's fossa. The hypothesis was put forward that, as the tympanic membrane receives the same blood supply from the internal carotid artery, which then goes on to supply the hypothalamus, which in turn regulates core temperature, then the tympanic temperature is a more true representation of core temperature than other sites, specifically the rectum, a hypothesis reiterated by M. Benzinger in 1969 [41]. Benzinger reported that the tympanic temperature was approximately 1.5°C lower than the rectal temperature but was easy to obtain, reproducible and showed consistent patterns of response to external warming or cooling.

These types of contact probes were used in clinical practice into the 1970s, although patient discomfort and complications such as perforation of the tympanic membrane restricted their use [42]. During the 1980s the design of the probe was altered. Work originally undertaken by the United States of America Aerospace Program of studies of the EAC as a potential site of temperature measurement in astronauts was incorporated into civilian medical applications such that by 1991 at least six makes of the new so-called infrared tympanic thermometers (ITT) were available on the market [43, 44].

6.4.4.1 Clinical Infrared Thermometry

Infrared thermometry (IT) uses the 'black box' principle where for each wavelength the maximum amount of radiation depends only on the temperature of the emitter (the 'black box') and is a precise value [45]. The emissivity of a surface is the ratio of emitted radiation to radiation emitted by a black box at the same temperature. Thus, if you know the emissivity geometry and the spectrum of radiation it is possible to derive the temperature of a surface. In the case of infrared thermometry the wavelengths are 0.7–20 μm. Using this principle, the ITT utilises a thermopile to detect infrared emissions from the tympanic membrane and then calculates the body temperature as a function of the intensity of the infrared radiation detected.

The first commercially available ITT was produced in 1986 by Intelligent Medical Systems (Carlsbad, CA) and was aptly named the FirstTemp® thermometer [46]. This first design comprised a hand-held probe attached by a cable to a desktop unit containing a calibration system, microprocessor, A-D converter, power supply, display and a charger. The probe was covered by a disposable tip/cover and inserted into the ear canal where it detected the temperature over a 1–2 second interval. In-built offsets allowed for the estimation of oral, rectal or core temperature. It was expensive, heavy and consumed a lot of power, although it became popular, especially within the paediatric community. It was replaced in 1991 by the Genius Infrared thermometer (Genius™ IT).

Modern-day ITTs share a similar design structure to the Genius™ IT. They consist of an otoscope-like probe tip covered by a disposable polyethylene speculum cover, a probe handle in which is housed the infrared sensor, a microprocessor and a calibration mechanism. The temperature is displayed usually via an integral liquid crystal display in either centigrade or Fahrenheit. The probe is inserted into the EAC and the scan button depressed. The emitted radiation is sensed over a 1–2 second period and then the temperature displayed. They are quick to use and have a reduced risk of cross-patient infection compared to other types of thermometers [47]. Prior to commercial use the Genius™ was calibrated against the National Physical Laboratory calibrated mercury-in-glass thermometer scaled to 0.1°C. It was designed to give rapid temperature readings in an operating range of 27.5–40°C.

6.4.4.2 Problems with Clinical IT Readings

Following the introduction of IT into clinical practice a number of publications compared different makes of IT, and it began to become apparent that there may be potential problems related to the accuracy of the readings with these types of thermometers [48–50]. The first problem lay in the name of the thermometer itself. Originally called infrared '*tympanic*' thermometers, it soon became apparent that, due to the wide view of the EAC that the probe saw, the thermometers were reading heat radiated from the skin of the wall of the EAC as well as that of the tympanic membrane. As it was considered that a heat gradient existed within the EAC this would lead to the potential underestimation of the temperature if the probe was not fully inserted or directed towards the tympanic membrane [51]. Thus, although the most accurate reading is obtained if the probe is aimed at the anterior inferior aspect of the tympanic membrane, in light of the realization of where the majority of the radiation is being received from, in the latter 1990s the term '*tympanic*' was dropped and the name changed to infrared thermometers (IT) [52].

The next problem concerned which ear to take the reading from. Although not statistically significant, there can be a temperature difference of up to 0.47°C between the left and right EAC [53]. In a normothermic child or adult this temperature difference does not matter, but it becomes important during the assessment of febrile illness where this small difference could lead either to the diagnosis being missed or to it being over-diagnosed.

It then became questioned as to whether or not the temperature of the EAC represents core temperature as it was found that there could be up to 1.2°C difference between the EAC temperature reading and other conventional sites such as the rectum, bladder, oesophagus, pulmonary artery (PA), axilla and sublingual areas [54–66].

Finally, it was considered whether or not local and systemic variables influenced the temperature readings. The probe itself is of a rigid, non-variable design whereas the human EAC changes in size and shape with the age of the subject. The EAC of the neonate are small and straight, whereas that of the adult is longer and curved. Hence, it was found that errors in temperature recording could occur when the thermometers were used with neonates, compared to infants, compared to adults [67–69].

As the probe must be inserted such that the sensor looks at the tympanic membrane, operator training becomes important [70,71]. A more accurate temperature reading may be achieved with the use of the ear tug [72,73]. The probe itself will be at a lower temperature than the inside of the EAC. This can lead to a lowering of the temperature in the EAC when the probe is inserted and can cause the formation of water droplets on the probe window, which can again alter the temperature reading [74].

Any obstruction present within the EAC could have an effect on the ability of the sensor to see the tympanic membrane. Hair does have an effect on the temperature, as does impacted wax (cerumen), but non-impacted wax is said to have no effect on infrared radiation detection within the EAC [75–78]. Local infection, particularly otitis media, does not appear to have a significant effect on the readings although if the tympanic membrane is bulging due to the presence of fluid or middle ear infection, this may alter the readings [79–82]. The application of local cream or removal of grommets has no effect but local scarring, due to alteration in local blood flow, can alter temperature readings [83,84]. An episode of vertigo causes the temperature to rise [85].

The next variables to be considered are the effect of the environmental ambient temperature and the effect of wind on the face. It has been shown that a rise in environmental ambient temperature from 18–35°C will result in false-high temperature readings from the EAC [86–89]. These false readings have been reported by other authors who also draw our attention to the observation that a lower ambient temperature does not significantly affect the EAC temperature reading [90]. Kahyaoglu et al. considered that this could be due to an effect on the ear lobe and an alteration of blood flow through it. In a series of experiments observing the effects of crying on the EAC, they found that the auricle would go red during an episode of crying due to increased blood flow, but that the temperature within the EAC remained unaltered [91]. The other potential environmental variable is that of the effect of hot and cold wind on the face. Sato et al. reported that if the face and neck were warmed or cooled by hot or cold wind, there was no alteration in the EAC temperature, although this has been disputed by Thomas et al. who found that if one fanned air onto the face there was a fall in EAC temperature [92,93].

Remaining with variables within the head and neck area, if one drinks a hot or cold drink or smokes a cigarette then this will result in an alteration of the oral temperature [94]. However, EAC temperature has not been reported to date to be influenced by these potential variables [95].

A large number of publications report the effect of hypo/hyperthermia and exercise on the temperature within the EAC [96–100]. These have shown that in the case of hypothermia the EAC temperature remains stable and can be used to take a temperature reading. However, in hyperthermia and during periods of exercise the rectal temperature will rise but the EAC temperature does not follow this rise and can thus yield a false-low result. This is thought to be due to the local physiological effect known as selective counter current cooling of the brain. As core temperature rises the body reacts by keeping the brain cool.

Finally, there are miscellaneous reports touching upon the temperature in the EAC. In those with meningitis, the EAC temperature has been reported to be higher than the expected core temperature. In those with a spinal cord injury the afferent input to the hypothalamus may be altered. This may in turn affect the efferent messages for shivering, sweating and vasoconstriction and this may alter both core and EAC temperature [101]. The sex and age of the individual may have an influence as it has been reported that children and females have higher resting EAC temperatures than males and adults [102]. The natural circadian rhythm of body temperature results in the EAC temperature at its lowest at approximately 0200 hours with a steady rise throughout the day until 1800 hours when it drops down through the evening to its lowest point at 0200 hours again [102]. Sato also noted that foot bathing altered the temperature recording from the EAC [92]. Wright et al. used the ability of the IT to record the temperature of intravenous fluid bags and found that they could be used as long as the temperature remained under 40°C [103].

6.4.5 Early Human Cadaveric Experimental Data

As far as the author can ascertain, the first proposal for the use of temperatures recorded from the EAC to estimate a PMI was made by Baccino et al. at a meeting in Paris in 1991 [1]. Although referenced in the group's later paper, to the author's knowledge this meeting presentation is not accessible within the published literature (personal communication, August 2014). The first published reference to the use of the EAC for estimation of a PMI is in the 1991 edition of Knight's *Forensic Pathology*. In this edition it is suggested that the ear can be used as an alternative site for recording a temperature for estimating the PMI [104]. However, this suggestion is unreferenced.

In 1992, Nokes et al. were the first to publish research in the peer-reviewed literature concerning the use of the outer ear as a means of determining the post-mortem period in human corpses [2]. Five cadavers on entering the mortuary were stripped, weighed and measured. In each case a calibrated thermocouple was inserted into the external auditory canal to a point just in front of the tympanic membrane and the temperature measured every 15 minutes for a constant period of time. The resulting cooling curves showed a consistent shaped cooling curve without an initial plateau (Figure 6.73).

From these curves they developed the formula:

$$t_1 = \frac{\left(ln\theta_0 - ln\theta_1\right)\Delta t}{\left(ln\theta_1 - ln\theta_2\right)}$$

where $\Delta t = t_2 - t_1$.

In this equation *ln θ* is the log of the temperature of the outer ear at the time of death ($_0$) and arbitrary times after death ($_1$ and $_2$), where t_1 and t_2 are arbitrary times after death.

During this work they realized that the outer ear temperature in life cannot be assumed to be 37°C. Through readings taken from 5 healthy living volunteers they reported that the outer ear temperature in life ranged between 35–36°C which led them to adopt 35.5°C as the temperature at death for their calculations. However, in doing this they observed errors between the actual and estimated post-mortem interval and considered this assumption to be a major source of error in their calculations. They also questioned whether or not a single exponential equation could be applied to the calculation with knowledge of the temperature plateau effect known to affect calculations derived from the rectum. Having raised this they considered it highly unlikely that such a plateau existed with the

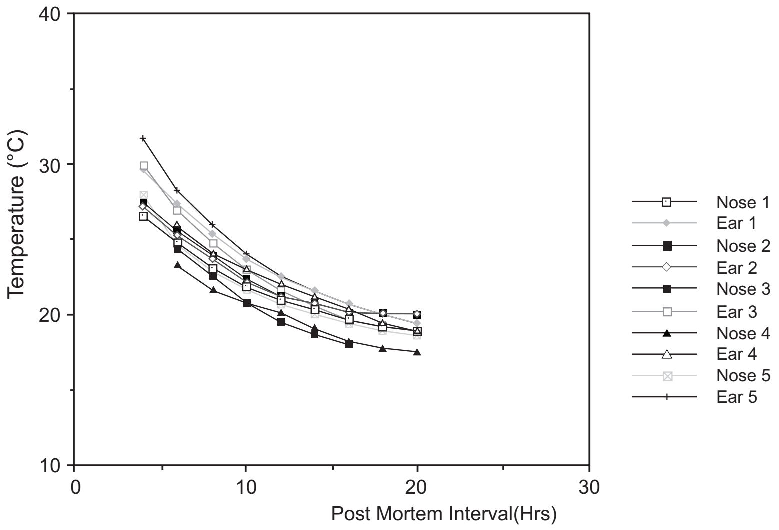

Figure 6.73 Post-mortem cooling curves for five corpses using nose and ear as temperature measurement sites.

(From Nokes LDM, Flint T, Jaafar S, Knight BH. The use of either the nose or outer ear as a means of determining the post-mortem period of a human corpse. *Forensic Sci Int* 1992; **54**: 153–158.)

ear. They also questioned the possibility of environmental factors influencing the temperature. Due to their observations, they concluded that the errors present in their experiments rendered the ear an unsuitable site for temperature-based post-mortem interval calculations. Despite the suggestion of Nokes et al. regarding the unsuitability of the EAC as a temperature recording site, this did not deter future researchers.

6.4.6 Cadaveric Animal Experimental Data

Two principal research groups now appear to have arisen, each working independent of each other. The first group was in France led by Baccino, and the second in the United Kingdom led by Rutty. Baccino's early work focused on humans, then evolved to consider an animal model and then returned to human cadaver studies. Rutty, on the other hand, initially revisited the work of Nokes using an animal model. Starting in 1994 and presenting the first data on the use of infrared tympanic thermometers for recording temperatures from the EAC in the post-mortem period in 1996 [5], this work formed the basis of his doctorate studies.

Working with the Ministry of Defence (MoD), Veterinary and Remount Services (VRS), UK, Rutty was permitted access to five British Army male German shepherd dogs who were euthanised for veterinary reasons. Following the administration of intravenous sodium pentobarbitone, each deceased animal was immediately transported to a secure room on the MoD base and placed on an examination table, that is no significant time elapsed between death and the transportation of the body. The temperature within the room was essentially the same as the outside ambient temperature and subject to ambient temperature variation. In each dog the following were recorded: ambient room temperature using the thermocouple, the wind speed over the body using a digital anemometer, rectal temperature using the thermocouple and the right external ear canal temperatures were recorded using a First Temp® Genius™ Tympanic Thermometer (Sherwood Medical, England), and an Ototemp Veterinary Infrared Tympanic Temperature Scanner (Henry Schein Rexodent, England), as well as the thermocouple, that is three readings per time period. Only one reading was taken from each site with each thermometer at each time period. Readings were taken hourly for the first six hours, 2 hourly from 6 to 12 hours, and then in two cases readings were taken from the EAC only at 22 and 24 hours.

From this work and similar to the work of Nokes et al. a post-mortem temperature plateau was not observed in the temperature recorded from the dogs' ears (Figure 6.74). The starting and subsequent ear temperatures were shown to be consistently lower than the rectal temperatures, an observation reported both in animals [105] and humans (see earlier). The two infrared thermometers used yielded different readings, one greater than the thermocouple and the other lower. This pattern was observed by later investigators [15].

When the ear temperatures were applied to the Rule of Thumb algorithm (see Part 6.1), the PMI was overestimated in every case. However, one has to take into account that there was a difference between the ear and the rectal temperatures at any given time. Thus, the Rule of Thumb was modified to take account of these differences, first using the difference between the two readings for each individual case and then using a constant derived from the mean temperature difference between the rectal and ear temperatures for all dogs at all time periods.

$$\text{PMI} = (\text{EAC}\cdot \text{t}O\cdot{}^\circ\text{C})\cdot-\cdot(\text{EAC}\cdot t1\cdot{}^\circ\text{C}\cdot+\cdot\text{C})\cdot+3$$

where *t0* is the temperature at the time of death, *t*1 is the temperature at a time period after death and *C* is the constant derived from the mean difference between the rectal

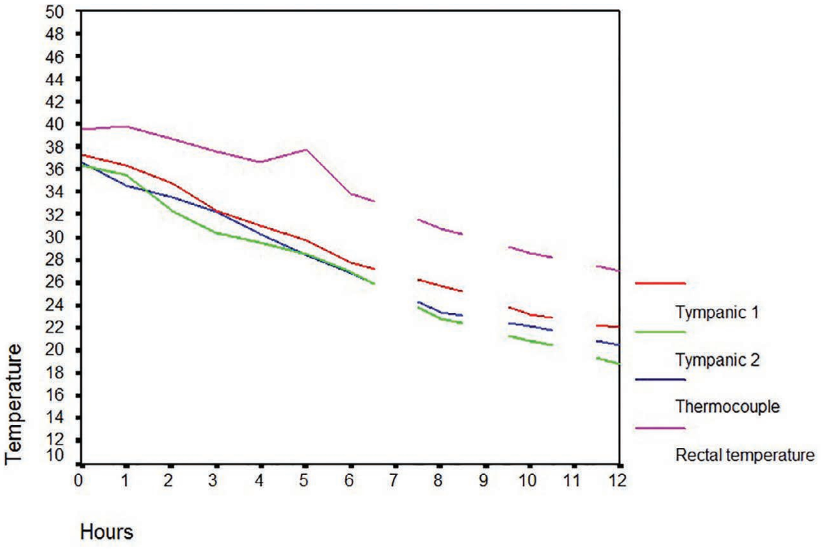

Figure 6.74 External auditory canal and rectal temperature (°C) for time (hours) for a dog.

(From Rutty GN. *The use of temperatures recorded from the external auditory canal in the estimation of the time since death*. Sheffield, University of Sheffield, medical doctorate thesis 2001, as modified in Rutty GN. The estimation of the time since death using temperatures recoded from the external auditory canal. Part I. Can a temperature be recorded and interpreted from this site? Forensic *Sci Med Pathol* 2005; **1**: 41–51.)

and EAC temperatures during the post-mortem period. The subsequent calculation still overestimated the PMI although the time generated was closer to the known actual time. The ear temperatures were then applied in an unmodified manner to the other published algorithms. Using this dataset, the best results, either on their own or as a range, were obtained from both Henssge nomograms, especially the nomogram for the brain [106] an observation reiterated by the later work of LaPlace et al. [16].

This early animal work supported the earlier observations of Nokes et al. with regard to the temperature plateau. Unlike the work of Nokes however it suggested that it could be possible to apply temperatures recorded from the ear to previously published PMI methods, but the operator had to take into account the difference between the rectal and ear temperatures at death which would affect calculations using methods designed for use with rectal temperatures.

In 2007 Baccino et al. published work concerning the cooling rates of pig heads submerged in water [11]. Baccino's group undertook two sets of experiments. The first was designed to consider if the isolated pig head ear and brain temperatures behaved after death in a similar manner to that of the intact pig cadaver. Having concluded that they did, they then used nine pairs of isolated pig heads in air and water in temperatures ranging from 0°C to 20°C to study ear and brain temperatures. From this work they supported Rutty's doctorate observations in humans that the head was less affected by variables [5] than other temperature recording sites further suggesting it to be a more reliable body region for PMI estimation. They also supported the previous work of Henssge reporting that cooling rates in water were quicker than those in air. They also showed in pigs that tympanic cooling is almost equal to cerebral cooling although they pointed out that this cannot be translated into humans due to differences in pig ear anatomy and brain size.

In 2009 Proctor et al. published their observations of post-mortem cooling curves in 16 dogs recorded using temperature probes and a data logger [14]. Aural temperatures were recorded using a probe inserted 4 cm into the external auditory canal for 32 hours in still air. The temperature graph for all dogs is shown in Figure 6.75. Similar to others' work they observed that the temperature in the EAC was lower than that of the rectum. Within the paper's discussion the first three paragraphs appear to convey the authors' confusion as to why this observation occurred. Although they suggest a number of reasons for this occurrence, they do not make reference to the previous published work of Rutty who observed the same phenomenon in his canine research [5,9]. They do however appear to realise the lack of a plateau stage of EAC cooling as observed by previous authors.

6.4.7 Human Cadaveric Experimental Data

In 1993 Baccino et al. made a presentation at the Dusseldorf meeting of the International Association of Forensic Sciences, concerning temperatures from the outer ear and time of death [3]. Like Nokes earlier and Rutty later they reported that temperatures from the EAC did not show a post-mortem plateau. Unlike Nokes however they reported that the use of a single temperature reading from the EAC showed a higher correlation with the actual post-mortem interval than with a single temperature measurement from the liver [3].

In 1996 Baccino et al. published the first substantive research with regard to the use of the human outer ear temperature to estimate a time since death [4] having presented the data at the 1994 American Academy of Forensic Sciences meeting, San Antonio, Texas. Using a research cohort of 138 hospital deaths with known times of death, transported to the mortuary within 60–180 minutes of death and using a thermistor thermometer they measured the temperature in

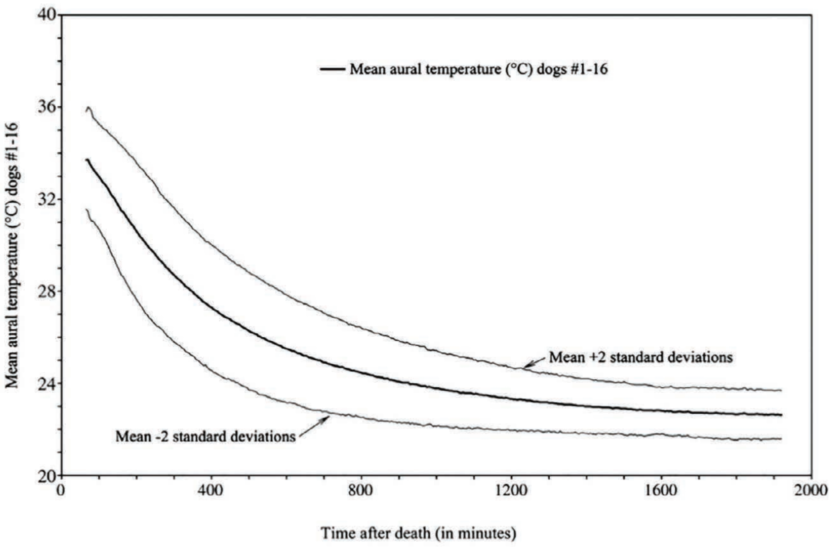

Figure 6.75 Data logger mean aural temperature readings (°C) for all dogs every 5 mins (n°=°16).

(From Proctor KW, Kelch WJ, New JC. Estimating the time of death in domestic canines. *J Forensic Sci* 2009; **54**: 1433–1437.)

Table 6.27 Research Sample: Results of Linear Regression Analysis of Relationship between Actual and Estimated PMI Using 6 Methods*

Methods		Ambient temperature intervals			
		0–5°C ($n = 34$)	6–10°C ($n = 34$)	11–15°C ($n = 33$)	16–23°C ($n = 37$)
Outer ear T°	*r*	0.88	0.95	0.76	0.73
	S.D. (min)	190	18	113	52
Rectal T°	*r*	0.82	0.84	0.65	0.28
	S.D.	37	31	105	123
Vitreous K^+	*r*	0.73 (NS)	0.68	0.58	0.40
	S.D.	224	117	184	108
CSF K^+	*r*	0.76 (NS)	0.51 (NS)	0.38 (NS)	0.74
	S.D.	198	166	190	29
Plasma log Na^+/K^+	*r*	0.63	0.46	–0.12 (NS)	–0.55
	S.D.	257	297	11	42
Plasma log Cl^-	*r*	0.44 (NS)	–0.03 (NS)	–0.0027 (NS)	–0.004 (NS)
	S.D.	299	249	190	132

---

[1] Rule of thumb 1': Post mortem interval (h) = [rectal T° at time of death (F°) – rectal T° at time T1 (F°)]/1.5.

[2] Rule of thumb 2': Post-mortem interval (h) = rectal T° at time of death (C°) – rectal T° at time T1 (°C) +3.

Source: From Baccino E, De Saint Martin L, Schuliar Y, Guilloteau P, Le Rhun M, Morin JF, Leglise D, Amice J. Outer ear temperature and time of death. *Forensic Sci Int* 1996; **83**: 133–146.

the rectum and both EAC's during an actual post-mortem period of 60–1115 minutes. The corpses were divided into four groups with group one stored at 0–5°C, group two between 6°C and 10°C, group three 11–15°C and group four between 16°C and 23°C. The temperatures recorded were applied to both multivariate and linear regression formula, the latter of which provided an 'interval' formula:

$$PMI\,(\text{min}) = A\cdot(37^\circ\text{C} - \text{OE}\cdot T^\circ) + B$$

where *OE* is the temperature in the EAC. They reported that as they were not able to maintain the corpses at above 23°C to avoid decomposition, the formula required modification to take this into account. It was thus modified to:

$$PMI\,(\text{min}) = A\cdot\text{OE}\cdot T^\circ + B\cdot\text{ambient}\cdot T^\circ + C$$

with the correlation coefficient of 0.9 and a standard deviation of 127 minutes. This was named the 'global' equation for EAC temperatures.

For the research cohort (138 corpses) Baccino et al. reported that the correlation coefficient (*r*) values for the EAC method always provided better correlation with the time of death no matter what the ambient temperature was compared to the rectal temperature or other methods investigated in their paper (Table 6.27). They observed that the estimated PMI calculated from EAC temperatures differed from the actual by less than 1 hour in 77% of cases using the EAC temperature alone and in 93% of cases using the multivariate equation.

Having established the 'interval' and 'global' formulae Baccino et al. applied these along with two variants of the Rule of Thumb formula and the Henssge nomogram to a different test population comprising 141 corpses with an actual post-mortem interval of 120–1330 minutes [4]. He separated the data into four ambient temperature groups and reported that the 'interval' and 'global' formulae using temperatures from the EAC provided better results than using the Rule of Thumb and Henssge nomogram with temperatures recorded from the rectum particularly for ambient temperatures over 15°C and post-mortem periods up to 20 hours (Table 6.28). If the post-mortem period is over 15 hours, from this work his group recommended that an EAC temperature should not be used. They promoted the use of EAC temperatures at the scene for its simplicity, lack of disturbing effect on evidence gathering and better accuracy.

In a letter to the editor following publication, Rutty supported the work of Baccino but drew to their attention other variables which may influence temperatures from the EAC and concluded with recommending caution, at this time, in obtaining and interpreting temperatures recorded from this site [6]. Their response to this letter [8] addresses these concerns and also those of Henssge who criticised the 'interval' and 'global' formulae for using constants which were not defined and thus could not be known to others [7]. Baccino in his response informs us that the reason that this was done was that there were commercial obligations related to those formulae for a prototype thermometer described at the end of the original paper. He did however provide an exampled formula for an ambient temperature range of 16–23°C, which had been presented at a meeting in France:

$$PMI\,(\text{min}) = 56.44\cdot[37^\circ\text{C} - \text{OE}\cdot T^\circ C] - 150$$

66% Interval confidence = ± 25%

95% Interval confidence = ± 40%

Table 6.28 Effect of Post-mortem Interval Length on the Results of Five Algorithms Applied to a Test Sample (*n*°=°141)*

PMI (min)		Ambient temperature intervals		
		≤420 (7 h) *n* = 43	≤600 (10 h) *n* = 79	≤900 (15 h) *n* = 128
Actual (PMIA)		274 ± 87	377 ± 134	521 ± 210
Estimated (PMIE)				
Outer ear T°	'Interval'	264 ± 110	355 ± 171	462 ± 204
	'Global'	296 ± 113	366 ± 176	467 ± 206
Rectal T°	Rule of thumb 1	116 ± 145	194 ± 243	308 ± 237
	Rule of thumb 2	276 ± 121	342 ± 202	436 ± 214
	Henssge	138 ± 127	166 ± 117	280 ± 174
Error				
Mean (PMIA – PMIE min)				
Outer ear T°	'Interval'	10 ± 111	21 ± 139	59 ± 146
	'Global'	−22 ± 127	10 ± 167	54 ± 102
Rectal T°	Rule of thumb 1	158 ± 173	182 ± 234	213 ± 209
	Rule of thumb 2	2 ± 153	35 ± 201	84 ± 188
	Henssge	130 ± 168	201 ± 157	256 ± 161
Relative (Error/PMIA %)				
Outer ear T°	'Interval'	−1 ± 44	2.5 ± 39	7 ± 33
	'Global'	−16 ± 51	−4 ± 47	3 ± 40
Rectal T°	Rule of thumb 1	51 ± 65	48 ± 61	42 ± 49
	Rule of thumb 2	−12 ± 65	0 ± 59	8.5 ± 48
	Henssge	39 ± 73	48 ± 55	46 ± 43

Source: From Baccino E, De Saint Martin L, Schuliar Y, Guilloteau P, Le Rhun M, Morin JF, Leglise D, Amice J. Outer ear temperature and time of death. *Forensic Sci Int* 1996; **83**: 133–146.

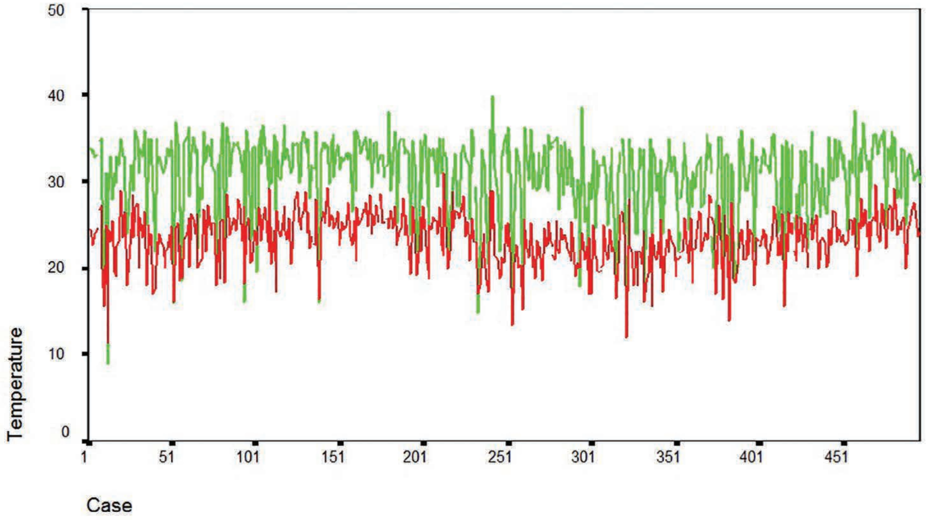

Figure 6.76 A plot of the rectal (green) and mean EAC (red) temperatures (°C) for all cases.

(From Rutty GN. *The use of temperatures recorded from the external auditory canal in the estimation of the time since death.* Sheffield, University of Sheffield, medical doctorate thesis 2001, as modified in Rutty GN. The estimation of the time since death using temperatures recoded from the external auditory canal. Part I. Can a temperature be recorded and interpreted from this site? *Forensic Sci Med Pathol* 2005; **1**: 41–51.)

Following this work, between 1996 and 1999, Rutty collected scene and ambient temperature and humidity data as well as serial ambient, EAC and rectal temperatures every 15 minutes from 600 human cadavers in the supine position. The ambient room temperature, the temperature within both EACs and the rectal temperature were recorded over a minimal period of 60 minutes (maximum 225 minutes) using a logging thermometer (HI 92840C logging thermometer, Hanna Instruments, UK) using an APK1 air probe for each EAC and an LPK1 general probe for the rectum and ambient temperature (Supplier: Hanna Instruments, UK). It was found that there was no statistical difference between the temperatures recorded from either EAC with the body in the supine position. The second observation was that the rectal temperature was always found to be higher than that of the EAC (Figure 6.76). The EAC was also found to cool at a rate of approximately 0.5°C per hour whereas the rectum cooled by 0.7°C per hour.

The time of death was known in 127 of cases as the death had been witnessed by either a relative/spouse/husband or by a member of the general public. The following methods were used to estimate a PMI using an EAC temperature: Rule of Thumb, Henssge nomogram for the rectum [107], Henssge nomogram for the brain [106], Al-Alousi temperature ratio method [108] and the method of De Saram [109]. The Rule of Thumb overestimated the PMI using both rectal and EAC temperatures. This was more pronounced with the EAC temperatures. If a constant derived from the difference between the rectal and EAC temperatures was added to the equation then the value approached, but still overestimated, the actual PMI. When EAC temperatures were applied to the Henssge nomograms, the rectal nomogram significantly overestimated the time whereas the brain nomogram reduced this overestimation. When the Al-Alousi algorithm was used, the rectal values underestimated the time since death whereas the EAC overestimated them again and in the case of the algorithm of De Saram both the EAC and rectal values underestimated the PMI [20].

Although the general observations made by Rutty were similar to Baccino and others with regard to the use of EAC temperatures and previously published formulae, he identified that the use of the K probes used with the logging thermometer may have caused a number of problems. First, although the EAC probes were chosen specifically because of their perforated ends, which recorded the temperature only within this area of the probe, the shafts were made of metal. Thus, when they were inserted into the EAC they were at room ambient temperature and required a period of stabilization. He postulated that this may have resulted in heat exchange between the EAC and the metal of the probe. The perforations of the probes were observed to become clogged with wax and required regular cleaning, which was difficult to perform. Finally, the placement of the probes was dependent upon the skill of the operator and thus it was possible that some probes were not fully inserted into the EAC.

Chronologically the next group to visit the concept of using the EAC for estimating the PMI were Kanawaku et al. from Japan [12]. This group used a computer simulation to analyse the cooling pattern of the EAC in a body placed in a near constant environment. Using computed tomography images from a single head they built a three-dimensional human head model. Thermophysical properties, initial condition and boundary condition were all postulated and calculations made based on an unsteady heat transfer equation using a finite element method to solve the equation. The cooling process was calculated for a 13-hour period. To verify the model, they continuously recorded temperatures from a single case using a temperature data logger and sensor over a 17-hour period. Again this group observed in the test subject that EAC cooling followed a single exponential curve. In terms of the computer simulation, it was observed that at a heat transmission coefficient of 6 W/m^2°C the simulation cooling curve nearly overlapped that of the case study (Figure 6.77). They concluded that measuring a temperature from the EAC at a scene of death was easy and that, assuming the body was relatively fresh, a useful result could be expected to be generated for the estimation of the PMI.

In 2009 Cattaneo et al. revisited the work of Rutty to consider whether an infrared tympanic thermometer could be used to record temperatures from the EAC of cadavers [13]. Recording multiple EAC temperatures from 25 cadavers at set intervals between 10 and 20 hours following arrival at the mortuary with two different types of commercially available infrared thermometers, they confirmed the previous work of Rutty that cadaveric EAC temperatures could be recorded with such devices and that the ear temperatures in both ears were similar when recorded with the two devices, that is that in a supine body the side from which the EAC temperature is recorded is not significant.

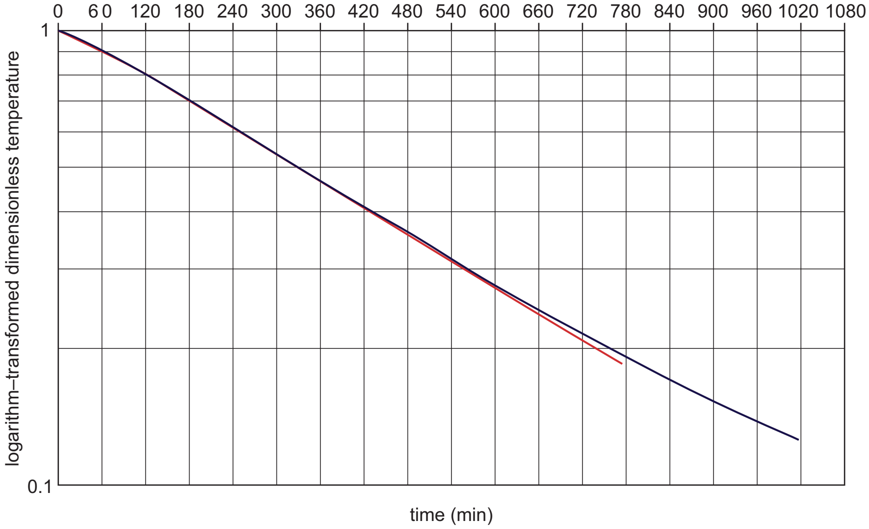

Figure 6.77 Logarithm-transformed curves for the case subject and the model. Red dot: simulation case. Blue dot: measured case.

(From Kanawaku Y, Kanetake J, Komiya A, Maruyama S, Funayama M. Computer simulation for post-mortem cooling processes in the outer ear. *Leg Med* 2007; **9**: 55–62.)

Table 6.29 Accuracy and Systematic Bias of Atrial and Temporal Infrared Thermometers Compared to the Metal Probe

	LA95 inf	LA95 sup	ICC [IC95]	Erreur relative moyenne (ET)	Erreur absolue moyenne
Thermoscan Pro 4000 (IR ouriculaire)					
OD	–2,2	5,0	0,24 [–0,48 ; 0,61]	1,38 (1,84)	1,64
OG	–2,0	4,4	0,48 [–0,18 ; 0,75]	1,19 (1,61)	1,44
Thermoflash (IR temporal)					
OD	–7,4	0,0	0,64 [0,19 ; 0,83]	–3,73 (1,86)	3,73
OG	–7,4	–0,2	0,85 [0,56 ; 0,93]	–3,81 (1,81)	3,87

LA95 : limited' accord á 95% ; CCI: coefficient de corrélation intraclasse; ET : écart-type de l'erreur relative moyenne.

Source: From Meusy A, Peyron PA, Molinari N, Colomb S, Rondepierre L, Couderc P, Contiero J, Guillote M, Bouelita L, Lossois M, Baccino E. Preliminary study of the accuracy and the systematic bias of two infrared thermometers for early postmortem interval estimation: Can commercially available infrared thermometers be used to determine the time of death? *La Revue de Medecine Legale* 2017; **8**: 97–104 Copyright© Elsevier Masson SAS. All Rights Reserved.

Following this work there was then a gap of 8 years before Baccino and others returned to this area of research. In 2017 Meusy et al. undertook a study considering whether commercially available infrared thermometers could be used to determine the time of death [15]. Studying 53 cadavers with a known post-mortem period of less than 12 hours and no ear pathology, no ear wax (removed if present) or head trauma each had two ear temperatures taken from both ears with two infrared thermometers by five different operators. A control tympanic temperature was taken with a thermocouple metal probe along with a rectal temperature. They observed that the infrared auricular thermometer used overestimated the tympanic temperature by an average of +1.38°C, and the temporal infrared thermometer used underestimated the tympanic temperature by an average of −3.37°C (Table 6.29). They concluded that these clinical thermometers could not replace a thermocouple thermometer with a metal probe. They suggested the need to design a cadaver-specific infrared thermometer, something Rutty had touched upon in his doctoral studies previously [20].

In 2020 Franchi et al. studied the post-mortem fall in tympanic temperature compared to that of the rectum in 117 cadavers with known times of death, without ear disease under standardized non-refrigerated ambient temperature conditions [17]. Two readings were taken from each ear using an infrared auricular thermometer. They reported that the reproducibility of measurements of ITT was excellent permitting to use the mean value of ITT. They noted no difference in ITT value between the same ear, the same cadaver and two trained staff. As part of their study, they developed a formula to predict the post-mortem interval

$$\mathrm{PMI} = 16.14 - 0.39 \cdot x \cdot \mathrm{ITT}$$

Finally, three papers appeared in 2021 again considering whether tympanic temperatures are suitable for the determination of a time since death [16,18,19]. First LaPlace et al. recorded the ear temperatures twice from both ears with an infrared thermometer and a metal probe thermometer from 100 cadavers with a known time of death and no ear wax (removed if present) [18]. They observed good repeatability with negligible differences in temperatures successively measured in each ear, with a strong and significant correlation between temperatures measured in each ear. However, they identified an underestimation of ear temperature compared to the metal probe ranging from 2.03°C to 2.43°C, concluding that their findings did not support the use of auricular infrared thermometry for post mortem interval estimation based on algorithms developed for probe thermometers.

Peyron et al. in their work considering the use of tau proteins in cerebrospinal fluid as a novel biomarker of the time of death recorded rectal and tympanic temperatures in 37 cadavers and applied the measurements to Henssge's nomogram and Baccino's formula [19]. As expected, a negative correlation was observed between the tympanic temperature and the post-mortem interval. They reported that Baccino's formula could be used for all their study cases and proved to be the more reliable temperature-based method to estimate the post-mortem interval although it failed to provide an appropriate time in 45.9% of cases. This was however better than Henssge's nomogram which yielded aberrant results in 62.2% of their cases with 25% of cases where it could not be used due to rectal temperatures higher than 37.2°C. When only normothermic cases were considered (18/37 cases) Baccino's formula provided reliable results in 15 cases (83.3%) compared to 11 cases (61.1%) with Henssge's nomogram.

The last paper in this series of three is authored by LaPlace et al. and considers the application of ear and rectal temperatures (in °C) from 100 non-refrigerated cadavers without ear wax (removed if present) to four temperature-based methods; Henssge's rectal and brain nomograms and Baccino's interval and global formulae [16]. This chapter uses the formula from Baccino's 1997 as the 'interval formula' and provides the reader with Baccino's 'global formula' as follows.

Baccino's interval formula:

$$PMI = 56.44 \cdot x \cdot [37 \cdot - \cdot \mathrm{EAC} \cdot \mathrm{temperature}] \cdot - \cdot 150$$

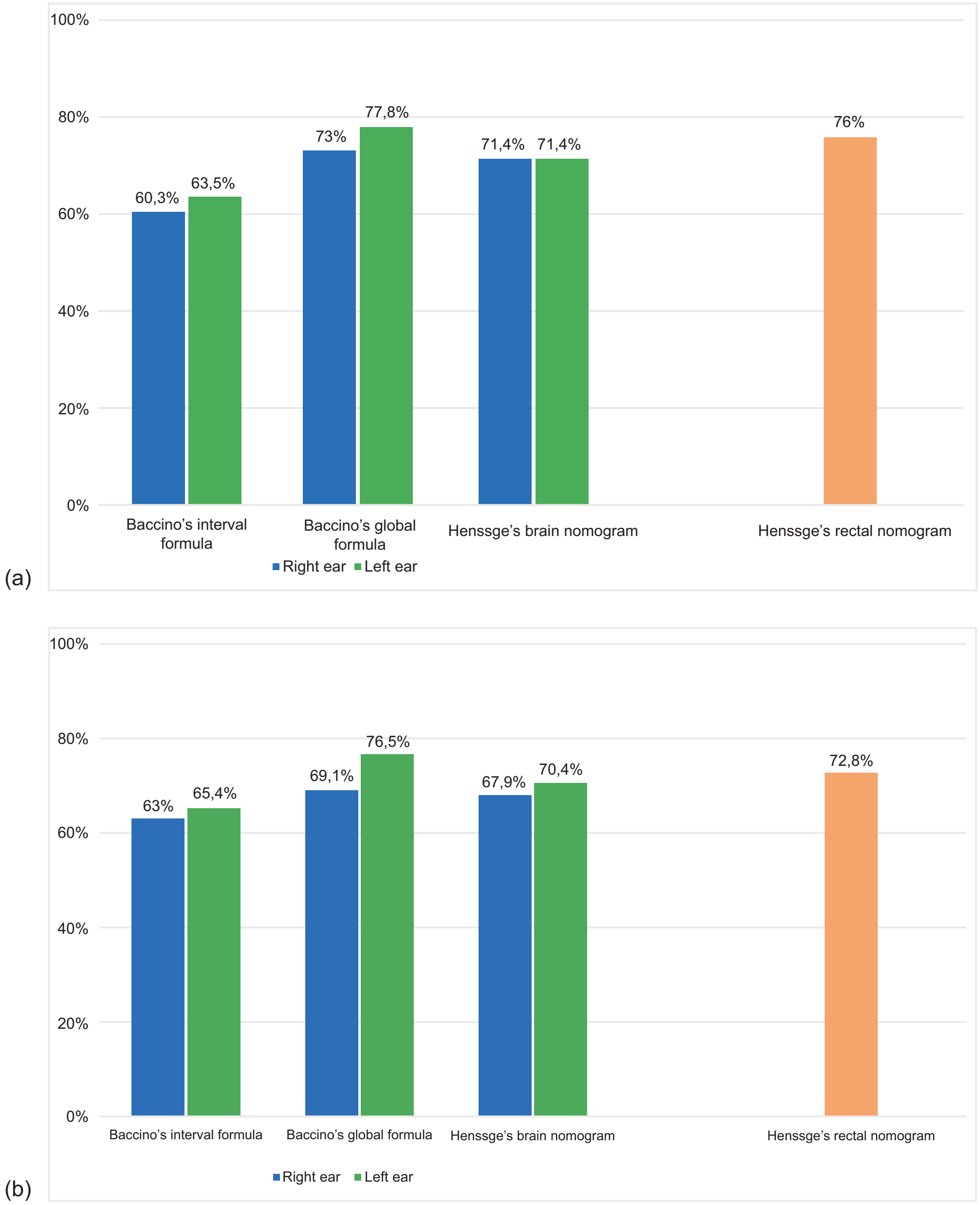

Figure 6.78 (a) proportion of correct PMI estimates provided by each temperature-based method (*n*°=°81). For each ear temperature–based methods, results are presented for both ears. (b) proportions of correct PMI estimates provided by each temperature-based method in the subgroup of normothermic patients at the time of death (*n*°=°61). For each ear temperature–based methods, results are presented for both ears.

(From LaPlace K, Baccino E, Peyron P-A. Estimation of the time since death based on body cooling: a comparative study of four temperature-based methods. *Int J Leg Med* 2021; **135**: 2479–2487.)

Baccino's global formula:

$$PMI = 57 \times [37 - \text{EAC temperature}] + 6.7 \times \text{ambient temperature} - 240$$

Ear temperatures were measured with a metal probe thermometer. Although there was a moderate but significant correlation between ear and rectal temperatures, rectal temperatures were, on average, 4.9°C higher than ear temperatures. Of the 100 cases studied, 63 (77.8%) were normothermic at death. Due to hyperthermia at the time of death all four formulae could only be applied to 81 cases. The results are shown in Figure 6.78 and indicate that, depending upon the method used, the different methods were not able to correctly predict the actual post-mortem period in a significant percentage of cases. However, they discuss how this study supports that ear-based temperature methods are as reliable as those based on rectal temperature for estimating early post-mortem intervals and that, as Rutty had previously shown, Henssge's nomogram for the brain could be used with ear temperatures and often provided an adequate post-mortem interval even when the rectal nomogram could not be applied.

6.4.8 Variables that Could Influence a PMI Calculation

A number of concerns have been raised over the years by researchers as to possible influences over temperatures recorded from the EAC, both clinically (see above) and in cadavers. Baccino et al. suggested that in the presence of otorrhagia or if the body is lying on its side with one ear in close contact with a surface then an EAC temperature should not be recorded [4]. Further concerns were raised by Rutty [6] in his letter regarding Baccino's work. Cattaneo et al. were concerned over the influence blood or perforation of the tympanic membrane may have if a probe, rather than an infrared device was used [13]. Finally, Kanawaku et al. questioned whether the length of hair on the scalp may have an influence on head cooling [12], although Henssge had previously advised, in terms of post-mortem brain temperature, that the estimated time of death did not become significantly more accurate even if the amount of hair was considered.

In the series of 600 cadavers studied by Rutty, he considered the role of a number of possible variables on EAC temperatures on two data sets: 499 cadavers where the wind speed was below the level of detection for the anemometer and 127 cases where the time of death was known. The variables assessed for both groups were gender, body weight, body length, absence or presence of clothing, whether the body was covered or not at the scene, whether the body was wet or dry, environmental humidity at the scene and mortuary, body position at the scene, head position at the scene and wind speed over the body. For 100 random cadavers he also assessed the distribution of head hair, the estimated length of the hair, the head circumference, the ear pinna and lobe morphology, ear index [110], skull bone thickness [111, 112] and brain weight. For 99 cases the length of each EAC was measured. For a further 70 cases the EAC measurements were derived from clinical computed tomography scans. The degree of atheroma within the right and left common carotid arteries below and at the bifurcation as well as to the internal and external carotid arteries immediately above the bifurcation were assessed in 103 paired vessels. Finally, a small data set considering the effect of body activity, position, and drinking of hot fluids was assessed on living volunteers [20, 10].

The results for the 499 and 127 data sets identified three variables that could have an influence on the temperature from the EAC. Within the 127 data sample the wearing of a dress, the humidity of the mortuary and whether a body was found indoors or outside were identified as statistical influences, but as they were not found to be so in the larger dataset they were dismissed. However, in the 499 cases the only significant variable that was found potentially to influence the EAC temperature was the position of the body at the scene. The cadavers were categorized into those lying on their back, front, right side or left side. Unlike the suggestion made by the earlier work of Baccino et al., there was no significant difference between the temperature within the right and left EAC for body position, an observation confirmed by later authors [17,18]. A difference was observed however between the rectal and mean EAC for the bodies on their back compared to the other positions although this was influenced by the small numbers of cases found on their front and sides compared to those on their back.

For 101 cadavers a fan was used to generate wind across the head and body. This was shown to have no effect on the temperatures recorded from the EACs. In 34 cases, cadavers had been refrigerated prior to assessment and thus the starting EAC temperature was below ambient temperature. It was observed that the EAC temperatures rose over a 120-minute period to approach ambient temperature.

In the case of head hair, no significant effect was observed, even if the external auditory meatus was covered by hair. Similarly ear shape and lobe attachment, head circumference, brain weight, skull bone thickness and the degree of atheroma within the carotid arteries had no effect on EAC temperatures.

Considering the EAC length then in any individual, there may be a difference between the left and right side, but this was not found to be statistically different. This could be an important observation as the EAC is expected to have a temperature gradient within the canal between the external ambient temperature and the tympanic membrane. Thus, the choice of thermometer to take an EAC reading becomes important as reported by Meusy et al. [15] and LaPlace et al. [18]. Due to the under- and overestimation of ear temperatures reported with the use of infrared thermometers it is currently recommended that a metal probe thermometer is used to record ear temperatures for application to algorithms developed for probe thermometers [18].

Age and gender are reported to have no significant effect on the ITT value [17], nor does operator reproducibility [17,18]. The choice of algorithm used with the temperature is reported however to affect the subsequent post-mortem interval calculation [16,18]

In the living the temperature within the EAC was found to vary with the time of day and activity. Interestingly, this appeared to be related to mental, rather than physical, activity. It was also found to rise after drinking a hot drink. Unlike the cadaver work and in support of Baccino et al., the EAC in contact with the ground when lying on one side was found to be warmer than the one exposed to ambient temperature. This was a time-dependent effect with a difference of 0.1°C at 1 minute, 0.6°C at 5 minutes and 0.9°C after 10 minutes for an unsupported head.

6.4.9 Application in Practice

To the authors knowledge, with the exception of the work of Rutty, the published research in this area is based on hospital acquired cadavers investigated in controlled mortuary environments. Rutty's doctoral thesis however has a subset of data more akin to real-world forensic practice.

Between 1996 and 1999 Rutty recorded single-reading temperatures from both EACs and the rectum, as well as the ambient temperatures using a First Temp® Genius™ Tympanic Thermometer (Sherwood Medical, England) and an alcohol-in-glass thermometer for 80 unselected suspicious and homicide death scenes and autopsies that he attended [20]. An ambient temperature could be recorded with the infrared thermometer as long as it was above 17°C. However, the value was found always to be significantly higher than that of the traditional glass thermometer.

In the majority of cases the rectal temperature was higher than its equivalent EAC temperature, an observation reiterated by LaPlace [16]. This difference may be explained with the knowledge that in life the temperature in the EAC is lower than the rectum. Thus, the temperature at the time of death at the two sites may not be the same. Although the rectum may (or may not) be 37°C, the EAC may be lower. In addition, if we consider the 'cooling curve' observed from the dog and human research discussed earlier, we can anticipate that the EAC will, unlike the rectum, show no lag phase prior to cooling. Thus, we can redraw our theoretical cooling curves for the two sites to explain potentially the difference in the temperatures at the two sites at any given time (Figure 6.79).

Although it has been shown that there is no significant difference between the temperatures within both EACs when both are measured using the same thermometers, Rutty found there was a thermometer dependent variant as the temperature in the EAC tended to be higher if measured with the tympanic rather than the alcohol-in-glass. He had previously noted in his dog research that there was also a difference between two different infrared thermometers, which was reenforced by both Meusy et al. [15] and LaPlace et al. [18] who also considered the difference between infrared and metal probe thermometers. This observation will affect any subsequent PMI estimation using an EAC temperature. An explanation for this can be hypothesized in the way that the various types of thermometers record temperatures within the EAC (Figure 6.80).

Using the temperatures recorded from the rectum and both EACs with the different instruments the PMI was now estimated using a number of previously published formulae. An 'actual' estimation of the time since death,

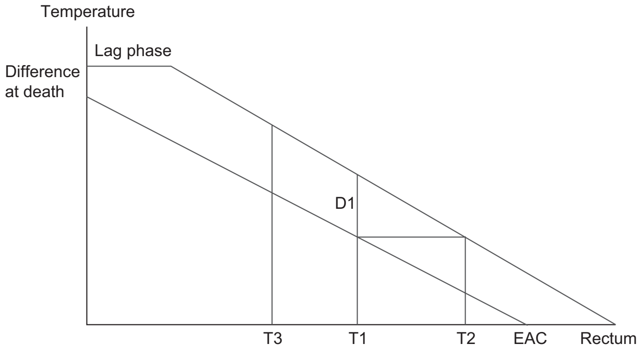

Figure 6.79 The theoretical cooling slopes for the rectum and the EAC showing a rectal plateau prior to temperature decline. Temperature °C. *T*1°=°time (hours) of reading from EAC, *T*2°=°equivalent rectal temperature at *T*1, *T*3°=°EAC temperature at rectal temperature *T*1 and *D*1 difference between rectal and EAC temperature at *T*1.

(From Rutty GN. *The use of temperatures recorded from the external auditory canal in the estimation of the time since death*. Sheffield, University of Sheffield, medical doctorate thesis 2001, as modified in Rutty GN. The estimation of the time since death using temperatures recoded from the external auditory canal. Part I. Can a temperature be recorded and interpreted from this site? *Forensic Sci Med Pathol* 2005; **1**: 41–51.)

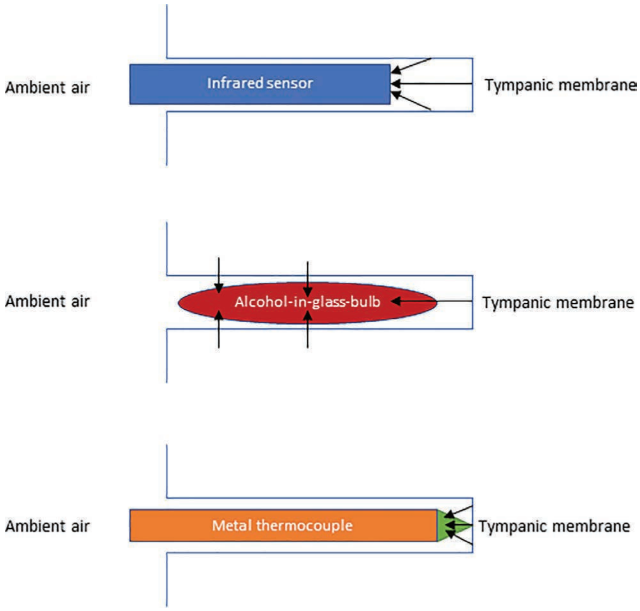

Figure 6.80 Hypothesized reason why there is a difference between the readings from the EAC with the different types of thermometer. Upper = infrared thermometer, middle = alcohol-in-glass, lower = metal probe thermocouple. The arrows represent heat from the tympanic membrane and ear canal. The metal thermometer probe tip in this model is seen to be nearest to the true tympanic membrane temperature.

(Modified from Rutty GN. The use of temperatures recorded from the external auditory canal in the estimation of the time since death. Sheffield, University of Sheffield, medical doctorate thesis 2001.)

which was based on information available at the time of the autopsy, was available in a total of 62 cases. For up to approximately 16 hours after death the centigrade Rule of Thumb calculation for all sites and instruments tended to overestimate the PMI, under-estimating it after approximately 16 hours. The infrared thermometer significantly overestimated the PMI more than the rectum and the alcohol-in-glass was even more pronounced. The PMI could however be more closely estimated by introducing a constant to the calculation derived from the total mean difference between the rectal and EAC temperatures, although it still tended to overestimate the true PMI.

The temperatures were then applied to the Henssge nomogram for the rectum and the brain. The infrared temperatures from the EAC overestimated the PMI in the majority of cases. However, using those cases where there was certainty of the actual PMI, applying infrared EAC temperatures to the brain nomogram predicted the 'actual' time in 77% of cases, a figure comparable to the later work of LaPlace et al., depending upon which algorithm is applied (Figures 6.81 and 6.82) [10,18].

6.4.10 Summary

A period of nearly 30 years has passed since the concept of using temperatures recorded from the EAC was first postulated by Baccino et al. [3]. During this period of time a wealth of evidence has been collected from a number of study centres in the UK, Europe and Japan which independently have come to comparable conclusions. Recording a temperature from the EAC can be undertaken quickly and easily without contamination of more critical evidence, for example in the case of a sexual assault, using a variety of thermometers including commercially available infrared thermometers.

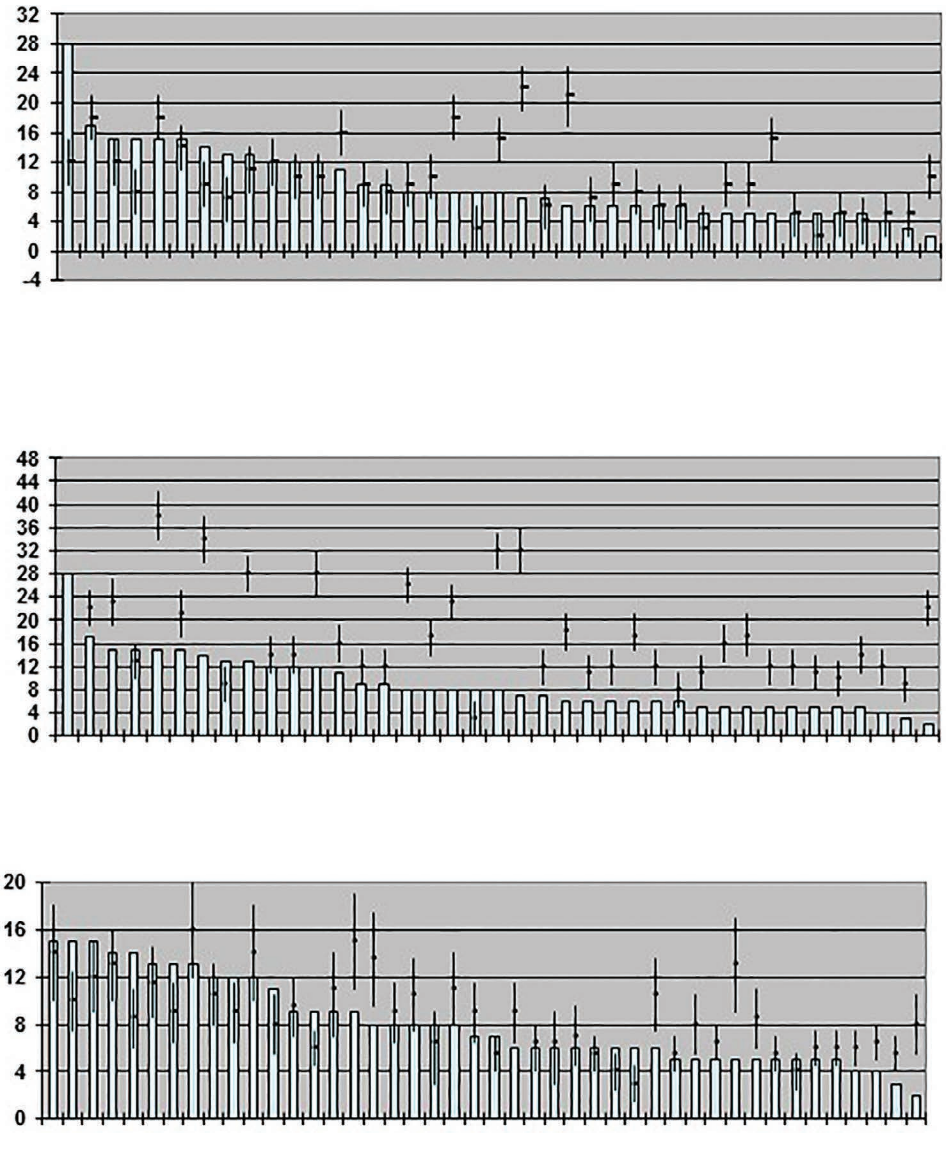

Figure 6.81 Plot of the 'actual' time since death (blue box) with the estimated time since death including the 95% confidence limits for cases used with the Henssge nomogram for the rectum (a and b) and the brain (b) for the rectal and infrared right EAC values.

(From Rutty GN. The estimation of the time since death using temperatures recoded from the external auditory canal. Part II. Using single temperatures from this site to estimate the time since death with consideration of environmental and body "factors" that could affect the estimation. *Forensic Sci Med Pathol* 2005; **2**: 113–123.)

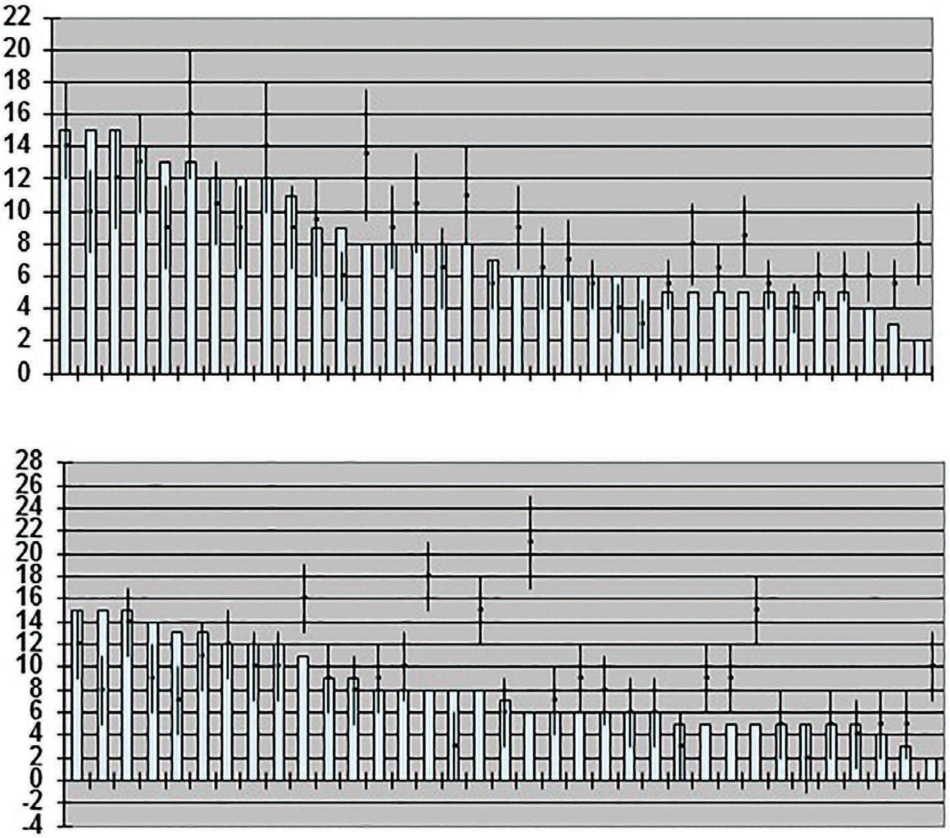

Figure 6.82 Plot of the 'actual' time since death (blue box) with the estimated time since death including the 95% confidence limits for 35 rectal and infrared right EAC values used with both the Henssge nomogram for the rectum (a) and the brain (b).

(From Rutty GN. The estimation of the time since death using temperatures recoded from the external auditory canal. Part II. Using single temperatures from this site to estimate the time since death with consideration of environmental and body "factors" that could affect the estimation. *Forensic Sci Med Pathol* 2005; **2**: 113–123.)

Unlike the rectum, the EAC has no discernible post-mortem plateau phase, follows a linear regression cooling curve, and the temperatures can be applied to published algorithms. However, the choice of thermometer and algorithm will affect the subsequent result as will the person being hyper- or hypothermic at the time of death, daily body temperature variations, and using the EAC nearest the ground. The current literature supports that when using an EAC temperature with an algorithm designed for probe thermometers that a metal probe thermometer should be used to record the temperature, not a clinical infrared thermometer. If the cadaver was normothermic at death, the use of a temperature recorded with such a probe applied to an algorithm such as Baccino's formula could result in a reliable post-mortem interval calculation in up to 83% of cases [19].

References

1. Baccino E, Frammery MF, Guedes Y, Morin JF, Barthelemy L. *Determination de l'Heure du Deces sur les Lieux: Apports Respectifs de la mesure de la Temerature Tympanique et Hepatique*. Societe de Medicine Legale et de Criminologie de France, Paris, 1991.
2. Nokes LDM, Flint T, Jaafar S, Knight BH. The use of either the nose or outer ear as a means of determining the post-mortem period of a human corpse. *Forensic Sci Int* 1992; 54: 153–8.
3. Baccino E, Guilloteau P, Le Moigne E, Schuliar Y. Postmortem delay determination: interest of the outer ear temperature. *Presented at the 13th I.A.F.S. Meeting Dusseldorf*, 1993.
4. Baccino E, De Saint Martin L, Schuliar Y, Guilloteau P, Le Rhun M, Morin JF, Leglise D, Amice J. Outer ear temperature and time of death. *Forensic Sci Int* 1996; 83: 133–46.
5. Rutty GN, Smith NC, Rutty JE. The use of infrared thermometry for determination of time since death in the early post mortem period. *J Pathol* 1996; 179(sup): 13A.
6. Rutty GN. Concerning the paper by Baccino et al., entitled: 'Outer ear temperature and time of death'. *Forensic Sci Int* 1997; 87: 171–2.
7. Henssge C. Concerning the paper by Baccino et al., entitled: 'Outer ear temperature and time of death'. *Forensic Sci Int* 1997; 87: 169.
8. Baccino E. response to Dr. Rutty's letter re: 'Outer ear temperature and time of death'. *Forensic Sci Int* 1997; 87: 173.
9. Rutty GN. The estimation of the time since death using temperatures recoded from the external auditory canal. Part I. Can a temperature be recorded and interpreted from this site? *Forensic Sci Med Pathol* 2005; 1: 41–51.
10. Rutty GN. The estimation of the time since death using temperatures recoded from the external auditory canal. Part II. Using single temperatures from this site to estimate the time since death with consideration of environmental and body "factors" that could affect the estimation. *Forensic Sci Med Pathol* 2005; 2: 113–23.
11. Baccino E, Cattaneo C, Jouineau C, Poudoulec J, Martrille L. Cooling rates of the ear and brain in pig heads submerged in

water. Implications for post-mortem interval estimation of cadavers found in still water. *Am J Forensic Med Pathol* 2007; 28: 80–95.

12. Kanawaku Y, Kanetake J, Komiya A, Maruyama S, Funayama M. Computer simulation for post-mortem cooling processes in the outer ear. *Leg Med* 2007; 9: 55–62.
13. Cattaneo C, Di Giancamillo A, Campari O, Orthmann N, Martrille L, Domeneghini C, Jouineau C, Baccino E. Infrared tympanic thermography as a substitute for a probe in the evaluation of ear temperature for post-mortem interval determination: a pilot study. *J Forensic Leg Med* 2009; 16: 215–17.
14. Proctor KW, Kelch WJ, New JC. Estimating the time of death in domestic canines. *J Forensic Sci* 2009; 54: 1433–7.
15. Meusy A, Peyron PA, Molinari N, Colomb S, Rondepierre L, Couderc P, Contiero J, Guillote M, Bouelita L, Lossois M, Baccino E. Preliminary study of the accuracy and the systematic bias of two infrared thermometers for early postmortem interval estimation: Can commercially available infrared thermometers be used to determine the time of death? *La Rev de Med Leg* 2017; 8: 97–104.
16. LaPlace K, Baccino E, Peyron P-A. Estimation of the time since death based on body cooling: a comparative study of four temperature-based methods. *Int J Leg Med* 2021; 135: 2479–87.
17. Franchi A, Clerc-Urmes I, Martrille L. Estimating the time of death with infrared tympanic thermometer: a new prospective study in France. *Int J Leg Med* 2020; 134: 591–5.
18. LaPlace K, Baccino E, Peyron P-A. Is infrared thermometry suitable for the determination of the time since death based on ear temperature? A comparative study of two measurement methods. *In J Leg Med* 2021; 135: 1669–74.
19. Peyron P-A, Hirtz C, Baccino E, Ginestet N, Tiers L, Martinez AY, Lehmann S, Delaby C. Tau protein in cerebrospinal fluid: a novel biomarker of the time of death? *Int J Leg Med* 2021; 135: 2081–9.
20. Rutty GN. *The Use of Temperatures Recorded from the External Auditory Canal in the Estimation of the Time Since Death*. Medical Doctorate Thesis, University of Sheffield, 2001.
21. The ear. In *Clinical Anatomy for Medical Students*. Ed. Snell RS. Little, Brown and Company, Boston, 1981, page 709–20.
22. Siegert R, Weerda H, Remmert S. Embryology and surgical anatomy of the auricle. *Facial Plastic Surg* 1994; 10: 232–43.
23. Kelley KE, Mohs DC. The external auditory canal. Anatomy and physiology. *Otolaryngol Clin North Am* 1996; 29: 725–39.
24. Huber GC. *Piersol's Human Anatomy*. 9th ed. J.B. Lippincott, Philadelphia, 1930, page 1488.
25. Bartlett EM. Temperature measurement: why and how in intensive care. *Intensive Crit Care Nurs* 1996; 12: 50–4.
26. Tortora GJ, Anagnostakos NP. *Principles of Anatomy and Physiology*. Harper and Row Publishers, London, 1990, pages 815–21.
27. Park S-J, Tokura H. Effects of two types of clothing on the day-night variation of core temperature and salivary immunoglobulin A. *Chronobiol Int* 1997; 14: 607–17.
28. Wunderlich C. *Das Verhalten der Eiaenwarme in Krankenheiten*. Otto Wigand, Leipzig, Germany, 1868.
29. Mackowiak PA, Wasserman SS, Levine MM. A critical appraisal of 98.6°F, the upper limit of normal body temperature, and other legacies of Carl Reinhold August Wunderlich. *JAMA* 1992; 268: 1578–80.
30. Kato M, Ando T, Yamashita Y, Tokura H. Thermophysiological effects of two different types of clothing under warm temperatures. *Appl Human Sci* 1995; 14: 119–24.
31. Li X, Tokura H. Acclimatization effect on the evening fall in core temperature under influence of two types of clothing. *Experientia* 1996; 52: 613–15.
32. Smith DL, Petruzzello SJ, Kramer JM, Misner JE. The effects of different thermal environments on the physiological and psychological responses of firefighters to a training drill. *Ergonomics* 1997; 40: 500–10.
33. White MD, Cabanac M. Exercise hyperpnea and hyperthermia in humans. *J Appl Physiol* 1996; 81: 1249–54.
34. Tanabe M, Shido O. Changes in body core temperatures and heat balance after abrupt release of lower body negative pressure in humans. *Int J Biometerol* 1994; 38: 48–54.
35. Szpak D, Groszek B, Obara M, Kusiak K. Thermoregulatory dysfunction secondary to acute ethanol poisoning. *Przegalnd Lekarski* 1995; 52: 281–3.
36. Roeggla G, Roeggla M, Binder M, Roeggla H, Muellner M, Wagner A. Effect of alcohol on body core temperature during cold-water immersion. *EJCP* 1995; 49: 239–40.
37. Wright K, Badia P, Myers BL, Plezler SC, Hakel M. Caffeine and light effects on nighttime melatonin and temperature levels in sleep-deprived humans. *Brain Res* 1997; 747: 78–84.
38. Benzinger TH, Taylor GW. Cranial measurements of internal temperature in man. In: *Temperature. Its Measurement and Control in Science and Industry*. Ed. Herzfeld CM. Reinhold Publishing Corporation, New York, 1963, pages 111–20.
39. Williams RJ, Thompson RC. A device for obtaining a continuous record of body temperature from the external auditory canal. *Science* 1948; 108: 90–1.
40. Wells N, King J, Hedstrom C, Youngkins. Does tympanic temperature measure up? *Am J Matern Child Nurs* 1995; 20: 95–100.
41. Benzinger M. Tympanic thermometry in surgery and anesthesia. *JAMA* 1969; 209: 1207–11.
42. Wallace CT. Perforation of the tympanic membrane; a complication of tympanic thermometry during anesthesia. *Anesthesiology* 1974; 41: 290–1.
43. Anonymous. Infrared ear thermometry. *Health Devices* 1991; 20: 431–41.
44. Fraden J. Infrared electronic thermometer and method for measuring temperature. *US Patent* 1989; 4: 797–840.
45. Edge G, Morgan M. The Genius infrared tympanic thermometer. An evaluation for clinical use. *Anaesthesia* 1993; 48: 604–7.
46. Betta V, Cascetta F, Sepe D. An assessment of infrared tympanic thermometers for body temperature measurement. *Physiol Meas* 1997; 18: 215–25.
47. Burke K. The tympanic membrane thermometer in paediatrics: a review of the literature. *Accid Emerg Nurs* 1996; 4: 190–3.
48. Newbold J. Evaluation of a new infrared tympanic thermometer: a comparison of three brands. *J Pediatr Nurs* 1991; 6: 281–3.
49. Jakobsson J, Nilsson A, Carlsson L. Core temperature measured in the auricular canal: comparison between four different tympanic thermometers. *Acta Anaesthesiol Scand* 1992; 36: 819–24.
50. Matsukawa T, Hanagata K, Miyaji T. A comparison of four infrared tympanic thermometers with tympanic membrane temperatures measured by thermocouples. *Can J Anaesth* 1996; 43: 1224–8.
51. Fraden J, Lackey RP. Estimation of body sites temperatures from tympanic measurements. *Clin Pediatr* 1991; 30 (Suppl 4): 65–70.
52. Terndrop TE, Crofton DJ, Mortelliti AJ, Kelley R, Rajk J. Estimation of contact tympanic membrane temperature with a

non contact infrared thermometer. *Ann Emerg Med* 1997; 30: 171–5.

53. Hasel K, Erickson R. Effect of cerumen on infrared ear temperature measurement. *J Geronto Nurs* 1995; 21: 6–14.
54. Milewski A, Ferguson KL, Terndrop TE. Comparison of pulmonary artery, rectal and tympanic membrane temperatures in adult intensive care patients. *Clin Pediatr* 1991; 30 (Suppl 4): 13–16.
55. Freed GL, Fraley JK. Lack of agreement of tympanic membrane temperature assessments with conventional methods in a private practice setting. *Pediatrics* 1992; 89: 384–6.
56. Rogers J. Evaluating tympanic membrane thermometry. *Nurs Times* 1992; 88: 52.
57. Brogan PA. Tympanic thermometry: poor correlations. *Clin Pediatr* 1993; 32: 699–670.
58. Klein DG, Mitchell C, Petrinec A, Monroe MK, Oblak M, Ross B, Youngblut JM. A comparison of pulmonary artery, rectal and tympanic membrane temperature measurement in the ICU. *Heart Lung* 1993; 22: 435–41.
59. Erickson RS, Kirklin SK. Comparison of ear-based, bladder, oral and axillary methods for core temperature measurement. *Crit Care Med* 1993; 21: 1528–34.
60. Yetman RJ, Coody DK, Stewart M, Montgomery D, Brown M. Comparison of temperature measurements by an aural infrared thermometer with measurements by traditional rectal and axillary techniques. *J Pediatr* 1993; 122: 769–73.
61. Erickson RS, Woo TM. Accuracy of infrared ear thermometery and traditional temperature methods in young children. *Heart Lung* 1994; 23: 181–95.
62. Darm RM, Hecker RB, Rubal BJ. A comparison of noninvasive body temperature monitoring devices in the PACU. *J Post Anesth Nurs* 1994; 9: 144–9.
63. Weiss ME, Poeltler D, Gocka I. Infrared tympanic thermometry for neonatal temperature assessment. *JOGNN* 1994; 23: 798–804.
64. Beckstrand RL, Wilshaw R, Moran S, Schaalje GB. Supralingual temperatures compared to tympanic and rectal temperatures. *Pediatr Nurs* 1996; 22: 436–8.
65. Hicks MA. A comparison of the tympanic and axillary temperatures of the preterm and term infant. *J Perinatol* 1996; 16: 261–7.
66. Romanovsky AA, Quint PA, Benikova Y, Kiesow LA. A difference of 5°C between ear and rectal temperatures in a febrile patient. *Am J Emerg Med* 1997; 15: 383–5.
67. Terndrop TE, Milewski A. The performance of two tympanic thermometers in a pediatric emergency department. *Clin Pediatr* 1991; 30 (Suppl 4): 18–23.
68. Nobel JJ. Infrared ear thermometry. *Ped Emerg Care* 1992; 8: 54–8.
69. Romano MJ, Fortenberry JD, Autry E, Harris S, Heyroth T, Parmeter P, Stein F. Infrared tympanic thermometry in the pediatric intensive care unit. *Crit Care Med* 1993; 21: 1181–5.
70. Terndrup T, Rajik J. Impact of operator technique and device on infrared emission detection tympanic thermometry. *J Emerg Med* 1992; 10: 683–7.
71. Petersen MH, Hauge HN. Can training improve the results with infrared tympanic thermometers? *Acta Anaesthesiol Scand* 1997; 41: 1066–70.
72. Pransky SM. The impact of technique and conditions of the tympanic membrane upon infrared tympanic thermometry. *Clin Pediatr* 1991; 30 (Suppl 4): 50–2.
73. Tourangeau A, MacLeod F, Breakwell M. Tap in on ear thermometry. *Canadian Nurse* 1993; Sept: 24–8.
74. Kiesow LA, Hurely C. Fogging in infrared tympanic and ear thermometry. *Annal Int Med* 1995; 122: 634–5.
75. Flo G, Brown M. Comparing three methods of temperature taking: oral, mercury – in-glass, oral Diateck and tympanic First Temp. *Nurs Res* 1995; 44: 120–2.
76. Doezema D, Lunt M, Tandberg D. Cerumen occlusion lowers infrared tympanic membrane temperature measurement. *Acad Emerg Med* 1995; 2: 17–19.
77. Yaron M, Lowenstein SR, Koziol-McLain J. Measuring the accuracy of the infrared tympanic thermometer: correlation does not signify agreement. *J Emerg Med* 1995; 13: 617–21.
78. Rohrberg M, Fritz U, Braun U. Temperaturmessung im Gehorgang: Verleich eines Infrarot-thermometers mit konventionellen Temeratursonden und Evalation klinischer einfuegroeen auf die infrarot-messund. *Anasthesioligie, Intersumedizme, Nothull Medigin, Schmerztherupie* 1997; 32: 409–13.
79. Kelley B, Alexander D. Effect of Otitis Media on infrared tympanic thermometry. *Clin Pediatr* 1991; 30 (Suppl 4): 46–8.
80. Talo H, Macknin ML, Mendendrop SV. Tympanic membrane temperatures compared to rectal and oral temperatures. *Clin Pediatr* 1991; 30 (Suppl 4): 30–3.
81. Pontious SL, Kennedy A, Chung K, Burroughs TE, Libby LJ, Vogel DW. Accuracy and reliability of temperature measurement in the emergency department by instrument and site in children. *Pediatr Nurs* 1994; 20: 58–63.
82. Jolin SW, Howell JM, Milzman DP, Stair TO, Butzin CA. Infrared emission detection tympanic thermometry may be useful in diagnosing acute otitis media. *Am J Emerg Med* 1995; 13: 6–8.
83. Castle S, Toledo S, Daskal L, Norman DC. The equivalency of infrared tympanic membrane thermometry with standard thermometry in nursing home residents. *J Am Geriatr Soc* 1992; 40: 1212–16.
84. Tomkinson A, Roblin DG, Quine SM, Flanagan P. Tympanic thermometry and minor ear surgery. *J Laryngol Otol* 1996; 110: 454–5.
85. Moriya K, Sekitani T, Yamashita H, Mizokami H. Tympanic membrane temperature in a patient with vertigo. *Acta Otolaryngol (Stockh)* 1993; 506 (Suppl): 24–5.
86. Zehner WJ, Terndrup TE. The impact of moderate ambient temperature variance on the relationship between oral, rectal and tympanic membrane temperatures. *Clin Pediatr* 1991; 30 (Suppl 4): 61–4.
87. Chamberlain JM, Grandner J, Rubinoff JL, Klein BL, Waisman Y, Huey M. Comparison of a tympanic thermometer to rectal and oral thermometers in a pediatric emergency department. *Clin Pediatr* 1991; (Suppl x): 24–9.
88. Henker R, Ciyne C. Comparison of peripheral temperature measurements with core temperature. *AACN Clin Ser* 1995; 6: 21–30.
89. Hashizume Y. Fluctuations of rectal and tympanic temperatures with changes of ambient temperature during night sleep. *Psychiatry Clin Neurosci* 1997; 51: 129–33.
90. Stavem K, Saxholm H, Smith-Erichsen N. Accuracy of infrared ear thermometry in adult patients. *Intensive Care Med* 1997; 23: 100–5.
91. Kahyaoglu O, Babka I, Demirci C, Boyer D. Effect of crying on infrared tympanic temperature measurement in pediatrics. *Clin Pediatr* 1997; 36: 48–9.
92. Sato KT, Kane NL, Soos G, Gisolfi CV, Kondo N, Sato K. Reexamination of tympanic membrane temperature as a core temperature. *Appl Physiol* 1996; 80: 1233–9.

93. Thomas KA, Savage MV, Brengelmann GL. Effect of facial cooling on tympanic temperature. *Am J Crit Care* 1997; 6: 46–51.
94. White N, Baird S, Anderson DL. A comparison of tympanic thermometer readings to pulmonary artery catheter core temperature readings. *Appl Nurs Res* 1994; 7: 165–9.
95. Roth NR, Verdile VP, Grollman LJ, Stone DA. Agreement between rectal and tympanic membrane temperature in marathon runners. *Ann Emerg Med* 1996; 28: 414–17.
96. Walpoth BH, Galdikas J, Leupi F, Muehlemann W, Schlaepfer P, Althaus U. Assessment of hypothermia with a new tympanic thermometer. *J Clin Monit* 1994; 10: 91–6.
97. Stone JG, Young WL, Smith CR, Solomon RA, Wald A, Ostapkovich N, Shrebnick DB. Do standard monitoring sites reflect true brain temperature when profound hypothermia is rapidly induced and reversed? *Anesthesiol* 1995; 82: 344–51.
98. Hansen RD, Olds TS, Richards DA, Richards CR, Leelarthaepin B. Infrared thermometry in the diagnosis and treatment of heat exhaustion. *Int J Sports Med* 1996; 17: 66–70.
99. Yeo S, Scarbough M. Exercise-induced hyperthermia may prevent accurate core temperature measurement by tympanic membrane thermometer. *J Nurs Meas* 1996; 4: 143–50.
100. Harasawa K, Kemmotusu O, Mayumi T, Kawano Y. Comparison of tympanic, esophageal and blood temperatures during mild hypothermic cardiopulmonary bypass: a study using an infrared emission detection tympanic thermometer. *J Clin Monit* 1997; 13: 19–24.
101. Chu A, Burnham RS. Reliability and validity of tympanic temperature measurement in persons with high spinal cord injury. *Paraplegia* 1995; 33: 476–9.
102. Chamberlain JM, Terndrop TE, Alexander DT, Silverstone FA, Wolf-Klein G, O'Donnell R, Grandner J. Determination of normal ear temperature with an infrared emission detection thermometer. *Ann Emerg Med* 1995; 25: 15–20.
103. Wright RO, Jay GD, Becker BM, Linakis JG. Use of infrared thermometry to measure lavage and intravenous fluid temperature. *Am J Emerg Med* 1995; 13: 281–4.
104. Knight B. The pathophysiology of death. In *Forensic Pathology*. Ed. Knight B. Edward Arnold, London, 1991, page 76.
105. Myers MJ, Henderson M. Assessment of two devices for measuring tympanic membrane temperature in swine, dairy cattle and dairy calves. *JAVMA* 1996; 208: 1700–1.
106. Henssge C, Beckmann ER, Wischhusen F, Brinkman B. Determination of time of death by measuring central brain temperature. *Z Rechtsmed* 1984; 93: 1–22.
107. Henssge C. Death time estimation in case work. I. The rectal temperature time of death nomogram. *Forensic Sci Int* 1988; 38: 209–2036.
108. Al-Alousi LM, Anderson RA, Land DV. A non-invasive method for postmortem temperature measurements using microwave probe. *Forensic Sci Int* 1994; 64: 35–46.
109. De Saram G, Webster G, Kathirgamatamby N. Post-mortem temperature and the time of death. *J Crim Law, Criminol Police Sci* 1955; 1: 562–77.
110. Farkas LG. Anthropometry of normal and anomalous ears. *Clin Plast Surg* 1978; 5: 401–12.
111. Ross AH, Jantz RL, McCormick WF. Cranial thickness in American females and males. *J Forensic Sci* 1998; 43: 267–72.
112. Ross MD, Lee KAP, Castle WM. Skull thickness in black and white races. *S Afr Med J* 1975; 50: 635–8.

6.5 Eye Temperature and the Time Since Death

■ *Michał Kaliszan*

6.5.1 Introduction

The idea of the estimation of the time since death (TSD) based on the measurement of the eye temperature was invented as this not previously studied site could have some valuable properties in comparison to widely used site as is rectum. Such properties include localization of the eyeball, which allows quite easy access for the temperature probe, closed compartment filled with vitreous humour, in which temperature in fact is measured, lack or minimal influence of body mass as head and eyeball mass is similar in different individuals and finally lack of influence of clothing layers covering the trunk, which is so important to consider when calculating the TSD based on rectal temperature.

The possibility of using the eye temperature in TSD estimation was initially tested in pigs with promising results [1,2] what was the key factor to continue the studies on human cadavers. During the studies in pigs the difference in the shape of the cooling curves of the eyeball versus rectum was observed. The eyeball temperature was decreasing more quickly than the rectal temperature; however, in the case of the eyeball, the so-called plateau effect (phase of initial slower cooling) on the temperature curve was not evident (Figure 6.83).

Several studies were performed on human cadavers regarding the value of the eye temperature in TSD determination [3,4], while the recent study published in 2019 is the most up to date, presenting 30 cases of death in the Intensive Therapy Department when the actual TSD was precisely known. [5]. Also, in the studies performed on human cadavers, the course of cooling already observed in previous studies in pigs was confirmed [1,2,4,5].

6.5.2 Method of Temperature Measurement and TSD Calculation

The temperature measurements can be taken with a high precision two-channel electronic thermometer with removable probes: a thin one with a sharp end (100 × 1.4 mm), with a 20 mm temperature sensor to be inserted into eyeball, and a thicker one (150 × 3.0 mm), ending in a 40 mm temperature sensor to be inserted into rectum. The thin probe should be inserted through the eyeball sclera

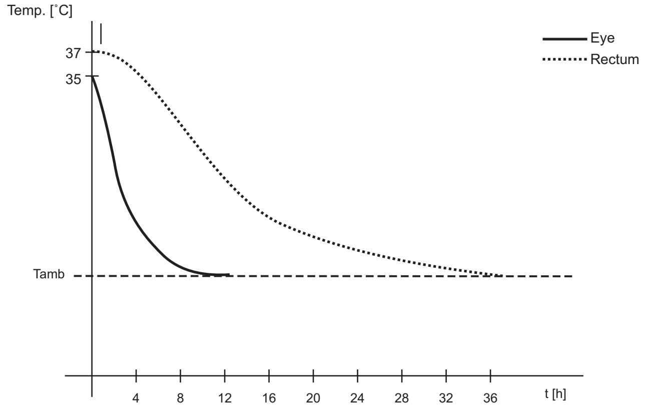

Figure 6.83 The graph presenting the approximate post-mortem cooling process of the eye and the rectum with marked plateau phase for the rectal temperature decrease.

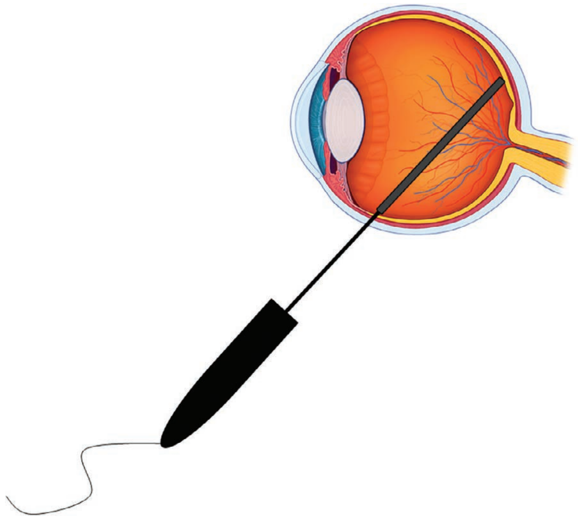

Figure 6.84 The thermometer probe with temperature sensor immersed in the eyeball vitreous chamber.

into the vitreous chamber until the 20-mm-long sensor is fully immersed (Figure 6.84).

To ease the insertion of the probe through the quite hard sclera into the eyeball, the injection needle (with a diameter of 2.1 mm) can be used as a guide for the pin probe. After injecting the needle in the sclera, the pin probe should be inserted to the eyeball through the needle and then the needle removed from the eyeball along the probe up to its handle to uncover the 20-mm long temperature sensor located at the end of the probe. Figure 6.85 shows the consecutive steps leading to the eyeball temperature measurement. The insertion of the thin probe through the sclera does not cause any visible damage to the eyeball.

Another thicker pin probe should be inserted into the rectum up to its handle (depth of 150 mm). Simultaneously the ambient temperature should be measured in close vicinity to the body.

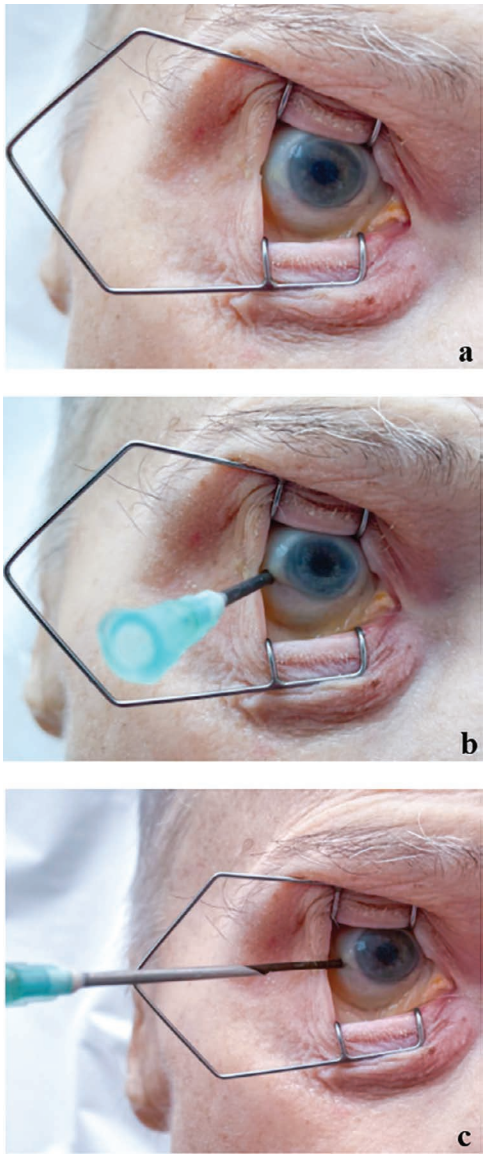

Figure 6.85 Method of inserting the thermometer probe into the eyeball: (a) eyelids open with use of speculum; (b) needle injected in the sclera; (c) probe inserted through the needle to the eye chamber.

After around 1 minute needed for the temperature reading to stabilize, the temperature values can be read and applied in the TSD calculations using the dedicated formula presented below.

A mathematical model developed using Newton's law of cooling to quantify the cooling of various pig body sites after death [1] and already tested in recent studies on human cadavers [4,5], can be applied to calculate the time which passed from the moment of death (TSD):

$$T = T_a + (T_0 - T_a)\exp(-k_c t) \quad \text{(Formula 1)}$$

where T is the temperature of the eyeball (if the temperature is measured in both eyeballs T°= T_1+T_2/2), T_a is the ambient temperature, assumed to be constant during the course of cooling until the moment of the measurement, T_0 is the initial human eye temperature, k_c is the first order cooling rate constant and t is the time in h which passed since death (TSD).

In the study involving examinations of 30 human cadavers, in which it should be assumed that the TSD was known with most possible precision, an optimum prediction of the determination of the TSD was obtained for the following parameters: $k_c = -0.2\ h^{-1}$ and $T_0 = 35°\text{C}$, where RMSE = 0.51 h. The 95% confidence interval for the current model of TSD estimation can be presented as ±1.96 × RMSE = ± 1 h [5].

Formula 1 developed using Newton's law of cooling during the experimental studies in pigs and human cadavers transformed and completed with the numerical value of $k_c = -0.2\ h^{-1}$ and $T_0 = 35°\text{C}$ allowing to calculate the TSD presents as follows:

$$t = -\frac{\ln\left(\frac{T - T_a}{35 - T_a}\right)}{0.2} \quad \text{(Formula 2)}$$

Results of the studies on which the parameters T_0 and k_c were established are presented in Table 6.30.

It should be stressed that such an accurate estimation of TSD in the early post-mortem period (±1 hour) could not have been achieved if only rectal temperature data had been relied upon, simply because of the several-hour-long plateau effect (Figure 6.83). As one can see from Table 6.30, in most of the 30 studied cases, the rectal temperature during the initial recording period of a few hours was still higher than 36°C, which often reflects a living individual's body temperature. Therefore, the only information concerning TSD in most of the studied cases when the rectal temperature was around 36–37°C, obtained using a Henssge nomogram, based on rectal temperature measurement, was that the moment of death could be placed within at least a 5-hour-wide time frame—as can be seen on various examples presented in Table 6.31 [5]. In the majority of the cases observed in the studies the rigor mortis was absent and the lividity was absent or scant, so even using the compound method integrating the rectal temperature measurement and non-temperature-based methods, one can only say that the time which passed from the moment of death can be placed between 0 and 3 hours. However, the presented study using the eyeball temperature measurements in TSD estimation clearly confirms that in the later phase of body cooling (after around 5 hours from the moment of death), the Henssge method based on single rectal temperature measurement is of no questionable value and has advantage over eyeball temperature, as well as is the compound method [6–8].

The presented results confirm that the proposed method of TSD estimation based on eyeball post-mortem temperature measurements might be applicable in the early post mortem period. Particularly, when applied to bodies found in normal environmental conditions (still air, normal humidity, no rain).

The effective application of the method developed during studies in pigs to human bodies and its reliability can be explained by the similar anatomical structure and location of pigs' and humans' eyeballs [9] and therefore their similar thermodynamic properties. The advantage of the presented method over the ones based on rectal temperature measurements in the early post-mortem period is the insignificant influence of clothes and body mass on the cooling rate of the eyeballs [1], what is influential in the case of body core (rectal) cooling [10]. Therefore, the actually proposed formula does not include corrective factors for body mass and clothes. Another issue deserving attention is the easy manner of the insertion of the pin probe into the eyeball, which doesn't require uncovering the rectal area of the deceased at the death scene and does not cause visible damage to the eyeball. Therefore, the method may be used in practice as a complementary one to already existing methods of TSD estimation, both temperature or non-temperature based. It might also be used as an alternative to rectal temperature measurements, in situations when rectal temperature measurements are not possible (i.e. traumatic lesion of this body site or a public place) or not indicated (i.e. sexual assault).

The application of the proposed method in casework, considering its good precision confirmed in the early post-mortem period, might be of use, particularly in criminal deaths, that is homicides, in which the bodies are often discovered shortly after the crime.

The TSD calculation according to the suggested method requires a mathematical formula which can be solved using at least a scientific calculator. The calculation can obviously be performed upon return from the body examination. However, investigators often expect the forensic pathologist to answer the question regarding the TSD of the crime victim immediately, at the death scene. Therefore, a specially designed thermometer can be used to display the estimated TSD conveniently and quickly. The thermometer should be equipped with a pin probe for the measurement of eye temperature, a probe measuring the ambient temperature and a built-in microprocessor containing the proposed mathematical formula complete with the cooling rate coefficient established in experimental studies and the initial eyeball temperature (Formula 2). Using this function, the TSD can be quickly calculated and displayed on the thermometer screen upon pressing the appropriate button. A prototype version of such an electronic thermometer with built-in microprocessor—a TOD (time of death) meter (Figure 6.86)—was constructed by Dostmann-electronic GmbH, Wertheim-Reicholzheim, Germany, according to the author's indications. It was built on the base of the routinely manufactured thermometer model (P755) but can be improved to more handy and dedicated to TSD estimation version [4,5].

Table 6.30 Results Acquired during the Study for 30 Bodies (40 Temperature Measurements) Calculated with the Use of Formula 2.

Case no.	T_1, °C (eyeball 1)	T_2, °C (eyeball 2)	T_r, °C (rectal)	TSD (actual)	TSD (predicted)	Δ TSD
1	33.4	33.1	36	50 min	43 min	–7 min
2	31.8	31.7	36.3	1 h 15 min	1 h 26 min	+11 min
3	32.5	31.9	37.5	2 h 15 min	1 h 13 min	–1 h 2 min
4	30	29.8	36.3	2 h 5 min	2 h 29 min	+24 min
5	28.7	28.3	37	2 h 30 min	3 h 28 min	+58 min
6	32.3	31.8	37	1 h 10 min	1 h 17 min	+7 min
7	29.9	29.3	36.5	2 h 30 min	2 h 40 min	+10 min
8	30.4	30.1	36.5	2 h	2 h 16 min	+16 min
9	33.7	33.7	35.9	30 min	32 min	+2 min
10	32.1	31.9	38.1	1 h 30 min	1 h 19 min	–11 min
11	30	29.5	36	2 h 30 min	2 h 35 min	+5 min
12	30.2	30.1	36.7	1 h	2 h 20 min	+1 h 20 min
13	32.5	32.3	36.8	1 h 10 min	1 h 7 min	–3 min
14	29.8	29.7	36.5	2 h	2 h 35 min	+35 min
15	30.1	30.1	36	1 h 50 min	2 h 22 min	+32 min
16	30.5	30.5	36	2 h	2 h 7 min	+7 min
17	30	29.7	36.2	3 h	2 h 31 min	+31 min
18	31.7	31.6	38	2 h	1 h 29 min	–31 min
19	31.1	31.1	37	3 h 20 min	3 h 55 min	+35 min
20	32.6	32.6	37.5	1 h	1 h 1 min	+1 min
21	30.7	30.6	37	2 h 30 min	2 h 2 min	–28 min
21′	29.8	29.8	36.5	3 h 30 min	2 h 33 min	–57 min
22	31.8	31.6	35.5	1 h 30 min	1 h 28 min	–2 min
22′	29.6	29.5	35	2 h 30 min	2 h 43 min	+13 min
23	30.7	30.7	35.5	1 h 45 min	2 h 1 min	+16 min
23′	30.2	30.1	35.1	2 h 45 min	2 h 20 min	–25 min
24	30.9	30.7	36.7	1 h 30 min	1 h 57 min	+27 min
24′	30	29.9	36.4	2 h 30 min	2 h 28 min	–2 min
25	31.1	31.1	37	2 h 30 min	2 h 47 min	+17 min
25′	29.9	29.8	36.1	3 h 30 min	2 h 31 min	–59 min
26	33.3	33.1	37.2	1 h	45 min	–15 min
26′	30.9	30.8	36.9	2 h	2 h 55 min	+55 min
27	31.2	31.1	36	2 h	1 h 46 min	–14 min
27′	29.7	29.7	35.6	3 h	2 h 37 min	–23 min
28	32.7	32.4	36.5	1 h	1 h 2 min	+2 min
28′	31.3	30.9	36.1	2 h	1 h 47 min	–13 min
29	28.8	28.6	34	2 h 15 min	3 h 19 min	+1 h 14 min
29′	27.7	27.4	33.3	3 h 15 min	4 h 15 min	+1 h
30	33.7	33.5	38	1 h	34 min	–26 min
30′	32.2	32	38	2 h	1 h 16 min	–44 min

$$\text{RMSE} = \sqrt{\frac{\sum_i (TSD_{act,i} - TSD_{pred,i})^2}{N}} = 0.51$$

Note: Ambient temperature was constant (22°C) in all cases.

Abbreviations: *T*1, *T*2—eyeballs temperature, *Tr*—rectal temperature, TSD—time since death in hours/minutes, Δ TSD—difference between actual and predicted TSD in hours/minutes, RMSE—root mean square error, *N*—number of cases.

Source: Kaliszan M, Wujtewicz M. Eye temperature measured after death in human bodies as an alternative method of time of death estimation in the early post mortem period. A successive study on new cases with exactly known time of death. *Leg Med* 2019;**38**:10–13.

Table 6.31 Examples of TSD Calculations Using Henssge Formula Based on Rectal Temperature Measurements in the Early Post-mortem Period (during Plateau Phase) in Standard Conditions: Room Temperature, without Corrective Factor

Rectal temperature, °C	Ambient temperature, °C	Body mass, kg	TSD calculated using Henssge formula [13]
37	22	70	1 h 15 min ± 2.8 h
37	22	90	1 h 36 min ± 2.8 h
36	22	70	3 h 31 min ± 2.8 h
36	22	90	4 h 28 min ± 2.8 h

Source: Kaliszan M, Wujtewicz M. Eye temperature measured after death in human bodies as an alternative method of time of death estimation in the early post mortem period. A successive study on new cases with exactly known time of death. *Leg Med* 2019;**38**:10–13.

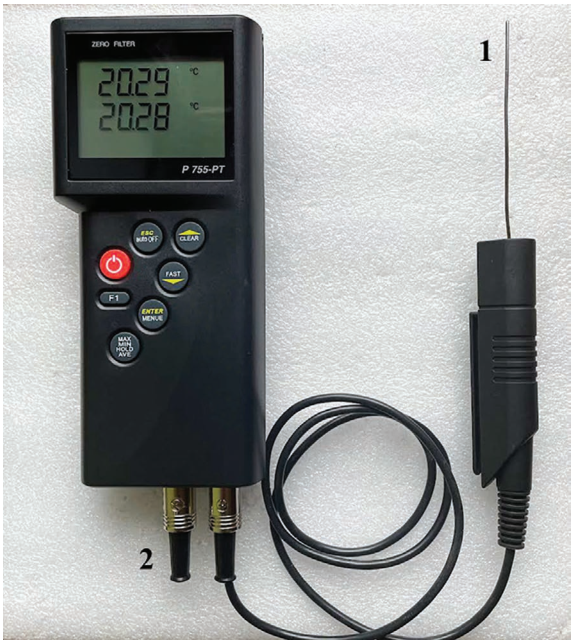

Figure 6.86 The prototype of the TOD-meter with probes: (1) pin probe for eyeball temperature measurement and (2) probe for ambient temperature measurement. The temperature values for both probes are displayed on the thermometer screen.

6.5.3 Limitations of the Method

As in other methods based on body cooling, the proposed method should be used with caution in the case of suspected ambient temperature fluctuation at death scene or lack of possibility of determination of the ambient temperature. The method must not be used in cases of open eyelids or head/face covered with some fabric, that is bedspread, face cuddled in a pillow or exposed to significant heat or cold radiation. The influence of moderate air flow in the room or length of hair on the process of cooling of the eyeball was not confirmed in the studies [4,5,11]. An example of the estimation of the TSD inconsistent with actual one in the case of individual with half-open eyelids after death can be seen in case 4.

6.5.4 Application in Practice

The four examples presented subsequently concern recent cases of death when attending the scene of death by forensic pathologist and the external body examination was required by the public prosecutor. The actual TSD was determined by the witnesses. The temperature measurements and TSD calculations were made personally by the author who was present at the scene and performed the external body examination.

6.5.4.1 Case 1

The body of a 58-year-old man was found at home in the bathroom hanging on a radiator mounted to the wall. He was last seen by his home mate at around 2:00 p.m. when the home mate left the locus. Upon return few minutes past 3:00 p.m. he discovered the body and immediately called 112. The body examination by forensic pathologist was performed and the body temperature was measured at 4:10 p.m. In the rectum it was 36.0°C, in the eyeball it was 32.3°C and the ambient temperature was 25.5°C. There was no rigor mortis present and the lividity was scant on the distal parts of the lower limbs, completely disappearing under pressure. Using Formula 2 [12] the TSD based on the eyeball temperature (32.3°C) was calculated as 1 h 40 min ± 1 h. From the Henssge formula [13] applying rectal temperature (36.0°C), corrective factor considering the body clothing (1.1) and body mass (74 kg), the TSD was calculated as 3 h 38 min ± 2.8 h.

6.5.4.2 Case 2

The body of a 26-year-old man was found at home hanging in the room around 3:30 p.m. by the relative who was alarmed receiving SMS with suicide note at 1:50 p.m. He cut off the ligature and laid the body on the floor, undertaking resuscitation and calling 112. The body examination by forensic pathologist was performed and the body temperature was measured at 5:40 p.m. In the rectum it was 34.6°C, in the eyeballs it was 28.3°C and 28.2°C. The ambient temperature was 22.5°C. There was already significant rigor mortis and the lividity was present on the posterior parts of the body, completely disappearing under pressure. Using Formula 2 [12] the TSD based on the mean eyeballs temperature (28.25°C) was calculated as 3 h 53 min ± 1 h. From the Henssge formula [13] applying rectal temperature (34.6°C), corrective factor considering the body clothing (1.1) and body mass (62 kg), the TSD was calculated as 5 h 54 min ± 2.8 h.

6.5.4.3 Case 3

The body of a 61-year-old man was found hanging in the attic of the family house around 5:30 p.m. by the relatives who were concerned by his prolonged absence after leaving home for a walk around 1:00 p.m. and not returning for a dinner as declared. The ligature was cut off and the body laid on the floor. No resuscitation was undertaken as the body was already stiff. The body examination by forensic pathologist was performed and the body temperature was measured at 7:10 p.m. In the rectum it was 35.4°C, in the eyeball it was 31.5°C. The ambient temperature was 26.4°C. There was intermediately marked rigor mortis and the lividity was present on the posterior parts of the body, completely disappearing under pressure. Using Formula 2 [12] the TSD based on the eyeball temperature (31.5°C) was calculated as 2 h 37 min ± 1 h. From the Henssge formula [13] applying rectal temperature (35.4°C), corrective factor considering the body clothing (1.1) and body mass (93 kg), the TSD was calculated as 6 h 28 min ± 2.8 h.

6.5.4.4 Case 4

A 48-year-old man suddenly collapsed at home what was witnessed by his wife. She immediately called emergency and the ambulance arrived after few minutes. The resuscitation was continued for around 20 minutes but with no effect. The death was confirmed at 1:30 a.m. The body examination by forensic pathologist was performed, during which it was noted that the eyelids are half open. The body temperature was measured at 3:30 a.m. In the rectum it was 35.8°C, in the eyeballs it was 27.6°C and 27.2°C. The ambient temperature was 20.0°C. There was no rigor mortis and the lividity was scant on the posterior parts of the body, completely disappearing under pressure. Using Formula 2 [12] the TSD based on the mean eyeballs temperature (27.4°C) was calculated as 3 h 32 min ± 1 h. From the Henssge formula [13] applying rectal temperature (35.8°C), corrective factor considering the body clothing (1.2) and body mass (76 kg), the TSD was calculated as 4 h 38 min ± 2.8 h.

References

1. Kaliszan M, Hauser R, Kaliszan R, Wiczling P, Buczyński J, Penkowski M. Verification of the exponential model of body temperature decrease after death in pigs. *Exp Physiol* 2005;**90**:727–38.
2. Kaliszan M, Hauser R, Buczyński J, Jankowski Z, Raczyńska K, Kernbach-Wighton G. The potential use of the eye temperature decrease in determining the time of death in the early post mortem period. Studies in pigs. *Am J Forensic Med Pathol* 2010;**31**:162–4.
3. Kaliszan M. First practical applications of eye temperature measurements for estimation of the time of death in casework. Report of three cases. *Forensic Sci Int* 2021;**219**:e13–e15.
4. Kaliszan M. Studies on time of death estimation in the early post mortem period—Application of a method based on eyeball temperature measurement to human bodies. *Leg Med* 2013;**15**:278–82.
5. Madea B. Methods for determining time of death. *Forensic Sci Med Pathol* 2016;**12**:451–85.
6. Henssge C. Death time estimation in case work. I. The rectal temperature time of death nomogram. *Forensic Sci Int* 1988;**38**:125–33.
7. Kaliszan M, Hauser R, Kernbach-Wighton G. Estimation of the time of death based on the assessment of post mortem processes with emphasis on body cooling. *Leg Med* 2009; **11**:111–17.
8. Sanchez I, Martin R, Ussa F, Fernandez-Bueno I. The parameters of the porcine eyeball. *Graefes Arch Clin Exp Ophtalmol* 2011;**249**:475–82.
9. Hubig M, Muggenthaler H, Sinicina I. Body mass and corrective factor: impact on temperature-based death time estimation. *Int J Legal Med* 2011;**125**:437–44.
10. Kaliszan M. Does a draft really influence post mortem body cooling? *J Forensic Sci* 2011;**56**:1310–14.
11. www.structure.mug.edu.pl/85, accessed on January 25th 2023.
12. www.pathguy.com/TimeDead.html, accessed on May 30th 2022.

7 Autolysis, Putrefactive Changes and Post-mortem Chemistry

Burkhard Madea

Contents

7.1 Autolysis (Self-digestion) 189
Burkhard Madea 189

- 7.1.1 Putrefaction 189
  - 7.1.1.1 Chemistry of Putrefaction 190
- 7.1.2 Decomposition 191
  - 7.1.2.1 Period up to Skeletonization 191
- 7.1.3 Animal Predation 192
- 7.1.4 Preservation Processes in Cadavers 192
  - 7.1.4.1 Mummification 192
  - 7.1.4.2 Decomposition of the Body in the Grave—Saponification 193
  - 7.1.4.3 Permafrost Bodies 194
  - 7.1.4.4 Bog Bodies 194
  - 7.1.4.5 Delayed Decomposition in a Zinc Coffin 194
- 7.1.5 Accumulated Degree Days to Estimate the Postmortem Interval from Decomposed Human Remains 194
- 7.1.6 Predicting the Post-mortem Submersion Interval for Human Remains Recovered from Water by Using Decompositional Time Tables Incorporating Accumulated Degree Days 196
  - 7.1.6.1 Decomposition in a Non-sequestered Aquatic Environment in the Mediterranean Sea 198
  - 7.1.6.2 Universal Equation to Estimate Post-mortem Interval 199

7.2a Eye Changes After Death 201
Burkhard Madea and Claus Henssge 201

- 7.2.1 Electrolyte Concentrations in Vitreous Humor 201
  - 7.2.1.1 Loss of Selective Membrane Permeability 201
  - 7.2.1.2 Short Review of the Literature on Vitreous Potassium 202
  - 7.2.1.3 Factors Influencing the Postmortem Rise of Vitreous Potassium 206
  - 7.2.1.4 Search for an Internal Standard of Electrolyte Homeostasis at the Moment of Death 209
  - 7.2.1.5 Urea as an Internal Standard 210
  - 7.2.1.6 Creatinine as an Internal Standard 212
  - 7.2.1.7 Recommendations for Further Studies 212
  - 7.2.1.8 Which Formula Should Be Used in Casework? 214
  - 7.2.1.9 Re-analysis of Original Data and Construction of a Local Regression Model 217
  - 7.2.1.10 Re-evaluation of the Data of Lange and Associates 218
  - 7.2.1.11 Accuracy of Estimating the Time Since Death by Using the Potassium Concentration as Independent Variable 219
- 7.2.2 Hypoxanthine 222
  - 7.2.2.1 Materials and Methods 223
  - 7.2.2.2 Results and Discussion 223

7.2b Potassium Levels Combined with Age and Temperature 229
Brita Zilg

- 7.2b.1 Influence of Ambient Temperature 230
- 7.2b.2 Influence of Decedent Age 230

DOI: 10.1201/9781003244974-7

- 7.2b.3 Influence of Other Factors 231
- 7.2b.4 A Multivariate Model for the Estimation of Time of Death Based on Vitreous Potassium Concentration, Decedent Age and Ambient Temperature 231
- 7.2b.5 Conclusion 232

7.2c Estimation of Time Since Death Based on Vitreous Humour Hypoxanthine and Temperature Measurement 232
Torleiv Ole Rognum *232*

- 7.2c.1 The Background 232
  - 7.2c.1.1 Methods of Measurement of Hypoxanthine (Hx) 234
- 7.2c.2 Algorithms for the Use of Vitreous Humour Hx for PMI 234
  - 7.2c.2.1 Ambient Temperature Is Decisive 234
  - 7.2c.2.2 Multivariable Linear Regression Models for Predicting PMI 235
  - 7.2c.2.3 What Are Normal Vitreous Humour Levels of Hx and K^+? 237
  - 7.2c.2.4 The Use of Vitreous Humour Hx and K^+ in Practical Case Work 237
  - 7.2c.2.5 Guidelines for the Use of Vitreous Humour for Estimation of PMI 238
  - 7.2c.2.6 Conclusion 238

7.3 Cerebrospinal Fluid Chemistry 240
Burkhard Madea and Claus Henssge

7.4 Estimation of Duration of Immersion 245
Elke Doberentz and Burkhard Madea

- 7.4.1 Correlation of Water Temperature and Stages of Putrefaction 246
- 7.4.2 Table for Estimating the Minimum Time Interval of Immersion 247
- 7.4.3 Evaluation of the Data of Reh 251
- 7.4.4 Results 252
- 7.4.5 Discussion 254
- 7.4.6 Conclusions 258
- 7.4.7 Recommended Procedure 258

7.5 H^3-Magnetic Resonance Spectroscopy 259
Frank Musshoff and Burkhard Madea

7.6 Post-mortem Protein Degradation 264
Stefan Pittner and Angela Pittner

- 7.6.1 Basics of Protein Degradation 264
- 7.6.2 Protein Degradation in a Forensic Context 265
- 7.6.3 Methodology 265
  - 7.6.3.1 Immunohistochemistry 265
  - 7.6.3.2 Western Blotting 266
  - 7.6.3.3 Mass Spectrometry 267
  - 7.6.3.4 Other Methods 268
- 7.6.4 Current and Future Challenges 269
  - 7.6.4.1 The Quest of Suitable Target Tissues 269
  - 7.6.4.2 Influencing Factors 274
  - 7.6.4.3 Routine Applicability 274
  - 7.6.4.4 Why It Is Difficult for a Method to Be Incorporated into Practice 275
- 7.6.5 An Attempt for Practical Application 275
  - 7.6.5.1 A Standard Protocol for the Collection and Storage of (Skeletal Muscle) Tissue Samples 276
  - 7.6.5.2 Post-mortem Protein Degradation Profiles 277
  - 7.6.5.3 Case Report 278

The early signs of death (post-mortem lividity, rigor mortis) together with the supravital reactions are of great importance for estimating the time since death. Immediately following the early signs of death, the later post-mortem changes develop, which cannot strictly be separated from the early changes. Later post-mortem changes lead not only to the decomposition of a corpse but also in some cases to its preservation. Endogenous processes resulting in decomposition are autolysis, putrefaction and decay, whereas exogenous factors include animal predation, exposure to the elements and mechanical injury. Late post-mortem changes may appear in chronological order in a cadaver as a result of changes in the surrounding conditions. However, if a corpse is exposed to separate environmental conditions by its position, quite different processes of decay may occur simultaneously.

7.1 Autolysis (Self-digestion)

■ *Burkhard Madea*

Autolysis is defined as the destruction of tissues and organs by their own enzymes. As a result of membrane destruction, the lysosomes discharge hydrolytic enzymes, which are activated by the low pH value in the cytosol: acid phosphatase, acid ribonuclease, acid desoxyribonuclease, cathepsin, collagenase and many other enzymes. They play a decisive role in the self-destruction of cell structures. Organs, such as the pancreas, which are already rich in enzymes during life, are thus subject to very quick cell digestion after death, as are the gastric mucosa and the adrenal medulla. Because of a breakdown of cell membranes with a post-mortem equalization of the concentration of substances that were unequally distributed in the different compartments during life, potassium increases and sodium and chloride concentrations decrease in extracellular fluid after death. As a result of anaerobic glycolysis, lactic acid concentrations rise, whereas pH values fall. Substantial factors in the progression of autolytic changes are the inner milieu of the cadaver at the time of death and the surrounding temperature. As bacteria continuously penetrate the tissues, autolysis is finally superseded by the processes of putrefaction and decomposition.

7.1.1 Putrefaction

Contrary to autolysis, putrefaction is defined as a 'heterolytic' alkaline, colliquative process on a reductive basis caused by bacteria. This extensive chemical process is accompanied by both visual (bloating) and olfactory (foul ammoniacal odours) features resulting from the generation of gases (hydrogen sulphide, hydrocarbons) and the release of ammonia. Bloating is especially seen in tissues with low turgor, such as the eyelids, mouth and tongue, which may become monstrously swollen (Figure 7.1). The abdomen may also be extremely bloated as a result of gas accumulation. The production of gas is the main reason that drowned bodies float to the surface of water after some time. There are intrinsic and extrinsic factors influencing the onset and extent of the post-mortem changes (Table 7.1) [37]. As a result of the build-up of sulph-haemoglobin, the abdominal wall shows greenish discolouration, beginning in the lower right belly (because oxygen is required for the build-up of sulph-haemoglobin). The discolouration may then expand to the entire surface of the body.

The spread of bacteria in the veins of the subcutaneous tissue and haemolysis of red blood cells cause venous marbling of the skin (Figure 7.2). A further

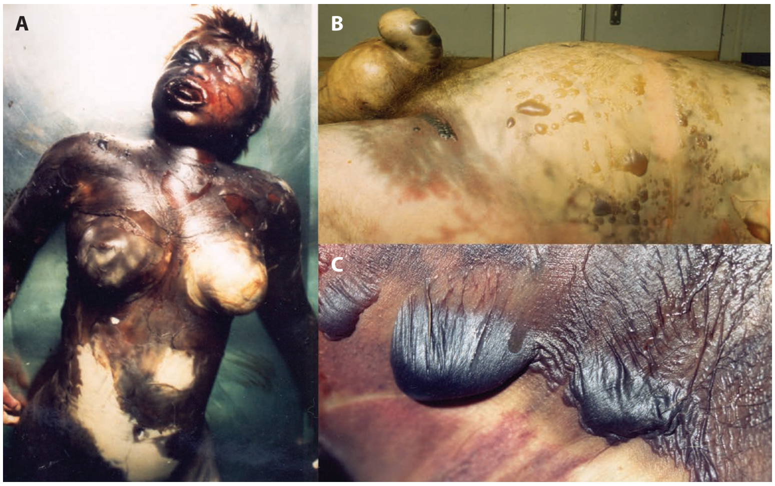

Figure 7.1 Bloating of tissues (A, B), discolouration (A) and putrefactive blisters of the skin (B, C).

Table 7.1 Intrinsic and Extrinsic Factors Influencing Onset and Extent of Post-mortem Changes

Acceleration of onset and extent of post-mortem changes
• Death occurred in a hot, moist environment or under high ambient temperatures.
• Body surface was insulated by warm clothing or other covering.
• Considerable time interval elapsed after death until artefactual cooling of the body.
• Subject was overweight or had a high fat content.
• Subject suffered from or died of underlying infection or sepsis.
• Subject was intoxicated (e.g. with illicit drugs such as heroin).
• Subject suffered from or died of open wounds (perforating/penetrating trauma such as multiple accidental injuries, stab wounds, gunshot wounds, impalement injuries) or during surgical procedures.
Deceleration of onset and extent of post-mortem changes*
• Death occurred in a cold, dry environment or under low ambient temperatures.
• Subject was scantily dressed, naked or undressed shortly after death.
• Subject was stored in a cooling device (refrigerator, freezer) shortly after death.

* These factors slow the speed of post-mortem changes but in general do not alter the underlying post-mortem biological processes.

Source: Data from Tsokos M. Post mortem changes and artefacts during the early post mortem interval. In: Tsokos M (ed.). *Forensic Pathology Reviews*. Totowa, New Jersey, Humana, 2005, pp 183–237.

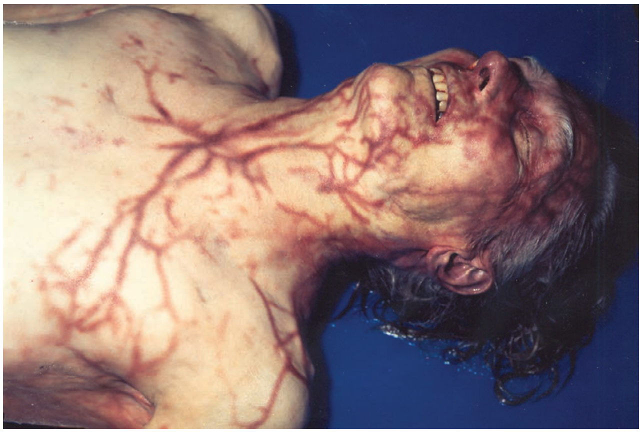

Figure 7.2 Venous marbling.

characteristic of putrefaction is the formation of putrefaction transudates (accumulation of fluids leaking out of the dermis with blister formation). During putrefaction, hair and nails loosen and can easily be dislodged. In the course of putrefaction, liquefaction of fatty tissues finally occurs. Because of the breakdown of proteins, biogenic amines (e.g. putrescine, cadaverine, histamine, choline) may accumulate, as well as cadaveric alkaloids, referred to as ptomaines ('cadaveric poisons'). However, although ptomaines have muscarinic atropine-like effects, they are not 'toxic'. During bacterial proteolysis, certain amino acids such as delta-aminovaleric acid or gamma-aminobutyric acid can be found in the brain and liver and may be used to make a rough estimate of the time elapsed since death. Further changes arising from gas accumulation are the formation of so-called foam organs and the discharge of putrefactive fluids from the mouth, nose, anus and genitals. In pregnant women, the pressure from putrefactive gas may cause the fetus to be expelled through the genitalia, a phenomenon known by the term 'coffin birth'. The progression of putrefaction even in a constant ambient temperature is so variable that no conclusion can be drawn about the time of death (Table 7.2) [4]. Table 7.2 gives only rough indications for the sequence of putrefactive changes in cadavers exposed above ground at relatively narrow ranges of temperatures (Table 7.3 gives indications of putrefaction in bodies exposed to air) [22]. A rule of thumb that goes back to the Berlin forensic physician Johann Ludwig Casper (1796–1864)—named Casper's rule—says that 1 week in air equals 2 weeks in water equals 8 weeks buried in the ground [7]. Casper's rule thus relates the decomposition process to different environmental conditions (air, water, earth), but does not allow a precise determination of time of death.

7.1.1.1 Chemistry of Putrefaction

Putrefaction is a bacterial process that starts with the normal microbial flora of the skin and the mucous membranes. Of particular importance are streptococci and various species of *Proteus*, whose flagellant motility enables these bacteria to spread quickly over an organism. Catabolic putrefying processes comprise proteins, carbohydrates and lipids. Protein breakdowns yield amino acids, which are then either de-aminated into their corresponding acids or decarboxylated into analogous amines by which the end products ammonia and carbon dioxide are created. The aromatic amino acids phenylalanine, tyrosine and tryptophan yield p-cresol, phenol, skatole and indole, which have been identified as main olfactory components of putrefaction. By anaerobic glycolysis, one

Table 7.2 Morphological Changes in the Putrefaction Phase: Aboveground Exposure at 20°C to 24°C (68°F to 75°F) without Insect Infestation*

Indication	Interval after death
Initial greenish discolouration on abdominal skin.	1–2 days
Cutaneous venous marbling.	2–4 days
Beginning of film-like slippage of the epidermis.	5–6 days
Loss of pigmentation in the stratum germinativum.	6–8 days
Putrefactive blisters and putrefactive transudates in the body cavities.	8–14 days
Putrefactive emphysema in the subcutis.	8–14 days
Bloating of abdominal cavities.	8–14 days
Diffusion of all fluids, collapse of organs.	Usually not until months later
Beginning of mummification with dehydration of soft tissues.	Usually not until months later

* This table gives only rough indications for the sequence of putrefaction effects in cadavers exposed above ground at a relatively narrow range of temperature. Numerous variations are possible, depending on the body's build, the underlying surface, coverings, terminal illness and other factors.

Table 7.3 Progression of the Putrefaction of Bodies in Air, at a Temperature of about 20°C

Interval after death	Indication
1–2 days	Green discolouration of abdominal wall; softening of eyeballs.
3–5 days	Dark green discolouration of large parts of the abdominal wall; some patchy green discolourations of the skin of other body regions; haemorrhagic fluid leaking out from mouth and nostrils; marbling.
8–12 days	Whole body surface dark green; face, neck and thoracic wall partly reddish green; bloating of abdomen, scrotum and face; fingernails still fixed; hair loose, beginning to peel.
14–20 days	Whole body green or reddish brownish; bloating of the whole body; blisters, partly filled with putrefactive fluid, partly bursting with desiccation of the dermis; eyes (iris, pupils, sclerae) red-brown discolouration; fingernails peeling.

Source: Data from Naeve, cited in Madea B. *Die Ärztliche Leichenschau*. 2nd ed. Berlin, Springer, 2006.

molecule of glucose yields two molecules of lactic acid. Various bacteria, among them clostridia, may, through alcohol fermentation, break down monosaccharides into alcohol to create those typical putrefactive alcohols in the cadaver. Lipids are broken down by hydrolases, esterases and catalases into their components [3,6,19,20,21]. Even putrefied bodies may be preserved very well under special circumstances, especially when they are hermetically submerged or when decomposition is interrupted or at least considerably delayed by wrapping the body or parts of the body in plastic bags or vinyl (Figure 7.3). Experimental investigations on the influence of vinyl materials on post-mortem alterations in rabbit and mice cadavers kept in plastic bags of different air volumes (3 litres/5 pints, 1 litre/1 3/4 pints, no air) at room temperature resulted in clearly delayed decomposition of these cadavers, with the volume of air within the bag clearly of greatest importance for the progression of putrefaction.

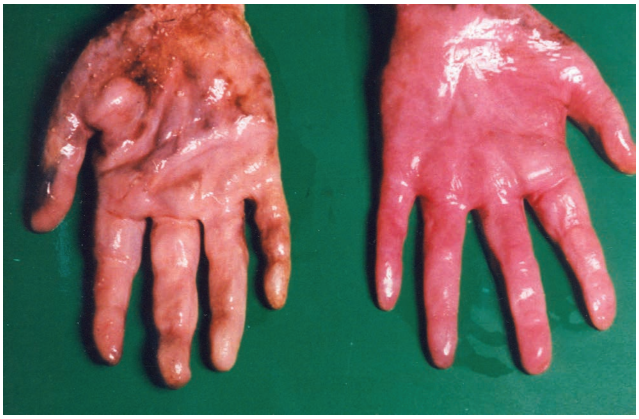

Figure 7.3 Hands of a homicide victim 2 years after the murder. The body was wrapped in several plastic bags. Although the epidermis is completely lost, dactyloscopic identification was possible.

7.1.2 Decomposition

Although putrefaction is a mainly anaerobic bacterial reduction process, decomposition is dominated by aerobic microbiological processes that may create pungent, rotten odours originating from the metabolic products of oxidation. Decomposition is a dry, acidic process on an oxidative basis, which leads to the splitting off of acids (carbonic acid, phosphoric acid, sulphuric acid). At the beginning of decomposition, large patches of fungus may form on the skin and mucous membranes (Figure 7.4).

7.1.2.1 Period up to Skeletonization

The period up to skeletonization shows great variability, depending on the storage conditions of the body. This concept is expressed by Casper's rule (defined earlier), which says that a cadaver lying on the ground decomposes more quickly than one lying in water or underground, although the ratios Casper gave are certainly also subject to numerous varying conditions. Corpses lying on the surface of the ground are, as a rule, skeletonized within 1 year, and after 2

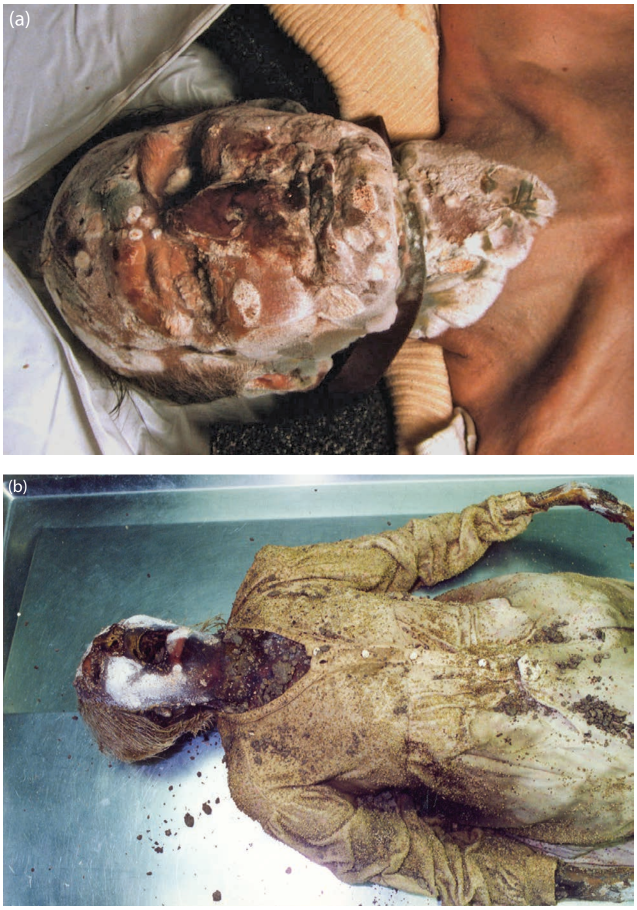

Figure 7.4 (a) Decomposition with patches of fungus on the face. (b) Advanced decomposition after exhumation with fungus patches on the skin.

years the bones are completely free of soft tissues. A considerable proportion of soft part reduction during the summer months results from maggot infestation and animal predation. Under such conditions, a cadaver can be completely skeletonized within a few weeks (Figure 7.5). In the case of a body lying underground, the time required for skeletonization essentially depends on the composition of the soil. Under normal conditions, in a usually water-permeable, aerated soil at a depth between 1 and 2 m (3 feet 3 inches to 6 feet 6 inches), about 5–7 years are needed until skeletonization is complete, although considerably longer periods can also be observed. In warmer climates, the period needed for skeletonization to occur is normally shorter. Results of exhumations in the past few years indicated, however, that even after burial periods of 5–7 years, some bodies, in addition to clothing, were often found to be well preserved; in some cases, the internal organs including the gastrointestinal tract were still intact. Bodies buried in crypts or sarcophagi may undergo mummification (see later). Special conditions apply to burials in mass graves. Even if many bodies are buried together at the same time, each body may display quite different degrees of decomposition; bodies lying on the periphery are usually extensively decomposed, whereas bodies lying more in the centre may display good preservation of soft tissues with pronounced grave wax formation. The bones of bodies lying above ground are, as a rule, completely skeletonized after 1–2 years; they show no remnants of soft tissues and no traces of cartilages or tendons. Remnants of soft tissues may still be found up to the second decade after burial in inhumed bodies, more rarely after the third or fourth decade. Remains of clothing may be preserved even longer [3,4,5,20,21].

7.1.3 Animal Predation

In the very early post-mortem interval (PMI), there may already be traces of animal predation, not only from rats or mice, or—in water—crabs and fish, but also from dogs and cats. Mice typically gnaw away the epidermis and leave characteristic gnawing marks (Figure 7.6).

Large areas of soft tissue damage may be caused, particularly by dogs. This damage can be explained by the dog's wish to provoke a reaction from its lifeless owner, first by licking the face, and then, when there is no result, behaving instinctively, by biting and later mutilating the owner.

7.1.4 Preservation Processes in Cadavers

Although autolysis, putrefaction and decomposition lead to dissolution and disintegration of the body down to its bones and tendons, the body may be preserved under special environmental conditions. Such preservation processes include mummification and adipocere formation. Preservation of the body can also be found in bog bodies and permafrost bodies.

7.1.4.1 Mummification

Mummification usually occurs when the water of the body's tissues evaporates in response to dryness of the environment and good ventilation. Mummification through natural processes may occur in bodies buried in churches or crypts (e.g. the lead cellar of Bremen Cathedral in Germany), but it is also seen in bodies that have lain at home, indoors, for some time before being discovered. Through mummification, the skin dries out into a hard, leathery state. The dehydration sometimes causes the body to be fixed in the position it was assumed to have been in at the onset of death (Figure 7.7). Furthermore, there is substantial weight loss as a result of desiccation and shrinking of tissues. It is especially a rapid loss of water that contributes to mummification, such as occurs by storage in dry, drafty air or on a warm and dry ground (Figure 7.8). Mummification leading to a leather-like, hard stiffening of the skin may, under appropriate

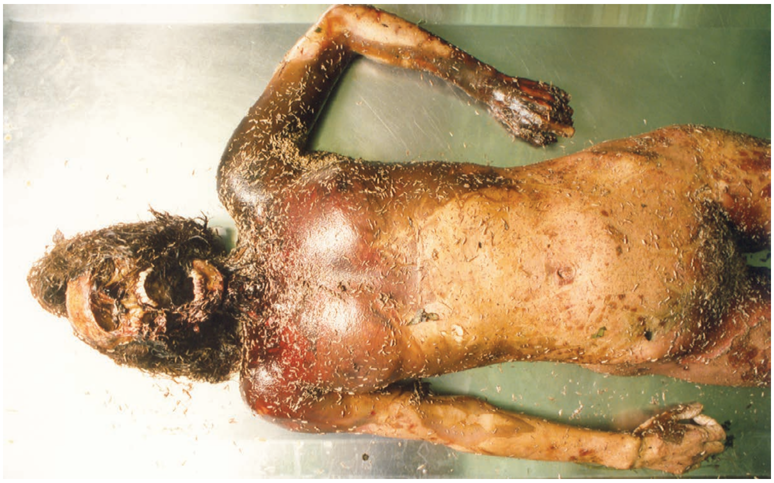

Figure 7.5 Advanced skeletonization of the skull after 1 week of lying on the surface in the wood in summer.

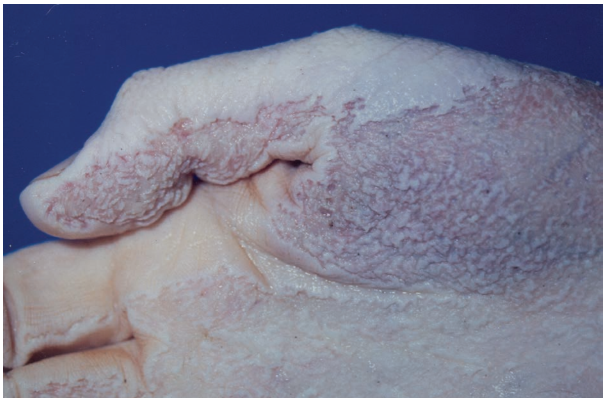

Figure 7.6 Gnawing marks in the epidermis of the hands by mice.

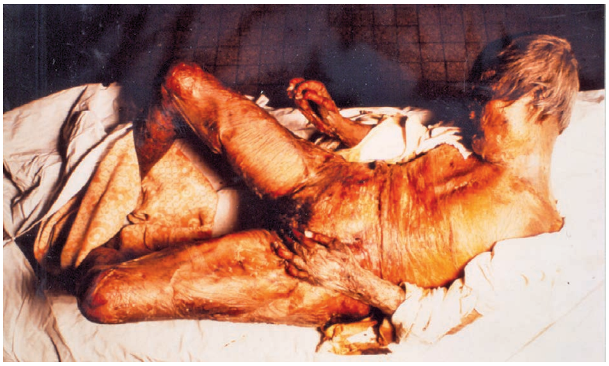

Figure 7.7 Mummification of a body in a fixed position. The man was lying on the couch of his apartment for half a year after death while doors and windows were open (in autumn and winter).

environmental conditions, commence relatively quickly (after 2–3 days), starting at the extremities (fingers, tips of nose and chin, ears, skin over the cheekbones); pronounced mummification, however, as a rule, is not detectable until after several weeks [1,3,5,10,15,20,21].

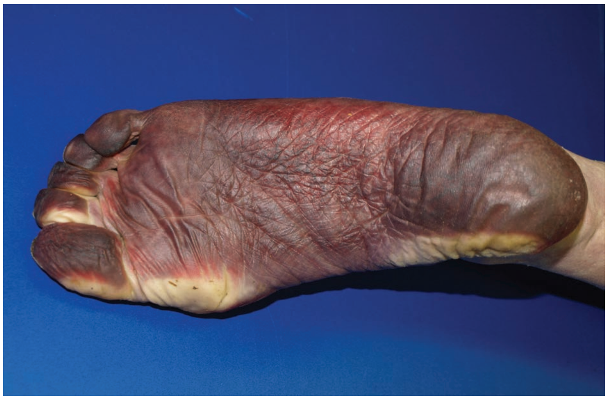

Figure 7.8 Mummification of a whole foot sole within 3 days after death.

7.1.4.2 Decomposition of the Body in the Grave—Saponification

A body buried in soil should be reduced to a skeleton after 15–20 years, at the latest. As is well known, skeletons may remain preserved for a much longer period of time (several centuries). Whether a corpse has largely decomposed within this time, however, also depends on the properties of the soil—its mineral composition and aeration—and on groundwater conditions. For these reasons, only those sites that have appropriate soil should be used for cemeteries. Examples of unsuitable sites are grounds in which the coffins are actually lying in groundwater or where the zone of decay constantly or temporarily contains groundwater and areas subject to flooding by bodies of water in public use. Nevertheless, under such conditions, a particular preservation process known as saponification—the formation of adipocere, or grave wax—may occur. Saponification can be observed in bodies that have lain in a completely or partially hermetic damp environment (e.g. water corpses and corpses in damp graves). During the formation of adipocere, unsaturated fats (oleic acids) are converted into saturated fats (palmitic and stearic acids). Saponification begins in the skin after about 6 weeks and in muscles after around 3–4 months. Entire extremities may be converted into adipocere, although this requires several months to years (Figure 7.9). The term 'adipocere' (*adeps*, fat; *cera*, wax) goes back to Fourcroy (1789) and Thouret (1792), who, during the closure of a cemetery in Paris, noticed that the bodies buried there, some of them in groups, had not 'wasted away', but had been preserved in the same characteristic way.

The German word *Fettwachs* ('fat wax') is still commonly used, although the substance contains neither fats (glycerin esters of higher fatty acids) nor waxes (esters between long-chain fatty acids and univalent alcohols), but instead contains higher fatty acids with C-chain lengths between 12 and 20. Macroscopically, fatty tissues are first converted into a greyish-white greasy mass, which later shows a waxy consistency. As a rule, adipocere begins to form in warmer water after around 1–2 months. The final state may result in conversion of soft body tissues into a hard shell of adipocere; if this happens in a limb, the central long bone sits loosely, such as in a tube of grave wax. For an entire body to convert into an adipocere corpse may take more than a year; its final state is also called a 'plaster corpse' because of its crumbly, hard consistency [11,16,22–24,20,21,27,29,31,32].

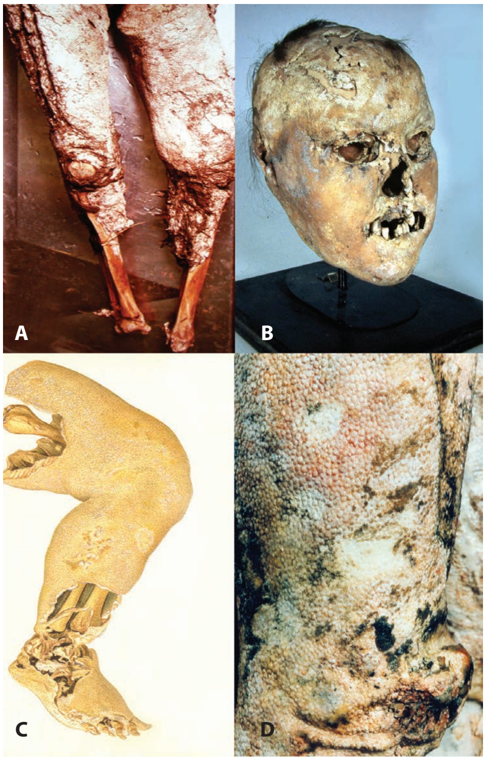

Figure 7.9 Saponification. (a) Soft tissues of the thighs were converted into hard shells of adipocere with the long bones hanging loosely. (b) Saponification of the head. (c) The leg of a newborn child, with saponification; after lying in flowing water for several months, the outer shapes of the legs were preserved; the chalk-like brittle mass, which looks like a stiff tube, contains loose bones. The muscles are missing. (d) The texture of the fat nodules in the subcutaneous fatty tissue was fixed by adipocere formation (état mamelonné).

7.1.4.3 Permafrost Bodies

Extensive body preservation may also be observed in permanently frozen ground. Permafrost bodies have been found in northern Canada (e.g. in the early 1980s). The bodies in question had been members of the Franklin expedition in the 1840s. The cadaver found in the Hauslabjoch area of the Italian Alps ('Ötzi') is a famous frozen body from central Europe [2,12,14,15,20,21,34–36].

7.1.4.4 Bog Bodies

In bog bodies, the effects of humic acid include bone demineralization, the tanning of soft tissues and a typical reddish dying of the hair. Because of the preservation of the body surfaces of bog corpses, it is often possible to collect significant evidence of the circumstances of death and the cause of death. Along with the presence of tannin and humic acid, a third important factor is the oxygen-poor peaty soil, which suppresses putrefaction processes and thus contributes to the good preservation of bog bodies [30,38,40,41].

7.1.4.5 Delayed Decomposition in a Zinc Coffin

As in plastic bags, plastic tubes, decomposition may be delayed due to the lack of oxygen also in zinc coffins [26,33].

Zinc coffins were used for burial especially by Sovereigns, for instance the Medici Dynasty in Florence or the Habsburg Dynasty in Vienna.

Zinc coffins were used in Europe in the last centuries also when a body had to be transported from one country to another. We had recently to investigate the case were on the cemetery exhumations were carried out. During one exhumation a zinc coffin was opened and a very well-preserved body was found. At first it was assumed due to the well preservation of the body, that the man had recently been buried. However, he has died about 40 years ago in a traffic accident in a neighbour country and was transported in a zinc coffin from Belgium to Germany and buried there in this zinc coffin. Müller (1913) has already described similar observations [26].

7.1.5 Accumulated Degree Days to Estimate the Postmortem Interval from Decomposed Human Remains

Megyesi et al. [25] attempted to estimate the PMI from decomposed human remains by using accumulated degree days (ADDs). Because soft tissue decomposition is a sequential process with numerous small changes

Table 7.4 Categories and Stages of Decomposition of the Head and Neck

A. Fresh	
1 point	1. Fresh, no discolouration.
B. Early decomposition	
2 points	1. Pink-white appearance with skin slippage and some hair loss.
3 points	2. Grey to green discolouration; some flesh still relatively fresh.
4 points	3. Discolouration and/or brownish shades, particularly at edges; drying of nose, ears and lips.
5 points	4. Purging of decompositional fluids out of eyes, ears, nose and mouth; some possible bloating of neck and face.
6 points	5. Brown to black discolouration of flesh.
C. Advanced decomposition	
7 points	1. Caving in of flesh and tissues of eyes and throat.
8 points	2. Moist decomposition with bone exposure less than one half that of the area being scored.
9 points	3. Mummification with bone exposure less than one half that of the area being scored.
D. Skeletonization	
10 points	1. Bone exposure of more than half of the area being scored with greasy substances and decomposed tissue.
11 points	2. Bone exposure of more than half the area being scored with desiccated or mummified tissue.
12 points	3. Bones largely dry, but retaining some grease.
13 points	4. Dry bone.

Source: Data from Megyesi MS, Nawrocki SP, Haskell NH. Using accumulated degree-days to estimate the postmortem interval from decomposed human remains. *J Forensic Sci* 2005;**50**(3):618–626.

Table 7.5 Categories and Stages of Decomposition of the Trunk

A. Fresh	
1 point	1. Fresh; no discolouration.
B. Early decomposition	
2 points	1. Pink-white appearance with skin slippage and marbling present
3 points	2. Grey to green discolouration; some flesh still relatively fresh.
4 points	3. Bloating with green discolouration and purging of decomposition fluids.
5 points	4. After bloating, following release of abdominal gases, with discolouration changing from green to black.
C. Advanced decomposition	
6 points	1. Decomposition of tissue producing sagging of flesh; caving in of the abdominal cavity.
7 points	2. Moist decomposition with bone exposure less than one half that of the area being scored.
8 points	3. Mummification with bone exposure less than one half that of the area being scored.
D. Skeletonization	
9 points	1. Bones with decomposed tissue, sometimes with body fluids and grease still present.
10 points	2. Bones with desiccated or mummified tissue covering less than one half of the area being scored.
11 points	3. Bones largely dry, but retaining some grease.
12 points	4. Dry bone.

Source: Data from Megyesi MS, Nawrocki SP, Haskell NH. Using accumulated degree-days to estimate the postmortem interval from decomposed human remains. *J Forensic Sci* 2005;**50**(3):618–626.

occurring throughout, these investigators scored decomposition in three specific areas of the body:

1. The head and neck, including the cervical vertebrae.
2. The trunk, including the thorax, pectoral girdle, abdomen and pelvis.
3. The limbs, including the hands and feet (Tables 7.4–7.6).

Tables 7.4–7.6 define the categories and stages of decomposition for each of the anatomical regions along with the assigned point value [25].

The stages of decomposition were slightly different for each of the three anatomical areas.

The scores of each of the three anatomical regions are combined to produce a total body score (TBS). The TBS for the cases reported by Megyesi et al. [25] ($n = 68$) ranged from 3 (fresh) to 53 (dry bones).

The ADDs were calculated as follows: all average daily temperatures above 0°C for all days from death and discovery were summed up. Temperatures below 0°C were always recorded as zero, because freezing temperatures severely inhibit biological processes. The TBS range of the investigated cases is shown in Table 7.7 [25]. The ADDs for all cases ranged from 27.1 to 3320.9, with a mean of 439.01 degree days.

By log-transforming both ADDs and PMI and by squaring TBS, an effective linear regression can be produced (Figures 7.10 and 7.11).

To predict the time of death for a new forensic case, one would first calculate the TBS for the individual by using the scoring strategy. Using several equations derived from the statistical analysis of their material, the time of death can be calculated together with 95 per cent confidence limits. The conclusion of the authors is that methods for determining the PMI from decomposition that take into account the temperature experienced after death produce more accurate estimates of the time of death than do methods that ignore accumulated temperatures. The proposed decomposition scoring system should be used cautiously

Table 7.6 Categories and Stages of Decomposition of the Limbs

A. Fresh	
1 point	1. Fresh, no discolouration.
B. Early decomposition	
2 points	1. Pink-white appearance with skin slippage of hands and/or feet.
3 points	2. Grey to green discolouration; marbling; some flesh still relatively fresh.
4 points	3. Discolouration and/or brownish shades, particularly at edges; drying of fingers, toes and other projecting extremities.
5 points	4. Brown to black discolouration; leathery appearance of skin.
C. Advanced decomposition	
6 points	1. Moist decomposition with bone exposure less than one half that of the area being scored.
7 points	2. Mummification with bone exposure of less than one half that of the area being scored.
D. Skeletonization	
8 points	1. Bone exposure over one half the area being scored; some decomposed tissue and body fluids remaining.
9 points	2. Bones largely dry, but retaining some grease.
10 points	3. Dry bone.

Source: Data from Megyesi MS, Nawrocki SP, Haskell NH. Using accumulated degree-days to estimate the postmortem interval from decomposed human remains. *J Forensic Sci* 2005;**50**(3):618–626.

only on complete adult-sized remains that have not been burned, buried or submerged. The pilot study found that more than 80 per cent of the observed variation in human decomposition could be accounted for by the combination of elapsed time and temperature as it is reflected in ADDs. The proposed method should be further investigated not only by anthropologists but also within a forensic context.

7.1.6 Predicting the Post-mortem Submersion Interval for Human Remains Recovered from Water by Using Decompositional Time Tables Incorporating Accumulated Degree Days

As long known, bodies decomposing in water show soft tissue modifications similar to those of bodies decomposing on land (see also Chapter 7.4). However, the visual markers appear at different time intervals, mainly because of ambient temperatures. For bodies decomposing on land, Megyesi et al. [25] developed an equation for calculating ADDs. This system measures a process of decomposition as the summation of progressive numerical scores (i.e. TBS), based on the appearance of three separate regions: the head, the trunk and the limbs.

Table 7.7 Characteristics of Decomposition and Corresponding Total Body Score Range

Decomposition characteristics	Total body score range
Purging from facial orifices.	8–13 ($n = 19$)
Bone exposure of head less than one half.	14–26 ($n = 34$)
Bloating of abdomen.	11–19 ($n = 34$)
Bone exposure of thorax.	20–35 ($n = 24$)
Bone exposure of limbs.	21–35 ($n = 22$)

Source: Data from Megyesi MS, Nawrocki SP, Haskell NH. Using accumulated degree-days to estimate the postmortem interval from decomposed human remains. *J Forensic Sci* 2005;**50**(3):618–626.

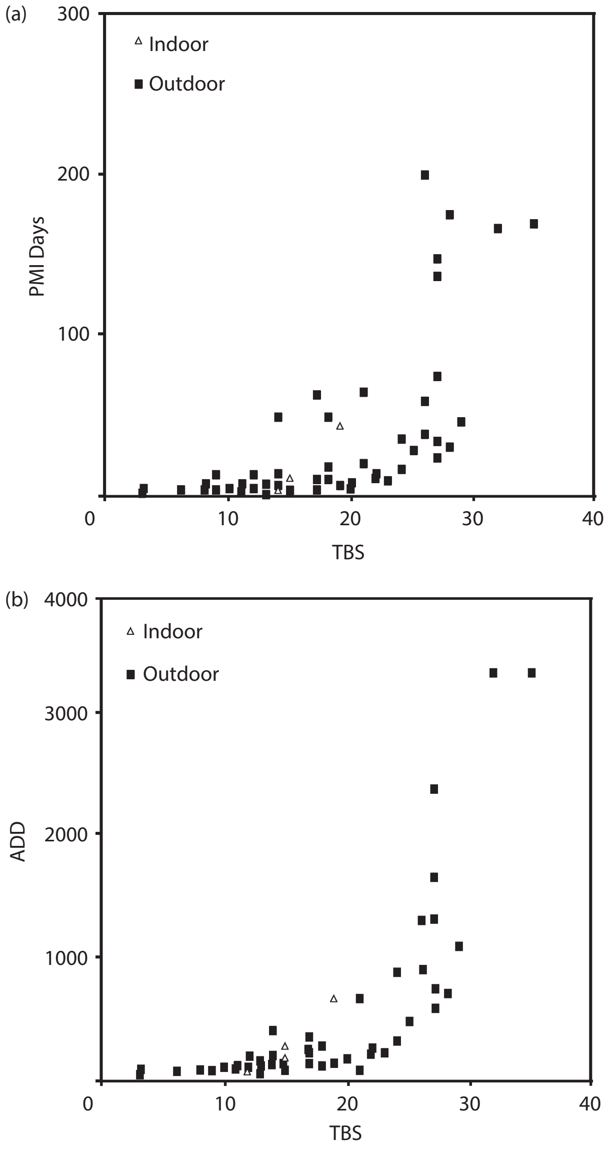

Figure 7.10 (a) Scatter of post-mortem interval (PMI) versus total body score (TBS) ($n = 68$). (b) Scatter plot of accumulated degree days (ADD) versus TBS ($n = 68$).

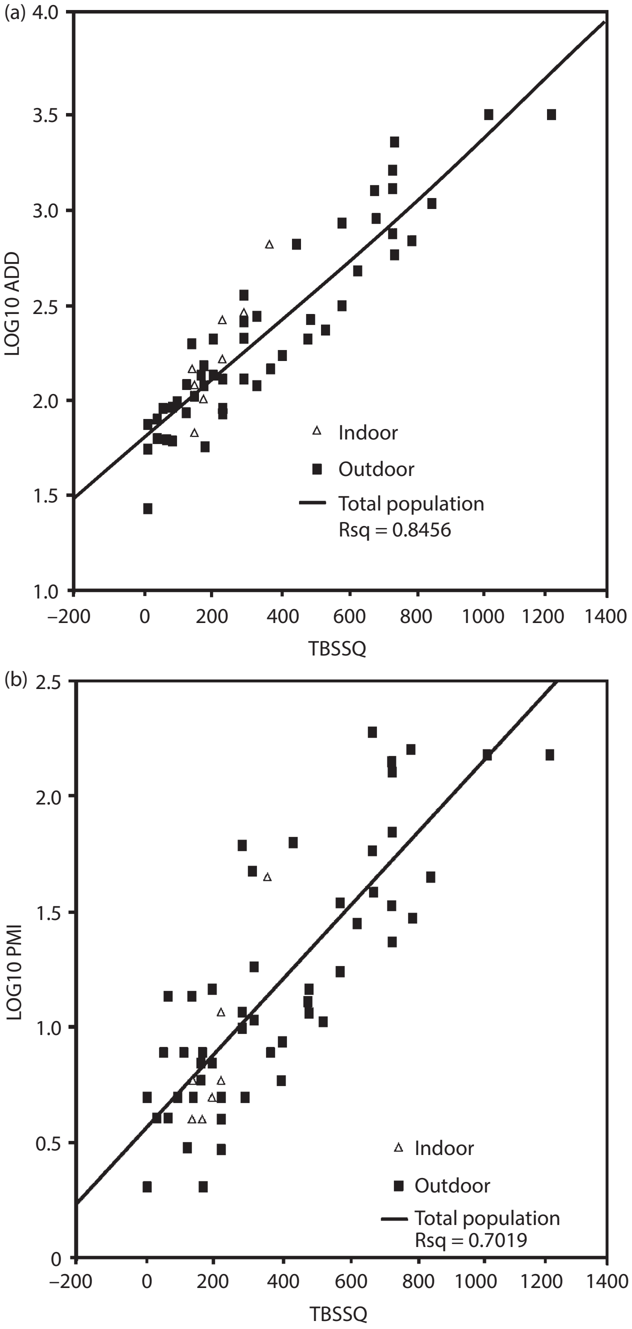

Figure 7.11 (a) LOG10-transformed post-mortem interval (PMI) versus total body score squared (TBSSQ) with a regression ($n = 66$). (b) LOG10-transformed accumulated degree days (ADD) versus TBSSQ with a regression ($n = 66$).

Table 7.8 Descriptive Stages for Decomposition Observed in the Face and the Assigned Facial Aquatic Decomposition Score

FADS	Description
1	No visible changes.
2	Slight pink discolouration, darkened lips, goose pimpling.
3	Reddening of face and neck, marbling visible on face; possible early signs of animal activity or predation concentrated on the ears, nose and lips.
4	Bloating of the face, green discolouration, skin beginning to slough off.
5	Head hair beginning to slough off, mostly at the front; brain softening and liquefaction; tissue becoming exposed on face and neck; green-black discolouration.
6	Bones becoming exposed, concentrated over the orbital, frontal and parietal regions, with some exposure of the mandible and maxilla; early adipocere formation.
7	More extensive skeletonization on the cranium; disarticulation of the mandible.
8	Complete disarticulation of the skull from the torso; extensive adipocere formation.

Abbreviation: FADS, facial aquatic decomposition score.

Source: From Heaton V, Lagden A, Moffatt C, Simmons T. Predicting the postmortem submersion interval for human remains recovered from U.K. waterways. *J Forensic Sci* 2010;**55**(2):302–307.

Table 7.9 Descriptive Stages for Decomposition Observed on the Torso and the Assigned Body Aquatic Decomposition Score

BADS	Description
1	No visible changes.
2	Slight pink discolouration, goose pimpling.
3	Yellow-green discolouration of abdomen and upper chest; marbling; initiation in internal organs of decomposition and autolysis.
4	Dark green discolouration of abdomen, mild bloating of abdomen, initial skin slippage.
5	Green-purple discolouration; extensive abdominal bloating, tense to touch; swollen scrotum in males; exposure of underlying fat and tissues.
6	Black discolouration; bloating becoming softer; initial exposure of internal organs and bones.
7	Further loss of tissues and organs; more bone exposed; initial adipocere formation.
8	Complete skeletonization and disarticulation.

Abbreviation: BADS, body aquatic decomposition score.

Source: From Heaton V, Lagden A, Moffatt C, Simmons T. Predicting the postmortem submersion interval for human remains recovered from U.K. waterways. *J Forensic Sci* 2010;**55**(2):302–307.

Heaton et al. [13] assessed and scored post-mortem decomposition by using described stages of decomposition observed on the head, the torso and the limbs (Tables 7.8–7.10). Eight stages of decomposition were identified for both the face (FADS) and the body (BADS), and nine stages were identified for the limbs (LADS). Thus, a total aquatic decomposition score (TADS) of 25 can be produced. From the 148 cases studied, TADS scores ranging from a score of 3 (no apparent decomposition) to 25 (complete decomposition—skeletonization and disarticulation) were calculated. The ADDs were calculated for 144 cases by summarizing the average temperatures for each 24-hour-period for the number of days that made up the post-mortem submersion interval (PMSI).

$$\text{ADD} = \sum \text{Average daily temperature} \\ \text{(degrees Celsius) for the entire PMSI}$$

Table 7.10 Descriptive Stages for Decomposition Observed in the Limbs and the Assigned Limb Aquatic Decomposition Score

LADS	Description
1	No visible changes.
2	Mild wrinkling of skin on hands and/or feet, possible goose pimpling.
3	Skin on palms of hands and/or soles of feet becoming white, wrinkled and thickened; slight pink discolouration of arms and legs.
4	Skin on palms of hands and/or soles of feet becoming soggy and loose; marbling of the limbs, predominantly on upper arms and legs.
5	Skin on hands/feet starting to slough off; yellow-green to green-black discolouration on arms and/or legs; initial skin slippage on arms and/or legs.
6	Degloving of hands and/or feet, exposing large areas of underlying muscles and tendons; patchy sloughing of skin on arms and/or legs.
7	Exposure of bones of hands and/or feet; muscles, tendons and small areas of bone exposed in lower arms and/or legs.
8	Bones of hands and/or feet beginning to disarticulate; bones of upper arms and/or legs becoming exposed.
9	Complete skeletonization and disarticulation of limbs.

Abbreviation: LADS, limb aquatic decomposition score.

Source: From Heaton V, Lagden A, Moffatt C, Simmons T. Predicting the postmortem submersion interval for human remains recovered from U.K. waterways. *J Forensic Sci* 2010;**55**(2):302–307.

The values for ADD ranged from 0.04 to 2151. There is an almost linear correlation between the TADS and the log ADD (Figure 7.12).

ADDs have a significant and essentially identical correlation with decomposition at each of the study sites. Bodies in water for a prolonged length of time at cooler temperatures and those subjected to warmer temperatures for a shorter time showed similar rates of decomposition.

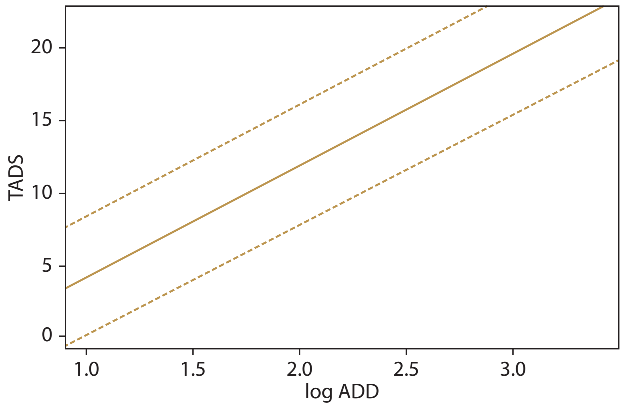

Figure 7.12 95 per cent confidence intervals around the regression slope as predicted by the model. Predicting the post-mortem submersion interval for human remains recovered from UK waterways. ADD, accumulated degree days; TADS, total aquatic decomposition score.

Table 7.11 Total Aquatic Decomposition Score and the Predicted Accumulated Degree Days and Confidence Intervals, Back Transformed from the Logarithmic Model

TADS	Predicted ADDs	Lower 95% confidence interval	Upper 95% confidence interval
5	13.16	3.550	45.88
6	17.70	4.825	61.52
7	23.79	6.552	82.58
8	31.99	8.889	110.9
9	43.01	12.05	149.2
10	57.83	16.31	200.8
11	77.76	22.07	270.5
12	104.5	29.82	364.9
13	140.6	40.26	492.6
14	189.0	54.31	665.6
15	254.1	73.18	900.3
16	341.7	98.51	1219
17	459.4	132.5	1652
18	617.7	178.0	2241
19	830.5	238.9	3043
20	1117	320.4	4135
21	1501	429.3	5625
22	2019	574.7	7659
23	2714	768.6	10 437
24	3649	1027	14 235
25	4906	1371	19 432

Abbreviation: ADDs, accumulated degree days; TADS, total aquatic decompositional score.

Source: From Heaton V, Lagden A, Moffatt C, Simmons T. Predicting the postmortem submersion interval for human remains recovered from U.K. waterways. *J Forensic Sci* 2010;**55**(2):302–307.

Once ADDs have been predicted from the TADS, the PMSI can be inferred by summarizing the average daily temperatures from the date the body was recovered retrospectively until the estimated ADD value is reached. This should indicate the time frame in which the body entered the water. Table 7.11 presents calculated predictions as confidence intervals for all values of TADS between 5 and 25 [13].

7.1.6.1 Decomposition in a Non-sequestered Aquatic Environment in the Mediterranean Sea

Starting from the work of Heaton et al. further studies provided descriptive stages and scoring methods to assess the post-mortem decay in open marine environments for the practical application of the PMSI estimation.

The decomposition rate of head/neck, trunk and limbs according to the decomposition scoring system developed by Heaton et al. and modified by De Donno et al. proved to be of great help in practice, especially in cases of drowned victims (migrants) in the Mediterranean Sea.

7.1.6.2 Universal Equation to Estimate Post-mortem Interval

Vass [39] has proposed that two simple formulas based on the level of decomposition, humidity and temperature could be used to accurately calculate the PMI for bodies outside (on or under the surface worldwide).

Formula I ($PMI_{Aerobic}$)—describes above ground (aerobic) human decomposition and is used to estimate the post-mortem interval. Result is in days.

$$PMI_{Aerobic} = \frac{1285 \cdot \times \cdot (\text{decomposition}/100) \cdot \cdot}{0.0103 \cdot \times \cdot \text{temperature} \cdot \times \cdot \text{humidity}}$$

where:

1285 is a constant, representing the empirically determined ADD value at which volatile fatty acid (VFA) liberation from soft tissue ceases.

decomposition is a single value, or range, between 1 and 100, representing the best estimation of the extent of a total body soft tissue decomposition.

0.0103 is a constant, representing an empirically determined measure of the effect of moisture on decompositional rates.

temperature is the value in degrees Celsius (°C) of either the average temperature at the site on the day the corpse was discovered or the average temperature over a period of time.

humidity is a value between 1 and 100, representing either the average humidity at the site on the day the corpse as discovered or the average humidity over a period of time.

Formula I requirements:

- Corpse found above ground (aerobic decomposition).
- Corpse must be in pre-skeletonization phase (≤1285 ADD).
- Soft tissue present—if mummified, the tissue must be soft and pliable.
- Corpse must be at least 1 day old.
- Corpse should be fairly intact (damage from large carnivores, dismemberment, etc. could affect the results).
- Must estimate the percentage of soft tissue decomposition that has occurred.
- Temperature must be above 0°C.
- Average temperatures (0°) and humidity ideally should be corrected for the discovery site.
- Little to no adipocere formation on the corpse.

A study by Cockle and Bell [8] attempted to validate Formula I proposed by Vass using 42 Canadian cases with known PMIs between 2 days and nearly 400 days.

The results indicated that bodies exposed to warm temperatures consistently overestimated the known PMI by a large and inconsistent margin for formula one estimations. For bodies exposed to cold and freezing temperatures (less than 4°C), the PMI was dramatically underestimated (Figure 7.13). The authors concluded that neither the universal formula performed well, and the results do not support the preposition of universality for PMI estimation.

Another validation study from cases from different locations (Nebraska and Hawaii) revealed that in Nebraska the equation was accurate at 100% of the cases, in Hawaii only in 50%.

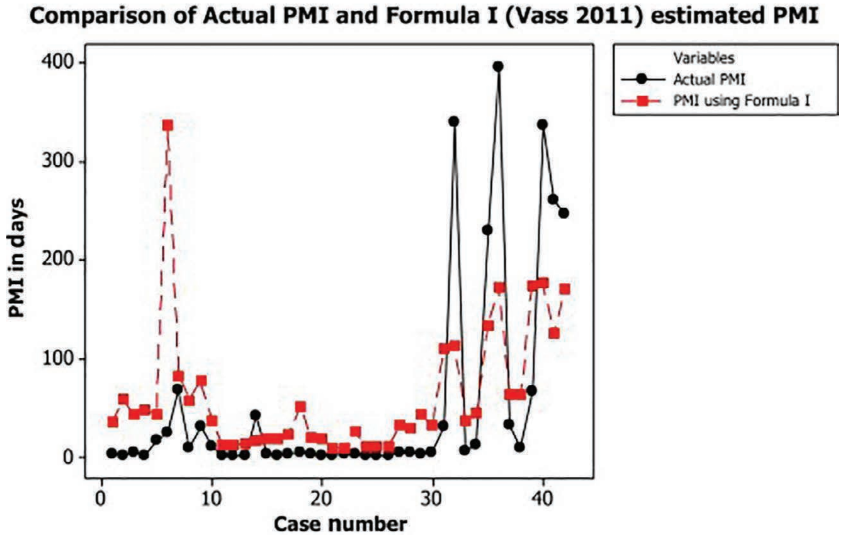

Figure 7.13 Comparison between the actual PMI (in black) and the estimated PMI using Formula I (Vass (in red) for each case. Formula I consistently underestimated the PMI for cases exposed to cold or freezing temperatures. The cases exposed to colder temperatures are those which were deposited in warmer conditions, but have been exposed to colder seasonal conditions with the passage of time in Canada. Formula 1 consistently overestimated the PMI for cases selected using the criteria provided by Vass. (For interpretation of the references to colour in this figure legend, the reader is referred to the web version of the chapter.)

In the study by Cockle and Bell [8] there were very great differences between actual PMI and PMI using formula one (Figure 7.13).

References

1. Aufderheide AC. *The Scientific Study of Mummies*. Cambridge, Cambridge University Press, 2003.
2. Beattie O, Geiger J. *Der eisige Schlaf. Das Schicksal der Franklin-Expedition*. Munich, Germany, Piper, 1992 (Originally published *Frozen in Time: The Fate of the Franklin Expedition*. London, Bloomsbury Publishing, 1987).
3. Berg S. Leichenzersetzung und Leichenzerstörung. In: Mueller B (eds.). *Gerichtliche Medizin*, vol. 1. Berlin, Springer, 1975, pp 62–106.
4. Berg S. Todeszeitbestimmung in der spätpostmortalen Phase. In: Brinkmann B, Madea B (eds.). *Handbuch Gerichtliche Medizin*, vol. 1. Berlin, Springer, 2004, pp 191–204.
5. Berg S, Rolle R, Seemann H. *Der Archäologe und der Tod, Archäologie und Gerichtsmedizin*. Munich, Germany, Verlag C. J. Bucher, 1981.
6. Bonte W. *Der postmortale Proteinkatabolismus. Experimentelle Untersuchungen zum Problem der forensischen Leichenzeitbestimmung*. Göttingen, Germany, Habilitation Schrift, 1978.
7. Casper JL. *Atlas zum Handbuch der gerichtlichen Medizin*. 3rd ed. Berlin, Verlag von August Hirschwald, 1860.
8. Cockle DL, Bell LS. Human decomposition and the reliability of a "Universal" model for post mortem interval estimations. *Forensic Sci Int* 2015;*253*:136.e1–136.e9.
9. De Donno A, Campobasso CP, Santoro V, Leonardi S, Tafuri S, Introna F. Bodies in sequestered and non sequestered aquatic environments: a comparative taphonomic study using decompositional scoring system. *Sci Justice* 2014;*54*:439–46.
10. Dotzauer G, Tamaska L. Hautveränderungen an Leichen. In: Marchionini A (ed.). *Handbuch der Haut- und Geschlechtskrankheiten* (Ergänzungswerk, vol. 1, T1). Berlin, Heidelberg, Springer, 1968.
11. Gaedke J. *Handbuch des Friedhofs und Bestattungsrechtes*. 9th ed. Cologne, Germany, Heymanns, 2004.
12. Haglund WD, Sorg MH. *Forensic Taphonomy*. Boca Raton, FL, CRC Press, 1997.
13. Heaton V, Lagden A, Moffat C, Simmons T. Predicting the postmortem submersion interval for human remains recovered from U.K. waterways. *J Forensic Sci* 2010;*55*:302–7.
14. Höpfel F, Platzer W, Spindler K. *Der Mann im Eis*, vol. 1. Bericht über das internationale Symposium 1992 in Innsbruck, Veröffentlichungen der Universität Innsbruck. Innsbruck, Austria, University of Innsbruck, 1992, p 187.
15. Krause D. Späte Leichenveränderungen. In: Brinkmann B, Madea B (eds.). *Handbuch Gerichtliche Medizin*, vol. 1. Berlin, Springer, 2004, pp 150–70.
16. Lötterle J, Schmierl G, Schellmann B. Einfluss der Bodenart auf die Leichendekomposition bei langen Liegezeiten. *Beitr Gerichtl Med* 1982;*40*:197–201.
17. Madea B, Brinkmann B (eds.). *Handbuch Gerichtliche Medizin*, vol. 2. Berlin, Springer, 2003.
18. Madea B, Cremer U, Schiwy-Bochat KH. Leichenverbergung durch Einmauern und Einbetonieren. *Arch Kriminol* 2003;*212*:129–40.
19. Madea B, Musshoff F. Postmortem biochemistry. *Forensic Sci Int* 2007;*165*:165–71.
20. Madea B, Preuss J, Musshoff F. From flourishing life to dust: the natural cycle of growth and decay. In: Wieczorek A, Rosendahl W (eds.). *Mummies of the World*. Munich, Germany, Prestel, 2010, pp 14–29.
21. Madea B, Preuss J, Musshoff F. Vom blühenden Leben zu Staub—Der natürliche Kreislauf von Werden und Vergehen. In: Wieczorek A, Tellenbach M, Rosendahl W (eds.). *Mumien—Der Traum vom ewigen Leben*. Mainz, Germany, Philipp von Zabern, 2007, pp 5–22.
22. Madea B. *Die Ärztliche Leichenschau*. 4th ed. Berlin, Springer, 2019.
23. Madea B. *Handbook of Forensic Medicine*. Chichester, John Wiley & Sons, 2014.
24. Madea B. *Praxis Rechtsmedizin: Befunderhebung, Rekonstruktion und Begutachtung*. 3rd ed. Berlin, Springer, 2014.
25. Megyesi MS, Nawrocki SP, Haskell NH. Using accumulated degree-days to estimate the postmortem interval from decomposed human remains. *J Forensic Sci* 2005;*50*(3):618–26.
26. Müller W. *Postmortale Dekomposition und Fettwachsbildung. Die Ausgrabungen auf dem Friedhof Hohe Promenade in Zürich*. Zürich, Albert Müller's Verlag, 1913.
27. Padosch SA, Dettmeyer R, Kröner L, Preuss J, Madea B. An unusual occupational accident: fall into a sewage plant tank with a lethal outcome. *Forensic Sci Int* 2005;*149*:39–45.
28. Palazzo C, Pelletti G, Fais P, Boscolo-Berto R, Fersini F, Gaudio RM, Pelotto S. Postmortem submersion interval in human bodies recovered from fresh water in an area of Mediterranean climate. Application and comparison of preexisting models. *Forensic Sci Int* 2020;*306*:110051.
29. Peterson F. Rechtsmedizinische Feststellung an einer 3 Jahre in Plastik gehüllten Kindesleiche. *Beitr Gericht Med* 1973;*29*:351–8.
30. Pieper P. Moorleichen. In: Beck H, Geuenich D, Steuer H (eds.). *Reallexikon der Germanischen Altertumskunde, vol 20*. Berlin, Walter De Gruyter, 2002, pp 222–9.
31. Preuss J, Brünig J, Madea B. Artifizielle Enterdigung durch Witterungseinflüsse. *Rechtsmedizin* 2004;*14*:14–19.
32. Rodriguez WC, Bass WM. Decomposition of buried bodies and methods that may aid in their location. *J Forensic Sci* 1985;*30*(30):836–52.
33. Schoenen D. *Verwesung und Verwesungsstörungen bzw. Entstehung von Eis- und Trockenmumien, Fettwachs-, Faul- und Moorleichen sowie fossilen Geweberesten und lithifizierten Gewebeabdrucken*. Düren, Shaker Verlag Düren, 2019.
34. Spindler K, Rastbichler-Zissernig E, Wilfing H, Zurnedden D, Nothdurfter H. *Der Mann im Eis: Neue Funde und Ergebnisse*. Vienna, Springer, 1995.
35. Spindler K, Wilfing H, Rastbichler-Zissernig E, Zurnedden D, Nothdurfter H. *Human Mummies: A Global Survey for the Status and the Techniques of Conservation*. Vienna, Springer, 1996.
36. Spindler K. *Der Mann im Eis: Die Ötztaler Mumie verrät die Geheimnisse der Steinzeit*. Munich, Germany, C Bertelsmann, 1993.
37. Tsokos M. Post mortem changes and artefacts during the early post mortem interval. In: Tsokos M (ed.). *Forensic Pathology Reviews*. Totowa, NJ, Humana, 2005, pp 183–237.
38. Van der Sanden, W. *Mumien aus dem Moor—Die vor- und frühgeschichtlichen Moorleichen aus Nordwesteuropa*. Amsterdam, Batavian Lion International, 1996.

39. Vass A. The elusive universal post-mortem interval formula. *For Sci Inter* 2011;204:34–40.
40. Wieczorek A, Rosendahl W (eds.). *Mumien—Der Traum vom ewigen Leben*. Mainz, Germany, Philipp von Zabern, 2007.
41. Wieczorek A, Rosendahl W (eds.). *Mummies of the World*. Munich, Germany, Prestel, 2010.

7.2a Eye Changes After Death

Burkhard Madea and Claus Henssge

7.2.1 Electrolyte Concentrations in Vitreous Humor

Autolysis starts with the cessation of energy metabolism in the cell and causes dissolution of the chemical, physical and morphological integrity of the body. Cessation of active membrane transport and loss of selective membrane permeability are direct consequences of the energy breakdown. With the loss of selective membrane permeability, diffusion of ions according to their concentration gradients begins. The time course of the autolytic processes is determined by many factors:

- Local anatomical factors (proximity of gallbladder, oesophagus, stomach, duodenum).
- Tissue- and cell-specific peculiarities.
- Biochemical factors (rate of glycolysis).
- Further ante-mortem and post-mortem factors influencing the 'interior milieu', especially temperature and pH.

As different tissues—and even the same tissues—at different topographical locations within the body have varying energy depots and rates of glycolysis, so too the duration of supravital activity varies considerably. As a result, the starting point and the time course (velocity of autolytic processes among different tissues, the same tissues at different locations of the body, as well as interindividually among different persons) differ widely.

Therefore, the following conclusions can be drawn concerning autolytic processes dependent on the time since death. Without strict differentiation of the structures investigated, the location of a collection of specimen temperature and ante-mortem factors (especially those that may affect post-mortem pH), the range of scatter of the autolytic parameter investigated will be wide and will rise considerably with an increasing PMI. This is true for most investigations dealing with autolytic processes and analyses regarding time since death. These issues are reviewed by Schleyer [94,95] and Coe [17–26] and therefore are not addressed here again.

7.2.1.1 Loss of Selective Membrane Permeability

The equalization of the concentration differences of ions in different compartments begins during and after the supravital period.

The equalization of concentration differences after the loss of selective membrane permeability follows Fick's first law of diffusion:

$$\mathrm{m} = \mathrm{D\,X}\,\frac{\mathrm{F}}{\mathrm{d}} \times (\mathrm{C1} - \mathrm{C2}) = \mathrm{D} \times \frac{\mathrm{F}}{\mathrm{d}}\,xc$$

where m is the diffusion stream; D is the diffusion coefficient, dependent on the medium and the particles diffusing; c is the concentration difference; F is the surface of the diffusion medium; d is the diameter; and $C1$, $C2$ is concentration in compartments 1 and 2.

Because of its isolated topography compared with blood and cerebrospinal fluid (CSF), and because of its resistance to microbiological contamination with bacterial degradation and biochemical structures, vitreous humour is a very suitable medium for post-mortem concentration studies [6,56,67,111].

The most favoured parameter studied is vitreous potassium (K^+), which diffuses post-mortem from the retina (and to a lesser extent from the lens) into the vitreous body [8]. Animal experiments [8] have shown that supravital metabolism may be maintained for 15 minutes at 37°C. Even during life, there are concentration gradients within and between the intraocular fluid compartments [8,9] (Figure 7.14), with a K^+ inflow from the lens and an outflow into retinal vessels. In dogs and rabbits, the highest intraocular fluid concentration of K^+ was found in the posterior chamber and in cats in the anterior segment of the vitreous. The latter finding can be explained only by active K^+ transport across the lens [9]. The K^+ outflow from vitreous to retinal vessels seems to be purely diffusion because the K^+ concentration of the posterior vitreous is higher than that of the plasma dialysate. Post-mortem, the K^+ gradient at the vitreous-retina interface reverses, with the lowest concentrations probably at the centre of the globe until diffusion equilibrium is achieved.

A striking finding was reported by Pau [83]. Although the K^+ content of the vitreous body was estimated to be 18–19 mg/dl, Pau noted that the vitreous layer adjacent to the retina contained about 100 mg/dl, which means that the whole vitreous behaves like a body fluid, but the vitreous layer acts as a body tissue. Whether this higher K^+ concentration of the layer is the result of electrochemical binding to the chemical substrate (tropocollagen,

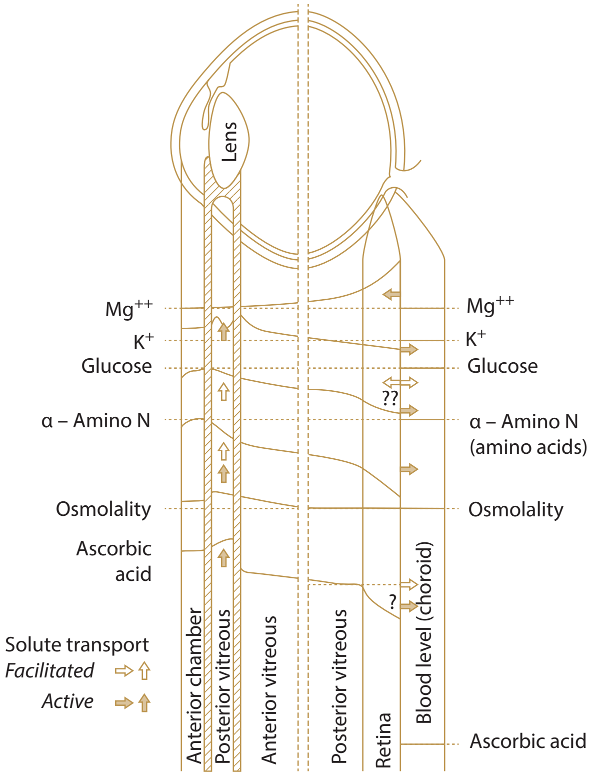

Figure 7.14 Schematic presentation of the gradients of some solute concentrations and total osmolality in the intraocular fluid system of a typical mammalian eye. The blood levels are shown by the dotted line and by the value given for the choroid. K^{+}, potassium; Mg^{++}, magnesium.

hyaluronic acid) is still unknown. These two findings (vitreous K^{+} gradients and higher concentrations of the layer) already play an important role in the removal of vitreous humor and further pre-analytical procedures.

The following recommendations of Coe [26] concerning vitreous sample acquisition should be strictly adhered to:

> Vitreous humour should be obtained by means of needle and small syringe with suction applied gradually. The use of Vacutainer tubes with their strong initial suction commonly causes fragments of retina or other tissues to contaminate the specimen and such particulate matter will distort biochemical values. With care, over 1 mL of vitreous humour can usually be aspirated from each eye, even in newborn infants. Centrifugation with the use of the supernatant portion prevents clogging of fine tubing used in most current analytical instruments. All the vitreous that can be extracted should be withdrawn as there is variation in the concentration of many solutes between the vitreous humour next to the retina and that obtained from the centre of the globe.

Only crystal-clear, colourless vitreous humour should be used for analysis. With the onset of decomposition, the fluid becomes cloudy and brownish. Further analytical and pre-analytical recommendations were published by Blana et al. [10], Coe and Apple [19], Thierauf et al. [109] and other sources [54,67,79,107,108].

7.2.1.2 Short Review of the Literature on Vitreous Potassium

The relationship between the rise of K^{+} concentration in the vitreous humour and the time since death has been established by numerous authors [1–5,11–18,20–26,30–33,37,40,43–47,50–53,55–65,71,73,75–82,85,96–108,112,113] (see the excellent historical review by Coe and Table 7.12). The most exciting results were presented by Sturner [105], 1 on a random sample of 54 bodies observed up to 100 hours post-mortem; the 95 per cent confidence limits of the K^{+} concentration were only ±9.5 hours.

The linear rise of vitreous K^{+} and the PMI up to 104 hours post-mortem were described by the following regression:

$$[\mathrm{K}^{+}] = 5.476 + 0.14\mathrm{h}, \quad \text{or} \quad \mathrm{h} = 7.14\,[\mathrm{K}^{+}] - 39.1$$

Follow-up investigations (see Table 7.12) could not confirm these 95 per cent confidence limits and revealed—even in the group of sudden or traumatic deaths—a much wider range of scatter. Figure 7.15, for example, shows the range of scatter of the values found by Hughes [43] with a regression line and 95 per cent confidence limits given by Sturner [102].

Figure 7.16 shows the values found by Coe [23]—only persons with normal electrolyte concentrations 6 hours before death are included—and the regression line and 95 per cent confidence limits given by Sturner [102]. In both instances, the values found do not fit into the 95 per cent confidence limits given by Sturner. However, one of the fundamental results of Sturner's investigation is that there are different 95 per cent confidence limits in the group of sudden or traumatic deaths and hospital deaths. Further important results were presented by Adelson et al. [1], who were able to show that the duration of the terminal episode also has a great influence on the range of scatter of K^{+} concentration over the PMI.

In cases with a terminal episode of less than 6 hours, the scatter was much smaller than in cases with a terminal episode lasting more than 6 hours. The great obstacle in using the K^{+} concentration in vitreous humour as an aid in estimating the time since death is the variation in 95 per cent confidence limits given by different authors. In a PMI of up to roughly 100 hours, these limits vary between ±9.5 hours and ±40 hours; in the early PMI of up to 24 hours, they vary from ±6 hours to ±12 hours (Figure 7.29).

Table 7.12 Summary of Investigations on Vitreous Potassium

Reference	PMI	*n*	Intercept (K^+ mmol/l)	Slope (K^+ mmol/l per hour)	Correlation coefficient (r)	95% confidence limits	Random sample	Comment
Jaffe [44]	Up to 125 h	31					17–81 years; no cases with uraemia or electrolyte imbalances.	K^+ concentration related to logarithm of time; no significant differences between refrigerated bodies and those kept at room temperature.
Adelson et al. [1]	24 h	209	5.36 I 5.27 II 5.72	0.17 0.16 0.18		±10 h ±5.75 h ±12 h	I: Agonal event <6 h. II: Agonal event > 6 h.	Straight line relationship between vitreous K^+ and PMI.
Sturner [105] Sturner and Gantner [104]	Up to 108 h	54	5.48	0.14	0.987	±9.5 h	Coroner cases	PMI = 7.14 K^+ –39.1.
Hughes [43]	Up to 117 h	135				±20 h	55 coroner cases. 80 hospital deaths.	Rise of K^+ could not be correlated with sufficient consistency with PMI.
Hansson et al. [37]	3–310 h	203	8	0.17		±40 h		In 180 cases with a PMI up to 120 h, linear rise of vitreous K^+.
Leahy and Farber [53]	30 h	52					Hospital patients; patients dead on arrival.	Vitreous K^+ concentrations appear to rise erratically after death.
Lie [55]	2–95 h	88	5.48	0.14		±3.6 h (1 SD)	Hospital cases.	Very good agreement with Sturner; slope, intercept and SD according to Henry and Smith: 'standard deviation calculated from author's data as variance from Sturner and Ganther's line of best fit'.
Marchenko [71]	6–48 h	300				Death time estimation possible within 3–6 hours.	Age 29–70 years.	Estimation of time since death possible within ±3 h.
Coe [23]	100 hpm	160	I 4.99 II 6.19	0.332 0.1625		±12 hours in the first day after death.	Hospital patients with normal electrolytes within 6 h of death and medical examiner cases.	I: PMI <6 h. II: PMI >6 h. Individual slope may vary between 0.085 and 0.45 mmol/l.
Krause et al. [51]	230 h	262			0.7	Range of scatter between 9 and 107 h for K^+ values between 5 and 28 mmol/l.		$K^+ = 2.96 + 1.65\sqrt{h}$ $h = \left[\frac{K - 2.96}{1.65}\right]^2$ Exponential rise of K^+ over the PMI.
Stegmaier [100]	82 h	98				±12		

(*Continued*)

Table 7.12 (*Continued*) Summary of Investigations on Vitreous Potassium

Reference	PMI	*n*	Intercept (K^+ mmol/l)	Slope (K^+ mmol/l per hour)	Correlation coefficient (r)	95% confidence limits	Random sample	Comment
Adjutanis and Coutselinis [2]	12 h	120	3.4 (taken from literature).	0.55 for the first 12 hours.		~±3.3		Timed bilateral withdrawal (interval 3 h) reveals a rise in precision of death time estimation from ±3.3 to ±2.2 h.
Komura and Oshiro [50]	≈30 h	90			0.78–0.92 (according to ambient temperature).			Linear relationship between vitreous K^+ and PMI, slope being steeper in ambient temperatures of 26 –29°C than in 13 –17°C.
Foerch et al. [31]		>50						Linear correlation between vitreous K^+ and PMI.
Blumenfeld et al. [11]	11–77 h	127			0.63	±26 h	127 children, age 1 hour–13 years.	K^+ increases with increasing PMI in an essentially linear fashion.
Forman and Butts [32]		82	4.8	0.21	0.787			Linear relationship between potassium level and PMI; y = 4.75x = 22.8.
Schoning and Strafuss [97]	48 h	60 (dogs)					Mongrel dogs.	Rise of K^+ temperature dependent.
Choo-Kang et al. [16]		105	9.67	0.09	0.85			
Balasooriya et al. [5]		59						Comparing vitreous K^+ values of both eyes, 18.6% of the results varied by more than 10% from the mean.
Farmer et al. [30]	24–120 h		238 mg/l	4.752	0.98			
Stephens and Richards [101]	35 h	1427	6.324	0.238		±20 h	Newborn–90 years.	
Madea et al. [58]	130 h	I 170	5.99	0.203	0.86	±34 h	I: Entire sample (clinical and forensic pathology).	
		II 138	5.88	0.188	0.89	±22 h	II: Urea < 100 mg/dl.	
		III 107	5.48	0.186	0.91	±20 h	III: Urea < 100 mg/dl and terminal episode < 6 h.	
Sparks et al. [99]	≈60 h	91			0.87	±10.5 within the first day.		Concomitantly the levels of 3-MT were studied in the putamen of the brain; combining K^+ and α3-MT determinations the accuracy of predicting PMI may be raised to ±8 h for individuals not dying of organic heart disease.

Table 7.12 (*Continued*) **Summary of Investigations on Vitreous Potassium**

Reference	PMI	*n*	Intercept (K$^+$ mmol/l)	Slope (K$^+$ mmol/l per hour)	Correlation coefficient (r)	95% confidence limits	Random sample	Comment
Schmidt [57]	88.5 h		5.35	0.17	0.83	±24.8	Sudden natural and traumatic death (forensic pathology).	
Montaldo et al. [75]	≈80 h	289	6.805 6.1–6.99	0.1652 0.15–0.20		±15 ±8 to ±23	Violent or unsuspected death.	K$^+$ over the PMI in the entire sample and in various subgroups was analysed; subgroups were formed according to age, sex, type of death, autopsy findings and climatic conditions (see Table 7.25).
Gamero et al. [33]	24 h	60					Coroner cases.	Best correlation between K$^+$ and PMI in cases dying of acute trauma with a PMI <17 h.
Rognum et al. [88]	120 h	87	5.8	0.17: 5°C 0.20: 10°C 0.25: 15°C 0.30: 23°C				Repeated sampling of vitreous humour (twice each eye); the higher the environmental temperature, the steeper the slope of vitreous K$^+$.

Abbreviations: K$^+$, potassium; 3-MT, 3-methoxytyramine; PMI, post-mortem interval; SD, standard deviation.

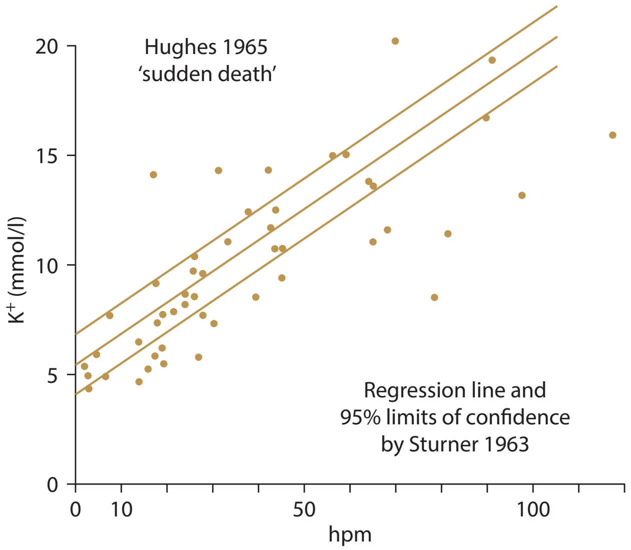

Figure 7.15 Fifty cases of sudden death published by Hughes [43] with a regression line and 95 per cent confidence limits by Sturner [102]. K$^+$, potassium.

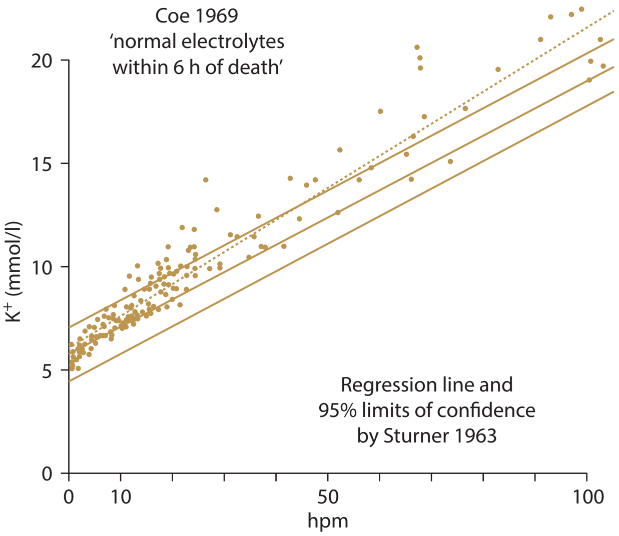

Figure 7.16 Vitreous potassium (K$^+$) values of normal individuals plotted against time since death with a regression line of all values having a post-mortem interval longer than 6 hours (dashed line) [23] and regression line and 95 per cent confidence limits (solid line) [98]. hpm, hours post-mortem.

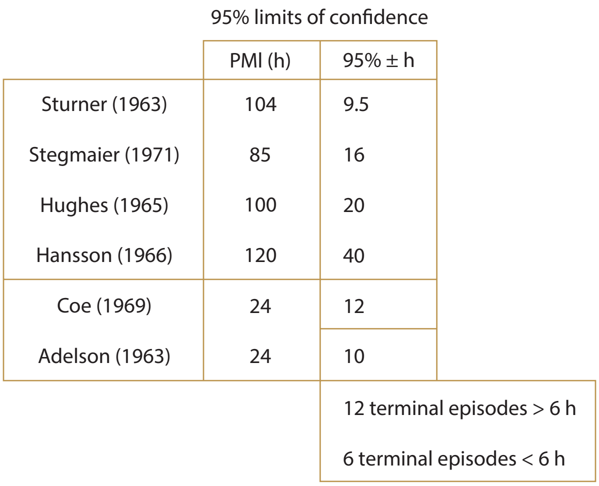

	95% limits of confidence	
	PMI (h)	95% ± h
Sturner (1963)	104	9.5
Stegmaier (1971)	85	16
Hughes (1965)	100	20
Hansson (1966)	120	40
Coe (1969)	24	12
Adelson (1963)	24	10
		12 terminal episodes > 6 h
		6 terminal episodes < 6 h

Figure 7.17 Potassium in vitreous humour. Different 95 per cent confidence limits quoted in the literature for the early and later postmortem interval (PMI).

The statistical parameters of the regression line vary correspondingly: (1) the K^+ concentration at the moment of death as the intercept of regression lines between 5 and 8 mmol/l; and (2) the rise of K^+ concentration per hour between 0.1 and 0.238 mmol/l (Table 7.13).

Table 7.13 Differing Statistical Parameters of the Regression Line as Quoted in the Literature

Reference	*n*	Intercept (mmol/l)	Slope (mmol/l per hour)
Sturner [102]	54	5.960* 5.600	0.132* 0.140
Adelson et al. [1]	209	5.360	0.170
Hansson et al. [37]	108	8.000	0.170
Lie [55]	88		0.140
Coe [23]	160	4.990 6.190	0.332 (first 6 h) 0.1625 (over 6 h)
Adjutantis and Coutselinis [2]			0.550 (for the first 12 h)
Stephens and Richards [101]	1427	6.342	0.238
Madea et al. [58]	170	5.880	0.190

* The author's own calculations on Sturner's material with differences from Coe's statement. In cases with vitreous potassium of both eyes, the mean value was used for regression analysis. The slope varies between 0.132 and 0.238 mmol/l per hour.

Note: The slope given by Adjutantis and Coutselinis [2] is as steep as 0.55 mmol/l per hour. Coe [23] found the slope in the first 6 hours to be 0.332 mmol/l per hour, which was much steeper than for the whole investigated period (0.1625 mmol/l per hour). In more than 100 individuals, sampling of the two eyes was made at different times, and the slopes for individual pairs ranged from 0.085 to 0.450 mmol/l per hour [23]. Differing individual slopes have also been reported by Madea et al. (Figure 7.18) [58].

Adjutantis and Coutselinis [2] confirmed the findings of an interindividual variation of the slope of K^+ concentration over the PMI and recommended a timed removal of vitreous humour of both eyes at an interval of 3 hours and calculation of the time since death along the individual slope on a 'normal value' of K^+ concentration at the moment of death (3.4 mmol/l). Death time estimation in the first 12 hours would be possible within an accuracy of ±1.1 hour.

The reasons for these confusing results concerning regression parameters and the precise estimation of death time are not clear because all authors claimed to have considered the same careful sample taking and pre-treatment of samples before analysis.

7.2.1.3 Factors Influencing the Postmortem Rise of Vitreous Potassium

Some reasons for the different regression parameters, especially the slope, have been identified:

- The duration of the terminal episode [1,58].
- The composition of the random sample of deaths: hospital cases, coroner cases (Table 7.14) [33,58,75,102].
- A much steeper slope in cases with raised urea values [58,60].
- Ambient temperatures (Figure 7.19) [8,13,14,26,50, 88,97,98,113].
- Possible influence of alcohol at the moment of death [103].
- Distribution of cases of the PMI.
- Instrumentation used to measure the concentrations (Figure 7.7) [10,19,107–109].
- Linear relationship between vitreous K^+ and the PMI. This is obviously not a simple straight line but is biphasic, with a steeper slope in the first 6 hours than for prolonged times [22].
- Age. The level of vitreous K^+ rises much more rapidly in infants than it does in adults, possibly because of a smaller diameter of the infant vitreous globe [26].

Our own investigations on vitreous K^+ were based on the following hypothesis: One reason for the varying range of scatter in the different studies may be electrolyte imbalances at the moment of death. Unlike in experimental studies, in casework information about the electrolyte status before death is lacking. Therefore, for investigations on vitreous humour, it would be valuable to perform measurements of different parameters, some of which act as an internal standard. This should give information about homeostasis of electrolytes—mainly K^+—at the moment of death. Such an internal standard should have a small standard range in life, be stable post-mortem and have a close relationship with electrolyte metabolism.

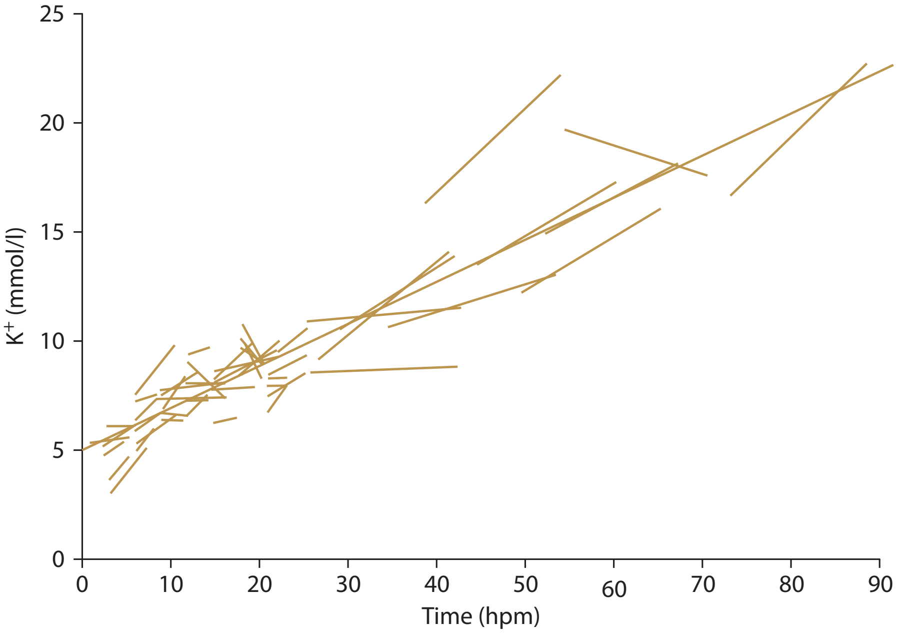

Figure 7.18 Potassium (K+) values of 53 cases of both eyes; vitreous humour of both eyes withdrawn at different time intervals after death (intervals between aspiration 2–3 hours, 4–5 hours and 12–24 hours). The 'rise' of the K+ concentration of vitreous humour obtained at different time intervals is within the normal range of scatter of values obtained at identical times after death. hpm, hours post-mortem.

Table 7.14 Regression Parameters and 95 Per Cent Confidence Limits in the Entire Sample and Various Subgroups According to the Mode and Cause of Death

Mode and cause of death	*n*	Intercept K+ (mmol/l)	Slope (mmol/l per hour)	95% confidence limits
Total number	289	6.805	0.1652	15
≤60 years	176	6.677	0.1657	14
>60 years	113	6.636	0.1663	16
Sudden death	138	6.683	0.1652	16
Violent death	151	6.661	0.1666	16
Sudden death ≤60 years	29	6.609	0.1727	14
Sudden death >60 years	42	6.183	0.1722	17
Violent death ≤60 years	111	6.801	0.1656	13
Violent death >60 years	40	6.663	0.1665	16
Sudden cardiac death ≤60 years	36	6.867	0.1803	17
Sudden cardiac death >60 years	31	6.383	0.1835	23
Violent asphyxial death	26	6.470	0.1689	12
Other violent death	125	6.692	0.1653	16
Death in winter	60	6.989	0.1626	16
Death in summer	74	6.567	0.1715	11
Violent death ≤60 years in winter	25	6.999	0.1500	21
Violent death ≤60 years in summer	34	6.100	0.2015	8

Abbreviation: K+, potassium.

Source: From Montaldo B, Umani Ronchi G, Marchiori A, Forgeschi M, Barbato M. La determinatione della concentrazione del potassio nel'umor vitreo: verifica di un methodo strumentale tanatocronologico. *Riv Ital Med Leg* 1989;**11:**180–199.

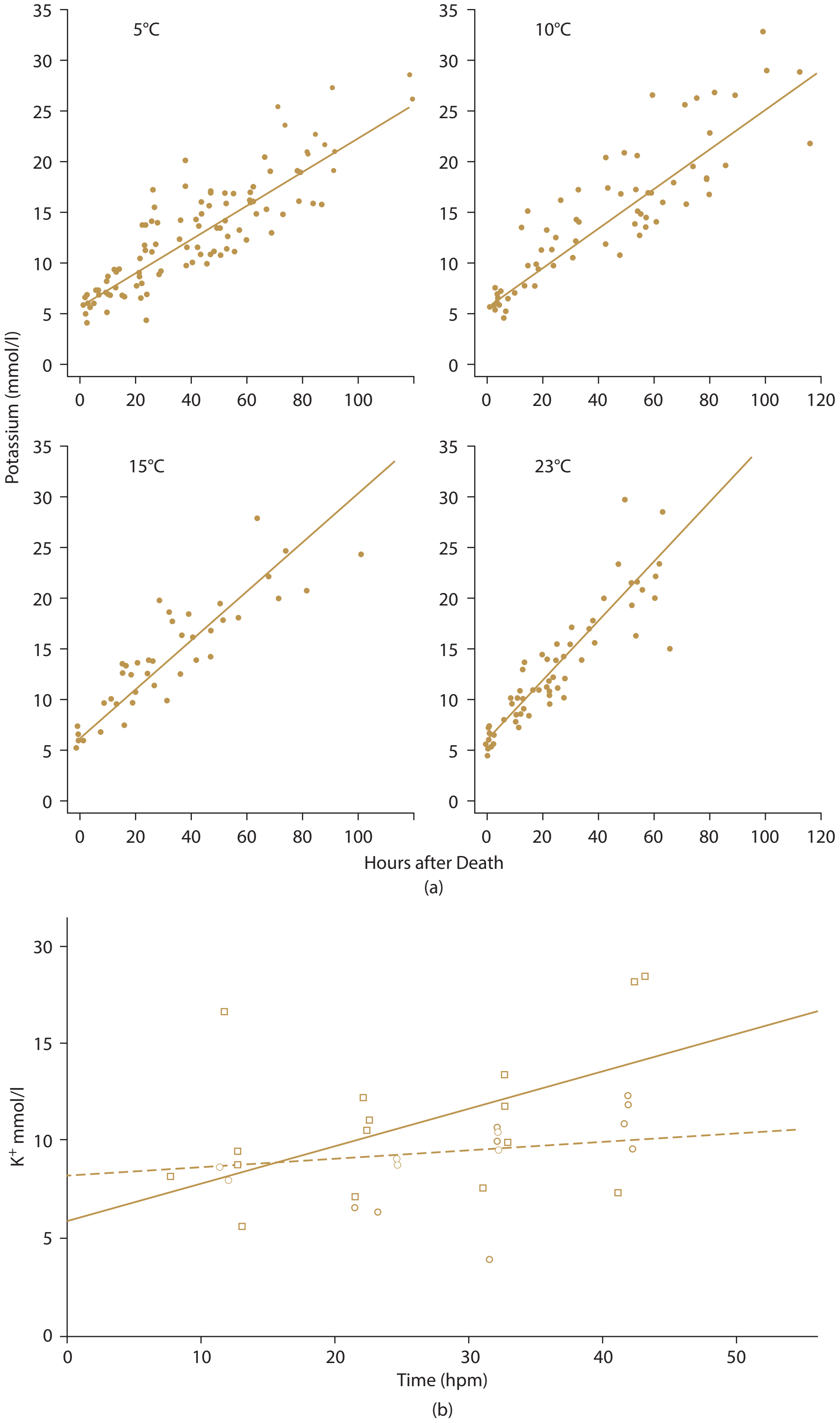

Figure 7.19 (a) Scatter plots of vitreous humour potassium (K^+) levels in subjects kept at 5°C, 10°C, 15°C and 23°C after death (the median slopes being 0.17 (5°C), 0.20 (10°C), 0.25 (15°C) and 0.30 (23°C) mmol/l per hour). The median slopes are indicated by lines [88]. (b) 32 K^+ values from 24 bodies brought within 3 hours of death into ambient temperatures of 5°C (squares) and 20°C (circles) [14].

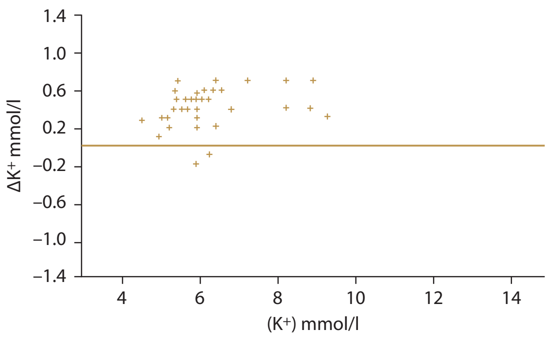

Figure 7.20 Differences of potassium (K^+) concentrations determined with ion-specific electrodes and flame photometry (ion-specific electrodes minus flame photometry) over the K^+ concentrations determined with ion-specific electrodes (calculation on the material of Coe and Apple [19]). Determination with ion-specific electrodes reveals slightly higher values than with flame photometry.

Table 7.15 Composition of the Random Sample (*n* = 270) with Regard to the Cause of Death

Cause of death	Forensic pathology	Clinical pathology	Total
Neoplasms	3	32	35
Accidents	47	3	50
Fall from height	21		21
Hanging	5		5
Myocardial infarction	71	21	92
Pulmonary thromboembolism	1	2	3
Cerebral infarction/ cerebral bleeding		5	5
Liver or renal failure	3	7	10
Gunshot	7		7
Intoxication	8		8
Burns	4		4
Other	17	13	30
Total	187	83	270

7.2.1.4 Search for an Internal Standard of Electrolyte Homeostasis at the Moment of Death

7.2.1.4.1 Materials and Methods

Vitreous humour was sampled from 270 consecutive cases with an accurately known time of death [58,60,62].

In the forensic case group (*n* = 187), the sudden deaths were mainly caused by coronary artery disease, head injury, traffic accidents, fall from height or other situations. In contrast, in the pathology group (*n* = 83), death occurred after chronic lingering disease (i.e. cancer, infectious diseases, renal failure, cardiac failure after myocardial infarction) (Table 7.15 and Figures 7.21 and 7.22).

After admittance to the mortuary, most of the bodies were kept at +15°C, but some of them were kept at +5°C. In all cases, vitreous humour from both eyes was completely aspirated at the same time by using a 10-mL syringe and a 20-gauge needle. Any specimens that were not crystal clear were rejected. Most of the samples were stored frozen at −70°C until analytical determinations could be performed. After thawing, the samples were centrifuged for 10 minutes at 3000 rpm, according to Adjutantis and Coutselinis [2]. The supernatant was then used for determinations. In all cases, there was enough material for the following parameters to be measured: K^+, sodium, chloride, urea, calcium. In some cases, creatinine was also determined. Sodium, K^+, chloride and calcium were determined using ion-sensitive electrodes. Because the linearity of the K^+ electrode of the Hitachi 705 system used in this investigation was confined to 10.9 mmol/l, most samples had to be measured once more after correct dilution with ion-free water.

Urea was determined using an enzymatic method according to Gutman and Bergmeyer [57]. The presence of ammonia did not affect the results. Creatinine

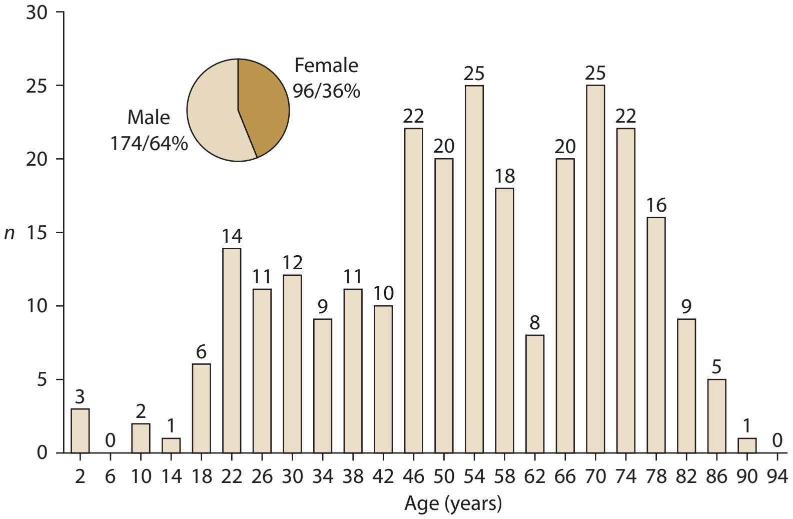

Figure 7.21 Distribution of the authors' random sample with regard to gender and age.

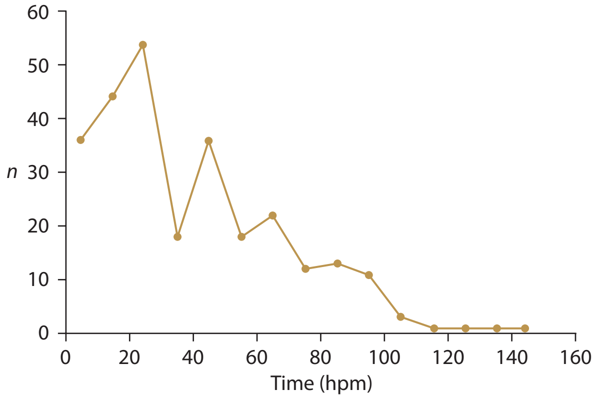

Figure 7.22 Distribution of the post-mortem interval of the authors' random sample ($n = 270$). hpm, hours post-mortem.

was measured using the kinetic (Jaffe) method [57]. In all instances, right and left eye aspirates were analysed independently.

7.2.1.4.2 Results and Discussion

7.2.1.4.2.1 Differences Between Eyes/Timed Bilateral Withdrawal

Because the left and right eye aspirates were determined independently, some remarks are made on the differences between the eyes. There were deviations of up to 10 per cent in the single values from the mean value, even in the early PMI (Figure 7.23). These percentage deviations of the single values of each eye from the mean value are not related to the time since death or the mode of death. These findings are in good accord with those of Stegmaier [100], but they are not as marked as those reported by Balasooriya et al. [5] (Table 7.16). We have also obtained similar differences between the eyes for sodium, chloride and calcium. Because we used the same pre-treatment for samples as did Adjutantis and Coutselinis [2] before analysis, these differences of the K^+ concentrations between the eyes do not allow us to use the method of Adjutantis and Coutselinis [2]. It consists of determining the individual slope up to 12 hours post-mortem after aspiration of vitreous humour of both eyes at different time intervals to obtain a more precise estimation of time since death. Another argument against their method is that the K^+ values in vitreous humour from both eyes obtained at different times after death (3–4 hours apart) are within the normal range of scatter of values obtained at identical times after death (see Figure 7.18). Correspondingly, Schleyer [96] mentioned that he could not confirm the results of Adjutantis and Coutselinis [2] by using their formula.

7.2.1.5 Urea as an Internal Standard

Although there are differences for single K^+ values taken at identical times, the statistical parameters of K^+ concentrations over the time since death for each eye do not differ from those of the mean value for both eyes: the regression lines are identical. Therefore, for further statistical analysis, only the mean values of both eyes were used.

Figure 7.24 shows the K^+ values of 270 cases (mean values of both eyes) plotted against time after death. There is a linear relationship between K^+ concentrations and time after death up to 120 hours. The slope is 0.20 mmol/l per hour; the intercept is 6.10 mmol per hour.

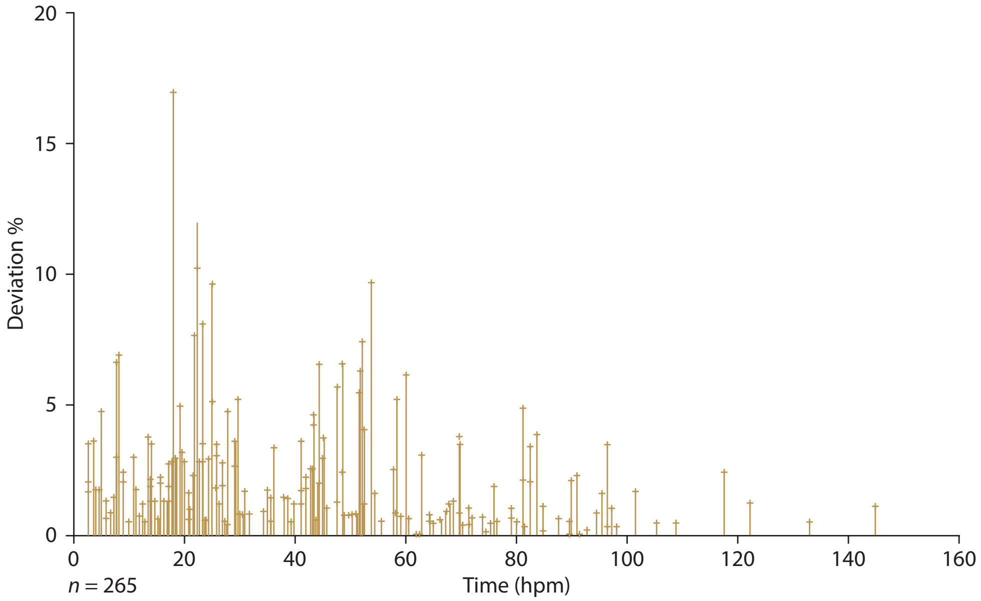

Figure 7.23 Histogram showing the percentage deviation of the single potassium values of each eye from the mean value of both eyes. hpm, hours post-mortem.

Table 7.16 Percentage Difference in Results of Potassium, Sodium and Urea in Each Eye Expressed as a Percentage of the Mean Result*

Potassium difference	**< 4%**	**4–10%**	**>10%**
n	29 (240)	19 (23)	11 (2)
%	49.2 (90.5)	32.2 (8.7)	18.6 (0.8)
Sodium difference	**<2%**	**2–5%**	**>5%**
n	35 (173)	18 (56)	6 (36)
%	59 (65)	31 (21.1)	10 (13.5)
Urea difference	**<6%**	**6–12%**	**>12%**
n	27 (217)	11 (27)	9 (20)
%	57 (82.2)	23 (10.2)	19 (7.6)

* Authors' data in parentheses. Data from Balasooriya BAW, Hill CAS, Williams AR. The biochemistry of vitreous humour: a comparative study of the potassium, sodium and urate concentration in the eyes at identical time intervals after death. *Forensic Sci Int* 1984;**26:**85–91.

The 95 per cent confidence limits in this entire group—which consists of both sudden traumatic deaths and hospital deaths—are ±25.51 hours up to 120 hours post-mortem (Table 7.17).

The first step to reduce these 95 per cent confidence limits was to look at the question of which of the other parameters could indicate an ante-mortem imbalance of metabolism. Sodium, calcium, chloride, urea and creatinine are stable in the PMI for up to 120 hours after death (Figures 7.25–7.29). Figures 7.28 (a) and (c) show a marked increase of urea in many cases and are indicative of ante-mortem urea retention. That these high urea values result from ante-mortem retention and not from post-mortem changes was shown by Coe [23], who compared urea values obtained from each eye at different time intervals after death. The differences in the values

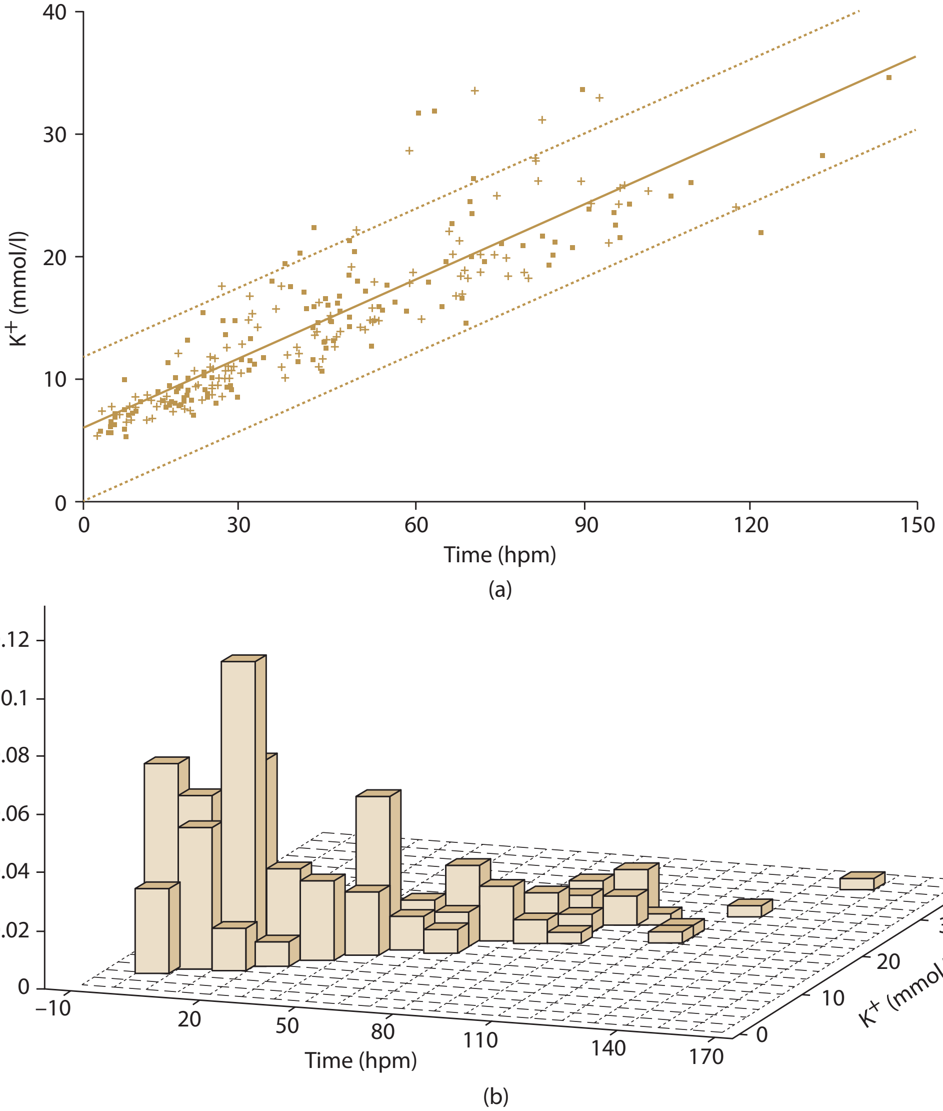

Figure 7.24 (a) Potassium (K⁺) value (mean value) of 270 cases plotted against time since death. This entire sample includes forensic and hospital cases. (b) Two-dimensional distribution of K⁺ values and post-mortem interval. hpm, hours post-mortem.

Table 7.17 Urea as Internal Standard: Statistical Parameters of the Entire Sample and the Subgroups*

		Urea <100 mg/dl	Change (%)	Urea <70 mg/dl	Change (%)
n	270 (170)	228 (138)	−15.5	206	23.7
Intercept	6.10 (5.99)	6.02 (5.88)	−1.3	5.92	−2.9
Slope	0.20 (0.2033)	0.18 (0.1877)	−10	0.18	−10.0
Correlation coefficient (*r*)	0.89 (0.86)	0.91 (0.89)	+2.2	0.93	+4.5
Variance (s^2_{yx})	8.57	5.09	−40.6	4.09	−47.7
Standard deviation (s_{yx})	2.93 (3.42)	2.25 (2.62)	−23.2	2.02	−31.0
95% confidence limits (h)	± 25.51 h (± 34)	± 21.78 h (± 22)	−14.6	± 20.4 h	−21.3

* Data in parentheses are from Madea B, Henssge C, Honig W, Gerbracht A. References for determining the time of death by potassium in vitreous humour. *Forensic Sci Int* 1989;**8:**231–243.

did not exceed 5 mg/dl, even in the cases with very long intervals between two samples. Thus, vitreous urea nitrogen can be used as an internal standard because it is stable post-mortem and has a close relationship with electrolyte metabolism. In the next step, all cases having a vitreous urea nitrogen level higher than 100 mg/dl were excluded from the entire group of K$^+$ values to check whether, in this diminished random sample, there is a closer connection between K$^+$ concentrations and time since death. In 42 cases of the entire group, there were vitreous urea nitrogen levels greater than 100 mg/dl (see Table 7.17).

In the diminished group (n = 228), the intercept was 6.02 mmol/l, and the slope 0.18 mmol/l per hour. The 95 per cent confidence limits up to 120 hours post-mortem were reduced from ±25.51 to ±21.78 hours.

The difference in the 95 per cent confidence limits of the entire group and of the diminished sample is significant. All patients with a urea level greater than 100 mg/dl had had chronic diseases. The different 95 per cent confidence limits in the entire group and in the diminished group are in general in good accord with Sturner's report, which highlighted that coroner cases of sudden and traumatic death showed a better correlation between K$^+$ concentration and time since death than did hospital cases.

In a third step, we excluded all cases with urea values greater than 70 mg/dl (see Table 7.17). However, the improvement in accuracy was not significant compared with the first step of elimination.

7.2.1.6 Creatinine as an Internal Standard

The value of creatinine as an internal standard was also checked. Creatinine and vitreous K$^+$ levels were determined in 170 cases. Different creatinine values were chosen as limiting values (Table 7.18). The comparison of urea and creatinine as an internal standard showed that urea is more sensitive (see Table 7.18). The combination of limiting values for urea levels lower than 70 mg/dl and creatinine values lower than 1 mg/dl revealed the most precise death time estimation with 95 per cent confidence limits of ±15 hours in the time interval up to 120 hours post-mortem. Considering from our random sample only sudden traumatic deaths (n = 71), and excluding all cases with urea values greater than 70 mg/dl, revealed a significant reduction in the 95 per cent confidence limits from ±22.34 to ±17 hours (see Table 7.7; Figures 7.30, 7.31 and 7.32).

The result of these steps of elimination to obtain a closer relationship between K$^+$ and time since death is that, by these means, a separation into cases with and without severe disturbances of metabolism is possible. Depending on the information obtained from the corpse in question—no other knowledge about health before death should be necessary—one can choose the reference for estimating time since death with different 95 per cent confidence limits (Table 7.19; see also Tables 7.17 and 7.18). A limiting value for urea of 100 mg/dl—which has been chosen arbitrarily—seems to be sufficient to separate cases with and without disturbances of metabolism at the moment of death.

Our conclusion that vitreous urea nitrogen is the most suitable internal standard of the disturbed homeostasis of electrolyte metabolism is confirmed by our augmented study.

7.2.1.7 Recommendations for Further Studies

Several internal and external factors have been identified that govern the post-mortem rise of vitreous K$^+$. The rise of vitreous K$^+$ in different temperature groups must be studied further to have reference material for casework. However, further studies on vitreous K$^+$, in our opinion, make sense only if all the external and internal factors influencing the post-mortem increase of K$^+$ are taken into consideration. For these studies, more case material is necessary not only to determine the effect of influencing factors but also to obtain useful statistical parameters to be applied in casework.

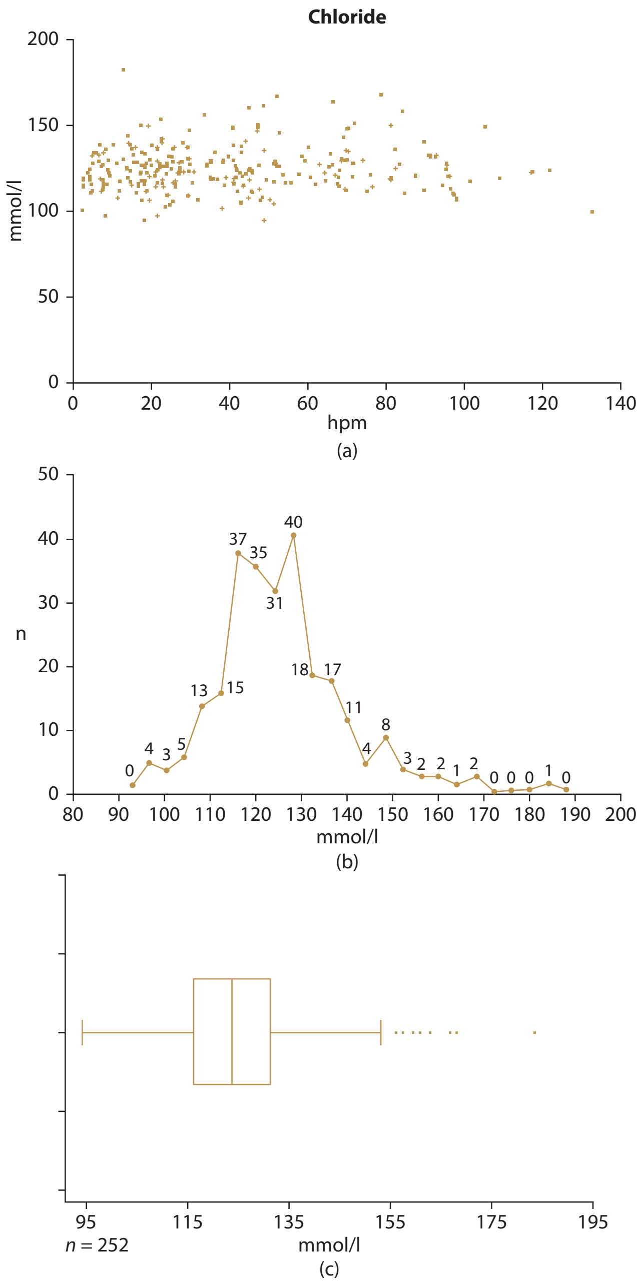

Figure 7.25 (a) Concentration, (b) frequency distribution of concentration and (c) box plots of chloride concentration. The rectangular box contains 50 per cent of all values found, marked by the upper and lower quartile. The box is divided by the median in two parts. The lines on the right and the left of the box correspond to the 90 per cent confidence interval and the median. The distribution becomes evident from the box plots.

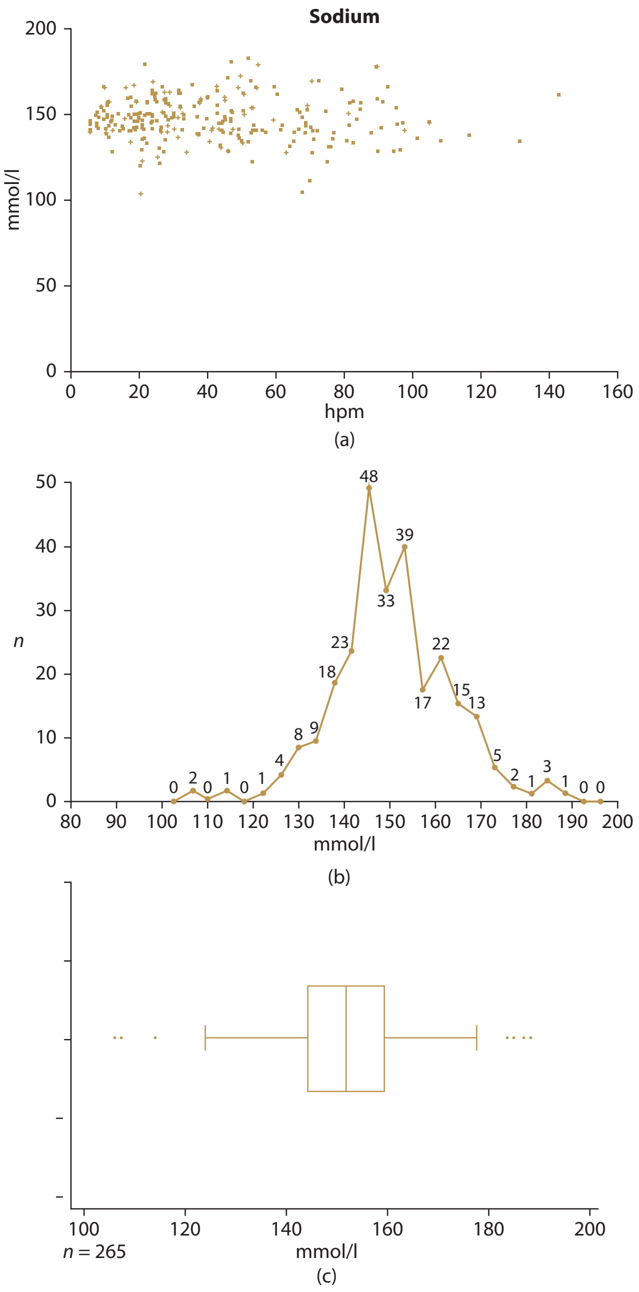

Figure 7.26 (a) Concentration, (b) frequency distribution of concentration and (c) box plots of sodium concentration. The rectangular box contains 50 per cent of all values found, marked by the upper and lower quartile. The box is divided by the median in two parts. The lines on the right and the left of the box correspond to the 90 per cent confidence interval and the median. The distribution becomes evident from the box plots.

Rognum et al. [88] published a paper on the post-mortem increase of vitreous hypoxanthine (Hx) in comparison with vitreous K^+; the vitreous humour was collected by repeated sampling. The scatter of the K^+ values was greater than for Hx. However, our own preliminary studies give contrary results, with the scatter of levels for Hx being greater than those for K^+ [63]. Perhaps by combining both methods and performing a multiple linear regression analysis, the procedure for the estimation of death time can be improved.

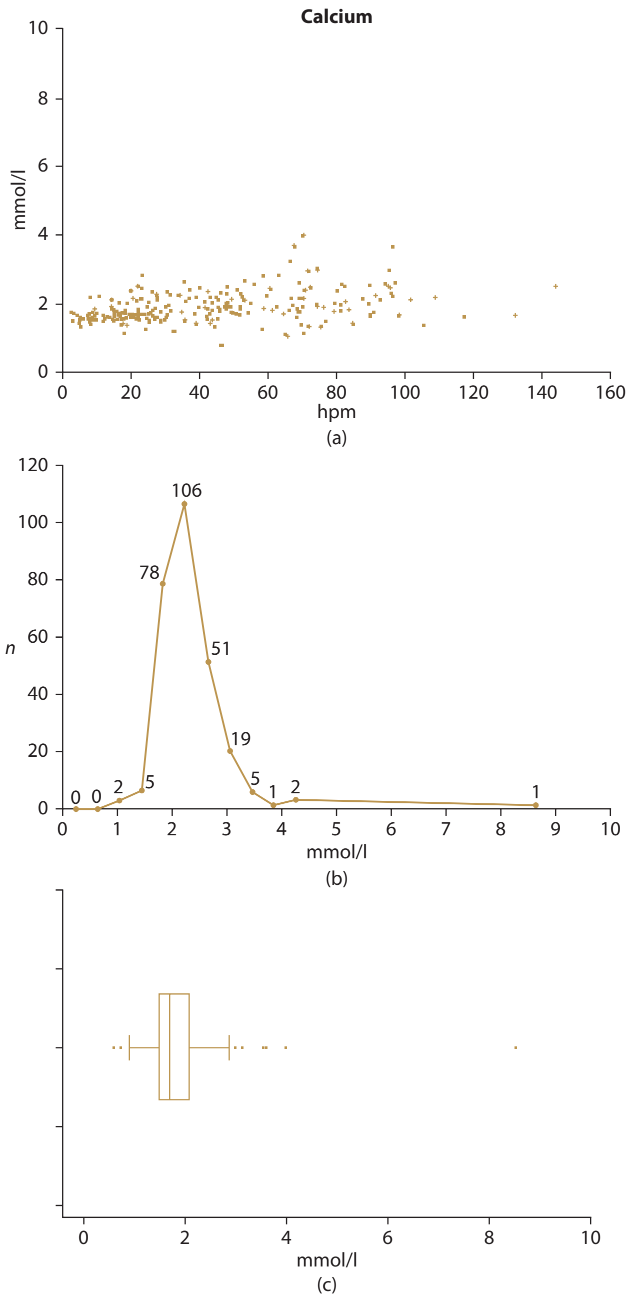

Figure 7.27 (a) Concentration, (b) frequency distribution of concentration and (c) box plots of calcium concentration. The rectangular box contains 50 per cent of all values found, marked by the upper and lower quartile. The box is divided by the median in two parts. The lines on the right and the left of the box correspond to the 90 per cent confidence interval and the median. The distribution becomes evident from the box plots.

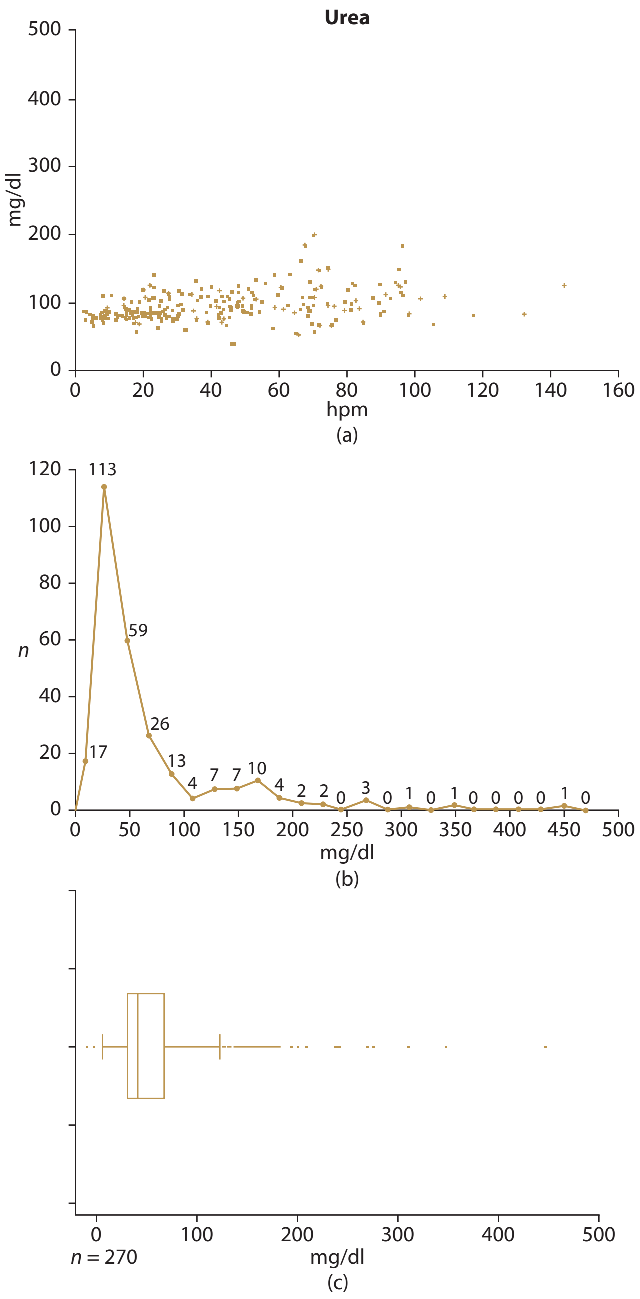

Figure 7.28 (a) Concentration, (b) frequency distribution of concentration and (c) box plots of urea concentration. The rectangular box contains 50 per cent of all values found, marked by the upper and lower quartile. The box is divided by the median in two parts. The lines on the right and the left of the box correspond to the 90 per cent confidence interval and the median. The distribution becomes evident from the box plots.

7.2.1.8 Which Formula Should Be Used in Casework?

In his historical review, Coe [26] asked whether vitreous K⁺ could be considered to have any value for the forensic pathologist at the present time. He recommended the test, and we share his opinion. Vitreous K⁺ is only of limited value for estimating the time since death in the first 24 hours post-mortem because other methods (e.g. body cooling, electrical excitability of skeletal muscles, chemical excitability of the iris) work quite satisfactorily in this post-mortem period, but the value of vitreous

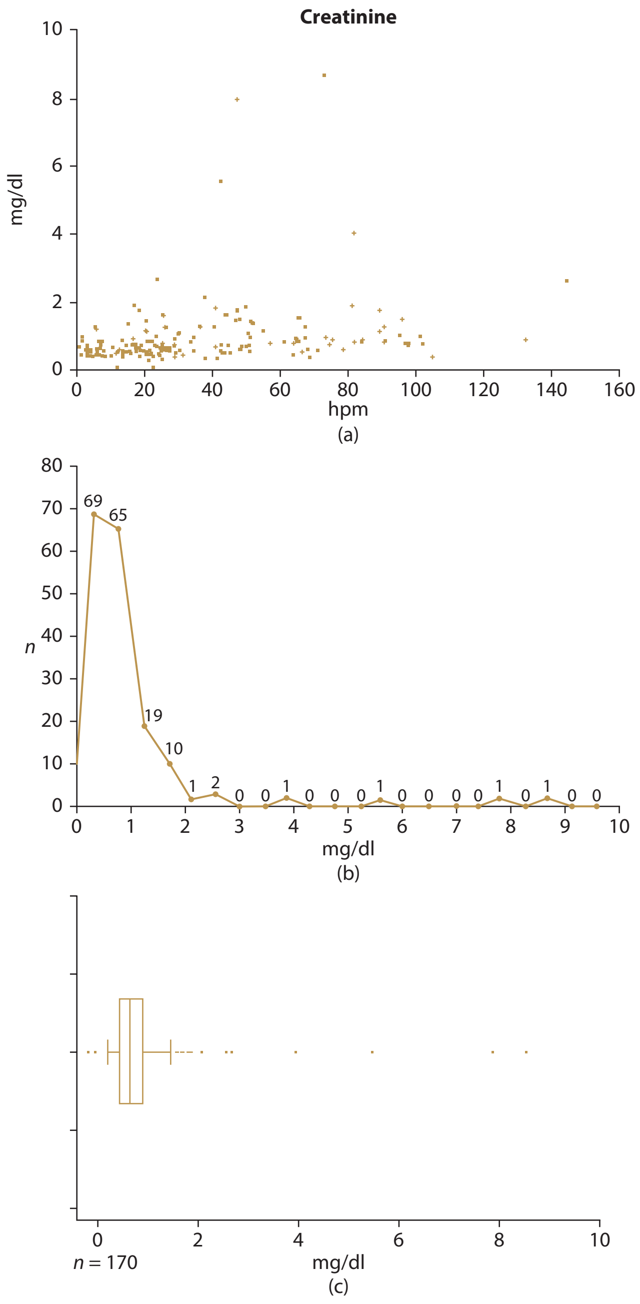

Figure 7.29 (a) Concentration, (b) frequency distribution of concentration and (c) box plots of creatinine concentration. The rectangular box contains 50 per cent of all values found, marked by the upper and lower quartile. The box is divided by the median in two parts. The lines on the right and the left of the box correspond to the 90 per cent confidence interval and the median. The distribution becomes evident from the box plots.

K^+ may increase with an increasing PMI, especially when the body has lain in a low to moderate environmental temperature. However, Coe proposed as the simplest procedure the well-known equation developed by Sturner [102]:

$$\text{PMI} = 7.14 \times \text{K}^+ \text{ concentration} - 39.1$$

Although the slope in Sturner's material is the flattest reported in the literature (see Table 7.13), Coe stated that results obtained from this formula are most satisfactory when the ambient temperature in which the body has lain is less than 50°F, and he emphasized that results even under these conditions may be inexact. The 95 per cent confidence limits will be much greater than ±4 hours on the first day and will increase with an increasing PMI. However, clear values for the precision of estimating the time since death (95 per cent confidence limits) using the Sturner formula are lacking. Madea et al. [62] compared the suitability and precision of death time estimation of the Sturner formula with their own equation with a much steeper slope (Figure 7.32). In 100 cases, mostly sudden traumatic or natural death with a short terminal episode and an ambient temperature lower than 50°F, the time since death was extrapolated using both the Sturner formula:

$$\text{PMI} = 7.14 \times \text{K}^+ \text{ concentration} - 39.1$$

and our own formula:

$$\text{PMI} = 5.26 \times \text{K}^+ \text{ concentration} - 39.9$$

From the deviation between real and extrapolated time since death, statistical parameters of precision of death time estimation were calculated. In a second step, we calculated the time since death for all cases in our random sample ($n = 270$) with a PMI of more than 30 hours and a urea value of less than 100 mg/dl ($n = 109$) by using Sturner's equation. This random sample is comparable to Sturner's material, in respect of cause and manner of death. Using the Sturner equation, there is a systematic deviation between real and extrapolated time since death (Figure 7.33 and Table 7.20). The mean difference between real and extrapolated time since death is 15 hours in the group of 100 cases compared with only −0.26 hours using our own equation. In the group of cases with a PMI of more than 30 hours and with urea values lower than 100 mg/dl, the mean difference (x) rises to 26 hours and the 95 per cent confidence limits to ±41 hours (Figure 7.34 and Table 7.21). This means that these parameters cover nearly the whole investigated PMI. The systematic overestimation of the time since death using Sturner's equation was expected: the reason is the flat slope (see Figure 7.32). Nearly all studies with larger case material reveal a much steeper slope between 0.17 and 0.238 mmol/l per hour. Therefore, when using the vitreous K^+ level to estimate the time since death, equations with a steeper slope than that reported by Sturner should be preferred to avoid systematic overestimations of the time since death.

Table 7.18 Creatinine as Internal Standard and Creatinine Compared with Urea as Internal Standard in a Random Sample of 170 Cases

Statistic parameters		**Creatinine <2 mg/dl**	**Creatinine <1.5 mg/dl**	**Creatinine <1.2 mg/dl**	**Creatinine <1.0 mg/dl**
Creatinine as internal standard (*n*)	170	163	154	142	133
Intercept	6.19	6.20	6.25	6.13	5.99
Slope	0.19	0.18	0.18	0.18	0.18
Correlation coefficient (*r*)	0.93	0.94	0.94	0.95	0.95
Variance (s^2_{yx})	4.39	3.37	3.20	2.79	1.62
Standard deviation (s_{yx})	2.10	1.84	1.79	1.67	
95% confidence limits (*h*)	± 19.89	± 18.08	± 17.99	± 16.94	± 16.22
Statistic parameters		Urea <100 mg/dl	Urea <70 mg/dl	Urea <70 and Creatinine <1 mg/dl	
Urea as internal standard compared with creatinine (*n*)	170	146	135	127	
Intercept	6.19	6.06	5.90	5.87	
Slope	0.19	0.187	0.18	0.18	
Correlation coefficient (*r*)	0.93	0.95	0.96	0.96	
Variance (s^2_{yx})	4.39	2.58	2.25	2.22	
Standard deviation (s_{yx})	2.10	1.60	1.50	1.49	
95% confidence limits (*h*)	± 19.89	± 16.33	± 15.22	± 14.99	

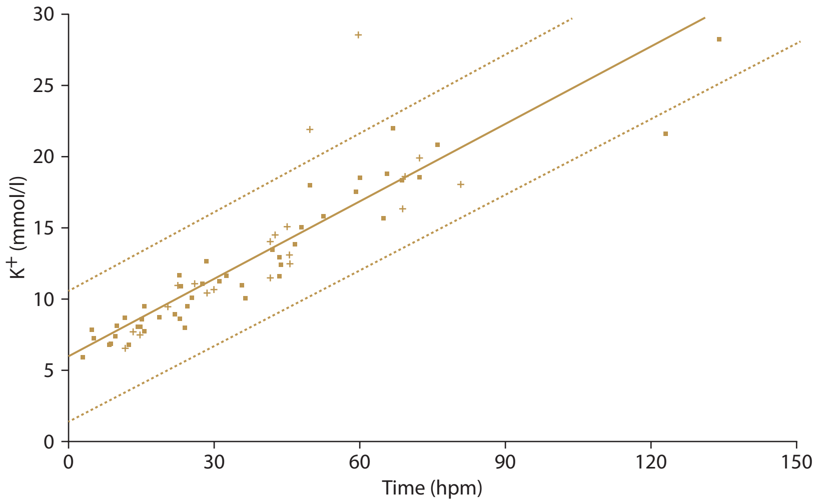

Figure 7.30 Potassium (K^+) values in cases of sudden traumatic death (*n* = 71). hpm, hours post-mortem.

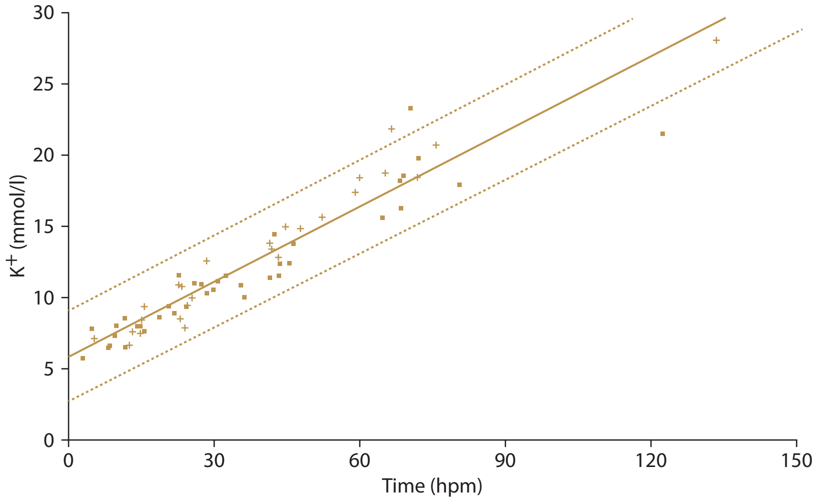

Figure 7.31 Potassium (K^+) values in cases of sudden traumatic death; elimination of all cases with urea values greater than 70 mg/dl. Significant rise in the precision of death time estimation. hpm, hours post-mortem.

Table 7.19 Urea Values Lower than 70 mg/dl as an Internal Standard in Cases of Sudden Traumatic Death

Value	Entire sample	Urea <70 mg/dl
n	71	68
Intercept	6.0	6.0
Slope	0.18	0.177
Correlation coefficient (r)	0.90	0.94
Variance (s^2_{yx})	5.341	2.528
95% confidence limits	22.72	17.14

Estimating the time since death with a slope of 0.19 mmol/l per hour and an intercept of 5.88 mmol/l (which is almost the same as the intercept calculated from Sturner's material of 5.96 mmol/l) provides an estimation of the time since death with no systematic deviations. The 95 per cent confidence limits are ±20 hours up to 100 hours post-mortem.

Other equations on PMI estimation are shown in Table 7.22.

A comparison of the precision of death time estimation using these different formulas is still missing.

7.2.1.9 Re-analysis of Original Data and Construction of a Local Regression Model

Lange et al. [52] re-analysed the data of six studies on the rise of vitreous K^+ comprising 790 cases total [1,23,58,100,102]. This re-analysis revealed that

- The relationship between vitreous K^+ and PMI is not completely linear.
- The residual variability of vitreous K^+ as a function of PMI is not constant.

Therefore, these investigators developed a new approach for modelling vitreous K^+ and PMI that accommodated non-linearities and changing residual variability. At first, a local regression model—specifically a loess smooth curve—was fitted separately to the data from each of the six studies. The data of all six studies were then combined to yield a single loess curve with 95 per cent confidence limits (Figure 7.35).

The estimated loess curve and confidence limits were then used in an inverse prediction method to construct low, middle and high PMI estimates at given values of vitreous K^+ (Table 7.23).

The reliability of estimated PMI decreases with an increasing K^+ concentration. However, PMI estimates are more precise over the entire range of vitreous K^+ and PMI than are estimates obtained from any single study alone. For K^+ values lower than 7 mmol/l, the extent of the lower and upper 95 per cent confidence limits is ±1 hour. For K^+ values greater than 7 mmol/l but less than 12 mmol/l, the extent of these confidence limits is ±2 hours. For a K^+ value greater than 12 mmol/l and less than 18 mmol/l, the extent is ±3 hours, whereas for a value greater than 18 mmol/l, the extent is ±5 hours. For concentrations greater than18 mmol/l, the extent is even greater.

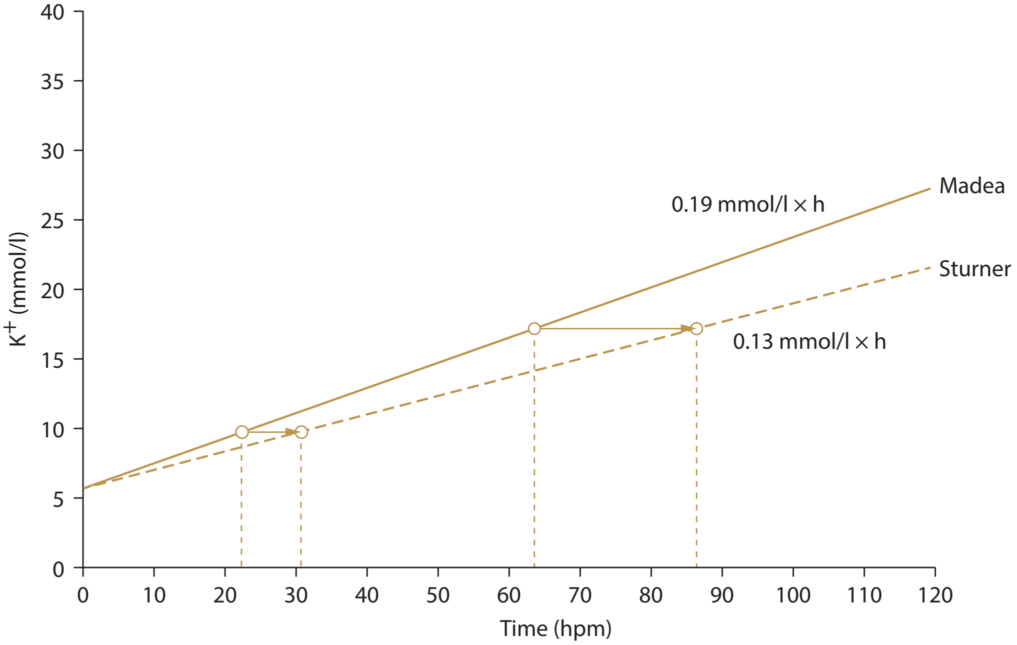

Figure 7.32 Vitreous potassium (K^+) level over the post-mortem interval (in hours [hpm]). Regression lines of Sturner and of the authors' own material. The intercept of both regression lines is nearly identical, but the slope varies between 0.13 mmol/l per hour (Sturner [102]) and 0.19 mmol/l per hour (authors' material). The much flatter slope of Sturner's regression for the same K^+ values causes a systematic overestimation of the time since death compared with the authors' regression. This overestimation increases with an increasing post-mortem interval.

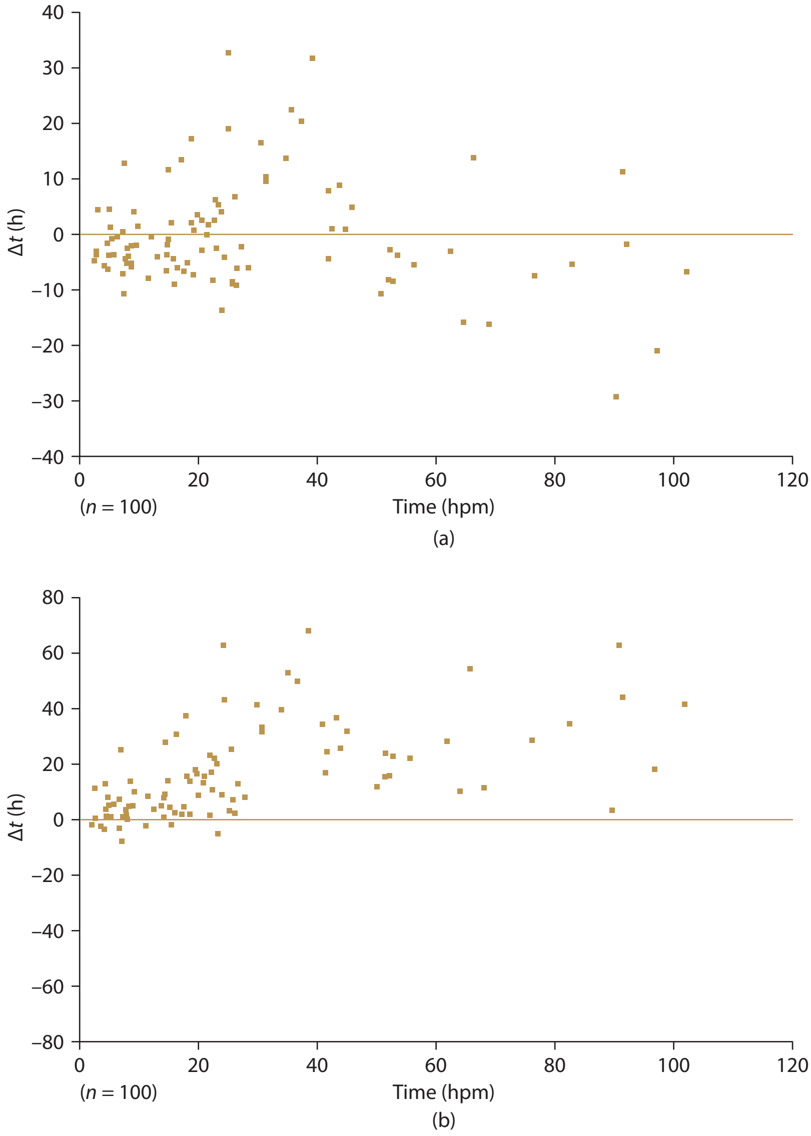

Figure 7.33 Deviations between extrapolated and real time since death (Δ*t* in hours) over the post-mortem interval for 100 independent cases in the post-mortem interval from 3 to 100 hours post-mortem (hpm). (a) Deviations using the authors' formula; no systematic deviations. (b) Deviations using the Sturner equation: systematic overestimation of the time since death.

Table 7.20 Mean Differences, Standard Deviation and 95 Per Cent Confidence Limits (in Hours) between Real and Extrapolated Time Since Death for 100 Independent Cases in the Post-mortem Interval of 3–100 Hours, Using Sturner's and the Authors' Own Equations for Extrapolating the Time Since Death

	Sturner's equation*	Authors' equation
n	100	100
$\overline{X}$	15.35	−0.258
SD	± 16.43	± 0.56
95% confidence limits	± 32.76	± 19.06

* Data from Sturner WQ [102].

Abbreviations: $\overline{X}$, mean differences; SD, standard deviation.

However, because of the much greater variability of the single K⁺ concentrations of the included studies from the 'single loess curve' with its 95 per cent confidence limits, the reliability of the statistical evaluation remains unclear. Obviously, the 95 per cent confidence limits concern the 'single loess curve' and not the deviations of the single values from the 'single loess curve'.

7.2.1.10 Re-evaluation of the Data of Lange and Associates

To re-evaluate the validity of the table of Lange et al. [52] (see Table 7.23) from 523 cases with measured K⁺ concentrations and known time since death, 492 cases (94 per cent) were selected [72]. In these 492 cases, the K⁺ concentrations were within a 10 per cent interval (±5 per cent) around the increasing K⁺ values given by Lange et al. (see Table 7.23).

Of the selected 492 cases, 153 had a PMI within the predicted PMI for the given K⁺ concentration, and 339 lay outside the interval (Table 7.24) [72].

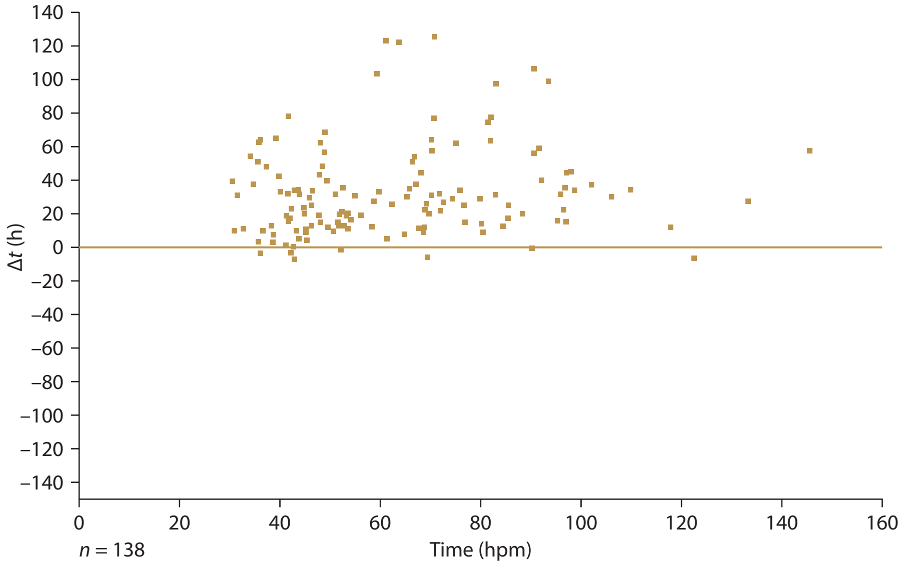

Figure 7.34 Deviations between real time (Δ*t*) and estimated time since death over the post-mortem interval in hours for 109 cases with a post-mortem interval of more than 30 hours and vitreous urea values below 100 mg/dl. Extrapolation of the time since death with Sturner's equation [102].

There has been a mean difference of −6 hours between estimated time since death according to Table 7.23 and actual time since death and a standard deviation of ±12 hours.

Table 7.21 Mean Difference, Standard Deviation and 95 Per Cent Confidence Limits (in Hours) between Real and Extrapolated Time Since Death for 109 Cases with a Post-mortem Interval of More than 30 Hours and a Vitreous Urea Value Lower than 100 mg/dl

	Sturner's equation
n	109 PMI >30 h Urea <100 mg/dl
$\overline{x}$	26.68
SD	± 20.88
95% confidence limits	± 40.92

Abbreviations: $\overline{x}$, mean differences; SD, standard deviation.

Source: Data from Sturner [102].

Figure 7.36 shows a widening gap between estimated and actual time since death with an increasing K^+ concentration corresponding to an increasing time since death.

It can be concluded that the calculation of the time since death based on the table published by Lange et al. [52] (see Table 7.23) reveals a systematic overestimation of the time since death, and the accuracy of death time estimation cannot be confirmed [72].

7.2.1.11 Accuracy of Estimating the Time Since Death by Using the Potassium Concentration as Independent Variable

Since the 1970s, reports on the rise of the K^+ concentration in vitreous humour have been published, with different statements concerning the accuracy of death time estimation. Although in most investigations the

Table 7.22 Formulae for Determining Post-mortem Interval (Hours) with Potassium Concentration (mmol/l)

Reference	Equation obtained*	Formula proposed
Sturner [102]	$y = 0.14x + 5.6$	PMI = 7.14 [K^+]–39.1
Adelson et al. [1]	$y = 0.17x + 5.36$	–
Hansson et al. [37]	$y = 0.17x + 8$	–
Coe [23]	$y = 0.332x + 4.99$ ($x < 6$ h)	–
Coe [23]	$y = 0.1625x + 6.19$ ($x \geq 6$ h)	–
Adjutanis and Coutselinis [2]	$y = 0.55x + 3.14$	–
Stephens and Richards [101]	$y = 0.238x + 6.342$	–
Madea et al. [58]	$y = 0.19x + 5.88$	PMI = 5.26 [K^+]–30.9
James et al. [45]	$y = 0.23x + 4.2$	PMI = 4.32 [K^+]–18.35
Muñoz Barús et al. [79]	$y = 0.17x + 5.60$	PMI = 3.92 [K^+]–19.04
Jashnani et al. [46]		PMI = 1.076 [K^+]–2.815

* *y* is potassium (K^+); variable *x* is post-mortem time/interval (h).

Abbreviations: PMI, post-mortem interval.

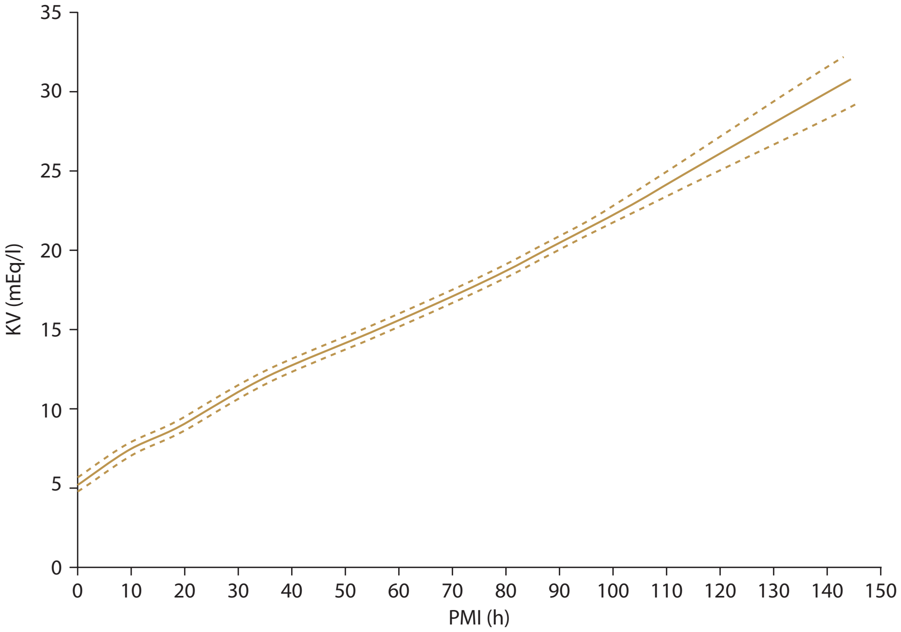

Figure 7.35 The estimated relationship between vitreous potassium (KV) and post-mortem interval (PMI) for six studies, with 95 per cent lower and upper confidence limits.

(From Lange N, Swearer ST, Sturner WQ. Human postmortem interval estimation from vitreous potassium: an analysis of original data from six different studies. *Forensic Sci Int* 1994;**66:**159–174.)

Table 7.23 Estimated Values of Post-mortem Intervals for Various Increasing Values of Potassium Obtained from Combining All 790 Cases and the Loess Procedure

	Estimated PMI (h)		
Measured vitreous potassium concentration mmol/l	**Lower 95% confidence limit value**	**Mean value**	**Upper 95% confidence limit value**
5.9	2	3	4
6.4	3	5	6
7.0	6	7	8
7.5	8	10	12
8.0	11	13	15
8.5	14	16	19
9.1	18	21	22
10.1	23	25	27
11.1	29	30	32
12.1	33	35	38
13.0	39	41	44
13.9	44	47	50
14.9	51	54	57
15.9	58	61	64
17.0	66	69	72
18.3	74	77	81
19.7	81	85	90
21.1	89	94	100
22.6	98	103	111
24.2	106	113	123

Source: From Lange N, Swearer ST, Sturner WQ. Human postmortem interval estimation from vitreous potassium: an analysis of original data from six different studies. *Forensic Sci Int* 1994;**66:**159–174.

Table 7.24 Overview of Cases (*n* = 492) with Potassium Concentrations within 10 Per Cent around the Mean Values According to Lange et al. (see Table 7.23)*

		Frequency	**Percentage**
Cases within the post-mortem interval corresponding to the potassium concentration according to Table 7.23.	No	$n = 339$	68.9%
	Yes	$n = 153$	31.1%
	Total	$N = 492$	100.0%

* The post-mortem interval (PMI) was calculated for the respective K^+ according to Table 7.23; 339 PMIs were outside the PMI according to Table 7.14, and 153 were inside.

Source: From Madea B, Rödig A. Time of death dependent criteria in vitreous humor: accuracy of estimating the time since death. *Forensic Sci Int* 2006;**164:**87–92.

PMI has been used as the independent variable and K^+ concentration as the dependent variable for regression analysis between PMI and K^+ concentration, it has been suggested to use the K^+ concentration as the independent variable for regression analysis [76,79]. Changing variables would lead to a higher accuracy in death time estimation. This hypothesis has meanwhile been checked on independent cases with K^+ and Hx in vitreous humour. Linear regression with the K^+ or Hx concentration as an independent variable has revealed a slightly more accurate death time estimation compared with linear regression with PMI as the independent variable (Table 7.25). Thus, for example, the accuracy could have been improved from ±25.96 to ±23.27 hours by using the K^+ concentration as the independent variable [72].

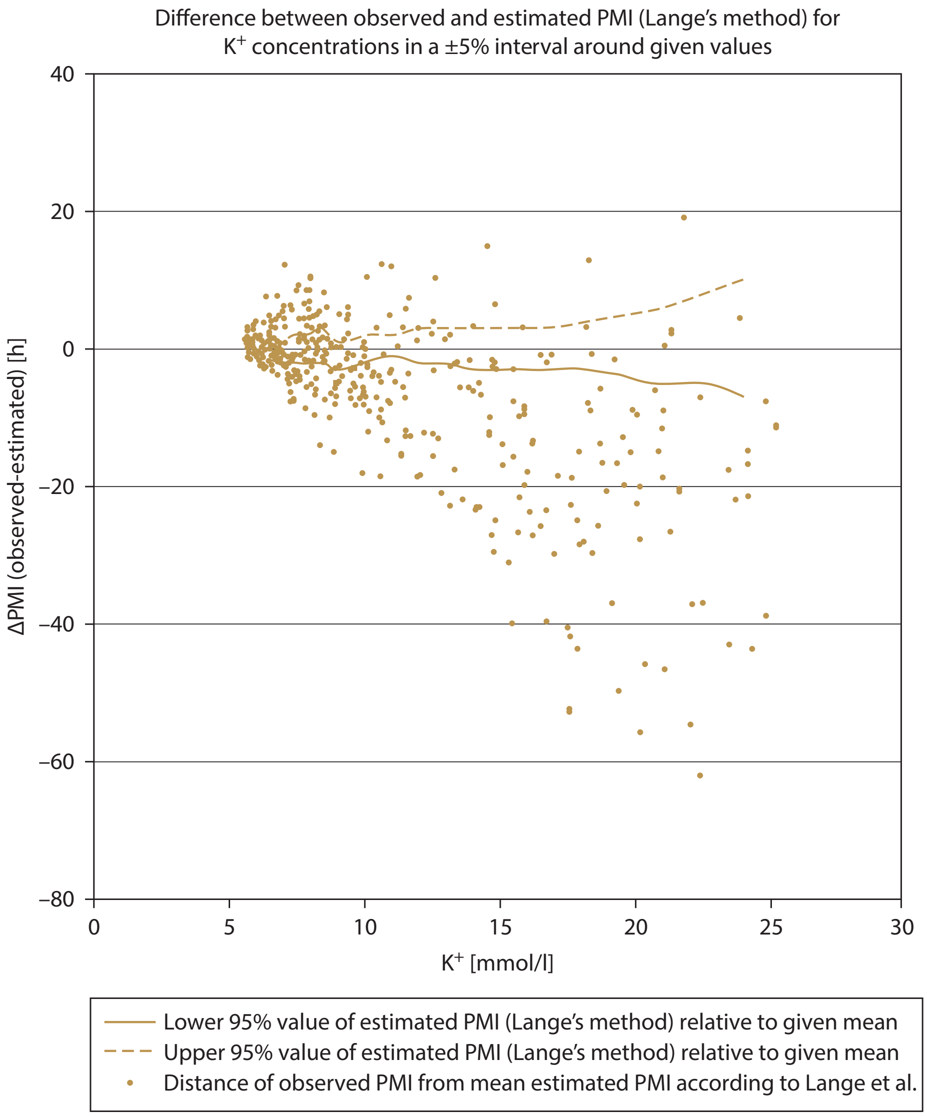

Figure 7.36 Deviations between real and extrapolated time since death over the potassium (K^+) concentration. Each point represents the difference between the observed post-mortem interval (PMI) and estimated PMI according to Lange et al. Those cases with K^+ concentrations in a ±5 per cent interval around the given concentrations were included. The two lines represent the upper and lower value of the 95 per cent confidence interval according to Lange et al. [49] relative to the given means [72].

Table 7.25 Regression Parameters of the Linear Regression for Estimating the Time Since Death from Vitreous Potassium: Correlation Coefficient, Standard Deviation and 95 Per Cent Confidence Limits*

	Own cases ($N = 170$)		Cases from Muñoz Barús et al., 2002 ($N = 171$)	
Data	**[K^+]-dependent variable**	**PMI-dependent variable**	**[K^+]-dependent variable**	**PMI-dependent variable**
Rise (PMI/K^+)	4.76	3.82	5.78	3.81
Intercept (PMI)	−29.05	−16.46	−32.28	−18.15
Mean value of residues (real minus calculated)	0.055	0.000	−0.014	0.000
Standard deviation (h)	13.25	11.87	4.36	3.54
95% confidence limits	± 25.96	± 23.27	± 8.55	± 6.94
PMI (h)	Up to 133		Up to 23	
Correlation coefficient (r^2)	0.801		0.660	

* Compared are precisions of estimating the time since death on two random samples with [K^+] as dependent or independent variable. Own sample and cases by Muñoz Barús et al. ($n = 176$).

Abbreviations: [K^+], potassium concentration; PMI, post-mortem interval.

Source: From Madea B, Rödig A. Time of death dependent criteria in vitreous humor: accuracy of estimating the time since death. *Forensic Sci Int* 2006;**164:**87–92.

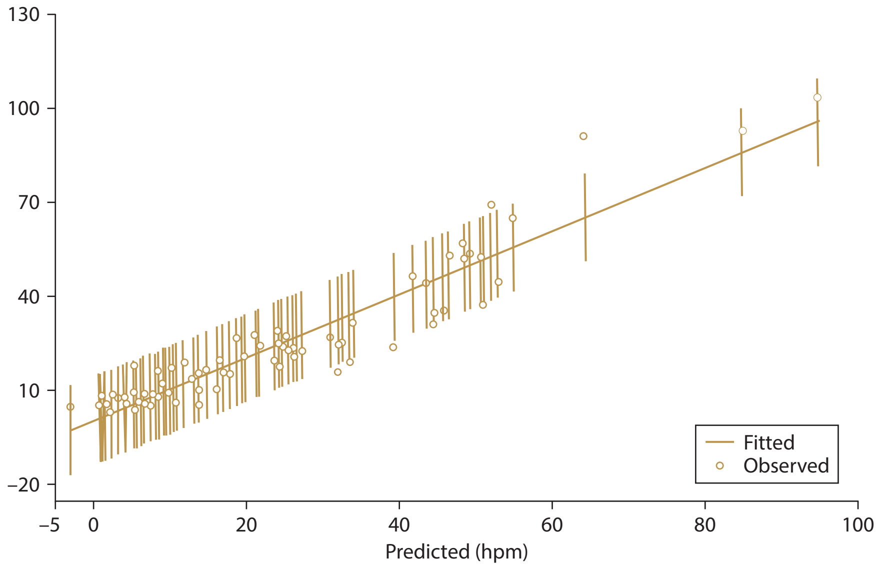

Figure 7.37 By multiple regression analysis, the calculated time since death over the real time since death. The vertical lines represent the 95 per cent confidence limits. hpm, hours post-mortem.

7.2.1.11.1 Multiple Linear Regression Analysis

Multiple linear regression analysis uses, apart from vitreous K^+, further time-dependent changing vitreous analytes. By using the multiple linear regression formula:

$$\mathrm{PMI} = 24.64 + (4.3741 \times \mathrm{K}^+) - (0.278 \times \mathrm{Na}^+) - (0.065 \times \mathrm{urea}) - (1.08 \times \log \mathrm{glucose})$$

95 per cent confidence limits of ±14 hours could be achieved (Figure 7.37). Using K^+ alone, the 95 per cent confidence limits on the same sample ($n = 85$) were ±16.2 hours. Therefore, it can be concluded that, by using multiple linear regression analysis, a slight increase in the precision of death time estimation can be achieved.

7.2.2 Hypoxanthine

Elevated Hx values resulting from tissue hypoxia have been demonstrated by several authors in different body fluids (plasma, urine, CSF, fetal scalp blood) [38,56,63,67–70,74,79,82,84,88–92]. These elevated Hx values are thought to be good markers of hypoxia, mainly in paediatric cases [89–93]. The increase of Hx during hypoxia is thought to be caused by the following three mechanisms:

1. An increased concentration of cellular adenosine monophosphate.
2. A decreased transformation of Hx into uric acid.
3. Inhibition of xanthine oxidase (Figure 7.38).

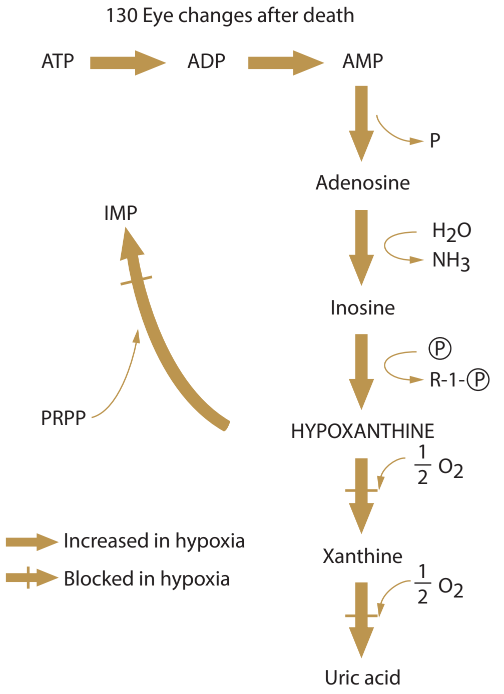

Figure 7.38 Cellular mechanisms for an increase of hypoxanthine concentration during hypoxia. ADP, adenosine diphosphate; AMP, adenosine monophosphate; ATP, adenosine triphosphate; IMP, inosine monophosphate; NH_3, ammonia; P, phosphate; PRPP, 5-phospho-a-d-ribosyl pyrophosphate.

(From Saugstad OD. Hypoxanthine as a measurement of hypoxia. *Pediatr Res* 1975;**9**:158–161.)

In 1957, Praetorius et al. [86] reported a post-mortem rise of Hx in CSF, and there are some reports on the post-mortem elevation of Hx in skeletal muscle as an aid for estimating the time since death. A 1991 study [88] of a then new biochemical method for estimation of post-mortem time on 87 cases revealed the following:

- A linear rise of Hx in vitreous humour in the PMI up to 120 hours post-mortem (hpm).

- A dependency of the slope of rise of vitreous Hx on temperature (the higher the ambient temperature, the steeper the slope).
- A strong correlation between vitreous Hx and vitreous K^+ values.
- A smaller range of scatter of the vitreous Hx than the vitreous K^+ values.

These results are based on 368 vitreous samples taken from 87 cases; two samples were taken from each eye, and four values per case were obtained.

The authors suggested further investigations on vitreous Hx in comparison with vitreous K^+. These investigations are indeed necessary because there are no statistical parameters on the precision of death time estimation by vitreous Hx compared with vitreous K^+.

7.2.2.1 Materials and Methods

Our own investigations [63] were performed on 92 bodies with a known time since death. Each globe was punctured only once, and the whole vitreous humour was withdrawn. Each sample was analysed independently. In these 92 cases, the vitreous humour of both eyes was withdrawn at the same time post-mortem.

In an additional 43 cases, vitreous humour of both eyes was withdrawn at timed intervals, ranging from 2 to 20 hours after death. The CSF samples were obtained by single puncture of the cisterna cerebello-medullaris.

The cases used for this study were all adults who had died either suddenly of natural causes, with a brief terminal episode, or of traumatic causes, also with a brief terminal episode.

The K^+ concentration was determined using ion-selective electrodes, and the Hx concentration was determined using a high-performance liquid chromatography method analogous to that of Rognum et al. [88].

7.2.2.2 Results and Discussion

7.2.2.2.1 Vitreous Humour

The vitreous samples of both eyes taken at the same time post-mortem showed a good correlation of Hx and K^+ values. For statistical analysis, the mean values of the K^+ and Hx concentrations from both eyes were used.

Hx increased in a linear mode over the PMI; the linear rise began immediately post-mortem rather than after a certain ‘stable interval’ of some 48–72 hours, as originally described (Figure 7.38). This immediate post-mortem rise of Hx concentration is in good accord with experimental animal findings of Gardiner et al. [34] and the findings of Rognum et al. [88].

The K^+ concentration increases linearly, as has long been known (Figure 7.39), and it has a much stronger correlation with the time since death than the Hx concentration (correlation coefficient [r] = 0.925 for K^+ compared with r = 0.714 for Hx). The 95 per cent confidence limits are ±17 hours for vitreous K^+ and ±32 hours for vitreous Hx (Table 7.26).

The conclusion of Rognum et al. [88] that the scatter of levels is greater for K^+ than for Hx cannot be confirmed based on our own material [see also 66,76 and 79].

In cases with timed bilateral withdrawal of vitreous humour (intervals from 2 to 20 hours), there are great interindividual differences in the rise of Hx concentrations. As is already known for vitreous K^+, there may be greater differences between the concentrations in both eyes, even when samples are withdrawn at the same time. This is also true for the Hx concentration. Indeed, if there

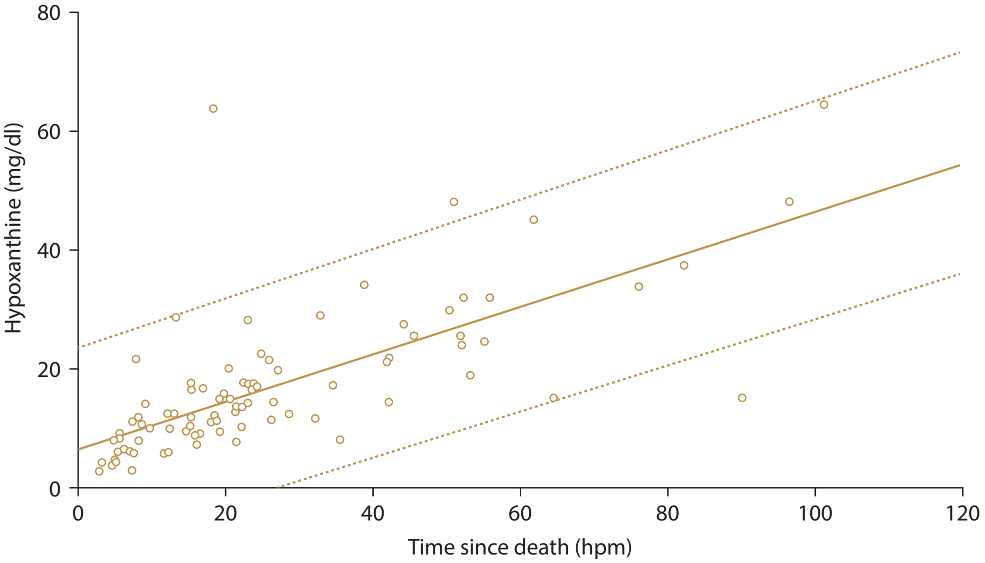

Figure 7.39 Hypoxanthine concentration in vitreous humour over the time since death (hours post-mortem [hpm]), with 95 per cent confidence limits.

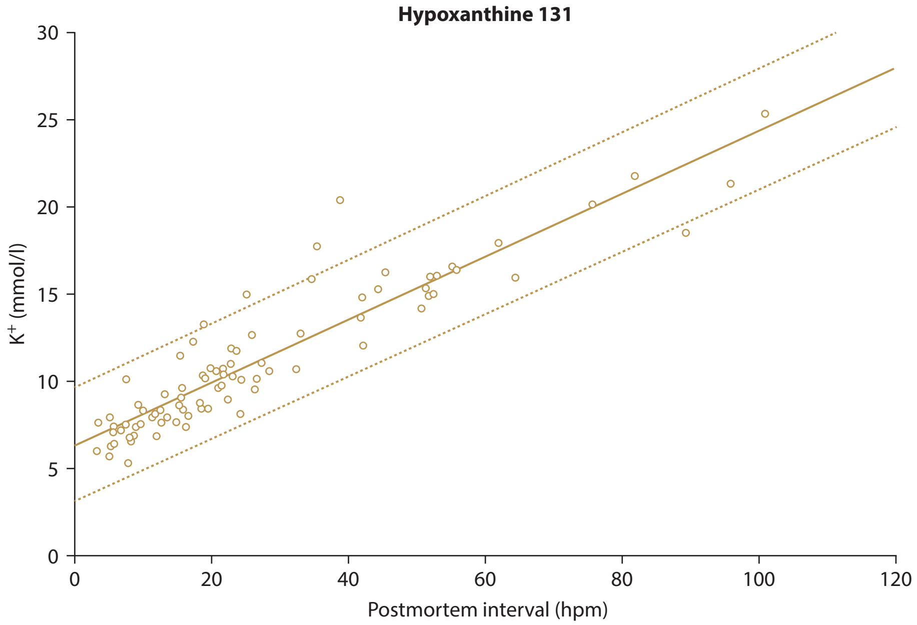

Figure 7.40 Potassium (K^+) concentration over the post-mortem interval (hours post-mortem [hpm]), with 95 per cent confidence limits.

Table 7.26 Statistical Parameters on the Precision of Estimating the Post-mortem Interval by Vitreous Hypoxanthine and Potassium

	Hypoxanthine	Potassium
N	92	92
Correlation coefficient (*r*)	0.7138	0.925
Intercept (*a*)	3.6991	6.3177
Slope (*b*)	1.293	0.179
95% confidence limits	±30.1	±16.3

are greater differences between both eyes, the later sample may have an even lower Hx concentration than the earlier sample.

The differences between the results from our study [63] and those of Rognum et al. [88] on vitreous Hx and K^+ are apparent. However, because we have used similar methods and the random samples consisted of comparable cases, an explanation for this discrepancy is not straightforward. One reason may be seen in the repeated sample taking, with disturbance of the vitreous concentration gradient. During life, in mammalian eyes, there are concentration gradients for several parameters among the different intraocular fluid compartments. After death, new gradients are established, mainly between the retina and the centre of the globe. Therefore, for biochemical analysis it is mandatory to aspirate the whole of the vitreous humour. Repeated sample taking disturbs the diffusion gradient and establishes a drainage effect, as described by Schourup [57] and by Dotzauer and Naeve [57] in their studies on CSF.

Rognum and Saugstad [90] seemed to be aware of this drainage effect in another study on vitreous Hx values in cases of sudden infant death syndrome. Although each globe was punctured twice, the Hx values of the second sample were found to be too high. These authors reported that 'multiple sampling during hypoxaemia was attempted, but this procedure led to artificially high values of hypoxanthine compared with control values from the left eye . . . and the procedure had to be abandoned' [84]. These authors added that 'furthermore, in the group in which sampling was started early after death, there was a slight tendency for the Hx increase to be greater at the second sampling within the same eye. This increase could be attributable to a certain degree of tissue mutilation during the sample procedure'.

A second possible reason for the different results may be that not only does Hx increase post-mortem in vitreous humour and CSF as a result of irreversible circulatory arrest, anoxaemia and diffusion, but also, during vital hypoxia, 'there is an accelerated catabolism of adenosine monophosphate to hypoxanthine which accumulates in tissues and body fluids [90]'.

In 1975, increased levels of plasma Hx were reported in newborn infants with clinical signs of intrauterine hypoxia during labour, compared with newborn infants after normal delivery. These increased values were interpreted as being caused by hypoxia, and the Hx accumulation in plasma was seen as a sensitive parameter of hypoxia.

The increase in Hx levels in different body fluids has been confirmed by several working groups. The vital elevation resulting from hypoxia is a factor of about 2.5–5, but it is rarely 10 or more. Compared with this vital elevation, the post-mortem rise has a 66-fold increase [34], which is much more marked. However, if hypoxia during life causes a marked increase in vitreous Hx, this may of course result in a greater scatter of post-mortem Hx values than of K^+ values.

The post-mortem rise of vitreous K^+ is mainly caused by diffusion from the retina into the centre of the globe, whereas Hx is a post-mortem degradation product of the adenine nucleotide metabolism. Hx is formed by the process of several enzymatic reactions (see Figure 7.25), and it then diffuses along the concentration gradient. In theory, it could be expected that a parameter such as a post-mortem increase that is solely the result of diffusion would correlate much more strongly with the time since death than would a parameter that increases in response to vital or post-mortem degradation and diffusion. Meanwhile, different formulae for determining PMI (hours) with Hx (μmol/l) have been proposed (Table 7.27) [45,63,66,79,88].

Table 7.27 Formulae for Determining Post-mortem Interval (Hours) with Hypoxanthine (μmol/l)

Reference	Equation obtained*	Formula proposed
Rognum et al. [88]	$y = 4.2x + 7.6$ at 5°C $y = 5.1x + 7.6$ at 10°C $y = 6.2x + 7.6$ at 15°C $y = 8.8x + 7.6$ at 23°C	
Madea et al. [66]	$y = 1.29x + 3.69$	
James et al. [45]	$y = 3.2x - 0.15$	PMI = 0.31 [Hx] + 0.05
Muñoz et al. [79]	$y = 3.01x + 26.45$	PMI = 7.14 [Hx] + 0.17

* *y* is hypoxanthine; variable *x* is the post-mortem interval (h).
Abbreviations: Hx, hypoxanthine; PMI, post-mortem interval.

In CSF, there is an exponential rise of the Hx concentration, with the steepest slope during the first 15 hours post-mortem (Figure 7.41). This steep rise during the early PMI is apparent from the results of Praetorius et al. [86], who found a more than 100-fold increase of Hx and xanthine values in CSF during the time interval up to 36 hours post-mortem.

Manzke et al. [69] observed no significant differences in the oxypurine concentrations of CSF samples during the first 3 days post-mortem (the samples were reserved during autopsy), but these authors clearly obtained their samples too late. Immediately after death, a rapid and marked rise of Hx in CSF occurs, and an equilibration seems to be achieved after about 20 hours. An exponential rise has also been reported in CSF K^+ levels. Among several other components of CSF examined by Schourup [57], the steepest rise occurs within the first few hours post-mortem, and equilibration is achieved after about 15 hours.

The mean normal value for CSF Hx in newborn infants was found to be 3.6 (range, 1.8–5.5) mmol/l, whereas that in adults was 1.8 (range, 0.6–5.1) mmol/l [38,39].

Compared with the rise of Hx in CSF that occurs as a consequence of hypoxia, the post-mortem rise and the post-mortem Hx levels are much more marked. Neither CSF K^+ nor CSF Hx concentrations can be recommended for practical use in death time estimation because the 95 per cent confidence limits are wide, and they also increase with increasing PMI. Other methods function satisfactorily during this early PMI, for up to 20 hours.

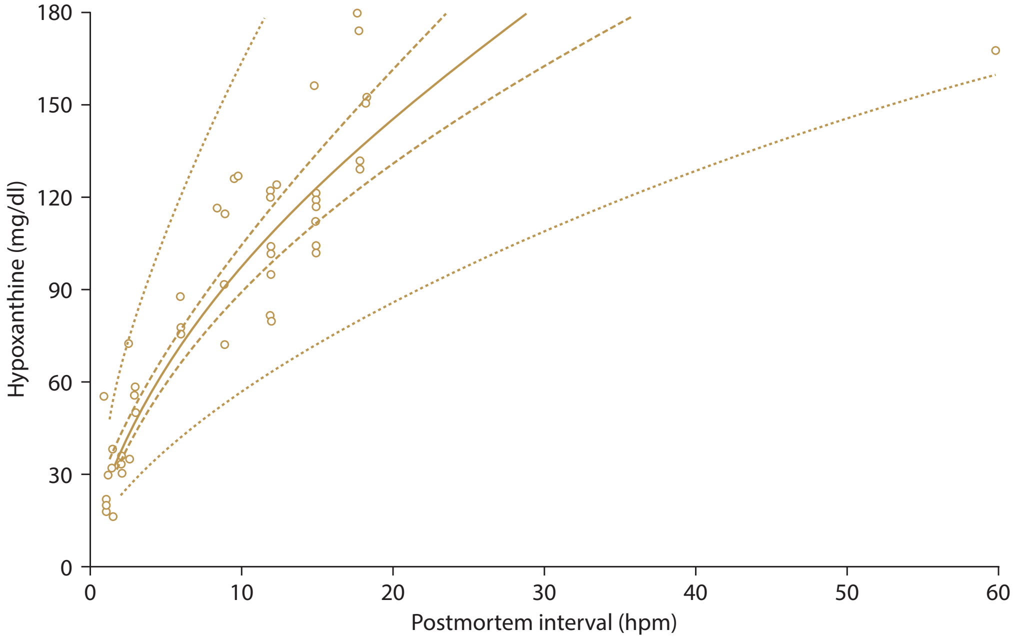

Figure 7.41 Increase of hypoxanthine in cerebrospinal fluid over various post-mortem intervals. An equilibration is achieved after 15–20 hours post-mortem (hpm).

References and further reading

1. Adelson L, Sunshine I, Rushforth NB, Marnkoff M. Vitreous potassium concentration as an indicator of postmortem interval. *J Forensic Sci* 1963;*8*:503–14.
2. Adjutantis G, Coutselinis A. Estimation of the time of death by potassium levels in the vitreous humour. *Forensic Sci Int* 1972;*1*:55–60.
3. Ahi RS, Garg V. Role of vitreous potassium level in estimating postmortem interval and the factors affecting it. *J Clin Diagn Res* 2011;*5*:13–15.
4. Ashima M, Agrawal YK. An overview of methods used for estimation of time since death. *Aust J Forensic Sci* 2011;*43*(4):275–85.
5. Balasooriya BAW, Hill CAS, Williams AR. The biochemistry of vitreous humour: a comparative study of the potassium, sodium and urate concentration in the eyes at identical time intervals after death. *Forensic Sci Int* 1984;*26*:85–91.
6. Balazs EA, Denlinger JL. The vitreous. In: Dawson H (ed.). *The Eye*, vol. 1a. 3rd ed. London: Academic Press, 1984, pp 533–89.
7. Berman ER, Voaden M. The vitreous body. In: Graymore CN (ed.). *Biochemistry of the Eye*. London, Academic Press, 1970, pp 373–471.
8. Bito LZ. Intraocular fluid dynamics I: Steady state concentration gradients of magnesium, potassium and calcium in relation to the sites and mechanisms of ocular cation transport processes. *Exp Eye Res*1970;*10*:102–16.
9. Bito LZ. The physiology and pathophysiology of intraocular fluids. In: Bito LZ, Davson H, Fenstermacher JD (eds.). *The Ocular and Cerebrospinal Fluids*. London, Academic Press, 1977, pp 273–89.
10. Blana SA, Musshoff F, Hoeller T, Fimmers R, Madea B. Variations in vitreous humor chemical values as a result of pre-analytical treatment. *Forensic Sci Int* 2011;*210*:263–70.
11. Blumenfeld TA, Mantell CH, Catherman RL, Blanc WA. Postmortem vitreous humour chemistry in sudden infant death syndrome and in other causes of death in childhood. *Am J Clin Pathol* 1979;*71*:219–23.
12. Bortolotti F, Pascali JP, Davies GG, Smith FP, Brissie RM, Tagliaro F. Study of vitreous potassium correlation with time since death in the postmortem range from 2 to 110 hours using capillary ion analysis. *Med Sci Law* 2011;*51*:S20–3.
13. Bray M. The effect of chilling, freezing, and rewarming on the postmortem chemistry of vitreous humor. *J Forensic Sci* 1984;*29*:401–11.
14. Bray M. The eye as a chemical indicator of environmental temperature at the time of death. *J Forensic Sci* 1984;*29*:396–403.
15. Chandrakanth HV, Kanchan T, Balaraj BM, Virupaksha HS, Chandrashekar TN. Postmortem vitreous chemistry: an evaluation of sodium, potassium and chloride levels in estimation of time since death (during the first 36 h after death). *J Forensic Leg Med* 2013;*20*:211–16.
16. Choo-Kang E, McKoy C, Escoffrey C. Vitreous humour analytes in assessing the postmortem interval and the antemortem clinical status. *Wiss Med J* 1983;*32*:23–6.
17. Coe JI. Postmortem chemistries on vitreous humour. *Am J Pathol* 1969;*51*:741–50.
18. Coe JI. Vitreous potassium as a measure of the postmortem interval: an historical review and critical evaluation. *Forensic Sci Int* 1989;*42*:201–13.
19. Coe JI, Apple FS. Variations in vitreous humour chemical values as a result of instrumentation. *J Forensic Sci* 1985;*30*:828–35.
20. Coe JI. Further thoughts and observations on postmortem chemistries. *Forensic Sci Gaz* 1973;*5*:2–6.
21. Coe JI. Postmortem biochemistry of blood and vitreous humour in pediatric practice. In: Mason JK (ed.). *Pediatric Forensic Medicine and Pathology*. London, Chapman & Hall Medical, 1989, pp 191–203.
22. Coe JI. Postmortem chemistries on blood with particular reference to urea nitrogen, electrolytes and bilirubin. *J Forensic Sci* 1974;*19*:33–42.
23. Coe JI. Postmortem chemistries on vitreous humour. *Am J Pathol* 1969;*51*:741–50.
24. Coe JI. Postmortem chemistry of blood, cerebrospinal fluid and vitreous humour. In: Wecht CH (ed.). *Legal Medicine Annual*. New York, Appleton-Century-Crofts, 1976, pp 53–91.
25. Coe JI. Postmortem chemistry: Practical consideration and a review of the literature. *J Forensic Sci* 1974;*19*:13–42.
26. Coe JI. Vitreous potassium as a measure of the postmortem interval: an historical review and critical evaluation. *Forensic Sci Int* 1989;*42*:201–13.
27. Cordeiro C, Ordóñez-Mayán L, Lendoiro E, Febrero-Bande M, Vieira DN, Muñoz-Barús JI. A reliable method for estimating the postmortem interval from the biochemistry of the vitreous humor, temperature and body weight. *Forensic Sci Int* 2019;*295*:157–68.
28. Deokar RB, Shendarkar AT, Patil SS. Estimation of the time since death by means of changes in the eye: vitreous humour calcium levels. *Int J Healthcare Biomed Res* 2013;*1*:141–6.
29. Ding Y, Li X, Guo Y, Duan W, Ling J, Zha L, Yan J, Zou Y, Cai J. Estimation of postmortem interval by vitreous potassium evaluation with a novel fluorescence aptasensor. *Sci Rep* 2017;*7*:1868.
30. Farmer JG, Benomran F, Watson AA, Harland WA. Magnesium, potassium, sodium and calcium in postmortem vitreous humour from humans. *Forensic Sci Int* 1985;*27*:1–13.
31. Foerch JS, Forman DT, Vye MV. Measurement of potassium in vitreous humour as an indication of the postmortem interval. *Am J Clin Pathol* 1979;*72*:651–62.
32. Forman DT, Butts J. Electrolytes of the vitreous humour as a measure of the postmortem interval. *Clin Chem* 1980;*26*:1024.
33. Gamero JJ, Romero JL, Arufe MI, Vizcaya MA. Incremento de la concentración de potasio en humor vitreo en función del tiempo postmortem. *Riv Ital Med Leg* 1990;*12*:785–801.
34. Gardiner EE, Newberry RC, Keng JY. Postmortem time and storage temperature affect the concentrations of hypoxanthine, other purines, pyrimidines, and nucleosides in avian and porcine vitreous humor. *Pediatr Res* 1989;*26*:639–42.
35. Girela E, Villanueva E, Irigoyen P, Girela V, Hernández-Cueto C, Peinado JM. Free amino acid concentrations in vitreous humour and cerebrospinal fluid in relation to the cause of death and postmortem interval. *J Forensic Sci* 2008;*53*(3):730–3.
36. Go A, Shim G, Park J, Hwang J, Nam M, Jeong H, Chung H. Analysis of hypoxanthine and lactic levels in vitreous humor for the estimation of post-mortem interval (PMI) using LC-MS/MS. *Forensic Sci Int* 2019;*299*:135–41.

37. Hansson LMA, Uotila U, Lindfors R, Laiho K. Potassium content of the vitreous body as an aid in determining the time of death. *Forensic Sci* 1966;*11*:390–4.
38. Harkness RA, Lund RJ. Cerebrospinal fluid concentrations of hypoxanthine, xanthine, uridine and inosine: high concentrations of the ATP metabolite, hypoxanthine, after hypoxia. *J Clin Pathol* 1983;*36*:1–8.
39. Harper DR. A comparative study of the microbiological contamination of postmortem blood and vitreous humour samples taken for ethanol determination. *Forensic Sci Int* 1989;*43*:37–44.
40. Henry JB, Smith FA. Estimation of the postmortem interval by chemical means. *Am J Forensic Med Pathol* 1980;*1*:341–7.
41. Henssge C, Knight B, Krompecher T, Madea B, Nokes L. *The Estimation of the Time Since Death in the Early Postmortem Period*. 2nd ed. London, Edward Arnold, 2002.
42. Henssge C, Madea B. Estimation of the time since death. *Forensic Sci Int* 2007;*165*:182–4.
43. Hughes W. Levels of potassium in the vitreous humour after death. *Med Sci Law* 1965;*150*:150–6.
44. Jaffe FA. Chemical postmortem changes in the intraocular fluid. *J Forensic Sci* 1962;*7*:231–7.
45. James RA, Hoadley PA, Sampson BG. Determination of postmortem interval by sampling vitreous humour. *Am J Forensic Med Pathol* 1997;*18*(2):158–62.
46. Jashnani KD, Kale SA, Rupani AB. Vitreous humor: biochemical constituents in estimation of postmortem interval. *J Forensic Sci* 2010;*55*(6):1523–7.
47. Klein A, Klein S. *Todeszeitbestimmung am menschlichen Auge*, MD thesis. Desden, Germany, Dresden University, 1978.
48. Knight B. *Forensic Pathology*. 2nd ed. London, Edward Arnold, 1996.
49. Knight B. *Legal Aspects of Medical Practice*. 3rd ed. London, Churchill Livingstone, 1982.
50. Komura S, Oshiro S. Potassium levels in the aqueous and vitreous humour after death. *Tohoku J Exp Med* 1977;*122*:65–8.
51. Krause D, Klein A, Meissner D, Roitzsch E, Herrmann WR. Die Bedeutung der Kaliumkonzentration im Glaskörper menschlicher Augen für die Todeszeitbestimmung. *Z Arztl Fortbild* 1971;*65*:345–8.
52. Lange N, Swearer ST, Sturner WQ. Human postmortem interval estimation from vitreous potassium: an analysis of original data from six different studies. *Forensic Sci Int* 1994;*66*:159–74.
53. Leahy MS, Farber R. Postmortem chemistry of human vitreous humour. *J Forensic Sci* 1967;*12*:214–22.
54. Lendoiro E, Cordeiro C, Rodríguez-Calvo MS, Vieira DN, Suárez-Penaranda JM, López-Rivadulla M, Munoz-Barús JI. Applications of tandem mass spectrometer (LC-MSMS) in estimating the postmortem interval using the biochemistry of the vitreous humour. *Forensic Sci Int* 2012;*223*:160–4.
55. Lie JT. Changes of potassium concentration in vitreous humour after death. *Am J Med Sci* 1967;*254*:136–42.
56. Madea B. Methods for determining the time since death. *For Sci Med Pathol* 2016;*12*:451–85.
57. Madea B (ed.). *Estimation of the Time Since Death*. 3rd ed. Boca Raton, London, and New York: CRC Press, Taylor & Francis Group, 2016.
58. Madea B, Henssge C, Honig W, Gerbracht A. References for determining the time of death by potassium in vitreous humour. *Forensic Sci Int* 1989;*8*:231–43.
59. Madea B, Henssge C, Püschel K, Honig W. Wie zuverlässig ist die Todeszeitbestimmung aus der Kaliumkonzentration in Zisternenliquor? *Beitr Gerichtl Med* 1988;*46*:375–81.
60. Madea B, Henssge C, Staak M. Postmortaler Kaliumanstieg in Glaskörperflüssigkeit: Welche Parameter sind als Indikatoren einer vitalen agonalen Elektrolytdysregulation geeignet? *Z Rechtsmed* 1986;*97*:259–68.
61. Madea B, Henssge C. Informationswert der Kaliumkonzentration in Glaskörperflüssigkeit für die Todeszeit—Präzisionsgewinn durch Erfassung antemortaler Dysregulationen? *Beitr Gerichtl Med* 1987;*45*:151–5.
62. Madea B, Herrmann N, Henssge C. Precision of estimating the time since death by vitreous potassium: comparison of two different equations. *Forensic Sci Int* 1990;*46*:277–84.
63. Madea B, Käferstein H, Hermann N, Sticht G. Hypoxanthine in vitreous humour and cerebrospinal fluid: a marker of postmortem interval and prolonged (vital) hypoxia? Remarks also on hypoxanthine in SIDS. *Forensic Sci Int* 1994;*65*:19–31.
64. Madea B, Kreuser C, Banaschak S. Postmortem biochemical examination of synovial fluid: a preliminary study. *Forensic Sci Int* 2001;*118*(1):29–35.
65. Madea B, Ortmann J, Doberentz E. Estimation of the time since death—Even methods with a low precision may be helpful in forensic casework. *Forensic Sci Int* 2019;302:109879.
66. Madea B, Rödig A. Time of death dependent criteria in vitreous humor: accuracy of estimating the time since death. *Forensic Sci Int* 2006;*164*:87–92.
67. Madea B. Is there recent progress in the estimation of the postmortem interval by means of thanatochemistry? *Forensic Sci Int* 2005;*151*:139–49.
68. Manzke H, Dörner K, Grünitz J. Urinary hypoxanthine, xanthine and uric acid excretion in newborn infants with perinatal complications. *Acta Paediatr Scand* 1977;*66*:713–17.
69. Manzke H, Krämer M, Dörner K. Postmortem oxypurine concentrations in the CSF. In: Nyhan WL, Thompson LF, Watts RWE (eds.). *Purine and Pyrimidine Metabolism in Man. V. Festschrift for JE Seegmiller*. New York, Plenum Press, 1986, pp 587–91.
70. Manzke H, Staemmler W. Oxypurine concentration in the CSF in children with different diseases of the nervous systems. *Neuropediatrics* 1981;*12*:209–14.
71. Martchenko HP. Veränderungen des Kaliumgehaltes der Glaskörperflüssigkeit in Abhängigkeit von der Todeszeit. *Gerichtl Med* 1966;*61*:295.
72. Mason JK, Klyne W, Lennox B. Potassium levels in the cerebrospinal fluid after death. *J Clin Pathol* 1951;*4*:231–3.
73. McLaughlin PS, McLaughlin BG. Chemical analysis of bovine and porcine vitreous humors: correlation of normal values with serum chemical values and changes with time and temperature. *Am J Vet Res*. 1987;*48*:467–73.
74. Meberg A, Saugstad OD. Hypoxanthine in cerebrospinal fluid in children. *Scand J Clin Lab Invest* 1978;*38*:437–40.
75. Montaldo B, Umani Ronchi G, Marchiori A, Forgeschi M, Barbato M. La determinatione della concentrazione del potassio nel'umor vitreo: verifica di un methodo strumentale tanatocronologico. *Riv Ital Med Leg* 1989;*11*:180–99.
76. Muňos JI, Suárez-Peňaranda JM, Otero XL, Rdríguez-Calvo MS, Costas E, Miguéns X, et al. A new perspective in the estimation of post-mortem interval (PMI) based on vitreous. *J Forensic Sci* 2001;*46*(2):209–14.

77. Muňoz Barús JI, Febrero-Bande M, Cadarso-Suárez C. Flexible regression models for estimating post-mortem interval (PMI) in forensic medicine. *Stat Med* 2008;*27*:5026–38.
78. Muňoz Barús JI, Rodríges-Calvo MS, Suárez-Penaranda JM, Vieira DN, Cadarso-Suárez C, Febrero-Bande M. PMICALC: An R code-based software for estimating post-mortem interval (PMI) compatible with Windows, Mac and Linux operating systems. *Forensic Sci Int* 2010;*194*:49–52.
79. Muňoz Barús JI, Suárez-Penaranda JM, Otero XL, Rodríguez-Calvo MS, Costas E, Miguénes X, Concheiro L. Improved estimation of postmortem interval based on differential behaviour of vitreous potassium and hypoxanthine in death by hanging. *Forensic Sci Int* 2002;*125*:67–74.
80. Munoz JI, Suárez-Penaranda JM, Otero XL, Rodgríguez-Calvo MS, Costas E, Miguéns X et al. A new perspective in the estimation of post-mortem interval (PMI) based on vitreous. *J Forensic Sci* 2001;*46*(2):209–14.
81. Ortmann J, Markwerth P, Madea B. Precision of estimating the time since death by vitreous potassium—Comparison of 5 different equations. *Forensic Sci Int* 2016;*269*:1–7.
82. Passos MLC, Santos AM, Pereira AI, Santos RJ, Santos AJC, Saraiva MLMFS, Lima JLFC. Estimation of postmortem interval by hypoxanthine and potassium evaluation in vitreous humor with a sequential injection system. *Talanta* 2009;*79*:1094–9.
83. Pau H. Betrachtungen zur Physiologie und Pathologie des Glaskörpers. *Graefes Arch Ophthalmol* 1951;*152*:201–47.
84. Poulsen JP, Rognum TO, Oyyasaeter S, Saugstad OD. Changes in oxypurine concentrations in vitreous humor of pigs during hypoxemia and postmortem. *Pediatr Res* 1990;*28*:482–4.
85. Pounder DJ, Carson DO, Johnston K, Orihara Y. Electrolyte concentration differences between left and right vitreous humor samples. *J Forensic Sci* 1998;*43*(3):604–7.
86. Praetorius E, Poulsen H, Dupont H. Uric acid, xanthine and hypoxanthine in the cerebrospinal fluid. *Scand J Clin Lab Invest* 1957;*9*:133–7.
87. Risoluti R, Canepari S, Frati P, Fineschi V, Matarazzi S. “2n analytical platform” to update procedures in thanatochemistry: estimation of post mortem interval in vitreous humor. *Anal Chem* 2019;*91*:7025–31.
88. Rognum TO, Hauge S, Oyasaeter S, Saugstad OD. A new biochemical method for estimation of postmortem time. *Forensic Sci Int* 1991;*51*:139–46.
89. Rognum TO, Saugstad OD, Oyasaeter S, Olaysen B. Elevated levels of hypoxanthine in vitreous humor indicate prolonged cerebral hypoxia in victims of sudden infant death syndrome. *Pediatrics* 1988;*82*:615–18.
90. Rognum TO, Saugstad OD. Hypoxanthine levels in vitreous humor: evidence of hypoxia in most infants who died of sudden infant death syndrome. *Pediatrics* 1991;*87*:306–10.
91. Rumran NK, Bardale RV, Dongre AP. Postmortem analysis of synovial fluid and vitreous humour for determination of death interval: a comparative study. *Forensic Sci Int* 2011;*204*(1–3):186–90.
92. Saugstad OD, Olaisen B. Postmortem hypoxanthine levels in the vitreous humor: an introductory report. *Forensic Sci Int* 1978;*12*:33–6.
93. Saugstad OD. Hypoxanthine as a measurement of hypoxia. *Pediatr Res* 1975;*9*:158–61.
94. Schleyer F. *Postmortale klinisch-chemische Diagnostik und Todeszeitbestimmung mit chemischen und physikalischen Methoden*. Stuttfart, Germany, Thieme, 1958.
95. Schleyer F. Determination of the time since death in the early postmortem interval. In: Lundquist F (ed.). *Methods of Forensic Science*. Vol. 2. New York, Interscience Publishers, John Wiley and Sons, 1963, pp 253–93.
96. Schleyer F. Wie zuverlässig ist die Kaliumbestimmung im Glaskörperinhalt als Mittel zur Todeszeitschätzung? *Z Rechtsmed* 1973;*71*:281–8.
97. Schoning O, Strafuss AC. Determining time of death of a dog by analysing blood, cerebrospinal fluid and vitreous humour collected postmortem. *Am J Vet Res* 1980;*41*:955–7.
98. Schoning P, Strafuss AC. Postmortem biochemical changes in canine vitreous humour. *J Forensic Sci* 1980;*25*:53–9.
99. Sparks DL, Oeltgen PR, Kryscio RJ, Hunsaker JC, III. Comparison of chemical methods for determining the postmortem interval. *J Forensic Sci* 1989;*34*:197–206.
100. Stegmaier K. *Untersuchungen über die postmortale Kaliumkonzentration in Glaskörperinhalt und Kammerwasser und ihre Beziehung zur Todeszeit*, MD thesis. Marburg, Germany, Marburg University, 1971.
101. Stephens RJ, Richards RG. Vitreous humour chemistry: the use of potassium concentration for the prediction of the postmortem interval. *J Forensic Sci* 1987;*32*:503–9.
102. Sturner WQ. The vitreous humour: postmortem potassium changes. *Lancet* 1963;*1*:807–8.
103. Sturner WQ, Dowdey ABC, Putman RS, Dempsey JL. Osmolality and other chemical determinations in postmortem human vitreous humour. *J Forensic Sci* 1972;*18*:387–93.
104. Sturner WQ, Gantner GE. The postmortem interval: a study of potassium in the vitreous humor. *Am J Clin Pathol* 1964;*42*:137–44.
105. Sturner WQ. Die gerichtmedizinische Bedeutung der Glaskörperflüssigkeit. In: Vamosi M (ed.). *Aktuelle Fragen der gerichtlichen Medizin II. Wiss Beitr Univ Halle-Wittenberg*, 1965, pp 57–62.
106. Sturner WQ. The vitreous humour: postmortem potassium changes. *Lancet* 1963;*1*:807–8.
107. Tagliaro F, Bortolotti F, Manetto G, Cittadini F, Pascali VL, Marigo M. Potassium concentration differences in the vitreous humour from the two eyes revisited by microanalysis with capillary electrophoresis. *J Chromatogr A* 2001;*924*:493–8.
108. Tagliaro F, Manetto G, Cittadini F, Marchetti D, Bortolotti F, Marigo M. Capillary zone electrophoresis of potassium in human vitreous humour: validation of a new method. *J Chromatogr B* 1999;*733*:273–9.
109. Thierauf A, Musshoff F, Madea B. Post-mortem biochemical investigations of vitreous humor. *Forensic Sci Int* 2009;*192*:78–92.
110. Tumram NK, Bardale RV, Dongre AP. Postmortem analysis of synovial fluid and vitreous humour for determination of death interval: a comparative study. *Forensic Sci Int* 2011;*204*:186–90.
111. Wurster U, Hoffmann K. Glaskörper. In: Hockwin O (ed.). *Biochemie des Auges*. Stuttgart, Germany, Enke, 1985, pp 100–34.
112. Yogiray V, Indumati V, Kodliwadmath MV. Study of vitreous humour to assess the postmortem interval and cause of death. *J Forensic Med Toxicol* 2008;*9*:171–4.
113. Zilg B, Bernard S, Alkass K, Berg S, Druid H. A new model for the estimation of time of death from vitreous potassium levels corrected for age and temperature. *Forensic Sci Int* 2015;*254*:158–66.

7.2b Potassium Levels Combined with Age and Temperature

■ *Brita Zilg*

At the Department of Forensic Medicine in Stockholm, Sweden, we examined potassium levels from 462 cases with known PMI (1). The cases consisted of a mixed population of various causes of death, traumatic as well as natural. Using these data, the aim was to generate a more accurate equation for calculating the PMI from vitreous potassium values by taking into account factors that may affect the post-mortem diffusion process in the vitreous. Many possible factors were considered, but in particular, ambient temperature, decedent age, the presence of alcohol, and agony were evaluated.

Vitreous fluid was consistently collected as soon as possible following the arrival of the bodies at the morgue. Briefly, 0.2 mL vitreous fluid was aspirated from the centre of each eye using a 1 mL syringe equipped with an 18-gauge needle. The samples were pooled in the same syringe and were not pre-treated or subjected to dilution, centrifugation, or sonication. The samples were then directly injected into an ABL 625 blood gas instrument (Radiometer, Copenhagen) (2). Samples that were macroscopically opaque or dirty were also analysed without pre-preparation. However, if there was a massive bleeding in the eye, no analysis of vitreous potassium analysis was performed. In addition, samples from severely decomposed bodies and infants were not consistently included.

Altogether, 462 cases were included (346 males and 116 females, median age 52 years (0–95). PMI ranged from 2 hours to 17 days. Subjects with a very long post-mortem interval were mainly bodies that were previously stored in a morgue at a different pathology department before they were transferred to the Forensic Medicine Department.

Since a lot of cases were included with a longer PMI than in most other studies, it could be observed that the rise in vitreous potassium levels was not linear. Therefore, a non-linear model was developed to better fit these data; see Figure 7.42.

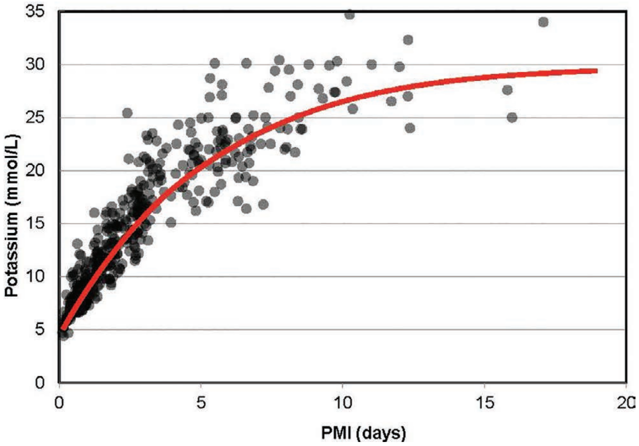

Figure 7.42 Potassium concentration (mmol/L) is plotted versus PMI ($n = 462$). The nonlinear regression line is shown in red.

Upon death, intracellular potassium ions diffuse from the surrounding cells in the retina into the vitreous fluid via passive mechanisms. Therefore, a two-compartment model (for the cell mass and the vitreous fluid) was established to account for the diffusion that occurs across an imaginary membrane present between the two compartments. Thus, the vitreous potassium concentration $[K^+]$ as a function of the PMI was expressed as:

$$[K^+] = M[1 - \exp(-L\mathrm{PMI})] + C_0 \exp(-L\mathrm{PMI})$$

where M is the steady state concentration of K^+ (mmol/L), L is the membrane crossing term (in 10^{-3}/day), and C_0 is the concentration of K^+ at death (mmol/L).

The PMI can then be calculated according to the following inverse relationship:

$$\mathrm{PMI} = \frac{\mathrm{In}\,((\mathrm{M} - \mathrm{C}_0)/(\mathrm{M} - [\mathrm{K}^+]))}{L}$$

where PMI is only defined when $[K^+] < M$ and $[K^+] \geq C_0$.

In this single-variable model, the parameters M, L, and C_0 are constant. The parameter values that gave the best fit (in the least-squares sense) based on the whole dataset examined ($n = 462$) were as follows: $M = 29.91$ mmol/L, $L = 0.22 \times 10^{-3}$/day, and $C_0 = 4.73$ mmol/L. This mathematical model was validated on a test dataset that included all of the cases for which information on PMI, decedent age, and potassium concentration was available ($n = 462$). The dataset was randomly divided into two subsets, a training dataset and a test dataset. The training dataset was used to form the PMI predictions for the test dataset. A total of 100 training and test datasets were generated, and for each pair, the percentage of samples with true PMI values outside of the 95% prediction interval were examined. The error rate was 4.05 ± 1.7% (mean ± SD). Since the average error rate was slightly less than 5%, the prediction interval was slightly conservative (too large). However, the difference was small and on average, less than 1% of the true PMI values were not appropriately categorized as outside the prediction interval. An additional 46 new cases with known post-mortem intervals were subsequently used to evaluate the precision of the model. The confidence intervals obtained according to the bootstrap method are shown in Figure 7.43. For the larger PMI values, the confidence intervals increased.

This study showed that the rise in potassium concentration does not follow a straight line but an exponential curve, and that this curve becomes asymptotic after about a week. Given that the amount of potassium present in the eye is finite, it is expected that intra- and extracellular potassium concentrations will eventually equilibrate after a certain period. It appears that equilibration occurs after about a week, and a concentration of ~ 35 mmol/L is achieved.

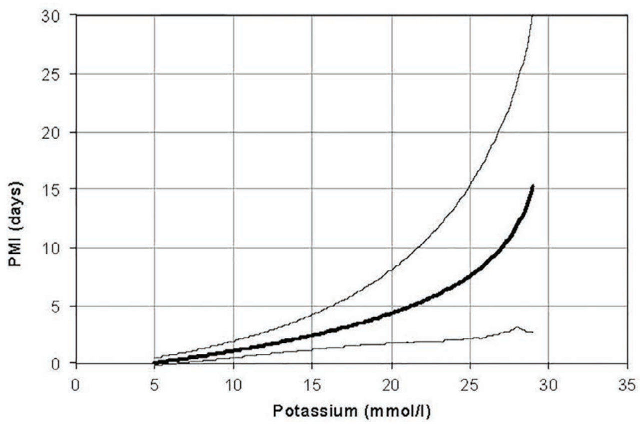

Figure 7.43 The 95% confidence intervals for the PMIs calculated from vitreous potassium levels were found to widen as potassium values increased.

7.2b.1 Influence of Ambient Temperature

Based on the basic potassium curve that was generated, various factors were assessed to evaluate their potential impact on potassium levels. First, the influence of ambient temperature was examined. Using mathematical modelling, ambient temperature was found to affect the rise of post-mortem vitreous potassium levels, although this factor only accounted for ~5% of the variability observed. Figure 7.44 shows that the higher the average ambient temperature, the steeper the rise in potassium concentration. In the early post-mortem period (up to approximately 4 days after death), the different temperature interval curves followed a clear pattern. However, for longer PMIs, this pattern became less clear because of the smaller number of cases with longer PMIs and a known ambient temperature.

7.2b.2 Influence of Decedent Age

When decedent age was examined as a factor of post-mortem rise in vitreous potassium levels, significant differences between all of the age groups were observed (t-statistics, $p < 0.001$) (Figure 7.45). Actually, age accounted for ~16% of the variability

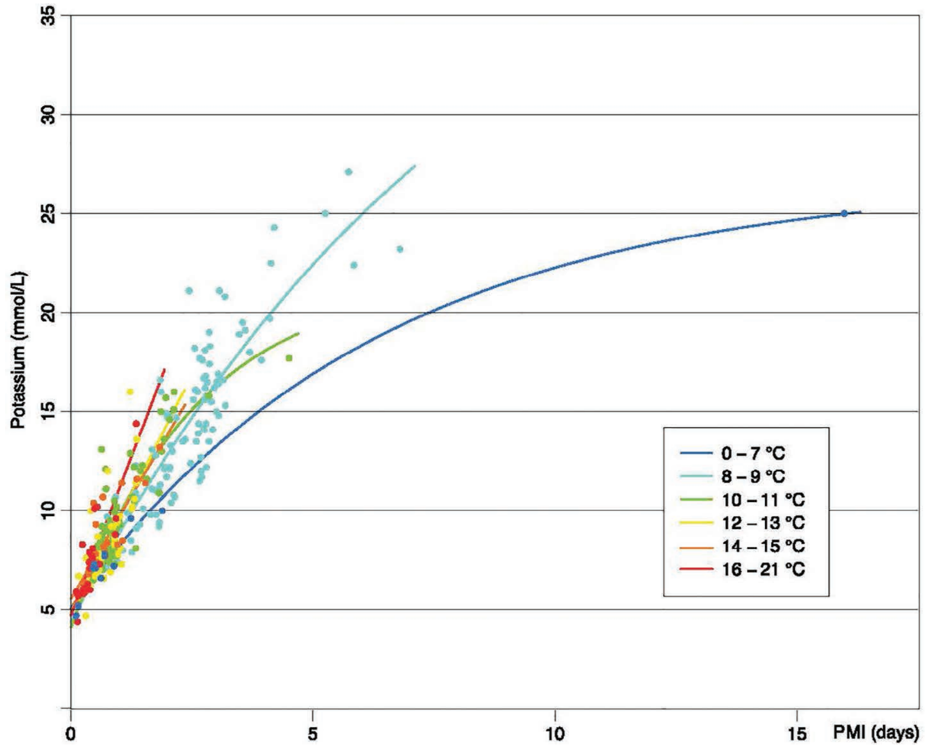

Figure 7.44 The influence of temperature on the post-mortem rise in vitreous potassium levels. The different colours represent the different ambient temperatures reported in 272 cases.

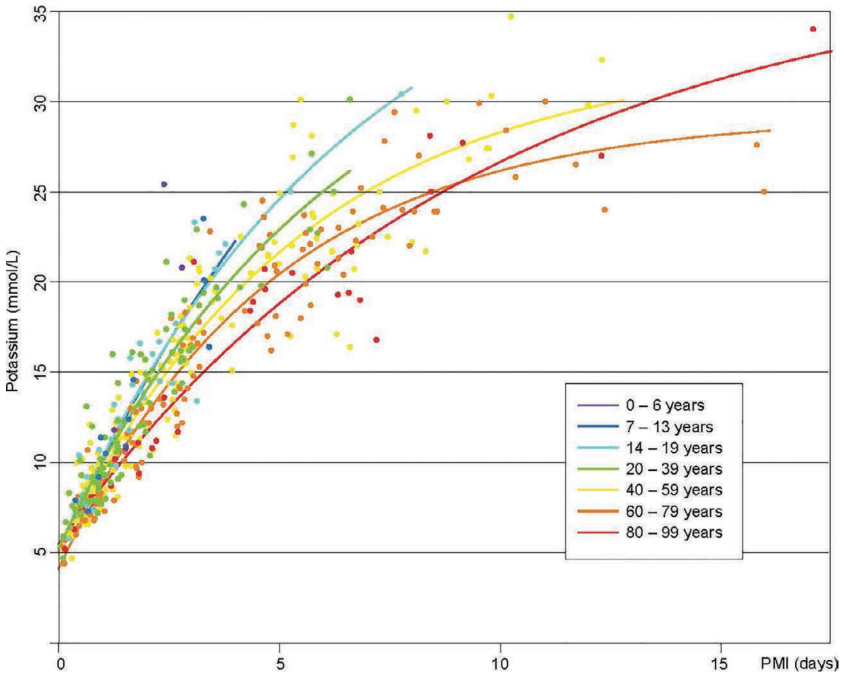

Figure 7.45 The influence of age on the post-mortem rise in vitreous potassium levels. The different colours represent the different age groups for the deceased as indicated in the key ($n = 462$).

observed. The age interval curves stayed separated even at longer PMIs.

7.2b.3 Influence of Other Factors

Additional factors that might influence the post-mortem rise in potassium concentrations following death were examined, including decedent gender, body weight, blood alcohol level and agonal period. Neither gender, nor body weight, were found to influence potassium concentrations. Blood alcohol level was found to account for only ~ 1% of the variability observed in the potassium curve. Agonal period is a variable that is difficult to evaluate. However, when the cases examined were divided into those that involved a rapid death (e.g., due to shootings or hangings) versus the remainder of the cases, 1% variability was observed between these two groups. Differences between various causes of death were also investigated, such as intoxications, drownings, instant traumatic death, massive skeletal trauma with delayed death, kidney failure and diabetic coma. There were only three cases of diabetic coma in the material, all with slightly higher potassium than the average relative to the true PMI. Otherwise, there were no obvious differences in potassium levels relative the PMI between different causes of death. There were no cases for which the rectal temperature had been recorded immediately prior to death, and therefore it was not possible to determine the possible impact of fever on the post-mortem rise of potassium.

7.2b.4 A Multivariate Model for the Estimation of Time of Death Based on Vitreous Potassium Concentration, Decedent Age and Ambient Temperature

Based on the results where decedent age and ambient temperature were identified as factors that significantly affected the PMI, these two factors were included in a final multivariate model:

$$\mathrm{PMI} = \frac{\mathrm{In}\left((\mathrm{M} - \mathrm{C_0}) / (\mathrm{M} - [\mathrm{K^+}])\right)}{L_0 + \mathrm{m_A A} + \mathrm{m_T T}}$$

where M = 34.44 mmol/L (steady-state concentration of K^+), C_0 = 4.4 mmol/L (the concentration of K^+ at death), L_0 = 0.135 × 10^{-3}/day (the membrane crossing term), m_A = −0.00112 × 10^{-3}/day × year (age coefficient year), A = decedent age, m_T = 0.00985 × 10^{-3}/day × degree (temperature coefficient degree) and T = ambient temperature

Simplified equation

$$\mathrm{PMI} = \ln\left(30.04 / (34.44 - \mathrm{K^+})\right) / (0.135 - 0.00112 \times \mathrm{AGE} + 0.00985 \times \mathrm{AMBIENT\ TEMP})$$

When the precision of the equation including age and temperature was examined by applying vitreous potassium concentrations available in 46 new cases with known post-mortem intervals, a good correlation ($r^2 = 0.87$) was found

(Figure 7.46). The numerical deviation between estimated and true PMI was low until about 4–5 days, and then increased markedly (Figure 7.47).

To simplify the calculation process for the user, a web application was created where the potassium concentration, decedent age and ambient temperature (if available) can be entered into a form and the PMI with confidence intervals will be calculated:

https://slbd.shinyapps.io/pmiPredictor/

The user is able to select a confidence interval (typically the interval selected is 67%, which corresponds with the SD). When ambient temperature and decedent age data are entered as well, the calculator can provide somewhat more precise results. This versatility can be valuable in the early phase of an investigation when the likelihoods of different scenarios are being considered.

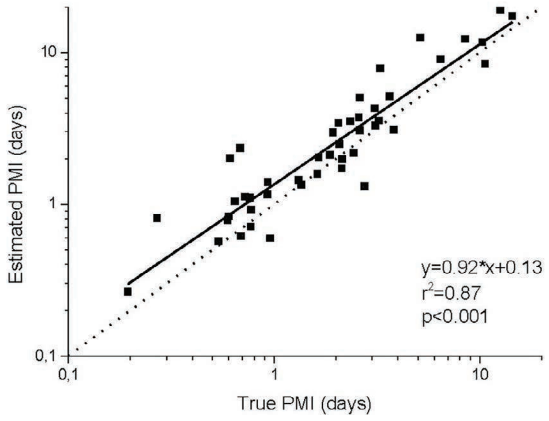

Figure 7.46 Comparison of the estimated PMIs with the true PMIs.

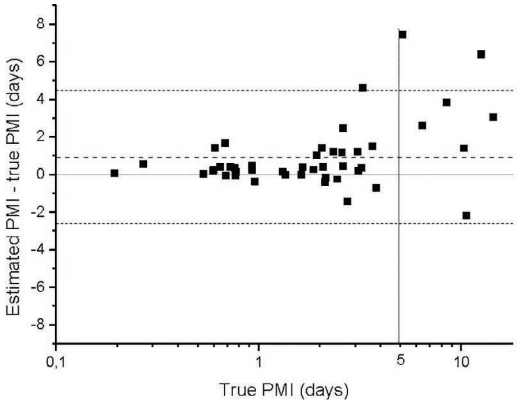

Figure 7.47 A Bland–Altman plot that shows the differences between the estimated PMIs and the true PMIs.

7.2b.5 Conclusion

The post-mortem rise in vitreous potassium is non-linear and decedent age and the ambient temperature significantly influence the rise. An equation for the estimation of the post-mortem interval that includes decedent age and ambient temperature and that provides confidence intervals was developed. To facilitate the calculation, a web application that rapidly provides a PMI estimate with confidence intervals based on these equations was developed.

References

1. Zilg B, Bernard S, Alkass K, Berg S, Druid H (2015) A new model for the estimation of the time of death from vitreous potassium levels corrected for age and temperature. *For Sci Int* 254:158–66.
2. Zilg B, Alkass K, Kronstrand R, Berg S, Druid H (2021) A Rapid Method for Postmortem Vitreous Chemistry-Deadside Analysis. *Biomolecules* 12(1):32

7.2c Estimation of Time Since Death Based on Vitreous Humour Hypoxanthine and Temperature Measurement

■ *Torleiv Ole Rognum*

7.2c.1 The Background

Hypoxanthine (Hx) is a metabolite in the degradation of adenosine monophosphate (AMP) and is accumulated in lack of oxygen (Figure 7.48) (1). Hx is showed to be elevated due to hypoxia prior to death (2, 3, 4) and it continues to increase in the post-mortem period (5).

In two studies of victims of sudden infant death syndrome (SIDS) from 1988 (4) and 1991 (5), the hypoxanthine levels were significantly higher in SIDS than in children that suffered a violent death. In the paper from 1991 (5), the authors recognized that the hypoxanthine levels increased after death, therefore the measured levels were corrected for an assumed post-mortem increase of 3.5 µmol/L per hour. The number 3.5 µmol/L/h was based on repeated sampling of vitreous humour in 13 adult bodies kept at 6°C. Nevertheless, Beckwith in a letter to the editor in *Pediatrics* (6) suggested that the observation of different hypoxanthine levels between SIDS and violent death might be due to post-mortem hypoxic metabolic activity in an anoxic and warm environment, the infant being tightly wrapped with the face down in a warm environment.

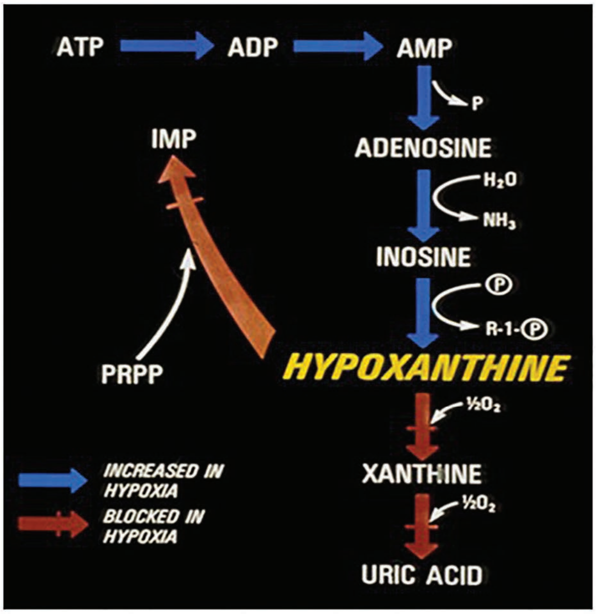

Figure 7.48 Purine metabolism from ADP. In lack of oxygen hypoxanthine is accumulated in body tissue and fluids. ADP, adenosine diphosphate; AMP, adenosine monophosphate; ATP, adenosine triphosphate; IMP, inosine monophosphate; NH3, ammonia; P, phosphate; PRPP, 5-phospho-a-d-ribosyl phosphate.

(Adapted from Saugstad OD (1).)

Furthermore, Beckwith pointed to the difficulty in deciding the time of death in SIDS cases since death occurs during sleep. This important objection raised by Beckwith was recognized by the authors (7), who already had designed studies to eliminate the error caused by post-mortem hypoxanthine increase (8).

Repeated vitreous humour sampling from 15 infants and small children that died from various reasons in hospital, kept at different times in room temperature before brought to the cold room, showed a median hypoxanthine increase of 7.5 µmol/L. This post-mortem increase is in accordance with findings by Carpenter et al. 1993 (9) who found a hypoxanthine increase of 8.3 µmol/L during the first 24 hours after death. These authors found that deaths from cardiopulmonary diseases had significantly lower vitreous humour hypoxanthine levels than SIDS but found no difference with a control group which consisted of 'other causes of death'.

To test the assumption that higher hypoxanthine levels in SIDS than in victims of violent death might be due to post-mortem hypoxic metabolic activity in an anoxic and warm environment as suggested by Beckwith (6), a study was performed to eliminate differences due to post-mortem increase (10). SIDS victims and controls were matched with regard to similar post-mortem time. The study demonstrated that SIDS victims had significantly higher vitreous humour hypoxanthine levels than violent deaths and deaths due to heart/lung diseases. Differences were neither seen between SIDS and 'borderline SIDS' (11), now named Category II SIDS (12), nor between SIDS and deaths due to infection (10). Furthermore, SIDS cases found in prone position did not differ from those found in supine position. SIDS that had been subjected to resuscitation did not differ from those who were not tried to be resuscitated, and there were no differences between infants found dead during the night or during the day (10).

Measurement of vitreous humour potassium for estimation of time since death was first proposed by Sturner in 1963 and 1964 (13,14) and thereafter by several others, for example Madea et al. (15) and Coe (16).

In a historical review article (16), Coe addressed external factors which influence the validity of the potassium method, sampling techniques, analytical instrumentation and environmental temperature during the PMI. Furthermore, Coe stated that internal factors may influence vitreous potassium, such as the age of the individual, the duration of the terminal episode and the presence or absence of nitrogen retention.

In 1991, Rognum et al. (17) published diagrams demonstrating the relationship between ambient temperature and slopes of both post-mortem potassium and hypoxanthine levels from 87 corpses with known time of death, divided in four groups kept at different temperatures. Vitreous humour was sampled four times, two times in each eye. Both the hypoxanthine and the potassium increase were fairly linear during 96 hours after death. Based on these observations, scatterplots of the relationship between ambient temperature and the Hx and K⁺ slopes for all 87 subjects investigated, and the corresponding 10th and 90th percentiles were constructed (Figure 7.49). PMI for a new case could be

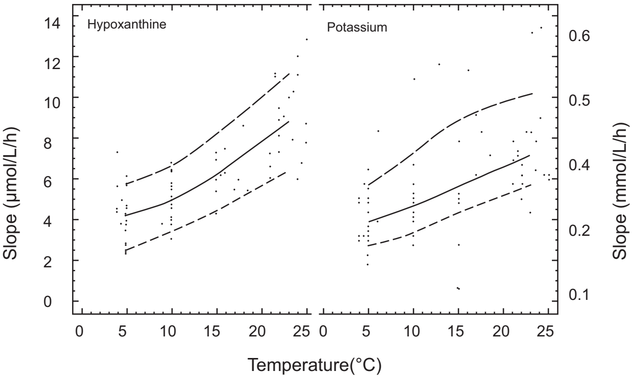

Figure 7.49 Scatter plots of the relationships between ambient temperature and the individual slopes of Hx levels (left) and K⁺ levels (right) in 87 subjects. The median slopes are connected with solid lines and the 10th and 90th percentiles with dotted lines.

(From Rognum et al. 1991) (17).

estimated by drawing a vertical line from the measured ambient temperature to the solid line connecting the median slopes. The corresponding number on the ordinate would indicate the slope of Hx and K^+, in the new case. The measured levels of Hx and K^+ divided by the slope would give a median PMI. The point on the ordinate corresponding to the point where the vertical line crossed the dotted lines indicates the range between the 10th and the 90th percentile (17).

At the Department of Forensic Medicine in Oslo the diagrams (17) have been applied in practical case work on vitreous humour sampled on the scene of death, as an adjunct to external post-mortem changes, such as hypostasis, rigor mortis (18), and temperature measurements based on Henssge's nomograms for rectal and brain temperatures (19, 20).

In a triple-murder case, estimation of time since death based on vitreous humour measurements of hypoxanthine and potassium were decisive for understanding of the incident. Brain and rectal temperature measurements could only confirm that time since death was 24 hours or more (21).

7.2c.1.1 Methods of Measurement of Hypoxanthine (Hx)

In the first studies in vitreous humour (2–5) hypoxanthine (Hx) was measured by a pO_2 electrode method or by high-performance liquid chromatography (HPLC) which were highly correlated (r=0.93, p<0.001), However, since the pO_2 electrode method also measure Xanthine, in all studies of PMI, only HPLC or capillary electrophoresis have been applied (17, 21, 22).

7.2c.2 Algorithms for the Use of Vitreous Humour Hx for PMI

After the first publication in 1991 of the combination of vitreous humour hypoxanthine and ambient temperature for estimating time since death (22), the significance of vitreous humour Hx has been studied by several authors (22, 23, 24, 25).

Madea et al. (23) in 1994 published an investigation of 92 adult subjects with known time of death. Each eye had been punctured only once and at the same time. In addition, they had sampled vitreous humour two times from each eye at different times in 43 subjects (23). Like Rognum et al. (17), Madea et al. found that Hx increased in a linear mode over the PMI, similar to potassium (15) as also reported by Rognum et al. (17). Furthermore, when all measurements were pooled, and ambient temperature was not included in the calculations, the potassium increase showed a slightly stronger correlation with PMI than the hypoxanthine increase (17, 22, 23, 24, 25). Formulae for estimating PMI in hours based on hypoxanthine (µmol/L) is summarized by Madea (26) based on equations obtained from Muñoz Barus (25)

Table 7.28 Formulae for Determining PMI (hrs) with Hypoxanthine [Hx] (µmol/L)

Reference	Equation obtained	Formula/diagram proposed
Rognum et al. (17)	$y = [Hx]$ $y = 4.2x + 8.6$ at 5°C $y = 5.1x + 8.6$ at 10°C $y = 6.2x + 8.6$ at 15°C $y = 8.8x + 8.6$ at 23°C	PMI by estimated using diagram (Figure 7.49)
Madea et al. (23)	$y = 1.29x + 3.69$	
James et al. (24)	$y = 3.2x - 0.15$	PMI = 0.31[Hx] + 0.05
Muñoz et al.(25)	$y = 3.01x + 26.45$	PMI = 0.172 [Hx] + 0.17

Note: Variable x is post-mortem interval (hrs)

7.2c.2.1 Ambient Temperature Is Decisive

In a new study from 2016, Rognum et al. (22) applied an extended reference material of vitreous humour from 132 subjects with known time of death, age 15–100 years, kept in rooms with different ambient temperatures during the period of sampling vitreous humour (Table 7.29).

In this extended reference group only the first sample from each eye was used for establishing algorithms for PMI. Hx levels were measured by HPLC or capillary electrophoresis, and potassium levels by flame photometry. When all measurements were pooled, regardless of ambient temperature, potassium showed a slightly stronger correlation with PMI than Hx, $r^2 = 0.75$, and $r^2 = 0.68$, respectively (Figure 7.50, A and B). However, when the subjects were divided according to the ambient temperature in the rooms in which they had been kept (Table 7.29), the correlation between hypoxanthine and PMI and potassium (K^+) and PMI, were similar (Figure 7.50, B and C). Thus, the linear correlation, as evaluated by r^2, were improved by considering temperature dependence both for Hx and K^+.

Table 7.29 Range of temperatures in four temperature groups

Temperature group	Range	Number of subjects
5°C	3.5–7C	34
10°C	9–12°C	18
15°C	13–18°C	25
23°C	20–27°C	55

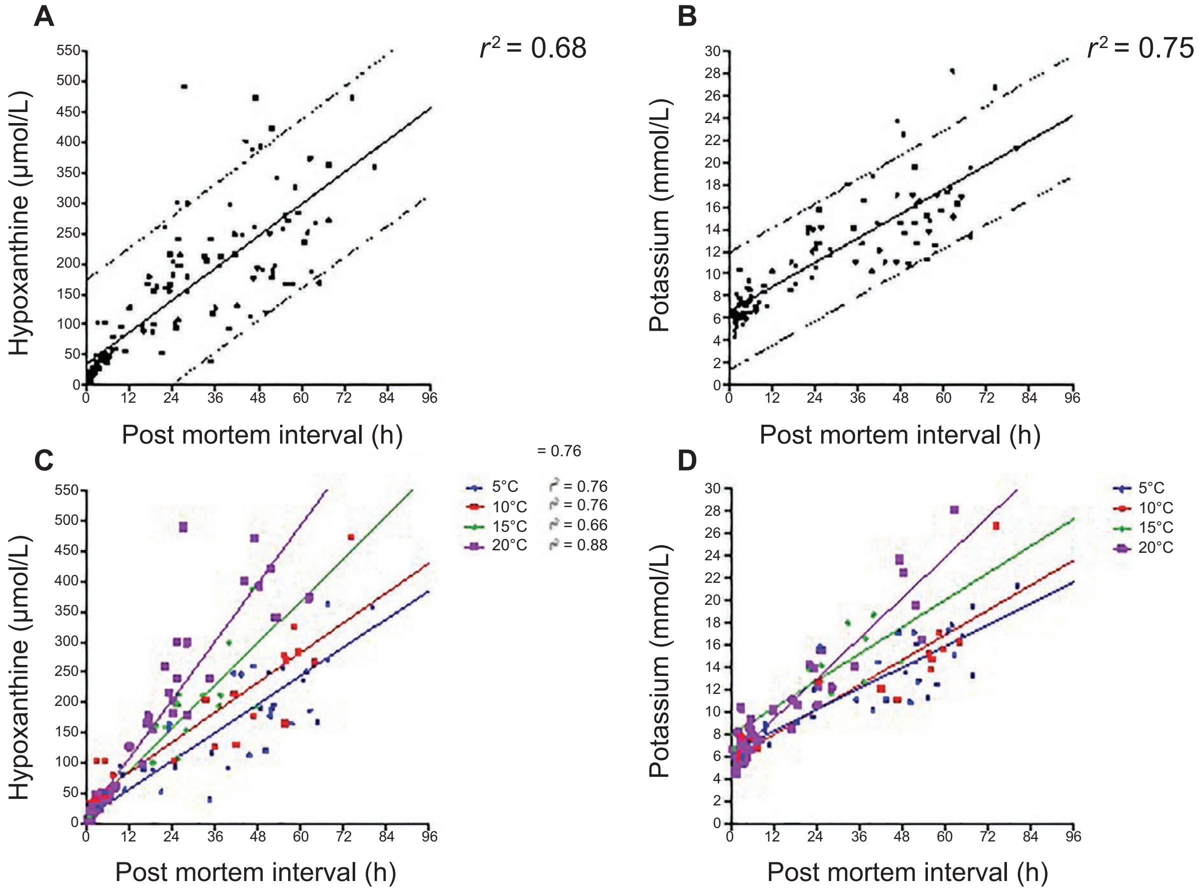

Figure 7.50 Scatter plots and linear regression lines showing the correlation between the PMI and the vitreous concentrations of Hx (A) and K+ (B). Figures C and D show the same dataset with the cases divided by temperature. A linear approximation of the 95% prediction intervals is indicated by the dashed lines (A and B) (from 22).

7.2c.2.2 Multivariable Linear Regression Models for Predicting PMI

The multivariable linear regression models using Hx and K^+ for predicting PMI are presented in Tables 7.30 and 7.31, respectively.

The regression models correlated with the observed PMIs (Figure 7.51, A and B). When ambient temperature was included in the regression models the correlation became stronger, r^2 being 0.85 for Hx and 0.86 for K^+ (Figure 7.51, C and D).

The corresponding standard error curves are non-linear, with the lowest standard error for Hx values around 150 μmol/L, corresponding to a 95% confidence interval of approximately 2.5 hours (Figure 7.52). K+ has the lowest standard error for values around 12 μmol/L, corresponding to a 95% confidence interval of approximately 3 hours (Figure 7.52).

The PMI estimated from vitreous humour Hx and K values correspond well to each other, with a correlation of $r^2 = 0.89$ (Figure 7.53).

Table 7.30 The Linear Regression Model Using Hx as a Predictor of PMI in Hours

	Coefficient	p-Value
Hx (μmol/L)	0.215	<0.001
T (temperature, °C)	−0.467	0.008
Interaction Hx and *T*	−0.005	<0.001
Constant	10.353	

Note: Post-mortem interval (PMI) may be estimated by the algorithm: PMI = 0.215 × Hx–0.467 × T–0.005 × Hx × *T* + 10.353

95% CI = PMI ± (((Hx × Hx × 0,00002)—(Hx × 0,00532) +1,5405) × 1,96)/24

Table 7.31 The Linear Regression Model Using K+ as a Predictor of PMI in Hours

	Coefficient	p-Value
K^+ (mmol/L)	5.164	<0.001
T (temperature, °C)	0.174	0.572
Interaction K^+ and *T*	− 0.100	<0.001
Constant	−19.588	

Note: Post-mortem interval (PMI) may be estimated by the algorithm: PMI = 5.164 × K^+ + 0.174 × *T*–0.1 × K^+ × *T*–19.588

95% CI = PMI ± (((K^+ × K^+ × 0,01160)—(K^+ × 0,25734)+2,79814) × 1,96)/24

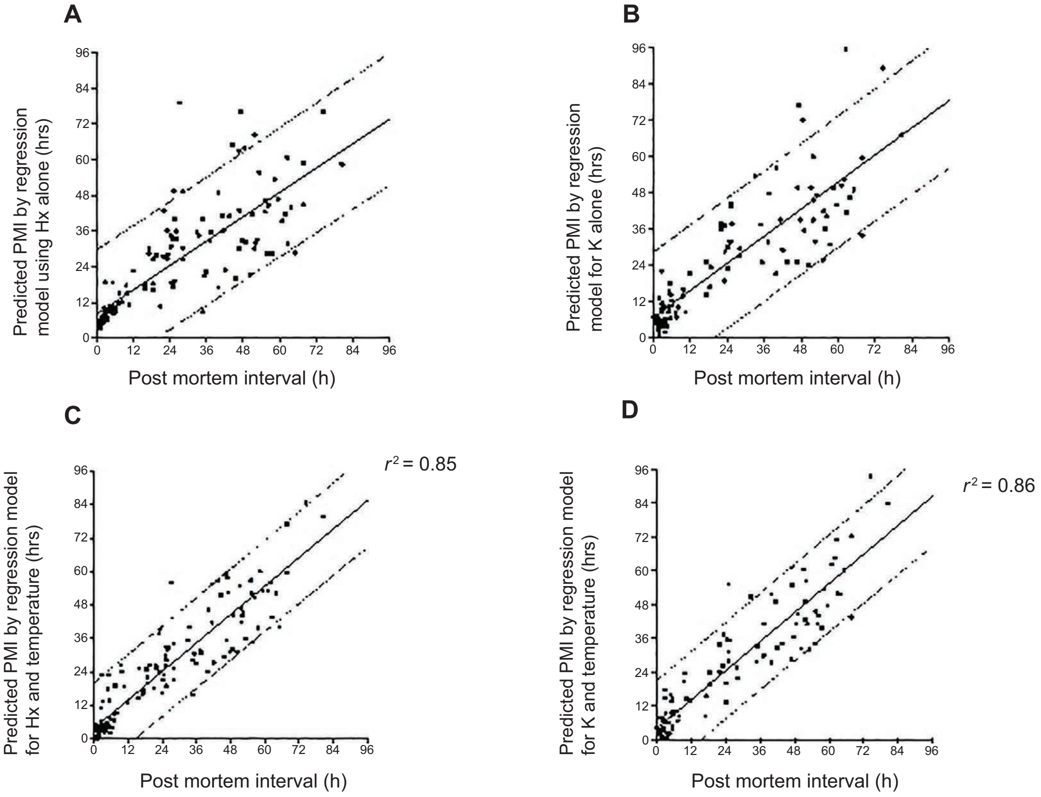

Figure 7.51 The correlation between the observed PMI and predicted post mortem intervals for Hx (A) and K$^+$ (B), without taking ambient temperature into the regression analyses, and for Hx (C) and K$^+$ (D) by regression analyses including ambient temperature. A linear approximation of the 95% prediction intervals is indicated by the dashed lines (from 22).

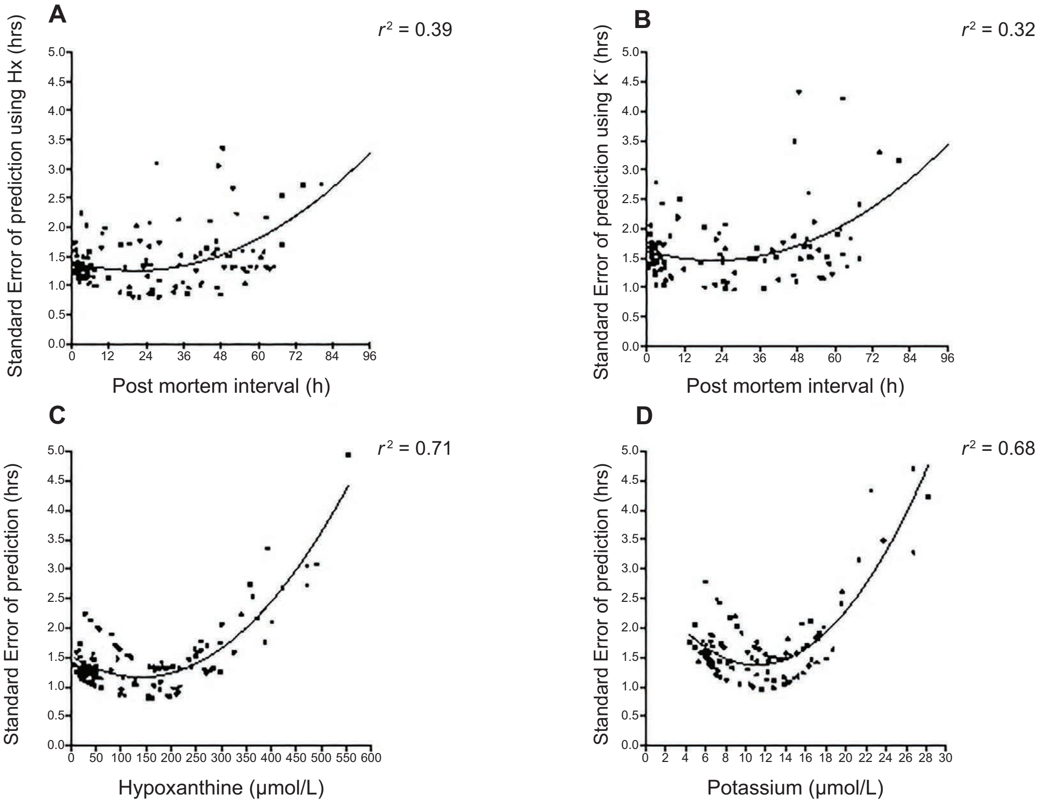

Figure 7.52 Scatterplots showing the standard errors of the predicted PMIs (in hours) as a function of predicted PMIs using the Hx-model (A), and K$^+$-model (B), an as function of the measured Hx value (C), and K$^+$ value (D). The r^2 values of the quadratic fit-lines are indicated in the upper right corners

(From Rognum et al.) (22).

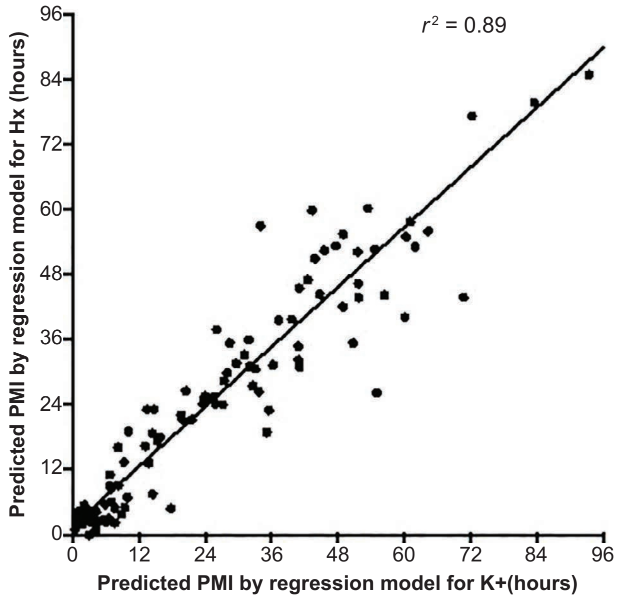

Figure 7.53 Correlation between predicted PMIs using Hx and K⁺. (From Rognum et al.) (22).

7.2c.2.3 What Are Normal Vitreous Humour Levels of Hx and K^+?

Median Hx concentration in eye fluid in 17 patients undergoing vitrectomy was 0.444 µmol/L, range 0.302–0.759 µmol/L. For K^+ the median concentration was 4.5 mmol/L, range 4.2–5.1 mmol/L (22).

7.2c.2.4 The Use of Vitreous Humour Hx and K^+ in Practical Case Work

Sampling of vitreous humour for measurement of Hx and K^+, measurement of ambient temperature near the body, brain temperature and rectal temperature for Henssge's nomograms, have been part of the Oslo-affiliated forensic pathologists work on the scene of crime since the 1990s. Until 2016, the diagrams for estimation of PMI published by Rognum et al. in 1991 were used for estimation of median time for PMI with range given as 10 and 90 percentiles (17). However, since 2016 the new algorithms (22) have been applied giving estimates for PMI as mean values and 95% CI (Table 7.30 and 7.31). An app, which helps estimation of time of death based on published algorithms, has been developed and is available for free (iTOD). Alternatively, it is possible to do the calculations using the web page *tod.international*.

Results of PMI estimations based on the 2016 algorithms (22) are currently compared with the tactical police investigations in cases where the time interval between last sign of life and the time when found dead was ≤3 hours. Preliminary results have been presented at an international conference (28), and a report is in the process of being published.

Eye fluid methods may be especially useful in cases where PMI are more than 24 hours. A triple murder case illustrates this point (Fig. 7.54). In June more than 20 years ago an elderly couple and their daughter were found shot dead in the couple's house (21). The daughter worked for the Ministry of Defense, and possible motives were both political and an inheritance dispute. The son of the couple, his wife, his sister-in-law, and her friend were sentenced for participation, but nobody has been prosecuted for performing the murders. During the court trial the order of the killings became important because of the inheritance dispute.

The daughter had probably arrived at her parents' house in the afternoon on June 3. All three were found dead on June 5 at 9.00 a.m. Forensic pathologist arrived on the scene in the afternoon on June 5.

All bodies were cold and showed decreasing death stiffness when found. Temperature measurements only indicated that death had occured more than 24 hours prior to the measurements.

When applying the diagrams PMI based of Hx and K^+ from 1991 (17), it was quite evident that the mother probably had survived the father and daughter by a substantial period of time. However, the 10th and the 90th percentiles showed overlap (21).

A re-evaluation was therefore performed by means of the algorithms from 2016 (22). With this algorithm the 95% did not overlap (Table 7.33). The estimations are easily performed by means of the calculator in the iTOD app (Figure 7.55).

Applying the algorithm (22) it is evident that the mother had survived the husband and the daughter for a

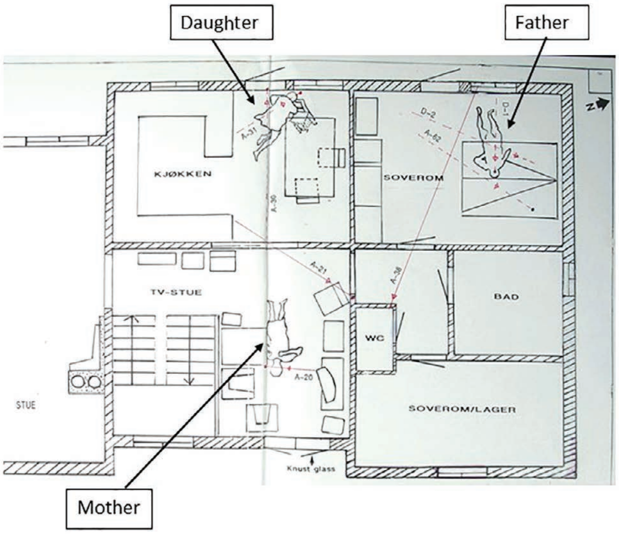

Figure 7.54 Scene of crime. Triple murder. Old couple probably shot in the double bed in the bedroom. The daughter shot while trying to escape out on a veranda. The mother shot while trying to escape through the back door.

Table 7.32 Time of Death Measurements

		Temperature °C			Vitreous humor	
Subject	**Time of measurements**	**Brain**	**Rectum**	**Ambient**	**Hx µmol/L**	**K⁺ mmol/L**
Mother	5.00 pm	16.6	20,5	16.5	205	12.5
Father	9.30 pm	18	20.6	18	310	16.5
Daughter	8.00 pm	19	21.7	16.8	210	16.2

Table 7.33 Triple-murder Case—Time of Death Based on Algorithms (22)

	Time of death Hx		Time of death K⁺	
Subject	**Mean**	**CI**	**Mean**	**CI**
Mother	June 4 at 1.48 p.m.	± 5.1 hrs	June 4 at 3.40 p.m.	± 4.6 hrs
Father	June 4 at 7.49 a.m.	± 5.4 hrs	June 4 at 8.55 a.m.	± 4.8 hrs
Daughter	June 4 at 3.29 a.m.	± 6.7 hrs	June 4 at 6.32 a.m.	± 5.6 hrs

significant period, without overlap of the 95% confidence intervals. The finding was strengthened by the fact that none of the six shotwounds were acutely fatal. Moreover, blood traces on the floor indicated that the mother had moved from the double bed to the place she was found (Figure 7.54).

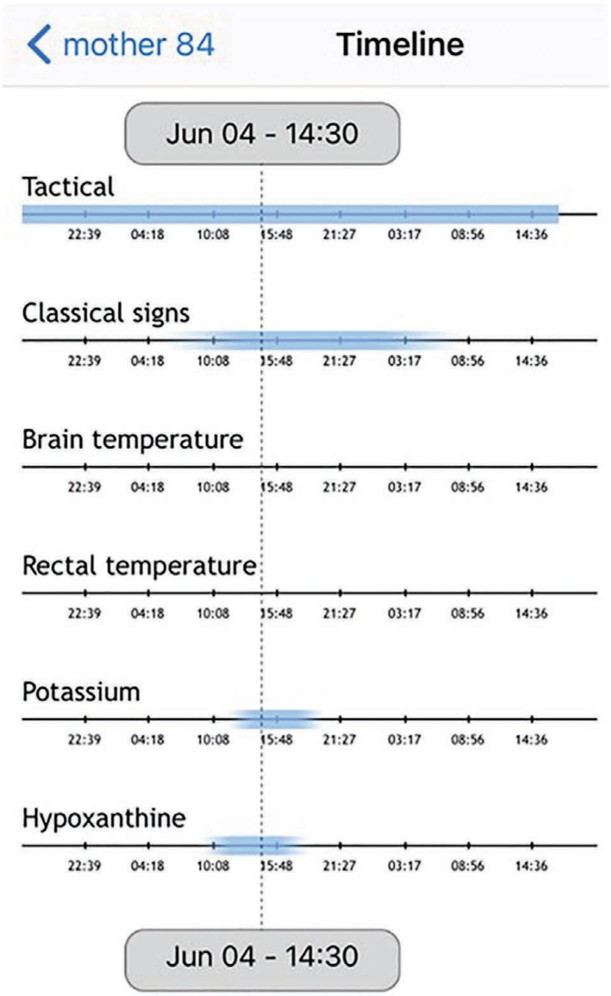

Figure 7.55 Screen dump from the iTOD app from the case presented above. Classical signs of death here mean the observed temperature and stiffness of the body; in this case cold and stiff. 14.30 (2.30 p.m.) is an intermediate time between estimations based on Hx and K⁺.

7.2c.2.5 Guidelines for the Use of Vitreous Humour for Estimation of PMI

Vitreous humour has to be sampled by a forensic pathologist on the scene of crime, who also performs temperature measurements and evaluates the conditions on the scene in co-operation with the police technicians. Blood contamination of the eye fluid must be avoided. The samples should be filtered through a filter unit with a 0.45 µm pore size, before being analysed.

In deaths after a significant period of hypoxia prior to death, for example intoxications, sudden infant death syndrome, cases with traumas near the eyes, the results of PMI based on Hx measurements is not possible.

According to the experience from Department of Forensic Medicine in Oslo, brain temperature measurement (20) is the most precise method for estimation of PMI during the first six hours after death. In the period between 6 hours and 24 hours post-mortem estimations by rectal temperature (19), vitreous humour Hx– and K⁺ are of equal significance (22). After 24 hours post-mortem vitreous humour Hx– and K⁺ seems to be the only alternative for the next two days (22).

7.2c.2.6 Conclusion

A relationship between vitreous humour Hx concentration and time since death has been confirmed by several authors Madea et al. 1994 (23); James et al. 1997 (24);

Muñoz et al. 2002 (25); Madea 2006 (27); 2005; Madea and Rödig 2006 (26); Muñoz et al. 2006 (29); Muñoz et al. 2008 (30). It is quite clear that the ambient temperature is of decisive significance for usable results. This means that eye fluid has to be sampled at the scene of crime together with measurement of ambient temperature near the head of the dead body.

Attempts to calculate the ambient temperature on arrival to the autopsy room or the morgue, give uncertain results with very wide PMI confidence intervals for potassium measurements (Zilg et al. [31]). This is also in accordance with our own experience both for Hx and K^+ (unpublished observations).

Another interesting attempt to integrate vitreous humour biochemistry with temperature and body weight has been proposed by (32) Cordeiro et al. (2019). It will be interesting to observe how this approach may function in practical forensic work.

Another attempt to avoid using ambient temperature measurement on the scene when using vitreous humour for PMI estimation has been suggested by Ortmann et al. (33). They propose different algorithms to be used in different areas according to the climate. In our experience it has turned out of decisively important to apply algorithms that combine the ambient temperature measured on the scene of crime and the simultaneously sampled vitreous humour.

Interestingly, Go et al. 2019 (34) in a study of vitreous humour biochemistry report that Hx showed stronger correlation with PMI than lactic acid.

Furthermore, the correlations with PMI were improved both for Hx and lactic acid when dividing the subjects according to season of death and in addition using the ambient temperature in the regression analyses.

References

1. Saugstad OD. Hypoxanthine as a measurement of hypoxia. *Pediatr Res* 1975;9:158–61.
2. Saugstad OD, Olaisen B. Postmortem hypoxanthine values in vitreous fluid. *Forens Sci Int* 1978;12:33–6.
3. Saugstad OD, Rognum TO. High postmortem levels of hypoxanthine in vitreous humor of premature babies with respiratory distress syndrome. *Pediatrics* 1988;81:395–8.
4. Rognum TO, Saugstad OD, Oyasaeter S, Olaisen B. Elevated levels of hypoxanthine indicate prolonged cerebral hypoxia in victims of sudden infant death syndrome. *Pediatrics* 1988;82:615–18.
5. Rognum TO, Saugstad OD. Hypoxanthine levels in vitreous humor: Evidence of hypoxia in most infants who died of sudden infant death syndrome. *Pediatrics* 1991;87:306–10.
6. Beckwith JB, SIDS and hypoxanthine. *Pediatrics*. Letter to the editor. 1991;88:1076–7.
7. Rognum TO, Saugstad OD. SIDS and hypoxanthine. Reply to Beckwith. *Pediatrics* 1991;88:1077.
8. Vege A, Chen Y, Opdal SH, Saugstad OD, Rognum TO. Vitreous humor hypoxanthine levels in SIDS and infectious death. *Acta Paediatr*. 1994;83(6):634–9.
9. Carpenter KH, Bonham JR, Worthy E, Variend S. Vitreous humour and cerebrospinal fluid hypoxanthine concentration as a marker of pre-mortem hypoxia in SIDS. *J Clin Pathol* 1993;46:650–3.
10. Opdal SH, Rognum TO, Vege A, Saugstad OD. Hypoxanthine levels in vitreous humor: a study of influencing factors in sudden infant death syndrome. *Pediatr Res*. 1998;44(2):192–6.
11. Gregersen M, Rajs J, Laursen H, Baandrup U, Fredriksen P, Gidlund E, Helweg-Larsen K, Hirvonen J, Isaksen CV, Kock K, Lundemose JB, Løberg EM, Rognum TO, Skullerud K, Vege Å. Pathologic criteria for the Nordic study of SIDS. In *Sudden infant death syndrome. New trends in the nineties*. Rognum TO (ed). Scandinavian University Press, Oslo, 1995, pp 50–8.
12. Bajanowski T, Vege A, Byard RW, Krous HF, Arnestad M, Bachs L, Banner J, Blair PS, Borthne A, Dettmeyer R, Fleming P, Gaustad P, Gregersen M, Grøgaard J, Holter E, Isaksen CV, Jorgensen JV, de Lange C, Madea B, Moore I, Morland J, Opdal SH, Råsten-Almqvist P, Schlaud M, Sidebotham P, Skullerud K, Stoltenburg-Didinger G, Stray-Pedersen A, Sveum L, Rognum TO. Sudden infant death syndrome (SIDS)—standardised investigations and classification: recommendations. *Forensic Sci Int* 2007;165(2–3):129–43.
13. Sturner WQ. The vitreous humour postmortem potassium changes. *Lancet* 1963;281(7285):807–8.
14. Sturner WQ, Gantner GE Jr. The postmortem interval. A study of potassium in the vitreous humor. *Am J Clin Pathol* 1964:42:137–44.
15. Madea B, Henssge C, Honig W, Gerbracht A. References for determinating the time of death by potassium in the vitreous humor. *Forens Sci Int* 1989;40:231–43.
16. Coe JI. Vitreous potassium as a measure of the postmortem interval: an historical review and critical evaluation. *Forens Sci Int* 1989;42(3):201–13.
17. Rognum TO, Hauge S, Oyasaeter S, Saugstad OD. A new biochemical method for estimation of postmortem time. *Forensic Sci Int* 1991;51(1):139–46.
18. Saukko P, Knight B. Post-mortem changes of forensic importance. In *Knight's forensic pathology*, 4th edition, Saukko P, Kinght B (eds). CRC Press, 2016, pp 58–66.
19. Henssge C. Death time estimation in case work. I. The rectal temperature time of death nomogram. *Forensic Sci Int* 1988;38(3–4):209–36.
20. Henssge C, Frekers R, Reinhardt, Beckmann ER. Todeszeitbestimmung auf der Basis simultaner Messung von Hirn- und Rektaltemperatur [Determination of the time of death based on simultaneous measurement of brain and rectal temperatures]. *Z Rechtsmed* 1984;93(2):123–33. In German with English Summary.
21. Rognum TO, Musse AM, Saugstad OD. Estimation of time since death by chemical analysis of potassium and hypxanthine (Hx) in vitreous humour in a triple murder case. *Scand J Forens Sci* 2002;1:17–22.
22. Rognum TO, Holmen S, Musse AM, Dahlberg PS, Stray-Pedersen A, Saugstad OD, Opdahl SH. Estimation of time since death by vitreous humor hypxanthin, potassium, and ambient temperature. *Forens Sci Int* 2016;262:160–5.
23. Madea B, Käferstein H, Hermann N, Sticht G. Hypoxanthine in vitreous humor and cerebrospinal fluid—a marker of postmortem interval and prolonged (vital) hypoxia? Remarks also on hypoxanthine in SIDS. *Forensic Sci Int* 1994;65(1):19–31.

24. James RA, Hoadley PA, Sampson BG. Determination of postmortem interval by sampling vitreous humour. *Am J Forensic Med Pathol* 1997;18(2):158–62.
25. Muñoz Barús JI, Suárez-Peñaranda J, Otero XL, Rodríguez-Calvo MS, Costas E, Miguéns X, Concheiro L. Improved estimation of postmortem interval based on differential behaviour of vitreous potassium and hypoxantine in death by hanging. *Forensic Sci Int* 2002;125(1):67–74.
26. Madea B, Rödig A. Time of death dependent criteria in vitreous humor: accuracy of estimating the time since death. *Forensic Sci Int* 2006;164(2–3):87–92.
27. Madea B. Is there recent progress in the estimation of the postmortem interval by means of thanatochemistry? *Forensic Sci Int* 2005;151(2–3):139–49.
28. Rognum TO, Holmen S, Opdal SH, Musse AN, Saugstad OD, Stray-Pedersen A. Evaluation of confidence of time of death estimation by measurement of hypoxanthine and potassium sampled at the scene of death. *20th Nordic Conference on Forensic Medicine*. Helsinki, June 13–16, 2018.
29. Muñoz Barús JI, Febrero-Bande M, Cadarso-Suárez C. Flexible regression models for estimating postmortem interval (PMI) in forensic medicine. *Stat Med* 2008;27(24):5026–38.
30. Muñoz JI, Costas E, Rodríguez-Calvo MS, Suárez-Peñaranda JM, López-Rivadulla M, Concheiro L. A high-performance liquid chromatography method for hypoxanthine determination in vitreous humour: application to estimation of post mortem interval. *Hum Exp Toxicol* 2006;25(5):279–81.
31. Zilg B, Bernard S, Alkass K, Berg S, Druid H. A new method for estimation of time since death from vitreous potassium levels corrected for age and temperature. *Forens Sci Int* 2015;254:158–66.
32. Cordeiro C, Ordónez-Mayaán L, Lendoiro E, Fereiro-Bande, Vieira DN, Munoz-Barús JU. A reliable method for estimating the postmortem interval from the biochemistry of the vitreous humor. Temperature and body weight. *Forens Sci Int* 2019;295:157–68.
33. Ortmann J, Markwerth P, Madea B. Precision of estimating the time since death by vitreous potassium-Comparison of 5 different equations. *Forensic Sci Int* 2016;269:1–7.
34. Go A, Shim G, Park J, Hwang J, Nam M, Eong H, Chung H. Analyses and lactic acid levels in vitreous humor for the estimation of post-mortem interval (PMI= using LC-MS/MS. *Forens Sci Int* 2019;299:135–41.

7.3 Cerebrospinal Fluid Chemistry

Burkhard Madea and Claus Henssge

Post-mortem changes of cerebrospinal fluid (CSF) electrolytes are caused by autolytic changes of cell membranes with resulting greater permeability so that intracellular ions of higher concentrations diffuse out into the extracellular fluid, whereas ions with a higher extracellular concentration decrease as a result of the increased volume of distribution. Post-mortem changes of CSF electrolytes are based mainly on hypoxic damage of the choroid plexus. Especially after 1950 several investigations on CSF and time since death were carried out [1,2,4–10–12–14–18, reviews in 11,13].

The investigations of Schleyer on chloride and magnesium concentrations in CSF [12], of Schleyer and Janitzki on inorganic phosphorus in CSF [15] and of Dotzauer and Naeve on sodium and calcium concentrations in CSF [1] revealed that determination of these parameters is of no use in estimating the time since death—not even in the early PMI. Calcium showed a tendency to increase in the later PMI, and sodium decreased with increasing PMI. Mason et al. [5] were the first to report on a relationship between time since death (t) and potassium (K^+) concentration [K+] (in mmol/l) in cisternal fluid with the following regression:

$$[K^+] = 48.56 + 61.45 \lg t$$

and a standard deviation of ±9.4 mg K^+/100 mL.

This standard deviation is equivalent to a halving or doubling of the time since death calculated from the cisternal fluid K^+. Neither Mason et al. [5] nor Dotzauer and Naeve [1] recommended cisternal fluid electrolyte determination for estimating the PMI.

A post-mortem increase of K^+ was also reported by Naumann [7] and by Murray and Hordynsky [6]. The latter authors drew the following conclusions from their investigations on 46 bodies in the time interval from 2 to 24 hours post-mortem:

1. Spinal fluid cannot be compared with cisternal fluid because of the obvious divergent gradients of diffusion.
2. The concentrations of sodium, magnesium and calcium have no obvious relationship with the time since death.
3. The amount of K^+ increases at a constant rate in relation to the temperature of the body.
4. Severe infections or toxic processes that exist for an extended period before death influence the subsequent rate of diffusion.

Schleyer's [12] results show, in addition to the previous studies on cisternal fluid K^+, a great scatter of values over the PMI. According to Schleyer, bloody cisternal fluid does not show excessively high K^+ values [11]. Further studies on CSF K^+ concentrations, with similar results, were published by Fraschini et al. [2], Paulson and Stickney [8] and Weischer [24].

In spite of these disappointing results, Urban and Tröger [19–23 and personal communication, R. Urban, 1987] carried out extensive investigations on CSF electrolytes. The results were obtained from cases of sudden death. From 147 bodies, cisternal fluid was withdrawn repeatedly at half-hourly intervals; from 143 bodies, only 1 sample was taken. Rectal temperatures were taken simultaneously. As expected from the literature, the concentrations of calcium and magnesium showed no correlation with the time since death. Sodium concentrations decreased exponentially during the first 20 hours post-mortem; two subgroups kept at ambient temperatures of 5°C and 20°C showed no differences (Figure 7.56).

The exponential rise of cisternal fluid K+ during the first 20 hours post-mortem showed a stronger relationship with the time since death (Figure 7.57). This rise of K+ was also not influenced by the environmental temperature. In Figure 7.57, the single values are plotted with 98 per cent confidence limits. During the first 10 hours, the variation was ±1 hour, with the exception of four individuals dying of liver failure or uraemia. All the other cases were sudden deaths. Figure 7.57 (b) appears to indicate that the rise of cisternal K+ is not influenced by the environmental temperature. Urban and Tröger [22] could reduce the deviations between real and extrapolated time since death from ±1.5 hours during the first 15 hours post-mortem to −0.75 to +1 hour by taking the actual rectal temperature and the cooling velocity into consideration. In 1987, the authors presented a 'Potassium—time since death nomogram' and claimed 95 per cent confidence limits of ±1.4 hours, which are wider than the published variations of ±1 hour up to 10 hours post-mortem.

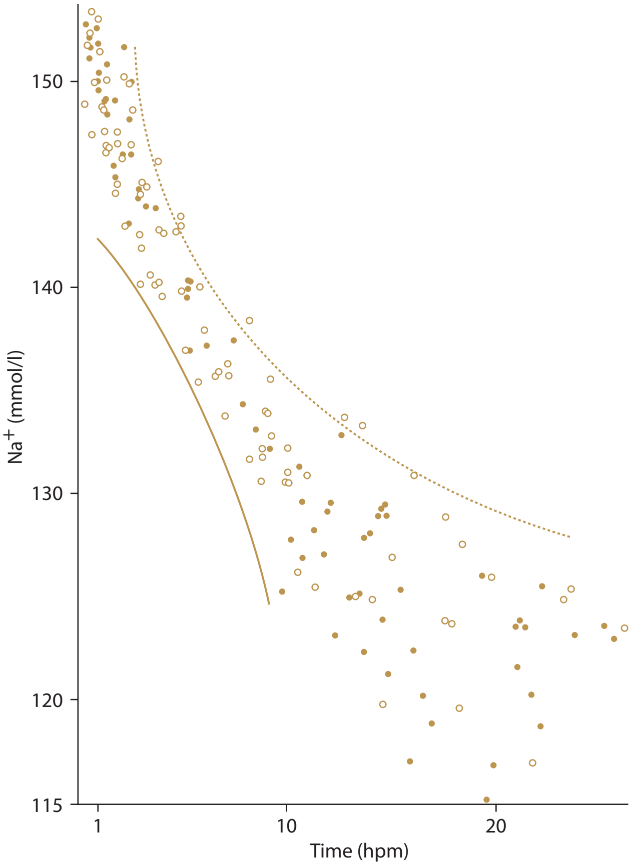

Figure 7.56 Temperature dependency of the decrease of the sodium (Na^+) concentration in cisternal fluid over the post-mortem interval. Open circles, ambient temperature of 5°C; closed circles, ambient temperature of 20°C. There is no temperature dependency. hpm, hours post-mortem.

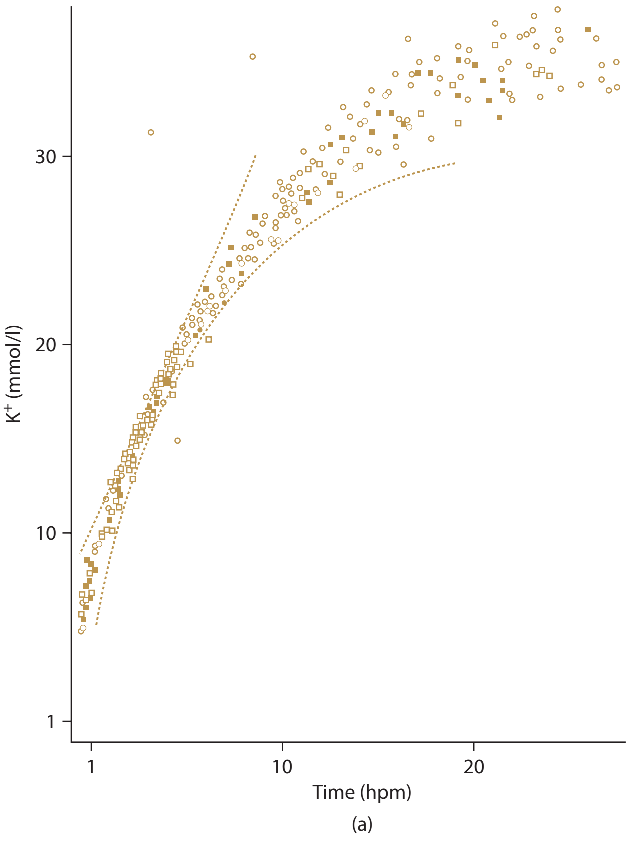

Figure 7.57 (a) Exponential rise of cisternal fluid potassium (K^+) over the post-mortem interval with cause of death. Closed squares, throttling, manual strangulation; closed circles, asphyxiation, drowning; open circles, cardiac failure: pulmonary thromboembolism, myocardial infarction; open squares, cardiac failure: shooting, stabbing; stars, liver failure, uraemia; four cases with liver failure/uraemia showed a marked deviation. (b) Rise of K^+ for two different environmental temperatures: squares, 5°C; circles, 20°C. hpm, hours post-mortem. (b) Rise of K^+ for two different environmental temperatures: squares, 5°C; circles, 20°C. hpm, hours post-mortem.

In 1987, 95 per cent confidence limits of death time estimation from cisternal fluid K+ of ±2.36 hours up to 15 hours post-mortem were reported. By taking the temperature into consideration, these limits could be reduced to ±1.4 hours for the interval up to 15 hours post-mortem; during the interval up to 10 hours post mortem, the 95 per cent limits were ±1.03 hours. Urban found a strong linear correlation between the estimated time since death based on cisternal K+ and the estimated time since death based on rectal temperature by using the nomogram method of Henssge (see Chapter 6.1) (Figure 7.58). The author assessed cisternal K+ to be the most precise method of death time estimation in the early PMI because the 95 per cent confidence limits are only ±1.4 hours compared with ±2.8 hours using Henssge's nomogram method. The

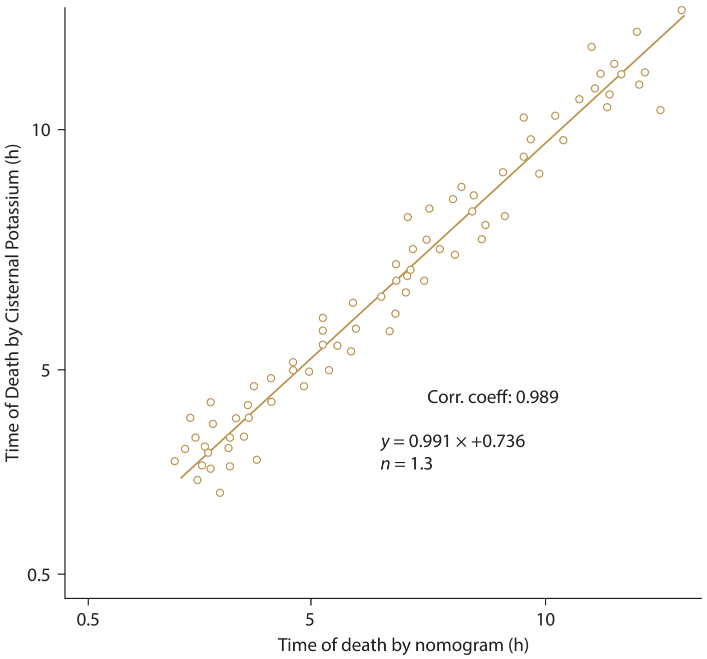

Figure 7.58 Correlation between estimated time since death from potassium concentration in cisternal fluid and rectal temperature (using the nomogram method of Henssge).

high correlation between death time estimation from cisternal K⁺ and body temperatures strengthens the value of combining different methods for a reliable statement on the time since death.

Urban and Tröger [19,21] recommended the application of his method for all cases except the following:

- Intracranial/intracerebral bleeding with haemorrhage into ventricles or cisterns
- Chronic lingering disease with electrolyte imbalances
- Death from hypothermia

The value of these investigations on the increase of cisternal K⁺ are without any doubt because Urban has, unlike other authors, studied the cisternal K⁺ concentration during its steepest rise and not during the interval when the equilibrium had already been achieved.

However, succeeding authors (Madea et al. [4] and Wiesböck et al. [25]) found a much wider range of scatter even in cases of sudden death (Figure 7.59). Comparing the raw data of Mason et al. [5] with Urban's results (Figure 7.3.5), Mason's values taken serially from 8 bodies show a greater scatter of values, although Mason et al. [5] claimed to have eliminated all cases with diseases that could influence serum K⁺.

In the 46 cases of Murray and Hordynsky [6] (Figure 7.61), as well as in Schleyer's cases [11], there is a much wider range of scatter than was found by Urban. However, the random sample of the latter authors included cases with causes of death such as encephalitis, glomerulonephritis, chronic hepatitis, stroke and bronchopneumonia, which may cause an ante-mortem dysregulation of electrolyte homeostasis.

The discrepancies between our results and those of Urban cannot be explained by differences in the random

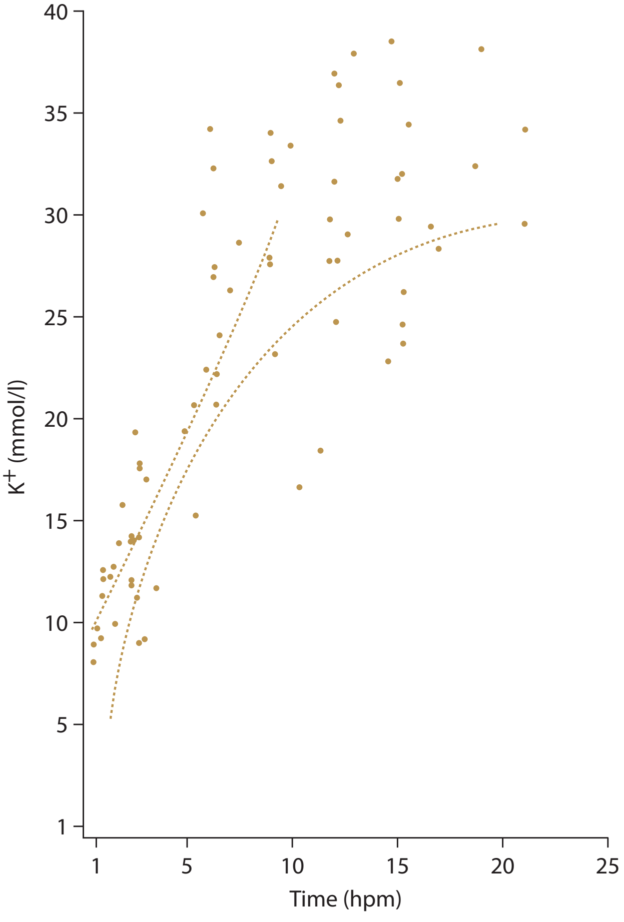

(a)

Figure 7.59 (a) Potassium (K⁺) concentration over the PMI ($n = 76$); sudden deaths; 98 per cent confidence limits by Urban. Although the sample consists only of sudden deaths, the range of scatter is much wider than that in Urban's sample.

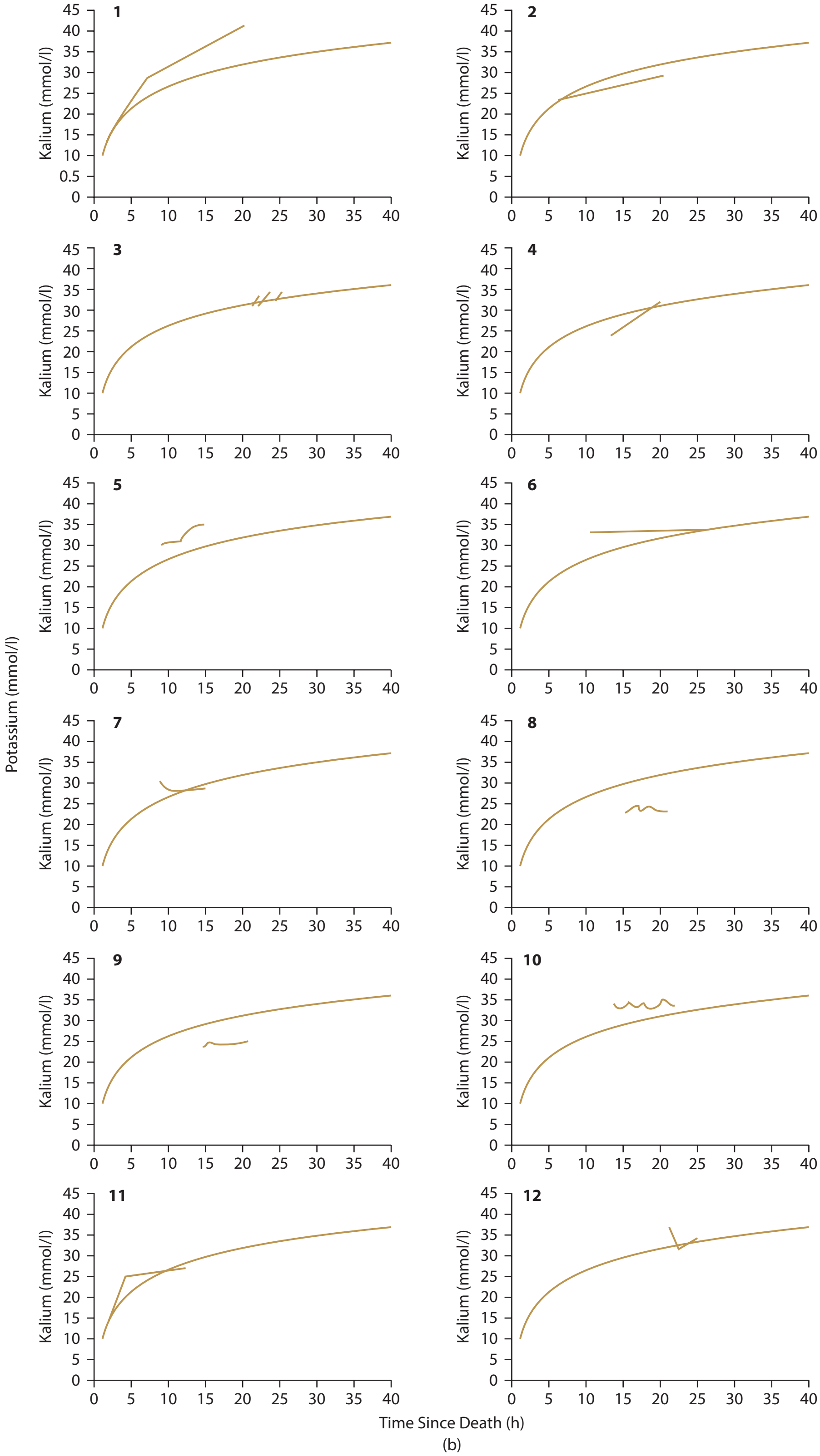

Figure 7.59 (*Continued*) (b) Individual courses of cisternal K+ levels in 12 cases of sudden death after repeated sample taking (ambient temperature 5°C) over the time since death. The regression curve was calculated from 76 independent K+ values (single sample taking). The 'rise' of cisternal K+ is irregular; in some cases, there is a drop of the potassium concentration (cases 7, 8, 10, 12), even in the early PMI (case 7). hpm, hours post-mortem.

(From Wiesböck J, Josephi E, Liebhart E. Intraindividuelle Kaliumverschiebungen im Liquor cerebrospinalis nach dem Tod. *Beitr Gerichtl Med* 1989;**47:**403–405.)

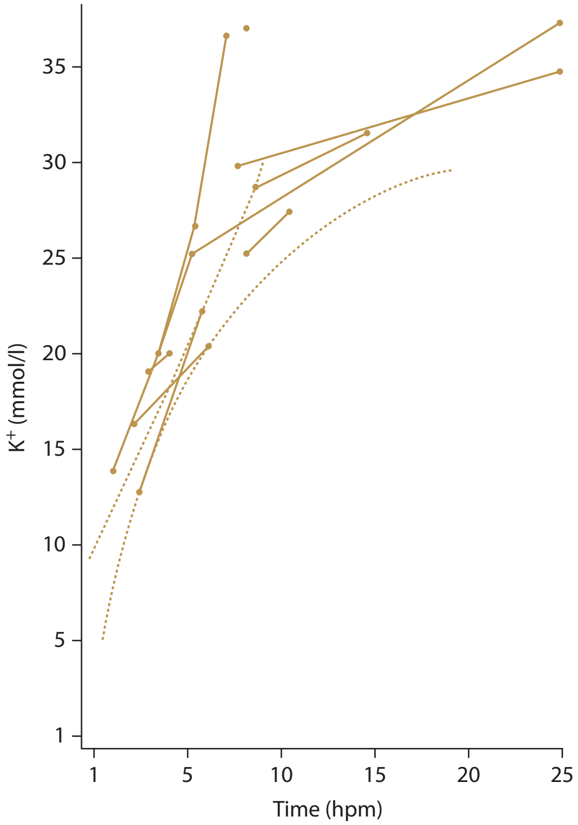

Figure 7.60 Potassium (K⁺) values (from Mason et al. [5]) with 98 per cent confidence limits). Nineteen values were taken from 8 bodies. hpm, hours post-mortem.

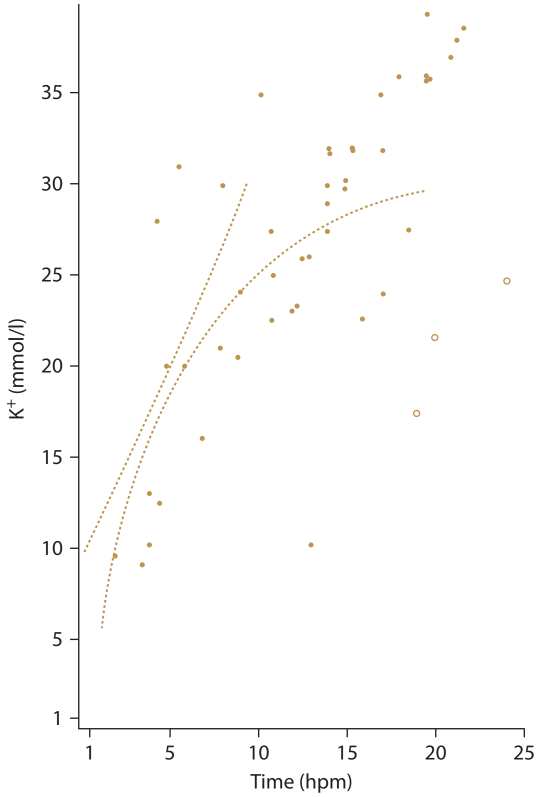

Figure 7.61 Forty-six potassium (K⁺) values (from Murray and Hordynsky[6]) with 98 per cent confidence limits by Urban. In three cases, only spinal fluid was available; this fluid has systematically lower potassium values than cisternal fluid. hpm, hours post-mortem.

samples because we studied cases of sudden death exclusively. Our sample consisted mostly of natural deaths, whereas Urban's group consisted of traumatic deaths such as strangulation, throttling, shooting and stabbing, which he was in part able to investigate within 1 hour after death.

According to Urban, the differences in taking the samples (single sample taking or repeated sample taking) cannot be taken into consideration as a cause of the different scatter: he found no systematic differences in the scatter of K⁺ values between single sample taking and repeated sample taking (unlike Schourup [18]).

The cause of the discrepancies in the scatter of values remains unclear, and further studies are necessary to clarify this situation. At present, we cannot recommend the use of the method of Urban and his narrow 98 per cent confidence limits.

A recent study by Garland et al. [3] examined 20 paired cases of vitreous humour and CSF to investigate their use in estimating PMI. From the examined ions only potassium showed a significant regression coefficient in vitreous humour and CSF. The conclusion of the authors is that their study showed changes in analytes in vitreous humour and CSF following similar trends.

Potassium (K+) in VH is most accurate in estimating the PMI. With no significant improvement in accuracy when potassium (K+) and CSF is combined. Thus, the role of CSF is electrolytes in estimating PMI may be very limited. A general conclusion may be that it doesn't make any sense to study CSF further because vitreous humour in any respect superior to CSF and measured values are more reliable.

References

1. Dotzauer G, Naeve W. Vergleichende Untersuchungen über den Natrium- und Kaliumgehalt im Serum wie im Liquor postmortem. *Dtsch Z Gerichtl Med* 1960;*49*:406–19.
2. Fraschini F, Muller E, Zanoboni A. Postmortem increase of potassium in human cerebrospinal fluid. *Nature* 1963;*98*:1208.
3. Garland J, Olds K, Rousseau G, Palmiere C, Ondruschka B, et al. Using vitreous humour and cerebrospinal fluid electrolytes in estimating post-mortem interval—an exploratory study. *Aust J Forensic Sci* 2020;*52*(6):626–33.
4. Madea B, Henssge C, Püschel K, Hönig W. Wie zulässig ist die Todeszeitbestimmung aus der Kaliumkonzentration in Zisternenliquor? *Beiträge zur gerichtlichen Medizin* 1988;*46*:283–7.
5. Mason JK, Klyne W, Lennox B. Potassium levels in the cerebrospinal fluid after duration of death. *J Clin Path* 1951;*4*:231–33.

6. Murray EF, Hordynsky W. Potassium levels in the cerebrospinal fluid and their relation to duration of death. *J Forensic Sci* 1958;*3*:480–5.
7. Naumann HN. Cerebrospinal fluid electrolytes after death. *Proc Soc Biol Med* 1958;*98*:16–18.
8. Paulson G, Stickney D. Cerebrospinal fluid after death. *Confin Neurol* 1971;*33*:149–62.
9. Poulsen JP, Oyasaeter S, Rognum TO, Saugstad OD. Hypoxanthine, xanthine, and uric acid concentrations in the cerebrospinal fluid, plasma, and urine of hypoxemic pigs. *Pediatr Res* 1990;*28*: 477–81.
10. Praetorius E, Poulsen H, Dupont H. Uric acid, xanthine and hypoxanthine in the cerebrospinal fluid. *Scand J Clin Lab Invest* 1957;*9*:133–7.
11. Schleyer F. *Postmortale klinisch-chemische Diagnostik und Todeszeitbestimmung mit chemischen und physikalischen Methoden*. Stuttgart, Germany, Thieme, 1958.
12. Schleyer F. Untersuchungen über die Beziehungen der postmortalen Chlor- und Magnesiumkonzentration in Liquor und Plasma zu Leichenalter und Todesursache. *Frankfurt Z Pathol* 1959;*69*:644–8.
13. Schleyer F. Determination of the time since death in the early postmortem interval. In: Lundquist F (ed.). *Methods of Forensic Science*, vol. 2. New York, Interscience Publishers, John Wiley and Sons, 1963, pp 253–93.
14. Schleyer F. Neuere Erkenntnisse über agonale und frühpostmortale chemische Vorgänge in den Körperflüssigkeiten. *Dtsch Z Gesamte Gerichtl Med* 1967;*59*:48–57.
15. Schleyer F, Janitzki U. Untersuchungen über den postmortalen Phosphatgehalt von Liquor und Serum in Beziehung zum Leichenalter. *Dtsch Z Gesamte Gerichtl Med* 1959;*49*:229–34.
16. Schoning O, Strafuss AC. Determining time of death of a dog by analysing blood, cerebrospinal fluid and vitreous humour collected postmortem. *Am J Vet Res* 1980;*41*:955–7.
17. Schoning P, Strafuss AC. Postmortem biochemical changes in canine cerebrospinal fluid. *J Forensic Sci* 1980;*25*:60–6.
18. Schourup K. *Dødstidsbestemmelse på grunlag af postmortelle cisternevaedskevorandringer og det postmortelle axiltemperaturfald. Summary: determination of the time since death*. Med. Diss. Copenhagen 1950, Dansk, Visdenskabs København.
19. Urban R. *Elektrolytbestimmung im Liquor cerebrospinalis—mathematische Analyse experimenteller Befunde unter Berücksichtigung forensisch relevanter Einflussfaktoren zur Todeszeitbestimmung im frühpostmortalen Intervall*. Hannover, Germany, Habilitation Schrift, 1987.
20. Urban R, Tröger HD. *Einfluss der Todesursache auf die Leichenliegezeitbestimmung im Zisternenliquor*. Vortrag 17. Jahrestreffen der Arbeitsgemeinschaft Nordund Westdtsch. Rechtsmed, 1986.
21. Urban R, Tröger HD. Todeszeitbestimmung im frühpostmortalen Intervall—Kalium–Todeszeit-Bezugsnomogramm. Vortrag 66. Jahrestag. *Dtsch Gesamte Rechtsmed* 1987:8.
22. Urban R, Tröger HD. Todeszeitbestimmung Möglichkeiten und Grenzen der Elektrolytbestimmung im Leichenliquor. *Beitr Gerichtl Med* 1987;*45*:157–161.
23. Urban R, Tröger HD, Krüger HJ. Todeszeitbestimmung im frühpostmortalen Intervall durch Elektrolytbestimmung im Zisternenliquor. Vortrag 64. Jahrestag. *Dtsch Gesamte Rechtsmed* 1985:7–11, Hamburg.
24. Weischer K. *Biochemische Liquoruntersuchungen an Leichen*, MD thesis. Münster, Germany, Münster University, 1982.
25. Wiesböck J, Josephi E, Liebhart E. Intraindividuelle Kaliumverschiebungen im Liquor cerebrospinalis nach dem Tod. *Beitr Gerichtl Med* 1989;*47*:403–5.

7.4 Estimation of Duration of Immersion

■ *Elke Doberentz and Burkhard Madea*

The estimation of the time of immersion is a common problem in forensic medicine. The factors that govern the rate of decomposition in water and the time in which the signs of immersion are developing were identified long ago:

- The water temperature, the most important factor
- The osmolarity of the water (fresh water, salt water)
- The bacterial content of the water (e.g. body found in a settling basin of a sewage plant)
- Stagnant water—running water

Decomposition, of course, proceeds much faster in warm water than in cold water.

For the estimation of the time of immersion 'in water of average temperature climates' some rules of thumb have been developed, for example [9]:

1. No wrinkling of the finger pads is present: up to a few hours.
2. Wrinkled fingers, palms and feet: from half a day to 3 days.
3. Early decomposition, often first in the dependent areas of head and neck, abdomen and thighs: 4–10 days.
4. Bloating of face and abdomen with marbling of veins and peeling of epidermis on hands and feet and slippage of the scalp: 2–4 weeks.
5. Gross skin shedding, muscle loss with skeletal muscle, partial liquefaction: 1–2 months.

In the German literature, the rules of thumb for estimation of immersion [4,19,21] are similar to those in the English literature [5,9,10,18,20,27]. However, the reliability and validity of these rules are low. According to Spitz [27], wrinkling of the skin cannot be used to determine the period of time a body was in the water. In the last three decades several authors have worked on the progression of washerwoman's skin depending on water temperature, osmolarity and other factors [18,22,29–31]. However, these investigations have never gained practical relevance because in the very early PMI other methods such as body cooling give quite satisfying results [8].

In the 1960s, a German forensic pathologist developed a table for the estimation of the time interval of immersion by taking into account the actual water temperature and morphological findings of bodies immersed in water identified during the external or internal examination [23–25]. This chart is part of German textbooks [1,16], but it seems to be relatively unknown in the English literature.

7.4.1 Correlation of Water Temperature and Stages of Putrefaction

The original investigations of the forensic pathologist Reh on 277 bodies recovered from the River Rhine with known PMIs were carried out to answer the question whether there is any correlation between time of immersion and water temperature on the one hand and signs of death, signs of immersion and stages of putrefaction on the other [23,24].

The corpses were mainly recovered from the Rhine and Rhine harbour in Düsseldorf, Germany (70 per cent), with a smaller percentage (30 per cent) from other stagnant or running waters, lakes and (swimming) pools.

Only those bodies were taken into consideration that were brought into a mortuary or a low environmental temperature (4°C, to prevent further putrefaction) immediately after recovery. Bodies of newborns or small children were excluded.

The external examination was normally carried out 2–3 days after recovery of the body, which is a common time interval between recovery and legal autopsy in Germany.

Certain criteria concerning autolysis, putrefaction and maceration were taken into consideration in each case (see Table 7.34).

The water temperature at the place and time of recovery—taken 0.5–1 m below the water surface—was considered as well.

Figure 7.62 shows the average annual water temperatures of the River Rhine in Düsseldorf from 1961 to 1964 and of the River Danube in Vienna from 1897 to 1910. Although the temperatures of the River Danube are slightly lower than those of the Rhine (lowest difference in March: 1°C; highest difference from August to February: >1.8°C), the curves are almost identical.

However, within 1 month, the water temperature can vary considerably even in one place, and it can vary even more among different sites of the same river. Therefore, Reh considered the average water temperature for each month from 1961 to 1964.

In stagnant waters, the temperature is a little higher than in running waters.

Table 7.34 Reh's Table to Estimate the Minimum Time Interval of Immersion*

	Month	Jan.	Feb.	March	April	May	June	July	Aug.	Sept.	Oct.	Nov.	Dec.
Ø	Median water temperature (C) of the month according to measurements of Reh	3.5°	3.9°	5.8°	9.9°	13.0°	17.4°	18.6°	18.6°	17.3°	13.2°	8.8°	4.7°
				Signs of putrefaction									
1.	Marbling	32	25	16 (23)	9–10	4–5	2	1–2	2	3	4–5	10	17
2.	Distension of tissues by gas	35	25	16 (23)	10	4–5	2–3	2	3	3–4	7	10	17
3.	Discolouration of the body	35	25	16 (23)	(14)	4–5	2	2	3	3–4	7	10	17
4.	Peeling of the epidermis	35	25	16 (23)	(16)	4–5	3	2	3	3–4	7	10	17
5.	Hair loss	35	25	16 (23)	10–12	4–5	2–3	2–3	3	3–4	7	10	17
6.	Hands: beginning of wrinkling	(1)	(1) 28–30	(12 h)			(6 h)			2 h		2 h	(1)
7.	Nails become loose	>35	(40) 30–32	23	16	5	2–3	3	3	3–4	11	17	28
8.	Peeling of skin in glove form	35	(45)	23	16	10	3	3	3–4	4	7	20	28
9.	Nail loss	>53	45	30 (40)	21	14	8	3	4	10	>11	20	>35
10.	Feet: beginning of wrinkling	(1)	(1)	(12 h)	(1)		(6 h)	½ h		2 h		2 h	(1)
11.	Nails become loose	>53	40	26 (35)	17	10	5	3	4	8	12	17	28
12.	Peeling of skin	>53	60	35	16	10	5	3	5–6	8–9	>11 (14)	20	28
13.	Nail loss	>53	>60	53	>35	>28	>10	3	>10	>10	>11	>20	>35
14.	Transudate in pleural cavities†	35	25 (40)	18 (35)	10	5	3–4	3	3	11	5	>20	
15.	Heart without blood	>39	32–34 (40)	23	14–15	9	4	3	3	5	11	20	28
16.	Brain liquefied	35	30 (40)	(23)	14–	5	3–4	3	3	6	10	17	28

* Minimum time of immersion in days; maximum time in days shown in parentheses.

† >500 mL in adults.

Source: Modified from Reh [24].

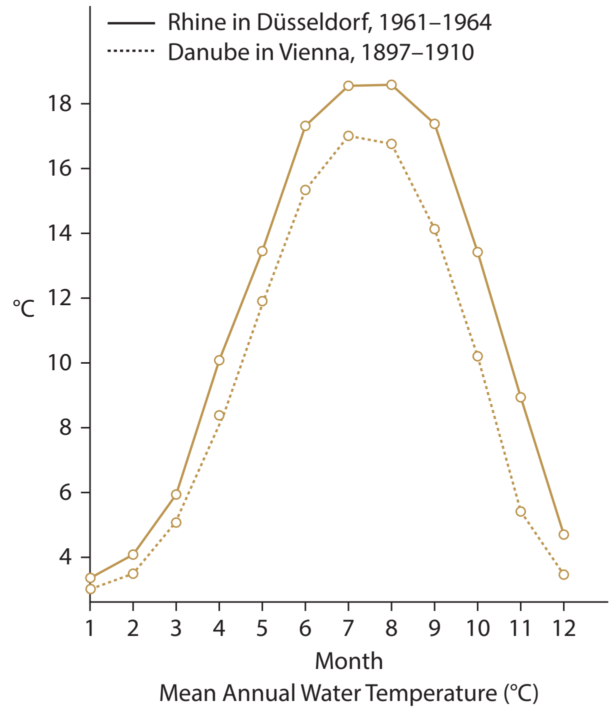

Figure 7.62 Average annual water temperatures of the River Rhine in Düsseldorf from 1961 to 1964 and of the River Danube in Vienna from 1897 to 1910.

Reh examined 277 corpses and established the following chronological order for the development of the signs of death and stages of putrefaction:

- Washerwoman's skin
- Loosening of rigor mortis
- Bloating and discolouration of the body
- Loosening and loss of skin, hairs and nails, with loss of toenails last
- Inner findings: transudate in pleural cavity greater than 500 mL
- Heart without blood and liquefaction of brain

A definite stage of putrefaction is achieved earlier in higher water temperatures.

In Figure 7.69, the dependency of putrefaction on water temperature and time of immersion is shown for three criteria:

- Bloating of the body (gas emphysema)
- Liquefaction of brain
- Loosening of toenails

For all three criteria, the minimal time interval is given, and it becomes evident that decomposition is accelerated in higher water temperatures. Although in March loosening of toenails or liquefaction of brain requires a time interval of more than 20 days (minimum, 24–26 days), the minimum time interval in July is only 2–4 days. The second factor is that the different signs of putrefaction take place simultaneously.

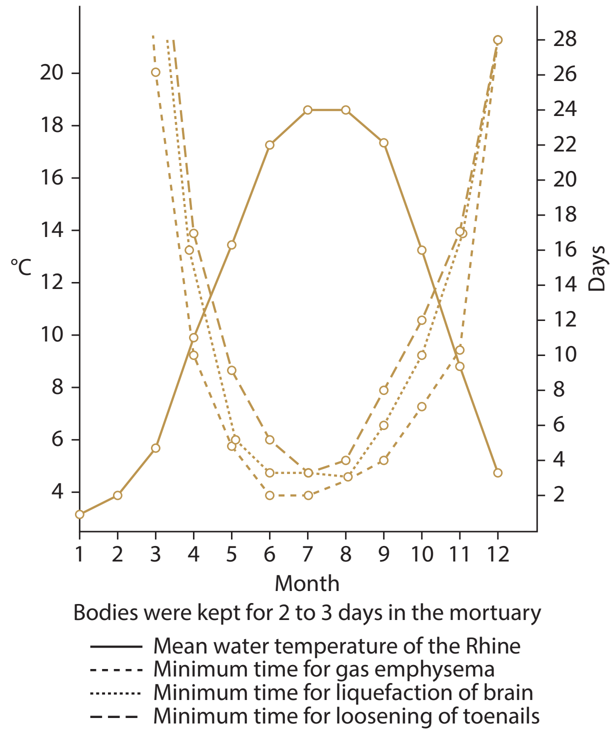

Figure 7.63 The dependency of putrefaction on water temperatures and times of immersion.

7.4.2 Table for Estimating the Minimum Time Interval of Immersion

From the average water temperatures for each month and the stages of decomposition, Reh developed a table with the minimum time intervals of immersion (Table 7.34). The left column contains the signs of decomposition (numbers 1–16), and the heading shows the months. Every month correlates with an average monthly water temperature (shown in the line below the month).

As many criteria as possible should be used for estimating the minimum time interval since death. With more than only one or two criteria, the result becomes more reliable. Every sign of putrefaction is correlated with a minimum time in which this sign can develop. This means, for example, that marbling can be found after a minimum of 32 days in January. After determining the signs of putrefaction and considering the several minimum times for each sign, the longest minimum time of all—the sign developing last—will be the minimum time for immersion in water. For example, the body shows marbling (32 days in January) and a liquefied brain (35 days in January)—the minimum time interval of immersion is 35 days because only after 35 days is brain liquefaction seen. The maximum time of immersion can also be determined: a heart without blood can be found after more than 39 days. If the heart contains blood, the body was not immersed for 39 days. Our example has a minimum time of immersion of 35 days and maximum time of immersion of 39 days. A better estimation of the immersion time can be made and help to support the investigations by using the chart instead of the old rules of thumb.

For estimating the minimum time interval of immersion, the average water temperature that is closest to the actual water temperature at the time of recovery is considered and not the water temperature of the actual month. Reh proposed using the water temperature of the day of recovery for an estimation [23,24]. With this table, not only can the minimum time interval of immersion be estimated, but also the maximum interval can be estimated by considering those criteria that have not yet developed in the corpse.

If in June marbling, bloating and discolouration have developed, and the nails are loose but not lost, it may be concluded that the interval of immersion is more than 3 days but less than 8 days.

Further examples are given in Tables 7.34–7.40.

It has been recorded during recent years that the water temperature of the Rhine has exceeded the temperatures indicated by Reh, especially in summer. Nevertheless, a careful estimation of the minimal time interval of immersion is possible if the highest temperature given in the table is considered.

Good experiences with Reh's table have been reported. The chart is much better than the formerly used rules of thumb and takes the actual water temperatures into account [2,3,13,15].

However, the following requirements have to be met to avoid miscalculations: the bodies should have been kept at a low environmental temperature (4°C) 2–3 days after recovery if the signs of death and stages of putrefaction have been observed 2–3 days after recovery. If the examination is carried out immediately after recovery, the table can be applied as well, but the bodies must not have been exposed to environmental temperatures for a longer period. However, it must be ensured that there is no time interval between death and immersion. Having this in mind and taking into account as many criteria as possible, a careful estimation of the minimum and maximum time intervals of immersion can be made.

In 1977, Reh et al. [26] published, as an addition to the table, diagrams (temperature and time diagrams for different stages of putrefaction and maceration) that also allow an estimation of the minimum interval of immersion. These diagrams are based on observations on 395 bodies recovered from water. The requirements are the same as for the tables.

Reh stated in this paper that there is no difference between running and stagnant water in the chronological development of the parameters of putrefaction and maceration. The main point to consider is the water temperature at the time of recovery.

Table 7.35 Example to Estimate the Minimum Time Interval of Immersion*

	Month	Jan.	Feb.	March	April	May	June	July	Aug.	Sept.	Oct.	Nov.	Dec.
Ø	**Median water temperature (C) of the month according to measurements of Reh**	**3.5°**	**3.9°**	**5.8°**	**9.9°**	**13.0°**	**17.4°**	**18.6°**	**18.6°**	**17.3°**	**13.2°**	**8.8°**	**4.7°**
	Signs of putrefaction												
1.	Marbling	32	25	16 (23)	9–10	4–5	2	1–2	2	3	4–5	10	17
2.	Distension of tissues by gas	35	25	16 (23)	10	4–5	2–3	2	3	3–4	7	10	17
3.	Discolouration of the body	35	25	16 (23)	(14)	4–5	2	2	3	3–4	7	10	17
4.	Peeling of the epidermis	35	25	16 (23)	(16)	4–5	3	2	3	3–4	7	10	17
5.	Hair loss	35	25	16 (23)	10–12	4–5	2–3	2–3	3	3–4	7	10	17
6.	Hands: beginning of wrinkling	(1)	(1) 28–30	(12 h)			(6 h)			2 h		2 h	(1)
7.	Nails become loose	>35	(40) 30–32	23	16	5	2–3	3	3	3–4	11	17	28
8.	Peeling of skin in glove form	35	(45)	23	16	10	3	3	3–4	4	7	20	28
9.	Nail loss	>53	45	30 (40)	21	14	8	3	4	10	>11	20	>35
10.	Feet: beginning of wrinkling	(1)	(1)	(12 h)	(1)		(6 h)	½ h		2 h		2 h	(1)
11.	Nails become loose	>53	40	26 (35)	17	10	5	3	4	8	12	17	28
12.	Peeling of skin	>53	60	35	16	10	5	3	5–6	8–9	>11 (14)	20	28
13.	Nails lost	>53	>60	53	>35	>28	>10	3	>10	>10	>11	>20	>35
14.	Transudate in pleural cavities†	35	25 (40)	18 (35)	10	5	3–4	3	3	11	5	>20	
15.	Heart without blood	>39	32–34 (40)	23	14–15	9	4	3	3	5	11	20	28
16.	Brain liquefied	35	30 (40)	(23)	14–16	5	3–4	3	3	6	10	17	28

* Minimum time of duration of immersion in days; maximum time in days shown in parentheses. Shaded areas show minimum time of immersion 10 days, in reality 5 days.

† >500 mL in adults.

Table 7.36 Example to Estimate the Minimum Time Interval of Immersion*

	Month	Jan.	Feb.	March	April	May	June	July	Aug.	Sept.	Oct.	Nov.	Dec.
Ø	**Median water temperature (C) of the month according to measurements of Reh**	**3.5°**	**3.9°**	**5.8°**	**9.9°**	**13.0°**	**17.4°**	**18.6°**	**18.6°**	**17.3°**	**13.2°**	**8.8°**	**4.7°**
	Signs of putrefaction												
1.	Marbling	32	25	16 (23)	9–10	4–5	2	1–2	2	3	4–5	10	17
2.	Distension of tissues by gas	35	25	16 (23)	10	4–5	2–3	2	3	3–4	7	10	17
3.	Discolouration of the body	35	25	16 (23)	(14)	4–5	2	2	3	3–4	7	10	17
4.	Peeling of the epidermis	35	25	16 (23)	(16)	4–5	3	2	3	3–4	7	10	17
5.	Hair loss	35	25	16 (23)	10–12	4–5	2–3	2–3	3	3–4	7	10	17
6.	Hands: beginning of wrinkling	(1)	(1) 28–30	(12 h)			(6 h)			2 h		2 h	(1)
7.	Nails become loose	>35	(40) 30–32	23	16	5	2–3	3	3	3–4	11	17	28
8.	Peeling of skin in glove form	35	(45)	23	16	10	3	3	3–4	4	7	20	28
9.	Nail loss	>53	45	30 (40)	21	14	8	3	4	10	>11	20	>35
10.	Feet: beginning of wrinkling	(1)	(1)	(12 h)	(1)		(6 h)	½ h		2 h		2 h	(1)
11.	Nails become loose	>53	40	26 (35)	17	10	5	3	4	8	12	17	28
12.	Peeling of skin	>53	60	35	16	10	5	3	5–6	8–9	>11 (14)	20	28
13.	Nail loss	>53	>60	53	>35	>28	>10	3	>10	>10	>11	>20	>35
14.	Transudate in pleural cavities†	35	25 (40)	18 (35)	10	5	3–4	3	3	11	5	>20	
15.	Heart without blood	>39	32–34 (40)	23	14–15	9	4	3	3	5	11	20	28
16.	Brain liquefied	35	30 (40)	(23)	14–16	5	3–4	3	3	6	10	17	28

* Minimum time of duration of immersion in days; maximum time in days shown in parentheses. Shaded areas show 2–3 days.

† >500 mL in adults.

Table 7.37 Example to Estimate the Minimum Time Interval of Immersion*

	Month	Jan.	Feb.	March	April	May	June	July	Aug.	Sept.	Oct.	Nov.	Dec.
Ø	**Median water temperature (C) of the month according to measurements of Reh**	**3.5°**	**3.9°**	**5.8°**	**9.9°**	**13.0°**	**17.4°**	**18.6°**	**18.6°**	**17.3°**	**13.2°**	**8.8°**	**4.7°**
	Signs of putrefaction												
1.	Marbling	32	25	16 (23)	9–10	4–5	2	1–2	2	3	4–5	10	17
2.	Distension of tissues by gas	35	25	16 (23)	10	4–5	2–3	2	3	3–4	7	10	17
3.	Discolouration of the body	35	25	16 (23)	(14)	4–5	2	2	3	3–4	7	10	17
4.	Peeling of the epidermis	35	25	16 (23)	(16)	4–5	3	2	3	3–4	7	10	17
5.	Hair loss	35	25	16 (23)	10–12	4–5	2–3	2–3	3	3–4	7	10	17
6.	Hands: beginning of wrinkling	(1)	(1) 28–30	(12 h)			(6 h)			2 h		2 h	(1)
7.	Nails become loose	>35	(40) 30–32	23	16	5	2–3	3	3	3–4	11	17	28
8.	Peeling of skin in glove form	35	(45)	23	16	10	3	3	3–4	4	7	20	28
9.	Nail loss	>53	45	30 (40)	21	14	8	3	4	10	>11	20	>35
10.	Feet: beginning of wrinkling	(1)	(1)	(12 h)	(1)		(6 h)	½ h		2 h		2 h	(1)
11.	Nails become loose	>53	40	26 (35)	17	10	5	3	4	8	12	17	28
12.	Peeling of skin	>53	60	35	16	10	5	3	5–6	8–9	>11 (14)	20	28
13.	Nail loss	>53	>60	53	>35	>28	>10	3	>10	>10	>11	>20	>35
14.	Transudate in pleural cavities†	35	25 (40)	18 (35)	10	5	3–4	3	3	11	5	>20	
15.	Heart without blood	>39	32–34 (40)	23	14–15	9	4	3	3	5	11	20	28
16.	Brain liquefied	35	30 (40)	(23)	14–16	5	3–4	3	3	6	10	17	28

* Minimum time of duration of immersion in days; maximum time in days shown in parentheses. Shaded areas show >20 days, in reality 25 days.

† >500 mL in adults.

Table 7.38 Example to Estimate the Minimum Time Interval of Immersion*

	Month	Jan.	Feb.	March	April	May	June	July	Aug.	Sept.	Oct.	Nov.	Dec.
Ø	**Median water temperature (C) of the month according to measurements of Reh**	**3.5°**	**3.9°**	**5.8°**	**9.9°**	**13.0°**	**17.4°**	**18.6°**	**18.6°**	**17.3°**	**13.2°**	**8.8°**	**4.7°**
	Signs of putrefaction												
1.	Marbling	32	25	16 (23)	9–10	4–5	2	1–2	2	3	4–5	10	17
2.	Distension of tissues by gas	35	25	16 (23)	10	4–5	2–3	2	3	3–4	7	10	17
3.	Discolouration of the body	35	25	16 (23)	(14)	4–5	2	2	3	3–4	7	10	17
4.	Peeling of the epidermis	35	25	16 (23)	(16)	4–5	3	2	3	3–4	7	10	17
5.	Hair loss	35	25	16 (23)	10–12	4–5	2–3	2–3	3	3–4	7	10	17
6.	Hands: beginning of wrinkling	(1)	(1) 28–30	(12 h)			(6 h)			2 h		2 h	(1)
7.	Nails become loose	>35	(40) 30–32	23	16	5	2–3	3	3	3–4	11	17	28
8.	Peeling of skin in glove form	35	(45)	23	16	10	3	3	3–4	4	7	20	28
9.	Nail loss	>53	45	30 (40)	21	14	8	3	4	10	>11	20	>35
10.	Feet: beginning of wrinkling	(1)	(1)	(12 h)	(1)		(6 h)	½ h		2 h		2 h	(1)
11.	Nails become loose	>53	40	26 (35)	17	10	5	3	4	8	12	17	28
12.	Peeling of skin	>53	60	35	16	10	5	3	5–6	8–9	>11 (14)	20	28
13.	Nail loss	>53	>60	53	>35	>28	>10	3	>10	>10	>11	>20	>35
14.	Transudate in pleural cavities†	35	25 (40)	18 (35)	10	5	3–4	3	3	11	5	>20	
15.	Heart without blood	>39	32–34 (40)	23	14–15	9	4	3	3	5	11	20	28
16.	Brain liquefied	35	30 (40)	(23)	14–16	5	3–4	3	3	6	10	17	28

* Minimum time of duration of immersion in days; maximum time in days shown in parentheses. Shaded areas show >2 to 3 days, in reality 3–4 days, June, water temperature 21°C.

† >500 mL in adults.

Table 7.39 Example to Estimate the Minimum Time Interval of Immersion*

	Month	Jan.	Feb.	March	April	May	June	July	Aug.	Sept.	Oct.	Nov.	Dec.
Ø	**Median water temperature (C) of the month according to measurements of Reh**	**3.5°**	**3.9°**	**5.8°**	**9.9°**	**13.0°**	**17.4°**	**18.6°**	**18.6°**	**17.3°**	**13.2°**	**8.8°**	**4.7°**
	Signs of putrefaction												
1.	Marbling	32	25	16 (23)	9–10	4–5	2	1–2	2	3	4–5	10	17
2.	Distension of tissues by gas	35	25	16 (23)	10	4–5	2–3	2	3	3–4	7	10	17
3.	Discolouration of the body	35	25	16 (23)	(14)	4–5	2	2	3	3–4	7	10	17
4.	Peeling of the epidermis	35	25	16 (23)	(16)	4–5	3	2	3	3–4	7	10	17
5.	Hair loss	35	25	16 (23)	10–12	4–5	2–3	2–3	3	3–4	7	10	17
6.	Hands: beginning of wrinkling	(1)	(1) 28–30	(12 h)			(6 h)			2 h		2 h	(1)
7.	Nails become loose	>35	(40) 30–32	23	16	5	2–3	3	3	3–4	11	17	28
8.	Peeling of skin in glove form	35	(45)	23	16	10	3	3	3–4	4	7	20	28
9.	Nail loss	>53	45	30 (40)	21	14	8	3	4	10	>11	20	>35
10.	Feet: beginning of wrinkling	(1)	(1)	(12 h)	(1)		(6 h)	½ h		2 h		2 h	(1)
11.	Nails become loose	>53	40	26 (35)	17	10	5	3	4	8	12	17	28
12.	Peeling of skin	>53	60	35	16	10	5	3	5–6	8–9	>11 (14)	20	28
13.	Nail loss	>53	>60	53	>35	>28	>10	3	>10	>10	>11	>20	>35
14.	Transudate in pleural cavities†	35	25 (40)	18 (35)	10	5	3–4	3	3	11	5	>20	
15.	Heart without blood	>39	32–34 (40)	23	14–15	9	4	3	3	5	11	20	28
16.	Brain liquefied	35	30 (40)	(23)	14–16	5	3–4	3	3	6	10	17	28

* Minimum time of duration of immersion in days; maximum time in days shown in parentheses. Shaded areas show >3 days and <8 days.

† >500 mL in adults.

Table 7.40 Example to Estimate the Minimum Time Interval of Immersion*

	Month	Jan.	Feb.	March	April	May	June	July	Aug.	Sept.	Oct.	Nov.	Dec.
Ø	Median water temperature (C) of the month according to measurements of Reh	3.5°	3.9°	5.8°	9.9°	13.0°	17.4°	18.6°	18.6°	17.3°	13.2°	8.8°	4.7°
				Signs of putrefaction									
1.	Marbling	32	25	16 (23)	9–10	4–5	2	1–2	2	3	4–5	10	17
2.	Distension of tissues by gas	35	25	16 (23)	10	4–5	2–3	2	3	3–4	7	10	17
3.	Discolouration of the body	35	25	16 (23)	(14)	4–5	2	2	3	3–4	7	10	17
4.	Peeling of the epidermis	35	25	16 (23)	(16)	4–5	3	2	3	3–4	7	10	17
5.	Hair loss	35	25	16 (23)	10–12	4–5	2–3	2–3	3	3–4	7	10	17
6.	Hands: beginning of wrinkling	(1)	(1) 28–30	(12 h)			(6 h)			2 h		2 h	(1)
7.	Nails become loose—*not yet*	>35	(40) 30–32	23	16	5	2–3	3	3	3–4	11	17	28
8.	Peeling of skin in glove form	35	(45)	23	16	10	3	3	3–4	4	7	20	28
9.	Nail loss	>53	45	30 (40)	21	14	8	3	4	10	>11	20	>35
10.	Feet: beginning of wrinkling	(1)	(1)	(12 h)	(1)		(6 h)	½ h		2 h		2 h	(1)
11.	Nails become loose—*not yet*	>53	40	26 (35)	17	10	5	3	4	8	12	17	28
12.	Peeling of skin	>53	60	35	16	10	5	3	5–6	8–9	>11 (14)	20	28
13.	Nails lost	>53	>60	53	>35	>28	>10	3	>10	>10	>11	>20	>35
14.	Transudate in pleural cavities†	35	25 (40)	18 (35)	10	5	3–4	3	3	11	5	>20	
15.	Heart without blood	>39	32–34 (40)	23	14–15	9	4	3	3	5	11	20	28
16.	Brain liquefied	35	30 (40)	(23)	14–16	5	3–4	3	3	6	10	17	28

* Minimum time of duration of immersion in days; maximum time in days shown in parentheses. Shaded areas show >4 days <10 days, in reality 5 days.

† >500 mL in adults.

7.4.3 Evaluation of the Data of Reh

The aim of a 2010 evaluation study was to evaluate the validity and reliability of Reh's table for the estimation of the time of immersion that was developed in the 1960s [2,3]. For this purpose, we evaluated retrospectively the autopsy protocols of 73 bodies from the years 1993–2007 mainly recovered from the River Rhine or other running waters and some lakes. In all cases, the time interval since the persons had been missing had exactly been known. In all cases, relatives had noticed the disappearance in a timely manner (e.g. the children had disappeared, or older people had disappeared from a residential facility for older adults). From police records and further investigations by the police, it was assumed that the time since the persons had been missing and the time of immersion had been more or less identical. The collected data included gender, age, last time seen alive, length of time missing, time of recovery, state of decomposition and signs of immersion, place of recovery, depth of water, water temperature, cause of death, toxicological findings and blood alcohol concentration. In all cases, comparable to Reh's original method, the examination had taken place a few days after recovery, and the bodies had been kept at low environmental temperatures.

The signs of putrefaction were marked in Reh's table to determine the minimum time of immersion by using the average water temperatures of the month (according to Reh's table) in which the body was recovered without regard to the real water temperatures.

Finally, the estimated minimal time interval of immersion was compared with the real missing time. In those cases in which the estimated time of immersion exceeded the missing time, the average monthly water temperatures in Reh's table were compared with the real water temperatures from official sources (agency of water management) and with the real water temperatures on the day of recovery and the average water temperature during the missing time [11,12]. The official water temperatures of every day are determined by different water temperatures measured on several times during the course of the day.

Furthermore, in 33 cases from 1999 to 2005, the time of immersion was estimated with the aid of Reh's table by using the real water temperatures from the day of recovery and, for comparison, by using the average water temperature during the missing time. The basis of the analysis was the nearest average water temperatures in Reh's table without taking into account the actual month.

Finally, we compared the actual water temperatures of the River Rhine (from 1999 to 2007) with the average monthly water temperatures of that river from 1961 to 1964.

7.4.4 Results

Most of the bodies were found in the River Rhine, and others were found in smaller rivers, ponds or (swimming) pools. Bodies were found all through the year but at high percentages during the months of January, June and July (Figure 7.64). Although it is within the bounds of possibility that the time of immersion could be shorter than the missing time, the opposite is quite impossible. In 49 cases, the chart gave quite reliable results, with the estimated time of immersion and the missing time in accord. In 12 cases, the time of immersion was underestimated compared with the time the person had been missing.

The greatest differences were found in these cases:

- Missing time 70 days, minimum time interval of immersion (according to Reh's table) 6 days.
- Missing time 97 days, minimum time of immersion 35 days.
- Missing time 54 days, minimum time of immersion 10 days.

However, in 12 cases, according to Reh's table the time of immersion exceeded the time the persons had been missing by more than 3 days when the estimation of the time of immersion was based on the average monthly temperature without taking into account the real water temperatures (Figure 7.67 and Table 7.41). Eight of these 12 bodies were found in the River Rhine, four in smaller tributaries. The greatest difference was 29 days (see Table 7.41):

- Water temperature from Reh's table: 5.8°C in March.
- Real average water temperature at the missing time: 7.1°C.
- Real water temperature on the day of recovery: 6.6°C.

Important differences were also found in case 7 (Table 7.42). The difference was 25 days. The real water temperature during the missing time had been higher than the average monthly water temperature in Reh's table:

- Water temperature from Reh's table: 3.9°C in February.
- Real average water temperature at the missing time: 7.9°C.
- Real water temperature on the day of recovery: 8.8°C.

In cases 4 and 10 (see Table 7.41), the times of immersion were overestimated for 11 and 10 days, respectively. In both cases, the average monthly water temperatures in Reh's chart were higher than the real water temperatures on the days of recovery and the average water temperature during the missing times.

In cases 2 and 6 (see Table 7.41), no real water temperatures were available.

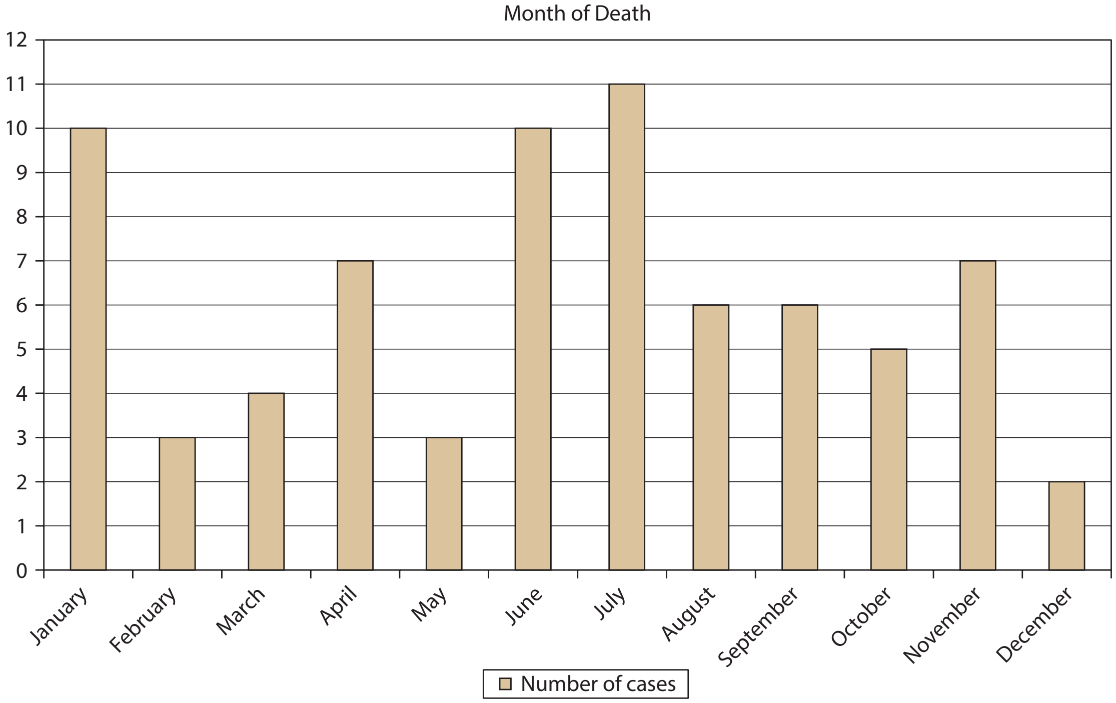

Figure 7.64 Monthly distribution of the 73 bodies recovered from water.

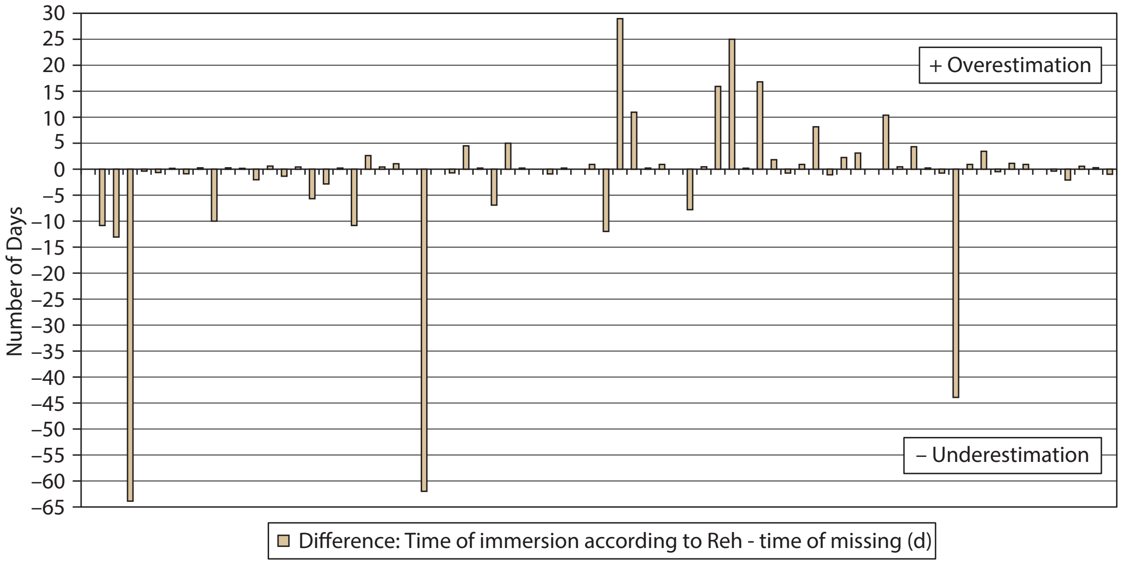

Figure 7.65 Difference between times of immersion according to Reh and the real missing times in 73 cases.

Table 7.41 Time of Immersion Was Longer than the Missing Time in 12 Cases

Case	River	Missing time (days)	Duration of immersion according to Reh (days)	Difference Reh—missing time (days)	Real water temperature on the day of recovery (°C)	Average monthly water temperature in Reh's table (°C)	Average water temperature during the missing time (°C)
1	Rhine	3.56	8.0	4.44	23.3	17.3	23.1
2	Sieg	15.02	20.0	4.98	—	8.8	—
3	Rhine	24.00	53.0	29.0	6.6	5.8	7.1
4	Rhine	2.95	14.0	11.05	9.7	9.9	9.2
5	Rhine	37.13	53.0	15.87	8.0	3.9	4.4
6	Sieg	6.17	23.0	16.83	—	5.8	—
7	Rhine	15.01	40.0	24.99	8.8	3.9	7.9
8	Rhine	1.79	10.0	8.21	24.1	18.6	24.1
9	Mosel	6.82	10.0	3.18	14.5	13.2	15.9
10	Rhine	12.74	23.0	10.25	3.5	5.8	4.3
11	Rhine	35.73	40.0	4.27	13.7	9.9	9.3
12	Mosel	2.72	6.0	3.28	22.3	17.3	22.1

In 33 further cases, the actual water temperatures, instead of the average monthly water temperatures, were taken into account for the estimation of the times of immersion; again, in 14 cases, the times of immersion according to Reh's table exceeded the time the persons had been missing (see Table 7.42). The maximum time difference was 32 days (missing time 3 days—time of immersion based on the actual water temperature on the day of recovery and also on the average water temperature of 35 days).

Interestingly, in most of these cases, no difference between times of immersion based on the actual water temperature on the day of recovery compared with the average monthly water temperature was found. The reason is that in these cases the actual and the average water temperatures had been nearly identical.

In one case (case 8), the water temperature on the day of recovery was remarkably higher than the average monthly water temperatures in Reh's table:

- The maximum average monthly water temperature from Reh's table is 18.6°C (for July and August).
- Real water temperature on the day of recovery: 25.9°C.
- Real average water temperature during the missing time: 25.13°C.

Table 7.42 Estimated Time of Immersion in 33 Cases on the Basis of the Water Temperatures of the Day of Recovery and the Average Water Temperature during the Known Missing Time

Case	Missing time (days)	Water temperature of the day of recovery (°C)	Duration of immersion according to Reh (days)	Average water temperature (°C)	Duration of immersion according to Reh (days)	Difference Reh—missing time for water temperature day of recovery	Difference Reh—missing time for average water temperature
1	12.7	3.7	30.0	4.38	28.0	17.3	22.3
2	0.05	12.65	0.5	12.65	0.5	0.45	0.45
3	35.73	13.7	11.0	11.2	21.0	−20.73	−24.73
4	0.92	22.12	0.03	20.88	0.03	−0.89	−0.89
5	54.0	22.9	3.0	17.62	10.0	−44.0	−44.0
6	1.06	8.55	0.08	8.67	0.08	−0.98	−0.98
7	3.0	19.7	6.0	19.46	6.0	3.0	3.0
8	1.79	25.9	—	25.13	—	—	—
9	15.01	5.1	30.0	5.45	30.0	14.99	14.99
10	37.12	8.0	20.0	5.9	53.0	−17.12	15.88
11	0.65	7.9	0.08	7.9	0.08	−0.57	−0.57
12	7.05	14.0	9.0	13.87	9.0	1.95	1.95
13	2.94	9.7	35.0	9.18	35.0	32.06	32.06
14	24.0	6.6	53.0	7.1	53.0	29.0	29.0
15	0.05	15.9	0.08	15.9	0.08	0.03	0.03
16	0.89	8.3	0.08	8.35	0.08	−0.81	−0.81
17	4.0	19.9	4.0	19.96	4.0	0	0
18	0.08	20.7	0.02	20.7	0.02	−0.06	−0.06
19	1.08	7.1	0.08	7.15	0.08	−1.0	−1.0
20	19.0	13.8	20.0	13.55	20.0	1.0	1.0
21	3.6	22.5	4.0	22.7	4.0	0.4	0.4
22	0.62	16.8	0.08	17.05	0.08	−0.54	−0.54
23	0.9	22.1	0.02	22.35	0.02	−0.88	−0.88
24	3.0	21.1	4.0	20.8	4.0	1.0	1.0
25	9.0	16.8	0.25	16.7	0.25	−8.75	−8.75
26	0.5	10.9	2.0	11.0	2.0	1.5	1.5
27	1.0	8.8	0.08	8.65	0.08	−0.92	−0.92
28	5.0	19.0	4.0	19.3	4.0	−1.0	−1.0
29	3.1	22.8	4.0	21.8	4.0	0.9	0.9
30	2.7	22.3	4.0	21.3	4.0	1.3	1.3
31	6.8	16.2	6.0	16.1	6.0	−0.8	−0.8
32	72.1	7.6	53.0	7.2	53.0	−19.1	−19.1
33	0.1	24.0	0.25	24.0	0.25	0.15	0.15

7.4.5 Discussion

In cases with a long PMI, the minimum time interval of immersion can be underestimated, especially if signs of putrefaction attributed to a defined water temperature are found fully developed. In these cases, it has to be kept in mind that Reh's chart allows estimation only of the minimum time interval of immersion.

By using the chart correctly (on the basis of the real water temperatures), the missing time can also be overestimated. In 14 cases (out of 33 cases; see Table 7.42), the determined times of immersion exceeded the real missing times. The water temperatures (on the day of recovery and the average water temperatures of the missing time) have been related to the nearest average monthly water temperature from Reh's chart. This point may be problematic because nearly identical water temperatures can be found in the chart (e.g. in July or August with 18.6°C or June and September with 17.3°C and 17.4°C), but they are related to different maximum and minimum time intervals of immersion. It is supposed that Reh respected the water temperatures of the preceding months (with lower or higher water temperatures). This is of significance only when a body is immersed for longer than 1 month. In cases 4 and 10, the estimated minimum time of immersion exceeded the known missing time, although the water temperature in Reh's table was higher than the real water temperature. If the estimation is based on a higher water temperature (Reh's table) even though the water temperatures had been lower, the time of immersion will be underestimated because in relation to the higher temperatures, not all signs of putrefaction have developed.

Reh proved for the first time a statistical correlation between putrefactive changes and water temperature. Based on this correlation, he developed a chart to estimate the minimum time of immersion. The estimations were based on the water temperatures at the day of recovery. However, using the water temperature of the day of recovery can reveal totally inaccurate conclusions because the water temperatures during the whole time of immersion can be higher or lower. Especially when the immersion time is comparatively long, fluctuation of water temperatures can be observed, and the water temperature on the day of recovery may not be representative of the water temperature during the whole time of immersion. This becomes evident from Figure 7.66, in which original water temperatures over 20 days at the turn of the years 2002–2003 are shown. The water temperature on the day of recovery (2.9°C) is about 4°C lower than the average temperature (6.8°C). By using the water temperature on the day of recovery, the *estimated* time of immersion would be much longer than the *real* time of immersion. The water temperature on the day of recovery is the average water temperature on the day the body was found, as measured by an official water company.

In contrast, in two cases (cases 4 and 10; see Table 7.46) we found an overestimation of the time of immersion, although the average monthly water temperature in Reh's chart was higher than the water temperature on the day of recovery and the average water temperature during the time the individual was missing.

Another problem is the recommendation to use average monthly temperatures for the estimation of duration of the immersion. If, for example, the water temperature on the day of recovery is 13.1°C, nearly the same temperature can be found in May (13°C) and October (13.2°C) in Reh's table. Although there is only a slight difference of the average temperature, the estimated times of immersion differ widely. Our analyses revealed that in some cases the actual water temperatures have been more than 7°C higher than the average monthly temperatures reported by Reh. The rise of the water temperatures of the River Rhine is also illustrated in Figures 7.67 and 7.4.7. Today, the average monthly water temperatures of the River Rhine measured near Bonn are approximately 2°C higher than in the 1970s and 3°C to 4°C higher than the average monthly water temperatures in Reh's table. Climate changes, as well as direct anthropogenic influences (industrial waters, power stations), may have contributed to an increase of the water temperature in the River Rhine. There are also considerable annual fluctuations in the

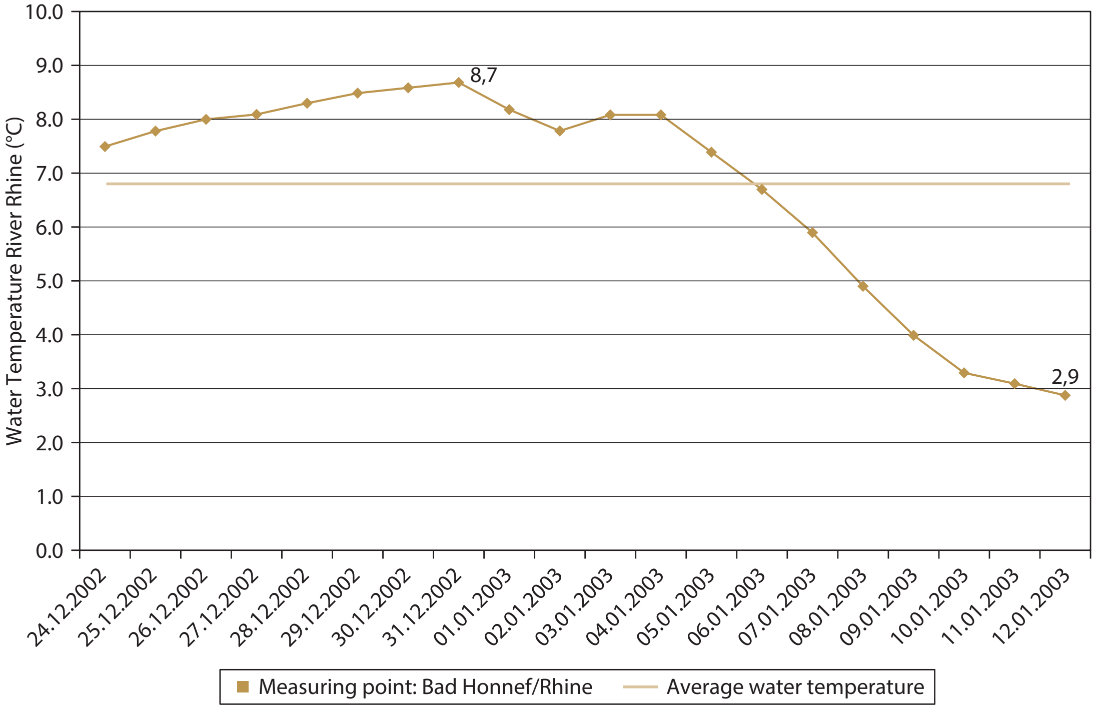

Figure 7.66 Example of the fluctuations of water temperatures during a period of 20 days (original water temperatures of the River Rhine from 24 December 2002 to 12 January 2003).

(From Doberentz E, Madea B. Estimating the time of immersion of bodies found in water: an evaluation of a common method to estimate the minimum time interval of immersion. *Rev Esp Med Leg* 2010;**36**(2):51–61.)

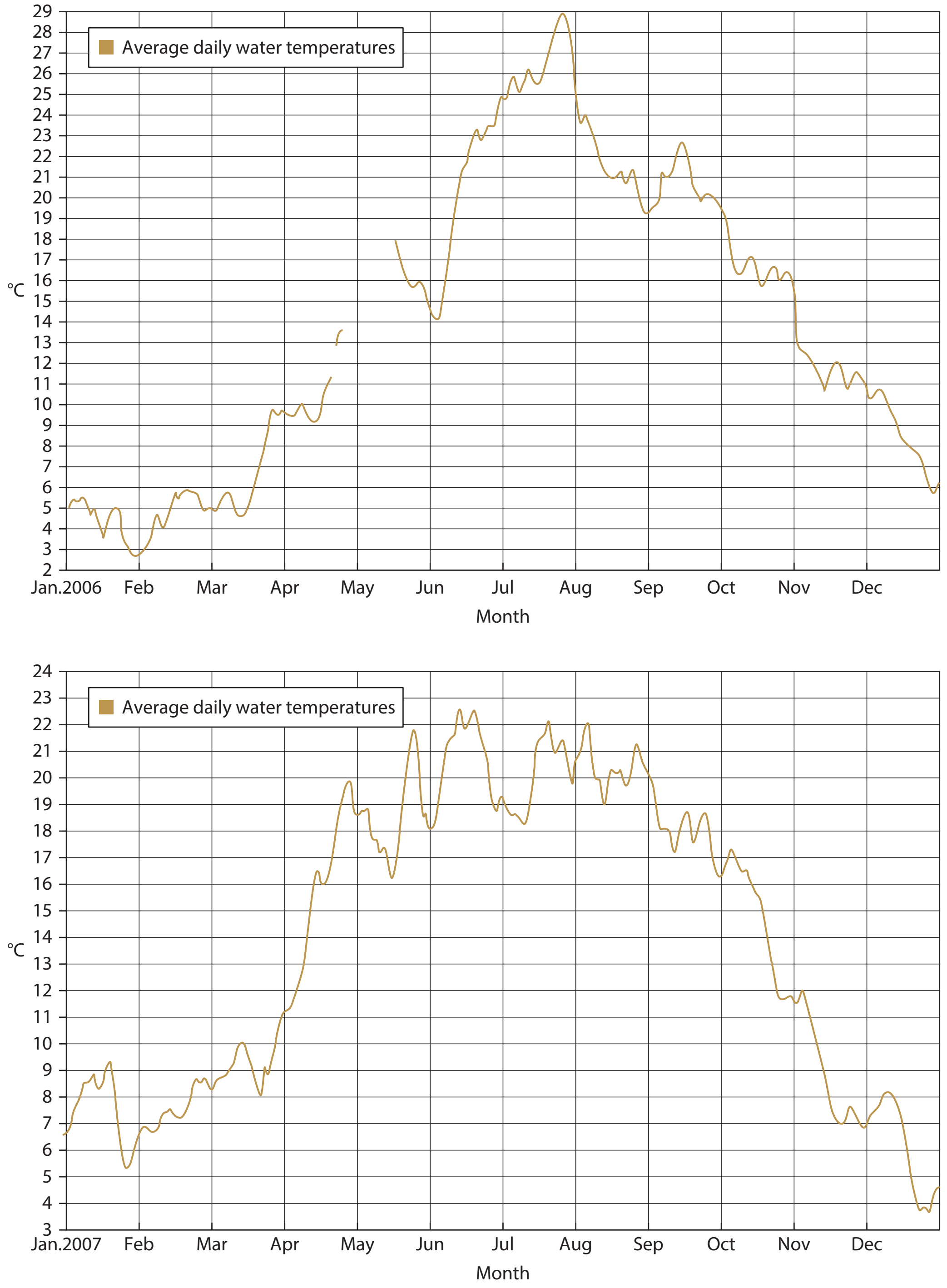

Figure 7.67 Water temperatures (°C) of the River Rhine measured near Bonn in 2006 and 2007.

(From Landesumweltamt NRW. *Jahresbericht 2007, Jahresbericht 2007, Klimawandel*. www.lanuv.nrw.de/veroeffentlichungen/jahresberichte/jabe2007/jabe2007S17S24.pdf, Jahresbericht 2007, Klimawandel, www.lanuv.nrw.de, 23.11.2008.)

average monthly water temperatures (Figure 7.69). The normal water level of the Rhine ranges between 200 and 550 cm [28], relating to the measuring stations along the Rhine.

Furthermore, we compared the average monthly water temperatures according to Reh's table with the actual water temperatures of the River Rhine for 1999–2007. The analysis is confined to this time period because digital and online data have been available only since 1999. Today's average monthly water temperatures of the River Rhine range about 4°C higher than in the 1960s (Table 7.43; see Figure 7.68).

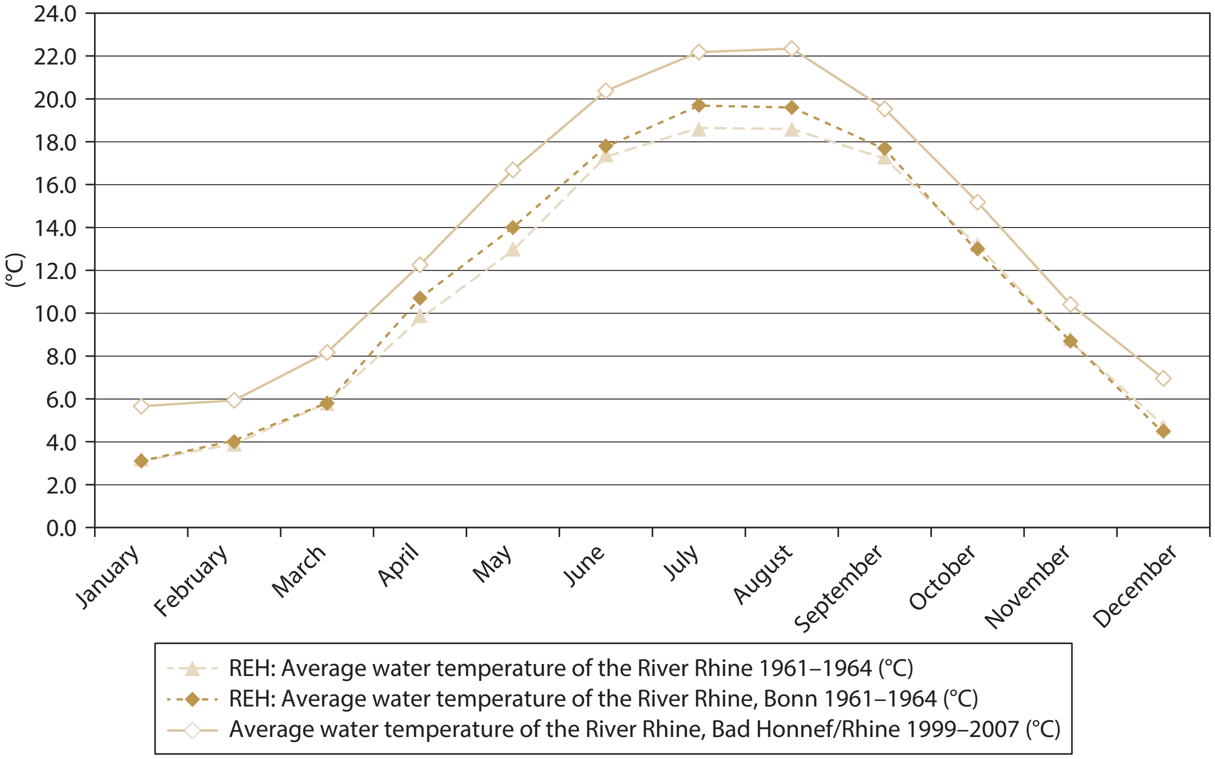

Figure 7.68 Average monthly water temperatures of the River Rhine from 1961 to 1964 and from 1999 to 2007.

(From Doberentz E, Madea B. Estimating the time of immersion of bodies found in water: an evaluation of a common method to estimate the minimum time interval of immersion. *Rev Esp Med Leg* 2010;**36**(2):51–61.)

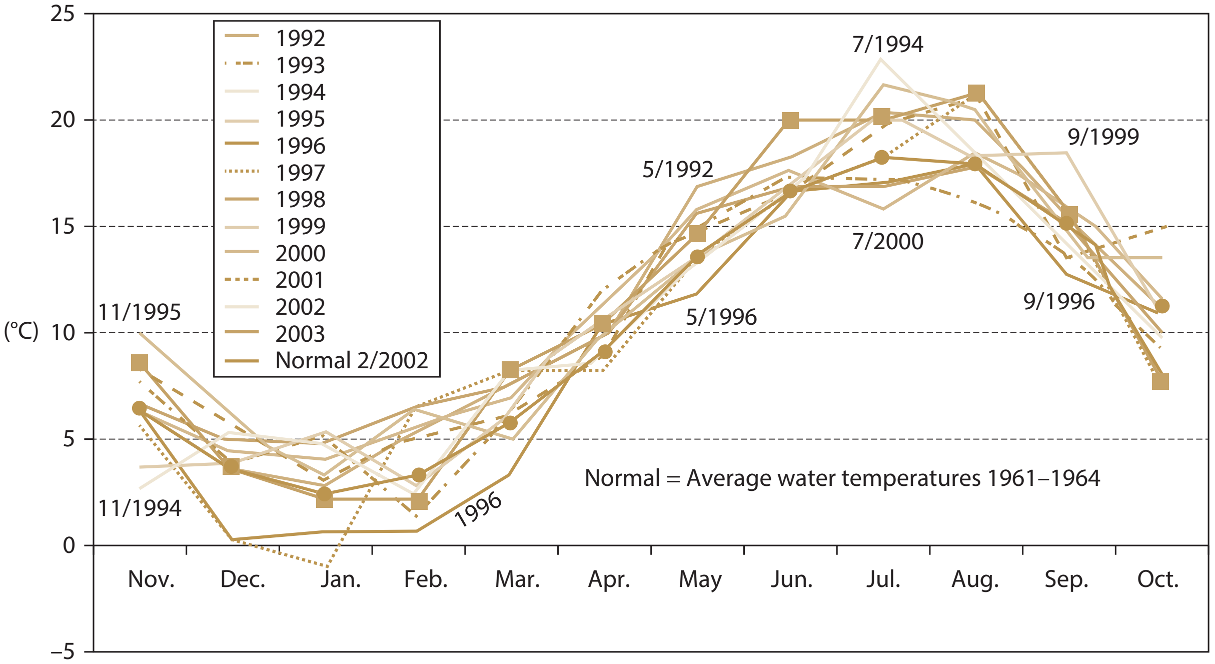

Figure 7.69 Average monthly water temperatures of the years 1992–2003 of the River Rhine, weather station Düsseldorf.

(From Landesumweltamt NRW. *Jahresbericht 2003: Das hydrologische Jahr und das außergewöhnliche Niedrigwasser des Rheins im Sommer*. www.lanuv.nrw.de/veroeffentlichungen/jahresberichte/2003/jabe03_s47.pdf2003, www.lanuv.nrw.de, 23.11.2008.)

Table 7.43 Average Monthly Water Temperatures of the Rhine from 1961 to 1964 and from 1999 to 2007

Month	Jan.	Feb.	March	April	May	June	July	Aug.	Sept.	Oct.	Nov.	Dec.
Average water temperature of the River Rhine, Bonn 1961–1964 (°C)	3.1	4.0	5.8	10.7	14.0	17.8	19.7	19.6	17.7	13.0	8.7	4.5
Reh: average water temperature of the River Rhine 1961–1964 (°C)	3.5	3.9	5.8	9.9	13.0	17.4	18.6	18.6	17.3	13.2	8.8	4.7
Average water temperature of the River Rhine, Bad Honnef/Rhine, 1999–2007 (°C)	5.7	5.9	8.2	12.3	16.7	20.4	22.2	22.3	19.5	15.2	10.4	7.0

Since 1978, the water temperature of the River Rhine increased by about 1.2°C [11,12]. Although this increase seems to be minor, there are considerable monthly and yearly climate changes with an influence on water temperatures (see Figures 7.67 and 7.69). Even fluctuations of about 8.0°C per year can be found.

7.4.6 Conclusions

The development of Reh's chart for the estimation of the minimum time of immersion of a body represented real progress because definite putrefactive changes and water temperature were taken into account [2,3,13,15]. Therefore, Reh's chart replaced the old and unreliable rules of thumb for the estimation of the duration of immersion. However, overall water temperatures have increased since the 1960s. For higher water temperatures (>20°C), Reh's table is unreliable and further investigations are necessary, especially for higher water temperatures regarding the correlation between temperatures and progression of putrefaction. For lower water temperatures, the given chart can be used even today. However, the actual measured water temperature on the day of recovery should be used for estimating the time of immersion; such data are available at agencies of water management. If a longer time of immersion is assumed or if considerable variations of water temperatures have to be taken into account, the average temperature during the missing time should be used.

Because of monthly fluctuations of the water temperature, it is not advisable to estimate the time of immersion based on data of the month of recovery without regard to the daily water temperatures.

7.4.7 Recommended Procedure

When finding a body immersed in water, it is necessary to measure the water temperature immediately on the same day. The water temperature depends on the type of water. For larger rivers, water temperatures on each day are available from the associated agencies of water management.

With the water temperature on the day of recovery and the signs of decomposition and putrefaction, an estimation of the time of immersion can be made by using Reh's chart. The water temperature on the day of recovery must be allocated to the closest average monthly water temperature from Reh's chart. If a longer time of immersion is suspected (e.g. advanced signs of putrefaction during the cold winter months), it could be useful to check the water temperatures during the last few weeks, because there can be significant variations in water temperatures. An alternative time of immersion can therefore be estimated.

Meanwhile in Germany, the institutes of forensic medicine located at the Rhine (Mainz, Bonn, Cologne, Düsseldorf, Duisburg) collaboratively study the decomposition of bodies recovered from the Rhine, taking into account the raised water temperatures.

Furthermore, a collaborative study predicting the postmortem submersion interval for human remains recovered from waterways or the sea [6,14] has started.

References and further reading

1. Brinkmann B, Madea B. Handbuch Gerichtliche Medizin, vol. 1. Berlin, Springer, 2004.
2. Doberentz E, Madea B. Estimating the time of immersion of bodies found in water: an evaluation of a common method to estimate the minimum time interval of immersion. *Rev Esp Med Leg* 2010;*36*(2):51–61.
3. Doberentz E, Madea B. Schätzung der Wasserliegezeit. Retrospektive Untersuchung zur Reliabilität. *Rechtsmedizin* 2010;*20*:293–9.
4. Dotzauer G, Tamaska L. Hautveränderungen an Leichen. In: Marchionini (ed.). *Handbuch der Haut-und Geschlechtskrankheiten* (Ergänzungswerk, vol. 1, T1). Berlin, Heidelberg, Springer, 1968.
5. Gee DJ. Drowning. In: Polson CJ, Gee DJ, Knight B (ed.). *The Essentials of Forensic Medicine*. 4th ed. Oxford, Pergamon Press, 1985, pp 421–48.
6. Heaton V, Lagden A, Moffatt C, Simmons T. Predicting the postmortem submersion interval for human remains recovered from U.K. waterways. *J Forensic Sci* 2010;*55*(2):302–7.
7. Henssge C, Madea B. Estimation of the time since death. *Forensic Sci Int* 2007;*165*:182–4.
8. Henssge C, Brinkmann B, Püschel K. Todeszeitbestimmung durch Messung der Rektaltemperatur bei Wassersuspension der Leiche. *Z Rechtsmed* 1984;*92*:255–76.
9. Knight B. Forensic Pathology. 2nd ed. London, Edward Arnold, 1996.
10. Knight B. Legal Aspects of Medical Practice. 3rd ed. London, Churchill Livingstone, 1982.
11. Landesumweltamt NRW. *Jahresbericht 2003: Das hydrologische Jahr und das außergewöhnliche Niedrigwasser des Rheins im*

Sommer, 2003. www.lanuv.nrw.de/veroeffentlichungen/jahresberichte/2003/jabe03_s47.pdf, www.lanuv.nrw.de, 23.11.2008.
12. Landesumweltamt NRW. *Jahresbericht 2007, Jahresbericht 2007, Klimawandel*, Jahresbericht, 2007, Klimawandel. www.lanuv.nrw.de/veroeffentlichungen/jahresberichte/jabe2007/jabe2007S17S24.pdf, www.lanuv.nrw.de, 23.11.2008.
13. Madea B. Estimation of duration of immersion. *Nord Rettsmed* 2002;*8*:4–10.
14. Madea B, Doberentz E. Commentary on Heaton V, Lagden A, Moffatt C, Simmons T. Predicting the postmortem submersion interval for human remains recovered from U.K. waterways. *J Forensic Sci* 2010;*55*(2):302–7; *J Forensic Sci* 2010;*55*(6):1666–7.
15. Madea B, Stockhausen S, Doberentz E. Estimation of the immersion time in drowned corpses—a further study on the reliability of the table of Reh. *Archiv für Kriminologie* 2016;*237*:1–12.
16. Madea B. *Praxis Rechtsmedizin: Befunderhebung, Rekonstruktion und Begutachtung*. 3rd ed. Berlin, Heidelberg, and New York, Springer, 2015.
17. Madea B. *Handbook of Forensic Medicine*. Chichester, John Wiley & Sons, 2014.
18. Mant AK. Taylor's Principles and Practice of Medical Jurisprudence. London, Churchill Livingstone, 1984.
19. Mueller B. Gerichtliche Medizin. 2nd ed., vol. 1. Berlin, Springer, 1975.
20. Polson CJ, Gee D, Knight B. Essentials of Forensic Medicine. 4th ed. Oxford, Pergamon Press, 1985.
21. Prokop O, Göhler W. *Forensische Medizin*. 3rd ed. Stuttgart, Germany, Gustav Fischer, 1976.
22. Püschel K, Schneider A. Die Waschhautentwicklung in Süss- und Salzwasser bei unterschiedlichen Temperaturen. *Z Rechtsmed* 1985;*95*:1–18.
23. Reh H. Anhaltspunkte für die Bestimmung der Wasserzeit. *Dtsch Z Gerichtl Med* 1967;*59*:235–45.
24. Reh H. *Diagnostik des Ertrinkungstodes und Bestimmung der Wasserzeit*. Düsseldorf, Germany, Triltsch, 1969.
25. Reh H. Über den frühpostmortalen Verlauf der Waschhaut an den Fingern. *Z Rechtsmed* 1984;*92*:183–8.
26. Reh H, Haarhoff K, Vogt CD. Die Schätzung der Todeszeit bei Wasserleichen. *Z Rechtsmed* 1977;*79*:261–6.
27. Spitz WU. Medicolegal Investigation of Death. 3rd ed. Springfield, IL, Charles C Thomas, 1993.
28. Waterlevel Rhein. www.wetteronline.de/pegel.htm, 07.412.2009.
29. Weber W. Zur Waschhautbildung der Fingerbeeren. *Z Rechtsmed* 1978;*81*:63–6.
30. Weber W. Flüssigkeitspenetration durch Leistenhaut. *Z Rechtsmed* 1982;*88*:185–93.
31. Weber W, Laufkötter R. Stadien postmortaler Waschhautbildung—Ergebnisse systematischer qualitativer und quantitativer experimenteller Untersuchungen. *Z Rechtsmed* 1984;*92*:277–90.

7.5 H^3-Magnetic Resonance Spectroscopy

■ *Frank Musshoff and Burkhard Madea*

As described before for the estimation of the early post-mortem interval (PMI) of 1–1.5 days, various methods are well established. For the later PMI, the accuracy of procedures is clearly lower [10,13]. Under these circumstances, the common indicators for the estimation (i.e. rigor mortis, livor mortis or the body's core temperature) will have reached steady state in most cases. Especially when putrefactive changes are apparent, only a rough estimation of the PMI is possible based on subjective experience of the forensic pathologist, but this is not a scientifically sound method.

In the twentieth century, various chemical tests were developed for an estimation of PMIs in the late post-mortem phase by identifying und quantifying by-products of the decomposition of the body, including substances in the soil underneath the decomposing corpse [21]. Some studies concentrated on specific groups of metabolites (e.g. fats or proteins [3,17]).

Early in the 1970s, extensive experimental work was carried out on protein degradation during putrefaction in various organs by Bonte [1,4]. It was speculated that the initially lagging proteolytic changes were caused by catalysis of autoenzymes, whereas bacteriological processes were thought to be responsible for a distinct acceleration from the twentieth day after death. At this time period, some amino acid concentrations showed a marked increase, which was followed by maximal bacterial growth that ultimately led to a sudden regression of special amino acids. Amines simultaneously appeared.

These findings were pursued by Daldrup [8], who took into account that interindividual differences in brain tissue composition are very small and that the skull represents a natural barrier against external factors. Daldrup proposed a method for the estimation of PMIs on the basis of amino acid concentrations in the brain that was based on empirical findings [5–7]. In an experiment, a corpse had been kept at room temperature (16°C to 23°C) for more than 48 days; at regular intervals, brain samples were taken, and the content of free amino acids and related compounds were analysed. It could be demonstrated that in a period from 4 to 20 days post-mortem, the PMI could be calculated from the concentrations of α-aminobutyrate (ABU), γ-aminobutyrate (GABA) and glutamic acid (GLU) in the brain according to the following formula:

$$T \sim \ln\left(\frac{ABU + GABA}{GLU} + 1\right)$$

where T is the post-mortem time lapse (days) and ABU, GABA and GLU are the concentrations in micromoles per gram (µmol/g) wet tissue of the corresponding amino acids. In a period from 4 to 20 days post-mortem, nearly a linear correlation was found (Figure 7.70).

The procedure is based on GLU reactions, specifically proteolysis and α-decarboxylation as well as γ-decarboxylation (Figure 7.71). In the range of about 17.5°C to 25°C, which guarantees bacterial growth and metabolism, the method was described as independent of ambient temperature. It was demonstrated that in addition to the temperature, a pH between 6 and 7.2 is essential for

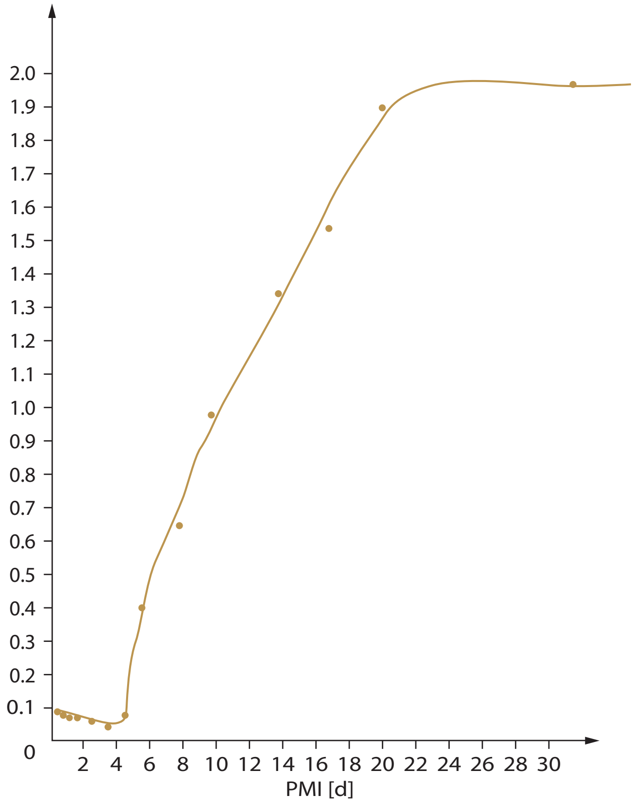

Figure 7.70 Correlation between the post-mortem interval (PMI) and the Daldrup formula calculated from the concentrations of α-aminobutyrate (ABU), γ-aminobutyrate (GABA) and glutamic acid (GLU) according to Daldrup [7].

high proteolytic activity. The brain samples from the cortex or parts of the putrefied brain mush can be taken without any special precaution during routine autopsy. The results of an experiment were supported by some practical cases where the PMI was well or reasonably well known.

However, these methods never gained real practical relevance. For one thing, they are time consuming, and labor-intensive chemical analysis is required. Moreover, most of these procedures attempted to characterize PMI by a few parameters, or even by just one specific parameter, which led to poor correlation as a result of interindividual differences.

In 2002, first results concerning post-mortem decomposition of brain tissue were described by using proton magnetic resonance spectroscopy (^{1}H-MRS) in a sheep head model and in selected human cases [11]. At first, changes in the concentrations of metabolites usually present *in vivo* and the appearance of previously reported decay products were observed. At about 3 days post-mortem, new metabolites including free trimethylammonium (fTMA), propionate (PROP), butyrate (BUT) and iso-butyrate (iBUT) started to appear *in situ* (Figure 7.72). Observed metabolites and time course were comparable in sheep and human brain tissues. These findings could be confirmed using isolated whole heads of young pigs, in which the time course of spectral changes was observed within 3 weeks [1]. *In situ* ^{1}H-MRS was considered as a possibly useful tool for the estimation of PMIs. Scheurer et al. [20] proposed mathematical functions to describe the time course of characteristic metabolites in decomposing brain (sheep head model) up to 3 weeks post-mortem. In a first step, analytical mathematical

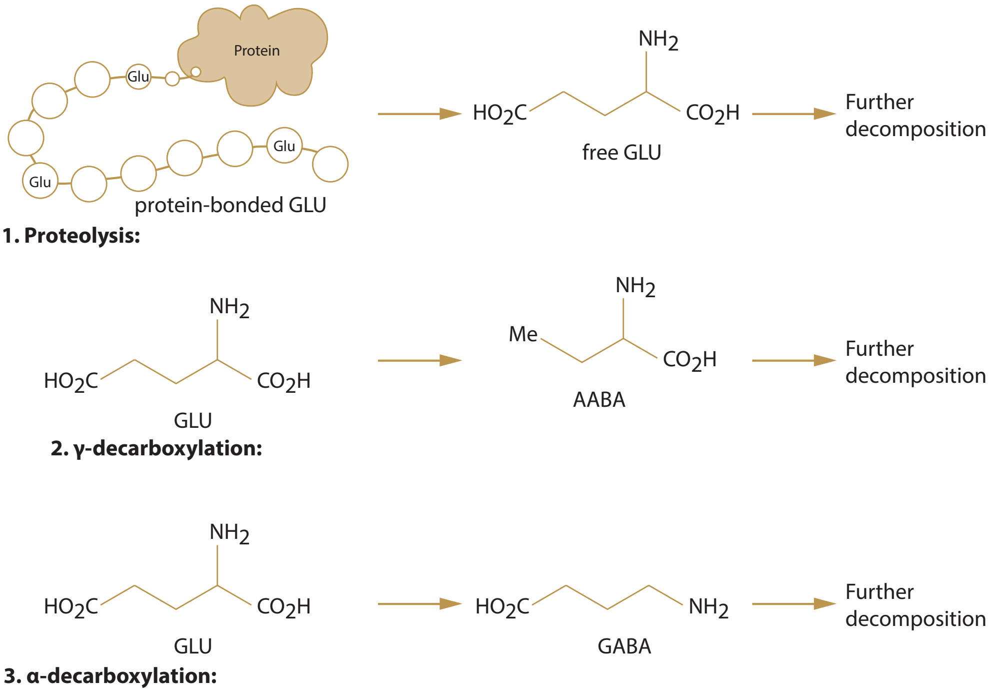
Protein
Glu
Glu
Glu
protein-bonded GLU
1. Proteolysis:
NH2
HO2C
CO2H
free GLU
Further decomposition
NH2
HO2C
CO2H
GLU
2. γ-decarboxylation:
NH2
Me
CO2H
AABA
Further decomposition
NH2
HO2C
CO2H
GLU
3. α-decarboxylation:
HO2C
NH2
GABA
Further decomposition

Figure 7.71 Reactions of glutamic acid (GLU) in the brain during decomposition. AABA, α-aminobutyrate; GABA, γ-aminobutyrate.

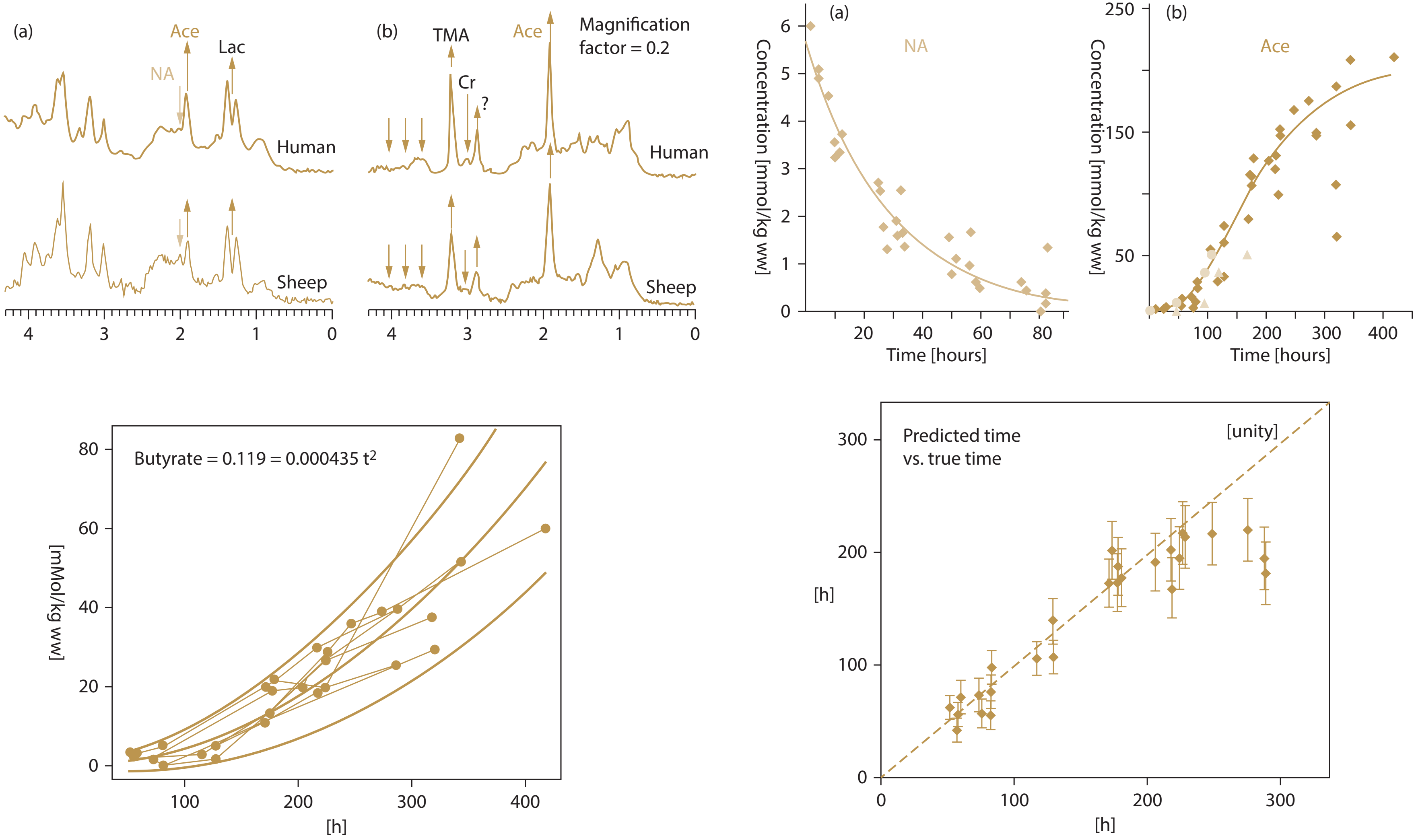

Figure 7.72 (a) Human and sheep spectra measured a) 2 days and b) 7 days post mortem. (b) Time course of a) NA (N-acetyl-aspartate) and b) Ace (acetate) concentration. (c) Concentration changes of butyrate over time post mortem. (d) Correlation of predicted time versus true time (±2 SD). Lac, lactate; TMA, trimethylammonium. ([a] and [b] from Ith M, Kreis R, Scheurer E, Dirnhofer R, Boesch C, Using ^{1}H-MR spectroscopy in forensic medicine to estimate the post-mortem interval: a pilot study in an animal model and its application to human brain. *Proc Int Soc Magn Reson Med* 2001;**9**:388; ([c] and [d] from Scheurer E, Ith M, Dietrich D, Kreis R, Huesler J, Dirnhofer R, Boesch C. Statistical evaluation of time-dependent metabolite concentrations: estimation of post-mortem intervals based on in situ ^{1}H-MRS of the brain. *NMR Biomed* 2005;**18**:163–172. These figures were reproduced by kind permission of the authors and International Society for Magnetic Resonance in Medicine.)

Table 7.44 The Parameterized Model Functions Used to Describe the Time Courses of Various Metabolites According to Scheurer et al. [20]

Variable	Model (time [t] in h)	Concentration limits for prediction (mmol/kg$_{ww}$)	Time limits for fit (h)
Acetate (ACE)	$f(t)=\dfrac{138}{1+exp\left[-(t-153)/35.1\right]}$	ACE <70	$t < 400$
Alanine (ALA)	$f(t) = 3.27 + 0.000435 * t^2$	ALA <20	$t < 200$
Butyrate (BUT)	$f(t) = 0.119 + 0.000435 * t^2$	BUT <70	$50 < t < 400$
Free trimethylammonium (fTMA)	$f(t) = -7.25 + 0.205 * t$	fTMA <30	$50 < t < 200$
Propionate (PROP)	$f(t) = -1.93 + 0.0851 * t$	PROP <30	$20 < t < 400$

Source: Data from Scheurer E, Ith M, Dietrich D, Kreis R, Husler J, Dirnhofer R, Boesch C. Statistical evaluation of time-dependent metabolite concentrations: estimation of post-mortem intervals based on *in situ* ^{1}H-MRS of the brain. *NMR Biomed* 2005;**18**:163–172.

functions were proposed to describe the time courses of ten metabolites in the decomposing brain (Table 7.44).

Subsequently, the inverted functions were used to predict PMIs based on measured metabolite concentrations. Individual PMIs calculated from five different metabolites (acetate [ACE], alanine [ALA], BUT, fTMA, PROP) were then pooled. Being weighted by their inverse variances (var):

$$PMI_{\text{estimated}} = \frac{\sum_i PMI^{\,i}_{\text{individual}} \big/ \text{var}_i}{\sum_i 1 \big/ \text{var}_i}$$

The variance of this weighted prediction (PMI$_{\text{estimated}}$) was calculated as follows:

$$\text{var}(PMI_{\text{estimated}}) = \frac{1}{\sum_i 1 \big/ \text{var}_i}$$

Correlation coefficient and average variance calculated from this formula for the combination of ACE, ALA, BUT, fTMA and PROP were 0.928 and 113, respectively. In the case of sheep experiments, individual PMIs calculated gave a good correlation up to 250 hours post-mortem. Additionally, results could be transferred to human cases. However, the bodies were measured only at one point in time and were stored at 4°C for between 20 and 70 hours before MR examination. The same working group then studied the effect of ambient temperature, which could be reliably included in the PMI determination [12]. These results have not yet been transferred to human cases. In addition, a Chinese group of investigators proposed a mathematical model for the estimation of PMIs by using ^{1}H-MRS at different temperatures [22].

For the preliminary experiments, isolated heads of animals were used, which were prepared by closing the spinal canal with plasticine, fixing in a plastic holder and storing in a plastic container or bag. In a comparison of the metabolic changes in an isolated whole head and a head of an intact animal, different results were obtained [18]: Gas bubbles occurring in the brain tissue after 6–7 days in the isolated animal head and after 4–5 days in the head of the whole animal complicated the selection of a voxel entirely within homogeneous brain tissue and impaired spectroscopic measurements at longer PMIs. During short PMIs, spectra obtained from the isolated head (Figure 7.73) showed signals already described by others and also occurring in healthy living brain, such as the singlets of N-acetyl-aspartate (NAA) at 2.01

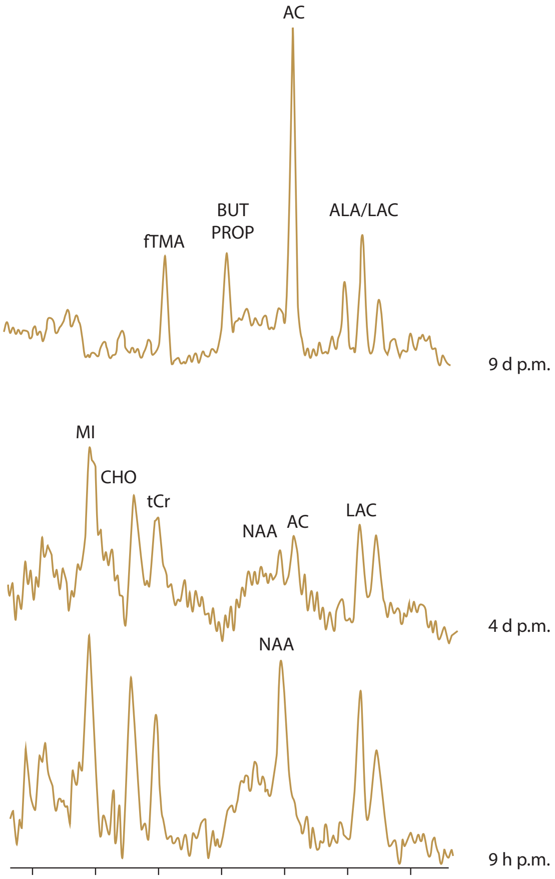

Figure 7.73 Metabolic decomposition in an isolated brain of a sheep measured by proton magnetic resonance spectroscopy on a 1.5-T magnetic resonance system (TR/TE 2500/25 ms) 9 hours, 4 days and 9 days post-mortem (p.m.). The data of other groups were highly reproducible (AC, acetate; ALA, alanine; BUT, butyrate; CHO, choline; fTMA, free trimethylamine; LAC, lactate; MI, myo-inositol; NAA, N-acetyl-aspartate; PROP, propionate; tCr, total creatine), according to Musshoff et al. [18].

ppm, (total) creatine (tCr) at 3.02 ppm and a single peak of bound TMA, mainly including choline compounds (CHO) at 3.19 ppm [16]. After a short time, the methyl (CH_3) doublets of lactate (LAC) at 1.33 ppm and ALA at 1.47 ppm appeared. Nine hours post-mortem, ACE was detected only as a small upfield shoulder of the NAA peak. At longer PMIs, ACE became the predominant peak, and additional signals evolved for succinate at 2.41 ppm and fTMA at 2.88 ppm, whereas other metabolites such as NAA, tCr and LAC disappeared.

In conclusion, the animal model appeared highly reproducible and in principle can be seen as a useful tool for further studies. However, quite different results were revealed by investigation of the metabolic alterations in the brain of the whole animal. Spectra showed differences already 48 hours post-mortem, but especially after longer PMIs (Figure 7.74). Fifteen days post-mortem, mainly fTMAs and LAC were found in the intact animal, but no further metabolites such as ACE, PROP, ALA and BUT, which were used for the mathematical model for the estimation of PMIs as described earlier [12,20]. These metabolites were detectable only in the isolated animal head 15 days post-mortem. However, significant differences in metabolic alterations during post-mortem decomposition in the brain were demonstrated between the animal model with isolated heads and the intact animal. Decomposition in the intact animal appeared faster and probably different compared with the model with isolated heads, as a result of bacterial invasion from the gastrointestinal tract, which can reach the brain in a few days in a cadaver. The significance of putrefiers such as *Clostridium sordelli* for the estimation of the PMI had been demonstrated by Bonte [3] and by Daldrup and Huckenbeck [9] several years earlier.

However, the investigation of post-mortem decomposition by ^{1}H-MRS may represent a real progress in research.

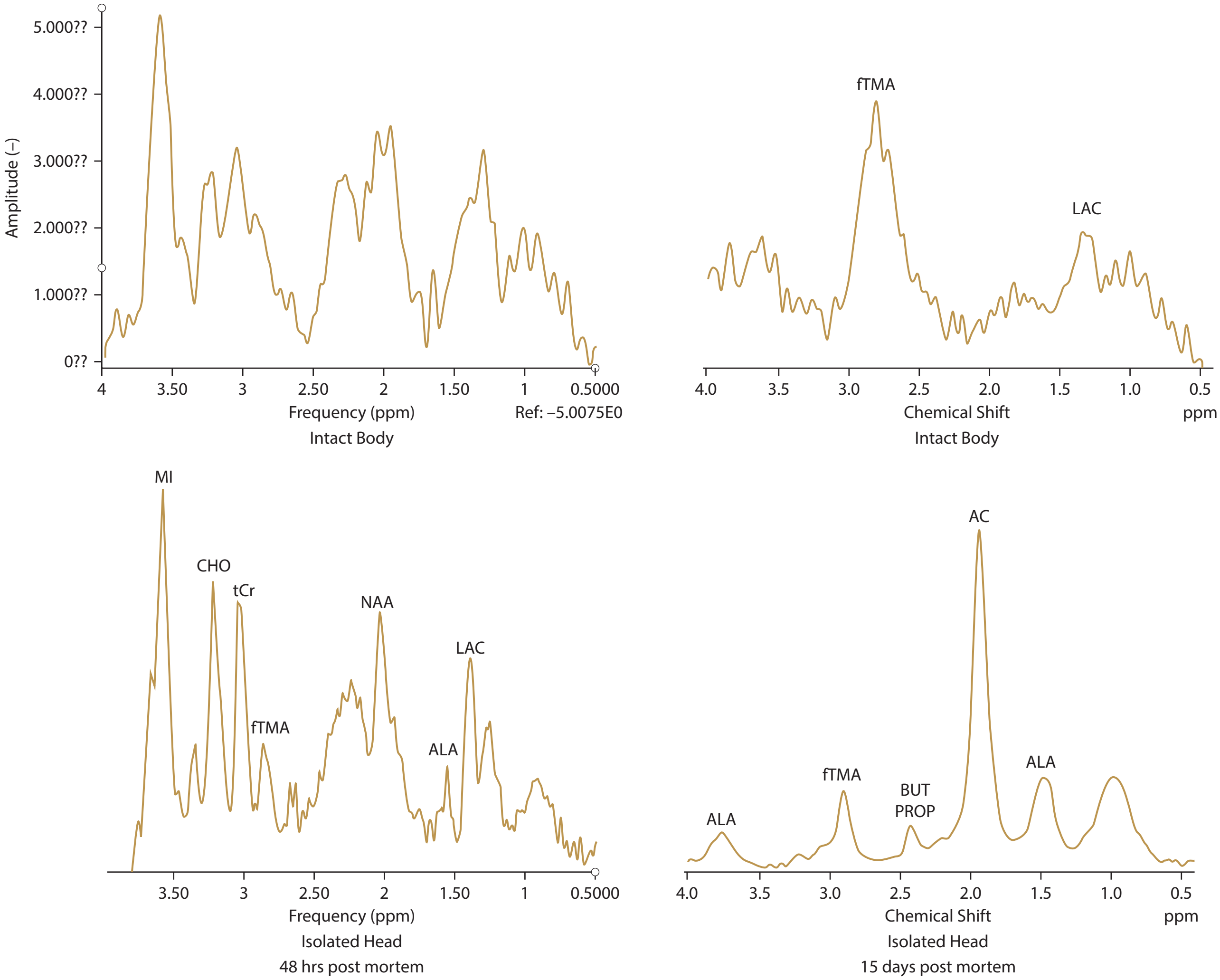

Figure 7.74 Proton magnetic resonance spectroscopy of sheep brain; analysis of an intact body and an isolated head 48 hours and 15 days post-mortem (AC, acetate; ALA, alanine; BUT, butyrate; CHO, choline; fTMA, free trimethylamine; LAC, lactate; MI, myo-inositol; NAA, N-acetyl aspartate; PROP, propionate; tCr, total creatine), according to Musshoff et al. [18].

The procedure allows non-invasive chemical analysis *in situ* with quantitation of analytes, as well as longitudinal studies of post-mortem changes with reproducible results. Influencing factors such as temperature and temperature-dependent invasion ability of bacteria can be easily studied, but in further studies intact bodies should be used instead of isolated heads. Old questions in forensic medicine such as death time estimation can benefit from recent developments in modern imaging systems [13–15].

Unfortunately, since the last edition, there were no further developments, although this technique is a superb research tool and promises interesting results also for the practice.

References and further reading

1. Banaschak S, Rzanny R, Reichenbach JR, Kaiser WA, Klein A. Estimation of postmortem metabolic changes in porcine brain tissue using ^{1}H-MR spectroscopy: preliminary results. *Int J Legal Med* 2005;*119*:77–9.
2. Bonte W. Der postmortale Eiweiss-Katabolismus. *Beitr Gerichtl Med* 1975;*33*:57–75.
3. Bonte W. *Der postmortale Proteinkatabolismus. Experimentelle Untersuchungen zum Problem der forensischen Leichenzeitbestimmung*. Göttingen, Germany, Habilitation Schrift, 1978.
4. Bonte W, Bleifuss J, Volck J. Experimental investigations in postmortem protein degradation. *Forensic Sci* 1976;*7*:9–22.
5. Daldrup T. Die Bedeutung der Bildung von α- und γ-Aminobuttersäure während der Fäulnis von eiweisshaltigem menschlichem Organmaterial. Eine Möglichkeit der Todeszeitbestimmung? *Beitr Gerichtl Med* 1979;*40*:379–82.
6. Daldrup T. Zur Kinetik des postmortalen bakteriellen Glutaminsäurestoffwechsels im Gehirn. *Z Rechtsmed* 1981;*86*:195–203.
7. Daldrup T. Praktische Erfahrungen mit der Leichenalterbestimmung durch Auswertung bakterieller Stoffwechselprodukte. *Z Rechtsmed* 1983;*90*:19–25.
8. Daldrup T. *Die Aminosäuren des Leichengehirns*. Stuttgart, Germany, Enke, 1984.
9. Daldrup T, Huckenbeck W. Bedeutung des Fäulnisbakteriums Clostridium sordellii für die Leichenaltersbestimmung. *Z Rechtsmed* 1984;*92*:121–5.
10. Henssge C, Madea B. Estimation of the time since death. *For Sci Int* 2007;165:182–4.
11. Höpfel F, Platzer W, Spindler K. *Der Mann im Eis*, vol. 1. Bericht über das internationale Symposium 1992 in Innsbruck, Veröffentlichungen der Universität Innsbruck. Innsbruck, Austria, University of Innsbruck, 1992, p 187.
12. Ith M, Bigler P, Scheurer E, Kreis R, Hofmann L, Dirnhofer R, Boesch C. Observation and identification of metabolites emerging during postmortem decomposition of brain tissue by means of *in situ* ^{1}H-magnetic resonance spectroscopy. *Magn Reson Med* 2002;*48*:915–20.
13. Ith M, Scheurer E, Kreis R, Thali M, Dirnhofer R, Boesch C. Estimation of the postmortem interval by means of ^{1}H-MRS of decomposing brain tissue: influence of ambient temperature. *NMR Biomed* 2011;*24*:791–8.
14. Madea B. Leichenzerstückelung mit ungewöhnlicher Konservierung der Leichenteile. *Arch Kriminol* 1994;*193*:72–8.
15. Madea B. Is there recent progress in the estimation of the postmortem interval by means of thanatochemistry? *Forensic Sci Int* 2005;*151*:139–49.
16. Madea B, Musshoff F. Postmortem biochemistry. *Forensic Sci Int* 2007;*165*:165–71.
17. Madea B, Preuss J, Musshoff F. Vom blühenden Leben zu Staub—Der natürliche Kreislauf von Werden und Vergehen. In: Wieczorek A, Tellenbach M, Rosendahl W (eds.). *Mumien—Der Traum vom ewigen Leben*. Mainz, Germany, Philipp von Zabern, 2007, pp 5–22.
18. Madea B, Preuss J, Musshoff F. From flourishing life to dust: the natural cycle of growth and decay. In: Wieczorek A, Rosendahl W (eds.). *Mummies of the World*. Munich, Germany, Prestel, 2010, pp 14–29.
19. Michaelis T, Helms G, Frahm J. Metabolic alterations in brain autopsies: proton NMR identification of free glycerol. *NMR Biomed* 1996;*9*:121–4.
20. Mittmeyer HJ, Strebel KH. Experimentelle Untersuchungen zur forensischen Liegezeitbestimmung durch Elektrofokussierung von löslichen Muskelproteinen. *Z Rechtsmed* 1980;*85*:235–40.
21. Musshoff F, Klotzbach H, Block W, Traeber F, Schild H, Madea B. Comparison of post-mortem metabolic changes in sheep brain tissue in isolated heads and whole animals using ^{1}H-MR spec-troscopy: preliminary results. *Int J Legal Med* 2011;*125*:741–4.
22. Odrizola A, Riancho JA, de la Vega R, Agudo G, Garcia-Blanco A, Cos de E, Fernandez F, Sanudo C, Zarrabeitia MT. miRNA analysis in vitreous humor to determine the time of death: a proof-of-concept pilot study. *Int J Legal Med* 2013;*127*:573–8.
23. Padosch SA, Dettmeyer R, Kröner L, Preuss J, Madea B. An unusual occupational accident: fall into a sewage plant tank with a lethal outcome. *Forensic Sci Int* 2005;*149*:39–45.
24. Petersohn F. Rechtsmedizinische Feststellungen an einer 3 Jahre in Plastik gehüllten Kindesleiche. *Beitr Gericht Med* 1972;*29*:351–8.
25. Preuss J, Brünig J, Madea B. Artifizielle Enterdigung durch Witterungseinflüsse. *Rechtsmedizin* 2004;*14*:14–19.
26. Scheurer E, Ith M, Dietrich D, Kreis R, Husler J, Dirnhofer R, Boesch C. Statistical evaluation of time-dependent metabolite concentrations: estimation of post-mortem intervals based on *in situ* ^{1}H-MRS of the brain. *NMR Biomed* 2005;*18*:163–72.
27. Yang TT, Li ZW, Liu L, Zhen N. Estimation of postmortem interval with single-voxel proton ^{1}H-MR spectroscopy at different temperature. *Fa Yi Xue Za Zhi* 2008;*24*:85–9 (in Chinese).
28. Vass AA, Bass WM, Wolt JD, Foss JE, Ammons JT. Times since death determination of human cadavers using soil solutions. *F Forensic Sci* 1992;*27*:1236–53.

7.6 Post-mortem Protein Degradation

Stefan Pittner and Angela Pittner

7.6.1 Basics of Protein Degradation

The breakdown of proteins within tissues is a ubiquitous and evolutionary conserved process and the main mechanisms are also exerted in living body cells [1]. The process of proteolysis breaks proteins down into smaller peptides, and ultimately amino acids as the destructive part of constant protein turnover. Hydrolysis of peptide bonds can occur under extreme pH and temperature conditions, or it can be catalyzed by proteolytic enzymes (proteases) [2]. In living tissue, proteolysis is usually mediated enzymatically by proteases via different mechanisms and biochemical systems including the ubiquitin-proteasome pathway, the autophagy-lysosomal pathway (cathepsins), the caspase system (e.g. responsible for apoptosis), and the Ca^{2+} triggered calpain system (e.g. necrosis) [3]. In post-mortem tissue, the calpains are recognized to be responsible for a large part of proteolytic activity due to the fact that this enzyme class is ATP-independent in its activation (*in vivo* the enzymes are largely inhibited by calpastatin and low cytoplasmic calcium concentrations [4–7]). Post-mortem, progressive membrane leakage and the ceasing of ATP driven Ca^{2+} removal from the cytoplasm out of the cell (plasma membrane Ca^{2+} ATPase [PMCA]), or into the sarcoplasmic reticulum (sarcoplasmic reticulum Ca^{2+} ATPase [SERCA]), leads to a rise of intracellular Ca^{2+} levels, and thus activation of the calpains [3,7]. Moreover, post-mortem protein decomposition can be accelerated by microbial enzymes (in particular of intestinal bacteria), and occasionally also by enzymes released from necrophagous insects [8].

7.6.2 Protein Degradation in a Forensic Context

The human body is approximately composed of 15–20% proteins (by weight) [9]. Post-mortem decomposition of a corpse therefore comprises the fragmentation of hundreds of thousands of proteins. Recent evidence has demonstrated that the post-mortem degradation of certain proteins proceeds in a regular, predictable fashion. Therefore, several research groups have suggested the analysis of the time course, respectively, the progress of protein degradation, as a tool for forensic PMI delimitation [10–12]. An estimate of the time of death can either be made when certain degradation processes have already occurred, and/or (others) are yet pending. To achieve respective models and reference data bases, the main principle behind any protein-based PMI estimation method is to (i) identify suitable marker proteins, (ii) analyse particular post-mortem alterations and (iii) correlate them to specific PMIs or PMI ranges, (iv) also including the investigation of respective influencing factors. Degradation profiles can either be compared to one another to obtain information on a time course of events (e.g. somebody died earlier than another person), but should certainly be aimed to allow back-calculation to a starting point along a time-dependent curve [13] to estimate the time interval that has elapsed since death.

7.6.3 Methodology

Currently, there is a variety of biochemical methods available for the detection of proteins in biological materials, differing in detection strategy, precision, cost and time investment. Several of these methods have already been successfully tested for forensic application. Regardless of what method is used to trace post-mortem protein decomposition, outcome acquisition and data analysis showed two different strategies: (i) calculation and comparison of gradual alterations of protein concentration levels and (ii) description and comparison of protein presence (or absence) at certain time points post-mortem [14]. Both strategies follow similar basic principles; however, the measurement of gradual changes always essentially depends on the knowledge of a starting value. In animal modelling under laboratory conditions, such values can conceivably be established, but exactly this is highly challenging with human samples and hardly possible in forensic cases in which ante-mortem reference or at death data are lacking [13,15]. By contrast, the evaluation of the presence and absence of a protein (and its degradation products) relies on strict detection limits based on rigorous concentration thresholds [14], making this strategy largely independent from an individual baseline level.

Based on a systematic search and literature review in 2020, the three most frequently used methods in protein degradation–based PMI research are immunohistochemistry (IHC), Western blotting and mass spectrometry [14]. While IHC and Western blotting use specific antibodies to establish whether predefined proteins are susceptible to time-dependent proteolysis, mass spectrometry is mostly used to profile the entire proteome, identifying changes in post-mortem protein/peptide patterns retrospectively.

7.6.3.1 Immunohistochemistry

Around 2000, the group of Wehner described post-mortem changes of immunohistochemical staining characteristics of the peptide hormones insulin [16], glucagon [17] and somatostatin [18] in human pancreas, thyroglobulin [19] and calcitonin [20] in human thyroid glands and glial fibrillary acidic protein (GFAP) in human brain [18] using. With advancing PMI and proteolysis, applied antisera could not bind to the proteins epitopes resulting in a loss of staining. For example, the stainability of GFAP in the frontal cortex persisted until 3 days post-mortem and after day 14 no staining was found consistently. Pancreatic somatostatin staining was detected between 1 and 2 days post-mortem, but it was consistently lost in samples with a PMI of 11 days post-mortem or longer.

Ortmann et al. (2017) [21] revisited the immunohistochemical approach by Wehner, investigating the degradation of proteins from thyroid gland and pancreatic tissue of human autopsy cases with different PMIs (ranging from several hours to 22 days), causes of death and a broad spectrum of environmental conditions before autopsy. The authors found that the immune stainability for insulin, glucagon, thyroglobulin and calcitonin was time dependent. For thyroglobulin and calcitonin, a weak stainability persisted for up to 8 days in some cases, but it was lost at 1 day post-mortem in others. Glucagon and insulin were successfully labelled up to a PMI of 12 and 18 days, respectively, while the immunoreactivity of these proteins was lost from day 18 and 22 onwards.

Lee et al. (2016) [22] investigated samples of rat psoas muscle and kidney at specific time points between 0 and 96 hours post-mortem. Renal glycogen synthase (GS) was found to remain stainable within 24 hours post-mortem but was no longer detected from 48 hours post-mortem onwards. Stainability of caspase-3 was completely lost at 96 hours post-mortem. In psoas muscle, staining capability was lost at 96 hours post-mortem for both proteins. For more details on the immunohistochemistry method by the group of Wehner refer to Chapter 10 of this book (*Immunhistochemical Methods as an Aid in Estimating the Time Since Death*).

7.6.3.2 Western Blotting

Western blot analysis was initially suggested as a method for PMI estimation in 2003. Sabucedo and Furton [23] investigated cardiac troponin I (cTnI) decomposition in cattle and found that the intact protein progressively fragmented with increasing PMI. In a second experiment, they analysed human myocardium from autopsy cases at the initial time of sampling and after an additional 24-hour incubation period at room temperature. Again, a time-dependent fragmentation of cTnI was detected.

Kang and colleagues (2003) [24] used Western blotting to investigate the degradation of calmodulin-binding proteins in lung and skeletal muscle tissue of rats. Sacrificed animals were stored at 21°C and tissues were sampled at 0, 24, 48 and 96 hours post-mortem. It was found that calcineurin A (CnA) significantly degraded in a predictable pattern (via a degradation product) in the lung, while it produced unpredictable band patterns in skeletal muscle. Ca^{2+}/CaM-dependent kinase II (CaMKII) remained stable within the investigated PMI of 96 hours post-mortem in both lung and muscle. Additionally, in the lung, myristoylated alanine-rich C-kinase substrate (MARCKS) exhibited a steady decrease, whereas band patterns of inducible nitric oxide synthase (iNOS) were irregular and largely unpredictable.

Poloz and O’Day (2009) [11] investigated a similar set of proteins in lung and skeletal muscle of mice. Animals were stored at temperatures of 5°C, 10°C and 21°C and sampled at 0, 24, 48 and 96 hours post-mortem. In lung tissue, CnA turned out to be almost fully degraded after 24 hours even when stored at low temperature (5°C), CaMKII was undetectable by 48 hours post-mortem at all temperatures, and MARCKS was found to be significantly degraded at 96 hours post-mortem at 10°C and 21°C. Phosphatase 2A (PP2A) remained unchanged until 96 hours post-mortem at 5°C but exhibited significant decreases at higher temperatures, after temporary increases at 24 and 48 hours post-mortem. In skeletal muscle, CnA underwent a rapid cleavage into smaller fragments, and the native band signal became significantly weaker within the first 24 hours post-mortem. CaMKII was undetectable by 48 hours post-mortem and MARCKS was not detectable in any of the samples. PP2A was found to be stable for up to 96 hours post-mortem at 5°C and 10°C, while a marked decline was found after 48 hours post-mortem at 21°C. A statistically significant effect of temperature was also confirmed for CnA, with faster degradation of both, the native protein and the emerged degradation product at higher temperatures.

Between 2015 and 2016 the group of Kumar published a sequence of four studies [25–28] on the post-mortem degradation of human cardiac troponin T (cTnT). The analysed heart tissue derived from forensic cases with different background: no disease [27] fatal burn [28] and electrocution [26]. Western blot analysis revealed that cTnT degraded in a pseudo-linear correlation between the ratio of intact cTnT and PMI, and that cTnT was cleaved into several degradation products over time. The authors also demonstrated that cTnT decomposition is temperature dependent, with increased degradation rates at higher temperatures [27].

Bolton and co-workers [29] investigated post-mortem cartilage degradation in pig trotters in 2015. Specimens were buried in graves and recovered at defined time points post-mortem (weekly over the course of 6 weeks), whereas fresh trotters were used as controls. Each week, cartilage tissue of the metacarpophalangeal and metatarsophalangeal joints was sampled and analysed by Western blotting. As a main result, the cartilage specific proteoglycan core protein aggrecan was found to degrade within the investigated PMI, as the native band disappeared at 30 days post-mortem onwards.

Lee et al. (2016) [22] investigated samples of rat psoas muscle and kidney at specific time points between 0 and 96 hours post-mortem via Western blot. Degradation of the following proteins were analysed: glyceraldehyde 3-phosphate dehydrogenase (GAPDH), caspase-3, peroxisome proliferator-activated receptor gamma (PPAR-γ), glycogen synthase (GS), Glycogen synthase kinase-3 β (GSK-3β), p 53, AMP-activated protein kinase α (AMPKα) and β-catenin. For most of these proteins, strong correlations of degradation with the PMI were found. Calculation of PMI50 (half maximum intensity of intact protein) values allowed to classify the investigated proteins into, what the authors called, short-term (PMI50 within 24 hours post-mortem), mid-term (PMI50 between 24 and

96 hours post-mortem) and long-term markers (PMI50 later than 96 hours post-mortem). As such, AMPKα, GSK-3β, GS and caspase-3 from psoas muscle were identified as 'short term', renal caspase-3, GAPDH and PPAR-γ as 'mid-term', and p 53 and β-catenin as 'long term' markers.

The groups of Foditsch et al. (2016) [30] and Pittner et al. (2016) [10] used SDS-PAGE (sodium dodecylsulphate polyacrylamide gel electrophoresis), Western blotting and casein zymography to trace PMI-dependent protein degradation patterns in porcine hindlimb muscle. In the study of Foditsch et al. [30] pigs were stored at 4°C and at 22°C and muscle samples (*M. biceps femoris*) were taken over periods of 21 days and 5 days, respectively. Pittner et al. [10] investigated protein decomposition in dismembered pig hindlimbs stored for 10 days at 21°C (humidity of 35% ± 5%). Samples were dissected from biceps femoris muscle at 18 predefined time points. Both studies investigated a similar set of proteins including α-actinin, calsequestrin 1, desmin, nebulin, sarcoplasmic/endoplasmic reticulum calcium ATPase (SERCA) 1, SERCA2, titin, tropomyosin, cTnT, laminin, and calpain. It was uniformly demonstrated that proteins degrade in a regular and predictable time-dependent fashion. Degradation products, present in different post-mortem time frames, were found for the proteins titin, desmin, SERCA1, nebulin and cTnT. At room temperature, tropomyosin, α-actinin, calsequestrin-1 and laminin remained stable for 5 [10], respectively 10 days [30]. These four proteins also remained unchanged in the samples stored for 21 days at 4°C [10]. Notably, the quantification strategy utilized by Pittner et al. [10] diverged from that applied in previous work. Instead of comparing ratios of band intensities [11,23–28,31], the authors focused on the timing of the appearance and disappearance of bands, calculating mean time points (+ 95% confidence interval) of protein pattern alterations. This allowed to define specific time intervals in which proteins and their degradation products are either significantly present or absent.

Follow-up work of the group of Pittner and co-workers expanded the knowledge on the degradation profiles of cTnT, desmin and tropomyosin by testing *M. vastus lateralis* samples from human forensic cases with known PMI [32]. Results were presented in the form of statistically calculated probabilities of presence and absence of protein bands with increasing accumulated degree days (ADD), employed as a combined measure of PMI and environmental temperature. This allowed to draw conclusions on the time frame in which a particular protein is present with high probability. While tropomyosin was present in all investigated cases regardless of ADD, cTnT and desmin presented distinct decomposition events (loss of native band, appearance of degradation products) associated with a presence/absence probability in different time frames. Factors possibly influencing protein degradation dynamics, such as age, sex and body weight (as represented by BMI), were additionally tested. Results indicate relevant influence of age and BMI, while sex and cause of death appeared to have no major effect.

Zissler et al. [33] used Western blotting to analyse the degradation of desmin, vinculin and tropomyosin in rat hindlimb muscle. After different pre-treatment (control, induced muscle injury, onset of atrophy by induced spinal cord injury) the rats were killed and stored for up to 4 days post-mortem at a constant temperature of 20°C. Desmin and (meta-)vinculin were found to degrade in a time-dependent manner, the native desmin band being lost at 2 days post-mortem, and both proteins giving rise to several degradation products. By contrast, tropomyosin remained stable over the investigated time period. In addition, results demonstrated an effect of altered ante-mortem metabolism (resulting from injury and atrophy) on post-mortem protein decomposition.

In 2019, Cho and Eom [31] used Western blots to test whether the multi-ligand receptor for advanced glycation end products (RAGE) could serve as a biomarker for PMI estimation in drowning cases. Lung tissue of drowned rats was dissected at 7 time points post-mortem (1–7 days post-mortem, 5 animals per time point) after controlled storage of the cadavers in seawater (15°C ± 5°C). Non-drowned rats immersed in seawater and untreated rats served as controls. Western blots showed that RAGE protein expression decreased significantly over the post-mortem submersion interval. Additional IHC analysis confirmed the Western blot results demonstrating a gradual decrease in the staining intensity of RAGE.

After successful identification of new forensic protein markers glycerinaldehyd-3-phosphat-dehydrogenase (GAPDH) and the eukaryotic translation elongation factor 1 alpha 2 (eEF1A2) by mass spectrometry, Choi et al. [34] tested the proteins' post-mortem behaviour by Western blot analysis using a standardized rat degradation model and human autopsy cases. Additionally, the protein changes were compared to degradation patterns of tropomyosin, desmin and vinculin. Muscle samples (*M. vastus lateralis*) of rats were collected at 5 time points post-mortem during a PMI of 0–96 hours post-mortem. Tropomyosin and GAPDH bands were present at all time points, whereas the intensity of the GAPDH band decreased significantly over the investigated period. eEF1A2 was completely degraded by 48 hours post-mortem, and native desmin bands were lost at 96 hours post-mortem. Similar to GAPDH vinculin bands decreased in intensity over the investigated PMI. The two latter proteins produced several degradation products.

7.6.3.3 Mass Spectrometry

In 2017 and 2018, the groups of Kwak [35], Li [36,37], Pérez-Martínez [38], Procopio [39] and Prieto-Bonete [12] introduced proteomic approaches for time since death estimation. Kwak et al. [35] specifically used HPLC-MS (high-performance liquid chromatography mass spectrometry) to trace the degradation of 26 proteins from rat heart and liver separated by two-dimensional polyacrylamide gel electrophoresis (2D-PAGE). Whole organs of three animals were dissected immediately after death, stored under controlled conditions and tissues were sampled at 0, 24 and 48 hours post-mortem. Intensity measurements of protein spots in the polyacrylamide gels presented a heterogeneous picture, revealing either an increase, or decrease over the investigated period.

The two studies of Li et al. employed liver [36] and skeletal muscle [37] to assess the applicability of Matrix-Assisted Laser Desorption/Ionization Time of Flight Mass Spectrometry (MALDI-TOF-MS) for PMI estimation. Rats and human liver lobes were stored under controlled conditions, and samples were dissected at different time points. Intensities of numerous peptide/protein peaks from both tissues were found to change significantly over the investigated PMI. Especially, peaks with specific mass-to-charge ratios (2826–1596 in rat liver, 3336–453 in human liver and 1564 and 2168 in rat muscle) evidently decreased in intensity over the sampled time and were therefore suggested as markers for PMI estimation. On the basis of *in vitro* decomposed human liver samples, various classification models were designed and validated using four additional human cases.

Procopio et al. [39] used pig carcasses to search for specific biomarkers that could aid in PMI delimitation. Animals were buried, and after 1, 2, 4 and 6 months, respectively, one of the carcasses was partially excavated and a tibia bone was collected. The second tibia of each animal was collected at a PMI of 1 year. Using liquid chromatography mass spectrometry/mass spectrometry (LC-MS/MS), 28 proteins were initially found to be more abundant in samples collected after a PMI of 1 month than at the later times. After methodological refinements, the authors focused on the degradation of 18 proteins, including plasma proteins, muscle proteins, and proteins involved in glycolysis and gluconeogenesis pathways. While some proteins decreased rapidly, others showed a lower depletion rate, until a rapid general decline in abundance occurred after 4 months. Only little further changes followed between 4 and 6 months. After one year, only 29% of the proteins could yet be analysed, ten of which showed inter-animal differences and nine proteins didn't achieve significant differences. For the protein biglycan, the authors additionally reported a statistically significant increase of deamidation with increasing PMI.

Pérez-Martínez et al.[38] and Prieto-Bonete [12] both investigated protein decay in human bones exhumed from a cemetery in the southeast of Spain. Pérez-Martínez et al. [38] used HPLC-MS/MS to assess the content of several proteins (and of non-protein biomolecules) in samples of long bones of individuals interred for 5–47 years. The amount of collagen type I was found to be significantly lower in bones with a PMI of ≥ 20 years compared to bones with shorter PMI. Mathematical modelling indicated a reliability of roughly 70%. Prieto-Bonete [12] used LC-MS/MS to analyse femur bone samples of humans interred for 5–20 years. Multiple correspondence analysis identified 32 proteins that allow to discriminate skeletal remains with a PMI of 5–12 years from those with a PMI of 13–20 years. Sixteen of the proteins, including those with high molecular weights, were only present in samples with PMIs <12 years. The remaining 16 proteins, including those with lower molecular weights, showed a statistically lower presence in samples with a PMI >13 years compared to the samples with shorter PMIs. In addition, the proportion of acidic and neutral amino acids increased with the PMI, while that of basic amino acids decreased.

In 2019, Choi et al. [34] presented a method to discover new protein markers for PMI estimation by mass spectrometry. Muscle tissue (*M. vastus lateralis*) samples of mice collected at 5 time points post-mortem (PMI 0-96 hpm, stored at 20°C) were analysed for the degradation of GAPDH and eEF1A2. Results showed that both proteins degrade consistently with increasing PMI. The usefulness of these proteins as PMI estimation markers was additionally validated by Western blot analysis in rats and humans.

7.6.3.4 Other Methods

Thaik-Oo et al. (2002) [40] introduced the enzyme-linked immunosorbent assay (ELISA) technique for forensic PMI estimation. The group investigated the degradation of the vascular endothelial growth factor (VEGF) in various organs (brain, kidney, heart, lung, liver) of individuals with PMIs ranging from 2.75 to 120 hours post-mortem. Organ specific but also PMI-correlated changes were reported. In brain, kidney, lung and liver, an initial increase of VEGF concentration levels was followed by a decrease at PMIs after 24 hours post-mortem. In contrast, no correlation between VEGF concentrations and PMI was found in cardiac tissue.

Boaks et al. (2014) [41] used a porcine model to investigate the ratio of collagenous to non-collagenous protein concentrations (Co/NCo) in skeletal remains. Pig carcasses were left to decompose in a field, and long bones were recovered and analysed after 2, 4, 6, 10 and 12 months, using fresh bones as controls. Bone cross sections were stained with a combination of two histological dyes differentiating collagen proteins and non-collagenous proteins. After destaining, photometrically analysed concentrations of Co and NCo proteins in the eluate showed an overall decrease of collagen over the investigated PMI. In addition, the authors reported that bones degraded non-uniformly, with signs of collagen loss appearing in the endosteal and/or periosteal regions, whereas mesosteal regions retained their collagen for longer time.

Between 2018 and 2019, Jellinghaus et al. published two studies on post-mortem degradation of collagen in pig [42] and human bones [43]. The first study [42] undertook a validation following the work of Boaks et al. [41], determining collagen to non-collagen (Co/NCo) ratios after differential staining of porcine bone sections. Specimens were buried in plastic boxes and stored under monitored conditions for 3 months and sampled at 3 time points. As outcomes of eluate photometry after destaining differed markedly from those of Boaks et al. [41], the authors examined the histological sections under a stereomicroscope and calculated Co/NCo ratios from digital imaging data: after a significant increase of the Co/NCo ratio until 56 days post-mortem a subsequent significant reduction over the rest of the investigated 3-month period was reported. In addition, the study tested whether the presence of microorganisms influenced bone collagen degradation and found no significant effects. In the second study [43], human femur samples were collected from exhumations (PMI 21–48 years) and autopsies, and additional samples were received from archaeological cases (PMI 135–153 years). The authors reported an ascending trend of the Co/NCo ratio if measured photometrically, but a decreasing trend if measurement is made with stereomicroscopic image analysis. If sorted by sex, the concentration of the Co/NCo ratio decreased in males but increased in females.

In a pilot approach, Lee et al. (2016) [22] successfully tested an lateral flow assay (LFA)-based diagnostic chip for its suitability to detect intact GAPDH in rat kidney, suggesting an attractive tool for future field application.

Abo El-Noor et al. (2016) [44] and da Fonseca et al. (2019) [45] used enzyme activity assays to investigate the post-mortem activity of glutathione-S-transferase (GST) [44], glutathione reductase (GR) [44], catalase (CAT) [44], acetylcholinesterase (AChE) [45], Na+/K+-ATPase [45] and glutathione-S-transferase (GST) [45] in heart [44], kidney [44,45], brain [45], liver [45] and gastrocnemius muscle [45]. Whereas the activity of most enzymes decreased with advancing PMI (e.g. Na+/K+-ATPase in brain and GR in heart and kidney) some enzymes showed a significant activity increase (e.g. GST and Na+/K+-ATPase in kidney), varying levels of activity (e.g. AchE and GST in brain and liver) or no time-dependent changes in activity levels (e.g. GST in brain and muscle).

The group of Alibegović [46] investigated cartilage degradation in bone samples of human donors stored for up to 36 days post-mortem at 11°C and 35°C in 2019. Intensities of histological collagen and proteoglycan staining was assessed by blinded observers using a grading scale. The authors found a significant reduction in staining intensity at day 36 post-mortem at both temperatures, compared to the baseline samples. They also reported that post-mortem time had a larger (significant) effect than temperature.

7.6.4 Current and Future Challenges

7.6.4.1 The Quest of Suitable Target Tissues

Decomposition of a cadaver starts at the time of death and usually progresses inevitably. The rate of tissue decomposition, however, can vary substantially depending on numerous factors regarding the body itself, the environment and the circumstances of death [47–50]. Disregarding external influences for now, it is known that several characteristics can accelerate or delay the rate of tissue decomposition, including (i) enzymatic activity, (ii) exposition to a distinct bacterial flora and (iii) the content of collagen and keratin (‘soft tissue’ versus ‘hard tissue’) [51–53]. In more detail, the post-mortem release of hydrolytic enzymes acidifies the surrounding tissue, which in turn promotes enzymatic activity [54]. The prevailing enteric bacterial flora accelerates decomposition of the gastrointestinal tract and its surrounding tissues via anaerobic fermentative processes and enhanced putrefaction [55]. On the contrary, the fibrous proteins collagen and keratin exhibit unique properties with strong inter- and intramolecular bonds that are difficult to hydrolyze, accounting for delayed decomposition in collagen- and keratin-rich tissues [51,56]. When defining specific target tissues, consideration of these tissue characteristics is reasonable. Indeed, research on post-mortem protein degradation has demonstrated that specific tissues have specific decomposition dynamics. The post-mortem stability of cartilage and bone enable PMI investigations in periods ranging from months to years [14]. In early and intermediate PMIs, ranging from hours to days [14], soft tissues containing proteins more susceptible to proteolysis proved suitable. Pancreas, for example, as an enzyme rich internal organ, is among the first soft tissue to be affected by post-mortem autolysis [57]. Already at 24 hours post-mortem, histological analysis showed advanced autolytic changes and complete autolysis of Langerhans islets at 36 hours post-mortem (room temperature) [58]. However, not general histological decay but the susceptibility of specific proteins to proteolysis seems to be a key determinant for choosing target tissues. This is indicated by successful staining of pancreatic tissue for insulin until up to 29 days post-mortem even in the presence of far advanced autolytic and putrefactive changes [16].

Even within one organ, tissue in-homogeneities may lead to different protein degradation patterns in samples dissected from various organ regions. Indication for this comes from non-simultaneous autolysis found in heart, pancreas and bone. Qualitative histological analysis of myocardial decay showed that autolysis advances faster in the subepicardial region than in the subendocardial region [58]. In pancreas, centrilobular areas underwent faster autolysis than other regions of the parenchyma [58]. At the protein level, accelerated loss of collagen was

Table 7.45 Overview of Reported Post-mortem Protein Changes in Various Organs and Tissues

Tissue	Protein	Method	PMI	Type of study outcome	Main study outcome	Reference
Bone	Collagen	Histology	approx. 90 days	Ratio of collagenous to non-collagenous (Co/NCo) protein concentration	Decrease in concentration of Co/NCo ratio	Jellinghaus et al., 2018
		Histology	171 years	Ratio of Co/NCo protein concentration	Decrease in concentration of Co/NCo ratio	Jellinghaus et al., 2019
		Photometry	1 year	Ratio of Co/NCo protein concentration	Decrease in concentration of Co/NCo ratio	Boaks et al., 2014
		MS	47 years	Abundance of proteins (number of peptides)	Significant decrease of collagen concentration over PMI	Pérez-Martínez et al., 2017
	Proteome	MS	20 years	Presence and absence of proteins at different PMI	Loss of proteins over PMI	Prieto-Bonete et al., 2018
			1 year	Abundance of different proteins at different PMI	Decrease in protein amount with PMI	Procopio et al., 2018
Brain	Acethylcholinesterase	Enzyme activity assay	2 days	Change of enzyme activity	Significant increase over PMI	da Fonseca et al., 2019
	Glial fibrillary acidic protein	Immunohistochemistry	21 days	Positive and negative immunostaining	Loss of stainability over PMI, no staining after 14 days	Wehner et al., 2006
	Na+/K+ ATPase	Enzyme activity assay	2 days	Change of enzyme activity	Significant decrease over PMI	da Fonseca et al., 2019
	VEGF	ELISA	5 days	Concentration of protein ng/mL	Increase up to 40 hours and subsequent decrease	Thaik-Oo et al., 2002
Cartilage	Aggrecan	Western blot	6 weeks	Qualitative assessment of band presence/ absence over PMI	Loss of protein over PMI	Bolton et al., 2015
	Collagen	Histology	approx. 40 days	Intensity of histological staining	Significant decrease in staining intensity over PMI	Alibegović et al., 2019
	Proteoglycan	Histology	approx. 40 days	Intensity of histological staining	Significant decrease in staining intensity over PMI	Alibegović et al., 2019
Heart	Catalase	Enzyme activity assay	7 hours	Change of enzyme activity	Significant decrease at 2 hours	Abo El-Noor et al., 2016
	cTnT	Western blot	approx. 8 days	Band intensity, % of intact protein	Significant decrease over PMI, degradation products	Kumar et al., 2016
			approx. 5 days	Band intensity, % of intact protein; migration distance of bands	Significant decrease of band intensity over PMI, degradation products	Kumar et al., 2015
			approx. 10 days	Band intensity, % of intact protein; migration distance of bands	Significant decrease of band intensity over PMI, degradation products	Kumar et al., 2015
			approx. 5 days	Band intensity, % of intact protein; migration distance of bands	Significant decrease of band intensity over PMI, degradation products	Kumar et al., 2015
	Glutathione reductase	Enzyme activity assay	7 hours	Change of enzyme activity	Significant decrease at 2 hours	Abo El-Noor et al., 2016
	Glutathione-S-transferase	Enzyme activity assay	7 hours	Change of enzyme activity	Significant decrease at 3 hours	Abo El-Noor et al., 2016
	Proteome	2D-PAGE	2 days	Spot intensity	Increase and decrease of spot intensity over PMI	Kwak et al., 2017

Table 7.45 (*Continued*) Overview of Reported Post-mortem Protein Changes in Various Organs and Tissues

Tissue	Protein	Method	PMI	Type of study outcome	Main study outcome	Reference
	TnI	Western blot	7 days	Band intensity, % of intact protein	Decrease and fragmentation of protein over PMI	Sabucedo and Furton, 2003
Kidney	AMPKalpha	Western blot	4 days	Band intensity, % of intact protein	Significant decrease/loss of intact protein after 2 days	Lee et al., 2016
	Caspase-3	Immunohistochemistry	4 days	Qualitative assessment of staining intensity	Loss of stainability over PMI, no staining after 4 days	Lee et al., 2016
		Western blot	4 days	Band intensity, % of intact protein	Significant decrease/loss of intact protein after 3 days	Lee et al., 2016
	Catalase	Enzyme activity assay	7 hours	Change of enzyme activity	Significant decrease at 7 hours	Abo El-Noor et al., 2016
	Glutathione reductase	Enzyme activity assay	7 hours	Change of enzyme activity	Significant decrease at 4 hours	Abo El-Noor et al., 2016
	Glutathione-S-transferase	Enzyme activity assay	7 hours	Change of enzyme activity	Significant decrease at 4 hours	Abo El-Noor et al., 2016
			2 days	Change of enzyme activity	Significant increase over PMI	da Fonseca et al., 2019
	Glycogen synthase	Immunohistochemistry	4 days	Qualitative assessment of staining intensity	Loss of stainability over PMI, no staining after 4 days	Lee et al., 2016
		Western blot	4 days	Band intensity, % of intact protein	Significant decrease/loss of intact protein after 2 days	Lee et al., 2016
	Na+/K+ ATPase	Enzyme activity assay	2 days	Change of enzyme activity	Significant increase over PMI	da Fonseca et al., 2019
	VEGF	ELISA	5 days	Concentration of protein ng/mL	Increase up to 20 hours and subsequent decrease	Thaik-Oo et al., 2002
Liver	Proteome	2D-PAGE	2 days	Spot intensity	Increase and decrease of spot intensity over PMI	Kwak et al., 2017
	VEGF	ELISA	5 days	Concentration of protein ng/mL	Increase up to 15 hours and subsequent decrease	Thaik-Oo et al., 2002
Lung	CaMKII	Western blot	4 days	Band intensity, % of intact protein	Increase over PMI	Kang et al., 2003
			4 days	Band intensity, % of intact protein	Significant decrease/loss of intact protein after 48 hours	Poloz et al., 2009
	CnA	Western blot	4 days	Band intensity, % of intact protein	Decrease of CnA-1, increase of CnA-2 over PMI	Kang et al., 2003
	iNOS	Western blot	4 days	Band intensity, % of intact protein	Increase and subsequent decrease over PMI	Kang et al., 2003
	MARCKS	Western blot	4 days	Band intensity, % of intact protein	Decrease over PMI	Kang et al., 2003
			4 days	Band intensity, % of intact protein	Significant decrease of band intensity over PMI	Poloz et al., 2009
	PP2A	Western blot	4 days	Band intensity, % of intact protein	Significant decrease of band intensity over PMI	Poloz et al., 2009
	RAGE	Immunohistochemistry	7 days	Qualitative assessment of staining intensity	Decrease of Immunohistochemistry staining intensity	Cho and Eom, 2019
		Western blot	7 days	Band intensity	Decrease of band intensity over PMI	Cho and Eom, 2019
	VEGF	ELISA	5 days	Concentration of protein ng/mL	Increase up to 20 hours and subsequent decrease	Thaik-Oo et al., 2002
Pancreas	Calcitonin	Immunohistochemistry	22 days	Positive and negative immunostaining	Loss of stainability over PMI, no staining after 8 days	Ortmann et al., 2017
	Glucagon	Immunohistochemistry	21 days	Positive and negative immunostaining	Loss of stainability over PMI, no staining after 13 days	Wehner et al., 2001

(*Continued*)

Table 7.45 (*Continued*) Overview of Reported Post-mortem Protein Changes in Various Organs and Tissues

Tissue	Protein	Method	PMI	Type of study outcome	Main study outcome	Reference
			22 days	Positive and negative immunostaining	Loss of stainability over PMI, no staining after 12 days	Ortmann et al., 2017
	Insulin	Immunohistochemistry	45 days	Positive and negative immunostaining	Loss of stainability over PMI, no staining after 29 days	Wehner et al., 1999
	Somatostatin	Immunohistochemistry	23 days	Positive and negative immunostaining	Loss of stainability over PMI, no staining after 11 days	Wehner et al., 2006
Skeletal muscle	Calpain-1	Casein zymography	2 days	Presence and absence probability of bands patterns with increasing ADD	Degradation products with increasing probability over ADD	Pittner et al., 2016b
	CaMKII	Western blot	4 days	Band intensity, % of intact protein	Stable over investigated PMI	Kang et al., 2003
					Significant decrease/loss of intact protein after 48 hours	Poloz et al., 2009
	Caspase-3	Immunohistochemistry	4 days	Qualitative assessment of staining intensity	Loss of stainability over PMI, no staining after 4 days	Lee et al., 2016
		Western blot	4 days	Band intensity, % of intact protein	Significant decrease over PMI	Lee et al., 2016
	CnA	Western blot	4 days	Band intensity, % of intact protein	Increase and subsequent decrease over PMI	Kang et al., 2003
					Significant decrease of band intensity over PMI, degradation products	Poloz et al., 2009
	cTnT	Western blot	2 days	Presence and absence probability of bands patterns with increasing ADD	Degradation products with increasing probability over ADD	Pittner et al., 2016b
	desmin	Western blot	2 days	Presence and absence probability of bands patterns with increasing ADD	Degradation products with increasing probability over ADD	Pittner et al., 2016b
			4 days	Change of band pattern over PMI	Loss of protein band after 2 days, degradation products after 1 day	Zissler et al., 2018
					Loss of protein band after 5 days, degradation products after 1 day	Choi et al., 2019
	eEF1A2	MS	4 days	Relative abundance	Decrease in relative abundance over PMI	Choi et al., 2019
		Western blot	4 days	Change of band pattern over PMI	Loss of protein band after 3 days	Choi et al., 2019
	GAPDH	MS	4 days	Relative abundance	Decrease in relative abundance over PMI	Choi et al., 2019
	Glycogen synthase	Immunohistochemistry	4 days	Qualitative assessment of staining intensity	Loss of stainability over PMI, no staining after 2 days	Lee et al., 2016
		Western blot	4 days	Band intensity, % of intact protein	Significant decrease/loss of intact protein after 2 days	Lee et al., 2016
	GSK-3beta	Western blot	4 days	Band intensity, % of intact protein	Significant decrease/loss of intact protein after 2 days	Lee et al., 2016
	Meta-vinculin	Western blot	4 days	Change of band pattern over PMI	Loss of protein band after 2 days	Zissler et al., 2018
					Loss of protein band after 3 days	Choi et al., 2019

Table 7.45 (*Continued*) Overview of Reported Post-mortem Protein Changes in Various Organs and Tissues

Tissue	Protein	Method	PMI	Type of study outcome	Main study outcome	Reference
	PP2A	Western blot	4 days	Band intensity, % of intact protein	Significant decrease of band intensity over PMI	Poloz et al., 2009
	PPAR-y	Western blot	4 days	Band intensity, % of intact protein	Significant decrease over PMI	Lee et al., 2016
	Proteome	MS	6 days	Signal strength of peptide/protein peaks	Decrease of signal strength over PMI	Li et al., 2017
	Vinculin	Western blot	4 days	Change of band pattern over PMI	Degradation products after 1 day	Zissler et al., 2018
					Degradation products after 1 day	Choi et al., 2019
	Capain-1	Casein zymography	10 days	PMI of band pattern change (+95% confidence interval)	Significant decrease/loss of intact protein after 91 hours, degradation products after 17 hours	Pittner et al., 2016
	Calpain-2	Casein zymography	10 days	PMI of band pattern change (+ 95% confidence interval)	Significant decrease/loss of intact protein after 180 hours, degradation products after 63 hours	Pittner et al., 2016
	cTNT	Western blot	10 days	PMI of band pattern change (+ 95% confidence interval)	Degradation products after 90 hours	Pittner et al., 2016
	Desmin	Western blot	21 days	Qualitative assessment of band intensity	Appearance of degradation products over PMI	Foditsch et al., 2016
			10 days	PMI of band pattern change (+ 95% confidence interval)	Degradation products after 22 hours	Pittner et al., 2016
	Nebulin	SDS-PAGE	21 days	Qualitative assessment of band intensity	Appearance of degradation products over PMI	Foditsch et al., 2016
			10 days	PMI of band pattern change (+ 95% confidence interval)	Significant decrease/loss of intact protein after 65 hours	Pittner et al., 2016
	SERCA-1	Western blot	21 days	Qualitative assessment of band intensity	Appearance of degradation products over PMI	Foditsch et al., 2016
			10 days	PMI of band pattern change (+ 95% confidence interval)	Degradation products after 138 hours	Pittner et al., 2016
	SERCA-2	Western blot	21 days	Qualitative assessment of band intensity	Decrease of band intensity over PMI	Foditsch et al., 2016
	Titin	SDS-PAGE	21 days	Qualitative assessment of band intensity	Appearance of degradation products over PMI	Foditsch et al., 2016
			10 days	PMI of band pattern change (+ 95% confidence interval)	Significant decrease/loss of intact protein after 18 hours, degradation products after 9 hours	Pittner et al., 2016
	Troponin T-C	Western blot	21 days	Qualitative assessment of band intensity	Decrease of band intensity over PMI	Foditsch et al., 2016
	μ-Calpain	Western blot	21 days	Qualitative assessment of band intensity	Appearance of degradation products over PMI	Foditsch et al., 2016
Thyroid gland	Calcitonin	Immunohistochemistry	21 days	Positive and negative immunostaining	Loss of stainability over PMI, no staining after 12 days	Wehner et al., 2001
	Insulin	Immunohistochemistry	22 days	Positive and negative immunostaining	Loss of stainability over PMI, no staining after 18 days	Ortmann et al., 2017
	Thyroglobin	Immunohistochemistry	21 days	Positive and negative immunostaining	Loss of stainability over PMI, no staining after 12 days	Wehner et al., 2000
			22 days	Positive and negative immunostaining	Loss of stainability over PMI, no staining after 8 days	Ortmann et al., 2017

found in endosteal and/or periosteal regions compared to mesosteal regions of long bones [41]. It remains to be investigated whether this phenomenon is organ specific and may decrease in more homogenous organs such as skeletal muscle. This is indicated by similar protein degradation rates at central and distal regions of the human thigh muscle *M. vastus lateralis* [59].

In tissues distributed throughout the body (e.g. bone), differences in protein degradation rates of samples dissected from different regions (e.g. femur versus humerus) must be taken into account. For example, a forelimb versus hindlimb divergence was found in collagen degradation rates of humeral and in femoral bone [41], reflecting the different amounts of cortical and cancellous bone in these skeletal elements. Likewise, degradation rates were shown to be non-simultaneous in different muscles of the human body [59]. Fibre-type composition, pH, and temperature effects (location at the surface or in the body centre) are reported as possible influencing factors [59–62].

7.6.4.2 Influencing Factors

Besides the variations due to biochemical tissue characteristics described earlier, there is a wide array of influencing factors, modifying the regular fashion of successive degradation stages and in turn protein degradation dynamics [47,63]. These factors can be intrinsic (body mass and surface area, but also age, sex, ante-mortem medical conditions, presence of injuries/trauma, level of bacterial activity, etc.), extrinsic (environmental conditions at the death scene, e.g. temperature, moisture, intensity of air flow, depth of burial, and activity of insects and microorganism) and related to the circumstances of death (cause of death, presence and type of clothing and other insulation of the body, etc.) [47–50,64]. In this context, a number of studies were conducted to investigate whether several influencing factors can affect protein degradation [63]. Results demonstrated that the vast majority of analysed factors modified degradation dynamics in the respective study settings. While temperature is probably the most popular and important influencing factor, accelerating and decelerating degradation processes in warm and cold environments respectively, also body mass, sex, age, cause of death, exposure and insect activity were found to alter degradation processes [11,18,27,30,32,43,46,65,66]. Only the presence of microorganisms did not affect the degradation of long bones [42]. However, it cannot be excluded that external microorganisms may contribute to post-mortem protein degradation in other organs, for example pathogens present in aspirated material invading the respiratory tract; all the more germs can easily enter these tissues in the absence of a functioning bronchobiliary barrier [56]. In general, caution is advised with tissues displaying openings to the outside and superficial tissues, as they, moreover, may be more affected by insect infestation, leading, on the one hand, to loss of sample material and, on the other hand, to accelerated degradation by enzymes released from these necrophagous insects [8].

Similarly, intrinsic factors and factors related to the circumstances of death such as body weight and cause of death (as well as ante-mortem medical condition) can have fatal or mild impact on different organs. For instance, obesity and underweight can modify cooling conditions of the corpse and in turn alter protein degradation rates especially in organs located in the body core [63,67]. Acute myocardial infarction, for example, leads to a detection loss of cardiac troponin T in cardiac tissue [68,69], severely falsifying PMI estimation [65] and supporting a heterogenous susceptibility of individual protein isoforms to influences exerted by death-causing processes. All these examples highlight the complexity of protein degradation dynamics and a strong need for the establishment of appropriate inclusion and exclusion criteria as well as for future studies in this field.

7.6.4.3 Routine Applicability

Priority in the selection of the target tissue should be given to availability and accessibility to enable a sensible, reproducible sampling procedure. Compared to confined organs (heart, kidney, etc.) especially tissues of the musculoskeletal system (bone, cartilage, and skeletal muscle) are distributed all over the human body and sampling can even be facilitated in cases with (substantial) ante-mortem and/or peri-mortem injuries, as well as extensive insect activity, or even in dismembered body parts. Regarding practical application, the sampling procedure in field cases should be quick and easy. Although samples of most tissues can routinely be harvested in course of an autopsy, sampling of internal organs in field cases can be extremely difficult, or impractical at least. Again, tissues of the musculoskeletal system have the advantage to be harvested with fewer expense and less invasive interventions. Especially skeletal muscle can easily be sampled without specialized equipment (e.g. bone saw) and long-lasting training of the mandated person. Indeed, skeletal muscle is found to be the most investigated tissue regarding post-mortem protein degradation-based PMI estimation in forensic research [14].

To enable routine applicability of a future PMI estimation method based on protein degradation, the ability to produce results and issue statements regarding the time since death directly at the crime scene can be a decisive factor. With their attempt to develop a simple test for the presence of a specific marker protein in rat post-mortem kidney, Lee et al. [22] provided a valuable basis for the development of a simple-to-use device to estimate the PMI directly at the scene of crime. A lateral flow assay is a paper-based platform for the detection of analytes in complex mixtures, where the sample is directly placed on the test device and the results are displayed within minutes [70]. For the development of such a device, however,

Table 7.46 Properties of Different Body Tissues to Consider as a Target for Protein-based PMI Estimation

	Internal influences (BMI, bacteria)	External influences (bacteria, insects)	Tissue mass/ tissue distribution	Accessibility (field application)
Bone	Low	Low	Moderate/all over body	Moderate
Brain	Low	Low	Low/restricted	Poor
Cartilage	Low	Low	Moderate/all over body	Moderate
Heart	High	Low	Low/restricted	Poor
Kidney	High	Low	Low/restricted	Poor
Liver	High	Low	Low/restricted	Moderate
Lung	High	High	Low/restricted	Poor
Skeletal muscle	Moderate (depending on location)	Moderate (depending on location)	High/all over body	Good
Pancreas	High	Low	Low/restricted	Poor
Thyroid gland	High	Moderate	Low/restricted	Poor

intensive research is required to present the groundwork for a technology that would withstand as valid method for PMI delimitation.

Once the target samples are harvested, a useful practical method can rely on the analysis of a set of multiple proteins with different susceptibility to post-mortem proteolysis within this specific tissue (e.g. a set of predefined proteins), selected depending on the PMI to be examined. To broaden the spectrum of proteins, identification of new markers can be facilitated in an appropriate time frame by profiling the post-mortem proteome using mass spectrometry [34]. Once suitable marker proteins are selected, statistically significant correlations between distinct degradation events and post-mortem time have to be validated and further evaluated, also in context with potential influencing factors. To generate reliable reference data, rigorous protein concentration thresholds should be used to decide about presence and absence of proteins and degradation products. The commercial availability and comparatively cheap purchase of specific antibodies generally plead for their usage in the laboratory (e.g. Western blot analysis) and in field application devices. The additional production of antibodies labelled against specific degradation products of marker proteins can further improve the precision of Western blot analysis or LFA-based quick tests. With multiple test lines to allow rapid and simultaneous detection of several analytes in a sample [70], a resulting specific protein degradation profile, in context with a reliable reference database, can produce valuable evidence to estimate the PMI.

7.6.4.4 Why It Is Difficult for a Method to Be Incorporated into Practice

In forensic research, it seems comparably easy to investigate potential PMI markers in model scenarios and to describe a PMI-correlated change as a ‘novel approach for time since death estimation’. As a consequence, numerous methods were proposed in recent years aiming to supplement and/or substitute existing methods for PMI estimation. But in fact, only a fraction of these methods (will) advance from basic research to practical routine use.

A new method requires certain properties: it should be easy and fast in handling and cost-effective, but at the same time precise and reliable. To accomplish these qualities, however, substantial effort on behalf of time and resources is necessary, as it requires more than the knowledge of a correlation between a measured marker and the PMI. Keeping the use case for forensic PMI estimation in mind, which is most often a corpse, discovered after an unknown time of death, usually without (ante-mortem) baseline measurements, a single measured value (e.g. marker protein concentration) would hardly be diagnostically conclusive. For actual application extensive research is required to develop standard procedures, define rigorous PMI marker criteria (e.g. concentration thresholds), calculate confidence intervals, investigate potential limitations (e.g. exclusion criteria) and influencing factors, all that on representative study populations.

Today, no approach using protein degradation-based PMI estimation is regularly applied in forensic routine. Based on the results of a systematic review [14], however, Western blotting has a sufficient evidence base, soon to be used in routine practice.

7.6.5 An Attempt for Practical Application

Western blot analysis of skeletal muscle tissue is the most extensively researched approach to apply post-mortem protein degradation for PMI estimation [14]. The Western blot method detects specific proteins form a sample of homogenized tissue. For this purpose, the proteins are separated by size (gel-electrophoreses), transferred to a solid membrane and detected by antibody labelling. Numerous laboratories around the word have methodical expertise for practical application, and sample preparation and processing are manageable with little equipment. Furthermore, storage of the samples is possible if done correctly. The method is relatively quick, with results available within a day (protein degradation profile of an individual corpse).

7.6.5.1 A Standard Protocol for the Collection and Storage of (Skeletal Muscle) Tissue Samples

The following protocol is derived from a study, specifically addressing process optimization and considerations for the application in forensic PMI estimation of post-mortem protein degradation [71].

1. *In course of an autopsy/at a crime scene/at a field experiment*
   a. Sample collection via muscle biopsy (optional): make a small incision opening skin, fatty tissue and muscle fascia, use a 5 mm diameter biopsy needle and excise muscle samples from the central muscle belly.
      Sample collection using a scalpel (optional): make a 2 cm incision opening skin, fat tissue and muscle fascia, dissect 5°×°5°×°5 mm samples (approximately 100 mg).
   b. Cut the dissected 100 mg sample into smaller pieces (<1 mm in one direction). This is done to enlarge the surface area and improve buffer infiltration.
   c. Transfer the sample into a vial containing 1 mL of extraction/lysis buffer (containing a protease inhibitor cocktail). Make sure that the sample is completely immersed. Incubate for 30 minutes at room temperature to allow buffer infiltration.
   d. Store the sample at −20°C.
2. *In a biochemistry or forensic laboratory*
   e. Sample homogenization: Thaw the sample. Disrupt the tissue using a tissue disperser. Secondary homogenization/cell lysis is recommended using ultrasound (ultrasound bath, sonicator probes, vial tweeter, etc.).
   f. Determine overall protein concentration (e.g. bicinchoninic acid assay) and dilute samples to an antibody specific overall protein concentration.
   g. Add SDS-sample buffer and denature the samples at 90°C for 5 minutes.
   h. Run SDS-PAGE to separate the proteins.
   i. Transfer the proteins from the gels to a blotting membrane (nitrocellulose or PVDF).
   j. Block the membranes in a buffer (e.g. PBS or TBS) containing a blocking agent (e.g. dry milk or BSA).
   k. Apply primary antibody in product specific dilution (in blocking buffer) and wash in PBS or TBS.
   l. Apply secondary antibody (e.g. HRP-conjugated) in product specific dilution (in blocking buffer) and wash in PBS or TBS.
   m. Visualize antibody binding by application of chemiluminescence substrate and analyse blot using a digital gel documentation system.

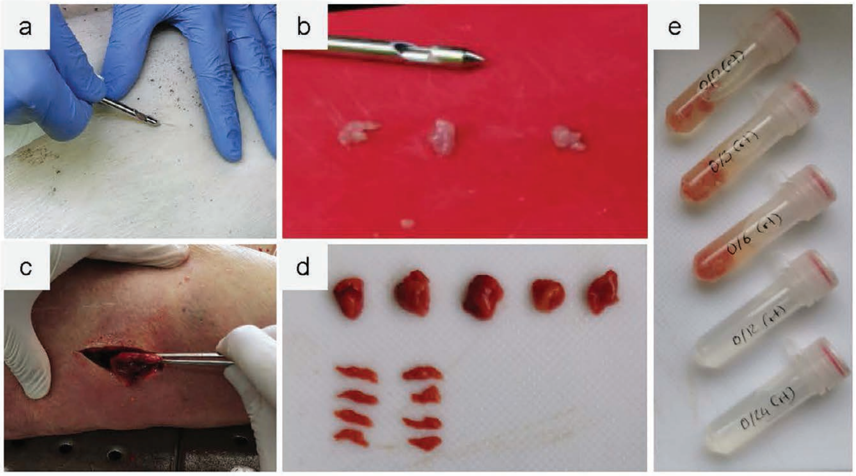

Figure 7.75 Sample collection (skeletal muscle) for protein analysis. (a) Muscle biopsy during a field experiment (on pigs). (b) Muscle biopsy samples. (c) Collection of skeletal muscle during autopsy. (d) Preparation of muscle samples (smaller pieces enable better buffer infiltration). (e) Samples in extraction/lysis buffer, ready to be frozen.

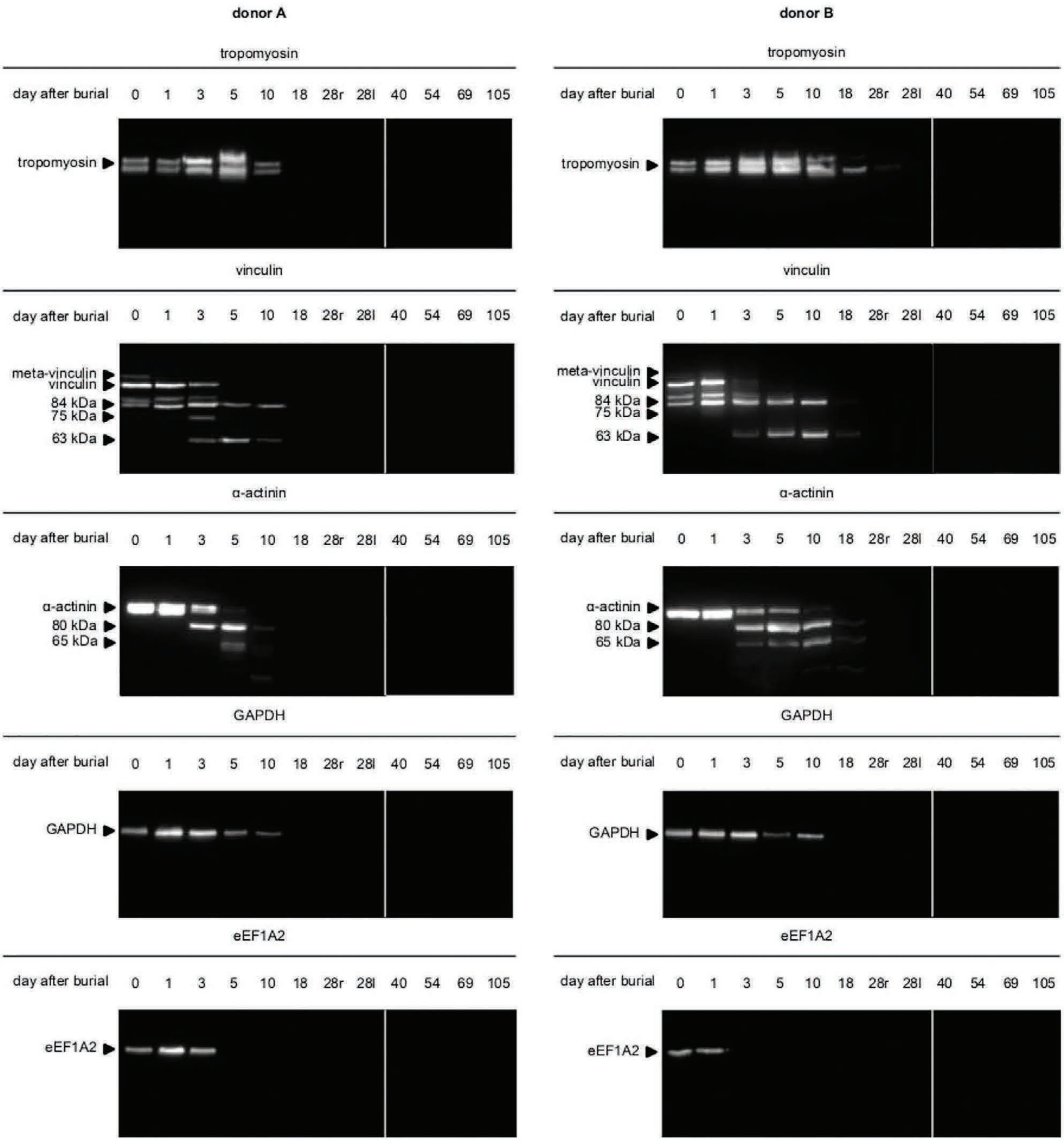

Figure 7.76 Representative protein degradation patterns obtained using the described standard procedure. Post-mortem muscle biopsy samples were collected from two body donors buried at the *Amsterdam Research Initiative for Sub-surface Taphonomy and Anthropology (ARISTA)* over a time period of 105 days. From day 0–28, samples were collected from the right thigh, from day 28–105 from the left thigh (hence two samples from day 28).

(Figure from Pittner et al. 2020 [72].)

7.6.5.2 Post-mortem Protein Degradation Profiles

A post-mortem protein profile summarizes degradation events of a variety of predefined proteins or protein fragments (degradation products) deriving from tissue samples collected from a forensic case. This profile can then be compared to a pre-established database to estimate the PMI. Knowledge and consideration of the precise timeframes in which degradation changes occur (eventually considering influencing factors) can facilitate the selection of appropriate marker proteins. Proteins for individual investigations may then be selected depending on the PMI range to be examined.

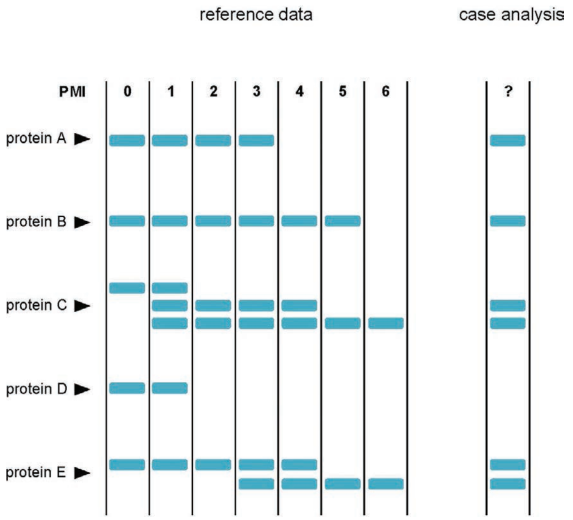

Figure 7.77 Hypothetical protein degradation patterns over the course of the post-mortem interval (PMI). Reference data depicts time-dependent changes of protein profiles, i.e. loss of a native band (proteins 1–5), or appearance of degradation products (proteins 2 and 3). These patterns allow comparison with protein profiles from cases with unknown PMI.

7.6.5.3 Case Report

The dismembered body of a 72-year-old woman was found deposited at the waterside of an Austrian lake (water temperature approximately 4°C). Torso and limbs were separately stored in large suitcases. Police divers found the head, casted into a concrete block at the bottom of the lake, together with a second corpse of a 73-year-old man in close vicinity. Bags filled with stones were tied around his wrists. None of the available methods to estimate the time of death could be applied for the woman. The body temperature was adjusted to environmental temperature. The corpse displayed no rigor mortis and livor mortis development. No macroscopic colonization of necrotrophic organisms was found. Also, the man's body was adjusted to ambient temperature and strong, complete rigor mortis was developed. The corpse displayed distinctive lividity, completely disappearing on thumb pressure. Except from wrinkling of the skin in the male, both corpses did not exhibit any water-induced morphologic changes enabling minimum PMSI determination. At autopsy, drowning was confirmed to be the cause of death of the male. In the female corpse, retroauricular and frontal petechiae were indicative for strangulation. Alike and similarly digested content of the stomach depicted weak indication for simultaneous deaths. However, from a medical examiner's point of view, there was no prospect to trace the progression of events.

Skeletal muscle protein degradation analysis revealed a substantially differing degradation profile of the two individuals. While desmin, cardiac troponin T (cTnT) and calpain analyses of the male corpse resulted in a 'native protein pattern', characteristic degradation products were detected in the woman's muscle tissue sample. The estimated ADD (a measure for elapsed time and mean environmental temperature) for both individuals differed by

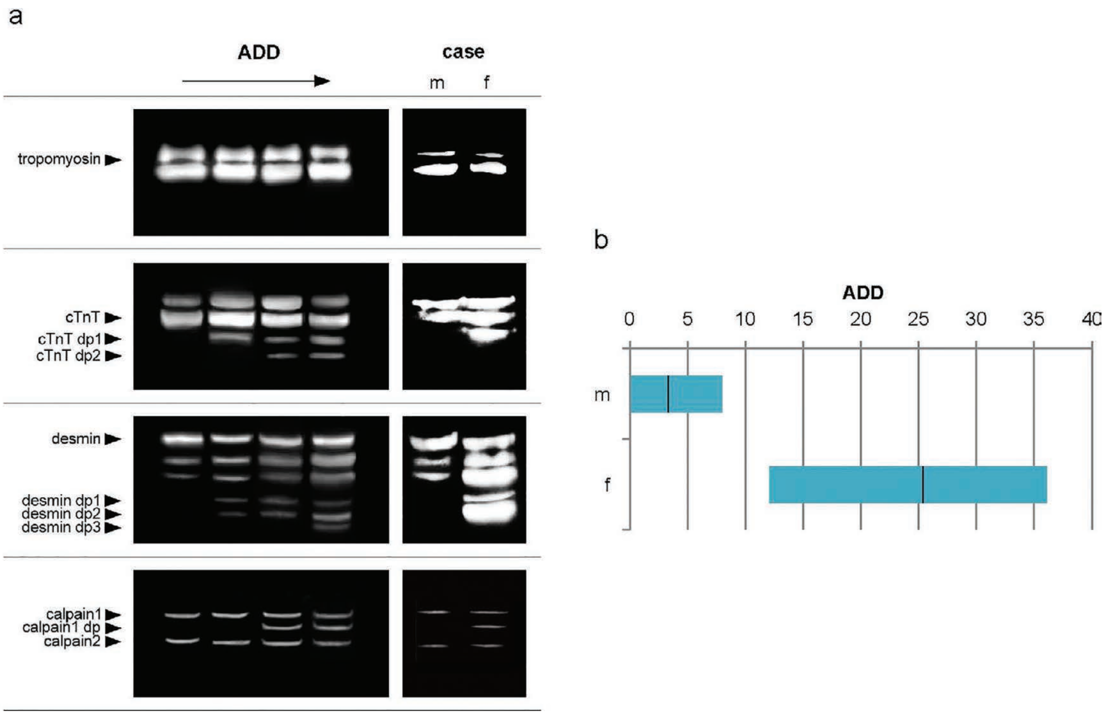

Figure 7.78 (a) Degradation patterns of selected proteins at increasing ADD (PMI × Temperature), collected from reference cases, as well as from the two forensic cases (m = male, f = female). (b) Estimation of the ADD and 95% confidence intervals of the two cases.

(Figure adapted from Pittner et al. 2016 [15].)

22.1 °d, based on a logistic model, including 51 previous cases. Furthermore, including 95% confidence intervals, the ADD of the female individual was at least 4.2 °d more than the male's ADD, providing mathematical evidence for the succession of the crime. Non-biomedical findings in the couple's house indicated domestic violence and confirmed the succession of the events. The man strangled and dismembered his wife, packed the body parts into suitcases and after a 6-hour drive, he arrived at the scene and deposited the remains. A taxi driver confirmed to have driven him to the scene 3 days later (at the night before the finding and autopsy) [15].

References

1. Peregrín-Alvarez, J.M.; Sanford, C.; Parkinson, J. The Conservation and Evolutionary Modularity of Metabolism. *Genome Biol.* **2009**, *10*, R63, http://doi.org/10.1186/gb-2009-10-6-r63.
2. Varshavsky, A. Proteolysis. In *Encyclopedia of Genetics*; Brenner, S., Miller, J.H., Eds.; Academic Press: New York, 2001; pp. 1573–5. ISBN 978-0-12-227080-2.
3. Lecker, S.H.; Goldberg, A.L.; Mitch, W.E. Protein Degradation by the Ubiquitin–Proteasome Pathway in Normal and Disease States. *J. Am. Soc. Nephrol.* **2006**, *17*, 1807–19, http://doi.org/10.1681/ASN.2006010083.
4. Sorimachi, Y.; Harada, K.; Yoshida, K. Involvement of Calpain in Postmortem Proteolysis in the Rat Brain. *Forensic Sci. Int.* **1996**, *81*, 165–74, http://doi.org/10.1016/S0379-0738(96)01981-0.
5. Lonergan, E. The Relationship between the Calpain Enzyme System and the Postmortem Degradation of Selected Myofibrillar Proteins. *Retrosp. Theses Diss.* **1995**.
6. Wendt, A.; Thompson, V.F.; Goll, D.E. Interaction of Calpastatin with Calpain: A Review. *Biol. Chem.* **2004**, *385*, 465–72, http://doi.org/10.1515/BC.2004.054.
7. Ji, J.-R.; Takahashi, K. Changes in Concentration of Sarcoplasmic Free Calcium during Post-Mortem Ageing of Meat. *Meat Sci.* **2006**, *73*, 395–403, http://doi.org/10.1016/j.meatsci.2005.09.010.
8. Aufderheide, A.C. *The Scientific Study of Mummies*; Cambridge University Press: Cambridge, 2003; ISBN 978-0-521-81826-1.
9. Wang, Z.; Shen, W.; Kotler, D.P.; Heshka, S.; Wielopolski, L.; Aloia, J.F.; Nelson, M.E.; Pierson, R.N.; Heymsfield, S.B. Total Body Protein: A New Cellular Level Mass and Distribution Prediction Model. *Am. J. Clin. Nutr.* **2003**, *78*, 979–84, http://doi.org/10.1093/ajcn/78.5.979.
10. Pittner, S.; Monticelli, F.C.; Pfisterer, A.; Zissler, A.; Sänger, A.M.; Stoiber, W.; Steinbacher, P. Postmortem Degradation of Skeletal Muscle Proteins: A Novel Approach to Determine the Time since Death. *Int. J. Legal Med.* **2016**, *130*, 421–31, http://doi.org/10.1007/s00414-015-1210-6.
11. Poloz, Y.O.; O'Day, D.H. Determining Time of Death: Temperature-Dependent Postmortem Changes in Calcineurin A, MARCKS, CaMKII, and Protein Phosphatase 2A in Mouse. *Int. J. Legal Med.* **2009**, *123*, 305–14, http://doi.org/10.1007/s00414-009-0343-x.
12. Prieto-Bonete, G.; Pérez-Cárceles, M.D.; Maurandi-López, A.; Pérez-Martínez, C.; Luna, A. Association between Protein Profile and Postmortem Interval in Human Bone Remains. *J. Proteomics.* **2018**, 192, 54–63, http://doi.org/10.1016/j.jprot.2018.08.008.
13. Madea, B. Methods for Determining Time of Death. *Forensic Sci. Med. Pathol.* **2016**, *12*, 451–85, http://doi.org/10.1007/s12024-016-9776-y.
14. Zissler, A.; Stoiber, W.; Steinbacher, P.; Geissenberger, J.; Monticelli, F.C.; Pittner, S. Postmortem Protein Degradation as a Tool to Estimate the PMI: A Systematic Review. *Diagn. Basel Switz.* **2020**, *10*, E1014, http://doi.org/10.3390/diagnostics10121014.
15. Pittner, S.; Ehrenfellner, B.; Zissler, A.; Racher, V.; Trutschnig, W.; Bathke, A.C.; Sänger, A.M.; Stoiber, W.; Steinbacher, P.; Monticelli, F.C. First Application of a Protein-Based Approach for Time since Death Estimation. *Int. J. Legal Med.* **2017**, *131*, 479–83, http://doi.org/10.1007/s00414-016-1459-4.
16. Wehner, F.; Wehner, H.-D.; Schieffer, M.C.; Subke, J. Delimitation of the Time of Death by Immunohistochemical Detection of Insulin in Pancreatic β-Cells. *Forensic Sci. Int.* **1999**, *105*, 161–9, http://doi.org/10.1016/S0379-0738(99)00124-3.
17. Wehner, F.; Wehner, H.-D.; Subke, J. Delimitation of the Time of Death by Immunohistochemical Detection of Glucagon in Pancreatic α-Cells. *Forensic Sci. Int.* **2001**, *124*, 192–9, http://doi.org/10.1016/S0379-0738(01)00608-9.
18. Wehner, F.; Steinriede, A.; Martin, D.; Wehner, H.-D. Two-Tailed Delimitation of the Time of Death by Immunohistochemical Detection of Somatostatin and GFAP. *Forensic Sci. Med. Pathol.* **2006**, *2*, 241–7, http://doi.org/10.1385/FSMP:2:4:241.
19. Wehner, F.; Wehner, H.-D.; Schieffer, M.C.; Subke, J. Delimitation of the Time of Death by Immunohistochemical Detection of Thyroglobulin. *Forensic Sci. Int.* **2000**, *110*, 199–206, http://doi.org/10.1016/S0379-0738(00)00177-8.
20. Wehner, F.; Wehner, H.-D.; Subke, J. Delimitation of the Time of Death by Immunohistochemical Detection of Calcitonin. *Forensic Sci. Int.* **2001**, *122*, 89–94, http://doi.org/10.1016/S0379-0738(01)00467-4.
21. Ortmann, J.; Doberentz, E.; Madea, B. Immunohistochemical Methods as an Aid in Estimating the Time since Death. *Forensic Sci. Int.* **2017**, *273*, 71–9, http://doi.org/10.1016/j.forsciint.2017.02.004.
22. Lee, D.-G.; Yang, K.E.; Hwang, J.W.; Kang, H.-S.; Lee, S.-Y.; Choi, S.; Shin, J.; Jang, I.-S.; An, H.J.; Chung, H.; et al. Degradation of Kidney and Psoas Muscle Proteins as Indicators of Post-Mortem Interval in a Rat Model, with Use of Lateral Flow Technology. *PLoS ONE* **2016**, *11*, e0160557, http://doi.org/10.1371/journal.pone.0160557.
23. Sabucedo, A.J.; Furton, K.G. Estimation of Postmortem Interval Using the Protein Marker Cardiac Troponin I. *Forensic Sci. Int.* **2003**, *134*, 11–16.
24. Kang, S.; Kassam, N.; Gauthier, M.L.; O'Day, D.H. Post-Mortem Changes in Calmodulin Binding Proteins in Muscle and Lung. *Forensic Sci. Int.* **2003**, *131*, 140–7, http://doi.org/10.1016/S0379-0738(02)00426-7.
25. Kumar, S.; Ali, W.; Singh, U.S.; Verma, A.K.; Bhattacharya, S.; Kumar, A.; Singh, R.; Rupani, R. Time-Dependent Degradation Pattern of Cardiac Troponin T in Cases of Death by Burn. *West Indian Med. J.* **2015**, *64*, 226–9, http://doi.org/10.7727/wimj.2014.232.
26. Kumar, S.; Ali, W.; Bhattacharya, S.; Singh, U.S.; Kumar, A.; Verma, A.K. The Effect of Elapsed Time on Cardiac Troponin-T (CTnT) Degradation and Its Relation to Postmortem Interval in Cases of Electrocution. *J. Forensic Leg. Med.* **2015**, *34*, 45–9, http://doi.org/10.1016/j.jflm.2015.05.009.

27. Kumar, S.; Ali, W.; Singh, U.S.; Kumar, A.; Bhattacharya, S.; Verma, A.K.; Rupani, R. Temperature-Dependent Postmortem Changes in Human Cardiac Troponin-T (CTnT): An Approach in Estimation of Time Since Death. *J. Forensic Sci*. **2016**, *61*, S241–5, http://doi.org/10.1111/1556-4029.12928.
28. Kumar, S.; Ali, W.; Singh, U.S.; Kumar, A.; Bhattacharya, S.; Verma, A.K. The Effect of Elapsed Time on the Cardiac Troponin-T (CTnT) Proteolysis in Case of Death Due to Burn: A Study to Evaluate the Potential Forensic Use of CTnT to Determine the Postmortem Interval. *Sci. Justice* **2015**, *55*, 189–94, http://doi.org/10.1016/j.scijus.2014.12.006.
29. Bolton, S.N.; Whitehead, M.P.; Dudhia, J.; Baldwin, T.C.; Sutton, R. Investigating the Postmortem Molecular Biology of Cartilage and Its Potential Forensic Applications. *J. Forensic Sci*. **2015**, *60*, 1061–7, http://doi.org/10.1111/1556-4029.12764.
30. Foditsch, E.E.; Saenger, A.M.; Monticelli, F.C. Skeletal Muscle Proteins: A New Approach to Delimitate the Time since Death. *Int. J. Legal Med*. **2016**, *130*, 433–40, http://doi.org/10.1007/s00414-015-1204-4.
31. Cho, H.-W.; Eom, Y.-B. Potential Forensic Application of Receptor for Advanced Glycation End Products (RAGE) as a Novel Biomarker for Estimating Postmortem Interval. *J. Forensic Sci*. **2019**, *64*, 1878–83, http://doi.org/10.1111/1556-4029.14063.
32. Pittner, S.; Ehrenfellner, B.; Monticelli, F.C.; Zissler, A.; Sänger, A.M.; Stoiber, W.; Steinbacher, P. Postmortem Muscle Protein Degradation in Humans as a Tool for PMI Delimitation. *Int. J. Legal Med*. **2016**, *130*(6), 1547–55, http://doi.org/10.1007/s00414-016-1349-9.
33. Zissler, A.; Ehrenfellner, B.; Foditsch, E.E.; Monticelli, F.C.; Pittner, S. Does Altered Protein Metabolism Interfere with Postmortem Degradation Analysis for PMI Estimation? *Int. J. Legal Med*. **2018**, *132*(5), 1349–56, http://doi.org/10.1007/s00414-018-1814-8.
34. Choi, K.-M.; Zissler, A.; Kim, E.; Ehrenfellner, B.; Cho, E.; Lee, S.; Steinbacher, P.; Yun, K.N.; Shin, J.H.; Kim, J.Y.; et al. Postmortem Proteomics to Discover Biomarkers for Forensic PMI Estimation. *Int. J. Legal Med*. **2019**, *133*, 899–908, http://doi.org/10.1007/s00414-019-02011-6.
35. Kwak, J.-H.; Kim, H.K.; Kim, K.; Noh, B.R.; Cheon, H.I.; Yeo, M.; Shakya, R.; Shrestha, S.A.; Kim, D.; Choe, S.; et al. Proteomic Evaluation of Biomarkers to Determine the Postmortem Interval. *Anal. Lett*. **2017**, *50*, 207–18, http://doi.org/10.1080/00032719.2016.1172080.
36. Li, C.; Li, Z.; Tuo, Y.; Ma, D.; Shi, Y.; Zhang, Q.; Zhuo, X.; Deng, K.; Chen, Y.; Wang, Z.; et al. MALDI-TOF MS as a Novel Tool for the Estimation of Postmortem Interval in Liver Tissue Samples. *Sci. Rep*. **2017**, *7*, 4887, http://doi.org/10.1038/s41598-017-05216-0.
37. Li, C.; Ma, D.; Deng, K.; Chen, Y.; Huang, P.; Wang, Z. Application of MALDI-TOF MS for Estimating the Postmortem Interval in Rat Muscle Samples. *J. Forensic Sci*. **2017**, *62*, 1345–50, http://doi.org/10.1111/1556-4029.13413.
38. Pérez-Martínez, C.; Pérez-Cárceles, M.D.; Legaz, I.; Prieto-Bonete, G.; Luna, A. Quantification of Nitrogenous Bases, DNA and Collagen Type I for the Estimation of the Postmortem Interval in Bone Remains. *Forensic Sci. Int*. **2017**, *281*, 106–12, http://doi.org/10.1016/j.forsciint.2017.10.039.
39. Procopio, N.; Williams, A.; Chamberlain, A.T.; Buckley, M. Forensic Proteomics for the Evaluation of the Post-Mortem Decay in Bones. *J. Proteomics* **2018**, *177*, 21–30, http://doi.org/10.1016/j.jprot.2018.01.016.
40. Thaik-Oo, M.; Tanaka, E.; Tsuchiya, T.; Kominato, Y.; Honda, K.; Yamazaki, K.; Misawa, S. Estimation of Postmortem Interval from Hypoxic Inducible Levels of Vascular Endothelial Growth Factor. *J. Forensic Sci*. **2002**, *47*, 186–9.
41. Boaks, A.; Siwek, D.; Mortazavi, F. The Temporal Degradation of Bone Collagen: A Histochemical Approach. *Forensic Sci. Int*. **2014**, *240*, 104–10, http://doi.org/10.1016/j.forsciint.2014.04.008.
42. Jellinghaus, K.; Hachmann, C.; Höland, K.; Bohnert, M.; Wittwer-Backofen, U. Collagen Degradation as a Possibility to Determine the Post-Mortem Interval (PMI) of Animal Bones: A Validation Study Referring to an Original Study of Boaks et al. (2014). *Int. J. Legal Med*. **2018**, *132*, 753–63, http://doi.org/10.1007/s00414-017-1747-7.
43. Jellinghaus, K.; Urban, P.K.; Hachmann, C.; Bohnert, M.; Hotz, G.; Rosendahl, W.; Wittwer-Backofen, U. Collagen Degradation as a Possibility to Determine the Post-Mortem Interval (PMI) of Human Bones in a Forensic Context—A Survey. *Leg. Med*. **2019**, *36*, 96–102, http://doi.org/10.1016/j.legalmed.2018.11.009.
44. Abo El-Noor, M.M.; Elhosary, N.M.; Khedr, N.F.; El-Desouky, K.I. Estimation of Early Postmortem Interval Through Biochemical and Pathological Changes in Rat Heart and Kidney. *Am. J. Forensic Med. Pathol*. **2016**, *37*, 40–6, http://doi.org/10.1097/PAF.0000000000000214.
45. da Fonseca, C.A.R.; Paltian, J.; dos Reis, A.S.; Bortolatto, C.F.; Wilhelm, E.A.; Luchese, C. Na+/K+-ATPase, Acetylcholinesterase and Glutathione S-Transferase Activities as New Markers of Postmortem Interval in Swiss Mice. *Leg. Med*. **2019**, *36*, 67–72, http://doi.org/10.1016/j.legalmed.2018.11.003.
46. Alibegović, A.; Blagus, R.; Martinez, I.Z. Safranin O without Fast Green Is the Best Staining Method for Testing the Degradation of Macromolecules in a Cartilage Extracellular Matrix for the Determination of the Postmortem Interval. *Forensic Sci. Med. Pathol*. **2019**, *16*(2), 252–8, http://doi.org/10.1007/s12024-019-00208-0.
47. Campobasso, C.P.; Di Vella, G.; Introna, F. Factors Affecting Decomposition and Diptera Colonization. *Forensic Sci. Int*. **2001**, *120*, 18–27.
48. Almulhim, A.M.; Menezes, R.G. Evaluation of Postmortem Changes. In *StatPearls*; StatPearls Publishing: Treasure Island, FL, 2020.
49. Zhou, C.; Byard, R.W. Factors and Processes Causing Accelerated Decomposition in Human Cadavers—An Overview. *J. Forensic Leg. Med*. **2011**, *18*, 6–9, http://doi.org/10.1016/j.jflm.2010.10.003.
50. Henssge, C. Death Time Estimation in Case Work. I. The Rectal Temperature Time of Death Nomogram. *Forensic Sci. Int*. **1988**, *38*, 209–36, http://doi.org/10.1016/0379-0738(88)90168-5.
51. Dent, B.B.; Forbes, S.L.; Stuart, B.H. Review of Human Decomposition Processes in Soil. *Environ. Geol*. **2004**, *45*, 576–85, http://doi.org/10.1007/s00254-003-0913-z.
52. Sorg, M.H.; Haglund, W.D.; Eds. *Forensic Taphonomy: The Postmortem Fate of Human Remains*; 1 edition.; CRC Press: Boca Raton, 1997; ISBN 978-0-8493-9434-8.
53. Benbow, M.E.; Tomberlin, J.K.; Tarone, A.M. *Carrion Ecology, Evolution, and Their Applications*; CRC Press: Boca Raton, 2015; ISBN 978-1-4665-7547-9.
54. Schotsmans, E.M.J.; Márquez-Grant, N.; Forbes, S.L.; Eds. *Taphonomy of Human Remains: Forensic Analysis of the Dead and the Depositional Environment*; John Wiley & Sons: Hoboken, 2017; ISBN 978-1-118-95332-7.

55. Bonte, W.; Bleifuss, J.; Volck, J. Experimental Investigations in Post-Mortem Protein Degradation. *Forensic Sci*. **1976**, *7*, 9–22, http://doi.org/10.1016/0300-9432(76)90003-0.
56. Gill-King, H. Chemical and Ultrastructural Aspects of Decomposition. In *Forensic Taphon. Postmortem Fate Hum. Remains*; Haglund, W.D., Sorg, M.H., Eds.; CRC Press: Boca Raton, 1997; pp. 93–108.
57. Dettmeyer, R.; Verhoff, M.A.; Schütz, H.F. *Forensic Medicine: Fundamentals and Perspectives*; Springer-Verlag: Berlin, Heidelberg, 2014; ISBN 978-3-642-38817-0.
58. Cocariu, E.A.; Mageriu, V.; Stăniceanu, F.; Bastian, A.; Socoliuc, C.; Zurac, S. Correlations Between the Autolytic Changes and Postmortem Interval in Refrigerated Cadavers. *Romanian J. Intern. Med. Rev. Roum. Med. Interne* **2016**, *54*, 105–12, http://doi.org/10.1515/rjim-2016-0012.
59. Pittner, S.; Gotsmy, W.; Zissler, A.; Ehrenfellner, B.; Baumgartner, D.; Schrüfer, A.; Steinbacher, P.; Monticelli, F. Intra- and Intermuscular Variations of Postmortem Protein Degradation for PMI Estimation. *Int. J. Legal Med*. **2020**, *134*, 1775–82, http://doi.org/10.1007/s00414-020-02355-4.
60. Christensen, M.; Henckel, P.; Purslow, P.P. Effect of Muscle Type on the Rate of Post-Mortem Proteolysis in Pigs. *Meat Sci*. **2004**, *66*, 595–601, http://doi.org/10.1016/S0309-1740(03)00175-X.
61. Tomaszewska-Gras, J.; Schreurs, F.J.G.; Kijowski, J. Post Mortem Development of Meat Quality as Related to Changes in Cytoskeletal Proteins of Chicken Muscles. *Br. Poult. Sci*. **2011**, *52*, 189–201, http://doi.org/10.1080/00071668.2011.561281.
62. Marino, R.; della Malva, A.; Albenzio, M. Proteolytic Changes of Myofibrillar Proteins in Podolian Meat during Aging: Focusing on Tenderness. *J. Anim. Sci*. **2015**, *93*, 1376–87, http://doi.org/10.2527/jas.2014-8351.
63. Zissler, A.; Stoiber, W.; Geissenberger, J.; Steinbacher, P.; Monticelli, F.C.; Pittner, S. Influencing Factors on Postmortem Protein Degradation for PMI Estimation: A Systematic Review. *Diagn. Basel Switz*. **2021**, *11*, 1146, http://doi.org/10.3390/diagnostics11071146.
64. Teo, C.H.; Pawita, A.H.; Khairul, O.; Atiah Ayunni, A.G.; Noor Hazfalinda, H. Post Mortem Changes in Relation to Different Types of Clothing. *Malays. J. Pathol*. **2013**, *35*, 77–85.
65. Kumar, S.; Ali, W.; Bhattacharya, S.; Verma, A.K. The Effect of Elapsed Time on Cardiac Troponin-T (CTnT) Degradation and Its Dependency on the Cause of Death. *J. Forensic Leg. Med*. **2016**, *40*, 16–21, http://doi.org/10.1016/j.jflm.2016.02.002.
66. Pittner, S.; Bugelli, V.; Weitgasser, K.; Zissler, A.; Sanit, S.; Lutz, L.; Monticelli, F.; Campobasso, C.P.; Steinbacher, P.; Amendt, J. A Field Study to Evaluate PMI Estimation Methods for Advanced Decomposition Stages. *Int. J. Legal Med*. **2020**, http://doi.org/10.1007/s00414-020-02278-0.
67. Mall, G.; Eisenmenger, W. Estimation of Time since Death by Heat-Flow Finite-Element Model. Part I: Method, Model, Calibration and Validation. *Leg. Med*. **2005**, *7*, 1–14, http://doi.org/10.1016/j.legalmed.2004.06.006.
68. Amin, H.A.A.; El-Hennawy, A.M.Y.; Nakhla, G.A.A.; Tabak, S.A.-H.; Hassan, H.H. Immuno-Histochemistry in the Detection of Early Myocardial Infarction (a Post-Mortem Study). *Egypt. J. Forensic Sci*. **2011**, *1*, 5–12, http://doi.org/10.1016/j.ejfs.2011.04.003.
69. Fishbein, M.C.; Wang, T.; Matijasevic, M.; Hong, L.; Apple, F.S. Myocardial Tissue Troponins T and I: An Immunohistochemical Study in Experimental Models of Myocardial Ischemia. *Cardiovasc. Pathol*. **2003**, *12*, 65–71, http://doi.org/10.1016/S1054-8807(02)00188-6.
70. Koczula, K.M.; Gallotta, A. Lateral Flow Assays. *Essays Biochem*. **2016**, *60*, 111–20, http://doi.org/10.1042/EBC20150012.
71. Pittner, S.; Merold, V.; Anders, S.; Lohner, L.; Amendt, J.; Klinger, M.; Hausmann, R.; Kissling, S.; Monticelli, F.; Geissenberger, J.; et al. A Standard Protocol for the Analysis of Postmortem Muscle Protein Degradation: Process Optimization and Considerations for the Application in Forensic PMI Estimation. *Int. J. Legal Med*. **2022**, *136*, 1913–23, http://doi.org/10.1007/s00414-022-02849-3.
72. Pittner, S.; Bugelli, V.; Benbow, M.E.; Ehrenfellner, B.; Zissler, A.; Campobasso, C.P.; Oostra, R.J.; Aalders, M.C.G.; Zehner, R.; Lutz, L.; Monticelli, F.C.; Staufer, C.; Helm, K.; Pinchi, V.; Receveur, J.P.; Geißenberger, J.; Steinbacher, P.; Amendt, J.; The applicability of forensic time since death estimation methods for buried bodies in advanced decomposition stages. *PLoS ONE*. **2020**, *15*(12), e0243395.

Taylor & Francis
Taylor & Francis Group
http://taylorandfrancis.com

8 DNA/RNA Degradation and Time Since Death

Akihiko Kimura and Toshikazu Kondo

Contents

8.1 DNA Degradation and Time Since Death 283
8.2 RNA Degradation and Time Since Death 284
  8.2.1 RNA Stability in Cadaver Organs 284
  8.2.2 Environmental Temperature Is the Most Influential Factor for RNA Degradation in Corpses 284
  8.2.3 Target RNA and Endogenous Reference for RNA Degradation-Based Estimation of PMI 284
  8.2.4 PMI Estimation Using miRNA 285
  8.2.5 Thanatobiological Approach for PMI Estimation 286
8.3 Circadian Rhythm-Based Estimation of Time of Death 287
8.4 Thanatomicrobiome for PMI Estimation 289
8.5 Conclusions 292

Remarkable advances in molecular biology and analytical techniques have enabled detailed analyses of various molecules that constitute living organisms, bringing about revolutionary progress and developments in biology, genetics, pathology, and clinical medicine. There have been great strides in the fields of forensics, forensic genetics, and drug analyses. In particular, the development and spread of DNA analysis technology have played an extremely important role in the progress of personal identification. Since the late 1980s, several attempts have been made to apply this technology to determine the time elapsed after death. Furthermore, the development of real-time RT-PCR methods has prompted studies on RNA-based analyses of post-mortem time. Although post-mortem analyses of DNA and RNA employ modern analytical methods, the underlying principle is the rate of degradation of these nucleic acids, which starts at death (**rate method**) and is similar to the principles of other methods developed to date. Therefore, the environment in which the deceased is placed, the cause of death, and the personality of the deceased greatly affect the accuracy of the estimation. On the other hand, a small number of studies have reported methods for estimating the time of death based on the expression levels of clock genes using real-time RT-PCR. This method is a **concurrency method** rather than a traditional postmortem interval (PMI) estimation and may eschew many of the limitations of rate methods. Recently, attempts to study in detail the postmortem changes in microbiota by comprehensively analyzing the DNA of bacteria and other microorganisms have produced promising results. This microbiota-based method appears to be a powerful tool for estimating the time after death.

In this chapter, we describe the current status of methods for estimating the time since death based on DNA/RNA degradation, circadian rhythms, and changes in postmortem microbiota.

8.1 DNA Degradation and Time Since Death

Since DNA is the most stable molecular species among biomolecules, this nucleic acid can be used to identify individuals from corpses or parts of corpses left behind under adverse conditions for a long period of time. However, even stable DNA gradually degrades over time after death. In early postmortem corpses, DNA is decomposed by endogenous enzymes derived from lysosomes, followed by bacterial enzymes with synergic effects. Therefore, the amount of DNA extracted from cadavers decreases over time. In 1988, Perry et al. first reported the relationship between postmortem DNA degradation and passage of time after death (1). Since then, many attempts have been made to estimate the time elapsed after death by analyzing the magnitude of DNA decrease over time using image analysis, single-cell electrophoresis, flow cytometry, RFLP, and the like. The stability of DNA in each cadaver organ is different; DNA stability decreases in the order of the brain, muscle, kidneys, and liver (2). Although the cause of death, sex, age, and health conditions before death may affect the rate of DNA degradation, it is clear that these factors have no substantial contribution. The environment in which cadavers

DOI: 10.1201/9781003244974-8

are placed is one of the most important factors that affect DNA degradation. Temperature, humidity, immersion in water or soil, and so on affect the rate of DNA degradation to different levels (3). Among these factors, temperature is the most influential. For example, DNA decomposition progresses at completely different rates at 20 and 4°C (2). Therefore, to determine the effects of temperature more accurately, some studies have sought correlations with accumulated-degree-days (ADD) rather than calendar days since death (4). For longer PMIs, DNA derived from bacteria and fungi contaminate DNA extracted from corpses; hence, it is necessary to use a detection method based on human-specific DNA sequences.

Most studies on DNA degradation-based PMI estimation conducted to date have used animals. The results obtained from animal experiments should be applied to establish a formula for estimating PMI based on DNA degradation and to verify its accuracy and practicality. However, such attempts have not yet been fully completed. Practical methods for forensic application are expected to be established through the introduction of improved technologies and statistical methods.

8.2 RNA Degradation and Time Since Death

Research using RNA as an indicator of PMI started more than a decade after that using DNA, since RNA has long been thought to be more labile than DNA and more rapidly degraded after death. In 2002, Inoue et al. first analyzed total RNA degradation in the heart, lungs, liver, and brain of dead rats over time using electrophoresis and northern blotting and showed that RNA degradation progresses in correlation with PMI. In addition, real-time RT-PCR analyses of the mRNAs of three housekeeping genes—*Gapdh* (glyceraldehyde-3-phosphate dehydrogenase), *Hgpt* (hypoxanthine-guanine phosphoribosyltransferase), and *Actb* (β-actin)—showed time-dependent decreases in detection levels in the rat corpses. In contrast, *Il1b* mRNA induced by LPS administration was degraded faster than the housekeeping gene mRNAs, indicating that the degradation rate differs depending on the type of mRNA (5). These results demonstrated that RNA degradation may be a new indicator for PMI estimation. Since then, many studies on postmortem RNA degradation have been performed, expanding the target RNA species to include ribosomal RNAs, microRNAs (miRNAs), circular RNAs (circRNAs), small nuclear RNA (snRNAs), and small regulatory RNA (srRNAs). Studies on miRNA stability in formalin-fixed paraffin-embedded tissues and the applicability of such miRNA in forensic analysis have also been conducted (6 and 7). In addition, valuable methods for evaluating their reliability and practicality have been reported following the introduction of new molecular biological analysis techniques.

8.2.1 RNA Stability in Cadaver Organs

RNA degradation is driven by endogenous RNases during early PMIs. Bacterial RNases also act in the late stages of PMI. Endogenous RNase activity varies from organ to organ and determines the postmortem RNA stability in each organ. Therefore, target organ selection is critical for estimating PMI based on RNA degradation. Previous studies on the postmortem degradation of RNA in the brain, heart, skeletal muscle, kidneys, spleen, and liver indicated that RNA is most stable in the brain and most labile in the liver (5 and 8). Dental pulp has a much higher RNA stability than other organs and is considered applicable for estimating late PMIs (9).

8.2.2 Environmental Temperature Is the Most Influential Factor for RNA Degradation in Corpses

Although many factors affect the degradation of RNA in a corpse, their degrees of influence vary; for example, the sex, age, physique, health condition, and cause of death of the deceased do not substantially affect RNA degradation. A salient influencing factor is the environment (especially the temperature of the environment) in which the corpse was placed after death. A correlation between environmental temperature and rate of RNA degradation has been observed; temperature is the main factor that reduces the accuracy of PMI estimation based on RNA degradation. In experimental studies using animals, multiple controlled environmental temperatures are set; however, in practical cases, it is common to place cadavers in an environment with varying temperature. This is the major difference between experimental research and practical forensics. Considering the large effect of temperature on RNA degradation, such degradation in late PMIs is considered to have a higher correlation with ADD than with PMI.

8.2.3 Target RNA and Endogenous Reference for RNA Degradation-Based Estimation of PMI

The mRNAs of housekeeping genes with high expression levels, such as *GAPDH* and *ACTB*, have been used as targets for PMI estimation. The mRNA levels of genes induced by various stimuli may vary in their initial expression levels owing to various personal factors, such as the cause of death and health conditions during life, and these are considered unsuitable targets. mRNA is unstable and is only suitable for estimating a relatively early PMI. miRNAs and circRNAs are more stable than mRNAs and may be useful for longer-term PMI estimation based on forensic aspects (10). When estimating the PMI using real-time RT-PCR, the amount of target mRNA must be measured relative to an internal standard. Therefore, finding a stable internal standard in cadavers is extremely important. Transcripts of housekeeping genes such as *GAPDH* and *ACTB* are rapidly degraded in cadavers; therefore, they are not ideal internal standards. Attempts to estimate PMI using miRNA, which is much more stable than mRNA, as an internal standard have become mainstream (11 and 12). Attempts have also been made to use DNA, which is more stable than RNA, as an internal standard (13).

8.2.4 PMI Estimation Using miRNA

miRNAs are more stable than mRNAs and less susceptible to environmental temperature. Therefore, they are excellent internal standards for PMI estimation using real-time RT-PCR. Owing to this characteristic of miRNA, many attempts have been made to estimate PMI by combining miRNA as an internal standard and the mRNA of a housekeeping gene as a target. Since the stability of various miRNAs and mRNAs varies depending on the organ, it is necessary to find different combinations for each organ.

Tu et al. estimated PMI for the mouse heart, liver, and skeletal muscle using real-time RT-PCR for up to 8 days at 25°C. Using the geNorm and NormFinder algorithms, they found the best internal standards for each organ. miR-122, miR-133a, and 18S in the heart; LC-Ogdh, circ-AFF1, and miR-122 in the liver; and miR-133a and circ-AFF1 in skeletal muscle were used as internal standards (Figure 8.1).

In addition, *U6* (snRNA) and *Rps18* in the heart and liver and *U6* and *Actb* in skeletal muscle were selected and analyzed as target mRNAs, and a formula for PMI estimation was derived based on ΔΔCq (Figure 8.2).

By averaging the values obtained for the three organs, the PMI was estimated with an error of within 0.5 days for periods up to 7.5 days. However, this estimation was performed at a constant temperature of 25°C and cannot be directly connected to practical examples that are strongly affected by temperature (14).

Lv et al. constructed a mathematical model that included a temperature term in the PMI estimation formula. Using the heart and liver of rats as target organs, PMI was estimated using real-time RT-PCR for up to 100 hours at 4, 15, 25, and 35°C. R software was used to derive the PMI estimation formulas from the ΔCt of *Actb* and ambient

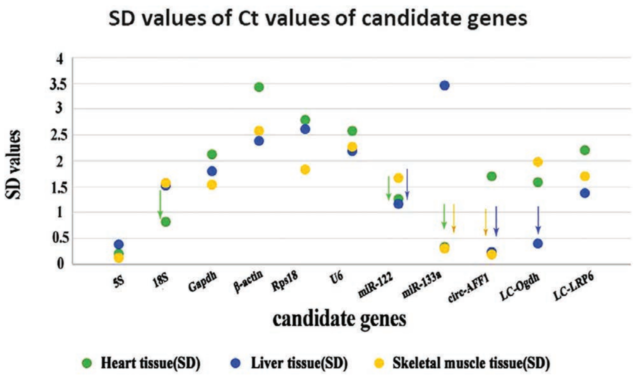

Figure 8.1 SD values of candidate genes within 0–8 days from death. The arrows indicate the most stable genes in three types of tissues (14).

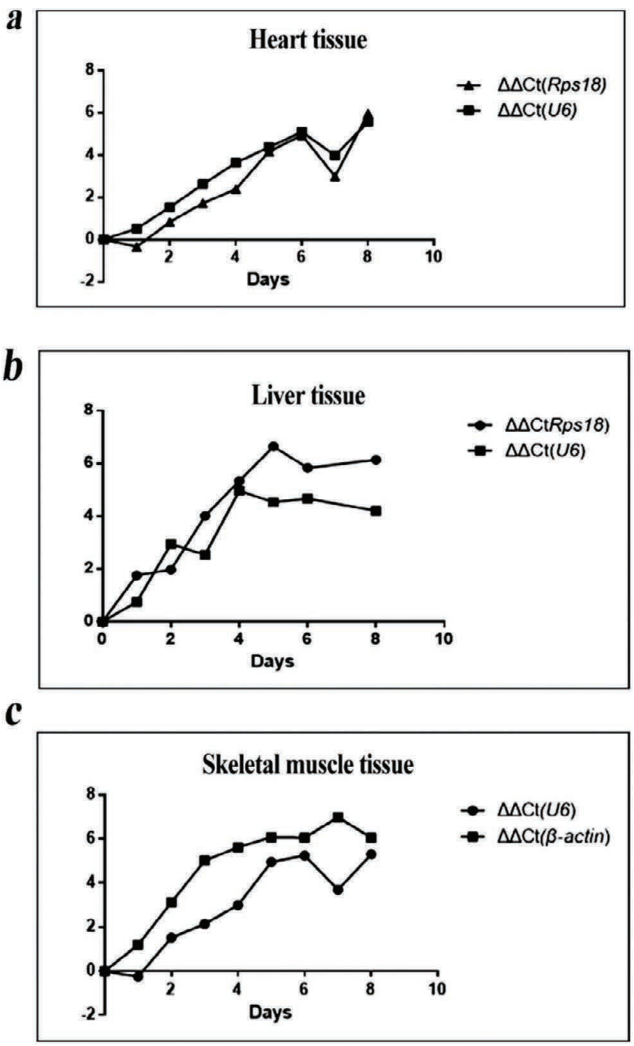

Figure 8.2 Selection of biomarkers correlating with PMI. We derived the correlation between ΔΔCq of all candidate genes and PMI for three types of tissues; U6 and Rps18 in heart and liver tissues showed the highest R^2 value, and U6 and β-actin in skeletal muscle tissues showed a better correlation with PMI. The correlation between these genes and PMI is shown in Panels a, b, and c (14).

temperature in both organs, with miR-1, miR-133a, and 5S rRNA in the heart and miR-122 and srRNA in the liver as internal standards (Figure 8.3).

Applying these formulas to 11 autopsy cases in which the PMI (6–71 hours) and mean temperature of the cadaver environment (8–25°C) were known, the PMI was estimated with a mean error of 5.06 hours. The results of this study indicate that real-time RT-PCR can be a powerful tool for estimating PMIs up to several days with a relatively small error using appropriate target RNA and internal standard miRNA (15).

8.2.5 Thanatobiological Approach for PMI Estimation

Comprehensive gene expression analysis in the field of thanatobiology has shown that the expression levels of specific genes change markedly after death (16). This change is independent of postmortem RNA degradation and may be a new index for the analysis of early PMI in forensic studies. Some level of postmortem mRNA transcription is detectable, and the results of comprehensive gene expression analysis have confirmed the active upregulation and downregulation of specific gene groups after death (17). Hunter et al. used the Gene Meter approach to profile thousands of postmortem gene transcriptions from RNA samples collected over time from 44 deceased zebrafish and 20 deceased house mice; they found the gene groups that showed the best correlation with PMI in zebrafish and mouse, and subjected them to microarray analysis. The profiles of 1063 genes whose transcription levels significantly increased in abundance after death were identified using a total of 74,179 calibrated microarray probes using Gene Meter approach. The transcription profiles were split into training and test datasets, groups of profiles were randomly selected, and over-defined and/or perfectly defined linear regression analyses were used to determine the modeling parameters of the genes for the fit (R^2) and slope predictions versus actual postmortem time (Figure 8.4).

Upon application of this experimental design thousands to millions of times, the gene groups that showed the best

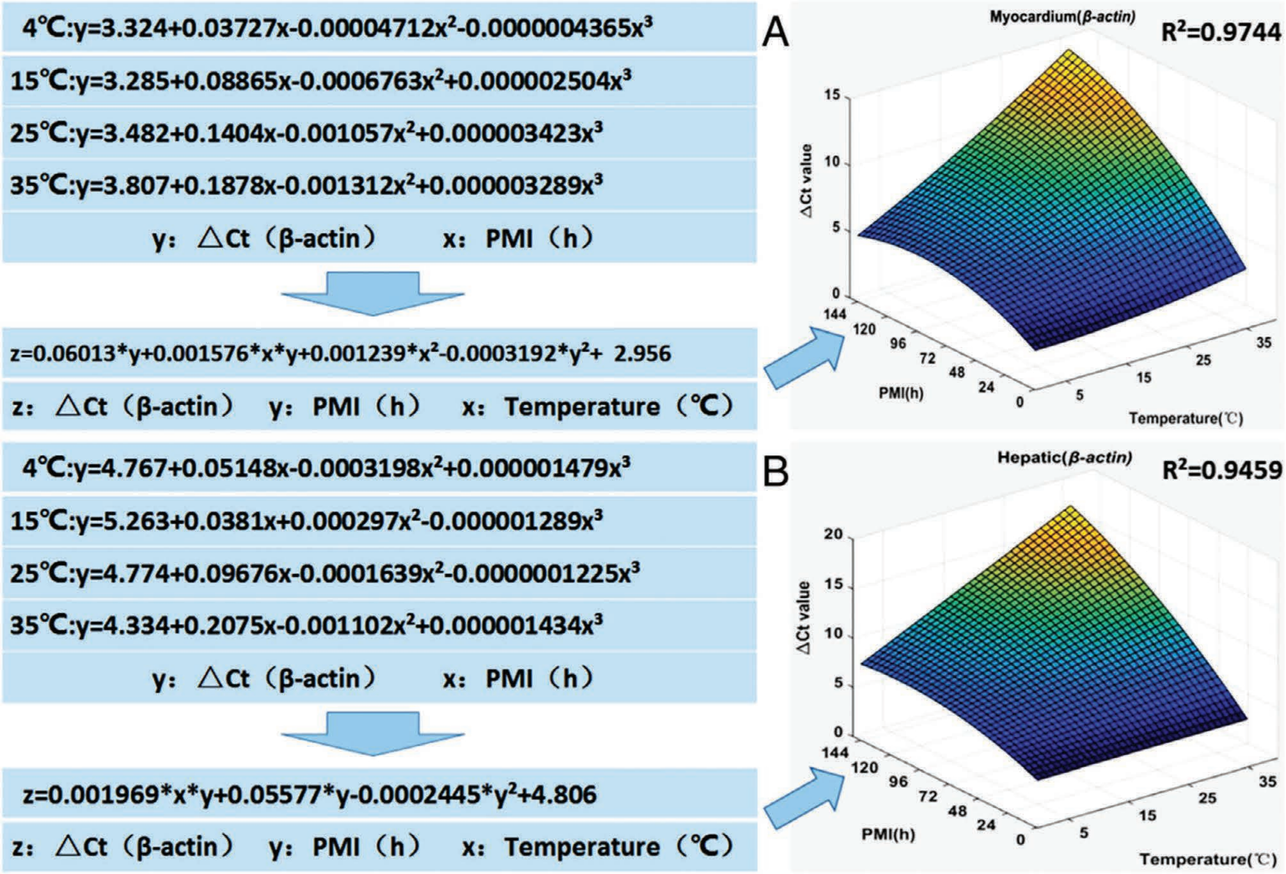

$4℃: y=3.324+0.03727x-0.00004712x^2-0.0000004365x^3$

$15℃: y=3.285+0.08865x-0.0006763x^2+0.000002504x^3$

$25℃: y=3.482+0.1404x-0.001057x^2+0.000003423x^3$

$35℃: y=3.807+0.1878x-0.001312x^2+0.000003289x^3$

y: $\triangle$Ct (β-actin) x: PMI (h)

$z=0.06013*y+0.001576*x*y+0.001239*x^2-0.0003192*y^2+2.956$

z: $\triangle$Ct (β-actin) y: PMI (h) x: Temperature (℃)

$4℃: y=4.767+0.05148x-0.0003198x^2+0.000001479x^3$

$15℃: y=5.263+0.0381x+0.000297x^2-0.000001289x^3$

$25℃: y=4.774+0.09676x-0.0001639x^2-0.0000001225x^3$

$35℃: y=4.334+0.2075x-0.001102x^2+0.000001434x^3$

y: $\triangle$Ct (β-actin) x: PMI (h)

$z=0.001969*x*y+0.05577*y-0.0002445*y^2+4.806$

z: $\triangle$Ct (β-actin) y: PMI (h) x: Temperature (℃)

Figure 8.3 The cubic curve fit of ΔCt (β-actin) and prolonged PMI under different temperature conditions was transformed into four equations for both the myocardium (A) and the liver (B). Animal data were generated for fitting using R software and then transformed into a three-dimensional visual mathematical model using MATLAB 7.0 (15).

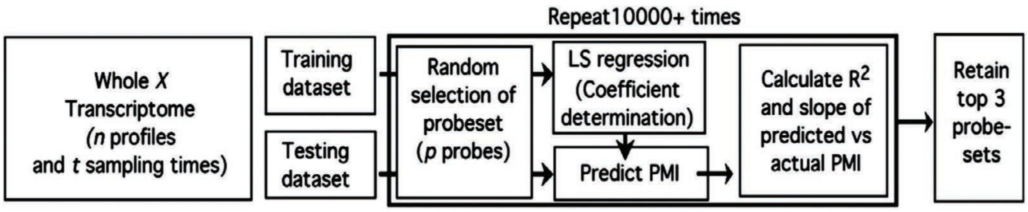
Repeat10000+ times
Whole X Transcriptome (n profiles and t sampling times)
Training dataset
Testing dataset
Random selection of probeset (p probes)
LS regression (Coefficient determination)
Predict PMI
Calculate R2 and slope of predicted vs actual PMI
Retain top 3 probe-sets

Figure 8.4 Scheme of experimental design for three datasets. The process in the bold box was repeated 10,000+ times. The top three probe datasets were determined based on the R^2 between predicted versus actual PMI and the slope closest to one for the test dataset. If *X* = “zebrafish” then *n* = 548, *t* = 11, and *p* = 11; if *X* = “mouse brain” then *n* = 478, *t* = 7, and *p* = 7; if *X* = “mouse liver” then *n* = 36, *t* = 7, and *p* = 7 (17).

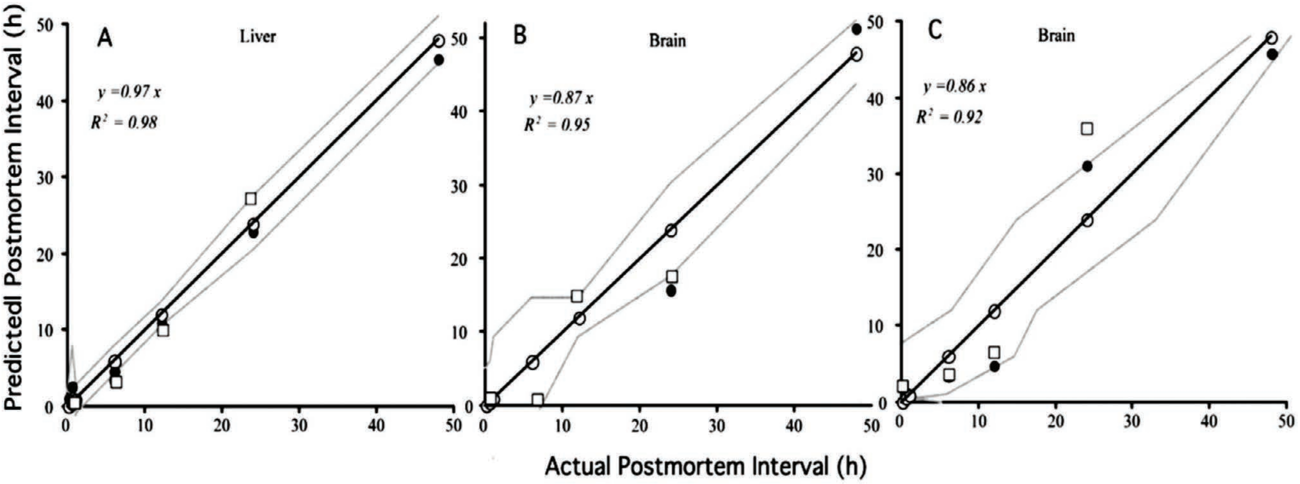

Figure 8.5 Predicted versus actual PMI determined for mice using three different equations, as represented by Panels A-C. R^2 and slopes are based on both training and testing datasets. The gray line represents the 99% confidence limits of the linear regression. Open circles: training data; closed circles: testing data; open squares: validation data (not used in training or selection) (17).

correlations with PMI in zebrafish and mouse livers and brains were identified. PMI estimation up to 50 h showed an R^2 of 1 and a slope of 0.99 for the zebrafish, an R^2 of 0.98 and a slope of 0.97 for the mouse livers, and an R^2 of 0.95 and a slope of 0.87 for the brain (Figure 8.5) (17).

This experiment was conducted without considering the influence of temperature—further studies that consider the temperature factor will be useful in forensic practice.

8.3 Circadian Rhythm-Based Estimation of Time of Death

The circadian rhythm is a basic biological phenomenon observed in various species, from bacteria to plants and humans. Circadian rhythms are the biological adaptations to environmental periodicity caused by Earth’s rotation. Humans exhibit a clear circadian rhythm in their physiology (e.g., body temperature, blood pressure, and endocrinological hormone secretion) and behavior (e.g., eating and sleeping). The molecular mechanism that controls this circadian rhythm exists in every cell in the body and is called the circadian clock or cellular clock. There is a master clock in the suprachiasmatic nucleus of the hypothalamus; this clock is calibrated by light stimulation via the eyes. Although the master clock controls the peripheral cellular clocks throughout the body, the peripheral clocks are organ specific. For example, the liver cell clock is strongly influenced by the feeding rhythm.

The study of the molecular mechanisms controlling the circadian clock originated from investigations on Drosophila mutants with abnormal behavioral cycles (18). In these studies, the period gene, a gene group involved in the regulation of the biological clock, was discovered for the first time. Many clock genes have been discovered in research on mammals (Table 8.1), and the entire mechanism of the molecular clock system, which comprises feedback loops between clock genes and their products (clock proteins), has been elucidated (19).

The expression levels of many clock genes that constitute feedback loops controlling the circadian clock oscillate with a circadian pattern. For example, the expression

Table 8.1 List of Clock Genes

Gene	Function	Human	Mouse
per	Transcription factor	*PER1, PER2, PER3*	*Per1, Per2, Per3*
tim	Transcription factor	*TIMELESS*	*Timeless*
clk	Transcription factor	*CLOCK, NPAS2*	*Clock, Npas2*
BMAL	Transcription factor	*ARNTL(BMAL1),* *ARNTL1(BMAL2)*	*Arntl (Bmal1)* *Arntl2 (Bmal2)*
cry	Transcription factor	*CRY1, CRY2*	*Cry1, Cry2*
vrille	Transcription factor	*NFIL3(E4BP4)*	*Nfil3(E4bp4)*
Pdp1	Transcription factor	*HLF, TEF, DBP*	*Hlf, Tef, Dbp*
DEC	Transcription factor	*BHLHE40(DEC1) BHLHE41(DEC2)*	*Bhlhe40(Dec1) Bhlhe41(Dec2)*
ID2	Transcription factor	*ID2*	*Id2*
Rev-erb α	Transcription factor	*NR1D1 (Rev-erb A)*	*Nr1d1 (Rev-erb A)*
RORα	Transcription factor	*RORA (NR1F1)*	*Rora (Nr1f1)*
SIRT1	Transcription factor	*SIRT1*	*Sirt1*

level of aryl hydrocarbon receptor nuclear translocator like 1 *(ARNTL)* also known as *BMAL1*, which is a major component of the feedback loop, is lowest in humans around 6 am and highest around 6 pm. In contrast, the expression level of nuclear receptor subfamily 1 group D member 1(NR1D1) also known as *REB-ERB alpha*, a nuclear transcription factor that represses *ARNTL* transcription, is highest at around 6 am and lowest at around 6 pm. The expression levels of these two genes are like the hands of a clock, and their expression thought to stop when an individual dies. Therefore, the time of death can be estimated by analyzing the expression levels of *ARNTL* and *NR1D1* in the organs of the deceased (20). Unlike PMI estimation based on DNA/RNA degradation, the method based on the expression level of clock genes is a pure concurrent method for estimating the time of death.

In this method, mRNA is extracted from cadaver organs and the expression levels of *ARNTL* and *NR1D1* are determined using real-time RT-PCR. The ratio of the expression levels of both genes, that is, the *NR1D1*/*ARNTL* ratio, is used as the hands of the cadaver's biological clock, which stopped at the time of death. This method does not require an internal standard and is advantageous because the two target genes oscillate in anti-phase and are thus detected as oscillations larger than the amplitude of the expression level of each gene (Figure 8.6).

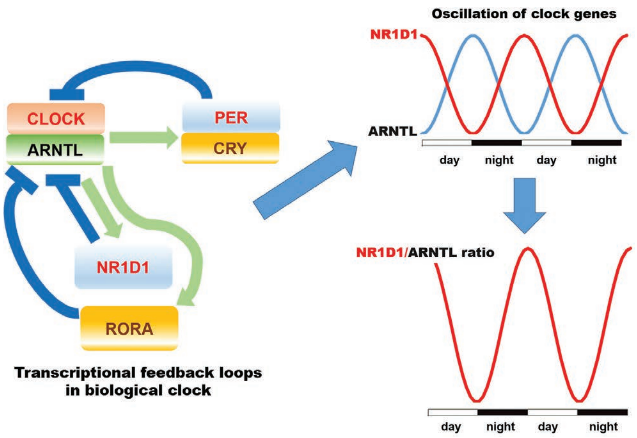

Figure 8.6 Transcriptional feedback loops in biological clock. *NR1D1/ARNTL* ratio is used as the hands of the biological clock.

The *NR1D1*/*ARNTL* ratio of hearts collected from 199 autopsy cases (140 males and 59 females, 2 months to 97 years old, PMI: 3–96 hours) with known death times plotted against the time of death revealed a pattern showing a maximum at around 6 AM and a minimum at around 6 pm (Figure 8.7a). Conversely, the *ARNTL*/*NR1D1* ratio showed a peak at around 6 pm (Figure 8.7b); these indices can be used to estimate mortality in the morning and evening. All cases with a *NR1D1*/*ARNTL* ratio of 25 or more died in the morning, with the majority distributed around 6 am (Figure 8.7a). On the other hand, all cases with an *ARNTL*/*NR1D1* ratio of 1.5 or more died in the afternoon, with most around 6 pm (Figure 8.7b).

This method is considered to be less affected by the environment; however, it is believed that individual lifestyles have a strong effect. The expression levels of basic clock genes in the peripheral circadian clock shows an opposite pattern in humans and mice. This is because humans are diurnal, whereas mice are nocturnal. When mice are fed only during the daytime, the expression levels of clock genes change to the human pattern. These observations suggest that night workers and shift workers may exhibit mouse-type clock gene expression patterns, which differ from those of daytime workers. In addition, attenuation of clock gene expression in patients with type 2 diabetes (21), disruption of clock gene expression in the pineal gland in patients with Alzheimer's disease (22), and disruption of the circadian pattern of gene expression in the brains of patients with major

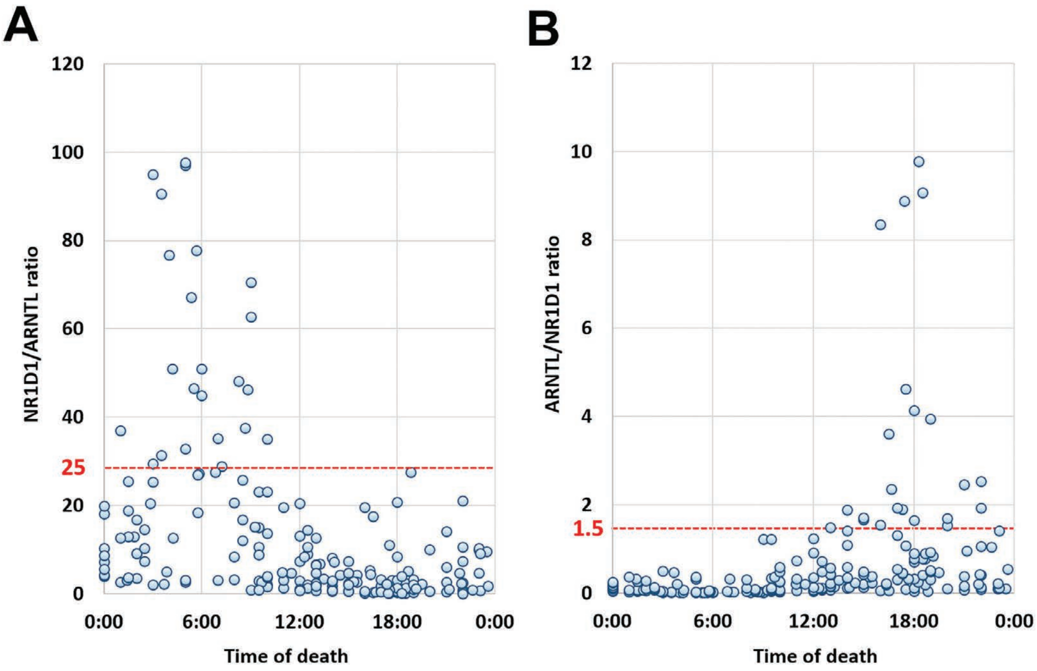

Figure 8.7 *NR1D1/ARNTL* ratio (A) and *ARNTL/NR1D1* ratio (B) of hearts collected from 199 autopsy cases with known death times plotted against the time of death.

depressive disorder (23) have been reported. Since the expression of clock genes is highly likely to be affected by individual factors, it is necessary to consider the lifestyle and chronic diseases of the deceased.

Circadian expression patterns are not restricted to clock genes. Many genes with expression controlled by clock genes exhibit circadian patterns. Melatonin is a primary example of this phenomenon. The time of death can be estimated by quantifying melatonin in the pineal gland, plasma, and urine of the deceased using radioimmunoassay (24). Genome-wide integrative studies have shown that the expression levels of many mRNAs and miRNAs in the mouse liver exhibit a circadian pattern (25). The phases of oscillation of these miRNAs vary. miRNAs have better postmortem stability than mRNAs. Based on these two points, a more accurate and precise method for estimating the time of death can be established by combining multiple miRNAs as indicators.

This method, based on the biological clock, can be used to estimate the time of death (clock); it can also be combined with other methods for estimating time since death (calendar) to estimate the date and time of death.

8.4 Thanatomicrobiome for PMI Estimation

Ecological methods, including forensic entomology, have been used to estimate late PMIs; however, they are prone to considerable errors. This limitation is due to the uncertainty of how long it takes for insects, such as flies, to lay eggs on carcasses, as well as the environment and season, which affect the growth rate of such insects. Metcalf et al. introduced the concept of a microbial clock into PMI estimation and showed that thanatomicrobiome (postmortem microbial community) analysis can be used to overcome the uncertainties of this forensic entomological method. Bacteria and other microorganisms, collectively called the microbiome, exist everywhere in the environment; the human skin and gastrointestinal tract have their own microbiomes. Humans and their microbiomes have a mutually supportive relationship and contribute to each other's homeostasis. When humans die, this homeostasis is lost, and their microbiomes undergo dramatic changes. Such changes correlate with the stage of decomposition of cadavers. Furthermore, the later stages of decomposition cause strong changes in the soil microbiome with which the carcasses are in contact. Metcalf et al. reported a study on a microbiome-based PMI estimation method (26). They used 40 mice euthanized by carbon dioxide and cervical dislocation. The corpses were placed on soil for 48 days in a constant environment, and the degree of corpse degradation was recorded periodically.

Simultaneously, samples were taken from the intraperitoneal cavity and skin of the head and abdomen. The collected samples were analyzed for microorganisms using high-throughput sequencing. Based on the results obtained, the relationship between postmortem decomposition processes in mice and changes in the carcass and soil microbiomes was analyzed. The microbiome (bacteria and eukaryotes) could serve as an index for PMI estimation, since the emergence of specific bacterial and eukaryotic groups and their quantitative changes were specifically observed at each decomposition stage

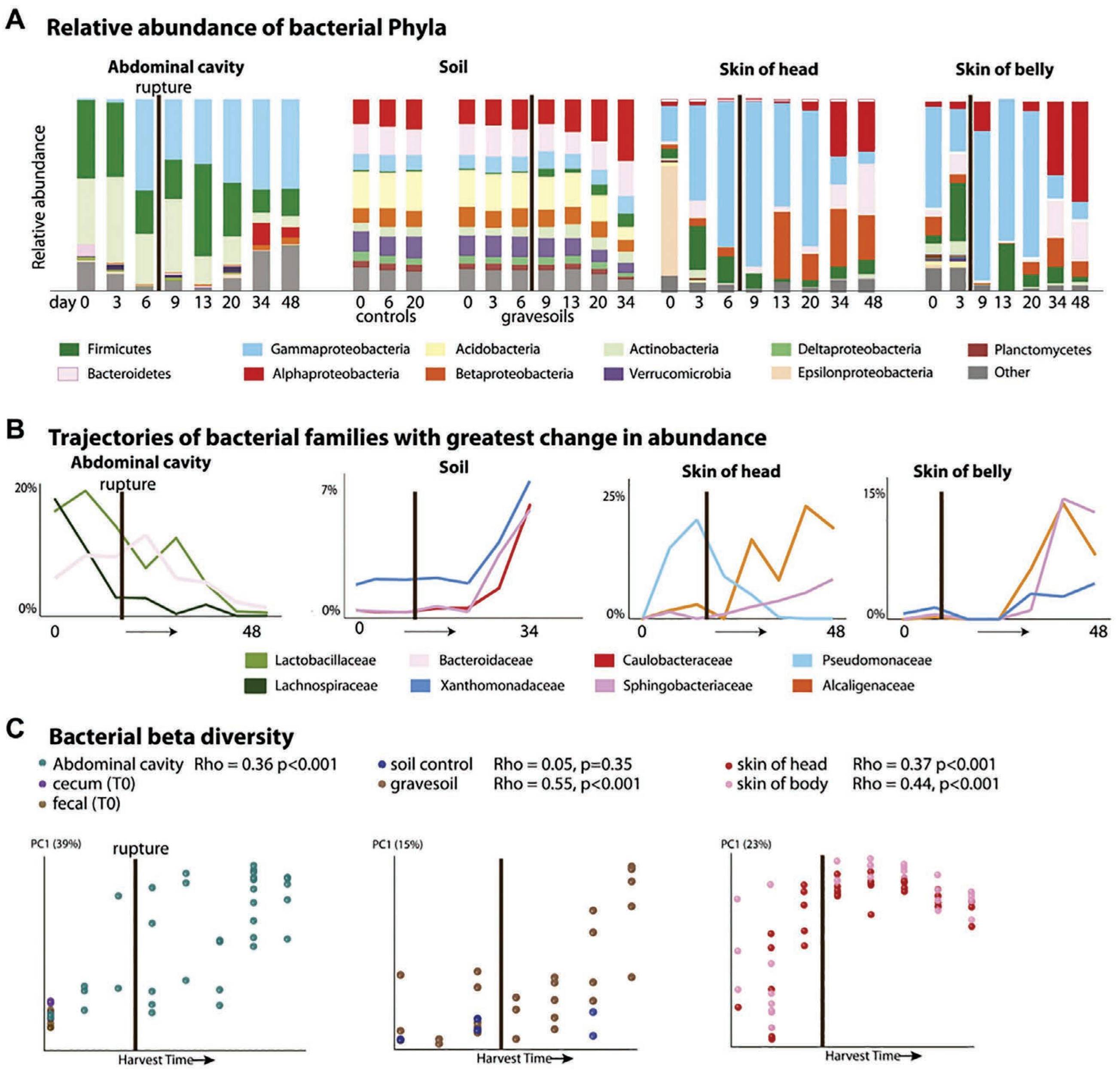

Figure 8.8 The bacterial community composition changes significantly and consistently over the course of decomposition. (A) Relative abundance of bacterial phyla over time for all body sites. For the abdominal site, Day 0 sampling includes cecum, fecal, and abdominal swab and liquid samples. For the soil site, control soils collected on Days 0, 6, and 20 are shown on the left of the plot. (B) The three bacterial families that show the greatest change in abundance over time are plotted for each site. (C) PCoA plot based on unweighted UniFrac distances displaying bacterial community changes at all sites during decomposition. Results from Mantel tests (Rho and p values) show that the changes in the bacterial community correlated significantly with time. The point of rupture is marked with a thick vertical black line on each plot (26).

(Figures 8.8 and 8.9). The relative abundances of taxa were directly regressed on known PMIs using the Random Forests model, and the best subset of features for PMI estimation from random decision trees was selected. This method allowed the estimation of PMIs within 3.30 +/− 2.52 days (mean absolute error +/− standard deviation) from temporal changes in the microbiome of the head skin. Eukaryotes contributed more to PMI estimation than bacteria, and the combination of both the 16S and 18S datasets showed higher estimation accuracy. Significant taxa were present at each sampling site, and among the many detected, models built using highly predictive taxa were analyzed using 5–10 taxa. The estimation accuracy was similar to that of the model using all taxa (Figure 8.10).

In this study, the type of soil, season (temperature conditions), and so on were constant. In subsequent research (27), experiments were conducted by placing

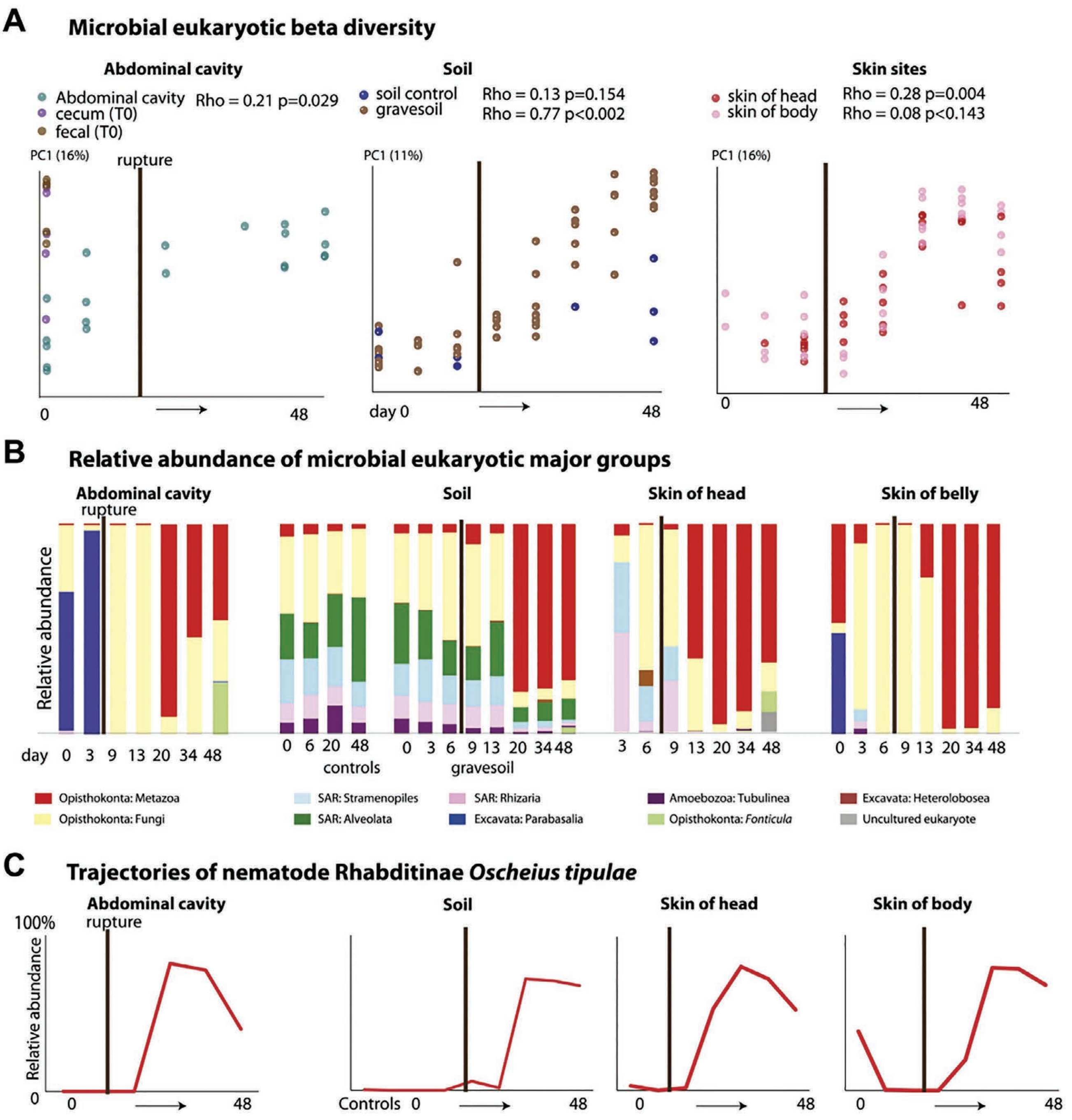

Figure 8.9 The eukaryotic community composition changes directionally and is dominated by the nematode, *Oscheius tipulae*. (A) PCoA plot based on unweighted UniFrac distances displaying microbial eukaryotic community changes during decomposition. Results from Mantel tests (Rho and p values) show that the changes in the microbial eukaryotic community correlated significantly with time, except for the skin of the belly. (B) Relative abundance of microbial eukaryote taxa at the class level over time. The microbial eukaryotic community composition changed significantly and predictably over the course of decomposition. (C) The eukaryotic nematode, *O. tipulae*, became highly abundant at each sample site at late stages of decomposition. The point of rupture is marked with a thick vertical black line on each plot (26).

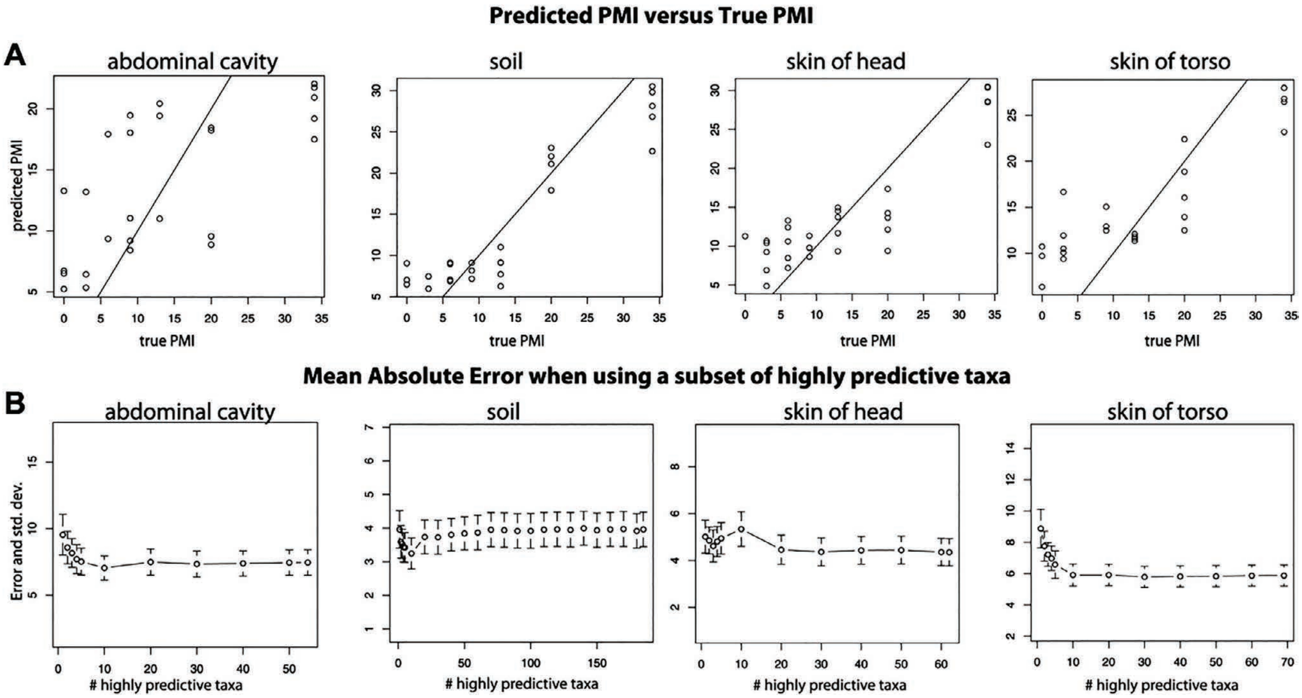

Figure 8.10 Trends of the postmortem interval (PMI) estimates. (A) A regression of PMI predictions vs true PMI using 16S data. The line represents a perfect prediction of PMI. The abdominal cavity shows the greatest scatter of points deviating from the line. (B) Estimates of the mean absolute error (MAE) for PMI predictions using subsets of highly predictive bacterial taxa. The results suggest that 5–10 highly predictive taxa are required to recover MAEs similar to those generated using the entire microbial community. Similar results were obtained for 18S data (not shown) (26).

humans and mice on multiple types of soils in different seasons (spring and winter), suggesting that PMI estimation by comprehensive thanatomicrobiome analysis is applicable beyond differences in soil, season, and corpse species, and that this is a very promising method.

8.5 Conclusions

Several studies conducted to date have clarified that miRNAs, which are more stable than mRNAs, are suitable for PMI estimation. In any estimation method, it is essential to introduce comprehensive and excellent mathematical analyses, such as calculations using artificial intelligence. Comprehensive analysis of the degradation and circadian oscillation of miRNAs in cadaver samples is expected to bring about great progress in estimating PMI and the time of death. Comprehensive analysis of the microbiome is expected to play a major role in estimating late PMIs. These new methods, combined with established, non-gene-based, and long-established methods, are likely to provide revolutionary advances in PMI estimation, one of the most important and difficult issues in forensics.

References

1. Perry WL, Bass WM, Riggsby WS, Sirotkin K. The autodegradation of deoxyribonucleic acid (DNA) in human rib bone and its relationship to the time interval since death. *J Forensic Sci*. 1988;33(1):144–53. PMID: 3351452
2. Itani M, Yamamoto Y, Doi Y, Miyaishi S. Quantitative analysis of DNA degradation in the dead body. *Acta Med Okayama*. 2011;65(5):299–306. http://doi.org/10.18926/AMO/47011. PMID: 22037266
3. Mansour H, Krebs O, Pinnschmidt HO, Griem N, Hammann-Ehrt I, Püschel K. Factors affecting dental DNA in various real post-mortem conditions. *Int J Legal Med*. 2019;133(6):1751–9. http://doi.org/10.1007/s00414-019-02151-9. Epub 2019 Sep 11. PMID: 31511983
4. Larkin B, Iaschi S, Dadour I, Tay GK. Using accumulated degree-days to estimate postmortem interval from the DNA yield of porcine skeletal muscle. *Forensic Sci Med Pathol*. 2010;6(2):83–92. http://doi.org/10.1007/s12024-009-9109-5. Epub 2009 Oct 23. PMID: 19851896
5. Inoue H, Kimura A, Tuji T. Degradation profile of mRNA in a dead rat body: basic semi-quantification study. *Forensic Sci Int*. 2002;130(2–3):127–32. http://doi.org/10.1016/s0379-0738(02)00352-3. PMID: 12477633
6. Kakimoto Y, Kamiguchi H, Ochiai E, Satoh F, Osawa M. MicroRNA stability in postmortem FFPE tissues: Quantitative analysis using autoptic samples from acute myocardial infarction patients. *PLoS ONE*. 2015;10(6):e0129338. http://doi

.org/10.1371/journal.pone.0129338. PMID: 26046358; PMCID: PMC4457786

7. Muciaccia B, Vico C, Aromatario M, Fazi F, Cecchi R. Molecular analysis of different classes of RNA molecules from formalin-fixed paraffin-embedded autoptic tissues: a pilot study. *Int J Legal Med*. 2015;129(1):11–21. http://doi.org/10.1007/s00414-014-1066-1. Epub 2014 Aug 19. PMID: 25135750
8. Sampaio-Silva F, Magalhães T, Carvalho F, Dinis-Oliveira RJ, Silvestre R. Profiling of RNA degradation for estimation of post mortem [corrected] interval. *PLoS ONE*. 2013;8(2):e56507. http://doi.org/10.1371/journal.pone.0056507. Epub 2013 Feb 20. Erratum in: *PLoS One*. 2013;8(6):null. PMID: 23437149; PMCID: PMC3577908
9. Young ST, Wells JD, Hobbs GR, Bishop CP. Estimating postmortem interval using RNA degradation and morphological changes in tooth pulp. *Forensic Sci Int*. 2013;229(1–3):163.e1–6. http://doi.org/10.1016/j.forsciint.2013.03.035. Epub 2013 May 4. PMID: 23647867
10. Mitchell PS, Parkin RK, Kroh EM, Fritz BR, Wyman SK, Pogosova-Agadjanyan EL, Peterson A, Noteboom J, O'Briant KC, Allen A, Lin DW, Urban N, Drescher CW, Knudsen BS, Stirewalt DL, Gentleman R, Vessella RL, Nelson PS, Martin DB, Tewari M. Circulating microRNAs as stable blood-based markers for cancer detection. *Proc Natl Acad Sci U S A*. 2008;105(30):10513–18. http://doi.org/10.1073/pnas.0804549105. Epub 2008 Jul 28. PMID: 18663219; PMCID: PMC2492472
11. Lv YH, Ma KJ, Zhang H, He M, Zhang P, Shen YW, Jiang N, Ma D, Chen L. A time course study demonstrating mRNA, microRNA, 18S rRNA, and U6 snRNA changes to estimate PMI in deceased rat's spleen. *J Forensic Sci*. 2014;59(5):1286–94. http://doi.org/10.1111/1556-4029.12447. Epub 2014 Feb 24. PMID: 24611529
12. Tu C, Du T, Shao C, Liu Z, Li L, Shen Y. Evaluating the potential of housekeeping genes, rRNAs, snRNAs, microRNAs and circRNAs as reference genes for the estimation of PMI. *Forensic Sci Med Pathol*. 2018;14(2):194–201. http://doi.org/10.1007/s12024-018-9973-y. Epub 2018 Apr 24. PMID: 29691731
13. Wei Deng, Meili Lv, Li Wang, Peng Bai, Weibo Liang, Lin Zhang. mRNA degradation pattern analysis in post-mortem normalized using the DNA. Forensic Sci Int Genet Suppl Ser. 2013;4(1):e266–7.
14. Tu C, Du T, Ye X, Shao C, Xie J, Shen Y. Using miRNAs and circRNAs to estimate PMI in advanced stage. *Leg Med (Tokyo)*. 2019;38:51–7. http://doi.org/10.1016/j.legalmed.2019.04.002. Epub 2019 Apr 2. PMID: 30986695
15. Lv YH, Ma JL, Pan H, Zeng Y, Tao L, Zhang H, Li WC, Ma KJ, Chen L. Estimation of the human postmortem interval using an established rat mathematical model and multi-RNA markers. *Forensic Sci Med Pathol*. 2017;13(1):20–7. http://doi.org/10.1007/s12024-016-9827-4. Epub 2016 Dec 28. PMID: 28032211
16. Javan GT, Hanson E, Finley SJ, Visonà SD, Osculati A, Ballantyne J. Identification of cadaveric liver tissues using thanatotranscriptome biomarkers. *Sci Rep*. 2020;10(1):6639. http://doi.org/10.1038/s41598-020-63727-9. PMID: 32313164; PMCID: PMC7170907
17. Hunter MC, Pozhitkov AE, Noble PA. Accurate predictions of postmortem interval using linear regression analyses of gene meter expression data. *Forensic Sci Int*. 2017;275:90–101. http://doi.org/10.1016/j.forsciint.2017.02.027. Epub 2017 Mar 4. PMID: 28329724
18. Takahashi JS. The 50th anniversary of the Konopka and Benzer 1971 paper in PNAS: "Clock Mutants of *Drosophila melanogaster*". *Proc Natl Acad Sci U S A*. 2021;118(39):e2110171118. http://doi.org/10.1073/pnas.2110171118. PMID: 34507977; PMCID: PMC8488695
19. Schibler U. The daily timing of gene expression and physiology in mammals. *Dialogues Clin Neurosci*. 2007;9(3):257–72. http://doi.org/10.31887/DCNS.2007.9.3/uschibler. PMID: 17969863; PMCID: PMC3202490
20. Kimura A, Ishida Y, Hayashi T, Nosaka M, Kondo T. Estimating time of death based on the biological clock. *Int J Legal Med*. 2011;125(3):385–91. http://doi.org/10.1007/s00414-010-0527-4. Epub 2010 Nov 11. PMID: 21069371
21. Ando H, Takamura T, Matsuzawa-Nagata N., et al. Clock gene expression in peripheral leucocytes of patients with type 2 diabetes. *Diabetologia*. 2009;52:329–35. https://doi.org/10.1007/s00125-008-1194-6
22. Wu YH, Fischer DF, Kalsbeek A, Garidou-Boof ML, van der Vliet J, van Heijningen C, Liu RY, Zhou JN, Swaab DF. Pineal clock gene oscillation is disturbed in Alzheimer's disease, due to functional disconnection from the "master clock". *FASEB J*. 2006;20(11):1874–6. http://doi.org/10.1096/fj.05-4446fje. Epub 2006 Jul 3. PMID: 16818472
23. Li JZ, Bunney BG, Meng F, Hagenauer MH, Walsh DM, Vawter MP, Evans SJ, Choudary PV, Cartagena P, Barchas JD, Schatzberg AF, Jones EG, Myers RM, Watson SJ Jr, Akil H, Bunney WE. Circadian patterns of gene expression in the human brain and disruption in major depressive disorder. *Proc Natl Acad Sci U S A*. 2013;110(24):9950–5. http://doi.org/10.1073/pnas.1305814110. Epub 2013 May 13. PMID: 23671070; PMCID: PMC3683716
24. Mikami H, Terazawa K, Takatori T, Tokudome S, Tsukamoto T, Haga K. Estimation of time of death by quantification of melatonin in corpses. *Int J Legal Med*. 1994;107(1):42–51. http://doi.org/10.1007/BF01247274. PMID: 7999645
25. Vollmers C, Schmitz RJ, Nathanson J, Yeo G, Ecker JR, Panda S. Circadian oscillations of protein-coding and regulatory RNAs in a highly dynamic mammalian liver epigenome. *Cell Metab*. 2012;16(6):833–45. http://doi.org/10.1016/j.cmet.2012.11.004. PMID: 23217262; PMCID: PMC3541940
26. Metcalf JL, Wegener Parfrey L, Gonzalez A, Lauber CL, Knights D, Ackermann G, Humphrey GC, Gebert MJ, Van Treuren W, Berg-Lyons D, Keepers K, Guo Y, Bullard J, Fierer N, Carter DO, Knight R. A microbial clock provides an accurate estimate of the postmortem interval in a mouse model system. *Elife*. 2013;2:e01104. http://doi.org/10.7554/eLife.01104. PMID: 24137541; PMCID: PMC3796315
27. Metcalf JL, Xu ZZ, Weiss S, Lax S, Van Treuren W, Hyde ER, Song SJ, Amir A, Larsen P, Sangwan N, Haarmann D, Humphrey GC, Ackermann G, Thompson LR, Lauber C, Bibat A, Nicholas C, Gebert MJ, Petrosino JF, Reed SC, Gilbert JA, Lynne AM, Bucheli SR, Carter DO, Knight R. Microbial community assembly and metabolic function during mammalian corpse decomposition. *Science*. 2016;351(6269):158–62. http://doi.org/10.1126/science.aad2646. Epub 2015 Dec 10. PMID: 26657285

Taylor & Francis
Taylor & Francis Group
http://taylorandfrancis.com

9 Gastric Contents and Time Since Death

Burkhard Madea, Bernard Knight, Elke Doberentz

Contents

9.1 Is There Post-mortem Transport of Gastric Contents? 296
9.2 Gastric Emptying Pattern 298
9.3 Estimation of Time of Death from Gastric Contents 300
9.4 Practical Procedure 302
9.5 Conclusions 302
9.6 A Case History: Steven Truscott 303
9.7 Further Case Histories 304
  9.7.1 Case History 304
  9.7.2 Value of Stomach Content in a Case of Child Homicide Case Report History at the Time of Autopsy 305
  9.7.3 Autopsy 305
  9.7.4 Further Police Investigation After Autopsy 306

The state of digestion and distribution of the last meal in the stomach and the upper intestine have long been proposed as a method for estimating the time since death [6,11,16,17,21,22,30,31]. The volume of the stomach contents compared with the volume of the last meal and the transportation distance into the small intestine must be known. Even if the volume of the last meal is not known from the type of meal (e.g. breakfast, lunch), rough estimations of the time of day when death occurred may be possible.

Estimations of the time since death based on stomach contents are often also required because the police did not call for a forensic pathologist to be present at the scene of a crime [4].

The state of digestion and the transportation rate of food from the stomach to the duodenum depend on several antemortem (anatomical, physiological, psychological, pathological, agonal, type of food) factors, which contribute to the great intraindividual and interindividual variability of gastric emptying. Therefore, it is not astonishing that diverging estimates on the time of death in relation to the last meal have been made by different pathologists in the same case. Estimations considering all circumstances should be made only with great reservation. Digestion itself does not cease with death but progresses after death; the state of digestion is therefore of only little value in estimating the time since death.

Opinions on this topic vary from author to author, but the following random extracts from standard English language textbooks indicate that strong evidential value can rarely be placed on the use of gastric contents in timing death.

> The state of digestion of the stomach contents and bowel may be used as an additional means of fixing the hour of death in relation to the last meal. Most elaborate tables have been prepared of the time taken by the stomach to digest certain articles of diet, but these are wholly unreliable. The rate of digestion varies in different persons and gastric and intestinal activity is much retarded in cases of trauma and insensibility. Even without the paralysis of movement that is common to grave injury or deep insensibility, the process of emptying of the stomach may be much delayed.
>
> (Simpson [29])

> If undigested food is found in the stomach at a postmortem examination, it is often claimed that the deceased must have died within 3–4 hours of his last meal. This claim is of limited value as there are great individual variations in the emptying time of the stomach. As the rate of digestion is variable and as it is not possible to determine the degree of digestion of various foods from a naked-eye examination of the stomach contents, little reliance can be placed upon estimates of the post-mortem interval which are based upon the apparent state of digestion. Gastric digestion may continue post-mortem, this creating further difficulties.
>
> (Gordon et al. [10])

> Attempts to fix this time (of death) based solely on examination of the stomach contents are unsatisfactory even when allowance is made for the factors which either hasten or retard digestion; allowance must always be made for individual variation . . . the foregoing (purported times of emptying), however, cannot be relied upon nor should it be relied upon, as crucial evidence which purports to fix the time of death within narrow limits.
>
> (Polson et al. [26])

DOI: 10.1201/9781003244974-9

The rate of emptying of the stomach is so variable that it cannot be used to give any certain indication of the time that has elapsed between the last meal and the death. The state of the stomach and its contents might, however, help in making a decision when, for example, death could have taken place at two or more times. When a person dies in bed after taking supper, an empty stomach would point to death having occurred towards the end of the night, rather than earlier. If there is food in the stomach of a person found dead one morning on the kitchen floor, it might point to death after breakfast, rather than before it.

(Camps [7])

Never to be disregarded are the variations which exist in the speed with which food normally passes through the gastrointestinal tract of different persons. Moreover, emotional upsets can produce changes in gastrointestinal motility. Thus psychogenic pylorospasm can prevent normal departure of a meal from the stomach for several hours. At the opposite, extreme hypermotility caused by emotional disturbance can result in hurried transit of food and chyme through the gut with resultant diarrhoea.

The physical and chemical facets of digestion are beset by so many imponderable and uncontrollable variables *in vivo*, that one cannot rely on the extent of mechanical dissolution and chemical breakdown of the gastric content, to help reach a reasonable estimate as to how long food was present in the stomach. Careful consideration of these factors indicates that one must be extremely wary about making statements about the time since death in relation to the last known meal on the basis of the "amount of digestion" of the gastric contents.

(Adelson [1])

In conclusion, the emptying of the stomach is a complex multifactorial process and its evaluation for determining the time of death requires caution and careful review of all limiting factors. Consideration must also be given to the possibility of one or more close consecutive meals.

(Spitz [32])

For many years, pathologists have argued over the reliability of the state of digestion of gastric contents as an indicator of the time between the last meal and death, the leading case in modern times being that of Truscott in Canada. There is now almost a consensus that with extremely circumscribed exceptions, the method is too uncertain to have much validity.

(Knight [15])

Thus this study demonstrates that the gastric emptying of either liquids or solids is subject to relatively wide differences in the same and different individuals, even if the same meal is ingested. If in addition to this we add differences in the weight, caloric content and composition of the meal we would see even greater differences in half-emptying time.

(Di Maio and Di Maio [8])

9.1 Is There Post-mortem Transport of Gastric Contents?

Previously published reports claimed that post-mortem transport of gastric contents to the duodenum occurs; these reports were based on animal experimental observations of post-mortem electrical and pharmacological excitability of gastric smooth muscles and volume-dependent peristalsis of the gastric wall [9,14]. When pressure was applied to the gastric wall with high filling volumes of the stomach, contractions of the wall were observed [9].

Table 9.1 Post-mortem Gastric Emptying: Observation of Stomach and Small Bowel under Direct View

Material	Method
10 rats (HAN-SPRD, body weight about 100 g); no feeding 2 days before death; anaesthesia with ether; death from KCl IV (5×) or ether/O_2 deficiency (5×).	Immediately after circulatory arrest: • Opening of the abdomen. • Pinching of the pylorus. • Positioning of a stomach sound. • Instillation of blue gelatine into the stomach. • Removing the clamp.
	In no case post-mortem was there peristaltic transport of gastric contents into the duodenum.

Abbreviations: IV, intravenously; KCl, potassium chloride.

Table 9.2 Observing the Stomach and Small Bowel under Direct View: Dependence of Antemortem Transport on Survival Time

Material	Method
4 rats (HAN-SPRD, body weight about 100 g); anaesthesia with ether.	During anaesthesia: • Positioning of a stomach sound. • Instillation of blue gelatine into the stomach. • Survival time 2, 5, 10, 20 minutes; then • Death due to KCl IV. • Opening of the abdomen.
	Transport distance into the small bowel depending on the survival time: 2 minute –2 cm. 20 minute –15 cm.
	No post-mortem gastric emptying, but post-mortem transport of small bowel content did occur.

Abbreviations: IV, intravenously; KCl, potassium chloride.

Table 9.3 Observing Stomach and Small Bowel under Direct View: Effect of Prostigmine on Post-mortem Transport

Material	Method
4 rats (HAN-SPRD, body weight 200 g); no feeding 2 days before death; anaesthesia with ether; death from KCl IV (2×) and exsanguination.	• 4 min before death, 0.28 mL prostigmine given IV. • Opening of the abdomen immediately after circulatory arrest. • Pinching of the pylorus. • Positioning of a stomach sound. • Instillation into the stomach. • Removing the clamp.
	No post-mortem transport of gastric contents.

Abbreviations: IV, intravenously; KCl, potassium chloride.

Table 9.4 Post-mortem Gastric Emptying: Radiological Control of Gastric Transport

Material	Method
10 rats (HAN-SPRD), body weight 150–180 g; no feeding for 1 day before death (7×); feeding immediately before death (3×); prostigmine IV 5 min before circulatory arrest (2×); death by ether/O_2 deficiency.	• Immediately after circulatory arrest, instillation of barium sulphate into the stomach by a stomach sound (3–5 mL, 10°C). • Radiological controls taken (anteroposteriorly and laterally) of the abdomen immediately after circulatory arrest, 10–15 minutes post-mortem, 30 minutes post-mortem (see Figure 9.1 [a] and Figure 9.2 [a]). • 2 hours post-mortem: preparation of stomach and small bowel (see Figure 9.1 [b and c] and Figure 9.2 [b]).
	No post-mortem transport of gastric contents (neither barium sulphate nor solid stomach contents).

Abbreviation: IV, intravenously.

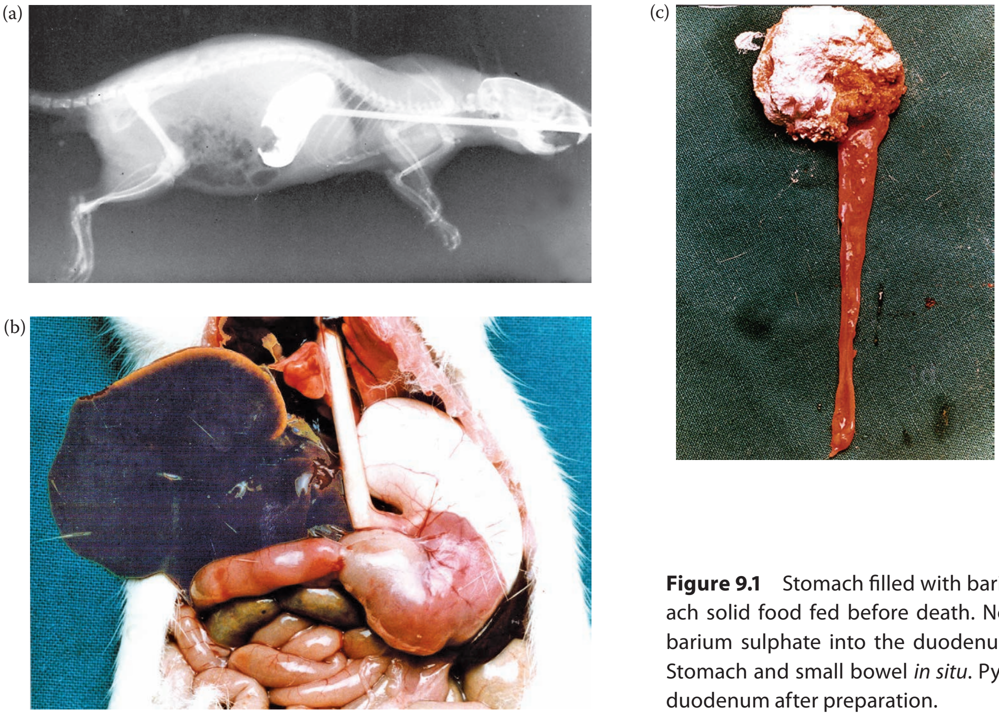

Figure 9.1 Stomach filled with barium sulphate; in the distal stomach solid food fed before death. No transport either of food or of barium sulphate into the duodenum. (a) Radiographic control. (b) Stomach and small bowel *in situ*. Pylorus fastened. (c) Stomach and duodenum after preparation.

Our own animal experiments [19,20] were carried out to answer these questions under the following circumstances (Tables 9.1–9.4):

1. Is there any post-mortem transport of stomach contents applied immediately after circulatory arrest to the stomach?
2. Is there any transport of stomach contents (gelatine) applied before death, depending on survival time?
3. Is there any effect of prostigmine on post-mortem peristalsis?
4. Is there any effect of feeding before death?

The stomach and small bowel were observed under direct vision after opening the abdomen, or the stomach contents (barium sulphate) were seen by means of a radiological control. In all cases, preparation of the stomach and small bowel was carried out 2 hours post-mortem.

Although peristaltic twitchings of the stomach were visible under direct view, no case of peristaltic emptying of the gastric contents was observed after death.

Even in the cases of feeding immediately before death, there was no transport of food to the duodenum (Figure 9.1). Correspondingly, when the whole stomach was filled with barium sulphate, no transport to the duodenum occurred (Figure 9.2). Post-mortem peristaltic transport of the small bowel contents may occur during the first minutes after death.

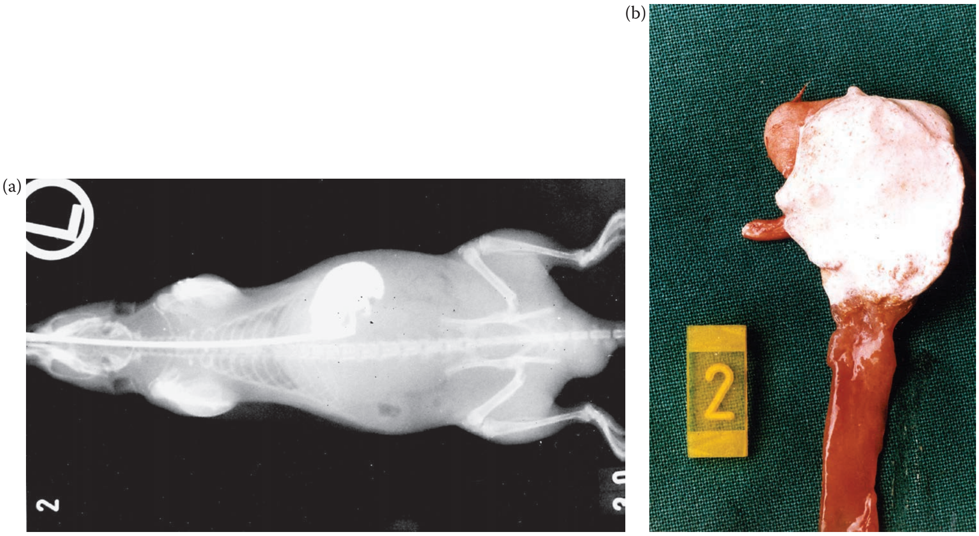

Figure 9.2 The whole stomach filled with barium sulphate. No transport into the duodenum. (a) Radiographic control. (b) Stomach and duodenum after preparation.

Under intravenous prostigmine, there was also no peristaltic gastric emptying, although the peristaltic twitchings may have been stronger. Depending on the survival time, liquid stomach contents (coloured gelatine) applied 2–20 minutes before death may have been transported to the duodenum. Overall, there was no evidence of any functionally relevant post-mortem gastric peristalsis with post-mortem transport of the gastric contents.

The ‘fastener’ function of the pylorus clearly remains stable after death. These findings correlate with those found at autopsy by the German pathologist Ludwig Aschoff (1921), who was able to perform autopsies at about 30 minutes after death during the First World War. Aschoff always found the pylorus fastened, whereas the supravital contraction of the pylorus occurred without relaxation, followed by rigor mortis [2].

Another argument for the post-mortem stable fastener function of the pylorus, and against post-mortem gastric emptying, is that in cases of newborn infants who survived only for a few minutes, air may be found in the stomach but not in the small bowel. Furthermore, in the previously mentioned investigations that claimed post-mortem peristaltic emptying of gastric contents, this could be observed only when high pressures were applied to the stomach wall.

9.2 Gastric Emptying Pattern

Gastric emptying has been studied and quantified since the 1980s by using different methods (radiological, intubation aspiration, radioisotopes, ultrasound, absorption kinetics of orally administered solutes and ferromagnetic traces) [13,23–25].

Liquids leave the stomach much more rapidly than do solids. For liquids, gastric emptying clearly follows an exponential function, but solids show a linear emptying pattern. A mixed meal shows an exponential emptying pattern, with the emptying time itself depending on the volume and composition of the last meal(s) and with carbohydrates, proteins and lipids leaving the stomach in that order. The following gastric emptying times have been cited in the literature:

- One to 3 hours for a light, small-volume meal.
- Three to 5 hours for a medium-sized meal.
- Five to 8 hours for a large meal.

Data relating to the gastric emptying pattern of solids and liquids are based on radionuclide studies (Table 9.5), but in the older German literature, tables were provided that indicated how rapidly different liquids, vegetables and mixed meals leave the stomach (Table 9.6).

Table 9.5 Solid and Liquid Gastric Emptying in Normal Subjects Assessed by Dual Radionuclide Methods

Authors	No. of subjects	Meal size (g)	Solids 50% emptying time (min)	Liquids 50% emptying time (min)
Fischer et al. (1982)	20	380	100 ± 4	30 ± 3
Heading et al. (1976)	10	185	120 ± 6	45 ± 4
Horowitz et al. (1984)	22	250	78 ± 4	19 ± 1
Moon et al. (1981)	8	300	77 ± 5	38 ± 4
	8	900	146 ± 26	81 ± 12
	10	1692	277 ± 44	178 ± 22
Wright et al. (1993)	31	410	87 ± 9	63 ± 6

Table 9.6 Solid and Liquid Gastric Emptying According to Pensold and Stinzing

Food leaving stomach	Quantity (g)
1–2 hours	
Water	100–200
Carbon dioxide, water	220
Tea	200
Coffee	200
Cocoa	200
Beer	200
Light wines	200
Milk (boiled)	100–200
Beef tea	200
2–3 hours	
Coffee with cream	200
Cocoa with milk	200
Wine	200
Water, beer or boiled milk	300–500
Egg (uncooked), scrambled or boiled	100
Beef/sausage	100
Boiled fish	200
Cauliflower	150
Potatoes	150
Cherries	150
White bread	70
Asparagus (boiled)	150
3–4 hours	
Date	100
Bread	40
Boiled chicken	220–230
Beef, boiled or uncooked	250
Ham, boiled or uncooked	160
Roast veal	100
Rice	150
Apple	150
Bean	150
Spinach	150
4–5 hours	
Ham, fatty	120
Eggs (5)	—
Beefsteak, roasted	250
Hare, roasted	150
Goose, roasted	250
Canard, roasted	280
Herring, salted	200
Lentils (porridge)	150
Peas (porridge)	200

Source: From Tröger HD, Baur C, Spann KW. *Mageninhalt und Todeszeitbestimmung*. Lübeck, Schmidt-Römhild, 1987.

Table 9.7 Aetiology of Delayed and Rapid Gastric Emptying

Transient delayed gastric emptying.

- Postoperative illness.
- Acute viral gastroenteritis.
- Hyperglycaemia.
- Drugs: morphine, anticholinergics, levodopa, beta-adrenergic agonists, nicotine.
- Stress: labyrinthine stimulation, cold, pain, pectin supplementation.

Chronic gastric stasis.

- Diabetes mellitus.
- Postsurgical—truncal vagotomy with pyloroplasty and antrectomy.
- Gastro-oesophageal reflux.
- Anorexia nervosa.
- Progressive systemic sclerosis.
- Chronic idiopathic intestinal pseudo-obstruction.
- Amyloidosis.
- Myotonia dystrophica.
- Familial dysautonomia.
- Dermatomyositis.
- Tachygastria.
- Paraplegia.
- Idiopathic myocardial infarction.
- Acute abdomen.
- Laparotomy.
- Physiological: liquids, acid, lipids, left-side position.

Rapid gastric emptying.

- After gastric surgery.
- Vagotomy.
- Antrectomy/subtotal gastrectomy.
- Zollinger–Ellison syndrome.
- Duodenal ulcer disease.
- Reserpine.
- Physiological: liquids, hunger.

Data from Horowitz M, Pounder DJ. Gastric emptying: forensic implications of current concepts. *Med Sci Law* 1985;**25:**201–214; and Tröger HD, Baur C, Spann KW. *Mageninhalt und Todeszeitbestimmung*. Lübeck, Schmidt-Römhild, 1987.

Modified from Horowitz M, Pounder DJ. Gastric emptying: forensic implications of current concepts. *Med Sci Law* 1985;**25:**201–214.

It should be kept in mind that different anatomical and functional disorders cause either delayed or rapid gastric emptying (Table 9.7). For example, in cases of raised intracranial pressure, gastric emptying may cease for several days. Püschel [27] reported data relating to solid stomach contents found at autopsy 10 days after scalding, 5 days after subdural haematoma, 9 days after scalding, 11 days after polytrauma and even a bolus death 14 days after subdural haematoma with entirely parenteral nutrition.

Horowitz and Pounder [13] summarized their review on gastric emptying as follows:

1. Simultaneously ingested liquid, digestible solid and non-digestible solid foods leave the stomach at different rates (see also Figure 9.3).
2. The emptying pattern of low-calorie liquids approximates a mono-exponential (volume-dependent) process that results primarily from the motoric activity of the proximal stomach.

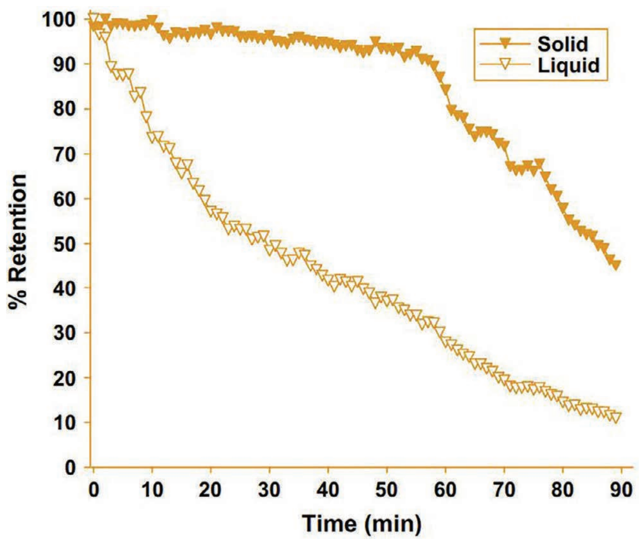

Figure 9.3 Gastric emptying curves for a solid and liquid meal in a healthy volunteer. Liquid emptying begins instantly in an exponential fashion, while the linear solid emptying begins after the lag phase.

(From Hellstrom et al. 2003).

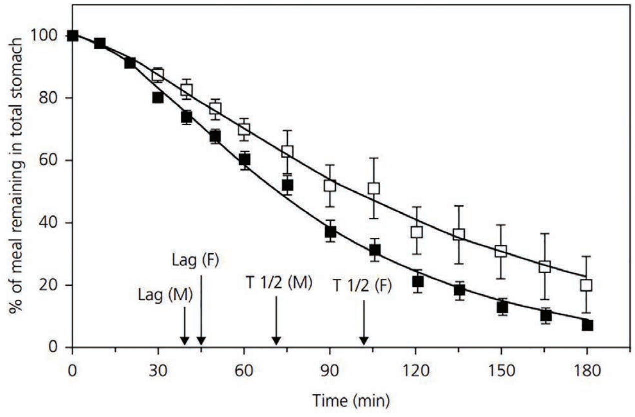

Figure 9.4 Emptying patterns of a test solid meal in normal males (■) and females (□). Almost 50% of the meal has been emptied by 70 minutes in males compared to 100 minutes in premenopausal females.

(From Knight et al. 1997).

3. The emptying of digestible solids usually occurs much more slowly than that of liquids and approximates a linear pattern following an initial lag period. It is primarily dependent on the motor activity of the distal stomach.
4. The emptying of larger, non-digestible particles chiefly occurs during the interdigestive periods, as a specific result of gastric motor activity.
5. Meals of higher osmotic and caloric content are emptied more slowly.
6. There is a substantial variation in emptying rates in normal subjects, and this variation may even be altered by diseases.

The emptying in solids is slower than that of liquids, with an initial lag phase as solids are retained before straight line elimination.

Furthermore, there is a gender difference in the gastric emptying pattern of solid food in premenopausal woman and man: it is slower in woman compared to men of the same age (Figure 9.4).

9.3 Estimation of Time of Death from Gastric Contents

From the examination of the stomach contents, only a rough estimation can be derived, and this may extend over a few hours. According to Horowitz and Pounder [12], only the solid components of a mixed solid and liquid meal should be considered, and the weight of the stomach contents should be compared with the estimated weight of the last meal and reference made to the known 50 per cent emptying times for the solid components of meals of various sizes (see Table 9.5).

Tröger et al. [33] compared the gastric contents (volume) found at autopsy with time and volume of last meals on an autopsy collective of 47 cases (sudden and unexpected death, exclusion of brain tumours, gastrointestinal tract surgery, intoxication, alcoholism). The gastric contents (as per cent volume of the last meal) were plotted against the survival time (see also [18]). Only a gastric content weight of more than 10 g was considered, and a regression line and 90 and 98 per cent confidence limits were calculated (Figure 9.5) [3].

The following conclusions were derived from the graph:

- If 90 per cent of the last meal is still found in the stomach, the last food intake was probably within the last hour before death, with 98 per cent confidence limits of 3–4 hours.
- At autopsy, if 50 per cent of the volume of the last meal is found in the stomach, the last food intake was about 3–4 hours before death, with 98 per cent confidence limits of not less than 1 hour and not more than 10 hours.
- If only 30 per cent of the last meal is found, the last food intake was about 4–5 hours before death, with 98 per cent confidence limits not less than 1–2 hours and not more than 10–11 hours.

The data shown in Figure 9.5 are valid only for mixed food. If the volume of the last meal is not known exactly, tables for the calculation of restaurant portions have been published by Tröger et al. [31].

Pure carbohydrate food leaves the stomach earlier than does mixed food. Therefore, a specialized graph was also derived for pure carbohydrate food (gastric contents in relation to the volume of the last meal, Figure 9.6), and a graph is also available for baby food (Figure 9.7). Because of the small sample sizes, confidence limits could not be calculated, and in the actual case only mean values could be estimated.

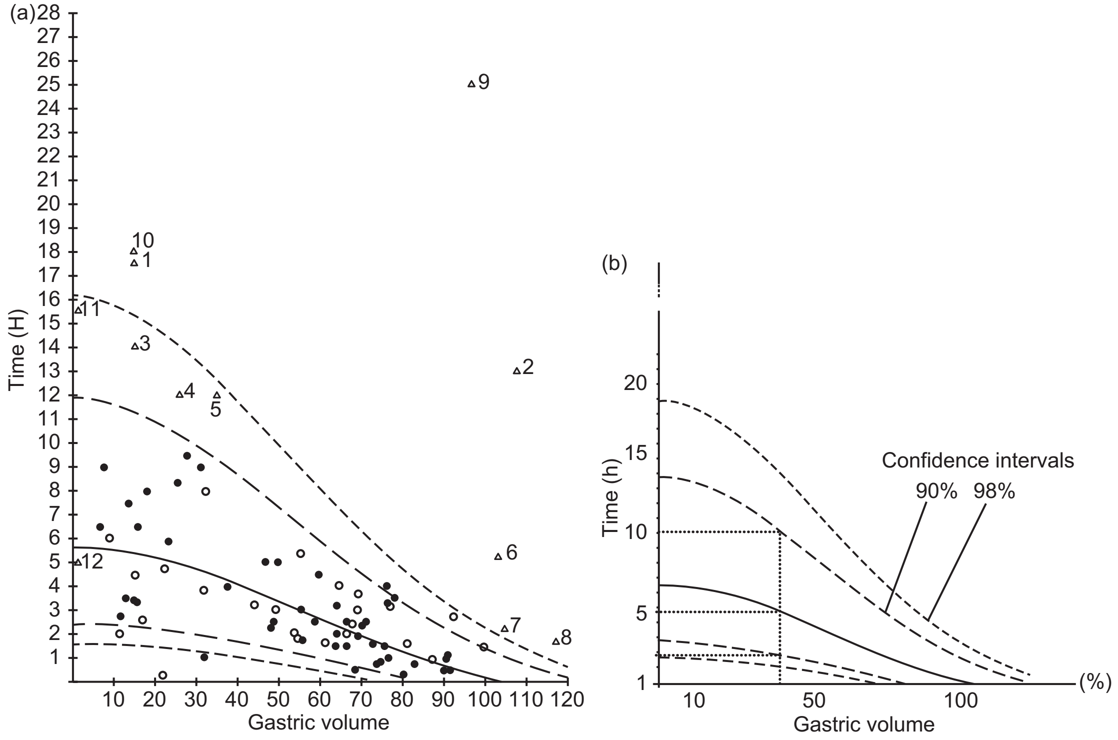

Figure 9.5 (a) Relation between gastric volume of a mixed meal in per cent of ingested volume and time after food intake with regression line, 90 and 98 per cent limits of confidence. Whole sample consists of 48 cases. Closed circles, normal cases; open circles, alcohol concentration between 0.3 and 3.18 per cent (*n* = 17); squares, death after hospitalization (*n* = 8); triangles, special cases (intoxication, trauma to the head). (b) Procedure in practice. From the stomach content in per cent of the ingested volume, an estimation of the survival period can be made.

(From Baur C, Spann KW, Tröger HD, Schuller E. Magenfüllung und Todeszeitpunkt. *Beitr Gerichtl Med* 1980;**38:**193–197.)

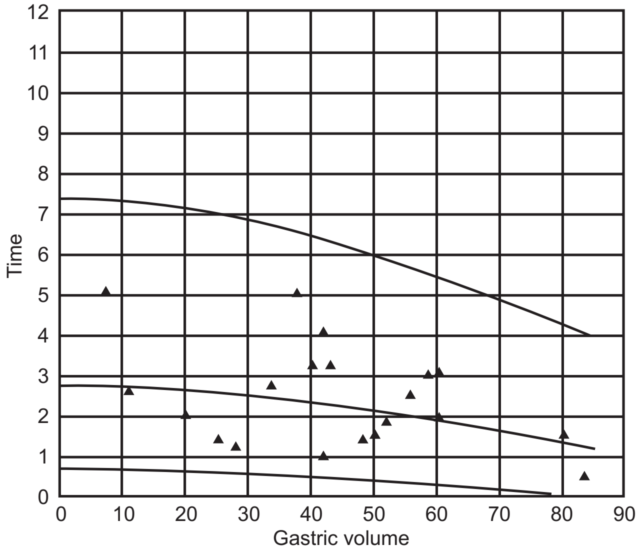

Figure 9.6 Pure carbohydrate food: rest volume in per cent of ingested volume plotted against the survival period after food intake. Regression line and 90 per cent limits of confidence.

(From Tröger HD, Baur C, Spann KW. *Mageninhalt und Todeszeitbestimmung*. Lübeck, Schmidt-Römhild, 1987.)

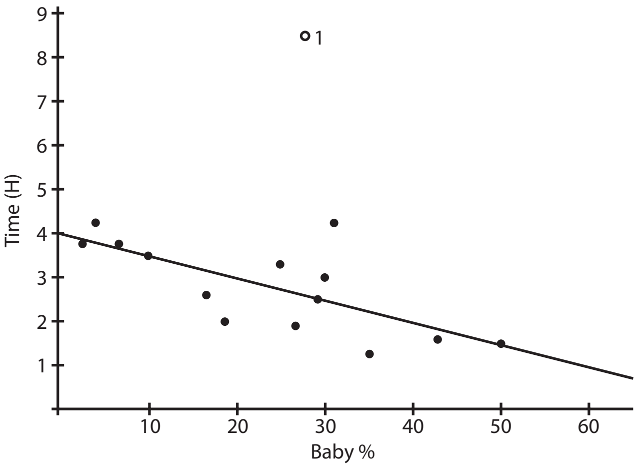

Figure 9.7 Babies up to 10 months—rest volume in per cent of the ingested volume in relation to the time since food intake. One case of fatal intoxication.

(From Tröger HD, Baur C, Spann KW. *Mageninhalt und Todeszeitbestimmung*. Lübeck, Schmidt-Römhild, 1987.)

9.4 Practical Procedure

In practical terms, the stomach contents at autopsy (mixed food with evidence of meat, carbohydrates, vegetables) are weighed and compared with the volume of the last meal. If the volume of the last meal is not known exactly, the gastric contents can be compared with typical restaurant portions. The remaining volume, expressed as a percentage of the ingested volume, provides the mean survival time after food intake, with the corresponding confidence limits. The actual case must be comparable to the case from which the graph was calculated.

For mixed food, these graphs are advantageous when estimating the time since death because the confidence limits derived from casework material can be used, and subjective rough estimations can be avoided. For the identification of food ingredients in stomach contents, the use of microscopic and/or immunological identification methods may be necessary, and these methods have been described in detail in a monograph [33]. For special identification methods, experts must be consulted.

To examine gastric contents, an additional sieve analysis is recommended [28], using a sieve tower. This equipment consists of a collecting basin and four sieves, each with a 20-cm diameter, which can be fitted together. The mesh diameters of the four sieves are 6.3, 4, 2 and 1 mm, respectively.

After weighing the gastric contents, the whole volume is placed into the upper sieve (6.3-mm mesh). If the contents are viscous, water will be added; this permits the contents to be separated into one liquid and up to four solid phases, and these can be further analysed as appropriate (Figures 9.8 and 9.9).

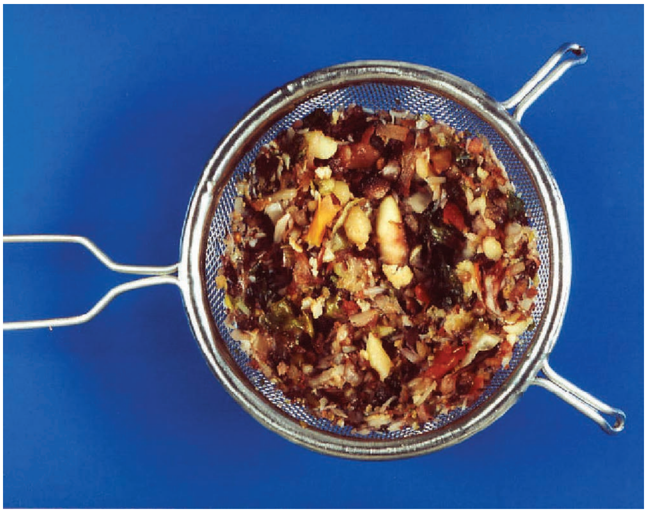

Figure 9.9 Solid phase of gastric contents consisting of vegetables (mixed salad) with only slight digestion. Victim stabbed soon after food intake (1–2 hours).

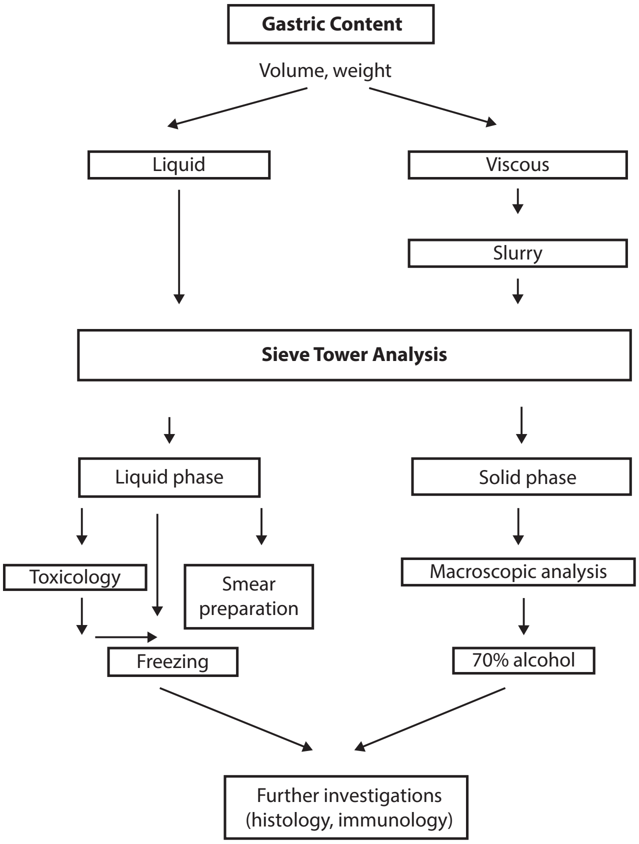

Figure 9.8 Sieve tower analysis of gastric contents allowing further preparation and investigation of the various phases of gastric content.

(From Rabl W, Sigrist T. Auftrennung des Mageninhaltes mittels Siebturm-Technik. *Arch Kriminol* 1992;**189**:164–168.)

9.5 Conclusions

It is thus apparent that the factors affecting gastric emptying are multiple and complex. Brophy et al. [5] tested the same subjects on different days with identical meals and liquids. These investigators showed marked variation even in the same individual at different times; the half-emptying times of solids ranged between 29 and 92 minutes, whereas for orange juice the times varied between 12 and 30 minutes.

Attempting to use the *state of digestion*, rather than the quantity of food, as a measure of time since ingestion is even more fraught with uncertainty. Assessing the stage of digestion in terms of time is subjective and almost impossible because virtually no one has any standardized control data for matching. Moreover, the original nature of the meal is usually unknown, so the appearance of the stage of digestion of, say, porridge and bread would be utterly different, at 1 hour from swallowing, from that of meat and raw root vegetables.

In summary, the quantity and digestive appearance of gastric contents are modified by the following factors:

- The total quantity of food taken at a meal.
- Additional 'snacks' taken between meals, especially from the modern habit of 'grazing', frequently on quick 'convenience' foods. Where frequent snacking occurs, food may still be in the stomach when the meal under consideration arrives.
- The ratio of solid to liquid in the meal and later 'top-ups' of liquids or solids.
- The carbohydrate and fat contents compared with more inert fibres, etc.
- Marked variations among individuals.
- Variations in the same individual from day to day (Brophy et al. [5]).
- Dramatic variations resulting from psychogenic and endocrine factors of emotion, fear, pain, anger, shock and trauma—with or without unconsciousness.

From the foregoing discussion, it is readily apparent that there is a whole range of variable factors making it impossible to use stomach contents as definitive evidence in estimating the time since death.

Even generalizations so often used by pathologists and other medical witnesses can be wildly incorrect, sometimes to the detriment of justice. However eminent a pathologist may be, their expertise on this matter is of necessity limited. This pathologist may have conducted thousands of post-mortem examinations, in each one of which the stomach contents have been noted. However, in most cases, the issue of the time since death does not need to be considered. Also, in most cases, the time and nature of the last meal are unknown and are usually of no interest. So, where does the medical witness obtain the sometimes dogmatic evidence that they deliver in court with such pontifical gravitas?

It may be true that for the majority of persons, the 'average meal' leaves the stomach in something between 30 minutes and 3 hours. However, these persons are not subjects of a forensic examination that is necessitated by a violent crime that may have all the connotations of emotion, fear, injury and so on that are well known to disrupt the digestive process. In addition, the 'majority of persons' leaves a very sizeable minority, whose gastric emptying may lie well outside the so-called normal parameters. Because proof in a criminal case must be 'beyond reasonable doubt', this leaves only little scope for firm testimony based on such shifting sands as gastric physiology.

Unfortunately for defence counsel, the value of such evidence tends to be one-sided—in other words, the unreliability of timing of death from stomach contents allows it to be legitimately claimed, in almost all situations, that death *could* have occurred during the period alleged by the prosecution—whereas the same evidence can virtually never be used to claim that it *could not* and thus remove the time of death into a period of alibi. This negative trend may be persuasive when added to other evidence, even though it has no probative value. A prime example of this is the Truscott case described here.

9.6 A Case History: Steven Truscott

The best-known instance where the estimation of time since death based on the post-mortem evaluation of stomach contents became a matter of international controversy is that of Steven Truscott.

In 1959 in Ontario, Canada, a 14-year-old boy was accused of sexually assaulting and strangling a 12-year-old girl, Lynne Harper. He was found guilty and was sentenced to be hanged, although on appeal several months later, this sentence was reduced to life imprisonment. Disquiet about his conviction led an investigative journalist, Isobel Lebourdais, to write a book on what was claimed to be an injustice; subsequently, a considerable political furore developed.

In 1966, the case was re-heard at the Supreme Court, and many forensic experts from Canada, the United States and Britain gave evidence, mainly on the reliability of estimating the time of death from gastric contents. These experts included Professor Milton Helpern from New York, Professor Francis Camps and Professor Keith Simpson from Britain, Dr Charles Petty (Baltimore, Maryland), Dr Frederick Jaffe (Toronto, Canada), Dr Sam Gerber (Cleveland, Ohio), Mr John Funk (Toronto, Canada) and Dr Noble Sharpe (Toronto, Canada). The Supreme Court upheld the conviction, and Truscott served about 10 years in prison and, on his release, assumed a new identity. The case remained in the public eye, however, with television and press coverage at intervals. In 2001, Steven Truscott declared his intention of clearing his name. He claimed that he was innocent of the crime for which he was convicted more than 40 years ago, and further expert medical opinion was being sought. The circumstances indicated that Truscott had only a period of 45 minutes in which he could have committed the crime; Lynne Harper was seen alive at 7:15 p.m., and Truscott was back home with numerous witnesses at 8:00 p.m. on the evening in question. The body was not discovered until 41 hours later, and a post-mortem examination was carried out 48 hours later, 2 days after the girl was last seen alive. The pathologist was Dr John Penistan, a hospital histopathologist who also performed medico-legal autopsies. He gave evidence to the effect that, based on rigor mortis, hypostasis and stomach contents, the time of death lay within a 30-minute interval, 2 days before the autopsy.

The facts relating to the gastric contents were that the girl ate a meal of turkey, cranberry sauce, peas, potatoes and pineapple pudding between 5:30 and 5:45 p.m. that day. There were other foods also on the table, but it is not known whether she took those, nor was there any knowledge of what fluids were taken.

The pathologist recorded that the stomach contents consisted of 'approximately one pint (568 mL)', although the evidence of two other doctors who examined the material in the forensic laboratory was that the volume was about 300 mL.

The material was described by Dr Penistan in his autopsy report as 'poorly masticated, only slightly digested food, including peas, onion, corn and a few shreds of apparent meat'. The forensic scientist, Mr Funk, described it as being of the consistency of 'a thick stew'. Dr Noble Share, a medically qualified forensic scientist, said it was like 'a lumpy porridge'.

Dr Penistan's actual words in his autopsy report, to which he adhered during the trial, were as follows:

> Note on time of death; this opinion, which would place the time of death between 7:15 and 7:45 p.m. on 9 June 1959, is based on the following observations and assumptions:
>
> The extent of decomposition which is entirely compatible with death approximately 45 hours prior to identification, having regard to the environmental and climatic conditions.
>
> The extent of rigor mortis. This had almost passed off—a finding again compatible with death at the suggested time.
>
> The limited degree of digestion and the large quantity of food in the stomach. I find it difficult to believe that this food could have been in the stomach for as long as 2 hours unless some complicating factor was present, of which I have no information. If the last meal was finished at 5:45 p.m., I would therefore conclude that death occurred prior to 7:45 p.m. The finding would be comparable (sic.) with death as early as 7:15 p. m.

Although Dr Penistan actually concludes with an opinion that death was *consistent* (although he uses the word 'comparable') with occurring as early as 7:15 p.m., his earlier phraseology was that the findings were *indicative* of death occurring between 7:15 and 7:45 p.m. This opinion was repeated throughout the trial and the later Supreme Court hearing, both by Dr Penistan and by those expert witnesses who supported his view—in spite of the defence witnesses and lawyers forcibly indicating that the medical evidence also allowed death to have taken place well outside those unreasonably narrow limits.

Although there was considerable other non-medical evidence involved in this case, there is no doubt that dogmatic adherence to unreliable pathological findings, which retrospectively placed the time of death within a 30-minute bracket from an autopsy 2 days later, contributed to the death sentence being passed on a 14-year-old boy.

9.7 Further Case Histories

In a homicide case the accused claimed death of the victim occurred between 5:00 and 8:00 a.m. since for this time period the owner of the house where the victim was found had no alibi. At autopsy: 300 mL content in the stomach of the victim, the duodenum empty, especially no solid content. In the stomach pieces of tomato, potatoes, cucumber, carrots, green salad, no meat.

Last meal between 9:00 and 11:00 p.m. The last meal consisted of salad and potatoes. Obviously, the whole meal was still in the stomach.

According to the graph, the mean survival time until death would be about half an hour, the maximum time about 2.5 hours (Figure 9.10). That would mean that death had occurred before 1:30 a.m., a time where the owner of the house had an alibi.

The accused was sentenced for murder.

9.7.1 Case History

A prostitute was found murdered in her apartment in an eros centre (cause of death: plastic bag suffocation and ligature strangulation).

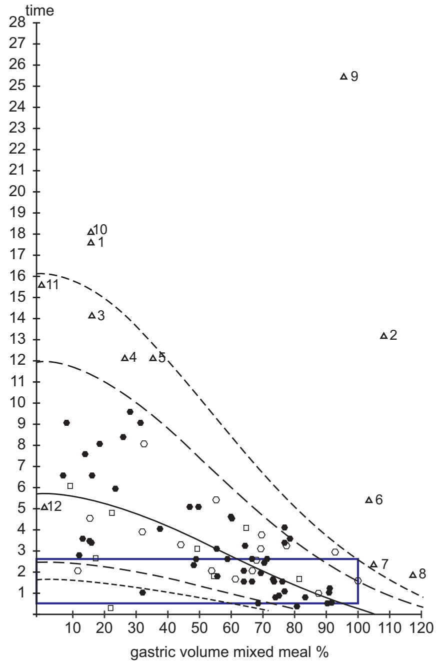

Figure 9.10 Relation between gastric volume and time after food intake. For details see 9.7.

One of the main questions was the time since death (see also the case history at the end of Chapter 1): 2:00 p.m. or 12 hours prior, 2:00 a.m.

In the stomach 100 mL of brownish content was found consisting of lentils. The duodenum was empty. Obviously, the last meal was eaten 3–5.5 hours prior to death. If she was murdered at 2:00 p.m., she must have eaten the lentils as breakfast. Her colleagues from South America said this would be a completely unusual breakfast: normal are bread, eggs and ham. Nobody would eat lentils at breakfast. This was another hint for time since death 12 hours prior after midnight.

9.7.2 Value of Stomach Content in a Case of Child Homicide Case Report History at the Time of Autopsy

A 22-year-old drug addict lived with her 4-month-old baby in a rehabilitation clinic. She became pregnant through rape. She had given birth to the infant on a prison term.

On August 5, around 9:10 a.m., the baby was found dead by the mother in the shared bed. She gave her child the bottle the night before at around 9:00 p.m. and then put the baby in bed to sleep. At around 1:30 a.m. she went to bed herself, the baby woke up and looked at her. When she woke up around 9:10 a.m., the mother found the lifeless child and called a nurse. The child had been lying face down in the mother's bed in prone position. White foam was found around mouth and nose.

The infant had previously been treated for bronchitis. However, on August 3 the doctor had already stopped all medication because the child did not present any symptoms.

9.7.3 Autopsy

Male infant with a body weight of 6.400 g and a body length of 60 cm. Brain weight 860 g, heart weight 33 g, weight of right lung 88 g, weight of left lung 67 g.

The autopsy showed a double system of livores: Livid livores on the front of the body corresponding to a prone position with pale area on the right side of the face. Livid livores on the back of the body corresponding to a supine position, also on the face with pale areas around the left ear.

The infant was in good condition and no injuries could be found on external inspection.

The scalp was without injuries. But the internal inspection revealed extensive blunt force against the head: small haemorrhages of the scalp in projection to the right and middle occipital bone (Figure 9.11). Extensive, thick-layered subperiostal haemorrhage on the left side of the middle

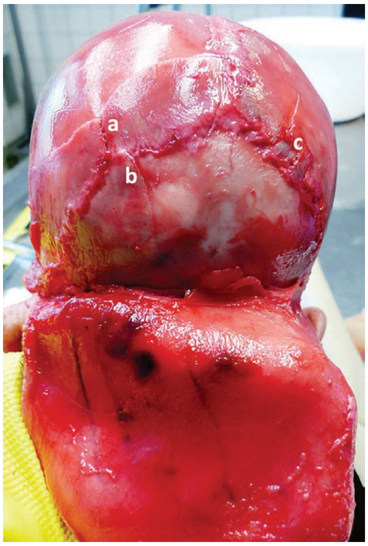

Figure 9.11 Some small haemorrhages in the scalp on the left side of the back of the head.

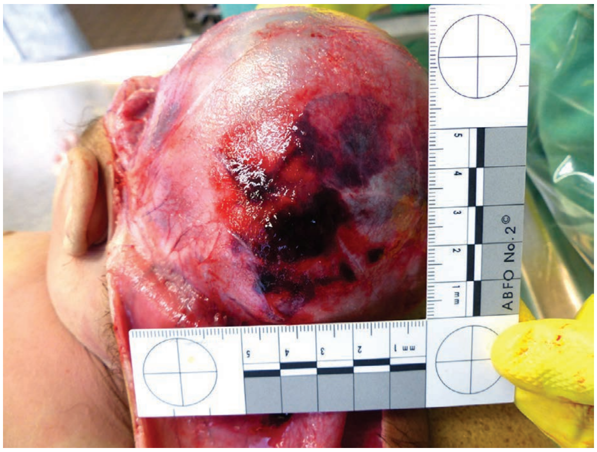

Figure 9.12 Subperiostal haemorrhage above fracture a (Figure 9.13).

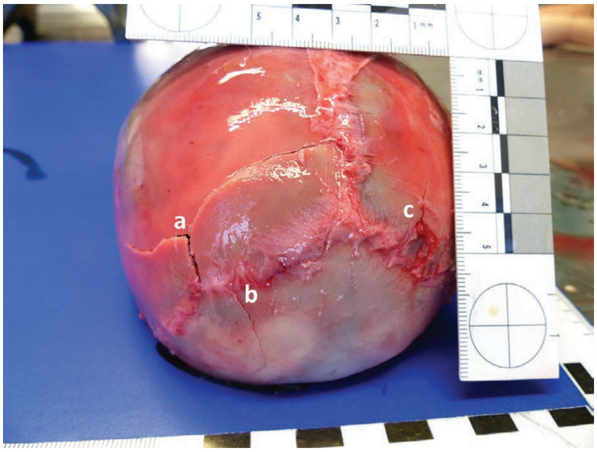

Figure 9.13 Three fracture areas at the back of the head (marked by small letters).

and upper back of the head (Figure 9.12). There were three fracture areas on the back of the head (Figure 9.13):

- One approximately 8 cm long, transverse, branched, partly gaping fracture of the left parietal bone at the back of the head with impression of 1–2 mm. Starting approximately in the middle of this fracture line, a fracture line of length approximately 1 cm running towards the neck, ending in the lambdoid suture.
- One arched, vertical, 4 cm long fracture line above the left occipital bone, running into the lambdoid suture.
- One linear, vertical fracture of the right parietal bone with a length of 2.5 cm above the middle back of the head, running into the lambdoid suture (Figure 9.14). Just before running into the suture two small areas of comminuted fracture of approximately 0.7 × 0.4 cm, respectively, approximately 1.2 × 0.4 cm.

Thin subdural haemorrhage covered both cerebral hemispheres. Pronounced cerebral oedema (860 g). No brain injuries were present.

Below the visceral pleura of both lungs were some spotted dark-livid discolouration on the anterior side of the lungs. In the bronchi, moderately whitish mucus. A moderate amount of blood and foamy liquid run off the cut surfaces.

In the stomach at least 150 mL of a whitish, milk-like liquid with white pasty fragments (Figure 9.15). Little greenish pasty content in the small and large intestines.

No evidence of organ malformations.

The cause of death was a craniocerebral trauma with three skull fractures and pronounced brain oedema.

Initially, the foam in front of mouth and nose led to the suspicion of an additional intoxication. Chemical-toxicological investigations were without results.

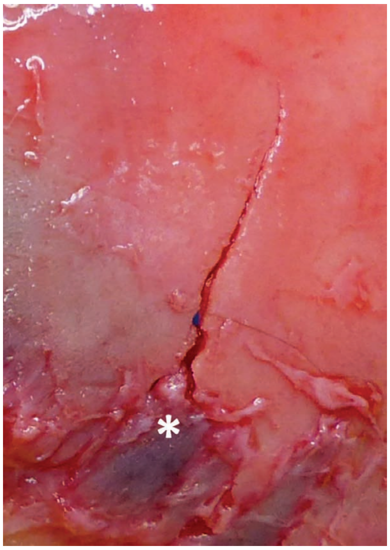

Figure 9.14 Fracture c on the right parietal bone. The white star shows the area of fragmentation close to the lambdoid suture.

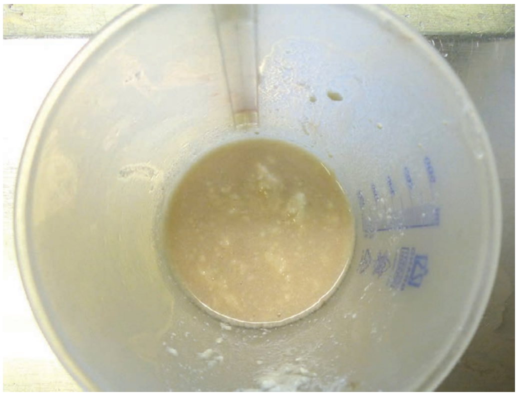

Figure 9.15 View into measuring cub with a part of the altogether 150 mL milky stomach content.

Histological examinations of the internal organs revealed cerebral oedema and pulmonary oedema with acute congestion of the lungs.

In suspicion of a possible additional shaking trauma, eye pathological examinations of both eyeballs were carried out, but did not reveal any pathological findings, especially no haemorrhages in the retina.

9.7.4 Further Police Investigation After Autopsy

The child's mother stated that the baby was completely normal during the day of August 4. The baby still had a little cough, and that's why she took the baby to the paediatrician last week. But the child no longer had to take medication for the bronchitis. It came out that the infant showed normal development. The baby suffered from colic and cried a lot.

On August 4, she gave the last bottle to the baby (180 mL milk formula) at around 9:00 p.m. The baby drank it well. The baby fell asleep laying in her bed. She then left the room and returned at midnight. Then she went to sleep on 1:30 a.m. At this time the baby woke up, looked at her and then fell asleep again. Normally, she would always get up around 6:00 a.m. However, that day she did not wake up until 9:00 a.m. because the night had been restless. When she woke up in the morning of August 5, she found that that the baby was dead and got help immediately. The troubled and crying mother called a nurse at 9:15 a.m. The baby was lying in prone position in the mother's bed with its head on the right side and was stiff and blue.

The mother had behaved abnormally on the night of August 4, but appeared neither drunk nor under the influence of drugs. At around 10:15 p.m., she said she wanted to go into town to drink alcohol, which a nurse refused to allow. She asked several times more urgently. After all, provided that she would not consume alcohol and organize childcare, she was allowed to go, but she could not guarantee that and stayed at home. At 11:25 p.m., she brought the nurse a letter of apology.

Other patients reported of an annoyed, rough and inappropriate behaviour of the mother towards the infant. She reported several times that she could not stand the screaming and snapped at and yelled at the crying baby. The mother reported feelings of hate, when the baby looked at her angrily while changing diaper, which reminded her of the child's father.

At autopsy approximately 150 mL milky fluid were found in the infant's stomach. Gastric contents alone allow only a rough estimation of the interval between the last meal and death. The state of digestion and the distribution of the last meal in the stomach and upper intestine have long been proposed as a method to estimate the time of death. For such estimation, the volume of the stomach contents compared with the volume of the last meal and transportation distance to the small intestine must be known. Even if the volume of the last meal is not known, the type of meal (i.e. breakfast, lunch, or dinner) may allow rough estimation of the time of day when death occurred. Gastric emptying has been studied and quantified during the past few decades using various methods, including radiology, intubation aspiration, radioisotopes, ultrasonography, absorption kinetics of orally administered solutes, and ferromagnetic traces.

Liquids leave the stomach much faster than solids. Whereas gastric emptying of liquids follows an exponential function, solids show a linear emptying pattern. The following gastric emptying times are given in the literature: 1–3 hours for a light small-volume meal, 3–5 hours for a medium-sized meal and 5–8 hours for a large meal. It must be kept in mind, however, that different anatomic and functional disorders can cause either delayed or more rapid gastric emptying. According to Horowitz and Pounder, only the solid compartment of a mixed solid and liquid meal should be considered, and the weight of the stomach contents should be compared with an estimated weight of the last meal, with reference made to the known 50 per cent emptying times for the solid components of meals of various sizes.

Tröger et al. compared the volume of the gastric contents found at autopsy with the time and volume of the last meals in an autopsy collection of 47 cases of sudden, unexpected death. Cases were excluded if there was a brain tumour, gastrointestinal tract surgery, intoxication, and/or alcoholism. Gastric content (% of the volume of the last meal) was plotted against the survival time. Only a gastric volume of 10 g was considered. The regression line and 90 and 98 per cent CIs were calculated. The authors arrived at the following conclusions. If 50 per cent of the volume of the last meal was found at autopsy, the last food intake occurred about 3–4 hours prior to death, with a 98 per cent CI of 1–10 hours. If 90 per cent of the last meal was found in the stomach, the last ingestion took place probably within the last hour prior to death, with a 98 per cent CI of 3–4 hours. However, conditions for delayed or rapid gastric emptying must be kept in mind.

It is thus apparent that the factors affecting gastric emptying are multiple and complex. Attempting to use the state of digestion, rather than the quantity of food ingested, to determine the time of death is fraught with uncertainty.

Based on the findings in 10 babies up to 10 months, Tröger et al. also presented the results of gastric contents in per cent and time after the last meal (Figure 9.7). There is a correlation with a correlation coefficient of 0.697 between gastric content and time. Obviously, there is a linear decrease of gastric content over the time, 4 hours after food intake the stomach seems to be empty. In the present case, the mother claimed she fed the infant with 180 mL formula. According to Tröger et al. amount of remaining stomach content of 83 per cent speaks for a time of death soon after feeding the infant at 9:00 p.m. Using a time-quantity diagram to estimate the duration of stomach emptying in infants (Figure 9.6), it can be assumed that the death occurred shortly (less than one hour) after food intake. One hour after eating 60 per cent of the amount fed (108 mL) would have been expected. According to the mother, the infant was still alive 4.5 hours after feeding. After this time the stomach would have been empty.

Furthermore, massive cerebral oedema was found as a result of the violence with skull fractures and subdural haemorrhage. This is to be regarded as the pathophysiological cause of death which could arise fast. The mother's reported reaction of the infant to her going to bed at 1:30 a.m. is not possible with regard to the severe traumatic brain injury, which took place directly after feeding 4.5 hours earlier.

In this way an estimation of the time of death was possible and the statements of the mother have been inexplicable.

Finally, on the last day of the main hearing at court, the mother confessed to the crime and stated that the baby smiled at her during the night, thus reminding her of the rape. She hit the baby against the edge of the table. Then she put the child back to bed and only informed the hospital staff the next morning. The child's mother was sentenced to six years in prison for manslaughter. After appeal by the public prosecutor and the infant's mother, the judgment was overturned by the Federal Court of Justice. Finally, the child's mother was sentenced to 11.5 years in prison for manslaughter of her own child.

References

1. Adelson L. *The Pathology of Homicide*. Springfield, IL, Charles C Thomas, 1974.
2. Aschoff L. Diskussionsbemerkung zu Mangold E: Über Automatie, Erregbarkeit und Totenstarre in verschiedenen Teilen des Froschmagens. *Dtsch Med Wochenschr* 1920;*16*:447–8.
3. Baur C, Spann KW, Tröger HD, Schuller E. Magenfüllung und Todeszeitpunkt. *Beitr Gerichtl Med* 1980;38:193–7.
4. Berg S. Der Beweiswert der Todeszeitbestimmung (Überlebenszeit). *Beitr Gerichtl Med* 1969;25:61–5.

5. Brophy CM, Moore JG, Christian PE, Egger MJ, Taylor AT. Variability of gastric emptying measurements in man employing standardized radiolabeled meals. *Dig Dis Sci* 1986;*31*:799–806.
6. Camps FE. Establishment of the time of death: a critical assessment. *J Forensic Sci* 1959;*4*:73–82.
7. Camps FE (ed.). *Gradwohl's Legal Medicine*. 3rd ed. Bristol, John Wright, 1976, p 98.
8. DiMaio D, DiMaio VJM. *Forensic Pathology*. New York, Elsevier, 1989, pp 36–42.
9. Forster B, Hummelsheim G, Döring G. Tierexperimentelle Untersuchungen über die postmortale Magenperistaltik bei Leuchtgas- und Parathion-Vergiftung. *Dtsch Z Gerichtl Med* 1965;*56*:148–59.
10. Gordon I, Shapiro HA, Berson SD. *Forensic Medicine: A Guide to Principles*. 3rd ed. Edinburgh, Churchill Livingstone, 1988, p 56.
11. Hellstrom PM, Gryback P, Jacobsson H. The physiology of gastric emptying. *Best Pract Res Clin Anaesthesiol* 2006;*20*(3):397–407.
12. Holczabek W. Zur Untersuchung des Magen-Darmtraktes für die Todeszeitbestimmung. *Beitr Gerichtl Med* 1961;*21*:23–7.
13. Horowitz M, Pounder DJ. Gastric emptying: forensic implications of current concepts. *Med Sci Law* 1985;*25*:201–14.
14. Joachim H. *Probleme der frühen Todeszeitbestimmung und die sogenannten supravitalen Reaktionen im Tierversuch*. Freiburg, Germany, Habil. Schrift, 1976.
15. Knight B. *Forensic Pathology*. 2nd ed. London, Edward Arnold, 1996, pp 89–90.
16. Knight B. The use of gastric contents in estimating time since death. In: Henssge C, Knight B, Krompecher T, Madea B, Nokes L, eds. *Estimation of the Time Since Death in the Early Postmortem Period*. 2nd ed. London, Edward Arnold, 2002, pp 209–15.
17. Knight LC, Parkmon HP, Brown KL, Miller MA, Trate SM, Maurer AH, Fisher MS. Delayed gastric emptying and decreased antral contractility in normal premonopausal woman compared with men. *Am J Gastroenterol* 1997;*92*(6):968–75.
18. Legge C. *The Use of Gastric Contents in Estimating Time Since Death*, Master of Science in Forensic Medical Sciences thesis. London, Queen Mary University of London, 2011.
19. Madea B, Oehmichen M, Henssge C. Postmortaler transport von Mageninhalt. *Z Rechtsmed* 1986;*97*:201–6.
20. Madea B, Oehmichen M, Henssge C. *Postmortale Magenperistaltik? Festschrift Prof Spann*. Berlin, Springer, 1986, pp 200–5.
21. Merkel H. Über Mageninhalt und Todeszeit. *Dtsch Z Gerichtl Med* 1922;*1*:346–58.
22. Modi JP. *Medical Jurisprudence and Toxicology*. Bombay, Tripathi, 1957.
23. Moore JG, Christian PE, Brown JA, Brophy C, Datz F, Taylor A, Alazraki N. Influence of meal weight and caloric content on gastric emptying of meals in man. *Dig Dis Sci* 1984;*29*:513–19.
24. Moore JG, Christian PE, Coleman RE. Gastric emptying of varying meal weight and composition in man. *Dig Dis Sci* 1981;*26*:16–22.
25. Moore JG, Tweedy C, Christian PE, Datz FL. Effects of age on gastric emptying of liquid-solid meals in man. *Dig Dis Sci* 1983;*28*:340.
26. Polson CJ, Gee DJ, Knight B. *The Essentials of Forensic Medicine*. 4th ed. Oxford, Pergamon Press, 1985, pp 32–3.
27. Püschel K. Nüchternheitsgebot und Aspirations prophylaxe aus rechtsmedizinischer Sicht. *AINS* 1996;*31*:248–50.
28. Rabl W, Sigrist T. Auftrennung des Mageninhaltes mittels Siebturm-Technik. *Arch Kriminol* 1992;*189*:164–8.
29. Simpson CK (ed.). *Taylor's Principles and Practice of Medical Jurisprudence*. 12th ed. London, J & A Churchill, 1965, p 210.
30. Sonderegger W. *Zeitbestimmungen nach biologisch-medizinischen Methoden in dem Gebiet der Rechtsmedizin*. Zürich, Medical Dissertation, 1916.
31. Sorge A. Die Verwertung des Mageninhaltes zur Bestimmung der Todeszeit und der Zeit der letzten Nahrungsaufnahme. Z *Medizinal Beamte* 1904;*17*:373–90.
32. Spitz WU. *Spitz & Fisher's Medicolegal Investigation of Death*. 3rd ed. Springfield, IL, Charles C Thomas, 1993, pp 28–31.
33. Tröger HD, Baur C, Spann KW. *Mageninhalt und Todeszeitbestimmung*. Lübeck, Schmidt-Römhild, 1987.

10 Immunohistochemical Methods as an Aid in Estimating the Time Since Death

Burkhard Madea

Contents

10.1 Immunohistochemical Detection of Insulin, Glucagon, Thyroglobulin and Calcitonin 309
10.1.1 Case Example 312
10.2 Conclusions 312

10.1 Immunohistochemical Detection of Insulin, Glucagon, Thyroglobulin and Calcitonin

Although morphological methods of death time estimation are of no practical value in forensic practice, there seems to be some change with the application of immunohistochemistry methods [1–8]. Wehner and colleagues studied whether a positive immunoreaction to antigens such as insulin, thyroglobulin or calcitonin is correlated with the time since death [4–8]. The philosophy behind these investigations is that with an increasing post-mortem interval, the tertiary structure of the antigen undergoes post-mortem changes, and as a result of protein denaturation, stainings become negative. For example, the colloid and the follicular cells of the thyroid give a positive immunoreaction for thyroglobulin until 5 days post-mortem, whereas none of the cases older than 13 days shows such a reaction (Figure 10.1). A negative reaction therefore means that a body has been dead for more than 6 days, and a positive reaction means that a body has been dead for less than 12 days.

Table 10.1 Immunohistochemical Detection of Insulin, Glucagon, Thyroglobulin and Calcitonin According to Wehner [2–6]

	Positive staining	Negative staining
Insulin	Up to 12 days in all cases	>30 days in all cases
Glucagon	Up to 6 days	>14 days
Thyroglobulin	Up to 5 days in all cases	>13 days in all cases
Calcitonin	Up to 4 days in all cases	>13 days in all cases

The pancreatic β-cells from up to 12-day-old corpses produce a positive immunoreaction towards insulin in all cases, whereas no corpse older than 30 days shows such a reaction. This means that in a case of negative immunoreaction, the time since death can be assumed to be more than 12 days before the autopsy. When there is a positive stain, the death must have occurred a maximum of 29 days earlier.

Calcitonin was always detectable in c-cells of the thyroid up to 4 days, and in bodies older than 13 days, there was always negative staining.

The results of the immunohistochemical detection of insulin, glucagon, thyroglobulin and calcitonin are summarized in Table 10.1.

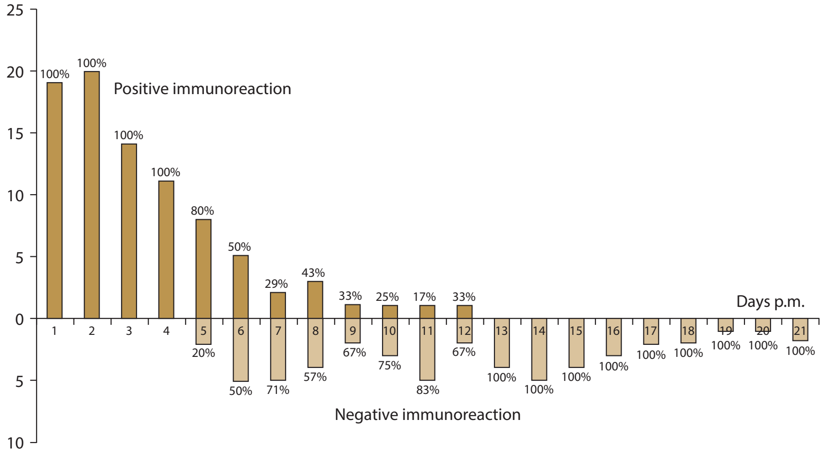

Figure 10.1 Overview of the time dependency of the stainability of thyroglobulin.

DOI: 10.1201/9781003244974-10

Meanwhile, a chart was developed to give a rough estimation of the time since death by immunohistochemical methods (Figures 10.2, 10.3 and 10.4).

We carried out a control study on 105 bodies. Positive immunoreactions for insulin and glucagon in the pancreatic tissue, and thyroglobulin and calcitonin in the thyroid gland are shown in Figure 10.5.

The original findings of Wehner et al. could be generally confirmed; however, for calcitonin and thyroglobulin earlier negative stainings were observed (Table 10.2).

When using the method in casework, the wider limits according to the results of both studies have to be taken into account to avoid false estimations of the time since death.

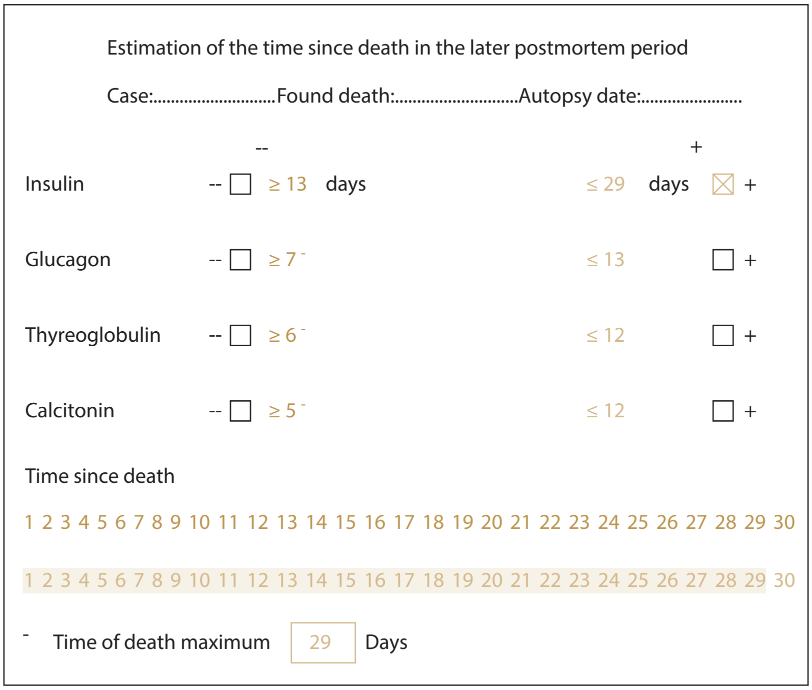

Estimation of the time since death in the later postmortem period

Case:............................Found death:............................Autopsy date:........................

-- +

Insulin -- ☐ ≥ 13 days ≤ 29 days ☒ +

Glucagon -- ☐ ≥ 7 ≤ 13 ☐ +

Thyreoglobulin -- ☐ ≥ 6 ≤ 12 ☐ +

Calcitonin -- ☐ ≥ 5 ≤ 12 ☐ +

Time since death

1 2 3 4 5 6 7 8 9 10 11 12 13 14 15 16 17 18 19 20 21 22 23 24 25 26 27 28 29 30

1 2 3 4 5 6 7 8 9 10 11 12 13 14 15 16 17 18 19 20 21 22 23 24 25 26 27 28 29 30

Time of death maximum 29 Days

Figure 10.2 Positive immunoreaction of insulin: time since death maximal 29 days.

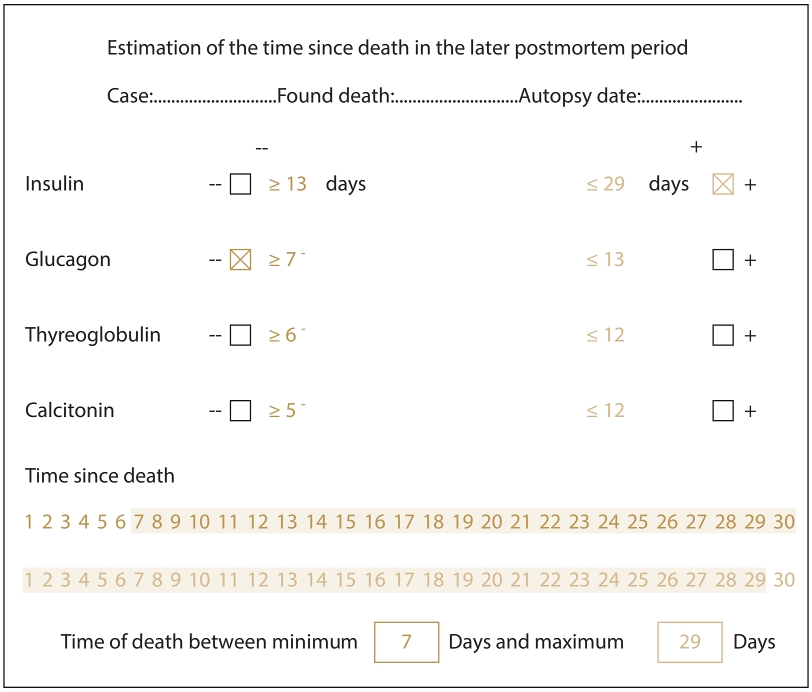

Estimation of the time since death in the later postmortem period

Case:............................Found death:............................Autopsy date:........................

-- +

Insulin -- ☐ ≥ 13 days ≤ 29 days ☒ +

Glucagon -- ☒ ≥ 7 ≤ 13 ☐ +

Thyreoglobulin -- ☐ ≥ 6 ≤ 12 ☐ +

Calcitonin -- ☐ ≥ 5 ≤ 12 ☐ +

Time since death

1 2 3 4 5 6 7 8 9 10 11 12 13 14 15 16 17 18 19 20 21 22 23 24 25 26 27 28 29 30

1 2 3 4 5 6 7 8 9 10 11 12 13 14 15 16 17 18 19 20 21 22 23 24 25 26 27 28 29 30

Time of death between minimum 7 Days and maximum 29 Days

Figure 10.3 Additional investigation of glucagon with a negative immunoreaction: delimitation of the time since death between 7 and 29 days.

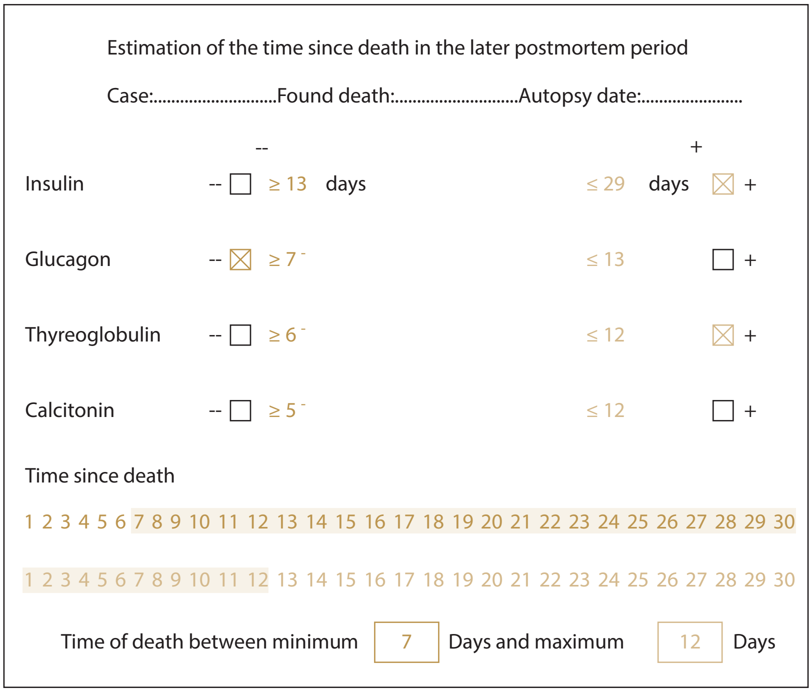

Estimation of the time since death in the later postmortem period

Case:............................Found death:............................Autopsy date:.......................

	--		+	
Insulin	-- ☐	≥ 13 days	≤ 29 days	☒ +
Glucagon	-- ☒	≥ 7 ⁻	≤ 13	☐ +
Thyreoglobulin	-- ☐	≥ 6 ⁻	≤ 12	☒ +
Calcitonin	-- ☐	≥ 5 ⁻	≤ 12	☐ +

Time since death

1 2 3 4 5 6 7 8 9 10 11 12 13 14 15 16 17 18 19 20 21 22 23 24 25 26 27 28 29 30

1 2 3 4 5 6 7 8 9 10 11 12 13 14 15 16 17 18 19 20 21 22 23 24 25 26 27 28 29 30

Time of death between minimum 7 Days and maximum 12 Days

Figure 10.4 Additional investigation of thyroglobulin with a positive immunoreaction: further delimitation between 7 and 12 days.

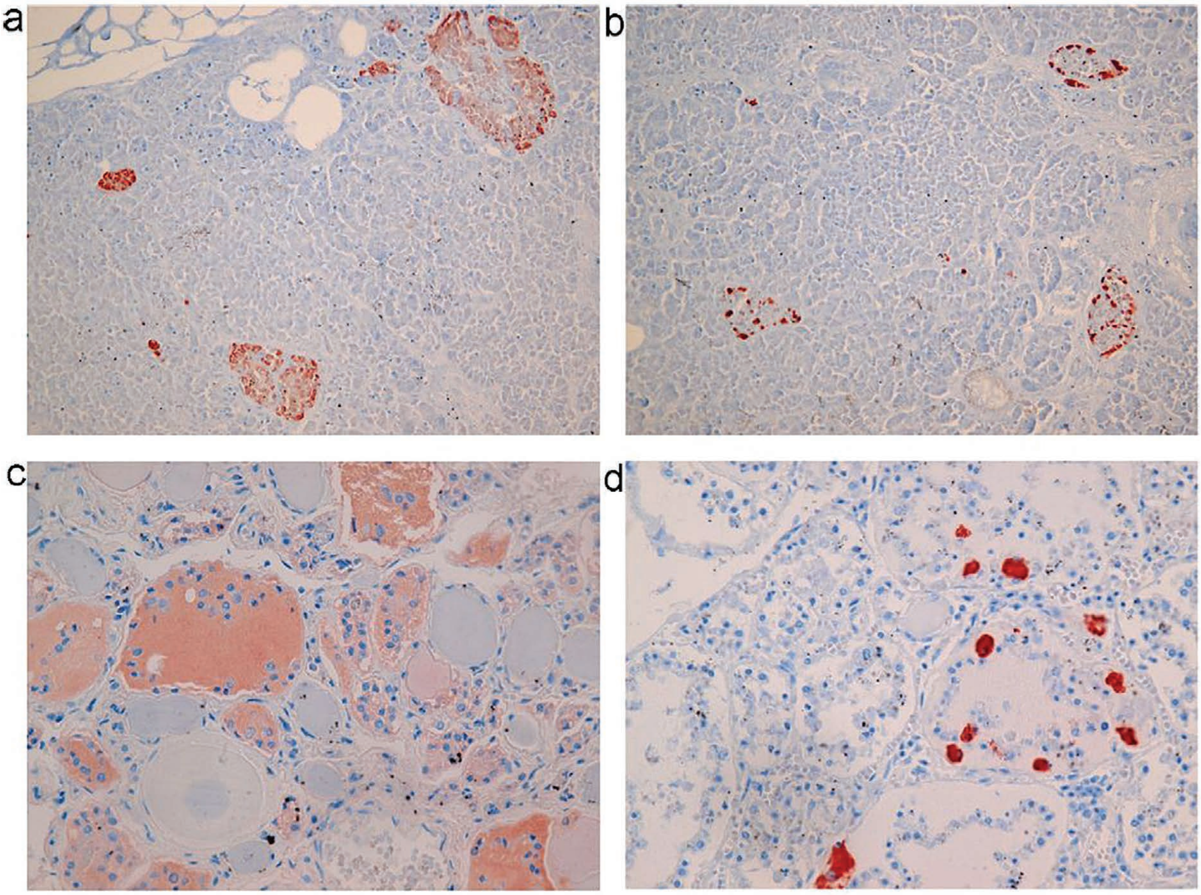

Figure 10.5 (a) Pancreas tissue anti-human insulin 200×, autopsy 8 days after death. (b) Pancreas tissue anti-human glucagon 200×, autopsy 8 days after death. (c) Thyroid gland tissue anti-human thyroglobulin 400×, autopsy 8 days after death. (d) Thyroid gland tissue anti-human calcitonin 400×, autopsy 11 days after death.

Table 10.2 **Comparison of the Results for Four Antigens between Wehner et al. and the Own Study**

Immunhistochemical marker	Wehner et al.		Own study	
	+	-	+	-
Insulin	29 days	13 days	18 days	22 days
Glucagon	13 days	7 days	12 days	8 days
Thyroglobulin	12 days	6 days	8 days	1 day*
Calcitonin	12 days	5 days	8 days	1 day*

Immunohistochemical methods are altogether a valid contribution to the repertoire of methods of estimation of time since death. However, in cases with microscopically observable and recognized pathologies immunohistochemical staining should not be used for time since death estimation.

10.1.1 Case Example

A 36-year-old woman was found dead in bushes near a railway line 8 days after having been seen last alive (Figure 10.6). Cause of death was a ligature strangulation; furthermore, there was a post-mortem incised wound of the anterior neck [2]. Due to lack of putrefactive changes post-mortem interval was thought to be not more than two days. The question of the police was of course: is an earlier time of death possible?

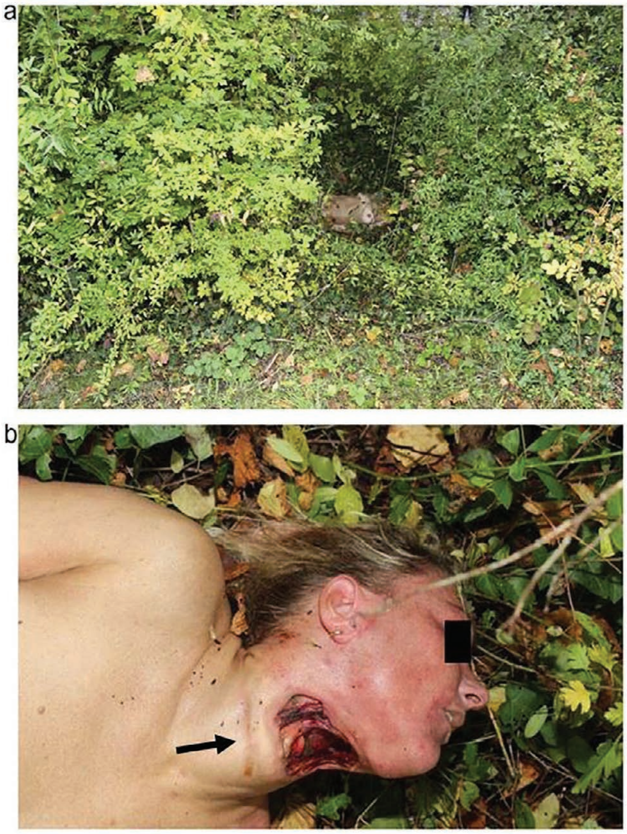

Figure 10.6 (a) Place of discovery, (b) Ligature strangulation mark (à) and post-mortem incised wound.

There would be completely different criminalistic approaches: either the murderer killed the woman immediately and hid her in the bushes or the murderer had the woman in his power for some days, killed her then and brought the body back to the place of discovery.

In this case, even methods with a low precision may be helpful in forensic casework (2). Immunohistochemical stainings were carried out on thyroid gland and pancreas and these stainings were positive for insulin, glucagon and thyroglobulin and negative for calcitonin.

Based on the immunohistochemical staining time since death was more than 5 days and less than 12 days.

Furthermore, vitreous potassium was with 33.8 mmol/l very high. Using different formulas time since death was over 6–7 days.

10.2 Conclusions

The immunohistochemical detection of antigens allows only a very rough estimation of the time since death, which may be helpful in single cases. However, these time limits may change in different environmental conditions. Therefore, control studies on independent case material in different environmental conditions are necessary but still missing.

References

1. Madea B. Is there recent progress in the estimation of the postmortem interval by means of thanatochemistry? *Forensic Sci Int* 2005;*151*:139–49.
2. Madea B, Ortmann J, Doberentz E. Estimation of the time since death—even methods with a low precision may be helpful in forensic casework. *Forensic Sci Int* 2019;*302*:109879.
3. Ortmann J, Doberentz E, Madea B. Immunohistochemical methods as an aid in estimating the time since death. *Forensic Sci Int* 2017;*273*:71–9.
4. Wehner F. Die Eingrenzung der Leichenliegezeit im spätpostmortalen Intervall. Neue Ansätze mittels immunhistochemischer Verfahren. *Med Welt* 2009;*11–12*:402–6.
5. Wehner F, Wehner HD, Schieffer MC, Subke J. Delimitation of the time of death by immunohistochemical insulin detection in pancreatic β-cells. *Forensic Sci Int* 1999;*105*:161–9.
6. Wehner F, Wehner HD, Schieffer MC, Subke J. Delimitation of the time of death by immunohistochemical detection of thyroglobulin. *Forensic Sci Int* 2000;*110*:199–206.
7. Wehner F, Wehner HD, Subke J. Delimitation of the time of death by immunohistochemical detection of calcitonin. *Forensic Sci Int* 2001;*122*:89–94.
8. Wehner F, Wehner HD, Subke J. Delimitation of the time of death by immunohistochemical detection of glucagon in pancreatic β-cells. *Forensic Sci Int* 2002;*124*:241–8.

11 Practical Casework

Claus Henssge and Burkhard Madea and Stefan Potente

Contents

11.1 Integration of Different Methods in Casework 313
Claus Henssge and Burkhard Madea
  11.1.1 Time-relevant Criteria of Different Methods 313
    11.1.1.1 Development of Rigor 313
    11.1.1.2 Lividity 314
    11.1.1.3 Mechanical Excitability of Skeletal Muscle 315
    11.1.1.4 The Electrical Excitability of Skeletal Muscle 316
    11.1.1.5 The Chemical Excitability of the Iris 316
  11.1.2 Arrangement of Data 316
  11.1.3 Principle of Using a Special Chart 317
  11.1.4 Experiences in Casework 318
  11.1.5 Discussion 323
11.2. Conditional Probability in Death Time Estimation 328
Stefan Potente
  11.2.1 Explaining Math in Court—A Thought Experiment 329
  11.2.2 Assumptions and Conditions in CPD Construction 330
  11.2.3 Compiling the CPD Interval 330
  11.2.4 Case Examples 330
  11.2.5 Results 331

11.1 Integration of Different Methods in Casework

■ *Claus Henssge and Burkhard Madea*

The great interindividual variability of the post-mortal changes as a consequence of many influencing factors restricts the accuracy of death time estimation and, if the limits of confidence of a method are not exactly known, impairs the reliability. Because no single method allows a sufficiently exact and reliable estimation of the interval of death in any particular case, it is recommended that several different methods are used. The selection of methods requires some consideration of the level of investigation and the consequent expenditure of effort.

The following scheme of integration of different methods is recommended for estimating the time of death in casework at the scene. The guidelines are as follows:

1. Whenever possible, use measurements instead of subjective evaluations.
2. Avoid a ‘mean value’ for the resulting time of death; instead, always offer a ‘range’ (i.e. the minimum and maximum limits).
3. Take into account important influencing factors on each criterion.
4. Use no more methods in a particular case than are potentially useful.
5. Give a preliminary statement of the interval of death at the scene.
6. The reliability of a stated range of time since death is more important than attempting to give an unrealistically narrow range.

The examination of the body at the scene usually begins with the use of the temperature-based method by using the nomogram as described in Chapter 6.1. The margins of error of this method can be reduced in many cases by using the following methods, although they themselves have wider margins of error. In a few cases, where the temperature-based method must not be used because of contrary circumstances, those methods should still be used.

11.1.1 Time-relevant Criteria of Different Methods

11.1.1.1 Development of Rigor

For more detailed information, see Chapter 4.

Hitherto, the grade of rigor has generally been evaluated subjectively for estimating the time of death in casework of human bodies. Measurement with a special device is

DOI: 10.1201/9781003244974-11

uncommon for a variety of reasons [1,3,23]. The description of the stages of the subjectively evaluated rigor differs from author to author [2,17,18]. For our purposes, only those stages of rigor that are relevant to the time of death are of interest. According to the statistical analysis by Mallach [17,18] of the data in the literature, this is given only for the following stages: 'beginning', 'full development', 'duration' and 'complete resolution' of rigor. The latter two stages are not relevant because of their late post-mortal onset of 57 (± 14) hours post-mortem and 76 (± 32) hours post-mortem, respectively. The stages of rigor are not exactly described either by Mallach [17,18] or in the only other experimental reports of Von Hofmann [11] in 1876 and 1877. (All the other data of Mallach's statistical analyses are figures from textbooks without any experimental basis.) 'Beginning' may mean 'you can observe slight rigor in the joints'. 'Full development' or 'complete development' (shortened to 'maximum' in Tables 10.1–10.3) may mean 'rigor is strongly developed in all joints'. There is a third useful marker—the re-establishment of rigor after breaking it. The re-established rigor is less strong than it was before breaking. To avoid a false-positive result, it is necessary to ensure that rigor was broken completely by fully moving the elbow joint several times. A negative result should be stated only if the examined joint had not been manipulated (e.g. by transport or removal of clothing) between breaking the rigor and examination for re-establishment.

The death time relationship of these three suitable marks of rigor can be seen in Table 11.1.

Table 11.1 Rigor Related to the Time of Death (hpm)

Stage	Mean	Standard deviation	Limits*	
			Lower	Upper
Beginning	3	2	0.5	7
Maximum	8	1	2.0	20
Re-establishment			2.0	8

* Lower and upper limits of variance computed from literature data (1811–1960) [17].

Table 11.2 Hypostasis Related to the Time of Death (hpm)

Stage	Mean	Standard deviation	Limits*	
			Lower	Upper
Beginning	0.75	0.5	0.25	3
Confluence	2.50	1.0	1.00	4
Maximum	9.50	4.5	3.00	16
Thumb pressure	5.50	6.0	1.00	20
Complete shifting	3.75	1.0	2.00	6
Incomplete shifting	11.00	4.5	4.00	24

* Lower and upper limits of variance computed from literature data (1905–1963) [17].

Table 11.3 Probability of a Time Interval of ±0.1 Hour Around the Mean Value of the Time Since Death (Examples) Related to the Standard Deviation

Criterion stage	Mean	Standard deviation	Probability*
Hypostasis			
Complete shifting	3.75	1.0	0.08
Thumb pressure	5.50	6.0	0.01
Maximum	9.50	4.5	0.02
Incomplete shifting	11.00	4.5	0.02

* The probabilities were computed according to Equation 10.1 for a time interval of ±0.1 hour (12 minutes) around the mean.

11.1.1.2 Lividity

For more detailed information, see Chapter 5.

Subjective methods are also employed for the evaluation of lividity. Attempts to make the evaluation of lividity objective [12,13] were not generally accepted in practical work until recently. Data in the literature—exceptionally figures from textbooks without experimental basis—were analysed statistically by Mallach [17,18], for the following degrees of lividity (see Tables 11.2 and 11.3): 'beginning', 'confluence', 'maximum of expansion and intensity' (shortened to 'maximum'), 'complete displacement by slight pressure' (using the thumb; shortened to 'thumb pressure'), 'complete shifting' and 'incomplete shifting' after turning the body over. Complete shifting means that lividity disappears completely in the upward-facing parts of the body after turning it over and then appears in the downward-facing parts; this is apparently dependent on the death time and may take from a few minutes to up to 1 hour. Incomplete shifting means that lividity fades only in the upward-facing parts and appears only slightly in the downward-facing parts after turning the body over. The maximum stage of lividity should be stated only after a second examination carried out later, especially in cases where bleeding had occurred. The criterion 'complete shifting' can be observed at the scene frequently when the body, or even parts of it, had been moved to a new position in the course of the investigative procedure. 'Incomplete shifting' is found to be more likely at autopsy if the body had been transported in another position than that examined at the scene. Two other criteria, 'incomplete displacement after strong pressure' and 'only small fading after turning the body', were not taken into account because they do not bring further information to the early death time interval in which we are interested.

The reason for non-displacement and non-shifting of lividity is not the early diffusion of haemoglobin, as supposed formerly, but rather the haemoconcentration by loss of fluid that penetrates the wall of those vessels related to the hydrostatic pressure, as shown by Hilgermann [10].

11.1.1.3 Mechanical Excitability of Skeletal Muscle

For more detailed information, see Chapter 3.

Sufficient data are given in the literature on the two phenomena of post-mortal mechanical excitability:

1. Tendon reaction, or Zsako's phenomenon, described first by Zsako [24] and examined as follows [21]: Striking at the lower third of the quadriceps femoris muscle about 10 cm above the patella with a reflex hammer causes an upward movement of the patella because of a contraction of the whole muscle.
2. Idiomuscular contraction (bulge), tested as described by Dotzauer [4] and Prokop [21]: Striking at the biceps brachii muscle with the back of a knife causes a muscular bulge at the point of contact resulting from local contraction of the muscle. The related times of death listed in Table 11.4 are taken from Popwassilew and Palm [19]. The muscular bulge is maintained for some hours if the examination takes place several hours post-mortem, as is usually the case, when adenosine triphosphate (ATP) levels are low. Nevertheless, to avoid a false-negative result, one should carefully check whether a local contracture appears after striking the muscle, but immediately disappears again, as may happen in the very early post-mortem period in response to high levels of ATP.

Table 11.4 Chronological Arrangement of the Lower and Upper Limits of the Time Since Death Related to the Different Stages of the Cited Methods According to Literature Data*

Parameter checked	Answer		Answer	
	↓		↓	
	Result reduction of the lower limit (t ≥ hpm)		Result reduction of the upper limit (t ≤ hpm)	
Lividity				
Beginning?	Yes	0.0	No	3.0
Confluence?	Yes	1.0	No	4.0
Thumb pressure?	No	1.0	Yes	20.0
Complete shifting?	No	2.0	Yes	6.0
Maximum?	Yes	3.0	No	16.0
Incomplete shifting?	No	4.0	Yes	24.0
Rigor mortis				
Beginning?	Yes	0.5	No	
Re-establishment?	No	2.0	Yes	9.5
Maximum?	Yes	2.0	No	20.0
Mechanical excitability				
Zsako's phenomenon?	No	0.0	Yes	2.5
Idiomuscular contraction?	No	1.5	Yes	13.0
Electrical excitability				
Eye VI?	No	1.0	Yes	6.0
Eye V	No	2.0	Yes	7.0
Eye IV?	No	3.0	Yes	8.0
Eye III?	No	3.5	Yes	13.0
Eye II?	No	5.0	Yes	16.0
Eye I?	No	5.0	Yes	22.0
Orbicularis oris muscle?	No	3.0	Yes	11.0
Chemical excitability				
Iris				
Atropine/cyclopentolate	No	3.0	Yes	10.0
Mydriaticum Roche (tropicamide)?	No	5.0	Yes	30.0
Acetylcholine?	No	14.0	Yes	46.0

* The upper limit of 8 hours related to re-established rigor was replaced by 9.5 hours according to a newer finding [9].

Source: From Madea B, Henssge C. *Estimation of the Time Since Death: Integration of Different Methods*. Digest of the International Meeting of P.A.A.F.S. and Police Medical Officers, Wichita, Kansas, August 10–14, 1987.

11.1.1.4 The Electrical Excitability of Skeletal Muscle

For more detailed information, see Chapter 3.

An extensive literature on this subject has accrued since the ‘second’ start of the investigations in this field by Prokop [20]. We refer here only to the results of the extensive experimental material of Klein and Klein [14] on 447 bodies. Because the type of electrical stimulus used influences the muscle reaction, the following data of death time are related to stimulation by ‘rectangular-like’ impulses of a duration of a ‘few milliseconds’ in a repetition rate of 30–70 per second and an amplitude of 50 volts (resistance 1 kOhm) [14]. A small battery-operated generator with constant-current rectangular impulses of 30 mA, 10-ms duration and a frequency of 50 per second is now available commercially (for details, see j-peschke .homepage.t-online.de). The time data shown in Table 11.4 can be transferred when using this device.

Needle electrodes are inserted 5–7 mm deep into the nasal part of the upper eyelid at a distance of 15–20 mm (Figure 11.1). The grade of reaction is divided into six degrees according to the spread of the reaction of the mimic muscles. The strongest reaction (degree VI) is obtained if the reaction includes the upper and lower eyelids, forehead and cheek. In the minimal reaction (degree I), only a small local fascicular contraction of the nasal angle of the upper eyelid appears (Figure 11.2). In addition, the electrodes can also be inserted 10 mm from each corner of the mouth.

We extracted the data in Table 11.4 from the original data produced by Klein and Klein [14] and computed the permissible variation of 95 per cent [5]. In cases with haematoma or emphysema of the eyelid, the time figures are much greater; in cases of a long terminal episode, the time figures are much smaller than those given in Table 11.4 [14]. At present, and regardless of the criticisms [5,15], this method seems to be the most suitable of all the reported ‘electrical’ methods for casework. Apart from the nomogram method, it is more useful than any of the other methods reviewed in this volume (see Table 11.7).

11.1.1.5 The Chemical Excitability of the Iris

For more detailed information, see Chapter 3.

From the extensive literature in this field, we refer only to the systematic investigations of Klein and Klein [14] on 5765 eyes of 3979 bodies. From these results, we used the data listed in Table 11.4. To examine this reaction, about 0.5 mL of the solution is injected subconjunctivally at the limbus corneae [14]; the concentration used is not important (e.g. 5 per cent). The onset of the reaction begins between 5 and 30 minutes after the injection, and it lasts at least 1 hour. Acetylcholine (miosis) and noradrenaline (mydriasis) have the same time interval of post-mortem reaction. However, the effect of acetylcholine is more reliable, and the application of noradrenaline is preferable only if the starting width of the pupil is small. The so-called double reaction, first miosis (e.g. acetylcholine), followed by mydriasis (e.g. atropine) on the same eye, or vice versa, gives no further time information than each reaction separately (using both eyes) (all according to Klein and Klein). To avoid mistakes, it is recommended that the starting diameter of the pupil is measured with a slide caliper to determine whether there was a reaction or not.

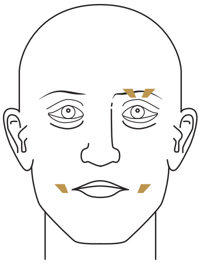

Figure 11.1 Position of insertion of electrodes for facial stimulation.

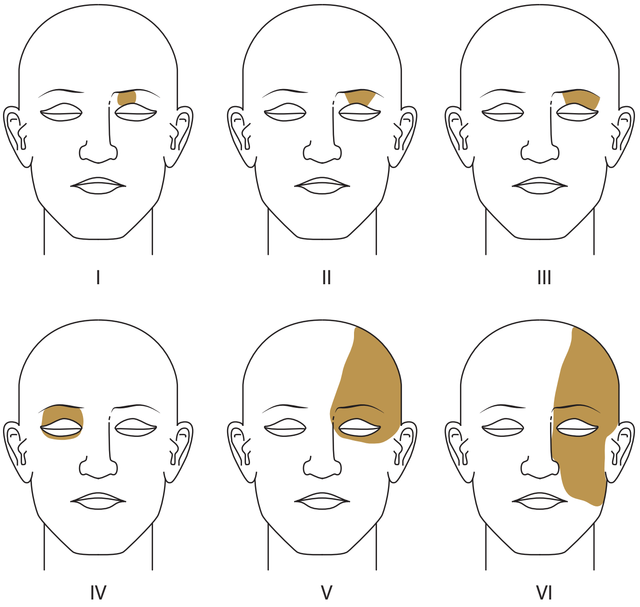

Figure 11.2 Degrees of reaction following electrical stimulation of facial muscles.

11.1.2 Arrangement of Data

As we concluded earlier in this section, there is no statistical evidence for the use of *mean* values of the time since death in a special case. Remembering the mathematical relationship between the probability of a short time interval ($X < X_k$) around the mean (x) and the standard deviation (SD):

$$\text{Prob}\left(X < X_k\right)| = X - x/\text{SD} \tag{11.1}$$

There is only a very small probability that the mean values will be accurate because of the great SDs (examples shown in Table 11.3).

In compliance with this, the mean value of the idiomuscular contraction (6.9 hours post-mortem) occurred in only 6 per cent of the cases of an experimental study [4]. To avoid great errors in our statements of the time since death, we have to avoid the use of mean values. Therefore, we recommend only the use of the upper and lower time limits of any criterion as the basis of statements. In the example of the idiomuscular contraction sought by striking the biceps muscle, no case was reported as having had idiomuscular contraction after the 13th hour post-mortem. In no case was this reaction missed before 1.5 hours post-mortem. This means that, if the reaction occurs, we can say only that the time since death must be less than 13 hours. If there is no reaction, we can state only that the time since death must be greater than 1.5 hours. Integrating the results of all examinations in the same manner, the greatest figure of any lower limit and the smallest figure of any upper limit reduce the interval within which the death occurred—with a high probability of at least 95 per cent.

From this point of view, and for practical purposes, data are best arranged chronologically, according to the lower and the upper limits (see Table 11.4).

11.1.3 Principle of Using a Special Chart

For casework, we rearranged the data of Table 11.4 into a special chart (Figure 11.3), which facilitates the choice of the subsequently helpful criteria in an actual case. In the example in Figure 11.3, the examination began with measurement of the rectal temperature, followed by use of the

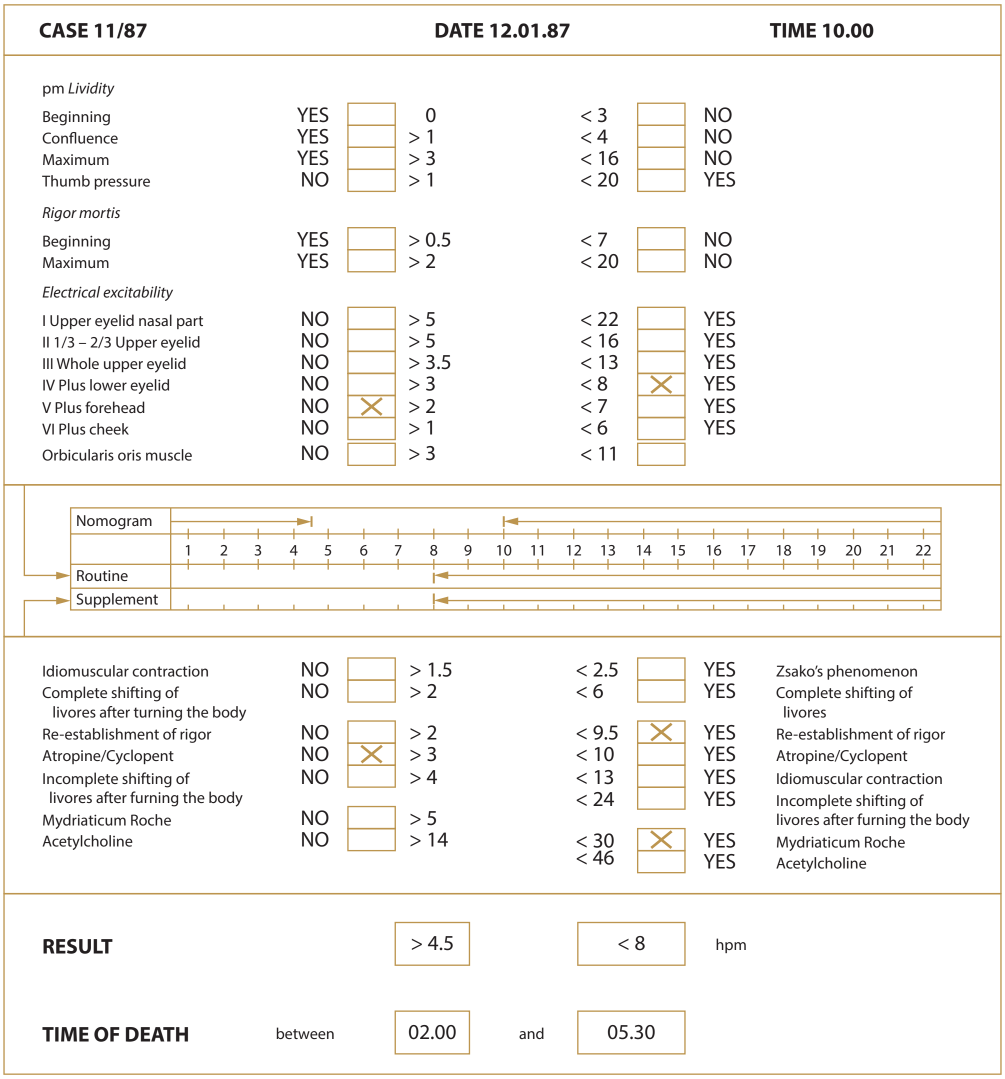

CASE 11/87 **DATE 12.01.87** **TIME 10.00**

pm *Lividity*						
Beginning	YES	☐	0	< 3	☐	NO
Confluence	YES	☐	> 1	< 4	☐	NO
Maximum	YES	☐	> 3	< 16	☐	NO
Thumb pressure	NO	☐	> 1	< 20	☐	YES
Rigor mortis						
Beginning	YES	☐	> 0.5	< 7	☐	NO
Maximum	YES	☐	> 2	< 20	☐	NO
Electrical excitability						
I Upper eyelid nasal part	NO	☐	> 5	< 22	☐	YES
II 1/3 – 2/3 Upper eyelid	NO	☐	> 5	< 16	☐	YES
III Whole upper eyelid	NO	☐	> 3.5	< 13	☐	YES
IV Plus lower eyelid	NO	☐	> 3	< 8	☒	YES
V Plus forehead	NO	☒	> 2	< 7	☐	YES
VI Plus cheek	NO	☐	> 1	< 6	☐	YES
Orbicularis oris muscle	NO	☐	> 3	< 11	☐	

Idiomuscular contraction	NO	☐	> 1.5	< 2.5	☐	YES	Zsako's phenomenon
Complete shifting of livores after turning the body	NO	☐	> 2	< 6	☐	YES	Complete shifting of livores
Re-establishment of rigor	NO	☐	> 2	< 9.5	☒	YES	Re-establishment of rigor
Atropine/Cyclopent	NO	☒	> 3	< 10	☐	YES	Atropine/Cyclopent
Incomplete shifting of livores after furning the body	NO	☐	> 4	< 13	☐	YES	Idiomuscular contraction
				< 24	☐	YES	Incomplete shifting of livores after furning the body
Mydriaticum Roche	NO	☐	> 5	< 30	☒	YES	Mydriaticum Roche
Acetylcholine	NO	☐	> 14	< 46	☐	YES	Acetylcholine

RESULT		> 4.5		< 8	hpm
TIME OF DEATH	between	02.00	and	05.30	

Figure 11.3 Integrating chart for casework at a scene of a crime with an example.

(From Madea B, Henssge C. *Estimation of the Time Since Death: Integration of Different Methods.* Digest of the International Meeting of P.A.A.F.S. and Police Medical Officers, Wichita, Kansas, August 10–14, 1987.)

nomogram method. The result was 4.5 hours post-mortem (lower limit) and 10.1 hours post mortem (upper limit). The lower limit can be confirmed or improved only by a criterion with a higher figure for its lower limit. Looking at the chart, in the left-hand column we can quickly find only two criteria that could improve the lower limit: the electrical excitability if there is a negative result, and the chemical excitability of the iris by tropicamide (Mydriaticum Roche, Hoffmann La Roche), also if there is a negative result. The upper limit (10.1 hours post-mortem) can be confirmed or improved only by a criterion with a lower figure for its upper limit. We can quickly find the possibly helpful criteria on the chart, in the right-hand column: the electrical excitability, again if there is a reaction of degree IV (or V or VI); or the chemical excitability of the iris by atropine or cyclopentolate (Cyclopent, United Pharmacies) if there is a reaction and the re-establishment of the rigor after breaking if it occurs. We examined the electrical excitability of the mimic muscles and the chemical excitability of the iris by atropine (one side) and by Mydriaticum Roche (other side), and we broke the rigor of one elbow joint. The other criteria need not be examined because they could not help in this case. (We always routinely examine the stages of rigor and hypostasis.)

The results of the examined criteria are put into the chart (see Figure 11.3). Only the electrical excitability (degree IV) and the re-established rigor were helpful: they reduced the upper time limit of the temperature-based nomogram result from 10 to 9.5 hours post-mortem (re-establishment) and further to 8 hours post-mortem (degree IV). The chemical examinations did not provide an improvement in this case. Insofar as this example is typical, the electrical examination gives rather more of an improvement than the other criteria (see Table 11.7). The final result in this case is as follows: with a high probability (95 per cent), the death occurred between 4.5 and 8 hours before the examination. The computer program www.AMAsoft.de automatically leads the procedure of examining the body at the scene according to this logistic (Figure 11.4) after performing all mathematical operations of the nomogram method (see Figure 6.33). The computer program was evaluated in a field study [8,9].

11.1.4 Experiences in Casework

In 32 cases with investigated death times between 2 and 13 hours, both the nomogram and the electrical excitability of mimic muscles were used (Figure 11.5 and Table 11.5) [16]. The results provide evidence that the range of death times resulting from the temperature

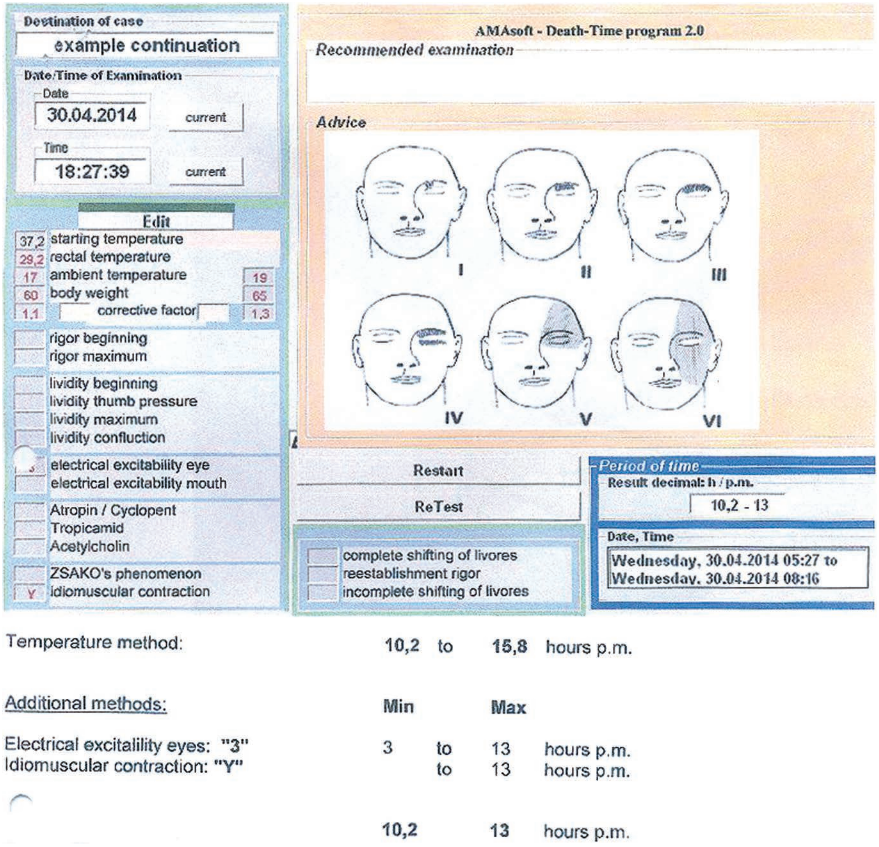

Destination of case
example continuation

Date/Time of Examination
Date: 30.04.2014
Time: 18:27:39

37,2 starting temperature
29,2 rectal temperature
17 ambient temperature 19
60 body weight 65
1,1 corrective factor 1,3
☐ rigor beginning
☐ rigor maximum
☐ lividity beginning
☐ lividity thumb pressure
☐ lividity maximum
☐ lividity confluction
3 electrical excitability eye
☐ electrical excitability mouth
☐ Atropin / Cyclopent
☐ Tropicamid
☐ Acetylcholin
☐ ZSAKO's phenomenon
Y idiomuscular contraction

☐ complete shifting of livores
☐ reestablishment rigor
☐ incomplete shifting of livores

Period of time
Result decimal: h / p.m.: 10,2 - 13
Date, Time: Wednesday, 30.04.2014 05:27 to Wednesday, 30.04.2014 08:16

```
Temperature method:                    10,2   to    15,8   hours p.m.

Additional methods:                    Min          Max

Electrical excitalility eyes:  "3"     3      to    13     hours p.m.
Idiomuscular contraction: "Y"                 to    13     hours p.m.

                                       10,2         13     hours p.m.
```

Figure 11.4 Case example (see Figure 6.33) of using the PC program www.AMAsoft.de for continuative examination of the non-temperature-based criteria according to this logistic.

nomogram becomes smaller in some cases by application of the method of electrical excitability of facial muscles according to Figure 11.2. Nevertheless, in the other cases the self-confidence of the investigator in their opinion on the time since death increases by using two independent methods with a common result. In addition, the 32 investigated cases confirmed the results of Klein and Klein [14].

Two special cases [7] may demonstrate that factors influencing the time course of electrical excitability in a contrary direction to body cooling may mislead or confuse the investigator when they are not taken into account (Figures 11.6 and 11.7).

In the case of Figure 11.6, the temperature-based nomogram method showed the death time interval to be from 8.8 to 14.3 hours, corresponding to 26.6°C rectal temperature, 10°C ambient temperature and 72 kg body weight. Rigor mortis had not begun, and electrical excitability showed a full reaction (degree VI) resulting in a death time of less than 7 and 6 hours, respectively. These results excluded each other. The suspicion of fatal hypothermia, as a result of purple-red patches of discolouration of the skin on and around the elbow and knee joints, was confirmed by autopsy findings such as haemorrhagic erosions of the stomach and haemorrhage of the pancreas and its ductus. The fatal hypothermia explains the contrary results of death time estimation between the temperature-based nomogram method and the electrical excitability method: the hypothermia simulated a long time since death because of the fall in central body temperature during life. The nomogram method must not be used in such a case (see Chapter 6.1). Electrical excitability is not influenced by hypothermia. The investigated time of death was really 2.5 hours.

In the other special case (see Figure 11.7), there was a large difference in the electrical excitability of the right and left eyelids. The right upper eyelid had emphysema resulting from an incised wound in the glabella region. Because of the higher figure obtained for death times with regard to the degree of electrical excitability in cases with emphysema or fresh haemorrhage [14], the reaction of the right eyelid (degree III) cannot be used as an upper limit of death time (13 hours). The investigated time since death was really 15 hours.

The experiences with the complete 'integrated method' used in a field study of 72 consecutive cases at the scene were published [8,9]. After using the temperature nomogram as primary method (see Tables 6.1.17 and 6.1.21), the non-temperature-based methods (see Table 11.4, Figure 11.3 and Figure 11.4) were selectively used to improve (or at least confirm) the range of death times resulting from the temperature nomogram. The case-oriented selection of the additional methods followed the principle discussed earlier (see Figure 11.3), and it was supported by the interactive notebook program (www.AMAsoft.de) discussed earlier in this chapter. The program defines the term 'confirmation of the range of death

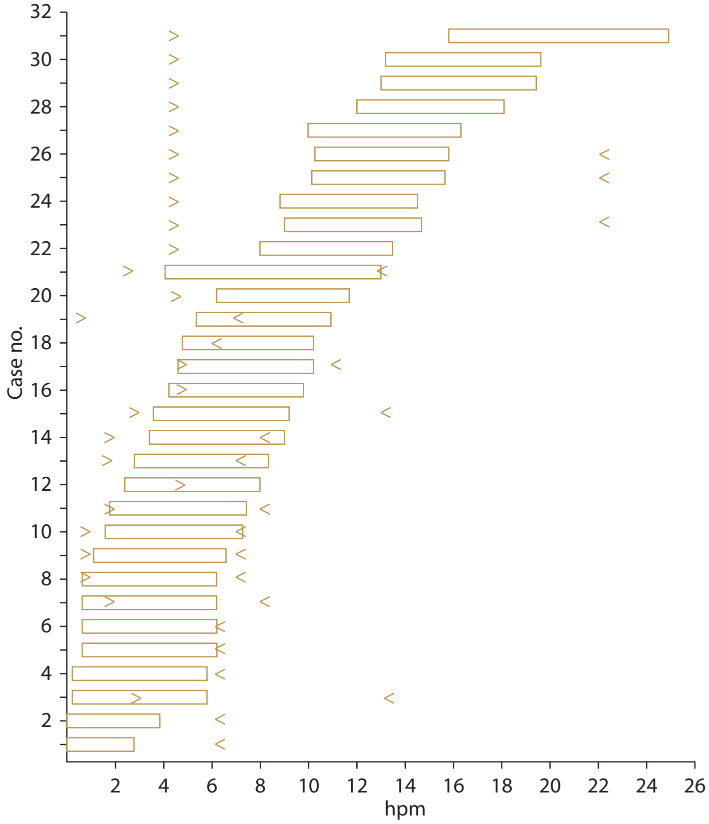

Figure 11.5 Combined application of the temperature-based nomogram and the electrical excitability for determining the time since death [16]. Case numbers are according to Table 11.5. Boxes: death time estimation by the nomogram method (lower and upper 95 per cent limits of confidence; see Table 11.5). > < Death time information based on the degree of electrical excitability. For instance, degree III positive (case 15) not only reveals the information that the time since death is <13 hpm but also means degree IV negative and therefore that the time since death is 3 hpm. Especially during the time period from 3 to 8 hpm, combining electrical excitability with the nomogram method reveals a more precise death time estimation than using one method alone. The real time since death was always within the calculated time since death.

Table 11.5 Death Time Estimation from Body Temperature (Using the Nomogram) and the Degree of Electrical Excitability

No.	Cause of death	Time of investigation	T_R	T_A	Body weight	*f*	Death time estimation (nomogram)	Degree of electrical excitability	Death time estimation (hours)
1	Female, 44 years, three homicidal shotgun wounds of the neck	13.20	37.2	35.5	60	0.5	0–2.8	VI	<6
2	Male, 45 years, suicidal shotgun wound of the head	13.30	37.1	17	70	1.2	0–3.8	VI	<6
3	Female, 30 years, stab wounds of the heart	16.10	35.6	14.5	54	1.1	0.2–5.8	III	>3<13
4	Female, 53 years, stab wounds of the neck and chest	15.55	36.5	18.5	74.3	1.2	0.2–5.8	VI	<6
5	Male suicidal shotgun injury of heart and lung	03.15	36	20.9	56	1.2	0.6–6.2	VI	<6
6	Male, 48 years, homicidal stab wounds of the chest	01.45	36.1	24.8	80	1	0.6–6.2	VI	<6
7	Female, 6 years, blunt force injury to the skull	06.15	26.4	2.3	19.8	1	0.6–6.2	IV	>2<8
8	Female, 80 years, coronary artery disease	16.20	36.7	23.6	71	1.9	0.6–6.2	V	>1<7
9	Male, 42 years, stab wounds of the neck	19.30	36.5	17.7	62.5	1.9	1–6.6	V	>1<7
10	Female, 20 years, fatal heroin intoxication	20.45	33.2	20.7	36.3	1	1.6–7.2	V	>1<7
11	Female, 35 years, stab wounds of chest and neck	04.25	33.3	9.5	60	1	1.8–7.4	IV	>2<8
12	Female, 72 years, homicidal strangulation	19.00	34.8	19.7	60.1	1.2	2.4–8	I neg.	>5
13	Male, 29 years, homicidal gunshot wound of the heart	10.25	34.7	18	75	1.05	2.8–8.4	V	>1<7
14	Female, 39 years, homicidal gunshot wound of the skull	09.20	34.9	21.5	75.5	1.1	3.4–9	V	>1<7
15	Male, 14 years, homicidal gunshot wound of the skull	09.00	33.4	20	61.2	1	3.6–9.2	III	>3<13
16	Female, 22 years, blunt force injury to skull and neck	04.45	32.1	20.6	50	1	4.2–9.8	I neg.	>5
17	Female, 45 years, alcoholic bleeding from gastric erosions	08.00	30.2	21.5	35.4	1	4.6–10.2	I orb. oris +	>5<11
18	Male, 44 years, homicidal shotgun wound of the heart	03.15	34.4	22.8	80	1	4.6–10.2	VI	<6
19	Male, 58 years, homicidal blunt force injury of the skull	13.15	28.3	6	65	1	5.4–11	V	>1<7
20	Homicidal stab wounds of the neck	11.15	32.9	24	71.5	1.1	6.2–11.8	I neg.	>5
21	Female, 3 years, drowning	00.30	26.2	22.9	16	1	4.1–13.1	III orb. oris +	>3<11
22	Male, 56 years, homicidal blunt force injury of the skull	10.45	33.2	22.5	90	1	8–13.6	I neg.	>5
23	Female, homicidal stab wounds of the neck	11.00	30.6	23.5	59.8	1.1	9–14.6	I	>5<22
24	Male, homicidal stab wounds of the neck	11.30	33.6	22.9	97.5	1.1	9.2–14.8	I neg.	>5
25	Male, homicidal stab wounds of the chest	12.10	32.7	21.5	87	1.2	10.2–15.8	I neg.	>5
26	Female, 79 years, throttling	04.00	31	21.8	65	1.2	10.4–16	I	>5<22

Table 11.5 (*Continued*) **Death Time Estimation from Body Temperature (Using the Nomogram) and the Degree of Electrical Excitability**

No.	Cause of death	Time of investigation	T_R	T_A	Body weight	*f*	Death time estimation (nomogram)	Degree of electrical excitability	Death time estimation (hours)
27	Female accidental traumatic asphyxia	12.30	25.9	19.6	42	1	10–16.4	I neg.	>5
28	Female, throttling	19.10	25.7	16.1	64	1	12–18.2	I neg.	>5
29	Male, 39 years, stab wounds of the neck	10.10	27.5	18	75.5	1	13–19.4	I neg.	>5
30	Female, 22 years, homicidal gunshot wound of the chest	23.20	26.5	19.1	62.6	1–1.2	13.2–19.6	I neg.	>5
31	Female, 73 years, homicidal strangulation	13.00	27.5	18	74	1.3	15.9–24.9	I neg.	>5
32	Male, 41 years, chronic alcoholism, pneumonia	12.05	38.9	24	72	1	—	IV orb. oris + thenar+++	>2<8

Abbreviations: +, positive; *f*, corrective factor; neg., negative; orb. oris, orbicularis oris; $T_{A,}$ ambient temperature (°C); $T_{R,}$ rectal temperature (°C).

Source: From Madea B, Henssge C. Electrical excitability of skeletal muscle postmortem on casework. *Forensic Sci Int* 1990;**47**:207–27.

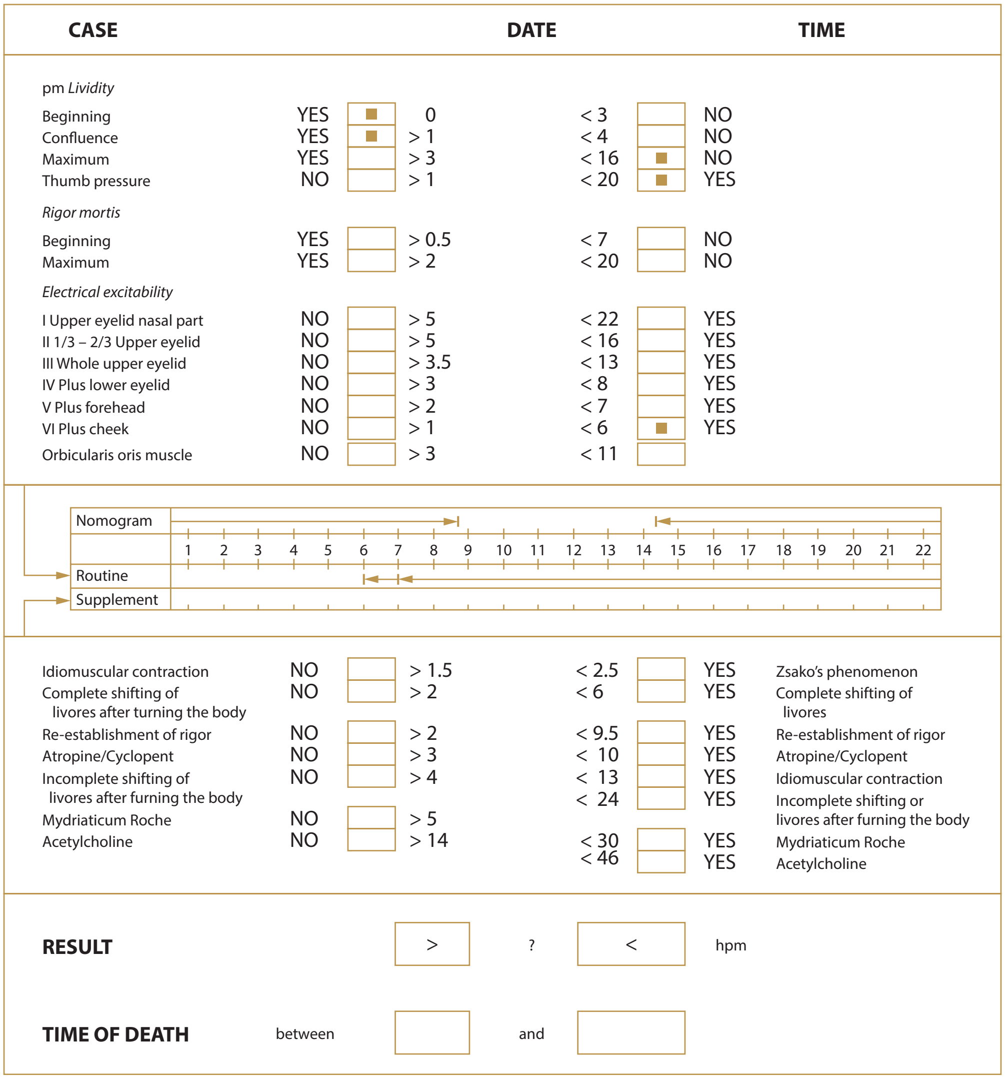

CASE **DATE** **TIME**

pm *Lividity*

Beginning	YES	■	0	< 3	☐	NO
Confluence	YES	■	> 1	< 4	☐	NO
Maximum	YES	☐	> 3	< 16	■	NO
Thumb pressure	NO	☐	> 1	< 20	■	YES

Rigor mortis

Beginning	YES	☐	> 0.5	< 7	☐	NO
Maximum	YES	☐	> 2	< 20	☐	NO

Electrical excitability

I Upper eyelid nasal part	NO	☐	> 5	< 22	☐	YES
II 1/3 – 2/3 Upper eyelid	NO	☐	> 5	< 16	☐	YES
III Whole upper eyelid	NO	☐	> 3.5	< 13	☐	YES
IV Plus lower eyelid	NO	☐	> 3	< 8	☐	YES
V Plus forehead	NO	☐	> 2	< 7	☐	YES
VI Plus cheek	NO	☐	> 1	< 6	■	YES
Orbicularis oris muscle	NO	☐	> 3	< 11	☐	

Idiomuscular contraction	NO	☐	> 1.5	< 2.5	☐	YES	Zsako's phenomenon
Complete shifting of livores after turning the body	NO	☐	> 2	< 6	☐	YES	Complete shifting of livores
Re-establishment of rigor	NO	☐	> 2	< 9.5	☐	YES	Re-establishment of rigor
Atropine/Cyclopent	NO	☐	> 3	< 10	☐	YES	Atropine/Cyclopent
Incomplete shifting of livores after furning the body	NO	☐	> 4	< 13	☐	YES	Idiomuscular contraction
				< 24	☐	YES	Incomplete shifting or livores after furning the body
Mydriaticum Roche	NO	☐	> 5	< 30	☐	YES	Mydriaticum Roche
Acetylcholine	NO	☐	> 14	< 46	☐	YES	Acetylcholine

RESULT > ? < hpm

TIME OF DEATH between and

Figure 11.6 Example of using the integrating chart (see text).

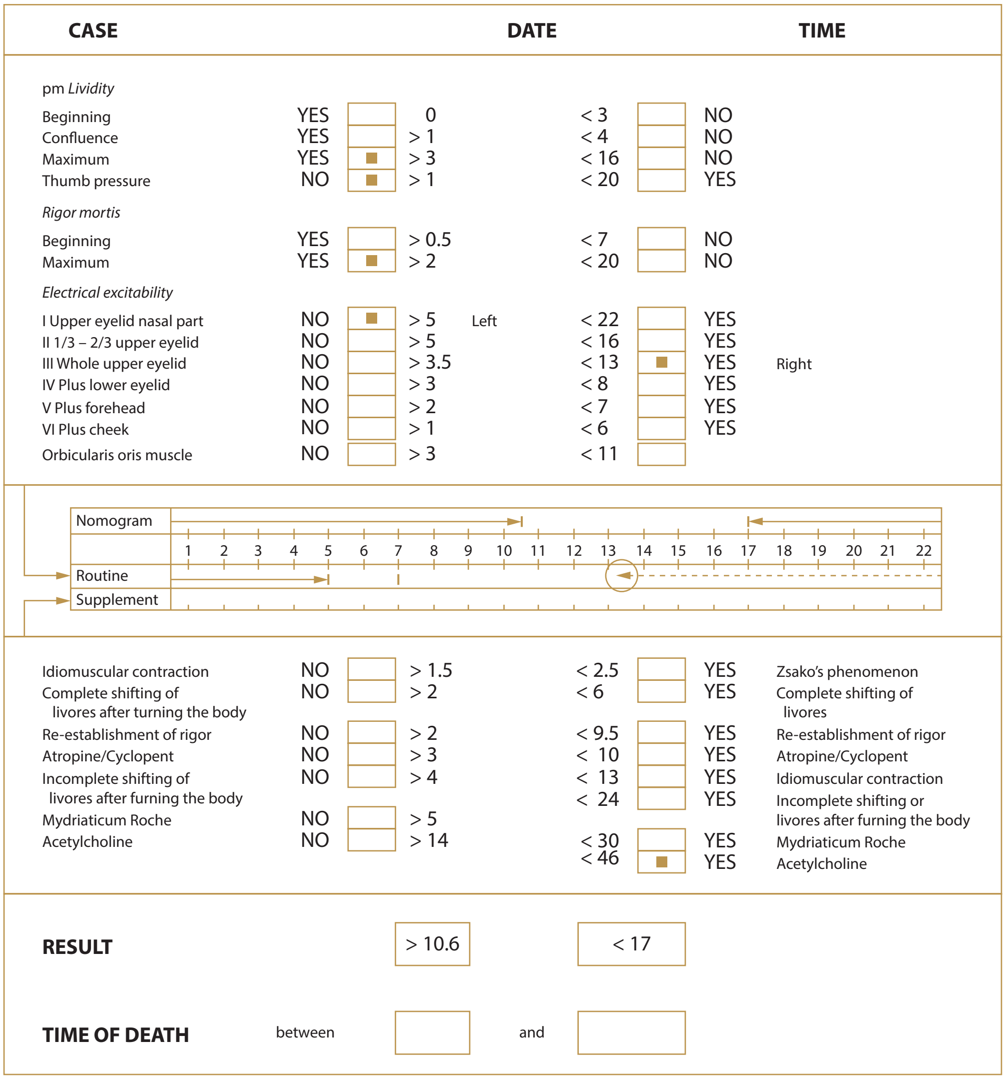

CASE				DATE				TIME
pm *Lividity*								
Beginning	YES	☐	0		< 3	☐	NO	
Confluence	YES	☐	> 1		< 4	☐	NO	
Maximum	YES	■	> 3		< 16	☐	NO	
Thumb pressure	NO	■	> 1		< 20	☐	YES	
Rigor mortis								
Beginning	YES	☐	> 0.5		< 7	☐	NO	
Maximum	YES	■	> 2		< 20	☐	NO	
Electrical excitability								
I Upper eyelid nasal part	NO	■	> 5	Left	< 22	☐	YES	
II 1/3 – 2/3 upper eyelid	NO	☐	> 5		< 16	☐	YES	
III Whole upper eyelid	NO	☐	> 3.5		< 13	■	YES	Right
IV Plus lower eyelid	NO	☐	> 3		< 8	☐	YES	
V Plus forehead	NO	☐	> 2		< 7	☐	YES	
VI Plus cheek	NO	☐	> 1		< 6	☐	YES	
Orbicularis oris muscle	NO	☐	> 3		< 11	☐		

Idiomuscular contraction	NO	☐	> 1.5	< 2.5	☐	YES	Zsako's phenomenon
Complete shifting of livores after turning the body	NO	☐	> 2	< 6	☐	YES	Complete shifting of livores
Re-establishment of rigor	NO	☐	> 2	< 9.5	☐	YES	Re-establishment of rigor
Atropine/Cyclopent	NO	☐	> 3	< 10	☐	YES	Atropine/Cyclopent
Incomplete shifting of livores after furning the body	NO	☐	> 4	< 13	☐	YES	Idiomuscular contraction
				< 24	☐	YES	Incomplete shifting or livores after furning the body
Mydriaticum Roche	NO	☐	> 5	< 30	☐	YES	Mydriaticum Roche
Acetylcholine	NO	☐	> 14	< 46	■	YES	Acetylcholine

RESULT		> 10.6		< 17
TIME OF DEATH	between	☐	and	☐

Figure 11.7 Example of using the integrating chart (see text).

time resulting from the temperature nomogram' as follows [6]: to confirm the upper and lower time limits obtained by the primary nomogram method, an additional criterion is requested only if its time limit is 20 per cent or at least 1 hour higher, or 20 per cent or at least 1 hour lower, respectively (Figure 11.8).

Using this logistic, only those criteria were used that could be potentially helpful in the actual cases examined. In three cases, none of the required examinations could be performed because of the particular situation at the scene. In several cases the required additional examinations could be performed only incompletely. Nevertheless, the range of death time as estimated by the nomogram method became smaller by application of additional methods in 49 cases (examples in Table 11.6). In a further six cases, the additional methods confirmed the time limits obtained by the temperature method. In three of four cases where the temperature method should not be used, the period since death was estimated by the non-temperature-based methods exclusively (see Table 11.6). As expected, the electrical examination gave rather more of an improvement, but the other criteria also contributed to improvement in many cases (Table 11.7). As can be seen from the examples in Table 11.6, the developing cascade of stepwise limitation of the period since death by examination of each further criterion contributes to the self-confidence of the investigator in their opinion on the period since death. The application of the integrated method including the nomogram method and the additional non-temperature-based criteria led to total spans of the period since death in the order of 1.5 hours in 5 cases, and up to 3.5 hours in a further 15 cases. In only 1 of the 72 cases (case number 23 in Table 11.6) did the upper limit of the estimated period since death concluded from the re-establishment of rigor (8 hours post-mortem) contradict the time of death investigated

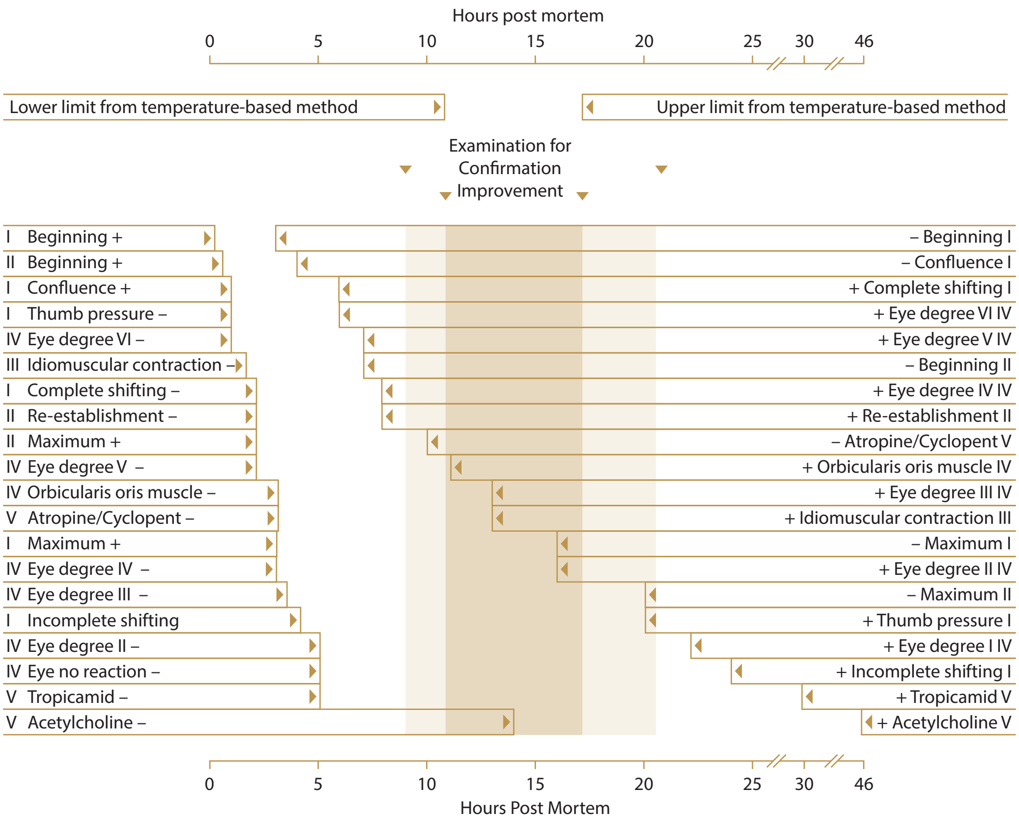
Hours post mortem
0
5
10
15
20
25
30
46
Lower limit from temperature-based method
Upper limit from temperature-based method
Examination for
Confirmation
Improvement
I Beginning +
II Beginning +
I Confluence +
I Thumb pressure –
IV Eye degree VI –
III Idiomuscular contraction –
I Complete shifting –
II Re-establishment –
II Maximum +
IV Eye degree V –
IV Orbicularis oris muscle –
V Atropine/Cyclopent –
I Maximum +
IV Eye degree IV –
IV Eye degree III –
I Incomplete shifting
IV Eye degree II –
IV Eye no reaction –
V Tropicamid –
V Acetylcholine –
– Beginning I
– Confluence I
+ Complete shifting I
+ Eye degree VI IV
+ Eye degree V IV
– Beginning II
+ Eye degree IV IV
+ Re-establishment II
– Atropine/Cyclopent V
+ Orbicularis oris muscle IV
+ Eye degree III IV
+ Idiomuscular contraction III
– Maximum I
+ Eye degree II IV
– Maximum II
+ Thumb pressure I
+ Eye degree I IV
+ Incomplete shifting I
+ Tropicamid V
+ Acetylcholine V
0
5
10
15
20
25
30
46
Hours Post Mortem

Figure 11.8 Logistic of the 'integrated method' (see Table 11.4). Only those criteria that can improve or confirm the time limits from the nomogram method should be used in an actual case.

by the crime police (9.4 hours post-mortem). However, the upper limits of the period since death concluded from the nomogram method (11.7 hours post-mortem) and from the criterion mydriasis of iris to atropine (10 hours post-mortem) were not in contradiction. The case gives cause for replacing 8 hours post-mortem with 9.5 hours post-mortem concerning the upper limit of re-established rigor in Tables 11.1 and 11.4 and in Figures 11.3, 11.6 and 11.7).

The field study clearly demonstrates the usefulness of estimating the period since death in the early post-mortem period by application of the 'integrated method' described in this volume.

11.1.5 Discussion

It must be emphasized that the proposed system is not the result of simultaneous measurements of experimental investigations, but rather is based only on separate data from the literature. Most of the data are again not the result of experimental investigations, but figures taken from textbooks. Therefore, not all cited limits will be the last word. For example, case number 23 in Table 11.6 points to a higher upper time limit of the criterion re-establishment of rigor (9.5 hpm) than the literature-based 8 hpm (see Tables 11.1 and 11.4).

Nevertheless, these data chosen and arranged from statistical and practical points of view are now evaluated in two field studies with simultaneous examination of the combined temperature-based nomogram method and the electrical excitability [16], as well as of combinations of all the parts of the integrated method [7,8].

Using the proposed combined method in casework at the scene, in several cases we were able to assist the criminal investigation in its earliest stage. In other cases, the additional examination of the listed criteria did not provide reduced limits for the nomogram reading. The overall result is an estimation of a time interval within which the death occurred—longer or shorter—but reliable within at least 95 per cent limits if the instructions about using the nomogram and the other methods are followed. We believe that this is the best we can do at present, when giving a statement concerning the time of death.

Table 11.6 Examples of Cases in which the Non-temperature-based Methods Provided a Reduction and/or a Confirmation of the Lower and/or Upper Limit of the Period Since Death Obtained by the Nomogram Method

Case number	Estimation lower limit (hpm)	Method/criterion	Upper limit (hpm)	Method/criterion	Ascertainment lower limit (hpm)	Upper limit (hpm)	Comments
4	2.0	Cooling by nomogram method					
	3.0	Lividity maximum					
	4.0	Lividity no incomplete shifting					
	5.0	**No electr. excit. eye**	**7.6**	**Cooling by nomogram method**	**5.8**	**6.3**	
15			11.0	Electr. excit. orbic. oris m.			
	0.3	Cooling by nomogram method	10.0	Mydriasis to atropine			
	1.0	Electr. excit. eye NO VI	8.0	Rigor re-establishment			
	1.0	Lividity confluence	7.0	Electr. excit. eye V			
	2.0	Rigor maximum+	6.0	Lividity complete shifting+			+After repeated examination at autopsy 2 hours later.
	3.0	**Lividity maximum+**	**5.9**	**Cooling by nomogram method**	**4.3**	**4.5**	
20			13.0	Idiomuscular contraction			
			11.2	Cooling by nomogram method			
			11.0	Electr. excit. orbic. oris m.			
	3.5	Electr. excit. eye NO III	10.0	Mydriasis to atropine			+Missing for 9.8 hours.
	5.6	**Cooling by nomogram method**	**8.0**	**Electr. excit. eye IV**	**2.8***	**9.8^{+}**	*Finding the body 2.8 hours before examination.
21			30.0	Mydriasis of iris to Mydriaticum Roche (tropicamide)			*The body found lying prone was transported lying back; the incomplete shifting of lividity was observed at autopsy.
	5.0	No electr. excit. eye	29.9	Cooling by nomogram method			
	18.1+	Cooling by nomogram method	24.0^{+}	Lividity incomplete shifting*	?	?	$^{+}$Survival of the fatal pressure on the neck for at least 30 minutes up to 3 hours; some contravascular emigration of polymorphic leucocytes in the subcutaneous fat of the ligature mark.
23			13.0	Electr. excit. eye III			
	3.0	Lividity maximum	11.7	Cooling by nomogram method			
	3.0	Electr. excit. eye NO IV	10.0	Mydriasis of iris to atropine			
	6.1	**Cooling by nomogram method**	**8.0**	**Rigor re-establishment+**	**9.3**	**9.4**	+Being inconsistent with the time of investigation.
26	2.0	Electr. excit. eye NO V					
	2.0	Rigor no re-establishment	11.9	Cooling by nomogram method			
	6.3	**Cooling by nomogram method**	**8.0**	**Electr. excit. eye IV**	**7.4**	**7.4**	

(Continued)

Table 11.6 ***(Continued)*** **Examples of Cases in which the Non-temperature-based Methods Provided a Reduction and/or a Confirmation of the Lower and/or Upper Limit of the Period Since Death Obtained by the Nomogram Method**

Case number	Estimation lower limit (hpm)	Method/criterion	Upper limit (hpm)	Method/criterion	Ascertainment lower limit (hpm)	Upper limit (hpm)	Comments
28	3.0	No electr. excit. orbic. oris m.	16.0	Electr. excit. eye II			
	3.5	Electr. excit. eye NO 1	10.0	Mydriasis of iris to atropine			
	3.5	Cooling by nomogram method	9.1	Cooling by nomogram method			
	5.0	**No mydriasis of iris to Mydriaticum Roche**	**8.0**	**Rigor re-establishment**	**6.6**	**6.9**	
34	1.0	Lividity confluence	8.9	Cooling by nomogram method			
	2.0	Electr. excit. eye NO V	8.0	Electr. excit. eye IV			
	3.3	**Cooling by nomogram method**	**6.0**	**Lividity complete shifting**	**4.8**	**5.5**	
40	3.0	No electr. excit. orbic. oris m.					
	5.0	No electr. excit. eye	14.5	Cooling by nomogram method			*Finding the body.
	8.9	**Cooling by nomogram method**	**10.0**	**Mydriasis of iris to atropine**	**7.5***	**12.3+**	+Infliction of the stab wounds.
44	0.5	Rigor beginning	13.0	Electr. excit. eye III			
	1.0	Lividity confluence	11.0	Electr. excit. orbic. oris m.			
	1.1	Cooling by nomogram method	8.0	Rigor re-establishment			
	3.0	**Electr. excit. eye NO IV**	**6.7**	**Cooling by nomogram method**	**3.6**	**4.3**	
46	3.0	No mydriasis of iris to atropine	13.0 13.0	Idiomuscular contraction			
	3.0	Electr. excit. eye NO IV	10.5	Electr. excit. eye III			
	3.0	No electr. excit. orbic. oris m.	8.0	Cooling by nomogram method			
	4.9	Cooling by nomogram method	6.0	Rigor re-establishment			
	5.0	**No mydriasis of iris to Mydriaticum Roche**		**Lividity complete shifting**	**5.8**	**6.1**	Same scene as 47.
47	2.0	Rigor maximum					Same scene as 46; examination 1.5 hours later than 46.
	3.0	Lividity maximum					
	3.5	Cooling by nomogram method	10.0	Mydriasis of iris to atropine			The man shot first the woman and then himself in the presence of witnesses: 'Contemporarily' proved.
	5.0	**Electr. excit. eye NO II**	**9.1**	**Cooling by nomogram method**	**7.3**	**7.6**	
48	3.0	Lividity maximum					+This finding would provide an extraordinarily small range of the period since death. As a precaution, the statement at the scene did not take this criterion into account.
	5.0	No electr. excit. eye					

(Continued)

Table 11.6 ***(Continued)*** **Examples of Cases in which the Non-temperature-based Methods Provided a Reduction and/or a Confirmation of the Lower and/or Upper Limit of the Period Since Death Obtained by the Nomogram Method**

Case number	Estimation lower limit (hpm)	Method/criterion	Upper limit (hpm)	Method/criterion	Ascertainment lower limit (hpm)	Upper limit (hpm)	Comments
	8.8	**Cooling**	**14.4**	**Cooling**	**11.0**	**14.0**	The upper limit of the time since death investigated later on (14.0 hpm) was identical to the lower limit of the estimated period since death based on this criterion.
	14.0^{+}	No miosis of iris to acetylcholine					
52	1.4	Cooling by nomogram method	11.0	Electr. excit. orbic. oris m.			
	2.0	Rigor maximum	8.0	Electr. excit. eye IV			
	2.0	Electr. excit. eye NO V	8.0	Rigor re-establishment			
	3.0	**Lividity maximum**	**7.0**	**Cooling by nomogram method**	**3.6**	**4.8**	
57	5.0	No electr. excit. eye					
	5.0	No mydriasis of iris to Mydraticum Roche					
	11.6	Cooling by nomogram method	20.0	Lividity positive thumb pressure			
	14.0	**No miosis of iris to acetylcholine**	**17.2**	**Cooling by nomogram method**	**3.2**	**18.7**	
58			24.0	Lividity incomplete shifting+			+The body found lying prone was transported lying back; the incomplete shifting of lividity was observed at autopsy.
	5.0	Electr. excit. eye NO II	20.1	Cooling by nomogram method			
	13.7	**Cooling by nomogram method**	**20.0**	**Lividity positive thumb pressure**	**14.3**	**16.1**	
59	1.8	Cooling by nomogram method					
	1.5	No idiomuscular contraction	8.0	Electr. excit. eye IV			
	2.0	Electr. excit. eye NO V	8.0	Rigor re-establishment			
	3.0	**No mydriasis of iris to atropine**	**7.4**	**Cooling by nomogram method**	**2.4**	**4.5**	
63			13.0	Idiomuscular contraction			
			11.2	Cooling by nomogram method			
	3.0	Lividity maximum	8.0	Rigor re-establishment			
	5.6	**Cooling by nomogram method**	**7.0**	**Electr. excit. eye V**	**6.7**	**7.1**	
67	3.0	No mydriasis of iris to atropine					
	3.0	No electr. excit. orbic. oris m.					
	3.5	Electr. excit. eye NO III					

(Continued)

Table 11.6 *(Continued)* **Examples of Cases in which the Non-temperature-based Methods Provided a Reduction and/or a Confirmation of the Lower and/or Upper Limit of the Period Since Death Obtained by the Nomogram Method**

Case number	Estimation lower limit (hpm)	Method/criterion	Upper limit (hpm)	Method/criterion	Ascertainment lower limit (hpm)	Upper limit (hpm)	Comments
	4.9	Cooling by nomogram method	16.0	Electr. excit. eye II			
	5.0	**No mydriasis of iris to Mydriaticum Roche**	**10.5**	**Cooling by nomogram method**	**9.3**	**10.3**	
68	2.0	Electr. excit. eye NO V					
	3.0	Lividity maximum	15.9	Cooling by nomogram method			
	6.9	**Cooling by nomogram method**	**8.0**	**Electr. excit. eye IV**	**5.7**	**11.2**	
69			11.0	Electr. excit. orbic. oris m.			
			10.0	Mydriasis of iris to atropine			
	1.7	Cooling by nomogram method	7.3	Cooling by nomogram method			
	3.0	**Lividity maximum**	**6.0**	**Electr. excit. eye VI**	**3.1**	**3.4**	
71	5.0	No electr. excit. eye	23.4	Cooling by nomogram method			
	14.4	**Cooling by nomogram method**	**20.0**	**Lividity positive thumb pressure**	**17.2**	**17.7**	
72			9.5	Cooling by nomogram method			
			8.0	Electr. excit. eye IV			
	2.0	Electr. excit. eye NO V	8.0	Rigor re-establishment			+Observed at the scene after turning the body from lying prone to lying back.
	3.9	**Cooling by nomogram method**	**6.0+**	**Lividity complete shifting+**	**5.1**	**5.4**	
			Cases where the nomogram method must not be used				
31	1.0	Lividity confluence	10.0	Mydriasis of iris to atropine			Because of the particular circumstances, the temperature-based nomogram method could not be used.
	3.0	**Electr. excit. eye NO IV**	**8.0**	**Rigor re-establishment**	**4.8**	**5.3**	
38			11.0	Electr. excit. orbic. oris m.			
	0.5	Rigor beginning	10.0	Mydriasis of iris to atropine			The temperature-based method was not used because of heat exposure by a room fire.
	1.0	**Electr. excit. eye NO VI**	**7.0**	**Electr. excit. eye V**	**3.0**	**?**	
45	1.0	Lividity confluence					The temperature method was not used because of the particular cooling conditions/
	2.0	Rigor maximum					
	3.0	No electr. excit. orbic. oris m.	10.0	Mydriasis of iris to atropine			
	5.0	**Electr. excit. eye NO II**	**8.0**	**Rigor re-establishment**	**4.5**	**7.5**	

Abbreviations: +, positive; electr. excit., electrical excitability; orbic. oris m., orbicularis oris muscle.

Table 11.7 Number of Instances Where a Criterion of a Non-temperature-based Method Led to Improvement or Confirmation of the Upper or Lower Limit of the Period Since Death Estimated from Body Cooling

Method/criterion	Improvement	Confirmation
Electrical excitability eye	33	18
Electrical excitability orbicularis oris muscle	6	5
Mydriasis of iris to atropine	9	3
Mydriasis of iris to tropicamide (Mydriaticum Roche)	4	1
Miosis of iris to acetylcholine	1	2
Rigor beginning	5	4
Rigor maximum	3	0
Rigor re-establishment	6	7
Idiomuscular contraction	1	1
Lividity beginning	0	0
Lividity confluence	6	3
Lividity maximum	9	3
Lividity complete displacement by thumb pressure	3	0
Lividity complete shifting after turning over	5	5

References

1. Beier G, Liebhardt E, Schuck M, Spann M. Measurement of rigor mortis on human skeletal muscles in situ [in German, with English summary]. *Z Rechtsmed* 1977;79:277–83.
2. Berg S. *Grundriss der Rechtsmedizin*. Munich, Germany, Müller und Steinicke, 1984.
3. Biermann FM, Potente S. The deployment of conditional probability distributions for death time estimation. *Forensic Sci Int* 2011;210(1–3):82–6. http://doi.org/10.1016/j.forsciint.2011.02.007.
4. Forster B, Ropohl D, Raule P. A new formula for the measurement of rigor mortis: the determination of the FFR-Index [in German, with English summary]. *Z Rechtsmed* 1977;80:51–4.
5. Dotzauer G. Idiomuskulärer Wulst und postmortale Blutung. *Dtsch Z Gerichtl Med* 1958;46:761–71.
6. Henssge C. *Methoden zur Bestimmung der Todeszeit*, MD thesis. Berlin, Humboldt University, 1982.
7. Henssge CA. *Beitrag zur Standardisierung eines komplexen Verfahrens zur Todeszeitbestimmung am Leichenfundort: Interaktives Computerprogramm*, MD thesis. Essen, Germany, University of Essen, 1999. www.AMAsoft.de
8. Henssge C, Madea B. Determination of the time since death: body heat loss and classical signs of death—an integrated approach. *Acta Med Leg Soc* 1988;I:9.
9. Henssge C, Althaus L, Bolt J, Freislederer A, Haffner HT, Henssge CA, Hoppe B, Schneider V. Experiences with a compound method for estimating the time since death. I. Rectal temperature time of death nomogram. *Int J Legal Med* 2000;113:303–19.
10. Henssge C, Althaus L, Bolt J, Freislederer A, Haffner HT, Henssge CA, Hoppe B, Schneider V. Experiences with a compound method for estimating the time since death. II. Integration of non–temperature-based methods. *Int J Legal Med* 2000;113:320–31.
11. Hilgermann R. *Histochemische Untersuchungen zur Frage der Diffusions-Totenflecke*, MD thesis. Marburg, Germany, Marburg University, 1973.
12. Hofmann EV. Die forensisch wichtigsten Leichenerscheinungen. *Vierteljahresschr Gerichtl Med* 1876;25:229–61 and 1877;26:17–40.
13. Hunnius PV. *Das Verhalten der Totenflecken bei quantitativen Druckmessungen in Abhängigkeit vom Leichenalter*. Tübingen, Germany, Dissertation, 1973.
14. Hunnius PV, Mallach HJ, Mittmeyer HJ. Quantitative pressure measurements of livores mortis relative to the determination of the time of death [in German, with English summary]. *Z Rechtsmed* 1973;73:235–44.
15. Klein A, Klein S. *Die Todeszeitbestimmung am menschlichen Auge*, MD thesis. Dresden, Germany, Medical Akademy, 1978.
16. Madea B, Henssge C. Estimation of the time since death: integration of different methods. *Digest of the International Meeting of P.A.A.F.S. and Police Medical Officers*, Wichita, Kansas, August 10–14, 1987.
17. Madea B, Henssge C. Electrical excitability of skeletal muscle postmortem on casework. *Forensic Sci Int* 1990;47:207–27.
18. Mallach HJ. Zur Frage der Todeszeitbestimmung. *Berl Med* 1964;18:577–82.
19. Mallach HJ, Mittmeyer HJ. Rigor mortis and livores [in German, with English summary]. *Z Rechtsmed* 1971;69:70–8.
20. Popwassilew J, Palm W. Über die Todeszeitbestimmung in den ersten 10 Stunden. *Z Arztl Fortbildung* 1960;54:73–7.
21. Prokop O. *Lehrbuch der gerichtlichen Medizin*. Berlin, VEB Verlag Volk und Gesundheit, 1960.
22. Prokop O. Supravitale Erscheinungen. In: Prokop O, Göhler W (eds.). *Forensische Medizin*. Berlin, Verlag Volk und Gesundheit, 1975, pp 1, 27.
23. Schuck M, Beier G, Liebhardt E, Spann W. On the estimation of lay-time by measurements of rigor mortis. *Forensic Sci Int* 1979;14:171–6.
24. Zsako S. Die Bestimmung der Todeszeit durch die muskelmechanischen Erscheinungen. *Munch Med Wochenschr* 1916;3:82.

11.2 Conditional Probability in Death Time Estimation

■ *Stefan Potente*

The conditional probability distribution (CPD) approach integrates additional information, namely the time interval in which death is at all possible to have occurred, into the nomogram interval.

Henßge's nomogram method for the estimation of time since death uses a normal distributed 2 standard deviation hours since measurement as target.

Additional methods, namely supravital reactions and properties of lividity and rigor as described in the compound method (CM), on the other hand aim at excluding certain time ranges. Here, findings may lead to statements about minimum or maximum hours since death.

The same principle is applied in police investigation where the time when the deceased was last seen alive and the time the body was found are checked regularly and additional information such as way-time-calculations, telecommunication data and such can be taken into account in a broader approach to the circumstances surrounding death.

When combining nomogram method results with said limitations to the time when death is at all possible to have occurred, effects on probability concerning the nomogram method findings have not yet been taken into account. In other words—‘under the condition that death might have occurred between time X and Y’ a given death time interval estimated using the nomogram method may hold considerably different properties than without said conditions. Vice versa, when conditions are discarded or taken out of the consideration, the unconditional death time interval will hold the properties of the ‘regular’, unconditional nomogram death time interval.

11.2.1 Explaining Math in Court—A Thought Experiment

Statements about probability, probability distribution and effects of certain changes in the setting can be difficult to explain to judges and juries. One should however try to do so properly, thereby avoiding the (incorrect) impression that the expertise was just “black magic with numbers” and something very theoretical applied to a very practical problem.

Even though the underlying math may not be easily understood by the layman, the problem as such may well be illustrated using analogies.

It has shown itself to be useful to illustrate the concept of normal distribution by using a (hypothetical) distribution of body height or the IQ while presenting the well-known bell-shaped curve. One may then proceed by applying this concept on real life problems, such as the design of car seats, the size of army uniforms to be held in stock and the problem of test design in high school education.

The next step would be to set a limitation to one of the systems just explained, for example the IQ distribution in the general public. The author prefers the example of IQ distribution:

The IQ may be normally distributed with an expected value of 100 and one standard deviation width of 10. Thus, 95.45% (2SD) of the population will fall into the IQ range of 80 through 120, with <2,5% being “smarter” or “dumber” respectively.

Consider Mr. Smith (IQ 125) who challenges random people on the street for being smarter, the odds being clearly in favor of Mr. Smith.

Consider Mr. Smith moving his scheme to a MENSA meeting, an organization of highly intelligent people with an IQ of 120 being the minimum IQ for joining. Will Mr. Smith have the same kind of success as on the streets?

Another good example is height distribution in the whole population which will be reflected in a population of rollercoaster riders. In a random seating of a very long (never-ending if you will) rollercoaster, the height distribution should reflect the bell shaped curve neatly. What will happen to this population when for technical reasons only people taller than 176 cm are allowed to take the ride?

Whatever example is chosen the minimum (take home) message should include a) limitations/conditions will reflect on probability and b) once the conditions are taken out of the equation everything goes back to its normal, unconditional state.

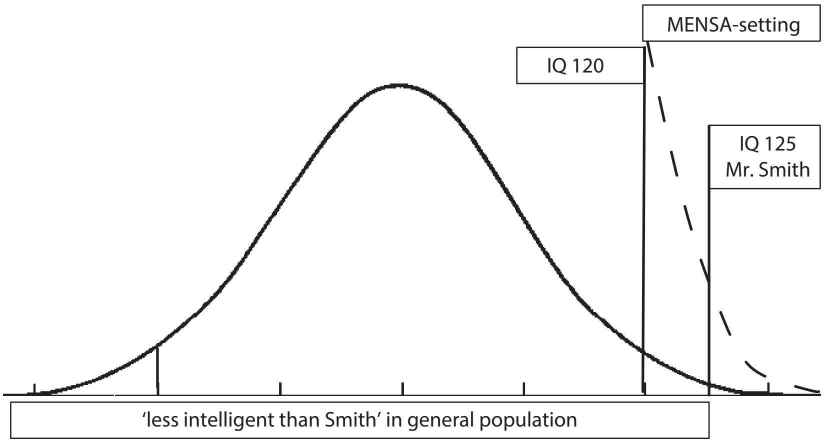

Figure 11.9 Example “Mr. Smith”: in the general population Mr. Smith outsmarts most people. Under MENSA-conditions (only IQ 120 and up), the area under the curve, representing probability, shows a very different picture.

11.2.2 Assumptions and Conditions in CPD Construction

Technically, from a strictly mathematical analytical point of view, every single death time interval estimated via the nomogram method is false since the unconditional interval by definition does not take into account that at time T0, when temperature was taken, the person was dead already. *Technically* there is always a probability unequal to zero attributed to the time after rectal temperature for death time estimation was taken.

In most practical settings this does not constitute any problem other than hypothetical. In *ultra-early death time estimation* however, when rectal temperature is taken shortly after death and cooling has just set in passing the plateau, this might constitute a very practical problem, when a death time interval is calculated which overlaps in larger parts with the time after measurement and this larger part is then simply "cut off" without further consideration of the probability.

Before constructing the CPD interval a regular, unconditional nomogram interval is either calculated or derived graphically.

The conditions which are to be applied to it should be laid out separately first, so they may be discussed separately in court, especially if different versions may have to be constructed. It has proven useful to handle this part of the presentation very much alike to testimony considering blood alcohol levels (different amounts of consumed drinks, different sizes of glasses and so on) so all parties in the trial/investigation may state an opinion on one or the other assumption and may find an agreement. A good example may be way-time-calculations (a receipt is found stating that the victim purchased some product at time X, 5 miles from the crime scene—there may be different assumptions as to the earliest time of death depending on the mode of travel).

After both the unconditional nomogram method interval and the assumptions are laid out, the assumptions may then be applied to the unconditional death time interval to compile the CPD interval.

11.2.3 Compiling the CPD Interval

For compilation of the CPD interval a computer spreadsheet is provided.

The conditions in terms of upper and lower limits (such as "found dead" and "last seen alive") are entered. The probabilities of the areas cut off using those limitations are calculated. The remaining time interval where "death is possible to have occurred" is then multiplied using the reciprocal value of the sum of cut off probabilities to construct the conditional probability distribution, since after applying the limitations/conditions the probability of the remaining interval (where "death is at all possible to have occurred") must hold 100 percent.

With the new distribution constructed the spreadsheet will then find the smallest possible interval holding 95.45% probability doing so by finding the modus (peak) of the distribution and spreading to both sides until either a limitation is hit or the interval holds 95.45% probability.

The results are produced as a new 95.45% interval. Information on the unconditional interval in the light of limitations is also given. Most commonly the unconditional interval will not hold 95.45% probability when limitations are taken into account.

11.2.4 Case Examples

> 58 year old male found dead at 08:02 on a forest path. Rectal temperature of 28.3° C in combination with 3° C ambient temperature and 65 kg body weight suggest a death time interval of 7.6 +/– 2:8 hours prior to measurement (13:15 on 24th November 2009).
>
> Re-establishment of rigor indicates a death time <= 8.0 hours, grade V reaction to electrical stimulation of facial muscles indicates a death time <=7.0 hours. The upper boundary was cut off accordingly.
>
> The death time interval was interpreted to be between 06:15 and 08:27. Confession of the perpetrator stated a time of death at 06:30.

The unconditional construction of the NM interval reveals a death time interval between 2:51 a.m. and 8:27 a.m. (5.6 hours width) with an attributed probability of 95.45%.

When applying the compound method as usual, in this case introducing a maximum time since death of 7 hours prior to measurement due to findings in electrical stimulation, the resulting interval is 6:15 a.m. to 8:27 a.m. (2.2 hours width). However, this interval does not hold 95.45% but a mere 93.19%.

The CPD interval, representing 95.45% stretches from 6:15 a.m. to 8:40 a.m. (2.43 hours width).

The example however did so far not exploit all the information available. The information of finding the body dead at 8:02 a.m. (5.22 hours prior to measurement) must be introduced as well.

In the compound method approach, theoretically at least, the introduction of data will transform into a death time interval between 6:15 a.m. (electrical stimulation) and 8:01 a.m. (finding of body one minute later). The interval width of 1.78 hours contain a probability of 100%, since death cannot have occurred any time outside of the interval.

When applying CPD the known probability distribution is integrated into the calculation and a smaller 95.45% death time interval considering the known limitations is constructed, ranging from 6:15 a.m. to 7:51 a.m. (1.6 hours width).

To highlight the benefits of CPD, we assume a variation of the case example above:

> *A group of young drug addicts has a party in the forest. One youngster leaves the group at 07:55 to urinate in the bushes. At 08:02 a policeman patrolling the forest path finds the youngster crouched over the dead body of an elderly gentleman. In his possession the purse of the elderly man is found. The young man claims that he did not harm the gentleman but rather found him already dead and took the money for drugs.*

Without CPD the probability of intervals cannot be addressed properly in this case. Without implementation of the time of finding the body (08:02) the information is cluttered and possibly misleading, as one death time interval stated as 06:15–08:30 wrongly suggests the youngsters time of absence as being "well inside the likely death time interval".

But we know that the body was found at 08:02. And we know it was dead for a maximum time of 7 hours prior to measurement.

A true 95.45% interval from 06:15 to 07:51 shows that the youngster was less likely the killer and the police should be informed that the case could be more complex than the first impression might have indicated.

It must be stated of course that interpretation of interval probability in respect to alibi should be handled with utmost care: had the youngster been the true killer and had left the group at an earlier time (say between 06:20 and 06:40) the probability of that time interval would have been rather "small" as well. So probability of time intervals should not be confused with probability of guilt.

Using a dedicated Excel-Sheet it is easy to construct a variety of real or hypothetical cases. Also it comes in handy when different versions are to be calculated such as way-time calculations assuming different modes of transport, different witness-accounts about the last time the victim was seen alive and even variations of expert opinions. Also a quick calculation using the sheet may be used to demonstrate certain information as practically irrelevant (for example that a runaway teen was last seen alive 3 weeks before finding the body).

It is often rewarding to look closely at case files and police statements in search of clues regarding "possible time interval of death". In one case the author was able to calculate a CPD interval partly based on the following information:

Two children returned from school around 2 p.m. to find the door of the apartment (4th floor) closed, their mother did not open. The children assumed that their mother had gone out to buy groceries and would soon return so they sat on the stairs by the door to wait for her. After waiting for 4 hours a neighbour offered to open the apartment door using a credit card to let the children in. As they entered, they found the mother dead. She had been stabbed multiple times.

In constructing the CPD interval 2 p.m. was used as latest possible death time since survival-time in this particular case was neglectable and no one had left the apartment after 2 p.m.

11.2.5 Results

There may be different results with varying degrees of change from unconditional to conditional probability distributions. In any case the conditional interval will show the correct 94.45% interval considering the conditions/limitations applied.

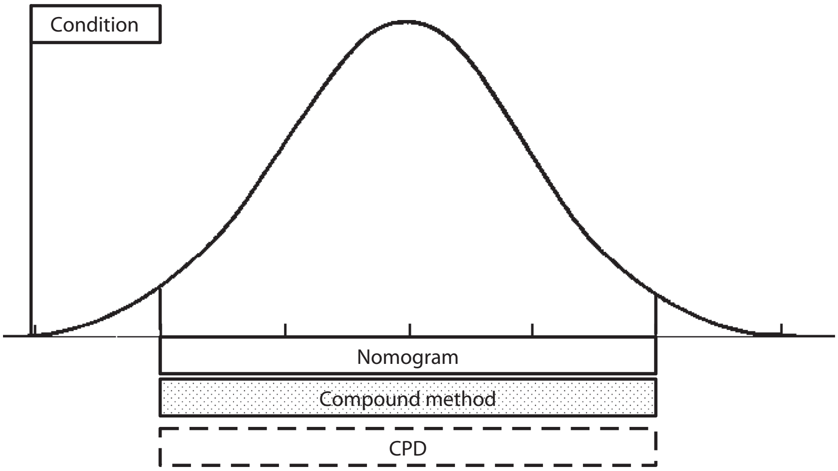

Figure 11.10 When limitations are introduced which lie far outside the 2-SD range, they do not cut off significant probability and therefore do not significantly alter probability distribution.

1. No change in respect to practical usability.

This is a usual result when the conditions/limitations introduced are rather weak, meaning that the time intervals cut-off did not hold much probability to begin with. This is easily understood both from a logical point of view and a mathematical point of view since, for example, in a body which has almost hit equilibrium with its environment, the information ‘found exactly at 2 p.m. this afternoon’ will not change the picture. Mathematically, a limitation at the far end ‘tail portion’ of the graph holds very little probability, so the reciprocal value to be multiplied with will be very close to 1, rendering the result to be changed only minimally. As a rule of thumb, conditions/limitations should fall into the unconditional 94.45%-interval on at least one side to yield practical results.

The results, when calculated for actual time intervals, transfer to very small values, such as one minute or even just seconds, holding no practical value for investigations or use in court. However, when conditions are known the CPD approach should be used in any case, if only to show that in fact they do not yield significant results.

2. The conditional interval is smaller than the unconditional interval simply “cut off”

This happens when the time interval determined to be “impossible death time” by limitations is significant but does not exceed 50%. In this case simply cutting off the unconditional interval will result in an interval which holds more than 95.45% probability, even 100% is possible (imagine a wide 95.45% interval which includes both the time of last seen alive and found dead). However, since 95.45% is the standard in the nomogram method, one might either state the interval´s probability in respect to conditions or calculate a new CPD 95.45% interval which will be considerably smaller.

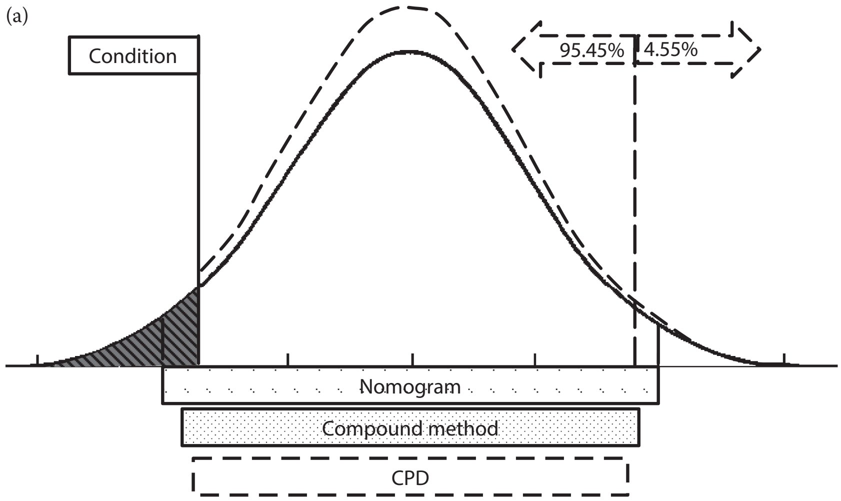

Figure 11.11a When less than 50% of probability is excluded using conditions (shaded area), the compound method interval will hold >95.45% probability. Integrating the conditional probability distribution (dashed curve) will calculate interval width for 95.45% probability and therefore further reduce interval width.

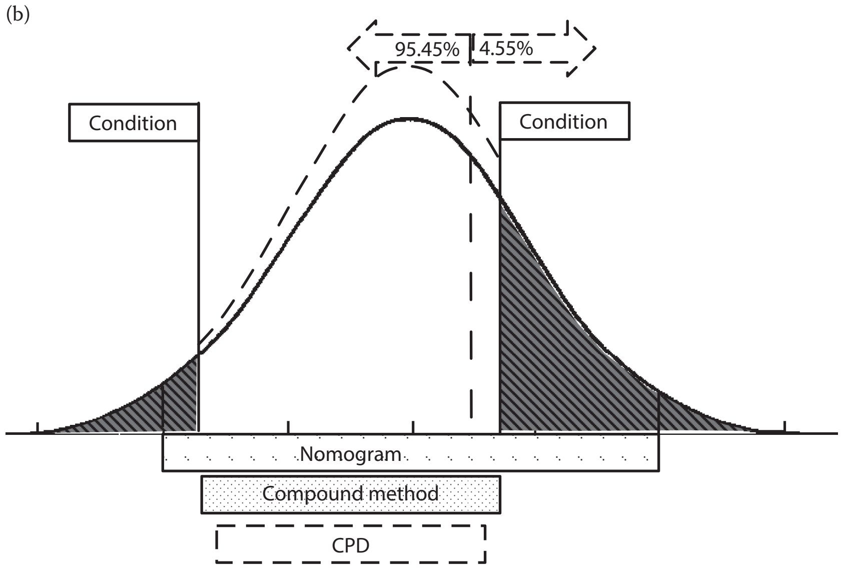

Figure 11.11b With restrictions to both sides of the probability distribution (shaded areas), each reaching inside the 2-SD-range, the interval probability of the compound method interval reaches 100%. Integrating the conditional probability distribution (dashed curve) will calculate interval width for 95.45% probability and therefore further reduce interval width.

3. There is no change in interval width

In rare cases there is no change in interval width when comparing the CPD interval to the unconditional interval which is simply cut off by limitations. This happens when the cutoff takes place exactly at the modus, the peak point of the distribution curve and exactly 50 percent is cut off. From a logical point of view, the proportions are not changed in this setting, when simply taking one half of the area inside and outside the interval away. It is however important to remember, and show on the graph, that the conditional 95.45% interval does no longer resemble a bell shape or any peaked curve at all for that matter, but probability will fall (or rise) rapidly in respect to one border. For example it might be reasonable to state that since a person who was last seen alive leaving a party was killed more likely shortly after that point in time than later.

4. The CPD interval is larger than the unconditional interval simply "cut off"

This happens when the time interval determined to be "impossible death time" by limitations does exceed 50%. Those cases can change the picture in the most dramatic way up to the point where the area outside the unconditional interval, which was simply cut off, yields a higher probability of death having occurred than the area of a falsely stated "death time interval".

For demonstration and as a proof-of-concept, the CPD method was applied to a set of external data. Henssge et al. applied the compound method to 72 crime scene cases in a field study. For 53 of these cases the CM data was given in detail with one case tested twice over time (leading to a total of 54). The CPD method was applied to all 53 cases.

The CPD algorithm achieved a narrowing of the death time interval compared to the CM interval in 43 out of 53

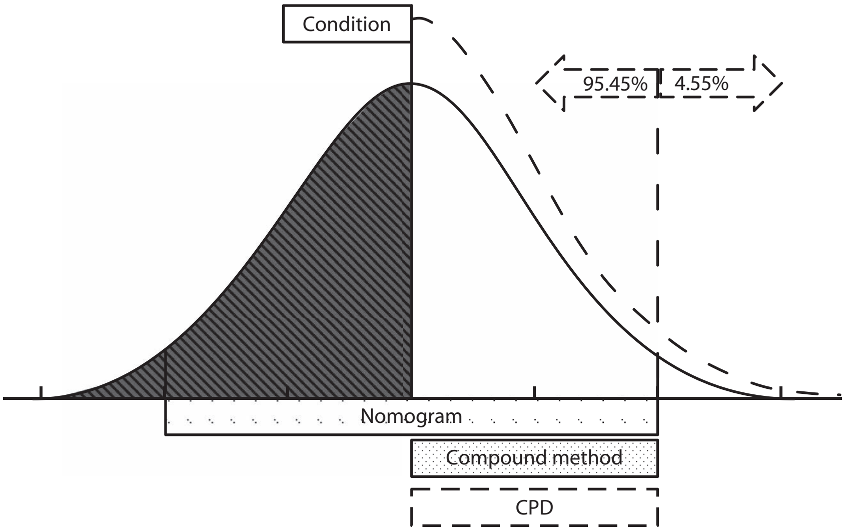

Figure 11.12 In the rare case of a condition excluding exactly 50% of probability on one side of the modus, the compound method interval and CPD interval are equal in location and probability. Note, however, since the conditional probability distribution (dotted line) is no longer symmetric, probability will gradually diminish in growing distance to the modus.

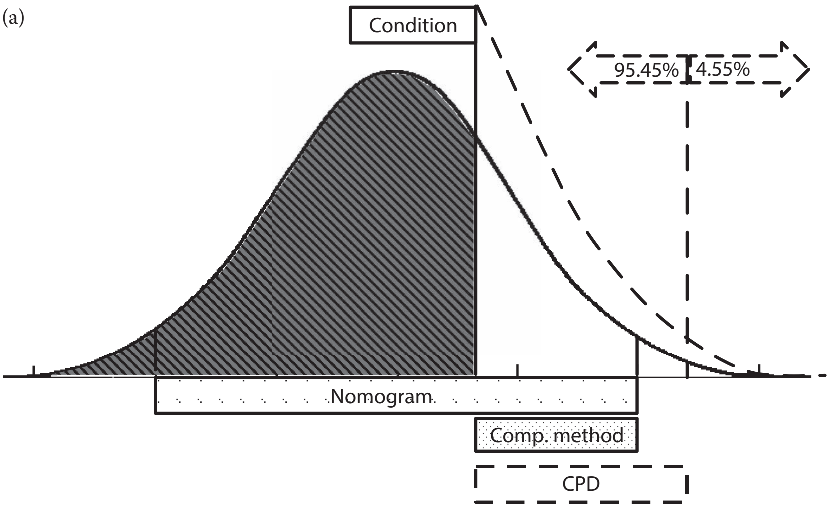

Figure 11.13a When more than 50% of probability is excluded by conditions, the resulting compound method interval will hold <95.45% probability. Therefore, when calculating the CPD interval holding 95.45% probability, the CPD interval width must be larger compared to the compound method interval.

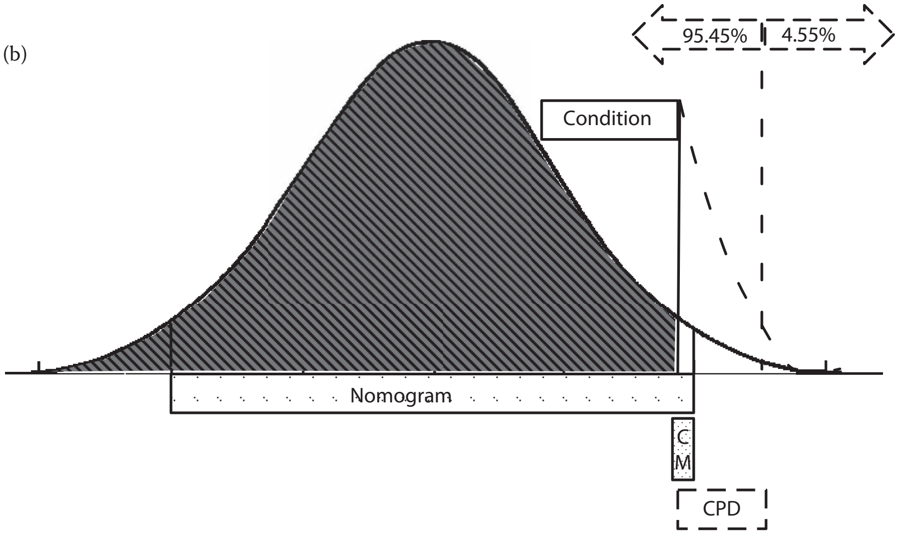

Figure 11.13b Under extreme conditions, when limiting conditions reach closely to the 2-SD-boundary of the nomogram interval, the resulting compound method interval may be extremely narrow, holding extremely low probability at the same time. The CPD interval holding 95.45% probability therefore is much wider than the compound method interval.

cases. The range of improvement was between −0.01% and −15.21% (between 0% and 5% in 9 cases, between 5% and 10% in 24 cases, and more than 10% in 10 cases). The six cases with no narrowing achieved by CM were all narrowed using CPD (between −1.75% and −8.52%). In 9 cases the dismissal in CM was so large that the probability in the given CM interval was less than 95.45% (between 47.38% and 94.87%). The true 95.45%-interval for these cases calculated using CPD was therefore wider compared to the CM interval (between +2.71% and +309.17%). However, in those cases the resulting CPD intervals were all smaller than the original nomogram method interval (between −51.79% and −71.43%). It should be noted that in 9 cases no information was provided about the time the person was found dead or was last seen alive respectively. In retrospect this information could have been obtained easily and might have led to further improvements when using CPD.

12 Forensic Entomology

Saskia Reibe

12.1 Identification of Insects 335
12.2 Blowfly Development 336
12.3 Influence of Temperature 336
12.4 Estimation of Post-mortem Interval 336
12.5 Succession 338
12.6 Sampling of Insects from Bodies 339
12.7 Case Reports 339
  12.7.1 Suicide 339
  12.7.2 Skeleton in Forest 340
  12.7.3 Dismembered Body 340
  12.7.4 Winter Suicide Indoors 341
  12.7.5 Winter Suicide Outdoors 342

In forensic entomology, which is the application of entomological science in medico-legal cases, arthropods, mainly insects, are treated as objective evidence in criminal investigations. Of main interest are insects that rely on decomposing tissue such as a dead body as feeding or breeding sites.

A dead body needs to be viewed as a system. It is influenced by numerous variables, such as ambient temperature or degree of exposure, which in turn influence insect colonization. These variables also interact with and influence each other.

After collecting the insects from a corpse, analysing their developmental stage and calculating their age by using the respective ambient temperature profile, a forensic entomologist can give reliable information about a minimum post-mortem interval (PMI). This is especially important in cases that are more than a few days old, where traditional medico-legal methods fail to give an accurate estimate [11].

A main question for forensic entomologists is estimating the PMI. The textbook scenario to answer this question involves an open space, summer temperatures, no rain and a person who falls dead on the spot during daylight. In this scenario blowflies would be attracted to the body within the first hour after death. These early visitors are looking for a convenient spot to deposit their egg patches. They will choose an area of the body that provides easy access to food for their offspring. This means the area should not be likely to dry out or be subject to predators. In general, the body's natural orifices are preferred choices for oviposition, and hatching larvae start feeding on the decomposing tissue. Eventually, bacteria will have broken down most of the tissue catalysed by insect activity and temperature, thus resulting in a corpse that will be fully infested by feeding larvae (Figure 12.1).

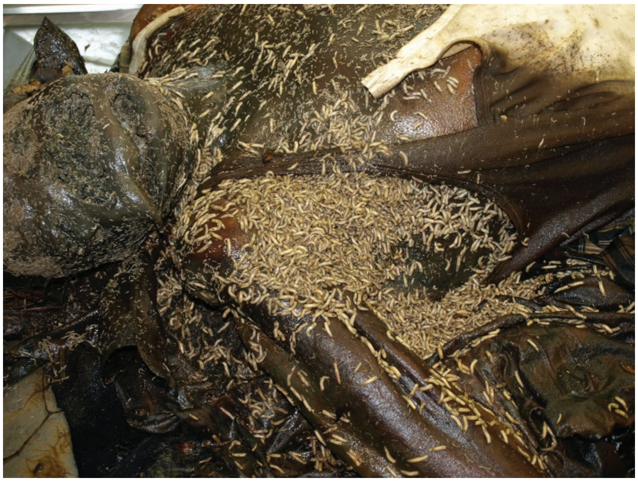

Figure 12.1 Body infested with blowfly larvae.

12.1 Identification of Insects

A reliable estimation of a PMI involving entomological evidence can be guaranteed only if the identification of the insect species collected in association with the corpse or the surroundings is accurate. A cheap and convenient method for reliable species identification is a morphological technique using appropriate identification keys. The only pieces of equipment necessary for morphological species determination are a dissecting microscope with a proper light source and a reliable identification key. Although insect identification is a skill every experienced forensic entomologist should have, it requires extensive practice. However, it may be impossible to identify a specimen by means of its morphology (e.g. as a result of damage). In such cases, it may be preferential to use molecular identification

DOI: 10.1201/9781003244974-12

tools. To ensure correct species identification, established molecular methods were transferred to the forensic field [4,22,23,27]. Analysis of mitochondrial DNA (mtDNA), and particularly of the cytochrome oxidase I gene (COI), appears to be a useful tool in species identification among the sub-families of Calliphoridae [9,10,28,30].

12.2 Blowfly Development

The developmental stages of a blowfly (Figure 12.2) can indicate the PMI [5,15,29], as a function of temperature [19]. During their feeding stages, the blowfly larvae undergo two periods of moulting, while their body size and weight increase constantly. Once a critical amount of food has been metabolized, the larvae leave the food source to enter the next developmental stage. This significant part of blowfly development is the pupal stage in which the larvae undergo metamorphosis and are re-programmed to become adult flies. The duration of this stage is, like the rest of the development, temperature dependent, but in general it takes up about half of the total development period. The larvae's growth rate depends on their body temperature, which is directly influenced by environmental conditions such as the ambient temperatures and the heat generated by maggot aggregations [21]. In addition, each species has its own temperature-dependent growth rate.

12.3 Influence of Temperature

Insects are poikilothermic organisms. Their body temperature changes with ambient temperature. The metabolic rate of poikilothermic animals shows the same temperature dependency as the reaction kinetics in a biochemical system: the rate of a chemical reaction is increased twofold for each rise of 10°C in temperature (van't Hoff's reaction-rate-temperature rule). For insect development, a relationship between ambient temperature and duration of developmental processes has long been known. There is a temperature zone where the development rate is optimal; furthermore, temperature thresholds exist below or above that optimum where no development will take place. During the twentieth century, significant effort was made to describe larval growth correctly and to find a function best representing the temperature-dependent growth rate [14]. Several empirical and physiochemical formulations of development were proposed, and two were discussed in particular by Sharpe and De Michele in 1977 [20] to present the reaction kinetics of poikilotherm development: the day-degree or temperature summation rule and the non-linear temperature inhibition model. The day-degree summation rule assumes that the rate of development (reciprocal of development curve) is proportional to temperature:

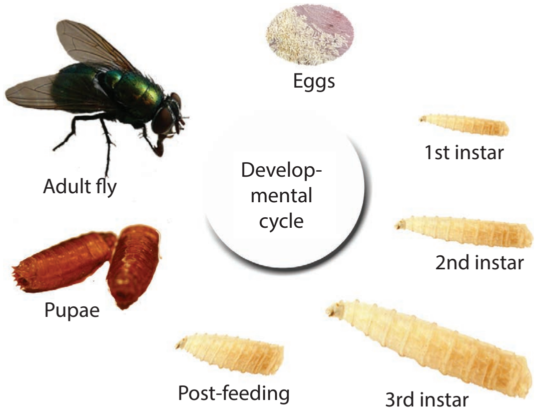

Figure 12.2 Overview of blowfly development.

$$k = \mathrm{b}(T - T0)$$

where k is the rate of development, b is a constant, T is the ambient temperature and $T0$ is a species-specific value, the so-called development zero, which is the x-intercept (i.e. an extrapolation of the linear approximation of the reciprocal of time for development).

12.4 Estimation of Post-mortem Interval

The term 'post-mortem interval' can be misleading when it is used in forensic entomology. The age of insect larvae feeding on a corpse can indicate a time frame of how long the corpse has been infested with insects. However, a person can already be infested while still alive. Examples include a neglected person who smokes and who has severe wounds of the leg [6] and, as reported from soldiers in the First World War, wounds that would have led to amputation if blowfly larvae had not fed on the necrotic tissue to clean the wounds [17]. In contrast, a person can be long dead and the larvae can still be only a few days old when the corpse was originally stored in a place with no access for the insects and was placed outside just a few days before the finding. Therefore, one must take into account every aspect before giving a statement about a PMI. In the latter case, if the insect evidence does not fit the decomposition stage of the corpse, the police can use that piece of information and can additionally use the information about how long the corpse has been exposed to insect activity. However, from the insect evidence alone, no reliable information can be given about the PMI in that case. Therefore, forensic entomologists refer to their estimations as minimum PMI (PMImin) (Figure 11.3).

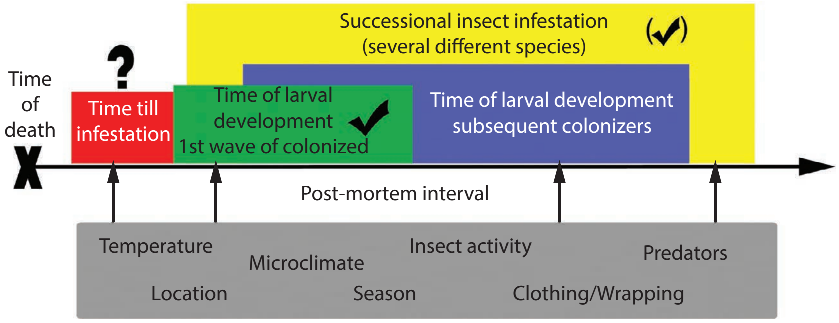
Successional insect infestation
(several different species)
(✓)
Time of death
?
Time till infestation
Time of larval development 1st wave of colonized
✓
Time of larval development subsequent colonizers
Post-mortem interval
Temperature
Microclimate
Insect activity
Predators
Location
Season
Clothing/Wrapping

Figure 12.3 Schematic overview of the PMI estimation process based on insect infestation. The estimation of time between death and the first insect infestation is highly challenging. The grey box contains a selection of factors that influence decomposition and insect activity simultaneously.

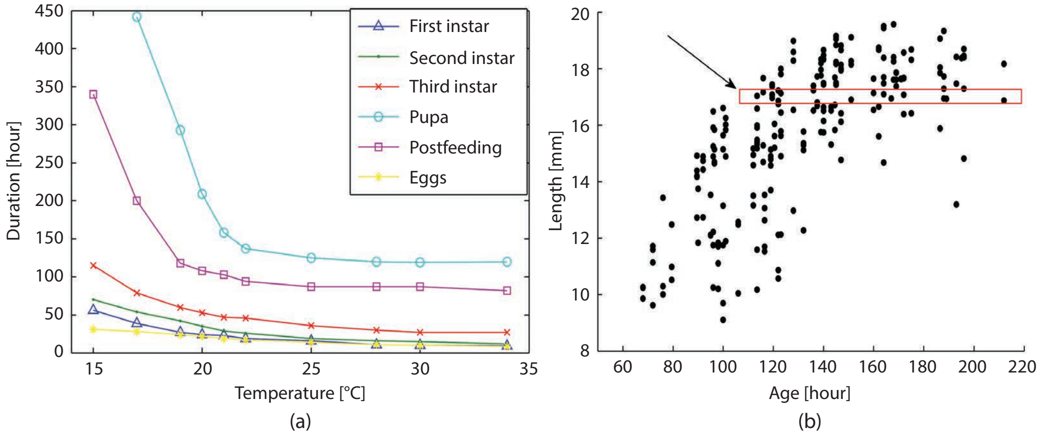

(a)

(b)

Figure 12.4 (a) Blowfly larval development as a function of temperature. (b) Scatterplot of blowfly larvae of different ages and sizes. The red box shows the distribution of larvae of the same length but different ages.

One way to estimate a PMImin is to calculate the age of the most highly developed insect (e.g. blowfly) larvae that are feeding on the corpse and thereby giving a minimum time interval the person has been infested by insect larvae. This estimation is possible only if the calculation is done for larvae of the first colonization wave. If the life cycle of the first larvae has already been completed and the adult flies continued oviposition on the corpse, it is safe to calculate only the time of the first completed life cycle. The basis of larval age calculation is their temperature-dependent development. This implies accurate knowledge of the temperature at the time and place of larval development. One method to approximate the ambient temperature is to record the temperature values at the desired place for a few days and compare them with data recorded at the nearest weather station. A regression analysis is applied to both data sets to obtain a formula that can be used to transform the data from the weather station covering the desired time frame into the temperature values that most likely influenced the developing larvae. In addition to temperature, the second requirement for calculating a PMImin based on larval age is the correct identification of the species, and the third requirement is the determination of the developmental progress of the collected larvae. Hence, determination of the stage (very rough estimation of age) or the length of the maggots is required, depending on the reference data set and the method that is to be used for the further calculation.

In forensic casework, two different methods are frequently used to calculate a PMImin. The correlation between larval developmental rate and temperature is well established, and all models include this factor (Figure 12.4 [a]).

The first method uses isomegalen or isomorphen diagrams, in which the lengths and the developmental stage of the larvae are combined as a function of time and mean ambient temperature in a single diagram [18]. According to its originators, this method is optimal only if the body and therefore the larvae were not undergoing fluctuating temperatures (e.g. in an enclosed environment where the temperature was nearly constant).

The second method of calculating a PMImin estimates the accumulated degree days (ADDs) or accumulated degree hours (ADHs). ADH values represent a certain number of 'energy hours' that are necessary for the development of insect larvae. The degree-day or degree-hour concept assumes that the developmental rate is proportional to the temperature within a certain species-specific temperature range [12]. However, the relationship of temperature and development rate (reciprocal of development time) is typically curvilinear at high and low temperatures and is linear only in between these extremes.

The formula for calculating ADH is as follows:

$$\mathrm{ADH} = T \cdot \left(\theta - \theta_0\right),$$

where T is the development time, θ is the ambient temperature, and the minimum developmental threshold temperature, θ_0, is a species-specific value, the so-called development zero, which is the x-intercept (i.e. an extrapolation of the linear approximation of the reciprocal of time for development).

This value has no biological meaning; it is the mathematical consequence of using a linear regression analysis [12]. One basic condition for using the ADH method is that the ADH value for completing a developmental stage stays constant within certain temperature thresholds. For example, a developmental duration for finishing a certain stage of 14 days at 25°C results in 238 ADDs when a base temperature of 8°C is assumed. A developmental duration of 19 days at 21°C results in 231 ADDs; both ADD values are in the same range.

In general, the ADH method seems to give good results only when the larvae of interest have been exposed to temperatures similar to those used in generating the reference value applied in the PMI calculation [2]. Moreover, the temperature range in which the development rate is actually linear is not wide enough to cover all temperatures during a typical summer in a temperate climate zone. Furthermore, neither developmental durations nor base temperatures for development have been calculated for most species in different geographical regions. The method must therefore be applied with caution. In addition, it is highly problematic that uncertainties for temperature measurements from a crime scene cannot be taken into account in either model. It is difficult to determine the actual temperature controlling the larvae at a real crime scene. Because temperature is the variable that most influences development, it is crucial to consider it as accurately as possible. The standard procedure is to use temperatures of the nearest weather station for the desired time frame and correct them by applying a regression starting from temperatures measured at the crime scene, when taking the larvae as evidence [3]. The corrected values still contain uncertainties that cannot be accounted for by the methods currently used for PMImin determination. No information exists for either model about the quality of the method or the error intervals of the calculated PMImin. In general, the greatest problem is the lack of data on the development of certain species, and especially data from different countries, because of the geographical variation in thermal requirements for insect development [13].

Calculation of PMImin also relies on determining the progress through the development cycle. Currently, this is achieved using morphological features. Figure 12.4 (b) shows the limitations of this approach: single data points illustrate the length of sampled larvae and their corresponding age. The box highlights larvae of 17 mm long and shows that the actual age of the larvae (which is used to estimate PMImin) has a very wide distribution from approximately 100 hours old to more than 200 hours old. Therefore, there is an obvious need to develop a more sophisticated and sensitive method to model developmental progress, to improve estimation of PMImin. Early efforts to integrate developmental gene expression patterns seem promising, but they have not been tested to ensure precise and applicable results in a judicial setting [7,24,25].

Another way to calculate PMImin is to use more sophisticated mathematical models that actually base their calculations on the non-linear development of blowfly larvae. Although the general consensus is that these models are not necessarily better than the previously described methods, their use should not be dismissed immediately. In 2010, a method was developed that models blowfly development based on exponential functions describing the growth curves [18]. A computer program was written that is able to use an individual temperature profile, calculate larval development for each temperature value at any desired time step and add them up to a total development time. The foremost advantage over the established methods is the additional information about the accuracy of the calculation. In addition, it is impossible to include uncertainties about the parameter in the calculation, which will influence the calculation and cannot be neglected. However, there is still a need to improve this new model and validate its use. Results of the method are shown in the case report section (first case report of suicide).

12.5 Succession

The composition of insect species present on a corpse at any given time point can be an indicator of the time frame the corpse has already been infested. Different decomposition stages of carcass attract different insect species, which also attract a range of predators. The species infesting a corpse can be manifold, and several factors influence their behaviour. Not only does the decomposition stage have an impact, but also season, temperature, microclimate, location of the body and so on can influence the succession pattern. This makes it difficult to estimate a time frame because it is impossible to conclude that species x arrives at a corpse only after time y. However, an experienced forensic entomologist who performed various field experiments observing pig carcasses at different locations, temperatures and seasons and who sampled insects from many real cases can draw conclusions from succession data if the ambient parameters are known. It is important to understand that it is impossible to use reference data published on succession experiments from regions, countries, microclimates and so on that differ from the finding situation of the case scenario in question because these data are not representative or applicable.

12.6 Sampling of Insects from Bodies

Here are eight simple rules to collect insect evidence:

1. Use a container that can be tightly closed so that no liquid will leak out of it.
2. Use a sheet of paper and a pencil, rip off some paper, label it with date, name and case number and put the labelled piece of paper inside the container (*really* use a *pencil*—ink from pens will be washed off by alcohol).
3. Sample the insects from the body and place them in the container (not more than half full); use forceps, a spoon or hands (the evidence is not likely to become contaminated or destroyed) (Figure 12.5).
4. Optional: Pour hot, nearly boiling water in the container filled with the entomological evidence and discard the water after 1–2 minutes, keeping the evidence inside the container.
5. *Mandatory*: Fill the container with 70–80 per cent ethanol or similar alcohol.
6. Close the container.
7. Repeat using more containers if you want to sample more specimens.
8. Sample as diversely as possible (regarding different specimens and locations on the body).

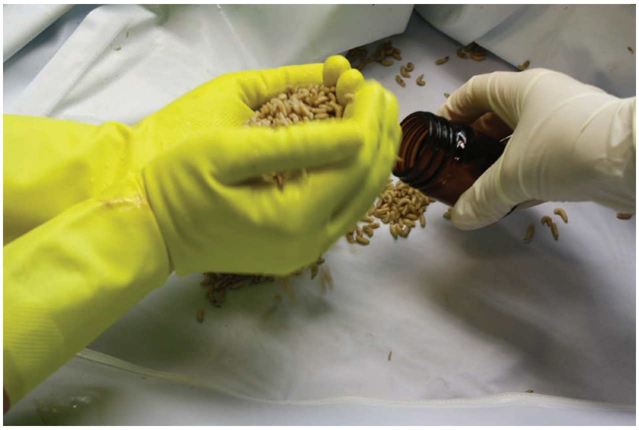

Figure 12.5 Sampling of insect larvae in a glass container by using just the hands.

12.7 Case Reports

All cases described here were examined by autopsy in the Institute of Forensic Medicine, Bonn, Germany, and the insects were sampled and analysed by the author.

12.7.1 Suicide

In July 2009, a young man was found hanging from a tree in a small forest near an urban area (Figure 12.6). The man could be identified without doubt, and his mother had reported him missing 3 days earlier, after she had found a suicide note in his bedroom. The body was transported to the Institute of Forensic Medicine nearby and was cooled at 4°C until autopsy. At time of the autopsy, it had been 147 hours since the mother last saw her son alive. During autopsy, larvae were sampled from the body and were immediately killed in nearly boiling water. After discarding the water, the larvae were stored in 80°C ethanol. Species identification revealed that the larvae were *Calliphora vicina*, a typical first-wave colonizer in Germany. The largest larvae sampled measured 12.5 mm and were in early third instar stage. The PMImin was calculated using the ADH method and also using the new computer-simulated method mentioned previously. The acquired temperature data (hourly records) from a nearby weather station were used without revising them. ADH calculation resulted in a PMImin of 139 hours, meaning

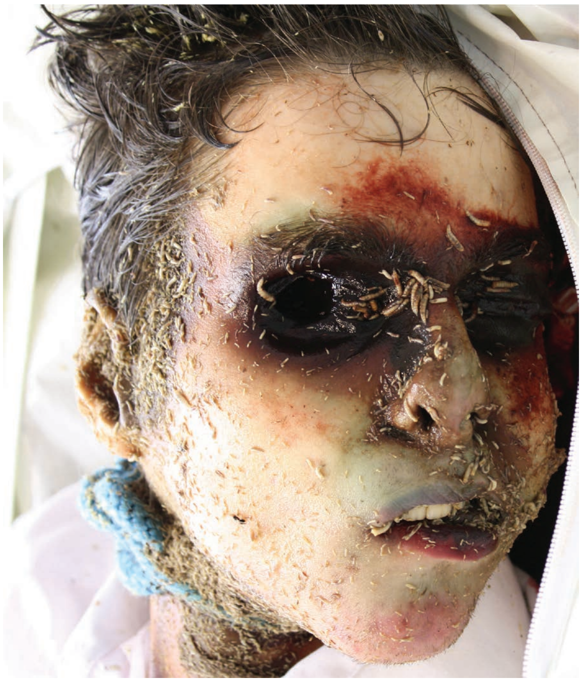

Figure 12.6 Blowfly larvae feeding in the facial region of the body; the eyes are already eaten away.

that the hanging took place in the afternoon of the day the young man went missing. The computer-simulated model resulted in a larval age of 145 hours, which shifted the time of the death to the morning, shortly after his mother had last seen her son. The standard deviation of the calculation was ±3 hours. This example shows first that the calculation based on entomological evidence can be very precise and second that a more complicated, computer-based model can be a reasonable alternative to the linear model.

12.7.2 Skeleton in Forest

At the end of July 2009, a nearly skeletonized body was found on a steep, bushy embankment under a highway bridge. The bones were partly held together by dried connective tissue. The skull was found separately, after it had rolled down the embankment and into a parking lot. The bones were nearly free of insect infestation, but below the dried scalp a few larvae of an unknown beetle species were collected, and at the connective tissue larvae of the fly species *Piophila casei* were sampled. The police wanted to clarify whether the body had most likely been lying on the embankment since earlier the same year or since the year before, to check the records of missing persons. During autopsy, it was established that the body was female and most likely of an older age.

Because the temperatures in this part of Germany did not rise to values that promote insect activity before the beginning of April 2009, it could be assumed that blowfly larvae would have fed on the body since then at the earliest, imagining a scenario where the body had been exposed in the same year. That would imply that the larvae had eaten away most of the body tissue and left the connective tissue to dry, all within 3–4 months. Moreover, the body must have been naked, and the number of maggots must have been immense. By implication, this would lead to very wet and 'marked' soil, as well as a massive amount of pupal cases at the finding site. However, after visiting the site and investigating the area and the corresponding soil, no such evidence could be found. The soil was dry and loose, and no pupal cases or tissue residuals could be detected. In Figure 12.7, a side-by-side comparison of the found skeleton (left) and the image of an 80-kg pig exposed in the open during summertime for 2 months is shown. It becomes apparent that the probability of an exposure time of the body in question is not very high for a period of about 3–4 months.

In conclusion, the entomological report stated that there is a high probability that the corpse was exposed at least during the summer of the previous year or even earlier than that.

After a few months the police could identify the body. The investigation revealed that the person had suffered from dementia and had run away, naked, from her nursing facility in summer 2008 and was reported missing. In this case report it becomes obvious that even the absence of insect involvement can be objective evidence for a forensic entomologist.

12.7.3 Dismembered Body

In September 2008, dog walkers found pieces of a dismembered body in a grove near the suburbs (Figure 12.8). The body parts were brought in plastic bags to the Institute of Forensic Medicine and inspected. Blowfly larvae were already crawling out of the bags. In the first bag was half a torso, two pieces of the lower legs und various small

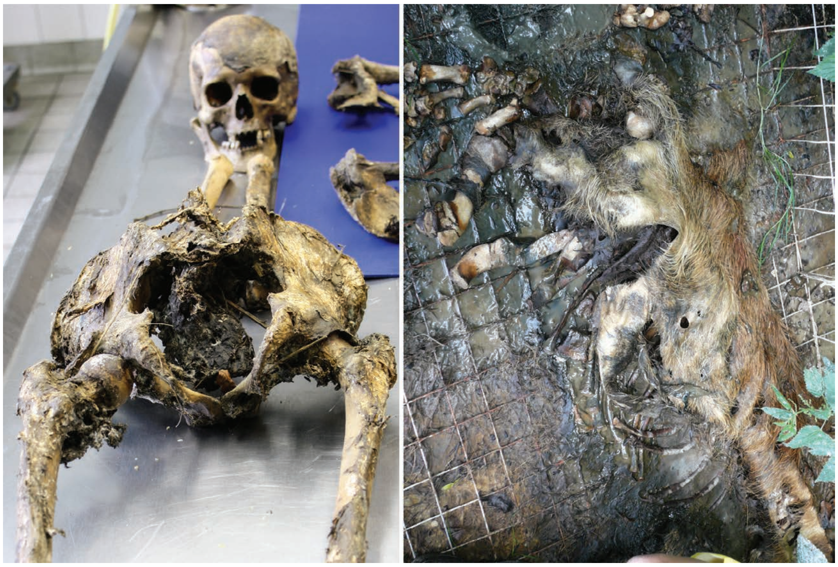

Figure 12.7 Left: Skeletonized body exposed for 10 months. Right: An 80-kg pig exposed for 2 months during summertime.

body pieces. All pieces were heavily infested with feeding blowfly larvae. One day later the police found the left arm and the head after they searched the surrounding area. At this time the identity of the corpse was unknown; it was apparent only that it was a middle-aged woman. The police ordered an estimation of the PMImin based on entomological evidence to limit the time interval for records of missing persons. For the estimation, larvae were used that were sampled on the first day the body pieces were brought to the Institute. The species was identified as *Calliphora vicina*. The finding place was investigated, and a data logger was put out to record the temperature hourly over a period of 24 hours to compare these records with the data recorded by the Institute of Metrology of the University of Bonn. The temperature values used for the PMImin estimation were adjusted accordingly. The PMImin estimation resulted in a time period of 5 days (start of the insect infestation on the Saturday morning before finding the first body parts). The estimation implied oviposition in the early hours of Saturday morning. Because blowflies usually do not oviposit at night, it could not be determined exactly whether the eggs were deposited Saturday morning or Friday very late in the evening. The entomological report stated that the sheer number of wounds and the amount of blood after the dismembering would have been very strong triggers for the blowflies to deposit their eggs. Because the location of the actual dismembering was unknown at the time, it could not be investigated whether the blowflies had started oviposition at the crime scene or after the placement of the body outside at the finding place.

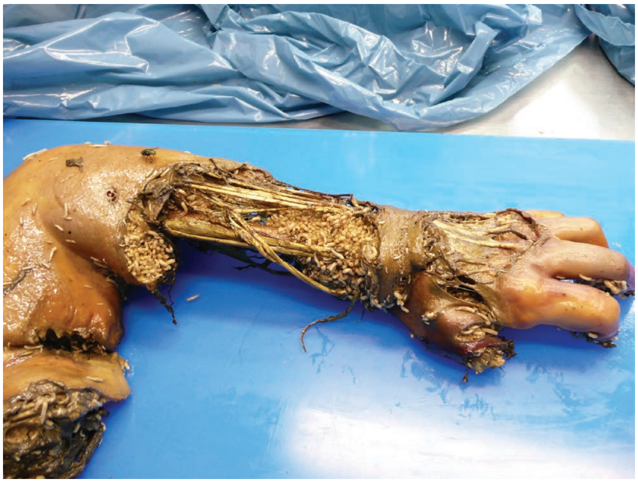

Figure 12.8 One of many body parts found in a forest after dismemberment.

Shortly afterwards the police could identify the victim and investigated her house. It became apparent that the killing and the dismembering took place in the house of the victim because a large amount of blood and more body parts were found inside and outside of the house. The partner of the victim was on the run and became a suspect immediately. Eventually, he was captured in the Netherlands and confessed to the crime. He stated that on Friday evening he and his partner started fighting and he stabbed her to death. Afterwards, to cover up his crime, he wanted to bury the body in the garden, but the pit he dug was too small, so he dismembered the body and took several body pieces outside the property, where they were finally found.

12.7.4 Winter Suicide Indoors

In January 2009, a woman was found dead in her apartment. She was found on a mattress on the floor and was dressed in thin capri pants, a T-shirt and woollen socks. Most of her body was mummified, and her face was partly skeletonized (Figure 12.9). The police investigated the case and determined that she had not been seen for 40 days.

The body was brought to the Institute for Forensic Medicine, and an autopsy was performed during which insect samples were collected. Empty pupal cases of *Lucilia sericata* sticking to the socks were sampled. A live specimen of *Necrobia rufipes* was crawling out of the clothes. Additionally, empty pupal cases and dead adult species of *Megaselia scalaris* were collected. After the abdominal cavity was opened, thousands of larvae and pupae of *M. scalaris* were revealed.

The police report stated that the temperature in the room where the body was found was 21°C. It was assumed that the temperature remained almost constant because the windows were closed and the shutters were down.

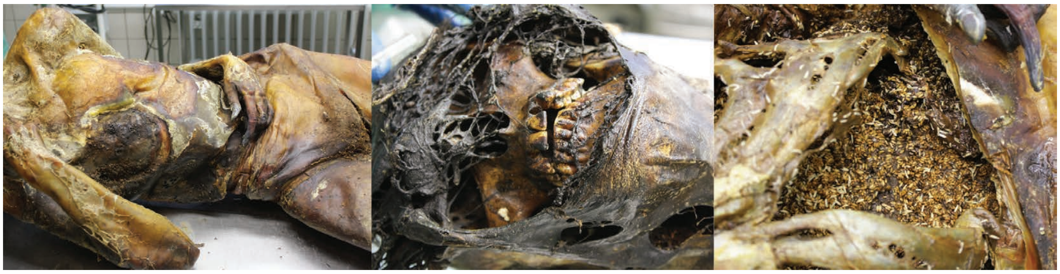

Figure 12.9 State of a body found indoors after 40 days.

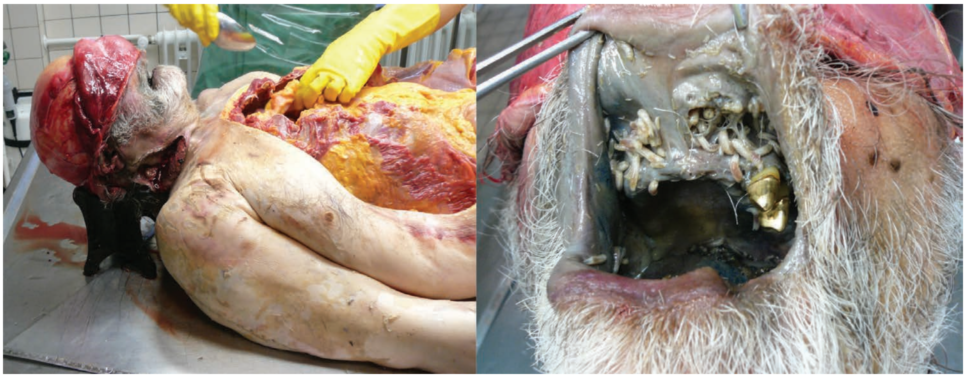

Figure 12.10 State of a body found outdoors after a missing period of about a month during wintertime.

For *L. sericata* the minimum developmental time at 21°C is 16 days [8]. It is unclear how soon the flies could enter the room and infest the body [16]. Presumably, they were active on the corpse shortly after death because the body dried out later, which is not an attractive state for blowfly larvae. *M. scalaris* completes development at a 12:12 photoperiod after about 37 days [26]. Because the period that the dead woman had been missing was about 40 days, PMImin estimation based on developmental data of *M. scalaris* was much more accurate than calculating the developmental time of *L. sericata*. It is also known that *M. scalaris* can reach corpses in closed room scenarios and even inside tightly knotted plastic bags very quickly because the specimens are very small and can usually infest a body only if they do not have to compete against the much larger blowflies [17].

12.7.5 Winter Suicide Outdoors

In December 2007, the body of a man was found on the waterfront of a lake in the outskirts of a rural area near Bonn, Germany. He had been reported missing about a month before the finding and was reported to have left a mental health institution without being dismissed. His body was clothed and partly hidden under bushes. In the autopsy report it was stated that no typical signs of decomposition were present, and livor mortis could be observed only sparsely (Figure 12.10, left). The cause of death was bleeding to death after cutting the throat. Furthermore, it was concluded to be a suicide. During the investigation of the oral cavity, several blowfly larvae of different sizes were revealed (Figure 12.10, right). During autopsy, living larvae were collected and placed on a feeding substrate to rear them at constant 25°C until adult flies would emerge. This was done for two reasons: first, it is easier to identify the species based on the adult fly; second, it would reveal the remaining developmental time until pupation and thus make a larval age calculation more reliable. The species was identified as *Calliphora vomitoria*. Ames and Turner [1] published an ADH value of 5638 from egg to pupation for this species. Analysing the daily temperature measurements of the nearest weather station and calculating a daily mean temperature accounted for the temperatures that influenced larval development during the time the body lay at the lake. For this calculation it was essential to take into consideration that on several days the daily mean temperature fell under the lower developmental threshold. Calculating the ADHs using the mean ambient temperature and excluding days with temperatures below the developmental threshold revealed as a starting point of larval development a time frame of 1 or 2 days after the man went missing. Usually, insects of central Europe are not overly active in November and December because the temperatures are very low. However, on the days the man went missing, it was unusually warm, which may have provoked certain insect activity. The results of the autopsy concluded a much shorter PMI that could have led to the question what happened between the days the man went missing and death occurred. However, the results of the entomological analysis supported the much more likely scenario that he had left the mental institution and killed himself shortly afterwards.

References

1. Ames C, Turner B. Low temperature episodes in development of blowflies: implications for postmortem interval estimation. *Med Vet Entomol* 2003;17:178–86.
2. Anderson GS. Minimum and maximum development rates of some forensically important Calliphoridae (Diptera). *J Forensic Sci* 2000;45:824–32.
3. Archer MS. Rainfall and temperature effects on the decomposition rate of exposed neonatal remains. *Sci Justice* 2004;44:35–41.
4. Benecke M. Random amplified polymorphic DNA (RAPD) typing of necrophageous insects (Diptera, Coleoptera) in criminal forensic studies: validation and use in practice. *Forensic Sci Int* 1998;98:157–68.

5. Benecke M. Six forensic entomology cases: description and commentary. *J Forensic Sci* 1998;43:797–805, 1303.
6. Benecke M, Josephi E, Zweihoff R. Neglect of the elderly: forensic entomology cases and considerations. *Forensic Sci Int* 2004;146(Suppl):S195–9.
7. Boehme P, Spahn P, Amendt J, Zehner R. Differential gene expression during metamorphosis: a promising approach for age estimation of forensically important *Calliphora vicina pupae* (Diptera: Calliphoridae). *Int J Legal Med* 2013;127:243–9.
8. Grassberger M, Reiter C. Effect of temperature on *Lucilia sericata* (Diptera: Calliphoridae) development with special reference to the isomegalen- and isomorphen-diagram. *Forensic Sci Int* 2001;120:32–6.
9. Harvey ML, Gaudieri S, Villet MH, Dadour IR. A global study of forensically significant calliphorids: implications for identification. *Forensic Sci Int* 2008;177:66–76.
10. Harvey ML, Mansell MW, Villet MH, Dadour IR. Molecular identification of some forensically important blowflies of southern Africa and Australia. *Med Vet Entomol* 2003;17:363–9.
11. Henssge C, Madea B. Estimation of the time since death in the early post-mortem period. *Forensic Sci Int* 2004;144:167–75.
12. Higley LG, Haskell NH. *Insect Development and Forensic Entomology in Forensic Entomology: The Utility of Arthropods in Legal Investigations*. Boca Raton, FL, CRC Press, 2009, pp 389–405.
13. Honek A. Geographical variation in thermal requirements for insect development. *Eur J Entomol* 1996;93:303–12.
14. Janisch E. Die Leben- und Entwicklungsdauer der Insekten als Temperaturfunktion. *Z Wissenschaft Zool* 1928;132:176–86.
15. Keh B. Scope and applications of forensic entomology. *Annu Rev Entomol* 1985;30:137–54.
16. Reibe S, Madea B. How promptly do blowflies colonise fresh carcasses? A study comparing indoor with outdoor locations. *Forensic Sci Int* 2010;195:52–7.
17. Reibe S, Madea B. Use of *Megaselia scalaris* (Diptera: Phoridae) for post-mortem interval estimation indoors. *Parasitol Res* 2010;*106*:637–40.
18. Reibe S, Doetinchem PV, Madea B. A new simulation-based model for calculating post-mortem intervals using developmental data for *Lucilia sericata* (Dipt.: Calliphoridae). *Parasitol Res* 2010;107:9–16.
19. Sharpe P, Hu L. Reaction kinetics of nutrition dependent poikilotherm development. *J Theor Biol* 1980;82:317–33.
20. Sharpe P, DeMichele D. Reaction kinetics of poikilotherm development. *J Theor Biol* 1977;64:649–70.
21. Slone D, Gruner S. Thermoregulation in larval aggregations of carrion-feeding blow flies (Diptera: Calliphoridae). *J Med Entomol* 2007;44(3):516–23.
22. Sperling FA, Anderson GS, Hickey DA. Partial sequencing of the cytochrome oxydase b subunit gene I: a tool for the identification of European species of blow flies for postmortem interval estimation. *J Forensic Sci* 1994;39:418–27.
23. Stevens J, Wall R. Species, sub-species and hybrid populations of the blowflies *Lucilia cuprina* and *Lucilia sericata* (Diptera: Calliphoridae). *Proc Biol Sci* 1996;263:1335–41.
24. Tarone AM, Foran DR. Gene expression during blow fly development: improving the precision of age estimates in forensic entomology. *J Forensic Sci* 2011;56(Suppl 1):S112–22.
25. Tarone AM, Jennings KC, Foran DR. Aging blow fly eggs using gene expression: a feasibility study. *J Forensic Sci* 2007;52:1350–4.
26. Trumble J, Pienkowski R. Development and survival of *Megaselia scalaris* (Diptera: Phoridae) at selected temperatures and photoperiods. *Proc Entomol Soc Wash* 1979;81(2):207–10.
27. Wallman J, Adams M. Molecular systematics of Australian carrion-breeding blowflies of the genus *Calliphora* (Diptera: Calliphoridae). *Austr J Zool* 1997;45:337–56.
28. Wallman JF, Leys R, Hagendoorn K. Molecular systematics of Australian carrion-breeding blowflies (Diptera: Calliphoridae) based on mitochondrial DNA. *Invertebr Syst* 2005;19:1–15.
29. Wells JD, Lamotte LR. *Estimating the Postmortem Interval in Forensic Entomology: The Utility of Arthropods in Legal Investigations*. Boca Raton, FL, CRC Press, 2009, pp 367–88.
30. Wells JD, Wall R, Stevens JR. Phylogenetic analysis of forensically important *Lucilia* flies based on cytochrome oxidase I sequence: a cautionary tale for forensic species determination. *Int J Legal Med Sci Law* 2007;121:229–33.

Taylor & Francis
Taylor & Francis Group
http://taylorandfrancis.com

13 Radiocarbon Dating
Basic Principles and Applications

Wilfried Rosendahl and Doris Döppes

Contents

13.1 Basic Principles 345
13.2 Calibration 347
13.3 Sample Material and Sample Pre-treatment 348
13.4 Radiocarbon Dating in Forensics: Closing Remarks 348
13.5 Case Studies from the Ice Age to the Present 348
  13.5.1 Old or Too Old? On the Dating of Cave Bears from Baumann's Cave in the Harz 348
  13.5.2 Easy to Date but Not a Baby: An Egyptian Mummy from Basel 349
  13.5.3 Mother and Children? An Unusual South American Mummy Group from Mannheim 350
  13.5.4 Three Dates but Still No Age: An Asian Mummy from Mannheim 351
  13.5.5 The Bog Dog from Burlage: Changing Dating of a Significant Bog Body 351
  13.5.6 Ötzi's Pet? The Find of a Frozen, Mummified Hare from the Alps 352

Scientific analysis of human remains, be they skeletal remains or mummified bodies or body parts, has major substantive importance for various disciplines, including not only archaeology but also anthropology, palaeontology and forensic medicine. In addition to specific data on such finds (e.g. gender, size and age at death), post-mortem interval (PMI) and geological age are also primary objects of enquiry. Whereas specific data can frequently be collected from morphological features on different bone elements (everything depending on the completeness and state of preservation), pure bone analysis cannot determine PMIs reliably. Whenever they are extant and typical for a specific period, accompanying finds such as grave goods, clothing remains or everyday objects facilitate relative dating. Depending on the age and preservation of a find, as well as the type and quality of accompanying finds, relative dates contain uncertainties of differing magnitude or imprecise time frames. This unsatisfactory situation for many of the aforementioned disciplines' scientific enquiries did not change fundamentally until the development of radiometric and chemical or physical dating methods based on natural decay chains. The method best suited for numerical or absolute dating of human skeletal remains and mummies from 50 000 years ago to the present is so-called radiocarbon or carbon-14 (^{14}C) dating. This technique was developed and applied by Willard Frank Libby from the University of Chicago at the end of the 1940s [1,14]. Libby was awarded the Nobel Prize in chemistry in 1960 for his work. The method has seen numerous improvements in measuring systems over the years. The development of the accelerator mass spectrometer (AMS) at the University of Oxford in 1977 was a particularly important advance. This equipment made it possible not only to minimize the quantity of samples required significantly but also to increase measurement speed and accuracy considerably (see Figure 13.1). Work is still being done at present to improve these parameters.

13.1 Basic Principles

The element carbon (C) is one of the biosphere's most important chemical constituents. Organic carbon compounds are the basis for all life. Three carbon isotopes occur naturally, the stable isotopes ^{12}C (98.89 per cent) and ^{13}C (1.11 per cent) and the unstable or radioactive isotope ^{14}C (10^{-10} per cent). Radiocarbon (^{14}C) is continually produced in the upper layers of the atmosphere by the interaction of neutrons from cosmic rays with nitrogen (N) atoms. During the nuclear reaction $^{14}N(n,p)^{14}C$, ^{14}N captures one neutron and releases one proton in return, thus transforming ^{14}N into radiocarbon (Figure 13.2). The average global rate of ^{14}C production is approximately 6–13.5 kg/year. Beta (β^-) decay causes unstable ^{14}C with a half-life of 5730 ± 40 years to decay into ^{14}N, one electron and one antineutrino. Chemically, ^{14}C acts like the other carbon isotopes and bonds with oxygen to form carbon dioxide. ^{14}C enters the biosphere through plant photosynthesis and, subsequently, the animal food chain. This is

DOI: 10.1201/9781003244974-13

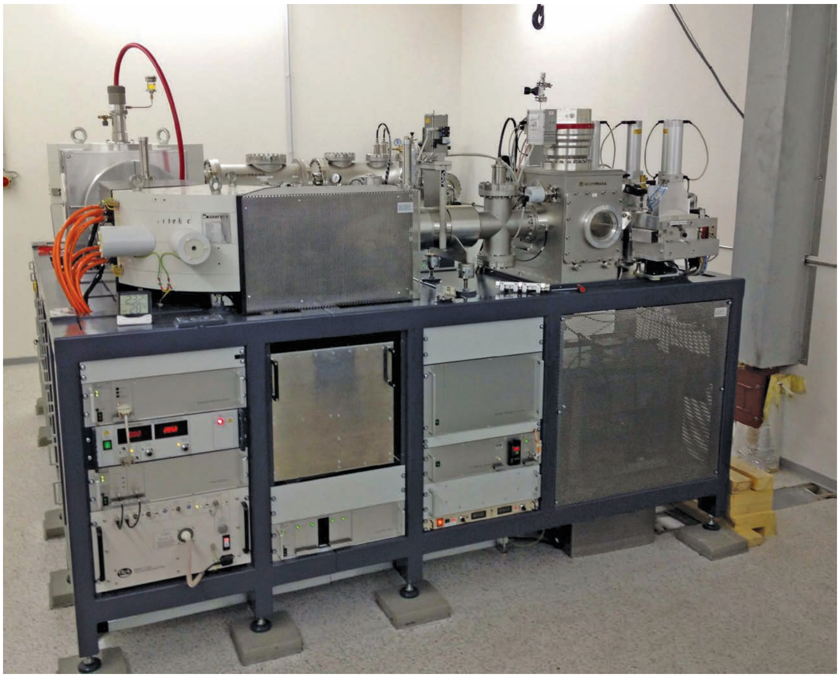

Figure 13.1 One of the most modern pieces of equipment for carbon-14 dating, the accelerator mass spectrometer of the MICADAS type at the Klaus-Tschira-Laboratory for Radiometric Dating Methods in the Curt-Engelhorn-Centre Archaeometry in Mannheim, Germany.

(Photograph courtesy of W. Rosendahl, Mannheim, Germany.)

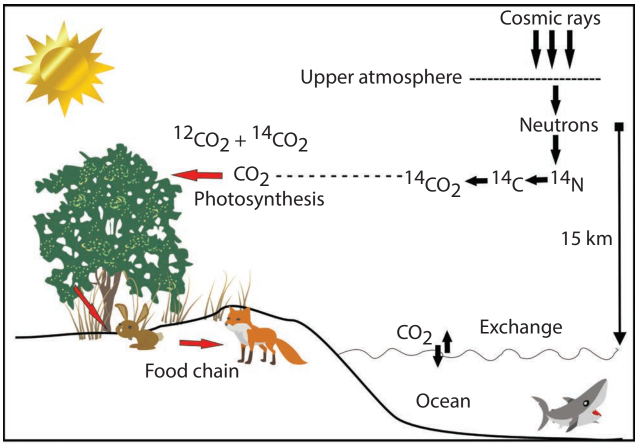

Figure 13.2 Radiocarbon cycle in the atmosphere and biosphere.

(Graphic by W. Rosendahl, Mannheim, Germany.)

also called the carbon cycle. The ^{14}C fraction in carbon remains in equilibrium as long as a living organism is an active part of this cycle. This changes when an organism dies. No more new ^{14}C is introduced, and the initial quantity starts decaying radioactively. Its physical half-life is 5730 ± 40 years (i.e. only half of the initial ^{14}C content exists after this period and, in turn, only half of that after another 5730 ± 40 years). The maximum age limit currently determinable by AMS is approximately 50,000 years.

According to Libby's model, the ^{14}C age can be calculated with the following equation:

$$t = 8033 \cdot \mathrm{In}\left({}^{14}C_0 / {}^{14}C\right)$$

where *t* is age, In is natural logarithm and $^{14}C_0$ is ^{14}C modern standard.

In 1958, De Vries demonstrated that the $^{14}C/^{12}C$ ratio fluctuates naturally over time. Thus, the model assumption of a spatiotemporally constant initial value of ^{14}C is not met [7]. This means that calculated ^{14}C ages are far younger than the corresponding solar or calendar years. They can deviate by significantly more than 1000 years in certain eras. There are three main causes of natural fluctuations of the atmospheric $^{14}C/^{12}C$ ratio. Whereas changes in Earth's magnetic field are chiefly responsible for long-term changes [17], short-term fluctuations are governed by solar activity (the so-called De Vries effect). The exchange of carbon from various geosphere and biosphere reservoirs with the atmosphere can also cause fluctuations.

Because ^{14}C mixes in the atmosphere very rapidly, ^{14}C fluctuations become noticeable at the same time all over the world, thus eliminating the problem of varying local concentrations.

In addition to natural fluctuations, there are also anthropogenically caused changes. Named after Hans E. Suess, the 'Suess-effect' describes the impact of industrialization and the use of fossil fuels on the ^{14}C content in the atmosphere since the mid-nineteenth century [23]. Given that fossil fuels no longer contain any detectable ^{14}C because of their old age, only ^{12}C and ^{13}C are released when they are burned. This dilution causes an artificial reduction of the ^{14}C content in the atmosphere (2–3 pMC [per cent modern carbon]). This can give the appearance of an unduly old age and therefore must be factored in when determining age.

The 'atom bomb effect' describes another important anthropogenic influence, namely, and as the name

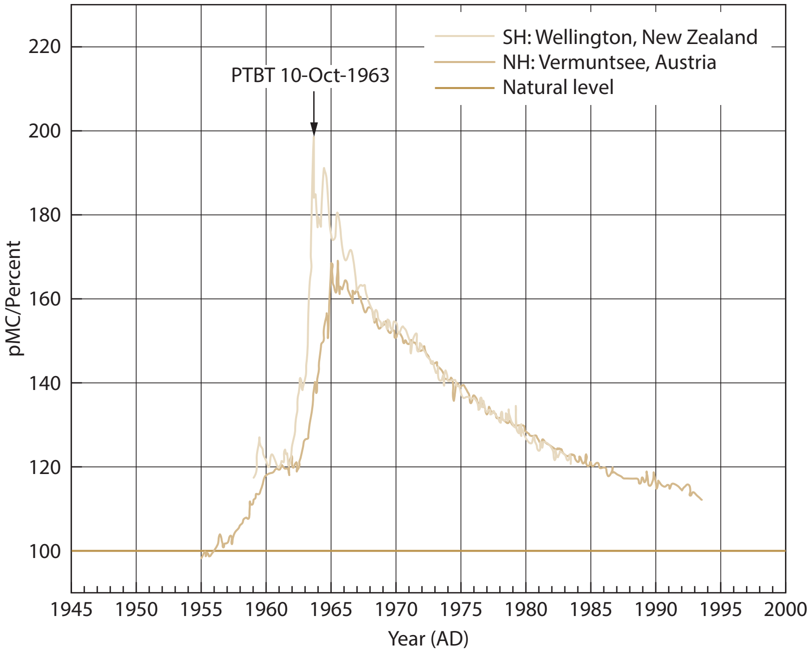

Figure 13.3 Bomb peak calibration curve. The New Zealand curve (red) is representative of the Southern Hemisphere; the Austrian curve (green) is representative of the Northern Hemisphere (data set from the Carbon Dioxide Information Analysis Center, Oak Ridge National Laboratory, Oak Ridge, Tennessee). The date of the Partial Test Ban Treaty (PTBT) is marked on the graph.

(Graphic public domain, Wikipedia.) pMC, percent of modern carbon.

implies, the impact on or substantial increase of atmospheric ^{14}C content from above-ground nuclear tests between 1950 and 1963. The ^{14}C content is still elevated 20 per cent today [26]. Because the values of the changes in the artificial ^{14}C content are known to the exact year, even samples after 1950 or the recent past can be radiocarbon dated very well using so-called bomb peak dating (Figure 13.3). The ^{14}C content of hair, skin or tendons can be used to determine time of death accurately to approximately 2 years [11]. The values obtained are compared with those of the bomb curve. Hair is better suited because, unlike bone, it grows continuously, and thus its ^{14}C content corresponds well with the biosphere at the time of death and allows relatively precise dating. This is especially important for the application of radiocarbon dating in forensic sciences.

Under certain conditions, spatial changes of the ^{14}C ratio can also occur, which must be allowed for and corrected when taking a measurement. Isotopic fractionation deserves mention. In other words, the three carbon isotopes with different masses can move differently or be released slightly during processes in the carbon cycle (e.g. during photosynthesis in different plant groups). Furthermore, there is the reservoir effect. This effect can be observed, for instance, in milieus where the ^{14}C had a higher average half-life (e.g. in deep ocean water) [2]. Allowance must also be made for possible contamination of samples by substances with a different ^{14}C age. For instance, many Pleistocene bone finds were still prepared with bone glue at the beginning of the twentieth century. Various purification processes (e.g. Soxhlet extraction) during sample pre-treatment can help minimize contamination problems.

13.2 Calibration

In keeping with international consensus, the readings obtained by radiocarbon dating are denoted as the conventional ^{14}C or AMS ^{14}C age, with 1950 as the zero reference point. The measured date is specified as a numerical value with a standard deviation (± value) and followed by the symbol BP. BP stands for 'before present', meaning the reference year 1950. Thus, a ^{14}C AMS age of 2250 BP indicates that a sample has an age of 2250 ^{14}C years before 1950. Because these ^{14}C dates are known to be systematically 3 per cent too low and the temporally variable dates are also not factored into the initial ^{14}C ratio, the dates have to be calibrated or corrected and converted into calendar years. Dendrochronology (i.e. dating using certain tree species' growth rings) and varve chronology (i.e. dating using seasonally laminated marine sediment) are primarily employed for this purpose [9]. Uranium-thorium-dated speleothems from China and the Bahamas, dated coral reefs, oxygen isotope analysis of benthic Foraminifera, tephra from known volcanic eruptions and laminated Greenland ice cores have also been referenced since 2009 [18]. In principle, dates can now be calibrated to the dating limit of 50,000 years. Calibrated raw dates are indicated by calBP. Free programmes that ascertain calendric dates are available or can be requested from various AMS laboratories online (e.g. www.calpal-online.de).

Calibrated ages are usually indicated by 1 sigma, corresponding to a confidence probability of 68.3 per cent. It rises to 95.5 per cent for 2 sigma. In such a case, measurements were taken over a longer period because enough material was available from the same sample, thus reducing the statistical error.

13.3 Sample Material and Sample Pre-treatment

Radiocarbon dating is used in many disciplines because it is suitable for a wide variety of materials: all organic materials, such as wood, charcoal, plant remains, peat, bone, teeth, ivory, antler, hair, leather and textiles, as well as inorganic materials, such as shells, corals, Foraminifera, calcareous sinter, inorganic carbon and carbon dioxide, dissolved in groundwater extracted from continental and glacier ice [10].

Because contamination can occur during soil sedimentation, datable carbonaceous samples are freed from coarse impurities, and foreign carbon that can distort age is removed. Acid and alkali pre-treatment separates carbonates from humins. Organic conservation substances can also distort age and are removed by the aforementioned Soxhlet extraction and ultrafiltration. Collagen, a water-insoluble structural protein, is extracted from bone. Bone was long considered to be unsuitable for ^{14}C dating because it is very porous and thus prone to exchange reactions with the groundwater. Collagen is hardly prone to exchanges. In the final step, organic samples are converted into carbon dioxide and subsequently converted into a solid graphite form.

Samples more in the milligram range are needed for measurement in an AMS. The atoms themselves are counted, not decay events as in Geiger or liquid scintillation counting. Thus, very small samples can be analysed. The graphite sample obtained is bombarded with caesium ions to obtain carbon ions. The ions of the ^{14}C isotope are separated in the accelerator according to their different masses. Age can be determined from the ratio of ^{14}C to ^{12}C. ^{13}C serves as the control for the separation processes. The values for the initial quantities, factoring in losses during sample pre-treatment, are summarized in Table 13.1.

Table 13.1 Approximate Amounts of Sample Used for the Accelerator Mass Spectrometer Technique

Material	Amount (mg)
Wood	100
Charcoal	100
Hair	20–50
Peat	50–100
Leather/skin	50–100
Textile	20–50
Plant remains	>10
Pollen	200
Bone	200–2000
Carbonate	>10

13.4 Radiocarbon Dating in Forensics: Closing Remarks

As explained earlier, radiocarbon dating basically provides a means for so-called bomb peak dating to determine the PMI after 1950 [6,16,24,25,27]. Depending on the type of sample, however, the value of the dates is highly dependent on various parameters. Allowance must be made for uncertainties, especially when the PMIs are short. Methodologically, problems are caused by humans' individual metabolisms and the resultant different rapid assimilation and exchange of ^{14}C in various parts of the body such as hair, skin, internal organs or bones. Hair, blood and nails are best suited for radiocarbon dating because their faster and continuous metabolism causes them to assimilate and exchange ^{14}C faster, too. By comparison, bones and collagen metabolize so much more slowly that ^{14}C is exchanged only every 10–30 years on average [5]. This means that the ^{14}C age of bone collagen dates the last assimilation or exchange of ^{14}C rather than the age at death. This results in an unduly old age. The shorter the PMI is, the more problematic the meaningfulness of the date becomes. It is therefore advisable in such cases to perform supporting analyses and tests in addition to radiocarbon dating. In relation to the result of the dating, the potential findings can narrow down a PMI. Depending on the condition and completeness of a skeletal find, anthropological analyses as well as morphological and microscopic bone analyses could be used to determine individual age and gender [13].

13.5 Case Studies from the Ice Age to the Present

Six examples of the use of radiocarbon dating related to the basic subject of the book based on the author's current research projects are presented here. The case studies have been selected to cover different periods, from the Late Pleistocene through the recent past, and to treat different issues and methodological approaches.

13.5.1 Old or Too Old? On the Dating of Cave Bears from Baumann's Cave in the Harz

The bone remains from Baumann's Cave in Bode Valley (Harz, Germany) have been well known since the sixteenth century. More was written about this cave than any other in the early days of natural science research. Parts of the 1950-metre-long cave are open to visitors.

Figure 13.4 Cave bear skeleton in Baumann's Cave (Harz, Germany).

(Photograph by W. Rosendahl, Mannheim, Germany.)

Chiefly cave bears (approximately 95 per cent) were found in Baumann's Cave. Such caves are called bear caves because associated fauna is usually represented minimally. The range of fossilized fauna (e.g. steppe bison, muskoxen, reindeer, cave lions, leopards, cave hyenas, arctic foxes, wolverines, wild horses, woolly rhinoceroses, mountain hares and diverse small mammals) known from the cave confirms that the finds generally date to the last major Ice Age (Würm glaciation).

Various bones, also from cave bears, were sampled for ^{14}C dating to ascertain whether the fauna dated from an older (older than 50 000 years) or younger phase of the last Ice Age. Pre-treatment revealed that the bones still contained enough collagen for dating that is basically methodologically reliable. The oldest sample was dated to 43 016 ± 814 years BP or 46 702 ± 1.681 years calBP, thus revealing that the finds date from the last half of the last Ice Age and can still be dated very well by radiocarbon analysis despite their old age [12]. This example demonstrates that allowance has to be made for relatively high standard deviations in older dates near the dating limit and that pure ^{14}C dates and calibrated ages differ significantly. This absolutely must be factored into any interpretation of the find context based on age values (Figure 13.4).

13.5.2 Easy to Date but Not a Baby: An Egyptian Mummy from Basel

Mummy III 8226 is a completely wrapped Egyptian mummy of a child in the Natural History Museum in Basel, Switzerland. More precise information on its provenance and entry in the collection is not available. The mummy presumably became part of the collections of the Museum of Ethnology in Basel in the nineteenth century.

The mummy's physical appearance—it has a length of 54 cm—initially suggests that it must be a baby. Not until computed tomography (CT) scans were taken did it become apparent that the bandages wrap the skeletal remains of a 3- to 4-year-old toddler rather than a baby [21]. The gender cannot be determined. The skeleton is disordered and has been shoved together. All the bones of the lower extremities—the feet are missing—have been moved to the upper body so that the upper ends of the femurs are at shoulder level.

The arrangements inside the mummy shrouds as described for the toddler are not untypical of the Greco-Roman era (end of the Ptolemaic Dynasty or Roman era). Importance was attached to the outer shroud in particular. Because no traces of embalming substances were found, the body was very likely subjected to decomposition until skeletonizing before it was shrouded. Afterwards, the skeletal remains were laid together in a more or less orderly fashion and wrapped carefully. This could also explain the absence of various skeletal elements. Traces of partly well-preserved painting are visible on the outer surfaces of the bandages. The motifs are closely related to the pantheon of ancient Egyptian gods and their symbolism. Identification with the death deity Osiris is particularly evident.

An unpainted piece of the bandage was radiocarbon dated to verify the relative dating possible from the find context. When dating Egyptian mummies, it is essential that potential samples are free of embalming substances (resin or bitumen). This includes both body and bandages samples. Mummy III 8226 was dated to 1968 ± 21 years before the present (18 ± 21 BC), thereby providing

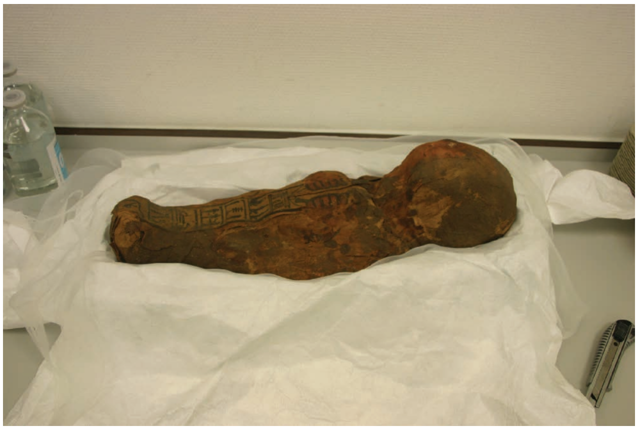

Figure 13.5 Mummy of the child III 8226 from the Natural History Museum in Basel, Switzerland. Well-preserved traces of painting and an inscription referencing the death deity Osiris are clearly visible on the surface of the bandages.

(Photograph by W. Rosendahl, Mannheim, Germany.)

excellent confirmation and narrowing the relative date to the Greco-Roman era (Figure 13.5).

13.5.3 Mother and Children? An Unusual South American Mummy Group from Mannheim

In many respects, the most important and most interesting mummified object in the Reiss-Engelhorn-Museen in Mannheim, Germany, is the group of M1 with M1a and M1b consisting of three mummies, a woman (M1) with two children. The child M1a is lying atop the stomach of the woman, who is lying on her side. Child M1b is lying beneath the woman's head. An old object label in the vitrine records the provenance as 'Toltec Indian with two children, Mexico, from an old tumulus near Oaxaca, 1895'. Mexican provenance is highly unlikely because this type of preservation is expected only in the Andean coastal region of South America. Woollen cloth is also not expected from Mexico because the country has none of the domesticated animals from which wool is obtained. The skin's post-mortem discolouration and the woman's position tend to evidence of provenance from Quiani in northern Chile.

Small bone samples were taken for ^{14}C dating and genetic analyses to clarify age and a possible genetic relationship among the three mummies.

Both the physical features of the body and the results of the CT scans revealed that mummy M1 is a woman. The woman has a height of approximately 156 cm. Her individual age is between 30 and 35 years. She was probably still nursing up until her death [20]. An abnormality of her hip joint on both sides was an unusual pathological finding. It may be avascular necrosis, a disease characterized by death of part of the femur head caused by an interrupted blood supply. Because the woman is mummified exceptionally well, remains of the brain, spinal cord and contents of the large intestine have been preserved. Another abnormality is a separation of the symphysis pubis in the pelvic region, which is visible in the CT scan. This is a crack in the symphysis pubis, which probably occurred during childbirth.

The mummy of the child M1b displays the same blackish patina as the mummy M1 and is lying with its upper body beneath the mummified woman's head. Its head, first and second cervical vertebrae, hands and feet are missing. Whereas gender and height cannot be determined, the individual age can be specified as 2–3 years old.

As mentioned, the mummified child M1a is lying on the stomach of the mummified woman. Unlike the mummies M1 and M1b, mummy M1a does not have a blackish patina. This child can therefore be assumed to have been added to the group later. Except for the missing feet and skin blemishes in the face, this mummy is also very well preserved. Large portions of the body except for the head are wrapped in a light brown woven fabric. Some cords made of plant fibres encircle the fabric. Three-dimensional animation during the CT scans revealed that the circle of cords is a regularly knotted carry net with a wide mesh. The child's gender and height could not be determined. It was 1–2 years old, based on the dental status, and approximately 18 months old, based on the length of the femur. Some pathological changes were detected. There is a bone tumour on the right upper jaw. The tumour may have been caused by fibrous dysplasia, chronic abnormal growth of new bone mass. It is the most frequent bone defect to appear in childhood and youth. Fibrous dysplasia manifests not only in frequent bone fractures but also in hormone imbalance (e.g. excess growth hormones). The cause of this disease is a non-heritable genetic defect. A discernible shift of the child's teeth may be connected with the disease. The exceptionally good mummification of the child is also evident in the preservation of remains of soft tissue in the lower abdomen and in the eye sockets and remains of the brain in the skull.

Molecular genetic tests confirmed that the three mummies came from South America but did not deliver any findings about a possible mother–child relationship in the mummy group.

This question can be answered by the findings of the ^{14}C dating, however. The mummified woman M1 dates to 1095 ± 50 years AD, a significant deviation from the date of 1347 ± 30 years AD of the mummified child M1a. This confirms the suspicion raised by the different skin colouration of the mummies that this mummified child was added to the mummy group later, most likely to make it more interesting for a buyer and to obtain a better price. The mummified child M1b's age of 1206 ± 36 years AD constitutes a difference that argues against a mother–child

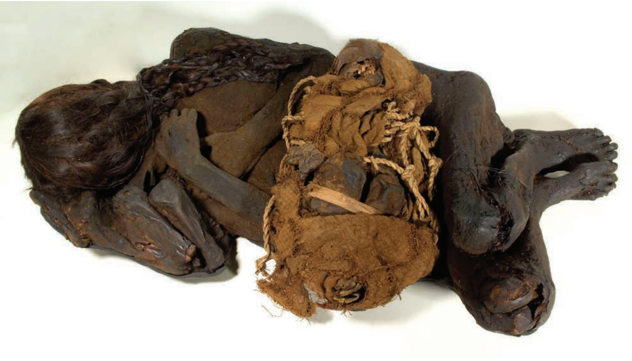

Figure 13.6 View of the South American mummy group 'Woman With Two Children' from the Reiss-Engelhorn-Museen in Mannheim, Germany. One mummified child (M1a) is lying on the woman's stomach and the other (M1b) is beneath her head.

(Photograph courtesy of J. Christen, Mannheim, Germany.)

relationship between mummies M1 and M1b. Concomitant analyses of diet revealed that mummy M1 primarily lived on a diet of fish and seafood [4]. Because ^{14}C travels more slowly in the marine cycle than in the terrestrial cycle, it is not impossible that mummy M1 was dated somewhat too old or that the date must be corrected towards the more recent date. For this reason, a mother–child relationship between these two mummies is definitely possible (Figure 13.6).

13.5.4 Three Dates but Still No Age: An Asian Mummy From Mannheim

Mummy M6 is a complete, light-skinned full-body mummy in an extended supine position. Impressions of a once-extant textile cushion are discernible in sections of the upper body. The collection's archive did not contain any other documents or information on this mummy's cultural geographical origins or proposed dating.

Bone and tissue samples were each taken from mummy M6 for genetic tests and ^{14}C dating to learn something about its possible geographical origins and dating. The mummy was subjected to a CT scan as the basis for a physical anthropological analysis [19].

The evaluation of the CT data revealed that it is a 15- to 17-year-old male adolescent with a height of approximately 153 cm (Figure 13.7).

Apart from a skull fracture in the right forehead, which probably occurred post-mortem, the teeth in particular are pathologically striking. Several teeth in both the upper jaw and lower jaw are significantly misaligned. The incisors in the upper jaw display the shovel shape typical of Asian or Indian peoples. The wisdom teeth have not broken through yet.

The ethmoidal sinuses in the nasal cavity have survived, but the cranial cavity is completely empty and does not contain any remains of the brain. The sacroiliac joint located in the pelvic ring is dislocated on both sides. Because it transmits the entire load of the torso to the legs, the sacroiliac joint is crucially important for the mechanics of the body and overall posture. The cause of this joint defect is unknown.

Genetic tests ascertained that the mummy can, in principle, be both American and East Asian in origin [22]. This mummy's individual sequence profile rules out a Pacific origin. A specific genetic mutation, conversely, indicates a northeast Asian origin.

Unfortunately, ^{14}C dating was unable to date the mummy plausibly. The dates ascertained in three different samples (bone and tissue) are scattered over a time frame from the Late Pleistocene until early 1950. The textile impressions discernible on the mummy are not the only evidence against a Late Pleistocene age. Because we know that the mummy entered the museum with Gabriel von Max's collection in 1917, it can in no way correspond to the most recent date ascertained. Still unidentified contamination makes correct dating impossible at present.

13.5.5 The Bog Dog from Burlage: Changing Dating of a Significant Bog Body

A peat cutter chanced on an incompletely preserved mummified dog in black peat approximately 70 cm beneath the terrace of Kloster Bog in Burlage (Cloppenburg District, Lower Saxony, Germany) in 1953 [15]. Its fur is well preserved, but all lower parts of the extremities as well as sections of its head are missing because of improper recovery. The find is a typical bog body (i.e. mummified by the bog water's special properties of chemical preservation).

Just under 70 cm in length, the so-called Bog Dog from Burlage has a shoulder height of no more than 40 cm. Although the skull resembles that of a present-day German Spitz, it is significantly more elongated. The dog's build most closely resembles that of a Hovawart, the typical 'farmer's dog' since the Middle Ages. The Bog Dog's coat deviates from that of this race considerably, however. Rather than fine, long and smooth, it is only 5–7 cm long and bristly. A genetic analysis is scheduled soon to identify the dog's breed (Figure 13.8).

The archaeological layer was palynologically dated shortly after the discovery of the mummified dog. It was dated to approximately 3200 years [15]. This would make it a bog body from the late Bronze Age.

As part of new testing of the Bog Dog in the German Mummy Project, a bone sample was radiocarbon dated at the Reiss-Engelhorn-Museen in Mannheim to verify this

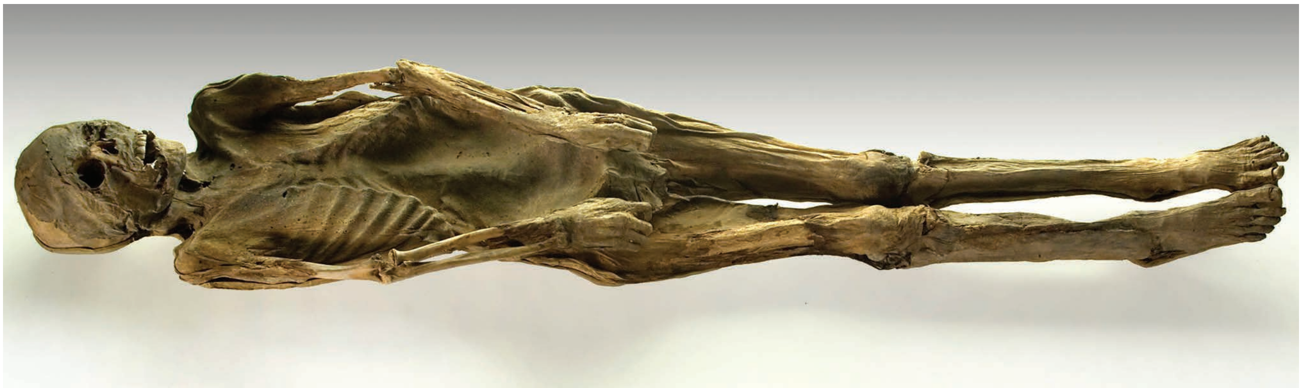

Figure 13.7 Mummy (M6) with geographical origins in northeast Asia from the collections of the Reiss-Engelhorn-Museen in Mannheim, Germany.

(Photograph by W. Rosendahl, Mannheim, Germany.)

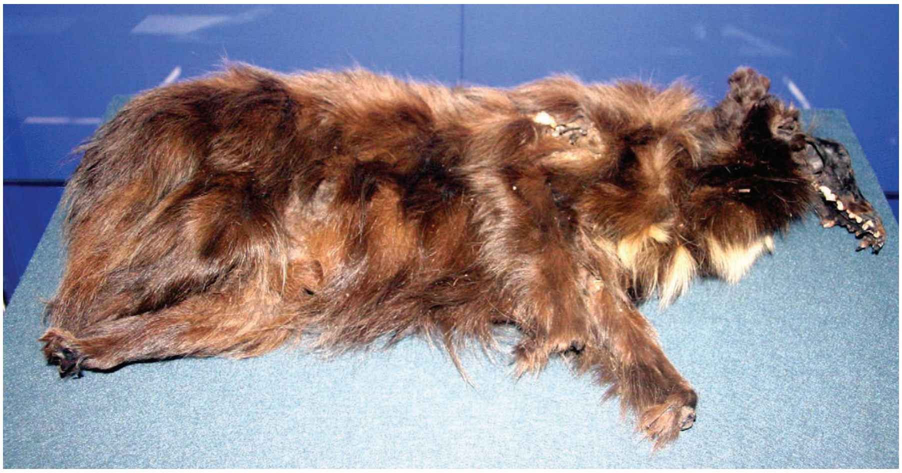

Figure 13.8 Bog Dog from black peat from Kloster Bog near Burlage in the Cloppenburg District (Lower Saxony, Germany), in the collections of the Geomuseum at the University of Münster, Germany.

(Photograph by W. Rosendahl, Mannheim, Germany.)

dating. The surprising result was that the mummified dog's age of 1544 ± 67 years AD dates it to the modern era [3]. The discrepancy between the two dates now available can be explained easily. The palynological analysis dated the archaeological layer correctly, but the dating of the mummy find proceeded from the false assumption that it had been embedded at the same time the archaeological layer formed. The new and first-time direct dating of the bog body itself revealed that the find was not embedded in older strata until much later. This example excellently demonstrates the importance of dating the find itself and not only the archaeological layer or accompanying finds.

A CT scan of the find produced more new information [3]. The skeleton turned out to be very well preserved. Nevertheless, a flattening of individual skeletal elements caused by the pressure of the applied load of the peat on the surface, as well as demineralization from the acidic surrounding soil, is discernible. Some vertebrae and ribs have disappeared from the anatomical group post-mortem. In terms of individual age and gender, this is a young-to-young adult male dog. Finally, the Bog Dog from Burlage is the sole surviving animal bog body in the world.

13.5.6 Ötzi's Pet? The Find of a Frozen, Mummified Hare from the Alps

This unusual mummified animal was discovered in South Tyrol (Italy) in August of 2005. The location of the find was 3000 m above sea level in the Hochferner glacier in Pfitsch. At 3463 m, the Hochfernerspitze is one of the highest mountains in the Zillertal Alps. The mummified hare melted out of the hanging Hochferner glacier on the northern face in 2005. The finders, S. Landthaler and E. Zössmaier, initially brought their find to the State Hunting and Fishing Agency in Bolzano and then to the South Tyrol Museum of Archaeology, where the first tests were supposed to be performed. Even before precise

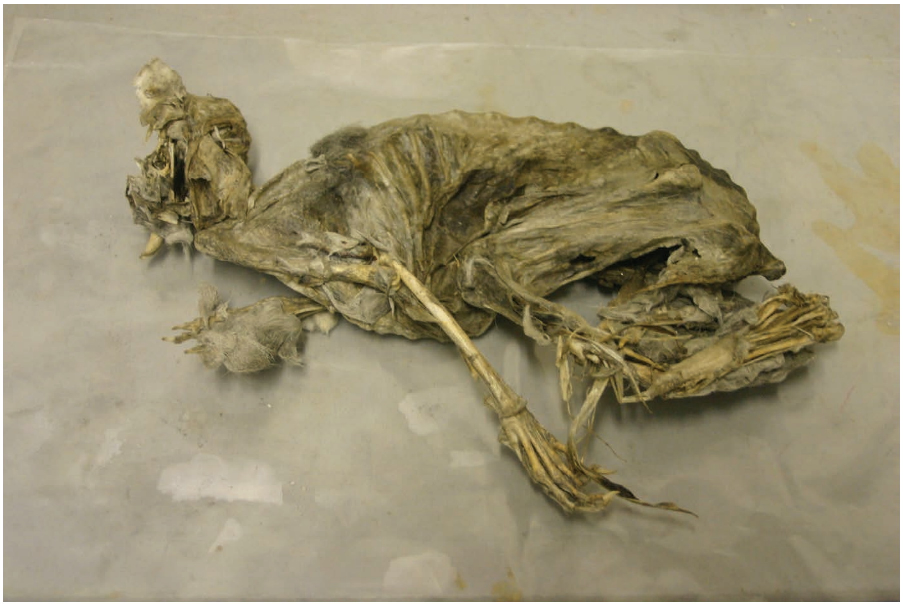

Figure 13.9 A mummified Alpine mountain hare from Hochferner glacier near Pfitsch, South Tyrol, Italy.

(Photograph by W. Rosendahl, Mannheim, Germany. Object from the South Tyrol Museum of Natural History in Bolzano, Italy.)

determinations and dates were available, this find went through the media as 'Pfitschi' or the 'Ötzi Hare', referring to the world famous Neolithic mummy of the so-called Iceman, also known by the name 'Ötzi', discovered in 1992. Initial ^{14}C dating of a tissue sample yielded an age more recent than 1950. The find was therefore considered to be meaningless and more or less fell into oblivion.

New tests as part of the German Mummy Project revealed that the find is definitely an Alpine mountain hare (*Lepus timidus varronis* Miller 1901). Not only the altitude but also the longer hind legs and shorter forelegs, as well as the cross section of the upper incisors, attest to this classification. With an average weight of 2.5–3 kg and a length of 460–560 mm, it is the smallest subspecies of mountain hare. Mountain hares are found in the Alps 1300 m above sea level. The decline in population of this hare in the Alpine countries of Germany, France, Italy, Austria, Switzerland and Slovenia is also connected with global warming.

The mummification process in the ice (freeze drying) shrunk the mummified hare down to 350 mm. Fur has survived only in small tufts on its back and paws. Wherever the parchment-like skin is missing, the bones are still joined only by tendons. Genetic tests revealed that the hare belongs to a now unfamiliar haplogroup [8], thus giving rise to doubts about the young dating obtained in 2005. It was therefore dated a second time, this time using bone material. The result confirmed the dating. Calibration with so-called bomb peak dating determined that the time of death was between 1984 and 1988 (Figure 13.9).

References

1. Arnold JR, Libby WF. Age determination by radiocarbon content: checks with samples of known age. *Science* 1949;110:678–80.
2. Ascough PL, Cook GT, Dugmore A. Methodological approaches to determining the marine radiocarbon reservoir effect. *Prog Phys Geogr* 2005;29(4):532–47.
3. Bertling M, Gill-Robinson H, Rosendahl W. The bog dog from burlage. In: Wieczorek A, Rosendahl W (eds.). *Mummies of the World*. Munich, Germany, Prestel, 2010, pp 298–9.
4. Bocherens H. Keratinisotopie: Antworten zu Lebensraum und Ernährung. In: Wieczorek A, Tellenbach M, Rosendahl W (eds.). *Mumien: der Traum vom ewigen Leben*. Mainz, Germany, Zabern, 2007, pp 235–8.
5. Chisholm BS. Variation in diet reconstructions based on stable isotopic evidence. In: Price TD (ed.). *The Chemistry of Prehistoric Human Bone*. Cambridge, Cambridge University Press, 1989, pp 10–37.
6. Cook GT, Dunbar E, Black SM, Xu S. A preliminary assessment of age at death determination using nuclear weapons testing ^{14}C activity of dentine and enamel. *Radiocarbon* 2006;48:305–13.
7. De Vries HL. Variation in concentration of radiocarbon with time and location on earth. *Proc K Ned Akad Wet* 1958;61:1–9.
8. Döppes D, Gill-Frerking H, Joger U, Rosendahl W, Stümpel N. A mountain hare mummy from Zillertaler Alps. *Yearb Mummy Stud* 2014;2:23–9.
9. Friedrich M, Remmele S, Kromer B, Hofmann J, Spurk M, Kaiser KF, Orcel C, Küppers M. The 12 460-year Hohenheim oak and pine tree-ring chronology from Central Europe: a unique annual record for radiocarbon calibration and paleoenvironment reconstructions. *Radiocarbon* 2004;46(3):1111–22.
10. Geyh MA. *Handbuch der physikalischen und chemischen Altersbestimmung*. Darmstadt, Germany, WBG, 2005, pp 1–211.
11. Hodgins G, Brook GA, Marais E. Bomb-spike dating of a mummified baboon in Ludwig Cave, Namibia. *Int J Speleol* 2007;36(1):31–8.
12. Joger U, Rosendahl W. The Rübeland Caves (Harz Mts.): historical excavations and modern analyses. *Braunschweig Nat Schrift* 2012;11:55–68.
13. Knight B. *Forensic Pathology*. 3rd ed. London, Edward Arnold, 2014, pp 1–672.

14. Libby WF. *Radiocarbon Dating*. Chicago, University of Chicago Press, 1952, pp 1–124.
15. Lotze F. Vorläufige Mitteilung über einen Moorhundfund bei Papenburg a. d. Ems. *Neues Jahrbuch Geol Palaontol Monatsh* 1955;137–8.
16. Lynnerup N, Kjeldsen H, Heegaard S, Jacobsen C, Heinemeier J. Radiocarbon dating of the human eye lens crystallines reveal proteins without carbon turnover throughout life. *PLoS ONE* 2008;*3*(1):e1529.
17. Mazaud A, Laj C, Bard E, Arnold M, Tric E. Geomagnetic field control of ^{14}C production over the last 80 ky: implications for the radiocarbon time-scale. *Geophys Res Lett* 1991;18(10):1885–8.
18. Reimer PJ, Austin W, Bard E, Bayliss A, Blackwell P, Bronk Ramsey C, Butzin M, Cheng H, Edwards R, Friedrich M, Grootes P, Guilderson T, Hajdas I, Heaton T, Hogg A, Hughen K, Kromer B, Manning S, Muscheler R, Palmer J, Pearson C, van der Plicht J, Reimer R, Richards D, Scott E, Southon J, Turney C, Wacker L, Adolphi F, Büntgen U, Capano M, Fahrni S, Fogtmann-Schulz A, Friedrich R, Köhler P, Kudsk S, Miyake F, Olsen J, Reinig F, Sakamoto M, Sookdeo A, Talamo S. The IntCal20 Northern Hemisphere radiocarbon age calibration curve (0–55 cal kBP). *Radiocarbon* 2020;62:725–57.
19. Rosendahl W, Alt KW, Meier S, Rühli F. Eine asiatische Mumie aus den Reiss-Engelhorn-Museen. In: Wieczorek A, Tellenbach M, Rosendahl W (eds.). *Mumien: der Traum vom Ewigen Leben*. Mainz, Germany, Zabern, 2007, pp 347–8.
20. Rosendahl W, Alt KW, Meier S, Rühli F, Michler E, Mitschke S, Tellenbach M. Südamerikanische Mumien aus den Sammlungen der Reiss-Engelhorn-Museen. In: Wieczorek A, Tellenbach M, Rosendahl W (eds.). *Mumien: der Traum vom ewigen Leben*. Mainz, Germany, Zabern, 2007, pp 358–66.
21. Rosendahl W, Gill-Robinson H, Hotz G, Pommerening T. The Egyptian mummies from Basel. In: Wieczorek A, Rosendahl W (eds.). *Mummies of the World*. Munich, Germany, Prestel, 2010, pp 326–8.
22. Rütze C, Forster P, Burger J. Molekulargenetische Herkunftsbestimmung von Mumien. In: Wieczorek A, Tellenbach M, Rosendahl W (eds.). *Mumien: der Traum vom ewigen Leben*. Mainz, Germany, Zabern, 2007, pp 229–33.
23. Suess HE. Radiocarbon concentration in modern wood. *Science* 1955;122:415.
24. Taylor RE, Suchey JM, Payen LA, Slota PJ. The use of radiocarbon (^{14}C) to identify human skeletal materials of forensic science interest. J Forensic Sci 1989;34:1196–205.
25. Ubelacker HD. Artificial radiocarbon as an indicator of recent origin remains in forensic cases. *J Forensic Sci* 2001;46:1285–7.
26. Wagner GA. *Altersbestimmung von jungen Gesteinen und Artefakten*. Stuttgart, Germany, Enke, 1995, pp 1–277.
27. Wild EM, Arlamovsky KA, Golser R, Kutschera W, Priller A, Puchegger S, Rom W, Steier P, Vycudilik W. ^{14}C dating with the bomb peak: an application to forensic medicine. *Nucl Instruments Methods Phys Res B* 2000;172:944–50.

14 Cross-Sectional Imaging and the Post-mortem Interval

Guy Rutty

Contents

14.1 Introduction 355
14.2 Post-mortem Computed Tomography 355
  14.2.1 Rigor Mortis 355
  14.2.2 Livor Mortis 356
  14.2.3 Airways, Lungs and Pleural Cavities 356
  14.2.4 Skin 359
  14.2.5 Liver 359
  14.2.6 Vascular Wall Changes 359
  14.2.7 Post-mortem Gas Formation 359
  14.2.8 Thyroid Gland Changes 361
  14.2.9 Adrenal Gland Changes 361
  14.2.10 Cerebral Parenchyma Attenuation 361
14.3 Post-mortem Magnetic Resonance Imaging 365
14.4 ^{1}H and ^{31}P Magnetic Resonance Spectroscopy 365
14.5 Micro-computed Tomography 366
14.6 Summary 368

14.1 Introduction

The first documented use of X-rays in relation to the investigation of death was in 1896 when X-rays were used by Professor Schuster to assist in the investigation of a gunshot homicide in Manchester, England [1]. During the next 100 years, radiography has become an important adjunct to autopsy practice, principally to facilitate identification and investigate the cause of death. In 1983 the application of computed tomography (CT), a new radiological approach to autopsy practice, was reported [2]. Although post-mortem computed tomography (PMCT) was then proposed as a replacement to the conventional invasive autopsy in 1994 [3], with a similar proposal following shortly afterwards in 1996 related to the use of magnetic resonance imaging (MRI) and perinatal autopsies [4], it was not until the new century that research was initiated to apply these radiological approaches, PMCT [5], post-mortem magnetic resonance (PMMR) and later micro-computed tomography (micro-CT), to assist with the consideration of the post-mortem interval (PMI).

This chapter focuses on summarizing research from a number of authors specific to the use of cross-sectional imaging and the estimation of the PMI. The chapter does not consider the wider subjects the differences between antemortem and post-mortem cross-sectional imaging. For this, the reader could turn to review articles such as, but not limited to, those written by Andrews [6], Ishida et al. [7] and Klein et al. [8].

14.2 Post-mortem Computed Tomography

Although a number of post-mortem changes can be observed with time after death using PMCT, there is as yet no established method whereby these changes can be used to estimate a PMI. However, that is not to say that consideration has not been given and advances have not been made to this area of study by a number of researchers using a variety of approaches.

14.2.1 Rigor Mortis

According to Levy, Harke and Mallak [9] PMCT shows no specific finding for rigor mortis assessment. These authors suggest that skeletal muscle attenuation, size and shape are not affected by rigor mortis. Okuma et al., on the other hand, report significant differences between antemortem and post-mortem cardiac and striated muscle attenuation [10]. Although they considered that this increase in attenuation could be related to rigor mortis, they found no

DOI: 10.1201/9781003244974-14

significant association between this post-mortem change and elapsed time since death.

14.2.2 Livor Mortis

A number of authors have considered the presence of livor mortis (also referred to as ‘lividity’ or ‘hypostasis’) as detected by PMCT. In 2002 Shiotani et al. reported that hypostasis could be observed using PMCT within 2 hours of death in approximately half of the cases in their 126 cases [11]. This corresponds to the time frame for the appearance of livor mortis on external examination of the body and thus in theory it could be used to estimate a minimal PMI. They also described how hypostasis manifests on PMCT images as a high-density fluid level in the lumen of the heart and great vessels. They proposed that this appearance was caused by the gravitational separation of serum and red cells following the cessation of blood flow.

The separation of blood into serum and blood cells, that is a haematocrit effect is now recognized to occur not only in the heart and great vessels but also in the veins, organs and tissues [9] (Figure 14.1). In the cranium it occurs within the posterior sagittal sinus, straight sinus and transvers sinus where it can be mistaken by the unwary as acute thrombosis [9] or as subarachnoid haemorrhage [12] (Figure 14.2). It can be seen with more clarity and precision using PMMR [13]. Shiotani et al. inform us that it does not occur in everyone and is influenced by factors such as age, clinical anaemia, blood volume, position after death and temperature. Ishida et al. have reported that clear cardiac and great vessel hypostasis on PMCT is related to high clinical fibrinogen states prior to death [14].

14.2.3 Airways, Lungs and Pleural Cavities

In the case of body organs, other than the chambers of the heart, hypostasis is best seen in the lungs. With the body in a supine position a horizontal line develops with a vertical density gradient from independent to dependent portions of the lung. Shiotani et al. reported that dependent ground-glass attenuation can be observed with PMCT immediately after death and becomes more pronounced with time [15]. This change is best appreciated in the sagittal view utilizing multi-planar reconstruction (Figure 14.3 [a]). If the body has been lying in a different position, for example in a prone position, then the opposite is true. This phenomenon can be reduced with the use of ventilated PMCT [16,17] (Figure 14.3 [b] and [c]).

Ishida et al. studied the development of fluid in the airways with time elapsed after death in 164 cadavers where PMCT was undertaken between 74 and 1921 minutes after death [18]. They found airway fluid to be present more frequently in those cadavers with pleural effusions than those without. In those without pleural effusion, they found a significant difference in time elapsed from death to PMCT between those with and without fluid. They reported an apparent linear relationship between the percentage of fluid present within the airways and the elapsed time (Figure 14.4). Although they are careful in the way they report their results, they suggest that the time between death and imaging is relatively short when neither pleural effusion

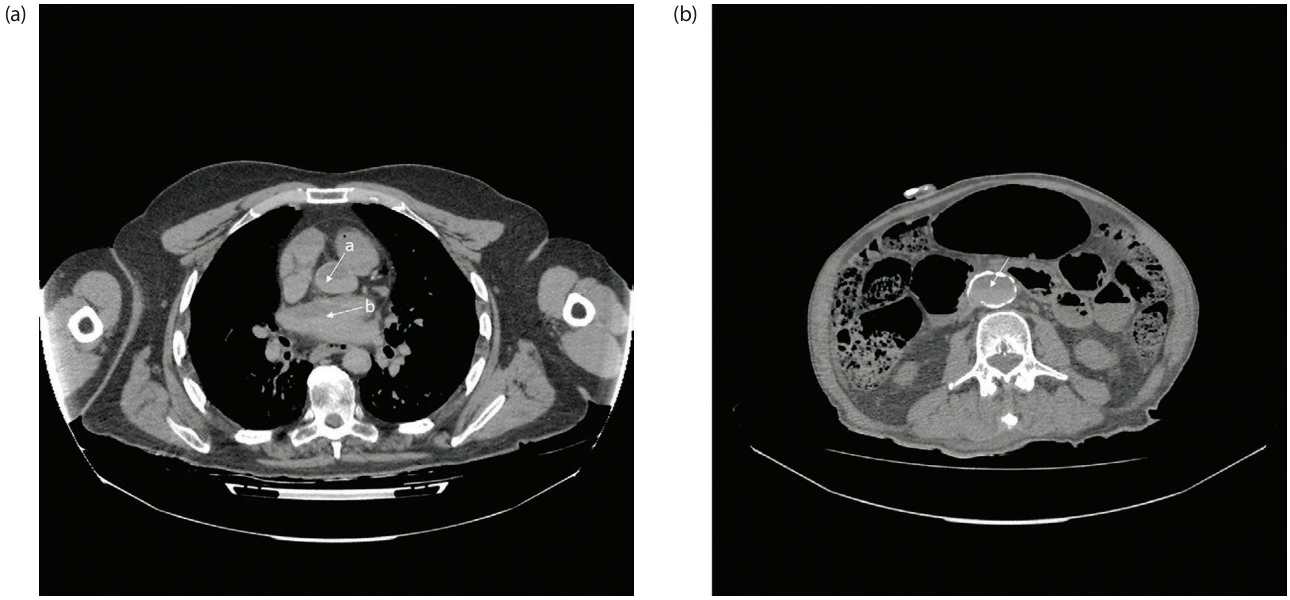

Figure 14.1 Axial section of the thorax showing post-mortem blood hypostasis levels within the aorta (arrow a) and pulmonary trunk (arrow b). (b) Axial section of the abdomen showing post-mortem blood hypostasis level within the abdominal aorta (arrow).

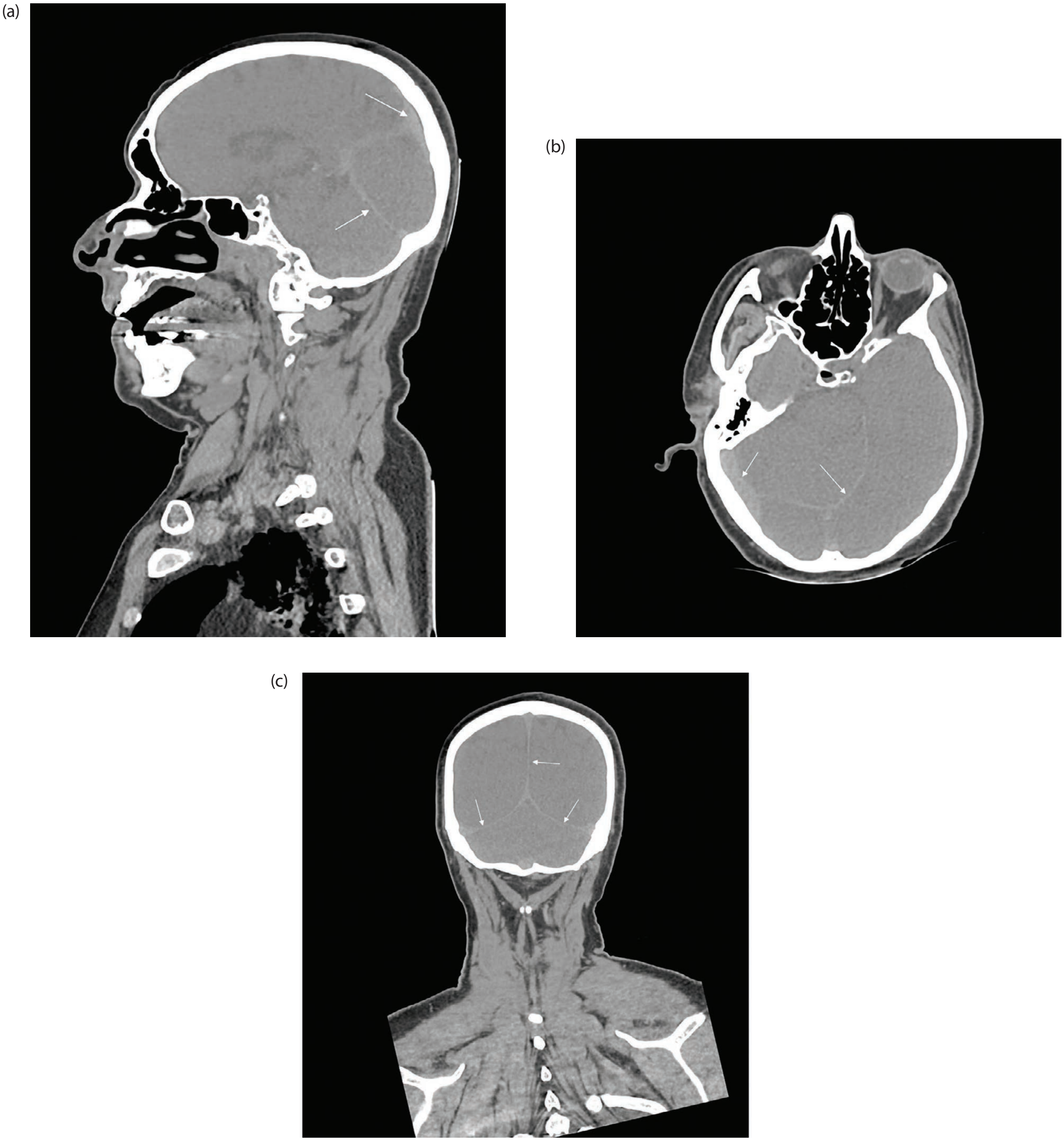

Figure 14.2 Sagittal (a), axial (b) and coronal (c) sections of the head showing post-mortem blood hypostasis (arrows) mimicking subarachnoid haemorrhage.

nor fluid in the airways is observed (mean 3.5 hours). They suggest that the percentage of fluid within the airways correlates with elapsed time from death.

Hyodoh et al. studied the time-related course of pleural space fluid accumulation and pulmonary aeration of 199 cadavers using PMCT [19]. They observed that pleural fluid collection was not a standard post-mortem change in the first 30 hours after death but then increased between 30 and 42 hours after death when it reached a maximum. They used this observation to suggest that if pleural fluid is seen on PMCT less than 30 hours after death, then it is likely due to an antemortem condition. They also noted with the increase in pleural fluid collection that the pulmonary volume decreased as the lung parenchyma was compressed. A later study of Okumura et al. reported that it was not possible to use PMI in the equations for either left or right lung volumes [20].

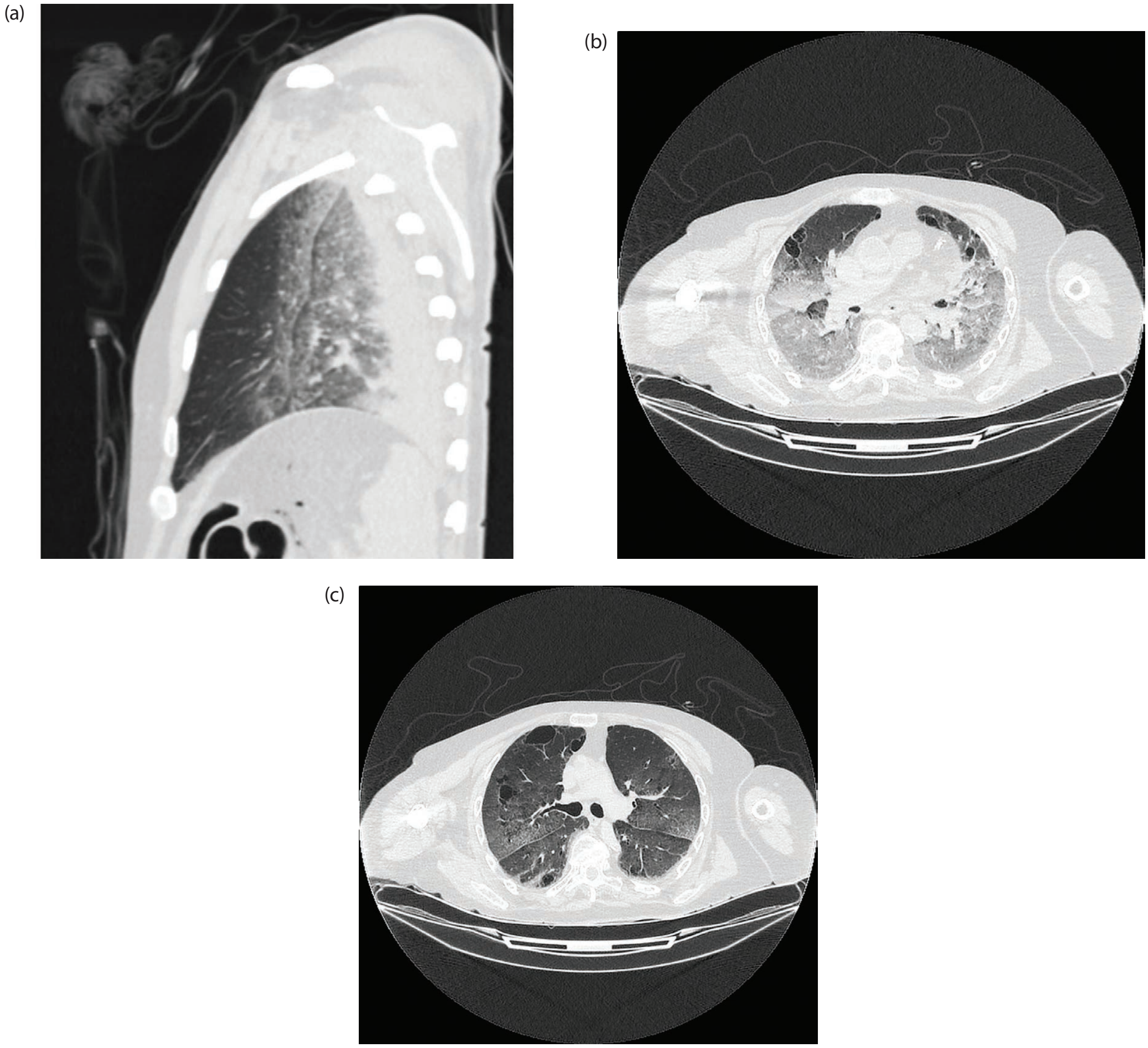

Figure 14.3 (a) PMCT sagittal view of lungs showing a horizontal line with a vertical density gradient from independent to dependent portions of the lung (b). Pre-ventilated and (c) post-ventilated PMCT axial images showing removal of the effect of post-mortem hypostasis within the lungs.

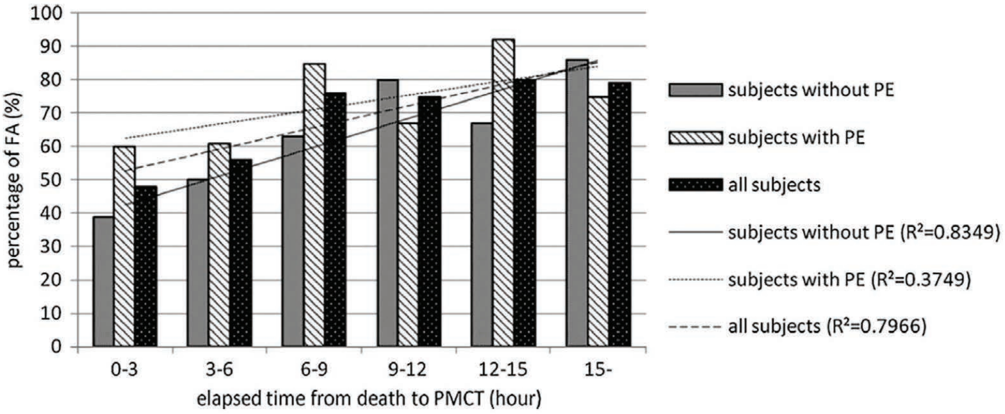

Figure 14.4 Distribution of the percentage of fluid within the airways in 168 cadavers with and without pleural effusions.

(From Ishida M, Gonoi W, Hagiwara K, Okuma H, Shitani Y, Abe H, Takazawa Y, Ohtomo K, Fukayama M. Fluid in the airways of nontraumatic death on postmortem computed tomography. *Am J Forensic Med Pathol* 2014; 35: 113–117.)

14.2.4 Skin

In terms of the skin, increased attenuation occurs between the subcutaneous fat and dermis, with the dermis becoming thicker in the dependent parts of the body. However, to date no published research exists concerning the distribution and fixation of lividity on PMCT images over time, as has been observed and documented during the external examination of the body.

14.2.5 Liver

Fisher et al. studied four areas of the liver using serial PMCT in five cadavers imaged hourly for 24 hours starting 3–20 hours after death [21]. They found that the liver parenchyma did not change significantly over time. The highest radiopacity was found to the right posterior lobe, which was attributed to physiological paradigms.

14.2.6 Vascular Wall Changes

It is now widely recognized that the so-called native or non-enhanced PMCT scan is insufficient for the diagnosis of vascular related pathology, specifically that of coronary artery disease. The use of post-mortem computed tomography with angiography (PMCTA) has been proposed as the new PMCT gold standard. However, due to the changes that occur within blood vessels after death, even with PMCTA the diagnosis of some natural diseases, such as pulmonary thromboembolus, remains difficult.

One of the changes that occur after death is that the great vessels may collapse. This can be observed on the native, non-enhanced scan. Shiotani et al. reported that the diameter of the ascending aorta was smaller than that of a living person [22]. In a later study Takahashi et al. reported that the aorta shrunk at all anatomical levels, noting that it became oval in shape in the descending and abdominal parts [23] (Figure 14.5). Ishikawa et al. have since studied the abdominal aorta just below the diaphragm in 140 cases within 5 days of death [24]. They report a relationship between the changes in aortic shape (narrowing), which they propose is due to the action of gravity at this point, with time. A similar relationship was not observed in the thoracic aorta or the bifurcation of the abdominal aorta, leading the authors to propose that this was due to the variation in the support of the aorta at differing points along its length, be it by local anatomical variations and/or the presence of atherosclerosis. Although they propose that post-mortem aortic narrowing may be time related, and thus amenable for use to estimate a PMI, they highlight a number of factors that need to be taken into account and investigated, such as the effect of physical build, cardiopulmonary resuscitation, haemorrhage and decomposition.

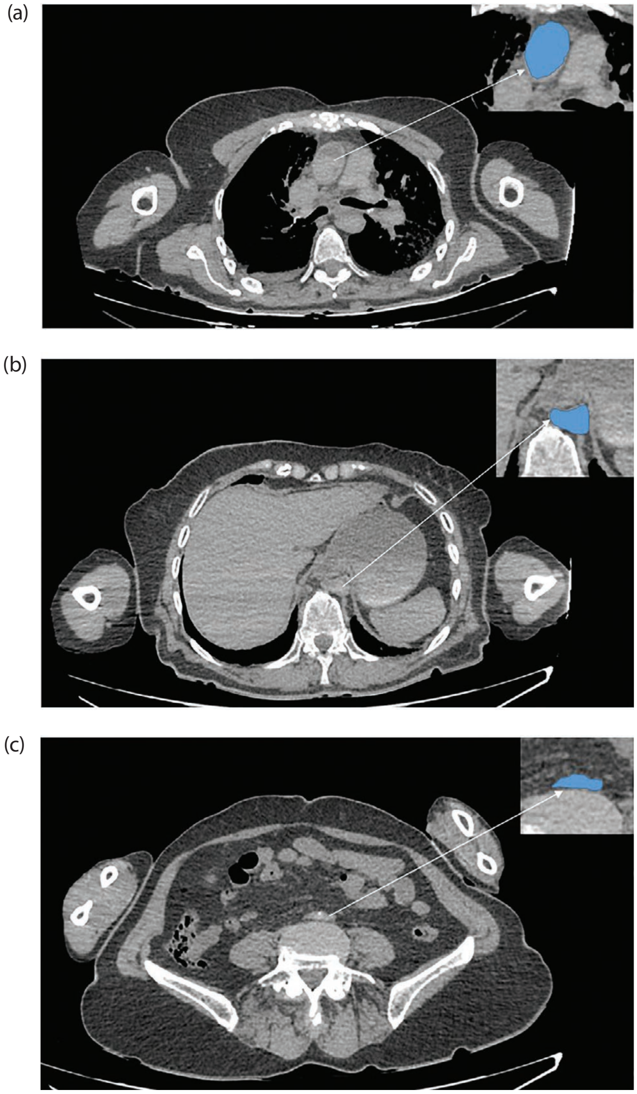

Figure 14.5 Post-mortem collapse of the aorta varies depending upon the anatomical position in the body. (a) Ascending aorta, (b) abdominal aorta at emergence through diaphragm and (c) abdominal aorta close to bifurcation into iliac vessels.

14.2.7 Post-mortem Gas Formation

Air and putrefactive gas (both referred to from this point onwards to as ‘gas’) is seen on PMCT within the vessels, organs, soft tissues and body cavities [9]. To date the literature has concentrated on the source, composition and distribution of gas within the vascular system rather than its appearance within the soft tissues [25,26,27,28,29,30,31].

The first true putrefactive gas site observed with PMCT is within the intestinal wall and mesenteric and portal venous systems [9] (Figure 14.6). It then develops within

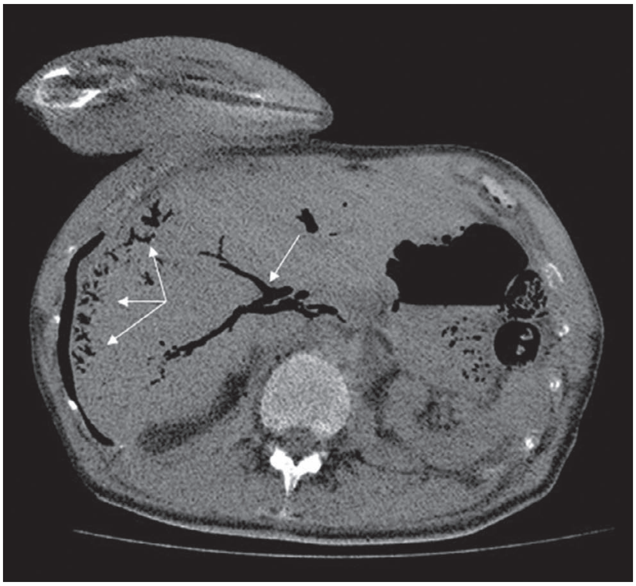

Figure 14.6 Axial image using minip projection showing air (arrow) in the portal veins as an early post-mortem change.

all vascular spaces and potential anatomical spaces, normally in a symmetrical distribution unless there is focal or asymmetric decomposition caused by an injury or local anatomical area of cooling or warming [9].

The principal problem when considering the presence of intravascular gas on PMCT is that it may not be derived from decomposition. Shiotani et al. described a relationship between gastrointestinal distension attributed to cardiopulmonary resuscitation (CPR) and the presence of hepatic portal venous gas (HPVG) observed within 2 hours of death [32]. A similar observation was reported by Asamura et al. [33].

Although HPVG is associated with clinical disease such as cholangitis, cholecystitis and sepsis, as well as trauma, Shiotani et al. reported that HPVG may be seen within 2 hours of death in the absence of CPR or local disease [32]. A similar time frame was observed by Yamazaki et al. in a case dying of ischaemic heart disease [34]. Yokota et al. observed gas formation within the arterial and venous systems and suggested that the pattern of distribution could be used to distinguish between true post-mortem gas formation and that associated with CPR [35]. Egger et al. have studied the distribution of gas within the vascular compartment proposing that it follows a specific distribution pattern [36]. Singh et al. through the study of a single adult case serially scanned over a 3-day period described the progressive formation of intrahepatic and intracardiac gas [37]. They illustrated how, in the absence of CPR or abdominal trauma, intrahepatic and intracardiac gas can form within 7 hours and 30.5 hours, respectively, after death.

Okumura et al. noted that intrarectal gas decreased with time after death [20]. They suggest that this was due to an increase in intra-abdominal pressure caused by putrefaction, pushing the gas out of the anus, which relaxes after rigor mortis is no longer present. Fisher et al. studied four areas of the liver using serial PMCT in five cadavers imaged hourly for 24 hours starting 3–20 hours after death [21]. In three of their five cadavers, intrahepatic gas increased over the initial 4–7 hours with no substantial gas increase in the other two cases within the 24-hour study period. They found that the largest amount of gas was found within the hepatic venous system, with no gas detected within the intra- and/or extrahepatic biliary system. No significant amount of gas was present within the intrahepatic arteries. They considered that the most common cause of gas in non-traumatic death was either resuscitation procedures or mucosal damage to the bowel.

Iwamoto et al. studied 3D-CT data of post-mortem portal venous and intestinal gas volume change in three sacrificed rats at seven time points at 24-hour intervals up to 168 hours after death [38]. They reported that the gas volume increased in a time-dependent manner (Figure 14.7). They

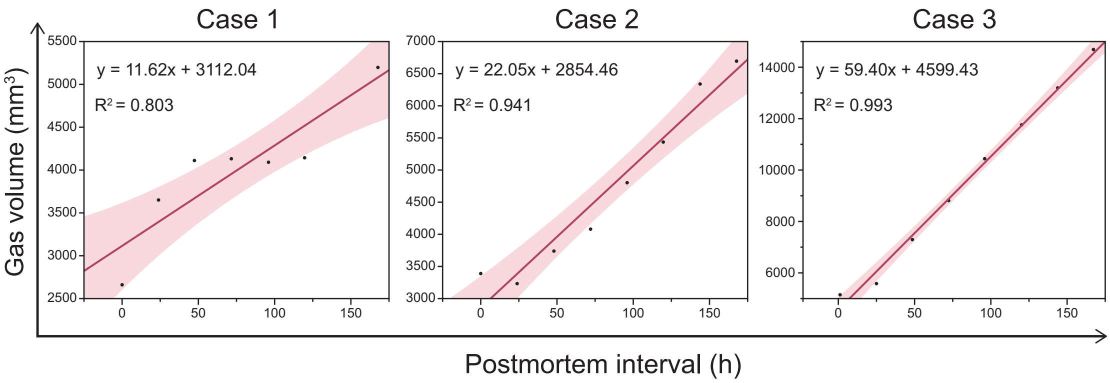

Figure 14.7 Volume changes in post-mortem intestinal gas. Time-dependent straight lines for the post-mortem interval and intestinal gas volume interaction determined on 3D-CT reconstructed images were calculated. Data shown are representative of three independent experiments.

(From Iwamoto C, Ohuchida K, Okumura M, Usumoto Y, Kishimoto J, Murata M, Ikeda N, Hashizume M. Postmortem interval estimation using the animal model of postmortem gas volume changes. *Leg Med* 2018; 32: 66–70.)

concluded that the PMI could be calculated from changes of intestinal and portal venous gas volume change.

14.2.8 Thyroid Gland Changes

A single study by Ishida et al. reports changes in the thyroid gland between antemortem clinical CT and PMCT that relate to the time elapsed [39]. This study of 50 patients dying in a tertiary care hospital identified that the density (Hounsfield Units, HU) of the left and right thyroid lobes decreased after death. However, they were unable to use this relationship to predict a time of death interval.

14.2.9 Adrenal Gland Changes

A single study by Ishida et al. reports changes in the volume of the left and right adrenal glands between antemortem clinical CT and PMCT [40]. This study of 28 patients dying of non-traumatic causes in a tertiary care hospital reported a significant reduction in PMCT adrenal gland volume compared to the antemortem CT values. The PMCT images were undertaken 94–1,191 minutes after death. The mean right adrenal gland volume reduced from 3.8 to 2.6 cm^3, whereas the left reduced from 4.2 to 3.1 cm^3. The authors suggested this may be as a result of lipid depletion. Despite this observed change, they reported that there was no significant correlation between time from the antemortem scan to death or between the time of death to PMCT.

14.2.10 Cerebral Parenchyma Attenuation

Those used to reporting PMCT scans will be aware that the brain has an appearance of global hypoxic injury. Blurring and loss of definition of the grey-white matter junction, decease in cerebral attenuation and sulcal effacement occurs early, with complete loss of grey-white matter differentiation seen within 2–3 days after death [9].

Using 61 cerebral PMCT scans Bayat and Klein studied the density (HU) of the dorsal aspects of the superior sagittal sinus, left and right vitreous humour (VH) and the anterior and posterior horns of the left and right lateral ventricles [41]. Their cases occupied a post-mortem time frame of 3.0–45.1 hours. They observed an increase in density of the lateral ventricle regions with a strong correlation between density (HU) and the post-mortem interval (W. M. Klein, 2014, personal communication) (Figure 14.8). In the published abstract, they hypothesize that this observation could be used to estimate a post-mortem interval, although validation studies would be required.

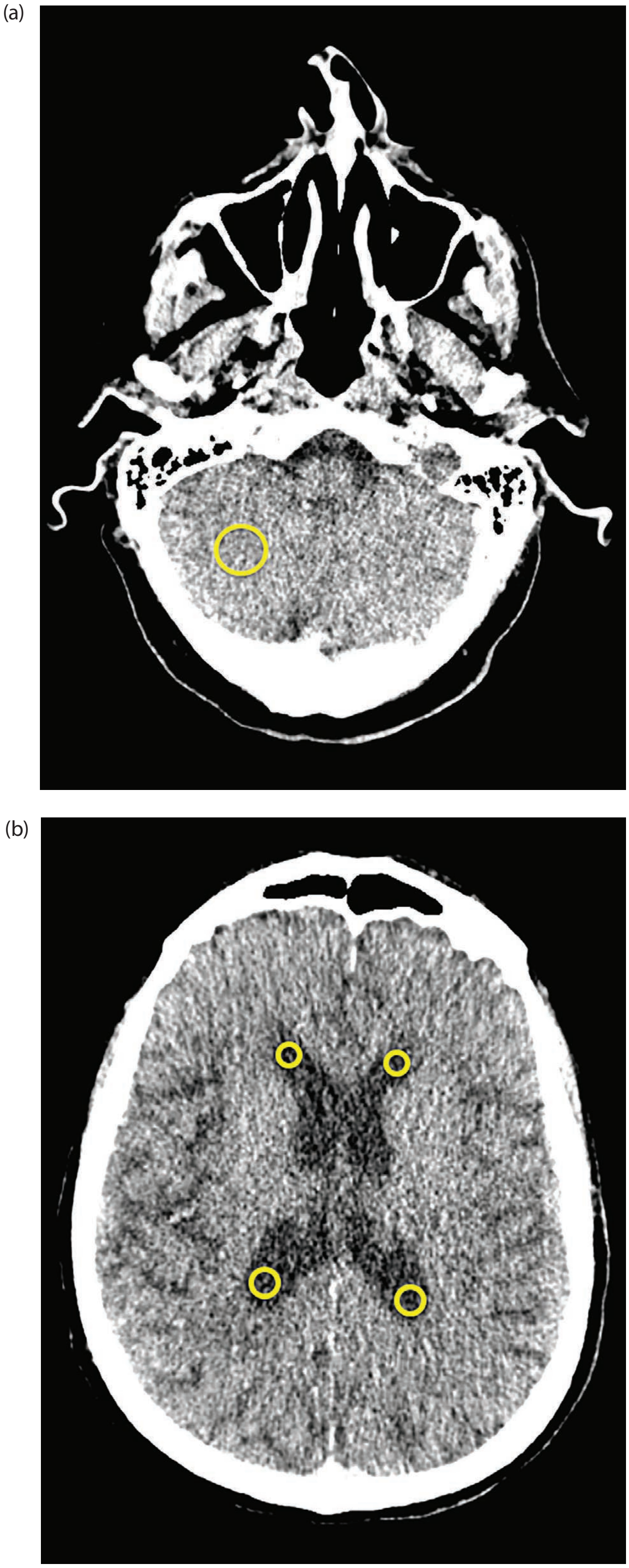

Figure 14.8 (a) Site for density measurement of the right cerebellar hemisphere at the level of nasopharynx. (b) Site for density measurements of cerebral spinal fluid in the anterior and posterior horns of the most lateral part of the left and right ventricles of the brain.

(From A. Bayat and W. M. Klein 2014.)

Hasegawa et al. evaluated the time-related changes to the lateral cerebral ventricles (LCV) in three cadavers scanned sequentially between 2 and 24 hours after death [42]. They reported that the frontal and posterior horns diminished in size with time and that the HU attenuation within the LCVs gradually increased over time (Figure 14.9).

Koopmanschap et al. further considered the PMCT change in cerebrospinal fluid (CSF) and VH radiodensity with time using three study groups [43]. Group A consisted of five donated cadavers all scanned with the same scanner using standardized conditions of temperature and humidity. Group B comprised 100 in-hospital deceased patients. The last group, group C, comprised 12 out-of-hospital forensic cadavers. They reported that the CSF radiodensity of group A increased with time since death (Figure 14.10). For the CSF they produced the following formulae:

$$\text{PMI}(h) = 4.29 \times \text{HU}^{\text{CSF}} - 16.17$$
$$\text{PMImax} = 4.82 \times \text{HU}^{\text{CSF}} - 11.47$$
$$\text{PMImin} = 3.77 \times \text{HU}^{\text{CSF}} - 20.88$$

Although CSF radiodensities of groups B and C also increased with time, they found the values to be higher than predicted with the model generated from group A. Using the PMI max formula, they estimated the PMI at, or below, the estimated PMI in 95% of group B and 100% of group C cases.

In terms of the VH, this also showed a slight increase with time in group A. From this they derived the following formulae.

$$\text{PMI}(h) = 3.03 \times \text{HU}^{\text{VH}} - 14.37$$
$$\text{PMImax} = 3.87 \times \text{HU}^{\text{VH}} - 4.30$$
$$\text{PMImin} = 2.19 \times \text{HU}^{\text{VH}} - 24.44$$

They again found that VH radiodensities of groups B and C also increased with time and that the values were higher than predicted with the model generated from group A. Using the PMI max formula, they estimated the PMI at, or below, the estimated PMI in 98% of group B and 100% of group C cases. They concluded from this work that the VH and CSF radiodensities correlated with the PMI and could be useful to estimate a time since death.

In the same year Morikawa et al. reported their study of PMCT CSF density of 189 cadavers with a postmortem interval of 0.5–30 days [44]. Although they again observed an increase in CSF density after day 3 with the highest recoded value to day 30, as the increase was not linear with discrete overlap in CSF radiodensity, they

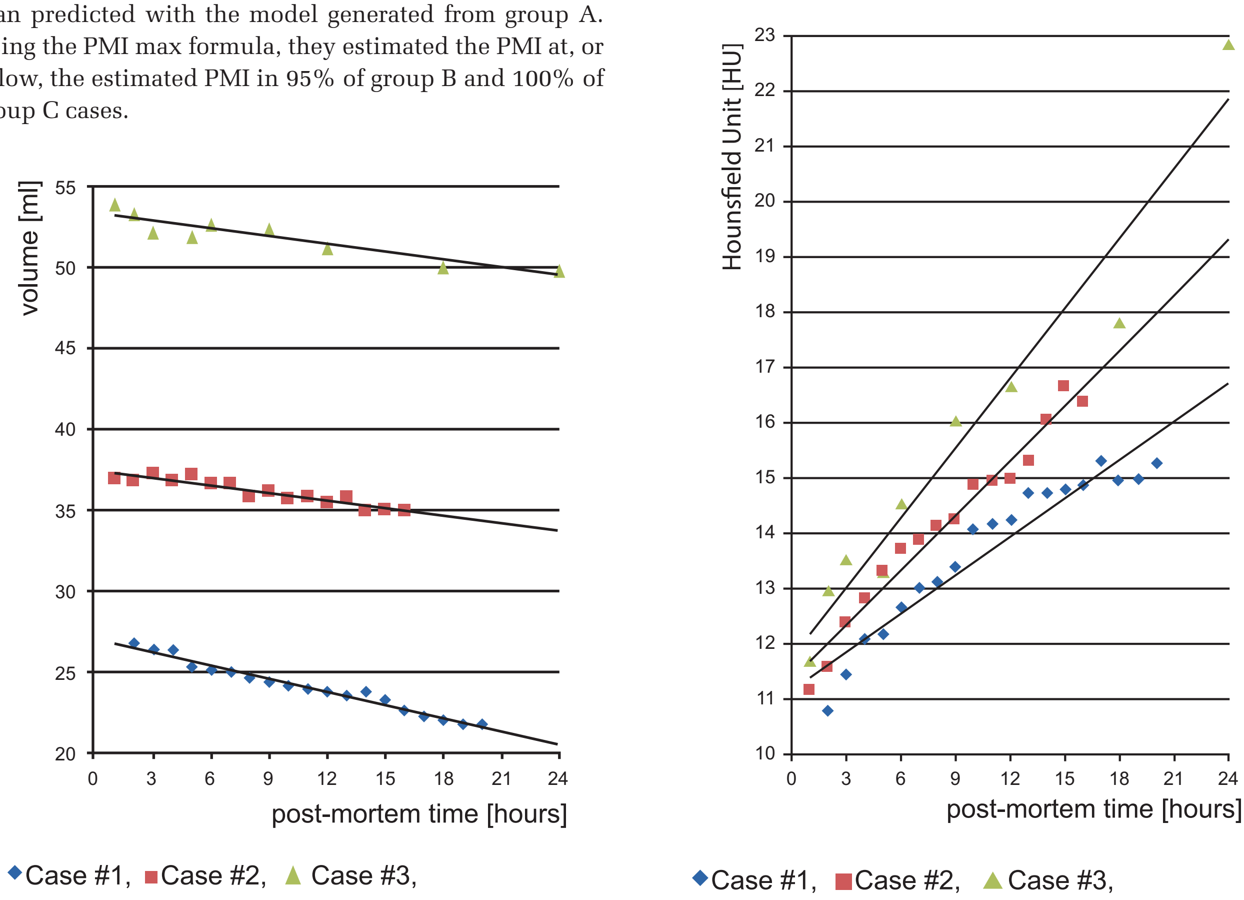

Figure 14.9 (a) Lateral cerebral ventricle volumes for three cases sequentially scanned. The volume deceases as a function of post-mortem time. (b) The HU attenuation increases within the lateral cerebral ventricles as a function of post-mortem time.

(From Hasegawa I, Shimizu A, Saito A, Suzuki H, Vogel H, Puschel K, Heinemann A. Evaluation of post-mortem lateral cerebral ventricle changes using sequential scans during post-mortem computed tomography. *Int J Leg Med* 2016; 130: 1323–1328.)

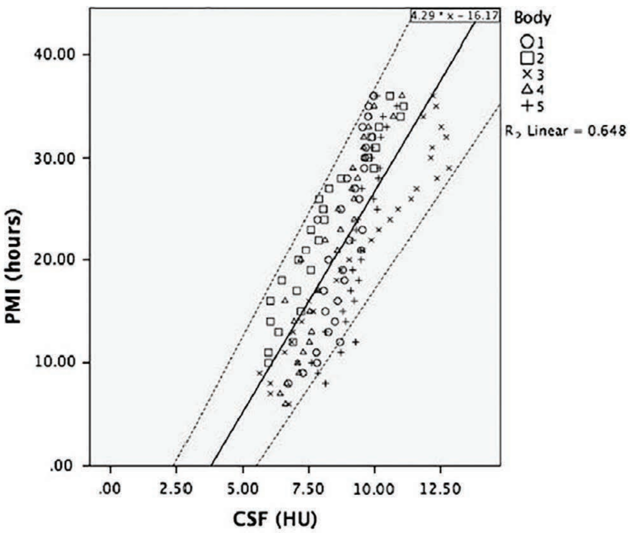

Figure 14.10a Scatterplot of the radiodensities of the CSF in the 5 donated cadavers that were scanned hourly, starting at a PMI of 6–10, to 36 h postmortem, R^2 is 0.65, which indicates a fairly accurate application of the model. The middle continuous line denotes the linear correlation line fitting the formula PMI (*h*) = 4.29 × HU^{CSF} – 16.17 and the upper and lower lines denote the 95 % confidence interval.

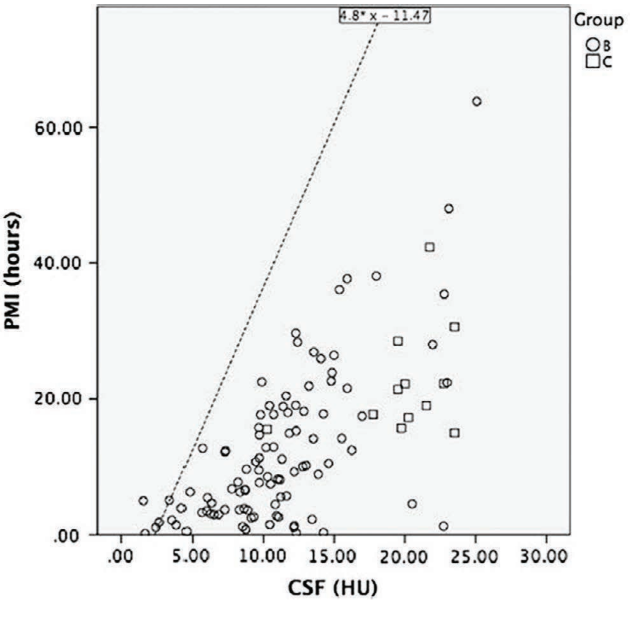

Figure 14.10b Scatterplot showing the CSF radiodensities of patient in groups B and C. The line denotes the upper limit prediction of the CSF radiodensity of group A, corresponding to the formula 4.82 × HU^{CSF} – 11.47, indicating estimated maximum post-mortem interval.

concluded that it was difficult to estimate the post-mortem time based on CSF density.

In 2021 De-Giorgio et al. published their PMCT sequential study of the LCV of ten cadavers between 5.5 and 273 hours after death [45]. They again report a linear decrease

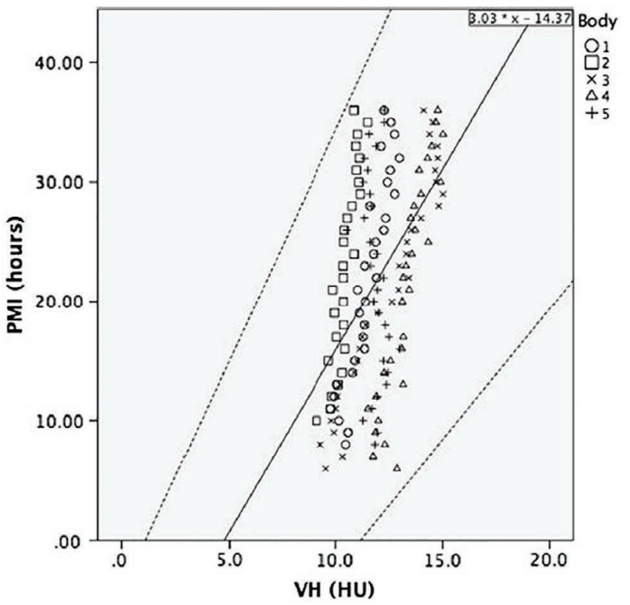

Figure 14.10c Scatterplot of the radiodensities of the VH in the 5 donated cadavers that were scanned hourly, up to 36 h portmortem, starting at a PMI of 6–10 h. The fixed effect regression line r^2 is 0.26, which indicates a low correlation. The *middle continuous line*, denotes the linear correlation line corresponding to the formula PMI (*h*) = 3.03 × HU^{VH} – 14.37 and the *upper* and *lower lines* indicate the 95% confidence interval.

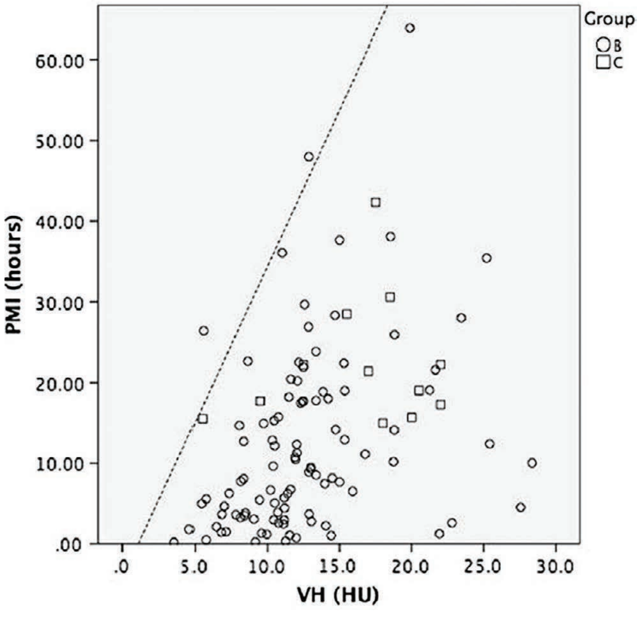

Figure 14.10d Scatterplot showing the VH radiodensities of patients in groups B and C. The *line* denotes the upper limit prediction of the CSF radiodensity of group A, corresponding to the formula 3.87 × HU^{VH} – 4.30, indicating the estimated maximum post-mortem interval.

(From Koopmanschap DHKLM, Bayat AR, Kubat B, de Bakker HM, Prokop MWM, Klein WM. The radiodensity of cerebrospinal fluid and vitreous humor as indicator of the time since death. *Forensic Sci Med Pathol* 2016; 12: 248–256.)

in LCV volume with time. They observed a strong inter-individual variability that was dependent on a number of factors, including subject age and size. Thus, they also considered the average LCV region radiodensity. Despite inter-individual variability, their data collapsed in a single master curve with a well-fitted logarithmic trend showing an initial fast growth rate which slowed down with time (Figure 14.11). They were able to plot both their data and that of Hasegawa et al. to illustrate that the joint sets of data were well fitted by the same logarithmic master curve. They concluded that the LCV CSF radiodensity could be a potential tool to determine the post-mortem interval.

Considering time-related change in brain parenchyma attenuation, Ramanaidu et al. undertook a PMCT study of 160 cadaver brains with a post-mortem interval of 0.3–30.8 hours [46]. Twenty measurements were taken from the frontal, temporal and parietal lobes; the basal ganglia; centrum semiovale and the high convexity. The linear regression plots for the sites all showed a positive linear monotonic correlation between the average attenuation values of the brain and the post-mortem interval. When the linear correlations of all the specific sites are plotted, there is an almost parallel slope of all the measured parts in correlation to the overall average (Figure 14.12). The authors conclude that there is a positive linear correlation between PMI and brain parenchyma attenuation. The most representative site of measurement to estimate a time since death was suggested from the high convexity.

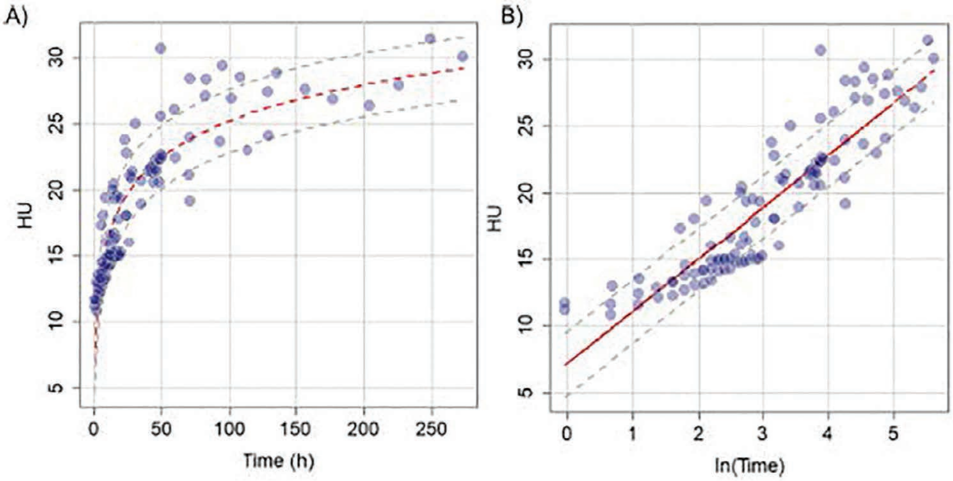

Figure 14.11 Global plot of the radiodensity evolution of ten cadavers in both (a) linear and (b) logarithmic scales. A logarithmic fit is superimposed to the data together with the corresponding confidence bands. The De-Giogio et al. data is plotted with data from Hasegawa et al. acquired in the time interval 0–24 hours post-mortem. The joint set of data is well fitted to the same logarithmic master curve.

(From De-Giorgio F, Ciasca G, Fecondo G, Mazzini A, De Spirito M, Pascali VL. Estimation of the time of death by measuring the variation of lateral cerebral ventricle volume and cerebrospinal fluid radiodensity using postmortem computed tomography. *Int J Leg Med* 2021; 135: 2615–2623.)

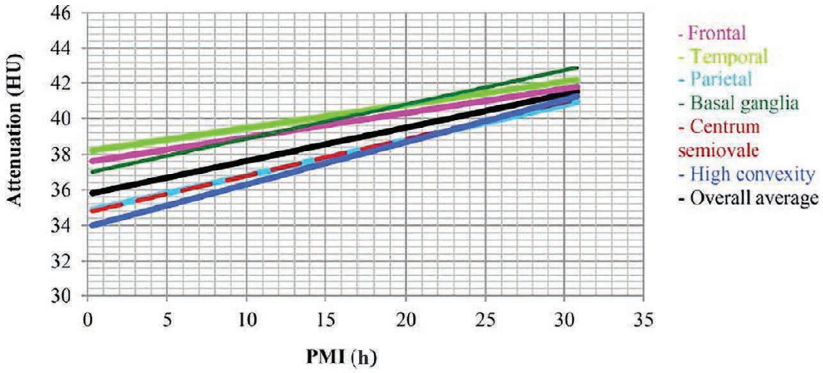

Figure 14.12 Multiple linear correlations of specific brain locations and overall attenuation average against PMI.

(From Ramanaidu V, Mustapha AWMM, Noor MHM, Abdullah N. Estimation of time of death using brain attenuation parenchyma attenuation in post mortem computed tomography of brain—In Malaysian setting. *Forensic Imaging* 2021; 26: 200470.)

14.3 Post-mortem Magnetic Resonance Imaging

A number of authors have reported time-related changes within the organs and blood vessels after death using post-mortem magnetic resonance imaging (PMMRI) to assist image interpretation compared to antemortem MRI. There are a few papers that consider how these changes could be applied to the estimation of a time since death.

Kobayashi et al. reported that cerebral post-mortem MRI showed characteristic signal intensity changes [47]. However, they did not attempt to use these changes to determine the post-mortem interval. Tashiro et al. also reported alteration of cerebral signal intensity after death attributing the T_1 and T_2 value changes to an increase in tissue water content, reduction in pH and post-mortem reduction of body temperature [48]. Shiotani et al. reported that a reduction in body temperature after death induced T_1 and T_2 value changes in the liver on PMMRI, although neither of these correlated significantly with the post-mortem interval [49]. Wagensveld et al. reported post-mortem MR changes in the brain, heart, great vessels, lungs, liver, kidneys, spleen and gallbladder [50]. Tumanova et al. considered the characterization of cadaveric hypostasis in the lungs, heart, vessels and liver of deceased newborns using MRI [51]. They described changes in the MR signal intensity in the ventral and dorsal regions of the liver and lungs with the appearance of a horizontal signal intensity gradient reflecting the position of the body after death. They described that often three layers were seen within the heart and vessels. The horizontal gradient was not only dependent upon the MRI mode but also on the organ studied and the duration of the post-mortem period.

Keller et al. investigated the changes in hepatic apparent diffusion coefficient (ADC) of 19 adult cadavers at multiple time points over a 16-hour period post-mortem [52]. Taking readings every 2 hours, they identified that the hepatic ADC showed characteristic changes in the immediate 16 hours post-mortem, which was influenced by the post-mortem liver temperature. They concluded that, in combination with their graph of post-mortem liver temperature, post-mortem liver diffuse-weighted imaging could be of interest for determination of the time of death.

Arthurs et al. performed post-mortem diffusion-weighted imaging (DWI) of the abdominal and thoracic organs on 15 foetal and childhood cases [53]. They identified that there was a significant non-linear correlation between the mean ADC of the lungs and the post-mortem interval (Figure 14.13). They provide a formula of this correlation.

$$y = 0.28\ln(\mathrm{x}) \times + \times 0.44; \times \mathrm{R}^2 = 0.66$$

No such correlation was found with the abdominal organs. They attributed the increase in lung ADC to the accumulation of fluid in the lungs. They suggest that this observation could be a useful imaging marker of post-mortem interval. However, in a subsequent larger study involving 80 perinatal deaths, the study results did not support the earlier findings [54]. In this latter study, they reported that post-mortem interval was not a significant predictor of ADC in any body area.

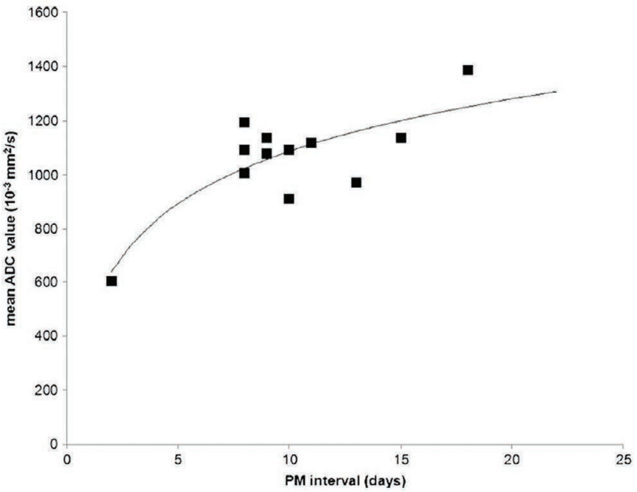

Figure 14.13 Lung apparent diffusion coefficient (ADC) changes with post-mortem interval.

(From Arthurs OJ, Price GC, Carmichael DW, Jones R, Norman W, Taylor AM, Sebire NJ. Diffuse-weighted perinatal postmortem magnetic resonance imaging as a marker of postmortem interval. *Eur Radiol* 2015; 25: 1399–1406.)

Using post-mortem MRI, Barber et al. investigated whether the accumulation of pleural fluid after death could be a possible marker of the interval since death [55]. Imaging 12 perinatal (24–48 weeks' gestation) and 11 childhood deaths (1 day to 4 years age) they reported a significant correlation for pleural effusion volume related to post-mortem interval in children and a subgroup of perinatal deaths. Acknowledging the small size of their study population, they suggest that if this relationship holds in a larger population, this observation may provide information regarding the time of death.

14.4 ^{1}H and ^{31}P Magnetic Resonance Spectroscopy

In 2002 Ith el al. considered the application of ^{1}H-MRS, as part of MRI, to forensic medicine in an attempt to estimate the post-mortem interval [56]. Studying eight abattoir-acquired decapitated sheep heads stored at 20°C and four human cadavers at 4°C, they considered the change in four brain metabolites over an 18-day period. They concluded that for the first 48 hours the sheep and human metabolite changes could be correlated with time, but after 3 days new metabolites appeared. Building upon this work a number of authors applied ^{1}H-MRS to both pig and sheep head models in an attempt to further study metabolite change with time and at different ambient temperatures [57,58,59]. They showed it was possible to define a single equation to describe eight metabolite concentrations as a function of post-mortem interval and ambient temperature, which could be used to determine a post-mortem interval. However, once bacterial decomposition ensues, reliable PMI calculation cannot occur. However, Musshoff et al. have shown problems using a decapitated head as the experimental model [60]. When these authors applied ^{1}H-MRS to a whole cadaver porcine model, significant differences in time-related metabolic changes were observed between the isolated heads and intact animal. Thus, although ^{1}H-MRS appears to be a promising avenue for the estimation of the post-mortem interval, to date insufficient data exists for ^{1}H-MRS to be reliably used to calculate a post-mortem interval in the human.

Schmidt et al. investigated the temporal post-mortem pattern of phosphor metabolites of the adductor magnus muscle of eight human cadavers dying of natural causes using phosphor MRS (^{31}P MRS) to determine if ^{31}P MRS of skeletal muscle could be used to determine a time of death [61]. MRI scans were undertaken every 1 hour over a period between 4.5 and 24 hours post-mortem, with the scans commencing as soon after death as possible. In addition, three control subjects were examined at a single time point. They identified that the acquired α-ATP/Pi ratio showed a significant post-mortem time course and that its inverse logarithmic function allowed the determination of the time of death up to 8 hours post-mortem within a 95% confidence interval. The measured α-ATP/Pi ratio of 1.0 determined the time of death within 1.4–2.5 hours post-mortem, whereas a ratio of only 0.1 increased the 95% timer interval from 5.7 to 12.8 hours post-mortem (Figure 14.14). They concluded that although further work was required, ^{31}P MRS might be added to post-mortem imaging methods.

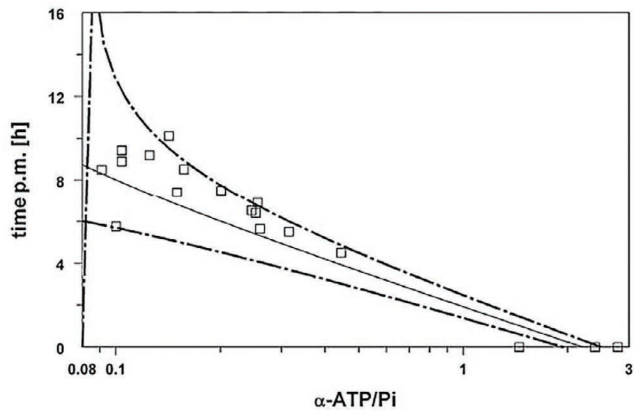

Figure 14.14 Inverse function of the post-mortem metabolic ratios of α-ATP/Pi (squares, thin solid line) allows the determination of the time of death point within its 95% confidence interval (dot-dashed lines).

(From Schmidt TM, Wang ZJ, Keller S, Heinmann A, Acar S, Graessner J, Schoennagel BP, Adam G, Fischer R, Yamamura J. Postmortem ^{31}P magnetic resonance spectroscopy of the skeletal muscle: α-ATP/Pi ratio as a forensic tool? *Forensic Sci Int* 2014; 242: 172–176.)

14.5 Micro-Computed Tomography

To date micro-CT has had a limited application to post-mortem investigation [62,63]. This is in part due to the restricted availability of this imaging modality to autopsy practitioners. Having said this, the forensic entomology work of Richards et al. [64] from the Natural History Museum, London, United Kingdom, has shown that cross-sectional imaging using micro-CT can be applied for the estimation of a minimal PMI.

After death blowflies are the first insect species to colonize the body [65]. Their ‘immatures’ pass through three developmental stages: egg, larval and pupal. By recording the duration of development of the oldest immature stage recovered from the body, it is possible to estimate a minimal PMI (PMImin) [66]. Methods can be applied to both larval and pupal stages to estimate a PMImin. In terms of the pupal stage, these have included measurement of the beginning and end of pupariation [67], as well as morphology studies, which have included the use of light and scanning electron microscopy [68], and histology [69]. These techniques when applied to pupae are time-consuming and destructive. In an attempt to overcome this problem, micro-CT has been used to facilitate the description of insect anatomy [70].

Richards et al. applied micro-CT to examine the development of blowfly pupae [65]. The imaging of the pupae was enhanced by staining them with iodine. By using micro-CT to investigate the internal anatomical changes during blowfly metamorphosis and considering the changes observed with those externally Richards et al. described how micro-CT can be applied to estimate a minimal post-mortem interval. The group highlighted that micro-CT is rapid, inexpensive and non-destructive, allowing for multiple pupae to be examined at the same time. Although currently pupae are killed for the examination, they suggest that, considering other work within the insect world, scanning the development of live pupae may be possible with micro-CT, thus producing more robust post-mortem interval estimation. Rutty et al. achieved this in the production of Figure 14.15 for this book.

In a follow-up study, the group selected two species commonly encountered in a forensic setting: the common bluebottle blowfly (*Calliphora vicina*) and the common green bottle blowfly (*Lucilia sericata*) [71]. Five random puparia from each species were stained with 0.5M iodine and subjected to micro-CT examination. Using the sagittal image plane, 17 age-informative internal morphological

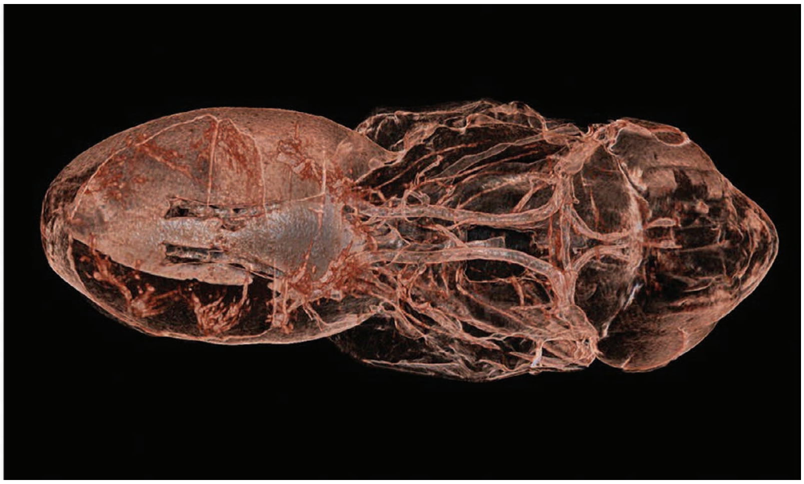

Figure 14.15 Fifteen-day-old blowfly pupae imaged live throughout pupation with micro-CT showing development of adult fly structures.

(Courtesy of G Clark, Department of Engineering, University of Leicester.)

landmarks were determined for *C. vicina* which allowed for age estimations with a 10% temporal resolution from 0% to 90% of the total intra-puparial period. They determined that with current resolution, age-diagnostic qualitative characters could be determined for most 10% time intervals of the intra-puparial period and that this could potentially be applied to other blowfly species such as *L. sericata*. The use of quantitative analysis of organ development was also discussed. They advised that neither qualitative nor quantitative analysis could be undertaken between the 90% and 100% stages and that special caution must be taken within the 50–60% stages. Overall, they concluded that the study highlighted micro-CT as a promising accurate and reliable age estimation system for blowfly during their intra-puparial period.

Another application of micro-CT for estimation of the post-mortem interval was reported by Longato et al. [72]. They analysed the bone density of three archaeological and three recent forensic bone samples using micro-CT showing that the samples with a short post-mortem interval had a higher bone density compared to those with a long post-mortem interval.

Le Garff et al. have published two studies concerning early post-mortem changes of human bone taphonomy studied with micro-CT [73,74]. In the first study, they extracted four bone samples from fresh human cranial vault and imaged them every week for 1 month. After 1 month the mean bone volume, bone surface and trabecular number deceased, whereas the mean trabecular separation and trabecular thickness increased, although due to the sample size no statistical results or real trends were reported. In the second study, ten human adult cranium bone samples were imaged every 2 weeks for 10 weeks. There was a statistical increase in the trabeculae separation along with a decrease in the ratio of the bone surface and bone volume in the first two weeks (Figure 14.16).

A machine learning approach has been used with micro-CT by Schmidt et al. [75]. In their analysis of 104 human skeletal remains with post-mortem intervals of between one day to 2000 years, they identified that the Cort Porosity increased with time and that the bone volume density (bone volume over the total volume) decreased over the

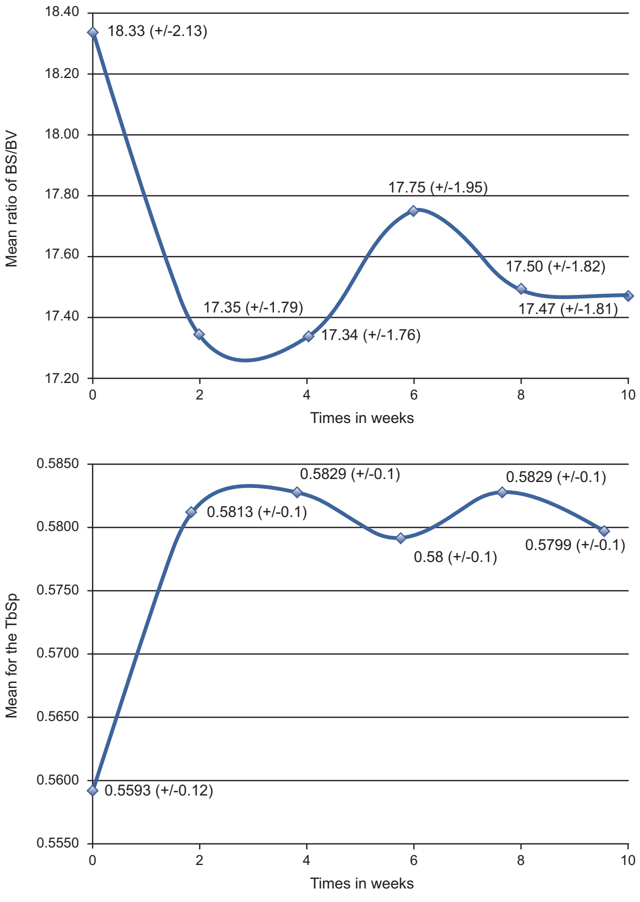

Figure 14.16 (a) mean ratio (+/– SD) of the bone surface/bone volume over time. (b) Mean trabeculae separation (+/– SD) over time.

(From Le Graff E, Mesli V, Marchand E, Behal H, Demondion X, Becart A, Hedouin V. Is bone analysis with µCT useful for short postmortem interval estimation? *Int J Leg Med* 2018; 1342: 269–277.)

years. The artificial neural network classification results of this study distinguished between forensic and archaeological samples but also between forensic bone samples of different PMI.

Micro-CT was used to investigate tooth enamel-cement thickness, abrasion and mineral density by Akbulut et al. [76]. Imaging the mandibles of 60 sacrificed female Wistar rats separated into 6 groups each containing 10 rats with a PMI of between 0 hours and 90 days, they reported that the enamel abrasion values combined with the findings of decreased enamel mineral density could be used for the determination of the PMI. However, further study was suggested to take into account the effect of environmental conditions.

14.6 Summary

Promising advances have been made in an attempt to develop a cross-sectional radiology imaging method to estimate the PMI. Of those that have been attempted, the most promising to date appear to be related to the use of PMCT and the consideration of the radiodensity changes that occur to the cerebrospinal fluid, brain parenchyma and VH as well as the time-based accumulation of fluid within the airways. As with other methods of estimating a PMI, no single radiological method can currently be used on its own to achieve this objective. However, a combination of PMCT assessments in conjunction with other available non-radiological assessment methods may assist the practitioner in estimating a time since death.

References

1. Eckert WG, Garland N. The history of the forensic application in radiology. *Am J Forensic Med Pathol* 1984; 5: 53–6.
2. Kranz P, Holtas S. Postmortem computed tomography in a diving fatality. *J Comput Assist Tomogr* 1983; 7: 132–4.
3. Donchin Y, Rivkind AI, Bar-Ziv J, Hiss J, Almog J, Drescher M. Utility of postmortem computed tomography in trauma victims. *J Trauma* 1994; 37: 552–5; discussion 555–6.
4. Brookes JA, Hall-Craggs MA, Sams VR, Lees WR. Non-invasive perinatal necroscopy by magnetic resonance imaging. *Lancet* 1996; 348 (9035): 1139–41.
5. Rutty GN, Brogdon G, Dedouit F, Grabherr S, Hatch GM, Jackowski C, Leth P, Persson A, Ruder TD, Shiotani S, Takahashi N, Thali MJ, Woźniak K, Yen K, Morgan B. Terminology used in publications for post-mortem cross-sectional imaging. *Int J Legal Med* 2013; 127: 465–6.
6. Andrews S. Postmortem changes as documented in postmortem computed tomography scans. *Acad Forensic Pathol* 2016; 6: 63–76.
7. Ishida M, Gonoi W, Okuma H, Shirota G, Shintani Y, Abe H, Takazawa Y, Fukayama M, Ohtomo K. Common postmortem computed tomography findings following atraumatic death: differentiation between normal postmortem changes and pathologic lesions. *Korean J Radiol* 2015; 16: 798–809.
8. Klein WM, Bosboom DG, Koopmanschap DH, Nievelstein RAJ, Nikkels PGJ, van Rijn R. Normal pediatric postmortem appearances. *Pediatr Radiol* 2015; 45: 517–26.
9. Levy AD, Harke HT, Mallak CT. Postmortem imaging. MBCT features of post-mortem change and decomposition. *Am J Forensic Med Pathol* 2010; 31: 12–17.
10. Okuma H, Gonoi W, Ishida M, Shirota G, Shitani Y, Abe H, Fukayama M, Ohtomo K. Comparison of attenuation of striated muscle between postmortem and antemortem computed tomography: results of a longitudinal study. *PLoS ONE* 2014; 9: e111457.
11. Shiotani S, Kohno M, Ohashi N, Yamazaki K, Itai Y. Postmortem intravascular high-density fluid level (hypostasis): CT findings. *J Comput Assist Tomogr* 2002; 26: 892–3.
12. Takahashi N, Satou C, Higuchi T, Shiotani M, Maeda H, Hirose Y. Quantitative analysis of intracranial hypostasis: comparison of early postmortem and antemortem CT findings. *AJR Am J Roentgenol* 2010; 195: W388–93.
13. Jackowski C, Thali M, Aghayev E, Yen K, Sonnenschein M, Zwygart K, Dirnhofer R, Vock P. Postmortem imaging of blood and its characteristics using MSCT and MRI. *Int J Legal Med* 2006; 120: 233–40.
14. Ishida M, Gonoi W, Hagiwara K, Takazawa Y, Akahane M, Fukayama M, Ohtomo K. Hypostasis in the heart and great vessels of non-traumatic in-hospital death cases on postmortem computed tomography: relationship to antemortem blood tests. *Leg Med (Tokyo)* 2011; 13: 280–5.
15. Shiotani S, Kobayashi T, Hayakaw H, Kikuchi K, Kohno M. Postmortem pulmonary edema: a comparison between immediate and delayed postmortem computed tomography. *Leg Med* 2011; 13: 151–5.
16. Germerott T, Preiss US, Ebert LC, Ruder TD, Ross S, Flach PM, Ampanozi G, Filograna L, Thali MJ. A new approach in virtopsy: postmortem ventilation in multislice computed tomography. *Leg Med (Tokyo)* 2010; 12: 276–9.
17. Rutty GN, Biggs MJ, Brough A, Robinson C, Mistry R, Amoroso J, Deshpande A, Morgan B. Ventilated post-mortem computed tomography through the use of a definitive airway. *Int J Legal Med* 2015; 129: 325–34.
18. Ishida M, Gonoi W, Hagiwara K, Okuma H, Shitani Y, Abe H, Takazawa Y, Ohtomo K, Fukayama M. Fluid in the airways of nontraumatic death on postmortem computed tomography. *Am J Forensic Med Pathol* 2014; 35: 113–17.
19. Hyodoh H, Shimizu J, Watanabe S, Okazaki S, Mizuo K, Inoue H. Time-related course of pleural space fluid collection and pulmonary aeration on postmortem computed tomography (PMCT). *Leg Med* 2015; 17: 221–5.
20. Okumura M, Usumoto Y, Tsuji A, Kudo K, Ikeda N. Analysis of postmortem changes in internal organs and gases using computed tomography data. *Leg Med* 2017; 25: 11–15.
21. Fisher F, Grimm J, Kirchhoff C, Reiser MF, Graw M, Kirchhoff S. Postmortem 24-h interval computed tomography findings on intrahepatic gas development and changes of liver parenchyma radiopacity. *Forensic Sci Int* 2012; 214: 118–23.
22. Shiotani S, Kohno M, Ohashi N, Yamazaki K, Nakayama H, Ito Y, Kaga K, Ebashi T, Itai Y. Hyperattenuating aortic wall on postmortem computed tomography (PMCT). *Radiat Med* 2002; 20: 201–6.
23. Takahashi N, Higuchi T, Hirose Y, Yamanouchi H, Takatsuka H, Funayama K. Changes in aortic shape and diameters after death: comparison of early postmortem computed tomography

with antemortem computed tomography. *Forensic Sci Int* 2013; 225: 27–31.

24. Ishikawa N, Nishida A, Miyamori D, Kubo T, Ikegaya H. Estimation of postmortem time based on aorta narrowing in CT imaging. *J Forensic Leg Med* 2013; 20: 1075–7.
25. Keil W, Bretschneider K, Patzelt D, Behning I, Lignitz E, Matz J. Air embolism or putrefaction gas? The diagnosis of cardiac air embolism in the cadaver. *Beitr Gerichtl Med* 1980; 38: 395–408.
26. Sakata M, Miki A, Kazama H, Morita M, Yasoshima S. Studies on the composition of gases in the post-mortem body: animal experiments and two autopsy cases. *Forensic Sci Int* 1980; 15: 19–29.
27. Thali MJ, Yen K, Schweitzer W, Vock P, Ozdoba C, Dirnhofer R. Into the decomposed body-forensic digital autopsy using multislice-computed tomography. *Forensic Sci Int* 2003; 134: 109–14.
28. Jackowski C, Sonnenschein M, Thali MJ, Aghayev E, Yen K, Dirnhofer R, Vock P. Intrahepatic gas at postmortem computed tomography: forensic experience as a potential guide for in vivo trauma imaging. *J Trauma* 2007; 62: 979–88.
29. Ishida M, Gonoi W, Hagiwara K, Takazawa Y, Akahane M, Fukayama M, Ohtomo K. Intravascular gas distribution in the upper abdomen of non-traumatic in-hospital death cases on postmortem computed tomography. *Leg Med (Tokyo)* 2011; 13: 174–9.
30. Shiotani S, Kohno M, Ohashi N, Atake S, Yamazaki K, Nakayama H. Cardiovascular gas on non-traumatic postmortem computed tomography (PMCT): the influence of cardiopulmonary resuscitation. *Radiat Med* 2005; 23: 225–9.
31. Fischer F, Grimm J, Kirchhoff C, Reiser MF, Graw M, Kirchhoff S. Postmortem 24-h interval computed tomography findings on intrahepatic gas development and changes of liver parenchyma radiopacity. *Forensic Sci Int* 2012; 214: 118–23.
32. Shiotani S, Kohno M, Ohashi N, Yamazaki K, Nakayama H, Watanabe K. Postmortem computed tomographic (PMCT) demonstration of the relation between gastrointestinal (GI) distension and hepatic portal venous gas (HPVG). *Radiat Med* 2004; 22: 25–9.
33. Asamura H, Ito M, Takayanagi K, Kobayashi K, Ota M, Fukushima H. Hepatic portal venous gas on postmortem CT scan. *Leg Med (Tokyo)* 2005; 7: 326–30.
34. Yamazaki K, Shiotani S, Ohashi N, Doi M, Honda K. Hepatic portal venous gas and hyper-dense aortic wall as postmortem computed tomography finding. *Leg Med (Tokyo)*. 2003; 5(Suppl 1): S338–41.
35. Yokota H, Yamamoto S, Horikoshi T, Shimofusa R, Ito H. What is the origin of intravascular gas on postmortem computed tomography? *Leg Med (Tokyo)* 2009; 11(Suppl 1): S252–5.
36. Egger C, Bize P, Vaucher P, Mosimann P, Schneider B, Dominguez A, Meuli R, Mangin P, Grabherr S. Distribution of artifactual gas on post-mortem multidetector computed tomography (MDCT). *Int J Legal Med*. 2012; 126: 3–12.
37. Singh MK, O'Donnell C, Woodford NW. Progressive gas formation in a deceased person during mortuary storage demonstrated on computed tomography. *Forensic Sci Med Pathol* 2009; 5: 236–42.
38. Iwamoto C, Ohuchida K, Okumura M, Usumoto Y, Kishimoto J, Murata M, Ikeda N, Hashizume M. Postmortem interval estimation using the animal model of postmortem gas volume changes. *Leg Med* 2018; 32: 66–70.
39. Ishida M, Gonoi W, Hagiwara K, Takazawa Y, Akahane M, Fukayama M, Ohtomo K. Postmortem changes of the thyroid on computed tomography. *Leg Med* 2011; 13: 318–22.
40. Ishida M, Gonoi W, Hagiwara K, Okuma H, Shirota G, Shintani Y, Abe H, Takazawa Y, Fukayama M, Ohtomo K. Early postmortem volume reduction of adrenal gland: initial longitudinal computer tomographic study. *Radiol Med* 2015; 120: 662–9.
41. Bayat A, Koopmanschap D, Klein WM. Postmortem interval: value of post-mortem cerebral CT. *J Forensic Radiol Imaging* 2014; 2: 98.
42. Hasegawa I, Shimizu A, Saito A, Suzuki H, Vogel H, Puschel K, Heinemann A. Evaluation of post-mortem lateral cerebral ventricle changes using sequential scans during post-mortem computed tomography. *Int J Leg Med* 2016; 130: 1323–8.
43. Koopmanschap DHKLM, Bayat AR, Kubat B, de Bakker HM, Prokop MWM, Klein WM. The radiodensity of cerebrospinal fluid and vitreous humor as indicator of the time since death. *Forensic Sci Med Pathol* 2016; 12: 248–56.
44. Morikawa K, Hyodoh H, Matoba K, Mizuo K, Okazaki S, Watanabe S. Time-related change evaluation of the cerebrospinal fluid using postmortem CT. *Leg Med* 2016; 22: 30–5.
45. De-Giorgio F, Ciasca G, Fecondo G, Mazzini A, De Spirito M, Pascali VL. Estimation of the timeof death by measuring the variation of lateral cerebral ventricle volume and cerebrospinal fluid radiodensity using postmortem computed tomography. *Int J Leg Med* 2021; 135: 2615–23.
46. Ramanaidu V, Mustapha AWMM, Noor MHM, Abdullah N. Estimation of time of death using brain attenuation parenchyma attenuation in post mortem computed tomography of brain—In Malaysian setting. *Forensic Imaging* 2021; 26: 200470.
47. Kobayashi T, Shiotani S, Kaga K, Saito H, Saotome K, Miyamotot K, Kohno M, Kikuchi K, Hayakawa H, Homma K. Characteristic signal intensity changes on postmortem magnetic resonance imaging of th e brain. *Jpn J Radiol* 2010; 28: 8–14.
48. Tashiro K, Shiotani S, Kobayashi T, Kaga K, Saito H, Someya S, Miyamoto K, Hayakawa H. Cerebral relaxation times from postmortem MR imaging of adults. *Magn Reason Med Scio* 2015; 14: 51–6.
49. Shiotani S, Kobayashi T, Hayakawa H, Homma K, Sakahara H. Hepatic relaxation times from postmortem MR imaging of adult humans. *Magn Reason Med Sci* 2016; 15: 281–7.
50. Wagensveld IM, Blokker BM, Wielopolski PA, Renken NS, Krestin GP, Hunink MG, Oosterhuis JW, Wewustink AC. Total-body CT and MR features of postmortem change in in-hospital deaths. *PLoS ONE* 2017; 12: e0185115.
51. Tumanova UN, Bychenko VB, Serova NS, Shchegolev AI. Postmortem MRI characterization of cadaveric hypostases in deceased newborns. *Bulletin Exp Biol Med* 2021; 170: 371–7.
52. Kellers S, Schmidt TM, Kim AC, Fischer R, Heinmann A, Adam G, Yamamura J. Postmortem MR diffusion-weighted imaging of the liver: time-behaviour of the hepatic apparent diffusion coefficient in the early death interval. *Int J Leg Med* 2018; 132: 263–8.
53. Arthurs OJ, Price GC, Carmichael DW, Jones R, Norman W, Taylor AM, Sebire NJ. Diffuse-weighted perinatal postmortem magnetic resonance imaging as a marker of postmortem interval. *Eur Radiol* 2015; 25: 1399–406.
54. Shelmerdine SCX, Main C, Hutchinson JC, Langan D, Sebire NJ, Arthurs OJ. The use of whole body diffusion-weighted post-mortem magnetic resonance imaging in timing perinatal deaths. *Int J Leg Med* 2018; 1432: 1735–41.

55. Barber JL, Hutchinson JVC, Sebire NJ, Arthurs OJ. Pleural fluid accumulation detectable on paediatric post-mortem imaging: a possible marker of internal since death? *In J Leg Med* 2016; 130: 1003–10.
56. Ith M, Bigler P, Scheurer E, Kreis R, Hofmann L, Dirnhofer R, Boesch C. Observation and identification of metabolites emerging during postmortem decomposition of brain tissue by means of in situ 1H-magnetic resonance spectroscopy. *Magn Reson Med* 2002; 48: 915–20.
57. Banaschak S, Rzanny R, Reichenbach JR, Kaiser WA, Klein A. Estimation of postmortem metabolic changes in porcine brain tissue using 1H-MR spectroscopy—preliminary results. *Int J Legal Med* 2005; 119: 77–9.
58. Scheurer E, Ith M, Dietrich D, Kreis R, Hüsler J, Dirnhofer R, Boesch C. Statistical evaluation of time-dependent metabolite concentrations: estimation of post-mortem intervals based on in situ 1H-MRS of the brain. *NMR Biomed* 2005; 18: 163–72.
59. Ith M, Scheurer E, Kreis R, Thali M, Dirnhofer R, Boesch C. Estimation of the postmortem interval by means of ^{1}H MRS of decomposing brain tissue: influence of ambient temperature. *NMR Biomed* 2011; 24: 791–8.
60. Musshoff F, Klotzbach H, Block W, Traeber F, Schild H, Madea B. Comparison of post-mortem metabolic changes in sheep brain tissue in isolated heads and whole animals using 1H-MR spectroscopy—preliminary results. *Int J Legal Med*. 2011; 125: 741–4.
61. Schmidt TM, Wang ZJ, Keller S, Heinmann A, Acar S, Graessner J, Schoennagel BP, Adam G, Fischer R, Yamamura J. Postmortem ^{31}P magnetic resonance spectroscopy of the skeletal muscle: α-ATP/Pi ratio as a forensic tool? *Forensic Sci Int* 2014; 242: 172–6.
62. Rutty GN, Brough A, Biggs MJ, Robinson C, Lawes SD, Hainsworth SV. The role of micro-computed tomography in forensic investigations. *Forensic Sci Int* 2013; 225: 60–6.
63. Hainsworth SV. The use of micro–computed tomography for forensic applications. In *Essentials of Autopsy Practice. Updates and Reviews to Aid Practice*, Vol 9. Ed. Rutty GN, Springer, London, 2022 (in press).
64. Richards CS, Simonsen TJ, Abel RL, Hall MJ, Schwyn DA, Wicklein M. Virtual forensic entomology: improving estimates of minimum post-mortem interval with 3D micro-computed tomography. *Forensic Sci Int* 2012; 220: 251–64.
65. Greenberg B. Flies as forensic indicators. *J Med Entomol* 1991; 28: 565–77.
66. Catts EP. Problems in estimating the post-mortem interval in death investigations. *J Agric Entomol* 1992; 9: 245–55.
67. Richards CS, Villet MH. Data quality in thermal summation development models for forensically important blowflies. *Med Vet Entomol* 2009; 23: 269–76.
68. Sukontason KL, Kanchai C, Piangjai S, Boonsriwong W, Bunchu N, Sripakdee D, Chaiwong T, Kuntalue B, Siriwattanarungsee S, Sukontason K. Morphological observation of puparia of Chrysomya nigripes (Diptera: Calliphoridae) from human corpse. *Forensic Sci Int*. 2006; 161: 15–19.
69. Levy M, Bautz AM. Degeneration of larval salivary glands during metamorphosis of the blowfly, Calliphora erythrocephala meigen (Diptera: Calliphoridae). *Int J Insect Morphol Embryol* 1985; 14: 281–90.
70. Friedrich F, Beutel RG. Micro-computed tomography and a renaissance of insect morphology. In S.R. Stock (Ed.), Developments in X-ray tomography VI. *Proc SPIE* 2008; 7078.
71. Martin-Vega D, Simonsen TJ, Wicklein M, Hall MJR. Age estimation during the blow fly intra-puparial period: a qualitative and quantitative approach using micro-computed tomography. *Int J Leg Med* 2017; 131: 1429–48.
72. Longato S, Woss C, Hatzer-Grubwieser P, Bauer C, Parson W, Unterberger SH, Kuhn V, Pemberger N, Pallua AK, Recheis W, Lackner R, Stadler R, Pallua JD. Post-mortem interval estimation of human skeletal remains by micro-computed tomography, mid-infrared microscopy imaging and energy dispersive X-ray. *Anal Methods* 2015; 7: 2917–27.
73. Le Graff E, Mesli V, Delannoy Y, Colard T, Demondion X, Becart A, Hedouin V. Technical note: early post-mortem changes of human bone in taphonomy with μCT. *Int J Leg Med* 2017; 131: 761–70.
74. Le Graff E, Mesli V, Marchand E, Behal H, Demondion X, Becart A, Hedouin V. Is bone analysis with μCT useful for short postmortem interval estimation? *Int J Leg Med* 2018; 1342: 269–77.
75. Schmidt V-M, Zelger P, Woess C, Pallua AK, Arora R, Degenhatt G, Brunner A, Zelger B, Schirmer M, Rabl W, Pallua JD. Application of micro-computed tomography for the estimation of the post-mortem interval of human skeletal remains. *Biology* 2022; 11: 1105.
76. Akbulut N, Cetin S, Bilecenoglu B, Altan A, Akbulut S, Ocak M, Orhan K. The micro-CT evaluation of enamel-cement thickness, abrasion, and mineral density of teeth in the post-mortem interval (PMI): new parameters for determination of PMI. *Int J Leg Med* 2020; 134: 645–53.

15 Drug Testing in Hair for the Estimation of the Time Since Death

Christopher Wiedfeld and Frank Musshoff

Besides conventional matrices such as blood, urine, or gastric content, hair has become a valuable material for postmortem toxicological analyses.[1] Hair strands are fiber-like structures consisting of keratinized cells within a cell membrane complex forming three layers: the inner medulla, the cortex that is responsible for the strain resistance and color, and the outer cuticle protecting the hair against environmental influences.[2]

Originating from particular follicles located within the skin, hair grows in cycles consisting of three phases: the anagen phase, in which the hair grows consistently up to several years; the catagen or transition phase (1–2 weeks), in which the growth stops; and the final telogen phase, in which the dead hair still plugs within the skin up to six months before it falls out.[2] Within the anagen phase, the hair grows with a rate of approximately 1 cm/month (between 0.6 and 1.4 cm/month). During this period xenobiotics can enter the growing hair cells from the blood by passive diffusion. Further incorporation occurs by diffusion from sweat and sebum also depending on the physicochemical properties of the substances making the process of drug incorporation rather complex.[2]-

Nonetheless, a high number of ingested exogeneous substances such as illicit drugs or pharmaceuticals can be detected by hair analysis, making it a useful tool for getting long-term information about the individual's drug use history before death.[1] By applying segmental analysis, for example, in sections of 1 cm, changes in the course of drug use can be revealed for the past months.

Furthermore, hair is a very stable matrix toward decomposition, especially under dry conditions. In cases of a long time interval since death, bones, teeth, and hair are often the only material left due to advanced putrefaction. Positive findings for benzoylecgonine or nicotine in hair of pre-Columbian mummies[3,4] and detection of cocaine or even ethylglucuronide in hair of mummies from the last centuries[5,6] impressively showed the power of hair analysis even after hundreds or thousands of years after death.

In postmortem cases, hair analysis can be applied to find answers to various issues[1]:

1. If high blood concentrations of drugs such as opiates or opioids are found that may be in a toxic range for opioid naive individuals, hair analysis can reveal if a previous chronic consumption with a respective development of tolerance took place or not.
2. If xenobiotics are found in blood or urine that are not known having been prescribed to the individual, hair analysis might confirm previous ingestions or prove abstinence.
3. In cases of unknown identity, potential long-term medication can be determined by hair analysis—might give hints if the individual was, for example, in psychiatric treatment, substitution program, or even a recreational drug user.[7,8]

Nonetheless, due to potential contamination by body fluids like sweat (especially during agony) or putrefaction fluid also causing diffusion of analytes into the hair, positive results must be interpreted with caution.[9] Thorough decontamination steps are mandatory to reduce interferences due to such external contamination. Furthermore, segmentation of the hair strand as well as comparison of the analyte concentration within the decontamination solvent versus the respective hair segment can help to estimate the extend of these influences but cannot completely defeat the problem.[9]

Due to continual improvement in analytical sensitivity, micro-segmental single hair analysis has become a relevant topic in modern forensic toxicology.[10] In contrast to routine methods not a hair strand, consisting of a bunch of hairs, is segmented and analyzed, but multiple single hairs. Hereby, most of the adverse effects restricting the temporal resolution of routine segmental analysis like misalignment of hairs, different growth rates and growth states, as well as a practicable segment length of at least 0.5–1 cm can be considered and a smaller segmentation is useful.[11] Hence, a much higher temporal resolution is achieved capable of resolving individual single intakes of a substance in such a way that also temporal back-calculation of the time of consumption is possible.[12] By analyzing a single hair in micro segments, an individual concentration profile is achieved. A single intake of a substance will likely result in a concentration peak in the time-corresponding section of the hair. By analyzing multiple hairs (n = 10) due to statistical reasons, telogen and very fast or slow growing hairs can be identified and excluded. The section with most overlapping peak maxima will indicate the timepoint of substance application.[13]

Several methods have been published yet covering only single or selected analytes up to complex screenings for over 150 analytes.[13,14] The applied segmentation length ranges between several millimeters down to

DOI: 10.1201/9781003244974-15

sub-millimeter segments, thus allowing back-calculations to periods of several days down to a specific single day.[15,16]

Here is where single hair analysis becomes relevant for the estimation of the time since death. If the deceased has taken a substance on a certain time before death, it should have been resulted in a concentration peak in the hairs. As hair stops growing after death, the position of the concentration peak will correspond to the time elapsed between ingestion and death, and hence, the time since death can be estimated.

Following requirements are necessary for a successful application if the hair sample is taken in a conventional way by cutting close to the scalp:

1. The deceased has taken a substance suitable to detect by hair analysis on a certain time before death.
2. It must have been a single or at least short-term application (1–2 days) and the exact day(s) of ingestion must be known.
3. The time of application must not be earlier than at least 3–4 weeks before death and otherwise not too long ago (ideally not more than six months, due to possible wash-out effects and other influences).
4. The hair sample must be long enough to cover the time of ingestion.

Kuwayama et al.[17] impressively demonstrated the application of single hair analysis on a case of a decomposed but identified corpse for which time since death could only be estimated roughly at 2 weeks to 2 months by autopsy. Besides a low concentration of lidocaine detected in blood, an administration of lidocaine during a surgery 57 days before discovery of the corpse was known due to medical records. Consequently, three head hairs (sampled by plugging them out) were cleaned, segmented in pieces of 0.4 mm, and analyzed for lidocaine and its metabolite.

Two lidocaine positive hair sections (A and B) could be detected: one near the root section and the other one around 2–3 cm apart, meaning that lidocaine must have been ingested at least at two different points of time before death, of which only one time point was known. In this study each section consisted of a higher and lower concentration peak due to different routes of incorporation of lidocaine into the hair: one derived from incorporation within the bulb section via blood and the second one from the dermal section by incorporation via sweat or sebum (Figure 15.1).

Nonetheless, these effects can only be seen using a very narrow segmentation and might have resulted in only one concentration peak if broader segmentation would have been applied.[13,14] The positions of the two bigger (blood derived) peak maxima were determined at the third and 57th segment from root in hair number 1, for example. The mean distances in the three analyzed hairs corresponded to estimated time intervals of 2.1 ± 0.5 days and 52.9 ± 3.2 days after surgery by applying a hair growth rate of 0.4 mm/day (Figure 15.2).[17]

Due to these findings two assumptions were possible. If the distal concentration peak (region B) would have been derived from the surgery taking place 57 days before the finding, death would have occurred around 4 days before. This could be excluded due to the state of putrefaction. Consequently, time of death must have been around 2 days after the surgery, meaning around 55 days before finding,

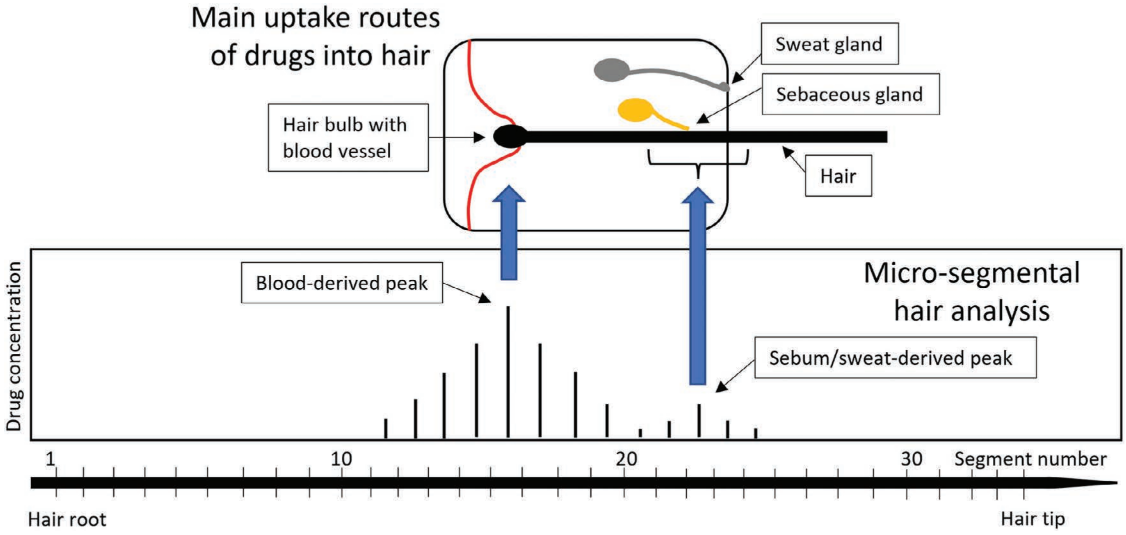

Figure 15.1 Sketch showing the main uptake routes of drugs into hair (upper part) and a corresponding schematic concentration profile obtained by micro-segmental hair analysis (lower part).

(Modified from Kuwayama et al.[17])

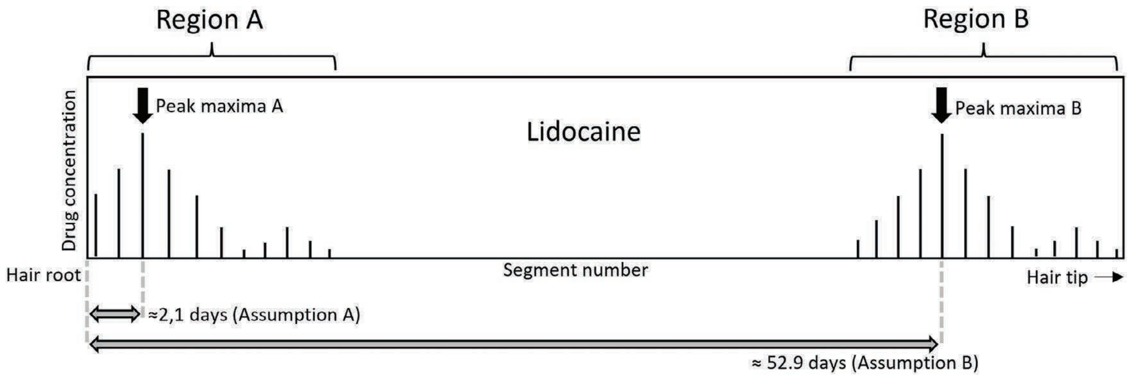

Figure 15.2 Schematic concentration profile of lidocaine in the three analyzed hairs with estimated mean time intervals after surgery. The arrows indicate the blood derived peak maxima.

(Modified from Kuwayama et al.[17])

which was in accordance with the results of autopsy and could also explain the low concentration of lidocaine detected in blood. In this case, there was no information about a further application of lidocaine several weeks before death, certainly responsible for the second peak (region B). Notably, the result of hair analysis would probably not have led to any conclusive result if hair had been sampled by cutting instead of plugging. With remark on the abovementioned requirements for a successful application of this method, plugging out some hairs as an additional sample material can be recommended.

In summary, micro-segmental single hair analysis is a powerful tool for retrospective evaluation of drug use history with a high temporal resolution. In special cases, it can also be utilized to estimate the time since death, although various requirements are necessary for a successful application. But if other forensic approaches fail to determine an exact time interval, this technique might be a promising tool.

References

1. Kintz P. Value of hair analysis in postmortem toxicology. *Forensic Sci Int*. 2004; 142:127–34. https://doi.org/10.1016/j.forsciint.2004.02.027
2. Pragst F, Balikova MA. State of the art in hair analysis for detection of drug and alcohol abuse. *Clin Chim Acta*. 2006; 370:17–49. https://doi.org/10.1016/j.cca.2006.02.019
3. Cartmell LW, Aufderhide A, Weems C. Cocaine metabolites in pre-Columbian mummy hair. *J Okla State Med Assoc*. 1991; 84:11–12.
4. Musshoff F, Rosendahl W, Madea B. Determination of nicotine in hair samples of pre-Columbian mummies. *Forensic Sci Int*. 2009; 185:84–8. https://doi.org/10.1016/j.forsciint.2008.12.016
5. Musshoff F, Brockmann C, Madea B, Rosendahl W, Piombino-Mascali D. Ethyl glucuronide findings in hair samples from the mummies of the Capuchin Catacombs of Palermo. *Forensic Sci Int*. 2013;232:213–17. https://doi.org/10.1016/j.forsciint.2013.07.026
6. Musshoff F, Fels H, Carli A, Piombino-Mascali D. The anatomical mummies of Mombello: detection of cocaine, nicotine, and caffeine in the hair of psychiatric patients of the early 20th century. *Forensic Sci Int*. 2017; 270:20–4. https://doi.org/10.1016/j.forsciint.2016.11.011
7. Methling M, Krumbiegel F, Alameri A, Hartwig S, Parr MK, Tsokos M. Concentrations of antidepressants, antipsychotics, and benzodiazepines in hair samples from postmortem cases. *SN Compr Clin Med*. 2020; 2:284–300. https://doi.org/10.1007/s42399-020-00235-x
8. Couper FJ, McIntyre IM, Drummer OH. Detection of antidepressant and antipsychotic drugs in postmortem human scalp hair. *J Forensic Sci*. 1995; 40:87–90.
9. Kintz P. Segmental hair analysis can demonstrate external contamination in postmortem cases. *Forensic Sci Int*. 2012; 215(1–3):73–6. https://doi.org/10.1016/j.forsciint.2011.01.041
10. Allibe N, Kintz P, Faure A, Paysant F, Michard-Lenoir A-P, Stanke-Labesque F, et al. Interest of single hair analysis to document drug exposure: literature review and a case report involving Zuclopenthixol. *Curr Pharm Des*. 2017; 23:5502–10. https://doi.org/10.2174/1381612823666170622100443
11. Thieme D, Baumer C, Sachs H, Teske J. Screening and long-term retrospection for psychoactive drugs in presumptive drug-facilitated crimes using segmented single hairs. *Drug Test Anal*. 2013; 5:736–40. https://doi.org/10.1002/dta.1502
12. Wiedfeld C, Skopp G, Kuepper U, Musshoff F. Application of single hair analysis reveals multiple administration of a drug mixture in a case of drug-facilitated sexual assault of a child. *Drug Test Anal*. 2021; 13(8):1580–4. https://doi.org/10.1002/dta.3057
13. Wiedfeld C, Skopp G, Musshoff F. Single hair analysis: validation of a screening method for over 150 analytes and application on documented single-dose cases. *Drug Test Anal*. 2021; 13(4):817–32. https://doi.org/10.1002/dta.2997
14. Shima N, Sasaki K, Kamata T, Matsuta S, Wada M, Kakehashi H, et al. Incorporation of zolpidem into hair and its distribution after a single administration. *Drug Metab Dispos*. 2017; 45:286–93. https://doi.org/10.1124/dmd.116.074211
15. Kuwayama K, Nariai M, Miyaguchi H, Iwata YT, Kanamori T, Tsujikawa K, et al. Micro-segmental hair analysis for

proving drug-facilitated crimes: evidence that a victim ingested a sleeping aid, diphenhydramine, on a specific day. *Forensic Sci Int*. 2018; 288:23–8. https://doi.org/10.1016/j.forsciint.2018.04.027

16. Kuwayama K, Nariai M, Miyaguchi H, Iwata YT, Kanamori T, Tsujikawa K, et al. Accurate estimation of drug intake day by microsegmental analysis of a strand of hair by use of internal temporal markers. *J App Lab Med*. 2018; 3:37–47. https://doi.org/10.1373/jalm.2017.025346
17. Kuwayama K, Nariai M, Miyaguchi H, Iwata YT, Kanamori T, Tsujikawa K, et al. Estimation of day of death using micro-segmental hair analysis based on drug use history: a case of lidocaine use as a marker. *Int J Leg Med*. 2019; 133:117–22. https://doi.org/10.1007/s00414-018-1939-9

Index

Note: Page numbers in *italics* indicate figures; page numbers in **bold** indicate tables.

A

accelerator mass spectrometer (AMS), 345, *346*, **348**
accumulated degree days (ADDs)
  postmortem interval from decomposed human remains, 194–196
  predicting post-mortem submersion interval for human remains, 196–200
acetate
  metabolic decomposition, *262*
  parameterized model functions, **262**
  proton magnetic resonance spectroscopy, *263*
adenosine triphosphate (ATP), 26, 52
adipocere, term, 194
age (decedent)
  influence on potassium levels, 230–231, *231*
  multivariate model of estimation of time of death, 231–232
  potassium levels with, and temperature, 229–232
alanine
  metabolic decomposition, *262*
  parameterized model functions, **262**
  proton magnetic resonance spectroscopy, *263*
ambient temperature
  evaluation of mean, 118, *119*, 120–121
  three-step procedure for, *120*
American Academy of Forensic Sciences, 169
amino acid concentrations, *see also* H^3-magnetic resonance spectroscopy
  brain, 259–260, 262–264
  post-mortem interval (PMI) and Daldrup formula, *260*
  proton magnetic resonance spectroscopy (^{1}H-MRS), *261*
  reactions of glutamic acid (GLU) during brain decomposition, *260*
animal predation, 192
animals, cadaveric experimental data, 168–169
Aschoff, Ludwig, 298
Asian mummy (Germany), radiocarbon dating, 351, *352*
asphyxia, 11
Atlas of Forensic Medicine (Hofmann), 21
auditory canal, *see* external auditory canal (EAC)
autolysis, definition, 189
autopsy
  gastric contents, 305–306
  police investigation after, 306–307

B

bacterial community, decomposition, *290*
barium sulphate, post-mortem gastric transport, 297, *297*, *298*
Baumann's Cave, radiocarbon dating of cave bears, 348–349, *349*
Benzinger, M., 165
black body, 135
black box principle, 165
blanching, post-mortem, 74–75
blowfly, *see also* forensic entomology
  body infested with larvae, *335*
  development, 336, *336*, *337*
  fifteen-day-old pupae, *367*
  larvae feeding on body, *339*
  micro-computed tomography, 366–367, *367*
bluebottle *Calliphora erythrocephala*, 22
body, *see also* protein degradation
  death time estimation from temperature of, **320**
  properties of tissues as target for protein-based PMI estimation, **275**
  reported post-mortem protein changes in organs/tissues, **270–273**
body compartments
  heat conductivity, **142**
  mass density, **142**
  number of elements, **141**
  specific heat capacity, **142**
  volume proportion, **141**
body cooling, 5, *see also* death time of cooling body; dummies; nomogram method
  accuracy of calculated time since death, 104–106
  basic conditions, 79–80
  clothed bodies, 92, **93**
  condition of lying on and covered by leaves, 101, **101**
  constant *B* (Newtonian cooling coefficient), 86, 88–92
  in constantly, slightly moving air, 92, **92**
  cooling dummy, 80, *80*
  corrective factors for naked/partly clothed bodies, **93**
  corrective factors of body weight, **112**, **113**
  death time calculation, 107, 112–113, 115
  estimation of constant *B* (Newtonian cooling coefficient), 86, 88
  finite element model, 140–146
  in flowing water, 94–95
  heat exchange to surroundings, 80–82
  heat flow measurements on body surfaces, 82, *83*, 84
  indirect estimation of *B* (standard conditions), 88–90
  individual value of plateau-related constant *A*, 101–103
  influence of supporting base on corrective factor, **112**
  instructive cases of field study, **108–111**
  investigations of bodies, 91–92
  investigations on dummies, 96–99
  mathematically modelling rectal cooling curve, 85–86
  modelling of, *87*, **88**
  physics of, 133–137
  principle of corrective factors of body weight, 91–92
  reconstruction, 129
  rectal temperature probe sites, 84–85
  in still air, 92, **93**
  in still water, 92, 94, **94**
  temperature at death, 103–104, *104*
  type of supporting base and influence of, 99, **99**, *100*, 101
  wet-through clothing/covering and wet body surface, **95**, 95–96
body cooling finite element model, 140–146
  body compartments, **141**, **142**
  boundary conditions, 143
  initial conditions of cooling process, 142–143, *143*
  initial temperature node sets in body, **142**
  mapping the cooling scenario, 140–141
  phases of body cooling, *144*, *145*, *146*
  reconstructing time since death, 143, 146
  thermodynamical properties of biological materials, 141–142
bog bodies, 194
Bog Dog from Burlage (Germany), radiocarbon dating, 351–352, *352*
Bonn Institute, 14
Boundary Element Method, 137
brain temperature
  investigating central, 129–130

  - method of inserting probe into centre of brain, *130*
  - rectal and, 130–131
  - time of death nomogram, *130*
- breaking effect, rigor mortis development, 63, *64*, 65
- Burman, Wilkie, 13
- butyrate
  - metabolic decomposition, *262*
  - metabolite, 260
  - parameterized model functions, **262**
  - proton magnetic resonance spectroscopy, *263*

C

- cadaver(s)
  - animal experimental data, 168–169
  - early human, experimental data, 167–168
  - preservation processes in, 192–194
  - RNA stability in organs, 284
- cadaveric rigidity, *see also* rigor mortis
  - description based on subjective examinations, 54
  - literature description of, 54–67
  - measure of, 58
  - proposed standardized measurements of, **58**
  - time course of, **55**
- cadaveric spasm, 19–20, 57
- calcitonin, 309
  - comparison of results, **312**
  - immunohistochemical detection of, **309**
  - thyroid gland tissue, *311*
- calcium, 211
  - box plots of concentration, *214*
  - concentration, *214*
  - frequency distribution of concentration, *214*
- calculated-real death time, standard deviation of, **106**
- calculated time since death
  - accuracy of, 104–106
  - nomogram method, 126–129
- calculus, 13
- *Calliphora erythrocephala*, 22
- *Calliphora vicina*, 339, 341, 366–367
- *Calliphora vomitoria*, 342
- Camps, Francis, 1, 303
- casework
  - arrangement of data, 316–317
  - chemical excitability of iris, 316, *316*
  - death time estimation from body temperature, **320**
  - death time estimation from electrical excitability, **320**
  - development of rigor, 313–314
  - electrical excitability for determining time since death, *319*
  - electrical excitability of skeletal muscle, 316, *316*
  - examples for non-temperature-based methods, **324–327**
  - experiences in, 318–319, 322–323
  - integration of methods, 313–323
  - lividity, 314
  - mechanical excitability of skeletal muscle, 315
  - PC program www.AMAsoft.de, *318*
  - principle of using special chart, *317*, 317–318
  - temperature-based nomogram, *319*
  - time-relevant criteria of methods, 313–316
- Casper, Johann Ludwig, 21, *21*
- Casper's rule, 21
- cave bears (Baumann), radiocarbon dating, 348–349, *349*
- Celcius, Anders, 9
- Centigrade scale, 9
- Centigrade system, 13
- central nervous system (CNS)
  - accelerating effect of, 57
  - influence on rigor mortis, 56–57
  - muscles and, in rigor mortis, 54
  - rigor mortis development, 65
- cerebrospinal fluid (CSF)
  - chemistry, 240–244
  - pH in post-mortem, *29*
  - potassium concentration, 240–242, *241*, *242*, *243*, 244
  - sodium concentration, 241, *241*
- Chatham General Hospital, 10
- chemical excitability, iris, **315**, 316, *316*
- child homicide case, gastric contents, 305
- chloride, 211
  - box plots of concentration, *213*
  - concentration, *213*
  - frequency distribution of concentration, *213*
- choline
  - metabolic decomposition, *262*
  - proton magnetic resonance spectroscopy, *263*
- circadian rhythm
  - clock genes, **288**
  - melatonin, 289
  - time of death estimation, 287–289
  - transcriptional feedback loops in biological clock, *288*
- *Clostridium sordelli*, 263
- Coates, Joseph, 11
- Coe, John, 22, *22*
- computed tomography, *see* post-mortem computed tomography (PMCT)
- conditional probability distribution (CPD)
  - assumptions and conditions, 330
  - case examples, 330–331
  - compiling the CPD interval, 330
  - death time estimation, 328–334
  - explaining math in court, 329
  - results, 331–334
- conduction, 133
- conductivity, 136
- conductivity matrix, 139
- convection, 133, 134
- convection coefficient *h*, 134
- convection heat transfer coefficient, 135
- Corday, Charlotte, 20
- core temperature (T_M), measured, 132
- corpses, temperature as factor in RNA degradation, 284
- court, explaining math in, 329
- creatinine, 211
  - box plots of, concentration, *215*
  - concentration, *215*
  - frequency distribution of concentration, *215*
  - internal standard, 212, **216**
- cross-sectional imaging, *see also* post-mortem computed tomography (PMCT)
  - ^{1}H and ^{31}P magnetic resonance spectroscopy, 365–366
  - micro-computed tomography, 366–368
  - post-mortem computed tomography (PMCT), 355–364
  - post-mortem magnetic resonance imaging, 365
- CSF, *see* cerebrospinal fluid (CSF)
- CT, *see* post-mortem computed tomography (PMCT)

D

- Davey, John, 9, 10
- David, Jacques Louis, 'Death of Marat' painting, 20, *20*
- death time determination
  - finite element method, 137–140
  - physical methods in temperature-based, 132–133
  - physics of body cooling, 133–137
  - solving heat equation, 137–140
- death time estimation
  - confirming precision of, 46, **46**
  - model curve, *133*
  - reference and control group, *46*
  - time since death as dependent variable, 45
- death time of cooling body, *see also* body cooling; nomogram method
  - calculations, 107, 112–113, 115
  - computation by Friedlander's computer program, *107*
  - dependence of corrective factors on body weight, **113**
  - empirical corrective factors of body weight, **112**
  - instructive cases of field study, **108–111**

  nomogram for reading, 113, *114*, 115, *115*, *116*
  PC program by C. Henssge, 112–113, *114*
  Schweitzer's free online program, 112, *113*
  supporting base influence on corrective factor, **112**
decomposition
  aquatic score and predicted ADDs and confidence intervals, **198**
  bodies recovered from water, 21, *22*
  categories and stages of, of head and neck, **195**
  categories and stages of, of limbs, **196**
  categories and stages of, of trunk, **195**
  characteristics of, **196**
  delayed, in zinc coffin, 194
  descriptive stages for, **197**
  descriptive stages observed in face, **197**
  descriptive stages observed in limbs, **198**
  descriptive stages observed in torso, **197**
  period up to skeletonization, 191–192
  saponification, 193–194, *194*
decompositional time tables, predicting post-mortem submersion interval for human remains, 196–200
degradation, *see* DNA degradation; protein degradation, post-mortem; RNA degradation
De Saram formula, 14
differential equation, heat transfer, 136–137
digestion, *see also* gastric contents
  state of, 295–296, 302–303
DNA degradation
  concurrency method, 283
  rate method, 283
  time since death and, 283–284
double-measurement method, 15
Dowler, Bennett, 10
drug testing in hair, estimation of time since death, 371–373
DuBois formula, 147
dummies, *see also* body cooling
  characteristics of cooling conditions, 96–99
  cooling, 80, *80*
  cooling curves of different-sized, *80*
  corrective factors on body weight, 96, *96*
  experimental arrangement for measurements, *82*
  experimental cooling curves of, *81*
  heat flow measurements on surfaces of, *83*
  heat flow on contact and non-contact surfaces of naked, 99, *100*
  individual value of plateau-related constant *A*, 102–103
  influence of supporting base on cooling of naked, **99**
  investigations, 96–99
  mean radius of cross section and virtual weight, *81*
  mean radius of cross section of different-sized, **81**
  overview of cooling, **156**

E

ear, *see also* external auditory canal
  anatomy of external, 163
Egyptian mummy (Switzerland), radiocarbon dating, 349–350, *350*
electrical excitability
  death time estimation from, **320**, **321**
  determining time since death, *319*
  eyelid, *38*
  eyes, **315**
  influence of cause of death on, 17
  longitudinal studies of, 40–47
  re-examination of, *39*
  regular loss of, 15
  self-constructed generator for examining, *38*
  skeletal muscle, **315**, 316, *316*
  skeletal muscles post-mortem, 39–40
electrical excitability of skeletal muscle
  development of, post-mortem in nineteenth century, **16**
  post-mortem experiments, *16*, *17*
electrocution, rigor mortis development, 61, 63, *64*
element transformation, 137, *137*
entomology, *see* forensic entomology
enzyme activity assays, post-mortem protein degradation, 268–269
enzyme-linked immunosorbent assay (ELISA), protein degradation, 268
error analysis, finite element (FE), 149–150
error propagation problem, 149
errors, estimating the time since death, 4–6
estimation of time of immersion, 245–246
  average monthly water temperature of River Rhine, *257*
  cases of recovered bodies, 252–253, **253**, **254**
  discussion, 254–256, 258
  evaluation of data of Reh, 251
  monthly distribution of recovered bodies, *252*
  recommended procedure for, 258
  Reh's table for, **246**, 253, 255–256
  rule of thumb, 245
  table to estimating minimum, 247–248, **248**, **249**, **250**, **251**
  water temperature and stages of putrefaction, 246–247
estimation of time since death, 1–3, *see also* gastric contents; prism method
  case material, 4
  circadian rhythm-based, 287–289
  design of study, 3–4
  drug testing in hair, 371–373
  errors in, 4–6
  gastric contents, 300, *301*
  grading of methods, **2**
  methods, 1–2
  objectives of, **2**
  rigor mortis intensity, 65–67
  vitreous humour hypoxanthine and temperature, 232–239
eukaryotic community, decomposition, *291*
evidence at court, time since death as, 6
excitation, parameters of, **37**
experimental data
  cadaveric animal, 168–169
  early human cadaveric, 167–168
  human cadaveric, 169–175
external auditory canal (EAC), 162–163, 177–178
  accuracy and systematic bias of atrial and temporal IR thermometers *vs.* metal probe, **173**
  anatomy of external ear, 163
  application in practice, 176–177
  Baccino's global formula, 174
  cadaveric animal experimental data, 168–169
  cooling slopes for rectum and EAC, *176*
  early human cadaveric experimental data, 167–168
  ear thermometry, 165–167
  human cadaveric experimental data, 169–175
  human thermoregulation, 163–165
  logarithmic-transformed curves for case subject and model, *172*
  plot of actual and estimated time since death, *177*, *178*
  plot of rectal and mean EAC temperatures, *171*
  post-mortem computed tomography, *164*
  post-mortem interval (PMI), 162–163, *174*
  research sample, **170**
  Rule of Thumb, 168, 170, 172
  variables influencing PMI calculation, 175–176
eye, *see also* vitreous potassium
  potassium values of 53

  cases of, *207*
  schematic presentation of mammalian, *202*
eye changes after death
  electrolyte concentrations in vitreous humor, 201–222
  hypoxanthine, *222*, 222–225
  internal standard of electrolyte homeostasis at moment of death, 209–210
  investigations on vitreous potassium, **203–205**
  literature review on vitreous potassium, 202, 206
  loss of selective membrane permeability, 201–202
eye temperature
  application in practice, 185–186
  limitations of method, 185
  method of inserting thermometer probe, *182*
  method of temperature measurement, 181–183
  post-mortem cooling process, *182*
  results of 30 bodies, **184**
  time since death (TSD) calculations, **184**
  time since death and, 181

F

Fahrenheit, Gabriel, 9
Fahrenheit scale, 9, 13
fatty pads, retardation of cooling, 15
FEM-Preprocessor MENTAT, 140
Fettwachs (fat wax), 194
fever, temperature at death, 104, *104*, **105**
fever at death, nomogram method, 125
Fick's first law of diffusion, 201
Finite Difference Scheme, 137
finite element, 138
finite element method
  element transformation, *137*
  solving heat equation, 137–140
  two-dimensional ellipsoid, *137*
finite element model (FEM)
  application examples, 150–151
  body cooling, 140–146
  comparison to Marshall and Hoare model, 147, *148*
  comparison to real body cooling, 147–149
  error analysis, 149–150
  FEM heat equation, 139
  geometry of cooling scenario, 140–141
  implementation, 140
  model validation, 146–149
  thermodynamic properties of biological materials, 141–142
First Temp® Genius™ Tympanic Thermometer, 168, 176
flow regimes, 134
fluid, 134
forced convection, 134
force transducer
  in corpore insertion of, *42*
  schematic presentation of, *41*
forensic entomology, 335
  blowfly development, 336, *337*
  case reports, 339–342
  dismembered body, 340–341
  estimation of post-mortem interval (PMI), 336–338
  identification of insects, 335–336
  sampling insects from bodies, 339, *339*
  skeleton in forest, 340, *340*
  succession, 338–339
  suicide, 339–340
  temperature influence, 336
  winter suicide indoors, 341–342
  winter suicide outdoors, 342, *342*
forensic mythology, 11
forensic pathology, electrical excitability, *39*
Forensic Pathology (Knight), 167
Forty Years of Murder (Simpson), 21
free trimethylamine
  metabolic decomposition, *262*
  proton magnetic resonance spectroscopy, *263*
free trimethylammonium (fTMA)
  metabolite, 260
  parameterized model functions, **262**
Friedlander, Ed, computer program, *107*
FRR (Freiburger Rigor Index), 58
Funk, John, 303, 304

G

Galvani, Luigi, 15
gastric contents
  autopsy, 305–306
  barium sulphate, 297, *297*, *298*
  case history of Truscott, 303–304
  case studies, 304–307
  child homicide case, 305
  dependence of antemortem transport on survival time, **296**
  dual radionuclide methods for solid and liquid emptying, **298**
  estimation of time of death from, 300, *301*
  gastric emptying pattern, 298–300, **299**, *300*
  observation of stomach and small bowel, **296**
  police investigation after autopsy, 306–307
  post-mortem transport of, 296–298
  practical procedure, 302
  prostigmine and post-mortem transport, 297, **297**
  radiological control of gastric transport, 297, **297**
  sieve tower analysis of, *302*
  solid phase of, *302*
  state of digestion, 295–296, 302–303
Gene Meter approach, PMI estimation, 286
geometry, mapping the cooling scenario, 140–141
Gerber, Sam, 303
Glasgow Royal Infirmary, 11
glucagon
  comparison of results, **312**
  immunohistochemical detection of, **309**
  negative immunoreaction, *310*
  pancreas tissue, *311*
glutamic acid (GLU), reactions of, *260*
Grashof number Gr, 135
grey body approximation, 136
Guy's Hospital, London, 10

H

H^3-magnetic resonance spectroscopy, 259–264
  acetate concentration, *261*
  amino acid concentrations, 259
  human and sheep spectra, *261*
  lactate (Lac), *261*
  metabolic decomposition of metabolites in sheep brain, *262*
  N-acetyl-aspartate (NA), *261*
  parameterized model functions for various metabolites, **262**
  proton MRS of sheep brain, *263*
  trimethylammonium (TMA), *261*
hair
  concentration profile of lidocaine in, 372, *373*
  drug testing in, 371–373
  main uptake routes of drugs into, *372*
hand, grading of random sample, **36**
hand muscle, grading, **35**
Harper, Lynne, 303
heart, latency, survival and resuscitation periods, *27*
heart blood, pH in post-mortem, *29*
heart tissue
  biomarker correlating PMI, *285*
  PMI and equations, *286*
heat conduction, 134
heat conductivity, 141, **142**
heat equation
  finite element method, 137–140
  homogeneous, 136
heat flow, sensor, *82*
heat flow measurements
  body surfaces, 82, 84
  heat flow sensor, *82*
heat transfer
  basic equation for, 136
  differential equation, 136–137
heat transfer mechanisms, 133–137
Helpern, Milton, 303
Hensley, Benjamin, 10
Henssge, Claus, 79
  PC program for death time, 112–113, *114*
homicide, 1, 305

homogeneous heat equation, 136
human(s), thermoregulation, 163–165
human cadaver, *see also* external auditory canal (EAC)
  early experimental data, 167–168
  experimental data, 169–175
human ear
  anatomy of external, 163
  clinical infrared thermometry (IT), 165–166
  infrared tympanic thermometers (ITT), 165
  post-mortem computed tomography imaging, *164*
  problems with clinical ITA readings, 166–167
  thermometry, 165–167
human thermoregulation, 163–165
Husband, H. A., 55
hypostasis, 71–73
  elements of, 73
  probability of time interval, **314**
  time of death and, **314**
  time of onset of, **72**
hypothermia, temperature at death, 104, *104*, **105**
hypoxanthine, 222–225, 232–234
  algorithms for use of vitreous humour, for post-mortem interval (PMI), 234–238
  cellular mechanisms for, during hypoxia, *222*
  concentration in vitreous humour, *223*
  estimation of time since death, 232–239
  formulae for determining PMI, **225**, **234**
  guidelines for use of vitreous humour for estimating PMI, 238
  increase in cerebrospinal fluid by PMI, *225*
  linear regression model using, as predictor for PMI, **235**
  material and methods, 223
  methods of measurement, 234
  multivariable linear regression models for predicting PMI, 235, *236*, *237*
  PMI for potassium and, *236*, *237*
  potassium concentration over PMI, *224*
  purine metabolism from ADP, *233*
  statistical parameters on precision of estimating PMI by, **224**
  use of vitreous humour, and K^+ in practical case work, 237–238
  vitreous humour, 223–225

I
idiomuscular pad, investigations on, **32**
immersion, *see also* estimation of time of immersion
  estimation of duration of, 245–246
immunohistochemical methods
  antigens, 312
  calcitonin detection, **309**, 309–310
  case example, 312
  glucagon detection, **309**, 309–310
  insulin detection, **309**, 309–310
  thyroglobulin detection, **309**, 309–310
immunohistochemistry, post-mortem protein degradation, 265–266
incised wound, post-mortem, *312*
infinite cylinder, concept of, 14
infrared tympanic thermometers (ITTs), 165, 166
inner energy production, 136
insects, *see also* forensic entomology
  identification of, 335–336
  sampling from bodies, 339, *339*
instantaneous rigor, 57
Institute of Forensic Medicine, 340, 341
Institute of Metrology, 341
insulin, 309
  comparison of results, **312**
  immunohistochemical detection of, **309**
  pancreas tissue, *311*
  positive immunoreaction of, *310*
Intelligent Medical Systems, 165
intermediary life, 25
International Association of Forensic Sciences, 169
intoxication
  hypostasis, 71
  rigor mortis development, 61, *63*
iris
  chemical excitability, 316, *316*, 318
  electrical excitability, 30, *31*
  pharmacological excitability of, **29**, **30**
  post-mortem excitability of, *30*
ischaemia, *26*
  post-mortem course of functions and structures, *27*

J
Jacobi matrix, 138–139
Jaffe, Frederick, 303
Journal of Forensic Sciences (journal), 15

K
Kirchhofrosen, 71
Knight, Bernard, 1, 19, 20

L
lactate
  metabolic decomposition, *262*
  proton magnetic resonance spectroscopy, *263*
lactic acid, cerebrospinal fluid over PMI, 28, *29*
lag period, plateau, 14
laminar flows, 134
latency period
  definition, 25
  heart, *27*
  organs, *26*
law of denervation, 29, 30
leaves, body cooling under, 101, **101**
Lebourdais, Isobel, 303
Lepus timidus varronis, 353
Libby, Willard Frank, 345
lidocaine, concentration profile in hair, 372, *373*
ligature strangulation, *312*
liquid chromatography mass spectrometry/mass spectrometry (LC-MS/MS), post-mortem protein degradation, 268
liver tissue
  biomarker correlating PMI, *285*
  PMI and equations, *286*
lividity, 314, **315**, *see also* post-mortem lividity
  causes, consequences and phenomena, **71**
  post-mortem, 71–72
  shifting after turning body, *73*
  time course of criteria, **74**
livor mortis, prone position of body, *21*
longitudinal studies, electrical excitability, 40–47
loss of blood, 11
Lucilia sericata, 341, 342, 366–367

M
magnetic resonance imaging (MRI), 355
magnetic resonance spectroscopy (MRS), *see also* H^3-magnetic resonance spectroscopy
  ^{1}H and ^{31}P, 365–366
Mall, Gita, 147
Marshall, T. K., 15
mass density, 141, **142**
mass spectrometry, post-mortem protein degradation, 267–268
Matrix-Assisted Laser Desorption/Ionization Time of Flight Mass Spectrometry (MALDI-TOF-MS), post-mortem protein degradation, 268
mechanical excitability, skeletal muscle, 315, **315**
mechanical muscle phenomenon, 18
Medical Examiner, The (journal), 10
Medici Dynasty, 194
Medicine, Science and the Law, 28
Megaselia scalaris, 341, 342
melatonin, circadian rhythm, 289
meshing, 140
methodology, estimation of time since death, 3–4
Methods of Forensic Science (Lundquist), 25
microbial eukaryotic community, decomposition, *291*

micro-computed tomography (micro-CT), 366–368
mimic muscles
  contraction of, *35*
  positions of electrodes for stimulation of, *37*
Ministry of Defence (MoD), 168
model curve T(*t*)
  body core, 132
  death time estimation, *133*
  mathematical approaches, 133
  physics-based approaches, 133
model error, finite element (FE), 149
model of Henßge, 147
model of Marshall and Hoare, 147, *148*
Mortiz, Alan R., 4
Mostly Murder (Smith), 14
MSC Software, MARC, 140
mummification, preservation of cadaver, 192–193, *193*
mummified hare (Alps), radiocarbon dating, 352–353, *353*
Munich Institute of Legal Medicine, 147
muscle(s)
  central nervous system and, in rigor mortis, 54
  parameters of excitation, **37**
  rigor mortis development and mass of, 60
  Zsako's phenomenon, 32–34, *33*, *34*
muscular contraction(s)
  composition of reference and control samples, **42**
  differences among muscle groups, 46
  differences between contralateral groups, 45–46
  experimental procedure and equipment, **42**
  graphical forms of, 40–41, *42*
  insertion of force transducer and puncture electrodes, *42*
  objectifying, 40
  one-peak shape of, 43
  positions of electrodes, 36, **36**
  post-mortem change in shape of, *43*
  recommendations, 47
  recommendations for practical use, 36–37
  relaxation time over PMI, *44*
  remodelled reference and control sample, **44**
muscular orbicularis oculi, degrees of electrical excitability, **37**
myo-inositol, proton magnetic resonance spectroscopy, *263*

N

N-acetyl-aspartate (NAA)
  metabolic decomposition, *262*
  proton magnetic resonance spectroscopy, *263*
natural convection, 134
Necrobia rufipes, 341
Newtonian cooling coefficient (constant *B*)
  broken cooling experiments, *89*, *90*
  estimation by multiple temperature measurements, 86, 88
  indirect estimation, 88–90
  investigations on bodies, 91–92
  principle of corrective factors of body weight, 91–92
Newton's law of cooling, 5, 13, 80, 85, *85*, 182, 183
  heat transfer equation, 134–135
nomogram method (NM), 152
  accuracy of calculated time since death, 126–129
  application in casework, 116–131
  combined brain and rectal temperatures, 130–131
  computer program www.AMAsoft.de, *119*, 124
  data of paired cases, **122**
  death time estimation, **320**, **321**
  determining time since death, *319*
  evaluating the corrective factor, 121, 123
  evaluation of mean ambient temperature, 118, *119*, 120–121
  fever at death, 125
  investigation of central brain temperature, 129–130
  known changes of cooling conditions, 123
  longer agony, 126
  reconstruction of body cooling, 129
  rectal temperature, 79
  special problems, 125–126
  time of death, 113, *114*, 115, *115*, *116*
  uncertainty in value of corrective factors, 123–124
  use of, *117*, *119*
  when not to use, 124–125
noradrenaline (NA), synthesis, metabolism and effects of, *31*
numerical stability, finite element (FE), 149
Nusselt number Nu, 135
Nysten, Pierre-Hubert, 19, 54
Nysten's law, 54, 65
Nysten's rule, 15

O

Ohm's law, 82, 84, *84*
orbicularis oculi
  degrees of positive reaction for stimulating, *38*
  grading, **35**
  grading of random sample, **36**
  positions of electrodes, **36**
  subjective grading of muscular responses to excitation, **36**
orbicularis oris
  grading, *35*, **35**
  grading of random sample, **36**
  positions of electrodes, *35*
organs
  reported post-mortem protein changes in, **270–273**
  RNA stability in cadaver, 284
Oscheius tipulae, decomposition, *291*
Ototemp Veterinary infrared Tympanic Temperature Scanner, 168
Ötzi's pet, radiocarbon dating, 352–353, *353*

P

PC program www.AMAsoft.de, *318*, 319
Pediatrics (journal), 232
Penistan, John, 303, 304
percentage cooling rate, 15
permafrost bodies, 194
Petty, Charles, 303
phase-contrast microscopy, 31
physical exercise, rigor mortis development, 60, *61*, **61**
Piophila casei, 340
plateau
  lag period, 14
  temperature, 11, 12, 13
PMCT, *see* post-mortem computed tomography (PMCT)
post-mortem blanching, *74*, 74–75
post-mortem caloricity, 10
post-mortem changes
  acceleration of onset and extent of, **190**
  deceleration of onset and extent of, **190**
post-mortem chemistry
  animal predation, 192
  autolysis, 189
  decomposition, 191–192
  putrefaction, 189–191
post-mortem computed tomography (PMCT)
  adrenal gland changes, 361
  airways, lungs and pleural cavities, 356–357, *358*
  cerebral parenchyma attenuation, *361*, 361–364, *362*, *363*, *364*
  liver, 359
  livor mortis, 356, *356*, *357*
  post-mortem gas formation, 359–361, *360*
  rigor mortis, 355–356
  skin, 359
  thyroid gland changes, 361
  vascular wall changes, 359, *359*
post-mortem course of functions, global ischaemia, *27*
post-mortem electrical excitability, skeletal muscle, 15–18
post-mortem experiments, electrical excitability of skeletal muscles, *16*, *17*
post-mortem interval (PMI)
  Baccino's global formula, 174, *174*
  Baccino's interval formula, 173, *174*

  comparison of actual and formula I of, *199*
  deviations between extrapolated and real time since death, *218*
  equation, 229
  estimated values for increasing potassium values, **220**
  estimating, from decomposed human remains, 194–196
  external auditory canal (EAC) for estimating, 162–163, 177–178
  forensic entomology, 336–338
  formula, 170
  formulae for determining, **219**
  formulae for determining, with hypoxanthine, **225**
  guidelines for using vitreous humour for estimation of, 238
  linear regression model using hypoxanthine, **235**
  potassium concentration *vs.*, *229*
  statistical parameters on precision of estimating, **224**
  thanatobiological approach for estimation, 286–287
  thanatomicrobiome for estimating, 289–292
  trends of estimates, *292*
  universal equation to estimate, 199–200
  variables influencing calculation, 175–176
  vitreous potassium, *217*
  vitreous potassium as measure of, 22
post-mortem lividity, 20–21, *21*, 71
  disappearance phenomena, 73, *73*
  discolouration, 71, **72**
  stages of, 75
  temperature and blanching influence, *75*
post-mortem magnetic resonance imaging (PMMR), 355, 365
post-mortem mechanical excitation, skeletal muscle, 32–34
post-mortem submersion interval (PMSI)
  decomposition in non-sequestered aquatic environment, 198
  predicting, for human remains from water, 196–200
  universal equation to estimate, 199–200
post-mortem temperature plateau (constant *A*)
  determination on dummies, 102–103
  estimation on bodies, 101–102
potassium levels, *see also* vitreous potassium
  age and temperature, 229–232
  cerebrospinal fluid (CSF) and, 240–242, *241*, *242*, *243*, 244, *244*
  influence of ambient temperature, 230
  influence of decedent age, 230–231
  influence of other factors, 231
  linear regression model using hypoxanthine, **235**
  multivariate model of estimation of time of death, 231–232
  PMI (post-mortem interval) for hypoxanthine and, *236*, *237*
  PMI *vs.*, *229*
  vitreous, 22
Prandtl number Pr, 135
preservation processes
  bog bodies, 194
  cadavers, 192–194
  decomposition, 193–194
  delayed decomposition in zinc coffin, 194
  mummification, 192–193
  permafrost bodies, 194
  saponification, 193–194
pre-shape functions, 138
prism method, 153
  ambient temperature (T_a), 153
  brute-forcing calculations, *153*
  calculations, 154
  computational workflow, 157
  cooling weight curves, *154*, *157*, *158*
  corrective factors (CF), 152
  elevated rectal temperature at time of death, 155
  errors for experimental settings, **157**
  experimental setup of cooling dummies, *155*
  future improvements, 160–161
  illustration of principle, *153*
  modelled cooling curves for different A values, *160*
  overview of cooling dummies, **156**
  proof of principle, 153
  rectal temperature at time of death ($T_{r@D}$), 152
  stages of cooling scenarios, *159*
probe sites, rectal temperature, 84–85
Prokop, Otto, *17*
propionate
  metabolic decomposition, *262*
  metabolite, 260
  parameterized model functions, **262**
  proton magnetic resonance spectroscopy, *263*
prostigmine, post-mortem transport of gastric contents, 297, **297**, 298
protein degradation, post-mortem
  attempting a practical application, 275–279
  basics of, 264–265
  case report, 278–279
  difficulty in method for practice, 275
  enzyme activity assays, 268–269
  enzyme-linked immunosorbent assay (ELISA), 268
  forensic context, 265
  immunohistochemistry, 265–266
  influencing factors, 274
  lateral flow assay, 269
  mass spectrometry, 267–268
  methodology, 265–269
  post-mortem, profiles, 277, *278*
  properties of tissues as target for protein-based PMI estimation, **275**
  protocol for collection and storage of tissue samples, 276
  quest for suitable target tissues, 269, 274
  ratio of collagenous to non-collagenous protein (Co/NCo) in skeletal remains, 268–269
  reported post-mortem protein changes in organs/tissues, **270–273**
  representative patterns using standard procedure, *277*
  routine applicability, 274–275
  Western blotting, 266–267
Proteus, 190
proton magnetic resonance spectroscopy (MRS), *see* H^3-magnetic resonance spectroscopy
putrefaction
  bloating, 189, *189*
  chemistry of, 190–191
  correlation of water temperature and stages of, 246–247, *247*
  definition, 189
  morphological changes in, **191**
  progression of, of bodies in air, **191**
  proton degradation during, 259
  venous marbling, 189, *190*
putrefactive changes, post-mortem, 21–22
Python programming language, 156

R

radiation, 133
radiocarbon dating
  Asian mummy from Mannheim (Germany), 351, *352*
  basic principles, 345–347
  bog dog from Burlage (Germany), 351–352, *352*
  bomb peak calibration, *347*
  calibration, 347
  case studies from ice age to present, 348–353
  cave bears from Baumann's Cave (Germany), 348–349, *349*
  cycle in atmosphere and biosphere, *346*
  Egyptian mummy from Basel (Switzerland), 349–350, *350*
  in forensics, 348
  mummified hare from Alps, 352–353, *353*
  sample material and sample pre-treatment, 348
  South American mummy group from Mannheim (Germany), 350–351, *351*
Rainy, Harry, 11, *12*

Réaumur, René, 9
Recherches de physiologie et de chimie pathologiques (Nysten), 19
recovering time, 26
rectal temperature
  brain and, 130–131
  mathematically modelling cooling curve, 85–86
  nomogram method, 79
  post-mortem cooling process, *182*
  probe sites, 84–85
  temperature at death, 103–104
reperfusion, *26*
Researches, Physiological and Anatomical (Davey), 9
resuscitation period, 26
  definition, 25
  duration of, 26
  heart, *27*
  organs, *26*
Reynolds number Re, 135
Richardson, W. B., 11
rigor, development of, 313–314, **314**
rigor mortis, 15, 18–19, 51, **315**, *see also* cadaveric rigidity
  adenosine triphosphate (ATP) theory, 52
  apparatus for measurement of intensity, *59*
  cadaveric spasm, 57
  chronology of development of, 54–55
  delay period (first phase), 53
  explanation of mechanism of, 51–54
  influence of central nervous system, 56–57
  influence of temperature, 55–56, **56**
  instantaneous rigor, 57
  objective measurements of, 57–59
  onset period (irreversible) (second phase), 53
  reestablishment, 55
  resolution (fourth phase), 53–54
  rigor (irreversible) (third phase), 53
  serial objective measurements following development of, 59–67
  sliding filament model, 52
  time course of, **19**
rigor mortis development, objective measurements, 59–67
  breaking effect, 63, *64*, 65
  central nervous system effect, 65
  electrocution effect, 61, 63, *64*
  estimating time since death by measuring intensity of, 65–67, *66*
  evolution of, in rat, *60*
  experimental evaluation of, **66**
  intoxication by strychnine, 61, *63*
  muscle mass difference effects, 60
  Nysten's law, 65
  physical exercise, 60, *61*, **61**
  temperature effects, 61, *62*
RNA degradation
  biomarkers correlating PMI, *285*
  concurrency method, 283
  environmental temperature as factor for, 284
  estimation of post-mortem interval (PMI), 284–285
  PMI estimation using microRNAs (miRNAs), 285–286
  predicted *vs.* actual PMI, *287*
  rate method, 283
  scheme of experimental design for datasets, *287*
  stability in cadaver organs, 284
  thanatobiological approach for PMI estimation, 286–287
  time since death, 284–287
Rule of Thumb, ear temperatures, 168, 170, 172

S

saponification, decomposition of body in grave, 193–194, *194*
sarcomere, schematic of contraction and relaxation of, *52*
Schweitzer, W., 112, *113*
segmentation problem, 141
Sellier, Karl, 14–15
Seydeler, R., 11
shape functions, 138
Sharpe, Noble, 303, 304
Simpson, Keith, 21, 22, 67, 303
Sinicina, Inga, 147
six-channel thermocouple device, 14
size factor, 15
skeletal muscle, *see also* protein degradation, post-mortem
  biomarker correlating PMI, *285*
  development of electrical excitability, post-mortem, **16**
  electrical excitability, 39–40, 316, *316*
  mechanical excitability, 315, **315**
  post-mortem electrical excitability, 15–18
  post-mortem electrical excitability in casework, 34–40
  post-mortem mechanical excitability, 32–34, *33*, **33**, *34*
  protocol for collection and storage, 276
  sample collection for protein analysis, *276*
skeletonization, decomposition, 191–192
skin, measuring site, 13
sliding filament model, rigor mortis, 52
Smith, Sir Sidney, 14
sodium, 211
  box plots of concentration, *213*
  concentration, *213*
  frequency distribution of concentration, *213*
South American mummy (Germany), radiocarbon dating, 350–351, *351*
spatial gradient, 139
specific heat, 141
specific heat capacity, 136, **142**
spontaneous supravital activity, 28
Sri Lanka (Ceylon), 13
standard cooling curves, 15
Stefan-Boltzmann constant, 135
Stefan-Boltzmann law, 135
strength-duration curve, 30, *31*
Stromer, Martin, 9
Student's Hand-Book of Forensic Medicine (Husband), 55
sudden cold of collapse, 11
sudden infant death syndrome (SIDS), 232–233
sudden traumatic death
  potassium values, 212, *216*
  urea as internal standard, **217**
suggillation, 71
suicide
  forensic entomology, 339–340
  hanging, *21*
  winter indoors, 341–342
  winter outdoors, 342
supravitality, 28, *28*, 32
supravital metabolism, 28–29
supravital muscular contraction, objectifying, 40–45
supravital period, 25, 26
supravital reagibility, 28
  physiological peculiarities of, 29–32
survival period, 26
  definition, 25
  heart, *27*
  organs, *26*
systematic deviation, 149

T

Taylor, Alfred Swaine, 10
Taylor's Principles and Practice of Medical Jurisprudence (Taylor), 10
temperature
  early work on time of death and, 9–15
  estimation of time since death, 232–239
  gradients, 15
  influence on rigor mortis, 55–56, **56**
  insect development, 336
  multivariate model of estimation of time of death, 231–232
  plateau, 11, 12, 13
  potassium levels with age and, 229–232
  rigor mortis development, 61, *62*
  RNA degradation in corpses in environment, 284
  time of death measurements, **238**
temperature measuring scales
  Centigrade, 9
  Fahrenheit, 9
  Réaumur, 9
temperature time diagram, body core cooling, 132
thanatomicrobiome, PMI estimation, 289–292
thermal conductivity, 84
thermocouple device, six-channel, 14

- thermodynamics
  - microscopical theory of, 134
  - science of, 133
- thermoregulation, human, 163–165
- thought experiment, explaining math in court, 329
- thyroglobulin, 309
  - comparison of results, **312**
  - immunohistochemical detection of, **309**
  - positive immunoreaction, *311*
  - thyroid gland tissue, *311*
  - time dependency of stainability, *309*
- time of death, nomogram method, 79
- time since death, *see also* estimation of time since death; eye temperature; prism method
  - calculations of, **6**
  - DNA degradation and, 283–284
  - estimation, 152
  - as evidence at court, 6
  - eye temperature and, 181–186
  - RNA degradation and, 284–287
- time since death t_s, 132
- tissues, reported post-mortem protein changes in, **270–273**
- TOD (time of death) meter, 183, *185*
- total creatine
  - metabolic decomposition of sheep brain, *262*
  - proton magnetic resonance spectroscopy, *263*
- Truscott, Steven
  - case history, 303–304
  - gastric contents, 296
- turbulent flows, 134
- tympanic, term, 166

U

- United States of America Aerospace Program, 165
- University of Bonn, 341
- University of Chicago, 345
- University of Glasgow, 11
- urea, *see also* vitreous potassium
  - box plots of concentration, *214*
  - concentration, *214*
  - frequency distribution of concentration, *214*
  - internal standard, 210–212, **212**, **216**, **217**

V

- Veterinary and Remount Services (VRS), 168
- virtual cooling time, concept of, 15
- vitreous humour, 223–225
  - algorithms for use of, for post-mortem interval (PMI), 234–238
  - ambient temperature, 234, **234**
  - electrolyte concentrations in, 201–222
  - estimation of time since death, 232–239
  - guidelines for use in estimation PMI, 238
  - multivariable linear regression models for predicting PMI, 235, *236*, *237*
  - normal levels of hypoxanthine and potassium, 237
  - time of death measurements, **238**
  - use of hypoxanthine and potassium in case work, 237–238
- vitreous potassium
  - accuracy of estimating time since death, 219–220, 222
  - casework and, 214–215, **216**, 217
  - creatinine at internal standard, 212
  - factors influencing postmortem rise of, 206, *208*
  - influence of temperature on post-mortem rise in, *230*
  - investigations on, **203–205**
  - local regression model, 217–218
  - multiple linear regression analysis, 222, *222*
  - multivariate model of estimation of time of death, 231–232
  - post-mortem interval, 22
  - potassium in vitreous humour, *206*, *207*
  - re-analysis of original data, 217–218
  - recommendations for future studies, 212–213
  - re-evaluation of data of Lange and Associates, 218–219
  - regression parameters of linear regression for estimating time since death, **221**
  - review of literature on, 202, 206
  - statistical parameters on precision of estimating PMI by, **224**
  - sudden traumatic death, 212, *216*
  - urea as internal standard, 210–212, **212**, **217**
  - values of normal individuals *vs.* time since death, *205*
- von Hofmann, Eduard, *18*, 18–19

W

- water, decomposition of bodies in, 21, *22*
- water temperature, *see also* estimation of time of immersion
  - average monthly water temperature of River Rhine, *257*, **258**
  - correlation with stages of putrefaction, 246–247, *247*
- Western blotting, post-mortem protein degradation, 266–267
- *Western Journal of Medicine and Surgery* (journal), 10
- Wirodouble® duplicating hydrocolloid, 156

Z

- zinc coffin, delayed decomposition, 194
- Zsakó, István, 18
- Zsako's phenomenon, muscle excitation, 32–34, *33*, *34*